THE 69TH INTERNATIONAL

CONFERENCE FOR STUDENTS OF PHYSICS AND NATURAL SCIENCES

OPEN READINGS

BOOK OF ABSTRACTS | 2026

Vilnius University

VILNIUS UNIVERSITY PRESS

Editors:

Rimantas Naina
Vincentas Adomaitis
Laurynas Vorobjovas
Tautvydas Kairys

Cover and Interior Design:

Goda Grybauskaitė
Agnė Schoroškaitė

Vilnius University Press
9 Saulėtekio Av., III Building, LT-10222 Vilnius
info@leidykla.vu.lt, www.leidykla.vu.lt/en/
www.knygynas.vu.lt, www.journals.vu.lt

Bibliographic information is available
on the Lithuanian Integral Library Information System (LIBIS) portal ibiblioteka.lt
ISSN 3030-2463

© Vilnius University, 2026

Dear Participant,

Welcome to the 69th International Conference for Students of Physics and Natural Sciences — Open Readings 2026!

The Open Readings 2026 organizing committee is proud to welcome students and accomplished scientists from around the world. This conference provides a platform for growth as a researcher — through sharing your work, exchanging ideas, and building connections with fellow scientists across disciplines.

This year's programme features lectures by world-renowned scientists covering a wide array of topics, alongside presentations from researchers who bring fresh perspectives and new ideas. We are confident the conference will offer an enriching and memorable experience for all participants.

We encourage you to approach this opportunity with curiosity and an open mind. By doing so, you contribute to the spirit of collaboration that drives scientific progress and helps shape a brighter future for us all.

We wish you a productive and inspiring conference. May Open Readings 2026 motivate you to carry curiosity and innovation with you throughout your life and career.

Sincerely,
The Open Readings Organizing Committee

OPEN READINGS

Conference Chair

Goda Grybauskaitė, *Faculty of Physics, Vilnius University, SPIE Student Chapter Vilnius University, Optica Student Chapter Vilnius University, European Physical Society Young Minds Vilnius Section*

Organizing Committee

Martynas Keršys (Conference Vice-Chair), *Faculty of Physics, Vilnius University, SPIE Student Chapter Vilnius University, Optica Student Chapter Vilnius University, European Physical Society Young Minds Vilnius Section*

Tautvydas Kairys (Secretary), *Faculty of Physics, Vilnius University, Optica Student Chapter Vilnius University*

Eimantas Urniežius (Human Resources), *Faculty of Physics, Vilnius University*

Džiugas Krencius (Head of Academic Relations), *Faculty of Physics, Vilnius University, SPIE Chapter of Vilnius University*

Teresė Kreišmontaitė (Head of Finance), *Faculty of Physics, Vilnius University, SPIE Student Chapter Vilnius University, Optica Student Chapter Vilnius University, European Physical Society Young Minds Vilnius Section*

Laura Grizickaitė (Head of Communication), *Faculty of Philology, Vilnius University*

Smiltė Gibavičūtė (Head of Participant Support), *Faculty of Physics, Vilnius University, SPIE Chapter of Vilnius University, European Physical Society Young Minds Vilnius Section*

Ignas Dailidėnas (Head of Pupils' Session), *Faculty of Physics, Vilnius University, SPIE Chapter of Vilnius University*

Kristupas Bagdonas (Head of Café Scientifique), *Faculty of Physics, Vilnius University, SPIE Chapter of Vilnius University*

Agnė Schoroškaitė (Head of Design), *Faculty of Physics, Vilnius University*

Vincentas Adomaitis (Head of Technical Support), *Faculty of Physics, Vilnius University, SPIE Chapter of Vilnius University*

Rimantas Naina (Head of Systems Engineering), *Faculty of Physics, Vilnius University, SPIE Chapter of Vilnius University*

Lukas Alaburda, *Faculty of Physics, Vilnius University*

Joana Barauskaitė, *Faculty of Physics, Vilnius University*

Miglė Bondarevaitė, *Faculty of Physics, Vilnius University*

Daniil Čiupalov, *Faculty of Physics, Vilnius University*

Paulius Daraška, *Faculty of Physics, Vilnius University*

Atėnė Dovydėnaitė, *Faculty of Physics, Vilnius University*

Julija Dvilevičiūtė, *Faculty of Physics, Vilnius University*

Aurėja Ertmanaitė, *Faculty of Physics, Vilnius University, European Physical Society Young Minds Vilnius Section*

Patricija Ivanauskaitė, *Faculty of Physics, Vilnius University*

Paulius Ivancius, *Faculty of Physics, Vilnius University*

Andrėja Janulevičiūtė, *Faculty of Physics, Vilnius University*

Deimantė Juknevičiūtė, *Faculty of Physics, Vilnius University, SPIE Chapter of Vilnius University, European Physical Society Young Minds Vilnius Section*

Linas Jūrėnas, *Faculty of Physics, Vilnius University*

Mantas Krejaras, *Faculty of Electronics, Vilnius Tech*

Erika Lengvinaitė, *Faculty of Physics, Vilnius University*

Dominykas Mačiulaitis, *Faculty of Physics, Vilnius University*

Jokūbas Mačiulis, *Faculty of Physics, Vilnius University*

Rojus Mervižinskas, *Faculty of Physics, Vilnius University*

Laura Milaknytė, *Life Sciences Center, Vilnius University*

Kristina Miliauskaitė, *Faculty of Electronics, Vilnius Tech*

Augustas Pupinas, *Faculty of Physics, Vilnius University*

Kamilė Simokaitytė, *Faculty of Physics, Vilnius University*

Emilijus Stankevičius, *Faculty of Physics, Vilnius University*

Akvilė Sukauskaitė, *Faculty of Physics, Vilnius University*

Eimantas Šiaulys, *Faculty of Physics, Vilnius University*

Ervinas Trusilo, *Faculty of Physics, Vilnius University*

Mykolas Vaitilas, *Faculty of Physics, Vilnius University*

Laurynas Vanagas, *Faculty of Physics, Vilnius University*

Laurynas Vorobjovas, *Faculty of Physics, Vilnius University*

Chairmen

Darius Abramavičius, *Institute of Chemical Physics, Faculty of Physics, Vilnius University*

Saulius Bagdonas, *Laser Research Center, Faculty of Physics, Vilnius University*

Rita Bukšnaitienė, *Department of Organic Chemistry, Faculty of Chemistry and Geosciences, Vilnius University*

Jevgenij Chmeliov, *Institute of Chemical Physics, Faculty of Physics, Vilnius University*

Marija Ger, *Institute of Biochemistry, Life Sciences Center, Vilnius University*

Lina Grinevičiūtė, *Department of Laser Technologies, Center for Physical Sciences and Technology*

Vytautas Jukna, *Laser Research Center, Faculty of Physics, Vilnius University*

Mindaugas Karaliūnas, *Department of Semiconductor Physics, Faculty of Physics, Vilnius University*

Aivaras Kareiva, *Institute of Chemistry, Faculty of Chemistry and Geosciences, Vilnius University*

Tatjana Kirtiklienė, *Department of Microbiology and Biotechnology, Life Sciences Center, Vilnius University*

Eglė Lastauskienė, *Institute of Biosciences, Life Sciences Center, Vilnius University*

Mažena Mackoit-Sinkevičienė, *Institute of Theoretical Physics and Astronomy, Faculty of Physics, Vilnius University*

Tadas Malinauskas, *Institute of Photonics and Nanotechnology, Faculty of Physics, Vilnius University*

Marius Maskoliūnas, *Institute of Theoretical Physics and Astronomy, Faculty of Physics, Vilnius University*

Saulius Miasojedovas, *Institute of Photonics and Nanotechnology, Faculty of Physics, Vilnius University*

Balys Momgaudis, *Laser Research Center, Faculty of Physics, Vilnius University*

Ieva Plikusienė, *Institute of Chemistry, Faculty of Chemistry and Geosciences, Vilnius University*

Edita Stonkutė, *Institute of Theoretical Physics and Astronomy, Faculty of Physics, Vilnius University*

Vincas Tamošiūnas, *Institute of Photonics and Nanotechnology, Faculty of Physics, Vilnius University*

Gražina Tautvaišienė, *Institute of Theoretical Physics and Astronomy, Faculty of Physics, Vilnius University*

Ieva Uogintė, *Department of Environmental Research, Center for Physical Sciences and Technology*

Lina Zabulienė, *Institute of Clinical Medicine, Faculty of Medicine, Vilnius University*

Programme Committee

Brigita Abakevičienė, *Institute of Materials Science, Faculty of Mathematics and Natural Sciences, Kaunas University of Technology*

Markus Ambrosh, *Institute of Theoretical Physics and Astronomy, Faculty of Physics, Vilnius University*

Erikas Atkočaitis, *Laser Research Center, Faculty of Physics, Vilnius University*

Dominykas Augulis, *Institute of Photonics and Nanotechnology, Faculty of Physics, Vilnius University*

Saulius Bagdonas, *Laser Research Center, Faculty of Physics, Vilnius University*

Gintautas Bagdžiūnas, *Institute of Biochemistry, Life Sciences Center, Vilnius University*

Aldona Balčiūnaitė, *Department of Optoelectronics, Center for Physical Sciences and Technology*

Eglė Balčiūnaitė, *Laboratory of Molecular Oncology, National Cancer Institute*

Rimantė Bandzevičiūtė, *Institute of Chemical Physics, Faculty of Physics, Vilnius University*

Dovydas Banevičius, *Institute of Photonics and Nanotechnology, Faculty of Physics, Vilnius University*

Veronika Borutinskaite, *Institute of Biochemistry, Life Sciences Center, Vilnius University*

Irina Buchovec, *Institute of Photonics and Nanotechnology, Faculty of Physics, Vilnius University*

Marius Butkevičius, *Institute of Biochemistry, Life Sciences Center, Vilnius University*

Rytis Butkus, *Institute of Photonics and Nanotechnology, Faculty of Physics, Vilnius University*

Jurgita Butkuvienė, *Institute of Biosciences, Life Sciences Center, Vilnius University*

Jurga Būdienė, *Department of Organic Chemistry, Center for Physical Sciences and Technology*

Ernesta Bužvaitė-Vertelienė, *Department of Laser Technologies, Center for Physical Sciences and Technology*

Enrika Celitan, *Department of Biochemistry and Molecular Biology, Life Sciences Center, Vilnius University*

Jevgenij Chmeliov, *Institute of Chemical Physics, Faculty of Physics, Vilnius University*

Tomas Čeponis, *Institute of Photonics and Nanotechnology, Faculty of Physics, Vilnius University*

Justinas Čeponkus, *Institute of Chemical Physics, Faculty of Physics, Vilnius University*

Dovilė Čibiraitė-Lukenskienė, *Department of Optoelectronics, Center for Physical Sciences and Technology*

Laurynas Dagys, *Institute of Chemical Physics, Faculty of Physics, Vilnius University*

Marius Dagys, *Institute of Biochemistry, Life Sciences Center, Vilnius University*

Neringa Daugelavičienė, *EMBL Partnership Institute, Life Sciences Center, Vilnius University*

Laimonas Deveikis, *Institute of Photonics and Nanotechnology, Faculty of Physics, Vilnius University*

Eimina Dirvelytė, *Institute of Biosciences, Life Sciences Center, Vilnius University*

Jelena Dodonova - Vaitkūnienė, *Department of Organic Chemistry, Faculty of Chemistry and Geosciences, Vilnius University*

Audrius Drabavičius, *Department of Characterization of Materials Structure, Center for Physical Sciences and Technology*

Simonas Draukšas, *Institute of Theoretical Physics and Astronomy, Faculty of Physics, Vilnius University*

Arnas Drazdauskas, *Institute of Theoretical Physics and Astronomy, Faculty of Physics, Vilnius University*

Virginija Dudutienė, *Institute of Biotechnology, Life Sciences Center, Vilnius University*

Mantas Gaidys, *Laser Research Center, Faculty of Physics, Vilnius University*

Andrius Gelžinis, *Institute of Chemical Physics, Faculty of Physics, Vilnius University*

Kristijonas Genevičius, *Institute of Chemical Physics, Faculty of Physics, Vilnius University*

Lena Golubewa, *Department of Molecular Compound Physics, Center for Physical Sciences and Technology*

Lina Grinevičiūtė, *Department of Laser Technologies, Center for Physical Sciences and Technology*

Tomas Grinys, *Institute of Photonics and Nanotechnology, Faculty of Physics, Vilnius University*

Ilja Ignatjev, *Department of Organic Chemistry, Center for Physical Sciences and Technology*

Gerda Jasinevičienė, *Life Sciences Center, Vilnius University*

Justinas Jorudas, *Department of Optoelectronics, Center for Physical Sciences and Technology*

Jurga Juodkazytė, *Department of Chemical Engineering and Technology, Center for Physical Sciences and Technology*

Saulius Juršėnas, *Institute of Photonics and Nanotechnology, Faculty of Physics, Vilnius University*

Eimutis Juzeliūnas, *Department of Electrochemical Material Science, Center for Physical Sciences and Technology*

Arūnas Kadys, *Institute of Photonics and Nanotechnology, Faculty of Physics, Vilnius University*

Virginija Kalcienė, *Institute of Biosciences, Life Sciences Center, Vilnius University*

Agnė Kalnaitytė-Vengelienė, *Laser Research Center, Faculty of Physics, Vilnius University*

Mindaugas Kamarauskas, *Institute of Chemical Physics, Faculty of Physics, Vilnius University*

Rūta Kananavičiūtė, *Institute of Biosciences, Life Sciences Center, Vilnius University*

Mindaugas Karčiauskas, *Department of Fundamental Research, Center for Physical Sciences and Technology*

Dovydas Karoblis, *Department of Inorganic Chemistry, Faculty of Chemistry and Geosciences, Vilnius University*

Renata Karpicz, *Department of Molecular Compound Physics, Center for Physical Sciences and Technology*

Irmantas Kašalynas, *Institute of Applied Electrodynamics and Telecommunications, Faculty of Physics, Vilnius University*

Asta Kaušaitė-Minkštimienė, *Institute of Chemistry, Faculty of Chemistry and Geosciences, Vilnius University*

Darius Kazlauskas, *Institute of Biotechnology, Life Sciences Center, Vilnius University*

Egidijus Kazlauskas, *Institute of Biotechnology, Life Sciences Center, Vilnius University*

Vytautas Klimavičius, *Institute of Chemical Physics, Faculty of Physics, Vilnius University*

Tatjana Kochanė, *Department of Polymer Chemistry, Faculty of Chemistry and Geosciences, Vilnius University*

Aleksejus Kononovičius, *Institute of Theoretical Physics and Astronomy, Faculty of Physics, Vilnius University*

Indrė Kučinskaitė-Kodzė, *Institute of Biotechnology, Life Sciences Center, Vilnius University*

Dovilė Lengvinaitė, *Institute of Chemical Physics, Faculty of Physics, Vilnius University*

Ramūnas Levinas, *Department of Catalysis, Center for Physical Sciences and Technology*

Mažena Mackoit-Sinkevičienė, *Institute of Theoretical Physics and Astronomy, Faculty of Physics, Vilnius University*

Tadas Malinauskas, *Institute of Photonics and Nanotechnology, Faculty of Physics, Vilnius University*

Viktoras Masevičius, *Department of Organic Chemistry, Faculty of Chemistry and Geosciences, Vilnius University*

Tadas Matijošius, *Department of Chemical Engineering and Technology, Center for Physical Sciences and Technology*

Ieva Matulaitienė, *Department of Organic Chemistry, Center for Physical Sciences and Technology*

Algirdas Mekys, *Institute of Photonics and Nanotechnology, Faculty of Physics, Vilnius University*

Saulius Miasojedovas, *Institute of Photonics and Nanotechnology, Faculty of Physics, Vilnius University*

Algirdas Mikalkėnas, *Institute of Biosciences, Life Sciences Centre, Vilnius University*

Lina Mikoliūnaitė, *Department of Organic Chemistry, Center for Physical Sciences and Technology*

Balys Momgaudis, *Laser Research Center, Faculty of Physics, Vilnius University*

Aušrinė Navickaitė, *Institute of Biosciences, Life Sciences Center, Vilnius University*

Irena Nedveckytė, *Institute of Biosciences, Life Sciences Centre, Vilnius University*

Edvinas Orentas, *Department of Organic Chemistry, Faculty of Chemistry and Geosciences, Vilnius University*

Edita Palaimienė, *Institute of Applied Electrodynamics and Telecommunications, Faculty of Physics, Vilnius University*

Rasa Pauliukaitė, *Department of Nanoengineering, Center for Physical Sciences and Technology*

Gražina Petraitytė, *Department of Organic Chemistry, Faculty of Chemistry and Geosciences, Vilnius University*

Augustinas Petrulėnas, *Department of Laser Technologies, Center for Physical Sciences and Technology*

Valentina Plaušinaitienė, *Department of Functional Materials and Electronics, Center for Physical Sciences and Technology*

Žydrūnas Podlipskas, *Institute of Photonics and Nanotechnology, Faculty of Physics, Vilnius University*

Sandra Pralgauskaitė, *Institute of Applied Electrodynamics and Telecommunications, Faculty of Physics, Vilnius University*

Vilmantas Pupkis, *Department of Neurobiology and Biophysics, Life Science Center, Vilnius University*

Steponas Raišys, *Institute of Photonics and Nanotechnology, Faculty of Physics, Vilnius University*

Simonas Ramanavičius, *Department of Electrochemical Material Science, Center for Physical Sciences and Technology*

Vilma Ratautaitė, *Department of Nanotechnology, Center for Physical Sciences and Technology*

Vytautas Rumbauskas, *Institute of Photonics and Nanotechnology, Faculty of Physics, Vilnius University*

Danielis Rutkauskas, *Department of Molecular Compound Physics, Center for Physical Sciences and Technology*

Tomas Sabirovas, *Department of Electrochemical Material Science, Center for Physical Sciences and Technology*

Skomantas Serapinas, *Life Sciences Center, Vilnius University*

Tomas Serevičius, *Institute of Photonics and Nanotechnology, Faculty of Physics, Vilnius University*

Virginija Siaurusevičiūtė, *Life Sciences Center, Vilnius University*

Gytis Sliaužys, *Institute of Chemical Physics, Faculty of Physics, Vilnius University*

Tomas Šalkus, *Institute of Applied Electrodynamics and Telecommunications, Faculty of Physics, Vilnius University*

Mindaugas Šarpis, *Institute of Photonics and Nanotechnology, Faculty of Physics, Vilnius University*

Gintautas Tamulaitis, *Institute of Photonics and Nanotechnology, Faculty of Physics, Vilnius University*

Tomas Tamulevičius, *Institute of Materials Science, Faculty of Mathematics and Natural Sciences, Kaunas University of Technology*

Viktorija Tamulienė, *Laser Research Center, Faculty of Physics, Vilnius University*

Ieva Uogintė, *Department of Environmental Research, SRI Center for Physical Sciences and Technology*

Nina Urbelienė, *Institute of Biochemistry, Life Sciences Center, Vilnius University*

Giedrė Valiulienė, *Department of Molecular Cell Biology, Life Sciences Center, Vilnius University*

Aušra Valiūnienė, *Institute of Chemistry, Faculty of Chemistry and Geosciences, Vilnius University*

Vladas Vansevičius, *Department of Fundamental Research, Center for Physical Sciences and Technology*

Gabrielė Vasiliauskaitė, *Department of Neurobiology and Biophysics, Life Science Center, Vilnius University*

Julius Vengelis, *Laser Research Center, Faculty of Physics, Vilnius University*

Linas Vilčiauskas, *Department of Chemical Engineering and Technology, Center for Physical Sciences and Technology*

Edita Voitechovič, *Department of Nanoengineering, Center for Physical Sciences and Technology*

Aistė Zentelytė-Vilkė, *Institute of Biochemistry, Life Sciences Center, Vilnius University*

Rokas Žalnėravičius, *Department of Electrochemical Material Science, Center for Physical Sciences and Technology*

Andrius Žemaitis, *Department of Laser Technologies, Center for Physical Sciences and Technology*

Albinas Žilinskas, *Institute of Chemistry, Faculty of Chemistry and Geosciences, Vilnius University*

Ieva Žutautė, *Department of Organic Chemistry, Faculty of Chemistry and Geosciences, Vilnius University*

69TH INTERNATIONAL

CONFERENCE FOR STUDENTS OF PHYSICS AND NATURAL SCIENCES

OPEN READINGS 2026

DAY 1 (2026-04-27)

Room: A101 — Opening Ceremony — **9:00-9:15**

Break — **9:15-9:30**

Room: A101 — **ORAL SESSION: O1** — **9:30-10:45**

Astrophysics and Theoretical Physics

9:30 Bruno Ćurjurić: THE CHRONICLES OF THE MILKY WAY: THE CARBON, THE NITROGEN, AND THE STELLAR AGES

9:45 Barkha Yakub Bale: TRACING INTERNAL MIXING THROUGH LITHIUM AND CNO ABUNDANCES IN RS CVN STARS

10:00 Ashutosh Sharma: PROBING NEUTRON-CAPTURE ELEMENTS IN PLANET-HOST STARS THROUGH HIGH RESOLUTION SPECTROSCOPY

10:15 Milda Valytė: FROM SIMULATION TO OBSERVATION: TESTING COMPATIBILITY OF AGN OUTFLOW RATE ESTIMATES

10:30 Vladas Šatas: THREE-DIMENSIONAL RECONSTRUCTION OF ROTATING ASTEROIDS FROM TWO-DIMENSIONAL IMAGE SEQUENCES

Session Chair: Marius Maskoliūnas

Room: D401 — **ORAL SESSION: O2** — **9:30-10:45**

Applied Electrodynamics

9:30 Daniel Daukševič: CYBERSECURITY REQUIREMENTS ASSURANCE IN CRITICAL INFRASTRUCTURE SYSTEMS THROUGH THE APPLICATION OF FORMAL VERIFICATION AND ARTIFICIAL INTELLIGENCE-BASED METHODS

9:45 Augustas Koklevičius: GENETICALLY OPTIMIZED MULTILAYER METASURFACE FOR X-BAND RADAR REFLECTION REDUCTION

10:00 Danas Černeckas: TRANSMISSION GRID POWER TRANSFORMER INSULATION HEALTH MONITORING AND ASSESSMENT USING ACOUSTIC EMISSION AND ULTRA HIGH FREQUENCY SENSORS

10:15 Patricija Ivanauskaitė: WIDEBAND PERFORMANCE EVALUATION AND CHARACTERISATION OF ANTENNA-COUPLED CMOS TERAFET DETECTORS FROM 0.1 TO 1.2 THZ

10:30 Justina Žemgulytė: HORIZONTALLY ORIENTED LOW PROFILE DIELECTRIC RESONATOR ANTENNA WITH EXTREME TEMPERATURE STABILITY FOR RADIO WAVE ENERGY HARVESTING

Session Chair: Mindaugas Karaliūnas

Coffee Break — **10:45-11:15**

Room: A101 —  **Willy Benz | PLENARY TALK** *University of Bern, Switzerland* — **The CHEOPS Mission: a Unique Interface Between Discovery and Characterisation of Exoplanets** — **11:15-12:30**

Chair: Edita Stonkutė

Lunch Break — **12:30-13:30**

Room: A101 — **ORAL SESSION: O3** — **13:30-15:00**

Astrophysics and Theoretical Physics

13:30 Dharma Prasetya Permana: OPTICAL SPIN-ORBIT DYNAMICS OF VECTOR VORTICES IN COHERENTLY PREPARED MEDIA

13:45 Austėja Mikalčiūtė: COMPLETE EXCITON HAMILTONIAN FOR PHOTOSYNTHETIC PIGMENT-PROTEIN COMPLEXES

14:00 Jorūnas Dobilas: CORRELATION-DRIVEN WEYL PHYSICS FROM AB INITIO DFT+DMFT THEORY

14:15 Meda Paulavičiūtė: VISUALIZATION OF ΛB BARYON DECAYS USING THE ECC METHOD FOR MISSING MOMENTUM RECONSTRUCTION

14:30 Dominykas Malinauskas: YUKAWA SECTOR RENORMALIZATION IN THE GRIMUS-NEUFELD MODEL

14:45 Justina Vaičaitytė: TIME-DEPENDENT PROJECTION SUPEROPERATOR APPROACH TO OPEN QUANTUM SYSTEMS

Session Chair: Jevgenij Chmeliov

Room: D401 — **ORAL SESSION: O4** — **13:30-15:00**

Spectroscopy and Imaging

13:30 Erikas Tarvydas: DYNAMIC FULL-FIELD OPTICAL COHERENCE MICROSCOPY FOR LIVE TISSUE IMAGING

13:45 Austėja Trečiokaitė: HIGH-THROUGHPUT SPATIO-TEMPORAL OPTICAL COHERENCE TOMOGRAPHY FOR ENHANCED RETINAL IMAGING SENSITIVITY

14:00 Aurimas Dubauskas: MULTINUCLEAR NMR STUDY OF THE $NA_{2.5}V_{1.5}Tl_{0.5}(PO_4)_3$ AQUEOUS ELECTROCHEMICAL DEGRADATION

14:15 Justinas Minkevičius: THE STUDY OF PROTEIN NMR RELAXATION - DURATION AND PRECISION CONSTRAINTS

14:30 Rodrigas Liudvinavičius: DIRECT LASER WRITING OF PLASMONIC GRATINGS: OPTICAL RESPONSE AND APPLICATIONS

14:45 Kernius Vilkevičius: RAPID FEMTOSECOND-LASER FABRICATION OF A PLASMONIC SENSOR FOR GLYCEROL DETECTION

Session Chair: Darius Abramavičius

Coffee Break — **15:00-15:30**

Public Lab Tour: Department of Nuclear Research (FTMC) — **15:00-15:30**

Room: A101 —  **Rainer Blatt | PLENARY TALK** *University of Innsbruck, Austria* — **Quantum Computation and Quantum Simulation With Strings of Trapped Ca+ Ions** — **15:30-16:45**

Chair: Mažena Mackoit-Sinkevičienė

Break — **16:45-17:00**

Main hall — **POSTER SESSION: P1** — **16:30-18:00**

Astrophysics and Theoretical Physics, Spectroscopy and Imaging, Applied Electrodynamics

69TH INTERNATIONAL

CONFERENCE FOR STUDENTS OF PHYSICS AND NATURAL SCIENCES

OPEN READINGS 2026

DAY 2 (2026-04-28)

Room: A101 — **ORAL SESSION: O5** — **9:00-10:30**

Chemistry

9:00 Anastasija Aleksandrovič: MODIFICATION OF SILICON OXIDE SURFACE WITH PHOSPHOLIPID BILAYERS FOR BIOSENSOR DEVELOPMENT

9:15 Miglė Stančiauskaitė: COMPARATIVE STUDY OF FC RECEPTOR BINDING AND IMMUNE MODULATION: NANOBODY-FC VS IgG IMMUNE COMPLEXES

9:30 Hassan Kouchakzadeh: DEVELOPMENT OF AN ADVANCED SURFACE ENGINEERED PLATINUM-BASED ELECTROCHEMICAL SYSTEM FOR ULTRA-SENSITIVE DETECTION OF MELOXICAM UTILIZING CHITOSAN TO SUPPRESS OXYGEN

9:45 Gerda Žižiūnaitė: EFFECTIVE DEFECT DENSITY AS A PREDICTIVE METRIC FORREPRODUCIBLE TOXIN DETECTION IN TETHERED BILAYER MEMBRANES

10:00 Kajus Momgaudis: HYBRID LIPID BILAYERS ON SILICON AS A PLATFORM FOR STUDYING PORE-FORMING TOXINS

10:15 Saari Anete Loog: ON-SITE DETECTION AND QUANTIFICATION OF SELECTED SEMI-SYNTHETIC AND NATURAL CANNABINOIDS IN CANNABIS PRODUCTS USING CAPILLARY ELECTROPHORESIS - DEEP UV FLUORESCENCE

Room: D401 — **ORAL SESSION: O6** — **9:00-10:30**

Materials Science and Nanotechnology

9:00 Jonas Jeffrey Haist: LASER ABLATION FOR RADIOACTIVE METAL SURFACE DECONTAMINATION

9:15 Martynas Talaikis: UV-SERS ON Cu, Co, AND Pd NANOSTRUCTURES FOR SELECTIVE DETECTION OF SMALL AROMATIC BIOMOLECULES

9:30 Benas Stanionis: TERAHERTZ EMISSION FROM Bi/GaAs HETEROSTRUCTURES

9:45 Andrius Masaitis: METAMATERIAL-BASED BEAM-SHAPING STRUCTURES FEATURED BY HIGHER-ORDER RESONANCES IN THZ FREQUENCY RANGE

10:00 Muhammad Haris: 2D-GRAPHENE SHIELDED GOLD METASURFACE FOR ENHANCED GREEN HYDROGEN EVOLUTION REACTION BY PHOTOELECTROCHEMICAL WATER SPLITTING

10:15 Kristupas Bagdonas: EFFICIENT THIRD-GENERATION BLUE OLEDS USING DIBENZOFURAN-BASED HIGH-TRIPLET-ENERGY HOSTS

Session Chair: Lina Grinevičiūtė

Coffee Break — **10:30-11:00**

Room: A101 —  **Sanjay Mathur | PLENARY TALK** — *University of Cologne, Germany* — **Catalysts of Change: Advanced Materials Steering Health and Energy Transition** — **11:00-12:00**

Chair: Aivaras Kareiva

Lunch Break — **12:00-13:00**

Room: A101 — **ORAL SESSION: O7** — **13:00-14:30**

Chemistry

13:00 Mihhail Fokin: ELECTROCHEMICAL FERRIER REARRANGEMENT IN FLOW

13:30 Jonas Žurauskas: PHOTOREDOX MANIFOLD FOR DEHYDROGENATIVE COUPLING USING PROTONS AS OXIDANTS

13:45 Amina Elkady: QM/MD STUDY OF STRUCTURE AND NMR SPECTRA OF TETRAPEPTIDE IN AQUEOUS IONIC LIQUID MIXTURES

14:00 Sana Abbas: GREEN AND SUSTAINABLE EXTRACTION OF MULTIFUNCTIONAL BIOACTIVE INGREDIENTS USING NATURAL DEEP EUTECTIC SOLVENTS FOR PHARMACEUTICAL APPLICATIONS

14:15 Ramunė Sidaraitė: APPLICATION OF CALCIUM OXIDE WASTE FOR THE SYNTHESIS OF HIGHER BASISITY CALCIUM SILICATEHYDRATES (CaO/SiO_2 =1.5)

Session Chair: Rita Bukšnaitienė

Room: D401 — **ORAL SESSION: O8** — **13:00-14:30**

Chemistry

13:00 Evelina Kasparavičiūtė: INFLUENCE OF DEPOSITION CONDITIONS ON THE PROPERTIES OF Sb_2S_3 LAYERS ON FTO SUBSTRATES

13:30 Sukomol Barua: ENHANCED ELECTROCATALYTIC HER PERFORMANCE: A COMPARATIVE STUDY OF OPTIMIZED BINARY AND TERNARY ELECTROCATALYSTS IN ALKALINE FRESHWATER AND SEAWATER

13:45 Ricardas Kleinauskas: TWO STAGE $CATIO_3$ SYNTHESIS IN DIFFERENT CRYSTALLINITY TIO_2 MIXTURES

14:00 Ernestas Brazys: ELECTROCHEMICAL SENSORS BASED ON MOLECULARLY IMPRINTED POLYMERS FOR DETECTION OF SMALL MOLECULES

14:15 Evelina Lukaitė: REAL-TIME ELECTROCHEMICAL MONITORING OF BIOFILM GROWTH

Session Chair: Ieva Plikusienė

Coffee Break — **14:30-15:00**

Public Lab Tour: Department of Chemical Engineering and Technologies (FTMC) — **14:30-15:00**

Room: A101 —  **Lora Heisler | PLENARY TALK** — *University of Aberdeen, Scotland* — **New Insights Into the Drug Treatment of Obesity** — **15:00-16:00**

Chair: Lina Zabulienė

Break — **16:00-16:15**

Main hall — **POSTER SESSION: P2** — **16:15-17:45**

Chemistry

69TH INTERNATIONAL

CONFERENCE FOR STUDENTS OF PHYSICS AND NATURAL SCIENCES

OPEN READINGS 2026

DAY 3 (2026-04-29)

Room: A101 **ORAL SESSION: O9** **9:00-10:30**

Laser Physics and Optical Technologies

9:00 **Jokūbas Pimpė**: HIGH REPETITION RATE DUV-NIR TUNABLE FEMTOSECOND LASER SYSTEM
9:15 **Simona Armalytė**: HIGH REPETITION RATE AND HIGH AVERAGE POWER FEMTOSECOND OPTICAL PARAMETRIC AMPLIFIER IN THE VIS AND NIR
9:30 **Kristupas Dagilis**: SUPERCONTINUUM GENERATION IN BULK SOLIDS WITH MID-INFRARED DRIVING PULSES
9:45 **Rugilė Pečiulytė**: COMPARATIVE PERFORMANCE OF BRILLOUIN ACTIVE MEDIA FOR ULTIMATE LASER PULSE COMPRESSION
10:00 **Tomas Latvys**: GENERATION OF REGULAR LASER PULSES IN A BACKWARD WAVE OPTICAL PARAMETRIC OSCILLATOR PUMPED BY INCOHERENT PULSES
10:15 **IOANNA ANGELIKI PETSI**: TWO-PHOTON POLYMERIZATION OF LOW-DENSITY MICROSTRUCTURES AND THEIR ASSEMBLY INTO RIGID HOLDERS FOR INERTIAL CONFINEMENT FUSION INVESTIGATION

Session Chair: Vytautas Jukna

Room: D401 **ORAL SESSION: O10** **9:00-10:30**

Materials Science and Nanotechnology

9:00 **Aivaras Špokas**: EXPLORING THE GROUP-V LIMITED GROWTH OF GaAsBi LAYERS
9:15 **Aistė Štaupienė**: STRUCTURAL AND OPTICAL INVESTIGATION OF GaAsBi/AlGaAs PARABOLICALLY GRADED QUANTUM WELL STRUCTURES
9:30 **Patricija Strumilaitė**: IMPACT OF RAPID THERMAL ANNEALING ON STRUCTURAL AND OPTICAL PROPERTIES OF GaAsBi/(Al,Ga)As QUANTUM WELLS
9:45 **Gabija Soltanaitė**: LOCAL V-DEFECT ENVIRONMENTS UNDER EXCITATION-DEPENDENT TRANSIENT CATHODOLUMINESCENCE
10:00 **Seda Türkcan**: CARRIER DYNAMICS IN N- AND P-TYPE InGaN LAYERS AND THE ROLE OF MAGNESIUM ACTIVATION
10:15 **Justas Žuvelis**: ELECTROLUMINESCENCE STUDY OF GaAsBi-BASED NEAR-INFRARED EMITTERS

Session Chair: Tadas Malinauskas

Coffee Break **10:30-11:00**

Room: A101



Jérôme Faist | PLENARY TALK
ETH Zürich, Switzerland

Semiconductor Quantum Walk Combs from the Near-Infrared to the Terahertz **11:00-12:00**

Chair: Vincas Tamošiūnas

Lunch Break **12:00-13:15**

Room: A101 **ORAL SESSION: O11** **13:15-14:45**

Laser Physics and Optical Technologies

13:15 **Tadas Latvys**: CONTROL OF SURFACE THERMAL EMISSION USING ULTRASHORT LASER PULSES
13:30 **Aleksandras Kondratas**: BOTTOM-UP DRILLING OF GLASS USING BURSTS OF ULTRASHORT LASER PULSES
13:45 **Abhinay Vats Mohan**: FABRICATION AND CHARACTERIZATION OF OPAQUE 3D MICROSTRUCTURES
14:15 **Florian Dötzer**: FULL-FIELD VIBRATION MEASUREMENTS USING SINGLE-SHOT SYNTHETIC WAVELENGTH INTERFEROMETRY
14:30 **Titas Tamošauskas**: MICROCOPPER ELECTRODES AND ELECTROCHROMIC MATERIALS INTERACTION WITH DIFFERENT ELECTROLYTES FOR SMART WINDOW APPLICATION

Session Chair: Balys Momgaudis

Room: D401 **ORAL SESSION: O12** **13:15-14:45**

Materials Science and Nanotechnology

13:15 **Aida Drevilkauskaitė**: CARBAZOLE-BASED PHOSPHONIC ACIDS IN PEROVSKITE SOLAR CELLS: IMPACT OF THE SUBSTITUTION PATTERN ON DEVICE PERFORMANCE
13:30 **Nida Vileniškytė**: THICKNESS-DEPENDENT PROPERTIES OF $ZnIn_2S_4$ THIN FILMS DEPOSITED BY CBD METHOD
13:45 **Guoda Gasauskaite**: NANOENGINEERED BIOPOLYMER-FULLERENE C60 COMPOSITE FILMS FOR BIOFOULING RESISTANCE
14:00 **Egle Martinaityte**: NBT-BT THIN FILMS: STRUCTURAL AND DIELECTRIC PROPERTIES
14:15 **Andrius Pečiulis**: BIOCHIPS WITH MICROSCALE SURFACE STIFFNESS PATTERNS FOR MECHANOBIOLOGICAL APPLICATIONS
14:30 **Krzysztof Gadomski**: IN-SITU XAS MEASUREMENTS OF VANADATE-PHOSPHATE GLASSES

Session Chair: Saulius Miasojedovas

Coffee Break **14:30-15:00**

Public Lab Tour: Department of Optoelectronics (FTMC) **14:30-15:00**

Room: A101



Francesca Calegari | PLENARY TALK
University of Hamburg, Germany

Tracing Electron Dynamics in Molecules: Novel Approaches for Attosecond Chemistry **15:15-16:30**

Chair: Mikas Vengris

Break **16:30-16:45**

Main hall **POSTER SESSION: P3** **16:45-18:15**

Laser Physics and Optical Technologies, Materials Science and Nanotechnology

69TH INTERNATIONAL

CONFERENCE FOR STUDENTS OF PHYSICS AND NATURAL SCIENCES

OPEN READINGS 2026

DAY 4 (2026-04-30)

Room: A101 | **ORAL SESSION: O13** | **9:00-10:30**

Biology and Medicine

9:00 Aistė Popandopula: INVESTIGATION OF THE RESPIRATORY MICROBIOME IN TUBERCULOSIS PATIENTS IN LITHUANIA

9:15 Danas Ivanauskas: IMPACT OF SURFACE-ASSOCIATED VIRULENCE FACTORS ON THE CYTOTOXICITY OF ACINETOBACTER BAUMANNII OUTER MEMBRANE VESICLES

9:30 Dominykas Grigorjevas: VIRULENCE FEATURES OF OPPORTUNISTIC PATHOGEN STENOTROPHOMONAS MALTOPHILIA: BIOFILM FORMATION, CAPSULE PRODUCTION, AND ANTIBIOTIC RESISTANCE

9:45 Goda Aleknavičiūtė: CHALLENGES IN ISOLATING EXTRACELLULAR VESICLES FROM HUMAN PLASMA BY DENSITY GRADIENT ULTRACENTRIFUGATION

10:00 Matas Merkelis: VIRAL RNA MIMETICS-INDUCED ALTERATIONS IN MICROGLIAL FUNCTION AND MITOCHONDRIAL NETWORK ARCHITECTURE

10:15 Urte Minkeviciute: PREBIOTIC SUPPLEMENTATION INDUCE MICROGLIAL MORPHOLOGICAL CHANGES IN HIGH-FAT DIET MODEL IN AGED MICE

Session Chair: Tatjana Kirtiklienė

Room: D401 | **ORAL SESSION: O14** | **9:00-10:30**

Ecology, Geology, and Environmental Sciences

9:00 Gelminė Vansevičiūtė: IS HYBRIDIZATION POSSIBLE BETWEEN INVASIVE (Heracleum sosnowskyi) AND NATIVE LITHUANIAN (H. sphondylium) HOGWEEDS. INSIGHTS FROM AN INSILICO STUDY

9:15 Agnė Minderytė: LOCAL VS. TRANSPORTED BLACK CARBON POLLUTION IN VILNIUS AND WARSAW

9:30 Durre Nayab Habib: CARBON ISOTOPIC COMPOSITION OF ANTHROPOGENIC AEROSOLS IN ATMOSPHERIC POLLUTION RESEARCH

9:45 Viktorija Arceryte: CURRENT STATUS OF GLACIAL RELICT CALANOID CRUSTACEANS IN LITHUANIAN LAKES

10:00 Emilija Mockutė: ASSESSING THE EFFICIENCY OF PHARMACEUTICAL ELIMINATION VIA QUATERNARY WASTEWATER TREATMENT

10:15 Rasa Miliukaitė: COMBINED AUTOFLUORESCENCE AND CARS ANALYSIS OF QUANTUM DOTS IMPACT ON MICROALGAE

Session Chair: Ieva Uogintė

Coffee Break — **10:30-11:00**

Public Lab Tour: Department of Environmental Research (FTMC) — **10:30-11:00**

Room: A101 — Chair: Eglė Lastauskienė



Celia Manaia| PLENARY TALK
Catholic University of Portugal, Portugal

Antibiotic Resistance in the Wild: When a Clinical Problem Becomes Everyone's Problem — **11:00-12:00**

Lunch Break — **12:00-13:00**

Room: A101 | **ORAL SESSION: O15** | **13:00-14:15**

Biology and Medicine

13:00 Aušrinė Navickaitė: EXCITABLE PLANTS: HOW ELECTRICAL SIGNALS MODULATE PHOTOSYNTHESIS

13:15 Hamidreza Sahaleh: DESIGN AND CHARACTERISATION OF LIPOSOMAL CURCUMIN AND ASTAXANTHIN MICROCAPSULES FOR ORAL DRUG DELIVERY

13:30 Paulina Malakauskaitė: CALCIUM ELECTROCHEMOTHERAPY USING ULTRA-FAST NANOSECOND ELECTRIC PULSES AND THEIR EFFECTS ON MITOCHONDRIA TRANSMEMBRANE POTENTIAL AND OXIDATION

13:45 Dominyka Adamonė: ASSESSMENT OF ELECTRICAL SIGNALS IN ELECTROPORATED LANGENDORF-PERFUSED RABBIT HEARTS

14:00 Anusiya Paneerselvam: PULSING BUFFER COMPOSITION IMPACT ON CELL VIABILITY AFTER ELECTROPORATIONBY SUPPLEMENTING THE BUFFERS WITH INTRACELLULAR MOLECULES

Session Chair: Saulius Bagdonas

Room: E302 | **ORAL SESSION: O16** | **13:00-14:15**

Ecology, Geology, and Environmental Sciences

13:00 Justas Stonkus: IDENTIFICATION OF A NOVEL RIBOSE-METHYLATED NUCLEOSIDE DEMETHYLATION REACTION CATALYZED BY 2OG-DEPENDENT PHYHD1 AND PHYH-LIKE OXYGENASES

13:15 Smiltė Januškevičiūtė: ARYL HYDROCARBON RECEPTOR EXPRESSION CHANGES IN GEMCITABINE-RESISTANT PANCREATIC CANCER CELLS

13:30 Gabija Žiūraitė: STUDY OF THE BIOLOGICAL PROPERTIES OF THE GLIOBLASTOMACELL LINE U87, WHICH INDUCIBLY SYNTHESIZES SOX2 AND OCT4

13:45 Justinas Malevskis: SELECTIVE INHIBITION OF TUMOR-ASSOCIATED CARBONIC ANHYDRASE IX BY FLUORINATED BENZENESULFONAMIDES

10:00 Gabrielė Skirmantaitė: NAMED ENTITY RECOGNITION IN ELECTRONIC HEALTH RECORDS FOR ALPORT SYNDROME

Session Chair: Marija Ger

Break — **14:15-14:30**

Room: A101 | **PANEL DISCUSSION** | **De-Extinction – Hope, Hype or Hazard?** — **14:30-15:30**

Chair: Elizabet Beržanskytė



Prof. Celia Manaia



Dr. Radvilė Rimgailė-Voicik



Prof. Juozas Lazutka



Prof. Andrej Spiridonov

Co-organizer:

Coffee Break — **15:30-16:00**

Main hall — **POSTER SESSION: P4** — **16:00-17:30**

Ecology, Geology, and Environmental Sciences; Biology and Medicine

Break — **17:30-17:45**

Room: A101 — **Closing Remarks and Awards** — **17:45-18:15**

Contents

Invited Speakers 44

STATE OF THE UNIVERSE
Brian Schmidt 45

THE CHEOPS MISSION: A UNIQUE INTERFACE BETWEEN DISCOVERY AND CHARACTERISATION OF EXOPLANETS
Willy Benz 46

QUANTUM COMPUTATION AND QUANTUM SIMULATION WITH STRINGS OF TRAPPED CA+ IONS
Rainer Blatt 47

CATALYSTS OF CHANGE: ADVANCED MATERIALS STEERING HEALTH AND ENERGY TRANSITION
Sanjay Mathur 48

NEW INSIGHTS INTO THE DRUG TREATMENT OF OBESITY
Lora Heisler 49

SEMICONDUCTOR QUANTUM WALK COMBS FROM THE NEAR-INFRARED TO THE TERAHERTZ
Jérôme Faist 50

TRACING ELECTRON DYNAMICS IN MOLECULES: NOVEL APPROACHES FOR ATTOSECOND CHEMISTRY
Francesca Calegari 52

ANTIBIOTIC RESISTANCE IN THE WILD: WHEN A CLINICAL PROBLEM BECOMES EVERYONE'S PROBLEM
Célia Manaia 53

Oral Session 1: Astrophysics and Theoretical Physics 54

O1-1 THE CHRONICLES OF THE MILKY WAY: THE CARBON, THE NITROGEN, AND THE STELLAR AGES
Bruno Ćurjurić, Arnas Drazdauskas, Gražina Tautvaišiene, Angela Bragaglia, Natalia Alvarez-Baena, Valentina DÓrazi, Marina Dal Ponte 55

O1-2 TRACING INTERNAL MIXING THROUGH LITHIUM AND CNO ABUNDANCES IN RS CVN STARS
B. Bale, G. Tautvaisiene, R. Minkeviciute, A. Drazdauskas, S. Mikolaitis, E. Stonkute, M. Ambrosch . . 56

O1-3 PROBING NEUTRON-CAPTURE ELEMENTS IN PLANET-HOST STARS THROUGH HIGH RESOLUTION SPECTROSCOPY
Ashutosh Sharma, Edita Stonkutė, Arnas Drazdauskas, Renata Minkevičiutė, Šarūnas Mikolaitis, Gražina Tautvaišienė, Ugne Jonauskaitė 57

O1-4 FROM SIMULATION TO OBSERVATION: TESTING COMPATIBILITY OF AGN OUTFLOW RATE ESTIMATES
Milda Valytė, Kastytis Zubovas 58

O1-5 THREE-DIMENSIONAL RECONSTRUCTION OF ROTATING ASTEROIDS FROM TWO-DIMENSIONAL IMAGE SEQUENCES
Vladas Šatas, Donatas Narbutis 59

Oral Session 2: Applied Electrodynamics 60

O2-1 CYBERSECURITY REQUIREMENTS ASSURANCE IN CRITICAL INFRASTRUCTURE SYSTEMS THROUGH THE APPLICATION OF FORMAL VERIFICATION AND ARTIFICIAL INTELLIGENCE-BASED METHODS
Daniel Daukševič . . . 61

O2-2 GENETICALLY OPTIMIZED MULTILAYER METASURFACE FOR X-BAND RADAR REFLECTION REDUCTION
Augustas Koklevičius, Paulius Ragulis, Žilvinas Kancleris, Audronė Sankauskaitė, Vitalija Rubežienė . 62

O2-3 TRANSMISSION GRID POWER TRANSFORMER INSULATION HEALTH MONITORING AND ASSESSMENT USING ACOUSTIC EMISSION AND ULTRA HIGH FREQUENCY SENSORS
Danas Černeckas, Kestutis Jasiūnas, Audrius Jonaitis . . . 63

O2-4 WIDEBAND PERFORMANCE EVALUATION AND CHARACTERISATION OF ANTENNA-COUPLED CMOS TERAFET DETECTORS FROM 0.1 TO 1.2 THZ
Patricija Ivanauskaitė, Dovilė Čibiraitė-Lukenskienė, Domantas Vizbaras, Alvydas Lisauskas . . . 64

O2-5 HORIZONTALLY ORIENTED LOW PROFILE DIELECTRIC RESONATOR ANTENNA WITH EXTREME TEMPERATURE STABILITY FOR RADIO WAVE ENERGY HARVESTING
Justina Žemgulytė, Paulius Ragulis, Modestas Sadauskas, Rimantas Simniškis, Anatolii G. Belous, Oleg I. Výunov, Žilvinas Kancleris . . . 65

Oral Session 3: Astrophysics and Theoretical Physics 66

O3-1 OPTICAL SPIN-ORBIT DYNAMICS OF VECTOR VORTICES IN COHERENTLY PREPARED MEDIA
Dharma P. Permana, Mazena Mackoit Sinkeviciene, Julius Ruseckas, Hamid R. Hamedi . . . 67

O3-2 COMPLETE EXCITON HAMILTONIAN FOR PHOTOSYNTHETIC PIGMENT-PROTEIN COMPLEXES
Austėja Mikalčiūtė, David Varas Rubio, Ulrich Kleinekathöfer, Darius Abramavičius . . . 68

O3-3 CORRELATION-DRIVEN WEYL PHYSICS FROM AB INITIO DFT+DMFT THEORY
Jorūnas Dobilas, Martin Braß, Frank T. Ebel, Silke Paschen, Karsten Held . . . 69

O3-4 VISUALIZATION OF ΛB BARYON DECAYS USING THE ECC METHOD FOR MISSING MOMENTUM RECONSTRUCTION
Meda Paulavičiūtė, dr. Augustas Vaitkevičius, dr. Mindaugas Šarpis . . . 70

O3-5 YUKAWA SECTOR RENORMALIZATION IN THE GRIMUS-NEUFELD MODEL
Dominykas Malinauskas, Simonas Draukšas . . . 71

O3-6 TIME-DEPENDENT PROJECTION SUPEROPERATOR APPROACH TO OPEN QUANTUM SYSTEMS
Justina Vaičaitytė, Andrius Gelžinis, Leonas Valkūnas . . . 72

Oral Session 4: Spectroscopy and Imaging 73

O4-1 DYNAMIC FULL-FIELD OPTICAL COHERENCE MICROSCOPY FOR LIVE TISSUE IMAGING
Erikas Tarvydas, Austėja Trečiokaitė, Egidijus Auksorius . . . 74

O4-2 HIGH-THROUGHPUT SPATIO-TEMPORAL OPTICAL COHERENCE TOMOGRAPHY FOR ENHANCED RETINAL IMAGING SENSITIVITY
Karolis Adomavičius, Austėja Trečiokaitė, Erikas Tarvydas, Egidijus Auksorius . . . 75

O4-3 MULTINUCLEAR NMR STUDY OF THE $NA_{2.5}$ $V_{1.5}TI_{0.5}(PO_4)_3$AQUEOUS ELECTROCHEMICAL DEGRADATION
Aurimas Dubauskas, Nadežda Traškina, Jurgis Pilipavičius, Linas Vilčiauskas, Vytautas Klimavičius . 76

O4-4 THE STUDY OF PROTEIN NMR RELAXATION - DURATION AND PRECISION CONSTRAINTS
Justinas Minkevičius, Marius Gedgaudas, Zigmantas Toleikis, Vytautas Petrauskas, Daumantas Matulis, Laurynas Dagys . . . 77

O4-5 DIRECT LASER WRITING OF PLASMONIC GRATINGS: OPTICAL RESPONSE AND APPLICATIONS
Rodrigas Liudvinavičius, Evaldas Stankevičius . . . 78

O4-6 RAPID FEMTOSECOND-LASER FABRICATION OF A PLASMONIC SENSOR FOR GLYCEROL DETECTION
Kernius Vilkevičius, Tomas Rakickas, Evaldas Stankevičius 79

Oral Session 5: Chemistry 80

O5-1 MODIFICATION OF SILICON OXIDE SURFACE WITH PHOSPHOLIPID BILAYERS FOR BIOSENSOR DEVELOPMENT
Anastasija Aleksandrovič, Aušra Valiūnienė, Gintaras Valinčius 81

O5-2 COMPARATIVE STUDY OF FC RECEPTOR BINDING AND IMMUNE MODULATION: NANOBODY-FC VS IgG IMMUNE COMPLEXES
Miglė Stančiauskaitė, Asta Lučiūnaitė, Mantvydas Usvaltas, Ieva Plikusienė 82

O5-3 DEVELOPMENT OF AN ADVANCED SURFACE ENGINEERED PLATINUM-BASED ELECTROCHEMICAL SYSTEM FOR ULTRA-SENSITIVE DETECTION OF MELOXICAM UTILIZING CHITOSAN TO SUPPRESS OXYGEN
Hassan Kouchakzadeh, Šarūnas Žukauskas 83

O5-4 EFFECTIVE DEFECT DENSITY AS A PREDICTIVE METRIC FORREPRODUCIBLE TOXIN DETECTION IN TETHERED BILAYER MEMBRANES
Gerda Žižiūnaitė, Aušra Valiūnienė 84

O5-5 HYBRID LIPID BILAYERS ON SILICON AS A PLATFORM FOR STUDYING PORE-FORMING TOXINS
Kajus Momgaudis, Aušra Valiūnienė 85

O5-6 ON-SITE DETECTION AND QUANTIFICATION OF SELECTED SEMI-SYNTHETIC AND NATURAL CANNABINOIDS IN CANNABIS PRODUCTS USING CAPILLARY ELECTROPHORESIS - DEEP UV FLUORESCENCE
Saari Anete Loog, Jelena Gorbatšova, Karoliin Remmelg, Maria Kuhtinskaja, Jekaterina Mazina-Šinkar 86

Oral Session 6: Materials Science and Nanotechnology 87

O6-1 LASER ABLATION FOR RADIOACTIVE METAL SURFACE DECONTAMINATION
Jonas Jeffrey Haist, Vilnius Žalėnas, Anton Koroliov, Emilis Sadrejevas, Artūras Plukis 88

O6-2 UV-SERS ON Cu, Co, AND Pd NANOSTRUCTURES FOR SELECTIVE DETECTION OF SMALL AROMATIC BIOMOLECULES
Martynas Talaikis, Evaldas Stankevičius, Rodrigas Liudvinavičius, Lina Mikoliūnaitė, Aikaterini-Maria Gkouzi, Shivani Yadav, Vladimir Sivakov, Gediminas Niaura 89

O6-3 TERAHERTZ EMISSION FROM Bi/GaAs HETEROSTRUCTURES
Benas Stanionis, Vaidas Pačebutas, Ričardas Norkus, Arūnas Krotkus 90

O6-4 METAMATERIAL-BASED BEAM-SHAPING STRUCTURES FEATURED BY HIGHER-ORDER RESONANCES IN THZ FREQUENCY RANGE
Andrius Masaitis, Vladislovas Čižas 91

O6-5 2D-GRAPHENE SHIELDED GOLD METASURFACE FOR ENHANCED GREEN HYDROGEN EVOLUTION REACTION BY PHOTOELECTROCHEMICAL WATER SPLITTING
Muhammad Haris, Klaudijus Midveris, Syeda Ammara Shabbir, Carlos Ponce de Leon, Mohamed Ahmed Baba, Gvidas Klyvis, Algirdas Lazauskas, Erika Rajackaitė, Mindaugas Andrulevičius, Mindaugas Juodėnas, Asta Tamulevičienė, Tomas Tamulevičius, Sigitas Tamulevičius 92

O6-6 EFFICIENT THIRD-GENERATION BLUE OLEDS USING DIBENZOFURAN-BASED HIGH-TRIPLET-ENERGY HOSTS
Kristupas Bagdonas, Goda Grybauskaitė, Domantas Berenis, Gediminas Kreiza, Edvinas Orentas, Eigirdas Skuodis, Karolis Kazlauskas, Dovydas Banevičus 93

Oral Session 7: Chemistry 94

O7-1 ELECTROCHEMICAL FERRIER REARRANGEMENT IN FLOW
Mihhail Fokin, Pallav Suman, Daniele Mazzarella, Maksim Ošeka 95

O7-3 PHOTOREDOX MANIFOLD FOR DEHYDROGENATIVE COUPLING USING PROTONS AS OXIDANTS
Jonas Žurauskas, Paulius Vaickūnas, Gustautas Snarskis, Nojus Radzevičius, Barbara Chatinovska, Gediminas Kreiza, Steponas Raišys, Mantas Šimėnas, Vidmantas Kalendra, Kęstutis Zakarauskas, Karolis Kazlauskas, Edvinas Orentas 96

O7-4 QM/MD STUDY OF STRUCTURE AND NMR SPECTRA OF TETRAPEPTIDE IN AQUEOUS IONIC LIQUID MIXTURES
Amina Elkady, Žyginta Murnikova, Kęstutis Aidas 97

O7-5 GREEN AND SUSTAINABLE EXTRACTION OF MULTIFUNCTIONAL BIOACTIVE INGREDIENTS USING NATURAL DEEP EUTECTIC SOLVENTS FOR PHARMACEUTICAL APPLICATIONS
Sana Abbas, Petras Rimantas Venskutonis, Luana Cristina dos Santos, Elena Ibáñez 98

O7-6 APPLICATION OF CALCIUM OXIDE WASTE FOR THE SYNTHESIS OF HIGHER BASISITY CALCIUM SILICATEHYDRATES (CaO/SiO_2 =1.5)
Ramune Sidaraite, Kestutis Baltakys, Tadas Dambrauskas 99

Oral Session 8: Chemistry 100

O8-1 INFLUENCE OF DEPOSITION CONDITIONS ON THE PROPERTIES OF Sb_2S_3 LAYERS ON FTO SUBSTRATES
Evelina Kasparavičiūtė, Remigijus Ivanauskas, Skirma Žalenkienė 101

O8-3 ENHANCED ELECTROCATALYTIC HER PERFORMANCE: A COMPARATIVE STUDY OF OPTIMIZED BINARY AND TERNARY ELECTROCATALYSTS IN ALKALINE FRESHWATER AND SEAWATER
Sukomol Barua, Aldona Balčiūnaitė, Jūratė Vaičiūnienė, Loreta Tamašauskaitė-Tamašiūnaitė, Eugenijus Norkus 102

O8-4 TWO STAGE $CATIO_3$ SYNTHESIS IN DIFFERENT CRYSTALLINITY TIO_2 MIXTURES
Ričardas Kleinauskas, Anatolijus Eisinas 103

O8-5 ELECTROCHEMICAL SENSORS BASED ON MOLECULARLY IMPRINTED POLYMERS FOR DETECTION OF SMALL MOLECULES
Ernestas Brazys, Vilma Ratautaitė, Arūnas Ramanavičius 104

O8-6 REAL-TIME ELECTROCHEMICAL MONITORING OF BIOFILM GROWTH
Evelina Lukaitė, Rugilė Jonaitytė, Marius Butkevičius, Eglė Malachovskienė, Algimantas Paškevičius, Marius Dagys, Rokas Žalnėravičius 105

Oral Session 9: Laser Physics and Optical Technologies 106

O9-1 HIGH REPETITION RATE DUV-NIR TUNABLE FEMTOSECOND LASER SYSTEM
Jokūbas Pimpė, Ieva Baltrukonytė, Audrius Dubietis, Julius Vengelis 107

O9-2 HIGH REPETITION RATE AND HIGH AVERAGE POWER FEMTOSECOND OPTICAL PARAMETRIC AMPLIFIER IN THE VIS AND NIR
Simona Armalytė, Julius Vengelis 108

O9-3 SUPERCONTINUUM GENERATION IN BULK SOLIDS WITH MID-INFRARED DRIVING PULSES
Kristupas Dagilis, Gintaras Tamošauskas, Rokas Danilevičius, Joris Roman, Andrejus Michailovas, Audrius Pugžlys, Audrius Dubietis 109

O9-4 COMPARATIVE PERFORMANCE OF BRILLOUIN ACTIVE MEDIA FOR ULTIMATE LASER PULSE COMPRESSION
Rugilė Pečiulytė, Paulius Mackonis, Aleksėj M. Rodin, Augustė Grigaravičienė 110

O9-5 GENERATION OF REGULAR LASER PULSES IN A BACKWARD WAVE OPTICAL PARAMETRIC OSCILLATOR PUMPED BY INCOHERENT PULSES
Tomas Latvys, Viktorija Tamulienė 111

O9-6 TWO-PHOTON POLYMERIZATION OF LOW-DENSITY MICROSTRUCTURES AND THEIR ASSEMBLY INTO RIGID HOLDERS FOR INERTIAL CONFINEMENT FUSION INVESTIGATION
Ioanna-Angeliki Petsi, Saule Petrauskaite, Dimitra Ladika, Donatas Narbutis, Mangirdas Malinauskas . 112

Oral Session 10: Materials Science and Nanotechnology 113

O10-1 EXPLORING THE GROUP-V LIMITED GROWTH OF GaAsBi LAYERS
Aivaras Špokas, Andrea Zelioli, Aistė Štaupienė, Andrėja Janulevičiūtė, Justas Žuvelis, Sandra Stanionytė, Giedrius Stalnionis, Evelina Dudutienė, Renata Butkutė 114

O10-2 STRUCTURAL AND OPTICAL INVESTIGATION OF GaAsBi/AlGaAs PARABOLICALLY GRADED QUANTUM WELL STRUCTURES
Aistė Štaupienė, Andrea Zelioli, Aivaras Špokas, Martynas Skapas, Bronislovas Čechavičius, Renata Butkutė, Evelina Dudutienė 115

O10-3 IMPACT OF RAPID THERMAL ANNEALING ON STRUCTURAL AND OPTICAL PROPERTIES OF GaAsBi/(Al,Ga)As QUANTUM WELLS
Patricija Strumilaitė, Aivaras Špokas, Justas Žuvelis, Andrea Zelioli, Sandra Stanionytė, Kipras Mažeika, Augustas Vaitkevičius, Renata Butkutė, Evelina Dudutienė 116

O10-4 LOCAL V-DEFECT ENVIRONMENTS UNDER EXCITATION-DEPENDENT TRANSIENT CATHODOLUMINESCENCE
Gabija Soltanaitė, Mantas Migauskas, Žydrūnas Podlipskas 117

O10-5 CARRIER DYNAMICS IN N- AND P-TYPE InGaN LAYERS AND THE ROLE OF MAGNESIUM ACTIVATION
Seda Türkcan, Kazimieras Nomeika 118

O10-6 ELECTROLUMINESCENCE STUDY OF GaAsBi-BASED NEAR-INFRARED EMITTERS
Justas Žuvelis, Andrius Bičiūnas, Aivaras Špokas, Mindaugas Kamarauskas, Andrea Zelioli, Evelina Dudutienė, Renata Butkutė 119

Oral Session 11: Laser Physics and Optical Technologies 120

O11-1 CONTROL OF SURFACE THERMAL EMISSION USING ULTRASHORT LASER PULSES
Tadas Latvys, Evaldas Kažukauskas, Simas Butkus 121

O11-2 BOTTOM-UP DRILLING OF GLASS USING BURSTS OF ULTRASHORT LASER PULSES
Aleksandras Kondratas, Juozas Dudutis, Paulius Gečys 122

O11-3 FABRICATION AND CHARACTERIZATION OF OPAQUE 3D MICROSTRUCTURES
Abhinay V Mohan, Robertas Virketis, Artur Harnik, Mantas Gaidys, Greta Merkininkaite, Gordon Zyla, Mangirdas Malinauskas 123

O11-4 FULL-FIELD VIBRATION MEASUREMENTS USING SINGLE-SHOT SYNTHETIC WAVELENGTH INTERFEROMETRY
Florian Dötzer, Muralidhar Madabhushi Balaji, Patrick Cornwall, Tianyi Wang, Stefan Sinzinger, Florian Willomitzer 124

O11-5 MICROCOPPER ELECTRODES AND ELECTROCHROMIC MATERIALS INTERACTION WITH DIFFERENT ELECTROLYTES FOR SMART WINDOW APPLICATION
Titas Tamošauskas, Dainius Balkauskas, Modestas Sadauskas, Edita Voitechovič, Romualdas Trusovas, Karolis Ratautas, Kuo-Ping Chen, Alexandr Belosludtsev 125

Oral Session 12: Materials Science and Nanotechnology 126

O12-1 CARBAZOLE-BASED PHOSPHONIC ACIDS IN PEROVSKITE SOLAR CELLS: IMPACT OF THE SUBSTITUTION PATTERN ON DEVICE PERFORMANCE
Aida Drevilkauskaitė, Lea Zimmermann, Eike Köhnen, Steve Albrecht, Artiom Magomedov, Vytautas Getautis 127

O12-2 THICKNESS-DEPENDENT PROPERTIES OF $ZnIn_2S_4$ THIN FILMS DEPOSITED BY CBD METHOD
Nida Vileniškytė, Ingrida Ancutienė, Rokas Kondrotas, Asta Bronušienė 128

O12-3 NANOENGINEERED BIOPOLYMER-FULLERENE C_{60} COMPOSITE FILMS FOR BIOFOULING RESISTANCE
Guoda Gasauskaite, Wanessa De Melo, María Belén Montero Rodríguez, Martynas Talaikis, Vidas Pakštas 129

O12-4 NBT-BT THIN FILMS: STRUCTURAL AND DIELECTRIC PROPERTIES
Eglė Martinaitytė, Vadzim Haronin, Rokas Dobužinskas, Arnas Naujokaitis, Jūras Banys, Šarūnas Svirskas 130

O12-5 BIOCHIPS WITH MICROSCALE SURFACE STIFFNESS PATTERNS FOR MECHANOBIOLOGICAL APPLICATIONS
Andrius Pečiulis, Tomas Rakickas, Tadas Jelinskas, dr. Martynas Gavutis 131

O12-6 IN-SITU XAS MEASUREMENTS OF VANADATE-PHOSPHATE GLASSES
Krzysztof Gadomski, Martyna Jankowska, Wojciech Tabiś, Alexey Maximenko, Sylwester Rzoska, Tomasz K. Pietrzak 132

Oral Session 13: Biology and Medicine 133

O13-1 INVESTIGATION OF THE RESPIRATORY MICROBIOME IN TUBERCULOSIS PATIENTS IN LITHUANIA
Aistė Popandopula, Edvardas Danila, Karolina Kėvelaitienė, Rūta Mereškevičienė, Vaiva Kumpauskaitė, Laima Vasiliauskaitė, Aleksandras Konovalovas, Julija Armalytė 134

O13-2 IMPACT OF SURFACE-ASSOCIATED VIRULENCE FACTORS ON THE CYTOTOXICITY OF ACINETOBACTER BAUMANNII OUTER MEMBRANE VESICLES
Danas Ivanauskas, Jūratė Skerniškytė 135

O13-3 VIRULENCE FEATURES OF OPPORTUNISTIC PATHOGEN STENOTROPHOMONAS MALTOPHILIA: BIOFILM FORMATION, CAPSULE PRODUCTION, AND ANTIBIOTIC RESISTANCE
Dominykas Grigorjevas, Laurita Klimkaitė, Jūratė Skerniškytė 136

O13-5 VIRAL RNA MIMETICS-INDUCED ALTERATIONS IN MICROGLIAL FUNCTION AND MITOCHONDRIAL NETWORK ARCHITECTURE
M. Merkelis, K. Pampuscenko, D. Umbrasas, V. Borutaite 137

O13-6 PREBIOTIC SUPPLEMENTATION INDUCE MICROGLIAL MORPHOLOGICAL CHANGES IN HIGH-FAT DIET MODEL IN AGED MICE
Urte Minkeviciute, Arnas Kunevicius, Akshay Kumar Vijaya, Aurelijus Burokas 138

Oral Session 14: Ecology, Geology and Environmental Science 139

O14-1 IS HYBRIDIZATION POSSIBLE BETWEEN INVASIVE (Heracleum sosnowskyi) AND NATIVE LITHUANIAN (H. sphondylium) HOGWEEDS. INSIGHTS FROM AN INSILICO STUDY
Gelminė Vansevičiūtė, Donatas Žvingila 140

O14-2 LOCAL VS. TRANSPORTED BLACK CARBON POLLUTION IN VILNIUS AND WARSAW
Agnė Minderytė, F. Moritz Hey, Emeka A. Ugboma, Nikolaos Evangeliou, Sabine Eckhardt, Ignacio Pisso, Steigvilė Byčenkienė, Iwona S. Stachlewska 141

O14-3 CARBON ISOTOPIC COMPOSITION OF ANTHROPOGENIC AEROSOLS IN ATMOSPHERIC POLLUTION RESEARCH
Durre Nayab Habib, Andrius Garbaras, Ulrike Dusek, Agne Masalaite 142

O14-4 CURRENT STATUS OF GLACIAL RELICT CALANOID CRUSTACEANS IN LITHUANIAN LAKES
Viktorija Arceryte, Kęstutis Arbačiauskas 143

O14-5 ASSESSING THE EFFICIENCY OF PHARMACEUTICAL ELIMINATION VIA QUATERNARY WASTEWATER TREATMENT
Emilija Mockutė, Inga Urniežaitė, Povilas Reškevičius 144

O14-6 COMBINED AUTOFLUORESCENCE AND CARS ANALYSIS OF QUANTUM DOTS IMPACT ON MICROALGAE
Rasa Miliukaitė, Saulius Bagdonas, Andrej Dementjev, Agnė Kalnaitytė-Vengelienė 145

Oral Session 15: Biology and Medicine 146

O15-1 EXCITABLE PLANTS: HOW ELECTRICAL SIGNALS MODULATE PHOTOSYNTHESIS
Aušrinė Navickaitė, Vytenė Macijauskaitė, Vilmantas Pupkis, Vilma Kisnierienė 147

O15-2 DESIGN AND CHARACTERISATION OF LIPOSOMAL CURCUMIN AND ASTAXANTHIN MICRO-CAPSULES FOR ORAL DRUG DELIVERY
Hamidreza Sahaleh, Dr. Jolita Stabrauskienė, Prof. Dr. Jurga Bernatonienė 148

O15-3 CALCIUM ELECTROCHEMOTHERAPY USING ULTRA-FAST NANOSECOND ELECTRIC PULSES AND THEIR EFFECTS ON MITOCHONDRIA TRANSMEMBRANE POTENTIAL AND OXIDATION
Paulina Malakauskaite, Vytautas Kaseta, Vitalij Novickij 149

O15-4 ASSESSMENT OF ELECTRICAL SIGNALS IN ELECTROPORATED LANGENDORF-PERFUSED RABBIT HEARTS
Dominyka Adamonė, Mantė Almanaitytė, Ieva Lankutytė, Vilma Zigmantaitė, Saulius Šatkauskas, Jonas Jurevičius, Regina Mačianskienė 150

O15-5 PULSING BUFFER COMPOSITION IMPACT ON CELL VIABILITY AFTER ELECTROPORATIONBY SUPPLEMENTING THE BUFFERS WITH INTRACELLULAR MOLECULES
Anusiya Paneerselvam, Baltramiejus Jakštys, Saulius Šatkauskas 151

Oral Session 16: Biology and Medicine 152

O16-1 IDENTIFICATION OF A NOVEL RIBOSE-METHYLATED NUCLEOSIDE DEMETHYLATION REACTION CATALYZED BY 2OG-DEPENDENT PHYHD1 AND PHYH-LIKE OXYGENASES
Justas Stonkus, Rasa Rutkienė, Rita Meškienė, Agota Aučynaitė, Justas Lazutka, Darius Balčiūnas, Giedrius Vilkaitis, Rolandas Meškys 153

O16-2 ARYL HYDROCARBON RECEPTOR EXPRESSION CHANGES IN GEMCITABINE-RESISTANT PAN-CREATIC CANCER CELLS
Smiltė Januškevičiūtė, Vaiva Grišunina, Vitė Vitkutė, Darius Stukas 154

O16-3 STUDY OF THE BIOLOGICAL PROPERTIES OF THE GLIOBLASTOMACELL LINE U87, WHICH INDUCIBLY SYNTHESIZES SOX2 AND OCT4
Gabija Žiūraitė, Arūnas Kazlauskas, Vilma Kaškonienė 155

O16-4 SELECTIVE INHIBITION OF TUMOR-ASSOCIATED CARBONIC ANHYDRASE IX BY FLUORINATED BENZENESULFONAMIDES
Justinas Malevskis, Joana Smirnovienė, Mantas Žvirblis, Virginija Dudutienė, Daumantas Matulis, Vytautas Petrauskas 156

O16-5 NAMED ENTITY RECOGNITION IN ELECTRONIC HEALTH RECORDS FOR ALPORT SYNDROME
Gabrielė Skirmantaitė, Gražina Korvel, Rimantė Čerkauskienė, Agnė Čerkauskaitė-Kerpauskienė . . . 157

Poster Session 1: Astrophysics and Theoretical Physics, Spectroscopy and Imaging, Applied Electrodynamics 158

P1-1 DETERMINATION OF Cd IONS BY SERS USING NANOPARTICLES
Kamilla Kalmykova, Tatjana Charkova 159

P1-2 UV-SERS PERFORMANCE OF NANOPARTICLES FORMED BY LASER ABLATION OF THIN Cu, Au, Ag, AND Fe FILMS
Rokas Čepėnas, Evaldas Stankevičius, Martynas Talaikis 160

P1-3 DIELECTRIC STUDIES OF PDMS-BASED COMPOSITE MATERIALS WITH Fe AND Fe_3O_4 NANOPARTICLES
Rokas Gedvilas, Edita Palaimienė, Jan Macutkevič, Jūras Banys 161

P1-4 VISION-BASED EVALUATION OF POSITIONING REPEATABILITY IN PROBE-BASED MICRO-SCALE SYSTEMS
Ujjawal Malani, Jurate Jolanta Peateroniene, Andrius Dezdicis, Vytautas Buchinskas 162

P1-5 TEMPERATURE-DEPENDENT FLUORESCENCE OF NITROGEN-RELATED COLOR CENTERS IN DIAMOND MICRONEEDLES
Paulius Rindzevičius, Sergei Malykhin, Polina Kuzhir, Renata Karpicz 163

P1-6 INFLUENCE OF MEDIUM pH ON THE PHOTOSTABILITY OF HEMATOPORPHYRIN AT DIFFERENT L-ASCORBATE CONCENTRATIONS
Marija Kalnaitytė, Saulius Bagdonas 164

P1-7 $ZnGa_2O_4$ SPINEL NANOPHOSPHORS WITH PERSISTENT LUMINESCENCE FOR BIOIMAGING
Vilius Čirgelis, Simona Streckaitė, Vitalii Boiko, Lena Golubewa, Vidas Pakštas, Mariusz Stefanski, Dariusz Hreniak, Vidmantas Gulbinas . . . 165

P1-9 DEVELOPMENT OF A GAS COMBUSTION SYSTEM FOR RADIOCARBON ANALYSIS OF HYDROCARBON GASES
Ąžuolas Ivickas, Žilvinas Ežerinskis, Laurynas Bučinskas, Laima Kazakevičiūtė-Jakučiūnien, Justina Šapolaitė . . . 166

P1-10 PHOTO-DEFLECTION ELECTRON PARAMAGNETIC RESONANCE SPECTROSCOPY
Laisvydas Giriūnas, Gediminas Usevičius, Vidmantas Kalendra, Mantas Šimėnas, Jūras Banys . . . 167

P1-11 CHOLINE GLYCINATE DOSY INVESTIGATION
Lukas Mikalauskas, Vytautas Klimavičius . . . 168

P1-13 MILLISECOND-SCALE SPIN COHERENCE OF ^{171} Yb QUBITS IN $CaWO_4$ AT A ZERO-FIELD CLOCK TRANSITION
Justinas Turčak, Vidmantas Kalendra, Jūras Banys, Philippe Goldner, John J. L. Morton, Mantas Šimėnas 169

P1-14 IMPACT OF AMINOACID SURFACTANTS ON THE MAGNETIC BEHAVIOR OF HYDROTHERMALLY SYNTHESIZED CoFe2O4 NANOPARTICLES
Aswathi Raveendran, Germante Paulikaite, Vidas Pakstas, Audrius Drabavicius, Martynas Talaikis, Aldona Balciunaite, Kestutis Mazeika, Vaclovas Klimas, Jurate Vaiciuniene, Agne Mikalauskaite, Simonas Ramanavicius . . . 170

P1-16 NMR INVESTIGATION OF ZIRCONIUM PHOSPHATES
Rokas Lemežis, Vytautas Klimavičius . . . 171

P1-17 DEVELOPMENT AND EVALUATION OF A HYBRID THZ IMAGING SYSTEM BASED ON 3D-PRINTED DIFFRACTIVE OPTICS
Kasparas Stanaitis, Vladislovas Čižas, Rusnė Ivaškevičiūtė-Povilauskienė, Sergėjus Orlovas, Ignas Grigelionis, Linas Minkevičius . . . 172

P1-18 THZ IMAGING SYSTEM BASED ON CW CLINOTRONS
Anna Kuleshova, Sergiy Vlasenko, Yuriy Kovshov, Sergiy Kishko, Eduard Khutoryan, Oleksiy Kuleshov 173

P1-19 TERAHERTZ SCATTERING SIMULATIONS IN ABSORBING AND LAYERED SKIN MODELS
Lukas Stacevičius, Rusnė Ivaškevičiūtė-Povilauskienė, Linas Minkevičius, Ignas Grigelionis . . . 174

P1-20 3D SURFACE RECONSTRUCTION FROM 2D IMAGES USING GEOMETRIC NORMAL ESTIMATION, SIGNED DISTANCE FUNCTION AND NEURAL NETWORK
Goda Palšytė, Donatas Narbutis . . . 175

P1-21 X-RAY SOURCE IMAGING USING GAS ELECTRON MULTIPLIER DETECTOR SYSTEM
Kristupa Šeškauskaitė, Algirdas Lazauskas, Muhammad Usman Uraf Ishafaq, Sigitas Tamulevičius, Brigita Abakevičienė . . . 176

P1-22 SENSORS IN REMOVABLE DENTAL APPLIANCES
Diana Belosludtseva, Edita Voitechovič, Rasa Pauliukaitė . . . 177

P1-23 INVESTIGATION OF STRONTIUM TITANATE CERAMICS BY IMPEDANCE SPECTROSCOPY
Roberta Diekontaitė . . . 178

P1-24 COBALT MONOSILICIDE SINGLE CRYSTAL GROWTH USING THE CZOCHRALSKI METHOD
Miglė Minalgaitė, Ramūnas Skaudžius, Jiří Pospíšil . . . 179

P1-25 APPLICATION OF THE CZOCHRALSKI METHOD FOR LITHIUM FLUORIDE SINGLE CRYSTAL GROWTH
Miglė Minalgaitė, Skirmantė Tutlienė, Ramūnas Skaudžius . . . 180

P1-27 FABRICATION OF SILVER BISMUTH SULFIDE THIN FILMS VIA Ag/Bi STACK PHYSICAL VAPOR DEPOSITION AND SULFURIZATION
Aistis Melnikas, Marta Miró Llorente, Diego Nistal Castro, Victoria Rotaru, Alex López García, Alejandro Perez-Rodriguez, Skirma Žalenkienė, Pedro Vidal Fuentes . . . 181

P1-28 SURFACE ENGINEERING OF TITANIUM-BASED IMPLANTS VIA SOL-GEL BIOACTIVE COATINGS
Martyna Sabaitė, Gabija Dragūnaitė, Brigita Abakevičienė, Odeta Baniukaitienė, Virginija Gylienė . . . 182

P1-29 INVESTIGATION OF PHOTONIC CRYSTAL FABRICATION BY UV PULSES IN SAPPHIRE
Lukas Bručas, Edvinas Aleksandravičius, Darius Gailevičius . . . 183

P1-30 SYNTHESIS OF ROOM-TEMPERATURE SINGLE PHOTONEMITTERS IN HEXAGONAL BORON NITRIDE
Ifra Bibi, Vakaris Šilys, Viktorija Nargelienė, Julius Janušonis, Danielis Rutkauskas, Edgaras Markauskas, Tadas Paulauskas . . . 184

P1-31 INVESTIGATION OF CHARGE TRANSPORT KINETICS IN PEROVSKITE SOLAR CELLS USING THE KINETIC PHOTOCONDUCTIVITY METHOD
Dovilė Vasiliauskaitė, Lauryna M. Svirskaitė, Ernestas Kasparavičius, Vidmantas Gulbinas . . . 185

P1-32 CHARACTERIZATION OF THERMALLY EVAPORATED ANTIMONY SELENIDE (Sb_2 Se_3) FILMS ON DIFFERENT BUFFER LAYERS
Amina Elkady, dr. Arnas Naujokaitis, dr. Vidas Pakštas . . . 186

P1-33 ELECTROMAGNETIC RADIATION DIRECTION FINDING SYSTEM
Mantas Krejaras, Justina Žemgulytė, Karolis Stankevičius, Rimantas Simniškis, Paulius Ragulis . . . 187

P1-34 INVESTIGATION OF THE OPTICAL CHARACTERISTICS OF SENSORS BASED ON COMPLEMENTARY METAL-OXIDE-SEMICONDUCTOR FIELD-EFFECT TRANSISTORS AT 2.52 THZ
Ričardas Petkus, Domantas Vizbaras, Ignas Grigelionis, Linas Minkevičius, Alvydas Lisauskas, Dovilė Čibiraitė-Lukenskienė . . . 188

P1-35 DESIGN OF A 2.4 GHz WILKINSON POWER DIVIDER WITH A DISTRIBUTED-ELEMENT BANDPASS FILTER
Kristina Miliauskaitė, Zigmas Balevičius . . . 189

P1-36 INVESTIGATION OF TEMPERATURE INFLUENCE ON SIGNAL DELAY OF COAXIAL CABLES
Dominykas Mačiulaitis, Rimantas Miškinis, Milda Tamošiūnaitė-Survilienė, Emilis Urba . . . 190

P1-37 COMPARISON OF SPECTRAL PROPERTIES IN THZ RANGE OF SQUARE AND CIRCULAR METASURFACE STRUCTURES ON CONDUCTOR/INSULATOR/CONDUCTOR STRUCTURES
Barbora Škėlaitė, Ignas Grigelionis . . . 191

P1-38 TEST-BASED RELIABILITY EVALUATION OF HYBRID IC PACKAGES WITH DIFFERENT INTERCONNECTION TECHNOLOGIES
Dominykas Mendelis, Mindaugas Žilys . . . 192

P1-39 HIGH-POWER ELECTRICAL PULSE WITH LOW HARMONIC DISTORTION FORMING METHODS FOR DYNAMICAL AND EMC TESTING
Rokas Grigaliunas . . . 193

P1-40 EMISSION HOMOGENEITY OF InGaAs/GaAs QUANTUM WELL STRUCTURES WITH DIFFERENT BARRIER PATTERNS
Kipras Mažeika, Augustas Vaitkevičius, Andrea Zelioli, Aivaras Špokas, Renata Butkutė, Jūras Mickevičius 194

P1-41 DIFFUSION IN A QUADRATIC POTENTIAL WITH A CHANGING DIFFUSION COEFFICIENT
Kristupas Kalvaitis, Rytis Kazakevičius . . . 195

P1-42 APPLICATION OF MACHINE LEARNING TO NUCLEAR REACTIONS
Darius Likandrovas, Arnoldas Deltuva . . . 196

P1-43 PENTAQUARK SEARCH IN BEAUTY LAMBDA TO CHARMED SIGMA DECAYS USING LHCB RUN3 DATA
Šarūnas Jacevičius . . . 197

P1-44 MECHANICS OF R-LOOP FORMATION BY CASCADE STUDIED WITH MAGNETIC TWEEZERS
Virginija Siaurusevičiūtė, Ugnė Gaižauskaitė, Gabija Naujokaitė, Inga Songailienė, Algirdas Toleikis . . 198

P1-45 SEPARATION OF HEAVY BARYON DECAY CHANNELS USING MODERN MACHINE LEARNING ALGORITHMS ON SIMULATED LHCB DATA
Neilas Beniušis, Mindaugas Šarpis . . . 199

P1-47 CMS INNER TRACKER UPGRADE AND TEPX ELECTRICAL TESTING AT VILNIUS
Samarendra Nayak, Andrius Juodagalvis, Marijus Ambrozas, Vincas Tamošiūnas, Matas Petrėnas, Kęstutis Ikamas, Domantas Vizbaras 200

P1-48 ADAPTING THE COFFEA FRAMEWORK FOR FCC
Eglė Lenkaitytė, David Lange, Prayag Yadav, Marijus Ambrozas, Andrius Juodagalvis 201

P1-49 APPLICATION OF SERS SPECTROSCOPY FOR FORENCIC ANALYSIS OF DOCUMENTS
Aistė Maldūnaitė, Valdas Šablinskas 202

P1-50 OFF-RESONANT NONLINEAR OPTICAL SPECTROSCOPY AND ITS APPLICATION TO TWO-DIMENSIONAL ELECTRONIC SPECTROSCOPY
Liutauras Pocius, Darius Abramavičius 203

P1-51 $CsPbCl_3$:Yb^{+3} STRUCTURAL ANALYSIS USING HYSCORE SPECTROSCOPY
Giedrė Kuktaitė, Mantas Šimėnas, Gediminas Usevičius, Simona Streckaitė, Marius Franckevičius, Vidmantas Gulbinas 204

P1-52 SPECTRAL CHARACTERIZATION OF NEUTRAL AND CATIONIC TPFPP: THE ROLE OF QUATERNARY AMMONIUM GROUPS
Martyna Petkutė, Gabrielė Vasiliauskaitė, Nojus Radzevičius, Irina Buchovec 205

P1-53 INVESTIGATION OF ORGANIC LIGHT-EMITTING DIODES AND OPTICAL SENSORS BASED ON RED AND NEAR-INFRARED EMITTING BENZOTHIADIAZOLE DERIVATIVES
Lesia Volyniuk, Melika Ghasemi, Stepan Kutsiy, Asta Dabuliene, Adam Pron, Dmytro Volyniuk, Juozas V. Grazulevicius, Irena Kulszewicz-Bajer, Audrius Bucinskas 206

P1-54 CEREBROSPINAL FLUID ANALYSIS USING ATR-IR SPECTROSCOPY
Julija Jakučionytė, Rimantė Bandzevičiūtė, Valdas Šablinskas, Gerald Steiner, Johannes Kasper, Konstantin Sulin, Robert Brilmayer, Žilvinas Chomanskis, Gediminas Lukšys, Saulius Ročka, Matthias Kirsch 207

P1-55 RELAXATION OF PARAHYDROGEN-ENABLED STATES USING VARIABLE FIELD NMR SPECTROSCOPY
Izabelė Navickaitė, Nojus Radzevičius, Edvinas Orentas, Laurynas Dagys 208

P1-56 THE PHOTO-INDUCED NMR RELAXATION IN LUCIGENIN
Viltė Zairytė, Laurynas Dagys 209

P1-57 EVALUATION OF THE INCORPORATION OF RED CURRANT POMACE AND EXTRACT IN MEATBALLS USING CONVENTIONAL QUALITY ASSESSMENT
Laura Jūrienė, Jovita Jovaišaitė, Petras Rimantas Venskutonis 210

P1-58 PRODUCTION AND FREEZE-DRYING OF YOGURT ENRICHED WITH BLUEBERRY POMACE
Laura Jūrienė, Austėja Kacucevičiūtė 211

P1-59 EFFECT OF PLANT-BASED ADDITIVES ON PHYSICOCHEMICAL AND SENSORY PROPERTIES OF KOMBUCHA DURING PRIMARY AND SECONDARY FERMENTATION
Laura Jūrienė, Mykolas Juknius 212

P1-60 FOOD REFORMULATION IN PRACTICE: DEVELOPMENT OF A FUNCTIONAL YOGHURT ICE CREAM
Iris-Gertrud Jussila, Anette Russ, Susanna Helena Toom, Kristel Vene 213

P1-61 VALORIZATION OF BILBERRY POMACE AS A FUNCTIONAL INGREDIENT FOR NUTRITIONALLY ENHANCED WHEATBREAD
Arnoldas Keibas, Laura Jūrienė, Petras Rimantas Venskutonis 214

P1-62 PREPARATION AND INVESTIGATION OF STABILITY OF EMULSIONS COMPOSED OF BLACKCURRANT EXTRACTS AND MODIFIED STARCH
Dovilė Liudvinavičiūtė, Laura Jūrienė, Ramunė Rutkaitė 215

P1-63 NANOZYME-DRIVEN AMPEROMETRIC GLUCOSE BIOSENSOR
Aiste Krikstaponyte, Asta Kausaite-Minkstimiene 216

P1-64 GOLD NANOPARTICLE BASED DETECTION OF REDUCING SUGARS AND THEIR MIXTURES
Isaac Garcia Contreras, Benediktas Brasiunas 217

P1-65 SYNTHESIS AND CHARACTERIZATION OF THERMO-RESPONSIVE β-CYCLODEXTRIN AND POLY(N-ISOPROPYLACRYLAMIDE) COPOLYMERS
Sofija Beatričė Dervinytė, Ramunė Rutkaitė, Miglė Savickė 218

P1-66 SYNTHESIS AND CHARACTERIZATION OF BIO-BASED VITRIMERS
Aysu Nasiribouyony, Jolita Ostrauskaitė, Sigita Grauželienė 219

P1-67 SYNTHESIS AND INVESTIGATION OF BIO-BASED VITRIMERS DERIVED FROMRENEWABLE RESOURCES
Viltė Šereikaitė, Sigita Grauželienė, Jolita Ostrauskaitė 220

P1-68 SYNTHESIS OPTIMISATION AND FUNCTIONAL CHARACTERIZATION OF DODECENYL SUCCINIC ANHYDRIDE AND ACETIC ANHYDRIDE MODIFIED CORN STARCHES
Muhammad Nasif, Ayodeji Amobonye, Joana Bendoraitiene, Laura Peciulyte, Remo Merijs Meri, Shu-Kai Yeh, Ramune Rutkaite 221

P1-69 POLYLACTIC ACID/HYDROXYAPATITE COMPOSITE FILAMENTS FOR BONE-RELATED APPLICATIONS
Jokūbas Lukošiūnas, Ugnius Dijokas, Odeta Baniukaitienė 222

P1-70 DEVELOPMENT AND RESEARCH OF THE PROPERTIES OF GELATIN-BASED HYDROGEL MATERIALS FOR TRANSDERMAL DRUG DELIVERY SYSTEMS
Daria Kuchynska, Olena Ishchenko, Ihor Okhrimenko, Mikael Yeganyan 223

P1-71 IDENTIFICATION OF SPECTRAL MARKERS IN FOURIER TRANSFORM INFRARED SPECTRA OF BIOLOGICAL SAMPLES BY MEANS OF STATISTICAL ANALYSIS
Tautvydas Taraškevičius, Justinas Čeponkus 224

P1-72 HYDROGENATED AND HYDROXYLATED NANODIAMONDS INTERACTING WITH WATER: A FIRST-PRINCIPLES STUDY
Naglis Januška, Šarūnas Masys 225

P1-74 AGN-ENHANCED STAR FORMATION
Martynas Laužikas, Kastytis Zubovas 226

P1-75 NON-LINEAR DYNAMICS AND PRIMORDIAL BLACK HOLE FORMATION DURING KINATION
Cheng Cheng, Panagiotis Giannadakis, Lucien Heurtier, Eugene Lim 227

P1-76 A DISFORMAL AFFAIR: HOW DARK MATTER MIMICS LORENTZ VIOLATION
Guillem Domenech, Apostolos Tsampodimos, Nathaniel Sherrill, Alexander Ganz, Fiona Kirk 228

P1-77 STAR CLUSTERS SIZE EVOLUTION IN M31
Karolis Daugevičius, Eimantas Kriščiūnas, Rima Stonkutė, Vladas Vansevičius 229

P1-78 KINEMATICS OF GALACTIC OUTFLOWS IN A TURBULENT ENVIRONMENT
Veronika Mykhailenko, Kastytis Zubovas 230

P1-79 EXTENDING GAIA XP SPECTRA BASED CLASSIFICATION OF HOT SUBDWARFS WITH MULTIPLE MACHINE-LEARNING APPROACHES AND AUXILIARY STELLAR DATA
Urtė Gedvilaitė, Erika Krikščiūnaitė, Aidas Medžiūnas, Kristupas Pribušauskas 231

P1-80 BRST SYMMETRY AND GRIMUS-NEUFELD MODEL
Nojus Danyla, Simonas Draukšas 232

P1-82 ELECTROCATALYTIC PERFORMANCE OF PdCo/Cu AND PdNi/Cu COATINGS TOWARD WATER SPLITTING AND OXYGEN REDUCTION REACTIONS
Raminta Stagniūnaitė, Virginija Kepenienė, Zita Sukackienė, Loreta Tamašauskaitė-Tamašiūnaitė . . . 233

P1-83 INSIGHTS INTO THE STABILISATION MECHANISM OF δ-Bi_2O_3-LIKE PHASE TO LOW TEMPERATURE BY CONFINEMENT OF NANOGRAINS IN GLASSY MATRIX
Maciej Nowagiel, Jerzy E. Garbarczyk, Marek Wasiucionek, Tomasz K. Pietrzak 234

P1-84 NANOSECOND LASER THERMAL DEWETTING OF THIN FILMS FOR PLASMONIC NANOPARTICLE FABRICATION AND COLOR ENGINEERING
Vita Petrikaitė, Ilja Ignatjev, Aušra Selskienė, Algirdas Selskis, Evaldas Stankevičius 235

P1-85 ATR-FTIR SCREENING OF INDUSTRIAL PVC
Vaidas Gasiūnas, Elena Jasiūnienė 236

P1-87 SIMULATION OF PURCELL-ENHANCED SPIN RELAXATION
Aistė Peštenytė, Gediminas Usevičius, Jūras Banys, John J.L. Morton, Mantas Šimėnas 237

P1-88 X-BAND BIMODAL MICROWAVE CAVITY FOR EPR SPECTROSCOPY
Ignas Pocius, Vidmantas Kalendra, Jūras Banys, Mantas Šimėnas 238

P1-90 GLUCOSE BIOSENSOR FOR THE DETERMINATION OF CADMIUM IONS VIA ENZYME ACTIVITY INHIBITION: EFFECT OF GOLD NANOSTRUCTURES ON THE ANALYTICAL SIGNAL
Katazyna Blazevic, Natalija German, Asta Kausaite-Minkstimiene, Almira Ramanaviciene 239

P1-91 THE DEVELOPMENT OF REAGENTLESS GLUCOSE BIOSENSORS BASED ON GOLD NANOSTRUCTURES IN THE ABSENCE AND PRESENCE OF POLYPYRROLE
Natalija German, Anton Popov, Almira Ramanaviciene 240

P1-93 POLYMERIC SCAFFOLDS FOR ARTIFICIAL MUSCLE TISSUE-CULTURED MEAT
Bramos Murthy 241

P1-94 IN VITRO MODELLING PREPARATION OF POLYMERIC HYDROGEL SCAFFOLDS SYSTEM FOR HUMAN JOINT DISEASE.
Aleena Ijaz, Edvinas Krugly 242

P1-95 FIRST-PRINCIPLES INSIGHTS INTO THE DESIGN OF MOLECULARLY IMPRINTED POLYPYRROLE FOR DETECTION OF CLORSULON
Enayat Mohsenzadeh, Vilma Ratautaite, Arunas Ramanavicius 243

P1-96 SABRE HYPERPOLARIZATION OF BIOLOGICALLY RELEVANT LIGANDS
Aura Matuliūkštytė, Laurynas Dagys 244

P1-97 Exploration of UV LEDs for disinfection
Rolands Gudermanis, Gita Revalde, Anda Ābola 245

P1-98 EXPLORATION OF ATOMIC OXYGEN IN HIGH-FREQUENCY ELECTRODELESS DISCHARGE LAMPS DURING PULSED EMISSION MODE
Rolands Gudermanis 246

Poster Session 2: Chemistry **247**

P2-1 STIMULI-RESPONSIVE H-BONDED SUPRAMOLECULAR SYSTEMS
Gabija Sergejevaitė, Domantas Valčeckas, Vaidas Klimkevičius, Edvinas Orentas 248

P2-2 INVESTIGATION OF SOLVENT-INDUCED SWELLING OF POLYPYRROLE THIN FILMS BY DRT ANALYSIS OF ELECTROCHEMICAL IMPEDANCE SPECTROSCOPY DATA
Domas Pirštelis, Ernestas Brazys, Vilma Ratautaitė, Arūnas Ramanavičius 249

P2-3 UHPLC-MS/MS METHOD DEVELOPMENT FOR TARGETED GIBBERELLIN PROFILING IN REPRODUCTIVE TISSUES OF HERACLEUM SOSNOWSKYI
Dominykas Laibakojis, Simonas Balčiūnas, Tautvydas Žalnierius, Jurga Būdienė 250

P2-4 MODELLING INTERMOLECULAR INTERACTIONS OF IBUPROFEN IN AQUEOUS HYDROTROPIC SOLUTIONS USING MD SIMULATIONS
Benjaminas Malmiga, Kęstutis Aidas, Žyginta Murnikova 251

P2-5 γ -GLUTAMYL TRANSFERASE CHARACTERIZATION USING SCANNING ELECTROCHEMICAL MICROSCOPY
Vaineta Vainalavičiūtė, Agnė Boguševičė, Inga Morkvėnaitė-Vilkončienė, Tomas Mockaitis 252

P2-7 VOLATILE FINGERPRINTS OF BOTANICAL HYDROLATES: HS-GC-MS VERSUS SOLVENT EXTRACTION-GC-MS
Konstantinas Brazinski 253

P2-8 COMPUTATIONAL STUDY INVESTIGATING ELECTRONIC SPECTRA AND STRUCTURE OF RETINOL AND RETINOIC ACID
Julius Ažukas, Žyginta Murnikova, Kęstutis Aidas 254

P2-9 MODELLING ^{1}H NMR SPECTRA OF WATER IN AQUEOUS MIXTURES OF 1-BUTYL-3-METHYL-IMIDAZOLIUM TETRAFLUOROBORATE IONIC LIQUID
Julius Ažukas, Kęstutis Aidas . . . 255

P2-10 PHOTOREDOX MANIFOLD FOR DEHYDROGENATIVE COUPLING USING PROTONS AS OXIDANTS
Jonas Žurauskas, Paulius Vaickūnas, Gustautas Snarskis, Nojus Radzevičius, Barbara Chatinovska, Gediminas Kreiza, Steponas Raišys, Mantas Šimėnas, Vidmantas Kalendra, Kęstutis Zakarauskas, Karolis Kazlauskas, Edvinas Orentas . . . 256

P2-11 INVESTIGATION OF THE HETEROGENEOUS CATALYTIC ADDITIONOF VINYL ACETATE TO AZOLES USING TRANSITION-METAL ACETATES IMMOBILIZED ONPOLY(1-VINYLAZOLES)
Nagharsh Mirakyan, Hovhannes Attaryan . . . 257

P2-12 A GENERAL ARENE C-H FUNCTIONALIZATION TO SUBSTITUTED METHYLENES
Nojus Radzevičius, Jonas Žurauskas, Paulius Vaickūnas, Gabija Sergejevaitė, Domantas Valčeckas, Edvinas Orentas . . . 258

P2-13 SYNTHESIS AND ANALYSIS OF AROMATIC ORGANIC ACIDS FOR THE PASSIVATION OF PEROVSKITE SURFACE DEFECTS
Ema Andriuškaitė, Dr. Matas Steponaitis . . . 259

P2-15 SYNTHESIS OF N-SUBSTITUTED 2-((4-(BENZIMIDAZO (2,1-b)(1,3)THIAZIN-4-YL)PHENYL)(BOC)AMINO)ACETAMIDES FOR THE RESEARCH OF AMYLOID AGGREGATION MODULATORS
Tadas Vasiliauskas, Ieva Žutautė . . . 260

P2-16 FACILE ONE-STEP HYDROTHERMAL SYNTHESIS OF NICKEL-INCORPORATED-NITROGEN-DOPED CARBON FOR DIRECTMETHANOL FUEL CELLS
Hamza Shehroz, Farah Mumtaz, Aldona Balčiūnaitė, Loreta Tamašauskaitė Tamašiūnaitė, Eugenijus Norkus . . . 261

P2-17 ELECTROCHEMICAL DESIGN OF INTERLAYER $Co(OH)_2$ -NiFe ELECTRODES TO TUNE REDOX AND ADSORPTION PROCESSES FOR EFFICIENT OER
Hafiz Muhammad Naeem, Loreta Tamašauskaitė-Tamašiūnaitė, Eugenijus Norkus, Ramūnas Levinas 262

P2-18 STABILITY OF HONEYCOMB-STRUCTURED COPPER FOAM ELECTRODES FOR CO_2 REDUCTION
Birutė Serapinienė, Jurga Juodkazytė, Algirdas Selskis, Rimantas Ramanauskas . . . 263

P2-19 CeO_2 /Pd-CA FOR OXYGEN REDUCTION REACTION IN ALKALINE MEDIA
Ana Nastasić, Jadranka Milikić, David Tomić, Meryem Samancı, Ayşe Bayrakçeken, Biljana Šljukić, Aldona Balčiūnaitė . . . 264

P2-20 NANOSIZED CoM/rGO COMPOSITES AS AN EFFICIENT OXYGEN REDUCTION ELECTRODE MATERIAL
Ana Nastasić, Jadranka Milikić, Kristina Radinović, David Tomić, Biljana Šljukić, Aldona Balčiūnaitė . . 265

P2-21 Ru-DECORATED Co/C CATALYST FOREFFICIENT HYDROGEN EVOLUTION REACTION
Julija Usavičiūtė, Virginija Kepenienė, Raminta Stagniūnaitė, Jūratė Vaičiūnienė, Loreta Tamašauskaitė-Tamašiūnaitė . . . 266

P2-22 OPERANDO XRD STUDY ON THE STRUCTURAL CHANGES OF ZINC HEXACYANOFERRATE IN AQUEOUS ZINC-ION BATTERIES
Dovilė Škarnulytė, Linas Vilčiauskas, Jurgis Pilipavičius . . . 267

P2-23 X-RAY DIFFRACTION STUDIES OF In_2S_3 LAYERS DEPOSITED ON POLYAMIDE 6 SURFACES
Ema Juocinskyte, Skirma Zalenkiene . . . 268

P2-24 STUDY ON REUSABILITY OF MAGNETIC CHITOSAN WITH DIFFERENT MAGNETIZATION LEVEL FOR RADIONUCLIDE REMOVAL
Matas Skripkauskas, Sergej Šemčuk, Galina Lujanienė, Martynas Talaikis, Vidas Pakštas, Kęstutis Mažeika . . . 269

P2-25 HETEROGENEOUS EPOXIDATION OF ALKENES USING BIOMASS-DERRIVED CATALYST
Eivydas Trioška, Carl Johan Wallentin, Edvinas Orentas . . . 270

P2-26 SYNTHESIS OF SUBSTITUTED BENZIMIDAZOTHIAZINES AND THIAZOLES FOR THE SEARCH OF AMYLOID AGGREGATION MODULATORS
Linas Petrauskas, Rita Bukšnaitienė 271

P2-27 SYNTHESIS OF NEW 4-(4-CHLOROPHENYL)-1-(3,4,5-TRIMETHOXYPHENYL)-1H-IMIDAZOLE-2-THIOL DERIVATIVES
Birutė Grybaitė, Natalia Maciejewska, Vytautas Mickevičius 272

P2-28 SYNTHESIS OF IMIDAZO(2,1-b)(1,3)THIAZINES VIA ELECTROPHILE-PROMOTED CYCLIZATION OF 2-ALKENYLTHIOIMIDAZOLES
Martyna Paulauskaitė, Ieva Žutautė 273

P2-29 PLANT-AVAILABLENUTRIENTS FROM ORGANIC MATERIALS: N, P, AND K EXTRACTION IN DIFFERENT MEDIA
Karina Kuzborskaja, Kristina Jančaitienė 274

P2-31 SYNTHESIS OF NOVEL BENZIMIDAZOTHIAZINE DERIVATIVES AS POTENTIAL MODULATORS OF AMYLOID AGGREGATION
Urtė Milerytė, Rita Bukšnaitienė, Ieva Žutautė 275

P2-32 EVALUATION OF KOMBUCHA FERMENTATION USING DIFFERENT TYPES OF TEA
Lukas Dapkus, Eglė Purvaneckaitė, Aivaras Anužis 276

P2-33 SYNTHESIS OF β-HYDROXY-α-AMINOACIDS UTILIZING L-THREONINE (TRANS)ALDOLASES
Ignas Katkevičius, Kamilė Butkutė, Rolandas Meškys 277

P2-34 THE SYNTHESIS AND MODIFICATION OF (IMIDAZO(2,1-b)(1,3)THIAZIN-4-YL)PHENOLS
Fausta Kairytė, Ieva Žutautė 278

P2-35 SYNTHESIS OF N-SUBSTITUTED RESORCINOLCARBOXAMIDES AS POTENTIAL HSP90 INHIBITORS
Ugnius Popovas, Ieva Žutautė 279

P2-36 EFFICIENT SYNTHESIS OF STEROIDAL 1,2,3-TRIAZOLES
Nana Barbakadze, Nanuli Nadaraia, Meri Kakhabrishvili 280

P2-37 SYNTHESIS AND INVESTIGATION OF BENZIDINE ANILINE AND BENZIDINE O-ANISIDINE COPOLYMERS WITH PANi LIKE STRUCTURE
Narine Durgaryan, Shushanna Vardanyan, Parandzem Minasyan, Gevorg Grigoryan 281

P2-38 CHARACTERISATION OF VOLATILE COMPOUNDS AND METABOLITE PROFILES OF VINCETOXICUM ROOTS ISOLATED BY SUPERCRITICAL CO_2 AND PRESSURISED LIQUID EXTRACTION
Jovita Jovaišaitė, Simon Duthen, Amélie Perez, Laura Jūrienė, Petras Rimantas Venskutonis 282

P2-39 ANTIOXIDANT PROFILE OF LIQUID FRACTION FROM DANDELION LEAF KOMBUCHA FERMENTATION
Taisa Vashkevich, Vilma Kaškonienė, Audrius Sigitas Maruška 283

P2-40 DESIGN AND SYNTHESIS OF NOVEL DERIVATIVES BASED ON1-(NAPHTHALEN-1-YL)-4-PHENYL-1H-IMIDAZOLE-2-THIOL
Aistė Starkauskaitė, Birutė Grybaitė, Vytautas Mickevičius 284

P2-41 PROPERTIES OF NONWOVEN MICROFIBER MATERIALS BASED ON PLANT EXTRACTS PRODUCED BY ELECTROSPINNING
Andrii Sikora, Irina Liashok, Viktoriia Plavan 285

P2-42 STRUCTURAL AND MORPHOLOGICAL CHARACTERIZATION OF POLY(PYRROLE-CO-ANTHRANILIC ACID) COPOLYMERS SYNTHESIZED USING DIFFERENT AMMONIUM PERSULFATE-TO-MONOMER RATIOS
Amelia Hendik, Justina Gaidukevič 286

P2-43 RAPID FABRICATION OF COC MICROFLUIDIC CHIPS USING ADHESIVE BONDING
Tadas Turonis, Kamilė Kasperavičiūtė, Eivydas Andriukonis, Arūnas Stirkė 287

P2-44 Pd-CATALYZED ASSEMBLY AND MECHANISTIC ELUCIDATION OF TWISTED DONOR-ACCEPTORCARBAZOLE SCAFFOLDS
Hamisu Aliyu Mohammed, Muhammad Hakim Muhamad Adzrill, Aqeel A. Hussein, Muhammad Kumayl Abdul Wahab, Nor Shafiq Mohd Jamel, Kai Lin Woon, Juozas V. Grazulevicius, Azhar Ariffin 288

P2-45 4-(7H-IMIDAZO(2,1-b)(1,3)THIAZIN-5-YL)ANILINE DERIVATIVES: SYNTHESIS AND MODIFICATION
Polina Pylskaja, Ieva Žutautė 289

P2-46 SYNTHESIS OF PYRAZOLE- AND BENZIMIDAZOLE DERIVATIVES FUSED VIA OXAZACYCLES
Agnė Užupytė, Povilas Viltrakis, Vilija Kederienė, Algirdas Šačkus, Eglė Arbačiauskienė 290

P2-47 SYNTHESIS AND INVESTIGATION OF 3-1-(2,4-DIFLUOROPHENYL)THIOUREIDOPROPANOIC ACID DERIVATIVES
Guoda Pranaitytė, Birutė Grybaitė, Vytautas Mickevičius 291

P2-48 CHARACTERIZATION OF CELLULOSE EXTRACTED FROM DIFFERENT WASTES SOURCES
Austėja Burbulytė, Ieva Uogintė 292

P2-49 SODIUM BOROHYDRIDE OXIDATION ON NiZn/Ti AND Au(NiZn)/Ti ELECTROCATALYSTS IN ALKALINE FUEL CELLS FOR CLEAN ENERGY CONSERVATION
Tripura Ganti, Aldona Balčiūnaitė, Huma Amber, Giedrius Stalnionis, Jūrate Vaičiūnienė, Loreta Tamašauskaitė-Tamašiūnaitė, Eugenijus Norkus 293

P2-50 ZINC - AND NITROGEN-DOPED BIOMASS-DERIVED CARBON CATALYSTS FOR OXYGEN REDUCTION
Daina Upskuvienė, Virginija Ulevičienė, Aldona Balčiūnaitė, Ance Plavniece, Loreta Tamašauskaitė-Tamašiūnaitė, Eugenijus Norkus 294

P2-51 ELECTRODE FABRICATION METHOD USING RESIN AND STEREOLITHOGRAPHIC 3D PRINTING
Rokas Bagdonas, Inga Morkvėnaitė-Vilkončienė 295

P2-52 Cd-N-DOPED BIOMASS-DERIVED CARBON AS AN ANODE CATALYST FOR HYDRAZINE OXIDATION
Virginija Ulevičienė, Aldona Balčiūnaitė, Daina Upskuvienė, Aleksandrs Volperts, Loreta Tamašauskaitė-Tamašiūnaitė, Eugenijus Norkus 296

P2-53 INFLUENCE OF SYNTHESIS TEMPERATURE ON THE PHOTOELECTROCHEMICAL PROPERTIES OF Cu_2 O
Urte Rinkeviciute, Irena Savickaja, Monika Skruodiene, Arnas Naujokaitis, Vidas Pakstas, Anatolijs Sarakovskis, Milda Petruleviciene 297

P2-55 SYNTHESIS AND ELECTROCHEMICAL PROPERTIES OF $ZnCo_2O_4$ SPINEL COATINGS PREPARED BY COMBUSTION AND SPRAY DEPOSITION
Kristijonas Kacevičius, Maria-Anthoniette Oghenetejiro Onoriode-Afunezie, Agnė Šulčiūtė 298

P2-56 OF VITAMINS AND POLYMERS: ELECTROPOLYMERIZED THIAMINE FILMS AND THEIR STRUCTURE-FUNCTION RELATIONSHIPS
Justina Stonytė, Paulina Morkytė, Nerija Ričkutė, Rasa Pauliukaitė 299

P2-57 INFLUENCE OF SN^{4+} IONS ON THE FORMATION OF CALCIUM SILICATE HYDRATES IN A 0.66CaO-SiO_2 -H_2O MIXTURE
Monika Bakierskyte, Tadas Dambrauskas 300

P2-58 SYNTHESIS OF SILVER-DOPED WHITLOCKITE
Gabriele Egle Budzyte, Aivaras Kareiva, Inga Grigoraviciute 301

P2-59 SILVER-DOPED CARBONATED HYDROXYAPATITE GRANULES FOR ANTIBACTERIAL BONE REGENERATION
Gabriele Meizyte, Maab Abdulsamad Ahmed Elsheikh, Aivaras Kareiva, Inga Grigoraviciute 302

P2-60 MAGNESIUM WHITLOCKITE FORMATION FROM AMORPHOUS CALCIUM PHOSPHATE: EFFECTS OF BUFFER COMPOSITION AND Mg^{2+}
Greta Linkaitė, Gabrielė Eglė Budžytė, Aleksej Žarkov, Aivaras Kareiva, Inga Grigoravičiūtė 303

P2-61 CORRELATION BETWEEN PHASE TRANSITION BEHAVIOR AND STRUCTURAL PROPERTIES IN Ba^{2+} -SUBSTITUTED La_2 Mo_2O_9
Ugnė Vazgelevičiūtė, Artūras Žalga, Giedrė Gaidamavičienė 304

P2-62 SOL-GEL SYNTHESIS AND CHARACTERIZATION OF ND_{1-x} NA_x MNO_3 PEROVSKITES
Aigul Dastankyzy, Dovydas Karoblis, Kestutis Mazeika, Aivaras Kareiva 305

P2-63 COMPARATIVE INVESTIGATION OF DOPING CONCENTRATION EFFECTS ON STRUCTURAL AND PHOTOLUMINESCENT PROPERTIES OF CAGDALO$_4$ AND CAYALO$_4$ PHOSPHORS
Domantas Černius, Monika Skruodienė, Milda Petruleviečienė, Meldra Kemere, Ramūnas Skaudžius . 306

P2-64 INFLUENCE OF TITANIUM DOPING ON THE STRUCTURAL PROPERTIES OF YAG:Pr
Tautvydas Pudžmys, Greta Inkrataitė 307

P2-65 PLATINUM-MODIFIED COBALT-IRON PHOSPHIDE ELECTROCATALYSTS FOR EFFICIENT OVERALL WATER SPLITTING AT INDUSTRIAL TEMPERATURES
Huma Amber, Dmytro Shyshkin, Loreta Tamašauskaitė-Tamašiūnaitė, Jūratė Vaičiūnienė, Giedrius Stalnionis, Eugenijus Norkus 308

P2-66 Ni(OH)$_2$-SUPPORTED Pd ELECTROCATALYSTS FOR METHANOL OXIDATION IN ALKALINE MEDIA
Muhammad Adeel Tariq, Hafiz Muhammad Naeem, Loreta Tamašauskaitė-Tamašiūnaitė, Eugenijus Norkus, Ramūnas Levinas 309

P2-67 LIGHT-DRIVEN OXIDATION OF GLYCEROL ON WO$_3$ -BASED PHOTOANODES FOR SUSTAINABLE APPLICATIONS
Kamila Turuta, Irena Savickaja, Jurga Būdienė, Viktorija Rapalytė, Milda Petrulevičienė, Jurga Juodkazytė 310

P2-68 Ni-BASED BIMETALLIC CATALYSTS FOR SODIUM BOROHYDRIDE HYDROLYSIS
Zita Sukackienė, Gitana Valeckytė, Loreta Tamašauskaitė-Tamašiūnaitė, Jolanta Stupakova 311

P2-69 NICKEL TUNGSTEN CATALYSTS FOR HYDROGEN GENERATION
Gitana Valeckytė, Zita Sukackienė, Jūratė Vaičiūnienė, Loreta Tamašauskaitė-Tamašiūnaitė, Eugenijus Norkus 312

P2-70 APPLICATION OF Co$_3$O$_4$ AND Cr$_2$O$_3$ PARTICLES SUPPORTED ON NITROGEN-DOPED CARBON FOR HYDROGEN EVOLUTION REACTION
Karina Vjūnova, Loreta Tamašauskaitė-Tamašiūnaitė 313

P2-71 Pd$_x$ Fe$_y$/CA FOR OXYGEN REDUCTION REACTION IN ALKALINE MEDIA
David Tomić, Jadranka Milikić, Meryem Samancı, Ana Nastasić, Ayşe Bayrakçeken, Biljana Šljukić, Aldona Balčiūnaitė 314

P2-72 Glutathione detection in Chinese Hamster Ovary Cells Using Scanning Electrochemical Microscopy
Indrė Padvilikytė, Agnė Boguševičė, Inga Morkvėnaitė, Tomas Mockaitis 315

P2-74 LUMINESCENCE INVESTIGATION OF CHROMIUM AND CERIUM CO-DOPED YLuAG GARNETS: EFFECT OF DOPANT Ce^{+3} / Cr^{3+} RATIO
Nerija Rickute, Greta Inkrataite, Ramunas Skaudzius 316

P2-75 EFFECT OF SYNTHESIS METHOD ON PHASE FORMATION AND HIGH-TEMPERATUREPHASE TRANSITION IN La$_2$ Mo$_2$O$_9$
Jonas Labutis, Giedrė Gaidamavičienė, Artūras Žalga 317

P2-76 THE INFLUENCE OF SiO$_2$ ADDITIVE ON THE MAYENITE FORMATION PROCESS AND ITS ADSORPTION CAPACITY FOR THE REMOVAL OF Cu^{2+} / SO$_4^{2-}$ IONS
Jolanta Doneliene, Bartas Gedminas, Andzelika Aleinikovaite, Kristina Vasiliauskiene, Anatolijus Eisinas 318

P2-77 INVESTIGATION OF THE LUMINESCENT PROPERTIES OF Gd3Ga5-2xMgxZrxO12:Cr3+ AND Gd3Ga5-2xZnxZrxO12:Cr3+ GARNETS SYNTHESIZED BY THE SOL-GEL METHOD
Austėja Šernaitė, Monika Skruodienė, Meldra Kemere, Ramūnas Skaudžius 319

P2-78 THERMAL FIELD CHARACTERISATION IN THE HIGH-TEMPERATURE MELT USED FOR BBO CRYSTAL GROWTH
Gabija Janušauskaitė, Martynas Misevičius 320

P2-79 BENZOPHENONE-(BENZO)CARBAZOLE-BASED HOST MATERIALS ENABLING EFFICIENT RED PHOSHORESCENT OLED THROUGH CO-HOST ENGINEERING
Gintare Krucaite, Dovydas Blazevicius, Raminta Beresneviciute, Saulius Grigalevicius, Yi-Qi Chao, Zih-Ru He, Kuan-Yu Su, Chih-Hao Chang 321

P2-80 CARBAZOLE-BENZOCARBAZOLE FRAGMENTS HAVING DERIVATIVES AS VERY EFFICIENT HOST MATERIAL FOR TADF BASED OLEDs
Daiva Tavgeniene, Sushanta Lenka, Hsuan-Min Wang, Jayachandran Jaykumar, Dovydas Blazevicius, Gintare Krucaite, Yu-Lin Chi, Saulius Grigalevicius, Jwo-Huei Jou 322

P2-81 MOLECULARLY IMPRINTED CONDUCTIVE POLYMER PLATFORM FOR PROTEIN SENSING
Artem Yerniiazov, Sarunas Zukauskas, Alma Rucinskiene, Arunas Ramanavicius 323

P2-82 DEVELOPMENT OF A MULTILAYERED, MOLECULARLY IMPRINTED POLYMER-BASED ELECTROCHEMICAL SENSOR FOR TETRACYCLINE DETECTION
Beatričė Kulikauskaitė, Domas Pirštelis, Ernestas Brazys, Vilma Ratautaitė, Arūnas Ramanavičius . . . 324

P2-83 SYNTHESIS OF NEWIMIDAZOLE-2-THIOLES CONTAINING HYDRAZONE MOIETY
Tomas Tutkus, Birutė Sapijanskaitė-Banevič 325

P2-84 GRAPHENEOXIDE AND CONDUCTING POLYMER COMPOSITES: SYNTHESIS AND INVESTIGATION
Greta Melkūnaitė, Justina Gaidukevič 326

P2-85 DIVERGENT SYNTHESIS OF HSP90 INHIBITORS CONTAINING RESORCINOL AND THIADIAZOLE MOIETIES
Vilius Petraška, Ieva Žutautė 327

P2-86 PROTEIN AGGREGATES CONCENTRATION DETERMINATION USING ELECTROCHEMICAL METHODS
Narvydas Dėnas, Povilas Virbickas, Aušra Valiūnienė 328

P2-87 MXENES-BASED ON-SITE HEAVY METAL SENSOR
Ilya Navitski, Šarūnas Žukauskas, Simonas Ramanavičius, Alma Ručinskienė, Arūnas Ramanavičius . 329

P2-88 MODIFICATION OF $Ti_3C_2T_X$ MXENE NANOSHEETS WITH POLYDOPAMINE FOR ANTIBODY IMMOBILIZATION
Kristina Sobol, Viktorija Liustrovaite, Benediktas Brasiunas, Anton Popov, Igor Iatsunskyi, Oleksiy Gogotsi, Almira Ramanaviciene 330

P2-89 GLASS-FORMING HOLE-TRANSPORT MATERIALS WITH TAILORED SURFACE ROUGHNESS FOR ENHANCED PERFORMANCE IN PEROVSKITE SOLAR CELLS
Adnan Ahmed, Naghash Miraqyan, Asta Dabuliene, Dmytro Volyniuk, Edwin Pineda De La O, Juozas Vidas Gražulevičius, Lethy Krishnan Jagadamma, Oleksandr Bezvikonnyi 331

P2-90 IMPACT OF QUATERNARY AMMONIUM GROUP POSITION IN SAMS ON THE PERFORMANCE OF PEROVSKITE SOLAR CELLS
Milda Žitinevičiūtė, Matas Steponaitis, Tadas Malinauskas, Vytautas Getautis 332

P2-91 NOVEL CARBORANE-BASED ELECTRON-TRANSPORTING MATERIALS FOR PEROVSKITE SOLAR CELLS
Julius Petrulevicius, Lea Zimmermann, Wander Max Bernardes de Araujo, Maxim Simmonds, Arman Mahboubi Soufiani, Maryte Daskeviciene, Tadas Malinauskas, Giedre Bubniene, Giedrius Juska, Vygintas Jankauskas, Dorothee Menzel, Florian Scheler, Eike Köhnen, Steve Albrecht, Vytautas Getautis 333

P2-92 SYNTHESIS AND INVESTIGATION OF ORGANIC HOLE SELECTIVE SEMICONDUCTORS WITH DUAL INTERACTIONS AND FUNCTIONALITY IN PEROVSKITE SOLAR CELLS
Gabija Linkaitė, Mantas Marčinskas, Tadas Malinauskas, Vytautas Getautis 334

P2-93 FABRICATION OF BISMUTH SULFIDE THIN FILMS USING L-CYSTEINE AS A NOVEL SULFUR SOURCE
Aistis Melnikas, Skirma Žalenkienė 335

P2-94 EVALUATION OF SUPPORT LAYERS FOR GRAPHENE TRANSFER
Evelina Vaicekauskaitė, Deivis Plaušinaitis, Milita Vagner, Valentina Plaušinaitienė 336

P2-95 SYNTHESIS AND APPLICATION OF AU-DECORATED 2D MXENE FOR THE PLASMONIC SENSING OF MERCURY IONS IN WATER
Saqib Ali, Martynas Talaikis, Oleksiy Gogotsi, Arunas Ramanavicius, Simonas Ramanavicius 337

P2-96 BENCHMARKING EXTENDED DENSITY FUNCTIONAL TIGHT-BINDING METHODS FOR PHOTOCHEMICAL PROPERTY PREDICTION OF MOLECULES
Deimantas Šmigelskas, Linas Vilčiauskas 338

P2-97 REMARKABLE THERMAL STABILIZATION OF COLLAGEN-LIKE PEPTIDES VIA 2-AZABICYCLO ALKANE INCORPORATION
Volodymyr Lyakh, Bartosz Łagan, Radosław Tymoszewicz-Gaida, Elżbieta Wojaczyńska 339

P2-98 SYNTHESIS AND ADMET EVALUATION OF CHLOROPYRIDINE-BASEDHYDRAZONE DERIVATIVES
Aida Šermukšnytė, Kristina Kantminienė, Ingrida Tumosienė 340

P2-99 SYNTHESIS OF 4-((BENZIMIDAZOL-2-YL)THIO)-6-ISOPROPYLRESORCINOLS
Gabija Griškonytė, Ieva Žutautė, Algirdas Brukštus 341

P2-100 GLUCOSE-BASED CHOLINESTERASES INHIBITORS
Rugilė Morkūnaitė, Marius Butkevičius 342

P2-101 A NEW LIGAND FOR BUCHWALD-HARTWIG AMINATION
Jonas Paukstys, Tomas Paskevicius, Linas Labanauskas 343

P2-102 ENGINEERING OXYTOCIN ANALOGS BY TARGETED PRO^{7} EXCHANGE WITH A CHIRAL 2-AZABICYCLIC RESIDUE: CONFORMATIONAL CONTROL AT THE BACKBONE LEVEL
Bartosz Łagan, Volodymyr Lyakh, Radosław Tymoszewicz-Gaida, Elżbieta Wojaczyńska 344

P2-103 SIDERITIS SCARDICA AND SIDERITIS SYRIACA PLANT EXTRACTS: STUDIES ON PHYTOCHEMICAL COMPOSITION AND PROPERTIES.
Greta Tverskytė, Vaida Kitrytė-Syrpa 345

P2-104 EVALUATIONOF ANTIOXIDANT, ENZYME INHIBITORY, AND UV-PROTECTIVE PROPERTIES OF ECHINOPSSPHAEROCEPHALUS L. EXTRACTS OBTAINED BY ACCELERATED SOLVENT EXTRACTION
Marius Užupis, Michail Syrpas, Joanna Topolska, Petras Rimantas Venskutonis, Małgorzata Starowicz, Vaida Kitrytė-Syrpa 346

P2-105 THIN-FILM POLYMER SYSTEM FOR DRUG DELIVERY
Felix Lücke, Šarūnas Žukauskas, Arūnas Ramanavičius, Almira Ramanavičienė 347

P2-106 STIMULI-RESPONSIVE ALGINATE-BASED CONDUCTIVE HYDROGELSINCORPORATING PANI AND PEDOT FOR TUNABLE DRUG RELEASE
Shahbaz Khan, Šarūnas Žukauskas, Arūnas Ramanavičius, Felix Luecke 348

P2-107 INVESTIGATION OF REAL-TIME INTERACTIONS BETWEEN DPP IV PROTEIN AND SPECIFIC ANTIBODIES
Justina Liesytė, Antanas Zinovičius, Ieva Plikusienė 349

P2-108 GOLD NANOPARTICLE-BASED STRATEGIES FOR IMPROVING SARS-COV-2 ANTI-RBD IMMUNOSENSOR SENSITIVITY
Agne Giniunaite, Asta Kausaite-Minkstimiene 350

P2-109 ENVIRONMENTALLY RELEVANT EFFECTS OF PHOTOLUMINESCENT GOLD NANOCLUSTERS: LINKING NANOMATERIAL PROPERTIES TO AQUATIC BIORESPONSES
Agne Mikalauskaite, Živile Jurgelene, Danguole Montvydiene, Simonas Ramanavicius 351

P2-110 REDUCED GRAPHENE OXIDE AND CALCIUM-DEFICIENT HYDROXYAPATITE COMPOSITES: SYNTHESIS, STRUCTURAL AND ELECTROCHEMICAL ANALYSIS
Dovilė Burakovaitė, Greta Linkaitė, Inga Grigoravičiūtė, Justina Gaidukevič 352

P2-111 CHEMICALLY DRIVEN SURFACE MODIFICATION OF POROUS POLYCARBONATE MEMBRANES IN DUAL-CHANNEL MICROFLUIDIC SYSTEMS TO ENHANCE CELL ADHESION
Kamilė Kasperavičiūtė, Tadas Turonis, Wanessa Melo, Arūnas Stirkė 353

P2-113 ULTRA-TRACE DETERMINATION OF RHODIUM IN CAR EXHAUST SAMPLES USING UV PHOTOLYTIC DIGESTION AND DIFFERENTIAL PULSE VOLTAMMETRY
Islam Hassan, Rasa Pauliukaitė, Gerd-Uwe Flechsig 354

P2-114 COMPARATIVE STUDY OF TITANIA SUBSTRATE WETTABILITY TO PROMOTE MXENE ADHESION FOR WATER SPLITTING APPLICATION
M. Sajid, P. Gaigalas, O. Gogotsi, V. Klimas, S. Ramanavicius 355

P2-115 ELECTROCHEMICAL INVESTIGATION OF POLYURETHANEBASED BINDERS FOR SODIUM ION BATTERIES
Paulina Nemaniutė-Daubarė, Nadežda Traškina, Jurgis Pilipavičius, Linas Vilčiauskas 356

Poster Session 3: Laser Physics and Optical Technologies; Materials Science and Nanotechnology 357

P3-1 TIME-DEPENDENT PROPERTIES OF $ZnIn_2S_4$ THIN FILMS DEPOSITED FROM POWDER
Tautvilas Breive, Rokas Kondrotas, Arnas Naujokaitis, Vidas Pakstas, Asta Bronusiene 358

P3-2 MODIFICATION OF MATERIAL PROPERTIES USING HIGH ENERGY ION BEAMS
Deividas Rūškys, Mindaugas Gaspariūnas, Vitalij Kovalevskij, Konstantinas Birzul 359

P3-3 EXPERIMENTAL ESTIMATION OF HOT CARRIER TEMPERATURE IN P-N SOLAR CELLS
Jonas Petrokas, Jonas Gradauskas, Oleksandr Masalskyi, Ihor Zharchenko, Steponas Ašmontas, Algirdas Sužiedėlis, Aldis Šilėnas, Aurimas Čerškus 360

P3-4 INVESTIGATION OF HYDROGENATED GRAPHENE/Si JUNCTIONS USING LOW-FREQUENCY NOISE SPECTROSCOPY
Ingrida Pliaterytė, Justinas Glemža, Šarūnas Meškinis, Rimantas Gudaitis, Šarūnas Jankauskas, Asta Guobienė, Andrius Vasiliauskas, Sandra Pralgauskaitė, Jonas Matukas 361

P3-5 INVESTIGATION OF COPPER MICRO-PATH ELECTRODE DESIGN AND LINE SPACING ON ELECTROCHROMIC DEVICE FUNCTIONALITY
Dainius Balkauskas, Titas Tamošauskas, Modestas Sadauskas, Edita Voitechovič, Romualdas Trusovas, Karolis Ratautas, Alexandr Belosludtsev 362

P3-6 ALCOHOLS OXIDATION OVER CoNb AND CoCe OXIDE-BASEDCATALYST SUPPORTS
Virginija Kepenienė, Raminta Stagniūnaitė, Jūratė Vaičiūnienė, Loreta Tamašauskaitė-Tamašiūnaitė . 363

P3-7 COMPARATIVE ANALYSIS OF SAMARIUM AND GADOLINIUM DOPED CERIUM OXIDE SYNTHESIZED BY COMBUSTION AND CO-PRECIPITATION CHEMICAL METHODS FOR SOFC APPLICATION
Augustinas Zinkus, Mantas Sriubas, Tomas Šalkus, Brigita Abakevičienė 364

P3-8 MANGANESE/COBALT-BASED CATALYSTS FOR METAL-AIRBATTERIES: SYNTHESIS, CHARACTERIZATION AND PROPERTIES
Kirill Grib, Loreta Tamašauskaitė-Tamašiūnaitė 365

P3-9 APPLICATION OF SPRAY DRYING FOR THE STABILIZATION OF NATURAL COLORANTS
Gabija Siaurusaitytė, Indrė Bernatavičiūtė, Rūta Gruškienė 366

P3-10 DIELECTRIC SPECTROSCOPY OF PHOSPHATE-BONDED $BaTiO_3$ -$CoFe_2O_4$ MAGNETOELECTRIC CERAMICS.
Žygimantas Logminas, Artyom Plyushch, Jūras Banys 367

P3-11 PROCESSING AND PROPERTIES OF STARCH ESTER-BASED THERMOPLASTIC COMPOSITIONS
Klaudija Cerkaite, Ayodeji Amobonye, Joana Bendoraitiene, Dovile Liudvinaviciute, Muhammad Nasif, Laura Peciulyte, Deimante Rosliuk, Remo Merijs Meri, Shu-Kai Yeh 368

P3-12 EFFECT OF ALKALINE TREATMENT ON STUCTURE OF HEMP SEED HULLS AND THE BIODEGRADABILITY OF THERMOPLASTIC BIOCOMPOSITES
Paulius Barvainis, Joana Bendoraitiene, Giedruna Pavuolyte, Laura Peciulytė, Dovile Liudvinaviciute, Ramune Rutkaite 369

P3-13 ELECTRICAL PROPERTIES OF LLTO CERAMICS
Indrė Petkevičiūtė, Edvardas Kazakevičius, Dovydas Karoblis, Ona Balachninaitė 370

P3-14 IMPACT OF HIGH PRESSURE ON THE STRUCTURE AND ELECTRICAL PROPERTIES OF LITHIUM VANADATE PHOSPHATE GLASS AND GLASS-CERAMICS
Łukasz Przeszłowski, Krzysztof Gadomski, Tomasz Pietrzak 371

P3-15 OPTIMALIZATION OF ELECTRICAL PARAMETERS OF Bi_2O_3-Al_2O_3-SiO_2
Norbert Gąsior, Marcin Małys, Marek Wasiucionek, Tomasz K. Pietrzak, Maciej Nowagiel 372

P3-16 SYNTHESIS OF $YFeO_3$ THROUGH OXIDE INTERMEDIATES
Evaldas Lugauskas, Dovydas Karoblis, Aivaras Kareiva 373

P3-17 PROCESS DESIGN OF MIGRATION-ENHANCED MOCVD GROWTH OF AIN AND AlGaN
Karolina German, Tadas Malinauskas, Arūnas Kadys 374

P3-18 EXCITATION-DEPENDENT PHOTOLUMINESCENCE IN GaN EPILAYERS WITH DIFFERENT DOPING CONCENTRATIONS
Aurėja Ertmanaitė, Jūras Mickevičius 375

P3-19 STUDY OF SbSeI THIN FILM CRYSTALLIZATION
Deividas Vainauskas, Vidas Pakštas, Rokas Kondrotas 376

P3-20 DOPING CONTROL OF Si- AND Mg-DOPED GaN EPITAXIAL LAYERS FOR PIN DETECTOR APPLICATIONS
Gustė Jovaišaitė, Arūnas Kadys, Tadas Malinauskas, Dominykas Augulis 377

P3-21 NARROW CAVITY CVD FOR MoS_2 FILM FORMATION FROM MoO_x PERCURSOR FILMS
Amelija Saulė Rupkutė, Mindaugas Kamarauskas, Tomas Daugalas, Vytautas Jakštas, Algimantas Lukša, Saulius Balakauskas, Ilja Ignatjev, Marius Treideris 378

P3-22 LOW MELTING TEMPERATURE LANTHANUM-LEAD-BISMUTH ALLOYS
Abdul Mannan Majeed, Sandra Stanionytė, Gediminas Kreiza, Šarūnas Vaitekonis, Vidmantas Kalendra, Patrik Ščajev, Algirdas Mekys 379

P3-23 YAG-BASED HIGH-ENTROPY GARNETS: SYNTHESIS AND CHARACTERIZATION
Diana Vištorskaja, Artūras Katelnikovas, Aivaras Kareiva 380

P3-24 VACUUM BASED SYNTHESIS OF $AgBiS_2$ THIN FILMS BY MAGNETRON SPUTTERING AND SULFURIZATION
J. Dubikaltis, R. Giraitis, M. Frankevičius, A. Sekskienė, V. Pakštas 381

P3-25 OPTICAL DLTS STUDY OF RADIATION-INDUCED DEFECTS IN BORON-DOPED LGAD DETECTORS
Joris Plaščinskas, Tomas Čeponis, Jevgenij Pavlov 382

P3-26 GERMANIUM(II) SULFIDE THIN FILMS FOR VISIBLE-LIGHT PHOTODETECTORS
Andrej Vedernikov, Audrius Drabavičius 383

P3-27 SURFACE ENGINEERING BY LASER BEAM IN PRISTINE AND PROTON IRRADIAED GaN
Mykolas Strigūnas, Jevgenij Pavlov, Tomas Čeponis 384

P3-28 CHARACTERIZATION OF INITIAL DEFECT LANDSCAPES AND METHODOLOGY DEVELOPMENT FOR LGAD-RELATED P-TYPE SILICON APPLICATIONS
Faustina Kiaušaitė, Tomas Čeponis, Jevgenij Pavlov 385

P3-29 DIRECT CURRENT INJECTION EFFECTS ON RADIATION-INDUCED DEFECT DYNAMICS IN SILICON AND SILICON GERMANIUM SENSORS
Adelija Garšvaitė, Tomas Čeponis, Jevgenij Pavlov 386

P3-30 SYNTHESIS AND CHARACTERIZATION OF NICKEL TUNGSTEN CATALYST
Lukas Šimkus, Gitana Valeckytė, Zita Sukackienė, Jūratė Vaičiūnienė, Loreta Tamašauskaitė-Tamašiūnaitė, Eugenijus Norkus 387

P3-31 ELECTROCHEMICAL SENSOR BASED ON MOLECULARLY IMPRINTED POLYMERS FOR PROTEIN DETECTION
Gintarė Ruginytė, Ernestas Brazys, Vilma Ratautaitė, Arūnas Ramanavičius 388

P3-32 MOLECULAR IMPRINTED POLYDOPAMINE-BASED SENSOR FOR TETRACYCLINE DETECTION
Danish Khalid, Arūnas Ramanavičius, Ernestas Brazys, Vilma Ratautaitė 389

P3-33 GREEN SYNTHESIS OF SILVER NANOPARTICLES USING LIPOPHILICITY-MODIFIED LINDEN EXTRACTS
Urtė Raubytė, Aistė Balčiūnaitienė, Jonas Viškelis 390

P3-34 FUNCTIONALIZATION OF CoP AND CoFeP WITH GOLD NANOPARTICLES VIA GALVANIC DISPLACEMENT FOR ALKALINE WATER SPLITTING
Dmytro Shyshkin, Huma Amber, Loreta Tamašauskaitė-Tamašiūnaitė, Eugenijus Norkus 391

P3-35 GREEN SYNTHESIS OF SILVERNANOPARTICLES USING PROCESSED TILIA CORDATA EXTRACTS AND THEIR ENHANCEDANTIOXIDANT AND ANTIMICROBIAL ACTIVITIES
Syeda Hijab Zehra, Jonas Viskelis, Aiste Balciunaitiene 392

P3-36 FABRICATION OF GRAPHENE FIELD EFFECT TRANSISTOR ARRAY FOR BIOSENSING
Ujjawal Malani, Aleksandra Širvinsytė, Vilius Vertelis, Skirmatas Keršulis, Nerija Žurauskienė 393

P3-37 MICROFLUIDIC SYNTHESIS OF CHITOSAN-TPP NANOPARTICLES FOR DRUG DELIVERY IN ANTIBIOFILM APPLICATIONS
Samanta Gelumbickytė, Adei Abouhagger, Arūnas Stirkė 394

P3-38 SURFACE PLASMON POLARITON APPLICATION FOR FLUORESCENT DYE LABELLED BOVINE SERUM ALBUMIN DETECTION
Ūla Elena Sauliūtė, Ernesta Bužavaitė-Vertelienė 395

P3-40 ELECTROCHEMICAL IMMUNOSENSING OF DIPEPTIDYL PEPTIDASE IV:TOWARD SENSITIVE AND ACCESSIBLE CANCER-RELATED BIOMARKER DETECTION
Vejas Strelciunas, Antanas Zinovicius 396

P3-41 3D-PRINTED DIFFRACTIVE OPTICAL ELEMENTS USING GRAYSCALE MULTIPHOTON PRINTING
Paulius Semenauskas, Mangirdas Malinauskas, Maria Farsari, Gordon Zyla 397

P3-42 REAL-TIME DATA HANDLING FOR FAST LIDAR
Vaidas Šutas, Jonas Jurkevičius 398

P3-44 TERAHERTZ METAMATERIAL ABSORBER BASED ON GRAPHENE PLASMONS
Mohammad Esmaeil Daraei, Mehdi Abedi-Varaki, Ignas Nevinskas 399

P3-45 A PM-PCF SAGNAC CONFIGURATION FOR HYBRID-WAVELENGTH PHOTON PAIR GENERATION
Gustas Liaugminas, Alexandr Belosludtsev, Julijanas Želudevičius, Kęstutis Regelskis 400

P3-46 RAPID DEOXYGENATION OF TTA-UC SOLUTIONS USING BMTS SCAVENGER
Dominykas Likas, Steponas Raišys, Manvydas Dapkevičius 401

P3-47 MOLECULARLY IMPRINTED CONDUCTING POLYMER HYDROGEL COMPOSITES FOR TETRACYCLINE LOADING AND ELECTRICALLY RESPONSIVE DRUG DELIVERY
Samuel A. Kosoko, Ernestas Brazys, Vilma Ratautaite, Arūnas Ramanavičius 402

P3-48 DURABILITY AND SUSTAINED ANTIMICROBIAL ACTIVITY OF NANOCOMPOSITE COATINGS
Mindaugas Ilickas, Wanessa De Cassia Martins Antunes De Melo, Karolis Gedvilas, Asta Guobienė, Mantvydas Merkis, Simas Račkauskas, Arūnas Stirkė, Brigita Abakevičienė 403

P3-49 OPTIMIZATION OF ANTIMONY SELENIDE DEPOSITION ON ZINC OXIDE BY VAPOR TRANSPORT DEPOSITION METHOD
Gerarda Jocytė, Rokas Kondrotas, Gintautas Jonkus, Vidas Pakštas 404

P3-50 INVESTIGATION OF ION-BEAM IRRADIATION EFFECTS ON THE ELECTRICAL PROPERTIES OF NOVEL N-TYPE LOW GAIN AVALANCHE DETECTORS
Margarita Biveinytė, Tomas Čeponis, Laimonas Deveikis, Miloš Manojlović, Vytautas Rumbauskas, Kęstutis Žilinskas 405

P3-51 MODIFICATION OF GaN THIN LAYERS WITH HYDROGEN IMPLANTATION
Margarita Biveinytė, Šarūnas Vaitekonis, Vitalij Kovalevskij, Arūnas Kadys, Algirdas Mekys 406

P3-52 BILAYER POLYSACCHARIDE FILMS CONTAINING FERMENTED AND NON-FERMENTED ARTHROSPIRA PLATENSIS EXTRACTS
Deimante Rosliuk, Dovile Liudvinaviciute, Ramune Rutkaite, Shahana Aboobacker, Vaida Kitryte-Syrpa, Michail Syrpas 407

P3-53 FABRICATION AND DYNAMIC MECHANICAL CHARACTERIZATION OF FLAX FIBER-REINFORCED HYBRID COMPOSITES
Robertas Gilys, Justas Ciganas, Urte Cigane 408

P3-54 METAL HIGH-REFLECTIVE MIRRORS FOR SPACE APPLICATIONS
Alexandr Belosludtsev, Ignas Bitinaitis, Vitalij Kovalevskij, Karolis Stravinskas, Anna Sytchkova 409

P3-55 SYNTHESIS AND CHARACTERIZATION OF ZINC SULFIDE FILMS ON FTO GLASS
Dominyka Zubrickaitė, Ingrida Ancutienė, Asta Bronušienė 410

P3-56 MXENE BASED SCHOTTKY-JUNCTIONS FOR UNASSISTED PHOTOELECTROCHEMICAL WATER SPLITTING
Syeda Ammara Shabbir, Muhammad Haris, Sohaib Khalid, Carlos Ponce de Leon, Klaudijus Midverisa, Muhammad Younas, Hamid Latif, Imed Boukhris, M S alburiahi, Norah Salem Alsaiari, Tomas Tamulevičius, Sigitas Tamulevičius 411

P3-57 CYANOPYRIDINE-BASED TADF EMITTERS FOR OLEDS AND OPTICAL SENSING
Akaki Kalatozishvili, Oleksandr Bezvikonnyi, Jurate Simokaitiene, Dmytro Volyniuk, Dalius Gudeika, Hlafira Krasnozhon, Juozas V. Grazulevicius 412

P3-58 SYNTHESIS AND PROPERTIES OF PHENANTHROIMIDAZOLE-BASED COMPOUNDS AS PROMISING EMITTERS FOR OLEDS
Svetlana Sargsyan, Viktorija Andruleviciene, Matas Guzauskas, Dmytro Volyniuk, Juozas Vidas Grazulevicius 413

P3-59 MOLECULAR ENGINEERING OF ETHYLCARBAZOLE DERIVATIVES FOR HIGHLY EFFICIENT OLED HOST MATERIALS
Dovydas Blazevicius, Raminta Beresneviciute, Ernestas Kasparavicius, Julius Petrulevicius, Gintare Krucaite, Saulius Grigalevicius, Chih-Hung Ko, Cai-Fan Lo, Chih-Hao Chang 414

P3-60 LINK BETWEEN SYNTHESIS PARAMETERS AND STRUCTURAL PROPERTIES OF ZINC OXIDE
Gintautas Jonkus, Vidas Pakštas, Rokas Kondrotas 415

P3-61 SELENIZATION OF THIN ANTIMONY FILMS FOR Sb_2Se_3 SOLAR CELLS
Linas Majauskas, Audrius Drabavičius, Vidas Pakštas, Rokas Kondrotas 416

P3-62 NANOCRYSTALLISATION OF AMORPHOUS ANALOGUES OF BSCCO SUPERCONDUCTORS
Maria Kacprzak, Tomasz K. Pietrzak 417

P3-63 STUDY OF RECOMBINATION CHARACTERISTICS OVER A WIDE FLUENCE RANGE IN REACTOR NEUTRON IRRADIATED Si
Justė Martinavičiūtė, Laimonas Deveikis, Tomas Čeponis 418

P3-64 OPTIMIZING QUALITY OF La:SrSnO3 FILMS VIA OXYGEN CONCENTRATION AND STOICHIOMETRIC CONTROL
Mindaugas Voznikas, Milita Vagner, Tomas Murauskas, Virgaudas Kubilius, Valentina Plaušinaitienė . 419

P3-65 INVESTIGATION OF ENERGY CONVERSION IN FREQUENCY CONVERTERS FOR DIFFERENT PUMP SPATIAL PROFILE
Gabrielius Rusonis, Arūnas Varanavičius 420

P3-66 OPTIMIZATION OF LASER CUTTING PARAMETERS FOR INCREASED CUTTING SPEED IN STAINLESS STEEL
Lukas Brundza, Mindaugas Gedvilas 421

P3-67 AEROSOL CHARACTERIZATION DURING LASER ABLATION OF STRUCTURAL STEEL FOR NUCLEAR DECOMMISSIONING APPLICATIONS
Emilis Sadrejevas, dr. Artūras Plukis, dr. Rita Plukienė, Vilius Žalėnas, dr. Anton Koroliov, Jon Jeffrey Haist 422

P3-68 MICROFABRICATION OF TRANSPARENT POLYMER FOR INTRAOCULAR LENS BY FEMTOSECOND PULSES
Dainius Ratkus, Andrius Žemaitis, Arnas Vyšniauskas, Paulius Gečys 423

P3-69 LASER INDUCED DAMAGE THRESHOLD CHANGE IN TIME IN NANOSTRUCTURED GLAD ALL-SILICA HIGHLY REFLECTIVE OPTICAL MIRRORS
Adomas Strazdas, Lukas Ramalis 424

P3-70 REAL-TIME FULL-FIELD VIBROMETRY USING A SMART-PIXEL LOCK-IN CAMERA
Florian Dötzer, Fridtjof Seufert, Stefan Sinzinger 425

P3-71 LASER TREATMENT OF HYBRID TI-AU-AG THIN FILMS AND INVESTIGATION OF THEIR OPTICAL PROPERTIES
Kasparas Okleiteris, Evaldas Stankevičius 426

P3-72 FORMATION OF MICROSTRUCTURES IN GLASS USING LASER INTERFERENCE ABLATION AND CHEMICAL ETCHING
Daumantas Sriubas, Simonas Indrišiūnas 427

P3-73 X-RAY EMISSION FROM A CU TARGET DRIVEN BY 2 µm FEMTOSECOND LASER PULSES
Miroslav Saniuk, Anton Koroliov, Artūras Plukis 428

P3-74 PARAMETRIC ANALYSIS OF FILAMENT ASSISTED X-RAY GENERATION
Šarūnas Logminas, Balys Momgaudis 429

P3-75 IMPROVED SEAM STRENGTH IN ULTRASHORT PULSED LASER WELDING OF GLASSES VIA INTERFACE PRE-ROUGHENING
Neda Mažeikytė, Edgaras Markauskas, Paulius Gečys 430

P3-76 METASURFACE OPTICS FOR APPLICATIONS ACCROSS THE INFRARED
Erika Jonaitytė, Klaudijus Midveris, Mindaugas Juodėnas 431

P3-77 LIFETIME MEASUREMENTS OF PLASMON-EXCITON POLIARITONIC EMISSION USING SUPER-CRITICAL ANGLE FLUORESCENCE MICROSCOPY
Evita Spalinskaitė, Justina Anulytė, Vytautas Žičkus, Zigmas Balevičius 432

P3-78 SUB-THZ BEAM FORMING FOR NEXT-GENERATION HIGH-FREQUENCY COMMUNICATION SYSTEMS USING DIFFRACTIVE OPTICAL ELEMENTS
Kotryna Nacienė, Kasparas Stanaitis, Ernestas Nacius, Linas Minkevičius 433

P3-79 FLUORESCENCE CONCENTRATION QUENCHING IN CHLOROPHYLL MOLECULE AGGREGATES
Liudas Ablačinskas 434

P3-80 MULTIFUNCTIONAL CARBON-BASED QUANTUM DOTS FOR ENVIRONMENTAL AND MEDICAL APPLICATION
Martynas Zalieckas, Hanna Maltanava, Nikita Belko, Polina Kuzhir, Renata Karpicz 435

P3-81 DESIGN AND FABRICATION OF MINIATURIZED OPTICAL SYSTEMS VIA MULTI-PHOTON LITHOGRAPHY
Austėja Kvedaraitė, Dimitra Ladika, Mangirdas Malinauskas, Gordon Zyla 436

P3-84 LASER-INDUCED GRAPHENE FOR RADAR ABSORBING MATERIALS APPLICATIONS
Rokas Klimas, Augustas Koklevičius, Paulius Ragulis, Romualdas Trusovas 437

P3-85 DIRECT LASER WRITING OF PLASMONIC NANOSTRUCTURES ON AG-AU ALLOY FILMS
Marijus Mozdeikis, Evaldas Stankevičius 438

P3-86 MULTI-PHOTON LITHOGRAPHY FOR PHOTONIC APPLICATIONS
Kristina Budiak, Gordon Zyla, Mangirdas Malinauskas, Dimitra Ladika 439

P3-87 DESIGN AND FABRICATION OF METASURFACES VIA MULTI-PHOTON LITHOGRAPHY
Jonas Vytautas Sviklis, Dimitra Ladika, Mangirdas Malinauskas, Gordon Zyla 440

P3-88 LASER-INDUCEDGRAPHENE FORMATION IN KEVLAR
David Bolanos, Romualdas Trusovas 441

P3-89 STRUCTURAL AND OPTICAL PROPERTIES OF Eu^{3+} /Tb^{3+} CO-DOPED $GdPO_4$ NANOPARTICLES
Mirza Abdul Qudoos Baig, Eglė Ežerskyte, Artūras Katelnikovas, Živilė Jurgelenė, Vaidas Klimkevičius 442

P3-90 PROTOTYPE OF A WHITE LED WITH GLASSY NAF-AL_2 O_3-P_2O_5: EU PHOSPHOR
Mateusz Słotwiński, Agata Jarocka, Tomasz Pietrzak 443

P3-91 EFFECT OF ORGANIC WASTE PARTICLE ADDITIVES ON THE PROPERTIES OF THERMOPLASTIC CELLULOSE ACETATE
Akvile Brazdauske, Laura Peciulyte, Ramune Rutkaite, Dovile Liudvinavičiūtė, Joana Bendoraitiene, Kastytis Pamakštys, Visvaldas Varzinskas 444

P3-92 PHOTOLUMINESCENCE STUDY OF InGaAs QUANTUM WELLS WITH LINEARLY AND PARABOLICALLY GRADED AlGaAs BARRIERS
Denis Goldobin, Aistė Štaupienė, Justas Žuvelis, Aivaras Špokas, Andrea Zelioli, Aurimas Čerškus, Evelina Dudutienė, Renata Butkutė 445

P3-93 SPECTROSCOPIC INVESTIGATION OF GOLD NANOCLUSTERS UNDER DIFFERENT PH CONDITIONS
Jelizaveta Fedotova, Giedrė Grincienė, Renata Karpicz 446

P3-94 INFLUENCE OF Co^{2+} IONS ON GYROLITE FORMATION UNDER HYDROTHERMAL CONDITIONS
Adrija Marija Paknytė, Tadas Dambrauskas 447

P3-95 EVALUATION OF THE PHYSICO-CHEMICAL PROPERTIES OF HYDRAULIC CALCIUM SILICATE-BASED SEALER MODIFIED WITH CALCIUM HYDROXYAPATITE, FLUOROHYDROXYAPATITE, AND MAGNESIUM WHITLOCKITE
Paulina Mozūraitė, Goda Bilvinaitė, Saulius Drukteinis, Simas Šakirzanovas 448

P3-96 CHEMICAL CHARACTERIZATION AND ANTIMICROBIAL ACTIVITY ASSESSMENT OF SPENT COFFEE GROUNDS USED IN BUILDING GYPSUM COMPOSITES
Neringa Matutytė, Rita Kazernavičiūtė, Aušra Šipailienė, Nora Kybartienė 449

P3-97 DEVELOPMENT OF MOLECULARLY IMPRINTED POLYMER ON MAGNETIC PARTICLES
Gabrielė Slaboševičiūtė, Ernestas Brazys, Vilma Ratautaitė, Arūnas Ramanavičius 450

P3-98 HIGH-ASPECT-RATIO c-Si METASURFACES FOR ULTRA-FAST PULSE LASERS
Klaudijus Midveris, Erika Jonaitytė, Gvidas Klyvis, Tomas Klinavičius, Andrius Žutautas, Mindaugas Juodėnas 451

P3-99 PHOTOLUMINESCENCE STUDY OF n/InGaN/p SINGLE QUANTUM WELLS
Deimantė Juknevičiūtė, Jūras Mickevičius 452

P3-100 SULPHUR-ENHANCED REVERSE INTERSYSTEM CROSSING IN TADF AND MULTI-RESONANCE TADF BLUE EMITTERS
Mykolas Vaitilas, Goda Grybauskaitė, Giedrius Puidokas, Gediminas Kreiza, Domantas Berenis, Kenkera Rayappa Naveen, Karolis Kazlauskas 453

P3-102 APPLICATION OF DIBENZOFURAN-BASED HOST MATERIALS FOR BLUE 3RD GENERATION THERMALLY ACTIVATED DELAYED FLUORESCENCE (TADF) ORGANIC LIGHT EMITTING DIODES
Goda Grybauskaitė, Kristupas Bagdonas, Domantas Berenis, Gediminas Kreiza, Edvinas Orentas, Eigirdas Skuodis, Karolis Kazlauskas, Dovydas Banevičius 454

P3-103 OPTIMIZATION OF MAGNETIC-FIELD QUANTUM SENSING WITH NV CENTERS
Vakaris Šilys, Julius Janušonis, Tadas Paulauskas 455

P3-104 DETERMINATION OF THE PROBABILITY OF SINGLET EXCITON FORMATION DURING TRIPLET-TRIPLET ANNIHILATION IN MODEL PHOTON UPCONVERSION COMPOUNDS
Manvydas Dapkevičius, Džiugas Krencius, Steponas Raišys, Justas Lekavičius, Karolis Kazlauskas . . 456

P3-105 ENHANCING RISC IN NARROWBAND BLUE MR-TADF EMITTERS
Giedrius Puidokas, Lukas Deltuvytis, Gediminas Kreiza, Karolis Kazlauskas 457

P3-106 INVESTIGATION OF THE DEPENDENCE OF PHOTOLUMINESCENCEPROPERTIES ON MAGNESIUM CONCENTRATION IN LuAG: CeSCINTILLATORS
Mikas Iršėnas, Augustas Vaitkevičius, Arnoldas Solovjovas, Saulius Nargelas 458

P3-107 DESIGN OF NOVEL 3-(DIPHENYLAMINO)CARBAZOLE COMPOUNDS FOR MULTI-CHANNEL GREEN TADF OLEDs
Raminta Beresneviciute, Inesa Sasnauskaite, Zeyad Taher Abdou, Dovydas Blazevicius, Saulius Grigalevicius, Wanting Ju, Xiangqin Gan, Junqiao Ding, Kaspars Traskovskis 459

P3-108 STRUCTURE-PROPERTY RELATIONSHIPS IN ANTHRACENE ANNIHILATORS FOR TRIPLET-TRIPLET ANNIHILATION PHOTON UPCONVERSION
Džiugas Krencius, Justas Lekavičius, Manvydas Dapkevičius, Steponas Raišys, Edvinas Orentas, Karolis Kazlauskas 460

P3-109 PHOTOPHYSICAL STUDY OF POLYCYCLIC AROMATIC COMPOUNDS
Tautvydas Kairys, Kamilė Boguševičienė, Kasper Moth-Poulsen, Paulius Baronas, Saulius Juršėnas . 461

P3-110 CRYSTALLINE GETE THIN FILMS FOR INFRARED PHOTODETECTION
Pijus Kuliavas, Marius Franckevičius, Vidas Pakštas, Rokas Kondrotas, Audrius Drabavičius 462

P3-111 SYNTHESIS AND INVESTIGATION OF PHENOTHIAZINE ORGANICSEMICONDUCTORS
Skirmantas Musteikis, Mantas Marčinskas, Tadas Malinauskas 463

P3-112 TEMPERATURE-DRIVEN CROSSOVER OF CHARGE SEPARATION MECHANISMS IN NON-FULLERENE ORGANIC SOLAR CELL BLENDS
Rokas Jasiūnas, Nakul Jain, Titas Klepeckas, Andrius Gelžinis, Vidmantas Gulbinas 464

P3-113 SUB-NANOSECOND PULSE PARAMETRIC AMPLIFICATION SYSTEM IN THE VISIBLE SPECTRUM RANGE
Ieva Baltrukonytė, Jonas Banys, Julius Vengelis 465

P3-114 TOWARDS FDML-ENABLED FLOW-TROUGH QUANTITATIVE PHASE IMAGING
Laurynas Puškorius, Jonas Jurkevičius 466

P3-115 MODELING AND CHARACTERIZATION OF SPECTRAL PARAMETERS IN GLAD NANOSTRUCTURED THIN FILMS
Dovydas Šablinskas, Lukas Ramalis, Adomas Strazdas, Simas Melnikas 467

Poster Session 4: Ecology, Geology, and Environmental Sciences; Biology and Medicine 468

P4-1 IMPACT OF BODY MASS INDEX ON ERYTHROCYTE MEMBRANE FATTY ACID COMPOSITION AND OXIDATIVE STRESS IN HEALTHY ADULTS
Inga Bikulčienė, Inga Fomčenko, Virginijus Šapoka, Arvydas Kaminskas, Dovilė Karčiauskaitė 469

P4-2 EFFECTS OF MODULATING KDM5B EXPRESSION IN PROSTATE CANCER CELLS
Aukse Versekenaite, Ruta Maleckaite, Kristina Daniunaite 470

P4-3 EXPRESSION ANALYSIS OF THE COMPONENTS OF HIPPO SIGNALING PATHWAY IN OVARIAN CANCER
Kornelia Gurska, Rūta Čiurlienė, Rasa Sabaliauskaitė, Ieva Vaicekauskaitė 471

P4-4 DNMT AND HDAC INHIBITION INDUCE DISTINCT TRANSCRIPTIONAL PROGRAMS AND ACTIVE CHROMATIN REMODELING IN CAR19-NK CELLS
Patricija Daugėlaitė, Veronika Viktorija Borutinskaitė 472

P4-5 CIRCULAR RNA QUANTIFICATION IN PROSTATE CANCER CELL LINES WITH MODIFIED EXPRESSION OF SELECTED MICRORNAS
Gerda Bertulyte, Ruta Maleckaite, Aukse Versekenaite, Arnas Stucinskas, Marta Tamosiunaite, Kristina Daniunaite 473

P4-6 IN VITRO GENOTOXICITY ASSESSMENT OF POLYSTYRENE MICRO- AND NANOPARTICLES IN HUMAN ALVEOLAR EPITHELIAL CELLS (A549)
Vaiva Horbačauskaitė, Emilija Striogaitė, Juozas Rimantas Lazutka 474

P4-7 ACTIVITY OF DOXORUBICIN AND 5-FLUOROURACIL IN HUMAN MELANOMA A375 SPHEROIDS FORMED BY DIFFERENT METHODS
Akvilė Žilytė, Vilma Petrikaitė 475

P4-8 IN VITRO GENOTOXICITY OF POLYETHYLENE MICROPARTICLES IN HUMAN HEPATOMA (HEPG2) AND ADENOCARCINOMA (A549) CELL LINES
Emilija Striogaitė, Juozas Rimantas Lazutka 476

P4-9 TDP-43 LIQUID-LIQUID PHASE SEPARATION AND PHOSPHORYLATION STUDY
Saulė Rapalytė, Dominykas Veiveris, Darius Šulskis 477

P4-10 EXPRESSION, PURIFICATION AND ACTIVITY ASSESMENT OF RECOMBINANT ESCHERICHIA COLI PURINE DEAMINASES
Ugnius Kamandulis, Jaunius Urbonavičius, Daiva Tauraitė 478

P4-11 PTTG1 RS2910200 POLYMORPHISM AS A POTENTIAL MARKER OF LOCALLY ADVANCED LARYNGEAL SQUAMOUS CELL CARCINOMA
Augustė Simanonytė, Enrika Pileckaitė, Vykintas Liutkevičius, Rasa Liutkevičienė 479

P4-12 EXPRESSION OF KINESIN SUPERFAMILY MEMBERS KIF2C, KIF14 AND KIF20 AS DIAGNOSTIC BIOMARKERS FOR OVARIAN CANCER
Areta Petrauskaitė, Ieva Vaicekauskaitė, Rūta Čiurlienė, Rasa Sabaliauskaitė 480

P4-13 LIQUID-LIQUID PHASE SEPARATION OF S100A4 PROTEIN
Arijus Jaloveckas, Darius Šulskis 481

P4-14 DIFFERENT PHARMACOLOGICAL MODULATION OF TRPM6 AND TRPM7 PROTEINS IN HUMAN CARDIOMYOCYTES
Inga Andriulė, Regina Mačianskienė 482

P4-15 MOONLIGHTING CHAPERONE ACTIVITY OF S100A12 WITHIN THE S100A FAMILY
Orestas Antipas Pelivanov, Darius Šulskis 483

P4-16 REPROGRAMMING INHIBITOR-ENZYME RECOGNITION PROFILE VIA CHIMERIC CARBONIC ANHYDRASE I
Ignas Glušnys, Aurelija Mickevičiūtė, Daumantas Matulis, Joana Smirnovienė 484

P4-17 FACTORS AFFECTING THE LONG-TERM COEVOLUTION OF STREPTOCOCCUS THERMOPHILUS AND ITS LYTIC PHAGE 2972
Yana Karnitskaya, Laurynas Vaitkus, Giancarlo Russo 485

P4-18 BREWING DIVERSITY: PHENOTYPIC AND MOLECULAR CHARACTERIZATION OF YEAST FROM TRADITIONAL LITHUANIAN BEERS
Paulina Morkytė, Justina Stonytė, Rasa Pauliukaitė 486

P4-19 GENETIC STRUCTURE AND DIVERSITY OF RED DEER (CERVUS ELAPHUS) POPULATIONS IN LITHUANIA
Jokūbas Čypas, Evelina Genevičienė, Loreta Griciuvienė, Irma Ražanskė, Artūras Kibiša, Algimantas Paulauskas 487

P4-20 GENETIC DIVERSITY OF MICROORGANISM ASSOCIATED WITH MAKEUP FOUNDATIONS AND APPLICATION TOOLS
Ugnė Januškaitė, Saulė Norkutė, Asta Aleksandravičienė, Žaneta Maželienė, Giedrė Jarienė 488

P4-21 PREVALENCE AND MOLECULAR CHARACTERIZATION OF ANAPLASMAPHAGOCYTOPHILUM IN TICKS FROM URBANIZED AND NATURAL HABITATS OF LITHUANIA
Queen Uyojo Omale, Justina Snegiriovaitė, Indrė Lipatova, Miglė Razgūnaitė, Algimantas Paulauskas, Jana Radzijevskaja 489

P4-22 USE OF BACTERIAL OUTER MEMBRANE VESICLES IN COMBINED ANTIBIOTIC AND PHOTODYNAMIC THERAPY AGAINST ACINETOBACTER BAUMANNII
Ingrida Tarabildienė, Irina Buchovec, Jūratė Skerniškytė 490

P4-23 A SECRET ALLIANCE BETWEEN SPLIT PROKARYOTIC ARGONAUTE PROTEINS AND TYPE I RESTRICTION - MODIFICATION SYSTEMS
Laura Juozepavičiūtė, Edvardas Golovinas, Mindaugas Zaremba 491

P4-24 MOLECULAR DETECTION OF RICKETTSIA PATHOGENS IN ECTOPARASITES OF RED FOXES
Raminta Likšaitė, Ugnė Medikaitė, Indrė Lipatova, Justina Snegiriovaitė, Renata Špinkytė, Algimantas Paulauskas 492

P4-25 REFINING PRECLINICAL SCREENING: 3D CELL CULTURE MODELS AS A TOOL FOR ASSESSING TARGETED THERAPIES IN ENDOMETRIAL CANCER
Laura Marija Račytė, Evelina Šidlovska, Margarita Montrimaitė, Gediminas Januška, Rūta Čiurlienė, Eglė Žalytė 493

P4-26 CRISPR-CAS SYSTEMS VALIDATION USING A FLUORESCENT REPORTER CELL LINE
Rugilė Tūskaitė, Neringa Daugelavičienė, Eimina Dirvelytė-Valauskė, Simonas Kutanovas, Urtė Neniškytė 494

P4-27 AMNIOTIC FLUID STEM CELL-DERIVED EXTRACELULAR VESICLES MODULATE GENE EXPRESSION IN A miR-146a-5p-INHIBITED SH-SY5Y MODEL
Greta Bertašiūtė, Aistė Zentelytė, Rūta Navakauskienė, Giedrė Valiulienė 495

P4-28 ACTIVITY OF NOVEL HYDRAZONE DERIVATIVES IN 3D TUMOR SPHEROIDS AND SINGLE-CELL MIGRATION IN HUMAN BRAIN, TRIPLE-NEGATIVE BREAST, AND SKIN CANCER CELL LINES
Tomas Ragauskas, Juozas Kiltinavičius, Ingrida Tumosienė, Kristina Kantminienė, Vilma Petrikaitė . . 496

P4-29 IN VITRO ANTICANCER ACTIVITY OF HYDRAZONE DERIVATIVES IN PANCREATIC CANCER CELLS UNDER NORMOXIA AND HYPOXIA
Digna Narkevičiūtė, Juozas Kiltinavičius, Ingrida Tumosienė, Kristina Kantminiene, Vilma Petrikaitė . . 497

P4-30 SHORT-TERM PHARMACOLOGICAL MODULATION OFARTERIAL STIFFNESS IN PIGS IN VIVO
Ieva Lankutytė, Dominyka Adamonė, Vilma Zigmantaitė, Jonas Jurevičius, Regina Mačianskienė . . . 498

P4-31 RESISTANCE OF *ENTEROCOCCUS FAECIUM* BACTERIA TO COMMONLY USED DISINFECTANTS IN CLINICAL SETTING
Ernest Oleinik, Agnė Kirkliauskienė, Tatjana Kirtiklienė 499

P4-32 THE EFFECT OF NOVEL SULFONAMIDE DERIVATIVES ON HUMAN PROSTATE AND TRIPLE-NEGATIVE BREAST CANCER CELL LINE VIABILITY UNDER NORMOXIA AND HYPOXIA
Kotryna Čiupkevičiūtė, Valdas Vainauskas, Birutė Grybaitė, Vytautas Mickevičius, Vilma Petrikaitė . . . 500

P4-33 SUSTAINABLE MAGNETIC BUCKWHEAT HULL-Fe_3O_4 NANOCOMPOSITES FOR ENHANCED BIOSORPTION OF HEAVY METALS IN BINARY AND TERNARY CONTAMINANT MATRICES
Tayyab Tahir, Rūta Druteikienė, Zita Žukauskaitė, Rūta Barisevičiūtė, Jūratė Vaičiūnienė 501

P4-34 ASSESSMENT OF METHANE EMISSIONS IN REWETTED SWAMPS USING STABLE CARBON ISOTOPE ANALYSIS
Laurynas Bučinskas, Ąžuolas Ivickas, Andrius Garbaras 502

P4-35 SEASONAL VARIATION OF HYDROCARBON DEGRADATION GENES IN URBAN GREEN AREA SOILS OF VILNIUS
Aistė Pazikaitė, Nomeda Kuisienė 503

P4-36 IMPACT OF DIETARY MAGNETIC CHITOSAN AND PROBIOTICS ON OXIDATIVE STRESS BIOMARKERS IN COMMON CARP
Aida Bradauskaitė, Sergej Šemčuk, Renata Butrimienė, Danguolė Montvydienė, Natalia Matvienko, Vesta Skrodenytė-Arbačiauskienė, Živilė Jurgelėnė 504

P4-37 THE EFFECT OF DIFFERENT RATES OF INDUSTRIAL WASTE (BIOFUEL ASH) ON CULTIVATED MAIZE IN ACIDIC SOIL
Gabija Žilytė, Kristina Bunevičienė, Urtė Čegytė 505

P4-38 CHARACTERIZING ECOSYSTEM-SPECIFIC PATTERNS OF ANTIBIOTIC RESISTANCE IN ENVIRONMENTAL BACTERIA
Alper Melih Ucar, Juliana Lukša-Žebelovič, Elena Servienė 506

P4-39 HARNESSING THE POTENTIAL OF BACTERIA ISOLATED FROM CONSTRUCTION BY-PRODUCTS AS A SUSTAINABLE APPROACH TOWARDS ENVIRONMENTAL PROTECTION
Sabina Myrzakhmetova, Saloua Biyada 507

P4-40 OPTIMIZED BIOETHANOL PRODUCTION FROM SUNFLOWER (HELIANTHUS ANNUUS) HEAD WASTE USING SACCHAROMYCES CEREVISIAE
Sunil Kumar, Vilma Kaškonienė 508

P4-41 ADSORPTION OF POLYETHYLENE TEREPHTHALATE, POLYSTYRENE, AND POLYETHYLENE NANOPLASTICS FROM FRESHWATER SYSTEMS
Mahrosh Javed, Galina Lujanienė, Sergej Šemčuk, Vidas Pakštas, Martynas Talaikis, Aušra Selskienė 509

P4-42 EFFECT OF RAW MATERIAL COMPOSITION ON THE PHYSICALPROPERTIES OF SOLID ORGANIC FERTILIZERS
Gabija Aleksaitytė, Rasa Šlinkšienė 510

P4-43 ASSESSMENT OF WARM-SEASON SST TRENDS IN THE CURONIAN LAGOON USING REANALYSIS DATA
Gustė Gečaitė, Donatas Pupienis 511

P4-44 ENVIRONMENTAL BEHAVIOR AND EFFECTS OF RARE-EARTH UPCONVERTING NANOPARTICLES TO FRESHWATER ALGAE
Taseer Mustafa, Živilė Jurgelenė, Danguolė Montvydienė, Vilius Poderys, Eglė Ežerskytė, Jūratė Karosienė, Artūras Katelnikovas, Augustas Morkvėnas, Lukrecija Miliūtė, Vitalijus Karabanovas, Vaidas Klimkevičius 512

P4-45 INTEGRATING REMOTE SENSING AND MACHINE LEARNING TO RELATE GROUNDWATER LEVEL DYNAMICS WITH HYDROCHEMICAL VARIABILITY
Assemzhan Kunsakova, Vytautas Samalavičius 513

P4-46 INFLUENCE OF LANDFILL OPERATION AND TREATMENT PRACTICES ON LEACHATE TOXICITY TO DAPHNIA MAGNA
Tomas Makaras . . . 514

P4-47 FIRST COMPREHENSIVE ASSESMENT OF MICROPLASTICS IN URBAN STREET DUST OF EASTERN SAUDI ARABIA: ABUNDANCE, TRAITS, AND HEALTH RISKS
Ali Ashry . . . 515

P4-48 RECYCLING INITIATIVES IN SUSTAINABLE POLYMER WASTE MANAGEMENT
Maksym Koliada, Viktoriia Plavan, Oleh Lozovyi . . . 516

P4-49 UNRAVELING 4-HYDROXYPHENYLPYRUVATE METABOLISM IN CUPRIAVIDUS NECATOR H16
Monika Tamašauskaitė, Ingrida Sabaliauskė, Ernesta Augustinienė . . . 517

P4-50 THE MECHANISMS OF TYPE I RESTRICTION-ENDONUCLEASES AT SINGLE-MOLECULE RESOLUTION USING MAGNETIC TWEEZERS
Farzaneh Alipoor Azizollahi, Paulius Toliušis, Mindaugas Zaremba, Algirdas Toleikis . . . 518

P4-51 APPLICATION OF MOLECULAR BIOLOGY METHODS FOR THE DETECTION OF BABESIA CANIS
Illia Hol, Miglė Razgūnaitė, Justina Snegiriovaitė, Indrė Lipatova, Karolina Jankauskaitė, Birutė Karvelienė, Algimantas Paulauskas, Jana Radzijevskaja . . . 519

P4-52 FUNCTIONAL CHARACTERISATION OF RECOMBINANT PSEUDOMONAS AERUGINOSA LIPOXYGENASE
Vytautė Blekaitytė, Dovilė Daunoraitė, Inga Matijošytė . . . 520

P4-53 EVALUATION OF THE ENZYMATIC ACTIVITY AND LYOPHILIZATION STABILITY OF SURFACE DISPLAYED ESTERASE FROM *GEOBACILLUS STEAROTHERMOPHILUS*
Viktorija Kurpickaja, Arūnė Verbickaitė, Antanas Padaiga, Vilius Malūnavičius, Renata Gudiukaitė, Rasa Petraitytė-Burneikienė . . . 521

P4-54 CHARACTERIZATION OF A SYRINGIC AND VANILLIC ACID-INDUCIBLE GENE EXPRESSION SYSTEM IN SPHINGOBIUM SP. SYK-6
Miglė Loveikytė, Ernesta Augustiniene . . . 522

P4-55 AUXOTROPH-BASED SCREENING STRATEGIES FOR MODIFIED HETEROCYCLIC BASE METABOLISM
Augustė Kavaliauskaitė, Ieva Petkevičiūtė, Daiva Tauraitė, Jaunius Urbonavičius . . . 523

P4-56 TNPB: A POTENTIAL TOOL FOR GENOME-EDITING IN E. COLI
Justė Dautaraitė, Gytis Druteika, Tautvydas Karvelis . . . 524

P4-58 AUXIN AND CYTOKININ PROFILES IN BARLEY TWEAKY SPIKE (tw) MUTANTS REVEAL AN AUXIN-SPECIFIC HORMONE DISTURBANCE
Dominykas Laibakojis, Tautvydas Žalnierius, Jurga Jankauskienė, Vėjūnė Pukenytė, Raimondas Šiukšta, Simonas Balčiūnas, Sigita Jurkonienė . . . 525

P4-59 ULTRASOUN-INDUCED CHANGES IN THE ABSORPTION SPECTRA OF MAGNESIUM AND COPPER CHLOROPHYLLINS
Dita Valiulytė, Irina Buchovec . . . 526

P4-61 CREATING INNOVATIVE ORGANIC BIODEGRADABLE SUBSTRATES FOR SEED GERMINATION
Eglė Didžiulytė, Rasa Šlinkšienė . . . 527

P4-62 NOVEL POLYMER DOTS FOR FLUORESCENCE BIOIMAGING WITHIN THE SECOND NEAR-INFRARED WINDOW
Skaiste Talanovaite, Greta Tamoliunaite, Vilius Poderys, Simona Steponkiene, Yaw-Kuen Li, Tung-Kung Wu, Yang-Hsiang Chan, Vitalijus Karabanovas . . . 528

P4-63 INVESTIGATION OF ENERGY TRANSFER AND SINGLET OXYGEN GENERATION IN BLOOD PLASMA PROTEIN GOLD NANOCLUSTERS-CE6-UCNP COMPLEXES
Greta Tamoliunaite, Skaiste Talanovaite, Vilius Poderys, Vaidas Klimkevicius, Vitalijus Karabanovas . 529

P4-64 TIME-DEPENDENT STABILITY AND OPTICAL PROPERTIES OF RIBOFLAVIN AND MAGNESIUM CHLOROPHYLLIN MIXTURE IN SOLUTION
Urtė Mitrofanaitė, Irina Buchovec . . . 530

P4-65 THE EFFECT OF DIETARY SUBSTRATES ON THE GROWTH OF THE YELLOW MEALWORM (TENEBRIO MOLITOR L.)
Felicija Kvedaraitė, Gabrielė Bumbulytė-Žukevičienė 531

P4-66 INDIVIDUAL PHENOLIC COMPOUNDS COMPARISON OF BUCKWHEAT HONEY AND FLORAL SOURCE
Ernesta Zaksaitė, Mindaugas Liaudanskas, Vaidotas Žvikas, Sonata Trumbeckaitė 532

P4-68 DETERMINATION OF BETULINIC ACID CONTENT AND IN VITRO ANTIRADICAL ACTIVITY IN JAPANESE QUINCE (CHAENOMELES JAPONICA (THUNB.) LINL. EX SPACH) FRUIT SAMPLES
Kornelija Kondrotaitė, Mindaugas Liaudanskas, Rima Šedbarė, Jonas Viškelis, Pranas Viškelis, Valdimaras Janulis 533

P4-69 CHANGES IN ANTIOXIDANT PROPERTIES OF BEE-COLLECTED POLLEN DURING STORAGE
Yelyzaveta Lopatina, Vilma Kaškonienė, Audrius S. Maruška, Neringa Sutkevičienė 534

P4-70 EFFECTS OF CHRONIC PSYCHOLOGICAL STRESS ON FATTY ACID COMPOSITION IN RATS WITH TYPE 2 DIABETES MELLITUS
Justina Kežutytė, Justinas Baleišis, Romualdas Rudys, Inga Bikulčienė, Dovilė Karčiauskaitė 535

P4-71 MATERNAL HIGH-FAT DIET EFFECT ON THE OFFSPRINGS VOLATILOME COMPOUNDS
Patricija Čepauskytė, Gintarė Urbonaitė, Mantas Norkus, Toma Petrulionienė, Urtė Neniškytė 536

P4-72 EVALUATION OF ELECTROPORATION-INDUCED MYOCARDIAL LESION SIZE
Mantė Almanaitytė, Dominyka Adamonė, Ieva Lankutytė, Vilma Zigmantaitė, Jonas Jurevičius, Regina Mačianskienė 537

P4-73 HS-SPME/GC-MS-BASED CHARACTERISATION OF VOLATILE COMPOUNDS IN AEGOPODIUM PODAGRARIA L. PARTS AND EVALUATION OF THEIR ANTIMICROBIAL PROPERTIES
Ugnė Gabrytė, Rūta Mickienė, Audrius Sigitas Maruška 538

P4-74 INDUCTION OF APOPTOSIS AND PYROPTOSIS IN MACROPHAGES BY THE POLYSACCHARIDE CAPSULE OF ACINETOBACTER BAUMANNII
Joris Naujalis, Jūratė Skerniškytė 539

P4-75 BIOCIDAL POTENTIAL OF YEASTS FROM PASTURE ENVIRONMENTS AGAINST OTHER YEASTS AND BACTERIA
Deividas Paliovkinas, Živilė Strazdaitė-Žielienė, Elena Servienė 540

P4-76 HIDDEN DIVERSITY: SARCOCYSTIS PARASITES IN CATTLE (Bos taurus) RAISED IN LITHUANIA
Mingailė Stanionytė, Petras Prakas, Dalius Butkauskas, Donatas Šneideris, Naglis Gudiškis 541

P4-77 SPECIES DIVERSITY OF MESOSTIGMATID MITES FROM SMALL RODENTS IN SUBURBAN HABITATS
Violeta Šataitytė, Evelina Kaminskienė, Jana Radzijevskaja, Michal Stanko, Algimantas Paulauskas . . 542

P4-78 BEHIND THE MUSCLES: SARCOCYSTIS PARASITES IN HORSES FROM LITHUANIA
Naglis Gudiškis, Mingailė Stanionytė, Petras Prakas, Eglė Rudaitytė-Lukošienė, Dalius Butkauskas, Donatas Šneideris 543

P4-79 IMPROVING CELL INTACTNESS IN CRYOGENIC FLUORESCENCE SPECTROSCOPY MEASUREMENTS
Patricija Žemaitytė, Yaraslau Padrez, Claudia Büchel, Andrius Gelzinis, Lena Golubewa 544

P4-80 SELECTED TOOTH SAMPLE DEHYDRATION METHODOLOGY: LITERATURE REVIEW AND EXPERIMENTAL EXAMPLE
Robertas Virkėtis, Airida Elžbieta Žygytė, Artūr Harnik, Donatas Narbutis, Mangirdas Malinauskas, Irma Dumbrytė, Greta Merkininkaitė 545

P4-81 DETERMINANTS OF PHAGE SENSITIVITY TO THE OLOKUN ANTIPHAGE DEFENSE SYSTEM
Vincentas Raudys, Edvinas Jurgelaitis, Mindaugas Zaremba 546

P4-82 INHIBITION OF THE CRISPR-CAS SYSTEM BY AN ANTI-CRISPRPROTEIN
Darija Andrušaitytė, Tomas Šinkūnas 547

P4-83 INVESTIGATION OF THE ACTIVATION MECHANISM OF SPLITPAGO PROTEINS AND ASSOCIATED HEPN EFFECTORS IN E. COLI
Rokas Bružaitis, Edvardas Golovinas, Mindaugas Zaremba 548

P4-84 CHARACTERIZATION OF A NON-CANONICAL TYPE IV-A1 CRISPR-CAS SYSTEM
Gintarė Žvejytė, Rimvydė Čepaitė, Aistė Skorupskaitė, Patrick Pausch 549

P4-85 INFLUENCE OF BACTERIAL DEFENSE SYSTEM COMPONENTS ON CELL VIABILITY
Austėja Narkevičiūtė, Tomas Šinkūnas 550

P4-86 STUDY OF INTERACTIONS BETWEEN SHORT PROKARYOTIC ARGONAUTE AND HFQ PROTEIN
Jokūbas Šiaučiūnas, Edvinas Jurgelaitis, Evelina Zagorskaitė, Mindaugas Zaremba 551

P4-87 MONOCLONAL ANTIBODIES AGAINST STREPTOLYSIN O
Adrija Buturlakina, Indrė Kučinskaitė-Kodzė, Martynas Simanavičius 552

P4-88 CHARACTERIZATION OF THE EC2APEA ANTIVIRAL PROTEIN THROUGH PHAGE INFECTIONS AND TOXICITY ASSAYS
Ema Ežerskytė, Jonas Juozapaitis, Giedrius Sasnauskas 553

P4-89 IN VITRO CHARACTERIZATION OF THE MOKOSH TYPE 1 ANTI-PHAGE DEFENSE SYSTEM
Matas Račickas, Edvinas Jurgelaitis, Arūnas Šilanskas, Mindaugas Zaremba 554

P4-91 QCM-D/SE COMPARISON OF SB14 AND SB68 FC-FUSION NANOBODY IMMUNOCOMPLEX FORMATION WITH SARS-COV-2 VIRUS-LIKE PARTICLES
Mantvydas Usvaltas, Asta Lūčiunaitė, Vincentas Mačiulis, Ieva Plikusienė 555

P4-92 METABOLIC CHANGES IN VANDETANIB AND ROSMANTUZUMAB-TREATED HUMAN ENDOMETRIAL AND ENDOMETRIOTIC STROMAL CELLS
Žemyna Kazlauskytė, Rūta Navakauskienė, Aistė Zentelytė-Vilkė 556

P4-93 REAL-TIME INTERACTION STUDY OF COVALENTLY IMMOBILIZED SARS-COV-2 SPIKE PROTEIN AND SPECIFIC NANOBODIES
Smiltė Drobnytė, Mantvydas Usvaltas, Vincentas Maciulis, Asta Luciunaite, Ieva Plikusiene 557

P4-94 PRODUCTION OF VB _ ECOS _ NBD2 BACTERIOPHAGE-ORIGINATED POLYTUBES USING DIFFERENT YEAST EXPRESSION HOSTS
Paulina Kočiūnaitė, Laima Čepulytė, Rasa Petraitytė-Burneikienė 558

P4-95 PROTECTIVE PROPERTIES OF PLANT-DERIVED NANOVESICLES AGAINST VIRAL INFLAMMATION BY MODULATING MITOCHONDRIAL RESPIRATION
Vaiva Kurlytė, Emilija Mikalauskienė, Zbignev Balion, Aistė Jekabsone 559

P4-96 CHARACTERIZATION OF A NOVEL BACTERIAL ANTI-PHAGE DEFENSE SYSTEM
Miglė Paulikaitė, Radvilas Bendorys, Patrick Pausch 560

P4-97 EEG-BASED NEURAL VARIABILITY AND INHIBITORY CONTROL ACROSS THE MENSTRUAL CYCLE: A HORMONE-VALIDATED LONGITUDINAL STUDY
Gabrielė Kukytė, Monika Palaimaitė, Ingrida Zelionkaitė, Rimantė Gaižauskaitė, Lauryna Filatovaitė-Vyčienė, Ramunė Grikšienė 561

P4-99 ANALYSIS OF IN VITRO GENOTOXICITY OF VARIOUS SIZE AND SHAPE GOLD NANOPARTICLES IN HUMAN HEPATOMA CELL LINE (HepG2)
Viltė Slančiauskaitė, Emilija Striogaitė, Juozas Rimantas Lazutka 562

P4-100 MODULATION OF INTERCELLULAR COMMUNICATION THROUGH CARDIOVASCULAR CONNEXIN - 43 GAP JUNCTION CHANNELS BY ANESTHETIC PROPOFOL
Orestas Makniusevičius, Tadas Kraujalis, Mindaugas Šnipas, Lina Kraujalienė 563

P4-101 EXPLORING SPATIAL VARIATION OF THE URBAN HEAT ISLAND IN RELATION TO URBAN STRUCTURE USING MACHINE LEARNING
Mehri Davtalab, Steigvilė Byčenkienė 564

P4-102 FOOT STRUCTURE ASSESSMENT AND MANAGEMENT OF FLAT FEET IN CHILDREN
Dominykas Ševelis, Raimonda Bružienė, Gintarė Petrošienė, Birutė Sinkutė 565

P4-103 INNOVATIVE APPROACHES TO THE DEVELOPMENT OF NEXT-GENERATION ORTHOPEDIC DEVICES
Minvydas Gražulevičius, Zigmas Bolzanas, Vaida Keršienė, Birutė Sinkutė 566

P4-104 EFFECTIVENESS OF ORTHOPEDIC TEXTILE COMPRESSION BRACES IN SCAR TREATMENT
Birutė Sinkutė, Vykinta Vaitiekūnaitė, Danutė Maurušaitienė 567

P4-105 IN SILICO PREDICTION AND VALIDATION OF TnpB AND Cas12a OFF-TARGETS IN THE HUMAN GENOME
Lukrecija Petrikaitė, Marius Baltramonaitis, Tautvydas Karvelis 568

P4-106 PARAGEOBACILLUS THERMOGLUCOSIDASIUS AS A RECOMBINANT HOST: OPTIMIZATION STRATEGIES
Elina Guogytė, Rūta Kananavičiūtė 569

P4-108 EFFECTS OF GRNA STRUCTURE ON ASCAS12A ACTIVITY IN E. COLI
Gabija Magelinskaite, Jonas Kubilius, John P. Cooper, Stephen K. Jones Jr. 570

P4-109 DEVELOPMENT OF CELL-BASED SCREENING SYSTEM FOR TnpB GENOME EDITING TOOLS
Bartė Žiliukaitė, Marius Baltramonaitis, Tautvydas Karvelis 571

P4-110 PSILOCYBIN INDUCES SYNAPTIC REMODELING BY MODULATING MICROGLIA
Milda Markutė, Ieva Šiugždaitė, Louise Ellen Schuberth, Maxime Veleanu, Stefan Vestring, Urtė Neniškytė 572

P4-111 IN VIVO STUDY OF A NOVEL THOERIS EFFECTOR
Ignė Jačunskytė, Deividas Vilutis, Arūnas Šilanskas, Giedrė Tamulaitienė 573

P4-112 DESIGN AND CHARACTERIZATION OF A SYRINGE PUMP FOR MICROFLUIDICS
Mykolas Peleckis 574

P4-113 MICROFLUIDIC FABRICATION OF ALGINATE MICRODROPLETS FOR PHOTODYNAMIC ANTIMICROBIAL THERAPY
Laura Milaknytė, Adei Abouhagger, Dr. Wanessa De Cassia Martins Antunes De Melo 575

P4-114 EVALUATION OF MICROBIAL CONTAMINATION IN USED MAKEUP FOUNDATION PRODUCTS AND ASSOCIATED APPLICATORS
Saulė Norkutė, Ugnė Januškaitė, Žaneta Maželienė, Asta Aleksandravičienė, Giedrė Jarienė 576

P4-115 THE ABATEMENT OF MICROBIAL AIR POLLUTION USING IONIZATION TECHNOLOGIES
Patricija Kirvelaitytė, Justinas Masionis, Martynas Tichonovas, Dainius Martuzevičius 577

P4-116 ADVANCES IN ENGINEERING OF CHEMOLITHOAUTOTROPHIC BACTERIA FOR CARBON DIOXIDE FIXATION
Tasawar Abbas, Naglis Malys 578

Invited Speakers

Keynote Lectures by World-Renowned Scientists

STATE OF THE UNIVERSE

Brian Schmidt[1]

[1] Australian National University (ANU), Canberra, Australia
Brian.Schmidt@anu.edu.au

Professor Schmidt's lecture "State of the Universe" will offer a comprehensive and accessible overview of current cosmological knowledge, tracing the Universe's development from the Big Bang through its subsequent evolution. The presentation will address fundamental properties of the Universe, including its size, age, density, shape, and composition, as well as insight from observational data concerning its history and possible future. The lecture will differentiate between established scientific findings and major unresolved questions in contemporary cosmology. This event is free of charge and open for anyone interested to attend – professionals, students and the general public.

About the Invited Speaker

The distinguished professor of Astronomy at the Australian National University (ANU) B. Schmidt has made substantial contributions to modern cosmology through pioneering research. Awarded the 2011 Nobel Prize in Physics for the discovery of the Universe's accelerated expansion, he provided the first robust evidence for dark energy. His research focuses on observational cosmology, supernovae, and large-scale astronomical surveys to clarify the composition, structure, and evolution of the Universe. He has also held significant academic and scientific leadership positions, including senior roles within the International Astronomical Union, where he was appointed president elect.



THE CHEOPS MISSION: A UNIQUE INTERFACE BETWEEN DISCOVERY AND CHARACTERISATION OF EXOPLANETS

Willy Benz[1]

[1]Physics Institute, University of Bern, Switzerland
willy.benz@unibe.ch

The Characterising ExOPlanet Satellite (CHEOPS) was selected as the first Small Mission (S-Mission) in ESA's Science Programme in 2012, and was successfully launched on time and on budget on 18 December 2020 on a Soyuz-Fregat rocket from Kourou in French Guiana. CHEOPS is the first mission dedicated to searching for exoplanet transits using ultra-high-precision photometry on bright stars that are already known to host planets. Monitoring planets with high-precision photometry improves the measurement of their properties, such as radii and masses (via TTVs), and enables the definition of precise transit ephemerides, particularly for small bodies. This often leads to the refinement of the overall architecture of the systems (e.g. the discovery of new planets). Similarly, measuring occultations and phase curves with a precision of a few parts per million has opened up new avenues in the study of hot planets' atmospheres. Due to its agility and ability to observe a large portion of the sky, CHEOPS uniquely interfaces the discovery of exoplanets (e.g. by the TESS satellite) with their subsequent spectroscopic characterisation by large space-based (e.g. JWST & ARIEL) or ground-based (e.g. VLT & ELT) facilities.

About the Invited Speaker

Professor Willy Benz earned his PhD in astrophysics from the University of Geneva in 1984 and held research and teaching positions in the US (Los Alamos, Harvard, University of Arizona) and Switzerland. Since 1997 he has been a professor of physics and astrophysics at the University of Bern, directing its Physics Institute since 2002 and leading NCCR PlanetS. His commitment to teaching and research was recognized in 1988 with the Milton Fund Award, followed in 1989 by the Thomas Temple Hoopes prize for Excellence in Undergraduate Teaching. He has served on numerous international advisory bodies (ESO, ESA, EKWF) and was a Swiss Delegate to the ESO Council. Benz co-investigated HARPS and contributed to instruments like ESPRESSO, NIRPS, and HIRES for exoplanet research. His career focuses on planetary systems within and beyond the Solar System.



QUANTUM COMPUTATION AND QUANTUM SIMULATION WITH STRINGS OF TRAPPED CA+ IONS

Rainer Blatt[1]

[1] Institute for Experimental Physics, University of Innsbruck, Austria
Rainer.Blatt@uibk.ac.at

This talk reviews the advanced capabilities of the trapped-ion quantum computer at Innsbruck [1]. We provide an overview of the quantum toolbox available and discuss the scalability of our approach. We utilize the quantum toolbox to optimize parameters for quantum metrology [2] and showcase quantum-enhanced sensing of an optical transition through collective quantum correlations [3]. To shield quantum computers from noise, we redundantly encode logical quantum information across multiple qubits using error-correcting codes, and demonstrate a fault-tolerant universal set of gates on two logical qubits in the ion-trap quantum computer [4,5]. Employing several states per ion, we simulate a two-dimensional lattice gauge theory on a qudit quantum computer [6]. For scalability, we propose and investigate an architecture (quantum spring arrays) with micro-structured chip-traps [7].

About the Invited Speaker

German-Austrian experimental physicist Professor dr. Rainer Blatt is well-known for his groundbreaking work in quantum information science and quantum optics. Blatt's research centers on using trapped ions to explore and harness the principles of quantum mechanics.His team at the University of Innsbruck made significant strides in quantum computing, including the first "quantum byte" and the first quantum teleportation between atoms. Precision spectroscopy, quantum metrology, and scalable quantum processors have all benefited from Blatt's work with trapped ions. He is a member of several prestigious scientific academies throughout the world and has won various international awards, such as the Herbert Walther Prize, the Micius Quantum Prize, and the Austrian Cross of Honour for Science and Art.



[1] I. Pogorelov *et al.*, *PRX Quantum* 2, 020343 (2021).
[2] C. D. Marciniak *et al.*, *Nature* 603, 604 (2022).
[3] J. Franke *et al.*, *Nature* 621, 740 (2023).
[4] L. Postler *et al.*, *Nature* 605, 675 (2022).
[5] L. Postler *et al.*, *PRX Quantum* 5, 030326 (2024).
[6] M. Meth *et al.*, *Nature Physics* 21, 570 (2025).
[7] M. Valentini *et al.*, *Physical Review X* 15, 041023 (2025).

CATALYSTS OF CHANGE: ADVANCED MATERIALS STEERING HEALTH AND ENERGY TRANSITION

Sanjay Mathur[1]

[1] Director, Institute of Inorganic and Materials Chemistry, University of Cologne, Germany
sanjay.mathur@uni-koeln.de

Advanced materials are driving innovation across all fields of technology, ranging from construction and mechanical engineering, automotive and electromobility, to medical technology, energy storage and conversion technologies, and microelectronics. Given their technological impact, functional materials represent an essential segment of industrial technologies with significant value creation potential for both established markets and emerging technologies. Especially in the context of sustainable production techniques, substitution of critical raw materials, and energy- and resource-efficient manufacturing, tailored surfaces and interfaces are gaining increasing importance in the future. In this context, chemical processing of nanostructured ceramics in tuning the functional and interfacial properties for better charge transport, higher corrosion protection and enhanced performance. The examples will include the role of functionalized inorganic surfaces in electrolysers for hydrogen production, and advances in photon-harvesting technologies for perovskite-based photovoltaics. Moreover, chemically functionalized SiO2 nanoparticles acting as efficient drug-carriers to transport higher amounts of therapeutic payloads to diseased sites will be presented. Hollow nanocarriers can reduce undesired off-site effects and enable theranostic and thera-regenerative approaches. This talk will emphasize the role of new materials in enabling energy and health transitions.

About the Invited Speaker

Sanjay Mathur is Director of the Institute of Inorganic Chemistry at the University of Cologne and a leading researcher in nanomaterials, ceramics, and inorganic chemistry.Professor Mathur's research focuses on chemical design concepts for nanostructured ceramics and composites, with applications in energy technologies, biomedicine, sensors, protective coatings, and functional surfaces. His group has developed single-source precursor libraries for controlled synthesis of nanostructured materials with tailor-made properties, advancing technologies in drug delivery, implant integration, gas and moisture detection, catalytic supports, and transparent conductive oxides. He has authored over 500 publications, holds multiple patents, and his work has wide applications in energy, biomedicine, and advanced materials. He is Editor-in-Chief of the Journal of Electroceramics and Fellow of several.



NEW INSIGHTS INTO THE DRUG TREATMENT OF OBESITY

Lora Heisler[1]

[1]Rowett Institute, University of Aberdeen, Scotland
lora.heisler@abdn.ac.uk

Obesity represents a major global health and economic challenge, and glucagon-like peptide-1 receptor (GLP-1R) agonists such as semaglutide (Wegovy) have emerged as highly effective therapeutics through their actions to reduce food intake. Although GLP-1R agonists clearly induce weight loss, the mechanisms through which they alter feeding behaviour and body composition remain incompletely understood. Here, we investigated the impact of short- and longer-term semaglutide treatment, as well as drug withdrawal, on food choice, body composition, and underlying neurocircuit mechanisms in dietary-induced obese mice.

As expected, semaglutide administration significantly reduced body weight, driven predominantly by decreases in fat mass and, to a lesser extent, lean mass. Correspondingly, semaglutide lowered white and brown adipose tissue depots and reduced liver weight. Bone mineral density and bone mineral content were unchanged, while reductions in individual muscle weights did not translate into impaired muscle function. These findings indicate that semaglutide produces rapid weight loss associated with tissue-specific effects.

In studies assessing drug withdrawal, semaglutide cessation resulted in rapid rebound weight gain, with fat mass exceeding pre-treatment levels and lean mass showing limited recovery. Conversely, less frequent semaglutide dosing over two months maintained robust fat-mass reductions while preventing lean-mass loss, suggesting dose-pattern optimisation may mitigate adverse body-composition effects.

To identify neural substrates engaged by GLP-1R agonists, we examined brainstem circuits and found that a subset of dorsal vagal complex (DVC) GLP-1R-expressing neurons is GABAergic. Functional manipulation of GABA DVC → hypothalamic arcuate nucleus (ARC) projections revealed their potent bidirectional control of food intake. Moreover, chemogenetic inhibition of GABA DVC neurons partially attenuated liraglutide- and semaglutide-induced hypophagia, demonstrating that this circuit contributes to GLP-1R–mediated feeding suppression. Together, these findings reveal integrated metabolic and neurocircuit mechanisms through which GLP-1R agonists regulate energy balance and highlight GABA DVC pathways as a contributor to the therapeutic benefit.

About the Invited Speaker

Professor Lora Heisler is the Chair in Human Nutrition and Director of Research at the Rowett Institute, University of Aberdeen, Scotland, where she leads the Obesity and Food Choice research theme. Her research focuses on the brain circuits regulating appetite, body weight, physical activity, and glucose homeostasis, with the goal of identifying new therapeutic targets for obesity and Type 2 diabetes. She has made seminal contributions to the neurobiology of energy balance, including discovery on how brain serotonin signaling can be harnessed for metabolic disease treatment. Professor Heisler's work bridges fundamental neuroscience and clinically relevant applications and has been recognized with major international awards, as well as election to the Royal Society of Edinburgh.



SEMICONDUCTOR QUANTUM WALK COMBS FROM THE NEAR-INFRARED TO THE TERAHERTZ

Jérôme Faist[1]

[1] IQE, ETH Zürich, Switzerland
jerome.faist@phys.ethz.ch

The random walk is a fundamental concept in mathematics and physics that describes a walker taking random steps in a discretized space. While the spread of a classical random walker is characterized by a square root standard deviation after N steps it is surpassed by its quantum counterpart, in which the standard deviation of the position scales linearly with the number of steps. We recently showed that the concept of quantum walk[1] can be applied to the problem of generating an optical frequency comb, an array of single frequencies locked into equidistance by a non-linear optical process. These optical combs have proven to be of great use for a number of applications such as optical synthesis, metrology and sensing. In our case, the quantum walk occurs in the synthetic dimension formed by the modes of a resonator where a phase modulation induced, for instance, through the electro-optical effect or the laser's pump can introduce coupling in the chain, giving rise to continuous-time quantum walk dynamics.

This system can be analogously mapped to a quantum harmonic oscillator[2]. We demonstrate both theoretically and experimentally that the full potential of the synthetic frequency lattice can be unlocked by employing ultrafast saturable gain. The giant nonlinearity of such gain locks the resonator modes and effectively counteracts the dispersion. This is in great contrast with the situation of slow gain where, as was shown many years ago, only the fundamental mode is the Gaussian-shaped fundamental mode of the parabolic potential[2].

Laser based on semiconductors active regions are, in general, excellent candidates to realize quantum walk combs, as they exhibit very naturally both the phase modulation as well as the fast gain saturation which are both key for the operation of the device. It is also true in interband devices despite the relatively long spontaneous emission time[3]. The coupling between the real and imaginary part of the gain, responsible for the linewidth enhancement factor, will ensure that a modulation of the gain will also generate the phase modulation necessary for the proliferation of the modes.

We report the operation of such combs across the electromagnetic spectrum from the Terahertz to the near-infrared, demonstrating the universal character of the quantum walk comb in semiconductor lasers.

Quantum walk combs are equally relevant for applications in sensing or telecommunication as well as a platform for emulation of quench dynamics, taking advantage of the liquid-like properties of light in a fast gain medium[4]. We show also that, because their spectral envelop can be controlled electrically, quantum walk combs enable new avenues into broadband spectroscopy.

[1] I. Heckelmann, M. Bertrand, A. Dikopoltsev, M. Beck, G. Scalari, and J. Faist, "Quantum walk comb in a fast gain laser," *Science*, vol. 382, no. 6669, pp. 434–438, Oct. 2023, doi: 10.1126/science.adj3858.

[2] H. Haus, "A theory of forced mode locking," *IEEE Journal of Quantum Electronics*, vol. 11, no. 7, pp. 323–330, Jul. 1975, doi: 10.1109/JQE.1975.1068636.

[3] B. Marzban, L. Miller, A. Dikopoltsev, M. Bertrand, G. Scalari, and J. Faist, "A Quantum Walk Comb Source at Telecommunication Wavelengths," Nov. 13, 2024, *arXiv*: arXiv:2411.08280. doi: 10.48550/arXiv.2411.08280.

[4] A. Dikopoltsev *et al.*, "Collective quench dynamics of active photonic lattices in synthetic dimensions," *Nat. Phys.*, pp. 1–7, May 2025, doi: 10.1038/s41567-025-02880-2.

About the Invited Speaker

Jérôme Faist is a Swiss physicist and professor at the Institute of Quantum Electronics at ETH Zürich, where he also heads the FIRST Center for Micro- and Nanoscience. He is a pioneer of the quantum cascade laser (QCL), a fundamentally new semiconductor light source operating from mid-infrared to the terahertz range, developed during his work at Bell Laboratories. His research has been instrumental in advancing intersubband physics, infrared and terahertz lasers, and spectroscopic technologies. At ETH Zürich, his group focuses on high-performance QCLs, frequency combs, and light-matter interaction, including ultra-strong coupling and vacuum fluctuations. His contributions have been recognized with major awards, including the National Swiss Latsis Prize.



TRACING ELECTRON DYNAMICS IN MOLECULES: NOVEL APPROACHES FOR ATTOSECOND CHEMISTRY

Francesca Calegari[1]

[1]Center for Free-Electron Laser Science,University of Hamburg, Germany
francesca.calegari@desy.de

The Nobel Prize in Physics awarded in 2023 underscored the importance of attosecond light sources, which now grant us access into the electron time scale within matter. This advancement has paved the way for the emergence of attochemistry, a novel field aiming at manipulating chemical reactivity by steering the electron dynamics in molecules.

In this presentation, I will first give an overview of our latest achievements in producing remarkably short light pulses across both ultraviolet (UV) and soft X-ray spectral ranges. Additionally, I will highlight a variety of applications for these ultrashort light transients, such as the real-time observation of ultrafast charge migration and dissociative dynamics in photoexcited molecules. A key focus will be on our novel approach to instigating well-controlled charge migration in chiral neutral molecules, which represents a significant step toward achieving charge-directed reactivity—the ultimate objective of attochemistry.

About the Invited Speaker

Francesca Calegari is an Italian physicist renowned for pioneering advances in attosecond science and ultrafast spectroscopy. She leads the Attosecond Science Division at DESY's Center for Free-Electron Laser Science and is a Professor of Physics at the University of Hamburg. Her work has been recognized with major distinctions, including the ICO Prize, the Ernst Abbe Medal, and Fellowship of Optica. Calegari's research centers on real-time tracking and control of electron dynamics in molecules, biomaterials, and nanostructures. By developing cutting-edge table-top light sources and combining attosecond spectroscopy with X-ray free-electron lasers, she advances fundamental understanding of ultrafast processes in chemistry and biology.



ANTIBIOTIC RESISTANCE IN THE WILD: WHEN A CLINICAL PROBLEM BECOMES EVERYONE'S PROBLEM

Célia Manaia[1]

[1]Centre for Biotechnology and Fine Chemistry,Catholic University of Portugal, Portugal
cmanaia@ucp.pt

Bacterial antimicrobial resistance (bAMR) is mostly reported in hospital and clinical settings. In 2021, it was estimated that 4·71 million deaths were directly or indirectly associated with bacterial bAMR [1]. However, bAMR is not confined to clinical settings - it originates outside these settings, enters them, and can subsequently spread to any environment where it can persist and thrive. This boundary-free vision of the bAMR distribution is aligned with the One Health concept, a multisectoral and holistic approach to promote human health in harmony with the animal health and welfare and environmental quality and protection.

The One Health approach is extraordinarily wise and of potential high impact, but its implementation to control bAMR is still suboptimal due to technical and organizational constraints. In particular, the role of the environment as a habitat and pathway for bAMR spread and transmission through trophic chains and interface domains still requires significant improvement. In parallel, environmental bAMR is only one part of the massive load of contaminants that reach soils, water bodies, and the air. Climate events, mass migrations, refugee crises, and war scenarios are all potential drivers for bAMR spread.

Actions to combat bAMR have been in place for decades and have had positive impacts; however, mitigation efforts appear insufficient to contain what can be considered a dangerous silent pandemic. Nevertheless, technical and scientific developments are opening new opportunities. In this sense, while microbiological approaches aimed at tackling unwanted microorganisms have mainly focused on their selective elimination, it may be high time to change this paradigm. A strong argument is that the best entities to fight unwanted microorganisms are the beneficial ones, those that can create barriers to invasion and antagonize cheaters and exploiters, thereby stabilizing the system.

About the Invited Speaker

Célia Manaia is Associate Professor of Microbiology and Genetics at the Universidade Católica Portuguesa, where she also serves as Vice-President for Research and Internationalization. She leads research on bacterial ecology and antibiotic resistance in environmental settings, has collaborated with international organizations such as WHO and FAO, and holds leadership and editorial roles in major microbiology societies and journals.



[1] GBD 2021 Antimicrobial Resistance Collaborators, *Lancet* 404, 1199 (2024).

ORAL SESSION 1

Astrophysics and Theoretical Physics

Chair: Dr. M. Maskoliūnas

THE CHRONICLES OF THE MILKY WAY: THE CARBON, THE NITROGEN, AND THE STELLAR AGES

Bruno Ćurjurić[1], Arnas Drazdauskas[1], Gražina Tautvaišiene[1], Angela Bragaglia[2], Natalia Alvarez-Baena[3,4], Valentina D'Orazi[3,4], Marina Dal Ponte[5]

[1]Vilnius University, Faculty of Physics, Institute of Theoretical Physics and Astronomy, Vilnius, Lithuania
[2]INAF - Osservatorio di Astrofisica e Scienza dello Spazio, Bologna, Italy
[3]University of Rome Tor Vergata, Department of Physics, Rome, Italy
[4]INAF - Osservatorio Astronomico di Roma, Rome,Italy
[5]INAF - Ossevatorio Astronomico di Padova, Padova, Italy
bruno.curjuric@ff.stud.vu.lt

Reliable stellar age estimates are essential across many areas of astrophysics, as they allow us to connect observed stellar properties with the evolutionary history of stars, galaxies, and their chemical enrichment. One of the promising methods for estimating stellar ages is through chemical clocks, which use abundance ratios of elements that evolve differently over time—such as [C/N] in giants [1] or [Y/Mg] in both giants and solar-type stars [2] — to provide independent age constraints. In evolved giants, the [C/N] ratio changes during the first dredge-up and subsequent extra mixing on the red giant branch in a way that depends on stellar mass [3], making it a useful indicator of mass and, indirectly, of stellar age.

Our objective is to significantly expand the pool of open clusters with homogeneous carbon, nitrogen, and oxygen abundance measurements in 89 evolved low- and intermediate-mass giants in 29 open clusters, advancing the use of chemical clocks in stellar age determinations.

High-resolution spectra of the stars were obtained for the Stellar Population Astrophysics programme (SPA) [4] with the Italian Telescopio Nazionale Galileo (TNG) and analysed using a model-atmosphere approach. Stellar properties were determined, and synthetic spectra were generated to match the observations. Carbon and nitrogen abundances were derived from molecular bands of C_2 and CN, while oxygen abundances were obtained from an atomic oxygen line. The stars were then classified by their evolutionary stage, allowing us to investigate how internal mixing processes alter their surface chemical composition over time. These results were used to study how the [C/N] ratio changes with age for stars at different evolutionary stages, providing an independent way to estimate stellar ages.

Our analysis indicate that precise age dating requires separate age calibrations of [C/N] ratios for the first-ascent giants of the lower part of red giant branch (RGB) and for the red clump (RC) stars (Fig. 1) to account for the additional carbon and nitrogen abundance alterations during the post-RGB luminosity bump evolution.

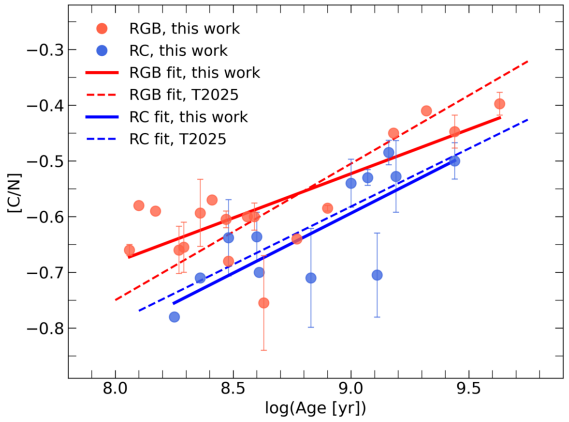


Fig. 1. [C/N] versus age for the RGB (red) and RC stars (blue). The dots represent the averaged [C/N] values and the scatter per cluster of this work and the obtained relations with the age (continuous lines). For a comparison, the corresponding relations obtained in [1], determined using the same method of analysis, are shown by dashed lines and corresponding colours.

Acknowledgements

A.D., G.T. acknowledge funding from the Research Council of Lithuania (LMTLT, grant No. S-MIP-23-24).

Keywords: Galactic chemical evolution, open clusters, stellar evolution and nucleosynthesis, stellar ages

[1] G. Tautvaišienė et al., "Carbon and nitrogen as indicators of stellar evolution and age," Astronomy and Astrophysics, vol. 703, p. A4, Oct. 2025, doi: 10.1051/0004-6361/202555685.
[2] G. Tautvaišienė et al., "Abundances of neutron-capture elements in thin- and thick-disc stars in the solar neighbourhood," Astronomy and Astrophysics, vol. 649, p. A126, Mar. 2021, doi: 10.1051/0004-6361/202039979.
[3] N. Lagarde, A. C. Robin, C. Reylé, and G. Nasello, "Population synthesis to constrain Galactic and stellar physics," Astronomy and Astrophysics, vol. 601, p. A27, Feb. 2017, doi: 10.1051/0004-6361/201630253.
[4] M. D. Ponte et al., "Stellar Population Astrophysics (SPA) with the TNG," Astronomy and Astrophysics, vol. 701, p. A289, Aug. 2025, doi: 10.1051/0004-6361/202554258.

TRACING INTERNAL MIXING THROUGH LITHIUM AND CNO ABUNDANCES IN RS CVN STARS

B. Bale[1], G. Tautvaisiene[1], R. Minkeviciute[1], A. Drazdauskas[1], S. Mikolaitis[1], E. Stonkute[1], M. Ambrosch[1]

[1]Vilnius University, Faculty of Physics, Institute of Theoretical Physics and Astronomy, Saulėtekio av. 3, 10257, Vilnius, Lithuania
barkha.bale@ff.vu.lt

Lithium (Li), together with the surface abundances of carbon, nitrogen, and oxygen (CNO), is considered a sensitive diagnostic of stellar evolution and internal mixing processes. In single red giant stars, the evolution of these abundances is generally well reproduced by standard stellar evolution models after the first dredge-up has occurred. In contrast, RS CVn-type binaries are recognized as a distinct class of close, chromospherically active systems characterized by rapid rotation and strong magnetic activity, and chemical abundance patterns that depart from classical evolutionary predictions are frequently exhibited.

In this study, Li and CNO abundances, as well as the $^{12}C/^{13}C$ and C/N ratios, are investigated in a sample of 33 RS CVn stars observed with the 1.65,m Moletai Astronomical Observatory telescope using the VUES spectrograph. These data are complemented by archival high-resolution spectra of 13 additional RS CVn stars obtained in previous analyses. Chemical abundances are determined through spectral synthesis, and stellar masses are estimated using the UniDAM tool.

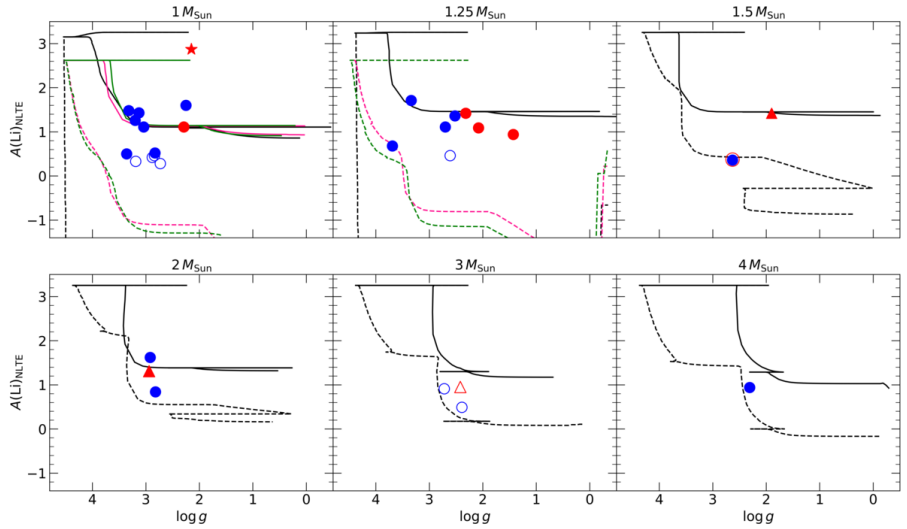


Fig. 1. Comparison between observed lithium abundances in RS CVn stars and theoretical model predictions including standard first dredge-up and additional mixing processes.

It is found that approximately half of the low-mass RS CVn giants exhibit lithium abundances consistent with predictions for the first dredge-up, whereas significantly enhanced Li depletion is observed in the remaining stars as seen in Figure 1, indicating that additional mixing processes, most likely thermohaline mixing, are operating. In intermediate-mass RS CVn stars, lithium abundances are found to be systematically lower than those predicted by standard stellar evolution models, with rotation-induced mixing considered the most plausible explanation. Overall, the lithium evolution observed in RS CVn systems is broadly consistent with the declining trend seen in normal red giants, although an earlier onset and increased efficiency of extra mixing processes are suggested.

Carbon isotopic ratios provide further support for this interpretation. Low $^{12}C/^{13}C$ ratios are exhibited by two stars, ι Gem and HD 179094, despite their location below the red giant branch luminosity bump, implying that extra mixing may be initiated earlier in magnetically active stars than in inactive counterparts. In contrast, unusually high C/N and $^{12}C/^{13}C$ ratios are retained by the Li-rich giant V* OP And, and the physical mechanism responsible for its lithium enrichment remains unresolved.

Acknowledgements
We acknowledge funding from the Research Council of Lithuania (LMTLT, grant No. S-MIP-23-24)

Keywords: stars: abundances – stars: evolution – stars: magnetic field

PROBING NEUTRON-CAPTURE ELEMENTS IN PLANET-HOST STARS THROUGH HIGH RESOLUTION SPECTROSCOPY

Ashutosh Sharma[1], Edita Stonkutė[1], Arnas Drazdauskas[1], Renata Minkevičiutė[1], Šarūnas Mikolaitis[1], Gražina Tautvaišienė[1], Ugne Jonauskaitė[1]

[1]Vilnius University, Faculty of Physics, Institute of Theoretical Physics and Astronomy, Vilnius, Lithuania
ashutosh.sharma@ff.vu.lt

The discovery of thousands of exoplanets in recent years has fundamentally revolutionized our understanding of planet formation and their evolution. Thanks to space missions like Kepler & Transiting Exoplanet Survey Satellite, and ground-based telescopes, more than 6 000 exoplanets have been confirmed so far. Understanding the chemical composition of stars hosting exoplanets is crucial for understanding the formation and evolution of planetary systems. High-resolution spectroscopy offers a powerful tool to probe the elemental abundances in these stars, shedding light on the conditions under which planets form and evolve.

In this talk, I present results from a homogeneous, high-resolution spectroscopic analysis of a set of neutron-capture element abundances in a sample of 160 F-, G-, and K-type stars hosting confirmed planets. The targets and planetary parameters were chosen from the confirmed exoplanet list available at the NASA Exoplanet Archive. Observations were carried out with the 1.65-m telescope installed at Molėtai Astronomical Observatory of Vilnius University in Molėtai, Lithuania. The telescope is equipped with a high-resolution Vilnius University Echelle Spectrograph.

The analysis is based on differential line-by-line spectrum synthesis using MARCS model atmospheres, with careful treatment of hyperfine splitting and non-local thermodynamic equilibrium effects for key species. We find that most elemental abundance ratios in planet-hosting stars follow Galactic chemical evolution trends; however, statistically significant overabundances of Zr, La, and Ce are detected in stars with planets when compared to chemically similar non-hosts at a given [Fe/H] (see Fig.1).

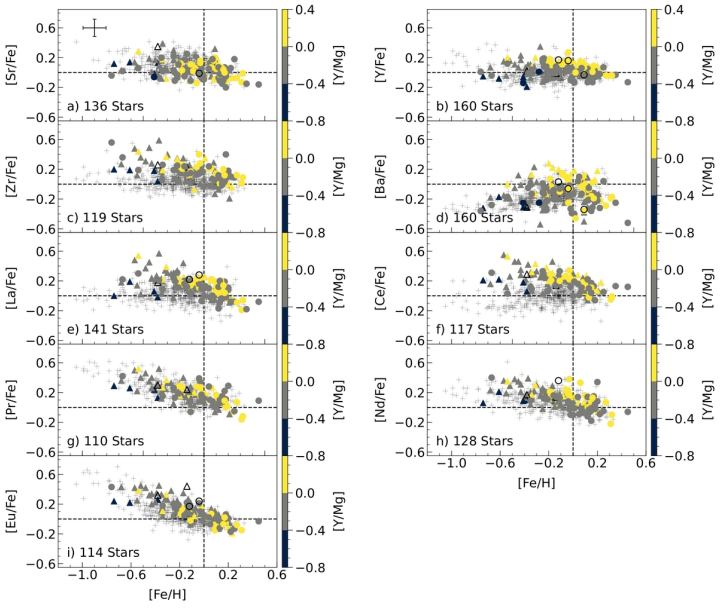


Fig. 1. Abundances of neutron-capture elements [El/Fe] as functions of metallicity [Fe/H] for target stars, colour-coded according to their [Y/Mg] ratio.

We further explore the connection between stellar chemistry and planetary properties. Several neutron-capture elements exhibit positive correlations with planetary mass, whereas Sr, Y, and Ba show insignificant correlations across all sub-samples. Condensation-temperature trends indicate a systematic enrichment of refractory material in planet-hosting stars. Multi-planet systems are found preferentially around metal-rich stars, and older systems tend to show flatter or negative abundance-condensation temperature slopes, hinting at evolutionary effects in planetary architectures.

Together, these results provide new observational constraints on the role of heavy elements in planet formation and highlight the importance of homogeneous abundance analyses in disentangling chemical evolution from genuine star-planet connections. The findings have direct relevance for current and upcoming exoplanet missions and for models linking stellar nucleosynthesis to planetary system diversity.

Keywords: High resolution spectroscopy; Chemical abundances; Planet-harbouring stars; Exoplanets.

FROM SIMULATION TO OBSERVATION: TESTING COMPATIBILITY OF AGN OUTFLOW RATE ESTIMATES

Milda Valytė[1,2], Kastytis Zubovas[1,2]

[1]Center for Physical Sciences and Technology, Fundamental Research division, Vilnius
[2]Vilnius University, Institute of Theoretical Physics and Astronomy, Vilnius
milda.valyte@ftmc.lt

Active galactic nuclei (AGN) can launch powerful galactic outflows that reshape the interstellar medium and regulate star formation. However, comparing outflows in simulations and observations is difficult because key derived quantities (most notably the mass outflow rate $\dot{M}$) depend strongly on how outflowing gas is defined and how $\dot{M}$ is computed [1]. This can change inferred scaling relations and make physical interpretation unclear.

The aim of this project is to test how different outflow definitions and $\dot{M}$ calculation methods affect the relations between outflow properties and galaxy/AGN parameters, and to determine which trends remain stable across methods.

High-resolution hydrodynamical IllustrisTNG50 simulations [2] are used as the main simulation data set, and idealized GADGET-3 simulations [3] are used as controlled test cases to diagnose systematic effects. Outflowing gas is selected using kinematic criteria refined by thermodynamic phase cuts to reduce contamination from non-outflowing material. Multiple $\dot{M}$ estimators are then evaluated: Eulerian shell-based fluxes, Lagrangian crossing methods and projection-based observational analogues, while aperture, velocity threshold, time sampling and line of sight are varied. It is found that $\dot{M}$ and the resulting scaling relations with $M_\star$, SFR and $L_{\rm AGN}$ can vary strongly depending on the chosen outflow definition and measurement method, even for the same system. This motivates clearer, more consistent reporting of $\dot{M}$ calculation methods.

Overall, a more consistent basis for comparing simulations and observations is provided, and the analysis choices that most strongly affect $\dot{M}$ and the scaling relations are identified.

Acknowledgements
This research was funded by the Research Council of Lithuania (LMT), project No. S-MIP-24-100.

Keywords: active galactic nucleus (AGN), galactic outflows, mass outflow rate.

[1] S. Veilleux, R. Maiolino, A. D. Bolatto, and S. Aalto, “Cool outflows in galaxies and their implications,” Astronomy and Astrophysics Review, vol. 28, p. 2, Apr. 2020, doi: 10.1007/s00159-019-0121-9.
[2] D. Nelson et al., “First results from the TNG50 simulation: galactic outflows driven by supernovae and black hole feedback,” MNRAS, vol. 490, no. 3, pp. 3234–3261, Dec. 2019, doi: 10.1093/mnras/stz2306.
[3] V. Springel, “E pur si muove: Galilean-invariant cosmological hydrodynamical simulations on a moving mesh,” MNRAS, vol. 401, pp. 791–851, Jan. 2010, doi: 10.1111/j.1365-2966.2009.15715.x.

THREE-DIMENSIONAL RECONSTRUCTION OF ROTATING ASTEROIDS FROM TWO-DIMENSIONAL IMAGE SEQUENCES

Vladas Šatas[1], Donatas Narbutis[1]

[1]Vilnius University, Faculty of Physics, Theoretical Physics and Astrophysics Institute, Vilnius, Lithuania
vladas.satas@ff.stud.vu.lt

The three-dimensional reconstruction of celestial bodies from two-dimensional image sequences is a critical capability for early mission characterization, enabling gravitational potential estimation and hazard detection before active sensors like LIDAR are operational. This research investigates the viability and accuracy of photogrammetric reconstruction using real archival data from the NASA OSIRIS-REx mission to asteroid (101955) Bennu.

The study adresses the specific challenges of space-based photogrammetry, including single-source harsh lighting, dynamic shadowing due to asteroid rotation, and the limitations of different mission phases. An automated pipeline was developed to process massive archival datasets, implementing a strict multi-stage filtering methodology to isolate photogrammetrically viable data. Out of approximately 26 000 approach phase archival images, only a fraction (<1%) were found suitable for Structure-from-Motion algorithms.

Comparative analysis of mission phases revealed that orbital sequences failed to generate coherent models due to insufficient image overlap and moving shadows. Conversely, the approach phase proved successful, as the combination of the spacecraft's linear trajectory and the asteroid's rotation created a "virtual orbit" effect with adequate baseline and consistent enough lighting.

Quantitative validation against the ground-truth LIDAR model yielded a mean geometric error of $\sim$2 meters, representing approximately 0.4% of the asteroid's diameter. The results indicate that while photogrammetry effectively captures the global volume and shape of the object, it acts as a geometric low-pass filter, smoothing out high-frequency topographic details. The study concludes that while optical reconstruction cannot replace high-precision LIDAR for tasks requiring sub-meter accuracy, it is a robust method for initial shape, volume and gravitational potential modeling during the approach phase of deep space missions.

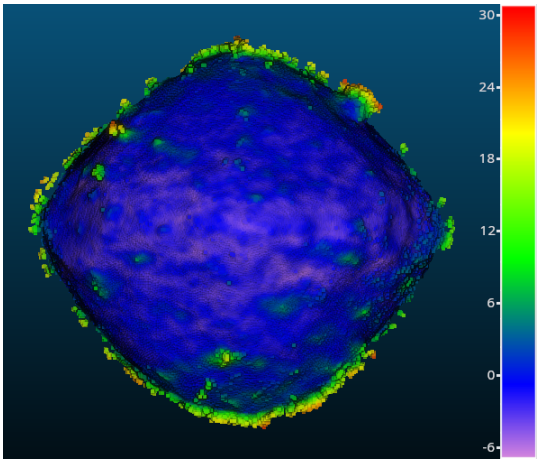


Fig. 1. Cloud-to-Mesh (C2M) error visualisation comparing the photogrammetric reconstruction to the OLA LIDAR reference model. The color scale represents geometric deviation in meters.

ORAL SESSION 2

Applied Electrodynamics

Chair: Dr. M. Karaliūnas

CYBERSECURITY REQUIREMENTS ASSURANCE IN CRITICAL INFRASTRUCTURE SYSTEMS THROUGH THE APPLICATION OF FORMAL VERIFICATION AND ARTIFICIAL INTELLIGENCE-BASED METHODS

Daniel Daukševič[1]

[1]Vilnius University, Faculty of Mathematics and Informatics, Institute of Computer Science, Vilnius, Lithuania
daniel.dauksevic@mif.stud.vu.lt

Cybersecurity of critical infrastructure has become a major concern of modern society and a matter of national interest, with direct impacts on social life, the economy, and government operations. Formal verification, a mathematically rigorous method for proving the correctness of algorithms and system designs, has been widely and successfully applied to the design and certification of safety-critical and cyber-physical systems to guarantee correctness, reliability, and fault tolerance. However, its systematic application to cybersecurity at the architectural and topological levels of such infrastructures remains limited. With the rapidly increasing impact of Artificial Intelligence (AI) in various domains, including cybersecurity, the idea of combining AI with formal verification has emerged as a promising research direction. This hybrid approach has already shown promising results in several domains, such as the verification of cryptographic protocols, software vulnerability detection and automated code repair.

The main hypothesis of the doctoral thesis is that some of these formal techniques and methods, actively used in the verification of safety-critical systems, as well as their combination with AI methods, can be successfully adapted and applied to the verification of cybersecurity properties in complex critical infrastructure systems. The thesis aims to contribute to the systematic application of formal methods at the topological and architectural levels for cybersecurity, proposing a framework that integrates existing formal verification techniques from safety-critical domains and AI methods with modern security requirements.

In this thesis, computer networks that form the backbone of critical infrastructures are defined using mathematical notation. This representation enables automated examination of these systems against logical formulas that capture key cybersecurity requirements, including confidentiality, integrity, and availability. AI-based methods are incorporated to assist in identifying potential attack paths and vulnerabilities, as well as optimizing the process of verification.

The expected outcome is a methodological foundation for future research at the intersection of formal verification, AI, and cybersecurity. This foundation will support rigorous security analysis of critical infrastructure systems, including power networks and industrial control systems, and provide guidance for the application of formal methods in the design and evaluation of secure and resilient cyber-physical infrastructures.

Acknowledgements
This work has been supported by the Lithuanian Research Council under grant No. P-PAD-23-173.

Keywords: Formal Methods, Formal Verification, Cybersecurity, Critical Infrastructure Systems, Artificial Intelligence

[1] J. Rushby, "Formal methods and their role in the certification of critical systems," in Safety and Reliability of Software-Based Systems. London, U.K.: Springer, 1997, pp. 1–42. doi: 10.1007/978-1-4471-0921-1_1.
[2] L. Lamport, Specifying Systems. Boston, MA, USA: Addison-Wesley Professional, 2003.
[3] A. Remke and B. Steffen, Eds., FMICS 2025: Formal Methods for Industrial Critical Systems, Lecture Notes in Computer Science, vol. 16040. Cham, Switzerland: Springer, 2025.

GENETICALLY OPTIMIZED MULTILAYER METASURFACE FOR X-BAND RADAR REFLECTION REDUCTION

Augustas Koklevičius[1], Paulius Ragulis[1], Žilvinas Kancleris[1], Audronė Sankauskaitė[2], Vitalija Rubežienė[2]

[1]Center for Physical Sciences and Technology, Department of Physical Technologies, Vilnius, Lithuania
[2]Center for Physical Sciences and Technology, Department of Textile Technologies, Vilnius, Lithuania
augustas.koklevicius@ftmc.lt

Reducing electromagnetic (EM) wave reflections is essential for stealth applications and minimising unwanted radar signals. Conventional metallic surfaces strongly reflect incident EM waves, making them easily detectable by radar systems. Metasurface-based structures made of subwavelength elements that can control the phase, amplitude, and polarization of electromagnetic waves, with properties not found in conventional natural materials-offer a promising way to reduce reflections without relying on bulky or thick absorbers [1].

This study presents a multilayer Salisbury-type structure incorporating a metasurface designed to reduce EM reflections in the X-band frequency range. The proposed structure is implemented on a rigid FR4 substrate, prioritizing mechanical stability. The multilayer configuration, shown schematically in Fig. 1(A), consists of a fully coated resistive textile layer serving as the first interface with the incident EM wave, followed by a dielectric spacer. Beneath this spacer, a metasurface patterned on FR4 is introduced, backed by a continuous metal plate.

The metasurface unit cell, illustrated in Fig. 1(B), is composed of 25 metallic squares with varying dimensions arranged in a non-uniform array. The elements were fabricated on an FR4 substrate with a copper layer using photolithography. Their dimensions were optimized using a genetic algorithm, a population-based optimization method inspired by natural evolution. The optimization objective was to minimize electromagnetic reflection within the X-band (8–12 GHz). Electromagnetic simulations were performed in CST Studio Suite, using periodic boundary conditions to model an infinite-size metasurface array, enabling efficient evaluation and convergence toward an optimal design.

Reflection reduction is achieved through destructive interference between incident and reflected waves. The wave reflected from the metal plate undergoes a 180° phase shift, destructively interfering with the wave reflected from the upper layers and suppressing overall reflection. As shown in Fig. 1(C), both simulated and measured reflection coefficients exhibit a pronounced resonance within the X-band, with a maximum reflection reduction of up to −15 dB around 8–9 GHz. The close agreement between simulation and measurement confirms the validity of the proposed multilayer design and the accuracy of the simulation model.

The optimized multilayer structure shows clear resonance behavior typical of Salisbury screens, further improved by the by the metasurface. The proposed design offers an effective and practical solution for reducing radar reflections in the X-band and can be adapted to other frequency bands and stealth applications.

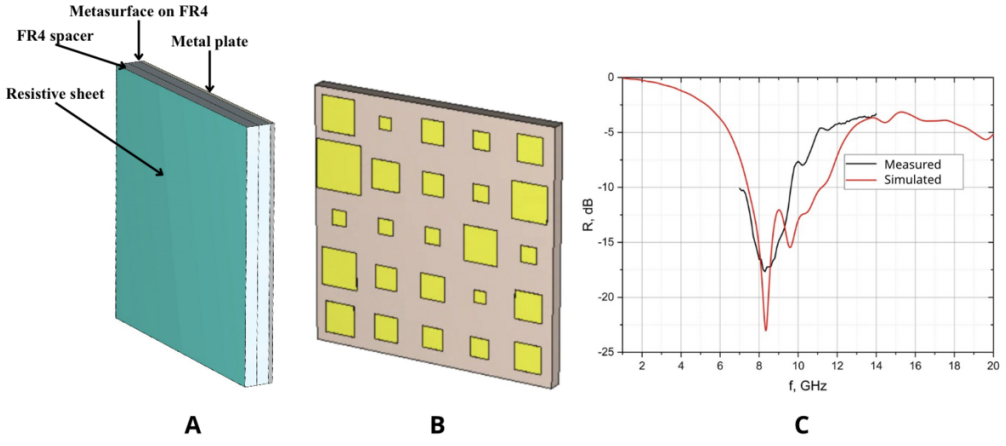


Fig. 1. (A) Layered configuration, (B) Unit cell design with 25 metallic elements, and (C) Comparison of simulated and measured reflection coefficient (R, dB).

[1] Z. Li, R. Pestourie, Z. Lin, S. G. Johnson, and F. Capasso, "Empowering Metasurfaces with Inverse Design: Principles and Applications," ACS Photonics, vol. 9, no. 7, pp. 2178–2192, Jun. 2022, doi: 10.1021/acsphotonics.1c01850.

TRANSMISSION GRID POWER TRANSFORMER INSULATION HEALTH MONITORING AND ASSESSMENT USING ACOUSTIC EMISSION AND ULTRA HIGH FREQUENCY SENSORS

Danas Černeckas[1], Kestutis Jasiūnas[1], Audrius Jonaitis[1]

[1]Kaunas University of Technology, Faculty of Electrical and Electronics Engineering, Kaunas, Lithuania.
danas.cerneckas@ktu.lt

The high-voltage power transformer is a crucial component for transmitting electric energy in a region or country, active surveillance to avert unforeseen breakdowns is critical to guarantee a continuous power supply. The majority of transformer failures can be attributed to partial discharge (PD) in the insulation of a transformer [1]. Partial discharges are destructive events within a part of the insulation system which release energy that can have a destructive effect to a utility and any other utility connected to it. An increase of PD provides an early warning for gradual insulation degradation. However, in practical application, PD is only measured at the transformer's bushings section which is applicable for on-line measuring but only provides partial data about the insulation quality of a transformer [2]. This paper presents a more detailed and reliable method of measuring and assessing on-line high voltage power transformer insulation quality using state-of-the-art acoustic and ultra high frequency (UHF) partial discharge detection. These measurements were done by applying acoustic emission and ultra high frequency sensors around 20 on-line 110-330 kV transformer tanks to measure, monitor and analyze local PD events. The research states that PD detection using aforementioned methods on the transformer tank were far more accurate for localizing a fault in an transformer. In addition, the suggested measuring method has saved time and resources due to the fact that a transformer disassembly was not required for this type of PD measuring. As a result, several cases were found where UHF and acoustic PD measuring was able to detect degrading insulation due to inner (transformer) and outer (other grid utilities) events. After all the measurements, to prove that this single outlier was not farce in detection of degrading insulation, a holistic assessment of the results was created. This was done by comparing acoustic and UHF PD measurements with provided PD voltage measurements of the bushings, the temperature and oil quality measurements of the transformers, it was possible to deduce the symptoms in order to confirm the diagnosis. This method has provided a way for substation engineers to better assess their transformer's health and do so more frequently. For future research it is important to address and implement AI data processing algorithms due to the huge amount of PD measurement results. AI integration could save loads of work time and also provide an efficient way of monitoring transformer health.

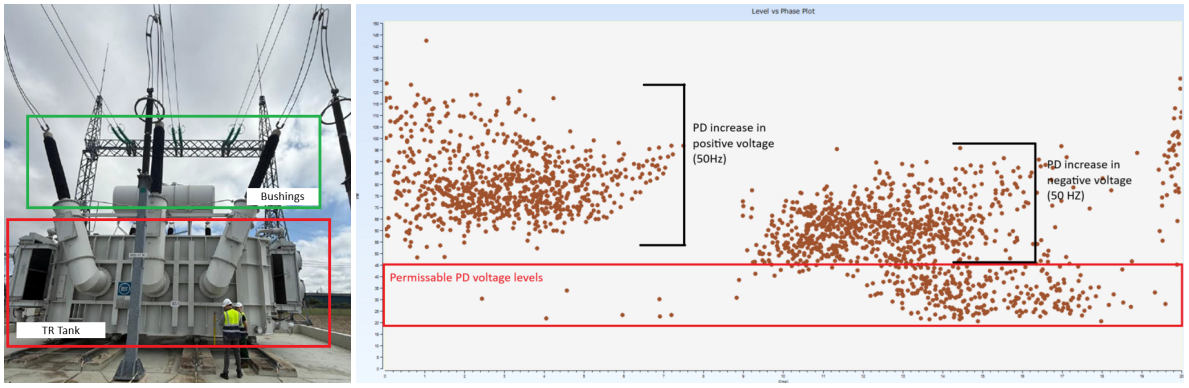


Fig. 1. An example of an acoustic emission PD measurement of a 110-330 kV power transformer

Keywords: Partial discharge, power transformer, transformer insulation, transformer oil, acoustic measurements, ultra high frequency measurements

[1] A. Akbari, P. Werle, H. Borsi, and E. Gockenbach, "Transfer function-based partial discharge localization in power transformers: A feasibility study," IEEE Elect. Insul. Mag., vol. 18, no. 5, pp. 22–32, Sep. 2002.
[2] M. R. Hussain, S. S. Refaat, and H. Abu-Rub, "Overview and Partial discharge Analysis of Power Transformers: A literature review," IEEE Access, vol. 9, pp. 64587–64605, Jan. 2021, do

WIDEBAND PERFORMANCE EVALUATION AND CHARACTERISATION OF ANTENNA-COUPLED CMOS TERAFET DETECTORS FROM 0.1 TO 1.2 THZ

Patricija Ivanauskaitė[1,2], Dovilė Čibiraitė-Lukenskienė[1,2], Domantas Vizbaras[2], Alvydas Lisauskas[1,2]

[1]Lithuania, Center for Physical Sciences and Technology, Department of Optoelectronics
[2]Lithuania, Vilnius University, Faculty of Physics, Institute of Applied Electrodynamics and Telecommunications (IAET)
patricija.ivanauskaite@ftmc.lt

The terahertz (THz) band (0.1-10 THz) [1], usually characterised by a lack of efficient, room-temperature sensing technology, is essential for “fingerprint” gas spectroscopy, as it coincides with molecular rotational and vibrational transitions [2]. While Complementary Metal-Oxide-Semiconductor (CMOS) field-effect transistors (TeraFETs) offer a path towards compact, high-speed detection, their deployment is hindered by the lack of standardised, high-precision characterisation methodologies [3].

Broadband characterisation is primarily challenged by a “power gap” between calibrated meters and low-power sources. Standard Thomas Keating (TK) absolute power meters require minimum power levels of ∼10 µW to distinguish signals from thermal fluctuations, yet TOPTICA TeraScan 780 photomixers typically produce power below 2 µW [4]. At these levels, TK sensors operate at their noise floor, where additive thermal noise causes an artificial overestimation of the actual power. While high-sensitivity Golay cells can bridge this gap, they require meticulous cross-calibration against a traceable standard and remain highly susceptible to environmental noise [3].

To address this, this study aimed to develop and implement a repeatable free-space platform to evaluate the broadband CMOS TeraFET sensors from 0.1 GHz to 1.2 THz. Using a TOPTICA TeraScan 780 system as a basis, with custom components for improved repeatability, three detector configurations, fabricated via 65-nm (bowtie antenna) and 90-nm (bowtie and log-spiral antennas) technology nodes, were characterised.

Results showed a 51.6 dB peak signal-to-noise ratio (SNR) for the log-spiral detector, with minimum noise equivalent power (NEP) comparable to that in the literature [3]. The platform successfully resolved the main narrow atmospheric water-vapour lines (notably 557 GHz), which were used for frequency offset calibration. While the log-spiral antenna provided the highest peak sensitivity, bowtie detectors exhibited flatter spectral response between 400 and 800 GHz.

An established characterisation platform provides a framework for benchmarking next-generation CMOS-based THz sensors. Successful resolution of atmospheric absorption features demonstrated that optimised TeraFETs can meet rigorous performance standards required for practical integration into compact gas spectroscopy systems. Future research will focus on TeraFET testing with a circular multipass cell for methanol detection.

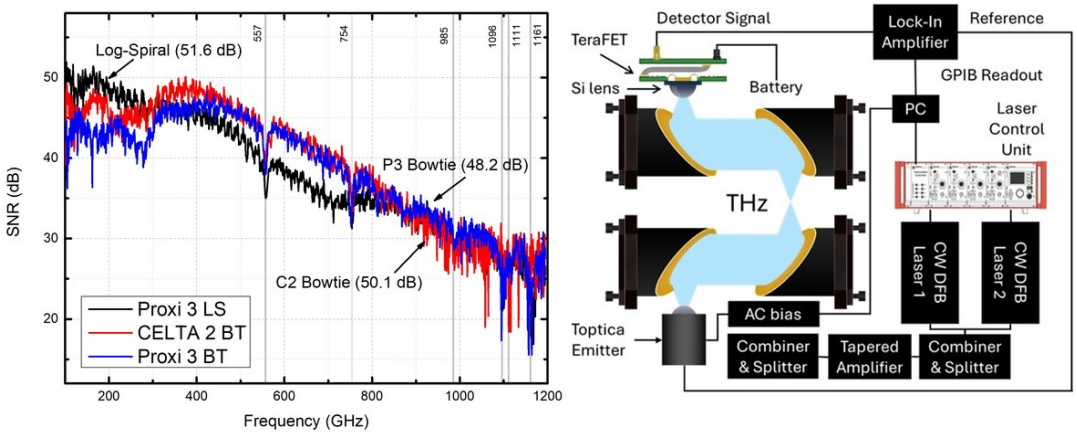


Fig. 1. Left: SNR for three different TeraFET detectors; Right: A schematic of the experimental setup featuring 4 OAP mirrors, GaAs Toptica Photonics photomixer emitter and a TeraFET detector with a hyper-hemispherical Si lens.

Acknowledgement: We would like to thank doc. dr. Dalius Seliuta and Terahertz Photonics Laboratory for all the assistance during the experimental preparation.

[1] G. Valušis et al., ”Roadmap of terahertz imaging 2021,” Sensors, vol. 21, no. 12, p. 4092, Jun. 2021, doi: 10.3390/s21124092.
[2] N. Rothbart, A. Glück, and H.-W. Hübers, ”Terahertz gas spectroscopy applied to medicine and metrology,” IEEE Trans. Terahertz Sci. Technol., vol. 14, no. 5, pp. 613–620, Sep. 2024, doi: 10.1109/TTHZ.2024.3411425.
[3] D. Čibiraitė-Lukenskienė, “Room-temperature passive terahertz imaging based on high sensitivity field-effect transistor detectors,” Ph.D. dissertation, Dept. Phys., Goethe Univ. Frankfurt, Frankfurt am Main, Germany, 2021. doi: 10.21248/gups.63353
[4] TOPTICA Photonics SE, ”TeraScan,” TOPTICA Photonics SE. https://www.toptica.com (accessed Feb. 1, 2026).

HORIZONTALLY ORIENTED LOW PROFILE DIELECTRIC RESONATOR ANTENNA WITH EXTREME TEMPERATURE STABILITY FOR RADIO WAVE ENERGY HARVESTING

Justina Žemgulytė[1], Paulius Ragulis[1], Modestas Sadauskas[2], Rimantas Simniškis[1], Anatolii G. Belous[3], Oleg I. V'yunov[3], Žilvinas Kancleris[1]

[1]Center for Physical Sciences and Technology, Department of Physical Technologies, Vilnius, Lithuania
[2]Center for Physical Sciences and Technology, Department of Laser Technologies, Vilnius, Lithuania
[3]V. I. Vernadsky Institute of General and Inorganic Chemistry NAS of Ukraine, Kyiv, Ukraine
justina.zemgulyte@ftmc.lt

The rising need for battery-free IoT and wireless sensor networks calls for antennas that are compact, efficient, and thermally stable, yet traditional metal-based designs tend to detune and suffer higher losses under temperature variations [1]. We present a horizontally oriented low-profile dielectric resonator antenna (HODRA) made from high-Q, temperature-stable (Mg,Ni)TiO_3–$Ca_{0.8}Sm_{0.13}TiO_3$ ceramic ($\varepsilon \approx 17$), whose performance and suitability for low-power autonomous sensing are confirmed through a radio frequency energy harvesting experiment.

The horizontally oriented dielectric resonator antenna model is shown in Fig. 1. The cylinder is placed on a one-sided metalized surface of laminate FR-4. Antenna has two circular metal contacts that are equal in size. The pin connects the hot contact of the antenna with the central conductor of the 50 Ω coaxial cable, whereas the other contact of the antenna is connected to the grounded pin.

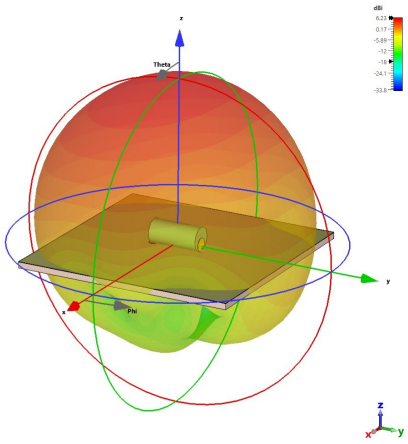


Fig. 1. Horizontally oriented dielectric resonator antenna model

Antenna electromagnetic characteristics were measured inside an anechoic microwave chamber. The resonance frequency of the antenna 5.39 GHz. The measured gain is around 6 dBi. The half power bandwidth (interval where the gain of the antenna is less than 3 dB below the maximum value) is approximately 1 GHz, providing near-complete coverage of the 5 GHz WiFi frequency band.

The antenna's excellent performance was further evaluated in an energy harvesting system. A simple voltage doubler circuit was designed using two SMS7630 Schottky diodes. The rectifier impedance was matched to the 50 Ω antenna input using a quarter-wavelength impedance matching network. A horn antenna was transmitting 200 mW at 1 m distance, the rectenna was loaded with a 3 kΩ resistor. With a measured received power of −10 dBm at the antenna input, the rectenna delivered 170 mV across a 3 kΩ load, corresponding to 9.6 µW DC and an RF-to-DC efficiency of around 9.6%. Harvested power is significant because it is sufficient to operate a low-power management circuit capable of accumulating energy over time [2].

The presented horizontally oriented, low-profile dielectric resonator antenna demonstrates excellent suitability for RF energy-harvesting systems, combining high gain, low electromagnetic losses, and exceptional material stability to reliably power autonomous wireless sensor nodes and IoT devices. Its performance shows that ceramic-based DRAs are a strong alternative to metal antennas at higher frequencies and paves the way for array-based designs and deeper integration with advanced power-management ICs to enable maintenance-free operation.

Acknowledgements

This work was supported by NATO Emerging Security Challenges Division, Science for Peace and Security Programme "3 D Metamaterials for energy Harvesting and Electromagnetic Sensing"

[1] S. A. Dasari, S. Y. Lee and N. Ghalichechian, "On-Chip Dielectric Resonator Antenna on Silicon Carbide Substrate for Extreme Environments," in IEEE Antennas and Wireless Propagation Letters, vol. 24, no. 9, pp. 2879-2883, Sept. 2025, doi: 10.1109/LAWP.2025.3576302.
[2] M. Caselli, M. Ronchi, and A. Boni, "Power management circuits for low-power RF energy harvesters," J. Low Power Electron. Appl., vol. 10, no. 3, pp. 1–20, Sep. 2020.

ORAL SESSION 3

Astrophysics and Theoretical Physics

Chair: Dr. J. Chmeliov

OPTICAL SPIN-ORBIT DYNAMICS OF VECTOR VORTICES IN COHERENTLY PREPARED MEDIA

Dharma P. Permana[1,2,3], Mazena Mackoit Sinkeviciene[1], Julius Ruseckas[4], Hamid R. Hamedi[1]

[1]Vilnius University, Faculty of Physics, Institute of Theoretical Physics and Astronomy, Lithuania
[2]Vilnius University, Faculty of Physics, Laser Research Center, Lithuania
[3]Aix-Marseille Universite, Faculte des Sciences, Departement Physique, France
[4]Baltic Institute of Advanced Technology, Lithuania
dharma.permana@ff.stud.vu.lt

Structured light carrying orbital angular momentum (OAM), known as an optical vortex, has gained growing interest in recent decades due to its potential applications in high-dimensional quantum communication and quantum information processing [1,2]. Recent full-vectorial studies of optical vortices interacting with electromagnetically induced transparency (EIT) media have revealed spatially dependent transparency and polarization transitions, enabling control of both OAM and spin angular momentum (SAM) encoded in the polarization states of light [3]. However, these effects have so far been restricted to four-level loop–tripod atomic systems that require a weak static magnetic field to establish the necessary quantum coherence. Here, the propagation of an optical vector vortex in a coherently prepared three-level-Λ configuration atomic medium is investigated, demonstrating an alternative EIT platform that supports quantum coherence without the need for a static magnetic field.

The weak vector probe beam is composed of paired vortex pulses carrying opposite OAM charges $\pm l$, with opposite SAM associated with orthogonal circular polarizations of opposite handedness. The medium linear response to the vector vortex under the steady-state regime was analytically derived to determine the beam's intensity and polarization evolution. We found that the topology of the vortex pairs is transferred to the atomic medium and produces $2|l|$-fold azimuthally structured transparency, transforming the beam's intensity profile from a ring-shaped into a petal like pattern. An effective optical anisotropy is induced by the OAM-structured atomic coherence, enabling the evolution of polarization texture during the propagation. This evolution is controlled by tuning the initial ground-state populations, allowing the transition between left-circular, linear, and right-circulation polarizations [4].

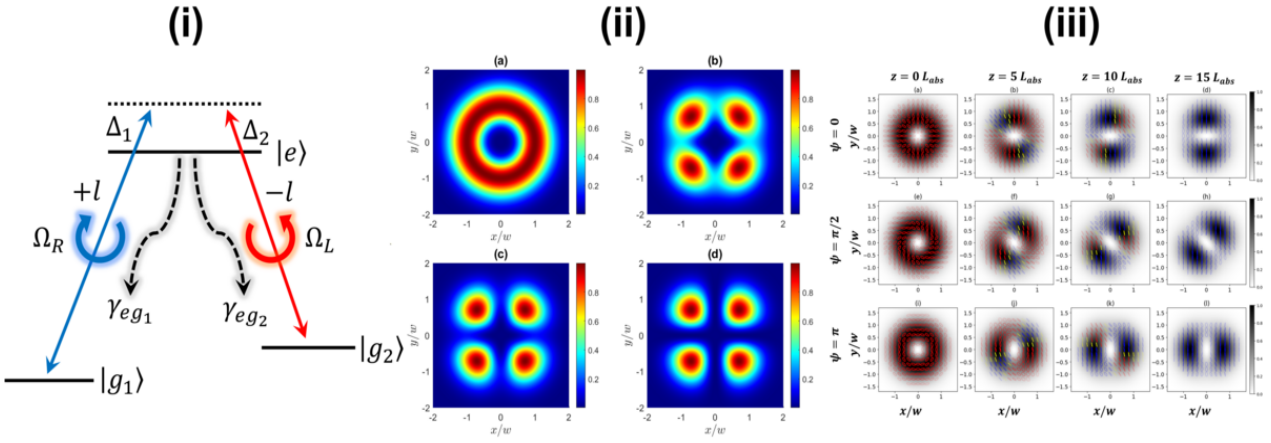


Fig. 1. (i) Three-level Λ configuration. (ii) The petal formation corresponding to $2|l|$-fold azimuthally dependent transparency for $|l| = 2$. (iii) the polarization state transitions from left-circular polarization (red) to right-circular polarization (blue) [4].

The results obtained suggest that the coherently prepared Λ configuration atomic medium can be considered as a potential EIT medium for OAM- and SAM-based application in a static magnetic field independent system.

Acknowledgements

This project has received funding from the Research Council of Lithuania (LMTLT), agreement No. S-ITP- 24-6. D.P.P. gratefully acknowledges the support of the Erasmus+: Erasmus Mundus programme of the European Union under Convention n° 101128124 — EUROPHOTONICS — ERASMUS-EDU-2023-PEX-EMJMMOB. The novelty found in this work has been submitted to Physical Review A (under review) [4].

Keywords: Light-matter interaction, orbital angular momentum of light, spin-orbit coupling, electromagnetically induced transparency, quantum optics

[1] M. Erhard, R. Fickler, M. Krenn, and A. Zeilinger, "Twisted photons: new quantum perspectives in high dimensions," Light Science & Applications, vol. 7, no. 3, p. 17146, Oct. 2017, doi: 10.1038/lsa.2017.146.
[2] S. Z. D. Plachta, M. Hiekkamäki, A. Yakaryılmaz, and R. Fickler, "Quantum advantage using high-dimensional twisted photons as quantum finite automata," Quantum, vol. 6, p. 752, Jun. 2022, doi: 10.22331/q-2022-06-30-752.
[3] P. Zhang, B.-H. Liu, R.-F. Liu, H.-R. Li, F.-L. Li, and G.-C. Guo, "Implementation of one-dimensional quantum walks on spin-orbital angular momentum space of photons," Physical Review A, vol. 81, no. 5, May 2010, doi: 10.1103/physreva.81.052322.
[4] D. P. Permana, M. M. Sinkevičienė, J. Ruseckas, and H. R. Hamedi, "Spin-orbit coupling of optical vector vortices in coherently prepared media," arXiv.org, Nov. 21, 2025. https://arxiv.org/abs/2511.17406

COMPLETE EXCITON HAMILTONIAN FOR PHOTOSYNTHETIC PIGMENT-PROTEIN COMPLEXES

Austėja Mikalčiūtė[1], David Varas Rubio[2], Ulrich Kleinekathöfer[2], Darius Abramavičius[1]

[1]Vilnius University, Faculty of Physics, Institute of Chemical Physics, Lithuania
[2]Constructor University, School of Science, Germany
austeja.mikalciute@ff.vu.lt

One of the core processes of photosynthesis is the “collection of the light energy” through excitations of multi-pigment light-harvesting antenna complexes. A vast diversity of photosynthetic pigments and light-harvesting complexes has evolved that adapted the process to occur both in water and on land, and it can be found in many bacteria, algae, and plant species. In this work, we extend the standard exciton model typically used to calculate various types of spectra of the light-harvesting complexes. The standard exciton theory used for describing the spectroscopy of molecular complexes usually assumes an infinite exciton lifetime, coming from complete isolation of Hamiltonian blocks describing a different number of excitations. We focus on extending the model by including environment-induced non-resonant couplings in the Hamiltonian, which couple different numbers of excitons. We analyze their impact on the absorption spectra of two small light-harvesting complexes from their crystallographic structure: Fenna–Matthews–Olson and fucoxanthin–chlorophyll protein. Quantum mechanics calculations of the pigment properties, combined with electro-static description of the protein, allowed us to construct the full Hamiltonian and calculate the exciton lifetimes and the absorption spectra using the secular Redfield theory. The results of the research indicated that off-resonant terms in the Hamiltonian are significant: they are at least one order of magnitude larger than the interchromophore resonant interactions and allow the estimation of each exciton lifetime, therefore should be included in the calculations of linear (or non-linear) spectra. Therefore, as the results proved to be consequential, the methodology of this model was advanced: molecular dynamics simulations have been performed for the protein and its ligands to get closer to real-life conditions than a single crystallographic structure. The molecular dynamics simulations allowed us to obtain correlation functions and spectral densities of the Fenna–Matthews–Olson complex with the off-resonant terms and to focus on developing the complex Redfield theory extension including the off-resonant terms for absorption calculations.

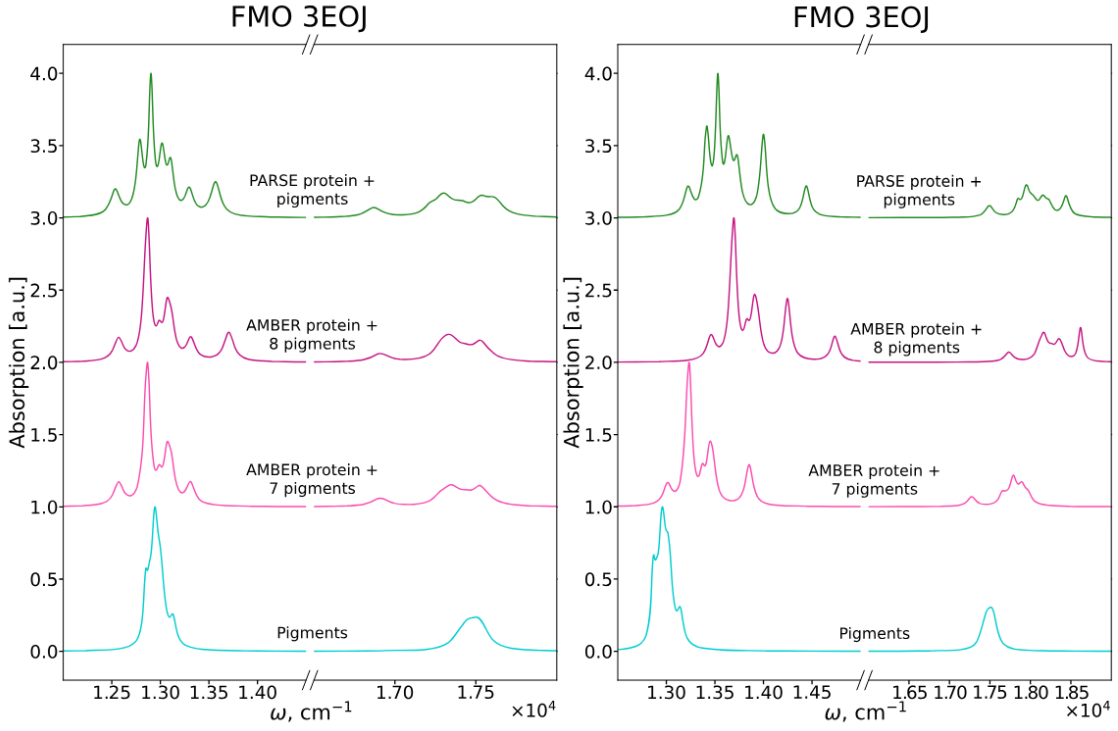


Fig. 1. Absorption spectra of the FMO 3EOJ PDB structure at 77 K calculated using the secular approximation of Redfield equation solutions: block-diagonal model (left) and full model (right).

Keywords: photosynthesis, spectroscopy, quantum chemistry, molecular dynamics, chlorophyll, Hamiltonian

CORRELATION-DRIVEN WEYL PHYSICS FROM AB INITIO DFT+DMFT THEORY

Jorūnas Dobilas[1], Martin Braß[2], Frank T. Ebel[2], Silke Paschen[2], Karsten Held[2]

[1]Center for Physical Science and Technology, Department of Fundamental Research, Lithuania
[2]Technical University of Vienna, Institute of Solid State Physics, Austria
jorunas.dobilas@ftmc.lt

Strongly correlated materials provide a platform for emergent quantum phases [1], including heavy-fermion metals, Kondo insulators, and unconventional superconductors. These phases arise from the interplay between crystal symmetries and complex many-body effects. Describing them from first principles is particularly challenging, as conventional density functional theory (DFT) fails to capture the low-energy quasiparticle physics. Here, using **state of the art** DFT combined with dynamical mean-field theory (DFT+DMFT) [2], we investigate the f-electron heavy-fermion compound $CeRu_4Sn_6$ to resolve its electronic structure and topology.

Our calculations show that Kondo hybridization opens a direct gap in the electronic structure, which is bridged by topological band crossings (Weyl nodes) along low-symmetry directions. We identify five inequivalent Weyl nodes of both type-I and type-II, generating a total of 64 symmetry-related Weyl points. A comprehensive analysis of these correlation-driven Weyl features is presented in our recent work [3]. The Weyl nodes emerge within correlated quasiparticle bands mainly composed of Ce-$4f$ orbitals and exhibit small electron velocities close to the Weyl nodes (below 10 km/s). The nodes closest to the Fermi energy lie approximately 0.5 meV below E_{F}, placing the Weyl physics at experimentally accessible energy scales.

These *ab initio* results establish $CeRu_4Sn_6$ as a model system for correlation-driven Weyl physics in f-electron materials, highlighting the importance of many-body correlations in $CeRu_4Sn_6$ and heavy-fermion systems in general. More broadly, this work provides a foundation for understanding interaction-driven topological phases and quantum transport phenomena in correlated quantum materials.

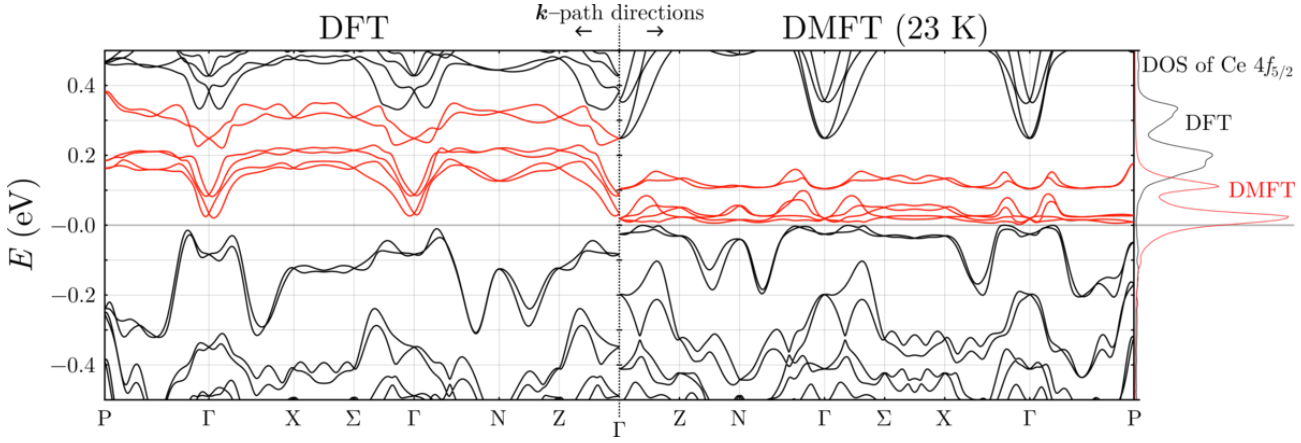


Fig. 1. Mirrored band structures of $CeRu_4Sn_6$ from DFT (left) and DFT+DMFT at 23 K (right) along identical high-symmetry paths centered at Γ. The Ce $f_{5/2}$ manifold is highlighted with red color to emphasize how Kondo hybridization reshapes the electronic structure. Correlation effects, included in DMFT solution, generate additional avoided band crossings and node-like features in the lower bands that are absent in DFT, revealing traces of Weyl physics. The side panel shows the corresponding Ce $4f_{5/2}$ density of states, confirming the emergence of Kondo effect at the Fermi level.

Keywords: Topology, Weyl Physics, DFT+DMFT

[1] J.G. Checkelsky et al., Nat Rev Mater 9, 509–526 (2024)
[2] K. Held, Advances in Physics 56(6), 829–926 (2007)
[3] J. Dobilas et. al., Phys. Rev. B (2026)

VISUALIZATION OF ΛB BARYON DECAYS USING THE ECC METHOD FOR MISSING MOMENTUM RECONSTRUCTION

Meda Paulavičiūtė[1], dr. Augustas Vaitkevičius[1], dr. Mindaugas Šarpis[1]

[1]Vilnius University, Faculty of Physics, Vilnius, Lithuania
meda.paulaviciute@ff.stud.vu.lt

Neutral particles such as π^0 mesons and γ photons are detected with low efficiency and poor resolution in particle detectors due to their lack of electric charge. This is particularly important in large-scale experiments like LHCb, where rare decay channels are investigated, and inefficiencies may cause events to remain undetected or misinterpreted. Therefore, improving reconstruction methods for decays involving neutral particles is essential for reliable physics analyses.

The objective of this work was to investigate and apply the Extended Cone Closure (ECC) method for deterministic reconstruction of missing momentum in heavy baryon decays and to develop visualization tools that enhance the understanding of reconstructed decay topologies. The study focused on the decay channel

$$\Lambda_b^0 \to \Lambda_c^+ D^0 K^-,$$

which is of interest in searches for pentaquark states predicted in the $\Lambda_c^+ D^{*0}$ system [1,2].

Monte Carlo–simulated Λ_b baryon decay samples were generated using the RapidSim framework and analyzed within the CERN ROOT environment. The Extended Cone Closure (ECC) method reconstructed the momentum of undetected neutral particles by applying energy–momentum conservation and geometric constraints derived from the decay topology. Using known particle masses and vertex information, the method determined the magnitude and direction of the missing momentum by scanning angular solutions and selecting the configuration that best matches the reconstructed Λ_b^0 flight direction. This allowed full kinematic reconstruction of the decay, despite the absence of direct detection of neutral particles. After confirming that the ECC method reconstructs the missing momentum of Λ_b, Python-based tools were used to visualize the reconstructed decays, enabling a more in-depth analysis.

The results demonstrate that the ECC method successfully reconstructs the missing momentum of neutral particles, such as π^0 mesons, in simulated Λ_b decays. The developed visualization approach provides clear insight into decay geometry and angular correlations of the decay products, enabling more detailed analysis.

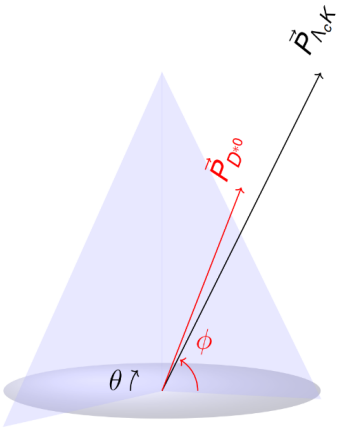


Fig. 1. Angles θ and ϕ between the $\bar{D}^{*0}$ momentum vector and the combined $\Lambda_c^+ K^-$ momentum vector, defining the cone used in the ECC reconstruction.

[1] R. Aaij et al., "Observation ofJ/ψpResonances Consistent with Pentaquark States inΛb0→J/ψK−pDecays," Physical Review Letters, vol. 115, no. 7, p. 072001, Aug. 2015, doi: 10.1103/physrevlett.115.072001.

[2] R. Aaij et al., "Observation of a narrow Pentaquark state, PC(4312)+, and of the Two-Peak structure of the PC(4450)+," Physical Review Letters, vol. 122, no. 22, p. 222001, Jun. 2019, doi: 10.1103/physrevlett.122.222001.

YUKAWA SECTOR RENORMALIZATION IN THE GRIMUS-NEUFELD MODEL

Dominykas Malinauskas[1], Simonas Draukšas[1]

[1]Vilnius University, Faculty of Physics, Institute of Theoretical Physics and Astronomy, Saulėtekio av. 9, Vilnius, Lithuania
dominykas.malinauskas@ff.stud.vu.lt

The study of fundamental particles and their interactions is deeply rooted in the framework of quantum field theory (QFT). In this framework, so far the most successful model is the Standard Model (SM), which has withstood numerous experimental checks. For example, it has correctly predicted the existence of the Higgs boson[1]. However, it does not explain the light masses of neutrinos[2], that are measured experimentally. Thus the SM needs to be extended to do so and the extension we use is the Grimus – Neufeld model (GNM)[3]. The model adds an additional Higgs doublet as well as a Majorana fermion to the SM. In the model, the seesaw mechanism and radiative corrections give the masses to the neutrinos. Having that, the next step is to cross-check the GNM predictions with the experimental data. This is troublesome, because QFT gives unphysical infinities that come from the high energy range, which must be included in QFT. Thus the model needs to be renormalized. Renormalization is a procedure, where we get rid of those infinities by shifting the values of our parameters to compensate for them.

During this study the objective was to renormalize the Yukawa constants that couple the first Higgs doublet with the fermions in the GNM. These constant are important, because after Spontaneous Symmetry breaking they give the fermions their physical mass. The renormalization of the Yukawa constant is achieved by renormalizing the three-point functions of Higgs–fermion interactions. The renormalization is done by using the Simonas Draukšas[4] scheme, which modifies the usual On-Shell renormalization scheme by introducing off-diagonal mass counterterms. Due to the connection between masses and the Yukawa couplings, these off-diagonal counterterms in principle can be related to the Yukawa coupling counterterms.

In this presentation we will present the Yukawa counterterms we have computed in this study. In future studies we will cross-check the the predictions of our model with experimental data.

[1] S. Chatrchyan et al. (CMS Collaboration), “Observation of a new boson at a mass of 125 GeV with the CMS experiment at the LHC,” Phys. Lett. B, vol. 716, no. 1, pp. 30–61, Sep. 2012.
[2] B. Batell, A. Bhoonah, and W. Huang, “Right-handed neutrino masses from the electroweak scale,” arXiv:2411.07294, 2024.
[3] W. Grimus and H. Neufeld, “Radiative neutrino masses in an SU(2) × U(1) model,” Nucl. Phys. B, vol. 325, no. 1, pp. 18–32, Oct. 1989.
[4] S. Draukšas, Renormalization of the Grimus–Neufeld Model, Ph.D. dissertation, Vilnius Univ., Lithuania, 2024.

TIME-DEPENDENT PROJECTION SUPEROPERATOR APPROACH TO OPEN QUANTUM SYSTEMS

Justina Vaičaitytė[1,2], Andrius Gelžinis[1,2], Leonas Valkūnas[2]

[1]Vilnius University, Faculty of Physics, Institute of Chemical Physics
[2]Center for Physical Sciences and Technology, Department of Molecular Compound Physics
justina.vaicaityte@ff.stud.vu.lt

Most quantum-mechanical systems interact with some kind of environment consisting of a large number of degrees of freedom. Such interactions between an open quantum system and its environment lead to damping, dissipation and strong decoherence [1]. The theory of open quantum systems is widely used in almost all areas of physics, including quantum optics, spectroscopy, chemical physics and quantum information [2]. The dynamics of such systems can be described by the so-called quantum master equation [3], which is usually obtained by employing projection superoperators.

In this work, we used a time-dependent projection superoperator proposed in Ref. [6] to derive quantum master equations for a molecular system and compare the results with the exact numerical solutions as well as with those obtained from the standard quantum master equation. It was found that the resulting equations are non-linear and differ from those obtained using a time-independent projector only by non-linear terms. We analyzed the obtained results for a variety of parameter values for a two-level molecular system. Fig. 1 shows an example comparing the exact solution and the solutions obtained from the linear and non-linear equations for the elements of the density operator at low temperature. It can be seen that the linear equations yield unphysical population values outside the range [0,1], while this issue does not arise for the non-linear equations. This represents a clear advantage of the time-dependent projector.

On the other hand, at high temperatures and for small values of the reorganization energy, both linear and non-linear equations yield excellent accuracy. For larger reorganization energies, however, the accuracy decreases significantly, with no noticeable difference between the linear and non-linear equations. In the fast bath relaxation regime, both linear and non-linear equations also produce accurate results.

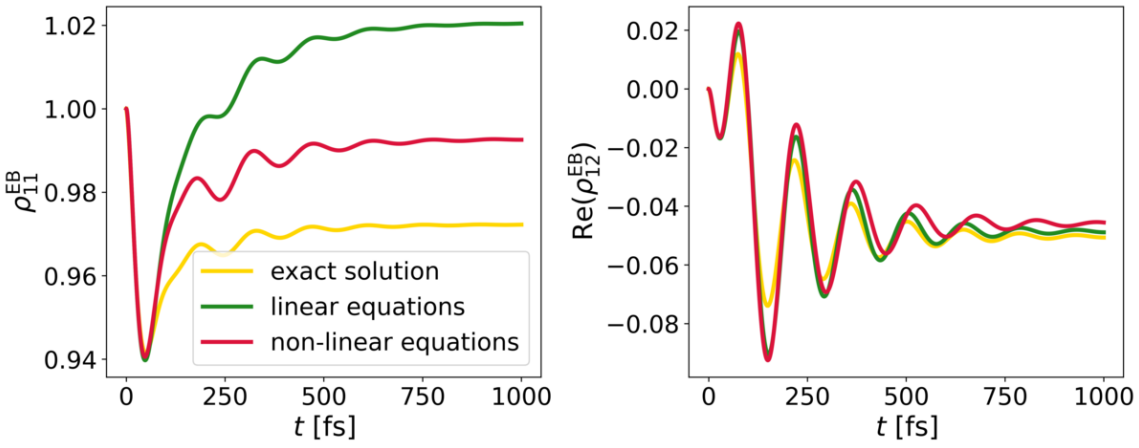


Fig. 1. Comparison of the exact solution for the density operator elements with the linear and non-linear equations. Left figure: population for the first excited state. Right figure: real part of the coherence. Parameter values: difference of excitation energies $\Delta E = 100\,\mathrm{cm}^{-1}$, interaction energy $J = 100\,\mathrm{cm}^{-1}$, reorganization energy $\lambda = 50\,\mathrm{cm}^{-1}$, inverse relaxation rate $\gamma^{-1} = 50\,\mathrm{fs}$, temperature $T = 50\,\mathrm{K}$.

[1] H.-P. Breuer, J. Gemmer, and M. Michel, “Non-Markovian quantum dynamics: Correlated projection superoperators and Hilbert space averaging,” Physical Review E, vol. 73, no. 1, p. 016139, Jan. 2006, doi: 10.1103/physreve.73.016139.
[2] H.-P. Breuer and F. Petruccione, The theory of open quantum systems. 2007. doi: 10.1093/acprof:oso/9780199213900.001.0001.
[3] O. Kühn and V. May, Charge and energy transfer dynamics in molecular systems. 2023. doi: 10.1002/9783527696277.
[4] C. R. Willis and R. H. Picard, “Time-dependent projection-operator approach to master equations for coupled systems,” Physical Review. A, General Physics, vol. 9, no. 3, pp. 1343–1358, Mar. 1974, doi: 10.1103/physreva.9.1343.

ORAL SESSION 4

Spectroscopy and Imaging

Chair: Dr. D. Abramavičius

DYNAMIC FULL-FIELD OPTICAL COHERENCE MICROSCOPY FOR LIVE TISSUE IMAGING

Erikas Tarvydas[1,2], Austėja Trečiokaitė[1], Egidijus Auksorius[1]

[1]Center for Physical Sciences and Technology, Vilnius, Lithuania
[2]Vilnius University, Faculty of Medicine, Vilnius, Lithuania
erikas.tarvydas@ftmc.lt

Dynamic full-field optical coherence microscopy (d-FF-OCM) is a label-free imaging technique that allows to visualize cells and their intracellular activity in various fresh biomedical tissues. Images acquired by using these methods provide crucial information in various biophysical and biomedical research areas. However, d-FF-OCM systems do not come without their challenges when imaging biomedical, highly scattering tissues [1, 2]. In this work we present a high-resolution d-FF-OCM system (Fig. 1a) which overcomes most of the challenges and generates enhanced contrast images (Fig. 1b, c) without the need of any sort of fluorescence dyes [3].

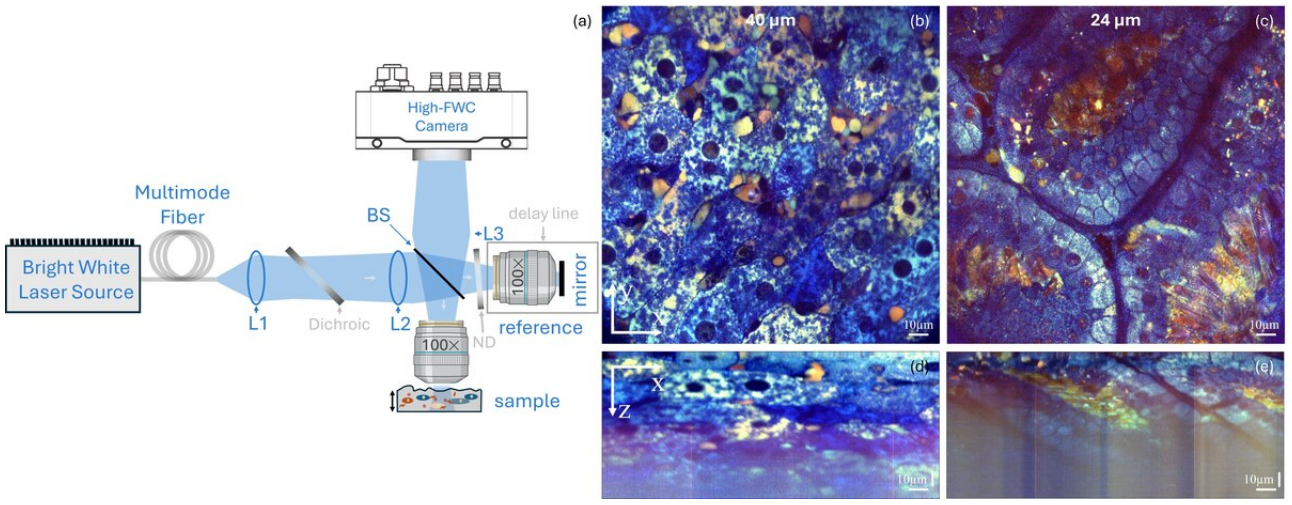


Fig. 1. Principle scheme of high-resolution FF-OCM system (a). Fluorescent like images acquired with d-FF-OCM system (b-c). Image (b) depicts liver tissue and hepatocytes, image (c) showcase mouse intestinal tissue imaged from villus side of the intestinal wall. (c) and (d) images - mathematically reconstructed axial views. Blue corresponds to low vibration frequencies (1 Hz), green to middle range (1-100 Hz) and red – high frequencies (100-250 Hz).

System is equipped with 100× oil-immersion objectives (NA=1.25) and a high-intensity, laser-pumped incoherent white light source which allowed us to achieve high resolution images in high-scattering tissues up to 120 µm deep. With this system we were able to acquire fresh ex vivo mouse liver (Fig. 1b, d) and small intestine (Fig. 1c, e) images with extended depth and detail. In these tissues, the dynamic contrast clearly revealed fine structures not visible with conventional OCT—for example, the sinusoidal microvasculature and organized cell layers in the liver, as well as neural plexuses, crypts and microvilli in the intestine—all visualized label-free.

Acknowledgements

We thank Seemantini Nadkarni and Arvydas Laurinavičius for discussions, and Urtė Neniškyte, Viktorija Kralikienė and Igor Nagula for providing mouse tissues.

Keywords: OCT, d-FF-OCM, microscopy, dynamics

[1] J. Scholler et al., “Dynamic full-field optical coherence tomography: 3D live-imaging of retinal organoids,” Light Science & Applications, vol. 9, no. 1, p. 14.0, Aug. 2020, doi: 10.1038/s41377-020-00375-8
[2] K. Groux et al., “Dynamic full-field optical coherence tomography allows live imaging of retinal pigment epithelium stress model,” Communications Biology, vol. 5, no. 1, p. 575, Jun. 2022, doi: 10.1038/s42003-022-03479-6.
[3] E. Tarvydas, A. Treciokaite, and E. Auksorius, “High-Resolution Dynamic Full-Field Optical Coherence Microscopy: illuminating intracellular activity in deep tissue,” arXiv.org, Aug. 05, 2025. https://arxiv.org/abs/2508.03657

HIGH-THROUGHPUT SPATIO-TEMPORAL OPTICAL COHERENCE TOMOGRAPHY FOR ENHANCED RETINAL IMAGING SENSITIVITY

Karolis Adomavičius[1], Austėja Trečiokaitė[1], Erikas Tarvydas[1], Egidijus Auksorius[1]

[1]Center for Physical Sciences and Technology, Optoelectronics department, Lithuania
austeja.treciokaite@ftmc.lt

Optical Coherence Tomography (OCT) has rapidly become a crucial tool in ophthalmologic diagnostics. Nevertheless, traditional scanning systems are strongly limited by scanning speed, susceptibility to motion artefacts and optical aberrations. Spatio-Temporal Optical Coherence Tomography (S-TOCT) enables high-speed retinal imaging with computational aberration correction, but at the cost of reduced sensitivity. When using standard 50/50 beamsplitters, more than 75% of the available light is lost due to double losses: 50% of the light is lost during illumination, and another 50% is lost in signal collection. In addition, the reference reflectance must be kept low for biological tissue samples [1]—which further increases light losses. Simply increasing the source power is typically not viable due to source limitations or phototoxic effects on the sample. Here, we present a high-throughput (HT) STOC-T configuration that recovers a significant portion of the available light budget without increasing source power. The design replaces the standard 50/50 beamsplitter with an asymmetric 90/10 beamsplitter and incorporates a pupil-plane pick-off mirror [2], allowing illumination and signal detection through the same beamsplitter facet (Fig. 1a). This maximizes light delivery to the retina while efficiently collecting backscattered photons scattered over a wide angular range by retinal tissue.

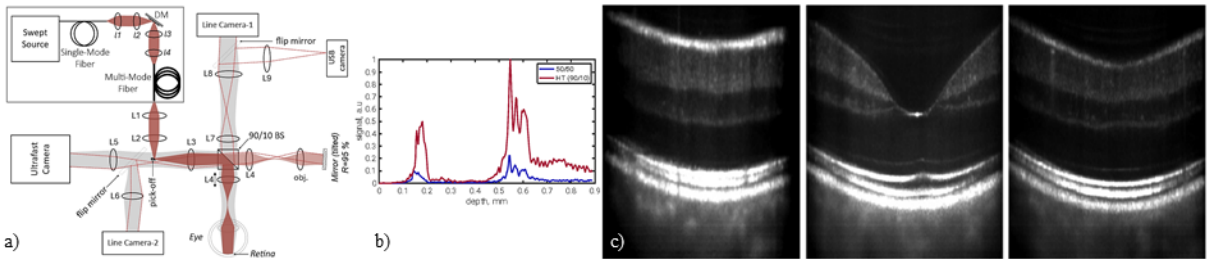


Fig. 1. (a) Principal system used. Comparison of in vivo human retina imaging with standard (b, blue curve) and high throughput S-TOCT (b, red curve) acquired with line cameras. (c) Retinal cross-sections acquired with HT mode and 2D camera.

The HT-STOC-T system achieves up to a 3.5× improvement in sensitivity (≈5.5 dB) compared to a conventional STOC-T configuration, reaching sensitivities close to 100 dB with moderate volume averaging [3]. In vivo retinal imaging confirms these findings: axial S-TOCT images reveal layered structures that are visible only in the HT configuration (Fig. 1b, c). In vivo retinal imaging using a 2D ultrafast camera demonstrates the practical impact of this sensitivity gain. Figure 1c shows three retinal cross-sectional (XZ) images acquired in HT mode with ultrafast 2D camera and centered around the macular region [3]. Each image represents a distinct cross-section through the retina. All major retinal layers—including the nerve fiber layer, inner and outer plexiform layers, the retinal pigment epithelium, and the choroid—can be clearly identified across the images, indicating improved depth-resolved contrast and signal quality throughout the retinal volume.

By substantially improving sensitivity while preserving ultrafast volumetric acquisition and computational aberration correction, the high-throughput STOC-T configuration enhances the capability of STOC-T for in vivo retinal imaging and low-signal biological applications.

[1] A. Dubois, L. Vabre, A.-C. Boccara, and E. Beaurepaire, "High-resolution full-field optical coherence tomography with a Linnik microscope," Applied Optics, vol. 41, no. 4, p. 805, Feb. 2002, doi: 10.1364/ao.41.000805.
[2] E. Auksorius and A. C. Boccara, "High-throughput dark-field full-field optical coherence tomography," Optics Letters, vol. 45, no. 2, p. 455, Dec. 2019, doi: 10.1364/ol.381888.
[3] K. Adomavičius, A. Trečiokaitė, E. Tarvydas, and E. Auksorius, "High-throughput spatio-temporal optical coherence tomography (STOC-T)," Optics Continuum, vol. 4, no. 9, p. 2099, Aug. 2025, doi: 10.1364/optcon.564109.

MULTINUCLEAR NMR STUDY OF THE $NA_{2.5}V_{1.5}TI_{0.5}(PO_4)_3$ AQUEOUS ELECTROCHEMICAL DEGRADATION

Aurimas Dubauskas[1], Nadežda Traškina[2], Jurgis Pilipavičius[2,3], Linas Vilčiauskas[2,3], Vytautas Klimavičius[1]

[1]Vilnius University, Faculty of Physics, Institute of Chemical Physics, Lithuania
[2]Center for Physical Sciences and Technology (FTMC), Vilnius, Lithuania
[3]Vilnius University, Institute of Chemistry, Lithuania
aurimas.dubauskas@ff.stud.vu.lt

Transition towards sustainable and renewable energy requires development of energy storage technologies such as Na-ion based batteries. Promising sodium ion batteries (SIB) are aqueous NASICON (Na Super Ionic CONductor) based batteries. NASICON materials feature a stable three-dimensional crystal structure, high ionic conductivity, thermal stability, and a wide range of redox potentials [1-3]. NASICON can be used as anodes, cathodes, solid electrolytes, or electrode coating materials in battery development. To efficiently and successfully use these technologies, it is necessary to understand the chemical processes that limit the effective usage time of the batteries. Solid-state Nuclear Magnetic Resonance spectroscopy can provide invaluable insights on the processes taking part in the solid-liquid interphases on the electrode. In addition, high-resolution (liquids) NMR is a powerful method to detect dissolved species in the electrolyte, thus giving insights on the solubility of the active electrode materials.

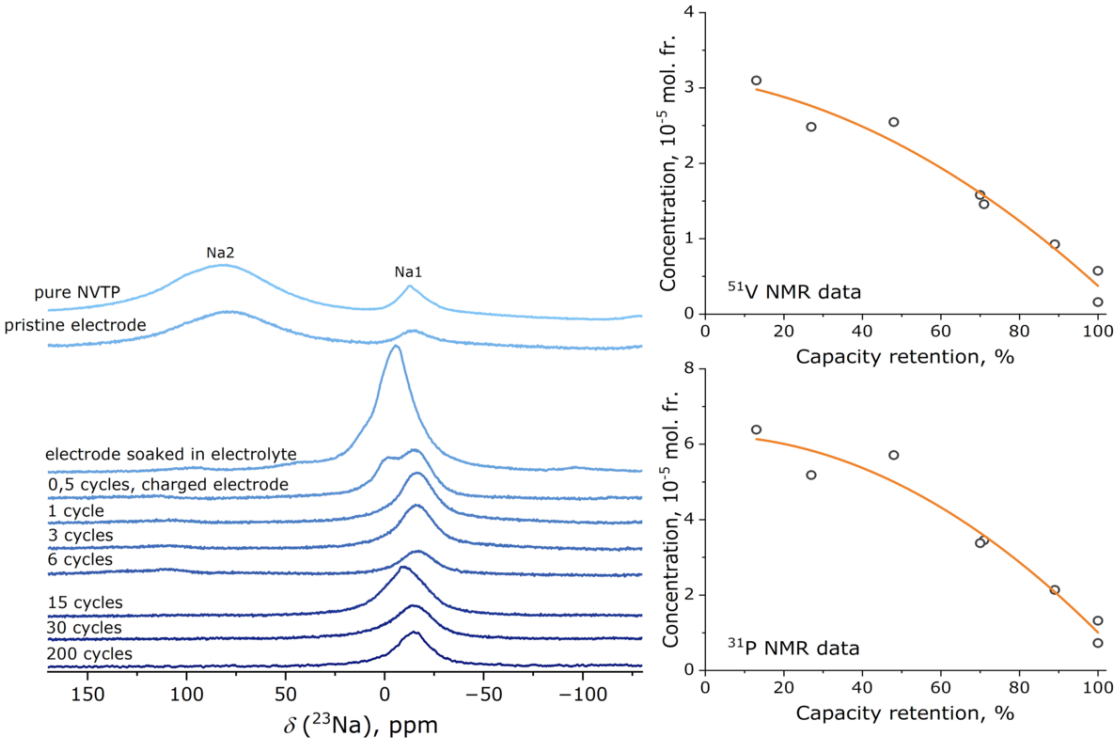


Fig. 1. Left - evolution of 23Na MAS NMR spectra during the GCD cycling. Right - calculated amount of vanadium and phosphate ions dissolved in the electrolyte solution upon GCD cycling.

In this study, we use multinuclear ^{31}P, ^{23}Na, ^{15}V, and ^{13}C *ex situ* solid state NMR of NVTP-based electrodes as well as ^{31}P and ^{15}V *ex situ* high resolution NMR of the electrolytes to analyze the degradation of the electrode material and the formation of the interphasial layers in aqueous electrolytes during electrochemical cycling. The obtained results provide some insights regarding the degradation products and processes in NVTP during its aqueous electrochemical operation.

[1] S. Chen et al., "Challenges and Perspectives for NASICON-Type Electrode Materials for Advanced Sodium-Ion Batteries," Advanced Materials, vol. 29, no. 48, p. 1700431, Dec. 2017.
[2] B. Singh et al., "A chemical map of NaSICON electrode materials for sodium-ion batteries," J. Mater. Chem. A, vol. 9, no. 1, pp. 281–292, Jan. 2021.
[3] G. Plečkaitytė et al., "Understanding and mitigation of NaTi2(PO4)3 degradation in aqueous Na-ion batteries," J. Mater. Chem. A, vol. 9, no. 21, pp. 12670–12683, Jun. 2021.

THE STUDY OF PROTEIN NMR RELAXATION - DURATION AND PRECISION CONSTRAINTS

Justinas Minkevičius[1], Marius Gedgaudas[2], Zigmantas Toleikis[2], Vytautas Petrauskas[2], Daumantas Matulis[2], Laurynas Dagys[1]

[1]Vilnius University, Institute of Chemical Physics, Lithuania
[2]Vilnius University, Life Sciences Center, Institute of Biotechnology, Department of Biothermodynamics and Drug Design, Lithuania
justinas.minkevicius@ff.stud.vu.lt

Nuclear magnetic resonance (NMR) relaxation measurements have become a powerful tool for probing protein dynamics, enabling the characterization of conformational exchange processes and kinetic behavior across a wide timescale ranging from picoseconds to milliseconds [1]. Such systems due to their size and spectral overcrowding are rarely analyzed using direct one-dimensional NMR spectroscopy. The use of higher-dimensional acquisition allows convenient spectral fingerprinting but inevitably leads to extended measurement time. Recently, researchers have found that overall time can be reduced by using sampling data points randomly. This so-called Non-Uniform-Sampling (NUS) in some cases can lead to even a 4-fold experimental time reduction but is a system-dependent parameter [2]. In this work we studied the experimental duration and precision by implementing NUS on a ^{15}N-labeled Carbonic Anhydrase II (CAII) protein. It is a well studied protein with determined backbone structure needed for peak selection and accessible 3D structure allowing it to be used as a benchmark system for method evaluation. CAII is one of the 14 isoenzymes of CAs that catalyze the reversible hydration of carbon dioxide to bicarbonate. Mutations in CAII in humans lead to osteopetrosis with renal tubular acidosis and cerebral calcifications, a disorder often associated with mental retardation [3].

The experiments involved measuring relaxation rate R_2 using Carr-Purcell-Meiboom-Gill (CPMG) method coupled with Heteronuclear Single Quantum Coherence (HSQC) pulse sequence. Measurements were performed on Bruker Avance Neo 600 MHz spectrometer equipped with a 5 mm high-resolution probe. The experimental duration was optimized by varying the level of NUS, number of scans and the number of data-points. The size of direct dimension for ^{1}H was fixed at 2 k. Acquired data were analyzed using CCPN software [4] for residuals peak position corrections and peak height calculation, and python, notably ”lmfit” and various other libraries for R_2 calculations and further results analysis. NMR peaks were assigned to different confidence limits, depending on spectral shape, positions and overlap. Peaks assigned to high confidence were compared between experiments.

We find that the errors of a single R_2 measurement do not highly depend on the level of NUS and number of scans used but the standard deviation of these experiments can vary. As these measurements are rarely repeated, the experimental precision can be easily overlooked and thus should be carefully noted. The presentation will focus and discuss the main factors contributing to precision and will inform our future studies.

[1] M. A. S. Hass and J. J. Led, “Evaluation of two simplified 15n-nmr methods for determining µs–ms dynamics of proteins,” Magnetic Resonance in Chemistry, vol. 44, no. 8, pp. 761–769, doi: 10.1002/mrc.1845
[2] T. E. Linnet and K. Teilum, “Non-uniform sampling of nmr relaxation data,” Journal of Biomolecular NMR, vol. 64, no. 2, p. 165–173, Feb. 2016, doi: 10.1007/s10858-016-0020-6
[3] E. Kida, S. Palminiello, A. A. Golabek, M. Walus, T. Wierzba-Bobrowicz, A. Rabe, G. Albertini, and K. E. Wisniewski, “Carbonic anhydrase ii in the developing and adult human brain,” Journal of Neuropathology Experimental Neurology, vol. 65, no. 7, pp. 664–674, 07 2006, doi: 10.1097/01.jnen.0000225905.52002.3e.
[4] S. P. Skinner, R. H. Fogh, W. Boucher, T. J. Ragan, L. G. Mureddu, and G. W. Vuister, “Ccpnmr analysisassign: a flexible platform for integrated nmr analysis,” Journal of Biomolecular NMR, vol. 66, no. 2, p. 111–124, Oct. 2016, doi: 10.1007/s10858-016-0060-y.

DIRECT LASER WRITING OF PLASMONIC GRATINGS: OPTICAL RESPONSE AND APPLICATIONS

Rodrigas Liudvinavičius[1], Evaldas Stankevičius[1]

[1]Center for Physical Sciences and Technology, Laser Technology Department, Vilnius, Lithuania
rodrigas.liudvinavicius@ftmc.lt

In recent years, nanotechnology has attracted significant attention due to the successful integration of plasmonic nanostructures into optical sensing platforms and advanced photonic devices. Metallic nanostructures, particularly those based on noble metals such as gold, exhibit strong plasmonic resonances arising from the interaction between electromagnetic radiation and collective electron oscillations. These properties make plasmonic gratings and periodic nanostructure arrays highly attractive for applications in sensing, spectroscopy, and nanophotonics.

Conventional fabrication of plasmonic nanostructures typically relies on electron-beam or focused ion beam lithography, which provide high resolution but are limited by low throughput, high cost, and limited scalability. In contrast, direct laser writing (DLW) has emerged as a versatile, mask-free, and chemically clean fabrication approach that enables fast fabrication of large-area plasmonic structures with controlled morphology. Based on recent experimental studies, this work focuses on the formation of plasmonic gratings composed of laser-induced micro- and nanostructures in thin metallic films using femtosecond laser pulses.

The research investigates the optical response of plasmonic gratings fabricated by DLW, exhibiting grating-coupled surface plasmon resonances and hybrid lattice plasmon modes [1, 2]. Recent results demonstrate that optimization of laser processing parameters allows the fabrication of highly uniform periodic arrays supporting narrow, high-quality plasmonic resonances. The influence of material choice, adhesion layers [1], and array geometry on resonance quality is discussed, highlighting strategies that improve both optical performance and structural integrity (resilience to the environment). Special attention is given to the role of array size and measurement conditions in evaluating plasmonic response. It is shown that resonance quality is not determined only by structure geometry, but also by the grating size. By matching array dimensions to the optical measurement beam and using measuring beam limiting diaphragms, fabrication time can be significantly reduced while preserving high-quality optical response [3].

The results demonstrate the potential of direct laser writing as a scalable method for plasmonic grating fabrication and open new possibilities for practical plasmonic devices in sensing [3], spectroscopy [4], and other fields.

Keywords: Lasers, Plasmonics, Resonance, Raman, Sensing

[1] R. Liudvinavičius, A. Selskis, and E. Stankevičius, “Titanium adhesion layer influence on the formation of hybrid lattice plasmon structures via laser-direct writing,” Optics & Laser Technology, vol. 175, p. 110807, Mar. 2024, doi: 10.1016/j.optlastec.2024.110807.

[2] R. Liudvinavičius, K. Vilkevičius, and E. Stankevičius, “High-quality grating-coupled surface plasmon resonances in silver and gold bumps arrays fabricated in thin metallic films using the third harmonic of femtosecond laser,” Applied Surface Science, vol. 711, p. 164127, Jul. 2025, doi: 10.1016/j.apsusc.2025.164127.

[3] R. Liudvinavičius and E. Stankevičius, “Influence of gold microbump array size on the hybrid lattice plasmon resonance quality,” Optical Materials, vol. 173, p. 117873, Jan. 2026, doi: 10.1016/j.optmat.2026.117873.

[4] M. Talaikis et al., “Femtosecond Laser-Induced nanostructures in copper film for UV-SERS,” ACS Applied Materials & Interfaces, vol. 18, no. 1, pp. 2501–2512, Dec. 2025, doi: 10.1021/acsami.5c21582.

RAPID FEMTOSECOND-LASER FABRICATION OF A PLASMONIC SENSOR FOR GLYCEROL DETECTION

Kernius Vilkevičius[1], Tomas Rakickas[2], Evaldas Stankevičius[1]

[1]Center for Physical Sciences and Technology, Department of Laser Technologies, Savanoriu Ave. 231, Lithuania
[2]Center for Physical Sciences and Technology, Department of Nanoengineering, Savanoriu Ave. 231, Lithuania
kernius.vilkevicius@ftmc.lt

Plasmonic nanostructures and their gratings attract a high interest due to their interactions with light at the nanoscale. Fast and repeatable fabrication of such structures is critical for practical applications and scalable mass production. While conventional lithographic or chemical techniques offer either high precision or simplicity, they are often limited in scalability, throughput, or repeatability. A proposed direct laser writing (DLW) [1] employing single femtosecond pulses for plasmonic array formation offers single-step fabrication with both high accuracy and reproducibility. Periodically arranged gold nanostructures' interaction with radiation results in the enhancement of local electromagnetic field and increased absorption at the resonant wavelengths. These phenomena are exploited in surface-enhanced Raman spectroscopy (SERS) and plasmonic sensing [2], therefore, the tunability of the produced structure properties are of high interest.

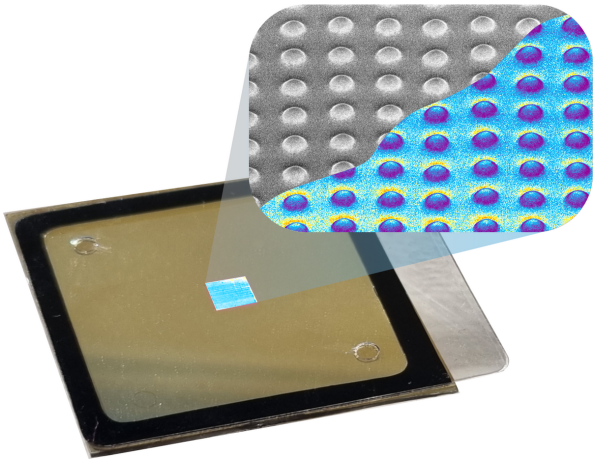


Fig. 1. Ag-Au nanobump sensing platform

Periodic plasmonic nanostructures on 50 nm thick gold, silver, and silver-gold bilayer films were fabricated by DLW using 343 nm femtosecond pulses. Changes in pulse energy impact the resulting morphology of the structure, thereby influencing the excitation and coupling of plasmonic modes [3]. While already effectively applied in SERS [4], such metallic arrays can also be used in sensing measurements. The optical response of the fabricated samples was characterized using spectroscopic techniques, revealing strong sensitivity to changes in the surrounding refractive index (RI), as the resonance shifts can be observed at various solutions to determine their concentration. Hemispherical bumps provide the sharpest resonant peaks and demonstrate remarkable peak redshift with increasing liquid RI, reaching a sensitivity of around 800 nm/RIU [5]. Individual resonant modes of both *s*- and *p*-polarizations have distinct sensitivities to glycerol solutions, with the most prominent response being for the out-of-plane origin resonance. By optimizing the angle of incidence, the sensing platform performance is further improved, reaching sensitivities of up to 933 nm/RIU and a figure of merit parameter of 57 RIU^{-1}. Such single-metal and bilayer nanobump platforms demonstrate excellent stability, repeatability, and durability, maintaining their optical properties for over six months, marking a potential for reliable and long-term accurate measurements.

The authors acknowledge the Research Council of Lithuania (LMTLT) for the received funding under project No. S-TPP-23-14.

[1] E. Stankevičius, K. Vilkevičius, M. Gedvilas, E. Bužavaitė-Vertelienė, A. Selskis, and Z. Balevičius, "Direct laser writing for the formation of Large-Scale gold microbumps arrays generating hybrid lattice plasmon polaritons in VIS–NIR range," Advanced Optical Materials, vol. 9, no. 12, Apr. 2021, doi: 10.1002/adom.202100027.
[2] K. Yang, X. Yao, B. Liu, and B. Ren, "Metallic Plasmonic Array Structures: Principles, fabrications, properties, and Applications," Advanced Materials, vol. 33, no. 50, May 2021, doi: 10.1002/adma.202007988.
[3] K. Vilkevičius, G. D. Tsibidis, A. Selskis, E. Stratakis, and E. Stankevičius, "Formation of highly tunable periodic plasmonic structures on gold films using direct laser writing," Advanced Optical Materials, vol. 12, no. 20, Apr. 2024, doi: 10.1002/adom.202400172.
[4] K. Vilkevičius, I. Ignatjev, A. Selskis, G. Niaura, and E. Stankevičius, "Tuning SERS performance through the laser-induced morphology changes of gold nanostructures," Applied Surface Science, vol. 660, p. 160003, Mar. 2024, doi: 10.1016/j.apsusc.2024.160003.
[5] K. Vilkevičius, T. Rakickas, and E. Stankevičius, "High-Quality Plasmonic Ag—Au Bilayer Nanobump Grating Sensor," Advanced Materials Technologies, vol. 10, no. 20, Aug. 2025, doi: 10.1002/admt.202501199.

ORAL SESSION 5

Chemistry

MODIFICATION OF SILICON OXIDE SURFACE WITH PHOSPHOLIPID BILAYERS FOR BIOSENSOR DEVELOPMENT

Anastasija Aleksandrovič[1], Aušra Valiūnienė[1], Gintaras Valinčius[2]

[1]Center for Physical Sciences and Technology, Department of Organic Chemistry, Vilnius, Lithuania
[2]Unaffiliated scientist
anastasija.aleksandrovic@ftmc.lt

Tethered phospholipid membranes (tBLMs) supported by self-assembled monolayers (SAMs) are gaining significant traction in the development of conductive biosensors. Tethered membranes offer a significant advantage over traditional black lipid membranes due to their enhanced mechanical stability and longevity. By anchoring the bilayer to the surface via silane chemistry, we create a sub-membrane space (a ”reservoir”) that mimics the aqueous environment of a cell, allowing for the potential integration of transmembrane proteins. Historically, gold has been the standard substrate for these systems, but it has some notable drawbacks: it is expensive and notoriously difficult to regenerate. As a result, metal oxides are emerging as a superior alternative. They offer a more budget-friendly foundation while providing the distinct advantage of easier membrane regeneration, making them a highly practical choice for next-generation biosensing applications [1-2].

This study explores the development and characterization of tethered bilayer lipid membranes (tBLMs) synthesized on silicon dioxide (SiO_2) substrates. By utilizing a silane-based self-assembled monolayer (SAM) as a foundational anchor, we aimed to create a robust, biomimetic platform capable of maintaining structural integrity across varying environmental conditions. The primary focus of this research was to evaluate the formation efficiency and stability of these membranes when subjected to different aqueous environments, specifically by modulating the buffer solution pH. The choice of a silicon-based substrate (specifically silicon plates coated with a precise SiO_2 layer) was strategic. This surface serves as a versatile interface that bridges the gap between solid-state electronics and biological systems. By leveraging the unique properties of SiO_2, we were able to employ a dual-mode analytical approach: electrochemical methods (used to probe the insulating properties, capacitance of the tBLM, providing insight into the ”sealing” quality of the membrane) and optical methods (utilized to monitor the thickness and viscosity ensuring a high degree of structural precision).

This multi-analytical framework not only validates the formation of the tBLM but also determines the operational limits of these sensors in varying chemical landscapes, paving the way for advanced applications in drug screening and biosensing.

[1] I. Gabriunaite, A. Valiūnienė, and G. Valincius, “Formation and properties of phospholipid bilayers on fluorine doped tin oxide electrodes,” Electrochimica Acta, vol. 283, pp. 1351–1358, May 2018, doi: 10.1016/j.electacta.2018.04.160.

[2] A. Aleksandrovic, I. Gabriunaite, G. Valincius, and A. Valiūnienė, “Regeneration of tethered bilayer lipid membrane biosensors for repetitive use in toxin detection,” Bioelectrochemistry, vol. 167, p. 109078, Aug. 2025, doi: 10.1016/j.bioelechem.2025.109078.

COMPARATIVE STUDY OF FC RECEPTOR BINDING AND IMMUNE MODULATION: NANOBODY-FC VS IgG IMMUNE COMPLEXES

Miglė Stančiauskaitė[1], Asta Lučiūnaitė[2], Mantvydas Usvaltas[3], Ieva Plikusienė[1]

[1]Lithuania, Vilnius University, Center of Nanotechnology and Materials Science - Nanotechnas
[2]Lithuania, Life Sciences Center, Institute of Biotechnology
[3]Lithuania, State Research Institute Center for Physical and Technological Sciences
migle.stanciauskaite@chgf.stud.vu.lt

Nanobodies (Nbs) are single-domain antibodies that are gaining traction in therapeutics and biosensing because they are small, robust, and can access cryptic epitopes[1]. When formatted as Fc fusions, Nbs can act as IgGs and trigger Fc receptor-driven responses to immune complexes (ICs). Here, we paired spectroscopic ellipsometry (SE) with quartz crystal microbalance with dissipation monitoring (QCM-D) to quantify binding kinetics and affinity, calculate dry mass, hydration, and map epitope relationships for Nb-Fc and SARS-CoV-2 spike (S) ICs engaging with FcγRI.

SE measured nanomolar IC-FcγRI dissociation constants, with Sb15/S exhibiting the strongest binding, comparable to IgGCR/S. QCM-D likewise showed pronounced FcγRI recognition of Sb/S complexes. Optical modeling of SE data indicated an FcγRI layer thickness of 3.3 nm and thinner IC layers for Nb complexes (18–22 nm) than for IgGCR/S (30 nm). The highest dry surface mass density was observed for Sb14/S (54.14 ng/cm^2), followed by CR3022/S (45.1 ng/cm^2), Sb15/S (39.06 ng/cm^2), and Sb68/S (30.68 ng/cm^2). Spike alone generated only a negligible QCM-D response and no dependable SE signal, consistent with FcγRI binding requiring pre-assembled ICs. Competitive QCM-D measurements further suggested that Sb14 and Sb15 share an epitope, whereas Sb68 targets a distinct region with partial overlap to human IgG CR3022.

In macrophage assays, Nb/S ICs were phagocytosed without induction of inflammatory cytokines, while spike alone entered predominantly via passive endocytosis. Only Sb15/S and Sb68/S increased CD83 (linked to inflammation resolution) and showed a trend toward elevated CCR2, whereas CD86, CCL5/CCR5, and CCL2 remained unchanged[2]. Notably, the largest/highest-affinity complexes did not increase CD83, implying that Fc-mediated signaling depends on IC architecture, not affinity alone.

Overall, Nb-based ICs engage FcγRI with IgG-like strength yet form thinner surface assemblies. SE/QCM-D readouts of IC structure provide a basis for selecting nanobodies to tune Fc-effector outcomes and deepen the knowledge on surface-assay design.

[1] M. I. Mustafa and A. Mohammed, “Nanobodies: A Game-Changer in Cell-Mediated Immunotherapy for Cancer,” SLAS DISCOVERY, vol. 28, no. 8, pp. 358–364, Aug. 2023, doi: 10.1016/j.slasd.2023.08.008.

[2] M. Luo et al., “CD83 mediates the inhibitory effect of the S1PR1 agonist CYM5442 on LPS-induced M1 polarization of macrophages through the ERK-STAT-1 signaling pathway,” International Immunopharmacology, vol. 143, no. Pt 3, p. 113526, Nov. 2024, doi: 10.1016/j.intimp.2024.113526.

DEVELOPMENT OF AN ADVANCED SURFACE ENGINEERED PLATINUM-BASED ELECTROCHEMICAL SYSTEM FOR ULTRA-SENSITIVE DETECTION OF MELOXICAM UTILIZING CHITOSAN TO SUPPRESS OXYGEN

Hassan Kouchakzadeh[1], Šarūnas Žukauskas[1]

[1]Department of Nanotechnology, State Research Institute Center for Physical Sciences and Technology, Sauletekio av. 3, Vilnius, LT-10257, Lithuania
hassan.kouchakzadeh@ftmc.lt

Rheumatoid Arthritis (RA) requires long-term management with Non-Steroidal Anti-Inflammatory Drugs (NSAIDs) like Meloxicam (MLX). It is a widely used NSAIDs and developing an electrochemical sensor for its sensitive detection is a strategic move to address the limitations of traditional pharmaceutical and clinical analysis [1-2]. While standard methods like High-Performance Liquid Chromatography (HPLC) are accurate, they are often time-consuming, expensive, and require sophisticated laboratory infrastructure [3]. In this work, an rGO/AuNPs electrochemical sensor for MLX is developed by the drug's intrinsic redox activity and the clinical need for rapid, cost-effective monitoring in arthritic patients as a theragnostic microneedle system (Figure 1). By replacing traditional, labor-intensive chromatographic methods with a portable electrochemical platform, real-time dosing adjustments can be made, enhancing therapeutic efficacy while minimizing systemic side effects. In this regard, for the designing and optimum fabrication of a high-performance nanocomposite transducer layer on a Platinum (Pt) electrode surface for MLX detection, graphene oxide (GO) concentration (0.5-1.5 mg/mL), HAuCl4 concentration (0.5-2.5 mM) and deposition time (100-500 second) considered as the independent variables considering the limit of detection (LOD) for MLX as the main response. Central Composite Design (CCD), which is more powerful than a Box-Behnken Design (BBD), is selected for design experiments [4]. For 3-factor optimization, a CCD designed 20 runs, 8 Factorial Points, 6 Axial (Star) Points, and 6 Center Points. A one-step potentiostatic co-reduction method [5] employs to achieve a high-performance rGO/AuNPs interface on a Platinum (Pt) electrode. The findings and optimum procedure ensure that the GO and Gold ions (Au3+) are reduced simultaneously, creating a cohesive, 3-dimensional conductive network suitable for highly sensitive MLX detection.

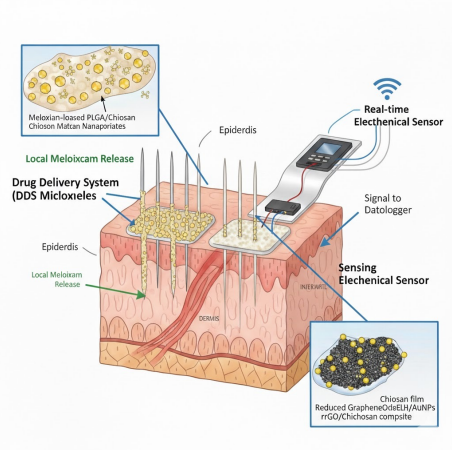


Fig. 1. schematic representation of theragnostic microneedle system

[1] J. S. Smolen, D. Aletaha, and I. B. McInnes, "Rheumatoid arthritis," The Lancet, vol. 388, no. 10055, pp. 2023–2038, May 2016, doi: 10.1016/s0140-6736(16)30173-8.
[2] Brune and P. Patrignani, "New insights into the use of currently available non-steroidal anti-inflammatory drugs," Journal of Pain Research, vol. 8, p. 105, Feb. 2015, doi: 10.2147/jpr.s75160.
[3] T. Lupoi, Y. R. Leroux, B. Feier, C. Cristea, and F. Geneste, "Electrochemical and photoelectrochemical aptasensors for the detection of environmental pharmaceutical pollutants," Electrochimica Acta, vol. 530, p. 146396, May 2025, doi: 10.1016/j.electacta.2025.146396.
[4] D. C. Montgomery, Design and analysis of experiments. John Wiley & Sons, 2017.
[5] C.-S. Lee, S. Yu, and T. Kim, "One-Step electrochemical fabrication of Reduced Graphene Oxide/Gold nanoparticles Nanocomposite-Modified electrode for simultaneous detection of dopamine, ascorbic acid, and uric acid," Nanomaterials, vol. 8, no. 1, p. 17, Dec. 2017, doi: 10.3390/nano8010017.

EFFECTIVE DEFECT DENSITY AS A PREDICTIVE METRIC FORREPRODUCIBLE TOXIN DETECTION IN TETHERED BILAYER MEMBRANES

Gerda Žižiūnaitė[1], Aušra Valiūnienė[1,2]

[1]Vilnius University, Faculty of Chemistry and Geosciences, Institute of Physical Chemistry, Lithuania
[2]State Research Institute Center for Physical Sciences and Technology, Lithuania
gerda.ziziunaite@chgf.stud.vu.lt

Tethered bilayer membranes (tBLMs) serve as mimetic platforms to study membrane-related phenomena, such as ions membrane-protein interactions. They consist of a solid substrate supporting a lipid bilayer, that is attached through molecular anchors. The anchors – such as polymers or self assembled silane or thiol monolayers – create a several nanometer aqueous reservoir that preserves bilayer fluidity and prevents direct contact between the substrate and membrane components, including transmembrane proteins commonly examined with tBLMs. The solid support provides stability and enables characterization by various methods. Conductive substrates, in particular, allow electrochemical analysis, with electrochemical impedance spectroscopy (EIS) offering a rapid, non invasive way to extract structural information. This makes EIS a promising tool for developing biosensors for pore forming toxins, which contribute to numerous diseases. One example is α hemolysin (αHL), a toxin implicated in sepsis, pneumonia, and related conditions. Although widely used, EIS analysis of tBLMs presents major challenges because the system's geometry introduces interpretive ambiguity. Ion movement in the submembrane space is restricted despite immersion in bulk electrolyte, and these conditions are not reliably captured by equivalent circuit models that assign fixed physical meaning to each element. In addition, poor tBLM reproducibility – arising from substrate roughness, stochastic anchor distribution, and variability in bilayer formation – leads to inconsistent responses to membrane active species. This variability, combined with the limitations of equivalent circuit models, complicates efforts to link initial membrane properties to their changes upon exposure to pore forming toxins during biosensor development. In this work we use a tBLM that consists of fluorine doped tin oxide (FTO) with a self-assembled monolayer of silane (the mixture of allyltrichlorosilane (ATS) and trichloro(3-(octadecylthio)propyl)silane (TOPS)) and a phospholipid bilayer made from 1,2-Dioleoyl-sn-glycero-3-phosphocholine (DOPC) and cholesterol. We analyze EIS data before and after incubation with αHL by employing a mathematical algorithm that represents the system as a probability distribution of defect density, P(N_{def}). Since the algorithm requires setting the resistance of the submembrane reservoir (ρ_{sub}), which cannot be unambigiously determined from EIS data because it scales co-linearly with the defect density, we introduce the concept of effective defect density N_{def}^{eff}, which is as close to the real physical parameter of defect density as the estimate of the value of (ρ_{sub}) is. While not providing the actual defect density values with certainty, N_{def}^{eff} scales linearly with the rate of α-hemolysin pore formation. As a result, the design of αHL biosensor whose response is predictable from the properties of the assembled tBLM is possible.

Keywords: Biosensors, tethered bilayer lipid membranes, pore-forming toxins, electrochemical impedance spectroscopy, alpha-hemolysin

HYBRID LIPID BILAYERS ON SILICON AS A PLATFORM FOR STUDYING PORE-FORMING TOXINS

Kajus Momgaudis[1], Aušra Valiūnienė[1]

[1]Vilnius University, Faculty of Chemistry and Geosciences, Department of Physical Chemistry, Vilnius, Lithuania
kajus.momgaudis@chgf.vu.lt

Research on phospholipid membranes is an essential subject for advancing the understanding of biological processes. The phospholipid bilayer is responsible for many crucial cell functions, including selective transport and protection against external agents. In this context, pore-forming toxins are of particular interest, as they directly compromise membrane integrity and serve as model systems for studying membrane disruption mechanisms [1] relevant to both pathology and antimicrobial activity. Phospholipid membrane models have been widely investigated on functionalized metal [2, 3] and metal oxide [4] surfaces. Silicon offers a well-defined and chemically versatile alternative, combining surface stability with tunable electrochemical properties. Its compatibility with controlled surface functionalization and semiconductor-based analysis enables systematic investigation of interfacial processes occurring at lipid membrane-solid interfaces.

The objective of this study was to form and characterize hybrid bilayer lipid membranes (hBLMs) composed of 1,2-dioleoyl-sn-glycero-3-phosphocholin (DOPC) on oxidized n-type silicon surfaces modified with an octadecyltrichlorosilane (OTS) self-assembled monolayer (SAM), and to investigate the concentration-dependent interaction of the pore-forming peptide, melittin, with these membranes.

Oxidized silicon wafers were functionalized with an OTS monolayer subsequently coated with a DOPC hBLM using the vesicle fusion technique [2]. Surface modification was evaluated using contact angle (CA) measurements and electrochemical impedance spectroscopy (EIS). EIS measurements were performed over a range of DC potentials to probe the change in interfacial resistance and capacitance of the surface after each modification step. The effect of melittin, the principal pore-forming component of bee venom [5], was assessed by exposing hBLMs to increasing peptide concentrations and monitoring the resulting changes in electrochemical response.

Successful formation of the silane-based SAM allowed for DOPC hBLM assembly and significantly altered both the surface chemistry and the electrochemical behavior of the semiconductor interface. EIS revealed characteristic impedance changes following monolayer and hBLM formation as well as disruption upon exposure to melittin. Melittin-induced defect formation led to a decrease in membrane resistance and changes in capacitance indicating increased ionic permeability. A clear correlation between the extent of membrane disruption and melittin concentration was observed.

These results demonstrate that oxidized n-type silicon functionalized with OTS provides a robust and reproducible platform for electrochemical studies of lipid membranes. The system enables sensitive detection of melittin-induced membrane damage and represents a promising approach for developing membrane-based sensing platforms relevant to toxin detection and membrane-active compound characterization.

[1] Rojko, N., & Anderluh, G. (2015). How Lipid Membranes Affect Pore Forming Toxin Activity. Accounts of Chemical Research, 48(12), 3073–3079. https://doi.org/10.1021/acs.accounts.5b00403

[2] Sabirovas, T., Valiūnienė, A., & Valincius, G. (2018). Mechanically Polished Titanium Surface for Immobilization of Hybrid Bilayer Membrane. Journal of The Electrochemical Society, 165(10), G109–G115. https://doi.org/10.1149/2.0101810JES/XML

[3] Sabirovas, T., Valiūnienė, A., & Valincius, G. (2021). Hybrid bilayer membranes on metallurgical polished aluminum. Scientific Reports 2021 11:1, 11(1), 1–11. https://doi.org/10.1038/s41598-021-89150-2

[4] Gabriunaite, I., Valincius, G., Žilinskas, A., & Valiūnienė, A. (2022). Tethered Bilayer Membrane Formation on Silanized Fluorine Doped Tin Oxide Surface. Journal of The Electrochemical Society, 169(3), 037515. https://doi.org/10.1149/1945-7111/AC5C96

[5] J. Chen, S. M. Guan, W. Sun, and H. Fu, “Melittin, the Major Pain-Producing Substance of Bee Venom,” Neurosci Bull, vol. 32, no. 3, p. 265, Jun. 2016, doi: 10.1007/S12264-016-0024-Y

ON-SITE DETECTION AND QUANTIFICATION OF SELECTED SEMI-SYNTHETIC AND NATURAL CANNABINOIDS IN CANNABIS PRODUCTS USING CAPILLARY ELECTROPHORESIS - DEEP UV FLUORESCENCE

Saari Anete Loog[1], Jelena Gorbatšova[1], Karoliin Remmelg[1], Maria Kuhtinskaja[1], Jekaterina Mazina-Šinkar[1]

[1]Estonia, Tallinn University of Technology, School of Science, Department of Chemistry and Biotechnology
saari.loog@taltech.ee

Hexahydrocannabinol (HHC) and tetrahydrocannabioctyl (THC-C8) are semi-synthetic cannabinoids (SSCs) that are increasingly added to cannabis products. These substances are often found in mislabelled and poorly regulated products, which have gained popularity—particularly among young people and children. Although frequently marketed as safe alternatives to Δ^9-tetrahydrocannabinol (Δ^9-THC), their psychotropic effects and potential health risks are often underestimated. Thus, the first aim of the study was to develop and validate a method for the rapid quantitative analysis of Δ^9-THC-C8, HHC, Δ^9-THC, and cannabidiol (CBD) in cannabis products that are suitable for use outside of traditional laboratory settings. The second aim was to screen some cannabis products and assess the method's practical applicability. For this purpose, a portable, in-house-built device based on capillary electrophoresis coupled with a deep-ultraviolet fluorescence detector was used. The developed methodology met the validation criteria. The validated method was applied to 16 cannabis products. In most cases, the declared cannabinoids were detected. However, the measured concentrations were significantly lower than those stated by the manufacturers. Current work presented the first opportunity to detect SSCs outside of the laboratory using a portable device operable by non-chemists. The device enables rapid on-site screening of cannabis products by law enforcement, particularly at events where such products are encountered. The methodology currently covers the two most prevalent SSCs and can be extended to include newly emerging cannabinoids.

ORAL SESSION 6

Materials Science and Nanotechnology

Chair: Dr. L. Grinevičiūtė

LASER ABLATION FOR RADIOACTIVE METAL SURFACE DECONTAMINATION

Jonas Jeffrey Haist[1,2], Vilnius Žalėnas[1], Anton Koroliov[1], Emilis Sadrejevas[1], Artūras Plukis[1]

[1]Center for Physical Sciences and Technology, Vilnius, Lithuania
[2]Vilnius University, Faculty of Physics, Vilnius, Lithuania
jonas.haist@ftmc.lt

Decommissioning nuclear power plants creates large quantities of radioactive metallic waste, 99% of which is classified as being of low or medium contamination [1], therefore suitable for deactivation and reusing. This study investigated the use of laser surface ablation as an alternative to existing techniques which generate significant secondary waste. For this study, a 200 W pulsed fiber laser (50 ns pulse duration, 150 kHz repetition rate, 0.1 mm spot size, 20 000 mm/s scanning speed), mounted on a mechanical platform, which could move 10 cm from the central position was used. A modified circuit breaker box was used for the cleaning chamber. Particles generated from laser ablation were removed from the chamber by a vacuum cleaner and filtered through a HEPA filter.

To analyze the ablation process, surface profiles were measured using an optical profilometer. A sample was prepared, consisting of 15 cleaned squares, 10 mm × 10 mm, on a rust-covered sheet of steel. The cleaned squares were produced at 3 distances away from the laser – at the focal point (210 mm from the laser), 215 mm and 205 mm. For each distance 5 different numbers of scans were performed: 1, 5, 10, 20 and 50. After performing the analyses, the results show that the greatest surface ablation with 50 scans was achieved with 210 mm distance cleaning (Figure 1a). The dependence of the ablation depth on the number of scans is logarithmic. The cleaning efficiency (depth per scan) decreases exponentially as the number of scans increases. In order to test deactivation efficiency, 6 non-core metal samples from Ignalina NPP were cleaned. A $CeBr_3$ gamma spectrometer mounted next to the laser was used to register the spectra of the samples during the cleaning process. The detector was calibrated using known sources of Cs-137 and Eu-152. Subsequently, the residue samples taken from the chamber walls were analyzed with an HPGe spectrometer (Figure 1b). The presence of Cs-137, Co-60 and Nb-94 confirmed removal from the surface, as these radionuclides do not appear naturally in such quantities [2].

Measured results showed an average dose rate reduction of 44%, Cs-137 surface activity reduction of 38%, and Co-60 reduction of 25%, with the best sample reaching 75% dose reduction. This confirms that surface ablation of contaminated metals removes not only rust but effectively cleans off radioactive particles. This leads us to believe that laser surface ablation is a practical and controlled method for radioactive metal surface deactivation [3], allows micrometer-scale surface layer removal and measurable reduction of radioactivity, making it a promising alternative for nuclear decommissioning waste treatment

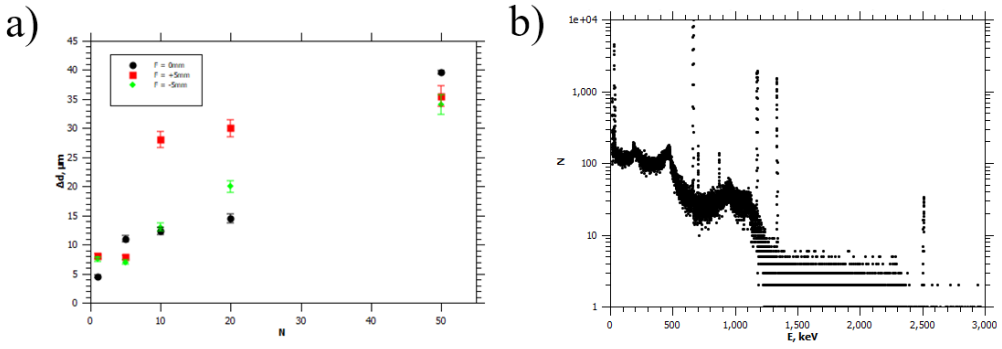


Fig. 1. a) Surface ablation depth dependence on number of scans b) Gamma spectrum of residue

Acknowledgements
A special thanks to the Research Council of Lithuania for funding provided via grant number P-REP-25-11

[1] R. Traboulsi, P. Lai, N. Tedford, M. Trovant, and N. Levin, "Metallic Low-Level Waste (LLW) Handling Options: An Optimal Life Cycle-Based Approach for North American Operations - 19413," Jul. 2019. [Online]. Available: https://www.osti.gov/biblio/23005316
[2] A.-M. Reinecke, M. Acker, S. Taut, M. Herrmann, W. Lippmann, and A. Hurtado, "Laser beam decontamination of metallic surfaces with a pulsed (150 W) Nd:YAG laser," Nuclear Engineering and Technology, vol. 55, no. 11, pp. 4159–4166, Aug. 2023, doi: 10.1016/j.net.2023.07.037
[3] K.-H. Song and J. S. Shin, "Surface removal of stainless steel using a single-mode continuous wave fiber laser to decontaminate primary circuits," Nuclear Engineering and Technology, vol. 54, no. 9, pp. 3293–3298, Apr. 2022, doi: 10.1016/j.net.2022.03.040

UV-SERS ON Cu, Co, AND Pd NANOSTRUCTURES FOR SELECTIVE DETECTION OF SMALL AROMATIC BIOMOLECULES

Martynas Talaikis[1], Evaldas Stankevičius[1], Rodrigas Liudvinavičius[1], Lina Mikoliūnaitė[1], Aikaterini-Maria Gkouzi[1], Shivani Yadav[2], Vladimir Sivakov[2], Gediminas Niaura[1]

[1]Center for Physical Sciences and Technology, Vilnius, Lithuania
[2]Leibniz Institute of Photonic Technology, Jena, Germany
martynas.talaikis@ftmc.lt

Surface-enhanced Raman spectroscopy (SERS) provides chemically specific molecular fingerprint information with sensitivity reaching the single-molecule level. Most SERS studies employ visible or near-infrared excitation; however, in these spectral regions fluorescence background and overlapping vibrational bands can reduce spectral contrast and limit discrimination between closely related biomolecules. In biomedical applications, these limitations are further compounded by substrate heterogeneity and the presence of complex biological matrices. Ultraviolet SERS (UV-SERS) addresses these constraints by exploiting the strong electronic absorption of aromatic biomolecules in the ultraviolet region, which selectively amplifies Raman scattering and improves molecular selectivity (Fig. 1). Many biologically and analytically relevant low-molecular-mass aromatics (nucleobases, aromatic amino acids, flavins, and numerous dyes) have strong electronic transitions in the UV. Thus, excitation at 229–325 nm can place these analytes under resonance or pre-resonance Raman conditions, producing strong, mode-selective amplification of vibrational bands that is not obtained for non-UV-active species. This is explicitly evidenced in your multiwavelength copper study, where π-conjugated analytes (adenine, guanine, riboflavin, 4-mercaptobenzoic acid) show pronounced UV and deep-UV enhancement, whereas an analyte lacking an extended π system (1-dodecanthiol) shows no vibrational signature bands, supporting the selectivity argument [1].

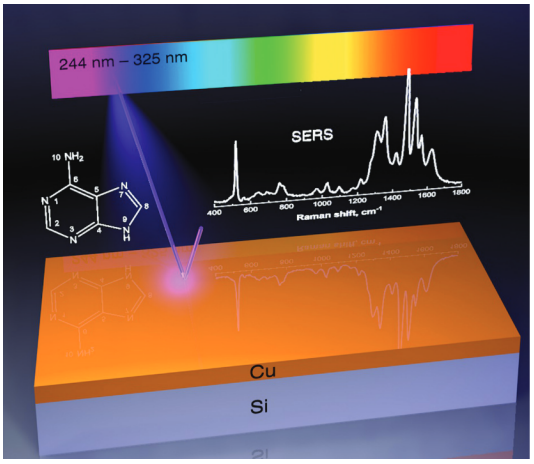


Fig. 1. A schematic representation of UV-SERS of copper-adsorbed adenine

UV-SERS was investigated on transition-metal (Cu, Co, and Pd) nanostructures with emphasis on experimentally validated enhancement mechanisms and substrate reproducibility. Femtosecond laser nanostructuring of 100 nm copper films produced morphology-dependent UV-SERS activity, with maximal adenine enhancement at 325 nm excitation observed for intermediate roughness surfaces exhibiting ring-like nanostructures [2]. Across all systems, reproducible UV-SERS signals were obtained with detection limits down to 10 μM for adenine and stability exceeding two months under ambient conditions. These findings establish copper, cobalt, and palladium-group nanostructures as chemically active, cost-effective UV-SERS substrates.

Acknowledgements

This work was supported by the Research Council of Lithuania (LMTLT) under an agreement number S-MIP-23-30 “Magneto-plasmonic nanoparticles for UV-SERRS detection of low-molecular-weight biomarkers (MAGUV-SERRS)”.

[1] S. Yadav, M. Talaikis, Y. V. Ryabchikov, M. Ziegler, G. Niaura, T. Deckert-Gaudig, V. Sivakov. “Copper-Based Multi-wavelength Ultraviolet Surface -Enhanced Resonance Raman Spectroscopy.” Advanced Optical Materials 2025, 13, 2500078. https://doi.org/10.1002/adom.202500078

[2] M. Talaikis, R. Liudvinavičius, E. Stankevičius, A. Selskienė, A. M. Gkouzi, T. Murauskas, V. Sivakov, G. Niaura. “Femtosecond Laser-Induced Nanostructures in Copper Film for UV-SERS.” ACS Applied Materials & Interfaces, 2026, acsami.5c21582. https://doi.org/10.1021/acsami.5c21582.

TERAHERTZ EMISSION FROM Bi/GaAs HETEROSTRUCTURES

Benas Stanionis[1], Vaidas Pačebutas[1], Ričardas Norkus[1], Arūnas Krotkus[1]

[1]Center for Physical Sciences and Technology, Department of Optoelectronics, Vilnius, Lithuania
benas.stanionis@ftmc.lt

Two-dimensional (2D) materials with atomic-scale thickness exhibit properties arising from quantum confinement and large surface to volume ratios. Thin bismuth (Bi) layers are particularly attractive for topological insulators, sensors, thermoelectric, and ultrafast optical devices. While bulk Bi is a semimetal, films thinner than 30 nm become semiconducting, with bandgaps tunable up to 0.8 eV in the ultrathin limit [1]. Bi growth has previously been demonstrated mainly on InAs, InP, and Si(111), with GaAs(111) also supporting high quality monolayer structures [2–4]. Under femtosecond excitation, Bi films can emit terahertz (THz) radiation through lateral photocurrents and nonlinear effects, while terahertz excitation spectroscopy (TES) enables investigation of band structure and carrier dynamics.

In this work, Bi layers were grown by molecular beam epitaxy on (100) oriented GaAs, a substrate orientation not previously reported. Heterostructures with 9 nm thick Bi layers were fabricated on semi-insulating, n-type, and p-type GaAs substrates. THz emission was studied as a function of excitation photon energy using femtosecond laser pulses in reflection geometry, with p-polarized light incident at 45° and constant average power of 20 mW. The excitation wavelength was tuned using an optical parametric amplifier.

The TES spectra revealed pronounced doping dependent behavior. Strong THz emission appeared only when photon energy exceeded the GaAs bandgap (1.42 eV), indicating that the dominant contribution originates from carrier dynamics within the GaAs substrate. Below this threshold, detectable THz emission was observed only for Bi/n-GaAs heterostructures. Opposite THz pulse polarities from n-type and p-type substrates were attributed to reversed internal electric fields at the Bi/GaAs interface, which drive photocurrent transients in opposite directions. Comparison with bare GaAs substrates estimated of the Bi optical absorption coefficient between 3×10^5 cm^{-1} and 4×10^5 cm^{-1} in the 1.5–1.7 eV range, which is over an order of magnitude higher than that of GaAs [5]. More pronounced deviations were observed for Bi semi-insulating GaAs, where excitation through the Bi layer reduced THz amplitude and reversed polarity near 1.7 eV, suggesting an additional emission mechanism associated with strong interfacial electric fields. Notably, Bi/p-GaAs heterostructures exhibited enhanced THz emission relative to bare p-GaAs, attributed to hole velocity overshoot in the strong internal electric field. Overall, thin Bi layers substantially modify THz emission through enhanced optical absorption and altered band alignment, highlighting Bi/GaAs heterostructures as promising platforms for efficient surface THz emitters.

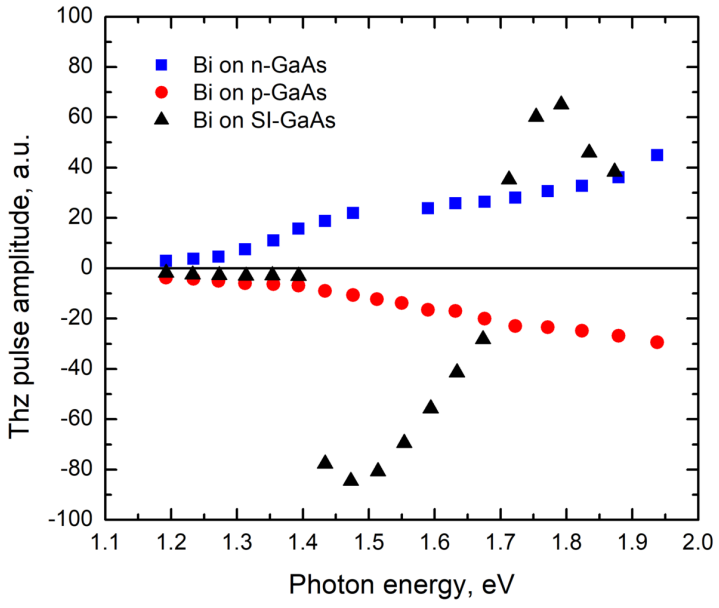


Fig. 1. THz excitation spectra of the heterostructures containing 9 nm thick Bi layers deposited on SI-GaAs, p-GaAs, and n-GaAs substrates.

[1] F. Reis et al., "Bismuthene on a SiC substrate: A candidate for a high-temperature quantum spin Hall material," Science, vol. 357, no. 6348, pp. 287–290, Jun. 2017, doi: 10.1126/science.aai8142.
[2] H. S. Inbar et al., "Inversion symmetry breaking in epitaxial Ultrathin Bi (111) films," arXiv (Cornell University), Feb. 2023, doi: 10.48550/arxiv.2302.00803.
[3] A. R. Jalil et al., "Phase-Selective Epitaxy of Trigonal and Orthorhombic Bismuth Thin Films on Si (111)," Nanomaterials, vol. 13, no. 14, p. 2143, Jul. 2023, doi: 10.3390/nano13142143.
[4] Y. Liu et al., "A 2D Bismuth-Induced honeycomb surface structure on GAAS(111)," ACS Nano, vol. 17, no. 5, pp. 5047–5058, Feb. 2023, doi: 10.1021/acsnano.2c12863.
[5] D. E. Aspnes, S. M. Kelso, R. A. Logan, and R. Bhat, "Optical properties of AlxGa1−x As," Journal of Applied Physics, vol. 60, no. 2, pp. 754–767, Jul. 1986, doi: 10.1063/1.337426.

METAMATERIAL-BASED BEAM-SHAPING STRUCTURES FEATURED BY HIGHER-ORDER RESONANCES IN THZ FREQUENCY RANGE

Andrius Masaitis[1,2], Vladislovas Čižas[1]

[1]Lithuania, Vilnius, Center for Physical Sciences and Technology, Department of Optoelectronics
[2]Lithuania, Vilnius University, Faculty of Physics
andrius.masaitis@ff.stud.vu.lt

Sub-terahertz (sub-THz) and terahertz (THz) frequency range, located between infrared and microwave frequency ranges, is becoming one of the main paths towards developing next generation devices for the huge amount of various applications [1]. Including imaging-related approaches as well as high-frequency communication systems, like 5G and 6G [2, 3]. Considering the data transmission, efficient beam-shaping is required to compensate the comparably high atmospheric absorption, which limits signal's path distance and lowers its intensity, especially in humid conditions. Metasurfaces, being considered as a viable alternative to the refraction-based beam-shaping solutions, experience fabrication difficulties at high-THz range due to the decreasing size of the metasurface--comprising metaatoms. In this work, higher modes of metasurfaces were investigated to evaluate their empolyment possibility in beam-shapping structures to achieve high intensity beam propagation signal and enhance directivity properties.

Employing complementary split-ring resonator (CSRR) metasurfaces six different metalense designs (T1 - T6) of varying geometrical parameters were investigated. Programming language's "Python" codes were written for C-shaped metaatom geometry-dependant resonance frequency analysis. Created designs were simulated using the Time Domain mode of the CST Studio Suite software and revealed focusing at 600 GHz. The particular frequency was selected as frequency of interest, as the resonator metaatom dimensions for the frequency are close to the limit of currently employed laser cutting system, but still large enough to ensure repeatability. Simulation results of the best-performing structures revealed full width at half maximum (FWHM) values of $FWHM_{K1}$ = 0.7 mm and $FWHM_{K2}$ = 0.6 mm, respectively and depth of focus values of DOF_{K1} = 2.7 mm and DOF_{K2} = 2.0 mm, respectively. Considering the wavelength of 0.5 mm, roughly equivalent to 1 full wavelength FWHM is considered close to optimal and represents the cases recorded during observation of the metalenses operating in the first order resonance conditions [4].

The exploitation of higher-order resonances of metaatoms in metasurface-based beam-shaping elements represents a promising approach for applications in the sub-THz and THz frequency ranges by demonstrating a near-wavelength-limited focusing performance. Employment of higher-order modes of the metaatoms is expected to extend the applicable frequency range of the laser-cut metasurface to at least several terahertz.

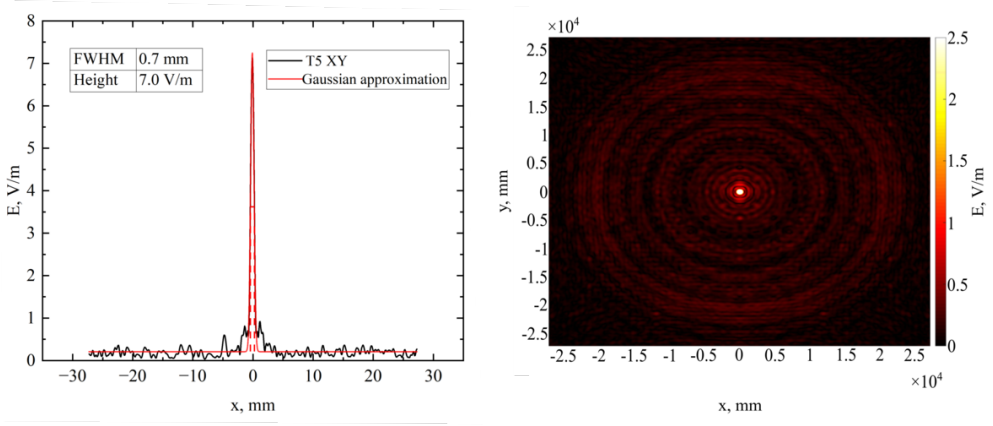


Fig. 1. Simulated electric field strength distribution map (left) and profile (right) at x-y plane - perpendicular to optical axis, located at the focal spot along the z axis of the element. Simulations performed using CST Studio Suite software. Gaussian approximation reveals FWHM = 0.7 mm value and peek signal intensity of 7 V/m.

[1] B. Ferguson and X.-C. Zhang, "Materials for terahertz science and technology," Nature Materials, vol. 1, no. 1, pp. 26–33, Sep. 2002, doi: 10.1038/nmat708.
[2] C. Yeh, G. D. Jo, Y.-J. Ko, and H. K. Chung, "Perspectives on 6G wireless communications," ICT Express, vol. 9, no. 1, pp. 82–91, Jan. 2022, doi: 10.1016/j.icte.2021.12.017.
[3] R. Appleby and H. B. Wallace, "Standoff detection of weapons and contraband in the 100 GHz to 1 THz region," IEEE Transactions on Antennas and Propagation, vol. 55, no. 11, pp. 2944–2956, Nov. 2007, doi: 10.1109/tap.2007.908543.
[4] R. Ivaškevičiūtė-Povilauskienė et al., "Flexible terahertz optics: light beam profile engineering via C-shaped metallic metasurface," Frontiers in Physics, vol. 11, May 2023, doi: 10.3389/fphy.2023.1196726.

2D-GRAPHENE SHIELDED GOLD METASURFACE FOR ENHANCED GREEN HYDROGEN EVOLUTION REACTION BY PHOTOELECTROCHEMICAL WATER SPLITTING

Muhammad Haris[1,2], Klaudijus Midveris[1,2], Syeda Ammara Shabbir[3,4], Carlos Ponce de Leon[3,4], Mohamed Ahmed Baba[2], Gvidas Klyvis[2], Algirdas Lazauskas[2], Erika Rajackaitė[2], Mindaugas Andrulevičius[2], Mindaugas Juodėnas[2], Asta Tamulevičienė[1,2], Tomas Tamulevičius[1,2], Sigitas Tamulevičius[1,2]

[1]Kaunas University of Technology, Department of Physics, Lithuania Studentų St. 50, LT, 51368, Kaunas, Lithuania
[2]Kaunas University of Technology, Institute of Materials Science, K. Baršausko St. 59, LT, 51423, Kaunas, Lithuania
[3]Forman Christian College, Department of Physics, Lahore, Pakistan
[4]University of Southampton, Faculty of Engineering and Physical Sciences, Southampton, SO17 1BJ, UK
muhhar@ktu.lt

This study presents a novel design of a graphene-capsulated gold plasmonic ordered nanoparticle (NP) array on conductive oxide as a photoelectrode for enhanced hydrogen evolution reaction (HER) via photoelectrochemical (PEC) water splitting. The 100 nm diameter and 400 nm pitch Au NP array self-assembled in the template and transferred on the fluorine tin oxide-coated glass substrate (FTO) substrate exhibited a shift from conventional surface lattice resonance to a hybrid plasmonic wave-guided mode at 631 nm wavelength .The microwave-enhanced chemical vapour deposition grown of a single atomic layer graphene film acted as a protective barrier for Au NPs, stabilized Fermi level pinning, and improved the junction from Schottky to ohmic, enabling faster charge transfer through thermionic and quantum tunneling effects. The photoelectrode with Au NP metasurface on FTO substrate with graphene film as a shielding barrier on top (FTO/Au(Metasurface)/G1L) achieved superior HER performance with an onset potential of −0.55 V(Ag/AgCl) and a photocurrent of −0.36 mA/cm2 under visible light. A maximum photocurrent of −6.2 mA/cm2 obtained under visible-light excitation confirms that HER solely originated from photoinduced excitation. This high activity resulted from rapid interband transitions in Au NPs, which generated hot carriers and promoted efficient charge mobility. Graphene semi encapsulation retained and protected Au NPs and their intrinsic plasmonic attributes in an electrochemical environment while enhancing photocatalytic kinetics. Overall, PEC tests confirmed that this tailored electrode minimized charge recombination, ensured steady current under bias, and delivered excellent solar-to-hydrogen performance with 0.35% applied bias photon-to-current efficiency, 70% external quantum efficiency, and nearly 100% internal quantum efficiency. This makes the FTO/Au(Metasurface)/G1L a promising photocathode for efficient and stable green hydrogen production.

Acknowledgements
This project has received funding from the Research Council of Lithuania (LMTLT), agreement no S-MIP-23-93

Keywords: Gold nanoparticles array, Surface lattice resonance, Capillarity-assisted particle assembly, Hybrid waveguided plasmonic mode, Graphene, Fermi level pinning, Helmholtz layer, Hydrogen evolution reaction, Thermionic emission, Thermionic field emission,

EFFICIENT THIRD-GENERATION BLUE OLEDS USING DIBENZOFURAN-BASED HIGH-TRIPLET-ENERGY HOSTS

Kristupas Bagdonas[1], Goda Grybauskaitė[1], Domantas Berenis[1], Gediminas Kreiza[1], Edvinas Orentas[2], Eigirdas Skuodis[3], Karolis Kazlauskas[1], Dovydas Banevičus[1]

[1]Vilnius University, Faculty of Physics, Institute of Photonics and Nanotechnology, Vilnius, Lithuania
[2]Vilnius University, Faculty of Chemistry, Department of Organic Chemistry, Vilnius, Lithuania
[3]Kaunas University of Technology, Faculty of Chemical Technology, Department of Polymer Chemistry and Technology, Kaunas, Lithuania
kristupas.bagdonas@ff.vu.lt

In the field of organic light-emitting diodes (OLEDs), thermally activated delayed fluorescence (TADF) has become an established pathway toward 100% internal quantum efficiency [1]. However, optimal device performance typically requires emitter to be doped in a suitable host matrix to suppress aggregation. The host should also provide balanced charge-carrier transport and a sufficiently high triplet energy to confine triplet excitons on the emitter and prevent back energy transfer to the matrix [2].

The aim of this research was to investigate four molecules composed of biphenyl core and dibenzofuran fragments with or without tert-Butyl units (Fig. 1A) as potential OLED host materials. OLED's and single carrier devices were fabricated by physical vapour deposition with DMeCzIPN employed as the emitter [3].

All organic diodes exhibited a turn-on voltage of 3.25 V and had emission peak in range 483–488 nm. The OLED's with 4FH matrix reached external quantum efficiency of 23.4% (Fig. 1B), luminous efficiency of 59 lm/W and had LT50 lifetime of 17.5 h at 1000 cd/m2 initial brightness. Having highest triplet energy of 2.87 eV this host was able to successfully confine excitation on emitter thus reducing exciton buildup preventing device nonradiative relaxation and degradation.

While the remaining compounds 2FH, 2FBu and 4FBu poses similar triplet energies to the emitter the differences in lifetime and efficiencies can be attributed primarily to carrier imbalance in the emissive layer. The addition of tert-butyl groups increased electron mobility up to four orders of magnitude (Fig. 1C) which results in localizing the exciton recombination zone close to hole transport layer [4]. This crowding increases the probability of destructive bimolecular interactions that accelerate device degradation.

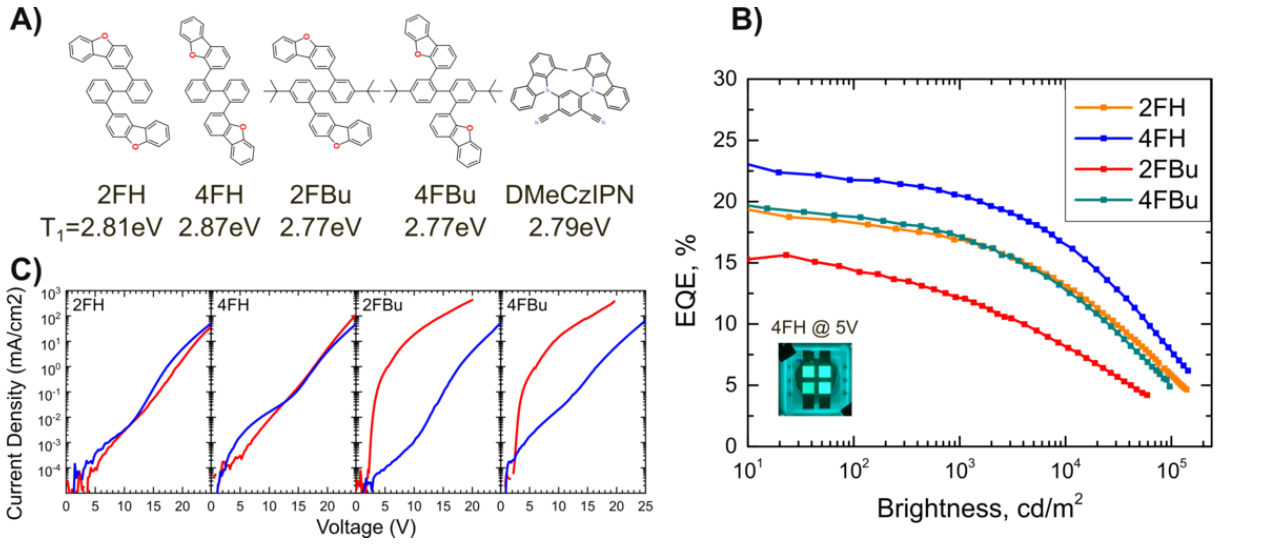


Fig. 1. A) the chemical structures and triplet energies of hosts and emitter molecules, B) OLED external quantum efficiency dependence on brightness, C) Current densities of electron and hole single carrier devices

The specific connection of the dibenzofuran unit to the biphenyl core in the 4FH molecule results in a higher triplet energy, making this host particularly well suited for blue emitters. While, the introduction of tert-butyl groups in this class of molecules promotes more n-type transport behaviour and can lead to a reduction in triplet energy.

Keywords: OLED, TADF, Blue, Hosts

[1] J. M. D. Santos et al., "The Golden Age of thermally Activated Delayed Fluorescence Materials: Design and exploitation," Chemical Reviews, vol. 124, no. 24, pp. 13736–14110, Dec. 2024, doi: 10.1021/acs.chemrev.3c00755.
[2] K. M. Youn et al., "High triplet energy bipolar host materials with the combination of dibenzofuran and benziimidazobenzoimidazole moieties for blue thermally activated delayed fluorescence emitter," Journal of Materials Chemistry C, vol. 8, no. 39, pp. 13811–13818, Jan. 2020, doi: 10.1039/d0tc02884c.
[3] G. Kreiza et al., "High efficiency and extremely low roll-off solution- and vacuum-processed OLEDs based on isophthalonitrile blue TADF emitter," Chemical Engineering Journal, vol. 412, p. 128574, Jan. 2021, doi: 10.1016/j.cej.2021.128574.
[4] M. Xu et al., "Analyzing exciton distribution in organic light-emitting devices using near-infrared probes," Applied Physics Letters, vol. 122, no. 26, Jun. 2023, doi: 10.1063/5.0155469.

ORAL SESSION 7

Chemistry

Chair: Dr. R. Bukšnaitienė

ELECTROCHEMICAL FERRIER REARRANGEMENT IN FLOW

Mihhail Fokin[1], Pallav Suman[1], Daniele Mazzarella[2], Maksim Ošeka[1]

[1]Tallinn University of Technology, School of Science, Department of Chemistry and Biotechnology, Estonia
[2]University of Rome Tor Vergata, Department of Chemical Sciences and Technologies, Italy
mifoki@taltech.ee

Synthetic organic chemistry is a crucial field of research, as it provides methods for the synthesis of a wide range of chemical compounds, including those used in industrial processes, biologically active molecules, and pharmaceutical drugs. As multiple synthetic routes often exist for any given compound, electrochemistry enabled in continuous-flow processes stands out as an exceptional approach for accessing certain compounds, offering very high productivity while remaining environmentally friendly.

Herein, we report a flow-enabled electrochemical Ferrier rearrangement (**Fig. 1**), a transformation that typically relies on stoichiometric amounts of toxic oxidants or strong acids, but in our case performed with only catalytical amount of charge and electrolyte.[1] This work demonstrates how medically relevant compounds, such as 2,3-unsaturated glycosyl derivatives, can be obtained using electrochemistry integrated into a continuous-flow process. This approach not only outperforms the earlier batch version of the transformation in terms of yield and productivity, but also represents a significant advancement in the field of flow electrochemistry research.[2]

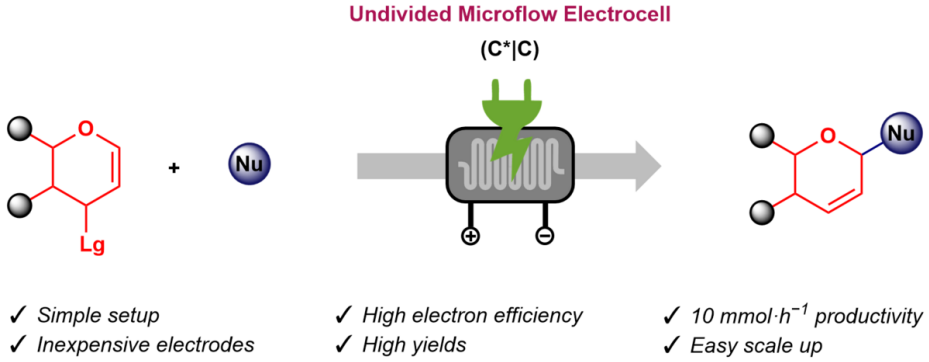


Fig. 1. Flow-enabled electrochemical Ferrier rearrangement

Acknowledgements

This work was supported by the Ministry of Education and Research of Estonia through the Centre of Excellence in Circular Economy for Strategic Mineral and Carbon Resources (SOURCES, TK228, 01.01.2024–31.12.2030) and by the Estonian Research Council grants (PSG828, PRG1031 and Estonian sub-project ETAG24073 of NordForsk project AGRI-WASTE2H2). The authors would also like to thank the Department of Chemistry and Biotechnology for supporting the conference visit, and Nora Deil for the assistance with disaccharide synthesis.

Keywords: Organic chemistry, Flow synthesis, Flow electrochemistry, electrochemical synthesis, sugar chemistry, Ferrier rearrangement

[1] P. Suman, M. Fokin, K. H. Hunt, T. Kanger, D. Mazzarella, M. Ošeka, “Electrochemical Ferrier rearrangement of glycals in flow”, Communications Chemistry, accepted.
[2] C. Qi, G. Goti, A. Sartorel, L. Dell’Amico, and D. Mazzarella, “Electrochemical ferrier rearrangement of glycals,” Organic Letters, vol. 26, no. 43, pp. 9328–9333, Oct. 2024, doi: 10.1021/acs.orglett.4c03511.

PHOTOREDOX MANIFOLD FOR DEHYDROGENATIVE COUPLING USING PROTONS AS OXIDANTS

Jonas Žurauskas[1], Paulius Vaickūnas[1], Gustautas Snarskis[3], Nojus Radzevičius[1], Barbara Chatinovska[1], Gediminas Kreiza[2], Steponas Raišys[2], Mantas Šimėnas[2], Vidmantas Kalendra[2], Kęstutis Zakarauskas[4], Karolis Kazlauskas[2], Edvinas Orentas[1]

[1]Vilnius University, Department of Organic Chemistry, Vilnius, Lithuania
[2]Vilnius University, Faculty of Physics, Vilnius, Lithuania
[3]Biomatter, Business Stadium West, Vilnius, Lithuania
[4]Lithuanian Energy Institute, Kaunas, Lithuania
jonas.zurauskas@chgf.vu.lt

The direct coupling of two unfunctionalized molecules under mild conditions embodies an ideal in synthetic chemistry. In this study, we report a metal-free photocatalytic process for arene C-H functionalization that employs an acridinium-type catalyst and produces dihydrogen as the only by-product. Throughout the catalytic cycle, the catalyst acts as an oxidizing agent, a hydrogen atom transfer agent, and a proton-reducing agent, enabling a cross-dehydrogenative transformation without the need for external oxidants. The reaction is conveniently performed using visible light, and the high oxidation potential of the catalyst allows it to engage even electron deficient arene substrates. The catalytic mechanism disclosed herein can become a general logic for developing various cross-dehydrogenative reactions adaptable for pharmaceutical and material sciences.

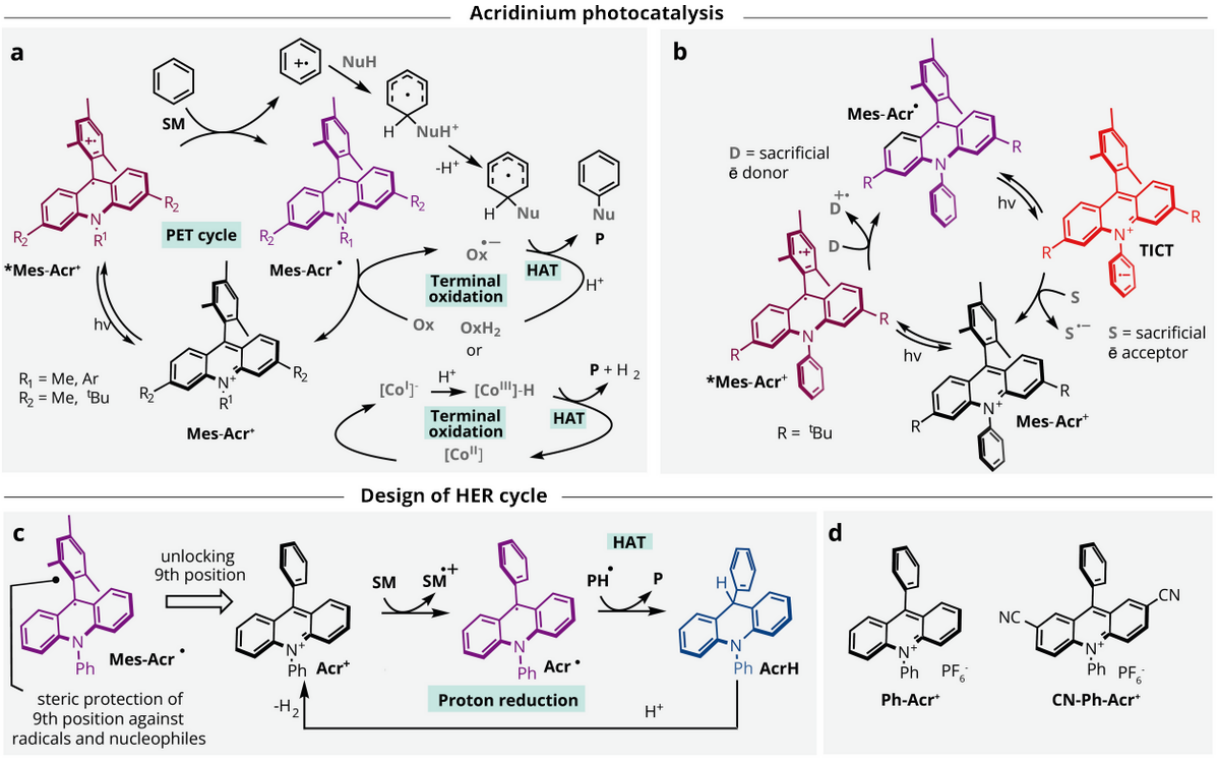


Fig. 1. Established and hypothesized reactivity modes of acridinium photocatalysis. a, A photocatalytic cycle based on reductive photocatalyst quenching. The regeneration of the catalyst is achieved either by sacrificial oxidant or cobalt-mediated dihydrogen formation. **b**, Exploration **5** of excited acridine radical as a potent reductant. **c**, Design of acridinium catalyst for hydrogen atom transfer and proton reduction to produce dihydrogen during the turnover (hydrogen evolution reaction (HER) cycle). **d**, Chemical structures of the photocatalysts. Mes, mesityl; SM, starting material; P, product

Acknowledgements

Financial support for this work was provided by the “Universities Excellence Initiative” programme by the Ministry of Education, Science, and Sports of the Republic of Lithuania under the agreement with the Research Council of Lithuania (project No. S-A-UEI-23-6). This work was partially supported by the project ”Industry 4.0 Lab Platform: EDIH VILNIUS” Nr. 02-016-P-0002. We thank the Arqus Talent Scholarship Fund for fellowship support for J.Ž.

[1] Žurauskas, J. et al. Electron-poor acridones and acridiniums as super photooxidants in molecular photoelectrochemistry by unusual mechanisms. Angew. Chem. Int. Ed. 62, e202307550 (2023).
[2] X. Yang et al., “Toward organic photohydrides: Excited-state behavior of 10-methyl-9-phenyl-9,10-dihydroacridine,” J. Phys. Chem. B, vol. 117, pp. 15290–15296, 2013.
[3] N. A. Romero, K. A. Margrey, N. E. Tay, and D. A. Nicewicz, “Site-selective arene C–H amination via photoredox catalysis,” Science, vol. 349, pp. 1326–1330, 2015.

QM/MD STUDY OF STRUCTURE AND NMR SPECTRA OF TETRAPEPTIDE IN AQUEOUS IONIC LIQUID MIXTURES

Amina Elkady[1], Žyginta Murnikova[2], Kęstutis Aidas[2]

[1]Vilnius University, Faculty of Chemistry and Geosciences, Institute of Chemistry, Lithuania
[2]Vilnius University, Faculty of Physics, Institute of Chemical Physics, Lithuania
amina.elkady@chgf.stud.vu.lt

Ionic liquids (ILs) have been known as “green” and biocompatible solvents for quite some time and their possible biological uses include making molecules permeate more easily through membranes, changing catalytic activity of enzymes, as well as stabilizing or destabilizing various proteins [1]. The nature of the interactions between ILs and proteins varies and is difficult to evaluate. Therefore, smaller peptides with amino acid sequences common in proteins are often used as model systems to discover how different ILs interact with these peptides and change their structure in aqueous solution. Nuclear magnetic resonance (NMR) spectroscopy is the method best suited for identifying both intermolecular interactions and intramolecular structural changes, since the chemical shifts of atoms, particularly hydrogen, are highly sensitive to changes in the local environment of the peptide.

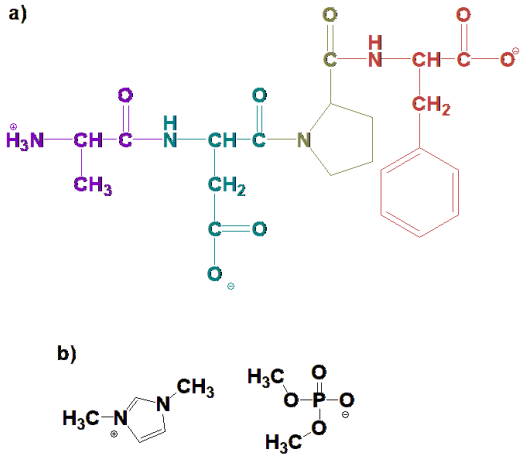


Fig. 1. Structural formulas of a) peptide Ala-Glu-Pro-Phe, b) 1,3-dimethylimidazolium dimethyl phosphate.

In this work, *trans*– and *cis*– Ala-Asp-Pro-Phe tetrapeptides were investigated using molecular dynamics (MD) simulations and quantum mechanics/molecular mechanics (QM/MM) calculations in both aqueous environment and in IL/water mixture. Such systems were analysed experimentally using NMR methods before [2], showing a difference of the peptide’s hydrogen atoms depending on its’ surroundings. The chosen ionic liquid [MMIM][DMP] constituted of 1,3-dimethylimidazolium and a common IL anion dimethyl phosphate. Computed chemical shift differences of atoms enabled us to evaluate various interactions present in peptide/IL/water systems. Meanwhile, trajectories from the MD simulations revealed structural changes in the peptide itself, as well as differences in its immediate surroundings.

Acknowledgements

This study was supported by the Research Council of Lithuania, grant no. S-MIP-22-74. Computations were performed on resources provided by the High-Performance Computing Center “HPC Saulėtekis” at Vilnius University, Lithuania.

[1] [1] J. M. Gomes, S. S. Silva, and R. L. Reis, “Biocompatible ionic liquids: fundamental behaviours and applications,” Chem. Soc. Rev., vol. 48, no. 15, pp. 4317–4335, 2019, doi: 10.1039/C9CS00016J.

[2] [1] A. Richardt, C. Mrestani-Klaus, and F. Bordusa, “Impact of ionic liquids on the structure of peptides proved by HR-MAS NMR spectroscopy,” J. Mol. Liq., vol. 192, pp. 9–18, Apr. 2014, doi: 10.1016/j.molliq.2013.12.027.

GREEN AND SUSTAINABLE EXTRACTION OF MULTIFUNCTIONAL BIOACTIVE INGREDIENTS USING NATURAL DEEP EUTECTIC SOLVENTS FOR PHARMACEUTICAL APPLICATIONS

Sana Abbas[1], Petras Rimantas Venskutonis[1], Luana Cristina dos Santos[2], Elena Ibáñez[2]

[1]Lithuania, Kaunas University of Technology, Department of Food Science and Technology,
[2]Spain, Institute of Food Science Research (CIAL, CSIC), Foodomics Lab
sana.abbas@ktu.edu

Growing interest in green solvents for the recovery of bio-actives from natural sources is a result of the growing need for environmentally friendly and sustainable extraction processes. This study applied the green and sustainable extraction of multifunctional bioactive ingredients using, natural deep eutectic solvents (NADES) as an attractive alternatives of traditional organic solvents. Four NADES namely, Choline Chloride: Lactic Acid (ChCl:LA), Choline Chloride: Acetic Acid (ChCl:AA), Choline Chloride: Citric Acid (ChCl:CA), and Choline Chloride: Propylene Glycol (ChCl:PG), along with propylene glycol (PG) were selected for the extraction of antioxidant-rich fractions from Paeonia officinalis and Paeonia anomala leaves and roots. Ultrasound-assisted probe extraction (5 min, 35% amplitude) with NADES was used for the extraction of phenolic rich fractions and NADES were removed using solid-phase extraction (SPE). Pressurized Liquid Extraction (PLE) with conventional solvent 75% ethanol was used as a reference method. All the extracts were analyzed for total phenolic content (TPC), total flavonoid content (TFC), and antioxidant activity using ABTS and ORAC assays. In most of the samples the highest TPC was expressed by ChCl:PG other than P. officinalis leaves. TFC results indicated ChCl:AA as the most effective solvent. ChCl:PG also showed superior ABTS radical scavenging activity across all tested leaves and roots samples than other NADES, whereas ORAC trends varied by species. UHPLC-ESI-QTOF-MS/MS analysis revealed that NADES extracts were richer in phenolics than PLE extracts with conventional solvents. Overall, ChCl:PG provided the most selective antioxidant-rich extracts, demonstrating the potential of polyol-based NADES as sustainable, selective alternatives to conventional solvents and advanced extraction techniques such as PLE.

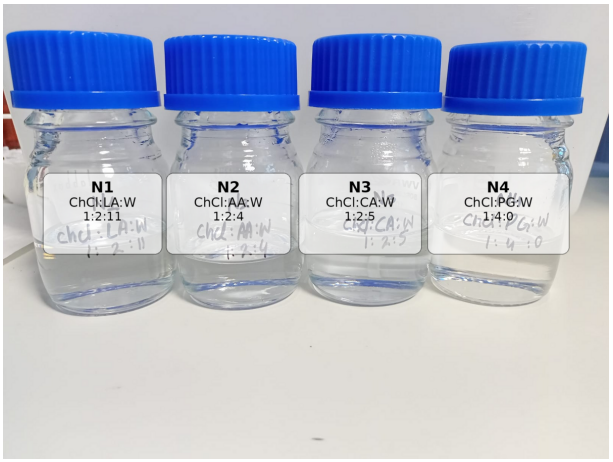


Fig. 1. NADES prepared in the laboaratory for the extraction of phytochemicals

Keywords: Paeonia officinalis, Paeonia anomala, antioxidant activity, NADES, PLE, UAE.

APPLICATION OF CALCIUM OXIDE WASTE FOR THE SYNTHESIS OF HIGHER BASISITY CALCIUM SILICATEHYDRATES (CaO/SiO_2 =1.5)

Ramune Sidaraite[1], Kestutis Baltakys[1], Tadas Dambrauskas[1]

[1]Kaunas University of Technology, Department of Silicate Technology, Kaunas, Lithuania
ramune.sidaraite@ktu.lt

The application of industrial wastes is a very challenging process because their chemical composition, as well as their chemical and physical properties, depend on the industrial process [1]. Calcium-containing industrial wastes are a promising source for the synthesis of calcium silicate hydrates, as they enable not only the reuse of waste material but also a decrease in CO_2 emissions due to the calcination of calcium carbonate [2]. One of the industrial wastes that has potential as a source of calcium is calcium oxide waste from sugar production. It is estimated that the amount of this waste is 5-6 mass percent of the amount of sugar produced [3]. To our knowledge, there is no information in the scientific literature regarding the application of this waste for the production of calcium silicate hydrates or calcium silicates, which are widely used in environmentally friendly technologies. Therefore, this work aimed to evaluate the potential for reusing calcium oxide-rich waste from the sugar industry for the hydrothermal synthesis of higher-basicity calcium silicate hydrates.

For the synthesis of calcium silicate hydrates, a mixture of quartz sand (98.5 wt% SiO_2) and calcium oxide-rich waste (91.8 wt% CaO) from sugar production was used. Quartz sand and waste were mixed to obtain a mixture with a molar ratio of CaO/SiO_2 equal to 1.5. The dry primary mixture was mixed with distilled water to reach a water-to-solid ratio of 10.0:1.0. The hydrothermal synthesis was carried out under saturated steam pressure at 200 °C, with reaction durations ranging from 0 to 72 hours.

It was determined that quartz and calcium oxide fully reacted after 4 hours of hydrothermal synthesis at 200 °C, resulting in the formation of anhydrous calcium silicate pavlovskyite ($Ca_8Si_5O_{18}$). The increase in synthesis duration led to the formation of a mixture of calcium silicates and calcium silicate hydrates consisting of xonotlite, kilchoanite, scawtite, and/or pavlovskyite. It was determined that the thermal stability of the synthesis products was strongly affected by the phase composition.

The obtained results showed that calcium oxide waste from sugar production can be used as a calcium source for the synthesis of calcium silicate hydrates.

Acknowledgements

This project has received funding from the Research Council of Lithuania (LMTLT), agreement No S-MIP-25-4

[1] A. Gil, “Challenges on waste-to-energy for the valorization of industrial wastes: Electricity, heat and cold, bioliquids and biofuels,” Environmental Nanotechnology Monitoring & Management, vol. 17, p. 100615, doi: 10.1016/j.enmm.2021.100615

[2] H. H. Abo-Almaged, R. E. A. Ngida, N. A. Ajiba, H. E. H. Sadek, and R. M. Khattab, “Utilization of industrial waste materials for the preparation of wollastonite by temperature-induced forming technique,” Scientific Reports, vol. 14, no. 1, p. 21752, Sep. 2024, doi: 10.1038/s41598-024-71243-3.

[3] F. A. Mostafa, A. N. Gad, A.-A. M. Gaber, and A.-M. A. Abdel-Wahab, “Preparation, Characterization and Application of Calcium Oxide Nanoparticles from Waste Carbonation Mud in Clarification of Raw Sugar Melt,” {\italic Sugar Tech}, vol. 25, no. 2, pp. 331–338, Jul. 2022, doi: 10.1007/s12355-022-01150-2.

ORAL SESSION 8

Chemistry

Chair: Dr. I. Plikusienė

INFLUENCE OF DEPOSITION CONDITIONS ON THE PROPERTIES OF Sb_2S_3 LAYERS ON FTO SUBSTRATES

Evelina Kasparavičiūtė[1], Remigijus Ivanauskas[1], Skirma Žalenkienė[1]

[1]Kaunas University of Technology, Kaunas, Lithuania
evelina.kasparaviciute@ktu.edu

The rapidly developing solar energy industry offers an excellent alternative to fossil fuels, the use of which contributes to climate change. Therefore, the search for efficient, resource-saving, and environmentally friendly materials suitable for use in solar energy technologies is ongoing. Antimony halide layers are an excellent alternative to toxic lead, cadmium, or mercury compounds in solar cells. Antimony sulfide (Sb_2S_3) is a p-type semiconductor with a direct optical band gap in the range of 1.6–2.46 eV [1] and a high absorption coefficient (~10^5 cm^{-1}) in the visible spectrum (400–700 nm) [2], making it a very efficient light absorber in photovoltaic cells and photodetectors. Furthermore, its layers 1 μm thick can absorb 95% of incident solar radiation. In addition, Antimony is widely distributed on Earth, and Sb_2S_3 is chemically stable, non-toxic, resistant to temperature fluctuations, and durable.

The morphology, crystal structure, defect concentration, thickness, adhesion to the substrate surface and, as a consequence, optical and electrical properties of the formed layer depend on the method of formation of Sb_2S_3 layers. In this work, Sb_2S_3 layers were formed on the surface of fluorinated tin oxide (FTO) slides by three methods: chemical bath deposition (CBD), sequential ion absorption and reaction (SILAR), and drop casting (DC). In addition, after depositing Sb_2S_3 films on the surface of FTO substrates, they were washed, dried, and annealed for 1 h in a nitrogen atmosphere at 250 °C. The conducted studies showed that the band gap values of Sb_2S_3 layers deposited by all methods are similar and vary from 1.66 eV to 1.8 eV, but the best adhesion to the FTO substrate surface and coating homogeneity were observed in layers formed by chemical bath deposition method.

[1] M. Wu et al., “Correlative and In Situ Microscopy Investigation of Phase Transformation, Crystal Growth, and Degradation of Antimony Sulfide Thin Films,” vol. 19, no. 27, pp. 25017–25027, July 2025, doi: 10.1021/acsnano.5c04342
[2] H. Min, “A Review On Antimony Trisulfide Thin Films,” vol. 32, pp. 597–601, 2020.

ENHANCED ELECTROCATALYTIC HER PERFORMANCE: A COMPARATIVE STUDY OF OPTIMIZED BINARY AND TERNARY ELECTROCATALYSTS IN ALKALINE FRESHWATER AND SEAWATER

Sukomol Barua[1], Aldona Balčiūnaitė[1], Jūratė Vaičiūnienė[1], Loreta Tamašauskaitė-Tamašiūnaitė[1], Eugenijus Norkus[1]

[1]Lithuania, Center for Physical Sciences and Technology (FTMC), Department of Catalysis
sukomol.barua@ftmc.lt

The electrocatalytic activity of two optimized, non-noble transition metal-based 3D bimetallic and trimetallic coatings (electrocatalysts) for hydrogen evolution (HER) in alkaline freshwater and seawater was investigated in this comparative study. Both electrodes were fabricated using a facile and inexpensive electrochemical deposition method based on the dynamic hydrogen bubble template (DHBT) technique. The electrodes were characterized using scanning electron microscopy with energy-dispersive X-ray spectroscopy, and inductively coupled plasma optical emission spectroscopy. Their HER performance was evaluated using linear sweep voltammetry at different temperatures in alkaline freshwater (1.0 M KOH), simulated seawater, SSW (1.0 M KOH + 0.5 M NaCl) and alkaline seawater, ASW (1.0 M KOH + natural seawater). A thin titanium (Ti) foil (0.127 mm thickness) was used as the substrate for synthesizing these binder-free, self-supported NiMn and NiMnCo electrocatalysts. The optimized binary NiMn/Ti-5 electrocatalyst's surface morphology exhibits a unique microsized porous architecture with abundant pores of distinctly different sizes. In contrast, the optimized ternary NiMnCo/Ti-2 electrocatalyst demonstrates a cauliflower-like, curd-shaped microspherical architecture that is directly deposited on the substrate. These compactly grown microspheres uniformly cover the entire surface of the conductive Ti substrate.

From the comparative perspective, the optimized NiMnCo/Ti-2 electrocatalyst exhibits excellent HER activity in alkaline media, achieving a low overpotential of 66 mV at the benchmark current density of 10 mA/cm^2. In contrast, the optimized NiMn/Ti-5 electrocatalyst requires a relatively higher overpotential of 127 mV to reach the same current density. In simulated seawater and alkaline seawater, the required overpotentials decreased significantly for both binary and ternary electrodes. Specifically, the 3D NiMn/Ti-5 electrode exhibited overpotentials of 64 mV (SSW) and 79 mV (ASW), whereas the 3D NiMnCo/Ti-2 electrocatalyst required only 29 mV (SSW) and 59 mV (ASW). These synthesized non-noble metal-based optimized binary and ternary electrocatalysts also demonstrated excellent long-term stability at a constant potential of -0.232 V (vs. RHE) and a constant current density of 10 mA/cm^2 showing exceptional current retention and minimal potential fluctuation. Furthermore, multi-step chronopotentiometric measurements were performed in alkaline media and SSW within a current density range of 20 mA/cm^2 to 100 mA/cm^2 for the optimized NiMnCo/Ti-2 electrocatalyst. The results confirm its sustainable durability and suitability for practical alkaline freshwater and seawater electrolysis applications.

Keywords: 3D Electrocatalyst, Hydrogen Evolution Reaction (HER), Simulated Seawater, Alkaline Seawater

TWO STAGE $CATIO_3$ SYNTHESIS IN DIFFERENT CRYSTALLINITY TIO_2 MIXTURES

Ričardas Kleinauskas[1], Anatolijus Eisinas[1]

[1]Kaunas University of Technology, Faculty of Chemical Technology, Kaunas, Lithuania
ricardas.kleinauskas@ktu.lt

Due to high caustic resistance, high thermal stability and low production cost, $CaTiO_3$-based materials are being actively developed for nuclear waste treatment [1], dielectric [2] and photocatalytic applications [3]. A growing number of research groups are focusing on optimizing the production of $CaTiO_3$ by modifying raw materials or combining various synthesis techniques. This work aims to develop a two stage calcium titanate synthesis using titanium dioxide with different crystallinity via hydrothermal and solid-state methods.

In this work, amorphous TiO_2 was prepared in accordance with our earlier experiments [4]. Samples were prepared by calcinating amorphous TiO_2 in 25, 130, 330 and 530 °C and mixing it and CaO equal to molar ratio of 1. Hydrothermal treatment was performed under saturated steam pressure of 15 bars at a temperature of 200 °C for 1-96 hours. The samples were filtered, dried and sieved (<80 μm) then sintered at a temperature of 900 °C for 1 hour in an air atmosphere. Synthesis products were characterized by XRD, FT-IR and STA instrumental methods.

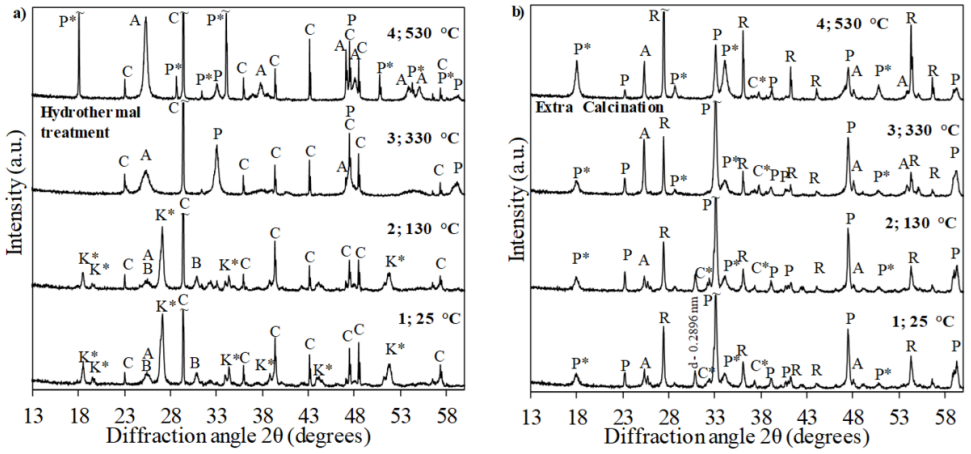


Fig. 1. XRD patterns of the synthesis products (CaO/TiO_2=1) after 48 h of hydrothermal treatment at 200 °C (a) and extra calcination at 900 °C (b) when the amorphous TiO_2 was calcinated, °C: 1 – 25; 2 – 130; 3 – 330; 4 – 530. Indexes: C – $CaCO_3$; P – $CaTiO_3$; P* – $Ca(OH)_2$; A – anatase; B – brookite; K* – kassite $CaTi_2O_5(OH_2)$

It was determined that amorphous TiO_2 treated at low temperatures (25-130 °C) enhances the formation of kassite during hydrothermal treatment (I stage). (**Fig. 1 a; 1, 2**). Meanwhile, TiO_2 calcinated at higher temperatures (330-530 °C) promotes formation of $CaTiO_3$ (**Fig. 1 a; 3, 4**). The most intense $CaTiO_3$ diffraction maximum was identified in the samples with TiO_2 calcinated at 330 °C (**Fig. 1. a; 3**). When hydrothermal synthesis products were calcinated at 900 °C (II stage), the highest $CaTiO_3$ diffraction peaks were identified in samples with lower TiO_2 crystallinity (**Fig. 1 b; 1, 2**). By comparison, more intense diffraction peaks attributed to rutile and portlandite suggest a limited reaction between CaO and crystalline TiO_2 (**Fig. 1 b; 3, 4**).

The results suggest that the crystallinity of TiO_2 has an influence on the formation of $CaTiO_2$ during hydrothermal and solid-state synthesis.

[1] N. Bensemma et al., “Radiation stability of Nd-doped perovskite ceramics for trivalent actinide waste (An+3) storage,” Nuclear Instruments and Methods in Physics Research Section B Beam Interactions With Materials and Atoms, vol. 550, p. 165306, Mar. 2024.
[2] B. Fang et al., “Achieving excellent thermoelectric properties in CaTiO3-based materials via entropy engineering and recrystallization,” Chemical Engineering Journal, vol. 509, p. 161480, Mar. 2025.
[3] LV. Hua et al., “Multishelled hollow CaTiO3 cubes decorated with Co0. 2Cd0. 8S nanoparticles for efficient photocatalytic H2 evolution via S-scheme charge transfer,” Separation and Purification Technology, vol. 345, p. 127429, 2024.
[4] J. Doneliene, E. Fataraite-Urboniene, M. Rudzikas, S. Pakalka, N. Danchova, and J. Ulbikas, “Effect of precursor nature and Sol-Gel synthesis conditions on TIO2 aerogel’s structure,” Molecules, vol. 26, no. 16, p. 5090, Aug. 2021.

ELECTROCHEMICAL SENSORS BASED ON MOLECULARLY IMPRINTED POLYMERS FOR DETECTION OF SMALL MOLECULES

Ernestas Brazys[1,2], Vilma Ratautaitė[2], Arūnas Ramanavičius[1,2]

[1]Lithuania, Vilnius University, Faculty of Chemistry and Geosciences, Institute of Chemistry, Department of Physical Chemistry

[2]Lithuania, SRI Center for Physical Sciences and Technology (FTMC), Department of Nanotechnology

ernestas.brazys@chgf.stud.vu.lt

Molecularly imprinted polymers (MIPs) are synthetic polymeric materials prepared via polymerisation in the presence of a template molecule, resulting in selective recognition sites complementary in shape, size, and functional groups. Often described as “plastic antibodies”, MIPs mimic the molecular recognition behaviour of natural antibodies while offering high selectivity and binding affinity [1]. Compared to biological receptors, MIPs exhibit enhanced chemical and thermal stability, greater resistance to harsh environmental conditions, and lower production costs. Consequently, they have been widely used to detect low-molecular-weight analytes, including food contaminants, pharmaceutical compounds, and environmental pollutants [2,3]. MIP fabrication typically involves self-assembly of functional monomers with the template, chemical or electrochemical polymerisation to form a rigid polymer matrix, and subsequent template removal to generate selective binding cavities [3].

In this work, electrochemical sensors employing polypyrrole-based molecularly imprinted polymers (MIPs) were developed for the selective detection of low-molecular-weight analytes, including melamine [2] and salicylic acid. The MIPs were synthesised via electropolymerisation of a pre-polymeric solution comprising pyrrole as the functional monomer and the corresponding template molecules. The resulting polymer films were amperometrically deposited directly on graphite and screen-printed carbon electrodes. After polymerisation, the template molecules were removed, generating specific recognition sites within the polymer matrix. For comparison, non-imprinted polymer (NIP) electrodes were fabricated under identical conditions, in the absence of the template molecules.

The electrochemical properties of all polypyrrole films were characterised using cyclic voltammetry (CV) and electrochemical impedance spectroscopy (EIS). Interactions between the template molecules and the polymer layers were evaluated by comparing oxidation peak currents measured via differential pulse voltammetry (DPV). The obtained results, together with the calculated apparent imprinting factors, indicate that the fabricated MIPs are well suited for developing electrochemical sensors to detect low-molecular-weight analytes.

Acknowledgements

This project has received funding from the Research Council of Lithuania (LMTLT), agreement No. S-LL-25-3.

Keywords: molecularly imprinted polymer (MIP); polypyrrole (Ppy); conducting polymers; electrochemical sensor.

[1] J. J. BelBruno, “Molecularly imprinted polymers,” Chemical Reviews, vol. 119, no. 1, pp. 94–119, Sep. 2018, doi: 10.1021/acs.chemrev.8b00171.

[2] E. Brazys, V. Ratautaite, B. Brasiunas, A. Ramanaviciene, L. Rodríguez, A. Pinto, D. Milea, U. Prentice, and A. Ramanavicius, “Molecularly imprinted polypyrrole-based electrochemical melamine sensors,” Microchemical Journal, vol. 199, p. 109890, Jan. 2024, doi: 10.1016/j.microc.2024.109890.

[3] V. Ratautaite, E. Brazys, A. Ramanaviciene, and A. Ramanavicius, “Electrochemical sensors based on l-tryptophan molecularly imprinted polypyrrole and polyaniline,” Journal of Electroanalytical Chemistry, vol. 917, p. 116389, May 2022, doi: 10.1016/j.jelechem.2022.116389.

REAL-TIME ELECTROCHEMICAL MONITORING OF BIOFILM GROWTH

Evelina Lukaitė[1,2], Rugilė Jonaitytė[1,2], Marius Butkevičius[2], Eglė Malachovskienė[3], Algimantas Paškevičius[3], Marius Dagys[2], Rokas Žalnėravičius[1,2]

[1]Center of Physical and Technology Sciences, Department of Electrochemical Materials Science, Vilnius, Lithuania
[2]Vilnius University, Life Sciences Center, Department of Bioanalysis, Vilnius, Lithuania
[3]Nature Research Centre, Laboratory of Biodeterioration Research, Vilnius, Lithuania
evelina.lukaite@ftmc.lt

Biofilms contribute to approximately 80% of chronic or recurrent infections and exhibit high tolerance to antimicrobial therapy, often 10–1000 times greater than planktonic cells [1]. Rapid detection of biofilm growth is essential for effective treatment; however, conventional microbiological methods are time-consuming, labor-intensive, and often disruptive [2]. Electrochemical techniques offer a fast, non-invasive alternative, enabling continuous, real-time monitoring of bacterial activity at electrode surfaces [3]. The aim of this study was to evaluate biofilm formation of *P. aeruginosa*, *S. aureus*, and their mixed cultures, and to assess the influence of drugs (i.e., antibiotics) on bacterial electrogenicity.

To monitor biofilm growth, chronoamperometric measurements were performed using a three-electrode system consisting of a carbon cloth working, an Ag/AgCl (3 M KCl) reference, and a Ti foil counter electrodes, respectively. Biofilms were grown directly on the electrode surface. The chronoamperometry was used to study biofilms' electrogenicity, which reflects the main stages of bacterial growth, including lag, log, and the stationary phase as presented in Fig. 1 A. In case with *P. aeruginosa*-based biofilms, the collected current increased from 0 µA to 1 µA within 24 h, indicating extracellular electron transfer between bacterial cells and the electrode surface. Mixed-species biofilms produced 2.5-fold higher current than monocultures. In the presence of antibiotics, the observed current profile had reached a plateau at 5 hours and then decreased to almost 0.0 µA, indicating their complete metabolic suspension Fig. 1 B. These findings were supported by standard microbiology assays and confocal microscopy investigations.

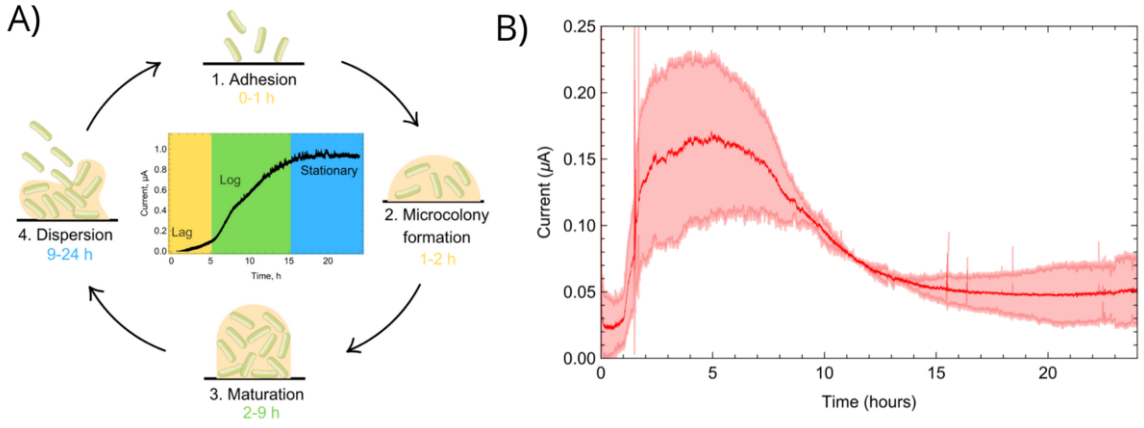


Fig. 1. Schematic illustration of biofilm development stages and current–time response.

Overall, the results demonstrate that chronoamperometry enables rapid, real-time and non-invasive monitoring of biofilm formation and their susceptibility to antibiotics, providing a simple electrochemical platform for assessing biofilms' electrogenicity and antibiotic efficacy.

[1] J. G. Thöming and S. Häussler, "Pseudomonas aeruginosa Is More Tolerant Under Biofilm Than Under Planktonic Growth Conditions: A Multi-Isolate Survey," Front. Cell. Infect. Microbiol., vol. 12, Feb. 2022, doi: 10.3389/fcimb.2022.851784.
[2] Y. Xu, Y. Dhaouadi, P. Stoodley, and D. Ren, "Sensing the unreachable: challenges and opportunities in biofilm detection," Curr Opin Biotechnol, vol. 64, pp. 79–84, Aug. 2020, doi: 10.1016/j.copbio.2019.10.009.
[3] A. Kulshrestha and P. Gupta, "Real-time biofilm detection techniques: advances and applications," Future Microbiol, vol. 19, Jun. 2024, pp. 1003–1016, doi: 10.1080/17460913.2024.2350285.

ORAL SESSION 9

Laser Physics and Optical Technologies

Chair: Dr. V. Jukna

HIGH REPETITION RATE DUV-NIR TUNABLE FEMTOSECOND LASER SYSTEM

Jokūbas Pimpė[1,2], Ieva Baltrukonytė[1], Audrius Dubietis[1], Julius Vengelis[1]

[1]Lithuania, Vilnius University, Faculty of Physics, Laser Research Center
[2]Lithuania, Vilnius, Light Conversion Ltd., Keramikų st. 2B
jokubas.pimpe@ff.vu.lt

The growing demand for high-power, high-repetition-rate femtosecond laser systems arises from their potential to enhance signal-to-noise ratios and acquisition speeds in scientific and biomedical imaging [1-3]. However, the fixed central wavelength of most solid-state femtosecond oscillators limits their versatility. To address this, we present a pre-chirp managed rod-type Yb-doped fiber amplifier system [4] capable of generating tunable wavelength femtosecond pulses through optical parametric amplification (OPA) and nonlinear harmonic generation.

The developed OPA, based on two LBO stages pumped with 30 W of second-harmonic signal and seeded with a broadband supercontinuum from a KGW crystal, delivers tunable wavelength output from 675 nm to 2.2 μm with sub-70 fs signal and sub-100 fs idler pulses. The total output power exceeds 11 W - the highest reported for femtosecond OPAs at a 76 MHz repetition rate - with excellent stability (∼1 % RMS) and low relative intensity noise (RIN) across the 1 kHz – 40 MHz bandwidth.

Further wavelength extension of femtosecond laser system is achieved through down-conversion of initial 1030 nm wavelength radiation to second (SH), third (TH), and fourth (FH) harmonic signals in BBO crystals, producing up to 41 W, 17.7 W, and 2.3 W of average power with conversion efficiencies of 60 %, 26 %, and 3 %, respectively. Generated harmonic signals exhibit nearly Gaussian shaped spatial intensity distribution with M^2 value lower than 1.3 and <1 % RMS long term stability over 10 hours of continuous operation.

This versatile, high-power, tunable femtosecond laser source offers new opportunities for applications such as stimulated Raman scattering microscopy, ultrafast spectroscopy, and deep-UV imaging with enhanced spatial resolution.

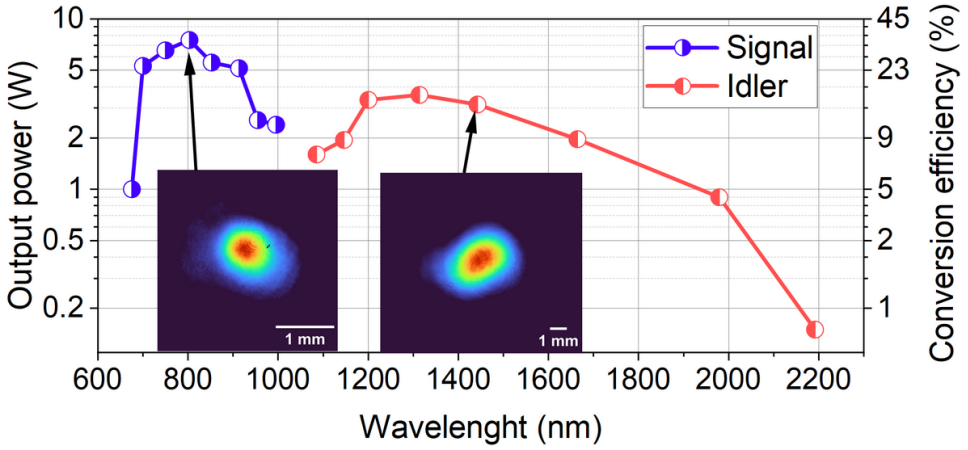


Fig. 1. Average output powers of 76 MHz LBO OPA signal (blue) and idler (red) waves as function of wavelength. The right y-axis displays conversion efficiency in OPA2 stage. The inset shows the near-field profiles of signal wave at 800 nm and idler wave at 1450 nm.

Keywords: Optical parametric amplifier, third harmonic generation, fourth harmonic generation, femtosecond pulses, fiber amplification.

[1] J. W. Ager, R. K. Nalla, K. L. Breeden, and R. O. Ritchie, “Deep-ultraviolet Raman spectroscopy study of the effect of aging on human cortical bone,” Journal of Biomedical Optics, vol. 10, no. 3, p. 034012, Jan. 2005, doi: 10.1117/1.1924668.
[2] G. Cerullo and S. De Silvestri, “Ultrafast optical parametric amplifiers,” Review of Scientific Instruments, vol. 74, no. 1, pp. 1–18, Jan. 2003, doi: 10.1063/1.1523642.
[3] X. Chen et al., “5.32 W ultraviolet laser generation at 266 nm using sum-frequency method with CsB3O5 crystal,” Optics Express, vol. 31, no. 2, p. 802, Dec. 2022, doi: 10.1364/oe.474095.
[4] J. Pimpė et al., “Highly stable, 72 W average power, 76 MHz repetition rate femtosecond hybrid PCMA-FCPA Yb-fiber amplifier,” Optics & Laser Technology, vol. 190, p. 113261, May 2025, doi: 10.1016/j.optlastec.2025.113261.

HIGH REPETITION RATE AND HIGH AVERAGE POWER FEMTOSECOND OPTICAL PARAMETRIC AMPLIFIER IN THE VIS AND NIR

Simona Armalytė[1], Julius Vengelis[1]

[1]Vilnius University, Faculty of Physics, Laser Research Center, Saulėtekio av. 10, Vilnius, Lithuania
simona.armalyte@ff.vu.lt

A high repetition rate of the laser source (>50 MHz) is a desirable characteristic in most applications, as it enables higher scanning speeds, the acquisition of a larger amount of data, and consequently improves statistical reliability [1] and the signal-to-noise ratio [2]. When working with biological samples, a high repetition rate can also reduce the probability of photodamage [3]. The development of high average power laser sources is therefore crucial for extending the capabilities of high repetition rate systems and enabling demanding applications that are otherwise power-limited. To this end, a unique hybrid pre-chirp managed amplification (PCMA) and fiber chirped pulse amplification (FCPA) system generating 114 fs pulses with a repetition rate of 76 MHz and an output power of 72 W has been developed at the Vilnius University Laser Research Centre [4]. In addition to high repetition rate and high average power, most commercial and scientific applications demand a broad wavelength tunability, low noise levels, and long-term operational stability. Since the wavelength tuning range of a laser is limited by the gain bandwidth of the laser medium, nonlinear optical frequency conversion processes, such as optical parametric generation and amplification (OPG/OPA), are employed to achieve broad wavelength tunability. Recently, an optical parametric amplifier operating at a high repetition rate and exhibiting record-high average power, seeded with a supercontinuum generated in a bulk crystal, was demonstrated [5]. Here, we demonstrate that the OPA output power can be further scaled by employing a fiber-based supercontinuum seed.

Therefore, a two-stage optical parametric amplifier (OPA) based on lithium triborate (LBO) crystal has been developed with unique pump characteristics: high repetition rate (76 MHz) and high average power femtosecond pulses. This OPA seeded with a supercontinuum generated in all normal dispersion photonic crystal fiber (ANDi PCF) has demonstrated a wide wavelength tuning range in the VIS and NIR spectral regions, covering wavelengths from 670 nm to 1030 nm for the signal wave and from 1030 nm to 2200 nm for the idler wave (Fig. 1.). High average output powers of signal and idler exceeding 14 W have been demonstrated after two-stage amplification, with a maximum conversion efficiency of around 40% at 900 nm central wavelength. The amplified pulses are compressible in time to near transform-limited durations. This OPA, featuring a unique combination of exceptional parameters, constitutes a first step toward the realization of a high repetition rate and high average power laser source operating in the mid-infrared spectral region.

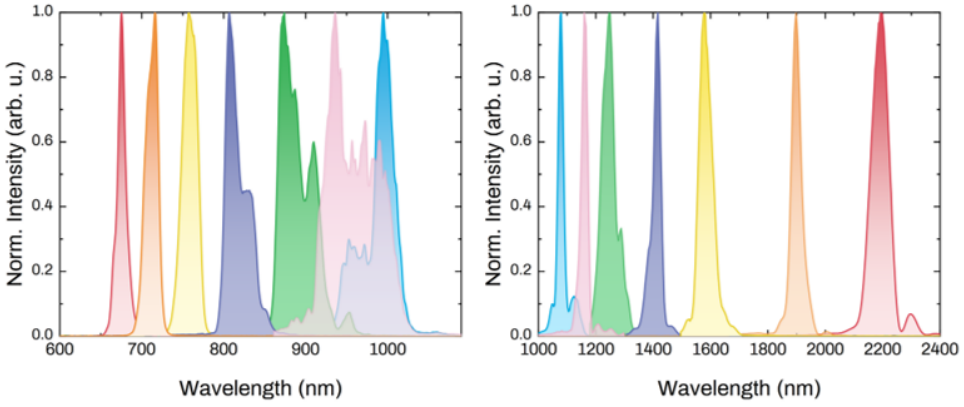


Fig. 1. Wavelength tuning range of fiber seeded high average power and high repetition rate OPA.

[1] R. Riedel, A. Stephanides, J. Prandolini, B. Gronloh, B. Jungbluth, T. Mans, F. Tavella, „Power scaling of supercontinuum seeded megahertz-repetition rate optical parametric chirped pulse amplifiers," Optics Letters, vol. 39, no. 6, Mar., pp. 1422-1424, 2014.
[2] H. Linnenbank, S. Linden, „High repetition rate femtosecond double pass optical parametric generator with more than 2 W tunable output in the NIR," Optics Express, vol. 22, no. 15, Jul., pp. 18072-18077, 2014.
[3] S.-W. Chu, T.-M. Liu, C.-K. Sun, C.-Y. Lin, H.-J. Tsai, „Real-time second-harmonic-generation microscopy based on a 2-GHz repetition rate Ti:sapphire laser," Optics Express, vol. 11, no. 8, Apr., pp. 933-938, 2003.
[4] J. Pimpė, J. Banys, S. Armalytė, J. Jakutis Neto, V. Jarutis, A. Dubietis, J. Vengelis, Highly stable, „72 W average power, 76 MHz repetition rate femtosecond hybrid PCMA-FCPA Yb-fiber amplifier," Optics & Laser Technology, vol 190, Apr., p. 113261, 2025.
[5] J. Pimpė, S. Armalytė, A. Dubietis, J. Vengelis, „11 W, broadly tunable, bulk supercontinuum-seeded femtosecond optical parametric amplifier at 76 MHz," Optics & Laser Technology, vol. 196, Jan., p. 114633, 2026.

SUPERCONTINUUM GENERATION IN BULK SOLIDS WITH MID-INFRARED DRIVING PULSES

Kristupas Dagilis[1], Gintaras Tamošauskas[1], Rokas Danilevičius[2], Joris Roman[3], Andrejus Michailovas[4], Audrius Pugžlys[3,4], Audrius Dubietis[1]

[1]Lithuania, Vilnius, Vilnius University, Faculty of Physics, Laser Research Center
[2]Lithuania, Vilnius, EKSPLA
[3]Austria, Vienna, TU Wien, Photonics Institute
[4]Lithuania, Vilnius, Center for Physical Sciences & Technology
kristupas.dagilis@ff.stud.vu.lt

The advent of ultrafast solid-state laser sources emitting at around 2 μm, which are based on chromium-doped chalcogenides [1], as well as holmium and thulium doped lasing materials [2], fostered the development of optical parametric amplifiers (OPAs) which make use of novel non-oxide crystals, offering greatly improved quantum efficiency and favourable signal-to-idler photon energy ratio. To utilize the entire tuning range of 2 μm-pumped OPAs, broadband supercontinuum seed with spectral red shifts extending at least up to 4 μm is required. However, recent experiments performed in various nonlinear optical crystals (NOC) show that achieving spectral broadening to such extent is a difficult task [3,4]. In this Contribution, an investigation of supercontinuum generation with ~2 μm driving pulses is presented in various dielectric and semiconductor bulk materials and a set material dispersion-related criteria are identified as a simple method of estimation of achievable red shifted spectral broadening.

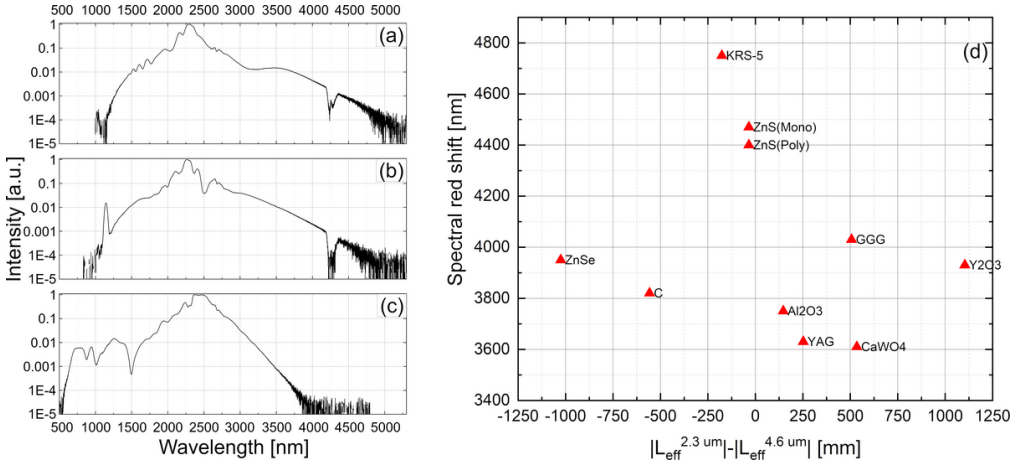


Fig. 1. Examples of supercontinuum spectra generated in (a) KRS-5, (b) single crystal ZnS, (c) YAG. (d) Measured supercontinuum spectral red shift as a function of effective dispersion length.

The experiments were performed with 180 fs, 2.3 μm driving pulses from an optical parametric amplifier. Supercontinuum generation was investigated in bulk nonlinear materials: KRS-5, ZnSe, ZnS (polycrystalline and single crystal), KGW, $CaWO_4$, Diamond, Y_2O_3, GGG, YAG and Sapphire. Material dispersion parameters: group velocity dispersion (GVD) and third-order dispersion (TOD), were analyzed as a potential limiting factor for supercontinuum spectral extent to the long-wavelength side. To fully investigate the influence of the dispersion parameters on supercontinuum spectral extent, materials that fall into both normal and anomalous GVD regimes were tested. Results show that for the tested central wavelength, NOCs that fall in the normal GVD range tend to produce larger spectral broadening to the long-wavelength side. The broadest red-shifted supercontinuum spectra were produced in ZnS and KRS-5 crystals, as shown in Fig.1(a) and Fig. 1(b), which are compared to typical supercontinuum spectrum generated in YAG, shown in Fig. 1(c). Additionally, larger spectral broadening to the long-wavelength side was achieved in materials with a low wavelength-dependence of the effective dispersion length, a parameter that incorporates both GVD and TOD, as summarized in Fig. 1(d).

Keywords: Ultrafast supercontinuum, dispersion parameters, nonlinear optical crystals

[1] S. Vasilyev, I. Moskalev, M. Mirov, V. Smolski, S. Mirov, and V. Gapontsev, "Ultrafast middle-IR lasers and amplifiers based on polycrystalline Cr:ZnS and Cr:ZnSe," Opt. Mater. Express, vol. 7, no. 7, p. 2636-2650, Jun. 2017, doi: https://doi.org/10.1364/ome.7.002636.
[2] Y. Wang et al., "Recent Progress in Sub-100 fs Mode-Locked Bulk Lasers Near 2 μm," Laser Photonics Rev., Nov. 2025, doi: https://doi.org/10.1002/lpor.202500111.
[3] S.-H. Nam, G. C. Nagar, D. Dempsey, O. Novák, B. Shim, and K.-H. Hong, "Multi-octave-spanning supercontinuum generation through high-energy laser filaments in YAG and ZnSe pumped by a 2.4 μm femtosecond Cr:ZnSe laser," High Power Sci. Eng., vol. 9, 2021, doi: https://doi.org/10.1017/hpl.2021.1.
[4] R. Danilin et al., "Supercontinuum generation in oxide and semiconductor materials (InP, Si, GaN, GaAs, PbMoO4, YVO4, ZGP, TiO2, diamond) pumped by radiation of the Cr:ZnS fs-MOPA system," J. Opt. Soc. Am. B, vol. 42, no. 6, pp. 1315–1322, Apr. 2025, doi: https://doi.org/10.1364/josab.553197.

COMPARATIVE PERFORMANCE OF BRILLOUIN ACTIVE MEDIA FOR ULTIMATE LASER PULSE COMPRESSION

Rugilė Pečiulytė[1], Paulius Mackonis[1], Aleksėj M. Rodin[1], Augustė Grigaravičienė[1]

[1]Center for Physical Sciences and Technology, Solid State Laser Laboratory, Savanorių ave. 231, 02300 Vilnius
rugile.peciulyte@ff.stud.vu.lt

High-energy picosecond lasers are in demand for satellite laser ranging, high-efficiency materials processing, and laser cosmetology. Stimulated Brillouin scattering (SBS) provides a cost-effective means of compressing nanosecond pump pulses while maintaining high output beam quality through phase conjugation. Previously, SBS-compressed, phase conjugated high-energy pulses of ~90 ps were demonstrated in C_8F_{18} [1]. This work aims to compare the performance of HT-230 and C_8F_{18}, two photodissociation-resistant and non-toxic Brillouin-active liquids used as coolants in the semiconductor industry [2]. The HT-230 medium appears most promising for ultimate compression of 890 ps pump pulses due to its short acoustic phonon lifetime of 0.3 ns.

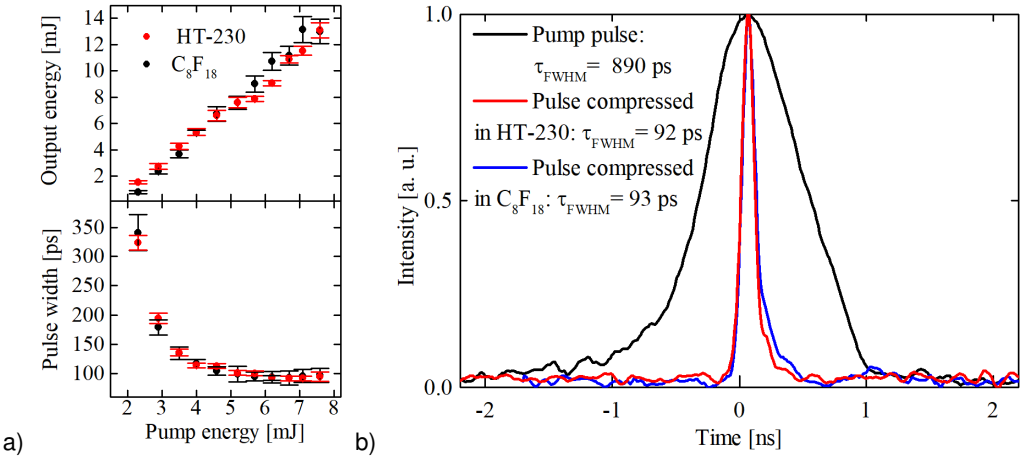


Fig. 1. a) Output energy (top) and pulse width (bottom) of the self-seeded SBS-compressor as a function of pump energy (error bars represent the standard deviation from the mean value). b) Temporal waveforms of the pump pulse (black) and the SBS-compressed pulses in HT-230 (red) and C_8F_{18} (blue).

Incident pulses from a passively Q-switched Nd:YAG laser were spatially cleaned and amplified using two side-diode-pumped gain modules. The counter-propagating, compressed Stokes pulses were amplified in the second path. The focusing and pumping conditions were optimized to achieve the best pulse compression (Fig. 1a). As a result, using an f = 200 mm focusing lens at a pump energy of 6.2 mJ, the incident pulses were compressed to ~90 ps in both media (Fig. 1b). Although the higher reflectivity in C_8F_{18} enabled nearly 11 mJ of output energy, compared with ~9 mJ from HT-230, pulses compressed in this way were less stable. Effective suppression of amplifier-induced aberrations and astigmatism was demonstrated in both media due to phase conjugation. Although the achieved pulses already exceed the requirements of cosmetology, future efforts will focus on nonlinear compression down to a few picoseconds for metal processing.

Acknowledgements
This research was funded by Research Council of Lithuania, grants S-MIP-25-17 and S-LU-26-1.

[1] A.M. Rodin, A. Černeckytė, P. Mackonis, P, A. Petrulėnas, "Optimizing Self-Seeded Perfluorooctane SBS Compressor Configurations to Achieve ~90 ps High-Energy Pulses", Photonics, 10(9), 1060, 2023.
[2] H. Park, C. Lim, H. Yoshida, M. Nakatsuka, "Measurement of Stimulated Brillouin Scattering Characteristics in Heavy Fluorocarbon Liquids and Perfluoropolyether Liquids", Jpn. J. Appl. Phys., 45, 5073, 2006.

GENERATION OF REGULAR LASER PULSES IN A BACKWARD WAVE OPTICAL PARAMETRIC OSCILLATOR PUMPED BY INCOHERENT PULSES

Tomas Latvys[1], Viktorija Tamulienė[1]

[1]Vilnius University, Faculty of Physics, Laser Research Center, Saulėtekio Ave. 10, 10223, Vilnius, Lithuania
tomas.latvys@ff.stud.vu.lt

Backward-wave optical parametric oscillators (BWOPOs) are unique nonlinear crystals that enable precise laser wavelength tuning with exceptional stability and spectral purity [1]. Previous studies have shown that, within a BWOPO crystal, the forward-propagating wave inherits the spectral modulation of the pump pulse; by contrast, the backward-propagating wave remains essentially transform-limited [2-4].

In this work, we simulate a numerical BWOPO model [5] to show that when a BWOPO crystal is pumped by a broadband incoherent pulse, the generated backward wave is regular and narrowband (Fig. 1). As shown in Fig. 1d, the forward wave spectrum closely follows the broadband spectrum shape of the pump, whereas the backward wave spectrum remains narrow. We further support this result by deriving analytical solutions for the forward and backward wave amplitudes in the linear regime using the Riemann's integration method that is presented in [6]. Our results establish a route to generating high-coherence, narrowband laser pulses using incoherent, broadband pump sources.

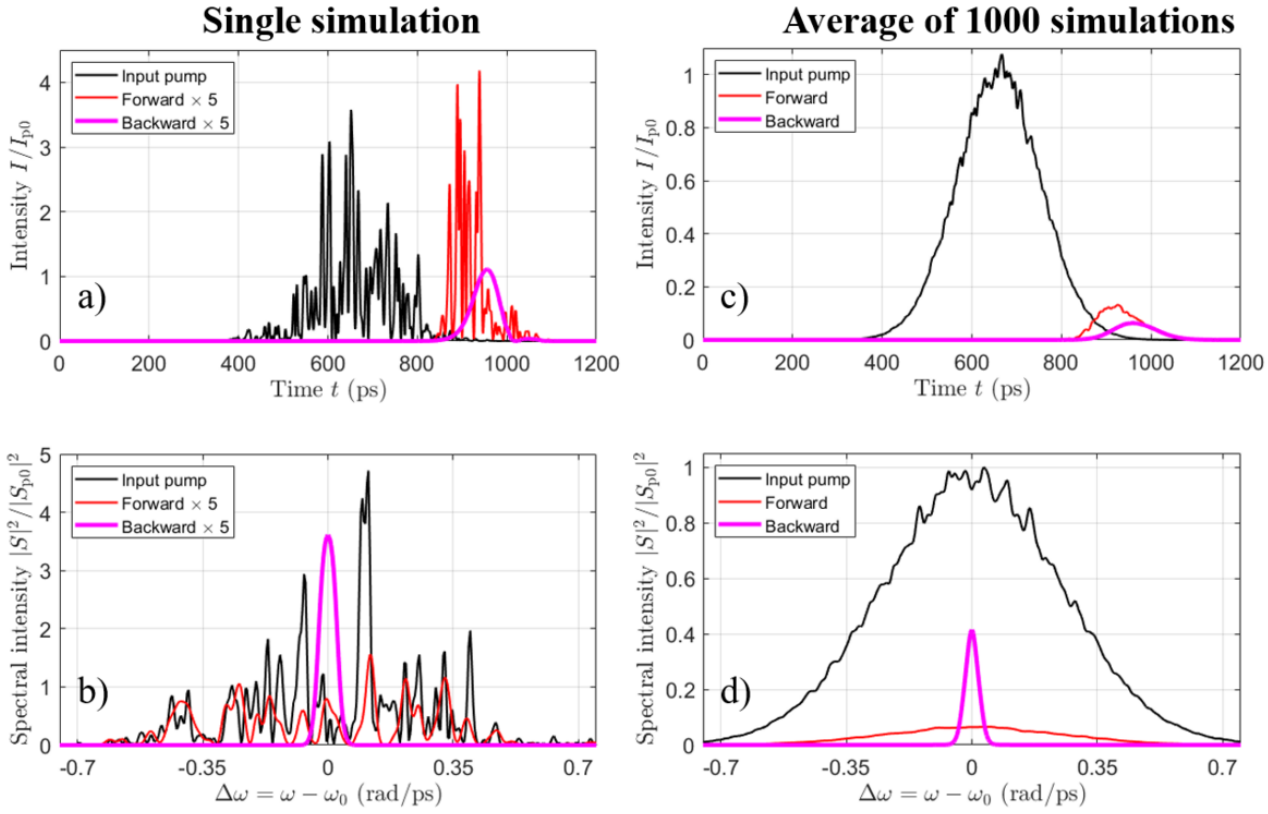


Fig. 1. Temporal pulse profiles (a, c) and angular-frequency spectra (b, d) of the input pump and the generated forward and backward waves. Panels (a, b) show results from a single simulation, while panels (c, d) present averages over 1000 simulations. The pump is incoherent, with pulse energy $E_p = 20\,\mu\mathrm{J}$ and central wavelength $\lambda_p = 532\,\mathrm{nm}$.

Keywords: Backward Wave Optical Parametric Oscillator (BWOPO), Incoherent Pump, Coherence Gain, Nonlinear Optics

[1] C. Canalias, V. Pašiškevičius, "Mirrorless optical parametric oscillator", Nat. Photonics, vol. 1, pp. 459-462, 2007.
[2] C. Montes, B. Gay-Para, M. Micheli, P. Aschieri, "Mirrorless optical parametric oscillators with stitching faults: backward downconversion efficiency and coherence gain versus stochastic pump bandwidth", J. Opt. Soc. Am. B, vol. 31, pp. 3186-3192, 2014.
[3] C. E. Minor, R. S. Cudney, "Mirrorless optical parametric oscillation in bulk PPLN and PPLT: a feasibility study", Appl. Phys. B vol. 123, no. 38, 2017.
[4] A. Viotti, F. Laurell, A. Žukauskas, C. Canalias, and V. Pašiškevičius, "Coherent phase transfer and pulse compression at 1.4 µm in a backward-wave OPO", Opt. Lett., vol. 44, pp. 3066-3069, 2019.
[5] T. Latvys, J. Banys, V. Jarutis, J. Vengelis, and V. Tamulienė, "X-wave formation in the subnanosecond backward-wave optical parametric oscillator", Phys. Rev. A, vol. 111, no. 6, 2025.
[6] C. Wang, "Theory of Stimulated Raman Scattering", Phys. Rev., vol. 182, pp. 482-494, 1969.

TWO-PHOTON POLYMERIZATION OF LOW-DENSITY MICROSTRUCTURES AND THEIR ASSEMBLY INTO RIGID HOLDERS FOR INERTIAL CONFINEMENT FUSION INVESTIGATION

Ioanna-Angeliki Petsi[1], Saule Petrauskaite[1], Dimitra Ladika[1], Donatas Narbutis[2], Mangirdas Malinauskas[1]

[1]Vilnius University, Laser Research Center, Vilnius, Lithuania
[2]Vilnius University, Institute of Theoretical Physics and Astronomy, Vilnius, Lithuania
petsiioannaangeliki@gmail.com

In the last decades, one major topic of research is Two-Photon Lithography, which is a non-linear laser direct writing technique that is based on two-photon absorption phenomenon [1]. It provides high resolution with sub-diffraction features and it can be used to create complex, true 3D-printed micro and porous structures [2], without the need of using masks.[3] TPL is often used for the fabrication of different geometries, like foams. High porosity foams have many applications in optics and photonics, biology, mechanics, acoustics, electronics etc.[1]

One of the properties that make them really significant is their ability to produce plasma during Inertial Confinement Fusion (ICF) [4], which is is a method of achieving nuclear fusion by using lasers or other energy sources to compress and heat a small fuel pellet until it implodes and fuses. The main requirements of the microstructures in order to be used as targets, are low and uniform density [5], as well as the absence of more heavy elements than Carbon.

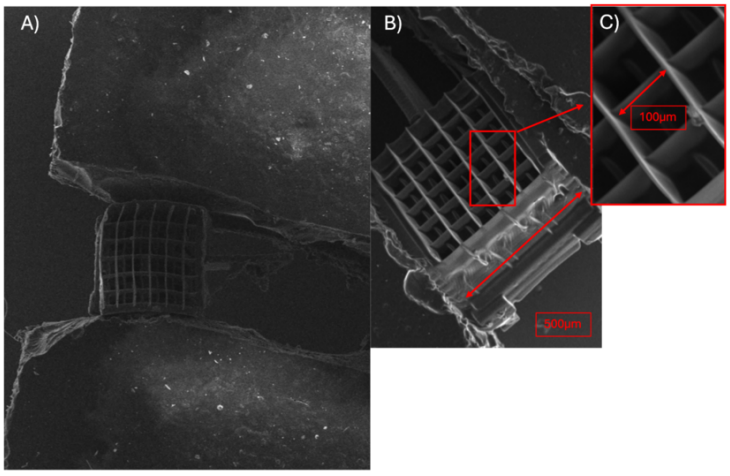


Fig. 1. Scanning Electron Mic1oscope (SEM) pictures of A) high-porosity woodpile microstructures integrated into the holder. B), C) Magnified woodpile inside the 3D printed holder. The estimated density of the structure is 0.07% g/cm^3. The distance between the filaments is 100 µm. The woodpile has dimensions 500 µm in X and Y axis and 250 µm in Z axis.

The aim of this work is to fabricate low-density woodpile geometry foams of acrylate materials using TPL, employing a 517 nm femtolaser source. To achieve this, laser power and scanning speed parameters were optimized to ensure the fabrication of stable, reproducible microstructures with high resolution. Specifically, the materials that were used were (PETA:PETTA)(60:40) and photoinitiator 0.5% thioxanthone-9h, which is a chemical compound that absorbs light and produces reactive species, such as free radicals, to initiate polymerization. The achieved density was 0.07% g/cm^3. Mechanical characterization was performed using Atomic Force Microscopy (AFM) by Maria Frasari and her colleagues at IESL-FORTH with data analysis currently ongoing. Finally, the woodpiles were integrated into a 3D printed holder, which is easy handling during ICF experiments, that will be conducted at ABC group of ENEA in Frascati by dr. Mattia Cipriani.

[1] H. Wang et al., “Two-photon polymerization lithography for optics and photonics: Fundamentals, materials, technologies, and applications,” Advanced Functional Materials, vol. 33, no. 22, Art. no. 2214211, 2023, doi: 10.1002/adfm.202214211.
[2] V. Skliutas et al., Polymerization Mechanisms Initiated by Spatio-Temporally Confined Light. Berlin, Germany: De Gruyter Brill, 2021.
[3] H.-B. Sun and S. Kawata, “Two-photon photopolymerization and 3D lithographic microfabrication,” Applied Physics A, vol. 79, no. 3, pp. 525–531, 2004.
[4] M. Cipriani et al., “Experimental and simulative study on laser irradiation of 3D-printed micro-structures at intensities relevant for inertial confinement fusion,” Matter and Radiation at Extremes, vol. 11, no. 2, Art. no. 027401, 2025, doi: 10.1063/5.0283201.
[5] S. Iaquinta, P. Amendt, J. Milovich, and E. L. Dewald, “Characterization of foam-filled hohlraums for inertial fusion experiments,” arXiv preprint arXiv:2406.03475, Jun. 2024, doi: 10.48550/arXiv.2406.03475.

ORAL SESSION 10

Materials Science and Nanotechnology

Chair: Dr. T. Malinauskas

EXPLORING THE GROUP-V LIMITED GROWTH OF GaAsBi LAYERS

Aivaras Špokas[1], Andrea Zelioli[1], Aistė Štaupienė[1], Andrėja Janulevičiūtė[1], Justas Žuvelis[1], Sandra Stanionytė[1], Giedrius Stalnionis[1], Evelina Dudutienė[1], Renata Butkutė[1]

[1]Center for Physical Sciences and Technology, Vilnius, Lithuania
aivaras.spokas@ftmc.lt

Near-infrared is one of the most important spectral regions in current technologies related to compact sensors for consumer electronics, LiDAR, and optical data transfer. GaAsBi is an attractive optoelectronic material for these applications due to its rapid bandgap reduction, ability to suppress Auger recombination, low emission wavelength sensitivity to temperature [1-3]. Even though some GaAsBi-based lasers and LEDs have been realised, the wider application of this alloy is limited by the challenging growth at reduced temperature and low group-V flux resulting in poor crystalline quality. It was noticed that when growing thicker layers (> 30 nm), the GaAsBi growth mode changes and the effective growth rate decreases, thickness deviates from the nominal value. Moreover, a large metallic droplet surface coverage is observed [4-7]. In this work we investigate the peculiarities of growing thick GaAsBi layers focusing on finding the optimal growth condition window for low roughness, high emission intensity at $\approx$ 1 eV and predictable layer thickness.

A series of GaAsBi samples were grown using a Veeco GENxplor R&D MBE system while varying the As, Ga and Bi fluxes at $\approx$ 350 °C substrate temperature. The structural properties were assessed by Nomarski and scanning electron microscopies, energy-dispersive X-ray (EDX) spectroscopy, X-ray diffraction, optical properties were investigated by photoluminescence (PL) spectroscopy. For samples grown in the As to Ga beam equivalent pressure ratio (BEPR) window from 1 to 8 several changes in the growth regime were noticed. In the As/Ga window of 1 to 2, a large metallic Ga droplet surface coverage is observed, pointing to an As deficiency and causing the reduced growth rate. At As/Ga > 3.5 a significant change of surface morphology is observed, with the droplet covered area decreasing by a factor of 8, while the composition of the droplets changes from mostly Ga to biphasic Ga-Bi, signalling the transition away from group-V limited growth. Further increasing the As pressure to As/Ga = 5, an improvement in surface roughness is observed, with very few droplets (d < 250 nm) detected. Additionally, at this point, the PL emission related with transitions in GaAsBi is no longer observed. Finally, at As/Ga > 6, the surface is completely free of metallic droplets, signifying that group-III limited growth conditions are achieved.

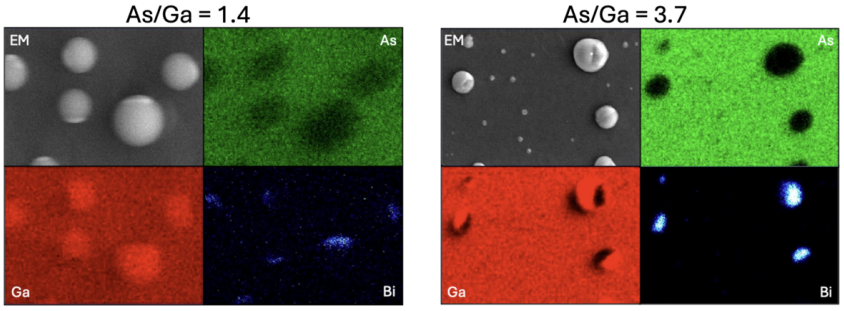


Fig. 1. SEM-EDX images of samples grown with different As to Ga BEPR. For the sample at As/Ga = 1.4 a high density of round droplets mostly comprised of Ga is observed. For sample grown at As/Ga = 3.7 a low density of biphasic Ga-Bi droplets is seen, signifying approach to the transition from group-V to group-III limited growth.

Acknowledgements

This project has received funding from the Research Council of Lithuania (LMTLT), agreement No. S-LT-TW-24-8.

[1] K. Oe, H. Okamoto, “New semiconductor alloy GaAs1-XBiX grown by Metal Organic Vapor Phase Epitaxy,” Jpn. J. Appl. Phys., vol. 37, p. L1283, 1998.
[2] S. Francoeur, M.-J. Seong, A. Mascarenhas, S. Tixier, M. Adamcyk, T. Tiedje, “Band gap of GaAs1-xBix, 0 < x 3.6%,” Appl. Phys. Lett., vol. 82, pp. 3874–3876, 2003.
[3] K. Alberi, O. D. Dubon, W. Walukiewicz, K. M. Yu, K. Bertulis, A. Krotkus, “Valence band anticrossing in GaBixAs1-x,” Appl. Phys. Lett., vol. 91, Art. no. 051909, 2007.
[4] G. Vardar, S. W. Paleg, M. V. Warren, M. Kang, S. Jeon, and R. S. Goldman, “Mechanisms of droplet formation and Bi incorporation during molecular beam epitaxy of GaAsBi,” Appl. Phys. Lett., vol. 102, no. 4, 2013.
[5] Y. Tominaga, Y. Horita, Y. Takagaki, F. Nishiyama, M. Yukimune, F. Ishikawa, “Crystalline quality of GaAs1−x Bi x grown below 250 °C using molecular beam epitaxy,” Appl. Phys. Express, vol. 15, no. 4, p. 045504, 2022.
[6] M. A. Stevens, K. A. Grossklaus, J. H. McElearney, T. E. Vandervelde, “Impact of rotation rate on bismuth saturation in GaAsBi grown by molecular beam epitaxy,” J. Electron. Mater., vol. 48, no. 5, pp. 3376–3382, J2019.
[7] M. A. Stevens, K. A. Grossklaus,T. E. Vandervelde, “Strain stabilization of far from equilibrium GaAsBi films,” J. Cryst. Growth, vol. 527, p. 125216, 2019.

STRUCTURAL AND OPTICAL INVESTIGATION OF GaAsBi/AlGaAs PARABOLICALLY GRADED QUANTUM WELL STRUCTURES

Aistė Štaupienė[1], Andrea Zelioli[1], Aivaras Špokas[1], Martynas Skapas[1], Bronislovas Čechavičius[1], Renata Butkutė[1], Evelina Dudutienė[1]

[1]Lithuania, Vilnius, SRI Center for Physical Sciences and Technology
aiste.staupiene@ftmc.lt

GaAsBi quantum well (QW) structures are one category of materials currently being studied for active area of light sources operating in the near-infrared (NIR) range [1]. A key advantage of GaAsBi is the strong band-gap redshift with increasing Bi content, together with enhanced spin–orbit splitting that can suppress Auger recombination and inter-valence-band absorption [2]. In addition, GaAsBi shows reduced temperature sensitivity [3], enabling tunable laser operation on the mature GaAs platform without the need for additional cooling. However, complicated growth conditions required for bismides [4] produce a high point-defect density, which degrades crystal quality and luminescence intensity. This has a detrimental effect on emission efficiency and therefore limits the practical implementation of GaAsBi-based optoelectronic devices.

This study investigates how technological modifications, such as, the use of non-conventional graded AlGaAs barriers or thermal treatments affect emission and structural properties of GaAsBi QW structures. We demonstrate that combining QWs with parabolically graded barriers (PQWs) together with optimized in-situ and/or ex-situ annealing can boost emission intensities by 25 times compared to conventional GaAsBi QWs. Annealing, however, promotes Bi redistribution that can distort the quantum structure by degrading the heterointerfaces. To suppress Bi segregation we therefore implemented ultrathin AlAs layers as Bi-blocking barriers. GaAsBi PQWs with these AlAs barriers show improved structural uniformity and even when Bi quantum dots (QDs) form after annealing they do not degrade the heterostructures (see figure 1). Unfortunately, although AlAs layers enhance structural quality, they tend to worsen optical performance of GaAsBi/AlGaAs QWs. The presence of AlAs reduces emission intensity, increases thermal quenching and carrier localization effects. However, this study showed that adverse optical effects introduced by AlAs can be partially mitigated by in-situ annealing and reducing the AlAs barrier thickness. These findings contribute to the optimization of GaAsBi growth processes, paving the way for enhanced optoelectronic device performance in the NIR region.

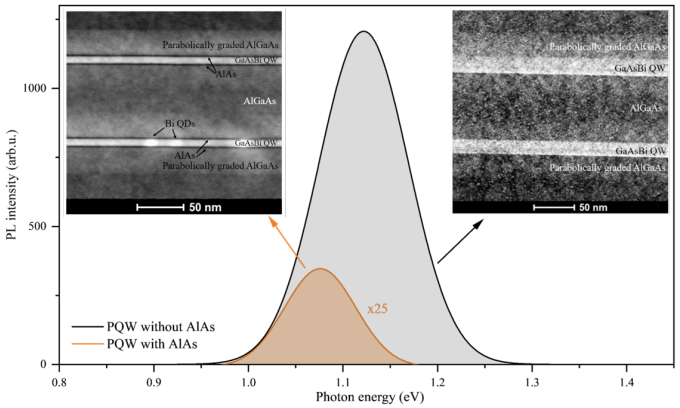


Fig. 1. Room temperature PL spectra and transmission electron microscopy micrographs of GaAsBi/AlGaAs PQW structures with and without AlAs Bi-blocking barriers.

Acknowledgements

This project has received funding from the Research Council of Lithuania (LMTLT), agreement No. S-MIP-24-99.

[1] R. D. Richards, N. J. Bailey, Y. Liu, T. B. O. Rockett, and A. R. Mohmad, “GAASBI: From molecular beam epitaxy growth to devices,” Physica Status Solidi (B), vol. 259, no. 2, Nov. 2021, doi: 10.1002/pssb.202100330.

[2] Z. Batool, K. Hild, T. J. C. Hosea, X. Lu, T. Tiedje, and S. J. Sweeney, “The electronic band structure of GaBiAs/GaAs layers: Influence of strain and band anti-crossing,” Journal of Applied Physics, vol. 111, no. 11, Jun. 2012, doi: 10.1063/1.4728028.

[3] J. Yoshida, T. Kita, O. Wada, and K. Oe, “Temperature dependence of GAAS1-xBixBand gap studied by photoreflectance spectroscopy,” Japanese Journal of Applied Physics, vol. 42, no. Part 1, No. 2A, pp. 371–374, Feb. 2003, doi: 10.1143/jjap.42.371.

[4] R. D. Richards et al., “Molecular beam epitaxy growth of GaAsBi using As2 and As4,” Journal of Crystal Growth, vol. 390, pp. 120–124, Dec. 2013, doi: 10.1016/j.jcrysgro.2013.12.008.

IMPACT OF RAPID THERMAL ANNEALING ON STRUCTURAL AND OPTICAL PROPERTIES OF GaAsBi/(Al,Ga)As QUANTUM WELLS

Patricija Strumilaitė[1], Aivaras Špokas[1], Justas Žuvelis[1], Andrea Zelioli[1], Sandra Stanionytė[1], Kipras Mažeika[2], Augustas Vaitkevičius[1,2], Renata Butkutė[1], Evelina Dudutienė[1]

[1]SRI Center for Physical Sciences and Technology, Department of Optoelectronics, Lithuania
[2]Vilnius University, Faculty of Physics, Institute of Photonics and Nanotechnology, Lithuania
patricija.strumilaite@ff.stud.vu.lt

Replacing a small fraction of As atoms in the GaAs lattice by Bi strongly reduces the band gap energy (E_g) and significantly suppresses its temperature dependence [1,2]. These properties make GaAsBi quantum structures promising for active regions of near-infrared light-emitting devices. However, the very low growth temperatures required (< 440 ^{o}C [3]) increase defect density and reduce photoluminescence (PL) efficiency [4]. Post-growth annealing is commonly used to improve epitaxial layer quality, yet its effects on GaAsBi remain controversial [5,6] and requires further investigation.

In this work, optical properties of GaAsBi/(Al,Ga)As multiple quantum well (MQW) structures grown by molecular beam epitaxy (MBE) were investigated using PL spectroscopy. The Bi concentration ranged from 8 to 11 %. Post-growth annealing was performed in a rapid thermal annealing (RTA) furnace under nitrogen atmosphere at 550, 600, 650, 700, and 750 ^{o}C for 3 minutes. Structural and morphological properties were additionally examined using high-resolution X-ray diffraction (XRD) and atomic force microscopy (AFM).

Annealing GaAsBi MQW with GaAs barrier resulted in degradation of crystalline and optical properties at all investigated temperatures. This behavior is attributed to Bi segregation from the GaAsBi to the surface, disrupting the periodic GaAsBi/GaAs structure. In contrast, GaAsBi MQW with AlGaAs barriers exhibited enhanced optical performance upon annealing at 650 ^{o}C and 700 ^{o}C, with PL intensity increases of 83% and 24%, respectively, indicating improved crystalline quality and effective Bi confinement. Annealing above 700 ^{o}C degraded the optical properties of all samples. A blueshift of the PL emission was observed in all structures annealed above 600 ^{o}C, indicating a reduction of Bi content in the GaAsBi lattice. Although literature reports suggest Bi quantum dot (QD) formation during annealing [7], no QD-relate emission was detected from 4 K to 300 K, implying an insufficient concentration of optically active Bi nanocrystallites.

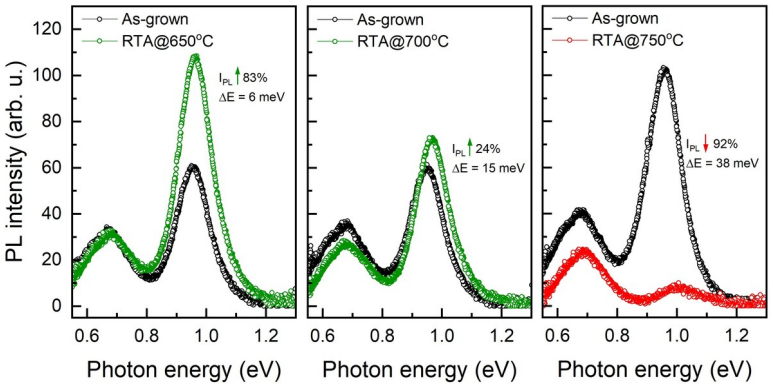


Fig. 1. Room-temperature PL spectra of GaAsBi/AlGaAs MQW before and after RTA at different temperatures.

Acknowledgements

This research has received funding from the Research Council of Lithuania (LMTLT), agreements No. S-SV-25-203 and No. S-MIP-24-99.

[1] S. Francoeur et al., "Band gap of GaAs1−xBix, 0<x<3.6%," Applied Physics Letters, vol. 82, no. 22, pp. 3874–3876, May 2003, doi: 10.1063/1.1581983.
[2] K. Alberi et al., "Valence band anticrossing in GaBixAs1−x," Applied Physics Letters, vol. 91, no. 5, Jul. 2007, doi: 10.1063/1.2768312.
[3] R. D. Richards et al., "Molecular beam epitaxy growth of GaAsBi using As2 and As4," Journal of Crystal Growth, vol. 390, pp. 120–124, Dec. 2013, doi: 10.1016/j.jcrysgro.2013.12.008.
[4] A. Štaupienė et al., "Internal quantum efficiency of GaAsBi MQW structure for the active region of VECSELs," Applied Physics Letters, vol. 125, no. 22, Nov. 2024, doi: 10.1063/5.0234853.
[5] P. C. Grant et al., "Rapid thermal annealing effect on GaAsBi/GaAs single quantum wells grown by molecular beam epitaxy," Journal of Vacuum Science & Technology B Nanotechnology and Microelectronics Materials Processing Measurement and Phenomena, vol. 32, no. 2, Mar. 2014, doi: 10.1116/1.4868110.
[6] B. Čechavičius et al., "Thermal annealing effect on photoexcited carrier dynamics in GaBixAs1−x," Semiconductor Science and Technology, vol. 26, no. 8, p. 085033, Jun. 2011, doi: 10.1088/0268-1242/26/8/085033.
[7] R. Butkutė et al., "Bismuth Quantum Dots in annealed GaAsBi/AlAs Quantum Wells," Nanoscale Research Letters, vol. 12, no. 1, p. 436, Jun. 2017, doi: 10.1186/s11671-017-2205-7.

LOCAL V-DEFECT ENVIRONMENTS UNDER EXCITATION-DEPENDENT TRANSIENT CATHODOLUMINESCENCE

Gabija Soltanaitė[1], Mantas Migauskas[1], Žydrūnas Podlipskas[1]

[1]Vilnius University, Faculty of Physics, Institute of Photonics and Nanotechnology
gabija.soltanaite@ff.vu.lt

V-defects, observed in group-III nitride compounds, originate from threading dislocations present in the epitaxial layers and may serve as an effective tool to mitigate the impact of dislocations on device performance. While the influence of V-defects on carrier dynamics is being actively studied, a complete understanding is still lacking. This study is set to investigate V-defects using time-resolved cathodoluminescence (TRCL), linking essential parameters - carrier lifetime, spectral characteristics, and defect architecture.

As defect size is considered to be directly related to defect properties, we study hundreds of V-defects from eight InGaN samples with different structure and material quality, grouped according to defect size. Each defect was individually measured, obtaining cathodoluminescence maps and streak images by beam-pointing across its geometry. Subsequently, profiles were constructed for each defect, showing cathodoluminescence intensity and carrier lifetime variations from the defect center to its periphery along both directions. Measurements were also performed using varying probe currents (1.5 - 33 pA) for selected defect groups in samples with contrasting internal quantum efficiency (IQE).

Each defect was evaluated using a measure of profile depth for intensity and lifetime, defined as I_p/I_c and τ_p/τ_c. Results for defects of different sizes (from 30 nm to 5 μm) reveal a positive correlation between defect size and profile depth for both intensity and lifetime profiles. Higher number of carriers reaching dislocations and participating in nonradiative recombination can be expected in defects with larger diameters due to weaker carrier localization in the quantum wells formed on the extended sidewalls. Thicker sidewall quantum wells formed early in the growth process and a smoother potential landscape can affect localization, increasing carrier interaction with defect-related nonradiative centers.

Defect profiles obtained under varying excitation conditions provide additional insight into carrier recombination processes. In this case, a minor negative correlation between probe current and profile depths τ_p/τ_c and I_p/I_c is observed for both high-IQE and low-IQE samples.

Keywords: Nitrides, cathodoluminescence, V-defects

CARRIER DYNAMICS IN N- AND P-TYPE InGaN LAYERS AND THE ROLE OF MAGNESIUM ACTIVATION

Seda Türkcan[1], Kazimieras Nomeika[1]

[1]Lithuania, Vilnius, Vilnius University, Faculty of Physics, Institute of Photonics and Nanotechnology
seda.turkcan@ff.stud.vu.lt

Indium gallium nitride (InGaN) is a key material for optoelectronic devices such as light-emitting diodes, laser diodes, and solar cells, where high-quality n- and p-type layers are essential for optimal performance. While efficient n-type conductivity in III-nitrides is readily achieved using dopants such as Si or C, reliable p-type doping remains challenging because the dopant magnesium (Mg) acceptors are passivated by hydrogen through the formation of Mg–H complexes. Activation of Mg typically requires post-growth rapid thermal annealing (RTA) to dissociate these complexes; however, such processing can introduce nitrogen-vacancy (N_V)–related defects that degrade material properties. Despite extensive studies on the electrical behavior of Mg-doped InGaN, a detailed understanding of how Mg activation influences carrier dynamics remains incomplete, particularly regarding recombination and transport following annealing.

In this work, carrier dynamics in both n-type and Mg-doped p-type InGaN layers, including as-grown and annealed samples with varying indium compositions are investigated, using time-integrated photoluminescence (TIPL) and light-induced transient grating (LITG) techniques. The results show increased carrier diffusivity in annealed p-type layers, accompanied by a reduction in carrier lifetime. Internal quantum efficiency (IQE) analysis is used in combination with ABC modeling to extract recombination coefficients and quantitatively evaluate the dominant recombination and transport processes. This comparative approach elucidates the differences in carrier dynamics between n- and p-type InGaN and highlights the impact of Mg activation and annealing-induced defects on recombination pathways.

ELECTROLUMINESCENCE STUDY OF GaAsBi-BASED NEAR-INFRARED EMITTERS

Justas Žuvelis[1], Andrius Bičiūnas[1], Aivaras Špokas[1], Mindaugas Kamarauskas[1], Andrea Zelioli[1], Evelina Dudutienė[1], Renata Butkutė[1]

[1]Lithuania, Center for Physical Sciences and Technology, Vilnius
justas.zuvelis@ftmc.lt

Emitters designed for the near-infrared (NIR) are essential for a wide variety of applications, spanning optical communications, medical imaging, and remote sensing. However, achieving efficient NIR emission, especially beyond 1 µm, on the GaAs platform remains challenging. The most widely used material system in this spectral region is InGaAs/GaAs quantum wells (QWs). However, device performance is limited by Auger recombination and the necessity for high indium content, resulting in degraded optical efficiency due to misfit dislocations [1]. An attractive alternative for NIR emission is GaAsBi. By substituting arsenic atoms with bismuth (Bi), the bandgap shrinks by 60-90 meV per % Bi, and above 10.5 % Bi the spin–orbit splitting energy exceeds the bandgap, suppressing a prominent Auger recombination channel [2]. Although achieving high crystalline quality remains challenging, growth optimization and rigorous studies over the past decades have enabled the fabrication of light-emitting devices (LEDs) and laser diodes [3]. Therefore, it is increasingly important to evaluate GaAsBi-based emitter performance under electrical injection.

In this work, temperature-dependent electroluminescence (EL) spectroscopy is used to characterize several molecular-beam-epitaxy grown LED and laser-diode structures with different GaAsBi active-region designs (see Fig. 1). The study focuses on quantifying how the emission wavelength and intensity depend on operating temperature and drive current, and on evaluating the internal quantum efficiency [4]. In addition, photoluminescence measurements are done to assess how the dominant recombination channels change under electrical injection. The optical investigation is further supported by electronic-structure modeling using the *nextnano* software, shown in the inset of Fig. 1, which enables estimation of the Bi content and provides insight into carrier confinement within the device structures.

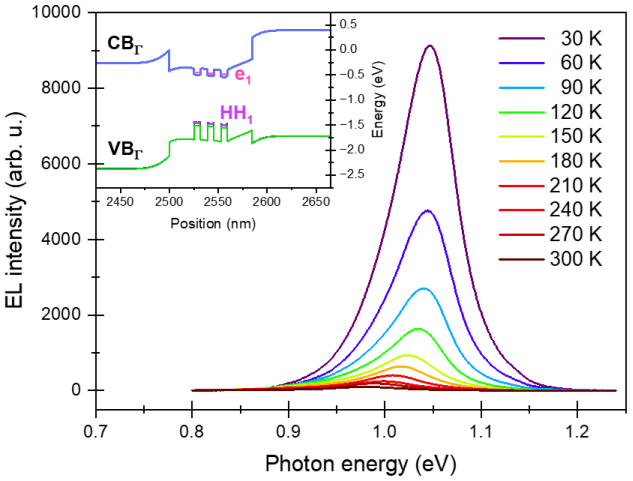


Fig. 1. Temperature-dependent electroluminescence spectra of a 6.8 nm multiple-quantum-well laser diode measured under a constant injection current of 30 mA. The inset shows the electronic structure of the forward-biased active region calculated using *nextnano++*, including the conduction-band (CB) and valence-band (VB) profiles at the Γ point, as well as the confined electron (e_1) and heavy-hole (HH_1) states.

Acknowledgements
This project has received funding from the Research Council of Lithuania (LMTLT), Agreement No. S-ST-25-78.

[1] Y. Q. Wei et al., "Long-wavelength InGaAs/GaAs quantum-well lasers grown by molecular beam epitaxy," Journal of Crystal Growth, vol. 278, no. 1–4, pp. 747–750, Mar. 2005, doi: 10.1016/j.jcrysgro.2004.12.094.
[2] Z. Batool, K. Hild, T. J. C. Hosea, X. Lu, T. Tiedje, and S. J. Sweeney, "The electronic band structure of GaBiAs/GaAs layers: Influence of strain and band anti-crossing," Journal of Applied Physics, vol. 111, no. 11, Jun. 2012, doi: 10.1063/1.4728028.
[3] A. Špokas et al., "Optimising (AL,GA) (AS,BI) Quantum Well laser structures for reflectance mode pulse oximetry," Micromachines, vol. 16, no. 5, p. 506, Apr. 2025, doi: 10.3390/mi16050506.
[4] J.-I. Shim and D.-S. Shin, "Measuring the internal quantum efficiency of light-emitting diodes: towards accurate and reliable room-temperature characterization," Nanophotonics, vol. 7, no. 10, pp. 1601–1615, Sep. 2018, doi: 10.1515/nanoph-2018-0094.

ORAL SESSION 11

Laser Physics and Optical Technologies

Chair: Dr. B. Momgaudis

CONTROL OF SURFACE THERMAL EMISSION USING ULTRASHORT LASER PULSES

Tadas Latvys[1], Evaldas Kažukauskas[1], Simas Butkus[1]

[1]Vilnius university, Laser Research Center, Saulėtekio al. 10, 10223 Vilnius
tadas.latvys@ff.vu.lt

The rapid growth of information technology has heightened the need for advanced anti-counterfeiting measures, shifting focus toward optical encryption that utilizes dimensions beyond the visible spectrum. While the mid-infrared range offers a natural advantage for data concealment, current methods for controlling thermal radiation often rely on complex multi-layer structures or expensive materials that are difficult to scale [1]. This study investigates the feasibility of controlling the thermal emissivity (ε) of fused silica through femtosecond laser surface engraving. The research seeks to establish a precise relationship between laser-induced surface morphology and thermal emission properties to create a platform for hidden, thermally activated data encoding.

Surface engraving was performed on fused silica using a femtosecond laser ($\lambda = 1030$ nm, $\tau = 211$ fs). By systematically varying the energy density (F) and pulse overlap (Ω), different surface roughness (S_a) values were achieved. Emissivity measurements were carried out using an infrared camera in the MIR atmospheric window (7.5–14.0 μm).

Experimental results show that surface emissivity can be precisely tuned even with minimal topographical changes ($\Delta S_a < 10$ nm). Notably, as seen in Fig. 1 (a) increasing the surface roughness of fused silica leads to a decrease in thermal emissivity, suggesting that the emission is governed by structural changes in the ablated layer and modified scattering angles.

The practical application of the findings was demonstrated by encoding complex patterns, including a chessboard seen in Fig. 1 (b) onto the fused silica surface using two distinct fluences (4.4 J/cm^2 and 12.5 J/cm^2) and $\Omega = 30\%$. While these encoded patterns remain invisible to the naked eye, heating the substrate to 400 °C provides the necessary thermal activation to reveal high-contrast, decodable information via a thermographic system.

This research demonstrates that laser engraving fused silica provides a robust and scalable method for programming thermal radiation. The findings offer a promising solution for high-security applications, such as heat-activated encryption and anti-counterfeiting labels that remain hidden under ambient conditions.

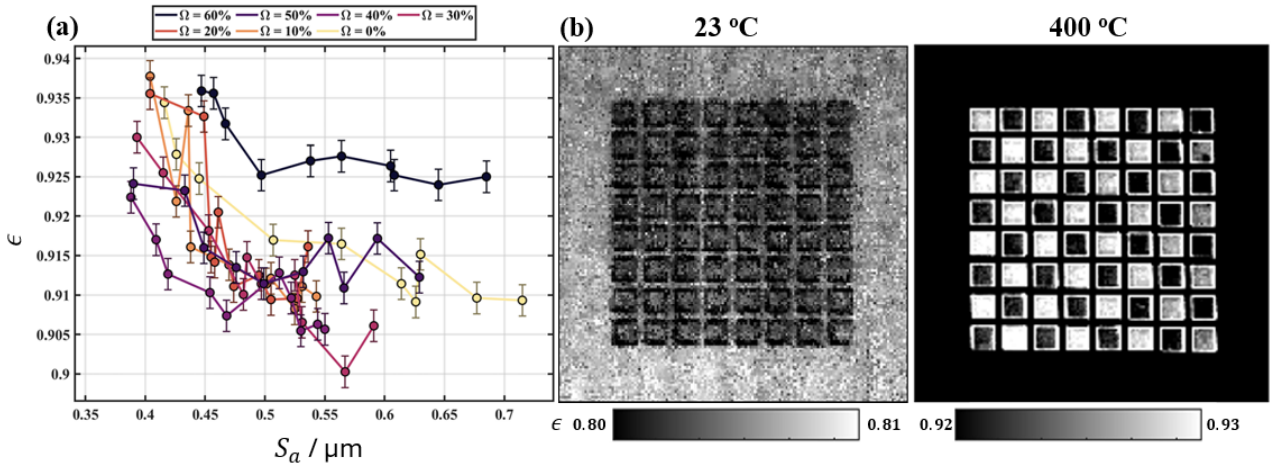


Fig. 1. Experimental results: (a) emissivity ε dependence on surface roughness S_a; (b) thermally encoded information.

[1] Z. Li and W. Chen, "Progress in dynamic emissivity regulation: control methods, material systems, and applications," Mater. Chem. Front., vol. 5, no. 17, pp. 6344–6366, 2021.

BOTTOM-UP DRILLING OF GLASS USING BURSTS OF ULTRASHORT LASER PULSES

Aleksandras Kondratas[1], Juozas Dudutis[1], Paulius Gečys[1]

[1]Center for Physical Sciences and Technology, Savanoriu ave. 231, LT-02300, Vilnius, Lithuania
aleksandras.kondratas@ftmc.lt

Through glass vias (TGVs) have gathered attention for applications in Micro-Opto-Electro-Mechanical Systems (MOEMS) as interposers [1], nozzles for laser wakefield accelerators [2] and connections for microfluidic devices [3]. This is because glass works as a better electrical insulator compared to widely used silicon wafers, has high mechanical strength, and its composition can be modified to change thermal expansion coefficient. Common TGV fabrication methods like electrochemical discharge (EDM) and laser-induced chemical etching (LISE) have difficulties producing over millimeter depth holes and result in tapered openings [4].

Laser drilled TGVs can have parallel walls and multimilimeter depths when utilizing bottom-up drilling technique. This technique offers enhanced milling rate compared to top-down drilling. Additionally, milling rate can be further improved by using laser bursts which consist of multiple ultrashort pulses with intra-burst repetition rates on the order of few tens of MHz up to THz [5]. Bursts work by first heating, introducing defects, or temporarily modifying the material which lowers the ablation threshold for subsequent pulses resulting in efficient ablation. For dielectric materials, ablation mechanism changes with higher number of pulses in the GHz burst to surface cracking and subsequent expulsion of micron sized particles. Debris is often the limiting factor for the creation of high depth channels [6]. Therefore, additional debris removal methods need to be employed.

In this study, laser milling parameters – GHz burst count, burst energy, pitch, spacing, and sample translation distance during milling, were optimised. 100 µm diameter through glass vias were milled in 1 mm and 6.3 mm thickness fused silica (FS) samples as seen in Fig 1. Ultrashort pulse laser FemtoLux 30 from Ekspla was used for the experiment operating in GHz burst regime. For part of the experiments, nozzles were used to blow pressurised air at the drilling areas to enhance debris removal.

Increase in GHz burst count in bottom-up drilling of fused silica resulted in more clean and efficient milling, however, at the cost of quality due to increased surface chipping. Reduced channel to channel distance was achieved by segmenting cavity milling, where only a part of the depth was milled for a cavity before moving on to another cavity. High airflow de Laval nozzle allowed us to mill through 6.3 mm fused silica sample.

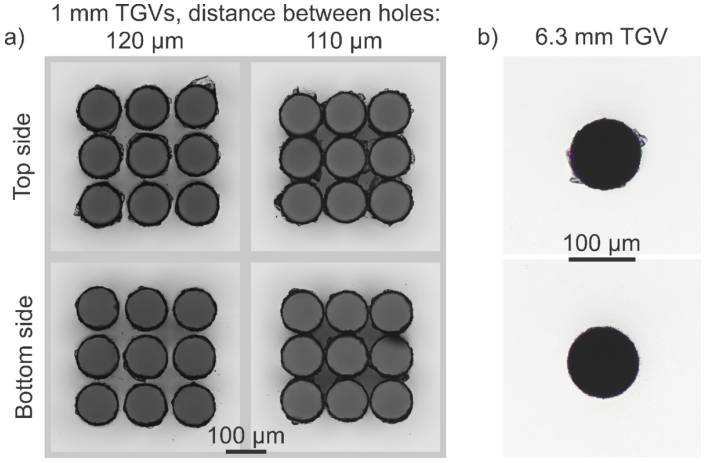


Fig. 1. Microscope images of top and bottom side of TGVs drilled in a) 1 mm thickness FS and no air flow and b) 6.3 mm thickness FS and air flow from de Laval nozzle.

[1] Xu, Q., Fang, D., Zhang, X., et al. “Etch the borosilicate glass to form a straight through-glass-via based on the FLACE technology”, Journal of Micromechanics and Microengineering, p. 055008, Vol. 32, 2022.
[2] Tomkus, V., Mackevičiūtė, M., Dudutis, J., et al. “Laser-machined two-stage nozzle optimised for laser wakefield acceleration”, Journal of Plasma Physics, Vol. 90, p. 965900102, 2024.
[3] Lu, Y., Li, Y. F., Wang, G., et al. “Femtosecond laser fabrication of microchannels in transparent hard materials”, Advanced Materials Technologies, Vol. 8, p. 2300015, 2023.
[4] Yu, C., Wu, S., Zhong, Y., et al. “Application of through glass via (TGV) technology for sensors manufacturing and packaging” Sensors, Vol. 24, p. 171, 2023.
[5] Balage, P., Bonamis, G., Lafargue, M., et al. “Advances in femtosecond laser GHz-burst drilling of glasses: Influence of burst shape and duration”, Micromachines, Vol. 14, p. 1158, 2023.
[6] Dudutis, J., Račiukaitis, G., Daknys, E., et al. “Quality and flexural strength of laser-cut glass: classical top-down ablation versus water-assisted and bottom-up machining”, Optics Express, Vol. 30, pp. 4564–4582, 2022.

FABRICATION AND CHARACTERIZATION OF OPAQUE 3D MICROSTRUCTURES

Abhinay V Mohan[1], Robertas Virketis[2], Artur Harnik[1], Mantas Gaidys[1], Greta Merkininkaite[2], Gordon Zyla[1], Mangirdas Malinauskas[1]

[1]Vilnius University, Faculty Of Physics, Laser Research Center, Vilnius, Lithuania
[2]Vilnius University, Faculty Of Chemistry and Geosciences, Vilnius, Lithuania
abhinay.mohan@ff.stud.vu.lt

3D laser direct writing has been employed as a technology of rapidly increasing importance [1], finding its applications in various fields, especially in micro-optics [2], with a growing demand for transparent and opaque three dimensional microstructures, where opaque microelements play essential roles, especially for stray light suppression, beam blocking and beam absorption. While Two Photon Polymerization (TPP) enables the fabrication of complex, high resolution free-form 3D structures [3], the construction of opaque microstructures remains challenging, due to the strong absorption of opaque photoresists in the UV to near-infrared spectral regime [4]. Moreover, most of the previous demonstrations of opaque microstructures have been achieved using organic photoresists, which limit the mechanical and thermal performance of the fabricated components [4,5].

In this work, truly opaque and inorganic microstructures are fabricated using a hybrid organic-inorganic photoresist as the precursor material [6], providing a viable alternative to organic precursors, with improved chemical inertness and mechanical robustness. The hybrid resist is optically transparent during fabrication, enabling efficient photopolymerization, which turns opaque only after thermal post-processing. Using femtosecond laser-based TPP, the smallest feature size of 755 nm was achieved with the hybrid resist. The fabricated structures were subjected to pyrolysis at 1400^{o}C, in an inert nitrogen atmosphere to remove the organic fraction of the structures, yielding opaque and ceramic microstructures, including solid cubes of dimensions 80 x 80 x 30 μm^3 as shown in Fig 1b.

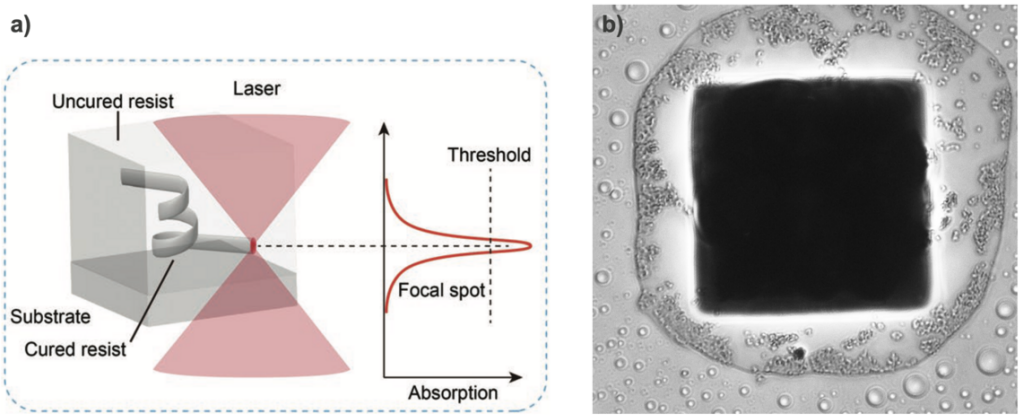


Fig. 1. (a) Process of two photon polymerization, adopted from [3]. (b) Opaque microstructure experimentally observed under transmission microscope

Systematic optimization of laser parameters was performed through the fabrication of an array of test structures, with varying laser power and scanning velocity, enabling the construction of robust free-form microstructures with sub-micrometer feature sizes. Post pyrolysis characterization of structures confirmed the formation of opaque and inorganic microstructures which were further analyzed for opaqueness, surface roughness, structure composition, and shrinkage behavior. These results demonstrate a versatile route for producing opaque and ceramic microstructures using the hybrid organic-inorganic precursor, combined with the high geometric freedom and resolution provided by TPP. They also highlight the potential applications of such structures especially in micro-optics, which require opaque and thermally stable microcomponents such as apertures, beam blockers and absorbers at the microscale.

[1] T. Q. Tran, “Recent advances in 3D printing and additive manufacturing technology,” Applied Sciences, vol. 15, no. 17, p. 9599, Aug. 2025, doi: 10.3390/app15179599.
[2] D. Gonzalez-Hernandez et al., “Laser 3D printing of inorganic Free-Form Micro-Optics,” Photonics, vol. 8, no. 12, p. 577, Dec. 2021, doi: 10.3390/photonics8120577.
[3] S. O’Halloran, A. Pandit, A. Heise, and A. Kellett, “Two-Photon Polymerization: Fundamentals, materials, and Chemical Modification Strategies (Adv. Sci. 7/2023),” Advanced Science, vol. 10, no. 7, Mar. 2023, doi: 10.1002/advs.202370039.
[4] M. D. Schmid, A. Toulouse, S. Thiele, S. Mangold, A. M. Herkommer, and H. Giessen, “3D direct laser writing of highly absorptive photoresist for miniature optical apertures,” Advanced Functional Materials, vol. 33, no. 39, Dec. 2022, doi: 10.1002/adfm.202211159.
[5] P. N. S. Nair et al., “Fabrication of opaque and transparent 3D structures using a single material via two-photon polymerisation lithography,” Light Advanced Manufacturing, vol. 4, no. 3, p. 1, Jan. 2023, doi: 10.37188/lam.2023.025.
[6] G. Merkininkaite et al., “Additive manufacturing of SIOC, SIC, and SI3N4 ceramic 3D microstructures,” Advanced Engineering Materials, vol. 25, no. 17, Jul. 2023, doi: 10.1002/adem.202300639.

FULL-FIELD VIBRATION MEASUREMENTS USING SINGLE-SHOT SYNTHETIC WAVELENGTH INTERFEROMETRY

Florian Dötzer[1], Muralidhar Madabhushi Balaji[2], Patrick Cornwall[2], Tianyi Wang[2], Stefan Sinzinger[1], Florian Willomitzer[2]

[1]TU Ilmenau, Department of Mechanical Engineering, Optical Engineering Group, Germany
[2]University of Arizona, Wyant College of Optical Sciences, 3DIM Group, USA
florian.doetzer@tu-ilmenau.de

Vibrations in daily life as well as in engineering often exhibit displacement amplitudes on the order of few micrometers and frequencies in the kilohertz-regime. The characterization of such vibrations poses a challenge, because micrometer displacement amplitudes are close to the lower detection limit for most incoherent full-field topography measurement methods. Regular interferometric techniques on the other hand are more useful for displacements in the nanometer-regime, as the variation in surface height between two frames must be significantly smaller than the optical wavelength to ensure unambiguous results. For displacement amplitudes of several micrometers this means that a large number of frames must be captured for each vibration period. This requires a camera with an excessively high frame rate much higher than the vibration frequencies to be studied.
Synthetic Wavelength Interferometry (SWI) solves this problem by making use of wavelength diversity to extend the unambigous measurement range. Specifically, interferometric measurements at two slightly different optical wavelengths λ_1 and λ_2 are recorded and evaluated. The phase difference between the two measured complex fields corresponds to the phase of the field at the synthetic wavelength $\Lambda = \lambda_1 \cdot \lambda_2 / |\lambda_1 - \lambda_2|$. It follows that the synthetic wavelength is tuneable in a wide range by tuning the optical wavelengths in a small range. It can especially be much larger than the optical wavelengths, leading to the desired extended unique measurement range.
By using a fiber-coupled dual off-axis carrier-fringe interferometry setup as sketched in figure 1, single shot SWI can be performed [1]. Each camera frame captures the full complex field information at both wavelengths from which the synthetic wavelength interferogram is calculated. This allows one to study dynamic processes such as vibrations. The synthetic wavelength can be chosen larger than the displacement amplitudes of the sample such that two measurements per vibration period are sufficient. As a result, cameras with a comparatively low frame rate can be used.

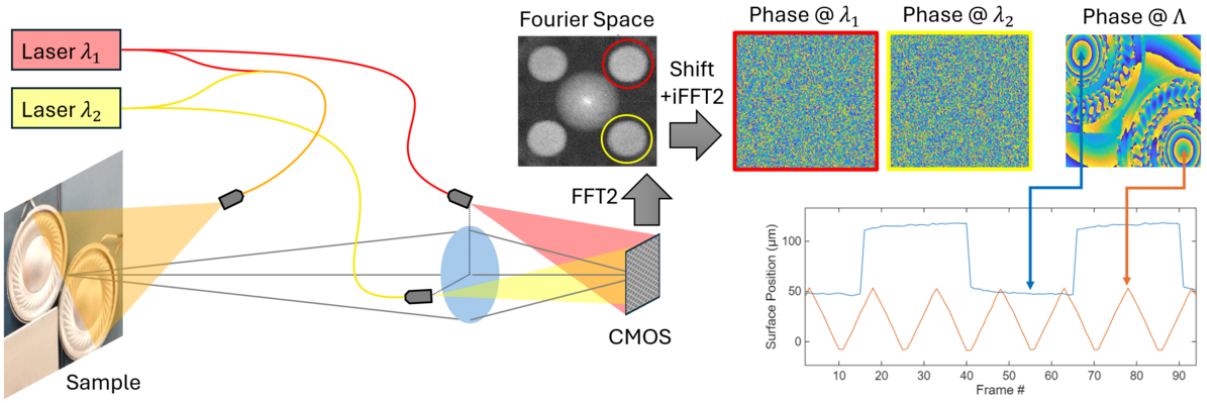


Fig. 1. Sketch of the single-shot synthetic wavelength interferometry setup (left), essential interferogram processing steps (top right) and an example of two vibration signals extracted from the same sequence of interferograms (bottom right).

We present SWI measurements of two small loudspeakers that are excited with different signal shapes and frequencies. The results demonstrate the method's capability to capture spatially highly resolved measurements of surface vibrations with micrometer displacements and arbitrary signal forms within the camera's bandwidth. By tuning the synthetic wavelength, the method can be adapted to a wide range of displacement amplitudes which makes it very versatile for a large range of applications

[1] M. Ballester, H. Wang, J. Li, O. Cossairt, and F. Willomitzer, "Single-shot synthetic wavelength imaging: Sub-mm precision ToF sensing with conventional CMOS sensors," Optics and Lasers in Engineering, vol. 178, p. 108165, Mar. 2024, doi: 10.1016/j.optlaseng.2024.108165.

MICROCOPPER ELECTRODES AND ELECTROCHROMIC MATERIALS INTERACTION WITH DIFFERENT ELECTROLYTES FOR SMART WINDOW APPLICATION

Titas Tamošauskas[1], Dainius Balkauskas[1], Modestas Sadauskas[1], Edita Voitechovič[2], Romualdas Trusovas[1], Karolis Ratautas[1], Kuo-Ping Chen[3], Alexandr Belosludtsev[1]

[1]Center for Physical Sciences and Technology, Department of Laser Technologies, Vilnius, Lithuania
[2]Center for Physical Sciences and Technology, Department of Nanoengineering, Vilnius, Lithuania
[3]National TsingHua University, Institute of Photonics Technologies, Hsinchu, Taiwan
titas.tamosauskas@ftmc.lt

Growing energy demand and environmental challenges drive the development of technologies aimed at reducing energy consumption in buildings [1]. Electrochromic smart windows are a promising solution, as their optical properties can be actively controlled by an electrical signal, enabling dynamic regulation of light transmission and reflectance.

In this work, the interaction between microcopper transparent electrodes and electrochromic materials is investigated for smart window applications. Microstructured copper electrodes were fabricated on glass substrates using Selective Surface Activation Induced by Laser (SSAIL) technology as an alternative to conventional transparent conductive oxide electrodes, such as ITO [2]. Tungsten oxide (WO_3) and PEDOT:PSS were studied as inorganic and organic electrochromic materials using lithium-based ($LiClO_4$) and proton-based (H_2SO_4) electrolytes, with optical transmittance measurements used to evaluate switching behavior and stability.

PEDOT:PSS-based devices exhibited fast and reversible electrochromic switching in proton-conducting electrolytes, with stable optical modulation at low operating voltages and high transparency in the bleached state. In contrast, WO_3-based devices operated with lithium-based electrolytes showed unstable behavior, resulting in partial degradation of the smart window and reduced electrochromic performance. These results highlight the strong influence of electrolyte selection on electrochromic stability and device reliability.

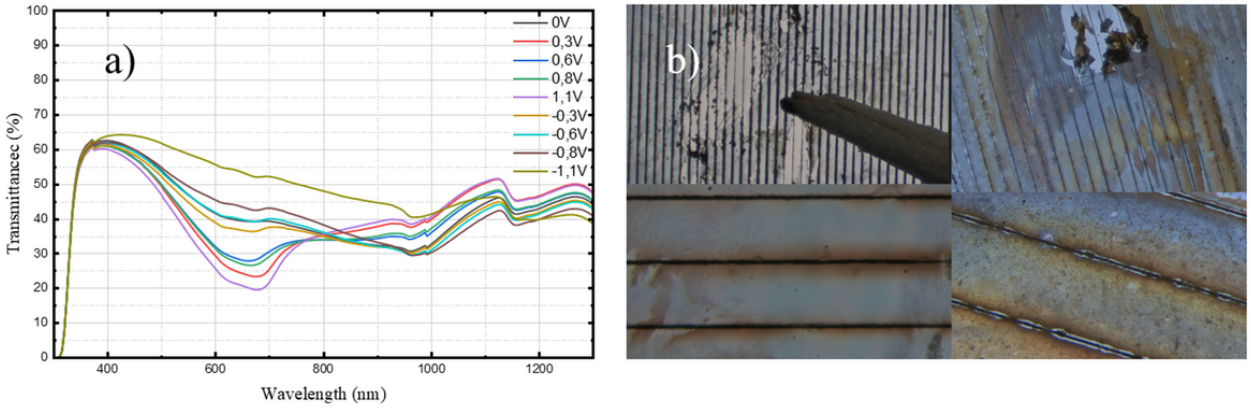


Fig. 1. a) PEDOT:PSS electrochromic smart window with H_2SO_4 electrolyte spectra; b) degraded WO_3 electrochromic smart window with $LiClO_4$ electrolyte microscope images

Future research will focus on improving device stability and durability by optimizing electrolyte systems and electrode-electrolyte interfaces. The implementation of gel or solid-state electrolytes, like PVA [3], together with improved electrode designs, is expected to further advance the performance of electrochromic smart windows.

Keywords: Smart windows, Electrochromic Materials, SSAIL Electrodes, Electrolyte

[1] T. Moore, L. Kleyn, and T. Simko, "On hot days, up to 87% of heat gain in our homes is through windows. on cold days, it's 40% of heat loss. Here's how we can fix that," The Conversation, Sep. 06, 2023. https://doi.org/10.64628/aa.s6wanx5dr (accessed Feb. 14, 2026).
[2] D. Balkauskas et al., "Transparent microscale electrodes formed by laser-induced metal deposition on glass for smart windows application," Optics & Laser Technology, vol. 192, p. 113669, Aug. 2025, doi: 10.1016/j.optlastec.2025.113669.
[3] K. Wang, H. Wu, Y. Meng, Y. Zhang, and Z. Wei, "Integrated energy storage and electrochromic function in one flexible device: an energy storage smart window," Energy & Environmental Science, vol. 5, no. 8, p. 8384, Jan. 2012, doi: 10.1039/c2ee21643d.

ORAL SESSION 12

Materials Science and Nanotechnology

Chair: Dr. S. Miasojedovas

CARBAZOLE-BASED PHOSPHONIC ACIDS IN PEROVSKITE SOLAR CELLS: IMPACT OF THE SUBSTITUTION PATTERN ON DEVICE PERFORMANCE

Aida Drevilkauskaitė[1], Lea Zimmermann[2], Eike Köhnen[2], Steve Albrecht[2], Artiom Magomedov[1], Vytautas Getautis[1]

[1]Kaunas University of Technology, Department of Organic Chemistry, Lithuania
[2]Helmholtz-Zentrum Berlin für Materialien und Energie, Division Solar Energy, Germany
aida.drevilkauskaite@ktu.edu

Self-assembled monolayers (SAMs) have emerged as the standard hole-selective layer in high-efficiency p-i-n perovskite solar cells (PSC). [1] However, a limited understanding of structure-property relationships remains a challenge for further performance optimization. Previous studies have shown that variations in functional groups, alkyl chain length, and molecular cores can influence device performance. [2] Despite these advances, clear structure-performance correlations have not yet been established. This study provides a comparison of a broader set of nine phosphonic-acid-based molecules, evaluating their performance within the same model PSC system. [3] The objective of this work is to clarify how different substitution patterns on the carbazole core affect layer properties and photovoltaic performance.

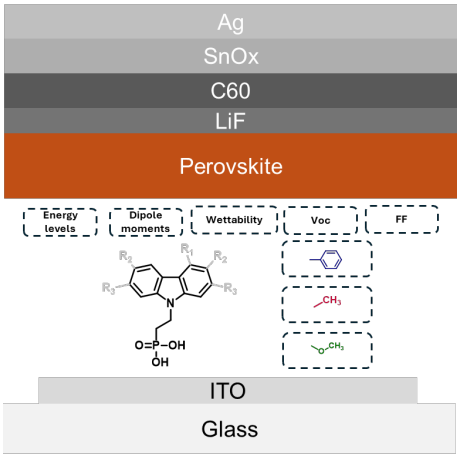


Fig. 1. Schematic illustration of the p-i-n PSC architecture incorporating carbazole-based phosphonic acid self-assembled monolayers (SAMs), highlighting different substitution patterns and functional groups used.

A series of differently substituted carbazole derivatives with phenyl-, methyl- and methoxy- functional groups was synthesized and integrated into devices. The influence of various functional groups was additionally examined using combined optical, thermal, and electrical characterization. Notably, SAMs substituted at the 3,6-positions delivered enhanced fill factors and power conversion efficiencies compared to other configurations. In addition, a correlation between the ionization potential and fill factor indicates the presence of a threshold value beyond which the fill factor decreases, likely due to energy level misalignment. Overall, this study provides valuable insights for future studies and the advancement of phosphonic acid-based materials for high-performance PSC.

Keywords: Monolayears, Solar Cells, Perovskite

[1] W. Fu et al., “Self-assembled monolayers for perovskite solar cells,” Review of Materials Research, vol. 1, no. 1, p. 100017, Jan. 2025, doi: 10.1016/j.revmat.2025.100017.
[2] C. E. P. Galvis, D. a. G. Ruiz, E. Martínez-Ferrero, and E. Palomares, “Challenges in the design and synthesis of self-assembling molecules as selective contacts in perovskite solar cells,” Chemical Science, vol. 15, no. 5, pp. 1534–1556, Nov. 2023, doi: 10.1039/d3sc04668k.
[3] A. Drevilkauskaitė et al., “Screening of the carbazole-based phosphonic acids in perovskite solar cells: impact of the substitution pattern on device performance,” Materials Advances, vol. 6, no. 23, pp. 8921–8929, Jan. 2025, doi: 10.1039/d5ma00703h.

THICKNESS-DEPENDENT PROPERTIES OF $ZnIn_2S_4$ THIN FILMS DEPOSITED BY CBD METHOD

Nida Vileniškytė[1], Ingrida Ancutienė[1], Rokas Kondrotas[2], Asta Bronušienė[1,2]

[1]Kaunas University of Technology, Faculty of Chemical Technology, Department of Physical and Inorganic Chemistry Radvilėnų pl. 19, LT-50254, Kaunas
[2]Center for Physical Sciences and Technology, Department of Characterization of Materials Structure Saulėtekio al. 3, LT-10257, Vilnius
nida.vileniskyte@ktu.edu

Zinc indium sulfide ($ZnIn_2S_4$) is a ternary metal sulfide semiconductor that has attracted significant attention due to its suitable band gap, good chemical stability, and potential applications in optoelectronics, photocatalysts, and energy-related devices. Among various synthesis techniques, the chemical bath deposition (CBD) method stands out as a simple, cost-effective, and low-temperature process that enables uniform thin film growth over large areas and allows precise control of deposition parameters [1-2].

In this study, $ZnIn_2S_4$ thin films were deposited on FTO glass via chemical bath deposition (CBD). After establishing an optimal precursor recipe, the deposition time was systematically varied to determine the relationship between growth duration, film thickness, and structural properties. Specifically, deposition intervals of 1 h 45 min, 2 h 30 min, 3 h 30 min, and 4 h 15 min were investigated.

The results indicate that increasing the CBD duration leads to the formation of a thicker sulfide film. Structural analysis revealed that despite these changes in thickness, the $ZnIn_2S_4$ phase remains stable and consistent. However, a stable film failed to form when the deposition time was extended to 4 h 15 min. This behavior is likely attributed to excessive film thickness, which results in poor adhesion and subsequent delamination from the substrate. Based on these observations, the critical adhesion limit for these films occurs between the 3 h 30 min and 4 h 15 min marks.

These findings demonstrate that while deposition time is a crucial tool for controlling film thickness, it also defines the mechanical stability limits of $ZnIn_2S_4$ thin films.

[1] G. Zhang et al., “A mini-review on ZnIn2S4-Based photocatalysts for energy and environmental application,” Green Energy & Environment, vol. 7, no. 2, pp. 176–204, Dec. 2020, doi: 10.1016/j.gee.2020.12.015.
[2] X. Xin et al., “Large electronegativity differences between adjacent atomic sites activate and stabilize ZnIn2S4 for efficient photocatalytic overall water splitting,” Nature Communications, vol. 15, no. 1, p. 337, Jan. 2024, doi: 10.1038/s41467-024-44725-1.

NANOENGINEERED BIOPOLYMER-FULLERENE C_{60} COMPOSITE FILMS FOR BIOFOULING RESISTANCE

Guoda Gasauskaite[1], Wanessa De Melo[1], María Belén Montero Rodríguez[2], Martynas Talaikis[1], Vidas Pakštas[1]

[1]State Research Institute Centre for Physical Sciences and Technology (FTMC), Department of Functional Materials and Electronics, Vilnius, Lithuania
[2]Universidade da Coruña, Departamento de Física y Ciencias de la Tierra-Escuela Politécnica de ingeniería de Ferrol (EPEF), Centro de Investigación en Tecnologías Navales e Industriales (CITENI), Ferrol, Spain
guoda.gasauskaite@ftmc.lt

Biofilm formation on medical devices and clinical surfaces remains a major contributor to persistent infections, as mature biofilms are highly tolerant to conventional antibiotics and disinfectants. Once established, these biofilms are difficult to eradicate, underscoring the need for antimicrobial surface strategies that do not rely on drug release or promote resistance. Antimicrobial photodynamic therapy offers such an approach by generating reactive oxygen species upon light activation, provided the photosensitizer can be stably immobilized within a solid material.

In this study, biopolymer–fullerene composite films were fabricated and structurally characterized as a materials platform for photodynamically active antimicrobial surfaces. Fullerene C_{60} nanoparticles were physically incorporated at 0.5 wt% into polylactic acid (PLA), poly(3-hydroxybutyrate-co-3-hydroxyvalerate) (PHBV), and chitosan matrices using a thermophysical melt-processing route. PLA and PHBV composites were obtained through extrusion followed by hot pressing, while chitosan films were prepared by hot pressing due to limited extrusion compatibility. This solvent-free approach enables stable photosensitizer immobilization without chemical modification.

Raman spectroscopy and hyperspectral Raman mapping confirmed successful incorporation of C_{60} across all matrices. Characteristic fullerene modes were clearly detected, with the intense Ag(2) band at 1467 cm^{-1} serving as a reliable spectral marker. Raman mapping further revealed localized fullerene-rich domains formed during melt processing.

X-ray diffraction and differential scanning calorimetry revealed matrix-dependent structural responses. PLA composites showed reduced crystallinity and pronounced cold crystallization, consistent with a largely amorphous structure. PHBV retained semicrystalline order with increased melting transitions and crystallite size, indicating a nucleating effect of C_{60}. Chitosan films displayed reduced structural order and modified dehydration-related transitions, suggesting partial disruption of the hydrogen-bonded network.

Overall, thermophysical processing provides a scalable route for producing biopolymer–fullerene composite films while preserving polymer integrity. The confirmed incorporation and matrix-dependent structural effects of fullerene establish a basis for further investigation of photodynamic activity and antimicrobial performance.

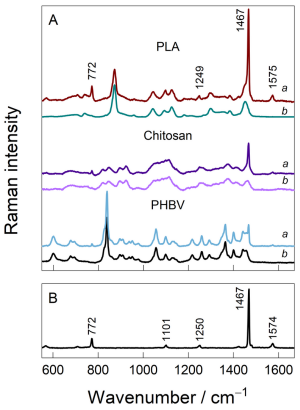


Fig. 1. (A) Raman spectra of PLA, chitosan, and PHVB samples with (a) and without fullerene (b). Spectra were collected by averaging the Raman mapping data of 500 individual spectra. (B) Raman spectrum of fullerene.

Keywords: Fullerene C_{60}, Photodynamic antimicrobial surfaces, Thermophysical melt processing, Biopolymer nanocomposites

NBT-BT THIN FILMS: STRUCTURAL AND DIELECTRIC PROPERTIES

Eglė Martinaitytė[1], Vadzim Haronin[1], Rokas Dobužinskas[2], Arnas Naujokaitis[3], Jūras Banys[1], Šarūnas Svirskas[1]

[1]Vilnius University, Faculty of Physics, Institute of Applied Electrodynamics and Telecommunications, Vilnius, Lithuania
[2]Vilnius University, Faculty of Physics, Institute of Chemical Physics, Vilnius, Lithuania
[3]Center for Physical Science and Technology, Department of Characterization of Materials Structure, Vilnius, Lithuania
egle.martinaityte@ff.stud.vu.lt

Ferroelectric thin films are used in sensors, actuators, and microelectromechanical systems because of their dielectric properties. The development of lead-free ferroelectric materials has gained increasing attention as an alternative to lead-based materials. However, achieving reproducible growth and consistent dielectric behavior in lead-free thin films remains challenging. In this work, the structural and dielectric properties of $Na_{0.5}Bi_{0.5}TiO_3$-$BaTiO_3$ (NBT-BT) thin films prepared by pulsed laser deposition are investigated.

Thin films of 0.8NBT-0.2BT were deposited on Pt/$LaNiO_3$/SiO_2/Si substrates. A relationship between the number of laser pulses and film thickness was established, allowing improved control of the growth process. The influence of deposition parameters, including substrate temperature, oxygen pressure, and laser fluence, on film structure and morphology was investigated using scanning electron microscopy and X-ray diffraction. Dielectric properties were evaluated using an LCR meter.

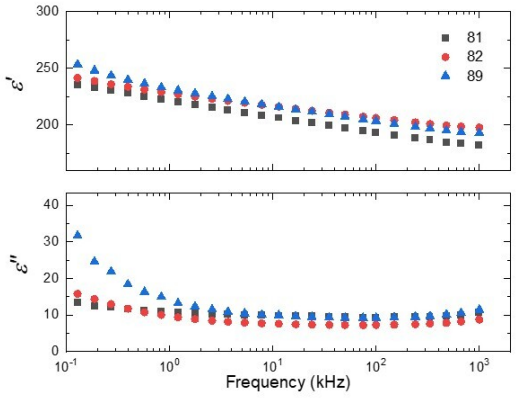


Fig. 1. Room-temperature dielectric behavior of films deposited under the same conditions.

The results show that films deposited under the same conditions have similar dielectric permittivity values, indicating reproducible dielectric response. The study highlights the importance of controlled deposition parameters for obtaining homogeneous NBT-BT thin films with reliable dielectric properties. These findings contribute to the understanding the influence of deposition parameters on thin films properties for future applications in electromechanical devices.

BIOCHIPS WITH MICROSCALE SURFACE STIFFNESS PATTERNS FOR MECHANOBIOLOGICAL APPLICATIONS

Andrius Pečiulis[1], Tomas Rakickas[1], Tadas Jelinskas[1], dr. Martynas Gavutis[1]

[1]Lithuania, Vilnius, Center for Physical Sciences and Technology, Department of Nanoengineering, LT-02300
andrius.peciulis@ftmc.lt

Mechanobiology is becoming well established field of science, with ever more research outlining the importance of mechanical properties of cellular environment in controlling cell fate [1], [2]. It has been shown that substrate stiffness influences cell migration, orientation and proliferation, with certain cell lines having certain preferences [3]. Here we present a simple and effective approach of creating Youngs modulus microscale patterns in a biological range, on soft biocompatible polyacrylamide hydrogel substrates. In this work we used photopolymerization of polyacrylamide enriched with methacrylic acid as the key mechanism for pattern generation. By polymerising samples in 2-step approach we were able to create zones that had higher degree of crosslinking, because of longer UV light exposure time (Fig. 1.). We were able to create this structured illumination by employing inverted microscope with "Optigrid" structured illumination module, by exchanging mask within this module with a custom one. Overall, 2 different masks were tested, which allowed for stiffness patterning of 10 µm width lines and 40 µm diameter disks. Samples had higher Young's modulus values in exposed zones (in ranges from 10 kPa to 90 kPa for different samples) as well as some degree of elevation (up to 4 µm for line pattern and more than 10 µm for disks), confirmed via AFM measurements. Inclusion of methacrylic acid allowed for surface patterning with ECM proteins by binding primary amines to carboxy group present in hydrogel [4]. Such hydrogels have been used for cell attachment experiments, in which cells showed different morphology based on Young's modulus value of their attachment zone. We believe that such hydrogel platforms could play a role in further mechanobiological advancements.

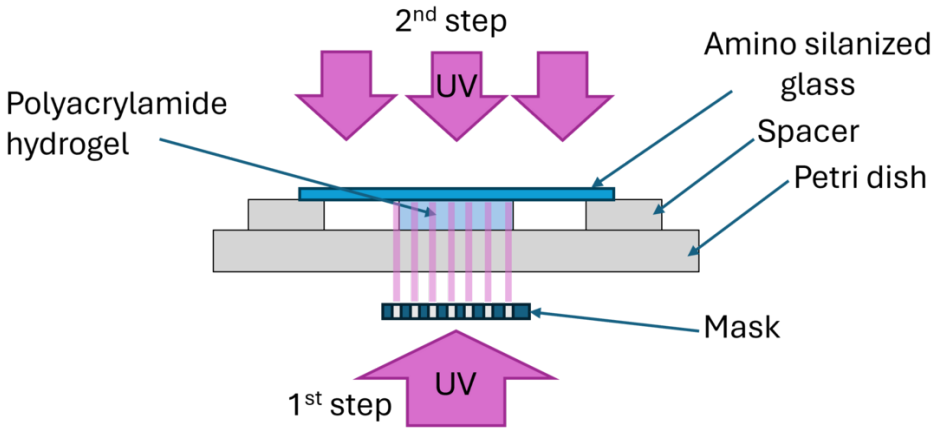


Fig. 1. Scheme of 2-step polymerisation, 1st step being exposure of hydrogel mixture to structured UV light, and 2nd step involving uniform polymerisation of the sample.

[1] N. Gjorevski et al., "Tissue geometry drives deterministic organoid patterning," Science (1979)., vol. 375, no. 6576, Jan. 2022, doi: 10.1126/science.aaw9021.
[2] M. T. Alameda, M. R. Osorio, J. J. Hernández, and I. Rodríguez, "Hierarchical micro-nano topographies to control Bacteria and mesenchymal stem cells biological responses," Sci. Rep., vol. 15, no. 1, Dec. 2025, doi: 10.1038/s41598-025-08415-2.
[3] F. Milos and A. del Campo, "Polyacrylamide Hydrogels as Versatile Biomimetic Platforms to Study Cell-Materials Interactions," Dec. 03, 2024, John Wiley and Sons Inc. doi: 10.1002/admi.202400404.
[4] M. Gavutis et al., "Biochip Surfaces Containing Recombinant Cell-Binding Domains of Fibronectin," Coatings, vol. 12, no. 7, Jul. 2022, doi: 10.3390/coatings12070880.

IN-SITU XAS MEASUREMENTS OF VANADATE-PHOSPHATE GLASSES

Krzysztof Gadomski[1], Martyna Jankowska[1,2], Wojciech Tabiś[3], Alexey Maximenko[4], Sylwester Rzoska[2], Tomasz K. Pietrzak[1]

[1]Warsaw University of Technology, Faculty of Physics, Poland
[2]Institute of High Pressure Physics, Polish Academy of Sciences, Poland
[3]AGH University, Faculty of Physics and Applied Computer Science, Poland
[4]SOLARIS National Synchrotron Radiation Centre, Jagiellonian University, Poland
krzysztof.gadomski2.dokt@pw.edu.pl

The rapid growth of renewable energy production is an undeniable reality of the modern world. However, a major limitation of these energy sources is their strong dependence on weather conditions, which significantly reduces their reliability. This challenge necessitates the use of energy storage systems, such as batteries, to stabilise the power grid during unfavourable weather conditions or periods without sunlight.

Vanadate phosphates constitute a broad class of materials that are considered promising cathode candidates for lithium-ion batteries and have therefore been extensively investigated. Notable examples include crystalline $VOPO_4$ [1] and $Li_3V_2(PO_4)_3$ [2]. Our group has also focused on glassy vanadate–phosphate systems, demonstrating that controlled thermal nanocrystallisation can substantially enhance their electronic conductivity. For example, 90 V_2O_5 ·10 P_2O_5 glasses initially exhibit an electrical conductivity of approximately $\sigma = 7 \times 10^{-5}$ S/cm, which increases dramatically to $\sigma = 7 \times 10^{-2}$ S/cm at room temperature following nanocrystallisation [3]. Despite this significant improvement, the underlying mechanism responsible for the conductivity increase during crystallisation is not fully understood yet.

The aim of this study was to investigate the structural and electronic changes occurring in vanadate–phosphate glasses during heating from room temperature to temperatures well above the crystallisation point. For this purpose, in situ X-ray Absorption edge Spectroscopy (XAS) measurements were performed. This technique provides valuable insight into the evolution of both the local atomic and electronic structures during the crystallisation process. Results of this measurement as well as methodology will be presented.

Acknowledgements

M.J., K.G., and T.K.P. are grateful to the National Science Centre (NCN), Poland, for support in the framework of a grant OPUS-23 no. 2022/45/B/ST5/04005. We acknowledge the SOLARIS Centre for access to the beamline ASTRA where the measurements were performed, under the provision of the Polish Ministry of Science and Higher Education project "Support for research and development with the use of research infra-structure of the National Synchrotron Radiation Centre SOLARIS" under contract nr 1/SOL/2021/2.

Keywords: XAS, glass, glass crystallisation

[1] Z. Chen, Q. Chen, L. Chen, R. Zhang, H. Zhou, N. A. Chernova and M. S. Whittingham, "Electrochemical Behavior of Nanostructured e-VOPO4 over Two Redox Plateaus," Journal Electrochemical Society, vol 160, pp. A1777, 2013.

[2] H. Huang, S.C. Yin, T. Kerr, N. Taylor and L.F. Nazar, "Nanostructured Composites: A High Capacity, Fast Rate Li3V2(PO4)3/Carbon Cathode for Rechargeable Lithium Batteries," Advanced Materials, vol 14, no 21, pp. 1525-1528, 2002.

[3] T.K. Pietrzak, Ł. Pawliszak, P.P. Michalski, M. Wasiucionek and J.E. Garbarczyk, "Highly Conductive 90 V2O5 10 P2O5 Nanocrystalline Cathode Materials for Lithium-ion Batteries." Procedia Engineering vol 98, pp. 28-35, 2014

ORAL SESSION 13

Biology and Medicine

Chair: Dr. T. Kirtiklienė

INVESTIGATION OF THE RESPIRATORY MICROBIOME IN TUBERCULOSIS PATIENTS IN LITHUANIA

Aistė Popandopula[1], Edvardas Danila[2,3], Karolina Kėvelaitienė[3], Rūta Mereškevičienė[3], Vaiva Kumpauskaitė[3], Laima Vasiliauskaitė[3,4], Aleksandras Konovalovas[1], Julija Armalytė[1]

[1]Lithuania, Vilnius University, Life Sciences Center, Institute of Biosciences
[2]Lithuania, Vilnius University Hospital Santaros Klinikos, Center of Pulmonology and Allergology
[3]Lithuania, Vilnius University, Faculty of Medicine, Institute of Clinical Medicine, Clinic of Chest Diseases, Immunology and Allergology
[4]Lithuania, Vilnius University Hospital Santaros Klinikos, Centre of Laboratory Medicine, Laboratory of Infectious Diseases and Tuberculosis
a.popandopula@gmail.com

Tuberculosis (TB) remains a major global health concern despite advances in treatment and prevention. Lithuania has one of the highest TB and drug-resistant TB rates in the European Union, underscoring the need for improved understanding of disease drivers [1]. Increasing evidence suggests that the respiratory tract microbiome may act as an ecological barrier or facilitator of *Mycobacterium tuberculosis* colonization [2]. Therefore, investigating lung microbiome composition may provide critical insight into TB susceptibility and progression.

This study aimed to analyze microbiota composition in sputum and oral swab samples using full-length 16S rRNA gene sequencing. Non-invasive and painless, sputum samples are commonly used to examine the microbiome of the lower respiratory tract. A total of 97 sputum samples obtained from patients with TB and other chronic lung diseases (CLD) were analyzed. Additionally, 18 paired oral swab samples were included to assess potential connection between respiratory tract microbiota from different areas.

The sputum microbiome of CLD patients was characterized by lower diversity and a higher proportion of *Pseudomonadota* bacteria, a pattern consistent with dysbiosis. In contrast, TB patients exhibited comparatively greater bacterial diversity. No significant differences in microbiome composition or diversity were observed between drug-sensitive and drug-resistant TB. In the majority of samples, the sputum microbiome differed from that of the oral cavity. Similarities observed between sputum and oral microbiomes may reflect not only the introduction of oral microorganisms during sampling but also the biological continuity between the upper and lower respiratory tracts.

In conclusion, these preliminary findings indicate that sputum is a suitable and informative sample for respiratory tract microbiome studies, and that TB and CLD patients exhibit distinct patterns of microbiome dysbiosis. These results provide a foundation for future research investigating the role of the respiratory tract microbiome in TB pathogenesis and progression.

[1] "Tuberculosis surveillance and monitoring in Europe 2025 - 2023 data," European Centre for Disease Prevention and Control, Mar. 24, 2025. https://www.ecdc.europa.eu/en/publications-data/tuberculosis-surveillance-and-monitoring-europe-2025-2023-data

[2] T. Shah, Z. Shah, Z. Baloch, and X. Cui, "The role of microbiota in respiratory health and diseases, particularly in tuberculosis," Biomedicine & Pharmacotherapy, vol. 143, p. 112108, Sep. 2021, doi: 10.1016/j.biopha.2021.112108.

IMPACT OF SURFACE-ASSOCIATED VIRULENCE FACTORS ON THE CYTOTOXICITY OF ACINETOBACTER BAUMANNII OUTER MEMBRANE VESICLES

Danas Ivanauskas[1], Jūratė Skerniškytė[1]

[1]Vilnius University, Life Sciences Center, Institute of Biosciences, Department of Biochemistry and Molecular Biology, Vilnius, Lithuania
danas.ivanauskas@gmc.stud.vu.lt

Acinetobacter baumannii is an opportunistic pathogen notable for its high levels of antibiotic resistance and its role in hospital-acquired infections [1]. Carbapenem-resistant *A. baumannii* was designated a top priority for antibiotic development by the WHO in 2017 [2]. Despite the identification of some virulence factors, the mechanisms underlying its pathogenicity remain poorly characterized compared to other Gram-negative bacteria [3]. It is known that *A. baumannii* releases outer membrane vesicles (OMVs) – nanoscale, outer-membrane-derived particles. OMVs are lipid bilayer vesicles released into the extracellular environment, containing outer membrane lipids and proteins, periplasmic enzymes, genetic material [4]. OMVs play an important role in pathogenesis by delivering virulence factors, inducing inflammation, promoting immune evasion and antibiotic resistance. By enabling host damage without direct bacterial contact, OMVs significantly enhance *A. baumannii* virulence [5]. This study aims to evaluate the influence of *A. baumannii* surface virulence factors on the cytotoxicity of OMVs.

In this study, five different *A. baumannii* strains were used: wild-type clinical isolates (52 wt and 169 wt), previously constructed polysaccharide capsule-deficient mutant strain (52 ΔgalU), outer membrane protein OmpA deficient mutant strain (52 ΔompA), spontaneous mutant strain with lipooligosaccharide (LOS) structural changes (169 ΔLOS). The *ompA* gene was knocked out of *A. baumannii* clinical isolate by generating a markerless gene-deletion mutant. The spontaneous mutant strain was obtained by colistin-dependent loss/modification of LOS, evaluated by SDS-PAGE and Alcian Blue dye. The OMVs were purified from each *A. baumannii* strain by ultracentrifugation of overnight cultures. The concentrations of OMVs were determined by overall protein content detected by Bradford assay. Cytotoxicity of OMVs was evaluated using A549 lung carcinoma epithelial cell line and assessing their viability via the MTT method.

The gene *ompA* was successfully knocked out from *A. baumannii* clinical isolate and confirmed by sequencing. Complete loss of LOS in the spontaneous mutant was not observed, but structural modifications were detected. OMVs from all strains exhibited cytotoxicity towards A549 cells compared to the PBS negative control. However, when comparing OMVs from the 52 wt strain and the capsular polysaccharide-nonproducing 52 ΔgalU strain, the latter showed a reduced cytotoxic effect. Similarly, the OMVs from the 169 wt caused lower viability of A549 cells when compared with OMVs from the 169 ΔLOS strain. Therefore, variation in OMV composition causes different outcomes towards cytotoxicity, highlighting the critical contribution of specific surface components to OMV-mediated host cell damage and represent promising targets for future therapeutic interventions.

[1] S. Monem et al., “Mechanisms Protecting Acinetobacter baumannii against Multiple Stresses Triggered by the Host Immune Response, Antibiotics and Outside-Host Environment,” International Journal of Molecular Sciences, vol. 21, no. 15, p. 5498, Jul. 2020, doi: 10.3390/ijms21155498.

[2] E. Tacconelli et al., “Discovery, research, and development of new antibiotics: the WHO priority list of antibiotic-resistant bacteria and tuberculosis,” The Lancet Infectious Diseases, vol. 18, no. 3, pp. 318–327, Dec. 2017, doi: 10.1016/s1473-3099(17)30753-3.

[3] C. M. Harding, S. W. Hennon, and M. F. Feldman, “Uncovering the mechanisms of Acinetobacter baumannii virulence,” Nature Reviews Microbiology, vol. 16, no. 2, pp. 91–102, Dec. 2017, doi: 10.1038/nrmicro.2017.148.

[4] Z. Weng et al., “Outer Membrane Vesicles from Acinetobacter baumannii: Biogenesis, Functions, and Vaccine Application,” Vaccines, vol. 12, no. 1, p. 49, Dec. 2023, doi: 10.3390/vaccines12010049.

[5] B. Cano-Castaño, M. López-Siles, F. Nonnoi, A. Pérez, A. C. Lugo, and M. J. McConnell, “Acinetobacter baumannii as a Model for the Study and Application of Gram-Negative Outer Membrane Vesicles: A Systematic Review,” Microbial Biotechnology, vol. 18, no. 9, p. e70207, Sep. 2025, doi: 10.1111/1751-7915.70207.

VIRULENCE FEATURES OF OPPORTUNISTIC PATHOGEN STENOTROPHOMONAS MALTOPHILIA: BIOFILM FORMATION, CAPSULE PRODUCTION, AND ANTIBIOTIC RESISTANCE

Dominykas Grigorjevas[1], Laurita Klimkaitė[1], Jūratė Skerniškytė[1]

[1]Vilnius University, Life Sciences Center, Institute of Biosciences, Lithuania
dominykas.grigorjevas@gmc.stud.vu.lt

Antibiotic resistance is one of the most urgent global health crises today, causing over a million deaths annually [1]. Multidrug-resistant pathogens can withstand multiple treatment options, increasing patient mortality, prolonging recovery, and burdening health care facilities [1]. One such multidrug-resistant pathogen is *Stenotrophomonas maltophilia*, an opportunistic bacterium that causes infections with mortality rates as high as 69% [2]. This pathogen can form biofilm and produce polysaccharide capsule [3], both of which can contribute to its persistence in the clinical environment, evasion of immune responses, and resistance to antibiotic treatment [2; 4]. Despite the clinical significance of *S. maltophilia*, there remains a lack of understanding regarding its resistance mechanisms and virulence factors.

This study aimed to assess biofilm formation and the distribution of biofilm-associated genes in 102 clinical isolates of *S. maltophilia* obtained from patients at Vilnius University Hospital Santaros Klinikos, as well as to examine the impact of the polysaccharide capsule on antibiotic resistance. Biofilm formation at 37°C was measured using crystal violet staining [5]. The following biofilm-associated genes in 71 isolates were selected for PCR analysis: *pilU*, *rmlA*, *smf1*, *fliC*, *ax21*, *spgM*, *fliA*, and *rpfF*. The impact of the polysaccharide capsule on antibiotic resistance was evaluated by comparing the minimal inhibitory concentrations (MICs) of 13 antibiotics (kanamycin, streptomycin, gentamicin, chloramphenicol, tetracycline, colistin, ampicillin, ceftazidime, cefazolin, imipenem, meropenem, and a combination of sulfamethoxazole/trimethoprim) between the wild-type isolate and its capsule-deficient mutant (*Δwzc*).

Out of the 102 *S. maltophilia* isolates analyzed, 98 % produced biofilms, indicating that biofilm formation is an important trait for *S. maltophilia* in clinical settings. The analyzed genes in 71 isolates were detected at high frequency, and no clear correlation was found between biofilm formation levels and the presence of biofilm-associated genes. This suggests that either other unexamined genes or gene regulation mechanisms might influence biofilm formation in *S. maltophilia*. MIC comparisons between the wild-type strain and its capsule-deficient mutant revealed that the loss of the polysaccharide capsule significantly increased the bacterial susceptibility to β-lactams (ceftazidime, imipenem, meropenem). Therefore, the polysaccharide capsule could be a target for next-generation drugs to improve the efficacy of antibiotic therapy.

[1] S. K. Ahmed et al., "Antimicrobial resistance: Impacts, challenges, and future prospects," Journal of Medicine Surgery and Public Health, vol. 2, p. 100081, Mar. 2024, doi: 10.1016/j.glmedi.2024.100081.

[2] J. Liu, Y. Xiang, and Y. Zhang, "Stenotrophomonas maltophilia: An Urgent Threat with Increasing Antibiotic Resistance," Current Microbiology, vol. 81, no. 1, p. 6, Nov. 2023, doi: 10.1007/s00284-023-03524-5.

[3] S. Shahid et al., "Antibiotic resistance genes prediction via whole genome sequence analysis of Stenotrophomonas maltophilia," Journal of Infection and Public Health, vol. 17, no. 2, pp. 236–244, Dec. 2023, doi: 10.1016/j.jiph.2023.12.010.

[4] E. Bjånes et al., "Exploring Roles of the Polysaccharide Capsule in Pathogenesis of Hypervirulent Acinetobacter baumannii Clinical Isolate Lac-4," Antibiotics, vol. 13, no. 1, p. 10, Dec. 2023, doi: 10.3390/antibiotics13010010.

[5] S. Stepanovic, I. Cirkovic, L. Ranin, and M. Svabic-Vlahovic, "Biofilm formation by Salmonella spp. and Listeria monocytogenes on plastic surface," Letters in Applied Microbiology, vol. 38, no. 5, pp. 428–432, Apr. 2004, doi: 10.1111/j.1472-765x.2004.01513.x.

VIRAL RNA MIMETICS-INDUCED ALTERATIONS IN MICROGLIAL FUNCTION AND MITOCHONDRIAL NETWORK ARCHITECTURE

M. Merkelis[1,2,3], K. Pampuscenko[3], D. Umbrasas[3], V. Borutaite[3]

[1]Lithuania, Lithuanian University of Health Sciences, Faculty of Pharmacy
[2]Lithuania, Kaunas University of Technology, Faculty of Chemical Technology
[3]Lithuania, Lithuanian University of Health Sciences, Neuroscience Institute
matas.merkelis@lsmu.lt

Neurodegenerative diseases are a group of neurological disorders that negatively affect the lives of many people worldwide and are associated with progressive loss of neurons in the central nervous system (CNS) or peripheral nervous system (PNS). Treatment of these neurological diseases is limited to symptomatic management, and this is mainly due to the lack of advances in the understanding of the molecular mechanisms underlying neurodegenerative processes.

Some of the main processes associated with neurodegenerative diseases are related to neuroinflammation. Key factors and triggers of neuroinflammatory responses are viral and bacterial infections, which activate innate immune response and innate immune effector cells, primarily microglia, which have a negative impact on neuronal viability and function. Viral components can activate pattern recognition receptors on microglia, such as TLR3 and TLR7, and modulate neuroinflammatory response. Several studies also suggest that changes in mitochondrial function and structure can modulate microglia cell response during neuroinflammatory response, but these molecular mechanisms remain poorly understood.

In this study, we investigated the microglial BV-2 cell line and their mitochondrial response to viral RNA-mimetic compounds Loxoribine and Poly (I:C) by various methods, including fluorescence microscopy, BrdU labeling assay, polymerase chain reaction (PCR) and Oroboros O2k oxygraphic system.

Our findings indicate that loxoribine and Poly (I:C) have no effect on BV-2 microglia cell culture viability and proliferation or mitochondrial content changes. Moreover, Poly (I:C) does not affect oxidative phosphorylation of BV-2 microglia cells. However, loxoribine exerts a concentration-dependent effect – lower concentrations stimulate oxidative phosphorylation and maximum respiratory rate, but higher concentrations of loxoribine inhibit mitochondrial respiration rate. Additionally, Loxoribine and Poly (I:C) have no effect on BV-2 microglia fusion (Mfn1, Mfn2, Opa1) or fission (Drp1, Fis1) marker gene expression change, but significantly increased fission marker (Mff) and tend to alter mitochondrial biogenesis regulatory factor (PGC-1α) expression.

The present results suggest that viral RNA-mimetic Poly (I:C) does not influence BV-2 microglia cells or their mitochondria, but loxoribine has a concentration-dependent effect and may alter genes related to mitochondrial dynamics and oxidative phosphorylation.

Acknowledgements

This work was supported by the Research Council of Lithuania, Researcher Groups projects No S-MIP-23-98 (APNEVIR) and Ministry of Education, Science and Sport of the Republic of Lithuania, grant agreement No: S-A-UEI-23-7.

Keywords: Neuroscience, Neurodegenerative diseases, Microglia

PREBIOTIC SUPPLEMENTATION INDUCE MICROGLIAL MORPHOLOGICAL CHANGES IN HIGH-FAT DIET MODEL IN AGED MICE

Urte Minkeviciute[1], Arnas Kunevicius[1], Akshay Kumar Vijaya[1], Aurelijus Burokas[1]

[1]Lithuania, Vilnius University, Life Sciences Center, Biochemistry Institute, Department of Biological Models
urte.minkeviciute@gmc.stud.vu.lt

Consumption of a chronic high-fat diet (HFD) and ageing are both associated with metabolic dysfunction and increased neuroinflammation. It contributes to the loss of gut microbiota diversity and the development of neurodegenerative diseases. Microglia are highly sensitive to metabolic and inflammatory signals, and their morphology is closely linked to its functional state. These molecular signals can derive from gut microbiota and influence microglia activation and disease progression. Gut microbiota-focused interventions have the potential to reduce the chronic inflammation and have a protective effect on microglia.

In this study, we examined how prebiotic supplementation with galactooligosaccharides and fructooligosaccharides (GOS+FOS) modulates microglial morphology in aged mice exposed to long-term HFD. The C57BL/6J mice were assigned to four dietary conditions for 18 months: control diet (CD), CD - GOS+FOS, HFD, and HFD - GOS+FOS. We utilized immunohistochemical staining to quantify three-dimensional branching architecture and two-dimensional shape descriptors.

Compared with CD, microglia in HFD-fed conditions exhibited measurable morphological changes consistent with a metabolically primed microglia phenotype. HFD supplementation with GOS+FOS reduced those HFD-induced structural alterations: average branch length decreased toward CD levels, and projected soma area was significantly smaller than in HFD, indicating partial structural recovery. In the CD - GOS+FOS group, microglial morphology were similar to CD group, indicating that the effects of GOS+FOS are specific to reducing HFD-associated microglial alterations rather than modifying baseline microglial structure.

Collectively, these findings suggest that prebiotic supplementation with GOS+FOS can modulate microglial structural remodeling in the aged brain under metabolic challenge, highlighting a protective role of gut microbiota-targeted interventions in diet-induced neuroinflammatory conditions.

Keywords: microglia, microglia morphology, gut-brain axis, high-fat diet, ageing

ORAL SESSION 14

Ecology, Geology and Environmental Science

Chair: Dr. I. Uogintė

IS HYBRIDIZATION POSSIBLE BETWEEN INVASIVE (Heracleum sosnowskyi) AND NATIVE LITHUANIAN (H. sphondylium) HOGWEEDS. INSIGHTS FROM AN INSILICO STUDY

Gelminė Vanseviciūtė[1], Donatas Žvingila[1]

[1]Vilnius University, Life Sciences Centre, Department of Botany and Genetics, Lithuania
gelmine.vanseviciute@gmc.stud.vu.lt

Invasive alien species are a major driver of biodiversity loss, ecosystem disruption, and economic damage worldwide [1]. One particularly harmful invasive plant in Europe is Sosnowsky's hogweed *Heracleum sosnowskyi*, which spreads rapidly, outcompetes native vegetation, and poses serious health risks to humans due to its ability to cause severe skin photosensitivity [2,3]. In contrast, the common hogweed *Heracleum sphondylium* is a widespread native species that plays a long-established role in European ecosystems.

When invasive and native species are closely related, they may interbreed. Such hybridization can create new plant forms with enhanced or reduced adaptability, facilitate the spread of invasive genes into native populations, and ultimately weaken native biodiversity. Furthermore, as *H. sphondylium* is already well established across most of Europe, it can serve as a vector for invasive species to spread into new environments [4]. Previous studies have shown that *H. sphondylium* can hybridize with other invasive hogweed species (*H. mantegazzianum* and *H. persicum*), raising concerns that similar processes may occur with *H. sosnowskyi* [5,6].

In this study, we used publicly available genomic data to investigate *in silico* whether hybridization between *H. sosnowskyi* and *H. sphondylium* is biologically plausible. Analysis revealed substantial genomic divergence and multiple chromosomal rearrangements between the two species, suggesting that hybridization is likely constrained and that resulting hybrids may be rare or sterile.

These findings indicate that, while hybridization between invasive and native hogweeds is theoretically possible, genomic barriers may limit its ecological impact. Understanding such barriers is essential for predicting invasion dynamics and for developing informed strategies to protect native biodiversity.

Acknowledgements

We would like to express our gratitude to Kotryna Kvedaravičiūtė for providing computational resources for this study.

Keywords: Hybridization, Gene flow, Hogweeds, Invasive plants, Invasive species

[1] E. S. Osipova, A. Y. Stepanova, D. V. Tereshonok, E. A. Gladkov, and O. N. Vysotskaya, "Genetic Diversity in Invasive Populations of Lupinus polyphyllus Lindl. and Heracleum sosnowskyi Manden.," Biology, vol. 10, no. 11, p. 1094, Oct. 2021, doi: 10.3390/biology10111094.

[2] L. Baležentienė, A. Stankevičienė, and V. Snieškienė, "Heracleum sosnowskyi (Apiaceae) seed productivity and establishment in different habitats of central Lithuania," Ekologija, vol. 59, no. 3, Jan. 2014, doi: 10.6001/ekologija.v59i3.2795.

[3] Z. Gudžinskas and E. Žalneravičius, "Seedling Dynamics and Population Structure of InvasiveHeracleum sosnowskyi(Apiaceae) in Lithuania," Annales Botanici Fennici, vol. 55, no. 4–6, pp. 309–320, Oct. 2018, doi: 10.5735/085.055.0412.

[4] K. A. Hodgins, P. Battlay, and D. G. Bock, "The genomic secrets of invasive plants," New Phytologist, vol. 245, no. 5, pp. 1846–1863, Jan. 2025, doi: 10.1111/nph.20368.

[5] F. Stewart, "Hybridization between Heracleum mantegazzianum Somm. & Lev. and H. sphondylium L. (Umbelliferae) in the British Isles," 1979. [Online]. Available: https://era.ed.ac.uk/bitstream/1842/11429/1/Stewart1979_001.pdf

[6] F. Stewart and J. F. Stewart and J. Grace, "An experimental study of hybridization between Heracleum mantegazzianum Somm. & Levier and H. sphondylium L. subsp. sphondylium (Umbelliferae)," Watsonia, vol. 15, pp. 73–83, Jan. 1984, [Online]. Available: http://archive.bsbi.org.uk/Wats15p73.pdf, "An experimental study of hybridization between Heracleum mantegazzianum Somm. & Levier and H. sphondylium L. subsp. sphondylium (Umbelliferae)," Watsonia, vol. 15, pp. 73–83, Jan. 1984, [Online]. Available: http://archive.bsbi.org.uk/Wats15p73.pdf

LOCAL VS. TRANSPORTED BLACK CARBON POLLUTION IN VILNIUS AND WARSAW

Agnė Minderytė[1], F. Moritz Hey[2,3], Emeka A. Ugboma[2], Nikolaos Evangeliou[4], Sabine Eckhardt[4], Ignacio Pisso[4], Steigvilė Byčenkienė[1], Iwona S. Stachlewska[2]

[1]Lithuania, Center for Physical Sciences and Technology (FTMC), Department of Environmental Research
[2]Poland, University of Warsaw (UW), Faculty of Physics
[3]Germany, IPA Johannes Gutenberg University (JGU)
[4]Norway, Stiftelsen NILU, Department for Atmospheric and Climate Research (ATMOS)
agne.minderyte@ftmc.lt

This study presents a new approach to separate urban black carbon (BC) pollution into locally produced and transported components, addressing a key challenge for effective air quality management. Cities can only directly reduce pollution emitted within their boundaries, yet measurements usually reflect a mixture of local emissions and pollution transported from other regions. To overcome this limitation, we develop a method that partitions measured BC concentrations into city-produced and transported fractions using a combination of observations and modeling [1]. We used measurement data from two simultaneous measurement campaigns (warm season 2022 and cold season 2022/23) conducted in two urban environments: Vilnius (Lithuania) and Warsaw (Poland).

During the cold season, black carbon (BC) concentrations increased substantially in both cities, being about 90% higher in Warsaw and 44% higher in Vilnius compared to the warm season. Derived aerosol properties indicate that wintertime air contained more complex mixtures of particles, including dust, BC, and brown carbon (BrC), which tended to form larger particles. We found that single scattering albedo (SSA; a measure of how particles scatter versus absorb light) decreases as BC from fossil fuel combustion increased. This relationship indicates that fossil fuel emissions amplify the warming effect of aerosols in both cities. In addition to local emissions, air mass transport also played an important role. On average, transported BC contributed 53±8% in Warsaw and 36±28% in Vilnius during the cold season, while its contribution was much lower in the warm season (23±7% and 13±21%, respectively). This means that most BC pollution – about 47% in Warsaw and 64% in Vilnius – originated from sources within the cities themselves.

Overall, the results show that winter air quality in both cities deteriorates significantly, driven by higher emissions and a stronger influence of transported pollution. These findings highlight the need for both local emission reductions and regional cooperation to effectively improve urban air quality.

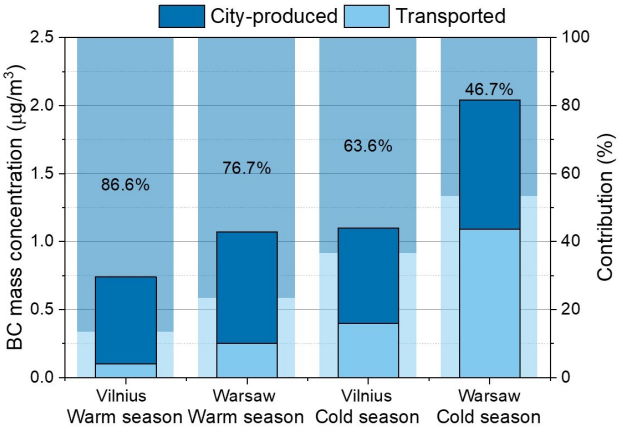


Fig. 1. Contributions of transported BC and city-produced BC in Vilnius and Warsaw during warm season (2022) and cold season (2022/2023).

Keywords: Aerosol, Black Carbon, Source apportionment, Aerosol Optical properties, Air mass transport

[1] F. M. Hey et al., "City-produced and transported black carbon: Synergy of in-situ optical measurements and modeling," Atmospheric Research, p. 108731, Jan. 2026, doi: 10.1016/j.atmosres.2025.108731.

CARBON ISOTOPIC COMPOSITION OF ANTHROPOGENIC AEROSOLS IN ATMOSPHERIC POLLUTION RESEARCH

Durre Nayab Habib[1], Andrius Garbaras[1], Ulrike Dusek[2], Agne Masalaite[1]

[1]Center for Physical Sciences and Technology, Department of Nuclear Research, Lithuania
[2]University of Groningen, Groningen,9747 AG, The Netherlands
durre.nayab@ftmc.lt

Carbonaceous aerosols from anthropogenic sources, including biomass burning (BB) and vehicular emissions, are a major component of fine particulate matter and play an important role in air quality, climate forcing, and human health [1]. However, uncertainties remain in identifying their sources and understanding how their chemical signatures evolve during atmospheric processing. Stable carbon isotopic composition ($\delta^{13}C$) of organic carbon (OC) offers a promising tracer to address these challenges. This study investigates the applicability of $\delta^{13}C$ in anthropogenic atmospheric pollution research through two independent experimental approaches.

Firstly, laboratory aging experiments were conducted on aerosols produced from the combustion of six different biomass fuels to examine isotopic changes during photochemical processing. $\delta^{13}C$ of OC was measured across three thermal fractions (200 °C, 350 °C, and 650 °C). OH-aged samples showed minimal isotopic change, in contrast to consistent ^{13}C depletion following UV aging. The intermediate-temperature OC fraction (350 °C) was generally enriched in ^{13}C compared to other fractions after UV aging. For example, wood-pellet emissions showed $\delta^{13}C$ values of −25.3 ‰, −25.1 ‰, and −25.0 ‰ for the 200 °C, 350 °C, and 650 °C fractions, respectively, compared to −25.6 ‰, −25.7 ‰, and −25.4 ‰ in un-aged samples.

Secondly, $\delta^{13}C$ of three-step OC was characterized for vehicle exhaust aerosols(un-aged) collected from eleven in-use vehicles. Substantial variability in isotopic composition was observed among vehicles and thermal fractions, with most values clustering between −26 ‰ and −28 ‰, alongside notable deviations in specific samples.

Overall, the results demonstrate that $\delta^{13}C$ of OC is sensitive to both photochemical aging and source-specific emission characteristics, supporting its use as a tracer for anthropogenic aerosol source apportionment and atmospheric pollution studies.

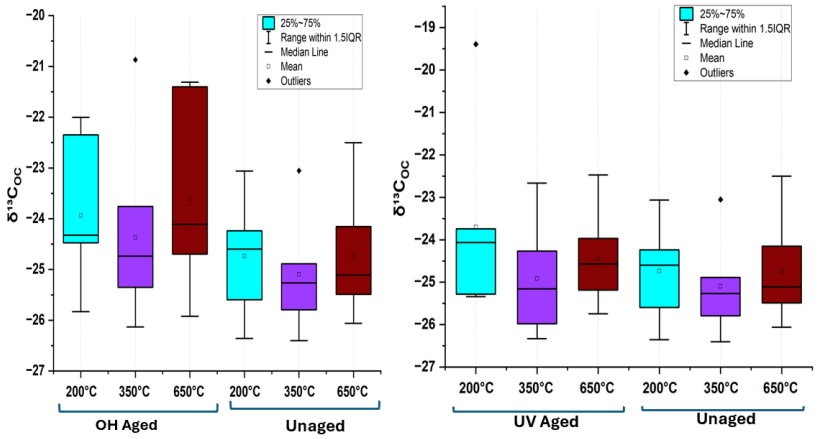


Fig. 1. Comparison of OH and UV aged biomass burning aerosol emissions samples with their respective un-aged samples

[1] H. Huang, Y. Jin, W. Sun, Y. Gao, P. Sun, and W. Ding, "Biomass Burning in Northeast China over Two Decades: Temporal Trends and Geographic Patterns," Remote Sensing, vol. 16, no. 11, p. 1911, May 2024, doi: 10.3390/rs16111911.

CURRENT STATUS OF GLACIAL RELICT CALANOID CRUSTACEANS IN LITHUANIAN LAKES

Viktorija Arceryte[1,2], Kęstutis Arbačiauskas[2]

[1]Vilnius University, Life Sciences Centre, Lithuania
[2]Nature Research Centre, Laboratory of Evolutionary Ecology of Hydrobionts, Lithuania
varceryte@gmail.com

Two species of glacial relict calanoid crustaceans, *Limnocalanus macrurus* (Sars G.O., 1863) and *Eurytemora lacustris* (Poppe, 1887) (Fig. 1), are still found in Lithuanian lakes of glacial origin [1]. These species are of considerable scientific interest. The status of their populations may provide valuable information about the ecological condition of lakes. In addition, relict crustaceans constitute an important part of the trophic web, serving as food for fish and significantly contributing to fish production [2]. Unfortunately, the survival of these crustaceans is threatened by eutrophication and global warming [3].

The aim of this work was to summarize available information and to investigate the distribution and abundance of *L. macrurus* and *E. lacustris* in Lithuanian lakes.

The research material was collected in 2022 and 2025 using two plankton nets of different diameters and analyzed under a stereomicroscope. Analysis of the material collected in 2022 revealed that relict calanoids inhabited all 22 studied lakes: *L. macrurus* was found in 14 lakes, while *E. lacustris* was recorded in 8 lakes. Relict calanoid crustaceans were detected in all their historically known habitats. In addition, new habitats were identified: *L. macrurus* was recorded in Lakes Juodieji Lakajai and Žeimenys, whereas *E. lacustris* was found in Lakes Alaušas, Avilys, and Galstas.

In 2025, previously unstudied lakes — Virintai, Smalvos, Sartai, and Drūkšiai — were examined to determine the presence of relict calanoid crustaceans. In addition, two previously studied lakes, Avilys and Žeimenys, were re-examined to confirm the presence of relict calanoids and to assess the abundance of their populations.

The results indicate that Lithuanian lakes remain insufficiently investigated, as new habitats of relict calanoid crustaceans continue to be discovered. Consequently, more comprehensive and systematic research is required to accurately assess the status of these species' populations in Lithuania.

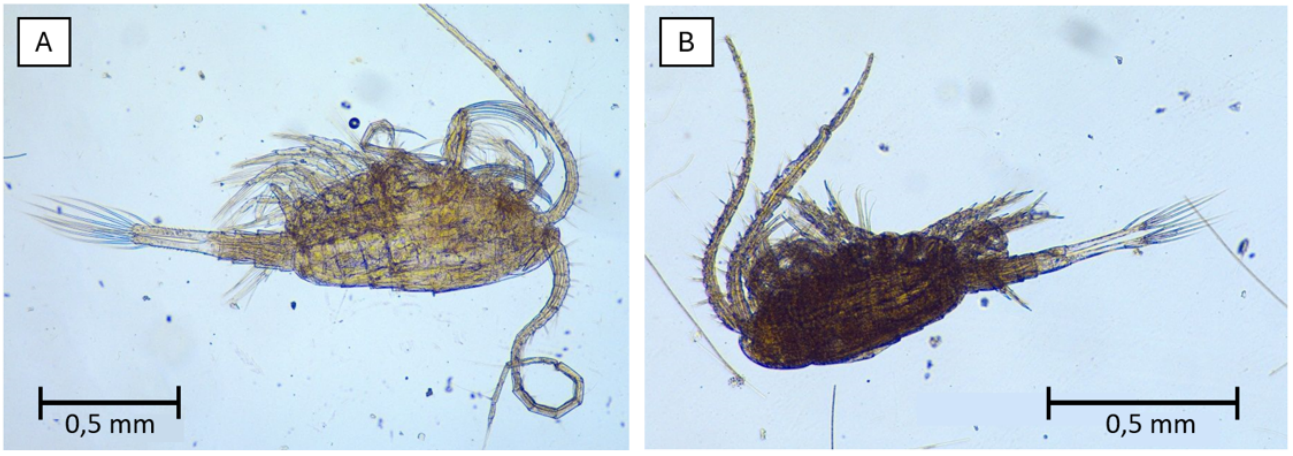


Fig. 1. A - Limnocalanus macrurus; B - Eurytemora lacustris (photo by V. Arcerytė).

[1] K. Arbačiauskas and D. Kalytytė, "Occurrence and Interannual Abundance Variation of Glacial Relict Calanoids Limnocalanus macrurus and Eurytemora lacustris in Lithuanian Lakes," Acta Zoologica Lituanica, vol. 20, no. 1, pp. 61–67, Jan. 2010, doi: 10.2478/v10043-010-0009-4.
[2] A. Audzijonytė, "Aukštesniųjų ledynmečio reliktinių vėžiagyvių gausumo ir populiacijos struktūros tyrimai Lūšių, Šakarvų, Akmenos ir Verniejaus ežeruose," Ekologija, no. 2, pp. 36–41, 1999.
[3] A. Audzijonyte, K. Arbačiauskas, and C. Smith, "Does the Ice Age legacy end in Central Europe? The shrinking distributions of glacial relict crustaceans in Lithuania," Aquatic Conservation Marine and Freshwater Ecosystems, vol. 33, no. 10, pp. 1003–1013, Aug. 2023, doi: 10.1002/aqc.4001.

ASSESSING THE EFFICIENCY OF PHARMACEUTICAL ELIMINATION VIA QUATERNARY WASTEWATER TREATMENT

Emilija Mockutė[1], Inga Urniežaitė[1], Povilas Reškevičius[2]

[1]Lithuania, Kaunas, Kaunas University of Technology, Department of Environmental Technology.
[2]Lithuania, Kaunas, JSC "Kauno vandenys" Wastewater Treatment Plant.
emilija.mockute@ktu.lt

Pharmaceutical compounds represent an important group of micropollutants of increasing concern due to their continuous release into the environment, biological activity, and potential adverse effects on aquatic ecosystems and human health [1]. These substances are widely detected in municipal wastewater; however, conventional biological wastewater treatment processes are not sufficiently effective in their removal. In response to this issue, the updated EU Urban Wastewater Treatment Directive introduces a quaternary treatment stage and identifies a list of 12 priority pharmaceutical compounds subject to monitoring and removal requirements [2]. The research, presented in this work, was funded by the EMPEREST project under the Interreg Baltic sea region programme 2021–2027. During the EMPEREST project, the impact of quaternary wastewater treatment technologies on the removal of micropollutants from wastewater was investigated. The same 12 pharmaceutical compounds, specified in the Directive, were investigated in this study, in order to assess the effectiveness of quaternary wastewater treatment technologies for the micropollutant removal. Samples were collected: untreated wastewater, after biological treatment and after each step of the quaternary treatment process: ozonation and activated carbon filtration. Pharmaceutical concentrations were determined using liquid chromatography–tandem mass spectrometry (LC-MS/MS) according to EPA Method 1694, operated in multiple reaction monitoring (MRM) mode.

Figure 1 illustrates changes in pharmaceutical concentrations across each stage of the quaternary wastewater treatment process, along with the applied ozone dose as a key technological parameter of the ozonation process. The results demonstrate a substantial reduction in overall pharmaceutical concentrations throughout the treatment train. Biological treatment removed approximately 60 % of the investigated pharmaceutical compounds. Subsequent ozonation increased the overall removal efficiency to about 95–96 %, while the complete quaternary treatment train including GAC filtration achieved an overall pharmaceutical removal efficiency of approximately 99 %. These findings confirm that a combined quaternary treatment approach is essential for the effective removal of pharmaceutical micropollutants.

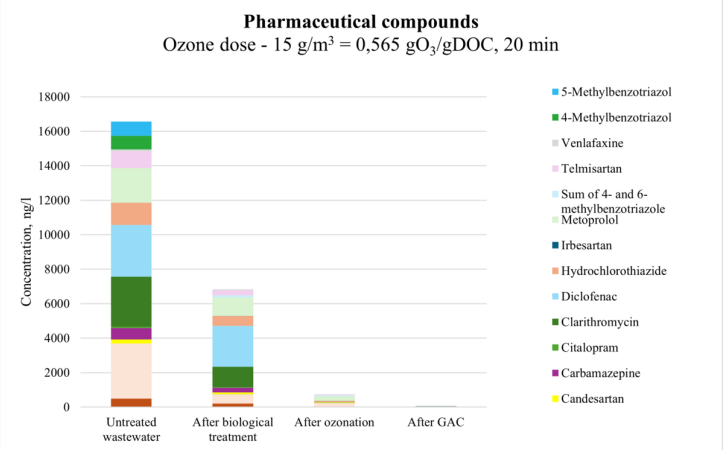


Fig. 1. Pharmaceuticals concentrations in wastewater before and after each stage of quaternary treatment.

[1] C. Vayssieres et al., "Assessment of wastewater treatment performance for PFAS removal: insights from pilot- and full-scale studies," NEXUS Nexus, vol. 2, p. 100076, 2022, doi: 10.1016/j.nexus.2022.100076.
[2] Council of the European Union, Proposal for a Directive of the European Parliament and of the Council concerning urban wastewater treatment (recast), Doc. 6848/24, Brussels, 2024.

COMBINED AUTOFLUORESCENCE AND CARS ANALYSIS OF QUANTUM DOTS IMPACT ON MICROALGAE

Rasa Miliukaitė[1,2], Saulius Bagdonas[1], Andrej Dementjev[3], Agnė Kalnaitytė-Vengelienė[1]

[1]Vilnius University, Faculty of Physics, Laser Research Center, Saulėtekio av. 9, bld. 3, LT-10222, Vilnius, Lithuania
[2]Vilnius University, Life Sciences Center, Institute of Biosciences, Saulėtekio av. 7, LT-10257 Vilnius, Lithuania
[3]Center for Physical Sciences and Technology, Department of Molecular Compound Physics, Saulėtekio av. 3, LT-10257, Vilnius, Lithuania
rasa.miliukaite@gmc.stud.vu.lt

Increasing use of nanoparticles (NPs) in industry and biomedicine raises new environmental safety challenges. Assessing NPs cytotoxicity is critical for developing safe technologies, particularly for quantum dots (QDs) - photoluminescent semiconductor NPs, that can interact with primary producers like algae. Although cadmium-free QDs are emerging as safer alternatives in biomedicine, their impact on photosynthetic organisms remains poorly understood. Additionaly, the role of an organism's physiological state in mediating QD-induced stress is often overlooked. This study examines how differently photoadapted algal cultures respond to Cu-based QDs, revealing links between environmental adaptation and NPs effects.

In this study, two *Desmodesmus communis* algae cultures (from Nature Research Center) were analyzed. Both were transitioned from high-light (100 µmol photons/m^{2}s) to lower-light conditions (34 µmol photons/m^{2}s, 12/12 h day/night photoperiod, MWC growth media) for different durations: one week (Culture No.1) and six months (Culture No.2), establishing distinct photoadaptation states. Samples were exposed to 4 µM CuInZnS/ZnS (Nanooptical materials, USA) QDs for 24 hours. The physiological impact and pigment dynamics were assessed using non-invasive *in vivo* techniques, including UV-VIS and PAM fluorometry, alongside fluorescence and Coherent anti-Stokes Raman (CARS) microscopy.

Our results demonstrate that although exposure to QDs generally causes disruption of energy distribution in PSII, as evidenced by decreased electron transport rate (ETR) and impaired non-photochemical fluorescence quenching coefficient (NPQ) in both cultures (Fig. 1), the nature of the resulting damage largely depends on the physiological state of the algae cells. In Culture No.1 (retaining high-light traits), this energetic imbalance quickly progressed to irreversible cellular damage, as evidenced by pigment degradation and pronounced alterations in autofluorescence as well as CARS data. In contrast, Culture No.2 (fully low-light adapted), primarily exhibited functional failure (registered sharp decrease in ETR) despite a more stable morphology. CARS microscopy further indicates that impaired photoprotection in the latter culture may be associated with functional uncoupling of carotenoids from their quenching complexes, leading to their locally enhanced vibrational visibility.

In conclusion, this study demonstrates that photoadaptation dictates whether QDs-induced stress leads to cellular degradation or functional impairment, providing a new mechanistic understanding of how NPs interact with the photosynthetic apparatus of algae.

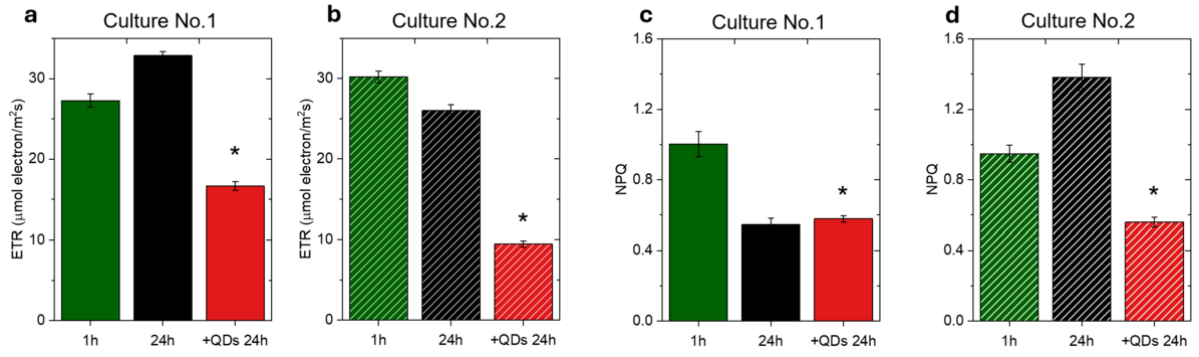


Fig. 1. Changes in ETR of (a) Culture No.1 and (b) Culture No.2 as well as NPQ of (c) Culture No.1 and (d) Culture No.2 algae, and after 24 hours incubation with QDs. Error bars represent 95% confidence interval, * p<0.05.

ORAL SESSION 15

Biology and Medicine

Chair: Dr. S. Bagdonas

EXCITABLE PLANTS: HOW ELECTRICAL SIGNALS MODULATE PHOTOSYNTHESIS

Aušrinė Navickaitė[1], Vytenė Macijauskaitė[1], Vilmantas Pupkis[1], Vilma Kisnierienė[1]

[1]Vilnius University, Life Sciences Center, Institute of Biosciences, Department of Neurobiology and Biophysics, Vilnius, Lithuania
ausrine.navickaite@gmc.vu.lt

Photosynthesis is a fundamental physiological process underlying plant growth and biomass production and is therefore central to plant performance under both optimal and adverse environmental conditions. Understanding the mechanisms that regulate photosynthesis is essential for improving predictions of plant performance under changing environment.

Beyond photochemical and biochemical regulation, plants generate electrical signals in response to diverse environmental stimuli, including both biotic and abiotic stressors. These signals – such as action potentials – arise from transient changes in the activity of ion transport systems (channels and pumps) and enable rapid information transfer within the plant, often leading to systemic responses such as increased stress hormone synthesis. The functional role of electrical signals in the regulation of photosynthesis remains underexplored. Experimental studies investigating the effects of action potentials on photosynthetic activity have yielded contradictory results: while most report a transient inhibition of photosynthesis following electrical excitation, others suggest an opposite effect.

This study used the freshwater characean macroalgae *Nitellopsis obtusa*, whose unique cellular morphology enables simultaneous application of electrical stimulation and pulse-amplitude-modulation (PAM) chlorophyll fluorometry in a single cell. This experimental approach enabled direct correlation between electrical signaling and photosynthetic responses. The results show that the generation of a single action potential causes a transient inhibition in the rise of non-photochemical quenching (NPQ), a key photoprotective mechanism responsible for dissipating excess light energy. Because NPQ depends on the transthylakoid pH gradient, it can be hypothesized that action potential generation reduced this gradient, for example by transiently suppressing the activity of plasma membrane H^+-ATPases (Fig. 1) and / or initiating Ca^{2+} signaling that modulates H^+ transport processes within the thylakoid membrane [1].

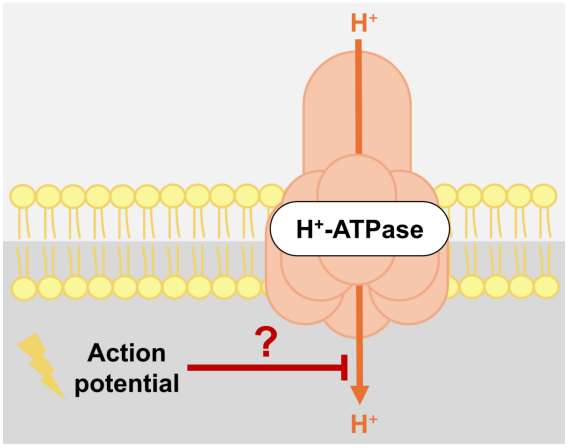


Fig. 1. Scheme illustrating the proposed hypothesis that action potential suppresses plasma membrane H^+-ATPases, which leads to reduced transthylakoid pH gradient.

[1] S. Stael, B. Wurzinger, A. Mair, N. Mehlmer, U. C. Vothknecht, and M. Teige, "Plant organellar calcium signalling: an emerging field," Journal of Experimental Botany, vol. 63, no. 4, pp. 1525–1542, Dec. 2011, doi: 10.1093/jxb/err394.

DESIGN AND CHARACTERISATION OF LIPOSOMAL CURCUMIN AND ASTAXANTHIN MICROCAPSULES FOR ORAL DRUG DELIVERY

Hamidreza Sahaleh[1], Dr. Jolita Stabrauskienė[1], Prof. Dr. Jurga Bernatonienė[1]

[1]Lithuanian University of Health Science, Faculty of Pharmacy, Kaunas, Lithuania
hamidreza.sahaleh@stud.lsmu.lt

Curcumin is a polyphenolic compound from Curcuma longa, and astaxanthin is a lipid-soluble xanthophyll carotenoid which widely studied for their antioxidant, anti-inflammatory, and anticancer properties [1],[2]. The clinical application of curcumin is limited due to poor aqueous solubility, rapid metabolism, and low systemic bioavailability [3]. Same issue for astaxanthin which is hydrophobic and chemically unstable and it restricts its oral bioavailability and requires advanced delivery strategies [4]. Liposomal and other nanoencapsulation approaches have been shown to improve dissolution, protect APIs such as curcumin and astaxanthin from degradation, improve cellular uptake, and increase bioavailability relative to their free forms [3],[5]. Recent studies report that liposomal formulations of both compounds can significantly improve physicochemical stability and increased therapeutic potential compared with non-encapsulated analogues [3],[5].

Previous studies have primarily focused on liposomal formulations of curcumin or astaxanthin individually but the aim of this study is to investigate the possible formulation and characterisation of liposomes with both compounds.

Liposomes are spherical, vesicular, colloidal delivery systems composed of an amphiphilic lipid bilayer, such as phospholipids which surrounded by an aqueous core. These structures have multiple advantages for drug delivery, such as improved solubility, stability, and bioavailability of encapsulated compounds. There are different methods to formulate liposomes but in this study, liposomal curcumin and astaxanthin was prepared by using the thin-film hydration method. The prepared liposomal solution was converted to microcapsules by lyophilization. The formulation process was challenging and carefully optimised. Some parameters such as phospholipid type, lipid-to-drug ratio, organic solvent content, and sonication time directly affect on liposome formation and their physicochemical properties.

In terms of particle size, the result for z-average was 114 nm which shows the liposomes are nanosized and suitable for efficient drug delivery. Polydispersity index (PDI) was 0.27 that proved the optimised formulation has a relatively uniform size distribution, and the zeta potential was -19.2 mv, which shows good stability. The encapsulation efficacy (%EE) was 85% for astaxanthin and 87% for curcumin. The yield after lyophilization was approximately 98% which shows high formulation efficiency. The moisture content of final product was 5.9 %. In addition, the results from scanning electron microscopy (SEM) confirmed the desirable structural of the formulations.

The liposomal curcumin and astaxanthin formulation is designed to improve solubility and protect the compounds from degradation. With liposomal curcumin and astaxanthin their poor solubility and bioavailability can be solved and as a result their anticancer efficacy will be improved.

[1] 1. A. Liakopoulou, S. Letsiou, K. Avgoustakis, G. P. Patrinos, F. N. Lamari, and S. Hatziantoniou, “Curcumin-Loaded Lipid Nanocarriers: a targeted approach for combating oxidative stress in skin applications,” Pharmaceutics, vol. 17, no. 2, p. 144, Jan. 2025, doi: 10.3390/pharmaceutics17020144.

[2] 2. Y. Zhu, L. He, X. Qin, M. Xu, and C. Tan, “Recent advances in nanodelivery systems for astaxanthin: A review,” Food Bioscience, vol. 67, p. 106305, Mar. 2025, doi: 10.1016/j.fbio.2025.106305.

[3] 3. M. Hao, C. Zhang, T. Wang, and H. Hu, “Pharmacological effects, formulations, and clinical research progress of curcumin,” Frontiers in Pharmacology, vol. 16, p. 1509045, Mar. 2025, doi: 10.3389/fphar.2025.1509045.

[4] 4. M. Vitale, J. Gomez-Estaca, J. Chung, S.-C. Chua, and D. M. Pampanin, “Encapsulation techniques to enhance astaxanthin utilization as functional feed ingredient,” Marine Drugs, vol. 23, no. 4, p. 143, Mar. 2025, doi: 10.3390/md23040143.

[5] 5. A. Ghosh, S. Banik, K. Takahama, Y. Nishida, and M. Honda, “Formulation and physicochemical characterization of astaxanthin-loaded liposomes: A comparative study of free and ester forms with different E/Z-isomer ratios of astaxanthin,” Food Research International, vol. 212, p. 116448, Apr. 2025, doi: 10.1016/j.foodres.2025.116448.

CALCIUM ELECTROCHEMOTHERAPY USING ULTRA-FAST NANOSECOND ELECTRIC PULSES AND THEIR EFFECTS ON MITOCHONDRIA TRANSMEMBRANE POTENTIAL AND OXIDATION

Paulina Malakauskaite[1,2,4], Vytautas Kaseta[3], Vitalij Novickij[1,2,4]

[1]State Research Institute Centre for Innovative Medicine, Department of Immunology and Bioelectrochemistry, Lithuania
[2]Vilnius Gediminas Technical University, Faculty of Electronics, Lithuania
[3]State Research Institute Centre for Innovative Medicine, Department of Stem Cell Biology, Lithuania
[4]Wroclaw Medical University, Department of Molecular and Cellular Biology, Poland
paulina.malakauskaite@imcentras.lt

Electroporation refers to the phenomenon wherein the application of high, short-duration pulsed electric fields (PEF) to biological cells induces a transient increase in plasma membrane permeability [1]. The pulse duration of nanosecond PEF (nsPEF) is significantly shorter than the time constant of biological cell membrane and can penetrate into the interior of the cell and organelles inducing various biological effects [2]. Thus, nsPEF alter mitochondrial function by permeabilizing its membrane. Mitochondria must maintain the electric potential across the inner membrane and a loss of the proton gradient often leads to the disruption of the mitochondrial membrane potential (MMP) and couples with the ROS-induced oxidative stress [3]. Both of these signalling systems profoundly influences the rate of ATP synthesis [4], which is also linked to calcium overload [5]. Mitochondrial calcium overload also work complementarily with ROS overproduction and dependent on the mitochondrial membrane potential [6]. All of these processes ultimately causes cell death involving apoptosis or necrosis. Therefore, stimulation of apoptosis through a mitochondrial-mediated pathway with nsPEF could enhance current electrochemotherapy protocols.

Pulses were generated using a custom-built high-frequency (up to 6.6 MHz) square-wave generator (≤3 kV). The voltage varied in 50 V – 1.6 kV range, corresponding to a 0.5–16 kV/cm electric field in the cuvette. We applied 50 ns or 300 ns monophasic pulses (100 pulses/burst, 100 ns delay) and a microsecond reference protocol (1.2 kV/cm × 100 µs × 8, 1 Hz). CHO-K1-Luc cells were used as a model. Permeabilization was detected with Yo-Pro-1, MMP disruption with TMRM, ROS with MitoSOX Red, ATP depletion via D-luciferin oxidation, and viability via PrestoBlue. For CaECT, $CaCl_2$ (5 mM) was added in low-conductivity HEPES buffer (10 mM HEPES, sucrose, 1 mM Mg^{2+}).

High permeabilization (>75 %) was achieved with pulsed electric field exceeding 6 kV/cm for 50 ns pulses and 4 kV/cm for 300 ns (n = 100), respectively. PEF amplitude was limited to 6–12 kV/cm protocols to ensure overlapping points in terms of permeabilization efficacy for both 50 ns and 300 ns protocols. 300 ns pulses caused a greater MMP reduction than 50 ns pulses, indicating that high permeabilization is required to trigger significant depolarization of mitochondria within the studied parametric range. In the context of ROS, 300 ns pulses trigger detectable oxidation of mitochondria even without added calcium. When calcium is added in both cases (50 ns and 300 ns) the oxidation of mitochondria increases up to 2000 %. A viability assay showed that 300 ns pulses at >6 kV/cm caused partly irreversible electroporation and cell death in all CaECT protocols, while 50 ns pulses (6–12 kV/cm) induced reversible electroporation. For 50 ns pulses, 10–12 kV/cm enabled sufficient calcium electrotransfer for effective CaECT in vitro.

[1] Kotnik, T., et al. Membrane Electroporation and Electropermeabilization: Mechanisms and Models. Annu Rev Biophys 48, 63–91, 2019.
[2] Ruiz-Fernández AR, et al. Nanosecond Pulsed Electric Field (nsPEF): Opening the Biotechnological Pandora's Box. Int J Mol Sci ;23(11):6158, 2022
[3] Fahimi, P., et al. Electrical homeostasis of the inner mitochondrial membrane potential. Physical biology vol. 22,2 10.1088/1478-3975/adaa47. 2025.
[4] Nicholls, D. G. Mitochondrial membrane potential and aging. Aging Cell 3, 35–40, 2004.
[5] Ohnishi, N et al., Variations of Intracellular Ca2+ Mobilization Initiated by Nanosecond and Microsecond Electrical Pulses in HeLa Cells. IEEE Trans Biomed Eng 66, 2259–2268, 2019.
[6] Tarasov AI, et al., Regulation of ATP production by mitochondrial Ca(2+). Cell Calcium. 52(1):28-35, 2012.

ASSESSMENT OF ELECTRICAL SIGNALS IN ELECTROPORATED LANGENDORF-PERFUSED RABBIT HEARTS

Dominyka Adamonė[1], Mantė Almanaitytė[1], Ieva Lankutytė[1], Vilma Zigmantaitė[1], Saulius Šatkauskas[2], Jonas Jurevičius[1], Regina Mačianskienė[1]

[1]Lithuanian University of Health Sciences, Institute of Cardiology, Laboratory of Membrane Biophysics, Sukilėlių pr.15, Kaunas, Lithuania
[2]Vytautas Magnus University, Faculty of Natural Sciences, Department of Biochemistry, Universiteto g. 10, Akademija, Kaunas, Lithuania
dominyka.adamone@lsmu.lt

Pulse Electric Field (PEF) ablation is gaining significant clinical interest as a non-thermal alternative to traditional radiofrequency or cryotherapy-based catheter ablation for the treatment of cardiac arrhythmias. Despite PEF offering improved tissue selectivity and reduced collateral damage, reliable functional validation of lesion depth and electrical effectiveness remains essential for controlling clinical outcomes.

We introduce a multimodal cross-validated approach for functional assessment of PEF-induced ablation zones by combining high-speed optical mapping (OM) with microelectrode (ME) transverse and transmural action potential (AP) recordings (Fig.1). Experiments were conducted in a Langendorff-perfused rabbit heart with synchronized PEF delivery, cardiac pacing, and OM acquisition. Critically, lesion depth and electrical impairment were independently verified by recording APs in a cut-off ventricular wedge prepared from PEF-treated regions, enabling direct cross-validation of surface and transmural electrophysiological changes. Both single-pulse and complex PEF protocols were evaluated.

The results indicate that PEF significantly affects lesion size, depth, and functional severity. It slows AP propagation, causes conduction block, and alters AP morphology in peri-ablated tissue. Regions without electrical activity were identified at depths of up to 3 mm, depending on the stimulation parameters used. Overall, OM and ME techniques are useful for investigating and evaluating PEF ablation effectiveness.

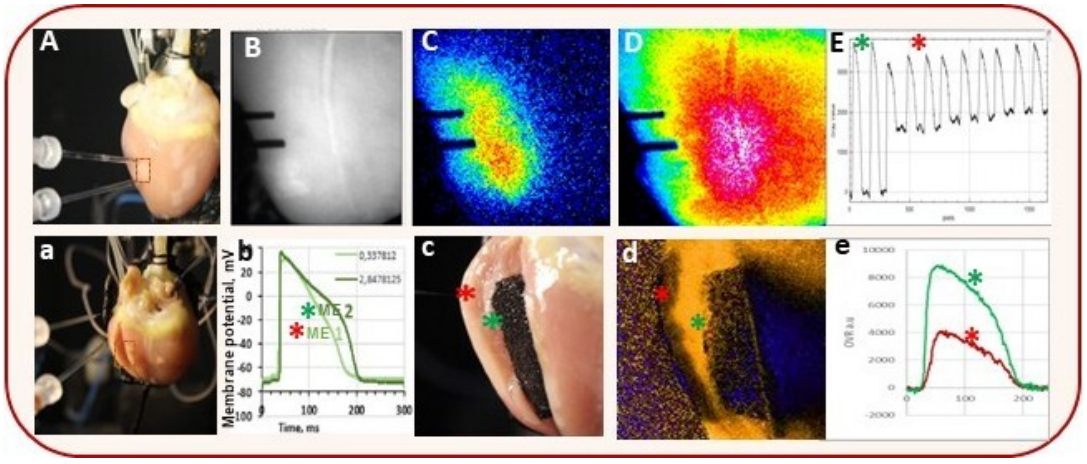


Fig. 1. Cross-validation demonstrating electroporation-induced electrical signal excitation in a whole heart (A-E) and of a cut-off ventricular wedge at PEF-treated regions (a-e). Square boxes indicate the locations from which the action potentials (APs) were obtained (A and a). Stars mark APs recorded with microelectrodes (ME) and optically, which were detected in undamaged (green) and PEF-affected (red) locations.

PULSING BUFFER COMPOSITION IMPACT ON CELL VIABILITY AFTER ELECTROPORATIONBY SUPPLEMENTING THE BUFFERS WITH INTRACELLULAR MOLECULES

Anusiya Paneerselvam[1], Baltramiejus Jakštys[1,2], Saulius Šatkauskas[1,2]

[1]Vytautas Magnus University, Nature Science Faculty, Biochemistry Cathedral, Kaunas, Lithuania
[2]Vytautas Magnus University, Kaunas, Research Institute of Natural and Technological Sciences, Cell and Tissue Biotechnology laboratory, Lithuania
anusiya.panneerselvam@stud.vdu.lt

Electroporation (EP) is a widely used method for intracellular delivery of biomolecules, yet the cell viability after treatment remains a critical limitation influenced by the involved pulsing conditions and respective medium composition [1]. While the extracellular environment plays a key role in gene electrotransfer optimization, its effects following membrane permeabilization have not been fully characterized [2, 3]. The objective of this study was to evaluate how EP supernatant affects cell viability post-electroporation under different pulsing media, with the aim of identifying conditions that improve cellular recovery while maintaining effective electroporation. To achieve this CHO cells were electroporated using three different media: a standard EP medium, EP HEPES buffer, and EP HEPES buffer supplemented with calcium. Following the electroporation with different parameters, cells were incubated with fresh medium or in EP-supernatant separately. Cell viability was assessed across a range of pulse strengths using flow cytometry-based analysis and MTS assay. The observed results after 24hrs represent the impact of EP-supernatant on cell viability. In the standard electroporation medium, exposure to pulses in EP-supernatant significantly improved cell viability, particularly at higher pulse strengths. In contrast, cells exposed to EP-supernatants from HEPES and HEPES supplemented with calcium showed significantly reduced viability compared to cells maintained in fresh medium. These findings clearly indicate that medium composition plays a crucial role in cellular responses post-electroporation. In conclusion, this study highlights the importance of selecting appropriate pulsing media to enhance post-electroporation cell survival [2, 3]. Ongoing work aims to assess gene electrotransfer efficiency and to investigate morphological changes associated with different media conditions, providing further insight into optimizing electroporation-based gene delivery protocols.

[1] E. Neumann, M. Schaefer-Ridder, Y. Wang, and P. H. Hofschneider, “Gene transfer into mouse lyoma cells by electroporation in high electric fields.,” The EMBO Journal, vol. 1, no. 7, pp. 841–845, Jul. 1982, doi: 10.1002/j.1460-2075.1982.tb01257.x.

[2] V. Rajeckaitė, B. Jakštys, A. Rafanavičius, M. Maciulevičius, M. Jakutavičiūtė, and S. Šatkauskas, “Calcein Release from Cells In Vitro via Reversible and Irreversible Electroporation,” The Journal of Membrane Biology, vol. 251, no. 1, pp. 119–130, Nov. 2017, doi: 10.1007/s00232-017-0005-8.

[3] B. Jakstys, M. Jakutaviciute, D. Uzdavinyte, I. Satkauskiene, and S. Satkauskas, “Correlation between the loss of intracellular molecules and cell viability after cell electroporation,” Bioelectrochemistry, vol. 135, p. 107550, May 2020, doi: 10.1016/j.bioelechem.2020.107550.

ORAL SESSION 16

Biology and Medicine

Chair: Dr. M. Ger

IDENTIFICATION OF A NOVEL RIBOSE-METHYLATED NUCLEOSIDE DEMETHYLATION REACTION CATALYZED BY 2OG-DEPENDENT PHYHD1 AND PHYH-LIKE OXYGENASES

Justas Stonkus[1], Rasa Rutkienė[1], Rita Meškienė[1], Agota Aučynaitė[1], Justas Lazutka[2], Darius Balčiūnas[2,3], Giedrius Vilkaitis[2], Rolandas Meškys[1]

[1]Vilnius University, Life Sciences Center, Institute of Biochemistry, Vilnius, Lithuania
[2]Vilnius University, Life Sciences Center, Institute of Biotechnology, Vilnius, Lithuania
[3]Temple University, College of Science and Technology, Department of Biology, Philadelphia, USA
justas.stonkus@gmc.stud.vu.lt

RNA chemical modifications are post-transcriptional alterations to RNA base or ribose components that serve as a crucial regulatory layer, influencing RNA stability, folding, and translation. Among the plethora of known modifications, 2′-*O*-methylation (Nm) is one of the most common and is found across diverse RNA species in all known domains of life, as well as in RNA viruses. In recent years, considerable progress has been made in mapping Nm sites and elucidating their biological roles [1]. However, the enzymatic pathways responsible for the catabolism of 2′-*O*-methylated nucleosides remain largely unexplored, as only a few bacterial nucleoside hydrolases have been characterized previously.

Therefore, functional screenings of metagenomic libraries were conducted to identify novel enzymes active toward 2′-*O*-methyl pyrimidines, using the auxotrophic *Escherichia coli* DH10B *ΔpyrFEC* strain, a method created to select for enzymes involved in the biodegradation of modified nucleosides [2]. During one of these searches, a novel 2′-*O*-methylated nucleoside demethylation reaction catalyzed by a bacterial 2-oxoglutarate- and Fe(II)-dependent dioxygenase FJS was identified. Following this, the same enzymatic activity was assigned to FJS-related enzymes annotated as members of the phytanoyl-CoA dioxygenase (PHYH) family or as phytanoyl-CoA dioxygenase domain-containing protein 1 (PHYHD1). Whilst human PHYH has a clearly defined function in phytanic acid α-oxidation within peroxisomes, until our study, the primary substrate of human PHYHD1 had not been identified [3].

It was found that, like FJS, eukaryotic PHYHD1 dioxygenases demethylate a broad range of ribose-methylated nucleosides but do not demethylate modified nucleotides or RNA *in vitro*. To determine whether the loss of PHYHD1 function affects 2′-*O*-methylation levels of RNA-incorporated or free nucleosides, a *phyhd1* knockout (*phyhd1*-KO) zebrafish line was generated. While no visible phenotype changes were observed and the RNA modification levels remained unchanged, the amounts of free 2′-*O*-methylated inosine, guanosine, cytidine, and uridine were significantly elevated in both *phyhd1*-KO embryo and adult zebrafish extracts. These findings indicate that PHYHD1 does not directly demethylate RNA but instead functions in the turnover of free 2′-*O*-methylated nucleosides [4].Thus, a previously unrecognized metabolic pathway for 2′-*O*-methylated nucleosides was identified, with PHYHD1 as the key dioxygenase responsible for their demethylation.

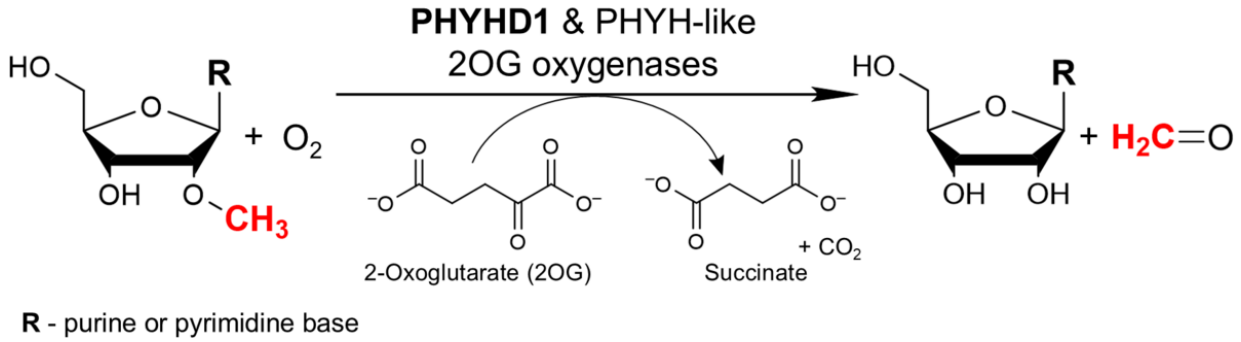


Fig. 1. Reaction scheme for the PHYHD1-catalyzed demethylation of 2′-*O*-methylated nucleosides.

[1] K. I. Zhou, C. V. Pecot, and C. L. Holley, "2′-O-methylation (Nm) in RNA: progress, challenges, and future directions," RNA, vol. 30, no. 5, pp. 570–582, Jan. 2024, doi: 10.1261/rna.079970.124.
[2] A. Aučynaitė, R. Rutkienė, R. Gasparavičiūtė, R. Meškys, and J. Urbonavičius, "A gene encoding a DUF523 domain protein is involved in the conversion of 2-thiouracil into uracil," Environmental Microbiology Reports, vol. 10, no. 1, Art. no. 1, 2018, doi: 10.1111/1758-2229.12605.
[3] T. Ala-Nisula, S. K. Sah-Teli, V.-P. Ronkainen, E. Y. Dimova, and P. Koivunen, "Human phytanoyl-CoA dioxygenase domain-containing 1 (PHYHD1) is a putative oxygen sensor associated with RNA and carbohydrate metabolism," FEBS Letters, vol. 597, no. 12, pp. 1651–1666, 2023, doi: 10.1002/1873-3468.14666
[4] J. Stonkus et al., "A new role for PHYHD1 and related dioxygenases: demethylation of 2′-O-methylated nucleosides," Nucleic Acids Res, vol. 53, no. 22, p. gkaf1379, Dec. 2025, doi: 10.1093/nar/gkaf1379.

ARYL HYDROCARBON RECEPTOR EXPRESSION CHANGES IN GEMCITABINE-RESISTANT PANCREATIC CANCER CELLS

Smiltė Januškevičiūtė[1], Vaiva Grišunina[1], Vitė Vitkutė[1], Darius Stukas[1]

[1]Lithuanian University of Health Sciences, Faculty of Medicine, Institute for Digestive Research, Surgical Gastroenterology Laboratory, Lithuania
smilte.januskeviciute@stud.lsmu.lt

Pancreatic ductal adenocarcinoma (PDAC) is a devastating disease and the sixth leading cause of cancer related deaths globally. The poor disease prognosis is a result of late diagnosis and limited therapeutic options. Due to late diagnosis systemic treatment with chemotherapy is usually the only option [1]. Gemcitabine (GEM) is the gold standard first-line single chemotherapy agent for pancreatic cancer [2]. Aryl-carbon receptor (AhR), a ligand-activated transcription factor. AhR is expressed in several tumor cells and regulates the expression of genes in the signal transduction pathways [3]. Elevated AhR levels in PDAC patients correlate with worse outcomes [4]. There are speculations that AhR can be linked the gemcitabine resistance, however, the role of AhR in modulating gemcitabine sensitivity and the development of gemcitabine resistance is not fully understood.

This research aims to assess alterations in AHR expression and gemcitabine IC_{50} values in gemcitabine-resistant pancreatic cancer cells.

This study used commercial pancreatic cancer cell lines Su.86.86 and BxPC-3. Cells planted in 96-well plates were treated with increasing doses of gemcitabine to measure gemcitabine resistance both before and after resistance development. IC_{50} values were computed by linear regression analysis, and cell metabolic activity was assessed using the resazurin reduction test. The expression of AHR mRNA was assessed before and after resistance acquisition. TaqMan probes were used in real-time PCR analysis after RNA was extracted using column-based kits and reverse-transcribed to cDNA. Using the $2^{-}\Delta\Delta Ct$ technique, relative gene expression changes were computed.RT-qPCR $2^{-}\Delta\Delta Ct$ analysis showed reduced basal AHR expression in gemcitabine-resistant pancreatic cancer cells compared with non-resistant cells.

Relative AHR expression was 0.578 in resistant BxPC-3 cells and 0.459 in resistant SU.86.86 cells. Treatment with IC_{50} doses of gemcitabine increased AHR expression in both resistant and non-resistant cells in both cell lines. Despite this induction, gemcitabine-resistant cells demonstrated considerably higher IC_{50} values than non-resistant cells. IC_{50} values increased from 27 nM to 1856 nM in BxPC-3 cells and from 37 nM to 24 268.9 nM in SU.86.86 cells.

Pancreatic cancer cells with acquired gemcitabine resistance exhibit decreased basal AHR mRNA expression, even though IC_{50} doses of gemcitabine induce AHR similarly, indicating a link between low AHR levels and resistance to gemcitabine in resistant cells

[1] V. Kannen et al., “Loss of aryl hydrocarbon receptor reduces pancreatic tumor growth by increasing immune cell infiltration,” Biochemical Pharmacology, vol. 236, p. 116872, Mar. 2025, doi: 10.1016/j.bcp.2025.116872.

[2] K. Samanta, S. Setua, S. Kumari, M. Jaggi, M. M. Yallapu, and S. C. Chauhan, “Gemcitabine Combination Nano therapies for pancreatic cancer,” Pharmaceutics, vol. 11, no. 11, p. 574, Nov. 2019, doi: 10.3390/pharmaceutics11110574.

[3] S. Masoudi et al., “An Increased Level of Aryl Hydrocarbon Receptor in Patients with Pancreatic Cancer,” Middle East Journal of Digestive Diseases, vol. 11, no. 1, pp. 38–44, Oct. 2018, doi: 10.15171/mejdd.2018.126.

[4] W. Mei et al., “The aryl hydrocarbon receptor inhibits antigen presentation to promote progression of pancreatic ductal adenocarcinoma,” Journal of Advanced Research, Nov. 2025, doi: 10.1016/j.jare.2025.10.079.

STUDY OF THE BIOLOGICAL PROPERTIES OF THE GLIOBLASTOMACELL LINE U87, WHICH INDUCIBLY SYNTHESIZES SOX2 AND OCT4

Gabija Žiūraitė[1,2], Arūnas Kazlauskas[2], Vilma Kaškonienė[3]

[1]Vytautas Magnus University, Faculty of Natural Sciences, Kaunas, Lithuania
[2]Lithuanian University of Health Sciences, Neuroscience Institute, Laboratory of Molecular Neurooncology, Kaunas, Lithuania
[3]Vytautas Magnus University, Research Institute of Natural and Technological Sciences, Open Access Center for Instrumental Analysis, Kaunas, Lithuania
gabija.ziuraite@vdu.lt

Glioblastoma multiforme (GBM) represents the most prevalent malignant tumor of the central nervous system (CNS). Despite a multimodal therapeutic approach, consisting of maximal surgical resection, radiotherapy, and concomitant chemotherapy, clinical outcomes remain suboptimal. The prognosis for GBM patients is still poor, with a median overall survival of approximately 15 months and a five-year survival rate of less than 5% [1]. Treatment is complicated by chemoresistance caused by Glioma Cancer Stem Cells (GCSCs) [2]. The GCSC phenotype is regulated by a specific group of transcription factors, traditionally identified as the ”Yamanaka factors”: Sox2, Oct4, c-Myc, and Klf4. However, according to research by Lopez-Bertoni et al. [3], the expression of only two genes—SOX2 and OCT4—is sufficient for stemness induction in glioblastoma cells, suggesting that the full reprogramming typically used to generate induced Pluripotent Stem Cells (iPSCs) is not required in this context.

The objective of this study was to investigate how ectopic expression of the SOX2 and OCT4 genes influences the biological functions of glioblastoma cells.

To investigate the causes of glioblastoma malignancy, experiments were conducted using U87-TSO cells, a modified U87 cell line engineered for the tetracycline-inducible expression of the transcription factors Sox2 and Oct4. The proliferation rates of both tetracycline-treated and control U87-TSO populations were quantified via MTT assay. The MTT assay was also used to evaluate the U87-TSO response to the anti-cancer drug temozolomide (TMZ). The ability to form spheroid structures was also evaluated by culturing the cells under conditions that promote a stem-like phenotype. Additionally, the influence of transcription factors on cellular motility was characterized by performing a scratch wound healing assay. All research findings were evaluated using arithmetic mean and standard deviation. Student’s t-test was used to determine the significance level (p) to evaluate data reliability. Results were considered statistically significant and reliable if $p < 0.05$.

Analysis via MTT assay revealed that the tetracycline-induced expression of SOX2 and OCT4 resulted in a reduction of cellular proliferation, accompanied by significant alterations in cell morphology. While the ectopic expression of these transcription factors did not yield a statistically significant change in the sensitivity of U87-TSO cells to TMZ, it appeared to promote cellular viability. Furthermore, U87-TSO spheroids exhibited prolonged viability compared to those formed from unmodified U87 cells. Results from the scratch assay indicated that the migration of U87-TSO cells is significantly slower compared to the parental U87 cell line.

These studies provide new insights into the stemness phenotype regulators Sox2 and Oct4 and the importance of their gene expression level in the process of glioblastoma pathogenesis.

Keywords: Glioblastoma multiforme (GBM), Stemness induction, Yamanaka factors, Tetracycline-inducible system, U87 cell line

[1] F. Girardi et al., “Global survival trends for brain tumors, by histology: analysis of individual records for 556,237 adults diagnosed in 59 countries during 2000–2014 (CONCORD-3),” Neuro-Oncology, vol. 25, no. 3, pp. 580–592, Nov. 2022, doi: 10.1093/neuonc/noac217.

[2] S. Abbas, S. K. Singh, A. K. Saxena, S. Tiwari, L. K. Sharma, and M. Tiwari, “Role of autophagy in regulation of glioma stem cells population during therapeutic stress,” Journal of Stem Cells and Regenerative Medicine, vol. 16, no. 2, pp. 80–89, Dec. 2020, doi: 10.46582/jsrm.1602012.

[3] H. Lopez-Bertoni et al., “DNMT-dependent suppression of microRNA regulates the induction of GBM tumor-propagating phenotype by Oct4 and Sox2,” Oncogene, vol. 34, no. 30, pp. 3994–4004, Oct. 2014, doi: 10.1038/onc.2014.334.

SELECTIVE INHIBITION OF TUMOR-ASSOCIATED CARBONIC ANHYDRASE IX BY FLUORINATED BENZENESULFONAMIDES

Justinas Malevskis[1], Joana Smirnovienė[1], Mantas Žvirblis[1], Virginija Dudutienė[1], Daumantas Matulis[1], Vytautas Petrauskas[1]

[1]Vilnius University, Life Sciences Center, Institute of Biotechnology, Department of Biothermodynamics and Drug Design, Lithuania
justinas.malevskis@chgf.stud.vu.lt

Carbonic anhydrases (CAs) are ubiquitous metalloenzymes present in living organisms; in humans, they belong to the α-CA family. These enzymes catalyze the reversible hydration of carbon dioxide to bicarbonate and a proton, thereby playing a key role in cellular pH regulation. Among the twelve catalytically active human isoforms, carbonic anhydrase IX (CA IX) is of particular interest due to its overexpression in hypoxic tumor cells, where it contributes to tumor progression and metastasis. Consequently, CA IX represents an attractive target for anticancer therapy. Primary benzenesulfonamides bearing various substituents are well-established CA inhibitors owing to their high affinity and relatively simple synthesis. However, the development of compounds that selectively inhibit CA IX while preserving the physiological activity of other CA isoforms remains a significant challenge [1].

The objective of this study was to identify selective CA IX inhibitors by evaluating newly synthesized fluorinated benzenesulfonamide derivatives bearing cyclic and aliphatic side chains High-throughput fluorescent thermal shift assay (FTSA) was employed to simultaneously screen multiple ligands across a range of concentrations. FTSA determines ligand-induced protein stabilization by monitoring changes in the protein unfolding temperature (ΔT_m), which is subsequently converted into binding constants K_b using advanced thermodynamic models [2]. Isoform selectivity was assessed by performing experiments with CA I, CA II, chimeric CA VI, CA VII, CA IX, CA XII, and CA XIII. In addition, stopped-flow CO_2 hydration assay was used to confirm inhibition of CA catalytic activity. All experimentally obtained binding and inhibition data were deposited into the Protein–Ligand Binding Database (PLBD, plbd.org), enabling their direct use in AI-driven drug discovery and predictive modeling of CA IX inhibitor affinity and selectivity.

Screening of the compound series enabled the identification of the lead compound MZ24-11, which exhibited nanomolar affinity (K_d = 1.4 nM) and pronounced selectivity toward CA IX (**Fig. 1**) over CA I, CA II, chimeric CA VI, CA VII, CA IX, CA XII, and CA XIII. Although the lead inhibitor demonstrated high potency, further structural optimization is required for its development as a viable anticancer drug candidate.

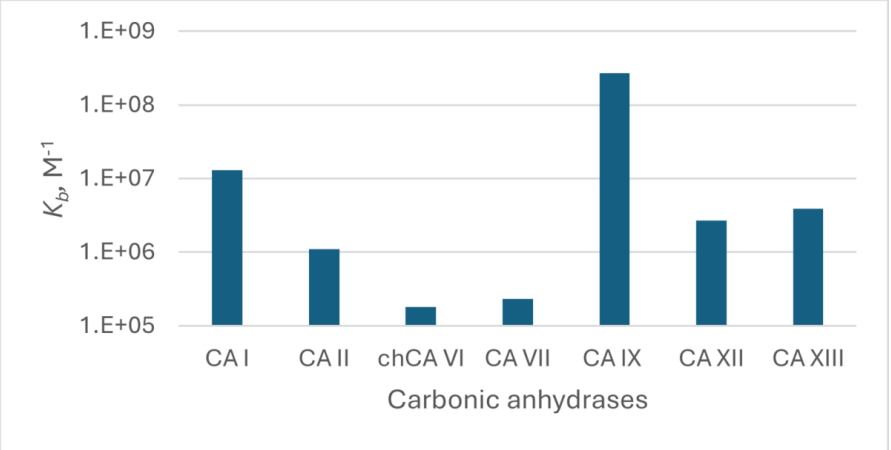


Fig. 1. A diagram comparing binding constants (Kb) of lead compound MZ24-11 binding to CA I, II, chCA VI, CA VII, CA IX, CA XII and CAXIII. CA IX is clearly inhibited by several orders of magnitude stronger than CA I, II, chCA VI, CA VII, CA XII, CA XIII, indicating inhibitor's selectivity towards CA IX.

[1] V. Linkuvienė et al., "Thermodynamic, kinetic, and structural parameterization of human carbonic anhydrase interactions toward enhanced inhibitor design," Quarterly Reviews of Biophysics, vol. 51, p. e10, Jan. 2018, doi: 10.1017/s0033583518000082.

[2] V. Petrauskas, E. Kazlauskas, M. Gedgaudas, L. Baranauskienė, A. Zubrienė, and D. Matulis, "Thermal shift assay for protein–ligand dissociation constant determination," TrAC Trends in Analytical Chemistry, vol. 170, p. 117417, Nov. 2023, doi: 10.1016/j.trac.2023.117417.

NAMED ENTITY RECOGNITION IN ELECTRONIC HEALTH RECORDS FOR ALPORT SYNDROME

Gabrielė Skirmantaitė[1], Gražina Korvel[1], Rimantė Čerkauskienė[2], Agnė Čerkauskaitė-Kerpauskienė[2]

[1]Vilnius university, Faculty of Mathematics and Informatics, Vilnius, Lithuania
[2]Vilnius university, Faculty of Medicine, Vilnius, Lithuania
gabriele.skirmantaite@mif.vu.lt

Rare diseases pose considerable diagnostic difficulties due to their infrequent occurrence, heterogeneous clinical presentation, and overlap with more prevalent conditions, often resulting in delayed or incorrect diagnoses that negatively affect patient management. Alport syndrome, a hereditary disorder affecting renal, auditory, and ocular systems, illustrates the clinical importance of the timely identification of disease-related information in patient records.

The increasing adoption of electronic health record (EHR) systems has led to the accumulation of large volumes of clinical data, a substantial proportion of which is recorded as unstructured free-text. Although structured EHR components can be readily processed computationally, a significant amount of clinically relevant information is documented in narrative form and is not directly accessible for automated analysis. Named entity recognition (NER), a core task in natural language processing, addresses this limitation by enabling the identification of clinically meaningful entities, such as diseases, symptoms, treatments, and medications, from unstructured clinical text and serves as a foundational step in clinical information extraction.

Against this background, the present study examines transformer-based NER applied to unstructured clinical documentation in Lithuanian electronic health records. Lithuanian constitutes a low-resource language in the clinical NLP domain, characterized by limited availability of annotated data and linguistic properties including rich morphology, extensive inflection, and high lexical variability. These features, combined with domain-specific medical terminology and the frequent use of abbreviations in clinical documentation, introduce additional challenges that prevent direct application of methods developed for high-resource languages.

The task is formulated as token-level sequence labeling using transformer-based architectures. Model performance is evaluated using standard entity-level precision, recall, and F1 metrics. The findings provide preliminary insights into the potential application of transformer-based models for named entity recognition in Lithuanian clinical documentation and indicate the relevance of language-specific methodological adaptation in low-resource clinical settings.

Keywords: Named Entity Recognition, Electronic Health Records, Natural Language Processing, Rare Diseases, Alport Syndrome, Low-Resource Languages

POSTER SESSION 1

Astrophysics and Theoretical Physics

Spectroscopy and Imaging

Applied Electrodynamics

DETERMINATION OF Cd IONS BY SERS USING NANOPARTICLES

Kamilla Kalmykova[1], Tatjana Charkova[1]

[1]Lithuania, Center for Physical Sciences and Technologies, Department of Organic Chemistry
kamilla.kalmykova@stud.vilniustech.lt

Heavy metal toxicity is a significant health concern arising from the accumulation of elements that the human body cannot effectively excrete. Even prolonged, low-level exposure to Cd can lead to fatigue, cognitive impairment, and damage to the kidneys, liver, and nervous system [1]. In this study, carboxyl-functionalized silver nanoparticles were employed, which exhibited detectable spectral changes in the presence of Cd^{2+} ions, as measured using UV-Vis spectroscopy and surface-enhanced Raman scattering (SERS) techniques.

Silver nanoparticles (Ag NPs) were prepared using the citrate reduction method and subsequently functionalized with 4-mercaptophenylacetic acid (MPAA) [2], providing carboxyl groups for effective Cd^{2+} cations binding. UV-Vis spectroscopy and high-resolution transmission electron microscopy (HR-TEM) verified the formation of spherical nanoparticles and enabled estimation of their average size (50 ± 5 nm) (Fig.1A).

In the presence of metal cations, carboxyl-functionalized silver nanoparticles bind ions and form Ag-MPAA-Me-MPAA-Ag complexes (Fig. 1B). This interaction reduces the interparticle distance, leading to nanoparticle aggregation and a strong enhancement of the MPAA Raman signal (Fig. 1C). As a result, low cation concentrations can be detected using the SERS technique.

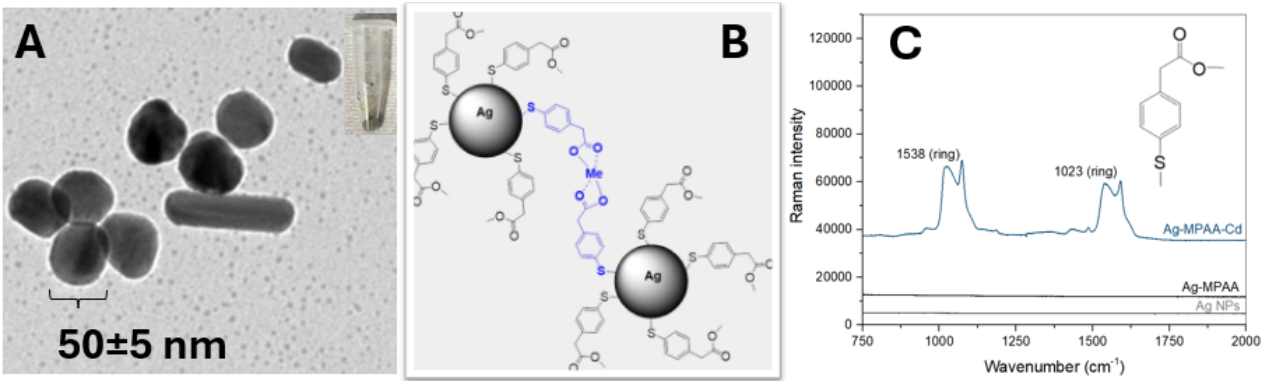


Fig. 1. (A) Photo and HR-TEM data of Ag NPs; (B) Scheme of Ag-MPAA-Me-MPAA-Ag complex; (C) SERS spectra of Ag NPs, Ag-MPAA and the complex with Cd^{2+} ions.

In this study, a detection limit of 10^{-11} M Cd^{2+} was determined by the SERS method, using synthesized and modified silver nanoparticles.

[1] Y. Yang, M. F. Hassan, W. Ali, H. Zou, Z. Liu, and Y. Ma, "Effects of cadmium pollution on Human Health: A Narrative review," Atmosphere, vol. 16, no. 2, p. 225, Feb. 2025, doi: 10.3390/atmos16020225.
[2] T. Charkova, "Determination of barium ions by SERS using silver nanoparticles," Nano-Structures & Nano-Objects, vol. 43, p. 101511, Jun. 2025, doi: 10.1016/j.nanoso.2025.101511.
[3] D. Paramelle, A. Sadovoy, S. Gorelik, P. Free, J. Hobley, and D. G. Fernig, "A rapid method to estimate the concentration of citrate capped silver nanoparticles from UV-visible light spectra," The Analyst, vol. 139, no. 19, p. 4855, Jul. 2014, doi: 10.1039/c4an00978a.

UV-SERS PERFORMANCE OF NANOPARTICLES FORMED BY LASER ABLATION OF THIN Cu, Au, Ag, AND Fe FILMS

Rokas Čepėnas[1], Evaldas Stankevičius[1], Martynas Talaikis[1]

[1]Center for Physical Sciences and Technology, Saulėtekio Ave. 3, 10257, Vilnius, Lithuania
rokas.cepenas@ff.stud.vu.lt

Surface-enhanced Raman spectroscopy (SERS) is an ultrasensitive vibrational spectroscopic technique that enables the detection of trace analyte concentrations while providing detailed molecular structure information. SERS employs nanoparticle-based substrates to enhance the Raman signal originating from molecules located at or near the surface. The enhancement arises from two main mechanisms: the electromagnetic mechanism, associated with localized surface plasmons, and the chemical mechanism, which involves direct interaction or binding of the molecule to the nanoparticle surface. Tuning excitation wavelength to the UV spectral range (e.g., 325 nm), known as UV-SERS, enables selective enhancement of Raman signals from biological molecules such as adenine or aromatic amino acids, even though plasmonic enhancement in the UV range is generally weaker. However, one of the key challenges in UV-SERS remains the production of chemically stable, nanostructured metallic substrates that provide sufficient enhancement in the UV range. For this purpose, nanoparticles can be produced by laser ablation in liquids, which ensures high chemical purity, and allows control over nanoparticle size and composition. In this work, 50 nm- and 100 nm-thick Cu, Au, Ag, and Fe films and their combinations were used to fabricate nanoparticles via laser ablation in acetone. These nanoparticles were then used for UV-SERS applications in biological molecule studies. The ability of these nanoparticles to enhance the Raman signal of adenine is analyzed, and their stability over time is evaluated in order to determine their suitability for long-term and repeatable measurements.

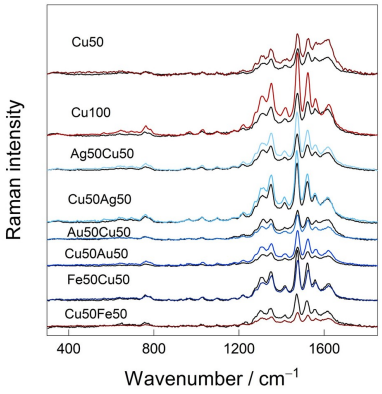


Fig. 1. Time-dependent UV-SERS spectra of adenine (0.1 mM) adsorbed on nanoparticles formed by laser ablation of thin metal layers immediately after preparation (color lines) and after 4 months of keeping nanoparticles in +4 °C. Spectra were collected using 325 nm laser excitation.

The study revealed that the strongest UV-SERS signal of adenine is obtained using copper nanoparticles from 100 nm thick Cu layer (Figure 1). After four months, the UV-SERS signal obtained from $Cu_{50}Ag_{50}$, $Au_{50}Cu_{50}$, and $Fe_{50}Cu_{50}$ nanoparticles remained unchanged or changed only slightly, demonstrating the highest stability among the investigated samples. Pure 50 and 100 nm iron, gold, and silver nanoparticles did not produce a detectable adenine spectrum using the UV-SERS method.

[1] S. Yadav, M. Talaikis, Y. V. Ryabchikov, M. Ziegler, G. Niaura, T. Deckert-Gaudig, and V. Sivakov, “Copper-based multiwavelength UV surface enhanced Raman spectroscopy,” Advanced Optical Materials, vol. 13, no. 25, Art. no. 2500078, 2025, doi: 10.1002/adom.202500078.

DIELECTRIC STUDIES OF PDMS-BASED COMPOSITE MATERIALS WITH Fe AND Fe_3O_4 NANOPARTICLES

Rokas Gedvilas[1], Edita Palaimienė[1], Jan Macutkevič[1], Jūras Banys[1]

[1]Vilnius university, Faculty of Physics, Institute of Applied Electrodynamics and Telecommunications, Lithuania
rokas.gedvilas@ff.stud.vu.lt

Polymer-based composites are being explored for applications involving electromagnetic (EM) wave interaction (shielding and absorption) for their low weight, flexibility, and tunable electrical properties [1]. Controlling dielectric behavior over broad frequency ranges is essential for applications involving radiofrequency and microwave interactions. However, systematic studies of the influence of filler type and concentration on the dielectric response of such composites across broad frequency ranges remain limited.

This work investigates the dielectric properties of polydimethylsiloxane (PDMS) composites filled with iron (Fe) and iron oxide (Fe_3O_4) nanoparticles. The dielectric response was examined as a function of filler type and volume fraction using dielectric spectroscopy over a broad frequency range from 100 Hz to 40 GHz at room temperature. Fe-PDMS composites contained 10-60 vol% iron, while Fe_3O_4-PDMS composites contained 1-38 vol% iron oxide.

The results demonstrate that the fundamental part of the dielectric permittivity of Fe_3O_4-PDMS composites is higher than that of Fe-PDMS composites over the entire investigated concentration range (Fig. 1). Electrical conductivity increases with increasing filler concentration in both systems; however, no sharp percolation-related conductivity jump is observed (Fig. 2). This suggests that continuous conductive networks are not formed at the studied filler concentrations.

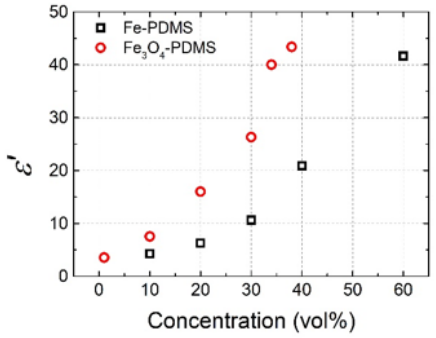


Fig 1. Dependence of the real fraction of Fe-PDMS and Fe_3O_4-PDMS composites on the filler concentration at room temperature at a frequency of 1765 Hz.

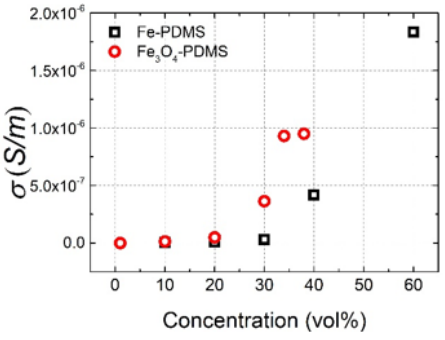


Fig 2. Dependence of the conductivity of Fe-PDMS and Fe_3O_4-PDMS composites on the filler concentration at a room frequency of 1765 Hz.

Fig. 1

Based on the concentration dependences of dielectric permittivity and electrical conductivity, it is concluded that the percolation threshold is not reached in either Fe-PDMS or Fe_3O_4-PDMS composites. To see potential percolation behavior, future studies should investigate lower filler volume fractions.

[1] V. M. G, M. Vatnalmath, and V. Auradi, “A review on conductive polymer composites focusing on advancements in electrical conductivity, and electromagnetic shielding capabilities,” Polymer Composites, vol. 46, no. 18, pp. 16507–16537, Jun. 2025, doi: 10.1002/pc.70059.

VISION-BASED EVALUATION OF POSITIONING REPEATABILITY IN PROBE-BASED MICRO-SCALE SYSTEMS

Ujjawal Malani[1,2], Jurate Jolanta Peateroniene[1], Andrius Dezdicis[1], Vytautas Buchinskas[1]

[1]Vilnius Gediminas Technical University, Mechanics faculty, Department of Mechatronics, Robotics, and Digital Manufacturing, Vilnius, Lithuania
[2]Center for Physical Science and Technology, Department of Functional Materials and Electronics, Vilnius, Lithuania
ujjawal.malani@stud.vilniustech.lt

Electrochemical investigation and surface engineering of living cells using ultramicroelectrodes require highly reliable probe positioning and accurate return-to-origin behavior. In probe-based systems such as Scanning Electrochemical Microscopy (SECM), SECM is a probing system used to measure chemical reactivity on the surface of the subject [1], small trajectory-dependent deviations in the positioning system can affect probe approach safety and measurement repeatability.

This study presents a vision-based approach for characterizing motion deviations in a Cartesian positioning system intended to support electrochemical probe-based experiments[2]. A CMOS camera was used to track the shadow of a platinum ultramicroelectrode at the return-to-origin position following repeated motion cycles. Image sequences were analyzed using a centroid-based intensity method to estimate positional deviations associated with different motion trajectories and feed rates.

The method was applied to representative linear and multi-axis trajectories relevant to probe positioning tasks. Experimental results show that, for most tested conditions, return-to-origin deviations remained below 2 µm, with maximum observed deviations on the order of 4 µm for certain trajectory and feed-rate combinations.

The results indicate that the vision-based deviation characterization enables reliable estimation of micrometer-scale positioning errors and provides a practical diagnostic tool for supporting ultramicroelectrode positioning in electrochemical investigations. This approach contributes to the development of stable motion platforms for living cell surface engineering and related probe-based micro-scale applications.

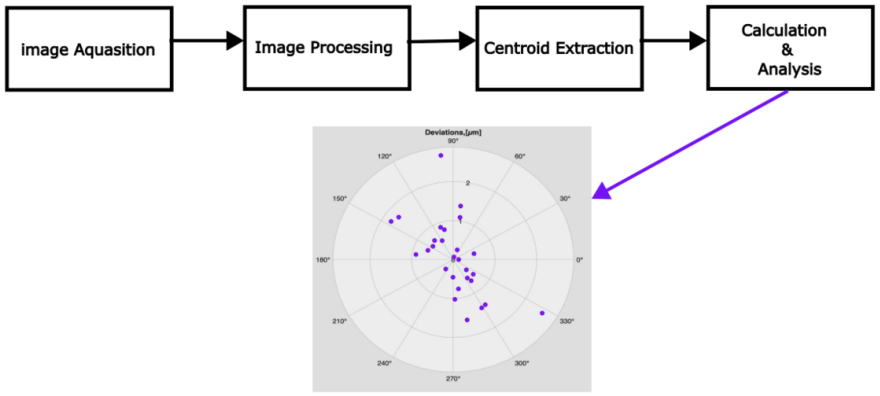


Fig. 1. Workflow diagram: Image acquisition using a CMOS sensor, image processing including grayscale conversion and filtering, centroid extraction based on intensity, calculation of positional deviations, and analysis of results. Most measured deviations were ≤ 2 µm.

[1] I. Morkvenaite-Vilkonciene, A. Valiūnienė, J. Petroniene, and A. Ramanavicius, "Hybrid system based on fast Fourier transform electrochemical impedance spectroscopy combined with scanning electrochemical microscopy," Electrochemistry Communications, vol. 83, pp. 110–112, Sep. 2017, doi: 10.1016/j.elecom.2017.08.020.

[2] V. Ivinskij et al., "Fast detection of micro-objects using scanning electrochemical microscopy based on visual recognition and machine learning," Ultramicroscopy, vol. 259, p. 113937, Feb. 2024, doi: 10.1016/j.ultramic.2024.113937.

TEMPERATURE-DEPENDENT FLUORESCENCE OF NITROGEN-RELATED COLOR CENTERS IN DIAMOND MICRONEEDLES

Paulius Rindzevičius[1,2], Sergei Malykhin[3], Polina Kuzhir[3], Renata Karpicz[1]

[1]Center for Physical Sciences and Technology, Department of Molecular Compound Physics, Lithuania
[2]Vilnius University, Faculty of Physics, Lithuania
[3]University of Eastern Finland, Faculty of Science, Forestry and Technology, Department of Physics and Mathematics, Finland
paulius.rindzevicius@ftmc.lt

Diamond's biological compatibility and easy functionalization make this material promising in quantum biosensing [1]. NV, SiV and GeV color centers can be useful for optical sensing of magnetic fields, electric fields and temperature [2-4]. In this work, the diamond plate and diamond microneedles samples fabricated with chemical vapor deposition (CVD) method were investigated. Steady-state and time-resolved fluorescence spectroscopy experiments using 375 nm excitation were conducted in the temperature range from 298 K to 328 K.

Fluorescence spectra of both diamond samples show phonon sidebands that reveal electron-phonon interactions of 389 nm color center. In case of diamond microneedles, a zero phonon line at 470 nm with a phonon sideband was observed. Color centers with zero phonon lines at 389 nm and 468 nm could be nitrogen-related [5]. Fluorescence kinetics measured at phonon sidebands can be described with biexponential decay. Measured fluorescence intensity decreases with increasing temperature. In case of diamond microneedles this dependence is linear. Fluorescence lifetimes at 410 nm do not show a clear dependence on temperature, while lifetimes at 500 nm show a linear decrease with increasing temperature.

The temperature-dependent luminescence behavior of 389 nm and 468 nm color centers in diamond was investigated and non-Arrhenius type behavior was identified. Linear dependence of fluorescence intensities and lifetimes could be useful in optical thermometry, since the device calibration is easier and complex data processing is not needed in case of a linear response.

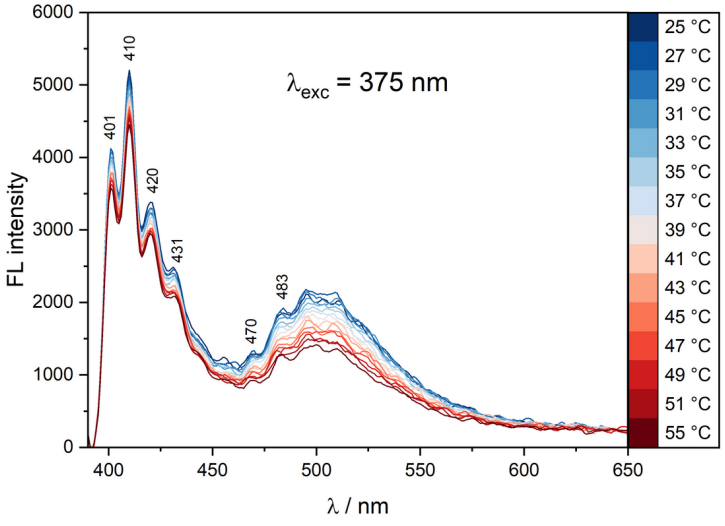


Fig. 1. Fluorescence spectra of diamond microneedles at different temperatures

Keywords: Fluorescence, temperature sensors, diamond microneedles, diamond color centers

[1] J. Zhang et al., "Nanodiamond-based sensing: A revolution for biosensors in capturing elusive bio-signals in living cells," Adv. Drug Deliv. Rev., vol. 221, 16 p., 2025.
[2] C. T. Nguyen et al., "All-optical nanoscale thermometry with silicon-vacancy centers in diamond," Appl. Phys. Lett., vol. 112, 2018.
[3] J.-W. Fan et al., "Germanium-vacancy color center in diamond as a temperature sensor," ACS Photonics, vol. 5, pp. 765–770, 2018.
[4] L. M. Pham et al., "Magnetic field imaging with nitrogen-vacancy ensembles," New J. Phys., vol. 13, 13 p., 2011.
[5] E. Filonenko et al., "Fluorescence dynamics of color centers in diamond needles," Nanotechnology, vol. 36, 8 p., 2025.

INFLUENCE OF MEDIUM pH ON THE PHOTOSTABILITY OF HEMATOPORPHYRIN AT DIFFERENT L-ASCORBATE CONCENTRATIONS

Marija Kalnaitytė[1], Saulius Bagdonas[1]

[1]Vilnius University, Faculty of Physics, Laser Research Center, Vilnius, Lithuania
marija.kalnaityte@ff.stud.vu.lt

Hematoporphyrin (HP) and its derivatives are tetrapyrrolic compounds that were among the first to be used as photosensitizers in photobiological research, diagnostics, and therapy [1].Upon absorbing photons of an appropriate wavelength, these photosensitizers transition to an excited state and can participate in both Type I and Type II photoreactions, as well as form chlorine-type photoproducts [2]. The properties of photosensitizers are influenced by environmental and structural changes, such as shifts in their aggregate state, which determine modifications of the photosensitizer's physicochemical properties in an aqueous medium [2]. However, there is still a lack of research evaluating the influence of electron donors present in the action environment, such as the contribution of L-ascorbate to HP photochemical processes, when the photosensitizer is studied in solutions of different pH.

In this work, we investigated the changes in optical density (OD) and fluorescence (FL) of hematoporphyrin monomethyl ether (HMME) ($5*10^{-5}$ M) in 50 mM KH_2PO_4-NaOH phosphate-buffered saline (PBS) at closely related pH levels (6.94 and 6.62), as well as its photostability. Additionally, spectral changes were compared upon the introduction of different concentrations (10^{-4} M and 10^{-3} M) of L-ascorbic acid into the system, evaluating both stability and photostability variations. Spectroscopic measurements of 1 ml samples were performed in 4x10 mm plastic semi-micro cuvettes. Between measurements, samples were stored in 1.5 ml microcentrifuge tubes in a refrigerator at +4 °C in the dark. During photostability experiments, a sample area of approximately 1 cm^2 in the cuvettes was irradiated with a green laser (532 nm, 28 mW). The total dose (100.8 J/cm^2) was measured at intervals of 8.4 J/cm^2 (from 0 J/cm^2 to 67.2 J/cm^2) and 16.8 J/cm^2 (up to 100.8 J/cm^2). Before each irradiation, the samples were homogenized by stirring, after which spectroscopic measurements were performed.

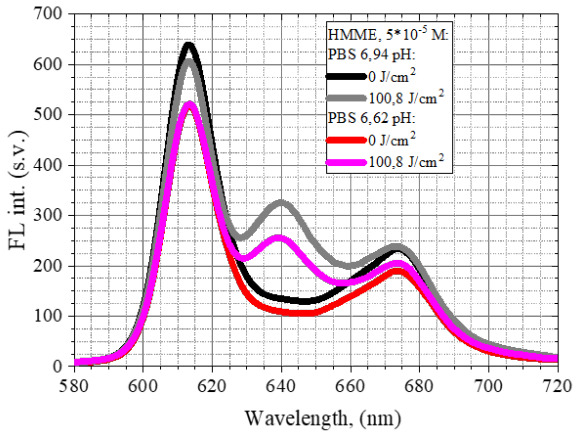


Fig. 1. Figure 1. Representative FL spectra of HMME, C = 0.5 μM in PBS, before and after irradiation with a dose of 100.8 J/cm^2 (λ_{ex} = 480 nm, excitation and emission slits 5 and 5).

The FL spectra recorded at different excitation wavelengths revealed that, regardless of the medium pH (6.94 and 6.62), the sample exhibits multiple fluorescent species. Formation of the peak at 640 nm characteristic of photoproducts depended on the solution pH. Subsequent measurements showed that L-ascorbate actively interferes with the photooxidation reaction pathways.

Keywords: Hematoporphyrin monomethyl ether (HMME), L-ascorbate, Aggregation, Fluorescence spectroscopy, Photostability, pH dependence.

[1] T. J. Dougherty et al., "Photodynamic therapy," J. Natl. Cancer Inst., vol. 90, no. 12, pp. 889–905, Jun. 1998
[2] R. Rotomskis, S. Bagdonas, and G. Streckyte, "Spectroscopic studies of photobleaching and photoproduct formation of porphyrins used in tumour therapy," J. Photochem. Photobiol. B, Biol., vol. 33, no. 1, pp. 61–67, Apr. 1996

$ZnGa_2O_4$ SPINEL NANOPHOSPHORS WITH PERSISTENT LUMINESCENCE FOR BIOIMAGING

Vilius Čirgelis[1,2], Simona Streckaitė[1], Vitalii Boiko[3], Lena Golubewa[1], Vidas Pakštas[1], Mariusz Stefanski[3], Dariusz Hreniak[3], Vidmantas Gulbinas[1]

[1]Center for Physical Sciences and Technology, Sauletekio Ave. 3, 10257 Vilnius, Lithuania
[2]Vilnius University, Faculty of Physics, Sauletekio Ave. 9, 10222 Vilnius, Lithuania
[3]Polish Academy of Sciences, Institute of Low Temperature and Structure Research, Okolna 2, 5-422 Wroclaw, Poland
vilius.cirgelis@ftmc.lt

Zinc gallium oxide ($ZnGa_2O_4$, ZGO) is a cubic spinel-structured oxide that has attracted interest for applications in optoelectronics [1], plasmonics [2] and biomedicine [3]. ZGO is chemically stable, inert to oxygen and humidity, and biocompatible, making it promising phosphor for applications, like bio-imaging and theranostic [4]. In ZGO lattice, Zn2+ occupies tetrahedral sites and Ga3+ occupies octahedral sites. Since chemical synthesis is entropy driven process, partial cation inversion can occur, where a fraction of Zn2+ occupies octahedral and a fraction of Ga3+ occupies tetrahedral positions, forming antisite defects. Antisites introduce trap states that capture charge carriers and hinder their recombination, enabling long-lived energy storage of excitation energy on timescales from hours to days [5]. The delayed photon emission, occurring from exciton recombination is called persistent luminescence (PersL). PersL is advantageous for in vivo bioimaging because the material can be pre-charged ex vivo and subsequently injected into organism, allowing imaging without continious excitation, thereby reducing tissue autofluorescence and minimizing phototoxicity and thermal damage [6]. ZGO optical properties can be altered by introduction of rare-earth ions into the lattice. Emission from Cr^{3+} and Yb^{3+} overlaps with the first and second biological windows—spectral ranges where tissue absorption and scattering are relatively low—enabling efficient deep-tissue imaging.

In this study, Cr^{3+} doped $ZnGa_2O_4$ was synthesized hydrothermally from aqueous solutions of $Zn(NO_3)_2$, $Ga(NO_3)_3$, and $Cr(NO_3)_3$. Stoichiometric amounts of the metal-nitrate precursors were combined and the pH was adjusted to 8 using NH_4OH. The mixture was transferred to a Teflon-lined vessel and sealed in a stainless-steel autoclave for hydrothermal treatment at 200 °C for 24 h. The resulting powder was washed with water and ethanol, dried for 24 h, and annealed at temperatures between 200 °C and 900 °C for 3 hours. The structural and optical properties of ZGO:Cr^{3+} were characterized by X-ray diffraction (XRD), steady-state and time-resolved photoluminescence (PL), thermoluminescence, and diffuse reflectance spectroscopy.

XRD measurements confirm that the synthesized $ZnGa_2O_4$ materials crystallize in the cubic spinel structure. With increasing annealing temperature, the diffraction peaks become narrower, indicating improved crystallinity and crystallite growth (i.e., reduced microstrain/defect-related broadening) over the range from 0 to 800 °C. At 800 °C, the XRD pattern matches that of the pre-annealed sample, indicating phase transition. The highest steady-state PL intensity is observed for ZGO:Cr^{3+} with 1.00 mol% Cr^{3+}, whereas the longest persistent-luminescence decay is obtained for the 0.25 mol% Cr^{3+}-doped sample. As ongoing work, ZGO:Yb^{3+} samples will be characterized using the same set of techniques.

Acknowledgements
This research was funded by Polish-Lithuanian research project DAINA-3, agreement No [S-LL-24-11].

Keywords: Spinels, persistent luminescence

[1] Y.-C. Shen, C.-Y. Tung, C.-Y. Huang, Y.-C. Lin, Y.-G. Lin, and R.-H. Horng, "Study on Optoelectronic Characteristics of ZNGA2O4 Thin-Film Phototransistors," ACS Applied Electronic Materials, vol. 1, no. 5, pp. 783–788, May 2019, doi: 10.1021/acsaelm.9b00128.
[2] M. Runowski et al., "Preparation of biocompatible, Luminescent-Plasmonic Core/Shell nanomaterials based on lanthanide and gold nanoparticles exhibiting SERS effects," The Journal of Physical Chemistry C, vol. 120, no. 41, pp. 23788–23798, Sep. 2016, doi: 10.1021/acs.jpcc.6b06644.
[3] Z. Li et al., "In vivo repeatedly charging Near-Infrared-Emitting mesoporous SIO2/ZNGA2O4:CR3+ persistent luminescence nanocomposites," Advanced Science, vol. 2, no. 3, Feb. 2015, doi: 10.1002/advs.201500001.
[4] D. Ding et al., "Mn3+-rich oxide/persistent luminescence nanoparticles achieve light-free generation of singlet oxygen and hydroxyl radicals for responsive imaging and tumor treatment," Theranostics, vol. 11, no. 15, pp. 7439–7449, Jan. 2021, doi: 10.7150/thno.62437.
[5] T. Zhao, R. Abdurahman, R. Aiwaili, S. Wu, and X.-B. Yin, "Spinel-type persistent luminescence nanoparticles: From mechanisms, compositions to applications," Coordination Chemistry Reviews, vol. 488, p. 215171, Apr. 2023, doi: 10.1016/j.ccr.2023.215171.
[6] S. Wu, Y. Li, W. Ding, L. Xu, Y. Ma, and L. Zhang, "Recent advances of persistent luminescence nanoparticles in bioapplications," Nano-Micro Letters, vol. 12, no. 1, p. 70, Mar. 2020, doi: 10.1007/s40820-020-0404-8.

DEVELOPMENT OF A GAS COMBUSTION SYSTEM FOR RADIOCARBON ANALYSIS OF HYDROCARBON GASES

Ąžuolas Ivickas[1], Žilvinas Ežerinskis[1], Laurynas Bučinskas[1], Laima Kazakevičiūtė-Jakučiūnien[1], Justina Šapolaitė[1]

[1]Lithuania, Center for Physical Sciences and Technology, Department of Nuclear Research, Accelerator Mass Spectrometry Laboratory
azuolas.ivickas@ftmc.lt

Radiocarbon (^{14}C) analysis is a powerful tool for distinguishing between biogenic and anthropogenic carbon sources, enabling the ability to track carbon dynamics in various systems and plays a critical role in carbon accounting, renewable energy certification, and greenhouse gas mitigation strategy development. Radiocarbon measurements of hydrocarbon gases such as methane are particularly valuable in differentiating between the contemporary and fossil fractions of gaseous carbon emissions. However, accurate ^{14}C determination in gaseous samples remains challenging as they require quantitative oxidation to CO_2 prior to accelerator mass spectrometry (AMS) or graphitization, as well as small sample sizes and the risk of isotopic fractionation during combustion [1].

Existing methods typically rely on catalyst-based oxidation systems that are time-consuming, prone to contamination, and require extensive laboratory infrastructure [1]. Therefore, the aim of this study was to develop and evaluate a novel gas combustion system (GCS) for the efficient and reliable conversion of hydrocarbon gases to CO_2 for AMS analysis. An alternative, catalyst-free GCS was designed and implemented utilizing controlled electric discharge ignition to oxidize sample gases mixed with oxygen, enabling more rapid sample preparation. The resulting CO_2 was compatible with automated graphitization equipment (AGE-3, Ionplus AG). The system was optimized to ensure complete combustion, high carbon recovery, minimal cross-contamination, and preservation of isotopic integrity.

Performance evaluation demonstrated quantitative combustion of methane at CH_4:O_2 ratios ≥ 1:2, yielding CO_2 recoveries of 78–88 % with negligible $\delta^{13}C$ fractionation. Cross-contamination between fossil and biogenic samples remained below 0.1 %, and analytical precision of radiocarbon measurements was sufficient to resolve mixed carbon sources. Environmental methane samples exhibited fully biogenic radiocarbon signatures, confirming system applicability under real-world conditions.

These results demonstrate that the developed GCS provides a rapid, robust, and reproducible alternative to conventional catalyst-based combustion systems. The GCS significantly enhances analytical capability for routine ^{14}C analysis of gaseous samples and supports improved source attribution of hydrocarbon gases in environmental, regulatory, and energy-related applications.

[1] C. Espic, M. Liechti, M. Battaglia, D. Paul, T. Röckmann, and S. Szidat, “Compound-Specific Radiocarbon Analysis of Atmospheric Methane: A New Preconcentration and Purification Setup,” Radiocarbon, vol. 61, no. 5, pp. 1461–1476, Jul. 2019, doi: https://doi.org/10.1017/rdc.2019.76.

PHOTO-DEFLECTION ELECTRON PARAMAGNETIC RESONANCE SPECTROSCOPY

Laisvydas Giriūnas[1], Gediminas Usevičius[1], Vidmantas Kalendra[1], Mantas Šimėnas[1], Jūras Banys[1]

[1]Lithuania, Vilnius, Vilnius University, Faculty of Physics, Institute of Applied Electrodynamics and Telecommunications
laisvydas.giriunas@ff.vu.lt

This study introduces photo-deflection electron paramagnetic resonance (EPR) spectroscopy as a new method for registering spectra of paramagnetic samples. The sample is placed in a resonance cavity and excited using microwave radiation, which is tuned via an external magnetic field to achieve resonance conditions. This process generates localized heating, creating a thermal gradient above the surface of the sample. A collimated laser beam directed through this gradient allows us to measure the deflection of the laser beam with a high-sensitivity photodetector. The resulting absorbance spectrum mirrors traditional EPR signals, with potentially enhanced sensitivity and providing new insights into thermal dynamics in materials with unpaired electrons. The implications of this technique are significant for various applications, particularly in materials science and biomedical fields, where understanding thermal behaviors at the microscopic level is crucial.

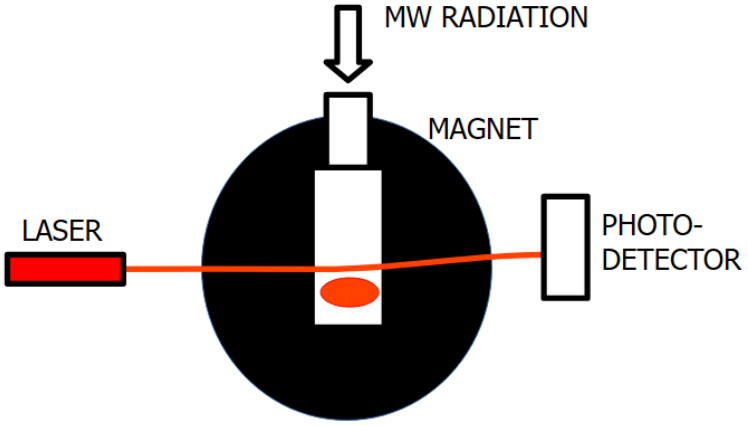


Fig. 1. Schematic cross-section of the photo-deflection EPR experimental setup

Acknowledgements
This work was funded by the European Union (ERC, Strong-ESPRESSO, 101162021)

CHOLINE GLYCINATE DOSY INVESTIGATION

Lukas Mikalauskas[1], Vytautas Klimavičius[1]

[1]Vilnius University, Faculty of Physics, Institute of Chemical Physics, Lithuania
lukas.mikalauskas@ff.stud.vu.lt

Bioactive room temperature ionic liquids (b-RTILs) are room temperature-molten salts compatible with living organisms. RTILs are becoming more popular in the scientific community due to the high number of ion combinations and tunability. Choline glycinate is one of the b-RTIL. It has potential in medicine, biofilm growth inhibition and in CO_2 absorption and separation. One of the most important parameters of ILs is the diffusion coefficient. It can give us information about the size or structure of molecules and how interaction between molecules change in different concentrations.

The main objective is to investigate the diffusion of choline glycinate ([Cho][Gly]) in a water mixture using DOSY and compare with other ionic liquids: choline lysinate ([Cho][Lys]) and choline tryptophanate ([Cho][Trp]). DOSY (Diffusion-Ordered Spectroscopy) is a powerful NMR (Nuclear Magnetic Resonance) tool for measuring the diffusion coefficient of a specific proton. The magnetic field gradient sequence is applied to the sample. With a different magnetic field, we get a different precession frequency. Due to the constant movement of molecules, the intensity of the spectra is lower than with a homogenous magnetic field across the sample. In the experiment, the intensity is measured using different gradient strengths. Using the Stejskal-Tanner equation, the diffusion coefficient can be calculated. The change in the intensity also depends on the size of the molecule and viscosity.

Using the DOSY method, it was found that the diffusion coefficient of a water molecule is the largest. The same can be said with water in [Cho][Lys] and [Cho][Trp] water mixtures. Also, there are two diffusion regimes in [Cho][Gly]: H_2O in choline glycinate and choline glycinate in H_2O. The breaking point is observed at χ_{RTIL}=0.16 mol.frac. concentration. Almost the same concentration as ^{1}H chemical shift minima of chemical groups around choline's nitrogen nucleus and ^{1}H chemical shift maxima of water. The breaking point can also be seen in [Cho][Lys] and water mixture, but at a lower concentration at around χ_{RTIL}=0.11 mol.frac. The occurrence of two separate regimes is due to strong hydrogen and Coulombic bonds between choline and glycine anion, and water's ability to break those bonds and form hydrogen bonds with those ions. At high water concentration, the cation's and anion's diffusion coefficients converge to one value. It can be due to anion self-aggregation.

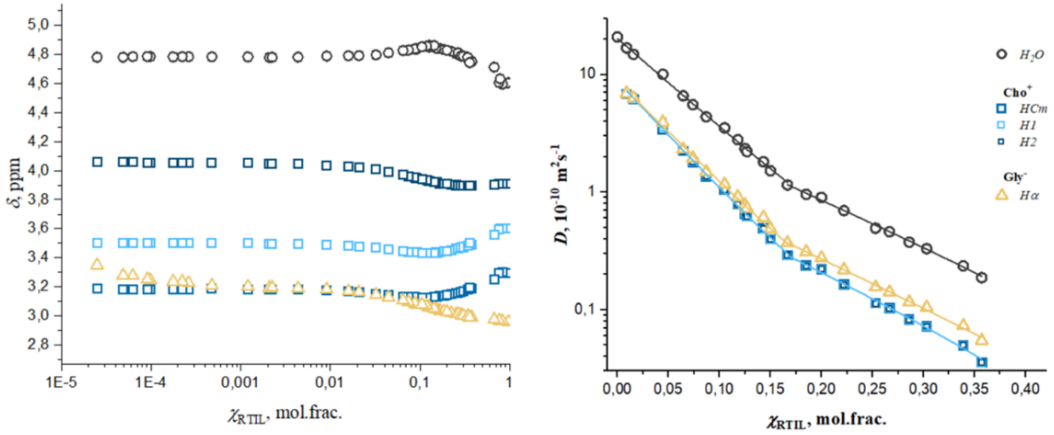


Fig. 1. ^{1}H chemical shift dependency from [Cho][Gly] concentration (left) and ^{1}H diffusion coefficient dependency from [Cho][Gly] concentration (right).

[1] M. H. Levitt, Spin Dynamics: Basics of Nuclear Magnetic Resonance. John Wiley & Sons, 2013.
[2] G. Latini et al., "Efficient and reversible CO2 capture in bio-based ionic liquids solutions," Journal of CO2 Utilization, vol. 55, p. 101815, Nov. 2021, doi: 10.1016/j.jcou.2021.101815.
[3] A. R. Pereira, I. B. Gomes, and M. Simões, "Choline-based ionic liquids for planktonic and biofilm growth control of Bacillus cereus and Pseudomonas fluorescens," Journal of Molecular Liquids, vol. 346, p. 117077, Jul. 2021, doi: 10.1016/j.molliq.2021.117077.
[4] F. Khorrami and M. H. Kowsari, "Tracing Local Nanostructure of the Aqueous Solutions of the Biocompatible [Cho][Gly] Ionic Liquid: Importance of Hydrogen Bond Attraction between Like-Charged Ions," The Journal of Physical Chemistry B, vol. 124, no. 18, pp. 3770–3783, Apr. 2020, doi: 10.1021/acs.jpcb.0c01796
[5] J. Chen, X. Zeng, and L. Chen, "Regulation nature of water-choline amino acid ionic liquid mixtures on the disaggregation behavior of starch," Carbohydrate Polymers, vol. 272, p. 118474, Jul. 2021, doi: 10.1016/j.carbpol.2021.118474.

MILLISECOND-SCALE SPIN COHERENCE OF ^{171}Yb QUBITS IN $CaWO_4$ AT A ZERO-FIELD CLOCK TRANSITION

Justinas Turčak[1], Vidmantas Kalendra[1], Jūras Banys[1], Philippe Goldner[2], John J. L. Morton[3], Mantas Šimėnas[1]

[1]Vilnius University, Faculty of Physics, Sauletekio 9, LT-10222 Vilnius, Lithuania
[2]PSL University, CNRS, Chimie ParisTech, Institut de Recherche de Chimie Paris, 75005 Paris, France
[3]UCL, London Centre for Nanotechnology, London, WC1H 0AH, United Kingdom
justinas.turcak@ff.vu.lt

Solid-state spin systems are attractive qubit candidates due to their scalable integration with existing microwave technologies and their long spin coherence times [1], defined as the duration over which a quantum superposition is preserved. In this context, rare-earth ions are particularly promising because their shielded 4f electrons lead to narrow transition linewidths and reduced coupling to the host lattice, enabling enhanced coherence in magnetically weak crystalline environments, which is necessary for quantum networks [2]. Further suppression of decoherence can be achieved by operating at clock transitions, where the spin transition frequency is first-order insensitive to magnetic field fluctuations, as demonstrated in both silicon-based [3] and rare-earth spin systems [4].

Ytterbium doped into $CaWO_4$ is a particularly attractive platform owing to the low magnetic noise environment of the host crystal with previous demonstrations of sub-second coherence using optical transitions [5]. In this study, we investigate the spin coherence enhancement at the 3.1 GHz clock transition for $^{171}Yb^{3+}$:$CaWO_4$ by direct measurements using pulsed electron spin resonance (ESR) spectroscopy. Spin coherence is probed using two ESR spectrometers: a Bruker ELEXSYS E580 operating at X-band frequencies (9-10 GHz) and a home-built low-frequency spectrometer covering the 1-6 GHz range. Low sensitivity parallel-mode ESR measurements are enabled by custom tunable loop-gap resonators equipped with a developed S-band cryoprobe. Temperature-dependent measurements reveal that below 4 K the coherence time is not limited by spin-lattice relaxation. At the clock transition, spin coherence times exceed 1 ms with decoherence dominated by direct spin flip-flop processes (Fig. 1).

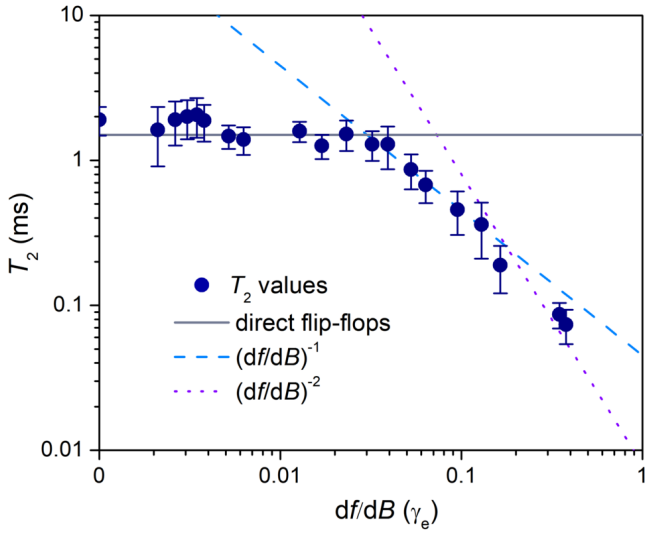


Fig. 1. Coherence time enhancement when approaching the zero-field clock transition.

Acknowledgements
This research was supported by Research Council of Lithuania (P-ITP-25-4).

Keywords: Spin qubit, rare-earth ion, clock transition, coherence time, electron spin resonance

[1] F. A. Zwanenburg et al., "Silicon quantum electronics," Reviews of Modern Physics, vol. 85, no. 3, pp. 961–1019, Jul. 2013, doi: 10.1103/revmodphys.85.961.
[2] W. Tittel et al., "Quantum networks using rare earth ions," Quantum Science and Technology, vol. 10, no. 3, 2025.
[3] G. Wolfowicz et al., "Atomic clock transitions in silicon-based spin qubits," Nature Nanotechnology, vol. 8, no. 8, pp. 561–564, Jun. 2013, doi: 10.1038/nnano.2013.117.
[4] D. L. McAuslan, J. G. Bartholomew, M. J. Sellars, and J. J. Longdell, "Reducing decoherence in optical and spin transitions in rare-earth-metal-ion–doped materials," Physical Review A, vol. 85, no. 3, Mar. 2012, doi: 10.1103/physreva.85.032339.
[5] A. Tiranov, E. Green, S. Hermans, E. Liu, F. Chiossi, D. Serrano, P. Loiseau, A. M. Kumar, S. Bertaina, A. Faraon, and P. Goldner, "Sub-second spin and lifetime-limited optical coherences in 171Yb3+:CaWO4," arXiv preprint arXiv:2504.01592, 2025.

IMPACT OF AMINOACID SURFACTANTS ON THE MAGNETIC BEHAVIOR OF HYDROTHERMALLY SYNTHESIZED CoFe2O4 NANOPARTICLES

Aswathi Raveendran[1], Germante Paulikaite[1], Vidas Pakstas[2], Audrius Drabavicius[2], Martynas Talaikis[3], Aldona Balciunaite[4], Kestutis Mazeika[5], Vaclovas Klimas[1], Jurate Vaiciuniene[4], Agne Mikalauskaite[1], Simonas Ramanavicius[1]

[1]Center for Physical Sciences and Technology, Department of Electrochemical Materials Research
[2]Center for Physical Sciences and Technology, Department of Structural Analysis of Materials
[3]Center for Physical Sciences and Technology, Department of Organic Chemistry
[4]Center for Physical Sciences and Technology, Catalysis department
[5]Center for Physical Sciences and Technology, Nuclear Research Department
aswathi.raveendran@ftmc.lt

Magnetic nanoparticles have been widely investigated for applications in data storage, magneto-optical devices, photocatalysis, and biomedicine due to their size-dependent properties[1][2],[3],[4]. Among ferrite materials, cobalt ferrite ($CoFe_2O_4$) is of particular interest because of its excellent magnetic stability and anisotropy. The structural and magnetic properties of $CoFe_2O_4$ nanoparticles are strongly influenced by particle size, morphology, and surface characteristics, which are governed by the synthesis method. Conventional preparation techniques such as hydrothermal, sol–gel, and co-precipitation methods allow control over nucleation and growth through parameters including temperature, pH, and stirring rate [5], [6], [7]. However, magnetic nanoparticles tend to agglomerate due to high surface energy and magnetic interactions. The use of surfactants effectively reduces aggregation by providing electrostatic repulsion and steric hindrance, while also enabling better control over particle growth and surface properties [4]. In this study, $CoFe_2O_4$ nanoparticles were synthesized via a hydrothermal co-precipitation method with and without amino acids acting as capping agents [2], [8]. The influence of amino acids on the structural and magnetic properties was investigated to improve nanoparticle stability and performance, highlighting their potential use as magnetically recoverable adsorbents and catalysts for wastewater treatment The charecterisation of the sythesised magnetic particles were done usng XRD and TEM.The magnetic measurements were made using VSM. We have mesured the surface area of the particles using BET analysis and the adsorption capabilities are checked by UV spectral analysis on two different organic dyes. We could conclude from our studies that the difference in amino acid surfactats significally influence the particle size, magnetic properties and surface area of the cobalt ferrite nanoparticles. This results are promising in modifying and synthesising nanoparticles of desired magnetism and surface properties.

Acknowledgements
This project received funding from the Research Council of Lithuania (LMTLT), agreement No S-MIP-24-14.

Keywords: Magnetic ferrites, Cobalt ferrites, Adsorption, Magnetism

[1] S. M. Ansari et al., “Controlled surface/interface structure and spin enabled superior properties and biocompatibility of cobalt ferrite nanoparticles,” Appl. Surf. Sci., vol. 459, pp. 788–801, Nov. 2018, doi: 10.1016/j.apsusc.2018.08.063.
[2] R. Žalnėravičius, A. Mikalauskaitė, G. Niaura, A. Paškevičius, and A. Jagminas, “Ultra-small methionine-capped Au0/Au+ nanoparticles as efficient drug against the antibiotic-resistant bacteria,” Materials Science and Engineering: C, vol. 102, pp. 646–652, Sep. 2019, doi: 10.1016/j.msec.2019.04.062.
[3] A. Raveendran, E. Semasko, A. Jagminas, A. Sukoviene, and S. Ramanavicius, “Current trends in cobalt and zinc ferrite based magnetic photocatalysts for wastewater treatment,” Inorg. Chem. Commun., vol. 183, p. 115876, Jan. 2026, doi: 10.1016/j.inoche.2025.115876.
[4] M. Kurtinaitiene, K. Mazeika, S. Ramanavicius, V. Pakstas, and A. Jagminas, “Effect of additives on the hydrothermal synthesis of manganese ferrite nanoparticles,” Adv. Nano Res., vol. 4, no. 1, pp. 1–14, Mar. 2016, doi: 10.12989/anr.2016.4.1.001.
[5] A. Sukoviene, S. Ali, A. Jagminas, and S. Ramanavicius, “Magnetic Cobalt and Other Types of Ferrite Nanoparticles: Synthesis Aspects and Novel Strategies for Application in Wastewater Treatment (Review),” Applied Sciences, vol. 15, no. 2, p. 857, Jan. 2025, doi: 10.3390/app15020857.
[6] M. Pleckaitis et al., “Magnetic Nanoparticles Decorated with Gold Nanoclusters–Applications in Cancer Theranostics,” Adv. Mater. Interfaces, vol. 10, no. 35, Dec. 2023, doi: 10.1002/admi.202300462.
[7] Shyamaldas, M. Bououdina, and C. Manoharan, “Dependence of structure/morphology on electrical/magnetic properties of hydrothermally synthesised cobalt ferrite nanoparticles,” J. Magn. Magn. Mater., vol. 493, p. 165703, Jan. 2020, doi: 10.1016/j.jmmm.2019.165703.
[8] K. Sangsuriyonk, N. Paradee, K. Rotjanasuworapong, and A. Sirivat, “Synthesis and characterization of CoxFe1−xFe2O4 nanoparticles by anionic, cationic, and non-ionic surfactant templates via co-precipitation,” Sci. Rep., vol. 12, no. 1, p. 4611, Mar. 2022, doi: 10.1038/s41598-022-08709-9.

NMR INVESTIGATION OF ZIRCONIUM PHOSPHATES

Rokas Lemežis[1], Vytautas Klimavičius[1]

[1]Vilnius University, Faculty of Physics, Institute of Chemical Physics, Saulėtekio ave. 3, LT-10257 Vilnius, Lithuania
rokas.lemezis@ff.stud.vu.lt

Zirconium phosphates (ZrP) are a family of materials used in variety of applications including batteries, supercapacitors, catalysis and medicine as drug carriers [1, 2]. They are 2D materials, which, due to their polymorphic structure, are classified as α-, γ- and λ- ZrP. These compounds are suitable for intercalation with various ions (Na^+, K^+, NH_4^+, Cl^- and others), enabling tailoring for a wide range of applications [3].

In this study solid-state Nuclear Magnetic Resonance (ssNMR) was used to characterize α- and γ- ZrP polymorphs doped with NH_4^+, K^+ and Na^+ ions. ^{31}P and ^{23}Na MAS NMR methods were used to determine the composition of the samples. Alongside 2D NMR techniques, such as ^{31}P-^{31}P 1Q-2Q and ^{23}Na MQMAS NMR, it was possible to assign ^{31}P MAS NMR spectral lines to different crystal motifs of ZrP polymorphs and determine number of distinct ^{23}Na environments present in the samples.

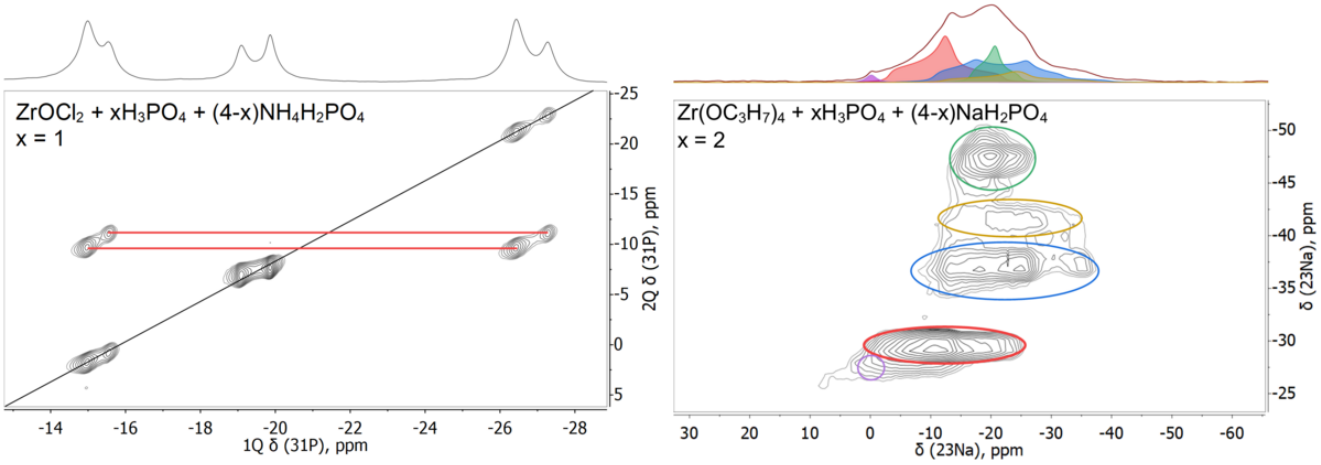


Fig. 1. ^{31}P-^{31}P 1Q-2Q (left) and ^{23}Na MQMAS (right) NMR spectra of α- and γ- ZrP polymorphs. Horizontal projections of 2D spectra correspond to 1D ^{31}P and ^{23}Na MAS NMR spectra.

It was found that α- and γ- polymorphs intercalated with NH_4^+, K^+ and Na^+ were formed during synthesis procedure. Additional ion exchange with hydrochloric acid (HCl) was performed to remove intercalated ions and confirm previous results. The ^{31}P-^{31}P 1Q-2Q NMR data enabled the identification of two structural phases of NH_4ZrP polymorphs and explanation of crystal structure of α-KZrP. Furthermore, intercalation with Na^+ ions yielded products with four distinct ^{23}Na chemical environments of NaZrP.

[1] M. Casciola, "From layered zirconium phosphates and phosphonates to nanofillers for ionomeric membranes," Solid State Ionics, vol. 336, pp. 1–10, Mar. 2019, doi: 10.1016/j.ssi.2019.03.005.
[2] M. V. Ramos-Garcés, J. González-Villegas, A. López-Cubero, and J. L. Colón, "New applications of zirconium phosphate nanomaterials," Accounts of Materials Research, vol. 2, no. 9, pp. 793–803, Sep. 2021, doi: 10.1021/accountsmr.1c00102.
[3] C. Bisio et al., "Recent advances and perspectives on intercalation layered compounds part 1: design and applications in the field of energy," Dalton Transactions, vol. 53, no. 35, pp. 14525–14550, Jan. 2024, doi: 10.1039/d4dt00755g.

DEVELOPMENT AND EVALUATION OF A HYBRID THZ IMAGING SYSTEM BASED ON 3D-PRINTED DIFFRACTIVE OPTICS

Kasparas Stanaitis[1,2], Vladislovas Čižas[1], Rusnė Ivaškevičiūtė-Povilauskienė[1], Sergėjus Orlovas[1], Ignas Grigelionis[1], Linas Minkevičius[1,2]

[1]Center for Physical Sciences and Technology, Department of Optoelectronics, Vilnius, Lithuania
[2]Vilnius University, Institute of Photonics and Nanotechnology, Vilnius, Lithuania
kasparas.stanaitis@ftmc.lt

Optical imaging systems are widely used in many scientific and practical applications, such as material inspection, security, and quality control. Many commonly used imaging methods rely on high energy radiation, for example X rays, which have several disadvantages related to safety, cost, and possible damage to the sample. Terahertz (THz) imaging is considered a safer alternative because it uses non ionizing radiation while still being able to penetrate many dielectric materials.

This work focuses on 3D printed thin diffractive optical elements that are used to generate different types of THz beams, such as Gaussian, Bessel, and Airy beams. These elements are integrated into a hybrid THz imaging system that allows both amplitude and interferometric measurements. The diffractive components are produced using extrusion 3D printing and are used for shaping the beam, focusing the radiation, and collecting the signal from the sample.

Imaging is carried out using various combinations of beam forming elements placed in different positions within the optical setup. The performance of the system is evaluated by comparing the quality of the obtained images for both amplitude based and interferometric imaging modes. The influence of different component combinations on image contrast, resolution, and sensitivity to alignment is analyzed in order to determine the most suitable configuration for hybrid THz imaging.

The results are expected to show how structured THz beams generated by diffractive components can improve imaging flexibility and provide additional information compared to conventional amplitude only systems.

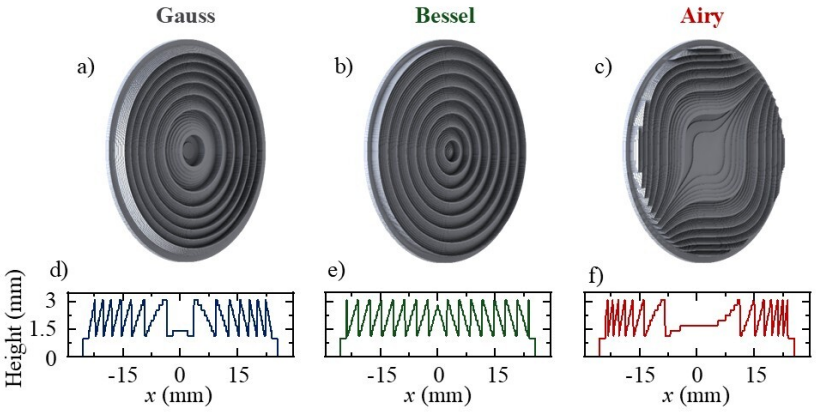


Fig. 1. (a) - (c) Physical models of THz optical components used for imaging evaluation, (d) - (f) corresponding height profiles along the *x*-axis.

[1] Valušis, G., Lisauskas, A., Yuan, H., Knap, W., & Roskos, H. G., Roadmap of terahertz imaging 2021 (Sensors, 21(12), 4092, 2021)

THZ IMAGING SYSTEM BASED ON CW CLINOTRONS

Anna Kuleshova[1], Sergiy Vlasenko[2,3], Yuriy Kovshov[2], Sergiy Kishko[2], Eduard Khutoryan[2], Oleksiy Kuleshov[2]

[1]Kharkiv National Medical University, II Medical Faculty, Ukraine
[2]O. Ya. Usikov Institute for Radiophysics and Electronics of NAS of Ukraine, Ukraine
[3]V. N. Karazin Kharkiv National University, School of Chemistry, Ukraine
jeanalexkh@gmail.com

Terahertz (THz) radiation possesses several unique features, including the ability to penetrate a wide range of materials while being strongly absorbed by water molecules, as well as a non-ionizing effect on inspected objects due to the very low photon energy compared to X-rays. These properties make THz sources highly promising for applications in physics, biology, medicine, plasma diagnostics, radar and remote sensing, high-data-rate communications, security systems etc. THz radiation provides novel information about substances that cannot be obtained using conventional microwave or X-ray techniques. In particular, rotational transitions of many biological molecules lie in the frequency range of 0.1–1 THz, making THz radiation attractive for medical and biological applications, where X-ray, ultrasound, optical, and magnetic resonance methods are currently employed. Owing to wavelengths shorter than 1 mm, THz imaging offers high spatial resolution and has demonstrated potential for differentiating non-melanoma skin cancers from normal tissue [1]. The THz spectral region lies between the microwave and infrared bands, where the output power of available radiation sources drops significantly, a phenomenon commonly referred to as the “THz gap.” The most powerful THz sources are gyrotrons, which can generate megawatt-level output power at frequencies up to 200 GHz, while gyrotrons operating at the second cyclotron harmonic achieve output powers of several tens of watts at frequencies around 0.8 THz [2]. However, gyrotrons require bulky and expensive superconducting magnets and offer a limited frequency tuning range. Compact THz sources can be developed based on solid-state and vacuum electron device (VED) technologies. While modern solid-state devices provide insufficient output power for many practical applications, VEDs such as backward-wave oscillators (BWOs), clinotrons, orotrons, diffraction radiation oscillators (DROs), and extended-interaction oscillators (EIOs) are widely used in the millimeter-wave range. Although EIOs can deliver watt-level output power in the sub-THz range, their frequency tuning bandwidth is typically very narrow [3]. The clinotron is a powerful modification of the BWO, originally developed at the O. Ya. Usikov Institute for Radio Physics and Electronics of the National Academy of Sciences of Ukraine (Kharkiv, Ukraine) [4]. Compact clinotrons combine wide frequency tunability with output powers of up to 1.5 W at 200 GHz and up to 100 mW at 0.4 THz [5]. Experimental investigations of the output characteristics were performed using Schottky barrier diodes and interferometers, while precise spectral measurements were carried out using high-frequency harmonic mixers and a spectrum-analyzer-equipped oscilloscope. The developed high-voltage power supply units enable stepped-frequency operation based on a PID control algorithm, which is particularly suitable for three-dimensional THz imaging applications.

Keywords: THz radiation, clinotron, frequency tuning, THz imaging

[1] G.-S. Park, M. Tani, J.-S. Rieh, and S. Y. Park, Advances in terahertz source technologies. CRC Press, 2024.
[2] M. Thumm, “State-of-the-Art of High-Power Gyro-Devices: 2025 Update of Experimental results,” Journal of Infrared Millimeter and Terahertz Waves, vol. 46, no. 6, May 2025, doi: 10.1007/s10762-025-01042-y.
[3] M. Blank and K. L. Felch, “Millimeter-Wave Sources for DNP-NMR,” eMagRes, vol. 7, pp. 155-166, 2018. doi: 10.1002/9780470034590.emrstm1582.
[4] G. Ya. Levin, The Clinotron. Kiev, Ukraine: Naukova Dumka Press, 1992.
[5] S. Vlasenko et al., “Development of Compact Cherenkov Devices with Sheet Electron Beams in Sub-THz and THz Frequency Ranges (Review),” Radioelectronics and Communications Systems, vol. 67, no. 3, pp. 105–119, Mar. 2024, doi: 10.3103/s073527272403004x.

TERAHERTZ SCATTERING SIMULATIONS IN ABSORBING AND LAYERED SKIN MODELS

Lukas Stacevičius[1], Rusnė Ivaškevičiūtė-Povilauskienė[1], Linas Minkevičius[1], Ignas Grigelionis[1]

[1]Center for Physical Sciences and Technology, Vilnius, Lithuania
lukas.stacevicius@ftmc.lt

Terahertz (THz) radiation has attracted increasing interest for biomedical imaging and spectroscopy applications, as it can penetrate dielectric materials opaque to visible light while remaining non-ionizing. Its low photon energy enables safe in vivo skin studies, where strong water sensitivity can provide contrast between healthy and cancerous tissue [1]. When modeling skin tissue across a broad THz range, scattering is often neglected due to strong water absorption. However, tissue structures with dimensions comparable to the wavelength can produce Mie scattering effects that should be considered to improve diagnostic accuracy.

To analyze light scattering, spherical scatterers with radii of 50–250 μm (size parameter $x \approx 1–15$ across 0.1–3 THz) were modeled using Mie theory modified for an absorbing host medium [2]. Both high and low refractive-index contrast cases were examined, corresponding to empty and filled sweat glands in dermis medium, respectively (Fig. 1a). A three-layer skin model, including stratum corneum, epidermis and dermis (layer thicknesses of 30 μm, 100 μm, and 1 mm, respectively) was also simulated using the discrete dipole approximation (DDA), adapted for irregular structures inserted inside the multilayered medium [3]. Layer permittivities were calculated using effective dielectric function of mixtures [4], based on double-Debye permittivities derived from THz spectroscopy data reported in the literature.

For the low refractive-index contrast case between filled sweat glands and dermis, the scattering asymmetry parameter became negative with radii >150 μm, reaching -0.65 at 3 THz (Fig. 1b), indicating enhanced backscattering at higher frequencies, whereas high-contrast case remained positive. In the multilayer skin model, a prolate ellipsoid representing basal-cell carcinoma (BCC) structure was inserted across all three layers, producing only a small reflectivity increase of ≈0.13 % when its surface area was increased from 0.21 mm^2 to 0.28 mm^2. Varying structure depth showed that beyond 200 μm backscattering contributed negligibly to the overall reflectivity due to strong THz absorption by water. In this case, calculated reflectivity was dominated by interface reflections rather than intrinsic scattering.

In conclusion, while larger structures increased THz scattering, its contribution to the total reflectivity in the multilayer skin model became negligible for deeper layers due to strong water absorption and interface reflections, highlighting the need for high-sensitivity detection and polarization-resolved approaches to detect weak scattering signals.

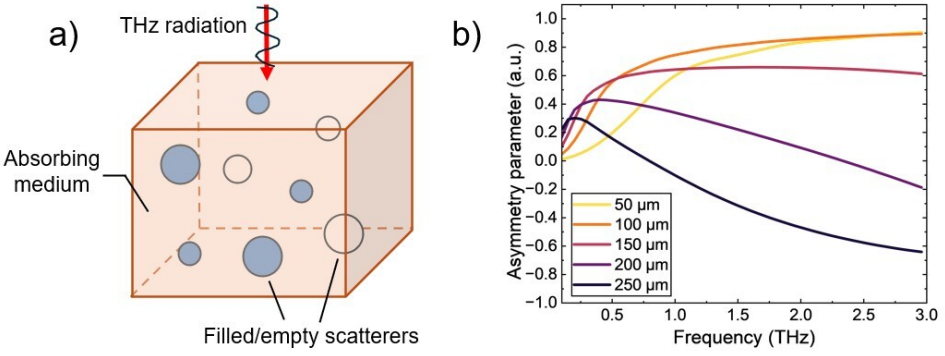


Fig. 1. (a) Skin model used for Mie theory calculations, modified for particles embedded in an absorbing host medium. (b) Scattering asymmetry parameter as a function of frequency (0.1–3 THz) for filled sweat gland in dermis medium, with radii ranging from 50 μm to 250 μm.

[1] Y. Sun, "A promising diagnostic method: Terahertz pulsed imaging and spectroscopy," World Journal of Radiology, vol. 3, no. 3, p. 55, Jan. 2011, doi: 10.4329/wjr.v3.i3.55.
[2] J. R. Frisvad, N. J. Christensen, and H. W. Jensen, "Computing the scattering properties of participating media using Lorenz-Mie theory," ACM Transactions on Graphics, vol. 26, no. 3, p. 60, Jul. 2007, doi: 10.1145/1276377.1276452
[3] P. C. Chaumet, D. Sentenac, G. Maire, M. Rasedujjaman, T. Zhang, and A. Sentenac, "IFDDA, an easy-to-use code for simulating the field scattered by 3D inhomogeneous objects in a stratified medium: tutorial," Journal of the Optical Society of America A, vol. 38, no. 12, p. 1841, Oct. 2021, doi: 10.1364/josaa.432685.
[4] S. Bosch, J. Ferré-Borrull, N. Leinfellner, and A. Canillas, "Effective dielectric function of mixtures of three or more materials: a numerical procedure for computations," Surface Science, vol. 453, no. 1–3, pp. 9–17, May 2000, doi: 10.1016/s0039-6028(00)00354-x.

3D SURFACE RECONSTRUCTION FROM 2D IMAGES USING GEOMETRIC NORMAL ESTIMATION, SIGNED DISTANCE FUNCTION AND NEURAL NETWORK

Goda Palšytė[1], Donatas Narbutis[1]

[1]Vilnius University, Faculty of Physics, Vilnius, Lithuania
goda.palsyte@ff.stud.vu.lt

3D object reconstruction from 2D images is a widely used process in fields such as robotics, autonomous systems, cultural heritage digitization, and medicine. However, reconstructions based on point clouds (PC) often suffer from low density caused by poor texture or low-quality imaging, resulting in inaccurate and hole-filled surfaces. Therefore, this work focuses on surface reconstruction from point clouds using geometric methods, signed distance functions (SDF), and neural networks.

High-resolution (6000×4000 pix) ammonite images from Kaggle (dataset name: 3D OBJECT RECONSTRUCTION FROM IMAGES) were processed with COLMAP to generate a point cloud. Noise and non-surface points were removed using Python and CloudCompare to improve data quality and ensure effective neural network training. Surface geometry was analysed using K-dimensional tree (KD-tree) neighbours search, centroid calculation, and covariance matrix estimation. Eigenvalue and eigenvector analysis was applied to determine surface normals, where the smallest eigenvalue direction represents the normal vector. Random points were generated around and beyond the surface, and signed distance function (SDF) values were computed for all points. A neural network was trained to distinguish surface points from surrounding space, enabling accurate and continuous surface reconstruction.

Thus, by applying the method of this work, it is possible to attempt reconstruction of 3D surfaces even for less textured objects with sparse point clouds.

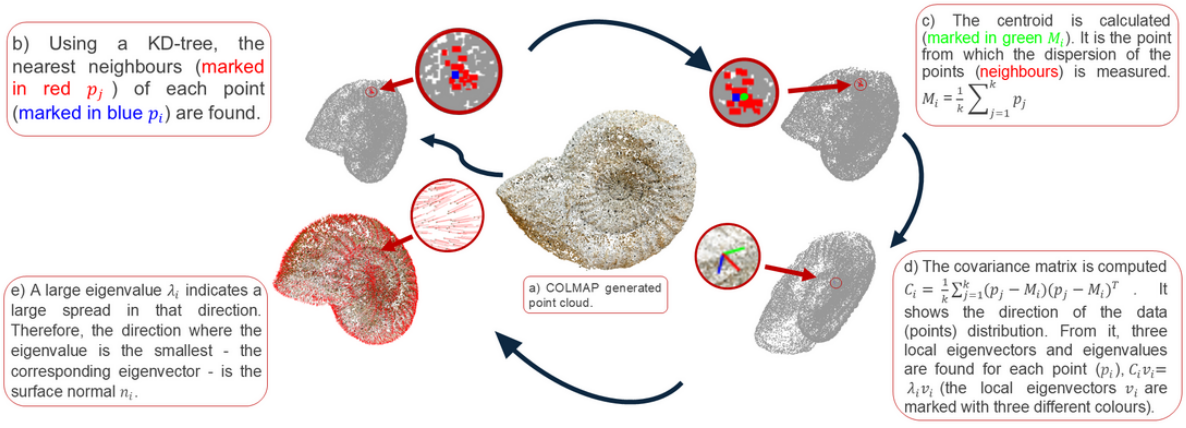


Fig. 1. Surface geometry analysis.

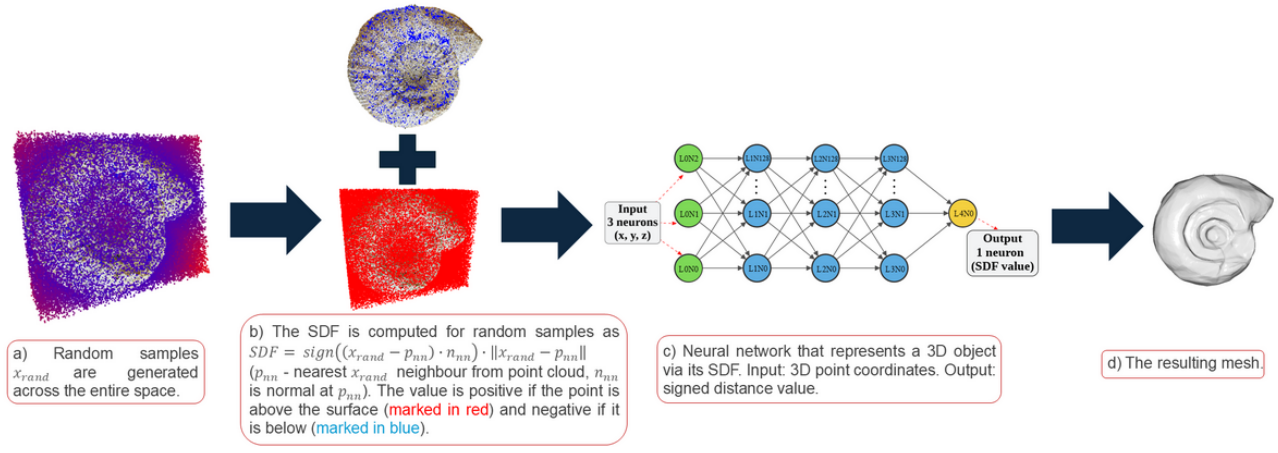


Fig. 2. Surface reconstruction with neural network.

X-RAY SOURCE IMAGING USING GAS ELECTRON MULTIPLIER DETECTOR SYSTEM

Kristupa Šeškauskaitė[1], Algirdas Lazauskas[1], Muhammad Usman Uraf Ishafaq[1,2], Sigitas Tamulevičius[1,2], Brigita Abakevičienė[1,2]

[1]Kaunas University of Technology, Institute of Materials Science, Kaunas, Lithuania
[2]Kaunas University of Technology, Faculty of Mathematics and Natural Sciences, Kaunas, Lithuania
kristupa.seskauskaite@ktu.edu

A fully integrated Gas Electron Multiplier (GEM) detector system was used for high-resolution X-ray imaging. The detector employs a triple-GEM foil structure with a 100 cm^2 active area enclosed in a sealed gas chamber. Each copper GEM foil contains a dense matrix of identical microscopic holes that enable electron avalanche multiplication under applied high voltage. Using a triple-GEM configuration provides high gain, low ion backflow, and excellent spatial resolution.

The detector features a Kapton entrance window and a drift cathode that generate a uniform electric field across the drift region, guiding primary ionization electrons toward the GEM stack. After amplification through the three foils, the electrons are collected on a readout plate, yielding accurate spatial information about the incident radiation.

Signal processing is performed by a custom 256-channel readout board developed by Techtra and connected to the detector via four Panasonic connectors. The board incorporates four Texas Instruments DDC264 ADCs, each providing 64 current-input channels with 20-bit resolution. Adjustable full-scale charge ranges from 12.5 pC to 150 pC and integration times between 160 µs and 1 s allow precise current measurement across a wide dynamic range.

The analog front end includes precision reference sources, low-pass filtering, and a biasing circuit capable of supplying a constant current to support negative-polarity input signals. A Xilinx FPGA manages timing, data acquisition, and communication. Digitized data are serialized and transferred to a PC over a 100 Mbit/s Ethernet interface, where TCP is used for system control and UDP for high-rate data streaming. The system operates at a 6.25 kHz sampling rate and is supported by software enabling real-time monitoring, visualization, and data storage.

The detector operates with an Ar/CO_2 (70/30) gas mixture and is powered by a Caen DT5470N high-voltage supply capable of delivering up to −5 kV at 200 µA. High voltage is routed to the GEM foils through a dedicated connector and cable. The assembly is housed in a gas-tight enclosure equipped with interfaces for gas inlet and outlet, HV distribution, and signal readout, ensuring stable performance within controlled gas condition.

To evaluate the detector's imaging performance, a COOL-X miniature X-ray source was used. This solid-state device employs a pyroelectric crystal to generate electrons, which then produce X-rays when accelerated into a copper target. The source delivers peak intensities of approximately 10^8 photons per second, with endpoint energies reaching up to 35 keV, providing a compact and reliable excitation source for characterization of the GEM-based imaging system.

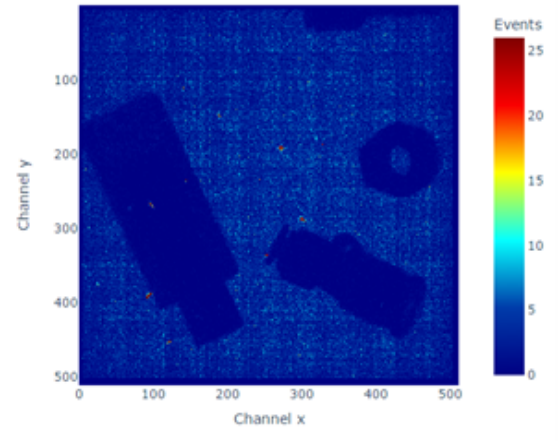


Fig. 1. Final reconstruction showing high-contrast, position-sensitive X-ray imaging achieved with the GEM detector

Acknowledgements

This work was supported by the project No. S-CERN-24-8, funded by the Research Council of Lithuania under the programme Prospective R&D Projects for Lithuania's Membership at CERN.

Keywords: GEM, X-ray, imagining, detector

SENSORS IN REMOVABLE DENTAL APPLIANCES

Diana Belosludtseva[1], Edita Voitechovič[1], Rasa Pauliukaitė[1]

[1]Center for Physical Sciences and Technology (FTMC), Department of Nanoengineering, Vilnius, Lithuania
d.beloslud@gmail.com

Removable dental appliances are custom-made devices that patients can insert and remove themselves to correct tooth alignment, replace missing teeth, or treat sleep-related conditions. They are typically made of acrylic resin and stainless steel wires or clear medical-grade plastic.

Sensors in removable dental appliances have evolved from simple timers into advanced monitoring systems that track everything from wear-time compliance to real-time biochemical changes in saliva. These embedded devices allow clinicians to transition from subjective patient reports to objective, data-driven treatment models.

Embedded biosensors can transform a standard dental appliance into a continuous health-monitoring platform. The integration of sensors into removable dental appliances represents a shift from mechanical correction to proactive health management. While the technology is already revolutionizing orthodontic compliance, its future lies in becoming a non-invasive window into a patient's systemic health.

Keywords: sensors, dental appliances, advanced monitoring systems, health-monitoring platform

INVESTIGATION OF STRONTIUM TITANATE CERAMICS BY IMPEDANCE SPECTROSCOPY

Roberta Diekontaitė[1]

[1]Vilnius University, Faculty of Physics, Insitute of Electrodynamics and Telecommunications
roberta.diekontaite@ff.vu.lt

Strontium titanate ($SrTiO_3$) is a perovskite oxide with a simple cubic crystalline structure at room temperature. This material is a mixed conductor, enabling a duality of the conductivity from predominantly electronic (via electrons or electron holes) to ionic (via oxygen vacancies)[1]. The purpose of this study is to examine electrical characteristics such as the ionic conductivity alongside the conductivity of electrons in a small sample of strontium titanate ceramics at different temperatures.

To obtain data, the sample is put in an impedance spectrometer, and a periodic sine waveform voltage signal is sent to it through a buffer. The measurements are performed in a frequency range of 10 Hz to 2 MHz. The temperature is varied from 300 K to 800 K in 20 K steps to acquire each impedance spectrum, as well as a second set of measurements is performed from 800 K down to 300 K. A computer-controlled power supply for the heater is used to control the temperature of the sample. The electrical signals are measured by a two-channel computer oscilloscope TiePie Handyscope HS3. The current is converted into voltage and measured. These steps result in frequency dependencies of the real and imaginary parts of impedance at different temperatures from which the ceramics can be characterized with the help of equivalent circuits. In this case a parallel (Maxwell) model is used. From the parameters of this equivalent circuit the value of conductivity can be found. It has been found, that the ionic conductivity follows the Arrhenius dependency:

$$\sigma = \frac{A_R}{T} e^{\frac{E_A}{k_B T}} \tag{1}$$

where A_R is constant proportional to the number of carrier ions, k_B – Boltzmann constant, and E_A – activation energy.

The results of this investigation show that the electrical characteristics of the material are dependent on the temperature of the sample and frequency of the applied signal through the sample.

Acknowledgements
This project has received funding from the Research Council of Lithuania (LMTLT), agreement No S-MIP-24-8.

Keywords: Ceramics; Impedance Spectroscopy; Ionic Conductivity

[1] I. Denk, W. Münch, and J. Maier, “Partial conductivities in SRTIO 3 : bulk polarization experiments, oxygen concentration cell measurements, and Defect-Chemical Modeling,” (Journal of the American Ceramic Society, vol. 78, no. 12, pp. 3265–3272, Dec. 1995)

COBALT MONOSILICIDE SINGLE CRYSTAL GROWTH USING THE CZOCHRALSKI METHOD

Miglė Minalgaitė[1,2], Ramūnas Skaudžius[2], Jiří Pospíšil[3]

[1]Center for Physical Sciences and Technology, Department of Chemical Engineering and Technology, Vilnius, Lithuania
[2]Vilnius University, Department of Inorganic Chemistry, Vilnius, Lithuania
[3]Charles University, Department of Condensed Matter Physics, Prague, Czech Republic
migle.minalgaite@ftmc.lt

Cobalt monosilicide (CoSi) is a semimetallic compound [1] that crystallises in a noncentrosymmetric cubic structure B20, described by the space group $P2_13$ [2].

Due to its unique topological and electronic properties, CoSi is currently the subject of extensive research in the field of chiral topological semimetals [3,4].

In the experimental procedure, pellets of CoSi were prepared by arc melting, using stoichiometric amounts of silicon and cobalt lumps as the starting materials. The annealed pellets of CoSi were crushed into medium-sized pieces and then placed inside a TriArc furnace. The crystal was grown in an argon atmosphere, and a piece of previously grown CoSi crystal was used as a seed. The obtained crystal was annealed, cut, and characterized using X-ray Laue diffraction and chemical analysis by EDX. The results showed that the CoSi monocrystal had been successfully grown.

Keywords: Czochralski, CoSi crystal;

[1] Z. J. Pan, L. T. Zhang, and J. S. Wu, “Electronic structure and transport properties of doped CoSi single crystal,” Journal of Applied Physics, vol. 101, no. 3, Feb. 2007, doi: 10.1063/1.2464186.
[2] A. T. Burkov, S. V. Novikov, V. K. Zaitsev, and H. Reith, “Transport properties of cobalt monosilicide and its alloys at low temperatures,” Semiconductors, vol. 51, no. 6, pp. 689–691, Jun. 2017, doi: 10.1134/s1063782617060094.
[3] Z. Ni et al., “Giant topological longitudinal circular photo-galvanic effect in the chiral multifold semimetal CoSi,” Nature Communications, vol. 12, no. 1, p. 154, Jan. 2021, doi: 10.1038/s41467-020-20408-5.
[4] L. Schnatmann et al., “Crystal Structure Analysis and Magneto-Transport Investigation of Co1−xFexSi (with x = 0% to x = 20%),” Advanced Electronic Materials, vol. 8, no. 4, Dec. 2021, doi: 10.1002/aelm.202101081.

APPLICATION OF THE CZOCHRALSKI METHOD FOR LITHIUM FLUORIDE SINGLE CRYSTAL GROWTH

Miglė Minalgaitė[1,2], Skirmantė Tutlienė[1], Ramūnas Skaudžius[2]

[1]Center for Physical Sciences and Technology, Department of Chemical Engineering and Technology, Vilnius, Lithuania
[2]Vilnius University, Department of Inorganic Chemistry, Vilnius, Lithuania
migle.minalgaite@chgf.stud.vu.lt

Lithium fluoride (LiF) is an inorganic compound that crystallises in a face-centred cubic structure described by the space group Fm-3m [1]. Due to its broad transmission range of 0.120-7 μm [2], LiF single crystals play an important role in advanced optical applications like laser systems, optoelectronics, X-ray and spectroscopic equipment [3, 4].

The aim of this work is to investigate the influence of the parameters of the growth by Czochralski method on the shape and form of lithium fluoride single crystals. LiF crystals were grown from the melt in a nitrogen atmosphere by adjusting the temperature, rotation speed and pulling speed parameters. The grown crystals were analysed using X-ray diffraction, X-ray Laue diffraction, Raman spectroscopy, FT-IR and UV-VIS spectroscopy. The process of optimising the parameters was successful, and LiF single crystals were successfully grown using our Czochralski equipment at the optimised single crystal growth parameters.

Acknowledgements

This research has received funding from the Research Council of Lithuania (LMTLT), agreement No. P-SV3-25-693.

Keywords: Czochralski, LiF single crystal

[1] L. Mei, X. Cai, D. Jiang, J. Chen, W. Guo, and W. Xiong, “Investigation of thermal neutron scattering data for BeF2and LiF crystals,” Journal of Nuclear Science and Technology, vol. 50, no. 4, pp. 419–424, Mar. 2013, doi: 10.1080/00223131.2013.773169.

[2] M. A. Vincenti, “Advanced spectroscopic investigation of color centers in LiF crystals exposed to 6 MV X-ray clinical beams,” Nuovo Cimento C Geophysics Space Physics C, vol. 40, no. 2, p. 93, Mar. 2017, doi: 10.1393/ncc/i2017-17093-6.

[3] G. Baldacchini, “Colored LiF: an optical material for all seasons,” Journal of Luminescence, vol. 100, no. 1–4, pp. 333–343, Dec. 2002, doi: 10.1016/s0022-2313(02)00460-x.

[4] Goodfellow, “Lithium Fluoride LiF - Lump - Material Information,” EU Website, Nov. 08, 2024. https://www.goodfellow.com/eu/resources/lithium-fluoride-lif-lump-material-information.

FABRICATION OF SILVER BISMUTH SULFIDE THIN FILMS VIA Ag/Bi STACK PHYSICAL VAPOR DEPOSITION AND SULFURIZATION

Aistis Melnikas[1], Marta Miró Llorente[2], Diego Nistal Castro[2], Victoria Rotaru[2], Alex López García[2], Alejandro Perez-Rodriguez[2,3], Skirma Žalenkienė[1], Pedro Vidal Fuentes[2]

[1]Kaunas University of Technology, Department of Physical and Inorganic Chemistry, Kaunas, Lithuania
[2]Catalonia Institute for Energy Research (IREC), Jardins de les Dones de Negre 1, 2ª pl., 08930 Sant Adrià del Besòs Barcelona, Spain
[3]Universitat de Barcelona, Departament d\'Enginyeria Electrònica i Biomèdica, IN2UB, C/ Martí i Franqués 1, 08028 Barcelona, Spain
aistis.melnikas@ktu.edu

Silver bismuth sulfide ($AgBiS_2$) has recently emerged as a promising, non-toxic light absorber material for thin-film photovoltaic applications due to its suitable optoelectronic properties and earth-abundant elemental composition [1]. $AgBiS_2$ has demonstrated exciting potential to be used in photovoltaics, as solar cells employing silver bismuth sulfide have achieved power conversion efficiencies exceeding 9% [2]. Many current methods of $AgBiS_2$ deposition rely on advanced and complex technology, such as atomic layer deposition (ALD), while physical vapor deposition routes offer reproducibility, low manufacturing costs, and an industrially applicable procedure. This opens the door to further optimize this technology through a larger and scalable process.

In this research, we investigate the growth of $AgBiS_2$ by employing physical vapour deposition routes. Glass substrates were first coated with molybdenum (Mo) by thermal evaporation, which acts as a back contact, onto which all films were subsequently deposited. Additionally, the formation of a MoS_2 layer beneath the absorber film during sulfurization can be beneficial by serving as a hole transport layer if properly optimized. Layers of silver (Ag) and bismuth (Bi) were deposited by e-beam evaporation and thermal evaporation, respectively. The Ag/Bi stack sequence, ratio, and total thickness were varied. The silver layer thicknesses of 6.5, 9.5, and 19 nm and the bismuth layer thicknesses of 13.7, 20, and 40 nm were employed, corresponding to the total stack thicknesses in the range of 20.2–69 nm, while expecting the $AgBiS_2$ thickness in the range of 35-100 nm. All layers were obtained on 1.5 x 2 cm^2 substrates. Furthermore, large area 5 x 10 cm^2 samples were fabricated by fixing the thickness of one metal layer while depositing a thickness gradient of the other (Ag or Bi). Large-area samples were employed to investigate the effect of the Ag/Bi stack ratio. Sulfurization of the deposited stacks was subsequently carried out as a reactive annealing in a tubular furnace over a temperature range of 300–500 °C for 30 min.

All samples were characterized by X-ray diffraction (XRD) analysis, Raman spectroscopy, and Scanning Electron Microscopy (SEM). XRD analysis reveals crystalline and preferred phases of $AgBiS_2$ with no significant influence in the Ag/Bi versus Bi/Ag sequence, Raman spectroscopy suggests the formation of MoS_2 at temperatures of 450 and 500 °C, and SEM analysis indicates homogenous film morphology in thicker stacks.

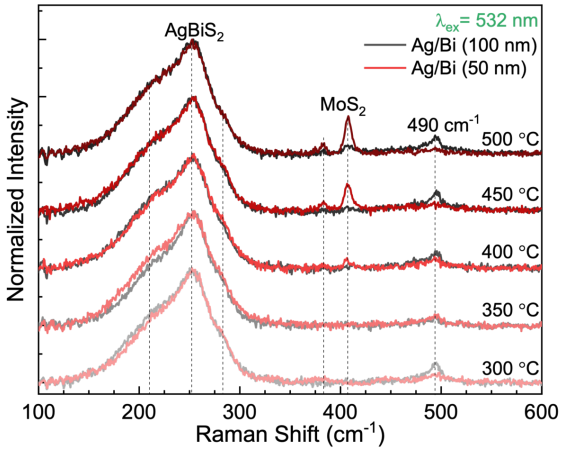


Fig. 1. Raman spectroscopy measurement of different $AgBiS_2$ samples fabricated by using different thicknesses of Ag/Bi precursor stacks and annealed at different temperatures

[1] U. Chalapathi et al., "Synthesis of AgBiS2 films by sulfurizing Bi/Ag stacks for thin film photovoltaics," Optical Materials, vol. 152, p. 115492, May 2024, doi: 10.1016/j.optmat.2024.115492.
[2] Y. Wang, S. R. Kavanagh, I. Burgués-Ceballos, A. Walsh, D. O. Scanlon, and G. Konstantatos, "Cation disorder engineering yields AgBiS2 nanocrystals with enhanced optical absorption for efficient ultrathin solar cells," Nature Photonics, vol. 16, no. 3, pp. 235–241, Feb. 2022, doi: 10.1038/s41566-021-00950-4.

SURFACE ENGINEERING OF TITANIUM-BASED IMPLANTS VIA SOL-GEL BIOACTIVE COATINGS

Martyna Sabaitė[1], Gabija Dragūnaitė[2], Brigita Abakevičienė[3], Odeta Baniukaitienė[1], Virginija Gylienė[4]

[1]Kaunas University of Technology, Faculty of Chemical Technology, Kaunas, Lithuania
[2]Lithuanian University of Health Sciences, Faculty of Medicine, Kaunas, Lithuania
[3]Kaunas University of Technology, Faculty of Mathematics and Natural Science, Kaunas, Lithuania
[4]Kaunas University of Technology, Faculty of Mechanical Engineering and Design, Kaunas, Lithuania
martyna.sabaite@ktu.edu

Implantable biomaterials play an important role in replacing or enhancing the function of major body systems. They can be made from polymers, ceramics, metals, metal alloys, or composite materials. Biomedical metal implant materials are of widespread application in clinical procedures that encompass dental implants, hip and knee replacements, bone plates, and screws, which plays a key role in the treatment of life-threatening disorders [1]. Different research challenges related to titanium-based implants are presented in Figure 1.

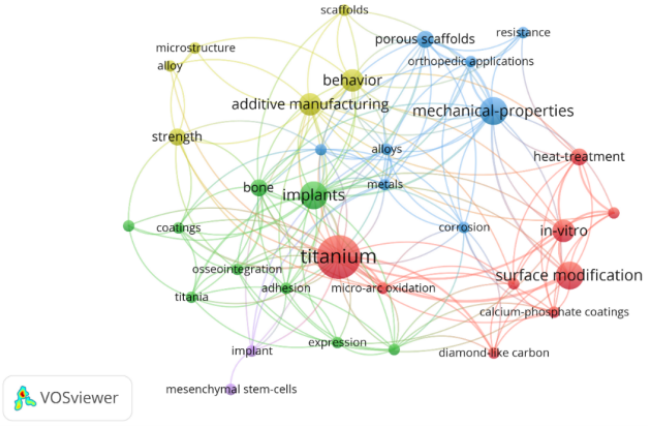


Fig. 1. Figure 1. Major Challenges in the Development of Titanium-Based Implants (generated using VOSviewer 1.6.20; © 2009–2023 Nees Jan van Eck and Ludo Waltman

One of the most commonly used alloys is Ti-6Al-4V, consisting of titanium with aluminum and vanadium as alloying elements (4–6 wt%). This alloy has relatively low density, is corrosion-resistant, and can withstand high mechanical loads. It is used to manufacture screws, plates, discs, needles, cylindrical, conical, and root-shaped implants. Commercially pure titanium (cpTi1) is also widely used due to its excellent biocompatibility in medical applications. However, unlike polymeric, ceramic, or composite implants, metallic implants may induce discomfort at the implantation site and cause tissue retraction. To enhance their biocompatibility, osseointegration, and chemical stability, the surfaces of medical implants often require modification [2] The aim of this project was to create a bioactive coating on biomedical implants and study their properties. Both Ti-6Al-4V alloy and cpTi1 were used as the substrate. The metal surfaces were first treated with acid and then coated with silicon dioxide-hydroxyapatite particles using the sol–gel method. FTIR, XRD, SEM, EDS, and surface roughness analyses were performed to evaluate the titanium alloy's surface and coating. A uniform and adherent bioactive coating was successfully formed on the surfaces of Ti-6Al-4V and cpTi1 alloys. Characterization confirmed the coating's structural integrity and surface properties, indicating its potential to enhance biocompatibility and osseointegration.

[1] S. Attarilar, M. Ebrahimi, F. Djavanroodi, Y. Fu, L. Wang, and J. Yang, "3D Printing Technologies in Metallic Implants: A Thematic Review on the Techniques and. Procedures," Int. J. BIOPRINTING, vol. 7, no. 1, pp. 21–46, 2021, doi: 10.18063/ijb.v7i1.306.
[2] T. Wegener, T. Wu, F. Sun, C. Wang, J. Lu, and T. Niendorf, "Influence of Surface Mechanical Attrition Treatment (SMAT) on Microstructure, Tensile and Low-Cycle Fatigue Behavior of Additively Manufactured Stainless Steel 316L," METALS, vol. 12, no. 9, p. 1425, Sep. 2022, doi: 10.3390/met12091425.

INVESTIGATION OF PHOTONIC CRYSTAL FABRICATION BY UV PULSES IN SAPPHIRE

Lukas Bručas[1], Edvinas Aleksandravičius[1], Darius Gailevičius[1]

[1]Vilnius University, Faculty of Physics, Laser Research Center, Vilnius, Lithuania
lukas.brucas@ff.stud.vu.lt

Photonic crystals are structures of periodically varying refractive index that are capable of altering and controlling the propagation of light, with potential applications as components in devices such as light emitters, optical waveguides, wavelength filters, dispersion compensators, and harmonic generators[1]. A desirable substrate for such structures is sapphire, due to its favorable mechanical, thermal, electrical, and optical properties[2]. Such photonic crystal fabrication is possible via femtosecond pulses, enabling multiphoton absorption and controllable volumetric modification of sapphire. Previous studies have focused on investigating fabrication with IR pulses, showing that cracks are a persistent obstacle in integrating photonic devices into sapphire[3]. However, use of more energetic UV photons could potentially enable crack-free fabrication of multi-layered structures using a wide range of production powers, allowing thorough control of light. In this work, fabrication via UV pulses is proposed as a viable method for 2D Laue photonic crystal integration in sapphire, enabling control of the Laue photonic crystal's filtering effect through various parameters.

A wide range of fabrication polarization and power, as well as structure size were investigated utilizing the 1st and 4th harmonics of the Yb:KGW laser for fabrication, representing near-IR (1030 nm) and mid-UV (257 nm) wavelengths respectively. The fabrication results were investigated using microscopy and the filtering effect was characterized. Fabrication using IR pulses resulted in cracks in all but the smallest structures. 4th harmonic yielded the most promising results, with successful fabrication in all cases. (Fig. 1 a.) The filtering effect was evaluated through transmittance measurements of structures fabricated using the 4th harmonic, which revealed heavy dependence of transmittance on fabrication polarization and power, as well as number of fabricated layers. (Fig. 1 b.)

The results prove the feasibility of photonic crystal fabrication in sapphire using UV pulses over a wide range of fabrication polarizations and powers, without limitation to structure size, allowing for thorough control of the filtering effect.

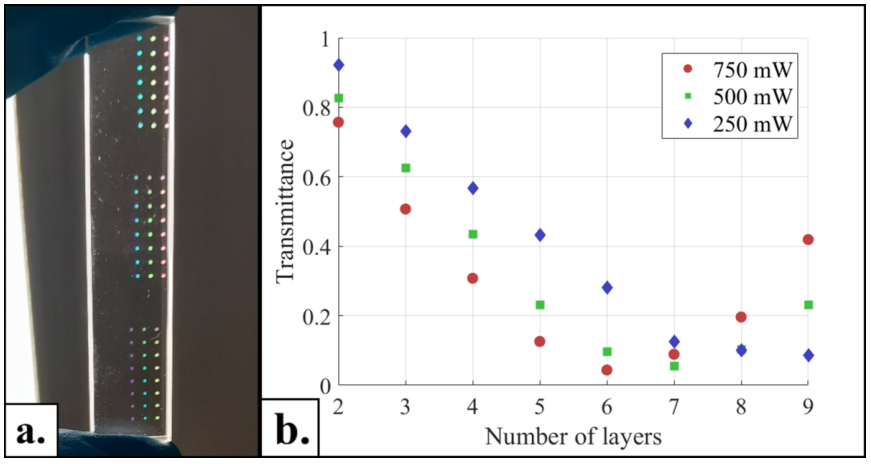


Fig. 1. a. Successfully fabricated structures; b. Transmittance dependence on layer index for different fabrication powers in case of fabrication polarization perpendicular to the structure lines.

[1] K. Inoue et al., "Photonic Crystals - Physics, Fabrication and Applications", Optical Sciences
[2] E. R. Dobrovinskaya et al., "Sapphire: Material, Manufacturing, Applications", Springer
[3] A. Puišys et al., "Integration of Fresnel Zone Plates in the Bulk of Sapphire Crystal by Femtosecond Laser Pulses", Journal of Laser Micro/Nanoengineering

SYNTHESIS OF ROOM-TEMPERATURE SINGLE PHOTONEMITTERS IN HEXAGONAL BORON NITRIDE

Ifra Bibi[1], Vakaris Šilys[1], Viktorija Nargelienė[1], Julius Janušonis[1], Danielis Rutkauskas[1], Edgaras Markauskas[1], Tadas Paulauskas[1]

[1]Center for Physical Sciences and Technology, Saulėtekio al. 3, 10257 Vilnius, Lithuania
ifra.bibi@ftmc.lt

Quantum key distribution requires reliable on-demand, room-temperature single-photon emitters (SPEs) hosted in wide-bandgap materials. Hexagonal boron nitride (hBN) has emerged as a promising platform due to its excellent optical performance and compatibility with integrated photonic devices [1]. hBN is a two-dimensional material that hosts a diverse range of fluorescent quantum defects that may form intrinsically during material growth or can be deterministically engineered [2] [3]. Here, we synthesized defect-based SPEs in high-quality hBN flakes using controlled defect-engineering approaches combining ion implantation, focused laser irradiation, and high-temperature annealing. Spatially localized single-photon emitters with favorable optical properties, including high brightness and photostability are obtained. Under optimized fabrication and annealing conditions emission in visible to near-infrared spectral range is observed, demonstrating that precise control of annealing parameters is critical for reproducible emitter formation. The resulting SPEs are characterized using scanning confocal photoluminescence microscopy, time-resolved lifetime measurements, and second-order correlation (Hanbury Brown and Twiss) experiments to confirm single-photon emission. These results address key requirements for practical quantum key distribution sources and paving the way towards scalable and integrated quantum photonic devices.

[1] H. Z. J. Zeng et al., ”Integrated room temperature single-photon source for quantum key distribution,” vol. 47, no. 7, pp. 1673-1676, 2022.
[2] G. L. Liu et al., ”Single photon emitters in hexagonal boron nitride fabricated by focused helium ion beam,” vol. 12, no. 9, p. 2302083, 2024
[3] L. Gan et al., ”Large-scale, high-yield laser fabrication of bright and pure single-photon emitters at room temperature in hexagonal boron nitride,” vol. 16, no. 9, pp. 14254-14261, 2022.

INVESTIGATION OF CHARGE TRANSPORT KINETICS IN PEROVSKITE SOLAR CELLS USING THE KINETIC PHOTOCONDUCTIVITY METHOD

Dovilė Vasiliauskaitė[1], Lauryna M. Svirskaitė[2], Ernestas Kasparavičius[1], Vidmantas Gulbinas[1]

[1]Center for Physical Sciences and Technology, Department of Molecular Compounds Physics, Lithuania
[2]Kaunas University of Technology, Faculty of Chemical Technology, Department of Organic Chemistry, Lithuania
dovile.vasiliauskaite@ftmc.lt

Renewable energy sources such as wind and solar energy have proven to be the cheapest and effective electrical power generation methods [1]. Alongside the ever increasing global power demand, further improvement and development of new technologies for power generation, such as organic and inorganic photovoltaics (PV), are highly incentivised. One example of rapidly developing PV technology field are the perovskite solar cells (PSCs). In less than two decades time, power conversion efficiency (PCE), value used to best describe the efficiency of solar cells, of PSCs improved from 3.8% to 27.2% [2,3]. This fast approach of the Shockley-Queisser limit in perovskite solar cells is significantly attributed to the development of new effective charge transport layers, as well as the tuning of the perovskite composition and structure, thus a better understanding of charge generation and transport kinetics is crucial for the further development and future applications of PSC photovoltaic technologies.

In this work the effect of different charge transport layers (CTLs) on the kinetics of charge extraction in modified perovskite solar cells is investigated using the kinetic photoconductivity method. The performed measurements showed that different materials used as charge transport layers significantly affected charge extraction kinetics. Comparison of charge transport kinetics of novel CTLs with good performing conventional materials like SnO2 and MeO-2PACz allowed to indirectly evaluate the work-functions and band bending in the semiconductor systems as well as the overall performance of the solar cells.

Based on the obtained kinetic data, schematic depictions of band bending profiles were created for each investigated CTL, enabling the assessment of their performance as charge transport layers in solar cells.

Keywords: Perovskite solar cell, charge transport, kinetic photoconductivity method

[1] G. R. Timilsina, “Are renewable energy technologies cost competitive for electricity generation?,” Renewable Energy, vol. 180, pp. 658–672, Sep. 2021
[2] A. Kojima, K. Teshima, Y. Shirai, and T. Miyasaka, “Organometal halide perovskites as Visible-Light sensitizers for photovoltaic cells,” Journal of the American Chemical Society, vol. 131, no. 17, pp. 6050–6051, Apr. 2009
[3] C. Tian et al., “Photostable donor–acceptor interface for minimizing energy loss in inverted perovskite solar cells,” Nature Photonics, Jan. 2026

CHARACTERIZATION OF THERMALLY EVAPORATED ANTIMONY SELENIDE (Sb_2 Se_3) FILMS ON DIFFERENT BUFFER LAYERS

Amina Elkady[1], dr. Arnas Naujokaitis[1], dr. Vidas Pakštas[1]

[1]Center for Physical Sciences and Technology, Department of Characterization of Material Structure, Photovoltaic Materials Laboratory, Vilnius, Lithuania
amina.elkady@ftmc.lt

Antimony selenide (Sb2Se3) has emerged as a promising absorber material for thin-film photovoltaics (PV) applications due to its optimal bandgap (1.1–1.2 eV), high absorption coefficient (>105^{-1} cm), low toxicity, and steadily increasing power-conversion efficiency (PCE) [1,2]. However, the performance of Sb2Se3-based devices strongly depends on the quality of the interface between the absorber and the buffer layer [3-5].

In this study, Sb_2Se_3 thin films were deposited by thermal evaporation onto soda-lime glass (SLG) substrates coated with fluorine-doped SnO_2 (FTO), which served as the conductive electrode. Prior to Sb_2Se_3 deposition, different buffer layers-tin oxide (SnO_2), cadmium sulfide (CdS), and titanium dioxide (TiO_2)-were deposited to systematically investigate their influence on thin-film growth, structural properties, and interfacial quality. Thermal evaporation was chosen due to its simplicity, high reproducibility, and compatibility with vacuum-based thin-film device fabrication. Furthermore, the relatively low melting point and high vapor pressure of Sb_2Se_3 make this technique particularly suitable, enabling controlled deposition and the formation of uniform, high-quality thin films. Structural and morphological characterizations were carried out to assess the impact of buffer layer selection on the structural integrity and overall quality of the Sb_2Se_3 thin films.

[1] A. Mavlonov, T. Razykov, F. Raziq, J. Gan, J. Chantana, Y. Kawano, T. Nishimura, H. Wei, A. Zakutayev, T. Minemoto, X. Zu, S. Li, and L. Qiao, “A review of Sb_2Se_3 photovoltaic absorber materials and thin-film solar cells,” Solar Energy, vol. 201, pp. 227–246, 2020, doi: 10.1016/j.solener.2020.03.009.

[2] C. Chen, K. Li, and J. Tang, “Ten years of Sb_2Se_3 thin film solar cells,” Solar RRL, vol. 6, 2022, doi: 10.1002/solr.202200094.

[3] G. Li, Z. Li, X. Liang, C. Guo, K. Shen, and Y. Mai, “Improvement in Sb_2Se_3 solar cell efficiency through band alignment engineering at the buffer/absorber interface,” ACS Appl. Mater. Interfaces, vol. 11, no. 1, pp. 828–834, 2019, doi: 10.1021/acsami.8b17611.

[4] K. Zeng, D.-J. Xue, and J. Tang, “Antimony selenide thin-film solar cells,” Semicond. Sci. Technol., vol. 31, no. 6, Art. no. 063001, 2016, doi: 10.1088/0268-1242/31/6/063001.

[5] Y. Wang, S. Ji, and B. Shin, “Interface engineering of antimony selenide solar cells: A review on the optimization of energy band alignments,” J. Phys. Energy, vol. 4, no. 4, Art. no. 044002, 2022, doi: 10.1088/2515-7655/ac8578

ELECTROMAGNETIC RADIATION DIRECTION FINDING SYSTEM

Mantas Krejaras[1], Justina Žemgulytė[1], Karolis Stankevičius[1], Rimantas Simniškis[1], Paulius Ragulis[1]

[1]Center for Physical Sciences and Technology, Department of Physical Technologies, Saulėtekis ave. 3, Vilnius, Lithuania
mantas.krejaras@ftmc.lt

Radiation direction finding (DF) is a difficult challenge in the fields of RF and Microwave engineering. It is often used for radar detection and locating unknown transmitters. While DF is not an innovative idea, research into developing simplified systems is an ongoing subject of interest [1]. In this work, a novel DF approach is presented that estimates the angle of arrival by comparing the ratio of measured received powers across circularly mounted antenna array applying the directivity pattern $G_{rx}(\alpha)$ of each antenna in the array.

The Friis equation states that the far–field received signal power depends inversely on the square of the distance between the transmitter and receiver, and it is directly related to the gains of the antennas involved [2]. Assuming differences in distances between the transmitter and the receiving antennas are negligible, signal's angle of arrival ϕ can be estimated from the ratio of received powers P_{r1} and P_{r2}, which equals to the ratio of antenna gains G_{r1} and G_{r2} at the same angle ϕ:

$$\frac{P_{r1}}{P_{r2}}(\phi) = \frac{G_{r1}}{G_{r2}}(\phi) \tag{1}$$

To validate the accuracy of this relationship, measurements using three X–band (8 – 12 GHz) antennas spaced 45° apart were made in a microwave anechoic chamber. An experiment was conducted using a 10 GHz, 0 dBm CW signal while rotating the antennas from –45° to +45° in 2° steps and recording received power. Using eq. 1, an algorithm was developed to estimate angle of arrival by matching antenna gain ratios to received power ratios. Results (Fig. 1) demonstrate that using high-gain antennas enables direction estimation with a maximum error of 6°. Overall, the measured performance verifies the proposed method as an effective and low-complexity approach for DF.

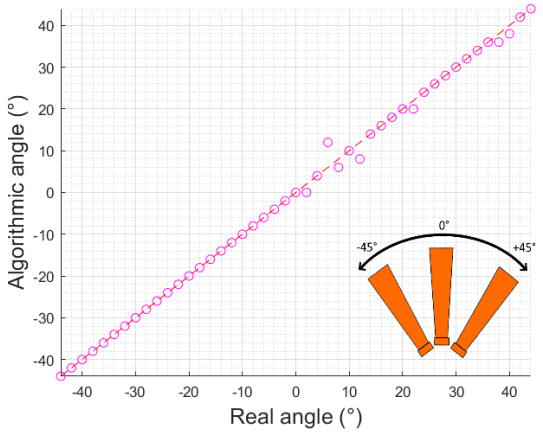


Fig. 1. Comparison of real signal's angle of arrival and algorithmically found angle of arrival using the ratio method for DF.

[1] [1] L. S. Driscoll, S. J. Thomas, and J. R. Smith, "Direction Finding System using an N-Channel Software Defined Radio Implemented with a Phase Interferometry Algorithm," in 2019 IEEE International Conference on Pervasive Computing and Communications Workshops (PerCom Workshops), Apr. 2019, pp. 917-922, doi: 10.1109/PERCOMW.2019.8730678
[2] Y. Huang and K. Boyle, Antennas: From Theory to Practice. Chichester, U.K.: John Wiley & Sons, 2008

INVESTIGATION OF THE OPTICAL CHARACTERISTICS OF SENSORS BASED ON COMPLEMENTARY METAL-OXIDE-SEMICONDUCTOR FIELD-EFFECT TRANSISTORS AT 2.52 THZ

Ričardas Petkus[1,2], Domantas Vizbaras[2], Ignas Grigelionis[1], Linas Minkevičius[1], Alvydas Lisauskas[1,2], Dovilė Čibiraitė-Lukenskienė[1,2]

[1]Center for Physical Sciences and Technology, Department of Optoelectronics, Lithuania.
[2]Vilnius University, Institute of Applied Electrodynamics and Telecommunications, Lithuania
ricardas.petkus@ftmc.lt

Terahertz (often defined as 100 GHz – 10 THz frequency range of the electromagnetic spectrum [1]) has the ability to penetrate non-conductive materials, it is non-ionizing in nature, and it has resonance with the rotational and vibrational modes of complex biomolecules. These properties are of interest for the development of high-power THz sources and high-sensitivity THz detectors. Field-effect transistors (FETs) with integrated antennas are being used in development of such THz radiation detectors [2]. FET technology is compatible with commercial complementary metal–oxide–semiconductor manufacturing processes and can operate efficiently at room temperature.

This work outlines the development of terahertz sensors based on FET technology and studies on their angular characteristics while operating at 2.52 THz.

This study involved several stages of detector development, including the investigation of suitable low-noise amplifier components, amplifier circuit modeling to validate the expected behavior, component soldering, and the assembly of the complete sensor device. Then, measurements were carried out to determine the angular dependency of detected power and scanning the antenna area using a mirror system that guided the THz wave from a 2.52 THz source.

The principle measurement diagram is shown in Fig. 1(a)). It depicts the laser used, the mirror system and the detector, which underwent both angular measurement (1)) and signal intensity mapping (2)). The conducted angular measurements (Fig. 1 b)) revealed an asymmetric, multi-lobed response peaking at 55° (370 μV) and –45° (161 μV). These results prompted a signal mapping (Fig. 1 c)) to determine why they differed from the expected Gaussian result. The spatial mapping revealed a doughnut-shaped terahertz beam with a central minimum, also observed in [3] for the same laser.

The future experiments will aim to involve the pinhole method at the intermediate focus, which will eliminate the modes and reduce their influence on beam profile characterisation.

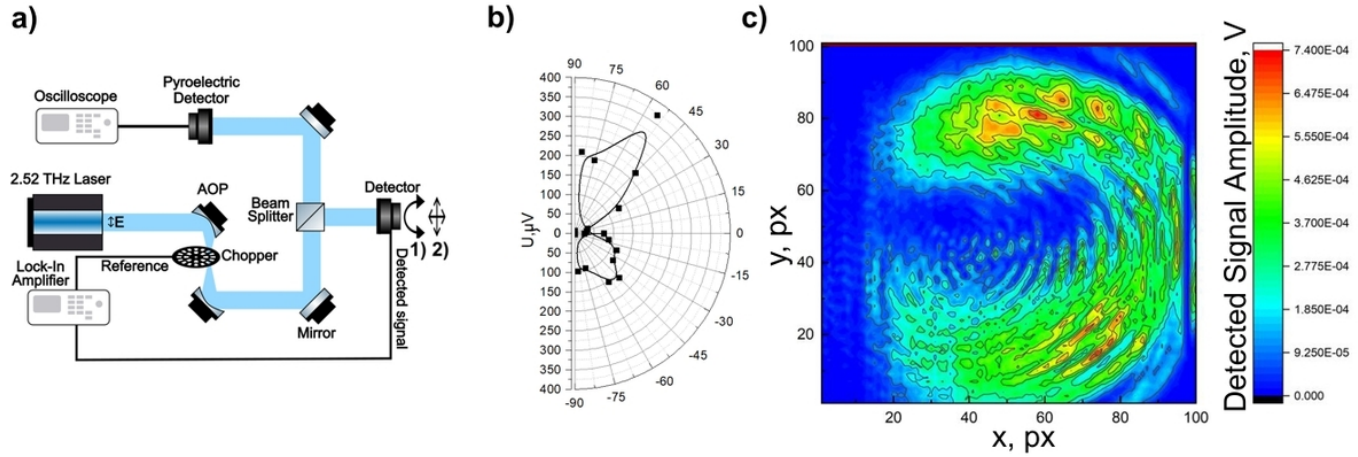


Fig. 1. a) Principle measurement diagram, here 1) is the angular measurement and 2) is the signal mapping; b) Measured angular dependence of THz response presented in this study; c) Signal intensity map of this study (size of a single pixel is 0.3 mm by 0.3 mm).

[1] R. Köhler et al., "Terahertz semiconductor-heterostructure laser," Nature, vol. 417, no. 6885, pp. 156–159, May 2002, doi: https://doi.org/10.1038/417156a.
[2] S. Boppel et al., "CMOS Integrated Antenna-Coupled Field-Effect Transistors for the Detection of Radiation From 0.2 to 4.3 THz," IEEE Transactions on Microwave Theory and Techniques, vol. 60, no. 12, pp. 3834–3843, Nov. 2012, doi: https://doi.org/10.1109/tmtt.2012.2221732.
[3] L. Minkevičius et al., "Titanium-Based Microbolometers: Control of Spatial Profile of Terahertz Emission in Weak Power Sources," Applied Sciences, vol. 10, no. 10, p. 3400, May 2020, doi: https://doi.org/10.3390/app10103400.

DESIGN OF A 2.4 GHz WILKINSON POWER DIVIDER WITH A DISTRIBUTED-ELEMENT BANDPASS FILTER

Kristina Miliauskaitė[1], Zigmas Balevičius[1]

[1]Vilnius Gediminas technical University (VILNIUS TECH), Faculty of Electronics, Department of Electronic Systems, Vilnius, Lithuania
k.miliauskaite@stud.vilniustech.lt

Power dividers are fundamental components in modern radio frequency (RF) and microwave systems. They are mostly used for even distribution of signal power among multiple ports. Of the various power divider architectures, the Wilkinson power divider has garnered significant attention due to its desirable characteristics, including high isolation between output ports and equal power division [1]. Despite the fact that this type of topology provides high isolation between output ports, a distributed-element bandpass filter is installed before the input of the Wilkinson power divider in order to improve signal quality and control the bandwidth more accurately.

The power divider with a bandpass filter is designed using microstrip lines. When low-loss dielectric materials are used, microstrips can provide excellent performance with minimal signal attenuation and good impedance control at RF and microwave frequencies. For circuit design, the low-loss dielectric material Rogers 4350B/C is used, which has a dielectric constant of $\varepsilon_r = 3.66$. Keysight Advanced Design System (ADS) software is used for circuit design and simulation [2]. The simulations examine S-parameters, which are commonly used to describe the input–output behavior of RF and microwave devices [3]. The following parameters are simulated: reflection coefficient S_{11}, forward transmission coefficients S_{21} and S_{31}, and isolation between terminals S_{23} and S_{32}. During simulation, the input reflection coefficient S_{11} shows that at 2.4 GHz only a small part of the signal is reflected back towards the source, meaning that the circuit is properly matched to the design frequency and most of the power is transmitted to the load. The forward transmission coefficients S_{21} and S_{31} indicate a nearly equal distribution of power between the two output ports, while the isolation parameters show that only a very small part of the signal leaks from one output to the other.

Integrating a distributed-element bandpass filter with a Wilkinson power divider is an effective way to achieve simultaneous power division and signal filtering in the 2.4 GHz band while maintaining good matching and high isolation between output ports. The proposed design can serve as a basis for further development of filtering power dividers for use in compact RF circuits which operate in the 2.4 GHz band, such as Wi-Fi and Bluetooth transceivers, multi-antenna access points, or measurement and testing setups where a single RF signal must be split into two or more band-limited paths. Integration and optimization of a filtering component directly into the power divider's architecture helps to address common signal quality issues in compact RF systems.

[1] "Hybrid power divider and combiner for passive RFID tag wireless energy harvesting," IEEE Journals & Magazine | IEEE Xplore, 2022. https://ieeexplore.ieee.org/document/9663231

[2] Keysight, "Advanced Design System (ADS) Circuit Design Cookbook 2.0," Keysight, Apr. 25, 2024. https://www.keysight.com/us/en/assets/7018-04800/application-notes/5992-0707.pdf

[3] J. Zhu, Y. Wang, K. Zhao, Y. Wang, C. Fu, and K. Man, "Assessment of measurement uncertainty for S-Parameter measurement based on covariance matrix," Sensors, vol. 24, no. 11, p. 3668, Jun. 2024, doi: 10.3390/s24113668.

INVESTIGATION OF TEMPERATURE INFLUENCE ON SIGNAL DELAY OF COAXIAL CABLES

Dominykas Mačiulaitis[1,2], Rimantas Miškinis[1], Milda Tamošiūnaitė-Survilienė[1], Emilis Urba[1]

[1]Center for Physical Sciences and Technology, National Metrology Institute, Time and Frequency Standard Laboratory, Vilnius, Lithuania
[2]Vilnius University, Faculty of Physics, Vilnius, Lithuania
dominykas.maciulaitis@ftmc.lt

Coaxial cables serve as critical infrastructure for high-speed data transmission and time synchronization in telecommunications, aerospace, and particle physics experiments. However, temperature fluctuations can degrade signal characteristics and timing accuracy through variable propagation delays in coaxial cables. The primary objective of this work is to investigate the influence of temperature on signal propagation delay for different cable types. The research aims at establishing how physical dimensions and manufacturing quality variances contribute to the temperature coefficient of delay. Although different methods can be used to estimate the delay of the cable, time interval counters disciplined by 10 MHz signal generated by cesium atomic clocks and two reference signals with the same repetition rate (one pulse per second) are used. The investigation uses temperature range from -6 ºC to 23 ºC, cable length from 5 m to 15 m and cable types RG174, H155. The results show that different cable types feature different temperature coefficients of delay. Thus, these results are important in evaluating measurement uncertainty for measurements carried out in the Time and Frequency Standard Laboratory.

COMPARISON OF SPECTRAL PROPERTIES IN THZ RANGE OF SQUARE AND CIRCULAR METASURFACE STRUCTURES ON CONDUCTOR/INSULATOR/CONDUCTOR STRUCTURES

Barbora Škėlaitė[1,2], Ignas Grigelionis[1]

[1]Center for Physical Sciences and Technologies, Deparment of Optoelectronics, Lithuania
[2]Vilnius University, Faculty of Physics, Lithuania
barbora.skelaite@ftmc.lt

Terahertz (THz) frequency range of the electromagnetic (EM) wave spectrum is known for its ability to pass through dielectric materials, that are otherwise non-transparent to visible light, such as plastic, paper, wood or textile, makes THz radiation a great tool in identifying and locating packed objects [1]. However, application of THz imaging systems is limited due to the absence of compact, efficient, and cost-effective solid-state emitters. Currently available solutions are expensive, suffer from limited operation frequency range and are of intricate structure [2]. As an alternative specifically tailored thermal radiation could be used, allowing for the mitigation of the above mentioned limitations. Here the semiconductor structures, particularly, devices comprising conductive/insulating/conductive layers structure, equipped with metasurfaces, could be used [3]. Such emitters can be operated at elevated temperatures, are of relatively simple inner structure, do not require additional expensive and usually bulky equipment and can provide thermal emission tailored to spectrally narrow resonant lines [4].

In this work the electromagnetic properties of GaAs-based conductor/insulator/conductor structures equipped with metasurfaces comprising either circular or square-shaped metacells are numerically simulated and investigated. The structures were simulated using Rigorous Coupled Wave Analysis (RCWA) [5] method and consisted of n-GaAs substrate, 4.3 µm thick GaAs insulator layer and 200 nm thick Ti/Au metasurface layer. The metasurface consisted of full or hollow metal metacells shaped like either squares or circles (Fig. 1) with dimensions (side length, diameter) varying from 20 µm to 40 µm. To compare the properties of differently shaped metacells the reflectance spectra, dielectric permittivity, magnetic susceptibility and EM field distribution throughout the structures were simulated.

Acquired reflection spectra (Fig. 1) showed that when the diameter of a circle matched the side length of the square metacell, the disk-shaped metasurface exhibited higher resonance frequency compared to the square-shaped one. It was noted that the increase in dimensions across all types of metacell configurations resulted in lower resonance frequency. Additionally, comparison of hollow and full shaped metacells, showed that by taking out a center part of the metal leads to EM field concentration mainly at the surface as opposed to the full metacells, where field distribution is more prominent throughout the whole structure. However, the resonance frequency values remained comparable, with the hollow-shaped metacells shifting slightly to lower frequencies.

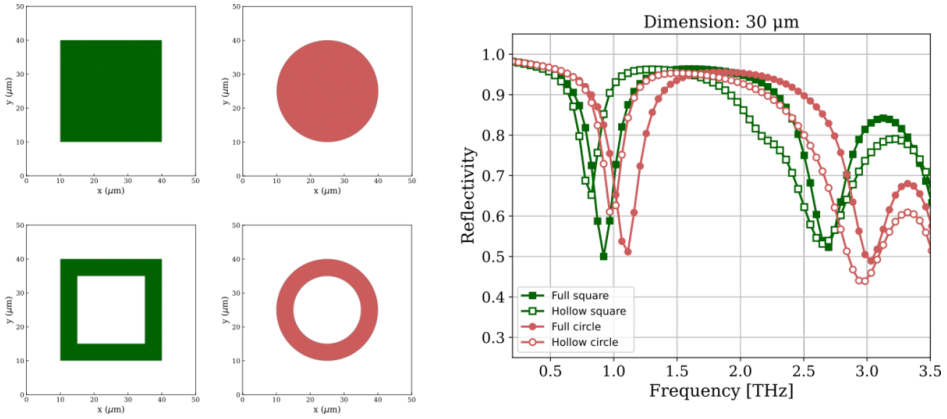


Fig. 1. Simulated metasurface unit cells (left) and their reflection spectra (right), where diameter and side length were 30 µm.

[1] J. Li et al., "Rapid sensing of hidden objects and defects using a single-pixel diffractive terahertz sensor," Nature Communications, vol. 14, no. 1, p. 6791, Oct. 2023, doi: 10.1038/s41467-023-42554-2.
[2] A. Leitenstorfer et al., "The 2023 terahertz science and technology roadmap," Journal of Physics D Applied Physics, vol. 56, no. 22, p. 223001, Feb. 2023, doi: 10.1088/1361-6463/acbe4c.
[3] F. Alves, B. Kearney, D. Grbovic, and G. Karunasiri, "Narrowband terahertz emitters using metamaterial films," Optics Express, vol. 20, no. 19, p. 21025, Aug. 2012, doi: 10.1364/oe.20.021025.
[4] B. J. Lee, L. P. Wang, and Z. M. Zhang, "Coherent thermal emission by excitation of magnetic polaritons between periodic strips and a metallic film," Optics Express, vol. 16, no. 15, p. 11328, Jul. 2008, doi: 10.1364/oe.16.011328.
[5] C. Kim and B. Lee, "TORCWA: GPU-accelerated Fourier modal method and gradient-based optimization for metasurface design," Computer Physics Communications, vol. 282, p. 108552, Sep. 2022, doi: 10.1016/j.cpc.2022.108552.

TEST-BASED RELIABILITY EVALUATION OF HYBRID IC PACKAGES WITH DIFFERENT INTERCONNECTION TECHNOLOGIES

Dominykas Mendelis[1], Mindaugas Žilys[1]

[1]Kaunas University of Technology, Electrical and Electronics Engineering Faculty, Electronics Engineering Department, Kaunas, Lithuania
dominykas.mendelis@ktu.edu

Hybrid integrated circuits (IC) enable the integration of diverse technologies within a single package, but their reliability is strongly influenced by packaging and interconnection processes. Variations in assembly technologies can introduce latent defects that are difficult to detect using conventional inspection methods, motivating the need for effective electrical testing approaches for early reliability evaluation. This study aims to evaluate the reliability of hybrid IC packages manufactured using different interconnection and assembly technologies, focusing on the capability of electrical testing to identify process-related reliability risks at an early stage.

Hybrid IC packages produced with distinct interconnection technologies were subjected to controlled electrical stress conditions. A set of electrical and functional parameters was monitored before and during stress application to assess degradation behavior. The collected measurement data were analyzed to compare reliability-related trends across different packaging implementations. The results reveal measurable differences in electrical response and degradation characteristics between the investigated interconnection technologies. Certain electrical parameters exhibited increased sensitivity to process-induced weaknesses, indicating their suitability as early indicators of reliability issues in hybrid IC packages.

The study demonstrates that test-based electrical evaluation provides valuable insight into the reliability of hybrid IC packaging technologies. The proposed approach supports early identification of reliability risks and can contribute to more efficient qualification and optimization of hybrid integrated circuit assembly processes.

HIGH-POWER ELECTRICAL PULSE WITH LOW HARMONIC DISTORTION FORMING METHODS FOR DYNAMICAL AND EMC TESTING

Rokas Grigaliunas[1]

[1]Kaunas University of Technology, Faculty of Electrical and Electronics Engineering, Department of Electrical Engineering, Kaunas, Lithuania
rokas.grigaliunas@ktu.edu

With the growth of the power of electronic power-switches and the speed of current control, the energy, electric transport, industry and other areas using powerful electrical converters are rapidly developing. However, the pulsations of electric and magnetic fields exceeding the limits can have a negative impact on both living organisms and nearby equipment. Therefore, an important stage in the research of these converters and power transistors is the testing of their maximum characteristics and environmental impact studies when the converters operate in nominal and maximum operating modes. The main challenges associated with testing these converters are the reduction of sufficiently small parasitic inductances and internal resistances in the circuit, the suppression of overvoltages and overloads, the maximization of the linearity of the parameter changes over time and the repeatability of all measured parameters. In the course of this research, mathematical models were created and two different circuits forming regular current pulses were practically tested. Minimized inductances and internal resistances of components allowing to achieve the real dI/dt speed of the electronic power switch. Also, the maximum generated electric, magnetic and electromagnetic fields at various distances from the source were investigated.

EMISSION HOMOGENEITY OF InGaAs/GaAs QUANTUM WELL STRUCTURES WITH DIFFERENT BARRIER PATTERNS

Kipras Mažeika[1], Augustas Vaitkevičius[1,2], Andrea Zelioli[2], Aivaras Špokas[1,2], Renata Butkutė[1,2], Jūras Mickevičius[1]

[1]Institute of Photonics and Nanotechnology, Saulėtekio al. 3, Vilnius, Lithuania
[2]State research institute Center for Physical Sciences and Technology, Saulėtekio al. 3, Vilnius, Lithuania
kipras.mazeika@ff.vu.lt

Indium gallium arsenide (InGaAs) is a III–V semiconductor alloy with a tunable bandgap from 1.425 eV (GaAs) to 0.36 eV (InAs) at room temperature [1], and, combined with its high electron mobility [2], serves as a key material in modern semiconductor technologies. InGaAs is commonly grown epitaxially, enabling precise control over composition and layer thickness. However, lattice mismatch with GaAs substrates can generate strain-induced defects, which degrade device performance [3]. These issues are particularly important in multilayered structures, which are widely used in applications such as lasers and heterostructure field-effect transistors (HFETs), where the optical response of individual layers is often indistinguishable. By employing photoluminescence (PL) measurements with excitation sources of different wavelengths, the contributions of individual layers can be separated, enabling a depth-sensitive and more precise analysis of both structural and optical characteristics.

In this work, three types of InGaAs/GaAs multiple quantum well (MQW) structures were investigated, each differing in barrier thickness and indium composition. The samples were grown by molecular beam epitaxy (MBE) on semi-insulating GaAs (100) substrates. The first structure featured 7 nm GaAs barriers between twelve QWs. The second comprised six QW pairs with alternating 7.3 nm and 119 nm GaAs barriers. The third retained the same ordering as the first structure while increasing the barrier thickness to 119 nm. The indium content ranged from 18.3% to 25.6%. PL measurements were performed using a WITec Alpha 300S confocal microscopy system, with optical excitation provided by four continuous-wave lasers emitting between 405 and 662 nm.

A theoretical model, based on known optical constants [4], was applied to estimate light penetration depth and transmission through the multilayered stacks. These predictions were experimentally validated using PL measurements at varying excitation wavelengths and power levels. Key parameters - including contrast, emission center of mass deviation, and spectral broadening - were analyzed to assess excitation behavior.

The results revealed that narrow barrier structures exhibited increased emission from a larger structural volume and greater spectral broadening with rising excitation power, whereas wide barrier structures maintained more stable emission characteristics due to limited light penetration imposed by the thicker barriers. These findings will be further investigated by evaluating the excitation threshold for QWs in different MQW structures, enabling a direct comparison between the different excitation conditions in the grown samples, giving a further insight into the reasoning behind previously observed trends.

[1] "Energy bandgap of InGaAs," Feb. 11, 2022. https://www.batop.de/information/Eg_InGaAs.html
[2] J. Katcki et al., "Formation of dislocations in InGaAs/GaAs heterostructures," Physica Status Solidi (A), vol. 171, no. 1, pp. 275–282, Jan. 1999, doi: 10.1002/(sici)1521-396x(199901)171:1.
[3] Ł. Gelczuk, M. Motyka, J. Misiewicz, and M. Dąbrowska-Szata, "Deep traps and optical properties of partially strain-relaxed InGaAs/GaAs heterostructures," Materials Science and Engineering B, vol. 147, no. 2–3, pp. 166–170, Oct. 2007, doi: 10.1016/j.mseb.2007.08.028.
[4] R. M. A. Azzam and N. M. Bashara, "Ellipsometry and polarized light". North Holland, 1987. See Section 4.6.

DIFFUSION IN A QUADRATIC POTENTIAL WITH A CHANGING DIFFUSION COEFFICIENT

Kristupas Kalvaitis[1], Rytis Kazakevičius[1]

[1]Vilnius University, Faculty of Physics, Lithuania
kristupas.kalvaitis@ff.stud.vu.lt

Diffusion with a changing diffusion coefficient can be used to model transport in heterogeneous media, such as living cells. In many systems, diffusing particles are confined to a limited region of space by an external potential. The simplest model for such confinement is a quadratic potential.[1]

In this work, we investigate two systems with a changing diffusion coefficient, described by systems of stochastic differential equations:

$$\begin{cases} dx_t = -\frac{1}{\tau_x}(x_t - \bar{x})\,dt + \sqrt{2D_t}\,dW_t^{(1)} \\ D_t = y_t^2 \\ dy_t = -\frac{1}{\tau_y} y_t\,dt + \sigma\,dW_t^{(2)} \end{cases} \quad \text{(1a)} \qquad \begin{cases} dx_t = -\frac{1}{\tau_x}\frac{D_t}{\bar{D}}(x_t - \bar{x})\,dt + \sqrt{2D_t}\,dW_t^{(1)} \\ dD_t = -\frac{1}{\tau_D}(D_t - \bar{D})\,dt + \sigma\sqrt{2D_t}\,dW_t^{(2)} \end{cases} \quad \text{(1b)}$$

Here, x_t represents the coordinate of a diffusing particle, and D_t represents the diffusion coefficient. Parameters τ_x, τ_y, τ_D, and σ determine the relative importance of the drift term and the noise term. In the system (1b), the drift term of the equation describing dx_t includes the diffusion coefficient. Similar systems were studied in [2].

For the first system we find the probability density functions for values of x_t in the long-time limit as well as the short-time limit. We compute time-dependent mean and variance of x_t. For the second system we find the PDF of x_t values in the long-time limit and approximate the mean and variance of x_t using multiple methods.

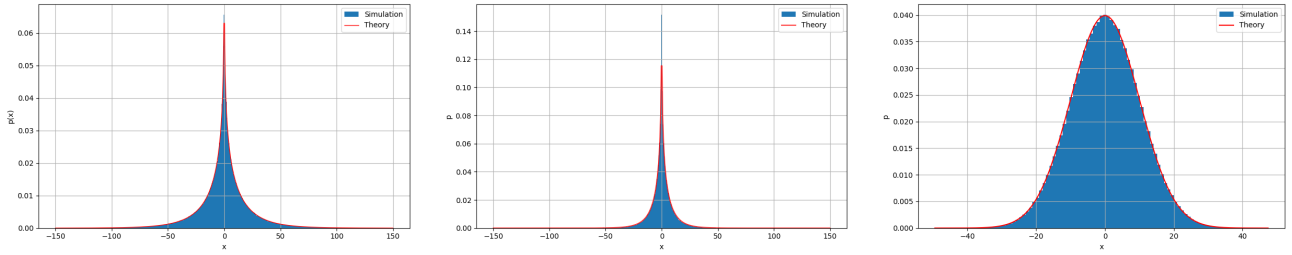


Fig. 1. (a) shows the long-time limit of the PDF of x values for the system (1a) with parameters $\tau_x = 1$, $\tau_y = 1000$, $\sigma = 1$, $\bar{x} = 0$, $T = 40$. T is the value of t when the simulation ended. (b) shows the short-time limit of the PDF of x values for the system (1a) with parameters $\tau_x = 1$, $\tau_y = 1000$, $\sigma = 1$, $\bar{x} = 0$, $T = 0.1$. (c) shows the long-time limit of the PDF of x values for the (1b) system with parameters $\tau_x = 1$, $\tau_D = 1000$, $\sigma = 1$, $\bar{x} = 0$, $\bar{D}$=100, $T = 30$.

These findings provide new insights into how varying diffusion affects confined systems and may inform future studies of complex stochastic dynamics

[1] Y. Lanoiselée, A. Stanislavsky, D. Calebiro, and A. Weron, “Temperature and friction fluctuations inside a harmonic potential,” Physical Review. E, vol. 106, no. 6, p. 064127, Dec. 2022, doi: 10.1103/physreve.106.064127.

[2] J. Ruseckas, R. Kazakevičius, and B. Kaulakys, “Coupled nonlinear stochastic differential equations generating arbitrary distributed observable with 1/f noise,” Journal of Statistical Mechanics Theory and Experiment, vol. 2016, no. 4, p. 043209, Apr. 2016, doi: 10.1088/1742-5468/2016/04/043209.

APPLICATION OF MACHINE LEARNING TO NUCLEAR REACTIONS

Darius Likandrovas[1,2], Arnoldas Deltuva[2]

[1]Vilnius University, Faculty of Physics, Vilnius, Lithuania
[2]Vilnius University, Institute of Theoretical Physics and Astronomy, Vilnius, Lithuania
darius.likandrovas@ff.vu.lt

The Coulomb interaction between charged particles complicates the theoretical description of scattering even in a two body system because its long range asymptotic behavior does not satisfy the standard assumptions of scattering theory [1]. In practical calculations, the screened Coulomb interaction and renormalization method is often used [2,3], in which the unscreened potential

$$w(r) = \frac{\alpha Z_1 Z_2}{r} \tag{1}$$

is replaced by a short range form

$$w_R(r) = w(r)\exp[-(r/R)^n], \qquad n \geq 1, \tag{2}$$

and the physical result is recovered by taking the limit $R \to \infty$.

Momentum space integral equation methods converge well at higher energies as the screening radius R is increased, allowing phase shifts to be computed with high accuracy. At lower energies, the influence of the Coulomb interaction becomes stronger and the numerical convergence with respect to R slows down, which reduces the accuracy of the calculations. This motivates the development of method that can reconstruct phase shift behavior at low energies using only a limited set of accurately computed values.

This work investigates the extrapolation of elastic two proton scattering phase shifts in the presence of the Coulomb interaction. The scattering problem is formulated within the Lippmann Schwinger integral equation and the t operator framework. The Coulomb interaction is included by using a screened Coulomb potential with screening radius R together with a renormalization procedure, and the extrapolation is performed with respect to $1/R$ at fixed scattering energy E. The task is defined as reconstructing the phase shift curve toward the limit $R \to \infty$ along decreasing $1/R$ using only the first three points of the curve.

To solve this problem, a fully connected regression neural network is constructed. Instead of predicting the phase shift directly, the network predicts not the phase shift itself but the residual with respect to a simple linear baseline approximation, while additionally given local geometry information, namely the first and second derivatives. The model is trained on data generated within effective field theory and tested on an independent dataset obtained with the realistic CDBonn potential.

The results show that the mean relative error is largest at the lowest energies, reaching about 1–2%, and decreases with increasing energy, stabilizing around 0.2%. The obtained results show that the chosen neural network method is suitable for extrapolating phase shift curves beyond the range of known region, and it may be applied in the future to more complex systems, including three and four body nuclear reaction problems.

Keywords: Lippmann Schwinger equation, two proton scattering, screened Coulomb potential, phase shift, extrapolation, neural network, regression

[1] J. R. Taylor, Scattering Theory: The Quantum Theory of Nonrelativistic Collisions. New York, NY, USA: John Wiley & Sons, 1972.
[2] J. R. Taylor, “A new rigorous approach to Coulomb scattering”, Il Nuovo Cimento B, vol. 23, pp. 313–334, 1974.
[3] A. Deltuva, A. C. Fonseca, and P. U. Sauer, “Nuclear many-body scattering calculations with the Coulomb interaction”, Annu. Rev. Nucl. Part. Sci., vol. 58, pp. 27–49, 2008.

PENTAQUARK SEARCH IN BEAUTY LAMBDA TO CHARMED SIGMA DECAYS USING LHCB RUN3 DATA

Šarūnas Jacevičius[1]

[1]Vilnius University, Faculty of Physics, Institute of Photonics and Nanotechnology, Lithuania
sarunas.jacevicius@cern.ch

Charmed pentaquark states (P_c^+) have first been observed by LHCb collaboration in 2015 in $\Lambda_b^0 \to J/\psi p K^-$ decay channel [1]. P_c^+ states have not yet been observed in other channels. $\Sigma_c^+ \bar{D}^{(*)0}$ systems are interesting for pentaquark search because they have the same quark content as $J/\psi p$ system ($uudc\bar{c}$) and their inertial masses are very close to the observed P_c^+ masses. $\Lambda_b^0 \to \Sigma_c^+ \bar{D}^{(*)0} K^-$ decay channels have not yet been analysed for pentaquark signals. Observation of P_c^+ signals in these channels or determination of signal upper limits would help constrain theoretical models that are currently unable to unambiguously describe the observed P_c^+ states.

The aim of this doctoral research is to analyse $\Lambda_b^0 \to \Sigma_c^+ \bar{D}^0 K^-$ decay channel for P_c^+ signals using LHCb Run3 data. This research topic branches off from Mindaugas Šarpis thesis where $\Lambda_b^0 \to \Lambda_c^+ \bar{D}^{*0} K^-$ decay channel was analysed using LHCb Run2 data [2]. A quark diagram that summarizes different possible $\Lambda_b^0 \to P_c^+ K^-$ decay channels is shown in Fig. 1.

One of the challenges of this research will be to isolate $\Lambda_b^0 \to \Sigma_c^+ \bar{D}^0 K^-$ decay channel in LHCb Run3 data. This channel has a major overlap with $\Lambda_b^0 \to \Lambda_c^+ \bar{D}^{*0} K^-$ channel in Λ_b^0 invariant mass spectrum. One approach to address this issue will be to utilize Monte Carlo (MC) event generator results for the overlapping decay channels and train a classifier model on experimental data in the narrow regions where the MC generated overlap is minimal. Analysis of $\Lambda_b^0 \to \Sigma_c^+ \bar{D}^{*0} K^-$ decay channel is also considered. These decays produce additional neutral particles (π_0 or γ) that are not efficiently detected. This results in $\Lambda_b^0 \to \Sigma_c^+ \bar{D}^{*0} K^-$ signal being shifted towards lower energies than $\Lambda_b^0 \to \Sigma_c^+ \bar{D}^{(*)0} K^-$ signal in the mass spectrum, avoiding signal overlap. The neutral particles can be reconstructed later by utilizing *Extended Cone Closure* method, introduced by Šarpis [2].

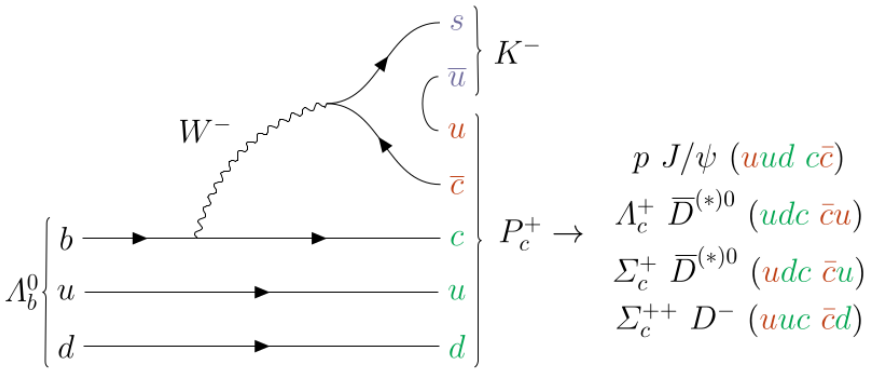


Fig. 1. Quark diagram of potential $\Lambda_b^0 \to P_c^+ K^-$ decay channels.

[1] LHCb collaboration, R. Aaij et al., Observation of J/ψ resonances consistent with pentaquark states in $\Lambda_b^0 \to J/\psi p K^-$ decays, Physical Review Letters, vol. 115, no. 7, p. 072001, 2015.

[2] M. Šarpis,Pentaquark Search in $\Lambda_b^0 \to \Lambda_c^+ \bar{D}^{*0} K^-$ Decays and LHCb Open Data Release, PhD Thesis, University of Bonn, Bonn, Germany, 2023.

MECHANICS OF R-LOOP FORMATION BY CASCADE STUDIED WITH MAGNETIC TWEEZERS

Virginija Siaurusevičiūtė[1], Ugnė Gaižauskaitė[1], Gabija Naujokaitė[1], Inga Songailienė[1,2], Algirdas Toleikis[1]

[1]Vilnius University, Life Sciences Center, Saulėtekio al. 7, LT- 10257 Vilnius, Lithuania
[2]University of Copenhagen, Novo Nordisk Foundation Center for Protein Research, Blegdamsvej 3B, DK-2200 Copenhagen, Denmark
virginija.siauruseviciute@gmail.com

Bacteria and archaea use CRISPR (clustered regularly interspaced short palindromic repeats) to defend against bacteriophages by targeting foreign nucleic acid for degradation. In type I CRISPR systems, the crRNA guide is bound and directed by the Cascade effector complex [1]. The Cascade complex recognizes the PAM sequence on the target DNA and identifies the target by formation of the R-loop structure – a three-stranded nucleic acid structure, composed of a DNA-RNA hybrid and the displaced non-target single-stranded DNA. The formation of a stable R-loop is a crucial step in the CRISPR mechanism because it permits recruitment of the nuclease-helicase Cas3, which initiates degradation of the target DNA [Fig. 1], [2].

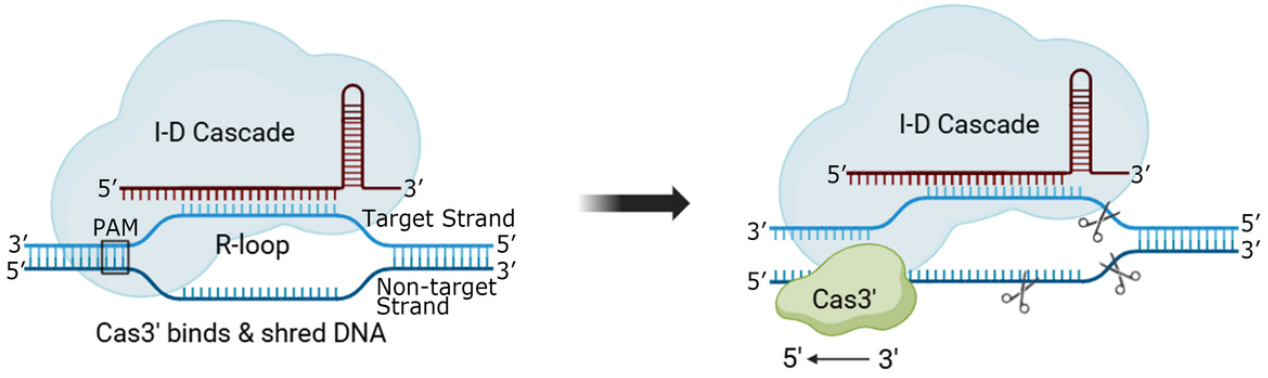


Fig. 1. The Type I-D Cascade binds its target and forms an R-loop, creating a platform for Cas3' to unwind and shred the DNA.

In this study, we investigate the mechanics of the R-loop formation in real-time at the single-molecule level using magnetic tweezers. This technology allows observation of dynamic conformational changes and the timing of individual R-loop-forming molecular events. By changing the force on a DNA-bound paramagnetic bead or introducing torque, we probe how R-loop stability depends on mechanical tension and torque. We compare Cascade complexes from different species to better understand the initiation and regulation of R-loops.

[1] Y. Zheng et al., "Endogenous Type I CRISPR-CAS: From foreign DNA defense to prokaryotic engineering," Frontiers in Bioengineering and Biotechnology, vol. 8, p. 62, Mar. 2020, doi: 10.3389/fbioe.2020.00062.
[2] K. Yoshimi et al., "Dynamic mechanisms of CRISPR interference by Escherichia coli CRISPR-Cas3," Nature Communications, vol. 13, no. 1, p. 4917, Aug. 2022, doi: 10.1038/s41467-022-32618-0.

SEPARATION OF HEAVY BARYON DECAY CHANNELS USING MODERN MACHINE LEARNING ALGORITHMS ON SIMULATED LHCB DATA

Neilas Beniušis[1], Mindaugas Šarpis[1]

[1]Vilnius University, Faculty of Physics, Institute of Photonics and Nanotechnology, Vilnius, Lithuania
neilas.beniusis@ff.stud.vu.lt

Separating resonant signals from background is a major challenge in studies of heavy baryon decays, especially when several states overlap. In this work, the decay $\Lambda_b^0 \to \Lambda_c^+ \bar{D}^{*0} K^-$ is studied using simulated LHCb detector data. This decay channel is relevant for understanding the formation of exotic states such as pentaquarks, first observed by the LHCb Collaboration in related Λ_b^0 decays [1], [2]. Monte Carlo simulations are used to model both resonant and non-resonant contributions to the decay.

The decay phase space is explored using Dalitz plots, which clearly show resonant structures and the kinematic boundary of the decay (Fig. 1). Based on these simulated data, several machine learning classifiers, including Random Forest, Gradient Boosting, and neural networks, are trained using invariant mass and angular variables. Their performance is evaluated using ROC curves and AUC values, showing good separation between signal and background. To better understand how the models make decisions, SHAP feature importance analysis is applied [3], indicating that invariant mass variables play the dominant role in the classification. This study shows that combining Dalitz plot analysis with interpretable machine learning methods is an effective approach for studying complex Λ_b^0 decay dynamics.

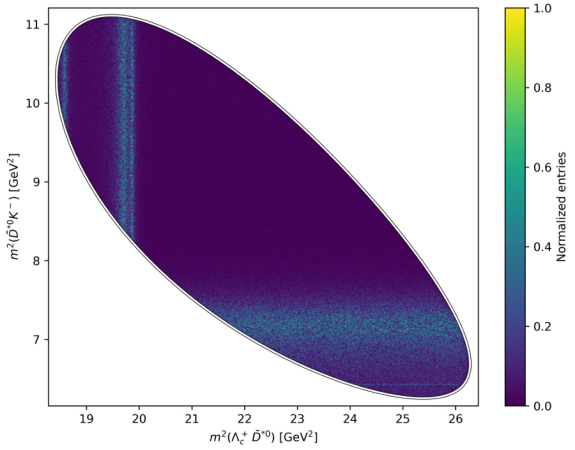


Fig. 1. Dalitz distribution of normalized entries for $\Lambda_b^0 \to \Lambda_c^+ \bar{D}^{*0} K^-$ phase space showing visible structures from $P_c(4312)^+$, $P_c(4440)^+$, $P_c(4457)^+$, $D_{s1}^*(2536)^+$ and $D_{s1}^*(2700)^+$ resonances.

Keywords: pentaquarks, Dalitz plot, Monte Carlo, machine learning, SHAP, RapidSim

[1] R. Aaij et al. (LHCb Collaboration), "Observation of J/ψp resonances consistent with pentaquark states in $\Lambda_b^0 \to J/\psi K^- p$ decays," Phys. Rev. Lett., vol. 115, p. 072001, 2015.

[2] R. Aaij et al. (LHCb Collaboration), "Observation of a narrow pentaquark state, $P_c(4312)^+$, and of the two-peak structure of the $P_c(4450)^+$," Phys. Rev. Lett., vol. 122, p. 222001, 2019.

[3] S. Lundberg and S.-I. Lee, "A unified approach to interpreting model predictions," Advances in Neural Information Processing Systems (NeurIPS), vol. 30, pp. 4765–4774, 2017.

CMS INNER TRACKER UPGRADE AND TEPX ELECTRICAL TESTING AT VILNIUS

Samarendra Nayak[1], Andrius Juodagalvis[1], Marijus Ambrozas[1], Vincas Tamošiūnas[1], Matas Petrėnas[1], Kęstutis Ikamas[1], Domantas Vizbaras[1]

[1]Vilnius University, Faculty of Physics, Experimental Nuclear and Particle Physics Center, Vilnius, Lithuania
samarendra.nayak@ff.vu.lt

The Large Hadron Collider (LHC) at CERN will enter the High-Luminosity LHC (HL-LHC) [1] era to enable more precise measurements and improve sensitivity to rare processes. This upgrade will expose the CMS experiment to extreme conditions, including peak luminosities of $7.5 \times 10^{34}\,\mathrm{cm}^{-2}\mathrm{s}^{-1}$, an integrated luminosity of $300\,\mathrm{fb}^{-1}$ per year, and about 200 proton-proton collisions per bunch crossing.

This work presents an overview of the CMS Inner Tracker (IT) upgrade [2], with a focus on the Tracker Endcap Pixel detector (TEPX), and highlights the ongoing electrical testing activities performed at the Vilnius test site.

To withstand radiation levels up to a 1 MeV neutron equivalent fluence of $2.6 \times 10^{16}\,\mathrm{cm}^{-2}$ and a total ionizing dose of 13 MGy, while operating at hit rates reaching $3.2\,\mathrm{GHz/cm}^2$, the upgraded IT will use thin, highly granular silicon sensors with pixel sizes of $25 \times 100\,\mu\mathrm{m}^2$ and fast, radiation-hard 65 nm CMOS readout electronics developed by the RD53 collaboration [3]. TEPX will be installed in the far forward region, where its innermost ring on the last disk extends beyond $|\eta| = 4$, enabling precision tracking and luminosity monitoring.

The upgraded TEPX system is designed to sustain HL-LHC operating conditions while functioning as a high-precision luminosity monitor. The Vilnius test site contributes through wire-bonding of bare modules and module-level electrical qualification, ensuring proper operation of the production chain under the required performance constraints.

The CMS IT upgrade, particularly the TEPX detector, is crucial for maintaining tracking and luminosity performance in the forward region of CMS at the HL-LHC. The wire-bonding and electrical testing activities at Vilnius support detector integration and validation, helping to ensure readiness for future operation.

Acknowledgements

This research has been carried out in the framework of the agreement of Vilnius University with the Lithuanian Research Council no. VS-13.

[1] C. Y. R. Monographs, "CERN Yellow Reports: Monographs, Vol. 10 (2020): High-Luminosity Large Hadron Collider (HL-LHC): Technical design report," CERN Document Server (European Organization for Nuclear Research), Dec. 2020, doi: 10.23731/cyrm-2020-0010.

[2] "The phase-2 upgrade of the CMS tracker," CERN Document Server, Jun. 2017, doi: 10.17181/CERN.QZ28.FLHW.

[3] M. Garcia-Sciveres, "RD53C Chip Manual," CERN Document Server, Feb. 27, 2024. https://cds.cern.ch/record/2890222

ADAPTING THE COFFEA FRAMEWORK FOR FCC

Eglė Lenkaitytė[1], David Lange[2], Prayag Yadav[3], Marijus Ambrozas[1], Andrius Juodagalvis[1]

[1]Vilnius University, Institute of Theoretical Physics and Astronomy, Lithuania
[2]Princeton University, United States of America
[3] University of Hyderabad, India
egle.lenkaityte@ff.stud.vu.lt

The Future Circular Collider (FCC) is a planned next-generation particle accelerator at CERN and a proposed successor to the Large Hadron Collider (LHC). With the potential to reach collision energies of up to 100 TeV, along with increased data rates and improved precision, it promises significant advances in our understanding of fundamental physics and the search for phenomena beyond the Standard Model. Although the FCC is not expected to begin operation for another 15–20 years, developing robust data analysis infrastructure at an early stage is essential to ensure effective preparation for future data-taking [1].

The Columnar Object Framework For Effective Analysis (Coffea) is a Python-based, unified analysis toolkit designed for high-energy physics data. In contrast to traditional event-loop-based analyses, columnar analysis follows a column-oriented, array-programming style, as illustrated in Figure 1. Coffea provides a collection of tools that simplify this approach, enabling more streamlined and reproducible workflows. As a result, analyses become more efficient, scalable, and easier to implement [2].

Coffea has already been successfully deployed within the CMS (Compact Muon Solenoid) experiment. However, its application to simulation data for the FCC, which relies on the Key4hep framework [3] and a dedicated software ecosystem (FCCSW) [4], is still under active development. Ensuring compatibility with these data formats and workflows is a necessary step toward its broader adoption in this context.

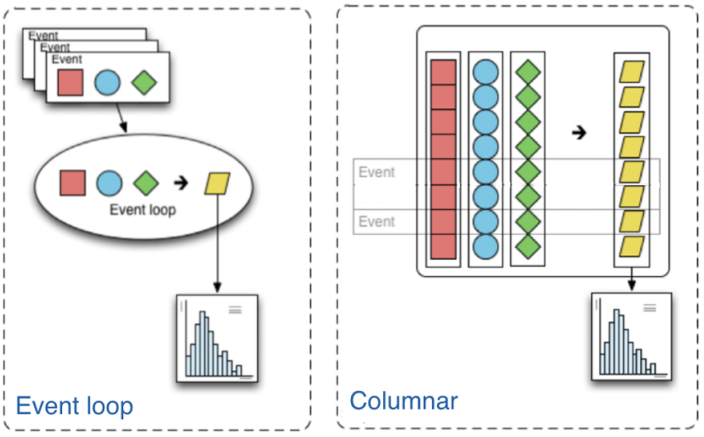


Fig. 1. Schematic of the event loop and columnar data processing paradigm [2].

The primary objective of this study is to adapt the Coffea framework for use with FCC simulation data. In particular, the project evaluates its suitability for the corresponding analysis workflows and explores extensions to its functionality where required.

The work begins with familiarization and practical use of Coffea through existing examples and tutorials, which are then adapted to simulation data produced within the Key4hep-based software environment. Initial results indicate that Coffea's columnar, array-based style can be successfully applied to FCC simulation data when appropriately integrated into the software ecosystem. Analyses adapted from existing workflows are able to process the relevant data formats efficiently, demonstrating clear improvements in scalability and performance compared to traditional event-loop approaches.

Overall, this study shows that Coffea can be effectively adapted and extended to meet the analysis requirements of future FCC studies. This research has been carried out in the framework of the agreement of Vilnius University with the Lithuanian Research Council no. S-IMPRESSU-24-4. The results will be presented at the conference.

[1] "The future circular collider," CERN, Jan. 28, 2026. https://home.cern/science/accelerators/future-circular-collider
[2] N. Smith et al., "COFFEA – Columnar Object Framework for Effective Analysis," Springer Link (Chiba Institute of Technology), Aug. 2020, doi: 10.48550/arxiv.2008.12712.
[3] "Key4hep — Key4hep documentation." https://key4hep.github.io/key4hep-doc/main/index.html
[4] "FCC Software." https://hep-fcc.github.io/FCCSW/

APPLICATION OF SERS SPECTROSCOPY FOR FORENCIC ANALYSIS OF DOCUMENTS

Aistė Maldūnaitė[1], Valdas Šablinskas[1]

[1]Vilnius University, Faculty of Physics, Institute of Chemical Physics, Vilnius, Lithuania
aistemaldunaite@gmail.com

Modern tools of falsification of written documents are rapidly improving, it becames easy to forge documents and are difficult to detect.There are chemical methods that allow to detect the loss of authenticity of a document, but usually they are invasive, what is not acceptable in case of old manuscripts. Raman spectroscopy is widely used for studies of chemical constitution of fluids, but it is difficult to apply it for ballpoint pen inks of conventional written documents since the ink layers are extremally thin. Additionally, weak Raman signal is followed by strong fluorescence background arising from the ink and the paper [1]. However, surface enhanced Raman spectroscopy (SERS) usually overcomes such sensitivity and background problems, also can be used to identify document forgery, just some technical problems of the spectroscopic experiment has to be solved [2].

In our study, it was intentionally falsificated one letter in text written by 'M&G Lavender' ball pen using identical-looking ink of 'M&G Poly Doba' pen. Different pen inks cannot be proved neither visually nor measuring conventional Raman spectra obtained without silver colloid solution. There are no Raman spectral bands due to strong fluorescence background. The SERS spectrum was measured, after adding silver colloidal solution onto the areas marked in purple and red in Fig. 1(a). The red arrow indicates the base of the word and the purple - shows the location of the falsification. A 633 nm laser, a 40x objective were used to measure the pen ink spectrum. The laser intensity was reduced to 5 mW in order to avoid sample heating and decomposition.The SERS method allowed to identify different pen inks, even though, the colours appear identical. It can be explained by their slightly different chemical constitution.

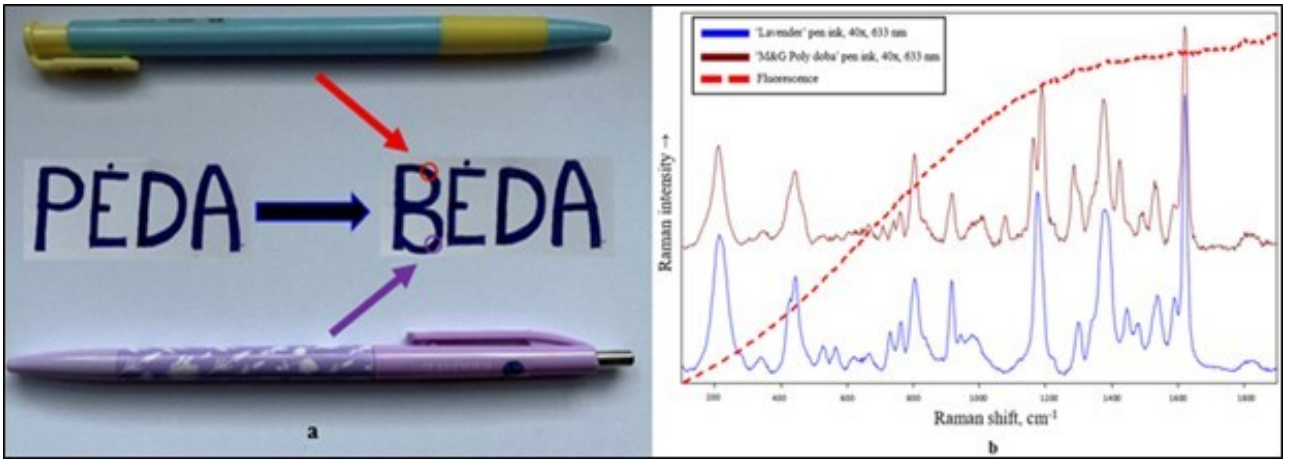


Fig. 1. (a) Word was falsificated to 'BĖDA' using identical-looking pen. Red and purple circles denote places where tiny drops of coloid were added and SERS spectra were measured;(b) SERS spectrum: blue - represents 'Lavender', while maroon – 'M&G Poly Doba' ink. Red broken curve represents fluorescence spectrum of the inks obtained from the same areas of the text before addition of silver colloidal solution.

The analysis of SERS spectra of two identical-looking pen inks reveals spectral differencies related to slightly different chemical constitution of the inks. Inks contain chemical components such as fatty acids and their esters, alcohols and coinsiding spectral bands for both inks can be attributes to these compounds. Clear spectral differences of the inks (Fig. 1(b)) in the spectral regions 500-600 cm^{-1} and 1060-1100 cm^{-1} possibly is related to benzyl alcohol, which is present just in one of the inks.

Analysis of the SERS results indicates that spectral differencies of chemically different ball pens are large enough for detection of forging documents.

Keywords: SERS, forgery, ballpoint pen inks

[1] M. A. Ettabib et al., "Grating-incoupled waveguide-enhanced Raman sensor," PLoS ONE, vol. 18, no. 8, p. e0284058, Aug. 2023, doi: 10.1371/journal.pone.0284058.

[2] Yumpu.com, "Forensic analysis of documents using Raman Spectroscopy - bruker," yumpu.com. https://www.yumpu.com/en/document/read/34072481/forensic-analysis-of-documents-using-raman-spectroscopy-bruker/1

OFF-RESONANT NONLINEAR OPTICAL SPECTROSCOPY AND ITS APPLICATION TO TWO-DIMENSIONAL ELECTRONIC SPECTROSCOPY

Liutauras Pocius[1], Darius Abramavičius[1]

[1]Lithuania, Vilnius University, Faculty of Physics, Institute of Chemical Physics
liutauras.pocius@ff.stud.vu.lt

At resonant conditions, different nonlinear spectroscopic signals can be unambiguously associated with specific Feynman diagrams describing distinct sequences of light–matter interactions. In contrast, under off-resonant conditions all interaction pathways can acquire comparable amplitudes and must be coherently summed in the signal calculation. This situation arises, for example, in second-harmonic generation from transparent media, where the microscopic origin of the signal—electronic versus vibrational—remains ambiguous, as in protein SHG experiments.

Partially off-resonant conditions are also encountered in third-order nonlinear measurements such as two-dimensional electronic spectroscopy (2DES). In the interpretation of 2DES, the waiting time T_2 is commonly associated with excited-state population dynamics, while the ground-state bleaching contribution is often considered dynamically trivial during this interval. This assumption is justified under resonant conditions, where electronic population and coherence dominate the signal. However, under partially off-resonant or transparent-window conditions, the system remains electronically in the ground state during T_2, and the role of nuclear degrees of freedom becomes less clear. In this case, virtual electronic polarization can mediate Raman-type vibrational coherences that evolve during T_2 and contribute to the measured errors of the third-order signal spectra. Understanding the role of these ground-state vibrational contributions is therefore essential for the correct interpretation of 2DES spectra obtained under off-resonant conditions. In this presentation, an off-resonant theoretical approach for calculating 2DES signals in transparent media is discussed. It is shown that solvent vibrational modes may lead to systematic, non-random contributions to the measured spectra, resulting in structured 2DES features rather than purely stochastic noise. These effects are illustrated by calculated 2DES spectra of a transparent medium in an off-resonant transparency window (Fig. 1).

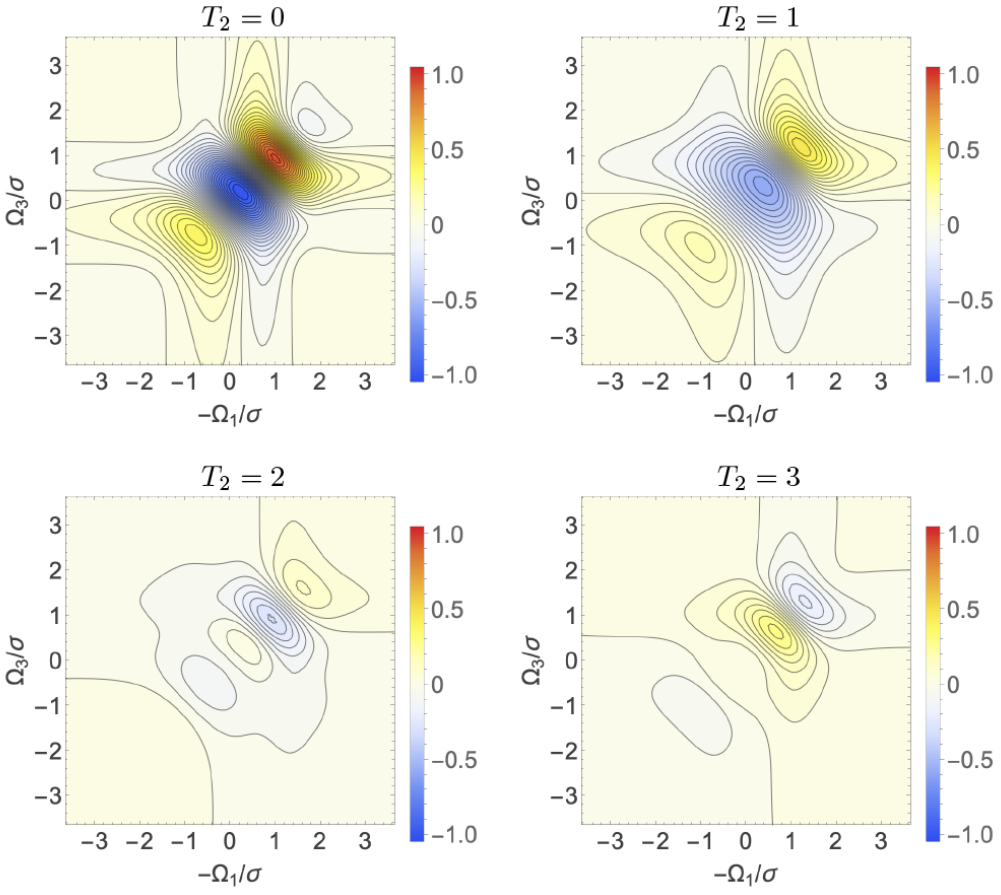


Fig. 1. Simulation of 2DES rephasing signal for a transparent nonliner medium including Raman process using chirped Gaussian pulses.

$CsPbCl_3$:Yb^{+3} STRUCTURAL ANALYSIS USING HYSCORE SPECTROSCOPY

Giedrė Kuktaitė[1], Mantas Šimėnas[1], Gediminas Usevičius[1], Simona Streckaitė[2], Marius Franckevičius[2], Vidmantas Gulbinas[2]

[1]Vilnius University, Faculty of Physics, Institute of Applied Elctrodynamics and Telecomunications, Lithuania
[2]Center for Physical Sciences and Technology, Lithuania
giedre.kuktaite@ff.stud.vu.lt

When Yb^{+3} ions are doped into the $CsPbCl_3$ crystal lattice the material exhibits especially effective infrared light emission during quantum splitting. Due to this property, this perovskite is a promising candidate for applications in quantum technologies, light-emitting diodes, lasers, photodetectors and solar-energy conversion. However, the lattice position occupied by Yb^{+3} ions has not been clearly established, despite its critical importance for optimizing the material's performance.

In this work, electron paramagnetic resonance (EPR) and hyperfine sublevel correlation (HYSCORE) spectroscopies, methods intended for structural analysis of materials with unpaired electrons, were employed to determine the lattice site of Yb^{+3} in $CsPbCl_3$ perovskite. Previous studies in our laboratory established key spectroscopic parameters, including the anisotropic g-factor and the hyperfine interaction associated with the Yb^{+3} center, but the structural assignment remained unresolved. Analysis of hyperfine and quadrupole interactions between the unpaired electron and surrounding Cs^{+}, Pb^{+2}, and Cl^{-} nuclei, via comparing experimental and simulated HYSCORE spectra, enabled identification of the Yb^{+3} local environment. The spectroscopic analysis indicates that Yb^{+3} ions substitute for Pb^{+2} sites within the $CsPbCl_3$ lattice rather than occupying interstitial positions or substituting Cs^{+} sites. This structural assignment provides direct insight into the local electronic environment of Yb^{+3}.

SPECTRAL CHARACTERIZATION OF NEUTRAL AND CATIONIC TPFPP: THE ROLE OF QUATERNARY AMMONIUM GROUPS

Martyna Petkutė[1], Gabrielė Vasiliauskaitė[1], Nojus Radzevičius[2], Irina Buchovec[1]

[1]Vilnius University, Faculty of Physics, Institute of photonics and nanotechnology, Vilnius, Lithuania
[2]Vilnius university, Faculty of Chemistry and Geosciences, Institute of chemistry, Vilnius, Lithuania
martyna.petkute@ff.stud.vu.lt

Porphyrins are widely studied as photosensitizers due to their high singlet oxygen quantum yield and broad absorption range, with a strong absorption band near 400 nm called the Soret band. However, their practical use is often limited by poor solubility and a strong tendency to aggregate in aqueous solutions, which leads to spectral changes, decreased absorbance and fluorescence intensity [1]. Chemical modification of the porphyrin structure, particularly the introduction of cationic substituents, is a common strategy to improve solubility and reduce aggregation [2]. The aim of this study is to investigate the photophysical properties of neutral tetrakis (pentafluorophenyl)porphyrin (TPFPP) and its cationic derivative (mTPFPP) (Fig. 1) in aqueous media.

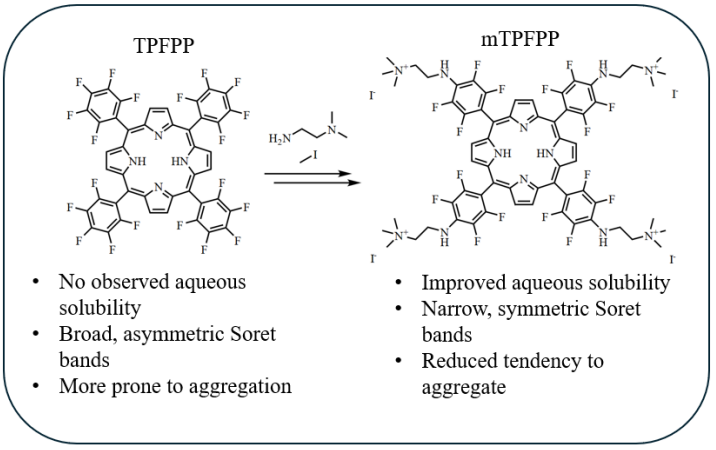


Fig. 1. Molecular structures of the parent porphyrin TPFPP and the modified cationic mTPFPP with quaternary ammonium substituents.

Preliminary visual observations showed that TPFPP is insoluble in distilled water (dH_2O) and phosphate-buffered saline (PBS), whereas mTPFPP exhibits partial solubility in dH_2O and good solubility in PBS. Due to the limited water solubility, stock solutions of both compounds were prepared in dimethyl sulfoxide (DMSO) and subsequently diluted into dH_2O and PBS to obtain working concentrations. UV–Vis absorption and fluorescence spectroscopy were used to examine their spectral features and concentration-dependent behavior in both media, while aggregation effects were further assessed by the addition of a non-ionic surfactant, Triton X-100. In dH_2O TPFPP exhibited broad and asymmetric Soret bands with varying position and shape, indicating aggregation effects. In contrast, mTPFPP showed narrower, symmetric Soret bands that remained constant, together with higher absorbance and fluorescence intensities. In PBS the same tendency was observed but with greater spectral broadening and lower absorbance and fluorescence intensities for both porphyrins, implying stronger tendency to aggregate than in dH_2O. The addition of the non-ionic surfactant Triton X-100 increased fluorescence intensity for both compounds and narrowed the Soret bands of TPFPP, indicating partial disaggregation.

These results suggest that cationic modification is associated with improved solubility and greater spectral stability of TPFPP in aqueous media.

[1] A. Glowacka-Sobotta et al., “Versatile Porphyrin Arrangements for Photodynamic Therapy—A Review,” Nanomaterials, vol. 14, no. 23, p. 1879, Nov. 2024.
[2] M. Luciano and C. Brückner, “Modifications of porphyrins and hydroporphyrins for their solubilization in aqueous media,” Molecules, vol. 22, no. 6, p. 980, Jun. 2017.

INVESTIGATION OF ORGANIC LIGHT-EMITTING DIODES AND OPTICAL SENSORS BASED ON RED AND NEAR-INFRARED EMITTING BENZOTHIADIAZOLE DERIVATIVES

Lesia Volyniuk[1], Melika Ghasemi[1], Stepan Kutsiy[3], Asta Dabuliene[1], Adam Pron[2], Dmytro Volyniuk[1], Juozas V. Grazulevicius[1], Irena Kulszewicz-Bajer[2], Audrius Bucinskas[1]

[1]Kaunas University of Technology, Department of Polymer Chemistry and Technology, Kaunas 51423, Lithuania
[2]Warsaw University of Technology, Faculty of Chemistry, Warsaw 00-664, Poland
[3]Lviv Polytechnic National University, Department of Electronic Engineering, Lviv 79013, Ukraine
lesia.volyniuk@ktu.lt

Numerous advanced technological fields, including telecommunications, healthcare, physiological monitoring, military systems, medicine, sensing technologies, and optogenetics, rely on light sources operating in the red and near-infrared (NIR) spectral regions. In this work, we studied three derivatives of 2,1,3-benzothiadiazole containing a central acceptor and two donors with varying electron-donating strengths, namely acridan, spiro[acridine-9,9'-fluorene] and phenoxazine. They exhibit thermally activated delayed fluorescence with photoluminescence maxima in the red or infrared regions. The phenoxazine derivative exhibits emission at 748 nm in toluene solution. The neat film of this compound emits near-infrared light, with a photoluminescence spectrum peaking at 726 nm. This compound was tested as an emitter in organic light-emitting diodes (OLEDs) using host-free, host-based, and multilayer light-emitting layers. OLEDs based on the neat film of the phenoxazine derivative emit near-infrared light, with an electroluminescence spectrum peaking at 745 nm. The external quantum efficiency (EQE) of this device is relatively low at 0.19%. In multilayer and host-containing light-emitting-layer-based OLEDs, this compound achieves maximum EQE values of 0.29% and 0.7%, respectively. Using the red-emitting derivative of 2,1,3-benzothiadiazole and spiro[acridine-9,9'-fluorene], red TADF OLEDs were developed with EL spectra at 621 nm and the highest EQEs of 3.42%. In addition, this compound demonstrated high oxygen sensitivity. Oxygen sensors containing this compound as the active material showed high Stern-Volmer coefficients of $3.4 \times 10{-}4$ ppm-1 in the range of oxygen concentrations from 0 ppm to 2000 ppm.[1] Three compounds were characterized by long-lived thermally activated delayed fluorescence, which is advantageous for organic light-emitting diodes and oxygen-sensing optical devices. The modifications to the molecular structure enabled us to shift the emission spectra of the films from the red to the near-infrared region. The near-infrared emitting compound was used for organic light-emitting diodes. The red-emitting compounds were used as the active materials in oxygen sensors.

Acknowledgements

This work is supported by Horizon Europe, the European Union's framework programme for research and innovation (R&I) for 2021-2027, project HELIOS, grant agreement No 101155017.

[1] Volyniuk, Lesia, et al. "Highly oxygen-sensitive red to near-infrared emitting benzothiadiazole derivatives for electroluminescent devices and optical sensors operating within the biological window". Sensors and Actuators B: Chemical, vol. 449, no.15, pp. 139066, Feb.2026, doi.org/10.1016/j.snb.2025.139066

CEREBROSPINAL FLUID ANALYSIS USING ATR-IR SPECTROSCOPY

Julija Jakučionytė[1], Rimantė Bandzevičiūtė[1], Valdas Šablinskas[1], Gerald Steiner[2,3], Johannes Kasper[2], Konstantin Sulin[2], Robert Brilmayer[2], Žilvinas Chomanskis[4], Gediminas Lukšys[4], Saulius Ročka[4], Matthias Kirsch[2]

[1]Vilnius University, Faculty of Physics, Institute of Chemical Physics, Lithuania
[2]Medical Campus Chemnitz at the TU Dresden, Klinikum Chemnitz, Department of Neurosurgery, Germany
[3]Technische Universität Dresden, University Hospital and Faculty of Medicine Carl Gustav Carus, Clinical Sensoring and Monitoring, Department of Anesthesia and Intensive Care, Germany
[4]Vilnius University, Faculty of Medicine, Clinic of Neurology and Neurosurgery, Lithuania
julija.jakucionyte@ff.stud.vu.lt

Infectious diseases of the central nervous system (CNS) are associated with significant morbidity and mortality. Early and precise distinction is essential to ensure appropriate therapy. However, infection cannot be clearly determined using clinical symptoms, physical examination, or routine laboratory studies alone [1]. Cerebrospinal fluid (CSF), due to its direct contact with brain tissue, reflects both normal and pathological CNS processes [2]. However, sensitive and informative methods are required to reliably evaluate CSF properties and distinguish infectious from non-infectious CNS disorders.

Infrared (IR) spectroscopy, especially when applying the attenuated total reflection (ATR) technique, is widely used for the analysis of biological materials, including biological fluids. The ATR-IR method enables rapid recording of IR absorption spectra, which reflect the molecular structure of biomolecules present in the sample, without requiring complex sample preparation. Therefore, this technique is suitable for CSF analysis aimed at identifying spectral differences in order to diagnose the type of CNS disease.

During the study, CSF samples were divided into two groups: normal (13 samples) and infectious (7 samples). To determine the differences between the ATR-IR absorption spectra of the two groups, the averages of all recorded spectra for each group were compared (Fig. 1). As CSF consists of many different components, absorption bands of different compounds may overlap, resulting in complex spectral absorption profiles. For example, at 1648 cm $^{-1}$ and 1556 cm^{-1}, individual subbands can be separated from the complex band profiles assigned to the amide I and amide II modes of the proteins. The appearance of the Amide I and Amide II bands, indicate an elevated protein concentration during CNS infection. In the spectral region of 1420-1180 cm^{-1}, higher absorption intensity, changes in the spectral contour, and a band at approximately 1450 cm^{-1} are observed in the infectious CSF spectrum. The spectral bands observed in this region are associated with lipids and proteins; therefore, their changes may be related to inflammatory processes, degradation products of cell membranes and increased protein level. In the 1200-1000 cm^{-1} region, the spectrum of infectious cerebrospinal fluid shows higher absorption intensity, especially for spectral bands at approximately 1117, 1079 and 1040 cm^{-1}. These bands are associated with phosphates, carbohydrates and lactate; therefore, the higher intensity can be explained by the elevated levels of nucleic acids, phospholipids and glucose metabolism products in infectious CSF, which is characteristic of CNS infections.

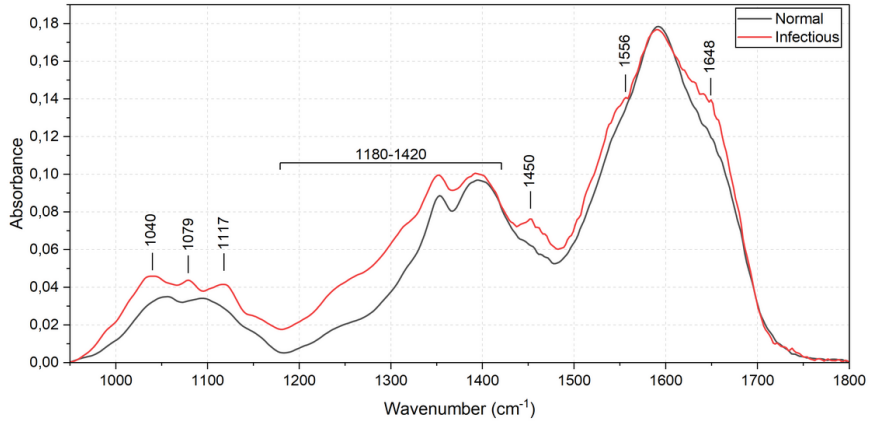


Fig. 1. Mean ATR-IR spectra of normal and infectious CSF samples

Acknowledgements

This study has been funded by the Baltic-German University Liaison Office (Project duration 01.02.2025. – 31.10.2025, agreement No. 2025/8).

[1] S. Kanjilal et al., "Diagnostic Testing in Central Nervous System Infection," Semin. Neurol., vol. 39, no. 3, pp. 297-311, 2019
[2] S. H. Howaidy, K. H. Abdulijabar, "The Biochemistry, Pathophysiology, and Clinical Importance of Cerebrospinal Fluid: A Review," Int. J. Med. Sci. Dent. Health, vol. 11, no. 11, pp. 250-255, 2025

RELAXATION OF PARAHYDROGEN-ENABLED STATES USING VARIABLE FIELD NMR SPECTROSCOPY

Izabelė Navickaitė[1], Nojus Radzevičius[2], Edvinas Orentas[2], Laurynas Dagys[1]

[1]Vilnius University, Faculty of Physics, Institute of Chemical Physics, Vilnius, Lithuania
[2]Vilnius University, Department of Organic Chemistry, Institute of Chemistry, Vilnius, Lithuania
izabele.navickaite@ff.vu.lt

Relaxation in Nuclear Magnetic Resonance (NMR) spectroscopy is a widely studied phenomenon. In addition to its practical implications for experimental duration, analysis of relaxation mechanisms allows characterisation of structure, crystal morphology and molecular dynamics. Difference in nuclear relaxation is also utilized as sophisticated contrast in Magnetic Resonance Imaging (MRI) [1].

Nuclear spin order relaxes depending on external factors such as magnetic field strength, temperature as well as internal factors such as viscosity, molecular size, nuclear interactions. Some nuclear spin-order displays exceptionally long lifetimes. For instance, nuclear magnetization converted to so-called singlet order can decay orders of magnitude longer enabling a better storage of spin-polarization in the system [1-3].

This is particularly relevant for Parahydrogen-Induced Polarization (PHIP) technique. PHIP experiments involve chemical reactions between substrates and parahydrogen gas in which 100% of nuclear spins are entangled in the nuclear singlet state. Therefore, slow relaxation leads to better accumulation of highly polarized substrates and influences practical utility of the method [2].

In this study, the relaxation properties of a compound containing three alkene groups at different magnetic fields are analysed by comparing longitudinal relaxation times T_1 to the nuclear singlet lifetimes T_s. The singlet state is acquired between the two cis-protons of the alkene group. The increasing relaxation contrast at low-fields suggests that for these derivatives PHIP experiments may be better performed at lower fields but predominantly relaxation is driven by ^1H dipolar interactions. Therefore, efficient PHIP experiments using similar molecular system may take a considerable advantage of isotope labelling to achieve higher efficiency for PHIP applications.

[1] M. H. Levitt, “Chapter 1: Long-lived States in Nuclear Magnetic resonance: An Overview,” in New Developments in NMR, 2020, pp. 1-32, doi: 10.1039/9781788019972-00001.
[2] L. Dagys, B. Ripka et al., “Geminal parahydrogen-induced polarization: accumulating long-lived singlet order on methylene proton pairs,” Magnetic Resonance, vol. 1, no. 2, pp. 175–186, Aug. 2020, doi: 10.5194/mr-1-175-2020.
[3] G. Stevanato et al., “A Nuclear Singlet Lifetime of More than One Hour in Room-Temperature Solution,” Angewandte Chemie, vol. 127, no. 12, pp. 3811–3814, Feb. 2015, doi: 10.1002/ange.201411978.

THE PHOTO-INDUCED NMR RELAXATION IN LUCIGENIN

Viltė Zairytė[1], Laurynas Dagys[1]

[1]Vilnius University, Faculty of Physics, Institute of Chemical Physics, Vilnius, Lithuania
vilte.zairyte@ff.vu.lt

Photochemical and photophysical phenomena are involved in all life and related processes such as photosynthesis, the degradation of plastics, photodegradation of drugs. Scientists are continually developing new concepts, molecules, and functional materials based on photochemical and photophysical processes. To characterize often UV-VIS spectroscopy, molecular dynamics (MD) calculations are used as well as Electron Paramagnetic Resonance (EPR) in some cases. Although photo-chemistry primarily involves excitation of electrons, the monitoring of slow dynamics can be performed by Nuclear Magnetic Resonance (NMR) which complements with insight in molecular structure and changes in molecular mobility [1].

In this work, NMR relaxation is studied in lucigenin, a known aromatic compound in a number of chemiluminescent and fluorescent assays. Some studies suggest that lucigenin and its luminescence is related to reduction of Luc2+ to radical form Luc*+ [2]. Therefore, one could expect that radical form of lucigenin should cause paramagnetic relaxation in NMR which can be observed over time.

Both longitudinal and transverse relaxation times were analysed using inversion recovery and Carr-Purcell-Meiboom-Gill (CPMG) pulse sequences. The measurements were performed after intense photo excitation using white light. Samples consisted of lucigenin and pentetic acid in variable concentrations which seemed to influence the rate at which system fully recovers back to an unexcited state. Moreover, we have noticed that the lack of oxygen considerably changes this rate. These findings favour the hypothesis that oxygen present in the solution may quench radical via chemical reaction [2] and demonstrate that NMR spectroscopy potentially can be used for analysis of similar systems.

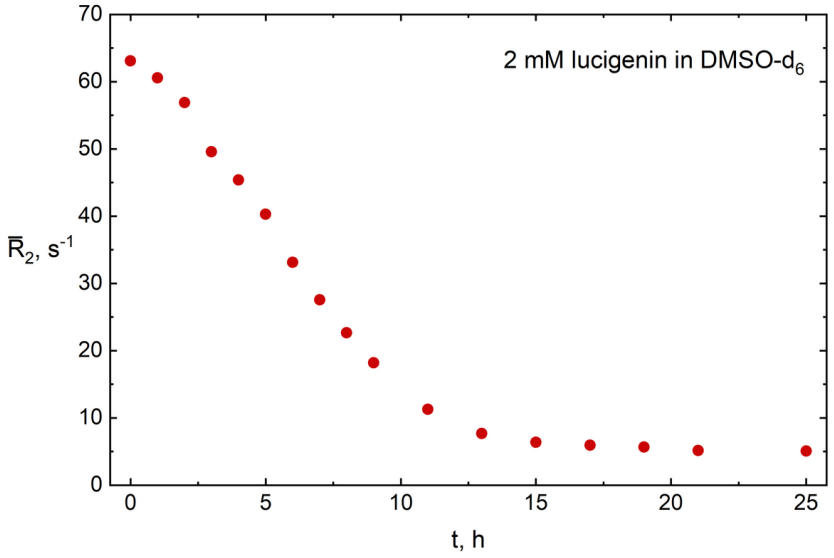


Fig. 1. Time dependence of the average transverse relaxation rate $\overline{R}_2$ of 2 mM lucigenin in DMSO – d6 following sample excitation.

[1] X. Ma and H. Tian, “Photochemistry and Photophysics. Concepts, Research, Applications. by Vincenzo Balzani, Paola Ceroni and Alberto Juris.,” Angewandte Chemie International Edition, vol. 53, no. 34, p. 8817, Jul. 2014, doi: 10.1002/anie.201405219.

[2] J. Zielonka and B. Kalyanaraman, “Small-molecule luminescent probes for the detection of cellular oxidizing and nitrating species,” Free Radical Biology and Medicine, vol. 128, pp. 3–22, Mar. 2018, doi: 10.1016/j.freeradbiomed.2018.03.032.

EVALUATION OF THE INCORPORATION OF RED CURRANT POMACE AND EXTRACT IN MEATBALLS USING CONVENTIONAL QUALITY ASSESSMENT

Laura Jūrienė[1], Jovita Jovaišaitė[1], Petras Rimantas Venskutonis[1]

[1]Kaunas University of Technology
laura.juriene@ktu.lt

Meat is a vital protein source in human diets, but its production is costly and environmentally impactful. Consequently, there is a discernible trend towards the development of meat-based products that incorporate plant-derived and unconventional ingredients such as antioxidant phytochemicals to inhibit oxidation processes and the formation of potentially carcinogenic compounds during meat processing. There is growing interest in biorefining agri-food by-products to extract nutrient-rich substances for various applications, including use in meat products. Ensuring safety and stability in meat products, given their susceptibility to microbiological contamination and oxidation, is crucial. This study aimed to determine the impact of additives on the quality and lipid oxidation of meat products. Red currant pomace was analyzed for its proximate composition, dietary fiber content and antioxidant capacity. For meat products containing additives, the color, pH, myoglobin form changes, texture profile and lipid oxidation during storage was quantified and a sensory evaluation was performed. Red currants had 25% dietary fiber, 16% protein and a lower antioxidant capacity and total phenolic content compared to the extract. The addition of red currant pomace and extract to meat products reduced their pH values. The addition of 1.5 and 3% pomace reduced their lightness (L*), yellowness (b*) and redness (a*) compared with those of the control sample. The firmness increased with the addition of the pomace, while the extract did not have any effect. Plant-based additives (pomace or extract) strongly inhibited lipid oxidation (by more than three times compared to the control) during the storage of meat products. Sensory evaluation of meat products showed that the control sample and the sample with the extract were the most acceptable for the panelists. Taken together, red currant pomace and extract may be considered promising antioxidant-containing and fibre-rich materials for use in pork meat products and may increase their nutritional quality due to red currants' health benefits.

PRODUCTION AND FREEZE-DRYING OF YOGURT ENRICHED WITH BLUEBERRY POMACE

Laura Jūrienė[1], Austėja Kacucevičiūtė[1]

[1]Kaunas University of Technology
laura.juriene@ktu.lt

The growing demand for functional foods has increased interest in incorporating plant-based by-products into dairy products. Blueberry (Vaccinium myrtillus L.) pomace is a valuable source of dietary fiber and phenolic compounds, making it a promising ingredient for yogurt enrichment. The aim of this study was to evaluate the effect of blueberry pomace (1%, 2%, and 4%) on the physicochemical, structural, antioxidant, and sensory properties of yogurt, as well as to assess the impact of freeze-drying on product acceptability.

Yogurt samples were prepared using 3.5% fat milk and thermophilic starter cultures. After fermentation, sugar and blueberry pomace were incorporated at different concentrations. The products were analyzed for pH, color, syneresis, particle size distribution, total phenolic content, and antioxidant activity (ABTS and CUPRAC methods). Freeze-dried samples were evaluated by sensory analysis.

Results showed that increasing pomace concentration reduced pH and lightness while significantly increasing total phenolic content and antioxidant activity. The yogurt with 4% pomace exhibited the highest phenolic content (573.97 µg GAE/g) and antioxidant activity, up to 40 times higher than the control. However, higher pomace concentrations increased syneresis and structural heterogeneity. Sensory evaluation indicated that freeze-dried yogurt with 4% pomace was the most acceptable to consumers.

The study demonstrates that blueberry pomace can be successfully used to produce functional yogurt with enhanced antioxidant properties, contributing to both product innovation and sustainable utilization of fruit processing by-products.

EFFECT OF PLANT-BASED ADDITIVES ON PHYSICOCHEMICAL AND SENSORY PROPERTIES OF KOMBUCHA DURING PRIMARY AND SECONDARY FERMENTATION

Laura Jūrienė[1], Mykolas Juknius[1]

[1]Kaunas University of Technology
laura.juriene@ktu.lt

Kombucha is a fermented tea beverage produced by a symbiotic culture of yeasts and acetic acid bacteria. The use of plant-based additives during secondary fermentation is a promising approach to improve its functional and sensory properties. The aim of this study was to produce kombucha beverages with different plant-based additives and to evaluate the changes in physicochemical parameters during fermentation, as well as the impact of additives on the final product quality and consumer acceptability.

Kombucha base was prepared using sweetened tea and a liquid starter culture and fermented for 18 days at 25 °C. During primary fermentation, soluble solids, relative density, pH, and titratable acidity were monitored periodically. Secondary fermentation was carried out for five days using four formulations: control, blueberry juice, pumpkin syrup, and a combination of blueberry juice and pumpkin syrup. The final beverages were evaluated for physicochemical properties and sensory characteristics.

During primary fermentation, soluble solids and density decreased, while titratable acidity increased nearly fourfold, indicating normal fermentation progress. Secondary fermentation results showed that blueberry juice significantly increased acidity, whereas pumpkin syrup exhibited a buffering effect and resulted in a milder taste. Sensory analysis revealed that plant-based additives enhanced color, aroma, and flavor intensity. The highest overall acceptability was observed in kombucha with pumpkin syrup, while blueberry kombucha was characterized by the most intense flavor and aroma.

The study demonstrates that plant-based additives can effectively modify kombucha properties and improve consumer acceptance, enabling the development of diversified functional beverages.

FOOD REFORMULATION IN PRACTICE: DEVELOPMENT OF A FUNCTIONAL YOGHURT ICE CREAM

Iris-Gertrud Jussila[1], Anette Russ[1], Susanna Helena Toom[1], Kristel Vene[1]

[1]Tallinn University of Technology, Faculty of Food Technology, Institute of Chemistry and Biotechnology, Tallinn, Estonia
irjuss@taltech.ee

Modern diets are increasingly dominated by ultraprocessed, energy-dense, nutrient-poor foods, which provide sensory satisfaction but lack dietary fiber, bioactive compounds, and microorganisms essential for gut microbiome health. The gut microbiome—a personalized ecosystem of billions of microbes—plays a key role in digestion, metabolism, immune function, and mental well-being, highlighting the importance of functional foods that support microbial diversity. Food reformulation is a key strategy for improving public health by reducing added sugars and saturated fat while increasing fiber and functional components. In the dairy dessert category, few products combine health-oriented composition with strong consumer appeal.

This study aimed to apply food reformulation principles to develop a functional ice cream under the TalTech brand that combines improved nutritional quality with strong consumer acceptance.

A rhubarb–red currant yoghurt ice cream in a waffle cone was developed in collaboration with an industrial partner. The formulation included dietary fiber and TENSIA® lactic acid bacteria. The development process involved competitive and nutritional benchmarking, prototype optimization, sensory evaluation, and large-scale consumer acceptance testing with several hundred participants.

The final product demonstrated reduced sugar content, moderate fat, higher protein, added dietary fiber, and maintained viable probiotics. Consumer responses were generally positive, indicating that reformulated ice cream can preserve sensory appeal while delivering nutritional benefits.

The project demonstrates that interdisciplinary food reformulation can create functional dairy desserts that support gut health, offer a healthier alternative to ultraprocessed products, and maintain market relevance, supporting the broader application of functional foods and food reformulation strategies in commercial dairy desserts.

VALORIZATION OF BILBERRY POMACE AS A FUNCTIONAL INGREDIENT FOR NUTRITIONALLY ENHANCED WHEATBREAD

Arnoldas Keibas[1], Laura Jūrienė[1], Petras Rimantas Venskutonis[1]

[1]Kaunas University of Technology
arnoldas.keibas@ktu.edu

Bilberries are widely appreciated for their high levels of dietary fiber and bioactive compounds, particularly phenolics and anthocyanins. Because of their short shelf life, a large portion of the harvest is processed into juices, beverages, and other products, generating significant amounts of pomace composed of skins, seeds, and pulp. Although often treated as waste, this by-product contains valuable nutrients and antioxidant compounds, making it a promising raw material for the development of functional foods.

The aim of this study was to assess the potential of bilberry (Vaccinium myrtillus L.) pomace as a functional ingredient in wheat bread and to evaluate its effects on technological and antioxidant properties. Two types of pomace were investigated: defatted pomace obtained after juice pressing and puree production, and non-defatted pomace obtained after puree production. These materials were incorporated into French-style wheat bread by replacing 5%, 7.5%, and 10% of wheat flour. Bread quality was evaluated based on loaf volume, weight, crumb porosity, and moisture content, while antioxidant activity was determined using the QUENCHER method (TPC, ABTS•+).

The incorporation of bilberry pomace significantly affected both the technological and nutritional characteristics of the bread. Moderate levels of pomace improved loaf volume, crumb porosity, and moisture retention, resulting in higher product yield. The enriched breads exhibited a darker crumb, softer texture, and a mild berry aroma that enhanced sensory properties. The most favorable quality parameters were observed in breads supplemented with 5% and 7.5% non-defatted pomace. In contrast, the addition of 10% pomace led to reduced loaf volume and crumb porosity, as well as excessive moisture, indicating that high inclusion levels may negatively affect product quality.

Pomace supplementation also increased antioxidant activity and phenolic content in the breads. The total phenolic content of the different pomace types ranged from 17.30 to 23.30 mg gallic acid equivalents (GAE)/g, with the highest values found in defatted pomace obtained after puree production.

These results demonstrate that bilberry pomace can serve as a valuable source of dietary fiber and antioxidant compounds in bakery applications. Its incorporation into wheat bread enhances nutritional value while maintaining acceptable technological and sensory properties, supporting its use in the development of functional, high value-added bakery products.

PREPARATION AND INVESTIGATION OF STABILITY OF EMULSIONS COMPOSED OF BLACKCURRANT EXTRACTS AND MODIFIED STARCH

Dovilė Liudvinavičiūtė[1], Laura Jūrienė[2], Ramunė Rutkaitė[1]

[1]Kaunas University of Technology, Faculty of Chemical Technology, Department of Polymer Chemistry and Technology, Kaunas, Lithuania
[2]Kaunas University of Technology, Faculty of Chemical Technology, Department of Food Science and Technology, Kaunas, Lithuania
dovile.liudvinaviciute@ktu.lt

Blackcurrant berries are widely recognized as a superfood, largely due to their high content of bioactive compounds. However, their short shelf life means that most berries are processed into derived products, generating substantial amounts of by-products. The valorization of blackcurrant pomace (skins and seeds) offers an opportunity to produce higher-value ingredients. In particular, extracts from blackcurrant skins are rich in anthocyanins, whereas seed extracts are a valuable source of polyunsaturated fatty acids. Anthocyanins are valuable natural pigments with strong antioxidant activity and growing application as natural colorants and functional ingredients for food industry and nutraceuticals. However, their application is constrained due to poor stability, as anthocyanin molecules readily degrade under adverse environmental conditions such as elevated temperature, light exposure, pH fluctuations, and oxygen, leading to loss of color and bioactivity during processing and storage [1].

To overcome these limitations, various encapsulation techniques have been widely explored. Among these, encapsulation of anthocyanins in emulsions with polysaccharide-derived wall materials has shown promise [2]. In addition, blackcurrant seed extracts could serve as an oil phase in emulsions. Starch sodium octenyl succinate, is known for emulsifying capability and ability to form protective matrices, also known as a safe food-grade additive and can be used to entrap anthocyanins within emulsion droplets, thus improving the stability and potential bioavailability of anthocyanins.

In this study, emulsions containing lipophilic (LE), water (WE) and ethanolic (EE) extracts of blackcurrant seeds and skins were prepared with sodium octenyl succinate starch (OSA-S) and their physical stability at different temperatures during a 28- day storage period was investigated.

Various emulsions, using rotor-stator homogenizer at 12,000 rpm for 10 min, were prepared with the following composition (w/w): 20% OSA-S, 2.5% or 5% LE, without or with 0.1% of emulsifier Tween 80 (tw) or lecithin (lec), and without and with 1% of EE or WE. Physical stability of prepared emulsions was investigated at temperatures of 4 °C and 20 °C over a 28-day period. Parameters such as particle size, polydispersity index, zeta potential, creaming index (CI) and clarification index (CLI) of the emulsion were determined after 1, 3, 8, 14, 21 and 28 days. Results showed that physical stability was highly depended on the composition of emulsion and the storage temperature. The most stable emulsion was composed of 20% OSA-S, 2.5% LE, 0.1% tw and 1% of WE and kept at 4 °C.

Acknowledgements

This project has received funding from Faculty of Chemical Technology (KTU) under the scientific project funding initiative, agreement No INP2025/2.

[1] D. Cai, X. Li, J. Chen, et al., “A comprehensive review on innovative and advanced stabilization approaches of anthocyanin by modifying structure and controlling environmental factors,” Food Chemistry, vol. 366, 130611, 2022.

[2] Y. Pan, X. Ma, J. Sun, and W. Bai, “Fabrication and characterization of anthocyanin-loaded double Pickering emulsions stabilized by β-cyclodextrin,” International Journal of Pharmaceutics, vol. 655, 124003, 2024.

NANOZYME-DRIVEN AMPEROMETRIC GLUCOSE BIOSENSOR

Aiste Krikstaponyte[1], Asta Kausaite-Minkstimiene[1]

[1]Vilnius University, Faculty of Chemistry and Geosciences, Institute of Chemistry, NanoTechnas - Center of Nanotechnology and Materials Science, Naugarduko St. 24, LT-03225 Vilnius, Lithuania.
aiste.krikstaponyte@chgf.vu.lt

A biosensor is a multicomponent analytical system designed to measure the concentration of a specific analyte. It consists of a biological recognition component selective for the analyte, a signal transducer, and a component responsible for signal processing and registration. Biosensors can be classified according to the biological recognition component employed, including enzymatic, immunological, or bacterial, as well as according to the analytical method used, such as optical, piezoelectric, or electrochemical techniques. Electrochemical biosensors are further divided into amperometric, potentiometric, conductometric, and other types. Among these, amperometric biosensors are considered one of the simplest types due to their straightforward operating principle. Amperometric enzymatic glucose biosensors based on glucose oxidase are widely used for monitoring blood glucose levels in patients with diabetes, as they are sensitive, exhibit a short response time, and do not require additional sample preparation. Nevertheless, they still exhibit some limitations, including interference effects and limited stability. To overcome these drawbacks and improve analytical performance, nanomaterials have attracted increasing attention. In particular, nanozymes, nanomaterials exhibiting enzyme-like catalytic activity, offer significant advantages over natural enzymes, as they are more stable, resistant to denaturation, less sensitive to environmental conditions, and easier to synthesize and modify.

In this work, metal nanoparticle-based peroxidase-like nanozyme was employed in the development of a nanozyme–enzyme-based glucose biosensor. The working electrode of the biosensor was fabricated by layer-by-layer modification of a graphite rod with trimetallic nickel–platinum–palladium nanoparticles, glucose oxidase, and an Aquivion® membrane. Furthermore, the electrode preparation and biosensor operating conditions were optimized, and the analytical performance of the developed biosensor was evaluated. The linear response range to glucose, as well as the limits of detection and quantification, were determined. The developed biosensor demonstrated good repeatability and reproducibility, high selectivity to glucose, and low interference from common electroactive substances. Moreover, sufficient storage stability and accurate glucose detection in real serum samples were achieved.

Acknowledgements

This research has received funding from the Research Council of Lithuania (LMTLT), agreement No. S-MIP-24-7.

GOLD NANOPARTICLE BASED DETECTION OF REDUCING SUGARS AND THEIR MIXTURES

Isaac Garcia Contreras[1], Benediktas Brasiunas[1]

[1]Vilnius University, Faculty of Chemistry and Geosciences, Institute of Chemistry, NanoTechnas – Center of Nanotechnology and Materials Science, Naugarduko st. 24, LT-03225, Vilnius, Lithuania.
isaac.contreras@chgf.stud.vu.lt

Because of their remarkable optical, electrical and magnetic characteristics nanomaterials can be applied across diferent fields of chemistry.Nanoparticles made from gold and silver are among the most widely used in organic fields such as organic catalysis, drug delivery, and biosensing due to their unique physicochemical properties and the possibility of precise size control [1].These tailorable features make it easy to adapt nanomaterials for intended applications.In particular, in the recent years gold nanoparticles have been extensively studied due to their vast properties like surface plasmon resonance, and their outstanding biocompatibility over others nanoparticle[2].Upon the reaction of gold ions(Au^{3+})with reducing agents, such as reducing sugars the synthesis and growth of gold nanoparticules takes place.This well-known reaction is employed as an analytical signal to detect the presence of sugars, and as a green synthesis method.The UV-Vis technique is a perfect fit to monitor and evalute the kinetics of such a reaction by further exploiting optical features.However,reducing sugars play a critical role in the development of the signal, and aspects such as the functional group and acyclic sugar content define the reaction's kinetics between gold atoms and the sugar itself and hence signal development [3].

This work aims to evalute the detection of reducing sugars leveraging the synthesis of AuNPs via reducing sugars.UV-vis spectroscopy was employed as technique to monitor the nanoparticle growth over time harnessing surface plasmon resonance of gold nanoparticles at 525 nm.In order to evaluate the overall reaction kinetics, parameters like sugar concentration, pH, temperature and surfactant amount were assessed to determine optimal reaction conditions. Experiments were conducted and evaluated with several reducing sugars specifically glucose, fructose, 2-deoxy-glucose, xylose, and mixtures of them.

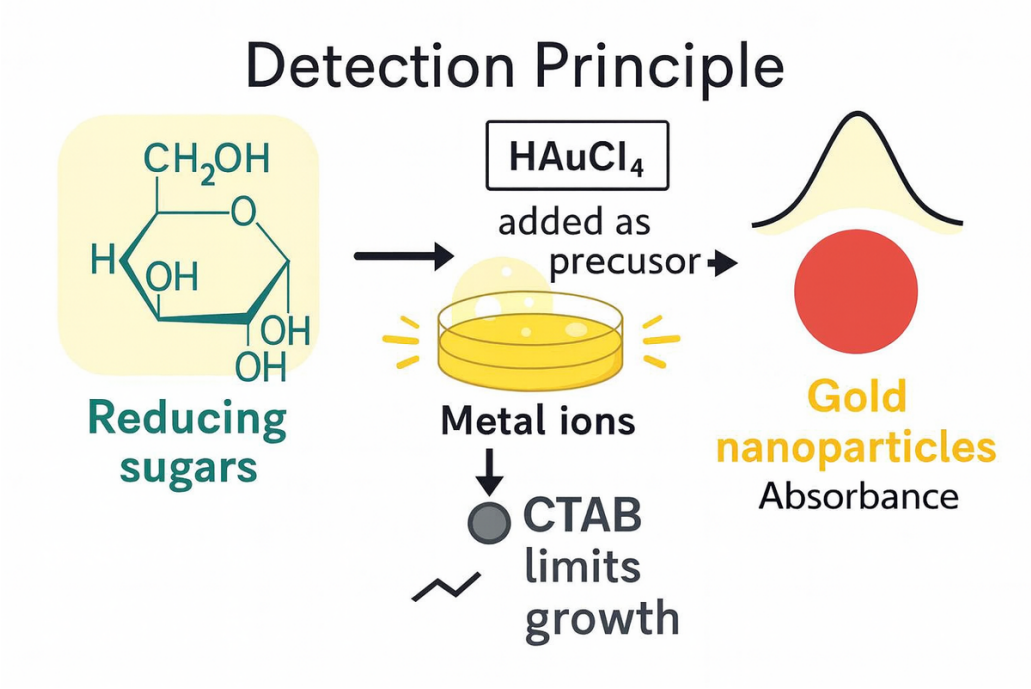


Fig. 1. Reducing sugar detection based on gold nanoparticle formation

[1] George Pasparakis. "Recent developments in the use of gold and silver nanoparticles in biomedicine". In: Wiley interdisciplinary reviews: Nanomedicine and nanobiotechnology 14.5 (2022), e1817
[2] Minakshi Das et al. "Review on gold nanoparticles and their applications". In: Toxicology and Environmental Health Sciences 3.4 (2011), pp. 193–205.
[3] Benediktas Brasiunas et al. "Gold nanoparticle based colorimetric sensing strategy for the determination of reducing sugars". In: Food Chemistry 351 (2021), p. 129238.

SYNTHESIS AND CHARACTERIZATION OF THERMO-RESPONSIVE β-CYCLODEXTRIN AND POLY(N-ISOPROPYLACRYLAMIDE) COPOLYMERS

Sofija Beatričė Dervinytė[1], Ramunė Rutkaitė[1], Miglė Savickė[1]

[1]Kaunas University of Technology, Department of Polymer Chemistry and Technology, Kaunas, Lithuania Lithuania
sofija.dervinyte@ktu.edu

In recent years, the field of polymer science has expanded rapidly, leading to the emergence of a group of polymers that respond to environmental stimuli, such as temperature. Thermo-responsive polymers are widely used due to their reversible and rapid phase transformations that occur near human body temperature, making them of great importance in the biomedical and pharmaceutical fields, especially drug delivery systems [1]. To improve the encapsulation properties of these polymers, combination copolymers are being developed.

In this work, seven β-cyclodextrin and poly(N-isopropylacrylamide) graft copolymers were synthesized by performing radical copolymerization in an aqueous medium, using potassium persulfate as the initiator. By varying the molar ratio of β-CD:NIPAAm from 1:0.25 to 1:10, copolymers with different amounts of PNIPAAm side chains were obtained. The synthesized copolymers were characterized using spectroscopic and thermogravimetric methods. Turbidity and differential scanning calorimetry studies revealed that heated aqueous solutions of the synthesized graft copolymers exhibited thermo-responsive behavior when the temperature reached 30.8–32.8 °C, at which point phase separation occurred. The steady-state fluorescence emission of pyrene, a fluorescent probe dispersed in both the copolymer solutions and dispersions, showed that the intensity ratio of the characteristic first and third peaks indicated effective immobilization of pyrene within the graft copolymer molecules in all the samples. Thermo-responsive β-cyclodextrin and poly(N-isopropylacrylamide) graft copolymers with immobilization potential and controlled phase transition in aqueous media were successfully developed, supporting their potential for controlled drug release and drug delivery applications.

[1] A. J. Rosario and B. Ma, “Stimuli-Responsive Polymer Networks: application, design, and computational exploration,” ACS Applied Polymer Materials, vol. 6, no. 23, pp. 14204–14228, Apr. 2024, doi: 10.1021/acsapm.4c00002.

SYNTHESIS AND CHARACTERIZATION OF BIO-BASED VITRIMERS

Aysu Nasiribouyony[1], Jolita Ostrauskaitė[1], Sigita Grauželienė[1]

[1]Kaunas University of Technology, Faculty of Chemical Technology, Department of Polymer Chemistry and Technology, Lithuania
aysu.nasiribouyony@ktu.lt

Polymers obtained from renewable resources have been increasingly investigated to reduce dependence on fossil feedstocks that generate a vast range of environmental impacts and attract remarkably attention due to their numerous advantages, such as biocompatibility, renewability, environmental friendliness and chemical functionality that promotes modifications for advanced materials and extraction [1,2]. Vitrimers are associative covalent adaptable networks (CANs) featuring dynamic crosslinks that enable exchange reactions at elevated temperatures, allowing network rearrangement at constant crosslink density and resulting in recyclability, repairability, self-healing, and malleability [3].

In this work, vitrimer networks were generated through photopolymerization of resin formulations incorporating bio-based monomers, with ethyl(2,4,6-trimethylbenzoyl) phenylphosphinate serving as the photoinitiator. Photocuring behavior was monitored by real-time photorheometry to assess curing kinetics and monomer-content effects. Structural verification of the vitrimers was achieved through FT-IR spectroscopy and Soxhlet extraction, whereas their thermal and mechanical performance was characterized using thermogravimetric analysis, dynamic thermomechanical analysis, and tensile testing.

The results indicated that photocuring behavior and the rheological, thermal, and mechanical properties of the vitrimers depended on the initial resin composition. Photocuring kinetics showed that higher monomer ratios in the formulations promoted longer induction periods and gelation times while simultaneously lowering viscosity, with minimal influence on the storage modulus. Vitrimers synthesized using aromatic ring containing monomers exhibited enhanced stiffness, reflecting changes in network structure and increased crosslink density. The improvement in mechanical properties after self-welding with increasing temperature highlights the repairability of vitrimers, as elevated temperatures activate dynamic bond exchange that enables network rearrangement and mechanical recovery. Moreover, the selected vitrimer displayed effective shape-memory performance, characterized by temporary shape stability and full recovery of the original shape upon heating.

Acknowledgements
This research was funded by the Research Council of Lithuania (project No. S-MIP-25-3)

Keywords: bio-based, photopolymerization, vitrimers, repairability, shape-memory

[1] E. Morici and N. Dintcheva, “Recycling of Thermoset Materials and Thermoset-Based Composites: Challenge and Opportunity,” Polymers, vol. 14, no. 19, p. 4153, Oct. 2022. [Online serial]. Available: https://doi.org/10.3390/polym14194153 . [Accessed Jan.22, 2026]
[2] Y. Xie, S. Gao, D. Zhang, C. Wang, and F. Chu, “Bio-based polymeric materials synthesized from renewable resources: A mini-review,” Resources, Chemicals and Materials, vol. 2, no. 3, pp. 223–230, Sep. 2023. [Online serial]. Available: https://doi.org/10.1016/j.recm.2023.05.001. [Accessed Jan. 22, 2026]
[3] A. V. Karatrantos, O. Couture, C. Hesse, and D. F. Schmidt, “Molecular simulation of covalent adaptable networks and vitrimers: A review,” Polymers, vol. 16, no. 10, p. 1373, May 2024. [Online serial]. Available: https://doi.org/10.3390/polym16101373. [Accessed Jan. 22, 2026]

SYNTHESIS AND INVESTIGATION OF BIO-BASED VITRIMERS DERIVED FROMRENEWABLE RESOURCES

Viltė Šereikaitė[1], Sigita Grauželienė[1], Jolita Ostrauskaitė[1]

[1]Lithuania, Kaunas University of Technology, Faculty of Chemical Technology, Department of Polymer Chemistry and Technology
vilte.sereikaite@ktu.edu

Polymers from natural sources provide ecological benefits, being renewable, accessible, relatively easy to extract, biocompatible, and non-toxic [1]. Vitrimers, a class of covalent adaptable networks with dynamic covalent bonds, allow reversible bond exchange, combining thermoset rigidity and thermal stability with stress relaxation, self-healing, reprocessability, and recyclability [2]. These features make vitrimers promising for sustainable and durable applications, including coatings, packaging, biomedical devices, and wearable systems [3].

In this study, a series of vitrimers was synthesized by photopolymerization of resins containing natural oil-based monomers and various bio-based comonomers, using ethyl-(2,4,6-trimethylbenzoyl)-phenylphosphinate as the photoinitiator. Real-time photorheometry was used to monitor the photocuring process, showing the photocuring rate and the influence of monomer content on resin properties. The chemical structure of vitrimers was confirmed by Fourier transform infrared spectroscopy and Soxhlet extraction. The thermal and mechanical properties of vitrimers were investigated by thermogravimetric analysis, dynamic thermomechanical analysis, and tensile testing.

It was determined that changes in the initial resin composition affected the photocuring rate, as well as the rheological, thermal, and mechanical properties of the vitrimers. The results of photocuring kinetics showed that monofunctional monomers exhibited a longer induction period and gelation time, although the values of these characteristics decreased in the mixed systems. In three-component formulations, increasing the amount of monofunctional monomers reduced viscosity and shrinkage, while the gelation time and induction period were extended, and the storage modulus remained almost unchanged. The presence of aromatic moieties provided rigidity to the network, while reducing intermolecular interactions, resulting in a rigid material. The self-welding experiment showed that parts of the vitrimer specimen can self-weld at elevated temperatures while maintaining the desirable mechanical properties of the original vitrimer. This phenomenon is attributed to dynamic covalent bond exchange reactions and, probably, thermal polymerization of the remaining free functional groups. This property is important for repairing materials and increasing their durability.

Acknowledgements
This research was funded by the Research Council of Lithuania (project No. S-MIP-25-3)

[1] B. Machado, S. M. Costa, I. Costa, R. Fangueiro, and D. P. Ferreira, “The potential of algae as a source of cellulose and its derivatives for biomedical applications,” Cellulose, vol. 31, no. 6, pp. 3353–3376, Mar. 2024, doi: 10.1007/s10570-024-05816-w.
[2] Y. Xu, R. Bai, L. He, J. Zhu, Z. Lei, and C. Yan, “Dynamic compressive mechanical testing and characterization of vitrimers under high and low temperatures,” Polymer, vol. 343, p. 129454, Dec. 2025, doi: 10.1016/j.polymer.2025.129454
[3] H. Qiang, J. Lv, Z. Ge, Z. Fan, Y. Zhu, and J. Du, “Renewable Biobased Vitrimers with Dual Dynamic Networks: High-Performance, Fully Recyclable, and Antimicrobial Materials for Potential Wearable Applications,” ACS Materials Letters, Jan. 2026, doi: 10.1021/acsmaterialslett.5c01380.

SYNTHESIS OPTIMISATION AND FUNCTIONAL CHARACTERIZATION OF DODECENYL SUCCINIC ANHYDRIDE AND ACETIC ANHYDRIDE MODIFIED CORN STARCHES

Muhammad Nasif[1], Ayodeji Amobonye[1], Joana Bendoraitiene[1], Laura Peciulyte[1], Remo Merijs Meri[2], Shu-Kai Yeh[3], Ramune Rutkaite[1]

[1]Kaunas University of Technology, Department of Polymer Chemistry and Technology, Lithuania
[2]Riga Technical University, Institute of Chemistry and Chemical Technology, Latvia
[3]National Taiwan University of Science and Technology, Department of Materials Science and Engineering, Taiwan
muhammad.nasif@ktu.edu

For the replacement of conventional plastics, the bioplastics based on renewable biopolymers such as natural polysaccharides are receiving increasing attention. In order to impart thermoplastic properties to polysaccharides such as starch dual chemical modification involving esterification reactionsis an effective strategy to overcome the limitations of native starch.

In this study, corn starch was first modified with dodecenyl succinic anhydride (DDSA) at two substitution levels (degree of substitution of DDSA of 0.025 and 0.072), followed by acetylation reaction using acetic anhydride, which was optimized using central composite design. The optimized acetylation conditions yielded dual-modified starches with high degree of acetylation around 2.4. Structural characterization by FTIR confirmed the introduction of ester groups, while XRD analysis indicated a partial shift toward amorphous structure correlated with the degree of acetylation. Scanning electron microscopy analysis revealed that DDSA modification helped to retain the starch granule morphology during acetylation, conferring structural resilience. Thermal analyses showed that double-modified starches exhibited improved thermal stability compared to native and succinylated starches, and DSC revealed that glass transition temperatures were dependent on both DDSA and acetyl group substitution. These findings demonstrate that dual dodecenyl succinic anhydride–acetic anhydride modification allows tuning of thermal and structural properties, offering potential for tailored thermoplastic applications such as biodegradable packaging materials.

Acknowledgements

Acknowledgements. This work was supported by the Project of Scientific Cooperation Program between Latvia, Lithuania, and Taiwan and received funding from the Research Council of Lithuania (LMTLT), agreement No S-LLT-25-4.

POLYLACTIC ACID/HYDROXYAPATITE COMPOSITE FILAMENTS FOR BONE-RELATED APPLICATIONS

Jokūbas Lukošiūnas[1], Ugnius Dijokas[1], Odeta Baniukaitienė[1]

[1]Kaunas University of Technology, Department of Polymer Chemistry and Technology, Lithuania
jokubas.lukosiunas@ktu.edu

Polylactic acid (PLA) composites reinforced with hydroxyapatite (HAp) are widely investigated for biodegradable bone-related applications. Nevertheless, achieving a uniform dispersion of HAp within filaments without compromising their extrusion processability remains a significant challenge. Uniform dispersion is critical for ensuring consistent mechanical performance and reliable 3D printing behavior. Moreover, optimizing the filler content can directly influence thermal properties, melt flow characteristics, and the overall structural integrity of printed scaffolds. The aim of this work was to develop PLA/HAp composite filaments with improved filler dispersion and suitable extrusion behavior. To achieve this, a solution-based mixing step was applied prior to filament fabrication, followed by melt extrusion of composites containing 5-30 wt% HAp. The composites were characterized using Fourier-transform infrared spectroscopy (FTIR), X-ray diffraction (XRD), scanning electron microscopy (SEM), melt flow rate (MFR) measurements, and tensile testing. SEM revealed that solution-based mixing produced a more uniform dispersion of hydroxyapatite (HAp) at low and moderate filler loadings. At higher HAp contents, filler-rich regions became more pronounced, reflecting the natural tendency of inorganic particles to agglomerate at elevated concentrations. These microstructural features correlated well with trends observed in thermal behavior, melt flow properties, and mechanical performance.

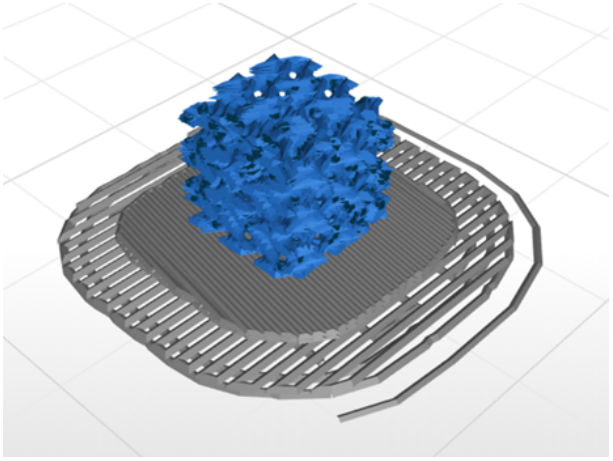


Fig. 1. Composite scaffold model for additive manufacturing

Overall, the findings provide practical guidance for fabricating PLA/HAp composite filaments and scaffolds for biomedical applications. The scaffold was printed according to the model shown in Figure 1, and among the compositions studied, PLA/HAp filaments with 20 wt% HAp exhibited the most balanced combination of structural uniformity and filament processability.

DEVELOPMENT AND RESEARCH OF THE PROPERTIES OF GELATIN-BASED HYDROGEL MATERIALS FOR TRANSDERMAL DRUG DELIVERY SYSTEMS

Daria Kuchynska[1], Olena Ishchenko[1], Ihor Okhrimenko[1], Mikael Yeganyan[1]

[1]Kyiv national university of technology and design, Department of industrial pharmacy, Kyiv, Ukraine
dkuchinska@gmail.com

The development of advanced transdermal therapeutic systems requires matrices that combine biocompatibility, mechanical integrity, and controlled release kinetics. This study focuses on the synthesis and characterization of multicomponent hydrogel films based on gelatin, polyvinyl alcohol (PVA), and hyaluronic acid (HA), crosslinked with glutaraldehyde. Gelatin provides essential biological signaling for cell adhesion and mimics the extracellular matrix, while PVA enhances the structural stability of the composite. The integration of HA, a high-molecular-weight anionic polysaccharide, aims to modulate the hydrophilicity and internal architecture of the polymer network to optimize drug diffusion. Rheological analysis of the Gelatin/PVA/HA compositions reveals non-Newtonian pseudoplastic behavior, where dynamic viscosity decreases as the shear rate increases. This characteristic is vital for the processing and application of biomedical gels. The introduction of HA significantly increases the initial viscosity in a concentration-dependent manner, indicating the formation of a more complex intermolecular network through hydrogen bonding between the HA functional groups and the base polymer chains. At high shear rates, the convergence of viscosity curves suggests the partial disruption of these physical interactions and a shift toward hydrodynamic dominance. Structural analysis through gel fraction determination shows that while glutaraldehyde effectively crosslinks the gelatin amino groups, HA remains primarily physically entrapped.

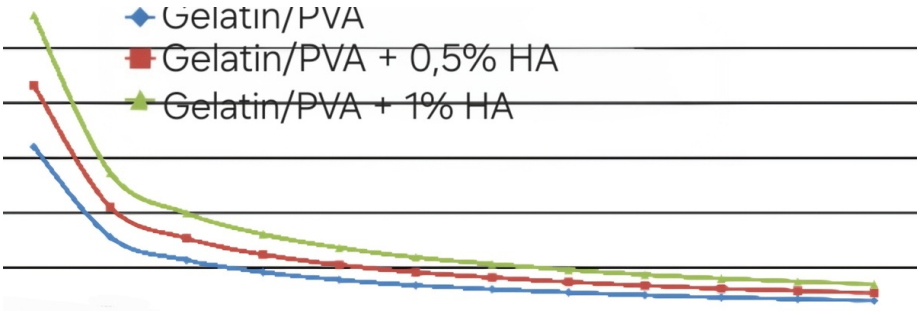


Fig. 1. Fig.1.Viscosity of hydrogel systems vs. shear rate for gelatin/PVA compositions without additives and with 0.5% and 1.0% HA.

Consequently, increasing HA content from 0.5% to 1.0% results in a proportional decrease in the gel fraction by 3–10% due to the leaching of uncrosslinked polysaccharide molecules. This structural modification directly influences the swelling behavior in phosphate-buffered saline (pH 7.4). Samples containing 0.5% HA demonstrate an optimal equilibrium swelling degree between 500% and 650%, maintaining structural stability alongside high hydrophilicity. Conversely, compositions with 1.0% HA exhibit excessive swelling exceeding 700%, leading to a degradation of mechanical properties caused by high osmotic pressure and electrostatic repulsion between polyanionic chains. The research concludes that Gelatin/PVA/HA hydrogels with a controlled HA concentration of 0.5% offer a superior balance of rheological properties, hydration capacity, and structural resilience. These materials represent a promising platform for transdermal drug delivery and wound dressing applications, allowing for the fine-tuning of API release through the adjustment of polymer ratios and crosslinking density.

Keywords: gelatin, polyvinyl alcohol, hyaluronic acid, hydrogels, polymer compositions, transdermal therapeutic systems, rheology, swelling kinetics

[1] K. J. Goudie, S. J. McCreath, J. A. Parkinson, C. M. Davidson, and J. J. Liggat, “Investigation of the influence of pH on the properties and morphology of gelatin hydrogels,” Journal of Polymer Science, vol. 61, no. 19, pp. 2316–2332, Jun. 2023, doi: 10.1002/pol.20230141.

[2] V. Dhote, S. Skaalure, U. Akalp, J. Roberts, S. J. Bryant, and F. J. Vernerey, “On the role of hydrogel structure and degradation in controlling the transport of cell-secreted matrix molecules for engineered cartilage,” Journal of the Mechanical Behavior of Biomedical Materials/Journal of Mechanical Behavior of Biomedical Materials, vol. 19, pp. 61–74, Nov. 2012, doi: 10.1016/j.jmbbm.2012.10.016.

[3] S. Bahmani, R. Khajavi, M. Ehsani, M. K. Rahimi, and M. R. Kalaee, “A development of a gelatin and sodium carboxymethyl cellulose hydrogel system for dual-release transdermal delivery of lidocaine hydrochloride,” International Journal of Biological Macromolecules, vol. 284, no. Pt 2, p. 138034, Nov. 2024, doi: 10.1016/j.ijbiomac.2024.138034.

IDENTIFICATION OF SPECTRAL MARKERS IN FOURIER TRANSFORM INFRARED SPECTRA OF BIOLOGICAL SAMPLES BY MEANS OF STATISTICAL ANALYSIS

Tautvydas Taraškevičius[1], Justinas Čeponkus[1]

[1]Vilnius University, Institute of Chemical Physics, Saulėtekio av. 3, 10257 Vilnius, Lithuania
tautvydas.taraskevicius@ff.stud.vu.lt

Fourier transform infrared (FTIR) spectroscopy is a versatile, non-destructive and non-specific vibrational spectroscopy method with great potential in biomedical research and diagnosis. FTIR spectroscopy has been successfully used in conjunction with statistical and machine learning methods for classifying different biological materials. In addition, many of those data analysis methods have the benefit of identifying the spectral regions associated with the biochemical differences between samples. However, the validity of these biomarkers is not well understood because of the complexity of vibrational spectra of biological samples, as well as the fact that usually there are no reference biomarkers to compare to. The aim of this study is to evaluate the validity of FTIR spectral biomarkers obtained by various statistical and machine learning methods and how they depend on spectral preprocessing.

For this study an experimental dataset was used containing FTIR spectra from two different types of microorganisms – bacteria and yeast – from four species: *Streptococcus pyogenes*, *Staphylococcus aureus* for bacteria and *Candida guilliermondii*, *Candida parapsilosis* for yeast. Three different methods of biomarker extraction were tested, each using one specific technique: univariate statistical hypothesis testing using the t-test; extracting loading vectors from classification models, in this case from a principal component analysis – linear discriminant classifier (PCA-LDC) model; multivariate feature selection using forward feature selection.

Based on the results, the following observations were made. First, while spectral preprocessing didn't appear to cause radical changes to the extracted biomarkers, it did qualitatively alter the interpretations of some of the spectral bands in the example spectra (see Fig. 1.). Furthermore, for the classification-based methods, these changes were observed even when the overall classification accuracy is optimal. Spectral markers obtained from the loadings of a classifier model had the advantage of indicating which spectral bands are correlated with the type of sample used. Multivariate feature selection is believed to be the most logically connected to spectral biomarker identification [1], but has the disadvantage of being computationally time consuming.

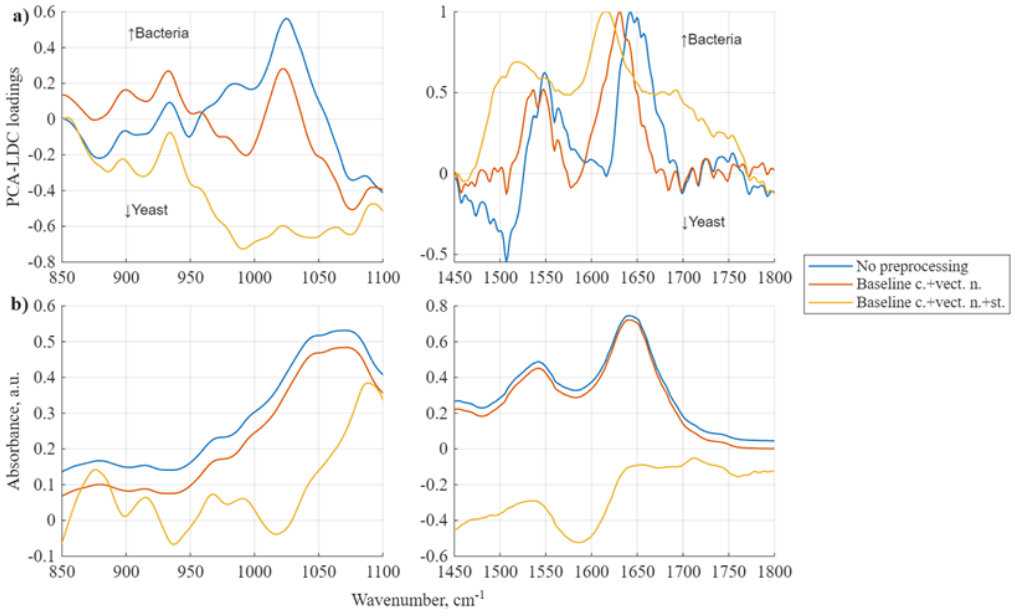


Fig. 1. a) Trained loadings (not to scale) of a PCA-LDC model classifying FTIR spectra of yeast and bacteria with different preprocessing: no preprocessing; linear baseline correction and vector normalization; linear baseline correction, vector normalization and standardization (Z-score normalization). Loadings with positive values are correlated with the spectrum belonging to bacteria and negative values – to yeast. b) Excerpts of a FTIR spectrum of bacteria that correspond to the PCA-LDC loadings in a).

[1] J. Trevisan et al., "Measuring similarity and improving stability in biomarker identification methods applied to Fourier-transform infrared (FTIR) spectroscopy," J Biophotonics, vol. 7, no. 3–4, pp. 254–265, Apr. 2014, doi: 10.1002/jbio.201300190

HYDROGENATED AND HYDROXYLATED NANODIAMONDS INTERACTING WITH WATER: A FIRST-PRINCIPLES STUDY

Naglis Januška[1], Šarūnas Masys[1]

[1]Vilnius University, Faculty of Physics, Institute of Theoretical Physics and Astronomy, Vilnius, Lithuania
naglis.januska@ff.stud.vu.lt

Diamond nanoparticles, or nanodiamonds (NDs), are perfectly suitable for nanomedicine due to the outstanding properties: exceptional biocompatibility, high carrying capacity, and a wide array of surface functional groups [1]. Studies in which NDs were used as delivery platforms for anthracyclines reveal that, compared to the efficacy of anthracyclines alone, ND-drug complexes substantially increase tumor-killing efficacy even in highly drug-resistant cases [2, 3].

One of the drawbacks of treating cancer with the help of NDs is the difficulty to track their localization and movement in vivo. Luckily, studies show that Overhauser effect-enhanced magnetic resonance imaging can in principle be used to monitor and track NDs in vivo [4]. Since this technology is based on the spin polarization transfer from unpaired electrons in NDs to protons in water hydrogen atoms, it is crucial for water molecules to be positioned as close as possible to the unpaired electrons at the ND surface. Theoretically, this can be examined by the first-principles calculations which determine whether paramagnetic defects with unpaired electrons can act as water attraction centers. It is also important to assess how the position of paramagnetic defect in ND and the functionalization of ND surface influence the interaction process.

In this work, water interactions with the dangling bonds (DBs) at the surface of NDs were modelled using semiempirical tight-binding GFN2-xTB [5] method via the automated DOCKER algorithm available in the ORCA quantum chemistry package [6]. The ND used in calculations was C35, which has 3 unique DB states at its surface. Two surface functionalizations were chosen – hydrogenation and hydroxylation. Overall, it was revealed that water prefers to interact with DBs at the hydrogenated surface, while in case of hydroxylation water tends to form bonds elsewhere.

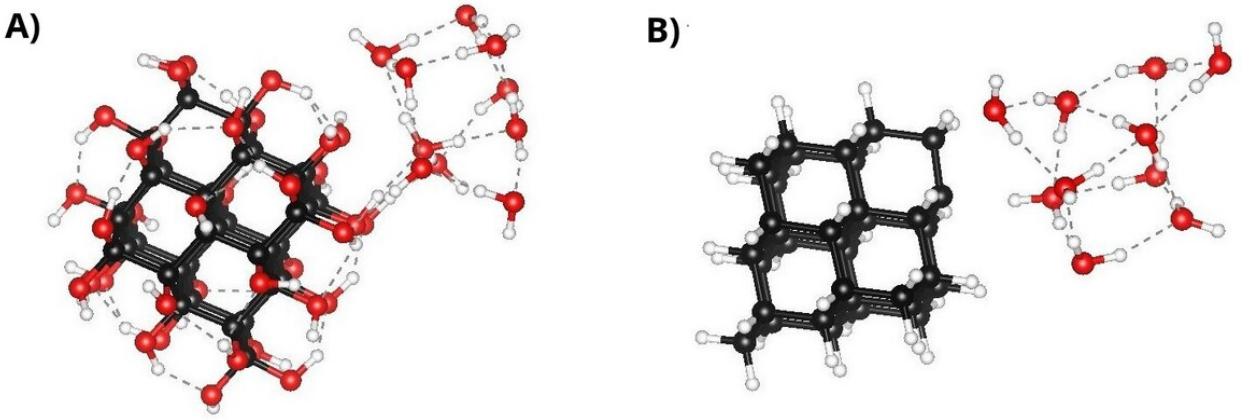


Fig. 1. Figure A) ND with OH-functionalized surface interacting with water.
Figure B) ND with H-functionalized surface interacting with water

[1] N. Nunn et al., “Nanodiamonds in biomedical applications,” Curr. Opin. Solid State Mater. Sci., vol. 21, p. 1, 2017.
[2] E. K. Chow et al., “Nanodiamond therapeutic delivery,” Sci. Transl. Med., vol. 3, p. 73ra21, 2011.
[3] X. Wang et al., “Nanodiamond–drug complexes for cancer therapy,” ACS Nano, vol. 8, p. 12151, 2014.
[4] D. E. J. Waddington et al., “Nanodiamond-enhanced Overhauser magnetic resonance imaging,” Nat. Commun., vol. 8, p. 15118, 2017.
[5] C. Bannwarth et al., “GFN2-xTB—An accurate and broadly parametrized self-consistent tight-binding quantum chemical method,” J. Chem. Theory Comput., vol. 15, p. 1652, 2019.
[6] F. Neese, “The ORCA quantum chemistry program package,” WIREs Comput. Mol. Sci., vol. 15, p. e70019, 2025.

AGN-ENHANCED STAR FORMATION

Martynas Laužikas[1], Kastytis Zubovas[1,2]

[1]Center for Physical Sciences and Technology, Vilnius, Lithuania
[2]Vilnius University, Astronomical Observatory, Vilnius, Lithuania
martynas.lauzikas@ftmc.lt

Active Galactic Nuclei (AGNs) are supermassive black holes at the centers of galaxies that actively consume matter and release enormous amounts of energy. AGNs flicker in bursts that each last approximately 0.1 million years [1], with quiescent periods in between. Despite low duty cycle behavior, the cumulative energy released across multiple AGN episodes is enough to disrupt the galaxies. However, most of the energy escapes as radiation, and the remaining energy fraction that does interact with the gas forms AGN wind-driven outflows [2] that redistribute gas in the galaxies.

Previous research has shown that fast outflows (moving faster than 500 km/s) can sweep gas out of the galactic bulge. They remove this raw material for star formation and simultaneously disrupt molecular clouds quenching the ongoing star formation in the galaxy. However, the effects of slower outflows remain poorly understood. It is unclear whether star formation is always suppressed or whether it might sometimes be triggered. Recent studies have provided evidence that outflows can trigger star formation - outflows and young stars are found co-spatially with comparable radial velocities, suggesting enhanced star formation in action [3]. The conditions required for such enhanced star formation to occur and kinematic properties of such newborn stars are the central questions my research addresses.

To investigate these questions, AGN-driven outflows and their interaction with the galactic environment are simulated. The Smoothed Particle Hydrodynamics method is used to model several AGN episodes and to track how the multiphase outflow propagates through the central kiloparsec of the galaxy. A dual nature of AGN feedback is confirmed by the simulations. As the outflow expands through the bulge, the surrounding material is swept up and compressed, and fast-moving stars are formed within the moving gas streams. Therefore, star formation can be stimulated rather than suppressed by AGN-driven outflows. On the other hand, molecular clouds are disrupted and gas is expelled from the galactic centre by powerful outflows, and the fuel needed for future star formation is removed.

The relative importance of these competing feedback mechanisms will be quantified. It will be shown how the spatial distribution of newly formed stars and the radial velocity dispersion of the stellar population are affected (see Fig.1). Understanding this balance is crucial for explaining how galaxies co-evolve with their central supermassive black holes and what effect is produced on the scatter of the observed $M - \sigma$ relation [4].

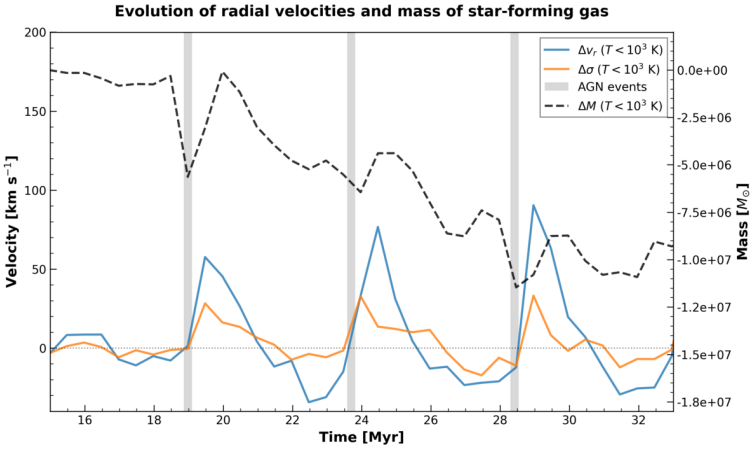


Fig. 1. Differences in radial velocity (Δv_r), velocity dispersion ($\Delta\sigma$), and molecular mass (ΔM) between models with and without AGN activity for cold gas ($T < 10^3$ K). Gray shaded regions indicate AGN event periods.

[1] K. Schawinski, M. Koss, S. Berney, and L. Sartori, "Active galactic nuclei flicker: an observational estimate of the duration of black hole growth phases of ~1e5 years," arXiv.org, May 25, 2015. https://arxiv.org/abs/1505.06733
[2] A. King and K. Pounds, "Powerful Outflows and Feedback from Active Galactic Nuclei," Annual Review of Astronomy and Astrophysics, vol. 53, no. 1, pp. 115–154, Apr. 2015, doi: 10.1146/annurev-astro-082214-122316.
[3] Maiolino, R., "Star formation inside a galactic outflow", Nature, vol. 544, no. 7649, pp. 202–206, 2017. doi:10.1038/nature21677.
[4] D. Merritt and L. Ferrarese, "TheM•-Σ relation for supermassive black holes," The Astrophysical Journal, vol. 547, no. 1, pp. 140–145, Jan. 2001, doi: 10.1086/318372.

NON-LINEAR DYNAMICS AND PRIMORDIAL BLACK HOLE FORMATION DURING KINATION

Cheng Cheng[1], Panagiotis Giannadakis[2], Lucien Heurtier[2], Eugene Lim[2]

[1]Center for Physical Sciences and Technology (FTMC), Department of Fundamental Research, Lithuania
[2]King\'s College London, Department of Physics, Theoretical Particle Physics and Cosmology Group, United Kingdom
cheng.cheng@ftmc.lt

The physics of the early universe may have included phases that differ from the standard radiation-dominated picture, with important consequences for the growth of fluctuations and the formation of compact objects. One such phase is kination, in which the expansion is driven by the kinetic energy of a scalar field. During kination, the evolution of density perturbations is altered in a scale-dependent way, potentially leading to strong non-linear effects and gravitational collapse.

In this work, the evolution of the scalar perturbations during a kination-dominated era was studied by solving the fully non-linear Einstein equations using numerical relativity. The dynamics of both sub-horizon and super-horizon perturbations were followed to identify the regimes where linear theory remains valid and where non-linear behaviour becomes essential.

Sub-horizon modes were well described by perturbative methods. Super-horizon perturbations were found to undergo significant non-linear growth, and in some cases lead to gravitational collapses and the formation of primordial black holes. Physical initial conditions required for such collapses were found numerically. These conditions have significant implications for primordial black hole production and post-inflationary reheating scenarios. The results highlight the importance of non-linear gravitational dynamics in non-standard cosmological epochs and provide a concrete framework for assessing the observable consequences.

Acknowledgements

We would like to thank the GRChombo team (http://www.grchombo.org/) and to DiRAC@Durham facility managed by the Institute for Computational Cosmology on behalf of the STFC DiRAC HPC Facility (www.dirac.ac.uk) under DiRAC RAC15 Grant ACTP316. The equipment was funded by BEIS capital funding via STFC capital grants ST/P002293/1, ST/R002371/1 and ST/S002502/1, Durham University and STFC operations grant ST/R000832/1. This work also used the DiRAC Data Intensive service at Leicester, operated by the University of Leicester IT Services, which forms part of the STFC DiRAC HPC Facility (www.dirac.ac.uk). The equipment was funded by BEIS capital funding via STFC capital grants ST/K000373/1 and ST/R002363/1 and STFC DiRAC Operations grant ST/R001014/1. DiRAC is part of the National e-Infrastructure.

Keywords: Numerical Relativity, Kination, Primordial Black Hole, Early Universe Cosmology, Non-Linear Dynamics

[1] C. Cheng, P. Giannadakis, L. Heurtier, and E. A. Lim, “Non-linear Dynamics and Primordial Black Hole Formation During Kination,” arXiv.org, 2025. https://arxiv.org/abs/2507.19166 (accessed Feb. 07, 2026).

A DISFORMAL AFFAIR: HOW DARK MATTER MIMICS LORENTZ VIOLATION

Guillem Domenech[1,2], Apostolos Tsampodimos[1,5], Nathaniel Sherrill[1], Alexander Ganz[1], Fiona Kirk[1,3,4]

[1]Institute for Theoretical Physics, Leibniz University Hannover, Appelstraße 2, 30167 Hannover, Germany
[2]Max Planck Institute for Gravitational Physics, Albert Einstein Institute, 30167 Hannover, Germany
[3]Physikalisch-Technische Bundesanstalt, Bundesallee 100, Braunschweig, 38116, Germany
[4]Department of Particle Physics and Astrophysics, Weizmann Institute of Science, Rehovot, Israel 7610001
[5]Center for Physical Sciences and Technology, Sauletekio 3, 10257 Vilnius, Lithuania
apostolos.tsampodimos@ftmc.lt

In this work the impact of general disformal metric transformations on fermions was studied, which shift the gravitational metric by an additional rank-2 tensor. This tensor can in principle be constructed from scalar-field gradients, vector fields, or field-strength contractions. It was shown that this transformation results in the conventional Dirac action being modified by additional kinetic and axial-current couplings that are quadratic in the shifted field. When the field sourcing the metric shift takes on a nontrivial background value, apparent Lorentz-violating effects can result, which were identified as terms in an effective field theory. Assuming the well-motivated cases of scalar and vector ultralight dark matter, it was demonstrated that experimental tests of rotation and boost violation imply constraints on the additional kinetic coupling. Even under conservative assumptions, the constraints for vector ultralight dark matter are extremely stringent.

STAR CLUSTERS SIZE EVOLUTION IN M31

Karolis Daugevičius[1], Eimantas Kriščiūnas[1], Rima Stonkutė[1], Vladas Vansevičius[1]

[1]Center for Physical Sciences and Technology (FTMC), Department of Fundamental Research, Vilnius, Lithuania
karolis.daugevicius@ftmc.lt

Most newborn stars form in star clusters (SCs), making them fundamental building blocks of their host galaxies. The properties of SC populations, such as the mass–radius relation (MRR), encode information on cluster structure at birth and effects of subsequent dynamical evolution. Observational constraints on the MRR, its evolution, and environmental dependence, provide crucial tests of star and cluster formation models, as well as theories of SC dynamical evolution. The Andromeda galaxy (M31) is ideal for such studies due to its proximity, large cluster sample, and similarity to the Milky Way.

This study is based on observations obtained with the Hubble Space Telescope as part of the Panchromatic Hubble Andromeda Treasury (PHAT) survey [1]. We use the M31 SC catalogue [2], which provides cluster physical (age, mass, and extinction) and structural parameters derived for 1922 SCs from integrated aperture photometry.

Within the first ∼50 Myr, SCs undergo rapid expansion (Fig. 1a-d), with the mean half-light radius, R_h, increasing by a factor of two (from ∼0.7 pc to ∼1.4 pc). We attribute this early expansion to stellar evolution effects, including massive star feedback, supernovae, and mass loss due to the expulsion of primordial gas.

For clusters older than ∼100 Myr (Fig. 1e-i), a shallow MRR emerges, with $R_h \propto M^{0.17\pm0.01}$. This slope is shallower than those reported for more distant galaxies ($R_h \propto M^{0.25-0.33}$; [3]). A comparison with the other Local Group galaxies reveals power-law indices ranging from 0.06 to 0.50. These results suggest a possible environmental dependence of the MRR. Furthermore, the observed relation for M31 SCs is significantly shallower than the initial MRR predicted from the cluster formation models ($R_h \propto M^{1/2}$ or $M^{1/3}$; [4]), but steeper than the equilibrium relation resulting from the combined effects of tidal shocks and two-body relaxation on cluster evolution ($R_h \propto M^{1/9}$; [5]). These discrepancies indicate that current theoretical models may be missing important physical processes relevant to cluster evolution in disc environments.

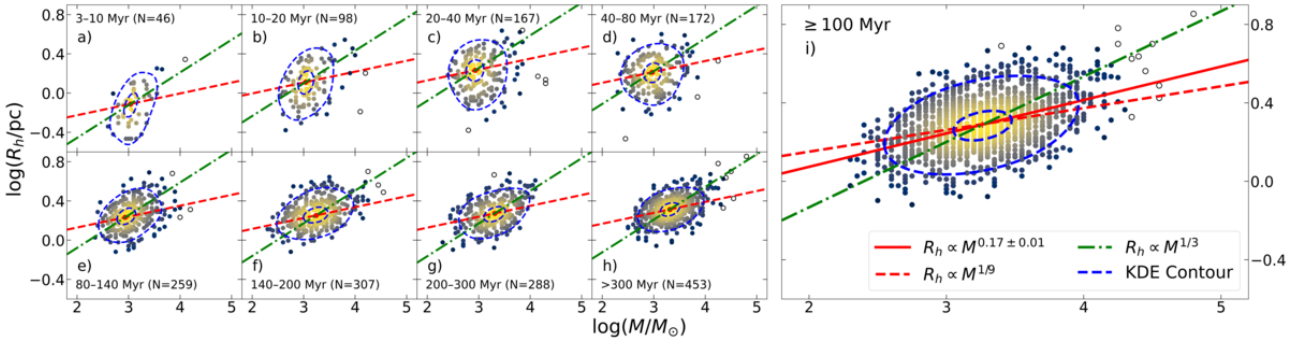


Fig. 1. Mass-radius relation for the M31 disc star clusters. Panels a-h) show cluster distribution in mass-R_h space for age intervals. Panel i) – R_h versus mass for clusters older than 100 Myr; solid red line marks best-fit MRR power-law. In all panels open circles mark 3σ-clipped points.

Acknowledgements

This project has received financial support from the Research Council of Lithuania (LMTLT), agreement No S-MIP-24-98.

[1] J. J. Dalcanton et al., "The Panchromatic Hubble Andromeda Treasury," The Astrophysical Journal Supplement Series, vol. 200, no. 2, p. 18, May 2012, doi: 10.1088/0067-0049/200/2/18.

[2] E. Kriščiūnas et al., "Deriving physical parameters of unresolved star clusters. X. The M 31 disc PHAT clusters," Astronomy & Astrophysics, submitted, in revision.

[3] G. Brown and O. Y. Gnedin, "Radii of young star clusters in nearby galaxies," Monthly Notices of the Royal Astronomical Society, vol. 508, no. 4, pp. 5935–5953, Oct. 2021, doi: 10.1093/mnras/stab2907.

[4] N. Choksi and J. M. D. Kruijssen, "On the initial mass–radius relation of stellar clusters," Monthly Notices of the Royal Astronomical Society, vol. 507, no. 4, pp. 5492–5506, Sep. 2021, doi: 10.1093/mnras/stab2514.

[5] M. Gieles and F. Renaud, "If it does not kill them, it makes them stronger: collisional evolution of star clusters with tidal shocks," Monthly Notices of the Royal Astronomical Society Letters, vol. 463, no. 1, pp. L103–L107, Jul. 2016, doi: 10.1093/mnrasl/slw163.

KINEMATICS OF GALACTIC OUTFLOWS IN A TURBULENT ENVIRONMENT

Veronika Mykhailenko[1], Kastytis Zubovas[1]

[1]Vilnius University, Faculty of Physics, Institute of Theoretical Physics and Astronomy, Vilnius, Lithuania
veronika.mykhailenko@ff.stud.vu.lt

Supermassive black holes at galaxy centers power Active Galactic Nuclei (AGN), releasing huge amounts of energy into the interstellar medium (ISM). AGN-driven outflows regulate star formation and shape galaxy evolution [1, 2]. Understanding outflow propagation through turbulent environments is essential for interpreting observations and validating AGN feedback models. Direct observations remain limited because of long evolutionary timescales, requiring numerical simulations.

This work investigates the kinematics of AGN-driven outflows in a turbulent interstellar medium through hydrodynamic simulations using the Smoothed Particle Hydrodynamics (SPH) method with the Gadget - 3 code [3]. Analysis was conducted using Python - based tools, which involved calculating radial velocities to identify outflowing gas, decomposing energy budgets, constructing phase diagrams, and locating shock fronts.

The results show a transition from kinetic to thermal energy dominance after AGN activation, confirming energy-driven outflow dynamics. The velocity dispersion increases from background ($\sim$50 - 70 km s^{-1}) to 200 - 300 km s^{-1} in shocks, with peaks at $\sim$1500 km s^{-1} in dense clump collisions. The outflow develops a multi-phase structure ($10^4 - 10^8$ K), and non-spherical filamentary morphology shaped by turbulence.

These findings agree with theoretical predictions, demonstrating that SPH simulations capture essential AGN feedback physics in turbulent galactic environments [4].

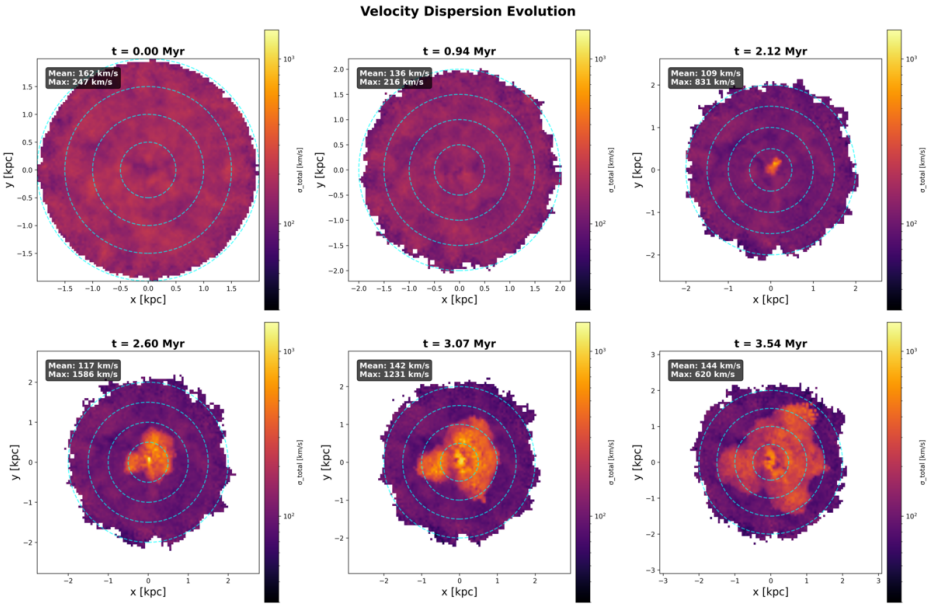


Fig. 1. Two-dimensional maps of total velocity dispersion σ_{total} in the x–y plane at six times. The mean and maximum dispersion values are indicated in each panel. High-dispersion regions (yellow/white) trace the shock front. The AGN activates at $t = 2.0$ Myr.

[1] A. King, "Black Holes, Galaxy Formation, and the M BH - relation," The Astrophysical Journal, vol. 596, no. 1, pp. L27–L29, Sep. 2003, doi: 10.1086/379143.

[2] K. Zubovas and A. King, "CLEARING OUT a GALAXY," The Astrophysical Journal Letters, vol. 745, no. 2, p. L34, Jan. 2012, doi: 10.1088/2041-8205/745/2/l34.

[3] V. Springel, "The cosmological simulation code gadget-2," Monthly Notices of the Royal Astronomical Society, vol. 364, no. 4, pp. 1105–1134, Nov. 2005, doi: 10.1111/j.1365-2966.2005.09655.x.

[4] C. Cicone et al., "Massive molecular outflows and evidence for AGN feedback from CO observations," Astronomy and Astrophysics, vol. 562, p. A21, Dec. 2013, doi: 10.1051/0004-6361/201322464.

EXTENDING GAIA XP SPECTRA BASED CLASSIFICATION OF HOT SUBDWARFS WITH MULTIPLE MACHINE-LEARNING APPROACHES AND AUXILIARY STELLAR DATA

Urtė Gedvilaitė[1], Erika Krikščiūnaitė[1], Aidas Medžiūnas[1], Kristupas Pribušauskas[1]

[1]Vilnius University, Faculty of Mathematics and Informatics, Institute of Applied Mathematics, Vilnius, Lithuania
kristupas.pribusauskas@mif.stud.vu.lt

This work is built on the Gaia XP spectra based machine-learning framework for hot subdwarf identification and classification introduced by Ambrosch et al. [1] Using this analysis as a reference point, the performance and complementarity of several additional machine-learning algorithms, including random forests, gradient-boosted trees, support-vector machines, and neural-network–based models, applied to Gaia XP spectral representations, are explored. Gaia XP spectra data remain the primary input, while the feature space is expanded to include selected astrometric and photometric parameters from Gaia as well as external information for stars of interest from complementary surveys.

Classification behaviour across algorithms is compared, robustness against known contaminants is assessed, and how alternative models and added data sources affect class boundaries is examined. Performance is evaluated using standard metrics and visualisation techniques, enabling direct comparison with the reference study. The results demonstrate how combining Gaia XP spectra with diverse machine-learning methods and auxiliary stellar data can refine classification confidence and uncover additional candidate objects for further investigation.

Keywords: hot subdwarfs, classification, machine learning, GAIA, spectra

[1] M. Ambrosch et al., “Detection of hot subdwarf binaries and sdB stars using machine learning methods and a large sample of Gaia XP spectra,” arXiv (Cornell University), Jan. 2026, [Online]. Available: http://arxiv.org/abs/2601.21727

BRST SYMMETRY AND GRIMUS-NEUFELD MODEL

Nojus Danyla[1], Simonas Draukšas[1]

[1]Vilnius University, Faculty of Physics, Institute of Theoretical Physics and Astronomy, Saulėtekio av. 9, Vilnius, Lithuania, LT-10222
nojus.danyla@gmail.com

It is not always clear whether intermediate theoretical quantities that lead to physical observables are gauge-dependent. One of the tools to analyze gauge dependence is the Nielsen identities [1], a generalisation of Slavnov-Taylor identities [2], [3], based on BRST symmetry [4]–[6]. Nielsen identities allow the gauge dependence to be expressed in terms of correlation functions involving BRST sources that are associated with the gauge parameters.

In this research, Nielsen identities are applied in the Grimus-Neufeld model [7], which explains small neutrino masses, specifically to investigate the gauge dependence of the neutrino self-energies in the mass eigenstate basis. For this, the Grimus-Neufeld model must be BRST quantized, and the BRST Lagrangian for the neutrino and Higgs sectors must be derived, which is required for calculating the Nielsen identity for the neutrino self-energy. To ensure that the implementation of BRST quantization is consistent, the gauge dependence of the neutrino self-energy is analyzed in two independent ways: 1) by deriving and calculating the Nielsen identity using the BRST Lagrangian; 2) by explicitly calculating the neutrino self-energy and taking the derivatives with respect to the gauge parameters.

The goal of this work is to automate the calculation of the Nielsen identity for the neutrino self-energy using *Mathematica*. The required theoretical framework, methodology, and results are presented.

[1] N. K. Nielsen, “On the gauge dependence of spontaneous symmetry breaking in gauge theories,” Nuclear Physics B, vol. 101, no. 1, pp. 173–188, Dec. 1975, doi: 10.1016/0550-3213(75)90301-6.
[2] A. A. Slavnov, “Ward identities in gauge theories,” Theoretical and Mathematical Physics, vol. 10, no. 2, pp. 99–104, Feb. 1972, doi: 10.1007/bf01090719.
[3] J. C. Taylor, “Ward identities and charge renormalization of the Yang-Mills field,” Nuclear Physics B, vol. 33, no. 2, pp. 436–444, Nov. 1971, doi: 10.1016/0550-3213(71)90297-5.
[4] C. Becchi, A. Rouet, and R. Stora, “The abelian Higgs Kibble model, unitarity of the S-operator,” Physics Letters B, vol. 52, no. 3, pp. 344–346, Oct. 1974, doi: 10.1016/0370-2693(74)90058-6.
[5] C. Becchi, A. Rouet, and R. Stora, “Renormalization of gauge theories,” Annals of Physics, vol. 98, no. 2, pp. 287–321, Jun. 1976, doi: 10.1016/0003-4916(76)90156-1.
[6] I. V. Tyutin, “Gauge invariance in field theory and statistical physics in operator formalism,” arXiv (Cornell University), Dec. 2008, doi: 10.48550/arxiv.0812.0580.
[7] W. Grimus and H. Neufeld, “Radiative neutrino masses in an SU(2) × U(1) model,” Nuclear Physics B, vol. 325, no. 1, pp. 18–32, Oct. 1989, doi: 10.1016/0550-3213(89)90370-2.

ELECTROCATALYTIC PERFORMANCE OF PdCo/Cu AND PdNi/Cu COATINGS TOWARD WATER SPLITTING AND OXYGEN REDUCTION REACTIONS

Raminta Stagniūnaitė[1], Virginija Kepenienė[1], Zita Sukackienė[1], Loreta Tamašauskaitė-Tamašiūnaitė[1]

[1]Center for Physical Sciences and Technology, Department of Catalysis, Vilnius, Lithuania
raminta.stagniunaite@ftmc.lt

Electrochemical water splitting and the oxygen reduction reaction are key processes for sustainable hydrogen and oxygen production and efficient operating of fuel cells in alkaline media, respectively. Pd based bimetallic catalysts supported on copper have emerged as promising alternatives to Pt due to their tunable electronic structure, improved activity, and reduced noble metal loading [1]. In this context, PdCo/Cu and PdNi/Cu catalysts have been shown to exhibit synergistic effects between Pd and 3d metals. These effects enhance the adsorption-desorption balance of hydrogen and oxygenated intermediates on the catalyst surface, rendering them attractive as multifunctional electrode materials capable of driving both water splitting and fuel cell systems. Therefore, studying PdCo/Cu and PdNi/Cu coatings offers valuable insights into structure–activity relationships and supports the development of efficient, durable, and cost effective electrocatalysts for next generation energy conversion devices [2].

In this study Co and Ni were electrolessly deposited on the copper surface to form Co/Cu and Ni/Cu coatings by using an electroless deposition bath at the temperature of 40 °C and morpholine borane as the reducing agent. 1 mmol $PdCl_2$ solution was used for deposition of Pd nanoparticles. The composition and morphology of prepared PdCo/Cu and PdNi/Cu coatings were characterized by Field Emission Scanning Electron Microscopy (FESEM) method. The electrocatalytical properties of the PdCo/Cu and PdNi/Cu catalysts toward the hydrogen evolution, oxygen evolution and oxygen reduction reactions were investigated in an alkaline medium by using linear sweep voltammetry.

Among the catalysts studied, PdCo/Cu displayed the lowest HER overpotential of 227 mV at a current density of 10 mA cm^{-2} (25 °C), outperforming PdNi/Cu which required 291 mV.

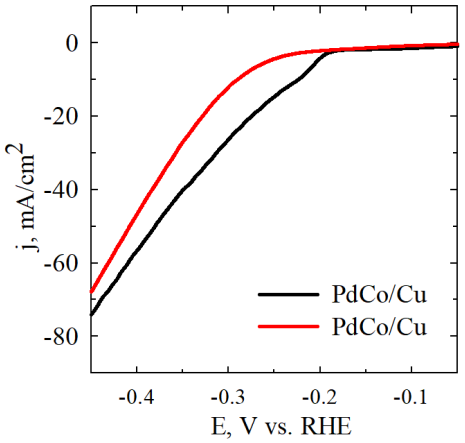


Fig. 1. HER polarization curves in a Ar-saturated 1 M KOH solution at scan rate of 2 mV s^{-1}; 25 °C.

[1] C. Renugadevi and L. Cindrella, "Nanoscale Pd-Co alloy supported on dual heteroatoms doped carbon – An efficient electrocatalyst for hydrogen evolution and oxygen reduction reactions.," Journal of Alloys and Compounds, vol. 1022, p. 179990, Mar. 2025, doi: 10.1016/j.jallcom.2025.179990.

[2] H. Amber et al., "PD-Modified COP and COFEP catalysts as efficient bifunctional catalysts for water splitting," Catalysts, vol. 15, no. 11, p. 1035, Nov. 2025, doi: 10.3390/catal15111035.

INSIGHTS INTO THE STABILISATION MECHANISM OF δ-Bi_2O_3-LIKE PHASE TO LOW TEMPERATURE BY CONFINEMENT OF NANOGRAINS IN GLASSY MATRIX

Maciej Nowagiel[1], Jerzy E. Garbarczyk[1], Marek Wasiucionek[1], Tomasz K. Pietrzak[1]

[1]Warsaw University of Technology, Faculty of Physics, Poland
maciej.nowagiel.dokt@pw.edu.pl

δ-Bi_2O_3 is a candidate material for oxide ion conducting membranes in intermediate-temperature fuel cells. This phase is, however, stable only in the high-temperature range (>730 °C). We observed the confinement of δ-like nanograins in an amorphous matrix down to room temperature [1]. There are a few working hypotheses to explain this phenomenon:

- stabilisation due to the nanometric size of grains and the influence of the surrounding glassy matrix,
- incorporation of glass-forming dopants into the crystal structure,
- formation of non-stoichiometric Bi_2O_{4-x} by Bi^{5+} ions.

The studied materials are based on the ternary bismuthate glassy system Bi_2O_3-Al_2O_3-SiO_2 [2-3]. Crystallisation of the glass has been studied by in situ high-temperature XRD. We investigated local atomic composition using TEM and EDS measurements. In combination with MAS NMR studies, it gave a consistent view of the location of the Si and Al dopants. XANES studies of the Bi L_3 absorption edge were carried out to determine whether Bi^{5+} ions are present in the material, which can be an alternative explanation for the stabilisation of the fluorite-type phase. In this work, I will present our current view on the subject, which was recently published in Ceramics International [4].

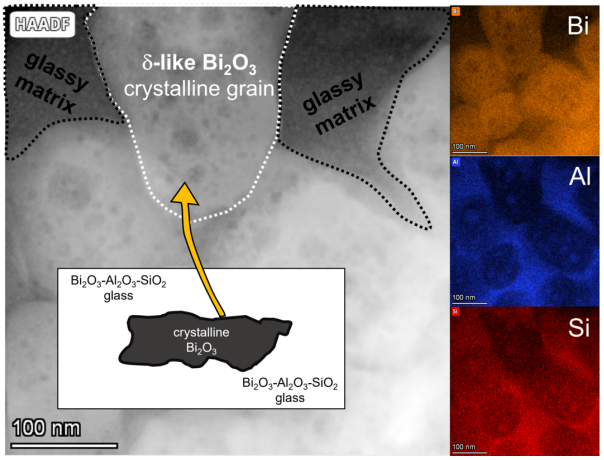


Fig. 1. A TEM image (HAADF mode) of a powdered glass-ceramics sample under study, together with elemental maps of Bi, O, Al, and Si (EDS). The inset shows schematically the microstructure of the sample.

Acknowledgements

This research was funded by POB TechMat of WUT within the IDUB program, and by the National Science Centre (NCN), Poland, in frames of a grant Preludium BIS 2 no. 2020/39/O/ST5/00897. NMR experiments were funded by the European Union's Horizon 2020 program, grant agreement No. 731019 (EUSMI).

[1] T. K. Pietrzak, J. E. Garbarczyk, and M. Wasiucionek, "Stabilization of the δ-Bi2O3-like structure down to room temperature by thermal nanocrystallization of bismuth oxide-based glasses," Solid State Ionics, vol. 323, pp. 78–84, May 2018, doi: 10.1016/j.ssi.2018.05.021.

[2] T. K. Pietrzak, A. Jarocka, C. Jastrzębski, T. Płociński, M. Wasiucionek, and J. E. Garbarczyk, "Facile and reproducible method of stabilizing Bi2O3 phases confined in nanocrystallites embedded in amorphous matrix," Scientific Reports, vol. 11, no. 1, p. 19145, Sep. 2021, doi: 10.1038/s41598-021-98435-5.

[3] V. Vlasenko, M. Nowagiel, M. Wasiucionek, and T. K. Pietrzak, "Stabilization of δ-like Bi2O3 Phase at Room Temperature in Binary and Ternary Bismuthate Glass Systems with Al2O3, SiO2, GeO2, and B2O3," Materials, vol. 17, no. 16, p. 4023, Aug. 2024, doi: 10.3390/ma17164023.

[4] M. Nowagiel et al., "Towards a deeper insight into the stabilisation mechanism of δ-Bi2O3-like phase to low temperature by confinement of nanograins in glassy matrix," Ceramics International, Jan. 2026, doi: 10.1016/j.ceramint.2026.01.182.

NANOSECOND LASER THERMAL DEWETTING OF THIN FILMS FOR PLASMONIC NANOPARTICLE FABRICATION AND COLOR ENGINEERING

Vita Petrikaitė[1], Ilja Ignatjev[2], Aušra Selskienė[3], Algirdas Selskis[3], Evaldas Stankevičius[1]

[1]Center for Physical Sciences and Technology, Department of Laser Technologies, Vilnius, Lithuania
[2]Center for Physical Sciences and Technology, Department of Organic Chemistry, Vilnius, Lithuania
[3]Center for Physical Sciences and Technology, Department of Characterization of Materials Structure, Vilnius, Lithuania
vita.petrikaite@ftmc.lt

Laser-induced dewetting of thin metal films is an efficient and versatile method for generating plasmonic nanoparticles directly on glass substrates. The technique is based on localized thermal heating of continuous thin metal films using nanosecond pulsed laser irradiation, which induces film breakup and self-organization into nanoparticles without the need for chemical reagents. This approach enables clean, scalable, and spatially controlled fabrication of plasmonic nanostructures with tunable optical properties.

In bimetallic Au–Ag systems, laser-induced dewetting allows precise control over nanoparticle composition, morphology, and size distribution by adjusting the initial film thicknesses and stacking order. As a result, localized surface plasmon resonance (LSPR) peaks can be tuned across a broad visible spectral range from 400 nm to 530 nm, with resonance widths varying between 40 nm and 130 nm. The obtained hybrid nanoparticles demonstrate strong surface-enhanced Raman scattering (SERS) performance, achieving enhancement factors exceeding 10^5 at a 532 nm excitation wavelength. The absence of chemical contaminants makes these laser-fabricated substrates particularly attractive for sensitive molecular detection and sensing applications.

Beyond noble bimetallic systems, the laser-induced dewetting method can be further optimized through substrate and interlayer engineering. Introducing a thin titanium adhesion layer beneath gold films significantly influences the dewetting dynamics, promoting the formation of smaller and more uniformly distributed nanoparticles. This morphological modification broadens the achievable plasmonic color palette beyond the intrinsic limitations of gold thin films [1], enabling vivid, tunable colors with improved film adhesion and durability [2]. By varying laser parameters such as pulse energy, scanning speed, repetition rate, and hatch spacing, high-resolution plasmonic color beyond the limited palette of gold thin films can be produced in a controlled and reproducible manner.

Overall, nanosecond laser-induced thermal dewetting of thin metal and multilayer films represents a robust, environmentally friendly, and cost-effective platform for fabricating plasmonic nanoparticles. The demonstrated versatility of this method opens pathways toward large-area SERS substrates [3,4], plasmonic color printing, anti-counterfeiting technologies [5], photonic devices, and other advanced optical applications [6].

Keywords: gold, silver, nanoparticles, laser, LSPR, dewetting

[1] N. Li, P. Zhao, and D. Astruc, "Anisotropic gold nanoparticles: synthesis, properties, applications, and toxicity," Angewandte Chemie International Edition, vol. 53, pp. 1756-1789, 2014.
[2] R. Liudvinavičius, A. Selskis, and E. Stankevičius, "Titanium adhesion layer influence on the formation of hybrid lattice plasmon structures via laser-direct writing," Optics & Laser Technology, vol. 175, p. 110807, 2024.
[3] P. Mulvaney, M. Giersig, and A. Henglein, "Electrochemistry of multilayer colloids: preparation and absorption spectrum of gold-coated silver particles," The Journal of Physical Chemistry, vol. 97, pp. 7061-7064, 1993.
[4] A. G. Da Silva, T. S. Rodrigues, T. J. Slater, E. A. Lewis, R. S. Alves, H. V. Fajardo, et al., "Controlling size, morphology, and surface composition of AgAu nanodendrites in 15 s for improved environmental catalysis under low metal loadings," ACS Applied Materials & Interfaces, vol. 7, pp. 25624-25632, 2015.
[5] V. Caligiuri, A. Patra, M. P. De Santo, A. Forestiero, G. Papuzzo, D. M. Aceti, et al., "Hybrid Plasmonic/Photonic Nanoscale Strategy for Multilevel Anticounterfeit Labels," ACS Applied Materials & Interfaces, vol. 13, pp. 49172-49183, 2021/10/20 2021.
[6] M. Song, D. Wang, S. Peana, S. Choudhury, P. Nyga, Z. A. Kudyshev, et al., "Colors with plasmonic nanostructures: A full-spectrum review," Applied physics reviews, vol. 6, 2019.

ATR-FTIR SCREENING OF INDUSTRIAL PVC

Vaidas Gasiūnas[1], Elena Jasiūnienė[2]

[1]Kaunas University of Technology, Lithuania
[2]Kaunas University of Technology, Prof. K. Baršauskas Ultrasound Research Institute, Lithuania
vaidas.gasiunas@ktu.lt

Industrial poly(vinyl chloride) (PVC) materials used in cable insulation and sheathing can differ due to supplier/feedstock variability and recycling-related changes, complicating incoming quality control and material traceability. This work evaluates Attenuated Total Reflectance–Fourier Transform Infrared spectroscopy (ATR-FTIR) as a rapid screening tool to capture chemical fingerprints and support grouping of industrial PVC samples. ATR-FTIR spectra were analysed using chemometric methods, including Principal Component Analysis (PCA) and supervised classification, to separate predefined groups (e.g., supplier/feedstock origin and material state such as original, scrap, and reprocessed). Future work will integrate ultrasonic guided waves (UGW) to link chemical variation with structural/functional indicators.

SIMULATION OF PURCELL-ENHANCED SPIN RELAXATION

Aistė Peštenytė[1], Gediminas Usevičius[1], Jūras Banys[1], John J.L. Morton[2,3], Mantas Šimėnas[1]

[1]Vilnius University, Faculty of Physics, Vilnius, Lithuania
[2]University College London, London Centre for Nanotechnology, United Kingdom
[3]University College London, Department of Electronic & Electrical Engineering, United Kingdom
aiste.pestenyte@ff.stud.vu.lt

As quantum technologies advance, electron spin resonance (ESR) is becoming a valuable tool for spin-based quantum device development due to its ability to directly probe spin states. Such ESR measurements often require mK temperatures to minimize thermal noise, enhance spin polarization, and maintain long coherence times. At such low temperature, the spin-lattice relaxation time (T_1) increases significantly, making ESR experiments impractical. To address these challenges, superconducting microwave resonators with high Q-factors are often used. Such resonators amplify microwave magnetic field experienced by the spins, boosting the spin-resonator coupling. An increase in coupling strength leads to the Purcell relaxation effect, which significantly accelerates spin relaxation enabling ESR experiments [1].

In this work, the Bloch equations are solved for an inversion recovery pulse sequence, where spin relaxation is limited by the Purcell effect in the presence of a straight inductor of a superconducting microwave resonator. Therefore, the impact of spatially varying coupling and driving magnetic fields on spin relaxation can be analyzed. New insights into Purcell-limited spin relaxation in microresonator-based measurements are provided by this approach, and a foundation for further studies is established.

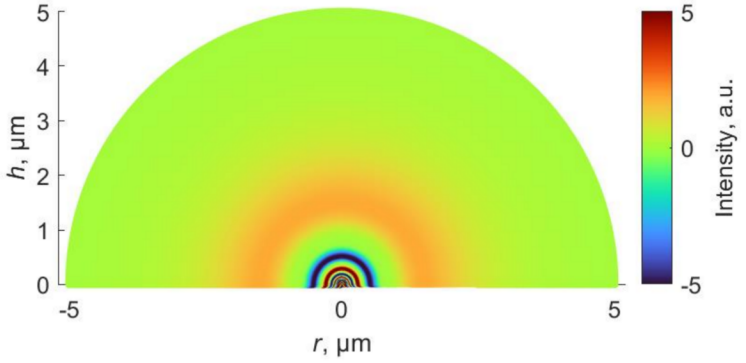


Fig. 1. Spatial distribution of the inversion recovery signal.

Acknowledgements
This work was funded by the European Union (ERC, Strong-ESPRESSO, 101162021)

[1] A. Bienfait, J. Pla, Y. Kubo, et al., “Reaching the quantum limit of sensitivity in electron spin resonance,” Nature, vol. 531, pp. 74–77, 2016.

X-BAND BIMODAL MICROWAVE CAVITY FOR EPR SPECTROSCOPY

Ignas Pocius[1], Vidmantas Kalendra[1], Jūras Banys[1], Mantas Šimėnas[1]

[1]Vilnius University, Faculty of Physics, Institute of Applied Electrodynamics and Telecommunications, Lithuania
ignas.pocius@ff.vu.lt

Electron paramagnetic resonance (EPR) spectroscopy is a widely used technique for studying paramagnetic centres in materials ranging from solids to proteins [1]. The method is based on the quantum nature of the electron spin, which causes splitting of its energy levels in the magnetic field. The essence of EPR spectroscopy is the excitation of the quantum transitions between these levels and the detection of the microwave absorption using microwave resonators [2].

Here, design and characterization of a microwave resonator with two orthogonal modes, which was modelled and manufactured based on the design proposed in Ref. [3] (see Figure 1) is presented. In such bimodal microwave resonators, one of the modes excites the spins in the sample, while the other mode is used to read out the EPR signal. In addition, this resonator geometry prevents the resonator ringing effect [3-5] and can be used to suppress thermal microwave noise greatly enhancing EPR sensitivity.

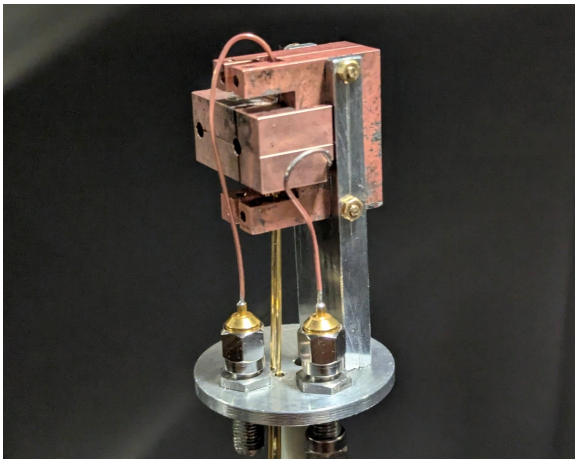


Fig. 1. Manufactured bimodal microwave resonator with tuning screws and microwave antennas.

[1] A. Lund, M. Shiotani, and S. Shimada, Principles and applications of ESR spectroscopy. Springer Netherlands, 2011.
[2] J. A. Weil and J. R. Bolton, Electron Paramagnetic Resonance: Elementary Theory and Practical Applications, 2nd ed. Hoboken, NJ, USA: John Wiley & Sons, 2007.
[3] G. A. Rinard, R. W. Quine, J. McPeak, L. Buchanan, S. S. Eaton, and G. R. Eaton, “An X-Band Crossed-Loop EPR Resonator,” Applied Magnetic Resonance, vol. 48, no. 11–12, pp. 1219–1226, Dec. 2017.
[4] G. A. Rinard, R. W. Quine, B. T. Ghim, S. S. Eaton, and G. R. Eaton, “Easily Tunable Crossed-Loop (Bimodal) EPR Resonator,” J. Magn. Reson., Ser. A, vol. 122, no. 1, pp. 50–57, Sep. 1996.
[5] C. Mailer, H. Thomann, B. H. Robinson, and L. R. Dalton, “Crossed TM110 bimodal cavity for measurement of dispersion electron paramagnetic resonance and saturation transfer electron paramagnetic resonance signals for biological materials,” Review of Scientific Instruments, vol. 51, no. 12, pp. 1714–1721, 1980.

GLUCOSE BIOSENSOR FOR THE DETERMINATION OF CADMIUM IONS VIA ENZYME ACTIVITY INHIBITION: EFFECT OF GOLD NANOSTRUCTURES ON THE ANALYTICAL SIGNAL

Katazyna Blazevic[1], Natalija German[2], Asta Kausaite-Minkstimiene[1,2], Almira Ramanaviciene[1,2]

[1]Vilnius University, Faculty of Chemistry and Geosciences, Institute of Chemistry, NanoTechnas - Center of Nanotechnology and Materials Science, Naugarduko str. 24, LT-03225 Vilnius, Lithuania
[2]State Research Institute Centre for Innovative Medicine, Department of Immunology and Bioelectrochemistry, Santariskiu str. 5, LT-08406 Vilnius, Lithuania
katazyna.blazevic@chgf.vu.lt

Cadmium (Cd^{2+}) is a highly toxic heavy metal that poses serious risks to human health and the environment, making rapid and reliable detection essential [1]. Electrochemical glucose biosensors based on glucose oxidase (GOx) are a well-established analytical platform. In this study, the same concept was applied to Cd^{2+} detection by exploiting the inhibitory effect of cadmium on GOx activity. The Cd^{2+} sensing principle is based on monitoring the decrease in electrochemical response during glucose oxidation in the presence of the soluble redox mediator phenazine methosulfate (PMS).

To enhance sensitivity toward Cd^{2+} induced inhibition, graphite rod (GR) electrodes were modified with gold nanomaterials: dendritic gold nanostructures (DAuNSs) and 13 nm gold nanoparticles (AuNPs), following GOx immobilization on the surface. The performance of the biosensor based on GR/DAuNSs/GOx electrode was compared with GR/AuNPs/GOx and GR/GOx (no nanomaterials). In all cases, Cd^{2+} decreased GOx activity, as evidenced by a reduced electrochemical signal, with the strongest signal suppression observed with DAuNS-modified electrodes. These results demonstrate that DAuNSs significantly improve the response of GOx-based biosensors for monitoring Cd^{2+} contamination, with potential applicability to other toxic metal ions.

Keywords: glucose oxidase, electrochemical biosensor, cadmium, inhibition, gold nanoparticles, dendritic gold nanostructures, PMS

[1] L. Anchidin-Norocel, G. Gutt, E. Tataranu, and S. Amariei, “Electrochemical sensors and biosensors : effective tools for detecting heavy metals in water and food with possible implications for children ’ s health,” Int. J. Electrochem. Sci., vol. 19, no. February, 2024, doi: 10.1016/j.ijoes.2024.100643

THE DEVELOPMENT OF REAGENTLESS GLUCOSE BIOSENSORS BASED ON GOLD NANOSTRUCTURES IN THE ABSENCE AND PRESENCE OF POLYPYRROLE

Natalija German[1], Anton Popov[1,2], Almira Ramanaviciene[1,2]

[1]State Research Institute Centre for Innovative Medicine, Department of Immunology and Bioelectrochemistry, Vilnius, Lithuania
[2]Vilnius University, Institute of Chemistry, Faculty of Chemistry and Geosciences, NanoTechnas—Center of Nanotechnology and Materials Science, Vilnius, Lithuania
natalija.german@imcentras.lt

The interest of the application of accurate, inexpensive, sensitive, selective, miniature and rapid response electrochemical biosensors and biofuel cells, in the clinical and pharmaceutical chemistry, drug discovery, food and environmental monitoring has been increased in the last few decades [1]. The blood glucose concentration is the major of diagnostic criterion for the diabetes mellitus due the accurate and chronic effects of diabetes and is a useful tool for the patient monitoring [2]. Enzymatic (glucose oxidase (GOx)) electrochemical biosensors containing redox inorganic, organic or metal-organic mediators are characterized by high current density and stability due the incensement of FAD-GOx rate catalysed glucose electrooxidation [2]. Dendritic gold nanostructures (DGNS) are considering as one of novel nanomaterials and are presenting great promise in electronics and biomedical applications [3]. Polypyrrole (Ppy) has been receiving great interest in clinical and environmental practises due efficient transfer of electric charge and flexibility in available chemical structure [1].

The main aim of the present study was to choose more suitable redox mediator (ferrocenecarboxylic acid, 1,10-phenathroline-5,6-dione (PD), N,N,N',N'-tetramethylbenzidine or tetrathiafulvalene) for the reagentless glucose enzymatic biosensors based on graphite rod (GR) electrode modified by electrochemically synthesized DGNS development and to investigate the influence of Ppy layer on those biosensors, to evaluate the analytical characteristics and to applicate the analytical system to determine glucose levels in the sample of serum.

It was investigated that enzymatic biosensor based 3 layer-by-layer PD and GOx (GR/DGNS/PD*/GOx, Fig. 1) was more suitable for the determination of glucose. To improve analytical characteristics of developed biosensor the surface of GR/DGNS/PD*/GOx electrode was modified 5 h by Ppy. Glucose biosensors based on GR/DGNS/PD*/GOx or GR/DGNS/PD*/GOx/$Ppy_{(5h)}$ electrodes were characterized by the linearity until 16.5 and 39.0 mmol L^{-1}, the sensitivity of 13.4 and 3.03 μA mM^{-1} cm^{-2}, the limit of detection of 0.114 and 0.683 mmol L^{-1}, the repeatability for 29.4 mmol L^{-1} glucose concentration of 9.10 and 10.3%, respectively. The Ppy-based glucose biosensor was characterized by good storage stability (until 9 days) and successful practical application in the sample of serum (97.5–98.0% of recovery).

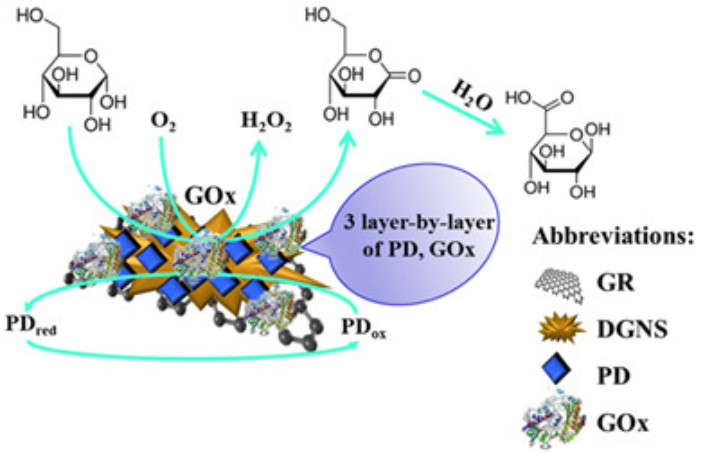


Fig. 1. The scheme of enzymatic biosensor based on GR/DGNS/PD*/GOx electrode.

[1] A. L. Galant, R. C. Kaufman, and J. D. Wilson. "Glucose: Detection and analysis." Food Chemistry, vol. 188, pp. 149–160. doi: 10.1016/j.foodchem.2015.04.071 (accessed Apr. 2015).
[2] A. Heller and B. Feldman. "Electrochemical glucose sensors and their applications in diabetes management." Chemical Reviews, vol. 108, no. 7, pp. 2482–2505. doi: 10.1021/cr068069y (accessed May 2008).
[3] A. Ramanaviciene, N. German, A. Kausaite-Minkstimiene, and A. Ramanavicius. "Glucose biosensor based on dendritic gold nanostructures electrodeposited on graphite electrode by different electrochemical methods." Chemosensors, vol. 9, no. 8, p. 188. doi: 10.3390/chemosensors9080188 (accessed Jul. 2021).

POLYMERIC SCAFFOLDS FOR ARTIFICIAL MUSCLE TISSUE-CULTURED MEAT

Bramos Murthy[1]

[1]Kaunas University of Technology, Faculty of Chemical Technology, Department of Environmental Engineering, Kaunas, Lithuania
bramos.murthy@ktu.edu

Raising animals for human consumption is a significant contributor to greenhouse gas emissions. In terms of greenhouse gas emissions, water consumption, and land use, cultured meat is likely to be more efficient than conventional meat [1]. The progress of edible scaffolds for cultivated meat in large scale-production is a major attraction. Electrospinning technology is recognised for it being an efficient, economical, and environmentally friendly technique to produce ultra-fine biopolymer fibres [2]. The work uses zein as a bio-polymer for electrospinning. Zein, a hydrophobic mixed protein derived from maize that is primarily composed of these proteins, is recommended for use as a mostly non-allergenic proteinaceous material in the food industry, according to a thorough analysis of alternatives [3]. The fibrous structure of electrospun fibres can mimic the natural ECM components due to the favourable properties of the main biomaterial mentioned above, making it easy to produce and suitable for expansion [4].

To make electrospinning solutions of 25 w/v from zein and other additives, including polyethylene oxide (PEO), sodium chloride (NaCl), glucose, and glycerol, the solutions were dissolved in an ethanol-water solvent mixture of varying ratios. The electrospinning process was carried out at 24.5 °C and approximately 38% relative humidity with an applied voltage of 14 kV. The effects of solution concentration and processing parameters on fibre production and morphology were thoroughly examined.

The initial results indicate promising outcomes under the solution concentration of 70:30 v/v ethanol-water mixture with the suitable parameters, including flow rate 6 (ml/h), distance from needle to collector 10 cm. This specific combination improves uniformity, reduced bead formation, minimized dripping of solvent while ejecting from the needle, demonstrating optimized spinnability and consistency. Thus, the existing studies are currently being thoroughly scrutinized and optimized, while their potential utilization will be examined for cell culture studies to be carried out later.

[1] A. M. M. N. Alam et al., “Scaffolding fundamentals and recent advances in sustainable scaffolding techniques for cultured meat development,” Food Research International, vol. 189, p. 114549, May 2024, doi: 10.1016/j.foodres.2024.114549.

[2] M. S. Islam, A. N. Naz, M. N. Alam, A. K. Das, and J. H. Yeum, “Electrospun poly(vinyl alcohol)/silver nanoparticle/carbon nanotube multi-composite nanofiber mat: Fabrication, characterization and evaluation of thermal, mechanical and antibacterial properties,” Colloids and Interface Science Communications, vol. 35, p. 100247, Feb. 2020, doi: 10.1016/j.colcom.2020.100247.

[3] F. A. Momany, D. J. Sessa, J. W. Lawton, G. W. Selling, S. a. H. Hamaker, and J. L. Willett, “Structural characterization of A-Zein,” Journal of Agricultural and Food Chemistry, vol. 54, no. 2, pp. 543–547, Dec. 2005, doi: 10.1021/jf058135h.

[4] W. Mao, S. Lee, S.-R. Kim, K.-N. Kim, and H. S. Yoo, “Electrospun nanohybrid hydrogels for enhanced differentiation of myoblasts,” Journal of Industrial and Engineering Chemistry, vol. 80, pp. 838–845, Jul. 2019, doi: 10.1016/j.jiec.2019.07.012.

IN VITRO MODELLING PREPARATION OF POLYMERIC HYDROGEL SCAFFOLDS SYSTEM FOR HUMAN JOINT DISEASE.

Aleena Ijaz[1], Edvinas Krugly[1]

[1]Kaunas University of Technology, Faculty of Chemical Technology, Department of Environmental Technology, Kaunas, Lithuania
aleenaijaz370@gmail.com

Osteoarthritis is one of the most painful human joint diseases, characterized by joint tissue interactions, inflammation, and biomechanical cartilage degradation. Conventional in vivo models do not support combined biochemical and biomechanical conditions of joint tissues and also lack physiological relevance. This study aims to create an integrated polymeric scaffold and hydrogel system to construct an in vivo model for human joint disease. Melt electro-writing (MW) technique is used for the fabrication of poly (ε-caprolactone) (PCL) scaffolds to check the pore size and fiber alignment of scaffolds. Alginate-based hydrogels were prepared for human joint tissue modelling because of their biocompatibility properties, and the requirements are also less harsh. To produce hydrogels through crosslinking, calcium chloride (CaCl) is crosslinked with alginate. Different concentrations of alginate were checked for crosslinking in 15-30 min at room temperature. The compatibility of these hydrogels was checked with and without polymeric scaffolds, and their morphology and porosity. The results vary with concentration, but do not show major changes. However, as the concentration increased, the hardness also increased. Currently, methyl cellulose-based hydrogels are prepared with a thermal gelation procedure. Different concentrations of screening gels are used for gelation to create a reproducible gel. Nowadays, check the mechanical strength and water absorption of these hydrogels. To check structural properties through characterization methods, which include optical microscopy, SEM, and ImageJ analysis. To improve the hydrophilicity and cell adhesion of the surface modification of scaffolds using melt electrospinning (ME). And FTIR analysis to check the crosslinking results for the formation of hydrogels. The purpose of polymeric-hydrogel scaffolds systems is to shift away from traditional single-material systems and toward hybrid biomaterials that better mimic complex tissue interactions.

Keywords: Osteoarthritis; polymeric scafflods; hydrogel; melt electro-writing; alginate.

FIRST-PRINCIPLES INSIGHTS INTO THE DESIGN OF MOLECULARLY IMPRINTED POLYPYRROLE FOR DETECTION OF CLORSULON

Enayat Mohsenzadeh[1], Vilma Ratautaite[1], Arunas Ramanavicius[1,2]

[1]State Research Institute Center for Physical Sciences and Technology (FTMC), Department of Nanotechnology, Sauletekio Ave. 3, Vilnius LT-10257, Lithuania
[2]Vilnius University (VU), Faculty of Chemistry and Geosciences, Institute of Chemistry, Department of Physical Chemistry, Naugarduko str. 24, LT-03225 Vilnius
enayat.mohsenzadeh@ftmc.lt

Molecularly imprinted polymers (MIPs) are artificial receptors designed to selectively recognise a specific target molecule. They are created by polymerising functional monomers in the presence of the analyte, resulting in a polymer matrix containing cavities complementary to the target, also called template [1]. The synthesis of MIPs includes the selection of suitable functional monomer and solvent, polymerisation, removal of the template, and evaluation of MIP sensitivity and selectivity through rebinding. These steps are time-consuming and costly, and the complexity of experiments requires deeper insights to overcome the challenges [2]. Semi-empirical metadynamics and density functional theory (DFT) were employed to calculate the molecular modelling properties. The electronic and physicochemical properties of polypyrrole conformers under αβ- and ββ-coupling of monomers were studied. The optimal imprinting conditions, including the best solvent and optimised monomers to template ratio, were calculated. The sensing mechanism of clorsulon through binding sites was described with density of states (DOS), UV-vis spectroscopy, and charge transfer analyses of optimised molecular systems. The study showed the binding sites had different sizes and densities, indicating variation of binding affinities and surface areas. At the optimised condition calculated, imprinted polypyrrole shows properties that promise a real-time sensing empowered with improved selectivity and sensitivity towards clorsulon.

[1] E. Mohsenzadeh et al., “Application of computational methods in the design of molecularly imprinted polymers (review),” TrAC Trends in Analytical Chemistry, vol. 171, p. 117480, Feb. 2024, doi: 10.1016/j.trac.2023.117480.
[2] G. Zvirzdine et al., “Electrochemical Salicylic Acid Sensor Based on Molecularly Imprinted Polypyrrole,” ACS Appl. Mater. Interfaces, vol. 17, no. 41, pp. 57475–57485, Oct. 2025, doi: 10.1021/acsami.5c11951.

SABRE HYPERPOLARIZATION OF BIOLOGICALLY RELEVANT LIGANDS

Aura Matuliūkštytė[1], Laurynas Dagys[1]

[1]Vilnius University, Faculty of Physics, Institute of Chemical Physics, Vilnius, Lithuania
aura.matuliukstyte@ff.vu.lt

Nuclear magnetic resonance (NMR) spectroscopy is widely used to study molecular structure and dynamics, but its sensitivity is limited by low nuclear spin polarization [1]. To improve sensitivity, stronger magnetic fields or hyperpolarization techniques are applied. One such technique is Signal Amplification by Reversible Exchange (SABRE), which uses parahydrogen as a source of spin order and enables fast signal enhancement without chemical modification of the target molecule. The efficiency of SABRE depends on reversible binding and chemical exchange at the metal catalyst center [1,2].

In this work, SABRE hyperpolarization of imidazole derivatives is studied. Imidazole is an aromatic heterocycle group often found in many antibiotic drugs and pharmaceutical compounds. In addition, the higher affinity to the iridium catalyst makes imidazole derivatives suitable SABRE target as it is demonstrated by the recent high spin-polarization achievements on antibiotic metronidazole [3]. This potentially enables fast NMR studies at millimolar concentrations for nitrogen-containing drugs, allowing single-scan NMR detection [1-3].

However, SABRE efficiency is strongly influenced by reversible ligand binding, exchange rates and by the selected method for polarization transfer from parahydrogen to the target [1–3]. In this work, SABRE was performed on a small variety of imidazole derivatives at room temperature by using a variety of different SABRE polarization protocols operating at low magnetic fields. The chemical dynamics were optimized by adjusting the co-ligand concentration in the solution. The SABRE efficiency was estimated by the achieved 15N signal enhancement compared to conventional NMR. The summarized SABRE performance will potentially serve as an important guide for future studies and lead towards novel pharmaceutical assays using hyperpolarized NMR.

[1] D. A. Barskiy, S. Knecht, A. V. Yurkovskaya, and K. L. Ivanov, “SABRE: Chemical kinetics and spin dynamics of the formation of hyperpolarization,” Progress in Nuclear Magnetic Resonance Spectroscopy, vol. 114–115, pp. 33–70, May 2019, doi: 10.1016/j.pnmrs.2019.05.005.

[2] T. Theis et al., “Microtesla SABRE enables 10% nitrogen-15 nuclear spin polarization,” Journal of the American Chemical Society, vol. 137, no. 4, pp. 1404–1407, Jan. 2015, doi: 10.1021/ja512242d.

[3] M. Fekete, F. Ahwal, and S. B. Duckett, “Remarkable Levels of 15N Polarization Delivered through SABRE into Unlabeled Pyridine, Pyrazine, or Metronidazole Enable Single Scan NMR Quantification at the mM Level,” The Journal of Physical Chemistry B, vol. 124, no. 22, pp. 4573–4580, May 2020, doi: 10.1021/acs.jpcb.0c02583.

Exploration of UV LEDs for disinfection

Rolands Gudermanis[1], Gita Revalde[1], Anda Ābola[1]

[1]University of Latvia, Faculty of Science and Technology, Institute of Atomic Physics and Spectroscopy, Latvia
r.gudermanis@gmail.com

The most recent pandemic highlighted the urgent need to develop additional methods for the disinfection and inactivation of human pathogens, in order to improve preparedness for future crisis scenarios. Although the germicidal effectiveness of UV-C radiation is well established, experimental studies and practical applications still predominantly rely on mercury low-pressure (or medium-pressure) lamps, whose principal emission line is at 254 nm [1].

The aim of this work is to investigate the use of UV LEDs for disinfection, with the goal of replacing the widely used mercury (Hg) lamps in the future, thereby limiting the spread of toxic mercury in the environment.

In this work, we studied irradiation of a UV-C (peak intensity at 272 nm) diode strip (Figure 1). The strip is 50 cm long, consisting of 70 individual UV-C diodes, which is being tested for application in a disinfection apparatus. The peak radiation power of the LED strip is 2.1 to 2.8 W. For implementation purposes, spatial irradiation distribution of the whole strip, groups of diodes, and singular diodes was measured using the Ocean Optics HR-4000 spectrometer.

As the wavelength of emitted light from diodes is not a singular emission line, each radiation measurement was integrated across the wavelengths of 260 nm to 290 nm to obtain absolute irradiation in μW/cm^2. This work helps with developing and designing a prototype of a UV disinfection apparatus for medical and civil purposes.



Fig. 1. Fragment of UV diode strip

Acknowledgements
The work was supported by ERDF project No.1.1.1.3/1/24/A/051.

[1] A. Skudra, G. Revalde et al., “Photochemical and photobiological effects of ultraviolet radiation in antimicrobial applications”, Journal of Photochemistry and Photobiology, 2022.

EXPLORATION OF ATOMIC OXYGEN IN HIGH-FREQUENCY ELECTRODELESS DISCHARGE LAMPS DURING PULSED EMISSION MODE

Rolands Gudermanis[1]

[1]University of Latvia, Faculty of Science and Technology, Institute of Atomic Physics and Spectroscopy, Latvia
r.gudermanis@gmail.com

High-frequency electrodeless discharge lamps (HFEDLs) are light sources that produce stable, intense, narrow emission lines, and have applications in atomic absorption spectroscopy, detection of contaminants with high precision, disinfection. Radiation emission happens from lowtemperature inductively-coupled plasma inside a small quartz glass bulb, which is excited using an external high-frequency coil.

However, there have been observed phenomena where HFEDLs enter pulsed emission mode, where emission periodically changes (Figure 1). This effect is uncharacteristic and unintended for HFEDLs, and is yet to be fully understood.

In this work, we study pulsed emission of HFEDLs dependence on various parameters, including atomic oxygen. Oxygen was found during spectral measurements of HFEDLs in pulsed emission mode, where atomic oxygen spectral lines at 777 nm appeared. Oxygen is not introduced during lamp production, so the presence of these spectral lines indicate that oxygen from HFEDLs' SiO2 walls participates in plasma excitation. As oxygen is highly electronegative, it may be the reason for plasma quenching in HFEDLs. For time-resolved spectral measurements, high-resolution ($\Delta\lambda$ = 0.008 nm) spectrometer Jobin Yvon SPEX 1000M was used.

Spectral data analysis confirms, that oxygen emission intensity coincides with lamps' working element (e.g. Se, Te) emission pulses. This work aims to improve understanding of the stability mechanisms in low-temperature inductively-coupled plasmas.

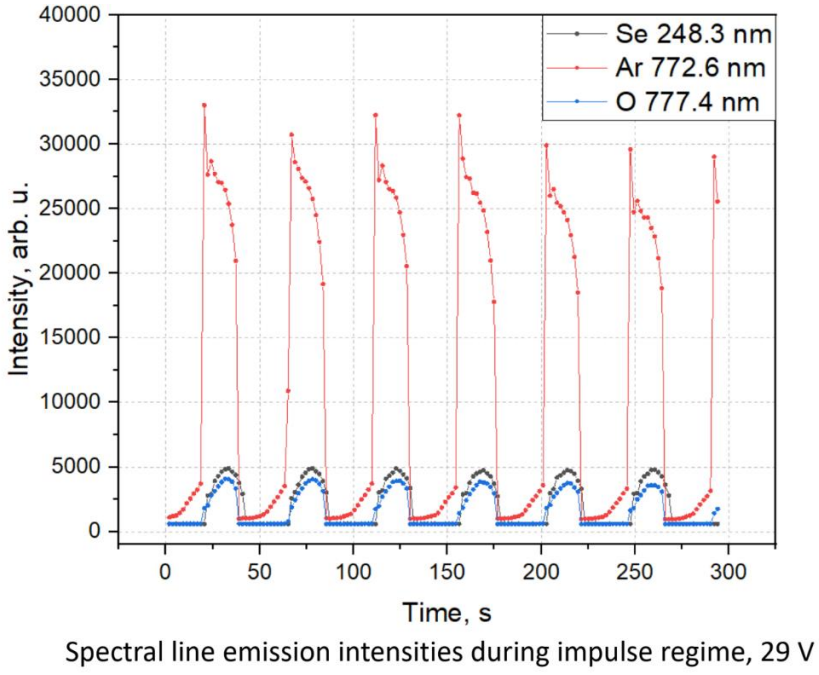


Fig. 1. An example of pulsed HFEDL emission

Chemistry

STIMULI-RESPONSIVE H-BONDED SUPRAMOLECULAR SYSTEMS

Gabija Sergejevaitė[1], Domantas Valčeckas[1], Vaidas Klimkevičius[2], Edvinas Orentas[1]

[1]Vilnius University, Faculty of Chemistry and Geosciences, Department of Organic Chemistry, Vilnius, Lithuania
[2]Vilnius University, Faculty of Chemistry and Geosciences, Department of Polymer Chemistry, Vilnius, Lithuania
gabija.sergejevaite@chgf.stud.vu.lt

Stimuli-responsive supramolecular systems have emerged as promising materials for adaptive and reconfigurable systems due to their dynamic and reversible non-covalent interactions [1]. However, designing smart hydrogen-bonded materials that exhibit controlled and predictable switching behavior under external stimuli remains challenging.

In our report, we design and investigate a series of H-bonded supramolecular systems constructed from ureidopyrimidinone (UPy) or 1,8-naphthyridine-2,7-diamine (DAN) motifs incorporated with stimuli-responsive functional groups. These systems dynamically reorganize their structures in response to light, temperature, or pH changes. NMR, UV–VIS spectroscopy, and viscosity measurements were employed to establish structure–property relationships and confirm quasi-reversible switching behavior.

These findings demonstrate the potential of hydrogen bond driven supramolecular architectures in advanced applications including smart coatings, self-healing materials or drug delivery systems. The rational design principles presented here provide a framework for engineering next-generation adaptive materials with programmable and reversible functionalities.

[1] M. Oggioni et al., “Photoacid-Induced Supramolecular Network Disassembly: A Systems Approach to Stimuli-Responsive Polymers,” Angewandte Chemie International Edition, vol. 64, no. 30, Jun. 2025, doi: https://doi.org/10.1002/anie.202506981.

INVESTIGATION OF SOLVENT-INDUCED SWELLING OF POLYPYRROLE THIN FILMS BY DRT ANALYSIS OF ELECTROCHEMICAL IMPEDANCE SPECTROSCOPY DATA

Domas Pirštelis[1,2], Ernestas Brazys[1,2], Vilma Ratautaitė[1], Arūnas Ramanavičius[1,2]

[1]Department of Nanotechnology, State Research Institute Center for Physical Sciences and Technology, Sauletekio av. 3, Vilnius LT-10257, Lithuania
[2]Department of Physical Chemistry, Institute of Chemistry, Faculty of Chemistry and Geosciences, Vilnius University, Naugarduko str. 24, Vilnius LT-03225, Lithuania
domas.pirstelis@ftmc.lt

Conducting polymers, such as polypyrrole(Ppy) are increasingly employed in modern bioelectronic devices [1]. However, their performance can be strongly affected by solvent induced swelling and the associated structural changes in the polymer matrix. One of the key challenges in such systems is therefore evaluating their robustness and stability in different media by characterizing the effect of pH, solvent or electrolyte-induced changes in the polymer matrix [2].

In this work, thin films of conducting polymer polypyrrole were electrochemically deposed onto screen printed carbon electrodes (SPCE). After synthesis, the Ppy/SPCE system was exposed to electrolyte solutions containing increasing concentrations of ethanol as a cosolvent. Fast Fourier transform electrochemical impedance spectroscopy (FFT-EIS) was applied to rapidly monitor time dependent changes in the electrochemical system.

For the analysis of the acquired EIS data, the two employed approaches were non-linear least squares fitting using equivalent circuit models and distribution of relaxation times (DRT) analysis [3]. Equivalent circuit model fitting provides information about changes in charge-transfer resistance, electric double-layer capacitance, and mass-transport limitations. In contrast, DRT analysis reveals dynamic shifts in the underlying relaxation processes of the Ppy/SPCE system without relying on a predefined equivalent circuit model. The combined data analysis provides valuable insights into ethanol-induced polymer swelling and reorganization of the Ppy film.

Acknowledgements
This research was supported by the Lithuanian Research Council under project No. S-MIP-24-111

[1] J. Sarvutiene, U. Prentice, S. Ramanavicius, and A. Ramanavicius, “Molecular imprinting technology for biomedical applications,” Mar. 01, 2024, Elsevier Inc. doi: 10.1016/j.biotechadv.2024.108318.
[2] E. Brazys, V. Ratautaite, E. Mohsenzadeh, R. Boguzaite, A. Ramanaviciute, and A. Ramanavicius, “Formation of molecularly imprinted polymers: Strategies applied for the removal of protein template (review),” Adv. Colloid Interface Sci., vol. 337, p. 103386, Mar. 2025, doi: 10.1016/J.CIS.2024.103386.
[3] T. H. Wan, M. Saccoccio, C. Chen, and F. Ciucci, “Influence of the Discretization Methods on the Distribution of Relaxation Times Deconvolution: Implementing Radial Basis Functions with DRTtools,” Electrochim. Acta, vol. 184, pp. 483–499, Dec. 2015, doi: 10.1016/J.ELECTACTA.2015.09.097.

UHPLC-MS/MS METHOD DEVELOPMENT FOR TARGETED GIBBERELLIN PROFILING IN REPRODUCTIVE TISSUES OF HERACLEUM SOSNOWSKYI

Dominykas Laibakojis[1,3], Simonas Balčiūnas[2], Tautvydas Žalnierius[3], Jurga Būdienė[1]

[1]Center for Physical Sciences and Technology, Department of Organic Chemistry, Lithuania
[2]Vilnius University, Department of Analytical and Environmental Chemistry, Lithuania
[3]State Scientific Research Institute Nature Research Centre, Laboratory of Plant Physiology, Lithuania
dominykas.laibakojis@ftmc.lt

Gibberellins (GAs) are a large group of plant hormones found in trace quantities that are involved in the control of plant growth and development [1–4]. Sosnowsky's hogweed (*Heracleum sosnowskyi* Manden.) is listed among Invasive Alien Species that are of high concern to the EU [5]. Concern is raised by its ability to destroy native ecosystems and by its toxicity to human health. Spreading occurs only by seeds, and death occurs after reproduction. For seed development and further spread, a crucial role is played by GAs [6]. Therefore, valuable information about the state of GA metabolism in response to various treatments or changes in environmental conditions is provided by the quantification of endogenous GAs in *H. sosnowskyi* tissues [2]. Thus, the efficient extraction, purification, and determination of minute GA amounts are essential [2]. In this study, the development of an UHPLC–MS/MS method for the quantification of GAs in *H. sosnowskyi* reproductive tissues is aimed at, and the optimization of an established GA extraction and purification protocol is performed.

In this study, a selective and sensitive UHPLC–MS/MS method was developed for the separation and quantification of 14 different GAs from 100 mg of *H. sosnowskyi* reproductive tissues. Optimal separation of GAs was achieved on a UHPLC reversed-phase column (ReproSil-Pur Basic-C18, 2.1 mm x 100 mm, 1.9 µm; Dr. Maisch) using a linear gradient of 0.1% formic acid (A) and acetonitrile (B) mobile phases at a flow rate of 0.4 mL min^{-1}, from 95:5 A:B (v/v) to 30:70 A:B (v/v) over 13 min, with column washing performed using 0:100 A:B (v/v) until 15 min. Quantification of GAs was performed using a highly selective multiple reaction monitoring (MRM) mode and an isotope dilution method. Furthermore, an existing GA extraction and purification method developed by Urbanova et al. [2] was modified and applied. The method is based on solid-phase extraction (SPE) with mixed-mode (Oasis MCX; Oasis MAX, Waters) and reversed-phase (Oasis HLB, Waters) cartridges. Insufficient recoveries of GAs for quantification were obtained from extraction using the originally developed protocol. Therefore, the method was modified, and improved recovery of GAs was achieved by adjustment of the composition of solvents used in SPE.

In conclusion, a robust UHPLC–MS/MS method was developed for the quantification of GAs in *H. sosnowskyi* reproductive tissues, and an extraction and purification protocol was optimized that provides a foundation for further investigations into GA-mediated regulation of reproductive development in this species.

[1] P. Hedden, "The current status of research on gibberellin biosynthesis," Plant Cell Physiol., vol. 61, pp. 1832–1849, 2020.
[2] T. Urbanová, D. Tarkowská, O. Novák, P. Hedden, and S. Miroslav, "Analysis of gibberellins as free acids by ultra performance liquid chromatography–tandem mass spectrometry," Talanta, vol. 112, pp. 85–94, 2013.
[3] V. M. Sponsel, "Signal achievements in gibberellin research: The second half-century," Annu. Plant Rev., vol. 49, pp. 1–36, 2016.
[4] P. Hedden, "Gibberellins," in Encyclopedia of Applied Plant Sciences, vol. 1, 2016, pp. 411–420.
[5] J. C. Serrani, M. Fos, A. Atarés, and J. L. García-Martínez, "Effect of gibberellin and auxin on parthenocarpic fruit growth induction in the cv. Micro-Tom of tomato," J. Plant Growth Regul., vol. 26, pp. 211–221, 2007.
[6] Z. Gudžinskas and E. Žalneravičius, "Seedling dynamics and population structure of invasive Heracleum sosnowskyi (Apiaceae) in Lithuania," Ann. Bot. Fenn., vol. 55, pp. 309–320, 2018.

MODELLING INTERMOLECULAR INTERACTIONS OF IBUPROFEN IN AQUEOUS HYDROTROPIC SOLUTIONS USING MD SIMULATIONS

Benjaminas Malmiga[1], Kęstutis Aidas[1], Žyginta Murnikova[1]

[1]Vilnius University, Faculty of Physics, Institute of Chemical Physics, Vilnius, Lithuania
benjaminas.malmiga@ff.stud.vu.lt

Poor solubility of candidate drug molecules in water is one of the most common obstacles in drug design, thus requiring methods to improve *in vitro* solubility[1]. The application of hydrotropy is one such method – mixtures of water and hydrotropes may improve drug molecule solubility by orders of magnitude[2]. Although hydrotropes are already seeing application, the hydrotropic effect itself has yet to be fully explained – there are currently three hypothesized mechanisms: self-aggregation, chaotropic effects, and the formation of low stoichiometry complexes[3]. Gaining insight into the working mechanism requires an investigation of changes within the first solvation layer of target drug molecules. In this work we investigate the hydrotropic effect of the ionic liquid cholinium salicylate on the model drug molecule ibuprofen. It has been shown in the literature that cholinium salicylate – an analog compound to the anti-inflammatory drug aspirin – is capable of increasing the solubility of ibuprofen in water by up to 6000-fold[4]. The investigation of the changes within the first solvation layer of ibuprofen is achieved via molecular dynamics (MD) simulations.

Initial geometries of ibuprofen, cholinium and salicylate molecules were constructed and optimized by using Gaussian[5], point charges and force field parametrization were acquired via the RESP method[6]. MD simulations were conducted using the AMBER MD packet[7]. The TIP4P-Ew water model was used for the water molecules and the General Amber Force Field (GAFF) was used for the remaining molecules[8]. In total – 7 simulation boxes were created: one reference system of ibuprofen in pure water; three systems containing 3%, 5%, and 7% molar fractions of sodium salicylate; and three 3%, 5%, and 7% systems of cholinium salicylate. MD simulations were conducted in two principal steps – equilibration and production phases. Equilibration was achieved by the minimization of potential energy, followed by a short 1 ns simulation in the NVT ensemble, at least 100 ns in the NPT ensemble (until equilibrium density is achieved), and 50 ns in the NVT ensemble before proceeding to the production run of 100 ns in the NVT ensemble. The resulting trajectories were analyzed using radial distribution functions which were integrated to obtain coordination numbers. Coordination numbers provide information about the first solvation layer of ibuprofen across systems of varying hydrotrope concentrations.

The trajectory analysis shows that the hydrotropic effect of cholinium salicylate is largely determined by the ejection of water molecules from the immediate surroundings of ibuprofen's aromatic ring, whereas the protection of the aliphatic chain of ibuprofen from interactions with water is not a determining factor. Furthermore, it was shown that salicylate ions maintain a significant distance from the aromatic ring of ibuprofen, which was contrary to prior expectations.

Acknowledgements
Thank you to VU HPC Saulėtekis for providing the neccessary computational resources

Keywords: Molecular dynamics, ionic liquids, hydrotropy, intermolecular interactions.

[1] V. Dhapte and P. Mehta, "Advances in hydrotropic solutions: An updated review," St Petersburg Polytechnical University Journal Physics and Mathematics, vol. 1, no. 4, pp. 424–435, Dec. 2015, doi: 10.1016/j.spjpm.2015.12.006.
[2] J. Mehringer and W. Kunz, "Carl Neuberg's hydrotropic appearances (1916)," Advances in Colloid and Interface Science, vol. 294, p. 102476, Jun. 2021, doi: 10.1016/j.cis.2021.102476.
[3] J. J. Booth, S. Abbott, and S. Shimizu, "Mechanism of hydrophobic drug solubilization by small molecule hydrotropes," The Journal of Physical Chemistry B, vol. 116, no. 51, pp. 14915–14921, Dec. 2012, doi: 10.1021/jp309819r.
[4] T. E. Sintra, D. O. Abranches, J. Benfica, B. P. Soares, S. P. M. Ventura, and J. A. P. Coutinho, "Cholinium-based ionic liquids as bioinspired hydrotropes to tackle solubility challenges in drug formulation," European Journal of Pharmaceutics and Biopharmaceutics, vol. 164, pp. 86–92, Apr. 2021, doi: 10.1016/j.ejpb.2021.04.013.
[5] M. J. Frisch et al., Gaussian 16 Revision C.01, Gaussian, Inc., Wallingford, CT, USA, 2016.
[6] M. Schauperl et al., "Non-bonded force field model with advanced restrained electrostatic potential charges (RESP2)," Communications Chemistry, vol. 3, no. 1, Apr. 2020, doi: 10.1038/s42004-020-0291-4.
[7] D. A. Case et al., "AmberTools," Journal of Chemical Information and Modeling, vol. 63, no. 20, pp. 6183–6191, Oct. 2023, doi: 10.1021/acs.jcim.3c01153.
[8] H. W. Horn et al., "Development of an improved four-site water model for biomolecular simulations: TIP4P-Ew," The Journal of Chemical Physics, vol. 120, no. 20, pp. 9665–9678, May 2004, doi: 10.1063/1.1683075.

γ -GLUTAMYL TRANSFERASE CHARACTERIZATION USING SCANNING ELECTROCHEMICAL MICROSCOPY

Vaineta Vainalavičiūtė[1,2], Agnė Boguševičė[2], Inga Morkvėnaitė-Vilkončienė[3], Tomas Mockaitis[1,2]

[1]Vilnius TECH, Department of Chemistry and Bioengineering, Vilnius 10223, Lithuania
[2]State Research Institute Centre for Physical Sciences and Technology, Department of Nanotechnology, Vilnius 10257, Lithuania
[3]Department of Electrical Engineering, Vilnius TECH, Vilnius 10223, Lithuania
vaineta.vainalaviciute@stud.vilniustech.lt

γ-Glutamyltransferase (GGT) is the main enzyme involved in glutathione (GSH) metabolism. This enzyme catalyzes the transfer of the γ-glutamyl group between glutathione and amino acids or peptides, maintains cellular redox balance, and protects cells from oxidative stress [1]. GGT activity is related to the functional state of the liver, biliary tract, and pancreas, therefore changes in the concentration of this enzyme in the blood can help assess disorders of various organs [2]. Currently, in clinical practice, GGT activity is determined by spectrophotometric, colorimetric, and other methods, which are sensitive but not very specific.

Scanning electrochemical microscopy (SECM) is a high-resolution microscopy technique that allows the visualization of local electrochemical activity on various surfaces (**Fig. 1**). SECM measurements are performed with an ultramicroelectrode that is capable of scanning at a distance to the sample surface, where catalytic, redox, or other electrochemically active sites may be present [3]. The use of scanning electrochemical microscopy (SECM) in this study allows for the investigation of local electrochemical processes, determination of GGT activity, and real time reaction kinetics.

The aim of this study is to analyse the electrochemical response of γ-glutamyltransferase using scanning electrochemical microscopy to develop sensitive biosensors for faster diagnosis of GGT related diseases.

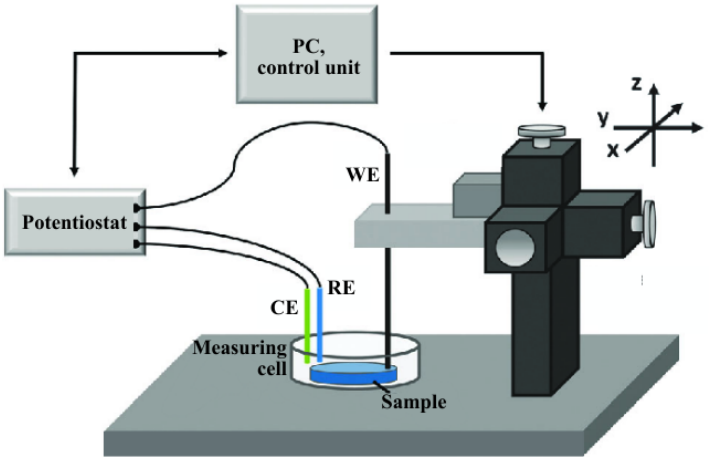


Fig. 1. Illustration of scanning electrochemical microscopy [4].

Acknowledgements

This research was funded by the Center for Physical Sciences and Technology (FTMC), agreement No 1600-BL14.

[1] Neuman, M. G., Malnick, S. & Chertin, L. Gamma glutamyl transferase – an underestimated marker for cardiovascular disease and the metabolic syndrome. J Pharm Pharm Sci 23, 65–74 (2020).
[2] Kumaragurubaran, N., Tsai, H.-T., Arul, P., Huang, S.-T. & Lin, H.-Y. Development of an activity-based ratiometric electrochemical probe of the tumor biomarker γ-glutamyl transpeptidase: Rapid and convenient sensing in whole blood, urine and live-cell samples. Biosensors and Bioelectronics 248, 115996 (2024).
[3] Morkvenaite-Vilkonciene, I., Ramanaviciene, A., Kisieliute, A., Bucinskas, V. & Ramanavicius, A. Scanning electrochemical microscopy in the development of enzymatic sensors and immunosensors. Biosensors and Bioelectronics 141, 111411 (2019).
[4] Ventosa, E. & Schuhmann, W. Scanning electrochemical microscopy of Li-ion batteries. Phys. Chem. Chem. Phys. 17, 28441–28450 (2015).

VOLATILE FINGERPRINTS OF BOTANICAL HYDROLATES: HS-GC-MS VERSUS SOLVENT EXTRACTION-GC-MS

Konstantinas Brazinski[1]

[1]Center for Physical Sciences and Technology (FTMC), Department of Organic Chemistry, Vilnius, Lithuania
konstantinas.brazinski@ftmc.lt

Botanical hydrolates are water-based distillates obtained as co-products during essential oil production. They contain a diverse mixture of dissolved volatile organic compounds (VOCs) transferred from plant material during distillation. Because of their pronounced aromas, they are widely used in cosmetics, fragrances, and food flavouring. Profiling of hydrolates is important to verify botanical origin, ensure batch-to-batch consistency, and screen for unexpected or potentially harmful volatile impurities [1]. However, VOC profiles can vary substantially depending on the GC–MS sample preparation method. Headspace (HS) sampling enables VOC determination by analysing the vapour phase above the sample, providing rapid analysis with minimal preparation, but it may under-represent less volatile constituents compared with other approaches.

The aim of this study was to evaluate differences in GC–MS profiles of botanical hydrolates obtained using HS sampling versus liquid–liquid extraction (LLE) with pentane followed by liquid injection. In addition, we aimed to identify marker compounds relevant for both routine screening and more comprehensive chemical fingerprinting. Seven hydrolates were analysed: apple blossom, apple mint, peppermint, two chamomile hydrolates, linden blossom, and rose blossom. Compounds were tentatively identified by mass spectral matching against the NIST mass spectral library.

Overall, HS–GC–MS produced fewer peaks and fewer tentatively identified compounds across samples, indicating reduced coverage of less volatile constituents. In contrast, pentane LLE yielded richer profiles and improved detection of semi-volatile constituents, supporting its use for more robust marker discovery, while HS provides a rapid option for routine screening.

[1] Tavares, C. S., Gameiro, J. A., Roseiro, L. B., & Figueiredo, A. C. “Hydrolates: a review on their volatiles composition, biological properties and potential uses.” Phytochemistry Reviews 21(5) (2022): 1661–1737.

COMPUTATIONAL STUDY INVESTIGATING ELECTRONIC SPECTRA AND STRUCTURE OF RETINOL AND RETINOIC ACID

Julius Ažukas[1], Žyginta Murnikova[1], Kęstutis Aidas[1]

[1]Vilnius University, Faculty of Physics, Institute of Chemical Physics, Vilnius, Lithuania
julius.azukas@ff.stud.vu.lt

Retinoids are chemical compounds related to vitamin A (see Fig. 1) which perform various vital functions in the human body. For instance, retinol is crucial for cell growth and differentiation, while the isomerization of 11-*cis*-retinal to all-*trans*-retinal and the subsequent restoration of 11-*cis*-retinal during the retinoid cycle allows us to see [1]. Spectroscopic methods are frequently used for investigating the structure of such compounds, which is useful for broadening the field of applications. While experimental methods provide us with accurate results, theoretical calculations complement experimental data by offering insights about the processes being investigated on a molecular level. Various carotenoids, which are similar in structure to retinoids, were successfully studied computationally in terms of vibrational and electronic spectra using density functional theory (DFT) [2]. However, attempts to study retinoids in common solvents, especially regarding different *cis-trans* isomers, in a similar manner have so far been unsuccessful, despite existing experimental results [3].

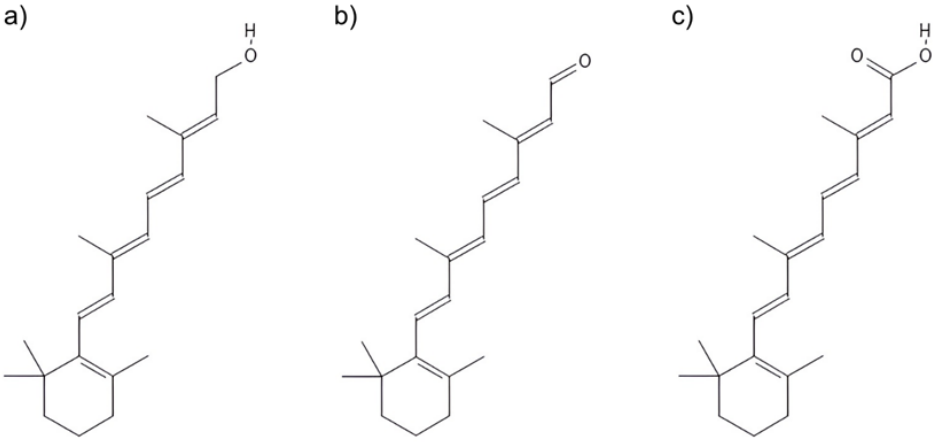


Fig. 1. Structural formulas of retinoids a) all-*trans*-retinol, b) all-*trans*-retinal, c) all-*trans*-retinoic acid.

The primary goal of this study was to properly evaluate the electronic absorption energy maxima of retinol and retinoic acid in organic solvents. Molecular dynamics (MD) simulations were performed for systems containing 1 molecule of either retinol or retinoic acid dissolved in 1000 molecules of ethanol. For each compound, 2 systems were analyzed with different *cis-trans* isomeric forms, as the absorption maxima of retinoids are dependent on molecular configuration. Quantum mechanics/molecular mechanics (QM/MM) calculations, as well as DFT methods, were then perfromed for various configurations of each system, obtained through the MD simulations. It was found that the calculated excitation energy maxima of both retinoids depend on the description of their molecular environment – modelling the surrounding molecules with a polarizable force field yields lower values, when compared with a non-polarizable force field. Further calculations were performed, leading to the conclusion that accounting for van der Waals interactions does not have a meaningful impact on the results.

Acknowledgements

Computations were performed using the resources provided by the High-Performance Computing Center “HPC Saulėtekis” at Vilnius University, Lithuania.

[1] E. H. Choi, A. Daruwalla, S. Suh, H. Leinonen, and K. Palczewski, “Retinoids in the visual cycle: role of the retinal G protein-coupled receptor,” Journal of Lipid Research, vol. 62, p. 100040, Jun. 2020, doi: 10.1194/jlr.tr120000850.

[2] M. Macernis, J. Sulskus, S. Malickaja, B. Robert, and L. Valkunas, “Resonance Raman Spectra and Electronic Transitions in Carotenoids: A Density Functional Theory study,” The Journal of Physical Chemistry A, vol. 118, no. 10, pp. 1817–1825, Feb. 2014, doi: 10.1021/jp406449c.

[3] M. A. Kane, J. L. Napoli, “[13] Quantification of physiological levels of retinoic acid,” Methods in Enzymology on CD-ROM/Methods in Enzymology, vol. 123, pp. 112–124, Jan. 1986, doi: 10.1016/s0076-6879(86)23015-3.

MODELLING ^{1}H NMR SPECTRA OF WATER IN AQUEOUS MIXTURES OF 1-BUTYL-3-METHYL-IMIDAZOLIUM TETRAFLUOROBORATE IONIC LIQUID

Julius Ažukas[1], Kęstutis Aidas[1]

[1]Vilnius University, Faculty of Physics, Institute of Chemical Physics, Vilnius, Lithuania
julius.azukas@ff.stud.vu.lt

Nuclear magnetic resonance (NMR) spectroscopy is an indestructive method of examining the molecular structure of a chemical compound. It relies on the excitation of an atom's nucleus to a higher energy spin state and the subsequent reemission of radio frequency radiation, which produces a signal. Since experimentally observed signals can be difficult to interpret, theoretical calculations allowing for extensive monitoring of the molecular environment of the compound being investigated are often employed. Lately, there have been numerous studies modelling ^{1}H NMR spectra of ionic liquids (ILs) and their aqueous mixtures aiming to overcome the computational challenges posed by local anisotropy and a wide array of different intermolecular interaction types with no clear dominant interaction [1]. In a recent computational ^{1}H NMR study [2], it was found that the chemical shift of water in an aqueous IL solution is very sensitive to the molar fraction of the IL, making water particularly useful as a probe of intermolecular configuration. As such, it is important to develop methods allowing for accurate modelling of ^{1}H NMR spectra of water in aqueous IL mixtures.

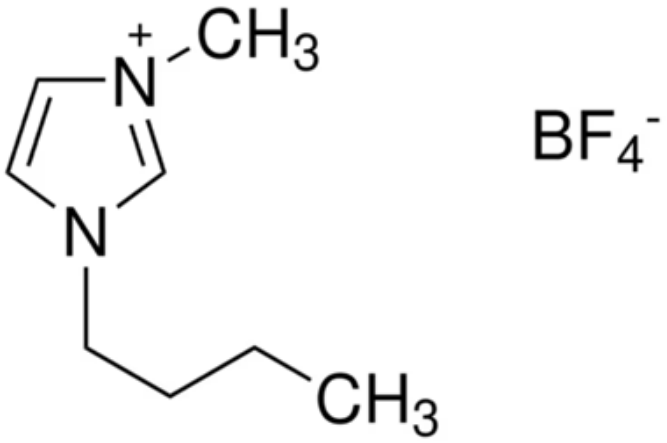


Fig. 1. Structural formula of [C4mim][BF4]

The primary goal of this study was to properly calculate the chemical shift of water in an aqueous solution of 1-butyl-3-methylimidazolium tetrafluoroborate, [C4mim][BF4] – see Fig. 1, at different molar fractions of the IL. A flexible water model was used so as to account for intramolecular processes. In order to compensate for slow intermolecular dynamics arising from the viscosity of the IL, extensive molecular dynamics (MD) simulations were performed to obtain a wide array of different configurations of the analyzed systems. Afterwards, the chemical shift of ^{1}H in the various configurations was calculated using quantum mechanics/molecular mechanics (QM/MM) methods and the results were compared with experimental data.

Acknowledgements

Computations were performed using the resources provided by the High-Performance Computing Center "HPC Saulėtekis" at Vilnius University, Lithuania.

[1] E. Sipavičius et al., "Towards accurate modelling of 1H NMR spectra of ionic liquids: The case of [C4mim][BF4] and its aqueous mixtures," Chemical Physics Letters, vol. 877, p. 142295, Jul. 2025, doi: 10.1016/j.cplett.2025.142295.

[2] S. S. Bystrov et al., "Translational Diffusion in a Set of Imidazolium-Based Ionic Liquids [bmim]+A− and Their Mixtures with Water," The Journal of Physical Chemistry B, vol. 123, no. 43, pp. 9187–9197, Oct. 2019, doi: 10.1021/acs.jpcb.9b06802.

PHOTOREDOX MANIFOLD FOR DEHYDROGENATIVE COUPLING USING PROTONS AS OXIDANTS

Jonas Žurauskas[1], Paulius Vaickūnas[1], Gustautas Snarskis[3], Nojus Radzevičius[1], Barbara Chatinovska[1], Gediminas Kreiza[2], Steponas Raišys[2], Mantas Šimėnas[2], Vidmantas Kalendra[2], Kęstutis Zakarauskas[4], Karolis Kazlauskas[2], Edvinas Orentas[1]

[1]Vilnius University, Department of Organic Chemistry, Naugarduko 24 LT-03225, Vilnius, Lithuania
[2]Vilnius University, Faculty of Physics, Saulėtekio av. 3, LT-10257, Vilnius, Lithuania
[3]Biomatter, Business Stadium West, Rinktinės g. 5-101, 09234, Vilnius, Lithuania,
[4]Lithuanian Energy Institute, Breslaujos 3, LT-44403, Kaunas, Lithuania
jonas.zurauskas@chgf.vu.lt

The direct coupling of two unfunctionalized molecules under mild conditions embodies an ideal in synthetic chemistry. In this study, we report a metal-free photocatalytic process for arene C-H functionalization that employs an acridinium-type catalyst and produces dihydrogen as the only by-product. Throughout the catalytic cycle, the catalyst acts as an oxidizing agent, a hydrogen atom transfer agent, and a proton-reducing agent, enabling a cross-dehydrogenative transformation without the need for external oxidants. The reaction is conveniently performed using visible light, and the high oxidation potential of the catalyst allows it to engage even electron deficient arene substrates. The catalytic mechanism disclosed herein can become a general logic for developing various cross-dehydrogenative reactions adaptable for pharmaceutical and material sciences.

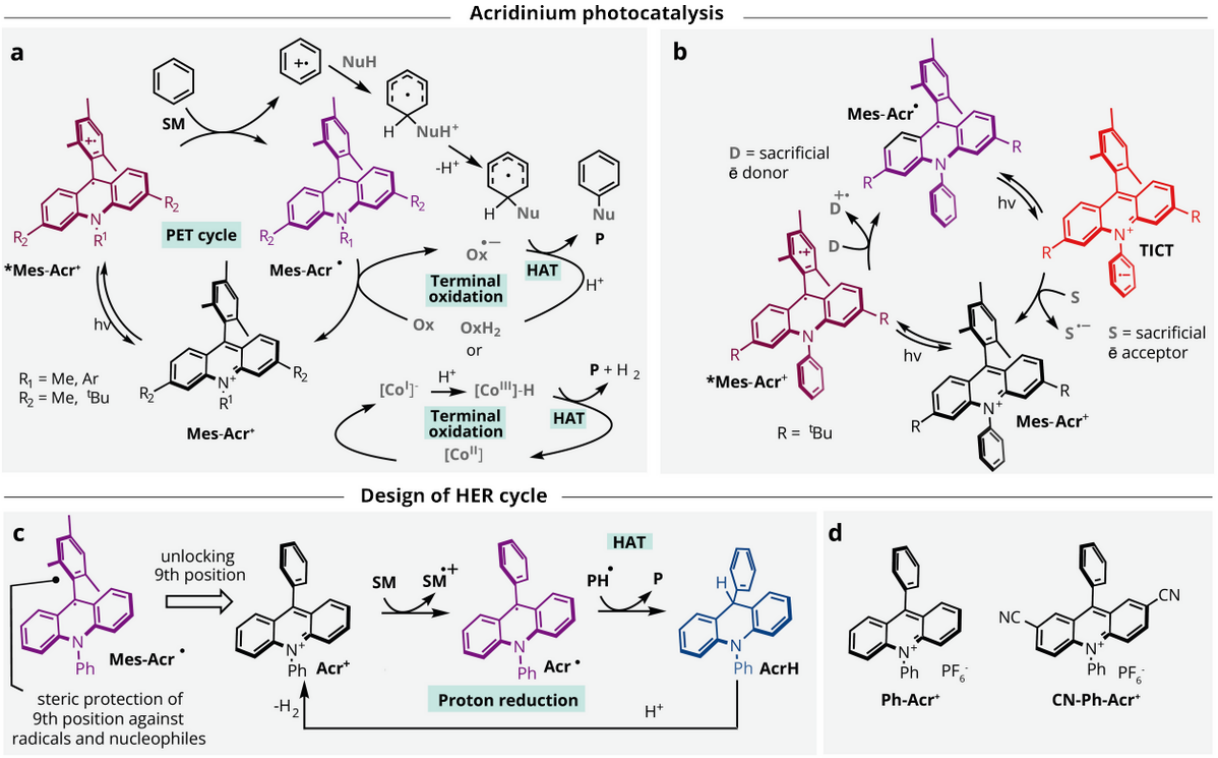


Fig. 1. Established and hypothesized reactivity modes of acridinium photocatalysis. a, A photocatalytic cycle based on reductive photocatalyst quenching. The regeneration of the catalyst is achieved either by sacrificial oxidant or cobalt-mediated dihydrogen formation. **b**, Exploration **5** of excited acridine radical as a potent reductant. **c**, Design of acridinium catalyst for hydrogen atom transfer and proton reduction to produce dihydrogen during the turnover (hydrogen evolution reaction (HER) cycle). **d**, Chemical structures of the photocatalysts. Mes, mesityl; SM, starting material; P, product

[1] J. Žurauskas et al., "Electron-poor acridones and acridiniums as super photooxidants in molecular photoelectrochemistry by unusual mechanisms," Angew. Chem. Int. Ed., vol. 62, e202307550, 2023.
[2] X. Yang et al., "Toward organic photohydrides: Excited-state behavior of 10-methyl-9-phenyl-9,10-dihydroacridine," J. Phys. Chem. B, vol. 117, pp. 15290–15296, 2013.
[3] N. A. Romero, K. A. Margrey, N. E. Tay, and D. A. Nicewicz, "Site-selective arene C–H amination via photoredox catalysis," Science, vol. 349, pp. 1326–1330, 2015.

INVESTIGATION OF THE HETEROGENEOUS CATALYTIC ADDITIONOF VINYL ACETATE TO AZOLES USING TRANSITION-METAL ACETATES IMMOBILIZED ONPOLY(1-VINYLAZOLES)

Nagharsh Mirakyan[1], Hovhannes Attaryan[1]

[1]Scientific and Technological Center of Organic and Pharmaceutical Chemistry, Yerevan, Armenia
nmiraqyan1@gmail.com

The catalytic activity of acetates of various transition metals (Zn2+, Mn2+, Co2+, Ni2+, Cu2+) on poly(1-vinylazole) carriers was studied in regard to the addition reaction of vinyl acetates via aza-Markovnikov mechanism. The immobilization of homogeneous transition-metal catalysts on organic polymers has attracted increasing attention, as it enhances product yields and enables catalyst reusability, thereby reducing overall catalyst consumption. The immobilization of transition metals on polymer matrices, such as poly(1-vinylazoles), for use as catalysts in aza-Markovnikov reactions has not been previously investigated, and this study addresses that gap [1]. 1-(α-Acetoxyethyl)-3,5-dimethylpyrazole is described in the literature [2]. The compound most likely decomposes at high temperatures. It was found out that during distillation at 80-90 °C temperature under 30 mm Hg vacuum 1-(α-Acetoxyethyl)-3,5-dimethylpyrazole undergoes cleavage, resulting in the formation of acetaldehyde and 1-acetyl-3,5-dimethylpyrazole. It should be noted that 1H-imidazole reacts with vinyl acetate even in the absence of $M(OAc)_2$ catalysts, so 1-(α-acetoxyethyl)imidazole and 1-acetylimidazole are formed in approximately the 1:1 ratio. The usage of Ⓟ→$M(OAc)_2$ catalysts shifts the reaction towards the formation of 1-acetylimidazole. Notably, this method enabled the first reported synthesis of 1-(α-acetoxyethyl)-3,5-dimethylpyrazole. The suggested optimized method has a number of advantages compare to previously known methods. The products are obtained with high yields without elaborate technological solutions. Moreover, the reactions proceed at room temperature and even without mixing the reagents. The ease of separating the products from the reaction mixture is another substantial benefit of the suggested method, since the use of chromatographic methods is not required. The obtained heterogeneous catalysts proved to be reusable, maintaining catalytic activity for more than three reaction cycles without requiring intermediate purification. Moreover, the polymeric part can be also regenerated and reused.

Acknowledgements

The authors thank for support by the NAS RA within the framework of the ''Young Scientists' Support Program'' under the code 25-YSIP-004.

Keywords: aza-Markovnikov, polyazoles, pyrazoles, vinyl acetate, catalysis

[1] "Heterogeneous catalysis of Aza-Markovnikov addition reactions by transition metal acetates immobilized on poly(1-vinylazoles)," ChemistrySelect, vol. 10, no. 41, Art. no. e04021, 2025, doi: 10.1002/slct.202504021.

[2] "SYNTHESIS OF VINYLPYRAZOLE BY HETEROGENEOUS CATALYSIS," 2000. https://arar.sci.am/dlibra/publication/201455/edition/183221/content (accessed Feb. 15, 2026).

A GENERAL ARENE C-H FUNCTIONALIZATION TO SUBSTITUTED METHYLENES

Nojus Radzevičius[1], Jonas Žurauskas[1], Paulius Vaickūnas[1], Gabija Sergejevaitė[1], Domantas Valčeckas[1], Edvinas Orentas[1]

[1]Lithuania, Vilnius, Vilnius University, Faculty of Chemistry and Geosciences, Department of Organic Chemistry
nojus.radzevicius@chgf.vu.lt

Late-stage functionalization has become a powerful strategy in modern drug development as it enables rapid diversification of complex, bioactive molecules without the need for de novo synthesis. Selective modification of advanced intermediates or lead compounds accelerates exploration of chemical space and study of structure–activity relationships, thus facilitating the fine-tuning of potency, selectivity, and pharmacokinetic properties. This approach reduces time, cost, and synthetic risk, making it especially valuable in lead optimization and the generation of analog libraries. As a result, many methods of late stage derivatization have recently been developed, especially such strategies as molecular editing [1] and C-H functionalization [2].

This work presents a novel photoredox catalysis-based method for mild and robust (hetero)arene C-H functionalization to provide the corresponding (hetero)benzyl pyridinium salts (Fig 1.). The method relies on a reagent that can be prepared from common, inexpensive laboratory chemicals, along with either organic or iridium-based visible light photocatalysts. The reaction, performed at room temperature, has successfully been performed on electron-rich, neutral, and some electron-poor (hetero)aryls, and has showed high functional group tolerance, which has allowed for it to be used on pharmaceutically active and drug-like substrates with good to excellent yields. A wide variety of mostly novel post-functionalization methods have been developed for the resulting pyridinium intermediates, including oxidation to aldehydes, multiple-level reductions, and nucleophilic functionalizations with both classical nucleophiles (e.g. amines, thiols and carboxylates) as well as palladium-catalyzed Suzuki/Hiyama/Sonogashira -type reactions.

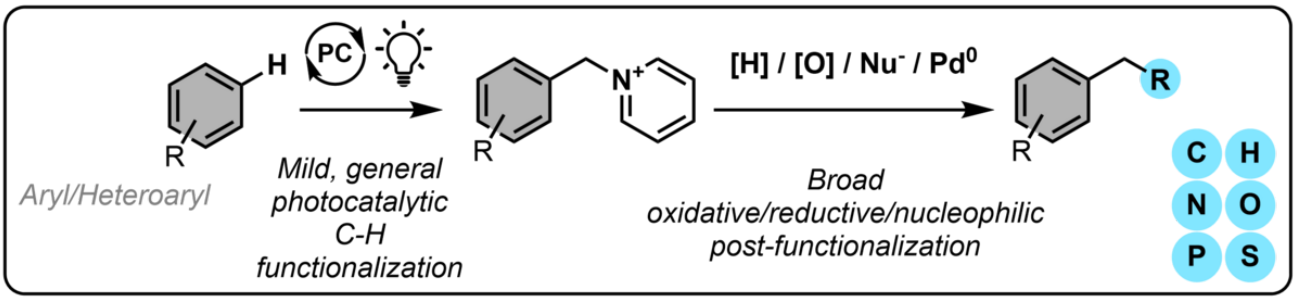


Fig. 1. C-H functionalization reaction scheme

Acknowledgements

Financial support for this work was provided by the “Universities’ Excellence Initiative” programme by the Ministry of Education, Science, and Sports of the Republic of Lithuania under the agreement with the Research Council of Lithuania (project No. S-A-UEI-23-6) and Delta Biosciences. We thank the Arqus Talent Scholarship Fund for fellowship support for J.Ž.

[1] J. Jurczyk, J. Woo, S. F. Kim, B. D. Dherange, R. Sarpong, and M. D. Levin, “Single-atom logic for heterocycle editing,” Nature Synthesis, vol. 1, no. 5, pp. 352–364, Apr. 2022, doi: 10.1038/s44160-022-00052-1.

[2] P. Bellotti, H.-M. Huang, T. Faber, and F. Glorius, “Photocatalytic Late-Stage C–H functionalization,” Chemical Reviews, vol. 123, no. 8, pp. 4237–4352, Jan. 2023, doi: 10.1021/acs.chemrev.2c00478.

SYNTHESIS AND ANALYSIS OF AROMATIC ORGANIC ACIDS FOR THE PASSIVATION OF PEROVSKITE SURFACE DEFECTS

Ema Andriuškaitė[1], Dr. Matas Steponaitis[1]

[1]Kaunas University of Technology, Faculty of Chemical Technology, Kaunas, Lithuania
ema.andriuskaite@ktu.edu

As fossil fuel reserves continue to decline, climate change intensifies, and the global demand for energy rapidly increases, the development of energy-efficient and renewable-energy-based technologies has become one of the greatest challenges in modern science [1]. Solar energy is particularly promising - within a single second, the Sun emits enough energy to theoretically meet humanity's energy needs for nearly one million years. These facts encourage researchers to develop new devices capable of efficiently converting solar radiation into electrical energy.

Over the past 15 years, thanks to extensive scientific research, perovskite solar cells (PSCs) have achieved efficiencies exceeding 27% [2]. Despite significant progress, there remain fundamental issues that must be addressed in science laboratories. One such issue is the presence of perovskite surface defects, (e.g. uncoordinated lead), which reduce device stability and limit efficiency [3]. Surface defects in PSCs are often passivated using relatively small organic molecules bearing functional groups (e.g., carboxylic acid, phosphonic acid, quaternary ammonium, etc.) that can form bonds with uncoordinated lead atoms [4]. Although the scientific literature contains numerous examples of materials used to reduce perovskite surface defects, there is still insufficient clarity regarding which functional group and molecular structure can deliver the best performance.

In this work various carbazole carboxylic acids were synthesized in order to investigate the influence of factors such as modifications in the carbazole core, distance between acid functional group and carbazole fragment on the interactions between the aromatic acids and perovskite surface defects. Nuclear magnetic resonance (NMR) experiments showed that interactions between PbI2 and carbazole carboxylic acids are selective and depend on the structure of the aromatic acid.

[1] N. Wunderling and A. S. von der Heydt, Climate tipping point interactions and cascades: a review, Earth System Dynamics, vol. 15, pp. 41–74, 2024.

[2] Z. Xiong, Q. Zhang, K. Cai, H. Zhou, Q. Song, Z. Han, S. Kang, Y. Li, Q. Jiang, X. Zhang, and J. You, Homogenized chlorine distribution for >27% power conversion efficiency in perovskite solar cells, Science, vol. 390, pp. 638–642, 2025.

[3] D. B. Khadka, Y. Shirai, M. Yanagida, H. Ota, A. Lyalin, T. Taketsugu, and K. Miyano, Defect passivation in methylammonium/bromine-free inverted perovskite solar cells using charge-modulated molecular bonding, Nature Communications, vol. 15, art. no. 882, 2024.

[4] Y. Deng, X. Li, and R. Wang, Carboxyl functional group-assisted defects passivation strategy for efficient air-processed perovskite solar cells with excellent ambient stability, Solar Energy Materials and Solar Cells, vol. 230, art. no. 111242, 2021.

SYNTHESIS OF N-SUBSTITUTED 2-((4-(BENZIMIDAZO (2,1-b)(1,3)THIAZIN-4-YL)PHENYL)(BOC)AMINO)ACETAMIDES FOR THE RESEARCH OF AMYLOID AGGREGATION MODULATORS

Tadas Vasiliauskas[1], Ieva Žutautė[1]

[1]Vilnius University, Faculty of Chemistry and Geosciences, Vilnius, Lithuania
tadas.vasiliauskas@chgf.stud.vu.lt

α-Synuclein is a small protein that can be found in the neurons of the central and peripheral nervous system. In Parkinson's disease, α-syn adopts a β-sheet conformation that, with additional monomers, forms oligomers and amyloid fibrils [1]. The accumulation of amyloid aggregates is associated with neuronal dysfunction. The search for compounds that inhibit α-synuclein aggregation is one approach to treating the disease. Such compounds range from small molecular-weight substances to complex drug mixtures. Work has been done to analyze the potential of a small-molecular-weight compound group, called imidazo[2,1-*b*][1,3]thiazines [2].

The purpose of this research is to synthesize modified imidazo[2,1-*b*][1,3]thiazines for further investigation of amyloid modulators. In this work, 4-iodoaniline is treated with di-*tert*-butyldicarbonate to introduce the *tert*-butoxycarbonyl (Boc) group. The nitrogen atom of the obtained product is alkylated with ethylbromoacetate. Then iodine is replaced with propargyl alcohol using the *Sonogashira* method, and the resulting product is brominated to replace the hydroxy group. During nucleophilic substitution, bromine is replaced with thiobenzimidazole. In the next step of cyclization, imidazo[2,1-*b*][1,3]thiazine is formed. In this work, the obtained product is modified in several steps with different amines, yielding amides.

During this research several *N*-substituted 2-((4-(benzimidazo[2,1-*b*][1,3]thiazin-4-yl)phenyl)(Boc)amino)acetamides were synthesized. The compounds will be further analyzed to determine their effectiveness in modulating amyloid aggregation.

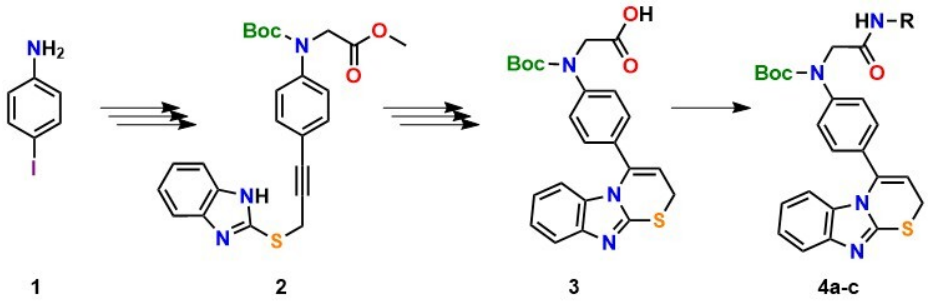


Fig. 1. Synthesis pathway for compounds 4a-c.

[1] P. Calabresi, A. Mechelli, G. Natale, L. Volpicelli-Daley, G. Di Lazzaro, and V. Ghiglieri, "Alpha-synuclein in Parkinson's disease and other synucleinopathies: from overt neurodegeneration back to early synaptic dysfunction," Cell Death and Disease, vol. 14, no. 3, p. 176, Mar. 2023, doi: 10.1038/s41419-023-05672-9.

[2] I. Misiūnaitė et al., "Imidazo[2,1-b][1,3]thiazine Derivatives as Potential Modulators of Alpha-Synuclein Amyloid Aggregation," ACS Chemical Neuroscience, vol. 15, no. 24, pp. 4418–4430, Nov. 2024, doi: 10.1021/acschemneuro.4c00451.

FACILE ONE-STEP HYDROTHERMAL SYNTHESIS OF NICKEL-INCORPORATED-NITROGEN-DOPED CARBON FOR DIRECTMETHANOL FUEL CELLS

Hamza Shehroz[1], Farah Mumtaz[1], Aldona Balčiūnaitė[1], Loreta Tamašauskaitė Tamašiūnaitė[1], Eugenijus Norkus[1]

[1]Center for Physical Sciences and Technology (FTMC), Department of Catalysis, Saulėtekio ave. 3, LT10257 Vilnius, Lithuania
hamza.shehroz@ftmc.lt

The urgent need to mitigate carbon emissions from conventional fuels has driven the development of efficient and low-cost energy conversion devices. Direct methanol fuel cells (DMFCs) are promising candidates due to their high energy density, potential for low-cost operation, and environmental benefits. However, their commercialization is hindered by reliance on expensive, CO-susceptible noble-metal catalysts. To address this challenge, the strategic design of non-noble multi-metallic catalysts has emerged as a critical approach. Herein, we report a facile, one-step hydrothermal synthesis method for producing a nickel-incorporated-nitrogen-doped carbon catalyst (Ni–NC) derived from nickel acetate, glucose, urea, and potassium hydroxide. The synthesized catalyst was characterized using scanning electron microscopy and X-ray diffraction. The synergistic integration of nickel species and nitrogen-doped carbon creates a multifunctional anode material exhibiting excellent methanol oxidation activity. Cyclic voltammetry measurements reveal that the Ni–NC catalyst exhibited a high current density of approximately 75 mA cm^{-2} using a 1 M KOH + 1 M CH_3OH solution as the electrolyte. The Ni–NC catalyst also demonstrates robust performance under varying operational conditions, maintaining current densities ranging from 66.6 to 76.3 mA cm^{-2} at scan rates ranging from 10 to 100 mV s^{-1}, and achieving an optimal value of 75.15 mA cm^{-2} at a methanol concentration of 1.5 M. Furthermore, the Ni–NC anode shows remarkable stability, with negligible activity loss over 500 cycles. This study presents a highly active, durable, and cost-effective catalyst system, advancing the development of practical non-precious-metal anodes for DMFC applications.

ELECTROCHEMICAL DESIGN OF INTERLAYER $Co(OH)_2$ -NiFe ELECTRODES TO TUNE REDOX AND ADSORPTION PROCESSES FOR EFFICIENT OER

Hafiz Muhammad Naeem[1], Loreta Tamašauskaitė-Tamašiūnaitė[1], Eugenijus Norkus[1], Ramūnas Levinas[1]

[1]Center for Physical Sciences and Technology (FTMC), Saulėtekio ave. 3, Vilnius, Lithuania
hafiz.naeem@ftmc.lt

To meet the Greener Europe initiative, there is a need for efficient and industrially viable renewable energy sources, and electrochemical water splitting is one of the cleanest emerging methods for producing hydrogen. However, the oxygen evolution reaction (OER) is kinetically sluggish and is the bottleneck in alkaline water electrolysis, for which more efficient and consistent catalysts with lower overpotentials, higher current density, and chemical stability are required [1-3]. Among non-noble metal candidates, NiFe oxides and (oxy)hydroxides have gained attention due to their efficient alkaline OER, low cost, and favorable redox chemistry. In spite of having outstanding OER characteristics, they are often limited by poor electrical conductivity and poor long-term stability. In this study, the broader shift from “material-only” to electrode architecture engineering was primarily explored, in which a $Co(OH)_2$ sponge interlayer is electrochemically deposited on the Cu electrode, followed by the deposition of a NiFe framework. The NiFe framework was optimized by adjusting the deposition voltage through measurement of the representative composition using EDX after each deposition. Successful deposition of $Co(OH)_2$ interlayer and NiFe top layer was confirmed using the SEM and elemental area mapping. Improved OER catalytic activity of the NiFe system was achieved upon incorporation of $Co(OH)_2$, yielding an overpotential of 261 mV at the current density of 10 mA cm^{-2}, and a Tafel slope of 47 mV dec^{-1}. EIS studies revealed that the double-layer capacitance was increased with the incorporation of $Co(OH)_2$, i.e., from 0.06114 Fcm^{-2} for NiFe1.5 alone to 0.11 Fcm^{-2} for NiFe1.5@C1, signifying the synergy between the NiFe and $Co(OH)_2$ interlayer. The presence of $Co(OH)_2$ was further confirmed by Raman spectroscopy, and Fe was observed to exist as Fe_3O_4 at higher deposition amounts. The absence of metallic Ni or Fe signals in XRD suggested the formation of a mixture of amorphous-like oxides and hydroxides. Overall, this study revealed the beneficial effect of interlayer interactions for the design of heterogeneous electrocatalytic materials for water splitting.

[1] D. Pan, T. Zhai, R. Zhang, Y. Yuan, H. Wang, and S. Lu, ”Advancing layered double hydroxides (LDHs) as the anodes for efficient anion-exchange-membrane water electrolyzers,” Nano Research, vol. 19, no. 1, p. 94907937, 2026, doi: 10.26599/NR.2025.94907937.

[2] U. Shamraiz, A. Majeed, B. Raza, N. u. Ain, and A. Badshah, ”Exploring the potential of cobalt hydroxide and its derivatives as a cost-effective and abundant alternative to noble metal electrocatalysts in oxygen evolution reactions: a review,” Sustainable Energy & Fuels, 10.1039/D3SE00942D vol. 8, no. 3, pp. 422-459, 2024, doi: 10.1039/D3SE00942D.

[3] H. Zhou et al., ”Strategies to maximize the oxygen evolution reaction in layered double hydroxides by electronic defect engineering,” eScience, vol. 5, no. 5, p. 100380, 2025/09/01/ 2025, doi: https://doi.org/10.1016/j.esci.2025.100380

STABILITY OF HONEYCOMB-STRUCTURED COPPER FOAM ELECTRODES FOR CO_2 REDUCTION

Birutė Serapinienė[1], Jurga Juodkazytė[1], Algirdas Selskis[1], Rimantas Ramanauskas[1]

[1]Center for Physical Sciences and Technology, Vilnius, Lithuania
birute.serapiniene@ftmc.lt

The high Faradaic efficiency and selectivity of Cu electrodes toward the formation of C_2+ products during CO_2 reduction have attracted considerable interest [1]. However, smooth polycrystalline Cu electrodes exhibit relatively low catalytic activity, underscoring the need for improved electrode models. Electrodeposition of copper under conditions where hydrogen evolution occurs leads to the formation of three-dimensional nanostructured Cu electrodes, commonly referred to as Cu foams. These materials are characterized by a high density of interconnected and isolated pores, resulting in a large real surface area. Owing to these features, such structures are widely employed in various applications, including CO_2 reduction.

When discussing the interrelation between catalyst structure and activity, both facet dependence and potential- and/or reaction-induced morphological and structural changes must be considered for a given electrocatalytic process. Because electrocatalytic properties strongly depend on surface structure, the reconstruction behavior of Cu metal plays a critical role in its CO_2 reduction performance [2]. Numerous studies have demonstrated that initially well-defined morphologies and highly active sites are often lost during electrocatalysis due to surface reconstruction, leading to a degradation in catalytic performance [3].

In order to investigate the stability of Cu foam structures in the process of electrochemical CO_2 reduction we have performed an ex-situ SEM, electrochemically active surface area measurements and Pb UPD analysis of Cu 3D electrodes before and after 2 hours of potentiostatic polarization in CO_2 saturated $KHCO_3$ solution. It was observed that Cu foam retains its dendritic morphology even after undergoing electrochemical CO_2 reduction, indicating structural stability and potential reusability of the catalyst.

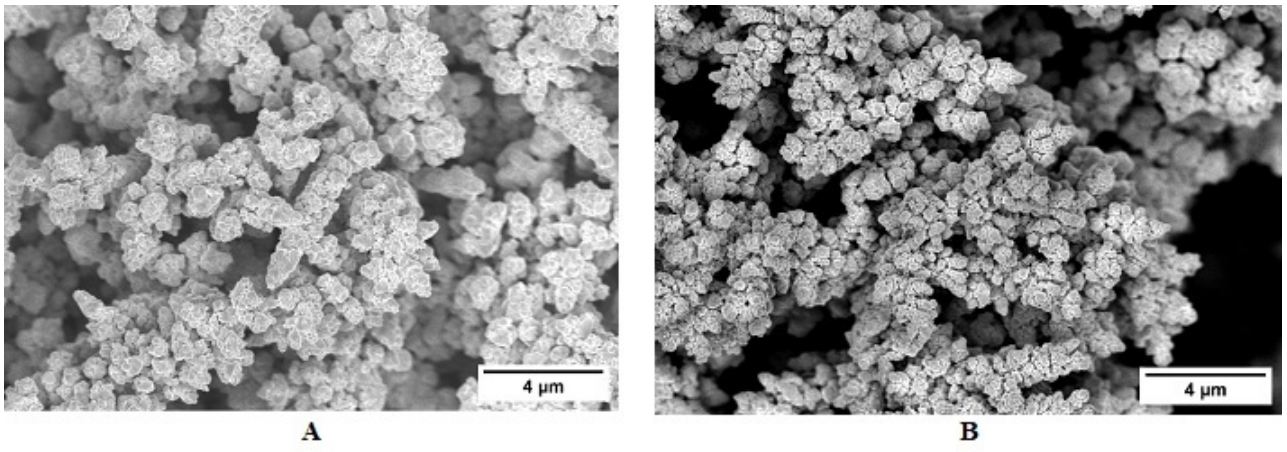


Fig. 1. SEM images of Cu I electrode before (A) and after (B) CO_2 reduction at -1.36 V in a 0.1 M $KHCO_3$ solution saturated with CO_2.

[1] Hori, Y. Electrochemical CO_2 Reduction on Metal Electrodes. In Modern Aspects of Electrochemistry. Modern Aspects of Electrochemistry; Vayenas, C.G., White, R.E., Gamboa-Aldeco, M.E., Eds.; Springer: New York; Vol. 42. (2008)

[2] Serapinienė, B.; Naujalis, E.; Selskis, A.; Juodkazytė, J.; Ramanauskas, R. Electrochemical reduction of CO_2 to C2 hydrocarbons using Cu 3D nanostructures. Materials, 18, 4210. (2025)

[3] Burwell, T.; Thangamuthu, M.; Aliev, G.N.; Ghaderzadeh, S.; Kohlrausch, E.C.; Chen, Y.; Theis, W.; Norman, L.T.; Fernandes, J.A.; Besley, E.; et al. Direct Formation of Copper Nanoparticles from Atoms at Graphitic Step Edges Lowers Overpotential and Improves Selectivity of Electrocatalytic CO_2 Reduction. Commun Chem, 7, 140. (2024)

CeO_2 /Pd-CA FOR OXYGEN REDUCTION REACTION IN ALKALINE MEDIA

Ana Nastasić[1], Jadranka Milikić[2], David Tomić[2], Meryem Samancı[3], Ayşe Bayrakçeken[3], Biljana Šljukić[2,4], Aldona Balčiūnaitė[5]

[1]University of Belgrade, Vinča Institute of Nuclear Sciences – National Institute of the Republic of Serbia, Department of Nuclear and Plasma Physics, Serbia
[2]University of Belgrade, Faculty of Physical Chemistry, Serbia
[3]Atatürk University, Department of Chemical Engineering, Turkey
[4]Universidade de Lisboa, Instituto Superior Tecnico, Chemical Engineering Department, Center of Physics and Engineering of Advanced Materials, Laboratory for Physics of Materials and Emerging Technologies, Portugal
[5]Department of Catalysis, Center for Physical Sciences and Technology, Lithuania
ana.nastasic@vin.bg.ac.rs

Carbon aerogels (CAs) have recently gained recognition as highly promising materials for numerous energy and environmental applications due to their three-dimensional porous architecture, high specific surface area, ultralow density, and outstanding electrical conductivity. In oxygen reduction reaction (ORR) electrocatalysis, doped and metal-decorated CAs represent potentially cost-effective alternatives to precious benchmark catalysts, offering versatility for both two- and four-electron reaction pathways, relevant for sustainable H_2O_2 production and electrochemical energy systems, respectively [1].

In this study, CeO_2 was grafted onto Pd-CA by the chemical co-precipitation method, at CeO_2:Pd-CA mass ratios of 1:2 and 2:1. ORR activity of CeO_2/Pd-CA materials was investigated in 1 M KOH using linear sweep voltammetry with a rotating disc electrode at 1600 rpm (**Figure 1**).

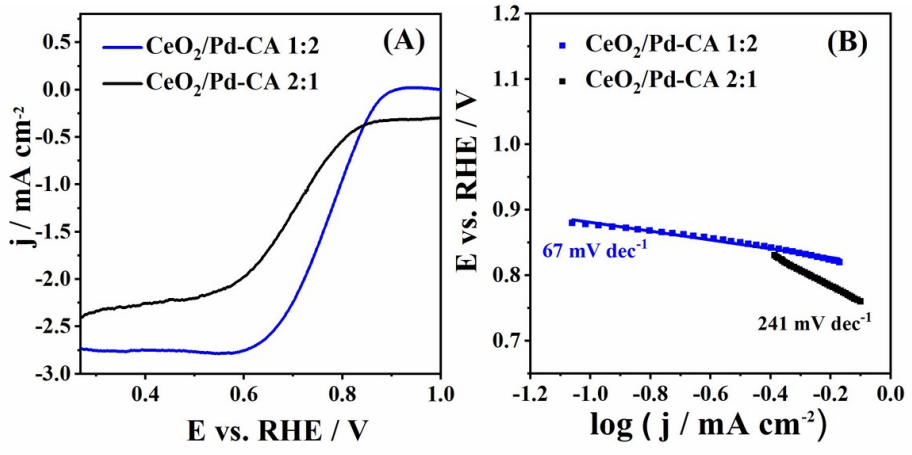


Fig. 1. ORR RDE curves of CeO_2/Pd-CA 1:2 and CeO_2/Pd-CA 2:1 in O_2- saturated 1 M KOH solution at 1600 rpm and 20 mV s^{-1} (A) with the corresponding Tafel plots (B).

Key ORR parameters, including onset potential (E_{onset}), half-wave potential ($E_{1/2}$), and Tafel slope, were determined. CeO_2/Pd-CA 1:2 material exhibited superior performance, with E_{onset} of 0.87 V,$E_{1/2}$ of 0.77 V, and a low Tafel slope of 67 mV dec^{-1}, indicating beneficial ORR kinetics. In contrast, the composite with a 2:1 weight ratios showed slightly lower activity (E_{onset} = 0.83 V, $E_{1/2}$ = 0.70 V) and a much higher Tafel slope (241 mV dec^{-1}), suggesting slower kinetics. CeO_2/Pd-CA composites exhibit promising ORR activity, with performance depending on the CeO_2:Pd-CA ratio, demonstrating their potential as effective electrocatalysts for ORR.

Acknowledgements

The authors would like to thank the Ministry of Science, Technological Development, and Innovation of the Republic of Serbia for support through contracts no. 451-03-136/2025-03/200146 and 451-03-137/2025-03/200146, as well as Fundação para a Ciência e a Tecnologia (FCT, Portugal) for contracts LAPMET-LA/P/0095/2020-IST-ID and https://doi.org/10.54499/UID/04540/2025. A.N. acknowledges support provided by the Vinča Institute of Nuclear Sciences, through contract no. 451-03-136/2025-03/200017 with the Ministry of Science, Technological Development, and Innovation of the Republic of Serbia.

[1] D. Tomić et al., "Carbon aerogels and xerogels: next-generation materials for sustainable energy and environmental solutions," Chemical Communications, vol. 61, no. 80, pp. 15510–15523, Jan. 2025, doi: 10.1039/d5cc02477c.

NANOSIZED CoM/rGO COMPOSITES AS AN EFFICIENT OXYGEN REDUCTION ELECTRODE MATERIAL

Ana Nastasić[1], Jadranka Milikić[2], Kristina Radinović[2], David Tomić[2], Biljana Šljukić[2,3], Aldona Balčiūnaitė[4]

[1]University of Belgrade, Vinča Institute of Nuclear Sciences – National Institute of the Republic of Serbia, Department of Nuclear and Plasma Physics, Serbia
[2]University of Belgrade, Faculty of Physical Chemistry, Serbia
[3]Universidade de Lisboa, Instituto Superior Tecnico, Chemical Engineering Department, Center of Physics and Engineering of Advanced Materials, Laboratory for Physics of Materials and Emerging Technologies, Portugal
[4]Department of Catalysis, Center for Physical Sciences and Technology, Lithuania
ana.nastasic@vin.bg.ac.rs

The oxygen reduction reaction (ORR) is a key cathodic reaction in alkaline fuel cells (AFCs) and metal-air batteries (MABs); yet its sluggish kinetics remain a major limiting factor of their performance. Although platinum-based materials exhibit high ORR activity, their high cost, scarcity and insufficient durability motivate the search for alternative materials [1-3]. In this context, earth-abundant transition metals, especially cobalt (Co), have emerged as relevant ORR electrocatalysts owing to their electronic structures and favorable interactions with ORR intermediates.

In this work, electrocatalysts based on Co combined with iron (Fe) or nickel (Ni) and supported on reduced graphene oxide (rGO) were investigated for ORR in alkaline media by linear sweep voltammetry using a rotating disc electrode. Key ORR kinetic parameters including onset potential (E_{onset}), half-wave potential ($E_{1/2}$) and Tafel slope (b) were determined. Both materials showed similar values of E_{onset} (0.81 V for CoNi/rGO and 0.83 V for CoFe/rGO) and $E_{1/2}$ (0.71 V for CoNi/rGO and 0.72 V for CoFe/rGO). However, CoNi/rGO exhibited a significantly lower Tafel slope (75 mV dec^{-1}) compared to CoFe/rGO (161 mV dec^{-1}), indicating a more favorable ORR rate. In conclusion, both tested Co-based composites demonstrated good performance for ORR, making them promising, more affordable alternatives to cathode materials for AFCs and MABs.

Acknowledgements

The authors acknowledge the financial support from the Science Fund of the Republic of Serbia, grant number 250, High-performance NANosize Oxygen Electrodes: transition metals deposited ON reduced graphene oxide vs. high-entropy alloy alternatives-NANO-E-ON (Diaspora: Support for Visits of Diaspora Scientists programme). The authors would also like to thank the Ministry of Science, Technological Development, and Innovation of the Republic of Serbia for support through contracts no. 451-03-136/2025-03/200146 and 451-03-137/2025-03/200146, as well as Fundação para a Ciência e a Tecnologia (FCT, Portugal) for contracts LAPMET-LA/P/0095/2020-IST-ID and https://doi.org/10.54499/UID/04540/2025. A.N. acknowledge support provided by the Vinča Institute of Nuclear Sciences, through contract no. 451-03-136/2025-03/ 200017 with the Ministry of Science, Technological Development, and Innovation of the Republic of Serbia.

[1] J. Milikić, A. Nastasić, M. Martins, C. a. C. Sequeira, and B. Šljukić, "Air cathodes and bifunctional oxygen electrocatalysts for aqueous Metal–Air batteries," Batteries, vol. 9, no. 8, p. 394, Jul. 2023, doi: 10.3390/batteries9080394.
[2] J. Milikić et al., "Efficient nano-size ZnM/rGO (M = Ni, Cu, and Fe) electrocatalysts for oxygen electrode reactions in alkaline media," International Journal of Hydrogen Energy, vol. 97, pp. 247–258, Nov. 2024, doi: 10.1016/j.ijhydene.2024.11.406.
[3] K. Gočanin et al., "Advanced nitrogen-doped transition metal oxides decorated with Pt: synthesis and composition strategies for maximised electrochemical performance," Dalton Transactions, vol. 54, no. 37, pp. 13934–13949, Jan. 2025, doi: 10.1039/d5dt01211b.

Ru-DECORATED Co/C CATALYST FOREFFICIENT HYDROGEN EVOLUTION REACTION

Julija Usavičiūtė[1], Virginija Kepenienė[1], Raminta Stagniūnaitė[1], Jūratė Vaičiūnienė[1], Loreta Tamašauskaitė-Tamašiūnaitė[1]

[1]Center for Physical Sciences and Technology, Department of Catalysis, Vilnius, Lithuania
julija.usaviciute@ftmc.lt

The accelerated evolution of renewable energy technologies has prompted extensive research into advanced catalytic materials that can facilitate efficient and sustainable energy conversion processes. A significant challenge in this field pertains to the extensive reliance on catalysts composed of pure noble metals. The high cost and limited availability of these metals hinder their large-scale deployment. In order to address this issue, current research efforts are focusing on reducing noble metal content by designing composite catalysts based on earth-abundant d-block metals, metal oxides, or their hybrids. These catalysts can provide comparable catalytic activity through synergistic effects [1-3].

Hydrogen has emerged as a clean and environmentally friendly energy carrier, and electrochemical water splitting represents a promising pathway for its sustainable production. The hydrogen evolution reaction (HER) is of particular significance in the context of green hydrogen generation. However, the effective catalysts required to surmount kinetic limitations are not yet available.

In this study, a Ru-decorated Co/C catalyst was synthesized to combine the high intrinsic activity of ruthenium with the cost-effectiveness of a cobalt-based support. The synergistic interaction between Ru and Co, combined with the high surface area and conductivity of the carbon support, is expected to promote favorable hydrogen adsorption and accelerate reaction kinetics [1-3]. Ru nanoparticles were deposited onto a Co/C substrate via a chemical reduction method using sodium borohydride as the reducing agent. The composition and morphology of prepared RuCo/C catalyst were characterized by Field Emission Scanning Electron Microscopy (FESEM) method and inductively coupled plasma optical emission spectroscopy (ICP-OES). The electrocatalytical properties of the RuCo/C catalyst were investigated toward the hydrogen evolution reaction by using linear sweep voltammetry.

It has been found that prepared RuCo/C catalyst with reduced amount of noble metal exhibited excellent HER overpotential of 70 mV at a current density of 10 mA cm^{-2} at the temperature of 25 °C.

[1] Zhao, J., Urrego-Ortiz, R., Liao, N., et al. Rationally designed Ru catalysts supported on TiN for highly efficient and stable hydrogen evolution in alkaline conditions. Nature Communications 2024, 15, 6391.

[2] Wang, J., Wang, D., Huang, T., He, Z., Cui, Y., Li, J., Boosting Hydrogen Evolution via Phase Engineering-Modulated Crystallinity of Ruthenium–Zinc Bimetallic MOFs. Catalysts 2025, 15(1), 58.

[3] Shi, Z., Nie, K., Shao, Z.-J., Gao, B., Lin, H., Zhang, H., Liu, B., Wang, Y., Zhang, Y., Sun, X., Phosphorus-modified ruthenium for hydrogen evolution catalysis. Energy & Environmental Science 2017, 10, 1262–1271.

OPERANDO XRD STUDY ON THE STRUCTURAL CHANGES OF ZINC HEXACYANOFERRATE IN AQUEOUS ZINC-ION BATTERIES

Dovilė Škarnulytė[1,2], Linas Vilčiauskas[1,2], Jurgis Pilipavičius[1,2]

[1]Vilnius University, Institute of Chemistry, Naugarduko 24, LT-03225, Vilnius, Lithuania
[2]Centre for Physical Sciences and Technology, Sauletekio av. 3, LT-10257, Vilnius, Lithuania
dovile.skarnulyte@chgf.vu.lt

Economic development and rapid population growth are among the factors contributing to the increasing demand for energy. [1] At the same time, growing awareness of the environmental impact of non-renewable resources is accelerating the transition toward renewable energy generation. However, energy supply from weather-dependent sources (sun, wind, etc.), creates imbalance between electricity production and consumption. [2] Possible solution to this problem is the development of large-scale battery parks that can store excess energy and supply it when needed.

Aqueous zinc-ion batteries (AZIBs) have attracted considerable attention as an environmentally benign alternative to widely used lithium-ion systems. [3] A promising cathode material in AZIB systems is a Prussian blue analogue zinc hexacyanoferrate(II, III) (ZnHCF, $Zn_{3+x}[Fe(CN)_6]_2$, $0 < x < 1$), which, depending on synthesis conditions, can crystallize in cubic and rhombohedral structures. [4] The open framework of ZnHCF allows the intercalation of various metal ions such as K^+, Na^+, Zn^{2+}. Nevertheless, practical implementation of these batteries remains challenging, as the mechanism of Zn-ion intercalation is still poorly understood.

This study aims to investigate structural changes occurring during charge/discharge processes using the operando XRD method. The obtained results demonstrate a phase transitions between cubic and rhombohedral crystal phases during cycling. These findings deepen the understanding of the structural and electrochemical properties of ZnHCF and provide guidance for enhancing its performance as a cathode material in safer and more sustainable aqueous zinc-ion batteries.

[1] A. Demirbas, „Energy issues and energy priorities“, Energy Sources, Part B: Economics, Planning, and Policy, vol. 3, no. 1, pp. 41–49, 2007.
[2] K. Hedegaard, P. Meibom, „Wind power impacts and electricity storage – A time scale perspective“, Renew Energy, vol. 37, no. 1, pp. 318–324, 2012.
[3] B. Tang et al., „Issues and opportunities facing aqueous zinc-ion batteries“, Energy Environ Sci, vol. 12, no. 11, pp. 3288–3304, 2019.
[4] J. Rodríguez-Hernández et al., „An atypical coordination in hexacyanometallates: Structure and properties of hexagonal zinc phases“, Journal of Physics and Chemistry of Solids, vol. 68, no. 9, pp. 1630–1642, 2007.

X-RAY DIFFRACTION STUDIES OF In_2S_3 LAYERS DEPOSITED ON POLYAMIDE 6 SURFACES

Ema Juocinskyte[1], Skirma Zalenkiene[1]

[1]Lithuania, Kaunas University of Technology, Faculty of Chemistry and Chemical Technology, Department of Physical and Inorganic Chemistry
ema.juocinskyte@ktu.edu

The scientific community has shown significant interest in indium sulfide, particularly due to its high photoconductivity, stability, and suitable wide optical bandgap for the fabrication of UV photodetectors [1]. Moreover, the wide bandgap of In_2S_3 enables greater transmission of incident light to the absorber layer, thereby enhancing the short-circuit current [2]. Despite the strong potential of In_2S_3 as a replacement for hazardous CdS, research on indium sulfide thin layers on flexible substrates is still insufficient.

In this study, In_2S_3 thin films were deposited on polyamide 6 via chemical bath deposition (CBD). Polyamide 6 (PA 6) films were boiled in distilled water for 2 h, then dried using filter paper and kept in a desiccator over silica gel. The PA 6 films were immersed in a mixture of indium sulfate ($In_2(SO_4)_3 \cdot 7H_2O$) and thioacetamide (C_2H_5NS) solutions at 70 °C. The samples were kept in the solution for 10 to 70 min.

The structural and morphological characteristics of the resulting layers were investigated using X-ray diffraction analysis. Two research methods were employed: conventional X-ray diffraction (XRD) and grazing incidence X-ray diffraction (GiXRD). The results were analyzed and compared. Both analyses confirmed the successful formation of crystalline In_2S_3 thin films on the surface of polyamide 6.

This study presents an environmentally friendly and cost-effective approach for depositing In_2S_3 layers on polyamide 6 surfaces. X-ray diffraction analysis confirms the successful formation and structural quality of the deposited films. The results support the development of sustainable and low-impact materials for future optoelectronic and energy-related applications, offering an eco-friendly alternative to conventional, resource-intensive technologies.

[1] P. Murahari, D. Alagarasan, S. S. Hegde, H. D. Shetty, M. Verma, N. A. Siddiqui, A. Khan, and S. P. Kollur, “High-performance photodetector applications of antimony doped indium sulfide thin films: Preparation, characterization and optical studies,” Optical Materials, vol. 162, Art. no. 116903, 2025, doi: 10.1016/j.optmat.2025.116903

[2] A. Ledesma-Juárez, J. F. Quintero-Guerrero, and A. M. Fernández, “Structural, morphological and optical comparison of In-S films deposited by CBD and ultrasonic pyrolytic spraying, as a buffer layer in CIGS solar cells,” Chalcogenide Letters, vol. 22, no. 12, pp. 1009–1018, 2025, doi: 10.15251/CL.2025.2212.1009.

STUDY ON REUSABILITY OF MAGNETIC CHITOSAN WITH DIFFERENT MAGNETIZATION LEVEL FOR RADIONUCLIDE REMOVAL

Matas Skripkauskas[1,2], Sergej Šemčuk[2], Galina Lujanienė[2], Martynas Talaikis[2], Vidas Pakštas[2], Kęstutis Mažeika[2]

[1]Vilnius University, Life Sciences Center, Vilnius, Lithuania
[2]State Research Institute Center for Physical Sciences and Technology (FTMC), Vilnius, Lithuania
matas.skrip8@gmail.com

The increasing presence of heavy metals and persistent pollutants in aquatic environments poses a significant threat to ecological integrity and public health. Traditional water purification methods often involve high costs, substantial energy consumption, or the generation of secondary waste streams, highlighting the need for more sustainable solutions. Recent studies show that these limitations can be addressed by developing recyclable and magnetically separable sorbents, which reduce chemical usage and simplify post-treatment recovery, supporting more environmentally responsible water treatment strategies [1]. In eco-chemistry, natural polymer-based sorbents that are biodegradable and reusable have emerged as promising environmentally friendly options for water remediation. Magnetic chitosan composites combine the adsorption capacity of chitosan with magnetic separability, reducing secondary waste and operational complexity [2]. Incorporating magnetic components also enables repeated regeneration and reuse, enhancing process sustainability and economic feasibility compared with conventional non-recoverable sorbents [3]. This study evaluated the reusability and performance consistency of magnetic chitosan nanocomposite (MCN) as a green sorbent, focusing on its capacity and applicability over multiple treatment cycles in water purification systems.

MCNs were synthesized by embedding various ratios of Fe3O4 nanoparticles within a chitosan (100,000–300,000 m.v.) matrix using a crosslinking method. The prepared MCNs were characterized by XRD, TEM, FT-IR, Mössbauer spectroscopy, and magnetization measurements; zero-point charge (pHzpc) and separation parameters were also determined. To assess reusability and potential changes in adsorption performance, multiple adsorption–desorption cycles were conducted using heavy metals (Cs(I) and Eu(III) ions) traced with radionuclides as adsorbates. The study confirms that reusable magnetic chitosan is a promising material for sustainable water treatment applications. Its biodegradability, low toxicity, and reusability are consistent with the principles of green chemistry, supporting the development of environmentally responsible technologies that reduce waste generation and resource consumption.

[1] M. C. Lefatle, L. M. Madikizela, V. E. Pakade, and P. N. Nomngongo, “Magnetic chitosan-zeolite composite as an adsorbent in ultrasound-assisted magnetic solid phase extraction of tetracyclines in water samples,” Journal of Analytical Science & Technology, vol. 14, no. 1, Jul. 2023, doi: 10.1186/s40543-023-00394-1.

[2] F. Karimi et al., “Removal of metal ions using a new magnetic chitosan nano-bio-adsorbent; A powerful approach in water treatment,” Environmental Research, vol. 203, p. 111753, Jul. 2021, doi: 10.1016/j.envres.2021.111753.

[3] D. A. Demirezen, D. D. Yılmaz, and Y. Ş. Yıldız, “Magnetic chitosan/calcium alginate double-network hydrogel beads: Preparation, adsorption of anionic and cationic surfactants, and reuse in the removal of methylene blue,” International Journal of Biological Macromolecules, vol. 239, p. 124311, Apr. 2023, doi: 10.1016/j.ijbiomac.2023.124311.

HETEROGENEOUS EPOXIDATION OF ALKENES USING BIOMASS-DERRIVED CATALYST

Eivydas Trioška[1], Carl Johan Wallentin[2], Edvinas Orentas[1]

[1]Vilnius University, Faculty of Chemistry and Geosciences, Vilnius, Lithuania
[2]Gothenburg University, Faculty of Science and Technology, Gothenburg, Sweden
eivydas.trioska@chgf.stud.vu.lt

Epoxides (also known as oxiranes) are cyclic three-membered ethers, that, due to significant ring strain, are more reactive than their non-cyclic counterparts. Phytic acid (PA) is an achiral meso-compound (*myo*-stereoisomer) with six phosphate ester groups that contain 12 acidic hydrogen atoms. Phytic acid is most often extracted from various seeds, nuts and grains and, due to its abundance, research into new uses for PA has been of great interest. In contrast to vanadyl (IV) acetylacetonate, the use of vanadyl (IV) phytate in organic reactions is poorly studied. In this study, the heterocatalytic reaction, consisting of dispersing VP catalyst in petroleum ether together with tert-butyl hydroperoxide (TBHP) and the substrate was investigated, while later reactions were performed using *Biotage®* Initiator microwave reactor at 60-80 ℃ for 5-10 min with yields up to 91 %. High selectivity for cinnamyl alcohol (α-methyl cinnamyl alcohol) and cyclohexenone (3-methylcyclohexenone) derivatives was observed.

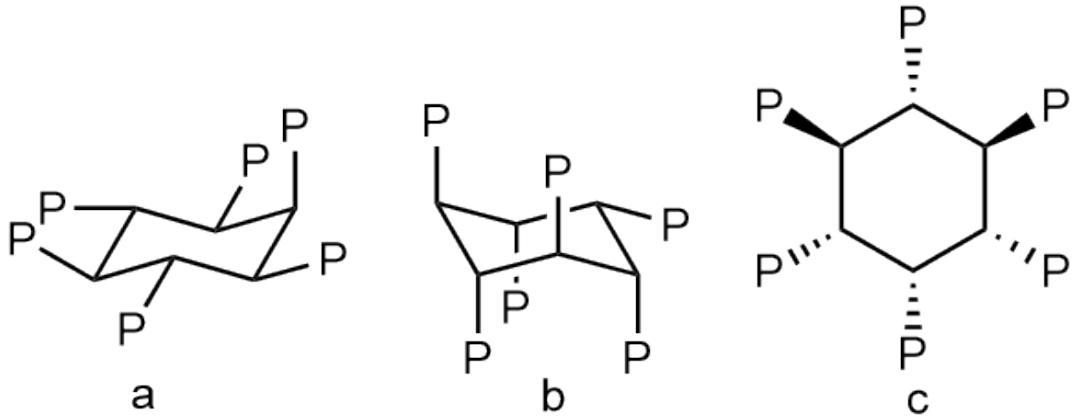


Fig. 1. (a) 1a5e PA conformation (b) 5a1e PA conformation (c) standard representation of PA molecular structure. Note that P stands for phosphate group $-P(=O)(OH)_2$.

SYNTHESIS OF SUBSTITUTED BENZIMIDAZOTHIAZINES AND THIAZOLES FOR THE SEARCH OF AMYLOID AGGREGATION MODULATORS

Linas Petrauskas[1], Rita Bukšnaitienė[2]

[1]Faculty of Medicine, Vilnius University, M. K. Čiurlionio str. 21, Vilnius, Lithuania
[2]Institute of Chemistry, Faculty of Chemistry and Geosciences, Vilnius University, Naugarduko str. 24, Vilnius, Lithuania
linas.petrauskas@mf.stud.vu.lt

Amyloid fibril formation is a common pathological feature of protein-misfolding disorders, where nucleation-dependent aggregation can generate heterogeneous intermediates such as oligomeric species, before mature cross-beta fibrils accumulate [1]. In synucleinopathies such as Parkinson's disease, the presynaptic alpha-synuclein undergoes misfolding, oligomerization and fibrillization, contributing to cellular stress pathways and progressive neurodegeneration [2], [3]. Because toxic effects are frequently linked to early assemblies rather than mature fibrils, targeting the aggregation pathway with small-molecule compounds is a promising therapeutic direction [1], [2]. Among emerging scaffolds, imidazo[2,1-b][1,3]thiazine derivatives were shown to inhibit primary nucleation and stabilize alpha-synuclein oligomeric states [4]. The pharmacophore could be a promising source of derivatives for modulating amyloid aggregation. This study aims to synthesize and characterize different benzimidazothiazines and appropriate thiazoles with potential amyloid aggregation reducing activity.

Firstly, the starting compound, a benzoimidazole-2-thione intermediate, was synthesized via the thiocarbonylation and intramolecular cyclocondensation of N-propargylated diaminobenzene with thiocarbonyldiimidazole. Multiple reaction pathways were chosen to produce the following compounds. Base-mediated intramolecular nucleophilic cyclization favors the formation of the benzoimidazothiazole core. Alternatively, electrophilic halocyclization with NCS produces a similar chlorinated derivative. Finally, the benzoimidazothiazine core was achieved through metal-activated intramolecular cyclization with gold(III) bromide.

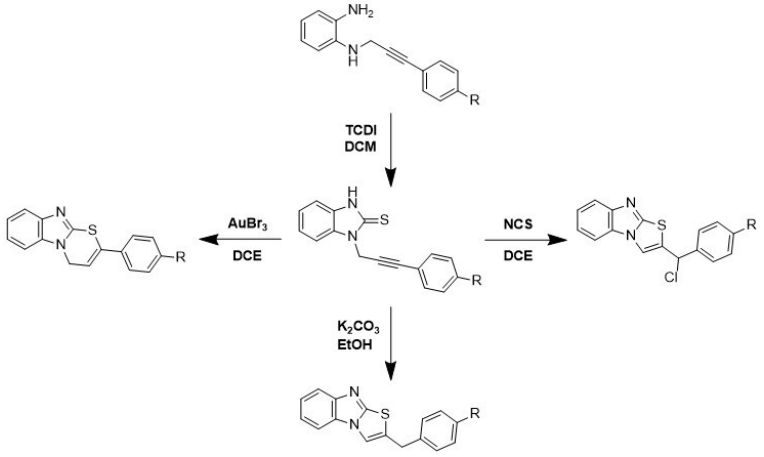


Fig. 1. General scheme of reactions

[1] P. C. Ke et al., "Half a century of amyloids: past, present and future," Chem. Soc. Rev., vol. 49, no. 15, pp. 5473–5509, 2020, doi: 10.1039/C9CS00199A
[2] O. Arias-Carrión, M. Guerra-Crespo, F. J. Padilla-Godínez, L. O. Soto-Rojas, and E. Manjarrez, "α-Synuclein Pathology in Synucleinopathies: Mechanisms, Biomarkers, and Therapeutic Challenges," IJMS, vol. 26, no. 11, p. 5405, Jun. 2025, doi: 10.3390/ijms26115405.
[3] J. Pitton Rissardo, A. McGarry, Y. Shi, A. L. Fornari Caprara, and G. T. Kannarkat, "Alpha-Synuclein Neurobiology in Parkinson's Disease: A Comprehensive Review of Its Role, Mechanisms, and Therapeutic Perspectives," Brain Sciences, vol. 15, no. 12, p. 1260, Nov. 2025, doi: 10.3390/brainsci15121260.
[4] I. Misiūnaitė et al., "Imidazo[2,1- b][1,3]thiazine Derivatives as Potential Modulators of Alpha-Synuclein Amyloid Aggregation," ACS Chem. Neurosci., vol. 15, no. 24, pp. 4418–4430, Dec. 2024, doi: 10.1021/acschemneuro.4c00451.

SYNTHESIS OF NEW 4-(4-CHLOROPHENYL)-1-(3,4,5-TRIMETHOXYPHENYL)-1H-IMIDAZOLE-2-THIOL DERIVATIVES

Birutė Grybaitė[1], Natalia Maciejewska[2], Vytautas Mickevičius[1]

[1]Kaunas University of Technology, Department of Organic Chemistry, Radvilėnų pl. 19, 50254 Kaunas, Lithuania
[2]Gdansk University of Technology, Faculty of Chemistry, Department of Pharmaceutical Technology and Biochemistry, Narutowicza St 11/12, 80-233 Gdansk, Poland
birute.grybaite@ktu.lt

Nitrogen-containing heterocycles constitute an essential class of structural motifs in medicinal chemistry and drug development. In particular, imidazole derivatives have gained sustained interest due to their favorable physicochemical properties and biological relevance. The imidazole ring is present in key endogenous molecules, enabling diverse noncovalent interactions with biological targets. As a consequence, imidazole-based compounds exhibit a broad range of pharmacological activities, including analgesic, antihypertensive, anticancer, antiviral, antitubercular, anti-inflammatory, and antidepressant effects [1-3].

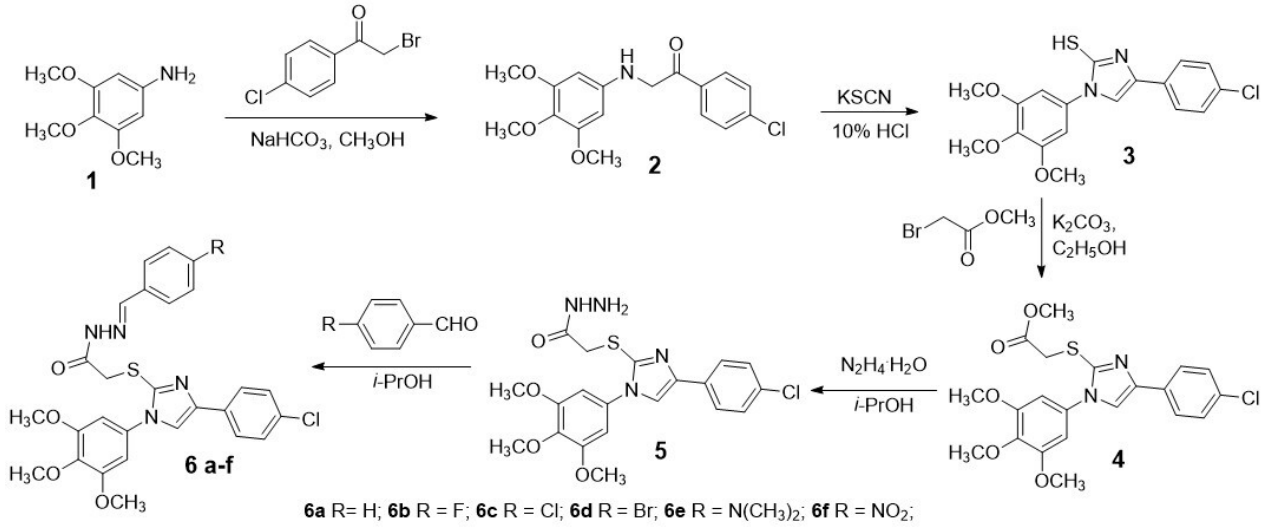


Fig. 1. Synthesis of compounds **2–6**.

In this study, 3,4,5-trimethoxyaniline **(1)** upon reaction with 2-bromo-4′-chloroacetophenone in methanol at room temperature for 2h formed the target 1-(4-chlorophenyl)-2-((3,4,5-trimethoxyphenyl)amino)ethan-1-one **(2)**. To obtain compound **3**, This *α*-amino ketone **2** reacted with potassium thiocyanate in diluted HCl. The reactions afforded imidazole-2-thione **3**. We found that the reaction of compound **3** with methyl bromoacetate in ethanol, in the presence of potassium carbonate, occurred uniquely to give the product of S-alkylation – methyl 2-((4-(4-chlorophenyl)-1-(3,4,5-trimethoxyphenyl)-1H-imidazol-2-yl)thio)acetate **(4)**. The obtained methyl ester **4** was transformed into hydrazide **5** using hydrazine monohydrate in 2-propanol (Fig. 1). Condensation of compound **5** with aromatic aldehydes in propan-2-ol led to the formation of *N*′-benzylidene hydrazides **6a–f**. The structures of the obtained compounds were confirmed by the data of the ^{1}H, ^{13}C NMR and FT-IR spectroscopy and elemental analysis.

[1] H. V. Tolomeu and C. A. M. Fraga, “Imidazole: Synthesis, Functionalization and Physicochemical Properties of a Privileged Structure in Medicinal Chemistry,” Molecules, vol. 28, no. 2, p. 838, Jan., 2023.
[2] V. Amita, S. Joshi, and D. Singh, “Imidazole: Having Versatile Biological Activities,” Journal of Chemistry, 2013.
[3] X. Zhang, Y. Li, H. Wei, W. Zhao, and J. Zhou, “Insight into the stabilization mechanism of imidazole-based ionic liquids at the interface of the carbon nanotubes: A computational study,” Journal of Molecular Liquids, vol. 375, p. 121320, Apr., 2023.

SYNTHESIS OF IMIDAZO(2,1-b)(1,3)THIAZINES VIA ELECTROPHILE-PROMOTED CYCLIZATION OF 2-ALKENYLTHIOIMIDAZOLES

Martyna Paulauskaitė[1], Ieva Žutautė[1]

[1]Vilnius University, Faculty of Chemistry and Geosciences, Vilnius, Lithuania
martyna.paulauskaite@chgf.stud.vu.lt

Compounds containing an imidazo[2,1-*b*][1,3]thiazine fragment exhibit a wide range of biological properties, including anti-tuberculosis [1], anti-inflammatory [2], antifungal [3], and amyloid aggregation inhibitory [4] activities. These diverse biological activities highlight the importance of this heterocyclic system in medicinal chemistry, as imidazo[2,1-*b*][1,3]thiazine derivatives display structure–activity trends that enable targeted modification of the core structure to improve biological efficacy. This system's high chemical stability and ability to interact with biomolecules selectively further support its importance in synthetic and medicinal chemistry. Due to the biological significance of this heterocyclic system, developing efficient synthetic strategies is important. Conventional approaches to constructing the imidazo[2,1-*b*][1,3]thiazine framework typically involve nucleophilic substitution or condensation reactions. These methods often require multiple synthetic steps and are associated with limited overall efficiency. In recent years, electrophile-promoted nucleophilic cyclization reactions have emerged as an effective strategy for the one-step formation of complex heterocyclic systems [5]. This approach not only enables efficient formation of the imidazo[2,1-*b*][1,3]thiazine core but also ensures good selectivity and high yields, making it a promising tool for the synthesis of structurally diverse derivatives.

In this study, electrophile-initiated cyclization reactions of 2-alkenylthioimidazoles were investigated. 2-Cinnamylthiobenzimidazole was selected as a model substrate for the optimization of cyclization reaction conditions. The optimized reaction conditions were applied to the cyclization of other 2-alkenylthioimidazole analogues. The resulting compounds underwent base-promoted elimination to efficiently yield the corresponding imidazo[2,1-*b*][1,3]thiazine derivatives (Fig. 1).

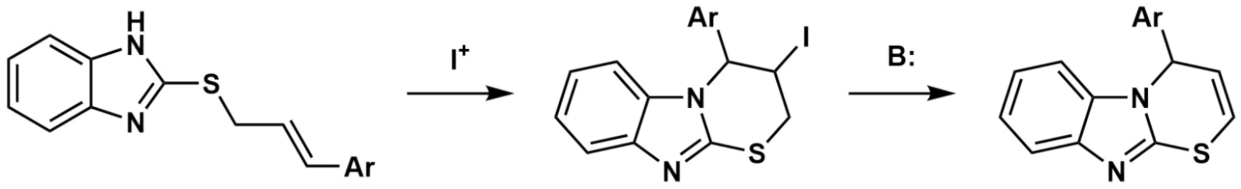


Fig. 1. Synthesis of benzimidazo[2,1-*b*][1,3]thiazine frameworks

[1] J.-X. Gong, Y. He, Z.-L. Cui, and Y.-W. Guo, "Synthesis, spectral characterization, and antituberculosis activity of thiazino[3,2-A]benzimidazole derivatives," Phosphorus, Sulfur, and Silicon and the Related Elements, vol. 191, no. 7, pp. 1036–1041, Feb. 2016, doi: 10.1080/10426507.2015.1135149.

[2] N. Slyvka, L. Saliyeva, S. Holota, M. Litvinchuk, S. Shishkina, and M. Vovk, "Synthesis and anti-inflammatory activity of S-oxides of pyridinyloxy substituted imidazo[2,1-b][1,3]thiazines," Current Chemistry Letters, vol. 12, no. 2, pp. 335–342, Jan. 2023, doi: 10.5267/j.ccl.2022.12.006.

[3] M. D. LaFleur, E. Lucumi, A. D. Napper, S. L. Diamond, and K. Lewis, "Novel high-throughput screen against Candida albicans identifies antifungal potentiators and agents effective against biofilms," Journal of Antimicrobial Chemotherapy, vol. 66, no. 4, pp. 820–826, Jan. 2011, doi: 10.1093/jac/dkq530.

[4] I. Misiunaite et al., "Imidazo[2,1-b][1,3]thiazine Derivatives as Potential Modulators of Alpha-Synuclein Amyloid Aggregation," ACS Chemical Neuroscience, vol. 15, no. 24, pp. 4418–4430, Nov. 2024, doi: 10.1021/acschemneuro.4c00451.

[5] B. Godoi, R. F. Schumacher, and G. Zeni, "Synthesis of heterocycles via electrophilic cyclization of alkynes containing heteroatom," Chemical Reviews, vol. 111, no. 4, pp. 2937–2980, Mar. 2011, doi: 10.1021/cr100214d.

PLANT-AVAILABLENUTRIENTS FROM ORGANIC MATERIALS: N, P, AND K EXTRACTION IN DIFFERENT MEDIA

Karina Kuzborskaja[1], Kristina Jančaitienė[1]

[1]Kaunas University of Technology, Faculty of Chemical Technology, The Department of Physical and Inorganic Chemistry, Kaunas, Lithuania
karina.kuzborskaja@ktu.edu

Soil degradation is an increasing global problem driven by intensive agriculture, excessive use of mineral fertilizers, and declining organic matter content, which together reduce soil fertility and nutrient availability for plants. Sustainable alternatives are therefore required to restore soil health and ensure long-term agricultural productivity. Organic fertilizers derived from biodegradable waste materials represent a promising solution, as they recycle nutrients and improve soil properties.

This study investigates the availability of plant-essential macronutrients – nitrogen (N), phosphorus (P), and potassium (K) – from selected organic residues, including banana peels, coffee bean husks, pine cones, and dried leaves and stems of violet and pink lupins. These materials were evaluated as potential raw resources for organic fertilizer production. Nutrient extraction was performed using three different approaches: aqueous extraction, alkaline extraction with 0,5 N KOH, and mineralization in concentrated H_2SO_4, allowing comparison of nutrient release under different chemical conditions.

The results indicate that potassium was most readily released in aqueous extracts, particularly from banana peels, while lupin and coffee bean husks biomass served as an efficient source of phosphorus. Nutrient solubilization was enhanced under alkaline conditions, while mineralization ensured the highest extraction efficiency for nitrogen and phosphorus, emphasizing the influence of chemical treatment on nutrient availability.

These findings confirm that common organic wastes can serve as valuable sources of plant-available N, P, and K. The study highlights the potential of converting organic residues into environmentally friendly fertilizers, contributing to sustainable nutrient management and soil fertility improvement.

SYNTHESIS OF NOVEL BENZIMIDAZOTHIAZINE DERIVATIVES AS POTENTIAL MODULATORS OF AMYLOID AGGREGATION

Urtė Milerytė[1], Rita Bukšnaitienė[1], Ieva Žutautė[1]

[1]Vilnius University, Faculty of Chemistry and Geosciences, Institute of Chemistry, Naugarduko str. 24, Vilnius, Lithuania
urte.mileryte@chgf.vu.lt

Parkinson's disease (PD) is a progressive neurodegenerative disorder closely associated with the misfolding and aggregation of α-synuclein, leading to Lewy body formation and dopaminergic neuron degeneration. As current therapies are primarily symptomatic and do not target the molecular mechanisms underlying disease progression, increasing attention has focused on modulating α-synuclein aggregation with low-molecular-weight compounds that cross the blood–brain barrier [1,2]. Despite numerous aggregation modulators reported in the literature, the set of chemically diverse, mechanistically well-characterized compounds remains limited, underscoring the need for new structural scaffolds [3].

Recent studies have identified the imidazo[2,1-*b*][1,3]thiazine scaffold as a promising pharmacophore for inhibiting the early stages of α-synuclein aggregation. However, its mechanisms of action remain incompletely understood [4]. This makes the scaffold particularly suitable for systematic structural modification and mechanistic investigation.

This study aimed to synthesize benzimidazo[2,1-*b*][1,3]thiazine derivatives capable of modulating α-synuclein aggregation. The synthesized compounds feature a novel structural modification – a substituent at the C_2 position adjacent to the double bond. As such compounds have not been previously described in the literature, the initial objective was to establish and optimize an appropriate synthetic methodology. For this purpose, a model compound, 1-(3-phenylprop-2-yn-1-yl)-1,3-dihydro-2*H*-benzo[*d*]imidazol-2-thione, was synthesized via alkylation of 1,2-diaminobenzene with (3-bromoprop-1-yn-1-yl)benzene, followed by condensation of the resulting intermediate with thiocarbonyldiimidazole. Using this model substrate, intramolecular cyclization reaction conditions were optimized by screening various coinage catalysts and solvents to maximize selectivity for six-membered ring formation. The highest selectivity for the six-membered ring product over the five-membered ring (12:1) was achieved when the reaction was conducted in DCE using $AuBr_3$ (15 mol%) as the catalyst. Based on these optimized conditions, subsequent studies systematically evaluated the influence of electron-donating and electron-withdrawing substituents on cyclization selectivity to elucidate the role of electronic effects in directing the formation of six- and five-membered ring products.

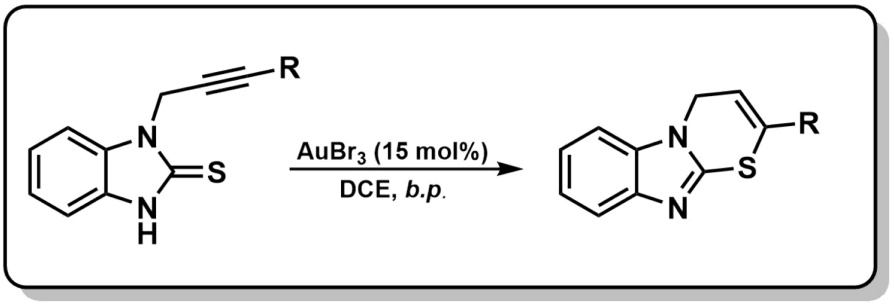


Fig. 1. $AuBr_3$-catalyzed cyclization for the synthesis of benzimidazo[2,1-*b*][1,3]thiazine derivatives.

[1] W. Poewe et al., "Parkinson disease," Nat. Rev. Dis. Primers, vol. 3, no. 1, p. 17013, Mar. 2017, doi: 10.1038/nrdp.2017.13.
[2] P. G. Coune, B. L. Schneider, and P. Aebischer, "Parkinson's Disease: Gene Therapies," Cold Spring Harb. Perspect. Med., vol. 2, no. 4, p. a009431, Apr. 2012, doi: 10.1101/cshperspect.a009431.
[3] L. De Luca et al., "Ligand-Based Discovery of a Small Molecule as Inhibitor of α-Synuclein Amyloid Formation," Int. J. Mol. Sci., vol. 23, no. 23, p. 14844, Nov. 2022, doi: 10.3390/ijms232314844.
[4] I. Misiūnaitė et al., "Imidazo[2,1-b][1,3]thiazine Derivatives as Potential Modulators of Alpha-Synuclein Amyloid Aggregation," ACS Chem. Neurosci., vol. 15, no. 24, pp. 4418–4430, Dec. 2024, doi: 10.1021/acschemneuro.4c00451.

EVALUATION OF KOMBUCHA FERMENTATION USING DIFFERENT TYPES OF TEA

Lukas Dapkus[1], Eglė Purvaneckaitė[1], Aivaras Anužis[1]

[1]St. Ignatius Loyola College, Department of Health Sciences and Technologies, Lithuania
lukas.dapkus@stud.ilk.lt

Kombucha is a fermented tea beverage that is widely valued for its refreshing sensory properties and potential functional attributes. However, variations in tea composition and fermentation conditions can lead to significant differences in fermentation dynamics and product quality. This emphasises the importance of systematically evaluating raw material selection. This study aimed to evaluate the influence of different tea substrates on the kombucha fermentation process and selected quality characteristics. Kombucha was produced using three types of tea, including hibiscus, green and black tea, under controlled fermentation conditions. Throughout fermentation, key physicochemical parameters such as pH, total acidity, alcohol content, and foam stability were monitored. In addition to the physicochemical analysis, the sensory properties of the kombucha samples obtained were assessed to determine differences in aroma, taste, mouthfeel and overall acceptability. A comparative analysis was performed to identify relationships between tea composition, fermentation behaviour and the resulting sensory and quality attributes of the beverages. This study improves our understanding of how tea selection affects kombucha fermentation and supports the development of kombucha products with optimised quality profiles and improved consumer acceptance.

SYNTHESIS OF β-HYDROXY-α-AMINOACIDS UTILIZING L-THREONINE (TRANS)ALDOLASES

Ignas Katkevičius[1,2], Kamilė Butkutė[2], Rolandas Meškys[2]

[1]Vilnius University, Faculty of Chemistry and Geosciences, Lithuania
[2]Vilnius University, Life Sciences Center, Institute of Biochemistry, Department of Molecular Microbiology and Biotechnology, Lithuania
ignas.katkevicius@chgf.stud.vu.lt

β-Hydroxy-α-aminoacids (β-HAAs) are a class of compounds widely used as intermediates in pharmaceutical synthesis (antibiotics, antiviral drugs), with the capacity to be incorporated into therapeutic peptides or functional proteins [1]. β-HAAs are typically obtained via chemical synthesis, although this process is unfavourable due to the use of several blocking groups during synthesis [2]. An alternative approach involves an enzymatic synthesis using L-threonine aldolases and transaldolases, which catalyse an aldol reaction between glycine or L-threonine and an aldehyde [3].

In this study, substrate selectivity was investigated using L-threonine aldolases from Neptunomas marina and Cellulosilyticum sp. (NmLTA and CsLTA) and L-threonine transaldolase from Pseudomonas fluorescens (ObiH). The substrate scope was evaluated using whole-cell biocatalysis, discovering that among the 23 aldehydes tested, 9 were suitable substrates for at least one enzyme. The analysis of enzymatic reactions showed that NmLTA and CsLTA catalyse the aldol reaction with pyridine-carbaldehydes (13-22%) as well as large aromatic aldehydes (3-7%), while ObiH was also active towards formyl-indoles (44-84%).

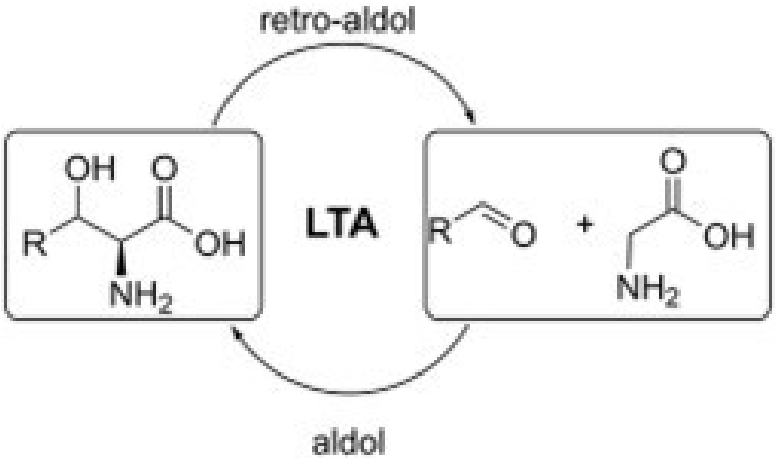


Fig. 1. Fig. 1 L-Threonine aldolase catalysed reactions [4].

[1] Chen, Q., Wang, J., Zhan g, S., Chen, X., Hao, J., Wu, Q., & Zhu, D. “Discovery and directed evolution of C–C bond formation enzymes for the biosynthesis of β-hydroxy-α-amino acids and derivatives”. Critical Reviews in Biotechnology., Vol. 44, Issue 8, pp. 1495–1514. 2024.
[2] He, Y., Li, S., Wang, J., Yang, X., Zhu, J., Zhang, Q., Cui, L., Tan, Z., Yan, W., Zhang, Y., Tang, L., Da, L. T., & Feng, Y. “Discovery and Engineering of the l-Threonine Aldolase from Neptunomonas marine for the Efficient Synthesis of β-Hydroxy-α-amino Acids via C-C Formation”. ACS Catalysis., Vol. 13, Issue 11, pp. 7210–7220. 2023.
[3] Wang, S., & Deng, H. “Peculiarities of promiscuous L-threonine transaldolases for enantioselective synthesis of β-hydroxy-α-amino acids”. Applied microbiology and biotechnology., vol. 105, no. 1, pp 1-11. 2020.
[4] [4] Fesko, K. “Comparison of L-threonine aldolase variants in the aldol and retro-aldol reactions”. Frontiers in Bioengineering and Biotechnology., vol. 7,pp 1-12. 2019.

THE SYNTHESIS AND MODIFICATION OF (IMIDAZO(2,1-b)(1,3)THIAZIN-4-YL)PHENOLS

Fausta Kairytė[1], Ieva Žutautė[1]

[1]Lithuania, Vilnius, Vilnius University, Faculty of Chemistry and Geosciences, Institute of Chemistry
fausta.kairyte@chgf.stud.vu.lt

Amyloidosis is a general term describing diseases that develop when there is an accumulation of proteins that have lost their biological function due to altered secondary structures [1]. Such proteins arise from misfolding or when broken down into separate, irregular fragments which connect and form insoluble, stable beta-fibrillar structure. The resulting aggregates of these structures are called amyloids. These deposits are resistant to proteolytic enzymes, such as proteases, which maintain protein homeostasis by degrading proteins. When this process is disrupted, systemic and localized forms of amyloidosis begin to develop, causing neurodegenerative diseases, such as Parkinson's and Alzheimer's diseases, localized in the brain [2]. During various scientific studies, it was observed that compounds containing small-molecular weight heterocyclic fragments are able to inhibit the formation of amyloid aggregates in the body [3, 4].

The aim of this work is to increase the variety of compounds that would exhibit the properties of modulators of amyloid aggregates. Therefore, the primary objective of this work is to synthesize compounds containing (imidazo[2,1-*b*][1,3]thiazin-4-yl)phenols with a heterocyclic fragment at different positions and modify them. 2-iodo and 4-iodophenols were chosen as starting compounds. Due to reactivity, the hydroxy groups were modified in the first step. This was followed by the addition of the triple bond and the subsequent replacement of the introduced propargyl bromide group with thioimidazole fragments. Following a gold-catalyzed cyclization reaction, the target (imidazo[2,1- *b*][1,3]thiazin-4-yl)phenols 1 and 2 were isolated. Their corresponding hydroxyl groups were further modified to target amides, esters and ethers for further evaluation in amyloid protein aggregation studies.

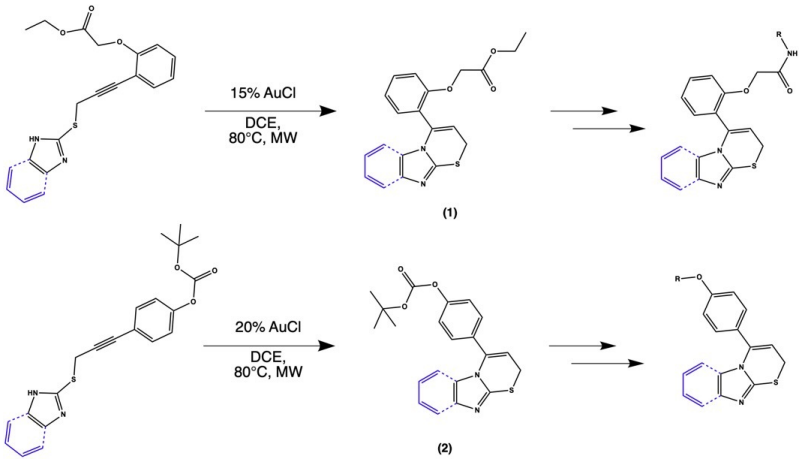


Fig. 1. Synthesis of target compounds: 2-(2-(imidazo[2,1-*b*][1,3]thiazinyl)phenoxy)acetate (1) and 4-(imidazo[2,1-*b*][1,3]thiazinyl)phenol (2).

[1] Ž. Petrulionienė et al., "ŠIRDIES AL AMILOIDOZĖ: KLINIKINIO ATVEJO APRAŠYMAS," Sveikatos Mokslai, vol. 24, no. 6, pp. 134–138, May 2014, doi: 10.5200/sm-hs.2014.127.

[2] G. Merlini and V. Bellotti, "Molecular mechanisms of amyloidosis," New England Journal of Medicine, vol. 349, no. 6, pp. 583–596, Aug. 2003, doi: 10.1056/nejmra023144.

[3] I. Misiūnaitė et al., "Imidazo[2,1-b][1,3]thiazine Derivatives as Potential Modulators of Alpha-Synuclein Amyloid Aggregation," ACS Chemical Neuroscience, vol. 15, no. 24, pp. 4418–4430, Nov. 2024, doi: 10.1021/acschemneuro.4c00451.

[4] Ž. Eva, "Amyloid-fibril formation," European Journal of Biochemistry, vol. 269, no. 14, pp. 3362–3371, Jul. 2002, doi: 10.1046/j.1432-1033.2002.03024.x.

SYNTHESIS OF N-SUBSTITUTED RESORCINOLCARBOXAMIDES AS POTENTIAL HSP90 INHIBITORS

Ugnius Popovas[1], Ieva Žutautė[1]

[1]Vilnius University, Faculty of Chemistry and Geosciences, Institute of Chemistry, Vilnius, Lithuania
ugnius.popovas@chgf.stud.vu.lt

Hsp90 (Heat Shock Protein 90) is a crucial molecular chaperone that plays a key role in the maturation and regulation of more than 300 client proteins. Many of these clients are associated with challenging illnesses, including cancer, neurodegenerative disorders, and infectious diseases. As a result, Hsp90 has emerged as an important target for the development of synthetic inhibitors. A central pharmacophore in many Hsp90 inhibitors is the resorcinol fragment, which suppresses Hsp90 activity through interaction in the ATP pocket in the protein's N-terminal domain. Therefore, resorcinol-containing compounds are extensively explored in the design of second-generation Hsp90 inhibitors [1].

To synthesize novel HSP90 inhibitors featuring a modified resorcinol structure, this study investigated synthetic routes for introducing an amide group at the 6-position of the aromatic ring. 4-Chlororesorcinol was selected as the core starting structure.

Several synthetic approaches were explored to obtain the target compounds, focusing on different strategies for functional group protection and amide formation. The initial route involved methylation of the hydroxyl groups of 4-chlororesorcinol, followed by formylation, oxidation to the corresponding carboxylic acid, and successful amide formation; however, non-selective deprotection of the methoxy groups using boron tribromide, as well as the failure of alternative deprotection methods, led to the abandonment of this strategy. Subsequently, direct amide coupling of dihydroxybenzoic acid derivatives with amines using HATU and EDCI activation systems was explored but did not yield the desired products. An alternative strategy employing acetyl protecting groups was therefore assessed and successfully validated in a model system lacking a chlorine substituent via a one-pot amide formation. However, extension of this approach to the chlorinated target was unsuccessful due to challenges associated with selective chlorination and oxidation without compromising the acetyl protections, underscoring the pronounced effect of the chlorine substituent on substrate reactivity. The advantages and limitations of the investigated synthetic approaches will be discussed during the presentation.

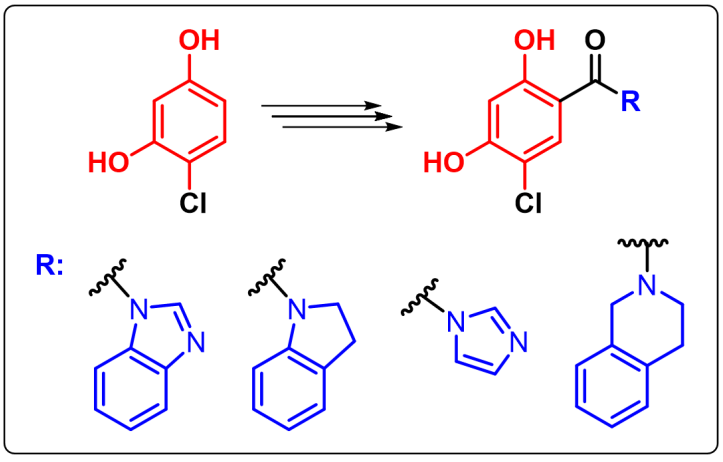


Fig. 1. Synthetic scheme of targeted compounds.

[1] L. Li, L. Wang, Q. D. You, and X. L. Xu, "Heat Shock Protein 90 Inhibitors: An Update on Achievements, Challenges, and Future Directions," J. Med. Chem., vol. 63, no. 5, pp. 1798–1822, Mar. 2019, doi: 10.1021/acs.jmedchem.9b00940.

EFFICIENT SYNTHESIS OF STEROIDAL 1,2,3-TRIAZOLES

Nana Barbakadze[1], Nanuli Nadaraia[1], Meri Kakhabrishvili[1]

[1]Tbilisi State Medical University Iovel Kutateladze Institute of Pharmacochemistry, Tbilisi, Georgia
n.barbakadze@tsmu.edu

Steroids play an important role in the physiological processes of living organisms and are widely used in medical practice. Purposeful chemical modification of steroidal substances obtained from plant raw materials, leading to changes in biological activity, is essential for the development of new pharmaceuticals. The majority of synthetic steroidal compounds, including nitrogen-containing derivatives, are biologically potent substances [1]–[3]. It has been established that steroidal azoles can interact with certain enzymes, exhibiting strong inhibitory properties, and are considered promising antitumor agents [4]. To obtain potentially biologically active compounds, new steroidal 1,2,3-triazoles were synthesized using a triazolization methodology [5], [6], which significantly reduced the number of synthetic steps required. The structures of the synthesized compounds were confirmed by ^{1}H and ^{13}C NMR spectroscopy. Evaluation of the agonistic and antagonistic properties of the synthesized steroidal 1,2,3-triazoles showed that several compounds reduced androgen receptor activity by 40%. Screening nitrogen-containing steroids for biological activity enables the creation of new libraries of potential therapeutic agents and facilitates the identification of lead compounds for the development of new drug precursors.

[1] R. Singh, S. Thota, and R. Bansal, “Studies on 16,17-pyrazoline substituted heterosteroids as anti-Alzheimer and anti-Parkinsonian agents using LPS-induced neuroinflammation models of mice and rats,” ACS Chem. Neurosci., vol. 9, no. 2, pp. 272–283, 2018.
[2] A. H. Banday, S. A. Shameem, and S. Jeelani, “Steroidal pyrazolines and pyrazoles as potential 5α-reductase inhibitors: Synthesis and biological evaluation,” Steroids, vol. 92, pp. 13–19, 2014.
[3] J. Cui et al., “Synthesis, characterization and antitumor activities of some steroidal derivatives with side chain of 17-hydrazone aromatic heterocycle,” Steroids, vol. 95, pp. 32–38, 2015.
[4] A. S. Latysheva and A. Yu. Misharin, “Steroidal inhibitors of CYP17A1—the template for novel anti-cancer agents development,” Biomed. Chem.: Res. Methods, vol. 1, no. 2, p. e00020, 2018.
[5] J. Thomas et al., “A single-step acid catalyzed reaction for rapid assembly of NH-1,2,3-triazoles,” Chem. Commun., vol. 52, no. 59, pp. 9236–9239, 2016.
[6] J. Thomas et al., “A general metal-free route towards the synthesis of 1,2,3-triazoles from readily available primary amines and ketones,” Chem. Commun., vol. 52, no. 14, pp. 2885–2888, 2016.

SYNTHESIS AND INVESTIGATION OF BENZIDINE ANILINE AND BENZIDINE O-ANISIDINE COPOLYMERS WITH PANi LIKE STRUCTURE

Narine Durgaryan[1], Shushanna Vardanyan[1], Parandzem Minasyan[1], Gevorg Grigoryan[2]

[1]Yerevan State University, Faculty of Chemistry, Department of Organic Chemistry, Yerevan, Armenia
[2]Yerevan State University, Faculty of Chemistry, Department of Physical Chemistry, Yerevan, Armenia
n.durgaryan@ysu.am

Conductive polymers are considered an important and innovative class of materials due to their significant impact on the field of polymers. These materials are characterized by extensive conjugation along their backbone, featuring alternating single and double bonds [1]. PANi and polymers synthesized from aromatic diamines are particularly notable among electroactive conjugated polymers. This distinction stems from their excellent environmental stability, simple and cost-effective synthesis methods, unique characteristics, and wide-ranging applications [2-4].

The studies show that conductive polymers can be obtained by using the method of oxidative polymerisation of aromatic diamines.However, the synthesized polymers were largely insoluble and displayed low electrical conductivities. In such cases copolymerization offers a facile route to the preparation of polymers with specifically desired properties [5,6]. The simple and inexpensive one-pot oxidative polycondensation of benzidine with aniline and o-anisidine has been done, to have PANi-like structured polymer with precise control over the ratio of quinonediiminic and aryleneiminic units [7].

The composition of the resulting copolymers was analyzed by proton magnetic resonance (PMR) spectroscopy for initial benzidine-to-o-anisidine molar ratios of 1:0.5, 1:1, and 1:2. The study demonstrates that the physicochemical properties of the copolymers—including ultraviolet–visible (UV–Vis) absorption characteristics, solubility, thermal stability, electrical conductivity, and morphology—can be tuned by adjusting the ratio of quinonediimine to substituted structural units within the polyaniline (PANi)-like chains. The copolymers exhibited high thermal stability, retaining 66–72 % of their weight up to 600 °C. When doped with hydrochloric acid (HCl), their electrical conductivity was comparable to that of the parent homopolymers, polyaniline and polyanisidine. These findings suggest the potential of structural modulation to enhance the functional performance of PANi-based copolymers for advanced materials applications.

Keywords: Conductive polymer, aniline, o-anisidine, benzidine, copolymerisation

[1] J. Huang, R.B. Kaner Conjugated polymers: Theory, synthesis, properties, and characterization (3rd ed.), CRC Press, Boca Raton (FL) (2006)
[2] A. Janošević, B. Marjanović, A. Rakić, G. Ćirić-Marjanović Progress in conducting/semiconducting and redox-active oligomers and polymers of arylamines J Serb Chem Soc., 78 (11) (2013), pp. 1809-1836
[3] A.G. MacDiarmid, A. Epstein Polyanilines: The new class of conducting polymers Faraday Discuss Chem Soc., 88 (1989), pp. 317-332
[4] X.G. Li, M.R. Huang, W. Duan, Y.L. Yang Novel multifunctional polymers from aromatic diamines by oxidative polymerizations Chem Rev., 102 (9) (2002), pp. 2925-3030
[5] Y. Wei, R. Hariharan, S.A. Patel Chemical and electrochemical copolymerization of aniline with alkyl ring-substituted anilines Macromolecules., 23 (3) (1990), pp. 758-764
[6] U.S. Waware, R. Arukula, A.M.S. Hamouda, et al. Cyclic voltammetry and XPS studies of poly (aniline-co-3-aminophenol) Polym. Bull., 80 (2023), pp. 3897-3910,
[7] P. Minasyan, Sh. Vardanyan, N. Durgaryan, G. Grigoryan, Synthesis and investigation of benzidine – aniline and benzidine – o-anisidine copolymers with PANi like structure, European Polymer Journal, Volume 239, 2025, 114249, ISSN 0014-3057,

CHARACTERISATION OF VOLATILE COMPOUNDS AND METABOLITE PROFILES OF VINCETOXICUM ROOTS ISOLATED BY SUPERCRITICAL CO_2 AND PRESSURISED LIQUID EXTRACTION

Jovita Jovaišaitė[1], Simon Duthen[2,3,4], Amélie Perez[2,3], Laura Jūrienė[1], Petras Rimantas Venskutonis[1]

[1]Kaunas University of Technology, Department of Food Science and Technology, Kaunas, LT-50254, Lithuania
[2]Université de Toulouse, Laboratoire de Recherche en Sciences Végétales, MetaToul-AgromiX platform, CNRS, INP, 24 Chemin de Borde Rouge, Auzeville, Auzeville-Tolosane 31320, France
[3]National Infrastructure of Metabolomics and Fluxomics, MetaboHUB-MetaToul, Toulouse 31000, France
[4]Université de Toulouse, Centre de Recherche sur la Cognition Animale (CRCA), Centre de Biologie Intégrative (CBI), UMR 5169, CNRS, Toulouse 31062, France
jovita.jovaisaite@ktu.lt

The growing interest in natural, biologically active compounds, coupled with the need for safer, more environmentally friendly alternatives to synthetic preparations, is driving more intensive research into medicinal plants. Particular attention is being paid to plant genera that have received limited study but have significant biological potential. One such genus is Vincetoxicum (Apocynaceae), whose species are characterised by a wide range of secondary metabolites and promising biological properties. This study aimed to isolate different fractions from the roots of three Vincetoxicum species and investigate their chemical composition using innovative extraction methods. Lipophilic fractions were obtained using supercritical carbon dioxide extraction (SFE-CO_2), while polar fractions were obtained using pressurised liquid extraction (PLE) with hydroethanol. The volatile compound composition of the plant raw materials and the SC-CO_2 extracts was analysed using GC×GC-TOF/MS, while the metabolite composition of the PLE extracts was determined using UHPLC-HRMS. GC×GC-TOF/MS analysis identified over 80 volatile compounds in the dry raw material and CO_2 extracts of Vincetoxicum roots. Preliminary phytochemical analysis of the hydrophilic extracts revealed over 20 compounds at identification level 1 (MS/MS match) and over 50 at level 2a. These results confirm the potential of Vincetoxicum species' roots as a significant source of biologically active compounds, providing a basis for further detailed biological activity and pharmacological studies.

Keywords: Vincetoxicum, phytochemistry, supercritical CO_2 extraction

ANTIOXIDANT PROFILE OF LIQUID FRACTION FROM DANDELION LEAF KOMBUCHA FERMENTATION

Taisa Vashkevich[1], Vilma Kaškonienė[1], Audrius Sigitas Maruška[1]

[1]Vytautas Magnus University, Instrumental Analysis Open Access Center, Lithuania
taisa.vashkevich@vdu.lt

Dandelion (*Taraxacum* genus) is a perennial plant that has a wild distribution on hillsides in the Northern Hemisphere [1]. Although it has medicinal uses [1], dandelion is considered a weed [2] and therefore can be classified as green waste and utilized as a source of phytochemical compounds. Kombucha fermentation, occurring via a symbiotic culture of bacteria and yeasts (SCOBY), can biotransform plant-derived substrates, altering the extraction and properties of antioxidant compounds [3]. In this study, dandelion leaves (*Taraxacum* sp.) were used as a substrate for fermentation using a SCOBY kombucha inoculum, in parallel with wild-type fermentation which served as a control. The incubation period lasted for 1, 3, and 5 days at 25 °C and 120 rpm. The analysis was performed on the liquid fraction of the fermentation samples. Spectrophotometric methods were applied to evaluate total polyphenolic content, 2,2-diphenyl-1-picrylhydrazyl (DPPH) and hydroxyl radical scavenging activities. Measurements were done in triplicate.

Statistical test of Shapiro–Wilk was used to assess the normality of the data. When the normality assumption was met, one-way ANOVA followed by Tukey's HSD post-hoc test was applied. When normality was violated, Welch's ANOVA with the Games–Howell post-hoc test was used instead.

According to total polyphenolic content and DPPH scavenging activity after fermentation there was no statistically significant difference between three days of fermentation with SCOBY innoculum. While across all the spectrophotometric tests the treatment group showed statistically significant increase after fementation comparing to control of the same day which ranged from 25.6 to 49.4%. The first day of fermenation using kombucha culture showed the highest total polyphenolic activity equal to 5.31 mg of rutin equivalents in ml comparing to all samples. The DPPH scavenging activity was highest on days 1 and 3 of treatment, equal to the same amount of 3.05 mg of rutin equivalents in ml comparing to all samples. According to the hydroxyl radical scavenging activity, the best perfomance was recorded on day 3 of treatment, and it was equal to 3.72 mg of ascorbic acid equivalents in ml among the samples.

Overall, application of kombucha inoculum to dandelion leaf improved antioxidant properties of the liquid part of fermented samples versus wild-type fermentation. However, there was no greater variation among the three days of kombucha inoculum fermentation.

[1] Q. Yan, Q. Xing, Z. Liu, Y. Zou, X. Liu, and H. Xia, "The phytochemical and pharmacological profile of dandelion," Biomedicine & Pharmacotherapy, vol. 179, p. 117334, Aug. 2024, doi: 10.1016/j.biopha.2024.117334.

[2] Shukla, S., Beohar, P., Pathak, R., Singh, D., and Chaturvedi, P., "Weed as potential source of phytochemicals," Journal of Biodiversity and Environmental Sciences, vol. 20, no. 4, pp. 88–95, 2022.

[3] S. A. Villarreal-Soto et al., "Impact of fermentation conditions on the production of bioactive compounds with anticancer, anti-inflammatory and antioxidant properties in kombucha tea extracts," Process Biochemistry, vol. 83, pp. 44–54, May 2019, doi: 10.1016/j.procbio.2019.05.004.

DESIGN AND SYNTHESIS OF NOVEL DERIVATIVES BASED ON1-(NAPHTHALEN-1-YL)-4-PHENYL-1H-IMIDAZOLE-2-THIOL

Aistė Starkauskaitė[1], Birutė Grybaitė[1], Vytautas Mickevičius[1]

[1]Kaunas University of Technology, Department of Organic Chemistry, Lithuania
aiste.starkauskaite@ktu.edu

Hydrazide–hydrazone derivatives represent an important class of bioactive compounds and have shown promising anticancer activity against a wide range of human cancer cell lines. Their structural versatility and ability to interact with multiple biological targets make them attractive scaffolds for further drug development.[1] Likewise, aminoketone derivatives have been reported to exhibit in vitro anticancer activity against selected cancer cell lines, suggesting their potential relevance in anticancer drug research.[2]

The starting compound **2** was prepared by the reaction of 1-naphthylamine **(1)** with 2-bromo-1-phenylethan-1-one at room temperature. Compound **3** was obtained by the reaction of aminoketone **2** with KSCN in 10% HCl under reflux. Methyl 2-((1-(naphthalen-1-yl)-4-phenyl-1H-imidazol-2-yl)thio)acetate **(4)** was obtained via S-alkylation of compound **3** with methyl bromoacetate. The reaction of ester **4** with hydrazine hydrate in 2-propanol under reflux gave 2-((1-(naphthalen-1-yl)-4-phenyl-1H-imidazol-2-yl)thio)acetohydrazide **(5)**, which crystallized from the reaction mixture after cooling it down. Condensation of hydrazide **5** with heterocyclic aldehydes gave hydrazones **6a-d**. The condensation of hydrazide **5** with 2,5-hexanedione in 2-propanol in the presence of a catalytic amount of acetic acid resulted in the formation of N-(2,5-dimethyl-1H-pyrrol-1-yl)-2-((1-(naphthalen-1-yl)-4-phenyl-1H-imidazol-2-yl)thio)acetamide **(7)**. The interaction of hydrazide **5** with 2,4-pentanedione in 2-propanol, in the presence of a catalytic amount of hydrochloric acid, resulted in the formation of pyrazole **8**.

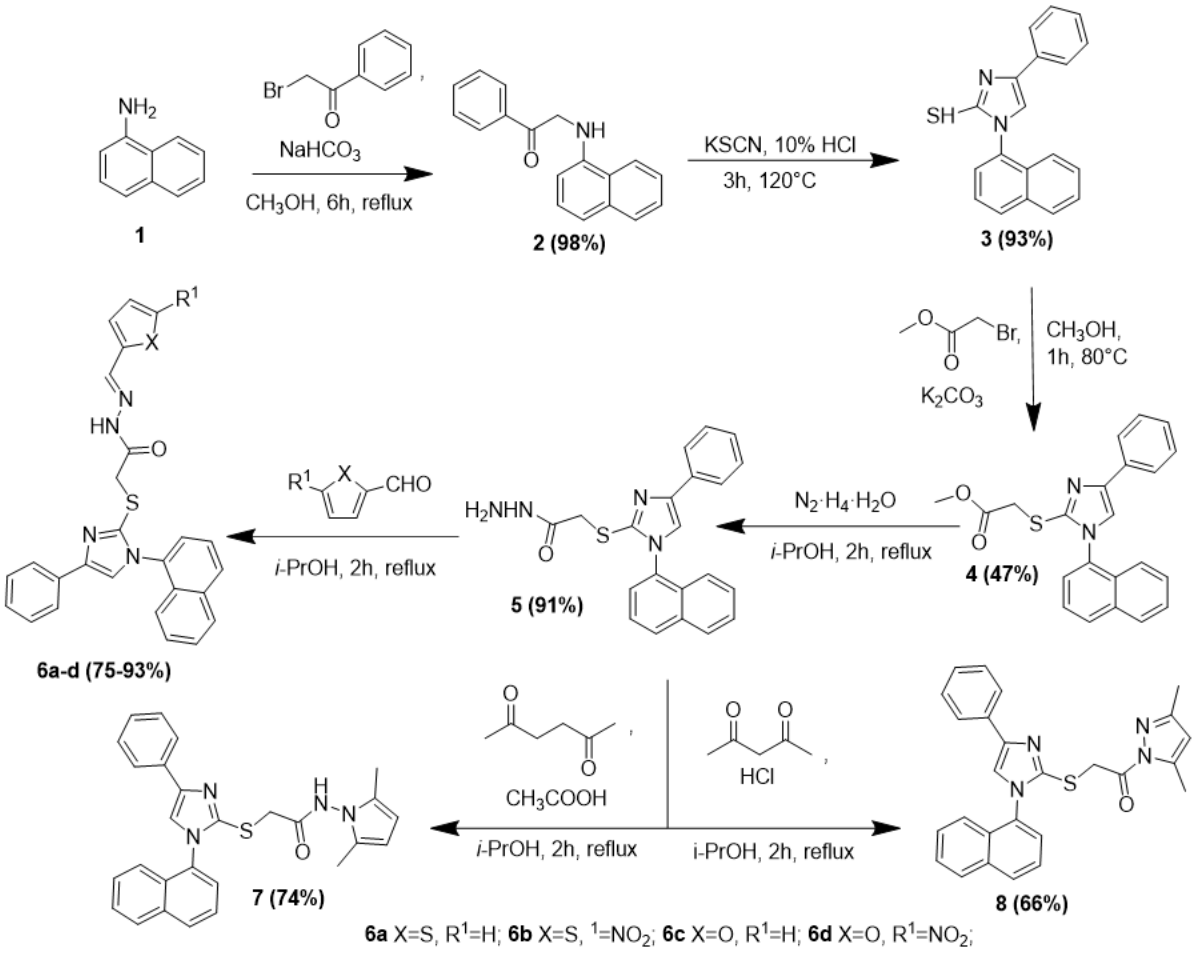


Fig. 1. Synthesis of compounds **2-8**.

The structure of the synthesized compounds was characterized by spectral data (IR, NMR spectra, and elemental analysis).

[1] S. Karakuş, F. Tok, B. İ. Abas, E. Tütüncü, and Ö. Çevik, "Synthesis and in vitro anticancer activity of some new hydrazide-hydrazones derived from articaine," J. Res. Pharm., vol. 28, no. 6, pp. 1901–1910, Jan. 2024, doi: 10.29228/jrp.863.

[2] W. Seebacher et al., "Formation of 5-Aminomethyl-2,3-dihydropyridine-4(1H)-ones from 4-Amino-tetrahydropyridinylidene Salts," Molecules, vol. 28, no. 19, art. no. 6869, Sep. 2023, doi: 10.3390/molecules28196869

PROPERTIES OF NONWOVEN MICROFIBER MATERIALS BASED ON PLANT EXTRACTS PRODUCED BY ELECTROSPINNING

Andrii Sikora[1], Irina Liashok[1], Viktoriia Plavan[1]

[1]Kyiv National University of Technologies and Design, Department of chemical technology and resource saving, Kyiv, Ukraine
lyashok.io@knutd.com.ua

Nonwoven fibrous materials (NFM), thanks to their unique structure and properties, such as high specific surface area, porous structure and the possibility of modification, are promising materials for a wide range of applications, especially in medicine and cosmetology. Their use for the manufacture of wound and cosmetic dressings, filters and other medical devices is the subject of active research and development. Of particular interest is the possibility of creating NFM containing functional groups, such as synthetic drugs or active substances of medicinal plants. This opens up new perspectives for the development of intelligent materials capable of not only protecting the wound or skin, but also promoting their healing and regeneration. This work presents the results of research on the vapor permeability and water absorption of NFM samples made by electrospinning from solutions of polyvinyl alcohol (PVA) containing extracts of medicinal plants. The electrospinning method is a relatively accessible and effective way to obtain nanoscale fibers. PVA was chosen as the polymer base due to its availability, ease of processing, non-toxicity and biocompatibility. These properties make PVA an ideal material for use in medical and cosmetic products.

For the study, NFM samples were made containing 10% by weight of PVA and extracts of medicinal plants, such as oak bark *Quercus robur L.*, blue gum *Eucalyptus globulus*, oregano *Origanum vulgare L.* and pot marigold *Caléndula*. These plants are known for their antiseptic, anti-inflammatory and wound-healing properties. The extracts of medicinal plants were prepared according to a special formulation, dry plant parts per boiling water (m/V): oak bark. (10 g per 100 ml); blue gum (10 g per 200 ml); oregano (10 g per 200 ml); pot marigold (5 g per 200 ml). To obtain an aqueous extract of medicinal plants, they were infused in a water bath at a temperature of about 95 °C, for 30 minutes, followed by cooling at room temperature. To remove mechanical impurities, the extracts were filtered through a filter paper. PVA solutions were prepared in a water bath for 40 minutes. The NFM samples were formed using a laboratory capillary-type setup. The electric field voltage was 30 kV, the distance between the electrodes was 17.5 cm, and the capillary diameter was 0.33 mm.The obtained test results are shown in Figure 1.

Medicinal plant	Electrical conductivity, S/m.	Nonwoven sample thickness, mm	Water vapor permeability of the nonwoven sample, mg/cm²·h	Water vapor permeability of the film, mg/cm²·h	Relative water vapor permeability, %
Oak bark	0,0394	0,15	1,843	0,3686	500
Blue gum	0,1216	0,07	1,4707	0,3465	424
Oregano	0,2072	0,07	2,9488	0,4239	696
Pot marigold	0,0587	0,11	1,843	0,4055	455

Fig. 1. Some properties of the resulting nonwoven materials

It was experimentally established that the vapor permeability value for NFM samples is greater than the vapor permeability value of the corresponding films by 400-700%. This indicates that NFM have a high ability to transmit water vapor, which is an important factor for ensuring comfort and skin breathing under the dressing.

STRUCTURAL AND MORPHOLOGICAL CHARACTERIZATION OF POLY(PYRROLE-CO-ANTHRANILIC ACID) COPOLYMERS SYNTHESIZED USING DIFFERENT AMMONIUM PERSULFATE-TO-MONOMER RATIOS

Amelia Hendik[1], Justina Gaidukevič[1,2]

[1]Lithuania, Vilnius University, Faculty of Chemistry and Geosciences, Institute of Chemistry
[2]Lithuania, Center for Physical Sciences and Technology
amelia.hendik@chgf.stud.vu.lt

Conducting polymers are materials that combine the electrical properties of metals or semiconductors with the processability and structural versatility of polymers [1]. Among them, poly(pyrrole) is a highly conducting polymer, notable for its excellent electrical conductivity, environmental stability, and ease of synthesis, making it widely used in electrochemical applications [2]. In contrast, poly(anthranilic acid) exhibits enhanced solubility and maintains electroactivity in neutral and alkaline media, while its carboxylic acid group provides chemical functionality, making it useful for biosensors, corrosion protection, and memory devices [3]. The structure and properties of copolymers formed from these materials are strongly influenced by synthesis conditions, particularly the type and concentration of oxidizing agent used during chemical oxidative polymerization [4]. Ammonium persulfate (APS) plays a key role in controlling polymer growth, oxidation state, and morphology.

In this study, we investigate the effect of the APS ratio on the structural and morphological characteristics of poly(pyrrole-co-anthranilic acid) (PPy-AA) copolymers, while keeping the monomer ratio constant at 3:1, to provide insights into optimizing synthesis conditions for improved material functionality. The structural, morphological, and surface characteristics of the synthesized PPy-AA copolymers were investigated using scanning electron microscopy (SEM), energy-dispersive X-ray spectroscopy (EDX), Raman spectroscopy, Fourier-transform infrared spectroscopy (FTIR). SEM images showed that the particles exhibit a granular, spherical structure, and increasing the APS ratio produced smaller particles with a higher tendency to agglomerate. Raman and FTIR spectra confirmed changes in the oxidation state and conjugation of the copolymers, suggesting modifications to the delocalized π-electron system. EDX analysis demonstrated systematic variations in elemental composition, demonstrating that excessive APS leads to increased oxidation of the pyrrole rings and partial degradation of the polymer chains. These results indicate that the APS ratio strongly influences the structural and morphological properties of PPy-AA copolymers.

Keywords: Poly(pyrrole-co-anthranilic acid); conducting copolymers; ammonium persulfate; oxidative polymerization; structural and morphological characterization.

[1] S. Jadoun, D. Singh Rathore, U. Riaz, and N. P. S. Chauhan, “Tailoring of conducting polymers via copolymerization – A review,” European Polymer Journal, vol. 155, art. no. 110561, 2021.
[2] M. R. Nateghi and M. Borhani, “Preparation, characterization and application of polyanthranilic acid copypyrrole,” Reactive & Functional Polymers, vol. 68, pp. 153–160, 2008.
[3] R. McCormick, E. Buckley, P. J. Donnelly, V. Gilpin, R. McMath, R. B. Smith, P. Papakonstantinou, and J. Davis, “Anthranilic acid: A versatile monomer for the design of functional conducting polymer composites,” Journal of Composites Science, vol. 8, art. no. 208, 2024.
[4] B. H. Patil, R. N. Bulakhe, and C. D. Lokhande, “Supercapacitive performance of chemically synthesized polypyrrole thin films: Effect of monomer to oxidant ratio,” Journal of Materials Science: Materials in Electronics, vol. 25, pp. 2188–2198, 2014.

RAPID FABRICATION OF COC MICROFLUIDIC CHIPS USING ADHESIVE BONDING

Tadas Turonis[1,2], Kamilė Kasperavičiūtė[1], Eivydas Andriukonis[1], Arūnas Stirkė[1]

[1]Center for Physical Sciences and Technology, Department of Functional Materials and Electronics, Vilnius, Lithuania
[2]Vilnius TECH, Faculty of Mechanics, Vilnius, Lithuania
tadas.turonis@ftmc.lt

Microfluidic chip technologies provide a new alternative for in vitro drug testing on a mass scale, biofilm research, and accessible screening devices for diseases [1]. With advances in materials science and microfluidic device manufacturing over the past two decades, microfluidic technologies have been increasingly adopted in drug testing and cosmetics, thereby reducing reliance on animal testing in these applications [2]. Therefore, there is a growing need for rapid, reliable, scalable fabrication approaches. Currently, most microfluidic chips are fabricated using polydimethylsiloxane (PDMS). However, PDMS has notable limitations, including absorption of small hydrophobic molecules such as nile red and rhodamine B, as well as low mechanical strength that can lead to channel deformation and inaccurate metrology. In addition to these intrinsic material drawbacks, PDMS fabrication involves manual steps like mixing, degassing, and curing, resulting in batch variability and unsuitability for mass production. To address these challenges, a cyclic olefin copolymer (COC) based microfluidic chip platform is presented. COC is a highly chemically resistant optically transparent thermoplastic, making it ideal for reproducible quantitative analysis. The objective of this work was the development of a rapid, low-barrier fabrication method for COC-based microfluidic chips. Using adhesive bonding combined with simple 3D-printed components, complete chip fabrication can be achieved in under 30 minutes with minimal training and materials, enabling rapid prototyping.

[1] R. Kojima, A. Kato, Y. Horie, and S. Takeuchi, “Organs-on-a-chip: A review,” Life, vol. 12, no. 5, p. 649, Apr. 2022, doi: 10.3390/life12050649.
[2] D. E. Ingber, “Human organs-on-chips for disease modelling, drug development and personalized medicine,” Nat. Rev. Genet., vol. 23, pp. 467–491, 2022, doi: 10.1038/s41576-022-00466-9.

Pd-CATALYZED ASSEMBLY AND MECHANISTIC ELUCIDATION OF TWISTED DONOR-ACCEPTORCARBAZOLE SCAFFOLDS

Hamisu Aliyu Mohammed[1], Muhammad Hakim Muhamad Adzrill[2], Aqeel A. Hussein[3], Muhammad Kumayl Abdul Wahab[2], Nor Shafiq Mohd Jamel[2], Kai Lin Woon[4], Juozas V. Grazulevicius[1], Azhar Ariffin[2]

[1]Kaunas University of Technology, Faculty of Chemical Technology, Department of Polymer Chemistry and Technology, Kaunas, Lithuania.
[2]University of Malaya, Faculty of Science, Department of Chemistry, Kuala Lumpur, Malaysia.
[3]Al-Qasim Green University, College of Science, Department of Biology, Al-Qasim, Babylon, Iraq.
[4]University of Malaya, Department of Physics, Low Dimensional Materials Research Center, Kuala Lumpur, Malaysia.
hammoh@ktu.lt

Herein, the synthesis, mechanistic study, and computational analysis of a series of sterically twisted donor–acceptor carbazole derivatives incorporating a 3,5-bis(trifluoromethyl)benzene acceptor are reported. The target scaffolds were assembled via a modular Pd-catalyzed route combining Buchwald–Hartwig amination with Pd-mediated cyclodehydrogenation via C–H activation. Parallel experimental investigations were conducted to compare Pd(0)- and Pd(II)-based catalytic protocols. Under the conditions examined, higher isolated yields and cleaner conversions were obtained using the Pd(0) pathway. Density functional theory (DFT) calculations were employed to probe the reaction mechanism, and the energetic preference of the Pd(0) manifold was demonstrated, with oxidative addition and reductive elimination steps shown to be kinetically and thermodynamically more accessible than the corresponding processes in the Pd(II) cycle. Taken together, the experimental and theoretical results define an efficient strategy for the construction of highly twisted donor–acceptor carbazole frameworks and provide mechanistic insight for further optimization of Pd-catalyzed C–H annulation chemistries for the preparation of optoelectronically active materials.

Acknowledgements

The work is supported financially by grant number FRGS/1/2019/STG01/UM/01/1, grant number IIRG001C-2022FNW, and agreement no. S-MIP-22-78

4-(7H-IMIDAZO(2,1-b)(1,3)THIAZIN-5-YL)ANILINE DERIVATIVES: SYNTHESIS AND MODIFICATION

Polina Pylskaja[1], Ieva Žutautė[1]

[1]Vilnius University, Faculty of Chemistry and Geosciences, Institute of Chemistry, Vilnius, Lithuania
polina.pylskaja@chgf.stud.vu.lt

Amyloid fibril formation is a central pathological feature of numerous neurodegenerative and systemic disorders, including Alzheimer's disease, Parkinson's disease, and type II diabetes. The accumulation of misfolded proteins into insoluble amyloid aggregates disrupts cellular homeostasis and causes cytotoxic effects, underscoring amyloidogenesis as a critical therapeutic target. Consequently, considerable research efforts have been directed toward the development of small-molecule inhibitors capable of modulating protein aggregation pathways or stabilizing non-toxic protein conformations [1].

Among various classes of bioactive compounds, heterocyclic systems containing imidazole or benzimidazole fragments have attracted significant attention due to their favorable electronic characteristics and ability to interact with biomolecular targets [2]. Compounds bearing the imidazo[2,1-*b*][1,3]thiazine scaffold have demonstrated a broad spectrum of biological activities, including anti-inflammatory, antifungal, anti-tuberculosis, and amyloid aggregation inhibitory effects [3]. These molecules are further distinguished by their chemical stability and selective binding properties, making them promising candidates for the development of novel modulators of amyloid fibril formation.

In this work, a series of compounds containing imidazo[2,1-*b*][1,3]thiazine or benzimidazo[2,1-*b*][1,3]thiazine fragments were synthesized and further modified. The synthetic strategy was based on an initial cyclization reaction to construct the corresponding heterocyclic core structures. Subsequent post-cyclization modifications focused on the functionalization of the amino group, enabling the introduction of various substituents through reactions with suitable electrophilic reagents. This approach allowed the generation of structurally diverse derivatives for further studies.

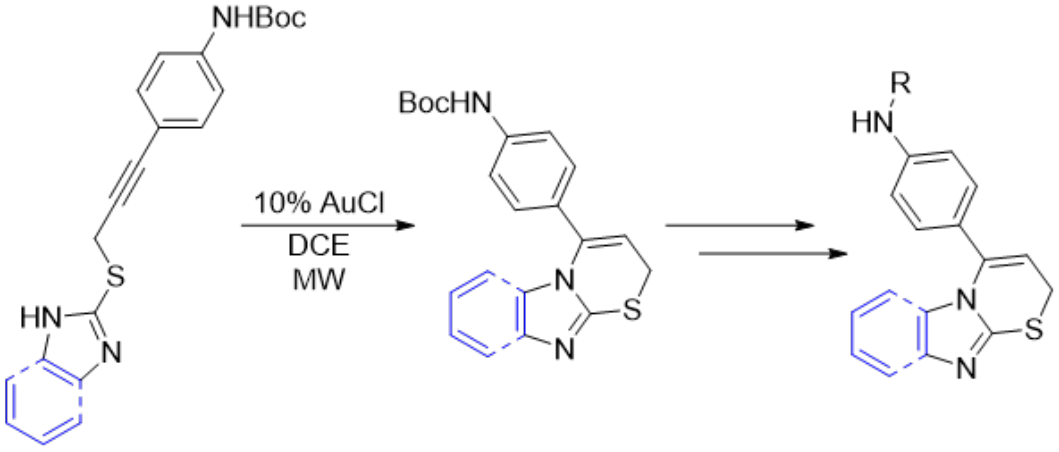


Fig. 1. Synthesis of 4-(7*H*-imidazo[2,1-*b*][1,3]thiazin-5-yl)aniline derivatives.

[1] M. G. Iadanza, M. P. Jackson, E. W. Hewitt, N. A. Ranson, and S. E. Radford, "A new era for understanding amyloid structures and disease," Nature Reviews Molecular Cell Biology, vol. 19, no. 12, pp. 755–773, Sep. 2018, doi: 10.1038/s41580-018-0060-8.

[2] X. Zhang et al., "How the imidazole ring modulates amyloid formation of islet amyloid polypeptide: A chemical modification study," Biochimica Et Biophysica Acta (BBA) - General Subjects, vol. 1860, no. 4, pp. 719–726, Jan. 2016, doi: 10.1016/j.bbagen.2016.01.008.

[3] I. Misiūnaitė et al., "Imidazo[2,1-b][1,3]thiazine Derivatives as Potential Modulators of Alpha-Synuclein Amyloid Aggregation," ACS Chemical Neuroscience, vol. 15, no. 24, pp. 4418–4430, Nov. 2024, doi: 10.1021/acschemneuro.4c00451.

SYNTHESIS OF PYRAZOLE- AND BENZIMIDAZOLE DERIVATIVES FUSED VIA OXAZACYCLES

Agnė Užupytė[1], Povilas Viltrakis[2], Vilija Kederienė[3], Algirdas Šačkus[4], Eglė Arbačiauskienė[5]

[1]Kaunas University of Technology, Faculty of Chemical Technology, Department of Organic Chemistry, Kaunas, Lithuania
agne.uzupyte@ktu.edu

Heterocyclic compounds play a central role in drug discovery due to their versatile structures and potential medicinal applications [1,2]. While pyrazole- or benzimidazole-fused heterocycles [3-5] and various six-, seven-, or eight-membered oxazacycles [6,7] have been reported individually, polycyclic molecules combining pyrazole, benzimidazole, and a variable oxazacycles have not yet been synthesized. Developing methods to access these novel fused scaffolds provides an opportunity to expand the chemical space of biologically relevant heterocycles.

The primary aim of this study is to develop a general and efficient syntheticstrategy for the preparation of novel polycyclic molecules combining pyrazole, benzimidazole, and variable six-, seven-, or eight-membered oxazacycles. This study seeks to expand the chemical space of biologically relevant heterocycles and provide new scaffolds for potential future pharmacological evaluation.

The pyrazole-benzimidazole systems fused via different oxazacycles systems were synthesized using a two-step modular approach. In the first step, a pyrazole carbaldehyde was condensed with a diamine to form a pyrazole-benzimidazole intermediate. In the second step, a dihalogenated alkane-induced annulation, linking the pyrazole hydroxyl group with the benzimidazole NH group, was used to form the four-ring scaffold. Reactions were monitored by TLC, and the structures of intermediates and final products were confirmed by NMR spectroscopy, mass spectrometry, and IR analysis. The modular two-step synthesis successfully yielded a series of pyrazole-benzimidazoles fused via oxazine, oxazepine, and oxazocine rings.

These results demonstrate the feasibility and versatility of the synthetic strategy for accessing previously unreported polycyclic systems. The approach expands the chemical space of biologically relevant heterocycles and provides a foundation for the future exploration of their pharmacological potential.

[1] R. Nath et al., “Therapeutic potential of nitrogen-containing heterocyclic compounds in Alzheimer’s disease: From molecular design to SAR studies,” Journal of Molecular Structure, vol. 1354, p. 144837, Nov. 2025, doi: 10.1016/j.molstruc.2025.144837.
[2] A. Kumar et al., “Nitrogen containing heterocycles as anticancer agents: A Medicinal Chemistry perspective,” Pharmaceuticals, vol. 16, no. 2, p. 299, Feb. 2023, doi: 10.3390/ph16020299.
[3] A. Da Fermo, A. Bisi, R. Orioli, S. Gobbi, and F. Belluti, “Triazole and pyrazole hybrids of electrophilic natural products as promising anticancer agents,” Molecules, vol. 31, no. 2, p. 355, Jan. 2026, doi: 10.3390/molecules31020355.
[4] V. Sundharaj, S. Mohanraj, S. Sarveswari, and V. Vijayakumar, “Catalyst-Assisted Synthesis of benzimidazole derivatives: recent advances and mechanistic insights,” Topics in Current Chemistry, vol. 384, no. 1, p. 5, Jan. 2026, doi: 10.1007/s41061-025-00535-7.
[5] M. Marinescu, “Benzimidazole-Quinoline hybrids: Synthesis and antimicrobial properties,” Pharmaceuticals, vol. 19, no. 1, p. 180, Jan. 2026, doi: 10.3390/ph19010180.
[6] G. Pan, L. Lu, W. Zhuang, and Q. Huang, “Synthesis of Indole-Fused six-, seven-, or Eight-Membered N,O-Heterocycles via Rhodium-Catalyzed NH-Indole-Directed C–H Acetoxylation/Hydrolysis/Annulation,” The Journal of Organic Chemistry, vol. 86, no. 23, pp. 16753–16763, Nov. 2021, doi: 10.1021/acs.joc.1c01982.
[7] R. R. Gataullin, “Advances in the synthesis of aryl-fused six- to nine-membered N,O-heterocycles,” Russian Chemical Bulletin, vol. 74, no. 3, pp. 585–622, Mar. 2025, doi: 10.1007/s11172-025-4555-0.

SYNTHESIS AND INVESTIGATION OF 3-1-(2,4-DIFLUOROPHENYL)THIOUREIDOPROPANOIC ACID DERIVATIVES

Guoda Pranaitytė[1], Birutė Grybaitė[1], Vytautas Mickevičius[1]

[1]Kaunas University of Technology, Department of Organic Chemistry, Kaunas, Lithuania
guoda.pranaityte@ktu.lt

In recent years, aromatic fluorine-containing compounds have been increasingly studied for their potential as pharmaceutical molecules, especially in the development of anticancer drugs. The physicochemical properties of fluorine, such as high bond strength, and minimal steric hindrance contribute to improved pharmacokinetics of medicinal molecules. Since many FDA-approved drugs are based on heterocyclic cores, the incorporation of heterocyclic motifs is essential in the synthesis of organic molecules with potential anticancer properties [1, 2].

In this work, compounds (**5–9**) containing a thiazolone moiety were synthesized. 3-[(2,4-Difluorophenyl)amino]propanoic acid (**2**) was first obtained by the reaction of 2,4-difluoroaniline (**1**) with acrylic acid. Subsequently, it was transformed into 3-[1-(2,4-difluorophenyl)thioureido]propanoic acid (**3**) by dissolving compound **2** in acetic acid, followed by the addition of potassium thiocyanate and stirring the reaction mixture under reflux. Since cyclic compound **4** was also formed during this reaction, complete cyclization of the product was achieved by heating it with hydrochloric acid. 3-[(2,4-Difluorophenyl)(4-oxo-4,5-dihydrothiazol-2-yl)amino]propanoic acid (**5**) was obtained by refluxing thioureido acid **3** with chloroacetic acid. The resulting product was further used in condensation reactions with various heterocyclic aldehydes (Fig. 1).

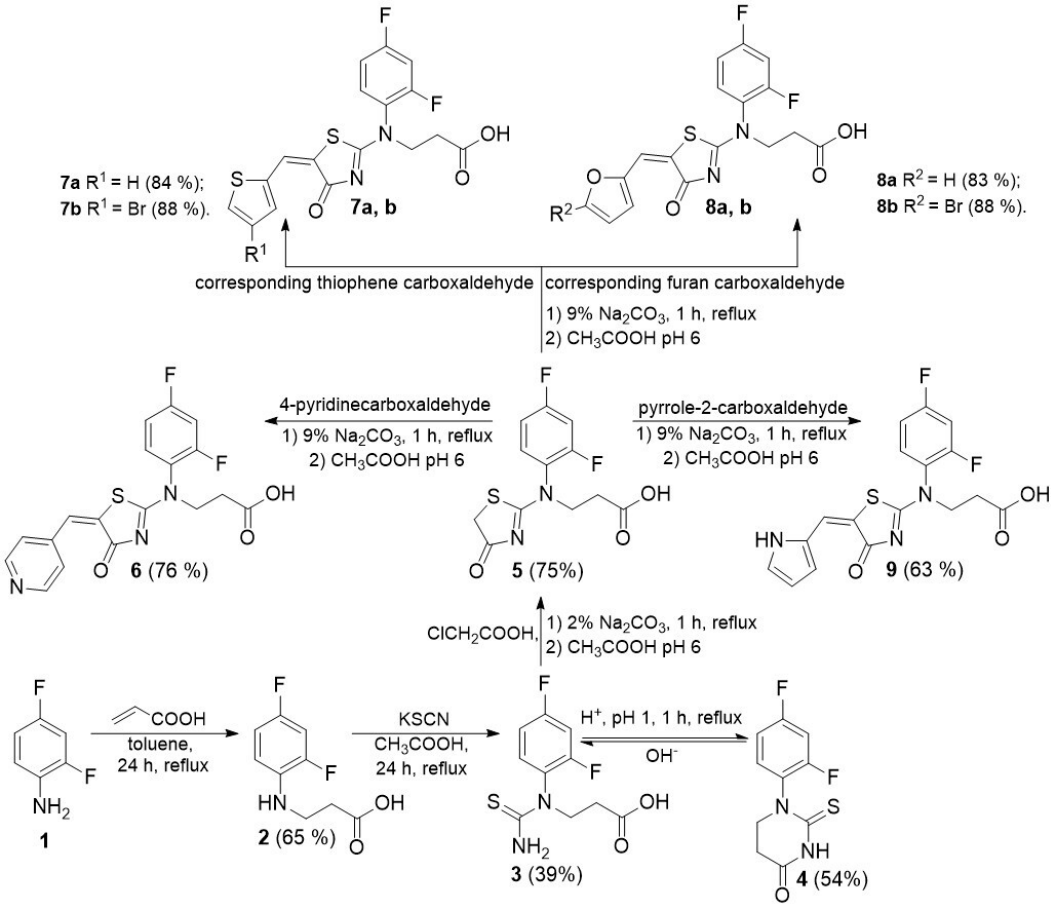


Fig. 1. Synthesis of 3-[1-(2,4-difluorophenyl)thioureido]propanoic acid derivatives **4–9**.

The structure of the synthesized compounds has been proven by ^{1}H NMR, ^{13}C NMR and other spectroscopic methods. Investigation of the anticancer activity of the synthesized compounds are planned.

[1] G. Shabir et al., "Chemistry and Pharmacology of fluorinated Drugs approved by the FDA (2016–2022)," Pharmaceuticals, vol. 16, no. 8, p. 1162, Aug. 2023, doi: 10.3390/ph16081162.

[2] Y. Du et al., "Fluorine in the pharmaceutical industry: FDA-Approved Fluorine-Containing Drugs in 2024," Chemistry - a European Journal, vol. 31, no. 25, p. e202500662, Mar. 2025, doi: 10.1002/chem.202500662.

CHARACTERIZATION OF CELLULOSE EXTRACTED FROM DIFFERENT WASTES SOURCES

Austėja Burbulytė[1], Ieva Uogintė[1]

[1]Center for Physical Sciences and Technology, Department of Environmental Reasearch, Lithuania
austeja.burbulyte@ftmc.lt

Lignocellulose is one of the natural and renewable sources of free major macromolecular polymers. The plant biomass consists of cellulose (35–60%), hemicellulose (20–40%), and lignin (10–25%) [1]. In the plant's cellulose acts as a main structural component, providing essential rigidity, tensile strength, and structural integrity to plants. Cellulose possesses a linear polymeric structure composed of β-D-glucose monomers linked by β-(1→4) glycosidic bonds. The abundance of hydroxyl (–OH) groups along the polymer chain enables the formation of extensive intra- and intermolecular hydrogen bonding. These interactions may be different in lignocellulose feedstocks and can have effect on crystallinity [2]. It is well known that cellulose can be obtained by using secondary materials such as waste. In view of this, this study was investigated and compared cellulose from softwood and hardwood.

Cellulose extraction procedure was performed by using bleaching method. First part was alkali pretreatment; different wood sawdust was placed in a chemical beaker and heated up with sodium hydroxide solution for 3 hours at 90℃. After that the solution was placed in oven for 24 hours at 60℃. When the solution was filtered and the wood sawdust washed to remove the residual of sodium hydroxide. The second part was bleaching. The wood sawdust was placed in a chemical beaker and heated up with hydrogen peroxide solution for 1,5 hours at 80℃. This step was repeated twice. When the solution was filtered and solid residue was heated up with sodium hydroxide and hydrogen peroxide solution for 3 hours at 80℃. After this, the solution was filtered, washed with distilled water and collected cellulose was dried in an oven.

The cellulose was extracted from three different sources: softwood (mix of pine and spruce) and hardwood (oak, mahogany). The extracted cellulose was characterized by SEM, EDX and XRD. Firstly, it was noticed that cellulose after extraction have white color. The efficiency of the extraction was around 76%. Additionally, the scanning electron microscopy describes the structure of cellulose surface. While from elemental analysis it is seen the dominance of carbon and oxygen atoms. Also, the X-ray diffraction analysis was performed and shows that cellulose have crystalline and amorphous regions. Characterization results show that different wood cellulose have nearly similar structures.

[1] A. Darmenbayeva et al., "Cellulose-Based Sorbents: A comprehensive review of current advances in water remediation and future prospects," Molecules, vol. 29, no. 24, p. 5969, Dec. 2024, doi: 10.3390/molecules29245969.

[2] V. K. Yadav et al., "Recent advances in synthesis and degradation of lignin and lignin nanoparticles and their emerging applications in nanotechnology," Materials, vol. 15, no. 3, p. 953, Jan. 2022, doi: 10.3390/ma15030953.

SODIUM BOROHYDRIDE OXIDATION ON NiZn/Ti AND Au(NiZn)/Ti ELECTROCATALYSTS IN ALKALINE FUEL CELLS FOR CLEAN ENERGY CONSERVATION

Tripura Ganti[1], Aldona Balčiūnaitė[1], Huma Amber[1], Giedrius Stalnionis[1], Jūrate Vaičiūnienė[1], Loreta Tamašauskaitė-Tamašiūnaitė[1], Eugenijus Norkus[1]

[1]Center for Physical Sciences and Technology (FTMC), Department of Catalysis, 10257,Vilnius, Lithuania.
tripura.ganti@ftmc.lt

The development of efficient anode electrocatalysts is critical for enhancing the sodium borohydride oxidation reaction (BOR) in fuel cells. In this study, NiZn/Ti electrodes and Au-modified NiZn/Ti electrocatalysts were fabricated by electrodeposition of a NiZn layer on Ti, followed by alkaline leaching and galvanic deposition of Au nanocrystallites. Alkaline leaching generated dendritic surface architectures, while subsequent Au decoration introduced enhanced surface heterogeneity, improving access to reactive surface regions. The Au loading was measured as 19.25 μg cm-2. The electrochemical performance of the resulting electrocatalysts was evaluated in alkaline media containing sodium borohydride at concentrations ranging from 0.01 to 0.05 M using cyclic voltammetry and chronoamperometry. The Au-modified electrode exhibited higher BOR activity compared to bare NiZn/Ti, even at low Au loadings. Increasing the sodium borohydride concentration led to higher current densities, accompanied by a slight positive shift in peak potential. Kinetic analysis indicated that the reaction proceeds via a diffusion-controlled mechanism. Chronoamperometric measurements further confirmed the stability of the Au–NiZn/Ti electrocatalyst under operating conditions. Overall, these results demonstrate that the Au–NiZn/Ti electrocatalyst is a highly effective anode material for BOR in fuel cell systems that use sodium borohydride as the energy carrier.

ZINC - AND NITROGEN-DOPED BIOMASS-DERIVED CARBON CATALYSTS FOR OXYGEN REDUCTION

Daina Upskuvienė[1], Virginija Ulevičienė[1], Aldona Balčiūnaitė[1], Ance Plavniece[2], Loreta Tamašauskaitė-Tamašiūnaitė[1], Eugenijus Norkus[1]

[1]Center for Physical Sciences and Technology, Department of Catalysis, Vilnius, Lithuania.
[2]Latvian State Institute of Wood Chemistry, Riga, Latvia.
daina.upskuviene@ftmc.lt

The oxygen reduction reaction (ORR) is a key electrochemical process in fuel cells and metal–air batteries, significantly influencing device efficiency and operational stability. The development of low-cost and sustainable electrocatalysts to replace noble metals remains a major scientific challenge. In this study, activated wood carbon (AWC), derived from alder wood char, was employed for the one-step synthesis of zinc- and nitrogen-doped carbon catalysts (AWC–Zn–N) via co-doping and thermal treatment. The synthesized materials were characterized using ICP-OES, XRD, XPS, SEM-EDS, BET surface area analysis, and Raman spectroscopy to evaluate their structural, compositional, and surface properties. The ORR performance of the AWC–Zn–N catalysts was investigated in an Ar- or O2-saturated 0.1 M KOH solutions using cyclic voltammetry (CV), linear sweep voltammetry (LSV), and the rotating disk electrode method (RDE). Furthermore, the AWC–Zn–N catalyst exhibited promising electrochemical performance toward the oxygen reduction reaction, demonstrating favorable onset potential and stable current response. The incorporation of Zn and N heteroatoms into the carbon matrix facilitates the formation of catalytically active sites and enhances electronic conductivity. These results highlight the potential of Zn- and N-doped biomass-derived carbon materials as efficient and environmentally friendly electrocatalysts for oxygen reduction, offering a promising alternative to precious metal-based materials in sustainable energy technologies.

ELECTRODE FABRICATION METHOD USING RESIN AND STEREOLITHOGRAPHIC 3D PRINTING

Rokas Bagdonas[1], Inga Morkvėnaitė-Vilkončienė[2]

[1]Vilnius Gediminas Technical University, Faculty of Mechanics, Department of mechanical and materials engineering
[2]Vilnius Gediminas Technical University, Faculty of Elektronics, Department of Electrical Engineering
rokas.bagdonas@vilniustech.lt

The microelectrodes used in scanning electrochemical microscope (SECM) measurements are usually made using a glass shell, which provides good insulating and mechanical properties. However, such electrodes are brittle and expensive, and manual manipulation of the electrode during the measurement, in particular positioning and surface modification, presents a high risk of damage, and the geometry and shape of the glass shell electrodes are practically fixed, making them difficult to adapt to non-standard or specific SECM measurements. These limitations are especially highlighted in experiments requiring frequent electrode surface refurbishment or customisation.

The aim of this work is to develop, experimentally test, and evaluate an alternative microelectrode manufacturing method that uses stereolithographic (SLA) or digital light processing (DLP) 3D printing and photopolymer resin, and to determine whether the resin-insulated electrode is suitable for electrochemical measurements.

The microelectrode was manufactured using a metal core, which was insulated with photopolymer resin and integrated into a stereolithographic (SLA) and digital light processing (DLP) 3D printed body. This method allows the electrode geometry to be freely changed and adapted to the requirements of the investigation, as well as reducing its cost. The active disc-shaped surface of the scanning electrochemical microelectrode was formed by sanding. The electrochemical properties were evaluated by measurements in $K_3[Fe(CN)_6]$ solution using a standard three-electrode system.

The experimental results showed that the ground microelectrode exhibits a clear, stable and repeatable oxidation and reduction response (a properly shaped Cyclic Voltammetry (CV) plot is obtained), comparable to the electrochemical properties of classical microelectrodes, while unpolished microelectrode did not show a significant electrochemical signal, thus confirming the effectiveness of the photopolymeric resin insulation and the tightness of the shell.

Results show that this method of microelectrode fabrication is promising for electrochemical applications. Due to its fast iteration capability, freedom of shape and lower cost, this method can be a useful alternative to classical glass-shell microelectrodes. The work provides a methodological basis for further research focusing on process optimisation and increasing the reproducibility of electrode fabrication.

Cd-N-DOPED BIOMASS-DERIVED CARBON AS AN ANODE CATALYST FOR HYDRAZINE OXIDATION

Virginija Ulevičienė[1], Aldona Balčiūnaitė[1], Daina Upskuvienė[1], Aleksandrs Volperts[2], Loreta Tamašauskaitė-Tamašiūnaitė[1], Eugenijus Norkus[1]

[1]Center for Physical Sciences and Technology, Department of Catalysis, Saulėtekio Ave. 3, LT-10257 Vilnius, Lithuania
[2]Latvian State Institute of Wood Chemistry, Dzerbenes Str. 27, LV-1006 Riga, Latvia
virginija.uleviciene@ftmc.lt

The hydrazine oxidation reaction (HzOR) is a promising anodic process for direct hydrazine fuel cells, offering a high energy density and a carbon-free reaction pathway. However, developing sustainable and cost-effective electrocatalysts remains a major challenge for practical applications. In this study, alder wood char was used to produce activated wood carbon (AWC), which was then employed as a substrate for synthesizing cadmium- and nitrogen-doped carbon catalysts (AWC–Cd–N) via one-step doping and thermal treatment. The structural, compositional, and surface features of the synthesized materials were evaluated using XRD, XPS, ICP-OES, SEM-EDS, BET, and Raman spectroscopy. Electrochemical performance towards HzOR was evaluated using cyclic voltammetry and chronoamperometry in a solution of 0.05 MN_2H_4 and 1 M KOH within an electrode potential range of -1.2 to 0.6 V (vs. SCE) at a scan rate of 50 mV $s^{-}1$. The AWC–Cd–N catalyst demonstrated a consistent current response and desirable electrochemical activity, proving its reliability over an extended testing period. The presence of Cd and N-heteroatoms within the carbon matrix leads to the formation of catalytically active sites and enhances the electronic properties. These results highlight the potential of Cd- and N-doped biomass-derived carbon as a sustainable and efficient electrocatalyst for HzOR, offering a practical pathway for non-precious metal-based fuel cell applications.

INFLUENCE OF SYNTHESIS TEMPERATURE ON THE PHOTOELECTROCHEMICAL PROPERTIES OF Cu_2O

Urte Rinkeviciute[1], Irena Savickaja[1], Monika Skruodiene[1,2], Arnas Naujokaitis[1], Vidas Pakstas[1], Anatolijs Sarakovskis[2], Milda Petruleviciene[1,2]

[1]Centre for Physical Sciences and Technology, Chemical engineering and technology, Lithuania
[2]University of Latvia, Institute of Solid-State Physics, Latvia
urte.rinkeviciute@ftmc.lt

Photoelectrochemical materials play an important role in converting solar energy into usable forms such as electricity or hydrogen fuel. Index Cu_2O is a promising semiconductor for these applications due to its absorption of visible light and low-cost synthesis; however, its stability and performance are often limited by photocorrosion and defect-related processes [1], [2]. Its photoelectrochemical properties are also highly sensitive to synthesis conditions, particularly the temperature used during electrode preparation [3]. The aim of this study was to evaluate the influence of synthesis temperature in the range of 30 - 80 °C on the photoelectrochemical properties of Index Cu_2O electrodes. Index Cu_2O electrodes were synthesized at different temperatures and characterized using open-circuit potential (OCP), cyclic voltammetry (CV), chronoamperometry (CA), electrochemical impedance spectroscopy (EIS).

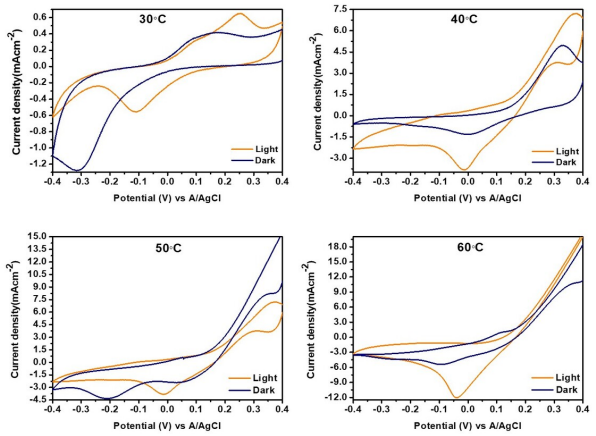


Fig. 1. CV responses of Index Cu_2O electrodes at various temperatures under light illumination (Orange) and in the dark (blue)

The CV results show a clear dependence of photoelectrochemical behavior on synthesis temperature (Fig. 1). Electrodes prepared at intermediate temperatures exhibited more stable open-circuit potentials, higher photocurrent responses, and lower charge transfer resistance, indicating improved interfacial charge transport. Investigation of temperature influence to the photoelectrochemical properties (OCP, CV, EIS and CA) will be presented and discussed in the conference.

Acknowledgements

The work of Milda Petruleviciene is supported by ERDF PostDoc project No. 1.1.1.9/LZP/2/25/232. Institute of Solid State Physics, University of Latvia has received funding from the European Union's Horizon 2020 Framework Programme H2020-WIDESPREAD-01-2016-2017-TeamingPhase2 under grant agreement No. 739508, project CAMART².

Keywords: Cu2O, photoelectrochemistry, electrochemical depositon;

[1] Q. Wang, Y. Zhang, and Y. Liu, "Photo Corrosion behaviour of CU2O nanowires during photoelectrochemical CO2 reduction," Journal of Electroanalytical Chemistry, vol. 912, no. 116239, pp. 1–7, 2022.
[2] C. Ying Toe, J. Scott, and R. Amal, "Recent advances in suppressing the photocorrosion of cuprous oxide for photocatalytic and photoelectrochemical energy conversion," Journal of Photochemistry and Photobiology C: Photochemistry Reviews, vol. 40, pp. 191–211, 2019.
[3] K. Syrek, M. Jażdżewska, and M. Kozieł, "Photoelectrochemical activity of CU2O electrochemically deposited at different temperatures," Journal of Industrial and Engineering Chemistry, vol. 115, pp. 561–569, 2022.

SYNTHESIS AND ELECTROCHEMICAL PROPERTIES OF $ZnCo_2O_4$ SPINEL COATINGS PREPARED BY COMBUSTION AND SPRAY DEPOSITION

Kristijonas Kacevičius[1], Maria-Anthoniette Oghenetejiro Onoriode-Afunezie[1], Agnė Šulčiūtė[1]

[1]Lithuania, Kaunas University of Technology, Faculty of Chemical Technology, Department of Physical and Inorganic Chemistry
maria.onoriode@ktu.edu

$ZnCo_2O_4$ spinel has emerged as a promising mixed-metal oxide for electrochemical and photoelectrochemical applications owing to its high redox activity, good electrical conductivity, and structural stability [1]. Compared to single-metal oxides, $ZnCo_2O_4$ exhibits enhanced charge-transfer properties and a higher density of electrochemically active sites, making it attractive for energy storage and photoelectrochemical systems. However, the functional performance of $ZnCo_2O_4$ strongly depends on the synthesis route and electrode fabrication strategy.

In this study, $ZnCo_2O_4$ was synthesized using a combustion method due to its simplicity, rapid reaction kinetics, and scalability. The precursor solution was calcined at 300 °C to remove volatile components and subsequently annealed at 600 °C to promote spinel phase formation. The synthesized material was deposited as thin-film coatings on conductive glass substrates using spray deposition, with the number of deposited layers varied to assess thickness-dependent behavior. Structural, morphological, and compositional characterization was performed using X-ray diffraction, scanning electron microscopy, energy-dispersive X-ray spectroscopy, and Fourier-transform infrared spectroscopy. Electrochemical and photoelectrochemical properties were evaluated using standard electrochemical techniques.

X-ray diffraction confirmed the formation of phase-pure $ZnCo_2O_4$ spinel after high-temperature annealing, while microscopic analysis revealed porous surface morphologies favorable for ion transport and charge transfer. Electrochemical testing demonstrated a strong dependence of capacitive behavior on coating thickness. An increase in the number of deposited layers enhanced electrochemical and photoelectrochemical performance up to an optimal value, beyond which charge transport limitations were observed. The highest capacitive response and photoelectrochemical efficiency were achieved for a 16-layer $ZnCo_2O_4$ coating. These findings are consistent with recent reports highlighting the importance of nanostructuring and optimized film architecture in $ZnCo_2O_4$-based electrodes [2], as well as the growing relevance of $ZnCo_2O_4$ for photoelectrochemical applications [3].

The results demonstrate that combustion synthesis combined with spray deposition is an effective and scalable approach for fabricating functional $ZnCo_2O_4$ spinel coatings. Proper optimization of synthesis conditions and coating thickness enables enhanced electrochemical and photoelectrochemical performance, confirming the potential of $ZnCo_2O_4$ coatings for energy storage and photoelectrochemical applications.

[1] Y. Zhang et al., “Facile synthesis of hierarchical porous $ZnCo_2O_4$ microspheres for high-performance supercapacitors,” J. Mater. Chem. A, vol. 3, pp. 982-985, 2015, doi: 10.1039/C4TA05279J.

[2] S. Anantharaj et al., “Electrochemical performance of 2D hierarchical sheet-like $ZnCo_2O_4$ microstructures for supercapacitor applications,” Crystals, vol. 10, no. 7, p. 566, 2020, doi: 10.3390/cryst10070566.

[3] S. Majumder et al., “Exploring $FeVO_4/ZnCo_2O_4$ n–p heterojunctions for superior photoelectrochemical performance,” J. Alloys Compd., vol. 1010, p. 177281, 2025, doi: 10.1016/j.jallcom.2024.177281.

OF VITAMINS AND POLYMERS: ELECTROPOLYMERIZED THIAMINE FILMS AND THEIR STRUCTURE-FUNCTION RELATIONSHIPS

Justina Stonytė[1], Paulina Morkytė[1], Nerija Ričkutė[2], Rasa Pauliukaitė[1]

[1]Center for Physical Sciences and Technology (FTMC), Department of Nanoengineering, Vilnius, Lithuania
[2]Vilnius University, Faculty of Chemistry and Geosciences, Institute of Chemistry, Vilnius, Lithuania
justina.stonyte@ftmc.lt

Bio-derived polymers offer an attractive pathway toward sustainable functional materials, yet many biologically relevant molecules remain underexplored [1]. Thiamine (vitamin B1) is a structurally complex, redox-active heterocycle that has been widely studied electrochemically as an analyte, but rarely considered as a monomer for polymer film formation [2]. In this work, we demonstrate the direct electropolymerization of thiamine (T), lysine (L), and thiamine–lysine (LT) systems to form polymer films.

Polymer films were synthesized electrochemically while varying pH and polymerization cycles, enabling controlled tuning of film growth. Scanning electron microscopy (SEM) and atomic force microscopy (AFM) revealed pronounced differences in surface morphology depending on monomer composition. Interfacial electrochemical behavior was evaluated using the $[Fe(CN)_6]^{3-/4-}$ redox couple, while differential pulse voltammetry was employed to examine responses toward biologically relevant analytes.

The results indicate that monomer selection and co-polymerization strategies directly influence polymer morphology and interfacial function, showing the importance of structure–function relationships in bio-derived polymer films.

[1] R. Celiešiūtė, A. Radzevič, A. Žukauskas, Š. Vaitekonis, and R. Pauliukaite, "A Strategy to Employ Polymerised Riboflavin in the Development of Electrochemical Biosensors," Electroanalysis, vol. 29, no. 9, pp. 2071–2082, Sep. 2017, doi: 10.1002/ELAN.201700218.

[2] W. T. Wahyuni, B. R. Putra, and F. Marken, "Voltammetric detection of vitamin B1 (thiamine) in neutral solution at a glassy carbon electrode via in situ pH modulation," Analyst, vol. 145, no. 5, pp. 1903–1909, Mar. 2020, doi: 10.1039/C9AN02186H.

INFLUENCE OF SN^{4+} IONS ON THE FORMATION OF CALCIUM SILICATE HYDRATES IN A 0.66CaO-SiO_2 -H_2O MIXTURE

Monika Bakierskyte[1], Tadas Dambrauskas[1]

[1]Kaunas University of Technology, Faculty of Chemical Technology, Department of Silicate Technology, Kaunas, Lithuania
monbak3@ktu.lt

Air pollution is one of the main environmental challenges of the 21st century, and volatile organic compounds (VOCs) are among the most important contributors to this problem [1]. To control VOC emissions, various VOC abatement technologies are employed: destruction methods (catalytic and thermal oxidation) and recovery methods (adsorption, absorption, condensation, and membrane separation). According to the literature, catalytic oxidation is one of the most effective and economical approaches, allowing VOCs to be oxidized to CO_2 and H_2O [2]. However, this technology relies on noble metals (palladium, platinum) as catalysts, which increases its cost and reduces its widespread use. Thus, the development of new environmentally friendly and cost-effective catalysts is in great demand. Such catalysts can be calcium silicate hydrates with intercalated transition metal ions [3]. However, only limited data are available in the scientific literature on the synthesis, properties, and catalytic applications of calcium silicate hydrates with intercalated metal ions. Thus, this work aims to determine the formation sequence of calcium silicate hydrates in a 0.66CaO-SiO_2-Sn^{4+}-H_2O mixture under hydrothermal conditions.

In this work, calcium oxide (produced by calcining calcium carbonate at 950 °C for 2 h), amorphous silicon dioxide ($SiO_2 \cdot nH_2O$), and tin nitrate [$Sn(Cl)_4 \cdot 5H_2O$] were used as raw materials. Calcium oxide and silicon dioxide were mixed to reach a molar ratio of calcium oxide to silicon dioxide (CaO/SiO_2) equal to 0.66. Later, 2 g of the solid mixture was mixed with 20 mL of a tin nitrate solution (c_{Sn} = 5 g/L) to achieve a water-to-solid ratio of 10. It was calculated that 50 mg of Sn^{4+} ions were present per gram of the solid mixture in the resulting suspension. The obtained suspension was hydrothermally treated in PTFE vessels placed in a Parr Instrument autoclave for 0–72 h at 200 °C. The obtained products were characterized by various instrumental analytical methods (XRD, STA, FT-IR, AAS, etc.).

It was determined that Sn^{4+} ions strongly affected the formation of calcium silicate hydrates under hydrothermal conditions. At the beginning of synthesis (up to 16 h), semicrystalline calcium silicate hydrate [C-S-H(I)] and Z-phase [$Ca_9(Si_{16}O_{34}(OH)_{14})(H_2O)_8$] were the dominant phases in the undoped system. Longer synthesis duration (24 h) led to the formation of gyrolite [$Ca_8Si_{12}O_{30}(OH)_4 \cdot 7H_2O$], which remained stable up to 72 h. Meanwhile, Sn^{4+} ions prevented the formation of calcium silicate hydrates because burtite [$CaSn(OH)_6$] was the dominant phase under all investigated conditions. Traces of Z-phase were identified after 4 h of synthesis, while those of gyrolite were observed after 16 h. The analysis of the liquid medium showed that all tin ions were intercalated or formed new compounds after 72 h of synthesis.

[1] L. Massolo, M. Rehwagen, A. Porta, A. Ronco, O. Herbarth, and A. Mueller, “Indoor–outdoor distribution and risk assessment of volatile organic compounds in the atmosphere of industrial and urban areas,” Environmental Toxicology, vol. 25, no. 4, pp. 339–349, May 2009, doi: 10.1002/tox.20504.

[2] X. Li, J. Ma, and X. Ling, “Design and dynamic behaviour investigation of a novel VOC recovery system based on a deep condensation process,” Cryogenics, vol. 107, p. 103060, Feb. 2020, doi: 10.1016/j.cryogenics.2020.103060.

[3] T. Dambrauskas, D. Davidoviciene, A. Eisinas, and K. Baltakys, “Thermal stability, porosity, and catalytic activity of compound formed in a CaO-SiO2-Cu(NO3)2-H2O system,” Surfaces and Interfaces, vol. 37, p. 102696, Jan. 2023, doi: 10.1016/j.surfin.2023.102696.

SYNTHESIS OF SILVER-DOPED WHITLOCKITE

Gabriele Egle Budzyte[1], Aivaras Kareiva[1], Inga Grigoraviciute[1]

[1]Vilnius University, Institute of Chemistry, Naugarduko st. 24, LT-30225, Vilnius, Lithuania
egle.budzyte@chgf.vu.lt

Calcium phosphate (CP) ceramics have been the focus of extensive research due to their structural similarity to the mineral phase of biological mammal hard tissues and their capacity to support bone regeneration through their bioactive surface properties. Within this group, particular attention has been drawn to whitlockite-type phosphates as a potential alternative to more conventional CPs, as demonstrated by numerous studies reporting enhanced osteogenic response and accelerated bone healing. It is important to note that the whitlockite crystal structure is capable of accommodating compositional variations without loss of its overall framework. This property allows for the substitution of calcium (Ca) by other ions, thereby enabling the emergence of newly acquired, substitution-induced properties.

A particularly noteworthy modification is that of silver (Ag) doping. The incorporation of Ag into the whitlockite matrix is of interest because it has the potential to introduce antibacterial functionality, which could reduce the risk of infection in scenarios involving bone repair. Nevertheless, the development of practical synthesis routes for Ag-doped whitlockite remains a significant challenge.

In this study, Ag-doped whitlockite was synthesized using calcium sulphate hemihydrate ($CaSO_4 \cdot 0.5H_2O$) as the calcium (Ca) source. The synthesis was carried out in a phosphate-containing medium, where $CaSO_4 \cdot 0.5H_2O$ dissolves and subsequently precipitates as the targeted whitlockite phase. The main synthesis parameters were investigated for their influence on phase formation and product composition. The parameters investigated included synthesis reaction time, Ca to Ag ratio, and the pH of the phosphate medium. Phase composition and purity, as well as morphology of the synthesized samples were evaluated using X-ray diffraction (XRD), Fourier-transform infrared spectroscopy (FTIR), inductively coupled plasma spectroscopy (ICP), and scanning electron microscopy (SEM).

SILVER-DOPED CARBONATED HYDROXYAPATITE GRANULES FOR ANTIBACTERIAL BONE REGENERATION

Gabriele Meizyte[1], Maab Abdulsamad Ahmed Elsheikh[1], Aivaras Kareiva[1], Inga Grigoraviciute[1]

[1]Lithuania, Vilnius University, Faculty of Chemistry and Geosciences, Institute of Chemistry
gabriele.meizyte@chgf.vu.lt

Bone repair requires scaffolds that mimic native mineral tissue. Carbonated hydroxyapatite (CHA, $Ca_{10-a}(CO_3)_b(PO_4)_{6-c}(OH)_{2-d}$) meets this need as the principal inorganic component of bone and is widely used as a graft material. It is more biocompatible than another common artificial bone substitute hydroxyapatite (HA, $Ca_{10}(PO_4)_6(OH)_2$) but less thermally stable. Overall, CHA offers a more suitable balance of biocompatibility and stability than HA for bone repair. [1, 2] Such unmodified materials, however, lack intrinsic antimicrobial activity, leaving implants vulnerable to infection. Silver ions were shown to possess antibacterial effects and were successfully incorporated into CHA. [3]

The CHA granules (150–500 μm) were synthesized via a low-temperature dissolution–precipitation method using naturally abundant calcium sulfate (gypsum). The reaction was conducted in aqueous media without organic reagents, aligning with environmentally friendly synthesis principles. Silver was incorporated relative to the initial CHA granule mass at 0.5, 1.0, 2.5, 5.0, and 7.5 wt% to systematically study its antibacterial effect. The characterization of CHA granules focused on structural, chemical, and morphological analysis via X-ray diffraction, Fourier transform infrared and Raman spectroscopies, scanning electron microscopy, and surface area measurements.

The study's outcome is to functionalize the CHA bioceramics by embedding silver into the CHA granules, and in this way produce an advanced antibacterial biomaterial suitable for bone regeneration.

[1] K. Ishikawa, Journal of the Ceramic Society of Japan, 127, 9, 595–601, 2019.
[2] E. Landi, G. Celotti, G. Logroscino, and A. Tampieri, Journal of the European Ceramic Society, 23, 15, 2931–2937, 2003.
[3] J. Kolmas, U. Piotrowska, M. Kuras, and E. Kurek, Materials Science and Engineering C, 74, 124–130, 2017.

MAGNESIUM WHITLOCKITE FORMATION FROM AMORPHOUS CALCIUM PHOSPHATE: EFFECTS OF BUFFER COMPOSITION AND Mg^{2+}

Greta Linkaitė[1], Gabrielė Eglė Budžytė[1], Aleksej Žarkov[1], Aivaras Kareiva[1], Inga Grigoravičiūtė[1]

[1]Vilnius University, Faculty of Chemistry and Geosciences, Vilnius, Lithuania
greta.linkaite@chgf.stud.vu.lt

Magnesium whitlockite (Mg-WH, $Ca_{18}Mg_2(HPO_4)_2(PO_4)_{12}$) is a biologically relevant calcium phosphate that is increasingly studied for bone regeneration and hard-tissue engineering owing to its osteoconductive and bioresorbable behavior [1][2]. Mg-WH can occur naturally in some tissues such as dentin and cartilage [3], and according to some sources, it has been associated with early-stage or actively forming bone, particularly in younger individuals [4], making it an attractive synthetic alternative to conventional calcium phosphates that lack structurally incorporated Mg^{2+} ions despite their known osteogenic role.

In this study, Mg-WH was synthesized at a relatively low temperature of 80 °C through a dissolution–precipitation synthesis route in a phosphate buffer, using amorphous calcium phosphate as a precursor. The effect of phosphate buffer composition and magnesium ion concentration on the final product was investigated in order to determine the most favorable conditions for single-phase Mg-WH formation. Optimized synthesis conditions resulted in the formation of phase-pure Mg-WH powder with particle size varying between 100-300 nm, whose purity was verified by XRD, Rietveld refinement, and FTIR analyses. Deviations from the selected conditions led to the formation of secondary impurity calcium phosphate phases.

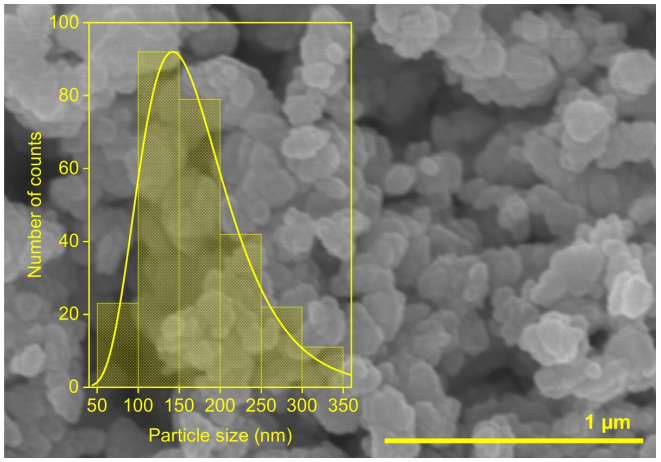


Fig. 1. Histogram of synthesized Mg-WH particle sizes (n = 270) with a lognormal fit (solid line), showing a right-skewed particle size distribution.

Keywords: Calcium Phosphates, Whitlockite, Biomaterials, Amorphous calcium phosphate, Dissolution–precipitation

[1] S. Palati, D. Ganapathy, and S. Sekaran, “Whitlockite as a next-generation biomaterial for bone regeneration: A systematic review of In Vivo evidence for bone regeneration,” Journal of Oral Biology and Craniofacial Research, vol. 15, no. 6, pp. 1176–1182, Aug. 2025, doi: 10.1016/j.jobcr.2025.08.002.

[2] A. Kizalaite et al., “Dissolution–Precipitation Synthesis and Characterization of Zinc Whitlockite with Variable Metal Content,” ACS Biomaterials Science & Engineering, vol. 7, no. 8, pp. 3586–3593, Jul. 2021, doi: 10.1021/acsbiomaterials.1c00335.

[3] F. A. Shah, “Magnesium whitlockite – omnipresent in pathological mineralisation of soft tissues but not a significant inorganic constituent of bone,” Acta Biomaterialia, vol. 125, pp. 72–82, Feb. 2021, doi: 10.1016/j.actbio.2021.02.02

[4] H. L. Jang, H. K. Lee, K. Jin, H.-Y. Ahn, H.-E. Lee, and K. T. Nam, “Phase transformation from hydroxyapatite to the secondary bone mineral, whitlockite,” Journal of Materials Chemistry B, vol. 3, no. 7, pp. 1342–1349, Dec. 2014, doi: 10.1039/c4tb01793e.

CORRELATION BETWEEN PHASE TRANSITION BEHAVIOR AND STRUCTURAL PROPERTIES IN Ba^{2+} -SUBSTITUTED La_2 Mo_2O_9

Ugnė Vazgelevičiūtė[1], Artūras Žalga[1], Giedrė Gaidamavičienė[1]

[1]Faculty of Chemistry and Geosciences, Institute of Chemistry, Vilnius University, Naugarduko str. 24, LT-03225 Vilnius, Lithuania
ugne.vazgeleviciute@chgf.stud.vu.lt

Lanthanum molybdate ($La_2Mo_2O_9$) is a well-established oxide-ion conducting material that has been extensively investigated due to its potential application in intermediate-temperature solid oxide fuel cells, oxygen separation membranes, and gas sensors [1]. Its functional properties are strongly influenced by a reversible first-order phase transition from a low-temperature monoclinic α-phase to a high-temperature cubic β-phase, which is accompanied by significant changes in crystal symmetry, lattice structure, and ionic transport behavior [2]. While the cubic phase exhibits higher oxide-ion conductivity, its stabilization over a broader temperature range remains a key challenge for practical applications.

Chemical substitution at the La^{3+} site has been widely recognized as an effective strategy to control the structural stability and phase transition characteristics of $La_2Mo_2O_9$-based materials [3]. In particular, alkaline earth cation substitution has attracted increasing attention due to its ability to induce lattice distortions, affect point defect distribution, and influence the thermodynamic characteristics of the phase transition. Recent studies have demonstrated that the size and valence mismatch between the host and substituent cations play a critical role in determining phase stability and transition temperature [4]. Despite growing interest, the influence of Ba^{2+} substitution on the crystal structure and phase transition in the $La_2Mo_2O_9$ system remains insufficiently explored, especially for materials synthesized via low-temperature chemical routes.

The aim of this study was to investigate the correlation between Ba^{2+} substitution, structural properties, and phase transition behavior in $La_2Mo_2O_9$. Ba^{2+}-substituted $La_2Mo_2O_9$ samples were prepared using an aqueous sol-gel synthesis route, ensuring homogeneous cation distribution at the molecular level. Structural and phase analysis was carried out by X-ray diffraction (XRD), while microstructural features were examined using scanning electron microscopy (SEM). Differential scanning calorimetry (DSC) was employed to evaluate the phase transition behavior.

XRD analysis indicated that the sol-gel synthesis method is suitable for the preparation of a single-phase compound without detectable secondary phases. SEM analysis revealed a relatively dense ceramic microstructure with the presence of a limited number of pores. Differential scanning calorimetry results suggested that partial substitution of lanthanum with barium contributed to the stabilization of the cubic β-phase at room temperature.

Keywords: LAMOX, phase transition, SOFC, sol-gel

[1] P. Lacorre, F. Goutenoire, O. Bohnke, R. Retoux, and Y. Laligant, “Designing fast oxide-ion conductors based on La2Mo2O9,” Nature, vol. 404, no. 6780, pp. 856–858, Apr. 2000, doi: 10.1038/35009069.

[2] S. Sen and T. Paul, “Electronic structures of trivalent cations doped bulk and cubic La2Mo2O9 oxide ion conductors,” Journal of Solid State Chemistry, vol. 295, p. 121918, Dec. 2020, doi: 10.1016/j.jssc.2020.121918.

[3] Y.-W. Liao, S. Kawabata, T. Yabutsuka, W.-J. Chen, H. Okumura, and S. Takai, “Low temperature phase transition phenomena in Ba- and Pb-substituted La2Mo2O9 oxide ion conductors,” Solid State Ionics, vol. 354, p. 115405, Jul. 2020, doi: 10.1016/j.ssi.2020.115405.

[4] A. Žalga and G. Gaidamavičienė, “Thermoanalytical and x-ray diffraction studies on the phase transition of the Calcium-Substituted LA2MO2O9 system,” Materials, vol. 16, no. 2, p. 813, Jan. 2023, doi: 10.3390/ma16020813.

SOL-GEL SYNTHESIS AND CHARACTERIZATION OF ND_{1-x} NA_x MNO_3 PEROVSKITES

Aigul Dastankyzy[1], Dovydas Karoblis[1], Kestutis Mazeika[2], Aivaras Kareiva[1]

[1]Vilnius University, Faculty of Chemistry and Geosciences, Vilnius, Lithuania
[2]Center for Physical Sciences and Technology, Vilnius, Lithuania
aigul.dastankyzy@chgf.stud.vu.lt

Rare-earth manganite perovskites with the general formula $RMnO_3$ (R = rare-earth element) represent a prominent class of strongly correlated oxides, in which charge, spin, orbital, and lattice degrees of freedom are strongly coupled, leading to rich magnetic and structural behavior [1]. These compounds crystallize in the ABO_3 perovskite structure, where distortions of the MnO_6 octahedra, governed by the A-site ionic radius and tolerance factor, play a decisive role in determining their structural stability and physical properties [1].

Rare-earth manganites have also attracted significant attention in the field of multiferroics and magnetoelectrics, as structural distortions and spin–lattice interactions in perovskite oxides can give rise to coupled magnetic and electric phenomena [2,3]. Among this family, $NdMnO_3$ is of particular interest due to the coexistence and interaction of Mn and Nd magnetic sublattices, which results in complex magnetic behavior and a high sensitivity to structural modifications [4].

A-site substitution offers an effective route for tuning the structure and properties of NdMnO3-based perovskites. Partial replacement of Nd^{3+} by monovalent Na^{+} alters the charge balance and the Mn^{3+}/Mn^{4+} ratio, leading to modifications of the magnetic structure and phase stability, as previously reported for $Nd_{1-x}Na_xMnO_3$ compounds [5]. However, most studies on $Nd_{1-x}Na_xMnO_3$ systems have primarily focused on low Na substitution levels, while investigations covering a wider range of Na concentrations remain limited.

In this work, a series of $Nd_{1-x}Na_xMnO_3$ (x = 0-0.6) perovskite oxides were synthesized using the sol–gel method with ethylene glycol as a complexing agent to ensure homogeneous cation distribution. Phase formation and crystal structure were investigated by X-ray diffraction (XRD). Fourier-transform infrared (FT-IR) spectroscopy was employed to confirm the formation of the perovskite framework and to probe changes in metal–oxygen bonding associated with Na substitution. Microstructural features were examined by scanning electron microscopy (SEM), while elemental composition and chemical homogeneity were verified using SEM–EDX and ICP–OES techniques. The results confirm the successful synthesis of Na-doped $NdMnO_3$ perovskites and provide insight into the influence of A-site substitution on their structural and compositional characteristics.

Keywords: Perovskites, sol-gel, manganites, multiferroics

[1] M. B. Salamon and M. Jaime, “The physics of manganites: Structure and transport,” Reviews of Modern Physics, vol. 73, no. 3, pp. 583–628, Aug. 2001, doi: 10.1103/revmodphys.73.583.
[2] A. J. C. Buurma, G. R. Blake, T. T. M. Palstra, and U. Adem, “Multiferroic materials: physics and properties,” in Elsevier eBooks, 2016. doi: 10.1016/b978-0-12-803581-8.09245-6.
[3] L. W. Martin et al., “Multiferroics and magnetoelectrics: thin films and nanostructures,” Journal of Physics Condensed Matter, vol. 20, no. 43, p. 434220, Oct. 2008, doi: 10.1088/0953-8984/20/43/434220.
[4] Y. Wang, H. Wang, W. Tan, and D. Huo, “Magnetization reversal, critical behavior, and magnetocaloric effect in NdMnO3: The role of magnetic ordering of Nd and Mn moments,” Journal of Applied Physics, vol. 132, no. 18, Nov. 2022, doi: 10.1063/5.0124002.
[5] B. Samantaray, S. Ravi, A. Das, and S. K. Srivastava, “Magnetic structure and magnetic properties of Nd1–xNaxMnO3 compounds,” Journal of Applied Physics, vol. 110, no. 9, Nov. 2011, doi: 10.1063/1.3656714.

COMPARATIVE INVESTIGATION OF DOPING CONCENTRATION EFFECTS ON STRUCTURAL AND PHOTOLUMINESCENT PROPERTIES OF $CAGDALO_4$ AND $CAYALO_4$ PHOSPHORS

Domantas Černius[1,2], Monika Skruodienė[2,3], Milda Petruleviečienė[2,3], Meldra Kemere[3], Ramūnas Skaudžius[1,2]

[1]Vilnius University, Department of Inorganic Chemistry, Lithuania
[2]Center for Physical Sciences and Technology, Department of Chemical Engineering and Technology, Lithuania
[3]University of Latvia, Institute of Solid-State Physics, LV-1063, Riga, Latvia
domantas.cernius@chgf.stud.vu.lt

$CaGdAlO_4$ (CALGO) and $CaYAlO_4$ (CALYO) have attracted significant attention as host matrices for rare-earth (RE^{3+}) ions due to their favorable combination of thermal and structural properties. Crystallizing in the tetragonal *I4/mmm* space group, these materials exhibit a ”disordered” crystal structure where Ca^{2+} and RE^{3+} ions share the same lattice sites. This disorder leads to a broadening of absorption and emission bands, a key requirement for high-efficiency laser crystals [1, 2]. Furthermore, CALGO and CALYO possess high thermal conductivity and excellent mechanical stability, allowing them to withstand the thermal loading typical of high-power optical applications [3]. Moreover, Yb-doped crystals are promising candidates for ultrashort-pulsed laser generation, where high thermal-conductivity is essential and both matrices exceed the minimum thermal requirements for such applications [2].

This study focuses on determining the optimal concentrations of Holmium (Ho^{3+}) and Ytterbium (Yb^{3+}) dopants, incorporated separately, to maximize optical performance while maintaining host crystallinity. X-ray Diffraction (XRD) is employed to monitor increasing dopant concentrations compromise phase purity. Previous studies show that in Yb^{3+}-doped CALYO, replacing the main ions with dopants causes a small but measurable changes in the volume of the elementary cell [2], whereas in Yb^{3+}-doped CALGO crystals, crystal structure remains well-preserved [4]. Scanning Electron Microscopy (SEM) is used to observe the surface morphology and determine the particle size. Luminescence measurements provide direct insight into the optical behavior of the dopant ions within the host lattice. By analyzing the emission spectra, it is possible to quantify the emission intensity of Ho^{3+} and Yb^{3+} ions and evaluate how it evolves with dopant concentration. These measurements reveal the efficiency of radiative transitions, identify characteristic emission bands, and allow detection of concentration-dependent effects such as energy transfer and quenching [1]. By correlating the structural information from XRD and SEM with the photoluminescence analysis, this study defines the optimal doping concentrations for CALGO and CALYO confirming their potential as high-performance optical materials.

[1] Z. Wang et al., “Yb:CALYO shaped crystal fibers: Growth and spectroscopic characterization,” Optical Materials, vol. 150, p. 115206, Apr. 2024, doi: 10.1016/j.optmat.2024.115206.
[2] D. Li et al., “Crystal growth and spectroscopic properties of Yb:CaYAlO4 single crystal,” Journal of Crystal Growth, vol. 312, no. 14, pp. 2117–2121, Apr. 2010, doi: 10.1016/j.jcrysgro.2010.04.028.
[3] J. Q. Di et al., “Crystal growth, polarized spectra, and laser performance of Yb:CaGdAlO4crystal,” Laser Physics, vol. 26, no. 4, p. 045803, Mar. 2016, doi: 10.1088/1054-660x/26/4/045803.
[4] X. Liu et al., “Growth, micromechanical aspects, spectroscopy, and laser performance of Yb: CALGO crystal,” Optics & Laser Technology, vol. 189, p. 113140, May 2025, doi: 10.1016/j.optlastec.2025.113140.

INFLUENCE OF TITANIUM DOPING ON THE STRUCTURAL PROPERTIES OF YAG:Pr

Tautvydas Pudžmys[1], Greta Inkrataitė[1]

[1]Vilnius University, Faculty of Chemistry and Geosciences, Institute of Chemistry, Vilnius, Lithuania
tautvydas.pudzmys@chgf.stud.vu.lt

Yttrium aluminium garnet (YAG) is one of the most widely used host materials for rare-earth ions due to its excellent thermal and chemical stability, as well as its beneficial optical properties, such as optical transparency over a broad UV–IR wavelength range [1,2]. The emissions of YAG:Pr arise from 4f–4f and 4f–5d electronic transitions (photoluminescence at UV and red-light wavelengths), making it suitable for lighting, scintillation, and potential laser technologies [3]. Consequently, YAG:Pr has been extensively researched. However, there haven't been many studies on co-doping YAG with praseodymium and transition metals, particularly with titanium. Titanium can substitute for aluminium in various structures and considering the success of titanium–doped sapphire uses in laser technologies, it is intriguing to study how this element can affect the structural properties of YAG:Pr [4]. Additionally, titanium can exist in two oxidation states: +4 and +3, which should influence how well it can be incorporated into garnet, as it replaces of Al^{3+} ions. The effects of this should be most visible in calcined samples, as during the calcination of YAG structures, many oxygen vacancies are filled [5]. Moreover, titanium compounds have shown great antibacterial activity [6]. And considering that YAG:Pr emits UV radiation after excitation, it is interesting to see how strong antibacterial properties YAG structures co-doped with praseodymium and titanium may exhibit [7].

In this work, yttrium aluminium garnets, doped with different amounts of Pr^{3+} and Ti^{4+} ions, have been synthesized by the aqueous sol-gel method and the effects of titanium doping in YAG:Pr have been examined. Phase composition was determined by X-ray diffraction analysis, which showed how a new phase appears at higher (≥10 %) titanium concentrations. Sample morphology was examined using scanning electron microscopy, and it was observed how different amounts of titanium change the morphology. In addition, the photoluminescence behaviour of the materials and the effect of titanium and praseodymium were studied.

[1] S. Murai, K. Fujita, K. Iwata, and K. Tanaka, "Optical properties of macroporous Y3Al5O12 crystals doped with rare earth ions synthesized via sol–gel process from ionic precursors," Optical Materials, vol. 33, no. 2, pp. 123–127, Sep. 2010, doi: 10.1016/j.optmat.2010.08.009.
[2] D. Franta and M.-G. Mureşan, "Wide spectral range optical characterization of yttrium aluminum garnet (YAG) single crystal by the universal dispersion model," Optical Materials Express, vol. 11, no. 12, p. 3930, Oct. 2021, doi: 10.1364/ome.441088.
[3] M. Wisniewska et al., "Luminescence and scintillation properties of YAG:Pr," IEEE Transactions on Nuclear Science, vol. 49, no. 3, pp. 926–930, Jun. 2002, doi: 10.1109/tns.2002.1039591.
[4] H. Bao and X. Ruan, "Absorption spectra and Electron-Vibration coupling of Ti:Sapphire from first principles," Journal of Heat Transfer, vol. 138, no. 4, Dec. 2015, doi: 10.1115/1.4032177.
[5] T. Huang et al., "Fabrication, microstructure and optical properties of titanium doped YAG transparent ceramic," Journal of Alloys and Compounds, vol. 478, no. 1–2, pp. L16–L20, Dec. 2008, doi: 10.1016/j.jallcom.2008.11.157.
[6] . Fujishima, T. N. Rao, and D. A. Tryk, "Titanium dioxide photocatalysis," Journal of Photochemistry and Photobiology C Photochemistry Reviews, vol. 1, no. 1, pp. 1–21, Jun. 2000, doi: 10.1016/s1389-5567(00)00002-2.
[7] A. Pakalniskis et al., "Sol-gel synthesis and study of praseodymium substitution effects in yttrium aluminium garnet Y3-xPrxAl5O12," Optical Materials, vol. 111, p. 110586, Nov. 2020, doi: 10.1016/j.optmat.2020.110586.

PLATINUM-MODIFIED COBALT-IRON PHOSPHIDE ELECTROCATALYSTS FOR EFFICIENT OVERALL WATER SPLITTING AT INDUSTRIAL TEMPERATURES

Huma Amber[1], Dmytro Shyshkin[1,2], Loreta Tamašauskaitė-Tamašiūnaitė[1], Jūratė Vaičiūnienė[1], Giedrius Stalnionis[1], Eugenijus Norkus[1]

[1]Center for Physical Sciences and Technology (FTMC), Department of Catalysis, Vilnius, Lithuania,
[2]Vilnius University, Faculty of Chemistry and Geosciences, Department of Inorganic Chemistry, Vilnius, Lithuania
huma.amber@ftmc.lt

The production of green hydrogen using electrocatalytic water splitting, driven by renewable electricity, has emerged as a promising approach. Unlike conventional strategies of developing electrocatalysts for the two half-reactions of water splitting (e.g., the hydrogen and oxygen evolution reactions, HER and OER) separately, there has been a growing interest in designing bifunctional electrocatalysts that can efficiently catalyze both reactions simultaneously. These catalysts are essential for bridging the gap between laboratory-scale research and industrial-scale alkaline water electrolysis. In this study, cobalt phosphide (CoP) and cobalt-iron phosphide (CoFeP) were directly fabricated on copper substrates via an electroless deposition method. Sodium hypophosphite (NaH_2PO_2) was utilized as both the phosphorus source and reducing agent. Subsequently, platinum (Pt) nanoparticles were introduced through a galvanic displacement process. The morphology, elemental composition, and crystal structure of the catalysts were characterized by scanning electron microscopy (SEM), energy-dispersive X-ray spectroscopy (EDS), inductively coupled plasma optical emission spectroscopy (ICP-OES), X-ray diffraction (XRD), and X-ray photoelectron spectroscopy (XPS). The bifunctional electrocatalytic performance toward overall water splitting was evaluated in a two-electrode setup in 1 M KOH electrolyte. Among the synthesized catalysts, Pt-CoFeP demonstrated superior bifunctional activity, with a low Pt loading of only 1.4 μg cm^{-2}, achieving a low cell voltage of 1.62 V at 10 mA cm^{-2}. This is attributed to synergistic interactions between Pt, Co, and Fe that enhanced HER and OER kinetics by improving charge transfer, stabilizing active sites, and optimizing the electronic structure, thus enhancing the utilization efficiency of Pt. It is imperative to assess the performance of electrocatalysts in the context of hydrogen generation under industrially relevant temperatures, as this evaluation is instrumental in substantiating their practical applicability. Remarkably, the electrolyzer employing Pt-CoFeP as the anode and Pt-CoP as the cathode requires only 1.54 V to achieve a current density of 10 mA cm^{-2} at an industrially relevant temperature of 75 °C. Furthermore, the cell voltage demonstrates a consistent decline from 1.62 V at 25 °C to 1.54 V at 75 °C. This indicates that the operational stability and efficacy of the system are enhanced across the temperature range of 25–75 °C, thereby confirming the robustness and industrial viability of the system. This present research offers a scalable strategy for the design of platinum-modified transition metal phosphides as efficient bifunctional electrocatalysts for industrial alkaline water electrolysis and sustainable hydrogen production.

Acknowledgements
This research was funded by a grant (No. P-MIP-23-467) from the Research Council of Lithuania.

Keywords: platinum nanoparticles, transition metal phosphides, Industrial temperature, overall water splitting, alkaline electrocatalysis

$Ni(OH)_2$-SUPPORTED Pd ELECTROCATALYSTS FOR METHANOL OXIDATION IN ALKALINE MEDIA

Muhammad Adeel Tariq[1], Hafiz Muhammad Naeem[1], Loreta Tamašauskaitė-Tamašiūnaitė[1], Eugenijus Norkus[1], Ramūnas Levinas[1]

[1]Center for Physical Sciences and Technology (FTMC), Department of Catalysis, Vilnius, Lithuania.
adeel.tariq@ftmc.lt

Direct methanol fuel cells (DMFCs) have gained characteristics attraction due to low operating temperature, high energy density and easy fuel storage and handling. However, comprehensive commercialization of DMFC technology is limited due to slow methanol oxidation reaction kinetics and severe poisoning of catalytic active sites resulting from adsorbed carbonaceous intermediates. Therefore, in order to overcome these challenges $Ni(OH)_2$ support material was hydrothermally synthesized followed by Pd nanoparticles decoration using chemical reduction treatment. The phase structure, crystallinity, morphological analysis with elemental composition and chemical composition of $Pd/Ni(OH)_2$ catalysts were analyzed using X-ray diffraction (XRD), scanning electron microscopy (SEM), energy-dispersive X-ray spectroscopy (EDS) and X-ray photoelectron spectroscopy (XPS). XRD patterns demonstrate that all the characteristics peaks of $Ni(OH)_2$ along metallic Pd peaks in $Pd/Ni(OH)_2$ catalysts. Highly irregular and agglomerated surface morphologies consisting of interlinked hydroxide aggregates revealed by SEM analysis, while EDS elemental mapping shows the presence of all constituent's elements with well dispersion. Also, XPS technique was used to evaluate the oxidation states of elements in $Pd/Ni(OH)_2$, indicating the presence of metallic Pd at binding energies of 335.00 eV and 340.22 eV. All these physiochemical characterizations confirmed the successful synthesis of $Pd/Ni(OH)_2$ along uniform distribution of Pd on $Ni(OH)_2$ substrate. Cyclic voltammetry (CV), chronoamperometry (CA), and electrochemical impedance spectroscopy (EIS) were used to evaluate the electrocatalytic performance of composite with different composition. $Pd/Ni(OH)_2$ electrodes exhibited good catalytic activity for methanol oxidation relatively to $Ni(OH)_2$ without Pd incorporation, due to synergistic interaction between Pd active sites and $Ni(OH)_2$/NiOOH support. Among the investigated catalyst $Pd/Ni(OH)_2$ (1:0.5) showed highest forward anodic peak current density (30 mA cm^{-2}) and mass activity normalized by Pd mass (450 mA mg^{-1} Pd), significant I_f/I_b ratios indicating good poisoning intermediates resistance along efficient long term stability. While, increasing $Ni(OH)_2$ contents in Pd-decorated $Ni(OH)_2$ catalyst leads to decrease the catalytic activity because of masking and dilution of Pd active sites. Kinetic studies suggest that methanol activation through initial C–H bond cleavage governs the overall reaction rate. Overall, the obtained Pd–decorated $Ni(OH)_2$ material presents a cost effective, promising, durable anode catalyst.

Keywords: Direct methanol fuel cells, methanol oxidation, Pd-decorated Ni(OH)2, Synergistic effect, catalytic activity

LIGHT-DRIVEN OXIDATION OF GLYCEROL ON WO_3 -BASED PHOTOANODES FOR SUSTAINABLE APPLICATIONS

Kamila Turuta[1], Irena Savickaja[1], Jurga Būdienė[1], Viktorija Rapalytė[1], Milda Petrulevičienė[1], Jurga Juodkazytė[1]

[1]Center for Physical Sciences and Technology (FTMC)
kamila.turuta@ftmc.lt

The increasing production of biodiesel has led to a substantial surplus of glycerol as an unavoidable by-product [1]. Crude glycerol streams, often containing methanol, inorganic salts, and fatty acid residues, pose disposal challenges and contribute to industrial wastewater pollution. At the same time, glycerol is an underutilized bio-derived carbon resource that is attractive for sustainable oxidation processes due to its non-toxicity, biodegradability, and high reducing capacity [2]. Selective oxidation of glycerol provides access to a broad range of oxygenated C3–C1 products, including value-added C3 compounds such as glyceraldehyde, dihydroxyacetone, and glyceric acid, C2 intermediates like glycolaldehyde arising from C–C bond cleavage, and deeper oxidation products such as formic acid [3]. However, conventional oxidation methods typically rely on harsh oxidants, suffer from limited selectivity, and generate secondary waste streams. Photoelectrochemical oxidation using semiconductor photoanodes offers a greener alternative by harnessing solar energy and operating in non-toxic aqueous electrolytes (Fig. 1A), enabling controlled oxidation under mild conditions.

In this study, WO_3 photoanodes were synthesized using a hydrothermal approach and characterized using complementary structural and morphological techniques to assess their phase composition and optical properties. The photoelectrochemical behaviour of the prepared WO_3 electrodes was investigated in neutral Na_2SO_4 electrolyte under controlled illumination and applied potential, both in the absence and presence of glycerol.

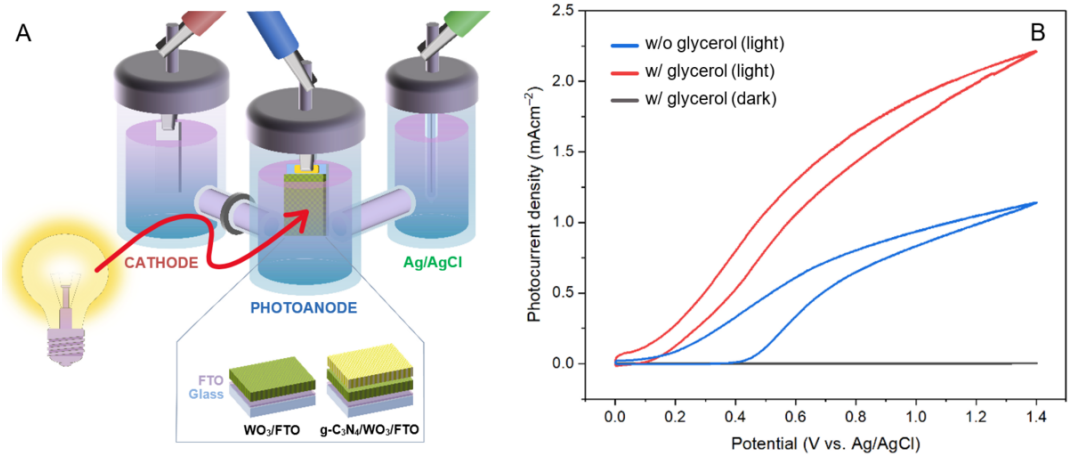


Fig. 1. (A) Setup of photoelectrochemical system, consisting of a three-compartment cell, electrodes immersed in electrolyte and a light source. (B) Cyclic voltammograms of WO_3 photoanode in 0.1 M Na_2SO_4 with and without 0.1 M glycerol recorded in dark and under illumination (1 sun, AM 1.5G illumination),potential scan rate: 50 mV/s.

Preliminary cyclic voltammetry measurements (Fig. 1B) reveal a pronounced enhancement of the photoanodic current upon glycerol addition, indicating a strong influence of glycerol on interfacial charge-transfer processes at illuminated semiconductor electrodes. This behaviour is commonly explained by the ability of glycerol to scavenge photogenerated holes on the semiconductor surface, thereby suppressing electron–hole recombination while simultaneously acting as an effective electron donor. As a result, the photoanodic current is significantly enhanced compared to water oxidation.

Building on this observation, the present work aims to systematically investigate photoelectrochemical glycerol oxidation on WO_3-based photoanodes under visible-light irradiation. At the conference, results on anode modification strategies, including WO_3/g-C_3N_4 systems, electrolyte composition effects, and chromatographic analysis of glycerol oxidation products will be reported.

[1] Y. Bansod, K. Ghasemzadeh, and C. D'Agostino, "Techno-economic assessment of biodiesel-derived crude glycerol purification processes," RSC Sustainability, vol. 3, no. 6, pp. 2605–2618, Jan. 2025, doi: 10.1039/d4su00599f.
[2] C. Venu, D. Palanisamy, S. Jaganathan, and S. Rajendran, "Production and evaluation of syngas derived from glycerol using aqueous phase reforming for fueling compression ignition engines," Renewable Energy, vol. 219, p. 119594, Nov. 2023, doi: 10.1016/j.renene.2023.119594.
[3] A. M. Hilbrands, M. K. Goetz, and K.-S. Choi, "C–C Bond Formation Coupled with C–C Bond Cleavage during Oxidative Upgrading of Glycerol on a Nanoporous BiVO4 Photoanode," Journal of the American Chemical Society, vol. 145, no. 46, pp. 25382–25391, Nov. 2023, doi: 10.1021/jacs.3c09631.

Ni-BASED BIMETALLIC CATALYSTS FOR SODIUM BOROHYDRIDE HYDROLYSIS

Zita Sukackienė[1], Gitana Valeckytė[1], Loreta Tamašauskaitė-Tamašiūnaitė[1], Jolanta Stupakova[2]

[1]Lithuania, Vilnius, Center for Physical Sciences and Technology, Department of Catalysis,
[2]Lithuania, Vilnius, Vilnius Gediminas Technical University
zita.sukackiene@ftmc.lt

The accelerated increase in global energy consumption, in conjunction with the gradual depletion of fossil fuel resources, has prompted an intensive search for clean, sustainable, and efficient energy alternatives. Among the proposed solutions, hydrogen has emerged as a particularly attractive energy carrier due to its high energy density and environmentally benign nature, producing only water as a by-product during use. Notwithstanding these advantages, the development of efficient and cost-effective hydrogen production technologies remains a significant challenge. In this context, the catalytic hydrolysis of sodium borohydride has garnered considerable interest, as it enables hydrogen generation under mild conditions with a high hydrogen yield.

In the present work, three nickel-based bimetallic catalysts $Ni_{96}Co_4$, $Ni_{95}Mo_5$ and $Ni_{93}W_7$ were synthesized and comparatively investigated for hydrogen generation via sodium borohydride hydrolysis. The catalysts were prepared using an electroless deposition method. The surface morphology and chemical composition of the samples were analyzed using scanning electron microscopy (SEM) and inductively coupled plasma optical emission spectroscopy (ICP-OES). A thorough examination through the use of scanning electron microscopy (SEM) revealed that all of the synthesized catalysts are composed of agglomerated particles with irregular, predominantly oval-shaped morphologies. These morphological features contribute to an increased surface area, which is favorable for catalytic activity.

Among the catalysts that were examined, $Ni_{93}W_7$ demonstrated the highest catalytic activity for the hydrogen generation reaction, achieving a hydrogen generation rate of 10.0 mL/min at 70 °C. Furthermore, this catalyst exhibited the lowest activation energy (50.14 kJ/mol) in comparison to the $Ni_{95}Mo_5$ and $Ni_{96}Co_4$ catalysts. The enhanced catalytic performance of $Ni_{93}W_7$ is attributed to the synergistic effect between nickel and tungsten, which facilitates the sodium borohydride hydrolysis reaction.

Keywords: electroless deposition, coatings, borohydride hydrolysis

NICKEL TUNGSTEN CATALYSTS FOR HYDROGEN GENERATION

Gitana Valeckytė[1], Zita Sukackienė[1], Jūratė Vaičiūnienė[1], Loreta Tamašauskaitė-Tamašiūnaitė[1], Eugenijus Norkus[1]

[1]Center for Physical Sciences and Technology (FTMC), Department of Catalysis, Vilnius, Lithuania
gitana.valeckyte@ftmc.lt

For more than a century, fossil fuels such as coal, natural gas and oil have been the world's main source of energy. But they are constantly running out. This is particularly due to the sharp increase in energy demand and the rapidly growing world population [1]. Scientists are working to find a way to replace this by developing clean, sustainable and efficient energy sources. One alternative is renewable energy from the sun and wind. It can be a sustainable, economical and environmentally friendly source of energy. It can also help reduce greenhouse gas emissions and mitigate the effects of climate change. But this has its drawbacks. Renewable energy from the sun and wind is intermittent. That is, electricity is only produced when the sun is shining or the wind is blowing. For this reason, it is difficult to ensure a constant supply of electricity [2]. The second alternative is hydrogen. Hydrogen is considered a "green" and sustainable energy [3]. It is a high-calorie, clean and environmentally friendly fuel with zero emissions. And during combustion, no greenhouse gases are released and no air pollution occurs, and only water vapor is formed as a by-product [1].

During this work, $Ni_{93}W_7$/Cu, $Ni_{91}W_9$/Cu, $Ni_{89}W_{11}$/Cu, $Ni_{87}W_{13}$/Cu, and $Ni_{85}W_{15}$/Cu catalysts were formed using the chemical method of metal deposition. The surface morphology, internal structure and chemical composition of the obtained catalysts were analyzed using scanning electron microscopy (SEM) and inductively coupled plasma optical emission spectroscopy (ICP-OES). It was determined that the prepared coating particles consist of oval-shaped agglomerates. The catalytic properties of the formed catalysts for sodium borohydride hydrolysis reaction were investigated. The two-component $Ni_{93}W_7$ coating was characterized by the highest catalytic activity.

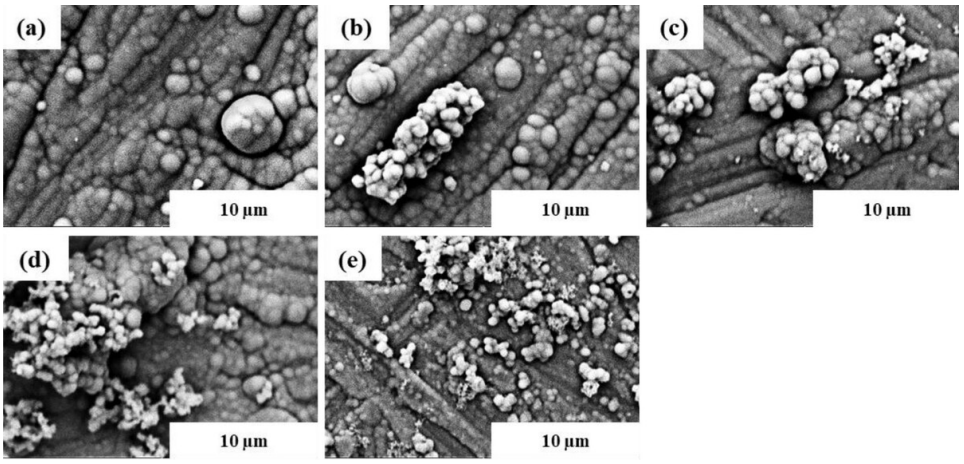


Fig. 1. SEM images of prepared $Ni_{93}W_7$/Cu (a), $Ni_{91}W_9$/Cu (b), $Ni_{89}W_{11}$/Cu (c), $Ni_{87}W_{13}$/Cu (d), $Ni_{85}W_{15}$/Cu (e).

Keywords: Nickel, tungsten, catalysts, hydrogen, sodium borohydride

[1] S. Rathod et al., "Catalytic hydrogen production via NaBH4 hydrolysis: Role of WO3 nanopellets," Renew. Energy, vol. 248, p. 123156, 2025.
[2] N. Ma et al., "Large scale of green hydrogen storage: Opportunities and challenges," Int. J. Hydrogen Energy, vol. 50, pp. 379-396, 2024.
[3] X. Zhang et al., "Efficient Hydrogen Generation from the NaBH4 Hydrolysis by Cobalt-Based Catalysts: Positive Roles of Sulfur-Containing Salts," ACS Appl. Mater. Interfaces, vol. 12, pp. 9376–9386, 2020.

APPLICATION OF Co_3O_4 AND Cr_2O_3 PARTICLES SUPPORTED ON NITROGEN-DOPED CARBON FOR HYDROGEN EVOLUTION REACTION

Karina Vjūnova[1], Loreta Tamašauskaitė-Tamašiūnaitė[1]

[1]Center for Physical Sciences and Technology (FTMC), Saulėtekio ave. 3, LT10257 Vilnius, Lithuania
karina.vjunova@ftmc.lt

The hydrogen evolution reaction (HER) is one of the key half-reactions in the process of electrochemical water splitting. It is responsible for generating hydrogen at the cathode. Efficient HER electrocatalysts are essential for reducing energy losses and enabling sustainable hydrogen production. Non-noble metal-based electrocatalysts offer an effective and low-cost alternative for HER, providing promising route towards green hydrogen production. In this study, Co_3O_4, Cr_2O_3, and Co_3O_4–Cr_2O_3 particles were prepared using a hydrothermal method and examined for their potential as non-noble metal electrocatalysts. Their structural and morphological properties were characterized using scanning electron microscopy (SEM). Additionally, the synthesized particles were supported on nitrogen-doped carbon (NC) with high surface area to enhance electrocatalytic activity. HER electrocatalytic activity was studied using linear sweep voltammetry (LSV) in an Ar-saturated 1 M KOH solution. The electrocatalytic activity for HER was found to be markedly increased when the Co_3O_4 and Co_3O_4–Cr_2O_3 particles were supported on NC, compared to the unsupported materials. Notably, Cr2O3 particles and the Cr2O3/NC electrocatalyst exhibited no activity towards HER, demonstrating the positive influence of cobalt-containing oxides on HER performance. The Co_3O_4/NC electrocatalyst demonstrated an onset potential (Eonset) of −0.189 V and an overpotential of 0.350 V at a current density of 10 mA cm^{-2}, compared to Eonset of −0.360 V and an overpotential of 0.476 V for Co_3O_4–Cr_2O_3/NC under the same conditions. Thus, hydrogen produced through this process can serve as a clean fuel for fuel cells, enabling efficient energy conversion with zero carbon emissions. These results demonstrate the potential of cobalt-containing non-noble metal oxides as efficient, low-cost electrocatalysts for hydrogen production, supporting their application in fuel cells.

Pd_x Fe_y/CA FOR OXYGEN REDUCTION REACTION IN ALKALINE MEDIA

David Tomić[1], Jadranka Milikić[1], Meryem Samancı[2], Ana Nastasić[3], Ayşe Bayrakçeken[2], Biljana Šljukić[1,4], Aldona Balčiūnaitė[5]

[1]University of Belgrade, Faculty of Physical Chemistry, Belgrade, Serbia
[2]Atatürk University, Department of Chemical Engineering, Erzurum, Turkey
[3]University of Belgrade, Vinča Institute of Nuclear Sciences – National Institute of the Republic of Serbia, Department of Nuclear and Plasma Physics, Belgrade, Serbia
[4]Universidade de Lisboa, Instituto Superior Tecnico, Chemical Engineering Department, Center of Physics and Engineering of Advanced Materials, Laboratory for Physics of Materials and Emerging Technologies, Lisbon, Portugal
[5]Center for Physical Sciences and Technology, Vilnius, Lithuania
david.tomic@ffh.bg.ac.rs

Carbon aerogels (CA) are highly porous 3D, conductive carbon materials with low density (<0.1 g cm^{-3}) and high specific surface area (500–2000 m^2 g^{-1}), serving as next-generation, multifunctional solutions for sustainable energy storage and conversion, environmental remediation, and catalysis. Their unique, tunable structures, derived from polymerization, drying and carbonization, enable superior performance in supercapacitors, gas adsorption, and water purification [1].

Metal-doped CAs have also shown significant potential as electrocatalysts for oxygen reduction reaction (ORR), which is kinetically very slow. These materials enable four-electron ORR pathway for energy conversion in fuel cells and metal-air batteries, and two-electron ORR pathways for green H_2O_2 production. Due to their properties, these materials represent a cheaper and more available alternative to Pt-based systems, which are considered as ORR benchmark electrocatalysts.

In this work, the electrochemical performance of CA doped with Pd and Fe in different ratios was investigated for ORR in an alkaline medium (1 M KOH) using cyclic voltammetry, linear sweep voltammetry with rotating disc electrode (RDE) and chronoamperometry. The number of electrons exchanged during ORR for $Pd_{30}Fe_{70}$/CA (3.38) and $Pd_{70}Fe_{30}$/CA (2.80) indicates a mixed mechanism where two-electron and four-electron ORR take place in parallel. The value of the onset potential at a current density of -0.1 mA cm^{-2} for $Pd_{70}Fe_{30}$/CA and $Pd_{30}Fe_{70}$/CA are 0.925 V and 0.885 V, respectively. The corresponding Tafel slope values for $Pd_{70}Fe_{30}$/CA and $Pd_{30}Fe_{70}$/CA are 115 mV dec^{-1} and 73 mV dec^{-1}, respectively. The low Tafel slope value for $Pd_{30}Fe_{70}$/CA is comparable to that of Pt/C (78 mV dec^{-1}) [2].

Thanks to their electrochemical properties and the optimization of experimental conditions, these materials show great potential for electrocatalysis of ORR and thus provide great opportunities for numerous applications.

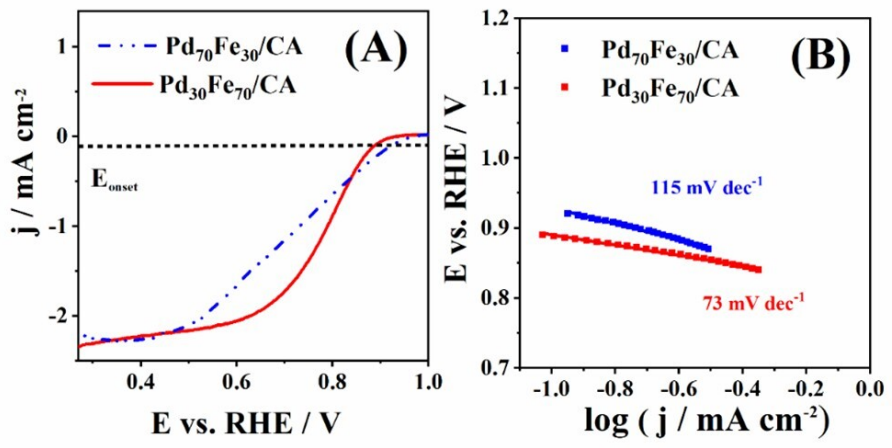


Fig. 1. ORR RDE curves of $Pd_{70}Fe_{30}$/CA and $Pd_{30}Fe_{70}$/CA (A) with the corresponding Tafel plots (B) in O_2- saturated 1 M KOH solution at 1600 rpm and 20 mV s^{-1} .

Acknowledgements

The authors would like to thank the Ministry of Science, Technological Development and Innovation of the Republic of Serbia (contracts no. 451-03-136/2025-03/200146 and 451-03-137/2025-03/200146) as well as Fundação para a Ciência e a Tecnologia (FCT, Portugal)) (contracts no. LAPMET - LA/P/0095/2020 - IST-ID and UID/PRR/04540/2025, https://doi.org/10.54499/UID/PRR/04540/2025).

[1] D. Tomić et al., “Carbon aerogels and xerogels: next-generation materials for sustainable energy and environmental solutions,” Chemical Communications, vol. 61, no. 80, pp. 15510–15523, Jan. 2025, doi: 10.1039/d5cc02477c.
[2] M. Shen et al., “Chemical vapor deposition strategy for inserting atomic FeN4 sites into 3D porous honeycomb carbon aerogels as oxygen reduction reaction catalysts in high-performance Zn-air batteries,” Chemical Engineering Journal, vol. 464, p. 142719, Apr. 2023, doi: 10.1016/j.cej.2023.142719.

Glutathione detection in Chinese Hamster Ovary Cells Using Scanning Electrochemical Microscopy

Indrė Padvilikytė[1,2], Agnė Boguševičė[2], Inga Morkvėnaitė[2,3], Tomas Mockaitis[1,2]

[1]Vilnius TECH, Department of Chemistry and Bioengineering, Vilnius 10223, Lithuania
[2]State Research Institute Centre for Physical Sciences and Technology, Department of Nanotechnology, Vilnius 10257, Lithuania
[3]Vilnius TECH, Department of Electrical Engineering, Vilnius 10223, Lithuania
indre.padvilikyte@stud.vilniustech.lt

Primary metabolites are essential molecules that support core cellular processes such as growth, energy metabolism, and reproduction (Martinez, 2023). Among them, reduced glutathione (GSH) and NADH play central roles in maintaining intracellular redox homeostasis. GSH is a major cellular antioxidant and participates in detoxification, nutrient metabolism, regulation of proliferation, and apoptosis. In reproductive biology, higher oocyte GSH levels have been associated with improved developmental competence, supporting a more reduced intracellular environment and serving as an electron donor for antioxidant enzymes (Yurttancikmaz et al., 2024; Wang et al., 2017).

Scanning electrochemical microscopy (SECM) is a powerful tool for investigating whole-cell surfaces by positioning an ultramicroelectrode (UME) above the sample and recording Faradaic currents generated by oxidation or reduction of a redox mediator at the tip (Morkvenaite-Vilkonciene et al., 2017). These measurements can provide spatially resolved information on cell topography and local redox activity.

In this study, intracellular GSH-related redox behaviour in Chinese hamster ovary (CHO) cells was probed using three mediators with distinct electrochemical properties: ferrocenecarboxylic acid (FcCOOH), ferrocenemethanol (FcMeOH), and menadione.

LUMINESCENCE INVESTIGATION OF CHROMIUM AND CERIUM CO-DOPED YLuAG GARNETS: EFFECT OF DOPANT Ce^{+3} / Cr^{3+} RATIO

Nerija Rickute[1], Greta Inkrataite[1], Ramunas Skaudzius[1]

[1]Lithuania, Vilnius, Vilnius University, Faculty of Chemistry and Geosciences, Institute of Chemistry
nerija.rickute@chgf.stud.vu.lt

Yttrium lutetium aluminium garnet (YLuAG) is a synthetic material that belongs to the garnet group. Synthetic garnet was first discovered in the 1950s, and since then the electronics industry has seen a rapid development of technologies using synthetic compounds with a garnet structure. YLuAG have good mechanical and optical properties. Cubic crystalline matrix allows incorporation in solid solution of luminescent ions such as transition metals (Cr^{3+}) and lanthanides (Ce^{3+}). Chromium and cerium co-doped YLuAG are widely used in luminescent systems such as phosphor-converted LEDs and scintillators. However, garnets doped with different amounts of luminescent metals show different results in luminescence properties. The measurements showed that even a small amount of chromium and cerium incorporated in garnets indicate luminescent properties. Ce^{3+} and Cr^{3+} co-doped YLuAG exhibit emission spectrum ranging from 480 nm to 830 nm, which almost covers full range of visible light and a slight shift towards the red light area. Due to that, it is a great candidate for white light LED lighting.

In the present work, garnets doped with different amounts of chromium have been synthesised and their structural and luminescence properties were studied. Ce^{3+} and Cr^{3+} co-doped YLuAG garnets were synthesized by the sol-gel method. The phase purity of the samples was analysed by means of X-ray diffraction. The morphology of the compounds was evaluated by using scanning electron microscopy. Photoluminescence properties such as emission and excitation spectra, decay curves, quantum efficiency have been investigated.

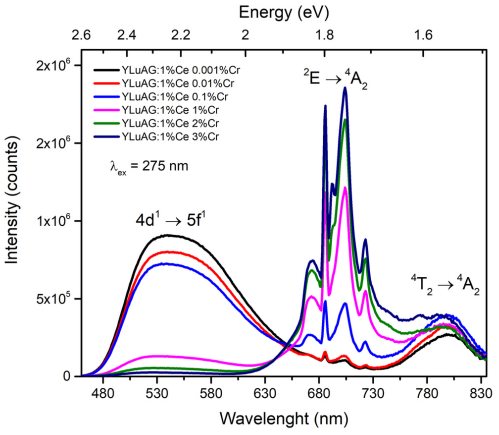


Fig. 1. Emission spectra of YLuAG co-doped with cerium and different amounts of chromium.

EFFECT OF SYNTHESIS METHOD ON PHASE FORMATION AND HIGH-TEMPERATUREPHASE TRANSITION IN La_2 Mo_2O_9

Jonas Labutis[1], Giedrė Gaidamavičienė[1], Artūras Žalga[1]

[1]Vilnius University, Faculty of Chemistry and Geosciences, Institute of Chemistry, Naugarduko Str. 24, 03225 Vilnius, Lithuania
jonas.labutis@chgf.stud.vu.lt

Oxygen-ion-conducting solid electrolytes have been investigated for over six decades due to their potential applications in galvanic cells for precise thermodynamic and kinetic measurements of oxygen-containing systems, oxygen sensors for gaseous and liquid-metal environments, and high-temperature fuel cells [1]. However, their practical relevance to energy conversion technologies has become particularly significant only in recent years [2]. Conventional solid electrolytes, such as yttria-stabilized zirconia (YSZ), exhibit optimal ionic conductivity at high operating temperatures (800 °C – 1000 °C) [3], while gadolinium-doped ceria operates at lower temperatures (600 °C – 800 °C) but suffers from mixed ionic–electronic conductivity and reduced stability under reducing conditions [4]. In this context, lanthanum molybdate ($La_2Mo_2O_9$), commonly referred to as LAMOX, has emerged as a promising alternative, owing to its exceptionally high oxygen-ion conductivity at elevated temperatures, first reported by Lacorre et al. in 2000 [5]. Nevertheless, the principal limitation of this binary oxide system arises from a reversible phase transition occurring in the 500 – 600 °C temperature range, during which the low-temperature monoclinic α-$La_2Mo_2O_9$ phase transforms into the high-temperature cubic modification responsible for enhanced oxygen-ion transport [6]. The complexity of the lanthanum molybdate system, along with its strong temperature dependence of physical properties, motivated this study to examine the influence of the final ceramic composition on the thermal effect associated with the phase transition, which is directly related to the physical properties of the cubic $La_2Mo_2O_9$ crystalline phase. X-ray diffraction (XRD) and thermogravimetric/differential scanning calorimetry (TGA/DSC) analyses were employed to evaluate the phase composition of the synthesized ceramic materials and the energetic characteristics of the high-temperature phase transition.

The results clearly indicate that both the initial molar composition and the used synthesis method have a strong influence on the final crystalline phase composition, as well as on the intensity of the phase transition thermal effect and the physical properties of the obtained ceramics at elevated temperatures.

Keywords: Sol-gel synthesis · Solid-state reaction · Phase transition · Thermal analysis · X-ray diffraction

[1] J. Li, Q. Cai, and B. A. Horri, “Highly conductive and stable electrolytes for solid oxide electrolysis and fuel cells: fabrication, characterisation, recent progress and challenges,” Materials Advances, vol. 6, no. 1, pp. 39–83, Nov. 2024, doi: 10.1039/d4ma00690a.

[2] P. Vinchhi, M. Khandla, K. Chaudhary, and R. Pati, “Recent advances on electrolyte materials for SOFC: A review,” Inorganic Chemistry Communications, vol. 152, p. 110724, Apr. 2023, doi: 10.1016/j.inoche.2023.110724.

[3] Z. Zakaria, S. H. A. Hassan, N. Shaari, A. Z. Yahaya, and Y. B. Kar, “A review on recent status and challenges of yttria stabilized zirconia modification to lowering the temperature of solid oxide fuel cells operation,” International Journal of Energy Research, vol. 44, no. 2, pp. 631–650, Oct. 2019, doi: 10.1002/er.4944.

[4] S. Zha, A. Moore, H. Abernathy, and M. Liu, “GDC-Based Low-Temperature SOFCs powered by hydrocarbon fuels,” Journal of the Electrochemical Society, vol. 151, no. 8, p. A1128, Jan. 2004, doi: 10.1149/1.1764566.

[5] P. Lacorre, F. Goutenoire, O. Bohnke, R. Retoux, and Y. Laligant, “Designing fast oxide-ion conductors based on La2Mo2O9,” Nature, vol. 404, no. 6780, pp. 856–858, Apr. 2000, doi: 10.1038/35009069.

[6] M. Ali, B. N. Wani, and S. R. Bharadwaj, “Phase transition in LAMOX type compounds,” Journal of Thermal Analysis and Calorimetry, vol. 96, no. 2, pp. 463–468, Feb. 2009, doi: 10.1007/s10973-008-9532-y.

THE INFLUENCE OF SiO_2 ADDITIVE ON THE MAYENITE FORMATION PROCESS AND ITS ADSORPTION CAPACITY FOR THE REMOVAL OF Cu^{2+} / SO_4^{2-} IONS

Jolanta Doneliene[1], Bartas Gedminas[1], Andzelika Aleinikovaite[1], Kristina Vasiliauskiene[1], Anatolijus Eisinas[1]

[1]Kaunas University of Technology, Faculty of Chemical Technology, Department of Silicate Technology, Radvilenu pl. 19, LT–50254 Kaunas, Lithuania
jolanta.doneliene@ktu.lt

Mayenite ($C_{12}A_7$) has recently attracted considerable research attention due to its outstanding accelerating effect and rapid hardening behaviour [1], as well as its high oxygen mobility, ionic conductivity, and catalytic properties compared with other calcium aluminates [2]. The synthesis route influences its practical applications, as well as the type and concentration of intercalated ions [3]. In previous work [4], it was observed that in unstirred $CaO–Al_2O_3–H_2O$ suspensions, when the molar ratio CaO/Al_2O_3=2.8, after 4 h of isothermal curing at 130 °C katoite was formed. Synthetic katoite at 350 °C fully recrystallised into mayenite. To the best of our knowledge, no data has been published, and it is still completely unknown how intercalated SiO_2 in the mayenite structure affects its adsorption properties.

This work aimed to determine the formation (from synthetic precursor) and adsorption properties of pure mayenite (M350) and mayenite with intercalated SiO_2 (MS350) after 1 h extra calcination at 350 °C. The synthesis was carried out in unstirred suspensions, with molar ratios of $CaO/(Al_2O_3+SiO_2)$=2.8 and SiO_2=0 or 0.25. The liquid-to-solid ratio of the suspension was 10:1. Hydrothermal synthesis conditions: 130 °C, 1 h. Adsorption experiments were carried out at 25 °C for different time periods. 1 g of adsorbent was added to 100 ml of a $CuSO_4$ aqueous solution containing 2.5 g/L Cu^{2+} ions.

It was observed that the SiO_2 additive did not influence the thermal stability of the products: in both systems, synthetic katoite fully decomposed to mayenite at 350 °C.

It was obtained that, after 3 min of adsorption, the amount of the adsorbed ions by M350 was equal to 22.5 mg Cu^{2+}/L (9%), and after 60 min duration, 100.5 mg/g Cu^{2+} ions (40.2%) were adsorbed (Table 1). In comparison with M350, MS350 has better adsorption capacity for copper ions: 3 min, 76.5 mg/g, and after 60 min, 131.5 mg/g of copper ions were absorbed. It is 30.6% and 52.6%, respectively. It was also observed that MS350 has better sorption properties for SO_4^{2-} anions: after 60 min, the adsorption capacity of MS350 was 1.5 times higher than that of M350.

It was observed that mayenite is unstable during adsorption and fully reacts under all experimental conditions (Fig. 1). After adsorption, the diffraction peaks characteristic of ettringite are higher in sample MS350.

Table 1. The adsorbed amount of Cu^{2+} ions (a) and SO_4^{2-} anions.

Initial concentration of Cu^{2+} = 2.5 g/L		The amount of adsorbed Cu^{2+} ions and SO_4^{2-} anions, mg/g		
	Duration of adsorption	3	20	60
M350	Cu^{2+}	22.5	83	100.5
	SO_4^{2-}	0	37.5	115
MS350	Cu^{2+}	76.5	95	131.5
	SO_4^{2-}	0	40	170

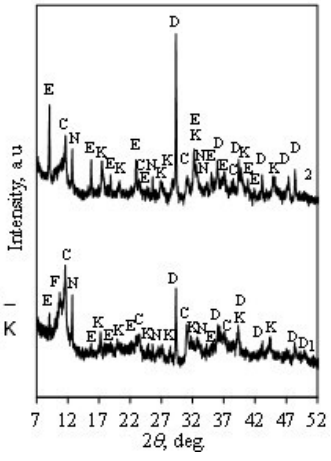


Fig. 1. XRD patterns of products after adsorption. Adsorbent: 1 – M350, 2 – MS350. Indexes: E – ettringite, C – calcium monocarboaluminate, N – posnjakite, K – katoite, D – calcite, F – calcium aluminum oxide carbonate hydroxide hydrate.

These results confirmed that after calcination of the synthesis products, pure mayenite and mayenite with intercalated SiO_2 were formed. SiO_2 additive gives a significant improvement in the adsorption properties of mayenite with intercalated SiO_2. Our research indicates that adsorption reactions are specific to chemisorption.

[1] A. Koehler et al., “How C12A7 influences the early hydration of calcium aluminate cement at different temperatures,” Cement and Concrete Research, vol. 162, p. 106972, Sep. 2022, doi: 10.1016/j.cemconres.2022.106972.

[2] . Abd-El-Raoof et al., “Fabrication and characterization of calcium aluminates cement via microwave-hydrothermal route: Mayenite, katoite, and hydrocalumite,” Construction and Building Materials, vol. 401, p. 132988, Aug. 2023, doi: 10.1016/j.conbuildmat.2023.132988.

[3] A. V. Kapishnikov et al., “Effect of the phase composition of Ca-Al hydroxide precursors on the mayenite formation,” Ceramics International, vol. 51, no. 22, pp. 35496–35505, May 2025, doi: 10.1016/j.ceramint.2025.05.272.

[4] A. Eisinas et al., “Cu2+ ion adsorption by synthetic mayenite and its thermal stability,” Ceramics International, vol. 46, no. 18, pp. 29429–29435, May 2020, doi: 10.1016/j.ceramint.2020.05.028

INVESTIGATION OF THE LUMINESCENT PROPERTIES OF Gd3Ga5-2xMgxZrxO12:Cr3+ AND Gd3Ga5-2xZnxZrxO12:Cr3+ GARNETS SYNTHESIZED BY THE SOL-GEL METHOD

Austėja Šernaitė[1,2], Monika Skruodienė[2,3], Meldra Kemere[3], Ramūnas Skaudžius[1]

[1]Vilnius University, Faculty of Chemistry and Geosciences, Department of Inorganic Chemistry, Lithuania
[2]Department of Chemical Engineering and Technology, Center for Physical Sciences and Technology, Lithuania
[3]University of Latvia, Institute of Solid-State Physics, Latvia
austeja.sernaite@chgf.stud.vu.lt

Gadolinium gallium garnets (GGG) doped with Cr^{3+} ions have shown great promise as a material for near infrared (NIR) light emitting diodes (LEDs). Although these diodes are still emerging and under extensive investigation, they have already demonstrated potential in applications such as plant growth regulation, night vision, food quality testing and healthcare applications [1 – 4]. However, most NIR LEDs have exhibited low quantum efficiency and limited thermal stability – properties that must be improved for these LEDs to achieve practical, real-world applications [5].

It is known that improving the luminescence properties of a material can lead to enhanced quantum efficiency. The present study aims to investigate the effect of Mg/Zr and Zn/Zr substitution for Ga in Cr^{3+} doped GGG on the luminescent properties of the material. Moreover, to the best of our knowledge, obtaining these materials in a single-phase form remains challenging, and they are synthesized here using Sol-Gel chemistry method assisted by Molten-Salt Route.

The results will be presented in detail. The phase formation and purity of the synthesized materials were examined by X-ray diffraction (XRD). Photoluminescence excitation and emission properties, along with quantum efficiency, were systematically investigated. The morphology of the samples was characterized using scanning electron microscopy (SEM).

[1] Y. Su et al., “Multi-site occupation of Cr3+ toward developing broadband near-infrared phosphors,” Ceramics International, vol. 47, no. 16, pp. 23558–23563, May 2021, doi: 10.1016/j.ceramint.2021.05.073.
[2] A. D. Zotte, M. Ottavian, A. Concollato, L. Serva, R. Martelli, and G. Parisi, “Authentication of raw and cooked freeze-dried rainbow trout (Oncorhynchus mykiss) by means of near infrared spectroscopy and data fusion,” Food Research International, vol. 60, pp. 180–188, Oct. 2013, doi: 10.1016/j.foodres.2013.10.033.
[3] X. Zou et al., “A highly efficient and suitable spectral profile Cr3+-doped garnet near-infrared emitting phosphor for regulating photomorphogenesis of plants,” Chemical Engineering Journal, vol. 428, p. 132003, Aug. 2021, doi: 10.1016/j.cej.2021.132003.
[4] A. Guelpa, F. Marini, A. Du Plessis, R. Slabbert, and M. Manley, “Verification of authenticity and fraud detection in South African honey using NIR spectroscopy,” Food Control, vol. 73, pp. 1388–1396, Nov. 2016, doi: 10.1016/j.foodcont.2016.11.002.
[5] Y. Wang et al., “Highly efficient and stable Near-Infrared broadband garnet Phosphor for multifunctional Phosphor-Converted Light-Emitting diodes,” Advanced Optical Materials, vol. 10, no. 11, Apr. 2022, doi: 10.1002/adom.202200415.

THERMAL FIELD CHARACTERISATION IN THE HIGH-TEMPERATURE MELT USED FOR BBO CRYSTAL GROWTH

Gabija Janušauskaitė[1], Martynas Misevičius[1]

[1]Center for Physical Sciences and Technology, Department of Chemical Engineering and Technologies, Vilnius, Lithuania
gabija.janusauskaite@ftmc.lt

β-BaB_2O_4 (BBO) single crystals are widely used in nonlinear optics; however, their growth by the Top-Seeded Solution Growth (TSSG) method requires precise control of the thermal environment. The temperature distribution inside the growth crucible plays a critical role in process stability, crystal morphology, and reproducibility. In this work, vertical and radial temperature gradients in the melt were systematically investigated under various lid configurations.

Temperature measurements were carried out using a Pt/Pt(Rh) thermocouple. The crystallisation temperature was determined by controlled cooling experiments performed at different cooling rates of 1, 3, 5, and 10 °C/h. The most reproducible crystallisation temperature was obtained at a cooling rate of 1 °C/h. Based on this result, all subsequent temperature gradient measurements were performed at a temperature 15 °C above the crystallisation temperature determined at 1 °C/h. Vertical and radial temperature gradients were investigated using different crucible lid designs with central opening diameters ranging from 8.5 mm to 35 mm. Radial temperature distributions were recorded at different heights above the crucible bottom, while the vertical temperature gradient was measured from approximately 2 cm above the melt surface down to the bottom of the melt. The influence of the lid central opening diameter on both vertical and radial temperature gradients was analysed quantitatively.

The results demonstrate that the diameter of the lid central opening has a significant effect on both the magnitude and uniformity of temperature gradients within the melt region. Larger central openings reduce radial temperature gradients but may lead to increased vertical temperature differences, whereas smaller openings promote steeper radial gradients. In addition, variations in cooling rate were shown to influence the apparent crystallisation temperature. Based on these results, optimal thermal configurations for stable and reproducible BBO crystal growth by the TSSG method are discussed.

This study provides detailed experimental insight into thermal field control and crystallisation behaviour in the solution growth melts and contributes to improved reproducibility, stability, and scalability of BBO single crystal growth.

BENZOPHENONE-(BENZO)CARBAZOLE-BASED HOST MATERIALS ENABLING EFFICIENT RED PHOSHORESCENT OLED THROUGH CO-HOST ENGINEERING

Gintare Krucaite[1], Dovydas Blazevicius[1], Raminta Beresneviciute[1], Saulius Grigalevicius[1], Yi-Qi Chao[2], Zih-Ru He[2], Kuan-Yu Su[2], Chih-Hao Chang[2]

[1]Lithuania, Kaunas University of Technology, Department of Polymer Chemistry and Technology.
[2]Taiwan, Yuan Ze University, Department of Electrical Engineering.
gintare.krucaite@ktu.lt

Organic light-emitting diodes (OLEDs) have rapidly gained widespread commercial adoption, however, efficiency losses and stability issues remain persistent challenges, particularly for long-wavelength emitters. Motivated by the increasing demand for efficient energy transfer and effective exciton management in phosphorescent OLEDs, we designed and synthesized four new benzophenone-(benzo)carbazole based host materials, namely BP-Cz2, BP-BCz2, BP-BCz, and BP-CzBCz, incorporating carbazole and extended π-conjugated benzo[a]carbazole electron-donating units, either individually or in a combination. All synthesized compounds exhibited excellent thermal stability and a strong tendency to form stable amorphous thin films, with glass transition temperatures exceeding 100 °C for most materials. Photophysical characterization revealed singlet energy levels ranging from 2.90 to 3.61 eV and triplet energy levels between 2.50 and 3.10 eV, corresponding to singlet–triplet energy gaps of 0.35–0.51 eV. These energy characteristics confirm that the benzophenone derivatives provide sufficient exciton confinement for red phosphorescent emitters. Furthermore, charge-transport measurements indicated hole and electron mobilities spanning from 10^{-3} to 10^{-12} cm^2 V^{-1} s^{-1}, highlighting the tunability of charge-transport properties through molecular design. The donor-acceptor compounds were evaluated as host materials in red OLED devices. Notably, devices employing a co-host configuration consistently outperformed their single-host counterparts. In particular, the BP-BCz-based co-host system utilizing OLED achieved a maximum external quantum efficiency of 17.9% with a reduced efficiency roll-off at high luminance. These results demonstrate that benzophenone-(benzo)carbazole based host materials, when implemented within a co-host architecture, facilitate balanced charge transport, suppress exciton quenching, and enable high-performance red OLEDs.

Acknowledgements

This work was supported by the Research Council of Lithuania (Grant No. S-MIP-25-23). C.H.C. gratefully acknowledges the funding support from the National Science and Technology Council of Taiwan, under the grant numbers (NSTC 112-2923-E-155-002-MY4, NSTC 113-2221-E-155-014-MY3, and NSTC 114-2923-E-155-001-MY3).

Keywords: Host material, glass transition temperature, amorphous layer, emitter, phosphorescent organic light emitting diode, efficiency.

CARBAZOLE-BENZOCARBAZOLE FRAGMENTS HAVING DERIVATIVES AS VERY EFFICIENT HOST MATERIAL FOR TADF BASED OLEDs

Daiva Tavgeniene[1], Sushanta Lenka[2], Hsuan-Min Wang[2], Jayachandran Jaykumar[2], Dovydas Blazevicius[1], Gintare Krucaite[1], Yu-Lin Chi[3], Saulius Grigalevicius[1], Jwo-Huei Jou[2]

[1]Lithuania, Kaunas University of Technology, Department of Polymer Chemistry and Technology
[2]Taiwan, National Tsing Hua University, Department of Materials Science and Engineering
[3]Taiwan, National Tsing Hua University, Department of Chemistry
daiva.tavgeniene@ktu.lt

Organic light-emitting diodes (OLEDs) have emerged as a transformative technology in modern display and lighting applications, spanning smartphones, televisions, tablets, and automotive systems. Multiple functional and interfacial layers have been incorporated to enhance the efficiency of OLEDs. While numerous emitter materials for thermally activated delayed fluorescence (TADF) OLEDs have been developed and documented, comparatively little attention has been directed toward the systematic design and advancement of suitable host materials. To address this, we designed and synthesized a carbazole–benzocarbazole-based derivative, DM323, as a potential host material for green TADF OLEDs. DM323 exhibits exceptional thermal resilience, with a decomposition temperature surpassing 400 °C and a glass transition temperature (Tg) of approximately 194 °C, highlighting its suitability for high-temperature processing and stable device operation. In addition to its thermal robustness, the compound possesses a wide optical bandgap of 3.6 eV and exhibits rapid exciton decay dynamics, both of which are critical attributes for efficient management and utilization of excitons in thermally activated delayed fluorescence (TADF) systems. Leveraging these advantageous properties, DM323 was employed as the host material in green TADF OLED devices. The resulting devices demonstrated remarkable electroluminescent performance, delivering a maximum external quantum efficiency (EQE) of 10.4%, a current efficiency (CE) of 20.6 cd/A, and a power efficiency (PE) of 12.7 lm/W, all achieved at relatively low driving voltages. These results underscore the effectiveness of DM323 as a high-performance host, combining excellent thermal stability, favorable electronic characteristics, and efficient exciton management to enhance overall device efficiency and operational stability. These findings underscore the potential of carbazole–benzocarbazole frameworks as versatile host platforms, combining straightforward synthesis, superior thermal stability, and excellent optoelectronic properties. Overall, DM323 emerges as a strong candidate for the next generation of cost-effective and high-performance OLED display technologies.

Acknowledgements

We are obliged to the Research Council of Lithuania for the support (Grant No. S-LLT-25-2) and the Ministry of Science and Technology (MOST), Taiwan for supporting our work under Project No 113B7021J4.

Keywords: carbazole–benzocarbazole compounds; green TADF; glass transition temperature; thermal stability; solution process OLED

MOLECULARLY IMPRINTED CONDUCTIVE POLYMER PLATFORM FOR PROTEIN SENSING

Artem Yerniiazov[1], Sarunas Zukauskas[1], Alma Rucinskiene[2], Arunas Ramanavicius[1,3]

[1]Center for Physical Sciences and Technology, Department of Nanotechnology, Lithuania, Vilnius.
[2]Center for Physical Sciences and Technology, Department of Electrochemical Material Science, Vilnius, Lithuania.
[3]Vilnius University, Faculty of Chemistry and Geoscience, Institute of Chemistry, Department of Physical Chemistry, Vilnius, Lithuania.
artem.yerniiazov@ftmc.lt

Molecularly imprinted polymer (MIP) platforms represent a low-cost and selective alternative to biosensors for protein sensing[1] in the 50–100 kDa range, such as bovine serum albumin (BSA). In this work, an overoxidized polypyrrole (PPy) nanofilm-based impedometric MIP fabricated on a glassy carbon electrode (GCE) is presented for the detection of BSA in the nanomolar range.

During MIP fabrication, chronoamperometric polymerization kinetically immobilizes the monomer–template complex by freezing the equilibrium between adsorption and desorption. After template extraction using protease, complementary cavities remain within the polymer matrix and function as specific binding sites during rebinding[2]. Electrochemical impedance spectroscopy (EIS) was employed as the primary transduction technique due to its minimal perturbation of the MIP layer. The sensing mechanism is primarily governed by changes in charge-transfer resistance (Rct) of the polymer by using a redox probe, the methodology schematics is in Fig.1. Capacitive sensing was additionally investigated under non-faradaic conditions in a low-ionic-strength electrolyte.

Analytical performance was evaluated using a concentration-dependent calibration curve[3]. In addition, binding kinetics studies revealed pseudo-first-order behavior, which is characteristic of nanofilm-based MIPs.

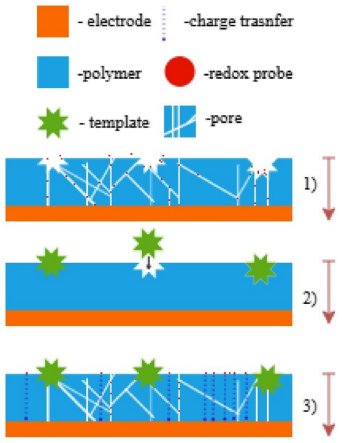


Fig. 1. Outer sphere charge transfer in a MIP. (1) The redox probe diffuses through open pores and transfers the charge to the electrode. (2) The analyte rebinding, obstructing the pores. (3) The charge transfer is through the conductive polymer to the underlying electrode.

[1] E. Mohsenzadeh et al., “Design of molecularly imprinted polymers (MIP) using computational methods: A review of strategies and approaches,” Wiley Interdisciplinary Reviews Computational Molecular Science, vol. 14, no. 3, May 2024, doi: 10.1002/wcms.1713.
[2] E. Mohsenzadeh et al., “Application of computational methods in the design of molecularly imprinted polymers (review),” TrAC Trends in Analytical Chemistry, vol. 171, p. 117480, Dec. 2023, doi: 10.1016/j.trac.2023.117480.
[3] G. Zvirzdine et al., “Electrochemical salicylic acid sensor based on molecularly imprinted polypyrrole,” ACS Applied Materials & Interfaces, vol. 17, no. 41, pp. 57475–57485, Oct. 2025, doi: 10.1021/acsami.5c11951.

DEVELOPMENT OF A MULTILAYERED, MOLECULARLY IMPRINTED POLYMER-BASED ELECTROCHEMICAL SENSOR FOR TETRACYCLINE DETECTION

Beatričė Kulikauskaitė[1], Domas Pirštelis[1,2], Ernestas Brazys[1,2], Vilma Ratautaitė[2], Arūnas Ramanavičius[1,2]

[1]Vilnius University, Faculty of Chemistry and Geosciences, Institute of Chemistry, Department of Physical Chemistry, Lithuania
[2]State Research Institute Center for Physical Sciences and Technology, Department of Nanotechnology, Lithuania
beatrice.kulikauskaite@chgf.stud.vu.lt

The widespread use of antibiotics, such as tetracycline, has resulted in persistent drug residues in the environment, which require monitoring to evaluate pollution levels. Molecularly imprinted polymer (MIP)–based sensors are considered a robust, low-cost, and easy-to-use solution for the development of analytical systems for the detection of various analytes [1,2]. The introduction of interfacial underlayers, such as self-assembled monolayers, between the electrode and the MIP layer enables the tuning of MIP properties [3].

In this work, a multilayered MIP sensor was constructed on a screen-printed carbon electrode (SPCE) platform. The SPCE was modified by drop-casting a poly(3,4-ethylenedioxythiophene):polystyrene sulfonate (PEDOT:PSS) mixture as an underlayer to tune charge-transfer characteristics. Subsequently, a molecularly imprinted polypyrrole (MIP-Ppy) layer, using tetracycline as the template, was electrochemically synthesized on the PEDOT:PSS/SPCE surface. A non-imprinted polypyrrole (NIP-Ppy) layer was prepared under identical conditions to demonstrate imprinting selectivity. The rebinding of tetracycline to the MIP/PEDOT:PSS/SPCE sensor was carried out in an acetate medium and was evaluated using electrochemical impedance spectroscopy.

The constructed sensor enabled the detection of tetracycline at micromolar concentrations. The proposed multilayered, easy-to-fabricate, MIP-based electrochemical sensor demonstrates promising potential for application in the environmental monitoring of antibiotic residues.

Acknowledgements
This project has received funding from the Research Council of Lithuania (LMTLT), agreement No. S-LL-25-3.

[1] E. Brazys, V. Ratautaite, E. Mohsenzadeh, R. Boguzaite, A. Ramanaviciute, and A. Ramanavicius, “Formation of molecularly imprinted polymers: Strategies applied for the removal of protein template (review),” Advances in Colloid and Interface Science, vol. 337, p. 103386, Dec. 2024, doi: 10.1016/j.cis.2024.103386.

[2] S. Ramanavicius, U. Samukaite-Bubniene, V. Ratautaite, M. Bechelany, and A. Ramanavicius, “Electrochemical molecularly imprinted polymer based sensors for pharmaceutical and biomedical applications (review),” Journal of Pharmaceutical and Biomedical Analysis, vol. 215, p. 114739, Mar. 2022, doi: 10.1016/j.jpba.2022.114739.

[3] V. Liustrovaite, V. Ratautaite, A. Ramanaviciene, and A. Ramanavicius, “Detection of the SARS-CoV-2 nucleoprotein by electrochemical biosensor based on molecularly imprinted polypyrrole formed on self-assembled monolayer,” Biosensors and Bioelectronics, vol. 272, p. 117092, Dec. 2024, doi: 10.1016/j.bios.2024.117092.

SYNTHESIS OF NEWIMIDAZOLE-2-THIOLES CONTAINING HYDRAZONE MOIETY

Tomas Tutkus[1], Birutė Sapijanskaitė-Banevič[1]

[1]Kaunas University of Technology, Department of Organic Chemistry, Lithuania
tomas.tutkus@ktu.lt

Imidazole fragment containing derivatives exhibit antibacterial, antifungal, antiviral, anti-inflammatory, antitumor activity and it is present in many pharmacologically important drugs such as Metronidazole, Ketoconazole, Megazol, Dicarbazine [1].

In this work, a series of imidazole-2-thiole derivatives containing a hydrazone moiety were synthesized.

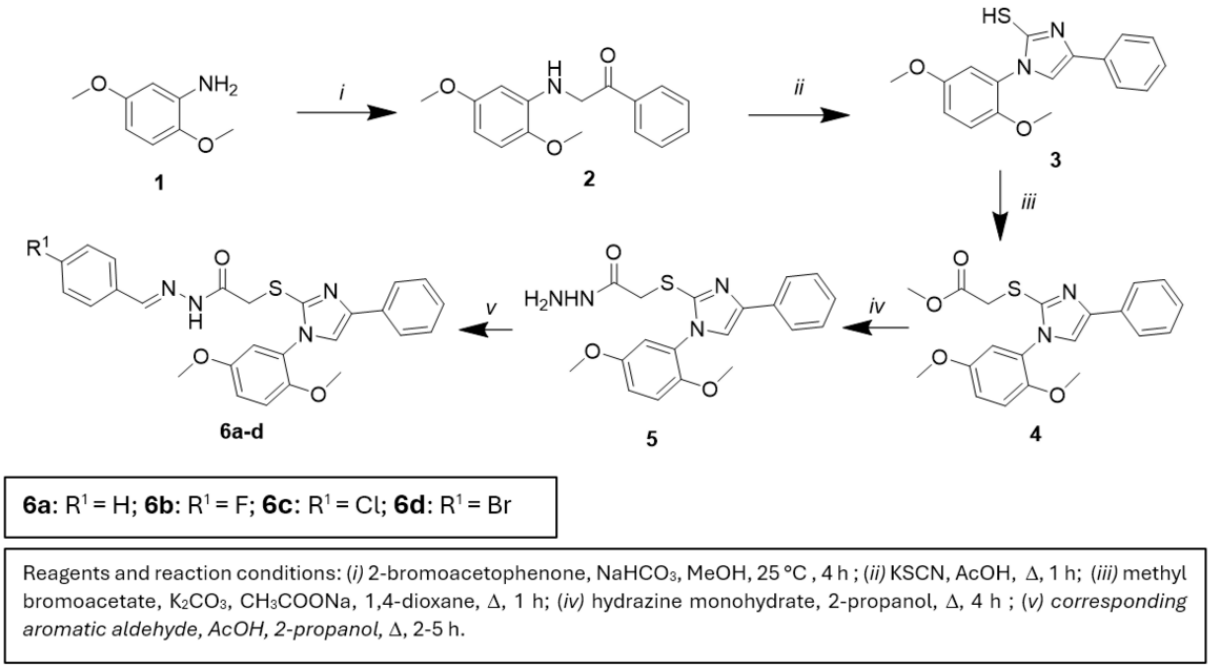


Fig. 1. Synthesis of imidazole-2-thioles containing a hydrazone moiety

Firstly, to obtain precursor **2**, primary amine **1** was treated with 2-bromoacetophenone in methanol at room temperature in the presence of catalytic amount of sodium bicarbonate. For the imidazole ring formation, cyclisation reactions of amine ketone **2** was carried out with thiocyanate in an acidic condition to afford compound **3**.

Methyl 2-[1-(2,5-dimethoxyphenyl)-4-phenyl-1*H*-imidazol-2-yl]thioacetate **4** was synthesized via alkylation of imidazole-2-thiole with methyl bromoacetate using potassium carbonate and sodium acetate as base. Acid hydrazide **5** was easily obtained by refluxing methyl ester **4** with hydrazine monohydrate in 2-propanol.

Condensation of hydrazide **5** with various aromatic aldehydes in 2-propanol under reflux for 2-5 hours resulted the hydrazones **6a-d**.

The structures of compounds **2-6** have been confirmed by elemental analysis, ^{1}H and ^{13}C NMR spectral data.

[1] D. Serdaliyeva, T. Nurgozhin, E. Satbayeva, M. Khayitova, A. Seitaliyeva, and L. Ananyeva, “Review of pharmacological effects of imidazole derivatives,” Journal of Clinical Medicine of Kazakhstan, vol. 19, no. 3, pp. 11–15, Jun. 2022, doi: 10.23950/jcmk/12117.

GRAPHENEOXIDE AND CONDUCTING POLYMER COMPOSITES: SYNTHESIS AND INVESTIGATION

Greta Melkūnaitė[1], Justina Gaidukevič[1]

[1]Vilnius University, Faculty of Chemistry and Geosciences, Institute of Chemistry, Vilnius, Lithuania
greta.melkunaite@chgf.stud.vu.lt

Graphene and its derivatives have attracted significant attention due to their wide range of potential applications, particularly in electrochemical sensing. Graphene oxide (GO), obtained by graphite oxidation, exhibits good dispersibility and chemical functionality, making it suitable for composite materials [1]. Conductive polymer composites offer improved surface area, more recognition sites, reduced detection limits, lower electrical resistivity or faster response time, and enhanced stability. Their mechanical properties are also improved, resulting in more durable and robust sensors [2]. Despite increasing interest in GO based polymer composites, achieving materials with uniform structure and reliable functional performance remains a key challenge that this study aims to adress. The aim of this study was to synthesize GO and poly(aniline-anthranilic acid) copolymer composites (GO/PANI-AA) and to perform their structural characterization.

GO was synthesized using a modified Hummer‘s method with graphite as the starting material. Graphite oxidation was carried out using sulfuric acid, potassium persulfate and phosphorus (V) oxide. The resulting intermediate GO product was further oxidized by adding sodium nitrate and potassium permanganate. GO/PANI-AA composites were prepared in hydrochloric acid by dissolving GO, aniline (PANI), anthranilic acid (AA), and ammonium persulfate. The ratio of GO to (PANI + AA) was 1:1, while the ratio of PANI to AA in the composite was varied.

The results demonstrated that the incorporation of GO significantly influenced the structural, morphological, electrochemical properties of the PANI-AA copolymer. SEM analysis revealed a more homogeneous surface morphology of the composites compared to the pristine copolymer, indicating improved dispersion of GO within the polymer matrix. XPS and Raman spectroscopies results confirmed the successful formation of the composite. Electrochemical measurements revealed that the composite with an PANI to AA ratio of 25:75 exhibited the best electrochemical performance for electrode modification.

The results suggest that GO/PANI-AA composites can be effectively used for electrode modification in electrochemical applications. The identified optimal composition provides a basis for further development of conducting polymer composite materials.

[1] A. Razaq, F. Bibi, X. Zheng, R. Papadakis, S. H. M. Jafri and H. Li, “Review on Graphene-, Graphene Oxide-, Reduced Graphene Oxide-Based Flexible Composites: From Fabrication to Applications,” Materials, vol. 15, no. 3, p.p. 1012-1029, 2022.

[2] D. W. Hatchett and M. Josowicz, “Composites of Intrinsically Conducting Polymers as Sensing Nanomaterials,” Chem. Rev., vol. 108, no. 2, p.p. 746-769, 2008.

DIVERGENT SYNTHESIS OF HSP90 INHIBITORS CONTAINING RESORCINOL AND THIADIAZOLE MOIETIES

Vilius Petraška[1], Ieva Žutautė[1]

[1]Vilnius University, Faculty of Chemistry and Geosciences, Vilnius, Lithuania
vilius.petraska@chgf.vu.lt

Hsp90 (Heat Shock Protein 90) is a molecular chaperone of the heat shock protein family that ensures proper protein folding, stabilizes proteins under stress conditions, and facilitates their degradation. While it constitutes 1-2% of all protein content in healthy human cells, cancer cells contain elevated levels of this protein [1]. Studies have shown that Hsp90 plays a key part in migration, metastasis, and other aspects of tumour progression. Consequently, over the last decade, Hsp90 has been thoroughly investigated as a potential target for anticancer treatments [2].

Research on natural compounds has found that resorcinol (**1**) is essential for a molecule to bind to the N-terminal domain of Hsp90. This region contains the ATP-binding pocket, which is vital for the protein's function. Further studies have shown that an aromatic ring near the resorcinol moiety greatly enhances the binding characteristics of Hsp90 inhibitors [3]. While many different compounds have been synthesized, the 4th position of the resorcinol ring is comparatively underexplored.

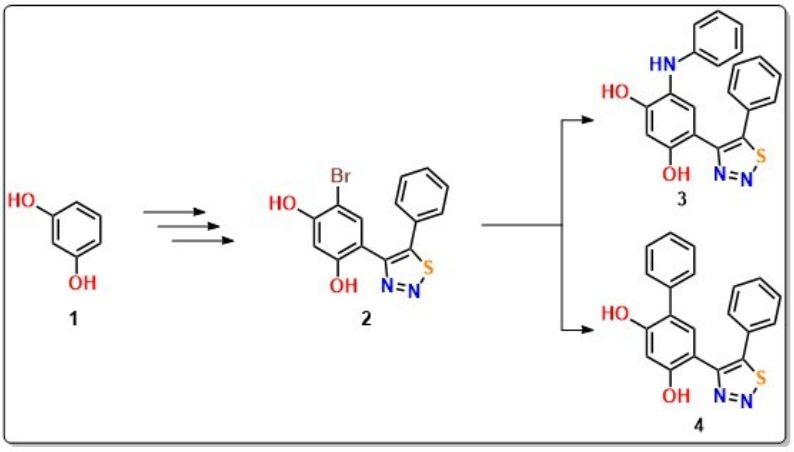


Fig. 1. Resorcinol **1** and target structures **3** and **4**

This work aimed to synthesize a range of Hsp90 inhibitors with hydrophobic substituents at the 4th position of the resorcinol fragment. Utilizing palladium chemistry, two different types of compounds were obtained using Buchwald-Hartwig (**3**) and Suzuki (**4**) coupling reactions with phenylamino and phenyl groups, respectively. The presentation will cover the divergent synthesis process, its challenges, and results.

Keywords: Hsp90, Organic Chemistry, Organic Synthesis

[1] S. Tsutsumi et al., "Charged linker sequence modulates eukaryotic heat shock protein 90 (Hsp90) chaperone activity," Proc. Natl. Acad. Sci. U. S. A., vol. 109, no. 8, pp. 2937–2942, 2012

[2] L. Neckers and K. Neckers, "Heat-shock protein 90 inhibitors as novel cancer chemotherapeutics - an update," Expert Opin. Emerg. Drugs, vol. 10, no. 1, pp. 137–149, 2005

[3] M. Ardestani, Z. Khorsandi, F. Keshavarzipour, S. Iravani, H. Sadeghi-Aliabadi, and R. S. Varma, "Heterocyclic Compounds as Hsp90 Inhibitors: A Perspective on Anticancer Applications," Pharmaceutics, vol. 14, no. 10, 2022

PROTEIN AGGREGATES CONCENTRATION DETERMINATION USING ELECTROCHEMICAL METHODS

Narvydas Dėnas[1,2], Povilas Virbickas[1,2], Aušra Valiūnienė[1,2]

[1]Vilnius university, Institute of Chemistry, Naugarduko str. 24, LT-03225, Vilnius, Lithuania
[2]State Research Institute Center for Physical Sciences and Technology, Sauletekio Ave. 3, LT-10257 Vilnius, Lithuania
narvydas.denas@chgf.stud.vu.lt

Determining protein aggregate concentrations is important in food industry and clinical studies. Fluorescence spectroscopy, employing amyloidophilic dyes, remains a primary technique for the detection and quantification of protein aggregates [1]. However, fluorescence method faces several limitations, for example, presence of other optically active contaminants or solution viscosity can significantly interfere with method accuracy [2] – [4]. In this work, instead of fluorescence methods, electrochemical methods were employed to determine protein aggregates concentrations.

A 3 electrode system, consisting of inert platinum electrodes as working and counter electrodes and Ag/AgCl, $KCl_{sat.}$ as reference electrode, was used. Amyloidophilic dyes, like thioflavin T (ThT), are not only suitable for fluorescence based detection, but also exhibit oxidation currents, which can be measured using electrochemical methods. Using the electrochemical activity of ThT, cyclic voltammetry curves were measured not only using different ThT concentrations, but also different protein aggregate concentrations in buffer solutions. Furthermore, electrochemical impedance spectroscopy at different protein aggregate concentrations were measured. Results demonstrate that protein aggregate addition to buffer solution, lead to measurable thioflavin T oxidation current decrease.

The obtained results suggest that using cyclic voltammetry in the potential range from 0.2 V to 0.9 V vs Ag/AgCl, $KCl_{sat.}$, allows for protein aggregate detection. This methodology allows for protein aggregate concentration quantification in the concentration interval ranging from 15 µg/mL to 595 µg/mL.

[1] S. Gregoire, J. Irwin, and I. Kwon, “Techniques for monitoring protein misfolding and aggregation in vitro and in living cells,” Korean J. Chem. Eng., vol. 29, no. 6, pp. 693–702, May 2012, doi: 10.1007/S11814-012-0060-X.
[2] V. Kumar, N. Sami, T. Kashav, A. Islam, F. Ahmad, and M. I. Hassan, “Protein aggregation and neurodegenerative diseases: From theory to therapy,” Eur. J. Med. Chem., vol. 124, pp. 1105–1120, Nov. 2016, doi: 10.1016/J.EJMECH.2016.07.054.
[3] J. A. J Housmans, G. Wu, J. Schymkowitz, and F. Rousseau, “A guide to studying protein aggregation,” FEBS J., vol. 290, no. 3, pp. 554–583, Feb. 2021, doi: 10.1111/FEBS.16312.
[4] P. Mukherjee and S. Ganai, “Thioflavin-T: A Quantum Yield-Based Molecular Viscometer for Glycerol-Monohydroxy Alcohol Mixtures,” ACS Omega, vol. 8, no. 39, pp. 36604–36613, Oct. 2023, doi: 10.1021/ACSOMEGA.3C06428.

MXENES-BASED ON-SITE HEAVY METAL SENSOR

Ilya Navitski[1], Šarūnas Žukauskas[2], Simonas Ramanavičius[1], Alma Ručinskienė[1], Arūnas Ramanavičius[3]

[1]State Research Institute Center for Physical Sciences and Technology (FTMC), Department of Electrochemical Material Sciences, Lithuania
[2]State Research Institute Center for Physical Science and Technology (FTMC), Department of Nanotechnology, Lithuania
[3]Vilnius University, Faculty of Chemistry and Geosciences, Lithuania
ilya.nov42@gmail.com

The impact of heavy metal contamination on biological systems can not be underestimated. Originating primarily from human industrial activities such as electroplating, batteries production and mining, these metals can cause damage to cardiovascular, skeletal, nervous and other systems in organisms. Consequently, monitoring those metals in water systems is therefore valuable for environmental stability and public health. Reliable sensors based on different detection methods for detecting those metals are ideal candidates for such a task. Among them, electrochemical sensors are considered one of the best options due to their high sensitivity and accuracy, as well as their rapid response and simple sample preparation procedures. In electrochemical sensing, the choice of material is critical – not only for overall sensor performance, but also for enhancing the sensitivity and selectivity of the sensing platform. MXenes, a family of two-dimensional nanostructures, are known for their graphite-like electrical conductivity and tunable surface functional groups, making them particularly attractive for electrochemical sensor applications [1-3]. In addition to material selection, the sensing strategy itself plays a crucial role. Developing methods that can be used outside laboratory environments is especially valuable for on-site monitoring. In this work, we explore the use of an MXene-based electrochemical sensor for on-site detection of zinc, lead, and cadmium ions in water sources. The sensor was fabricated by drop-casting a MXene+Nafion combination onto a glassy carbon electrode (GCE) surface in three layers. All electrochemical measurements were conducted in acetic buffer solution at pH 4.5. Measurements in various water sources were performed by adding a small amount of highly concentrated acetic buffer to the sample and mixing thoroughly. Sensor successfully detected cadmium, lead and zinc ions with detectable peaks emerging at concentration of 100 nM (Fig. 1), 250 nM and 30µM, respectfully. The sensitivity was within World Health Organization (WHO) requirements for water systems quality monitoring.

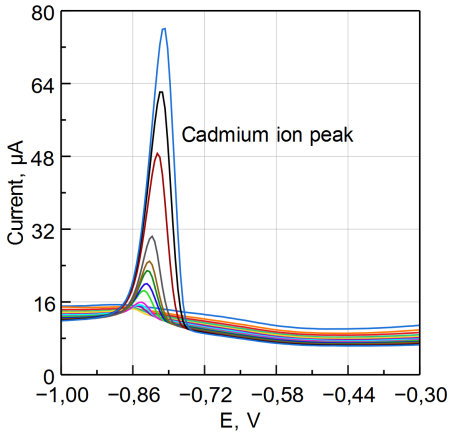


Fig. 1. Fig. 1. Cadmium detection by GCE/MXenes+Nafion sensor.

Keywords: MXenes, Heavy metals, Water systems

[1] I. Navitski, S. Zukauskas, S. Ramanavicius, O. Gogotsi, and A. Ramanavicius, "2D MXenes in the design of heavy metal ion sensors (review)," Trends in Environmental Analytical Chemistry, vol. 47, p. e00270, Jun. 2025, doi: 10.1016/j.teac.2025.e00270.
[2] I. Navitski, A. Ramanaviciute, S. Ramanavicius, M. Pogorielov, and A. Ramanavicius, "MXENE-Based Chemo-Sensors and other sensing devices," Nanomaterials, vol. 14, no. 5, p. 447, Feb. 2024, doi: 10.3390/nano14050447.
[3] S. Zukauskas et al., "Electrochemical real-time sensor for the detection of Pb(II) ions based on Ti3C2Tx MXene," The Science of the Total Environment, vol. 950, p. 175190, Jul. 2024, doi: 10.1016/j.scitotenv.2024.175190.

MODIFICATION OF $Ti_3C_2T_X$ MXENE NANOSHEETS WITH POLYDOPAMINE FOR ANTIBODY IMMOBILIZATION

Kristina Sobol[1], Viktorija Liustrovaite[1], Benediktas Brasiunas[1], Anton Popov[1], Igor Iatsunskyi[2], Oleksiy Gogotsi[3], Almira Ramanaviciene[1]

[1]Vilnius University, Faculty of Chemistry and Geosciences, Institute of Chemistry, NanoTechnas – Center of Nanotechnology and Materials Science, Institute of Chemistry, Naugarduko St. 24, LT-03225, Vilnius, Lithuania
[2]Adam Mickiewicz University, NanoBioMedical Centre, Poznan, Poland
[3]Nano Carbon Tech LLC, Poznan, Poland
kristina.sobol@chgf.vu.lt

MXenes are a novel family of two-dimensional (2D) inorganic nanomaterials, first discovered in 2011. The MXene family consists of transition metal carbides, nitrides, and carbonitrides with the general formula $M_{n+1}X_nT_x$, where M is an early transition metal, X is carbon and/or nitrogen, and T_X stands for surface terminations [1]. Owing to their unique properties, including large surface area, excellent conductivity, and abundant surface functional groups, MXenes are well-known as highly biocompatible nanomaterials with a wide range of biomedical applications. However, the practical use of pristine MXenes is often limited by their sensitivity to oxidation in aqueous and oxygen-rich environments, as well as the instability of their surface functional groups [2-3]. To address these limitations in developing immunosensors, we modified $Ti_3C_2T_X$ MXene nanosheets with polydopamine (PDA) via the self-polymerization of dopamine, thereby creating a versatile platform for antibody immobilization. Herein, electrochemical and optical analysis methods were assessed to confirm the successful immobilization of antibodies on PDA-coated MXenes. For electrochemical analysis, the preparation and drop-casting of $Ti_3C_2T_X$ MXene nanosheets onto screen-printed carbon electrodes were optimized. Subsequently, the PDA-coated MXenes were modified with antibodies against the SARS-CoV-2 spike protein. Electrochemical impedance spectroscopy was used to characterize the surface of the modified electrodes, enabling a simple and rapid evaluation of antibody immobilization. For optical analysis, $Ti_3C_2T_X$–PDA complexes were modified with horseradish peroxidase-conjugated secondary antibodies (Ab-HRP). Successful Ab-HRP immobilization on $Ti_3C_2T_X$–PDA was verified through an enzymatic reaction of HRP with tetramethylbenzidine in the presence of H_2O_2, which produced a distinct blue color, enabling direct visual assessment of antibody binding.

The obtained results demonstrate that PDA-coated MXenes are a promising platform for antibody immobilization and can be effectively evaluated using both optical and electrochemical methods.

Acknowledgements
This project has received funding from the Research Council of Lithuania (LMTLT), agreement No [S-LL-24-2].

[1] C. E. Shuck, K. Ventura-Martinez, A. Goad, S. Uzun, M. Shekhirev, and Y. Gogotsi, “Safe synthesis of MAX and MXENE: Guidelines to reduce risk during synthesis,” ACS Chemical Health & Safety, vol. 28, no. 5, pp. 326–338, Aug. 2021, doi: 10.1021/acs.chas.1c00051.
[2] K. Diedkova et al., “Effects of etching and delamination on biocompatibility of TI-Based MXEnes,” ACS Applied Materials & Interfaces, vol. 17, no. 34, pp. 47919–47937, Aug. 2025, doi: 10.1021/acsami.5c08807.
[3] A. Popov, V. Lisyte, M. Sapauskiene, S. Ramanavicius, S. Zukauskas, N. Slekie, I. Baginsky, V. Zahorodna, O. Gogotsi, A. Kausaite-Minkstimiene, A. Ramanaviciene, “MXene-Based Electrochemical Glucose Biosensors: Comparative Enhancement with Aquivion and Nafion”, Materials Today Nano, vol. 32, no. 100712, Oct. 2025.

GLASS-FORMING HOLE-TRANSPORT MATERIALS WITH TAILORED SURFACE ROUGHNESS FOR ENHANCED PERFORMANCE IN PEROVSKITE SOLAR CELLS

Adnan Ahmed[1], Naghash Miraqyan[1], Asta Dabuliene[1], Dmytro Volyniuk[1], Edwin Pineda De La O[2], Juozas Vidas Gražulevičius[1], Lethy Krishnan Jagadamma[2], Oleksandr Bezvikonnyi[1]

[1]Kaunas University of Technology, Department of Polymer Chemistry and Technology, Baršausko Str. 59, Kaunas LT-51423, Lithuania

[2]University of St Andrews, Energy Harvesting Research Group, School of Physics & Astronomy, SUPA, North Haugh, St Andrews, Fife KY16 9SS, UK

adnan.ahmed@ktu.edu

Charge transport materials in heterojunction solar cells, particularly perovskite solar cells (PSCs), are critical for optimal charge dynamics and device stability[1][2]. Conventional hole transport materials (HTMs) such as spiro-OMeTAD and PTAA demonstrate strong photovoltaic performance due to high thin-film quality and energy alignment[3][4]. However, they often show high material cost, low carrier mobility and poor stability, which greatly limit their practical applications. In our pursuit of low-cost, accessible organic HTMs with attributes such as enhanced thermal and photochemical stability, higher glass transition temperatures, and improved hole mobility, we designed and synthesized novel dibenzothiophene and spiro[1,3-dithiolane-2,9′-fluorene]-based compounds utilizing microwave-assisted Buchwald–Hartwig reactions. Notably, surface roughness analyses of the resulting materials revealed a general average roughness of 6.129 to 8.028 nm, influencing their charge transport dynamics. The synthesized materials exhibited excellent thermal stability, with decomposition temperatures between 309 and 408 °C and glass transition temperatures ranging from 99 to 163 °C. Photoelectron emission spectroscopy indicated ionization potentials from 5.03 to 5.16 eV. Additionally, time-of-flight (TOF) and charge extraction by linearly increasing voltage (CELIV) measurements demonstrated efficient hole transport in vacuum-deposited films, achieving hole mobilities as high as 4×10^{-4} cm^2 V^{-1} s^{-1} at an electric field of 9×10^5 V cm^{-1}. Among the materials evaluated, the compound 2′,7′-bis[(4-methoxyphenyl)(9-ethylcarbazol-3-yl)amino]-spiro[1,3-dithiolane-2,9′-fluorene] showcased the best device performance, attaining optimized power conversion efficiencies of 7.5% (forward scan) and 13.5% (reverse scan) under 1-sun illumination, alongside 14.55% (FW) and 26.5% (RV) under 3000 K LED illumination (1000 lx).

Acknowledgements

This project has received funding from the Research Council of Lithuania (LMTLT), agreement No S-MIP-24-6.

Keywords: Spiro-based organic semiconductors; charge transport and mobility; perovskite solar cells; thermal properties; surface roughness.

[1] X. Zhao and M. Wang, “Organic hole-transporting materials for efficient perovskite solar cells,” Mater. Today Energy, vol. 7, pp. 208–220, Mar. 2018, doi: 10.1016/j.mtener.2017.09.011.

[2] C. Zhang et al., “A review on organic hole transport materials for perovskite solar cells: Structure, composition and reliability,” Mater. Today, vol. 67, pp. 518–547, Jul. 2023, doi: 10.1016/j.mattod.2023.06.009.

[3] M. J. Choi et al., “Strategic approach for achieving high indoor efficiency of perovskite solar Cells: Frustration of charge recombination by dipole induced homogeneous charge distribution,” Chem. Eng. J., vol. 454, p. 140284, Feb. 2023, doi: 10.1016/j.cej.2022.140284.

[4] Q. Ma et al., “One-step dual-additive passivated wide-bandgap perovskites to realize 44.72%-efficient indoor photovoltaics,” Energy Environ. Sci., vol. 17, no. 5, pp. 1637–1644, 2024, doi: 10.1039/D3EE04022D.

IMPACT OF QUATERNARY AMMONIUM GROUP POSITION IN SAMS ON THE PERFORMANCE OF PEROVSKITE SOLAR CELLS

Milda Žitinevičiūtė[1], Matas Steponaitis[1], Tadas Malinauskas[1], Vytautas Getautis[1]

[1]Lithuania, Kaunas University of Technology, The Department of Organic Chemistry
milda.zitineviciute@ktu.lt

In recent years perovskite solar cells (PSCs) have emerged as a new and efficient way for green energy conversion. Extensive research has led said device performance to a remarkable 27%. However, interfacial engineering together with molecular and surface modifying strategies can further advance device performance. Incorporating self-assembled monolayers (SAMs) into PSC structure significantly increases both stability and device performance [1].

SAM architectures are typically defined by three key components: the functional group, the spacer, and the anchoring group. Molecules built following this principle can organize into a monolayer that promotes effective charge transport and further stabilizes the perovskite surface that is an essential factor for maintaining strong light absorption and overall exceptional device performance [2].

Years of sustained research have identified carbazole based SAMs containing phosphonic acid anchoring groups and alkyl chain spacers of varying length as particularly effective molecular structures [2]. In this work, phenylene groups were introduced into the structures in an attempt to reduce molecular aggregation and promote the formation of a more uniform monolayer. Additionally, ammonium salts were incorporated at different positions to improve the SAM/perovskite interface, an approach based on prior studies and theoretical insights expected to enhance overall device performance [3,4]. While this research is still ongoing, results should clarify whether ammonium functional groups and their position in the molecular structure have any positive effect on the performance of PSCs.

[1] L. Zhang et al., “Diverse perovskite solar cells: progress, challenges, and perspectives,” Advanced Materials, vol. 38, no. 1, p. e12221, Sep. 2025, doi: 10.1002/adma.202512221.

[2] Y. Yang et al., “Design and applications of hole-selective self-assembled monolayers for perovskite photovoltaics,” Chemical Engineering Journal, vol. 504, p. 158870, Dec. 2024, doi: 10.1016/j.cej.2024.158870.

[3] Z. Shi et al., “‘T-shaped’ carbazole alkylammonium cation passivation in perovskite solar cells,” ACS Energy Letters, vol. 9, no. 2, pp. 419–427, Jan. 2024, doi: 10.1021/acsenergylett.3c02357.

[4] H. Wu et al., “Tailored Lattice-Matched Carbazole Self-Assembled molecule for efficient and stable perovskite solar cells,” Journal of the American Chemical Society, vol. 147, no. 9, pp. 8004–8011, Feb. 2025, doi: 10.1021/jacs.5c00629.

NOVEL CARBORANE-BASED ELECTRON-TRANSPORTING MATERIALS FOR PEROVSKITE SOLAR CELLS

Julius Petrulevicius[1], Lea Zimmermann[2], Wander Max Bernardes de Araujo[2], Maxim Simmonds[2], Arman Mahboubi Soufiani[2], Maryte Daskeviciene[1], Tadas Malinauskas[1], Giedre Bubniene[1], Giedrius Juska[3], Vygintas Jankauskas[3], Dorothee Menzel[2], Florian Scheler[2], Eike Köhnen[2], Steve Albrecht[2], Vytautas Getautis[1]

[1]Lithuania, Kaunas University of Technology, Department of Organic Chemistry
[2]Germany, Helmholtz-Zentrum Berlin, Solar Energy Division
[3]Lithuania, Vilnius University, Institute of Chemical Physics
julius.petrulevicius@ktu.lt

Lead-based halide perovskite solar cells (PSCs) have gained significant attention due to their rapid performance advancements, with certified power conversion efficiencies (PCE) now reaching up to 27.3%, making them comparable to silicon solar cells. Recently, a perovskite/silicon tandem solar cell efficiency of 35.0% was reported, which exceeds the theoretical efficiency limit of 29.5% for a silicon single-junction cell [1]. Buckminsterfullerene (C_{60}) is the standard electron-transporting layer (ETL) used in high-efficiency p-i-n perovskite single-junction and perovskite/silicon tandem solar cells, owing to its ability to rapidly extract electrons from the perovskite absorber [2, 3], its relatively high electron mobility, and compatibility with thermal evaporation allowing for the deposition of thin, conformal layers over large substrate areas. However, C_{60} has several disadvantages such as high cost, interfacial non-radiative recombination, high parasitic absorption, and poor mechanical stability at the interface with the perovskite absorber as well as the SnO_x layer on top leading to interfacial delamination. Organic electron-transporting materials (ETMs) have recently attracted much attention as an alternative to fullerene C_{60} due to their low cost, straightforward synthesis as well as better adhesion with perovskite.

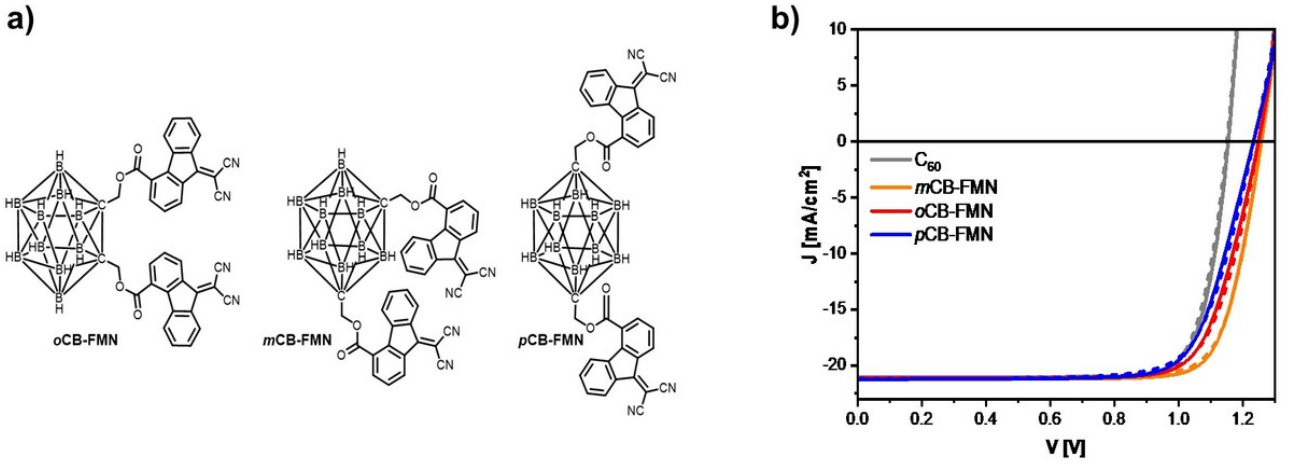


Fig. 1. a) The structures of carborane-based ETMs; **b)** *J-V* characteristics.

In this work, fluorenylidene malononitrilesubstituted carborane derivatives were synthesized and investigated as non-fullerene ETM for perovskite-based solar cells. Charge mobility of the layers based on o,m,p-series carborane derivatives was determined by xerographic time-of-flight (XTOF) measurements. The samples for the measurements were prepared by evaporating carborane compounds on polyester films with conductive Al layer. As a result, the electron mobility of **oCB-FMN**, **mCB-FMN** and **pCB-FMN** was found to be 1×10^{-5}, 5×10^{-5}, and 5×10^{-6} cm^2/Vs at zero-electric field. The new materials were tested as ETMs and successfully applied in single-junction PSCs. During device fabrication all ETMs were deposited by thermal evaporation. Furthermore, *m*-carborane derivative demonstrated best performance exhibiting a PCE 21.4% and revealing an efficiency potential that surpasses control devices with C_{60}. The new carborane derivatives demonstrate lower interfacial non-radiative recombination losses and reduced parasitic absorption in tandem devices for wavelength shorter than 650 nm, which highlights their potential as alternatives to C_{60}.

[1] "Best Research-Cell Efficiency Chart | Photovoltaic Research | NLR." https://www.nrel.gov/pv/cell-efficiency.html
[2] J. Siekmann et al., "Characterizing the influence of charge extraction layers on the performance of Triple-Cation perovskite solar cells," Advanced Energy Materials, vol. 13, no. 32, Jul. 2023, doi: 10.1002/aenm.202300448.
[3] Z. Guan et al., "Ultrafast Electron-Transfer via hybrid states at Perovskite/Fullerene Interface," Advanced Materials, vol. 36, no. 38, p. e2407406, Jul. 2024, doi: 10.1002/adma.202407406.

SYNTHESIS AND INVESTIGATION OF ORGANIC HOLE SELECTIVE SEMICONDUCTORS WITH DUAL INTERACTIONS AND FUNCTIONALITY IN PEROVSKITE SOLAR CELLS

Gabija Linkaitė[1], Mantas Marčinskas[1], Tadas Malinauskas[1], Vytautas Getautis[1]

[1]Lithuania, Kaunas, Kaunas University of Technology, Faculty of Chemical Technology
gabija.linkaite@ktu.lt

Lead halide perovskites have emerged in recent years as an exceptional semiconductor material used in solar cells and various optoelectronic applications. However, there are still major challenges in the practical application of PSCs, one of which is the toxicity of lead in such perovskites. In order to create lead-free PSCs, one of the possible strategies is to completely or at least partially replace lead with tin. Due to their atomic number, tin-based perovskites could exhibit optoelectronic properties similar to those of their lead-based counterparts. However, the inclusion of Sn^{2+} ions in the perovskite crystal lattice leads to certain undesirable effects: a reduced light absorption coefficient due to a reduced lead content, an inhomogeneous thin-film morphology due to the rapid Sn^{2+} crystallization process, a high defect concentration, a short charge carrier lifetime due to the easy oxidation of Sn^{2+} to Sn^{4+} and high energy barriers at the interfaces. To address these problems, effective strategies have been proposed recently in surface treatments, precursor design, compositional design, and structural optimization, employing various functional materials [1]. Of the many tin-containing perovskite compositions, only Sn-Pb (1:1) perovskite has so far demonstrated promising results close to those of lead-based performance. Since Sn-Pb mixture perovskites have 50% less lead than traditional Pb PSE, the toxicity problem is reduced but not eliminated [2].

In p-type perovskite solar cells, where hole transport layer is formed before the perovskite layer, self-assembled monolayer (SAM) forming compounds were introduced instead of conventional HTMs. SAMs are characterized by good hole extraction properties, higher efficiency, and stability. However, SAMs that show top-tier results in Pb-based PSCs do not replicate these results in Sn-containing PSCs. Not so long ago, a carbazole-based self-assembled monolayer-forming material $BrNH_3$-4PACz was synthesized, which has dual functionality: the carbazole functional group attached to the anchor phosphonic acid group creates a suitable dipole moment on the ITO electrode surface, ensuring optimal energy distribution and effective hole extraction from the narrow bandgap; the ionic ammonium bromide functional group passivates perovskite defects at the surface junction and regulates its crystallization [3]. Due to the dual interaction this compound demonstrated particularly good efficiency in Pb-Sn perovskite solar cells and not so long after was commercialized (by Tokyo Chemical Industry), demonstrating the importance and relevance of such ionic compounds and this concept in general.

In this study, we synthesized and investigated self-assembled monolayer-forming ionic compounds with dual interactions and functionality that could be used to construct Sn-containing perovskite solar cells.

[1] W. Gao, F. Yang, Z. Wang, Y. Lan, R. Nie, and C. Ran, “Interface matters: Boosting efficient PB-SN perovskite solar cells for All-Perovskite tandem photovoltaics,” Advanced Materials, p. e21789, Jan. 2026, doi: 10.1002/adma.202521789.

[2] H. Lee, S. B. Kang, S. Lee, K. Zhu, and D. H. Kim, “Progress and outlook of Sn–Pb mixed perovskite solar cells,” Nano Convergence, vol. 10, no. 1, p. 27, Jun. 2023, doi: 10.1186/s40580-023-00371-9.

[3] S. Zhumagali et al., “Efficient Narrow Bandgap Pb-Sn Perovskite Solar Cells Through Self-Assembled Hole Transport Layer with Ionic Head,” Advanced Energy Materials, vol. 15, no. 18, Jan. 2025, doi: 10.1002/aenm.202404617.

FABRICATION OF BISMUTH SULFIDE THIN FILMS USING L-CYSTEINE AS A NOVEL SULFUR SOURCE

Aistis Melnikas[1], Skirma Žalenkienė[1]

[1]Kaunas University of Technology, Department of Physical and Inorganic Chemistry, Kaunas, Lithuania
aistis.melnikas@ktu.edu

Bismuth sulfide (Bi_2S_3) thin films have recently attracted considerable attention, due to their suitable optical and electro-optical properties for the use in optoelectronic devices. Bi_2S_3 is a non-toxic, earth-abundant n-type semiconductor with a tunable band gap between 1.3 and 2.2 eV and a high absorption coefficient of 10^5 cm^{-1} [1]. It serves as an industrially available and environmentally friendly alternative n-type layer for the use in photovoltaic applications.

In our research, we investigate the chemical bath deposition method to fabricate FTO (fluorine doped tin oxide) glass substrates by using L-cysteine as a sulfur source. L-cysteine is a simple and promising, yet underexplored sulfur precursor, hence why it is chosen as a novel sulfur source in this experiment. Firstly, $Bi(NO_3)_3 \cdot 5H_2O$ was dissolved in 1 M nitric acid and diluted with distilled water to obtain a 0.1 mol/L solution. Secondly, a 0.025 mol/L solution of EDTA-Na_2 was added, thouroughly mixed, and heated to 80 °C. EDTA-Na_2 acts as a chelating agent, coordinating to bismuth ions to make the reaction slower, hence making the final Bi_2S_3 nuclei better dispersed [2]. Once the solution reached the optimal temperature, L-cysteine was added and mixed thoroughly. FTO glass substrates were subsequently immersed and kept for 8 h at 80 °C to form thin Bi_2S_3 films. The obtained samples were cleaned with distilled water and annealed in an inert atmosphere.

All samples were analyzed by UV-Vis absorption spectroscopy and X-ray diffraction (XRD) analysis on the Bruker D8 Advance diffractometer. Thin films were scanned over the range $2\theta = 3–70°$ at a scanning speed of 1° min^{-1} using a coupled two theta/theta scan type. This test determined structural characterization of the obtained materials. Results were studied and compared.

[1] T. O. Ajiboye and D. C. Onwudiwe, “Bismuth sulfide based compounds: Properties, synthesis and applications,” Results in Chemistry, vol. 3, p. 100151, Jan. 2021, doi: 10.1016/j.rechem.2021.100151.

[2] J. Jiang, G. Gao, R. Yu, G. Qiu, and X. Liu, “Chrysanthemum-like bismuth sulfide microcrystals: Synthesis, characterization, and properties,” Solid State Sciences, vol. 13, no. 2, pp. 356–360, Dec. 2010, doi: 10.1016/j.solidstatesciences.2010.11.035.

EVALUATION OF SUPPORT LAYERS FOR GRAPHENE TRANSFER

Evelina Vaicekauskaitė[1,2], Deivis Plaušinaitis[2], Milita Vagner[1], Valentina Plaušinaitienė[1]

[1]Lithuania, Center for Physical Sciences and Technology, Department of Functional Materials and Electronics
[2]Lithuania, Vilnius University, Faculty of Chemistry and Geosciences, Department of Physical Chemistry
evelina.vaicekauskaite@ftmc.lt

Graphene is a two-dimensional carbon material known for its excellent electrical conductivity. Graphene grown by chemical vapor deposition (CVD) is typically synthesized on copper substrates and requires a transfer step for integration onto target surfaces. Due to the atomic thickness and mechanical fragility of monolayer graphene, a temporary support layer is essential during the transfer process.

In this study, different support layers were evaluated for the transfer of CVD-grown graphene from copper foil onto target surfaces, such as gold (Au) and silicon (Si). The investigated support materials included paraffin, polymethyl methacrylate (PMMA), polycarbonate (PC), and six different photopolymer resins.The support layers were applied with varying thicknesses, and their solubility, removal behavior, and tendency to leave residues on the graphene surface were investigated. Raman spectroscopy was used to confirm the presence and continuity of the graphene layer after transfer, while optical microscopy was employed to observe surface features and residual contamination originating from the support layers.

The results demonstrate that the choice of support layer influences the quality of the transferred graphene. This work provides comparative insight into commonly used and alternative support materials for graphene transfer onto solid surfaces.

SYNTHESIS AND APPLICATION OF AU-DECORATED 2D MXENE FOR THE PLASMONIC SENSING OF MERCURY IONS IN WATER

Saqib Ali[1], Martynas Talaikis[2], Oleksiy Gogotsi[3], Arunas Ramanavicius[4], Simonas Ramanavicius[1]

[1]State Research Institute Center for Physical Sciences and Technology (FTMC), Department of Electrochemical Materials Research, Sauletekio av. 3, LT-10257 Vilnius, Lithuania
[2]State Research Institute Center for Physical Sciences and Technology (FTMC), Department of Organic Chemistry, Sauletekio av. 3, LT-10257 Vilnius, Lithuania
[3]Materials Research Center, Krzhizhanovskogo street, 3, 03680, Kyiv, Ukraine
[4]State Research Institute Center for Physical Sciences and Technology (FTMC), Department of Nanotechnology, Sauletekio av. 3, LT-10257 Vilnius, Lithuania
saqib.ali@ftmc.lt

Recent industrial development improves human quality of life, meanwhile posing a significant threat to the environment due to the involvement of synthetic chemicals and complex chemical procedures. Industrial effluents are the greatest source of heavy metal ions leaching into the aquatic system. Heavy metal ions are toxic even at low concentrations. Dissoled metal ions are among the most difficult contaminants to identify and remove from water[1]. Currently, lab-based detection technologies are used to secure the water supply for human consumption. There is a need to develop easy-to-use, field-deployable detection technologies. Plasmonic sensors are an emerging area of research for environmental applications, particularly in water quality testing, as they offer high sensitivity and selectivity. Advanced nanomaterials, such as 2D materials, have significantly advanced plasmonic sensor technology [2][3]. Herein, we demonstrated gold-functionalized 2D MXene synthesized at room temperature as a plasmonic sensor for the detection of trace amounts of Hg^{2+} metal ions in water. The detection mechanism relies on the adsorption of Hg^{2+} ions onto the gold-modified MXene surface, which alters its Localized Surface Plasmon Resonance (LSPR)[4]. The plasmonic sensor developed in this study showed a linear response to a change in the Hg^{2+} ions concentration up to 1 ppm in water. The LSPR signal at 580 nm exhibited a progressive redshift in λmax up to 20 nm. The MXene-based plasmonic sensors demonstrated high selectivity against competing metal ions in tap water. In conclusion, this research expands the application of MXene in versatile plasmonic sensor applications.

Keywords: Plasmonic Sensors, MXene, Water Quality, Heavy Metal Ions, 2D Materials

[1] N. Sharma, D. Yadav, M. Shandilya, A. Thakur, and C. M. Srivastava, “Ferrite-based hybrid structures for heavy metal ions removal,” Nanoferrites for Emerging Environmental Applications, pp. 161–175, Jan. 2025, doi: 10.1016/B978-0-443-22232-0.00008-3
[2] F. Q. Yang and L. Ge, “Colorimetric Sensors: Methods and Applications,” Sensors 2023, Vol. 23, Page 9887, vol. 23, no. 24, p. 9887, Dec. 2023, doi: 10.3390/S23249887
[3] I. Navitski, A. Ramanaviciute, S. Ramanavicius, M. Pogorielov, and A. Ramanavicius, “MXene-Based Chemo-Sensors and Other Sensing Devices,” Nanomaterials 2024, Vol. 14, Page 447, vol. 14, no. 5, p. 447, Feb. 2024, doi: 10.3390/NANO14050447
[4] S. Adomavičiūtė-Grabusovė, S. Ramanavičius, A. Popov, V. Šablinskas, O. Gogotsi, and A. Ramanavičius, “Selective Enhancement of SERS Spectral Bands of Salicylic Acid Adsorbate on 2D Ti3C2Tx-Based MXene Film,” Chemosensors 2021, Vol. 9, Page 223, vol. 9, no. 8, p. 223, Aug. 2021, doi: 10.3390/CHEMOSENSORS9080223

BENCHMARKING EXTENDED DENSITY FUNCTIONAL TIGHT-BINDING METHODS FOR PHOTOCHEMICAL PROPERTY PREDICTION OF MOLECULES

Deimantas Šmigelskas[1,2], Linas Vilčiauskas[1,2]

[1]Center for Physical Sciences and Technology (FTMC), Saulėtekio al. 3, LT-10257 Vilnius, Lithuania
[2]Vilnius University, Insitute of Chemistry, Saulėtekio al. 3, LT-10257 Vilnius, Lithuania
deimantas.smigelskas@ftmc.lt

Semi-empirical quantum mechanical methods based on extended tight-binding density functional theory offer similar accuracy at a computational efficiency that is 2–3 orders of magnitude faster than density functional theory (DFT) [1]. Earlier generation methods such as GFN2-xTB show limitations for redox-related applications. For example, GFN2-xTB systematically underestimates HOMO–LUMO gaps and requires empirical ionization potential and electron affinity corrections [2]. Recently developed general-purpose g-xTB method introduces fundamental theoretical improvements, achieving a weighted total mean absolute deviation of 9.3 kcal/mol on the GMTKN55 molecular dataset compared to 25 kcal/mol for GFN2-xTB [3].

This work aims to calibrate and validate the performance of g-xTB on energetic descriptors, particularly HOMO–LUMO gaps, which are central to photoredox catalyst screening. The goal is to establish whether this method can reliably determine photocatalyst ground-state properties.

A set of organic frameworks with variable light-oriented conjugated systems from the OCELOT database were optimized using g-xTB. This benchmark set consists of 4000 neutral, ground-state, closed-shell molecules containing π-conjugated systems with heavy heteroatoms such as S, Cl, and I, and is planned to be extended to the full OCELOT chromophore v1 dataset size (more than 25,000 scaffolds) in the near future. The obtained HOMO–LUMO gaps were compared with those computed at the LC-ωHPBE/def2-SVP level of theory [4]. An R^2 value of 0.485 with a mean absolute error (MAE) of 1.122 eV was obtained, representing moderate correlation between the selected SQM and DFT methods and somewhat poorer accuracy of g-xTB.

Current results suggest that the g-xTB method has potential for predicting energy-related properties of organic molecules relevant to photochemical applications. Pre-screening using g-xTB can provide quick and reasonably accurate insight into structure–property relationships and is expected to become even faster once analytical gradients are implemented.

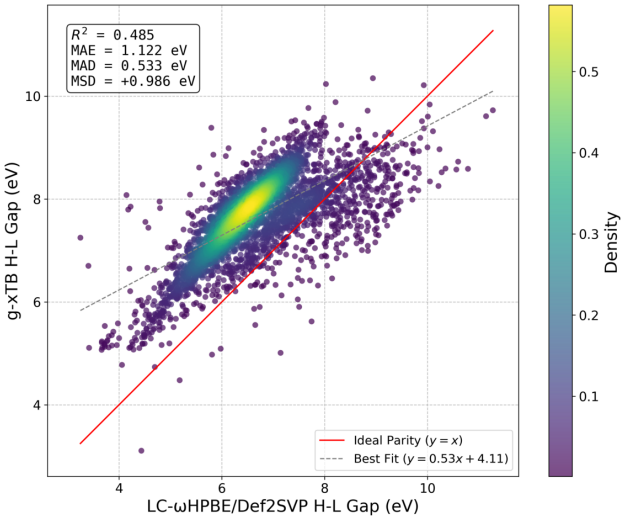


Fig. 1. Parity plot of HOMO–LUMO gaps computed by g-xTB and LC-ωHPBE/Def2SVP methods for a set of 4000 chromophores.

[1] C. Bannwarth, S. Ehlert, and S. Grimme, "GFN2-xTB—An Accurate and Broadly Parametrized Self-Consistent Tight-Binding Quantum Chemical Method with Multipole Electrostatics and Density-Dependent Dispersion Contributions," Journal of Chemical Theory and Computation, vol. 15, no. 3, pp. 1652–1671, Feb. 2019, doi: 10.1021/acs.jctc.8b01176.

[2] H. Neugebauer, F. Bohle, M. Bursch, A. Hansen, and S. Grimme, "Benchmark Study of Electrochemical Redox Potentials Calculated with Semiempirical and DFT Methods," The Journal of Physical Chemistry A, vol. 124, no. 35, pp. 7166–7176, Aug. 2020, doi: 10.1021/acs.jpca.0c05052.

[3] T. Froitzheim, M. Müller, A. Hansen, and S. Grimme, "g-xTB: A General-Purpose Extended Tight-Binding Electronic Structure Method For the Elements H to Lr (Z=1–103)," Chemrxiv, Jun. 23, 2025. doi: 10.26434/chemrxiv-2025-bjxvt.

[4] V. Bhat, P. Sornberger, B. S. S. Pokuri, R. Duke, B. Ganapathysubramanian, and C. Risko, "Electronic, redox, and optical property prediction of organic π-conjugated molecules through a hierarchy of machine learning approaches," Chemical Science, vol. 14, no. 1, pp. 203–213, Nov. 2022, doi: 10.1039/d2sc04676h.

REMARKABLE THERMAL STABILIZATION OF COLLAGEN-LIKE PEPTIDES VIA 2-AZABICYCLO ALKANE INCORPORATION

Volodymyr Lyakh[1], Bartosz Łagan[1], Radosław Tymoszewicz-Gaida[1], Elżbieta Wojaczyńska[1]

[1]Wrocław University of Science and Technology, Faculty of Chemistry, Department of Quantum and Physical Chemistry, Wrocław, Poland
volodimirlah@gmail.com

Collagen-like peptides (CLP) provide a controllable reductionist model of the collagen triple helix, serving as a fundamental tool for the rational design of stable, collagen-based biomaterials. In these systems, thermal stability can be tuned by sequence engineering (e.g., conformationally constrained residues) as well as by molecular architecture (e.g., covalent preorganization of three peptide strands on a tripodal scaffold).[1,2]

This study evaluates the impact of introducing a 2-azabicycloalkane residue (azBca) on the apparent melting temperature T_m and examines how concentration (0.5 vs 1.0 mg mL^{-1}) and architecture (linear vs scaffold-preorganized) influence higher-order association. Triple-helix formation and thermal unfolding were monitored by circular dichroism (CD) spectroscopy in PBS (10 mM, pH 7.4) after incubation at 4 °C for ≥48 h; thermal ramps (4–70 °C, 1 °C min^{-1}) were followed at 225 nm, with T_m obtained from the extremum of $\mathrm{d}Abs/\mathrm{d}T$ (Fig. 1).

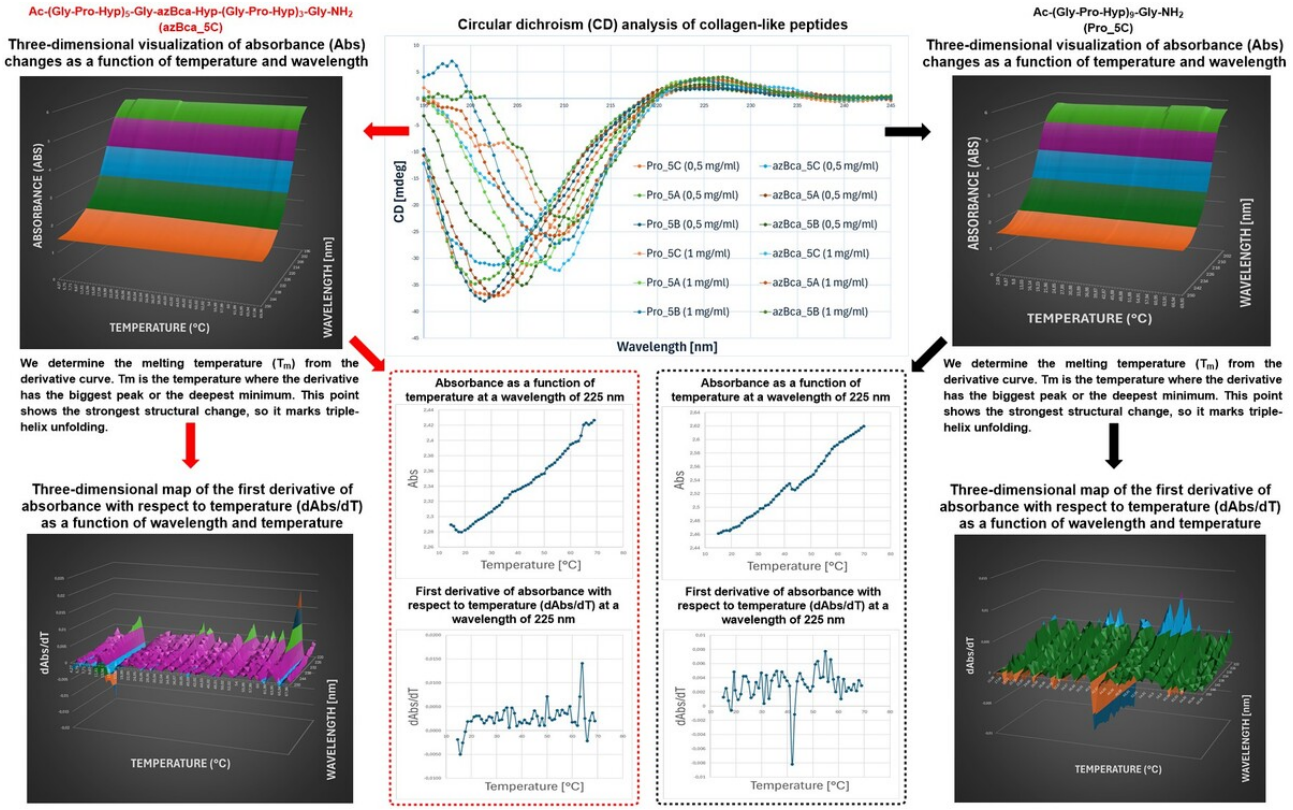


Fig. 1. CD spectra and thermal unfolding of CLP at 0.5 and 1.0 mg mL^{-1} in PBS (10 mM, pH 7.4). T_m was determined from the extremum of $\mathrm{d}Abs/\mathrm{d}T$ at 225 nm. Increasing concentration shifts the CD minimum toward ~205–210 nm, consistent with increased supramolecular ordering.

Results indicate that azBca incorporation strongly increases thermal stability, with T_m rising from 41.89 °C for Pro_5C to 63.95 °C for azBca_5C. With increasing concentration, the CD minimum shifts from approximately 198–205 nm toward approximately 205–210 nm, consistent with increased supramolecular ordering. Similar 204–210 nm features have been reported for type I collagen under fibrillogenesis conditions, although CD alone cannot confirm fiber formation.[3]

These azBca-stabilized CLPs provide a robust platform for introducing bioactive motifs and for integration into hydrogel/ECM-mimetic materials for tissue engineering applications.

[1] C. L. Jenkins et al., "Substituted 2-Azabicyclo[2.1.1]hexanes as Constrained Proline Analogues: Implications for Collagen Stability," The Journal of Organic Chemistry, vol. 69, no. 25, pp. 8565–8573, Aug. 2004, doi: 10.1021/jo049242y.

[2] J. Kwak, A. De Capua, E. Locardi, and M. Goodman, "TREN (Tris(2-aminoethyl)amine): An Effective Scaffold for the Assembly of Triple Helical Collagen Mimetic Structures," Journal of the American Chemical Society, vol. 124, no. 47, pp. 14085–14091, Nov. 2002, doi: 10.1021/ja0209621.

[3] K. E. Drzewiecki, D. R. Grisham, A. S. Parmar, V. Nanda, and D. I. Shreiber, "Circular Dichroism Spectroscopy of Collagen fibrillogenesis: A new use for an old technique," Biophysical Journal, vol. 111, no. 11, pp. 2377–2386, Dec. 2016, doi: 10.1016/j.bpj.2016.10.023.

SYNTHESIS AND ADMET EVALUATION OF CHLOROPYRIDINE-BASEDHYDRAZONE DERIVATIVES

Aida Šermukšnytė[1], Kristina Kantminienė[2], Ingrida Tumosienė[1]

[1]Kaunas University of Technology, Department of Organic Chemistry, Lithuania
[2]Kaunas University of Technology, Department of Physical and Inorganic Chemistry, Lithuania
aida.sermuksnyte@ktu.lt

Nitrogen-containing heterocycles are widely used in medicinal chemistry due to their presence in numerous biologically active compounds and approved drugs [1]. Among these, pyridine derivatives have attracted attention because of their favourable physicochemical properties and compatibility with a variety of pharmacological targets. Hydrazide and hydrazone functionalities are also well known for their biological relevance and are frequently explored as key structural motifs in the design of potential drug candidates [2,3].

In this study, a series of chloropyridine-based hydrazone derivatives were synthesized starting from 2-amino-5-chloropyridine. The reaction of the aminopyridine with acrylic acid in toluene under reflux conditions led to the formation of the corresponding β-alanine derivative. Its subsequent treatment with hydrazine monohydrate afforded the desired hydrazide, which further reacted with various aromatic and heteroaromatic aldehydes in methanol to yield a set of novel hydrazone derivatives. The synthesized compounds, bearing different aromatic substituents such as unsubstituted phenyl, halogenated phenyl, methoxyphenyl, and heteroaromatic moieties, were obtained in good yields and were characterized by standard spectroscopic methods.

To compare the drug-likeness and predict pharmacokinetic behaviour of the synthesized hydrazones, their *in silico* ADMET analysis was performed. The molecular weights of the evaluated compounds were in the range of 300 – 395 Da, and calculated LogP values ranged from 2.78 to 4.20, indicating moderate lipophilicity across the series. Topological polar surface area values remained below 100 $Å^2$ for all the derivatives. The differences in predicted blood-brain barrier permeability were observed depending on the aromatic substituent, with hydrazones bearing unsubstituted or less polar aromatic groups showing a higher likelihood of BBB penetration, while compounds containing more polar or heteroaromatic substituents were classified as non-BBB permeant. Human intestinal absorption and Caco-2 permeability predictions were comparable among the compounds, suggesting similar intestinal transport characteristics despite structural variation.

Overall, the synthesized chloropyridine-based hydrazone derivatives display suitable *in silico* drug-likeness and pharmacokinetic profiles. These results support their further evaluation in future biological studies.

Acknowledgements
This research was supported by the Research Council of Lithuania (LMTLT), agreement No S-MIP-25-22.

[1] E. Vitaku, D. T. Smith, and J. T. Njardarson, "Analysis of the Structural Diversity, Substitution Patterns, and Frequency of Nitrogen Heterocycles among U.S. FDA Approved Pharmaceuticals," Journal of Medicinal Chemistry, vol. 57, no. 24, pp. 10257–10274, Oct. 2014, doi: https://doi.org/10.1021/jm501100b.

[2] A. Šermukšnytė, M. Stasevych, O. Komarovska-Porokhnyavets, V. Zvarych, E. Jakubauskienė, K. Kantminienė, and I. Tumosienė, "Novel Antimicrobial and Antitumor Agents Bearing Pyridine-1,2,4-triazole-3-thione-hydrazone Scaffold: Synthesis, Biological Evaluation, and Molecular Docking Investigation," Biomolecules, vol. 14, no. 12, p. 1529, Nov. 2024, doi: https://doi.org/10.3390/biom14121529.

[3] A. Šermukšnytė, K. Kantminienė, I. Jonuškienė, I. Tumosienė, and V. Petrikaitė, "The Effect of 1,2,4-Triazole-3-thiol Derivatives Bearing Hydrazone Moiety on Cancer Cell Migration and Growth of Melanoma, Breast, and Pancreatic Cancer Spheroids," Pharmaceuticals, vol. 15, no. 8, p. 1026, Aug. 2022, doi: https://doi.org/10.3390/ph15081026.

SYNTHESIS OF 4-((BENZIMIDAZOL-2-YL)THIO)-6-ISOPROPYLRESORCINOLS

Gabija Griškonytė[1], Ieva Žutautė[1], Algirdas Brukštus[1]

[1]Faculty of Chemistry and Geosciences, Vilnius University, Vilnius, Lithuania
gabija.griskonyte@chgf.stud.vu.lt

An increasing number of cancer cases are being observed worldwide.Therefore, Hsp90 inhibitors are among the most promising approaches for cancer treatment. Hsp90 is a molecular chaperone expressed in a variety of cells and plays a critical role in regulating the cell cycle, including processes such as cell proliferation, signal transduction, and transcription [1]. Under environmental stress conditions such as high temperature and hypoxia, Hsp90 is overexpressed in cells [2], especially in tumor cells [3], to maintain a dynamic balance between protein folding and degradation. Due to the presence of mutated and unstable client proteins, cancer cells exhibit a greater dependence on Hsp90 than normal cells. This increased reliance renders Hsp90 an attractive therapeutic target as its inhibition can selectively disrupt oncogenic signaling pathways and reduce tumor development. The aim of this work is to synthesize variously substituted sulfur-containing resorcinol compounds that could act as Hsp90 inhibitors and inhibit cancer progression.

For the synthesis of targeted compounds, 1-isopropyl-2,4-dimethoxybenzene was selected as the starting material. Structural modification was introduced at the fifth position of aromatic ring, where thiobenzimidazoles moieties, were attached. Hydroxy groups were protected with methoxy groups to avoid additional reactions. The isopropyl substituent was obtained after the Wittig reaction with carbonyl and reduction. For the addition of sulfur-containing compounds, a Ullmann-type reaction was performed with iodinated and isopropyl-substituted dimethoxybenzene. Finally, the protecting groups were removed to yield the desired target compounds.

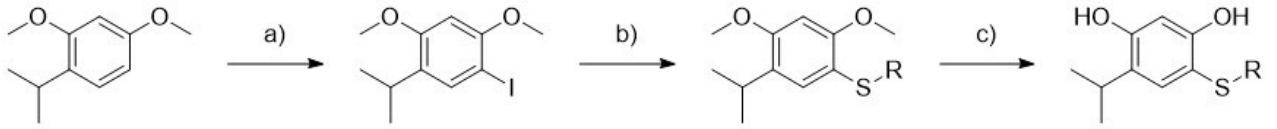


Fig. 1. Scheme of targeted compounds, a) NIS, CH_3CN; b) CuI, 2,9-dimethyl-1,10-phenanthroline hydrate, *t*-BuOK, DMF, 110°C, Ar; c) BBr_3, DCM, 0°C, Ar.

[1] L. Li, L. Wang, Q.-D. You, and X.-L. Xu, "Heat Shock Protein 90 inhibitors: an update on achievements, challenges, and future directions," Journal of Medicinal Chemistry, vol. 63, no. 5, pp. 1798–1822, Oct. 2019, doi: 10.1021/acs.jmedchem.9b00940.

[2] G. Garg, A. Khandelwal, and B. S. J. Blagg, "Anticancer inhibitors of HSP90 function," Advances in Cancer Research, vol. 129, pp. 51–88, Jan. 2016, doi: 10.1016/bs.acr.2015.12.001.

[3] Y. Zhang, L. Shan, W. Tang, Y. Ge, C. Li, and J. Zhang, "Recent Discovery and Development of Inhibitors that Target CDK9 and Their Therapeutic Indications," Journal of Medicinal Chemistry, vol. 67, no. 7, pp. 5185–5215, Apr. 2024, doi: 10.1021/acs.jmedchem.4c00312.

GLUCOSE-BASED CHOLINESTERASES INHIBITORS

Rugilė Morkūnaitė[1], Marius Butkevičius[2]

[1]Vilnius University, Faculty of Chemistry and Geosciences, Institute of Chemistry, Vilnius, Lithuania
[2]Vilnius University, Life Sciences Center, Institute of Biochemistry, Department of Bioanalysis, Vilnius, Lithuania
rugile.morkunaite@chgf.stud.vu.lt

Neurodegenerative diseases are closely associated with dysfunction of the cholinergic system, in which acetylcholine (ACh) acts as the primary neurotransmitter responsible for transmitting electrical impulses between nerve cells. In patients with Alzheimer's disease (AD), acetylcholine levels rapidly decrease due to excessive hydrolysis by acetylcholinesterase (AChE). Butyrylcholinesterase (BChE) is another enzyme closely related to AChE, it functions like a co-regulator of cholinergic system by hydrolysing ACh. Increased activity of BChE in the temporal cortex and the hippocampus is seen in patients with progressive AD. Focusing on both of these enzymes is important due to their different locations, AChE predominantly localised in the central nervous system, whereas BChE is present more in the peripheral tissues. [1] In this study, different glucose-6-esters were synthesised and their potential inhibitory effects on cholinesterases were evaluated. Glucose-6-esters were synthesised by a transesterification reaction catalysed by Candida antarctica lipase B (CALB). During a transesterification reaction one ester is converted into another ester through its reaction with an alcohol. In this case, a regioselective enzyme CALB was used to ensure selective modification of only the primary alcohol group of glucose. The acyl group was transferred from a short-chain vinyl ester, which were selected as acyl group donors. The reaction is driven towards product formation by spontaneous tautomerization of alcohol by-product into acetaldehyde, rendering the process irreversible consequently maximising product yield. [2] The main objective of this study was to use amperometric biosensors to measure the inhibitory effects of the synthesised glucose-6-esters on cholinesterase activity. Esterase activity was estimated using immobilised choline oxidase. In this system, ACh is hydrolysed by AChE to produce choline, which subsequently is oxidised by choline oxidase to generate hydrogen peroxide (H_2O_2). The peroxide undergoes oxidation at a platinum electrode, producing an amperometric signal directly proportional to the amount of peroxide formed. For the synthesis of glucose-6-esters, seven different short-chain vinyl esters were used: vinyl acetate, vinyl propionate, vinyl propionate, vinyl methacrylate, vinyl pivalate, vinyl 4-tert-butylbenzoate and vinyl benzoate. To determine synthesis efficiency two analytical methods were used, amperometric glucose biosensor and DNS method for reducing sugars. During the synthesis process, glucose is consumed, and its depletion, measured by the glucose biosensor, directly correlates with the quantity of ester product formed. The results showed that glucose-6-esters containing longer acyl chains provided more effective inhibition of cholinesterases. However, only three out of seven glucose-6-esters (acetate, propionate, butyrate) were obtained during the synthesis process with CALB.

[1] P. Anand and B. Singh, "A review on cholinesterase inhibitors for Alzheimer's disease," Archives of Pharmacal Research, vol. 36, no. 4, pp. 375–399, Feb. 2013, doi: 10.1007/s12272-013-0036-3.

[2] J. F. Kennedy et al., "Enzyme-catalyzed regioselective synthesis of sugar esters and related compounds," Journal of Chemical Technology & Biotechnology, vol. 81, no. 6, pp. 866–876, Apr. 2006, doi: 10.1002/jctb.1473.

A NEW LIGAND FOR BUCHWALD-HARTWIG AMINATION

Jonas Paukstys[1,2], Tomas Paskevicius[1], Linas Labanauskas[1]

[1]Center for Physical Sciences and Technology (FTMC)
[2]Vilnius University
jonas.paukstys@ftmc.lt

Heteroaromatic components are widely encountered in small-molecule drugs [1]. Efficient functionalisation of these compounds is key for the discovery and testing of new therapeutics. Palladium catalysis is widely applied for this purpose, particularly in amination reactions. Despite extensive research, ligands currently used for amination of heteroaromatic compounds are prone to deactivation, necessitating high catalyst loadings and extended reaction times. In 2024 novel O-bound electron deficient phosphine ligand (Figure 1A) was shown to be resistant to the deactivation processes [2]. However, the reported system relied on an air- and temperature-sensitive palladium precatalyst, making the reactions difficult to reproduce.

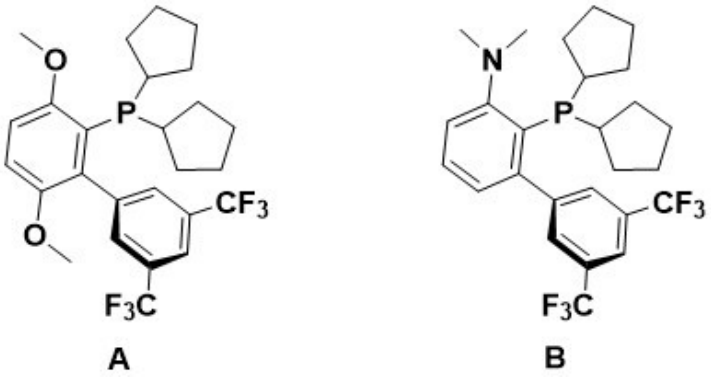


Fig. 1. Deactivation resistant ligand (A), new ligand synthesised in our work (B)

In this work, a series of ligands were synthesised and evaluated for their ability to support Buchwald–Hartwig amination of diverse heteroaromatic substrates. A catalytic system utilising a stable palladium source and a new ligand (Figure 1B) was developed. This system was shown to be compatible with a broad range of heteroaromatic compounds while requiring low catalyst loadings.

[1] E. Vitaku, D. T. Smith, and J. T. Njardarson, “Analysis of the Structural Diversity, Substitution Patterns, and Frequency of Nitrogen Heterocycles among U.S. FDA Approved Pharmaceuticals,” Journal of Medicinal Chemistry, vol. 57, no. 24, pp. 10257–10274, Sep. 2014, doi: 10.1021/jm501100b.

[2] K. Feng et al., “Development of a Deactivation-Resistant dialkylbiarylphosphine ligand for PD-Catalyzed arylation of secondary amines,” Journal of the American Chemical Society, vol. 146, no. 39, pp. 26609–26615, Sep. 2024, doi: 10.1021/jacs.4c09667.

ENGINEERING OXYTOCIN ANALOGS BY TARGETED PRO^7 EXCHANGE WITH A CHIRAL 2-AZABICYCLIC RESIDUE: CONFORMATIONAL CONTROL AT THE BACKBONE LEVEL

Bartosz Łagan[1], Volodymyr Lyakh[1], Radosław Tymoszewicz-Gaida[1], Elżbieta Wojaczyńska[1]

[1]Wrocław University of Science and Technology, Faculty of Chemistry, Department of Quantum and Physical Chemistry, Wrocław, Poland
bartoszlagan@gmail.com

Oxytocin is a clinically established cyclic nonapeptide whose therapeutic utility is fundamentally constrained by its very short in vivo half-life, resulting from rapid enzymatic degradation and conformational flexibility of the peptide backbone.[1] Despite decades of effort and the development of multiple oxytocin analogues, including sequence and side-chain modifications, improvements in metabolic stability remain limited and often accompanied by altered biological profiles.

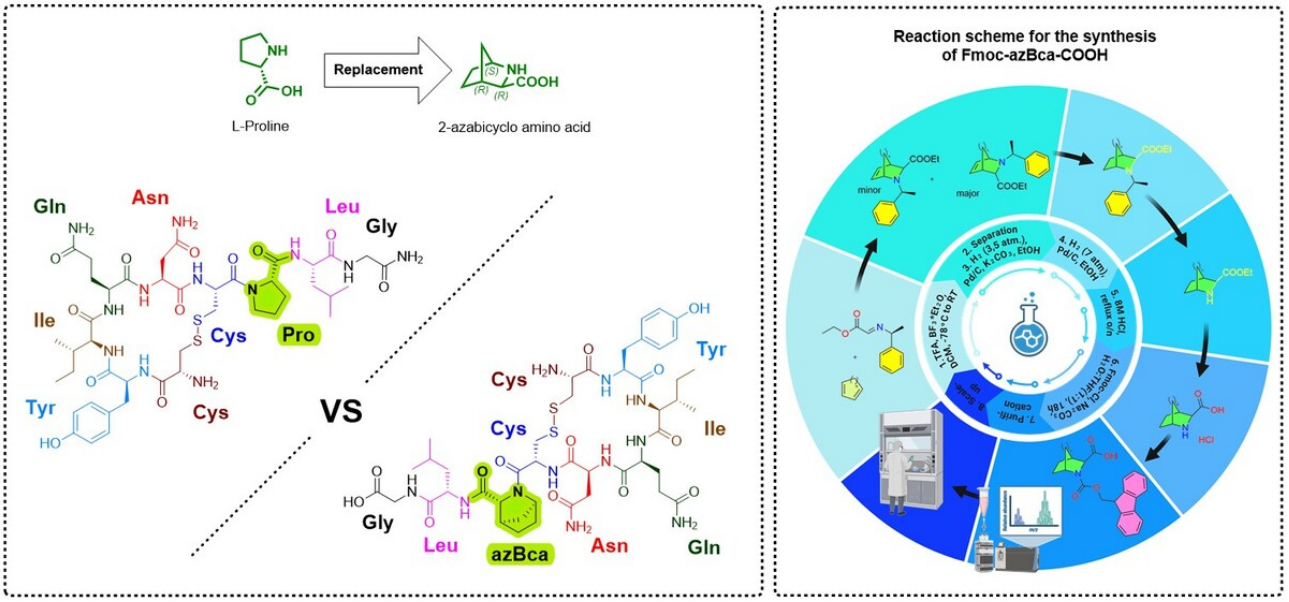


Fig. 1. Oxytocin (Pro^7) and the Pro^7→azBca analogue, alongside the synthetic route to the protected chiral azBca amino-acid building block.

An important yet underexploited factor contributing to oxytocin instability is the conformational heterogeneity associated with proline-containing motifs, which can modulate both receptor interaction and enzymatic recognition. In this context, replacement of native proline with conformationally constrained, non-natural amino acids represents a promising strategy to subtly control backbone geometry and evade proteolytic pathways.[2] Precedents from oxytocin and vasopressin-related systems indicate that minimal backbone rigidification can enhance peptide lifetime without compromising activity.[3] A conformational engineering approach is explored here as a route toward next-generation oxytocin analogues with improved stability.

[1] M. Manning et al., “Oxytocin and vasopressin agonists and antagonists as research tools and potential therapeutics,” Journal of Neuroendocrinology, vol. 24, no. 4, pp. 609–628, Feb. 2012, doi: 10.1111/j.1365-2826.2012.02303.x.
[2] C. L. Jenkins et al., “Substituted 2-Azabicyclo[2.1.1]hexanes as Constrained Proline Analogues: Implications for Collagen Stability,” The Journal of Organic Chemistry, vol. 69, no. 25, pp. 8565–8573, Aug. 2004, doi: 10.1021/jo049242y.
[3] V. J. Hruby, F. Al-Obeidi, and W. Kazmierski, “Emerging approaches in the molecular design of receptor-selective peptide ligands: conformational, topographical and dynamic considerations,” Biochemical Journal, vol. 268, no. 2, pp. 249–262, Jun. 1990, doi: 10.1042/bj2680249.

SIDERITIS SCARDICA AND SIDERITIS SYRIACA PLANT EXTRACTS: STUDIES ON PHYTOCHEMICAL COMPOSITION AND PROPERTIES.

Greta Tverskytė[1], Vaida Kitrytė-Syrpa[2]

[1]Kaunas University of Technology, Faculty of Chemical Technology, Kaunas, Lithuania
tverskyt.greta@gmail.com

In recent years, interest in natural bioactive compounds with beneficial effects on human health has been rapidly increasing. This trend encourages the development of innovative functional foods from plant-based raw materials. One such product is plant extracts. Plants of the Sideritis genus, also known as Greek mountain tea, are widely used in Southern Europe and are typically prepared as a decoction from stems, leaves, and flowers. Although further in vitro and in vivo studies are needed, existing data indicate that Sideritis species may exhibit antidiabetic, anxiolytic, and anti-agIn recent years, interest in natural bioactive compounds with beneficial effects on human health has been rapidly increasing. This trend encourages the development of innovative functional foods from plant-based raw materials. One such product is plant extracts. Plants of the Sideritis genus, also known as Greek mountain tea, are widely used in Southern Europe and are typically prepared as a decoction from stems, leaves, and flowers. Although further in vitro and in vivo studies are needed, existing data indicate that Sideritis species may exhibit antidiabetic, anxiolytic, and anti-aging effects, as well as a potential preventive role in Alzheimer's disease. Recent studies have identified bioactive compounds such as verbascoside and apigenin 7,4′-bis(trans-p-coumarate), which are of growing interest due to their anti-inflammatory and potential anticancer properties. Despite increasing research, systematic phytochemical studies of Sideritis species remain limited.[1-3]

This study aimed to evaluate the content of bioactive compounds in Sideritis scardica and Sideritis syriaca by analysing different plant parts (flowers, stems, and leaves) and their extracts. Special attention was given to the polarity of bioactive compounds, as it strongly influences extract composition and biological activity. Therefore, solvents of different polarity were used to ensure the extraction of a broad range of compounds. Sequential pressurized liquid extraction (PLE) was performed using four solvents: hexane, acetone, ethanol, and water. Antioxidant activity of the extracts and raw plant fractions was evaluated using ABTS and CUPRAC assays, while total phenolic content (TPC) and total flavonoid content (TFC) were also determined.

For both species the highest extraction yields were obtained with polar solvents, whereas hexane produced the lowest yields across all fractions. Leaves showed the highest extraction yields, particularly with ethanol and water ranged from 8,68 to 14,9% The highest antioxidant activity was observed in leaf samples, while stems showed the lowest activity. This trend was reflected in TPC results, where leaf extracts exhibited the highest values. For example, the acetone extract of S. syriaca leaves reached approximately 237.5 mg GAE/g extract, whereas stem extracts showed lower but still considerable values (about 182.6 mg GAE/g extract)

[1] P. Eleftheriou, E. Therianou, D. Lazari, S. Dirnali and A. Micha, '"Docking Assisted Prediction and Biological Evaluation of Sideritis L. Components with PTP1b Inhibitory Action and Probable Anti-Diabetic Properties," Current topics in medicinal chemistry, vol. 19, no. 5, Jan 1, pp. 383–392.

[2] J. Hofrichter, M. Krohn, T. Schumacher, C. Lange, B. Feistel, B. Walbroel and J. Pahnke, '"Sideritis spp. Extracts Enhance Memory and Learning in Alzheimer's β-Amyloidosis Mouse Models and Aged C57Bl/6 Mice," Journal of Alzheimer's disease, vol. 53, no. 3, Aug 3, pp. 967–980.

[3]] E.L. Wightman, P.A. Jackson, J. Khan, J. Forster, F. Heiner, B. Feistel, C.G. Suarez, I. Pischel and D.O. Kennedy, '"The Acute and Chronic Cognitive and Cerebral Blood Flow Effects of a Sideritis scardica (Greek Mountain Tea) Extract: A Double Blind, Randomized, Placebo Controlled, Parallel Groups Study in Healthy Humans," Nutrients, vol. 10, no. 8, Jul 24, pp. 955.

EVALUATIONOF ANTIOXIDANT, ENZYME INHIBITORY, AND UV-PROTECTIVE PROPERTIES OF ECHINOPSSPHAEROCEPHALUS L. EXTRACTS OBTAINED BY ACCELERATED SOLVENT EXTRACTION

Marius Užupis[1], Michail Syrpas[1], Joanna Topolska[2], Petras Rimantas Venskutonis[1], Małgorzata Starowicz[2], Vaida Kitrytė-Syrpa[1]

[1]Kaunas University of Technology, Faculty of Chemical Technology, Department of Food Science and Technology, Kaunas, Lithuania
[2]Polish Academy of Sciences, Institute of Animal Reproduction and Food Research, ul. Trylińskiego 18, 10-683 Olsztyn
marius.uzupis@ktu.edu

Echinops sphaerocephalus L. (glandular globe-thistle) is a medicinal plant belonging to the Asteraceae family, traditionally known primarily as a melliferous species. Phenolic compounds such as apigenin, chlorogenic acid, catechin, and quinic acids are recognized as key plant-derived bioactive compounds with strong antioxidants, anticancer, antibacterial, antiviral, and cardioprotective properties. However, the extraction of bioactive compounds from E. sphaerocephalus has been insufficiently investigated, and only limited information is available regarding the properties of its extracts. In this study, the phenolic content, antioxidant capacity, and sun protection factor (SPF) of E. sphaerocephalus extracts were evaluated using accelerated solvent extraction (ASE). Ethanol, water, and ethanol–water mixtures were selected as food- and pharmaceutical-grade solvents to obtain hydrophilic, antioxidant-rich extracts. ASE was performed under four conditions: 100% H_2O, 100% EtOH, and EtOH/H2O mixtures at 70/30% (v/v) and 50/50% (v/v). The extraction time was 45 minutes, and the temperature was set at 70 °C for EtOH and EtOH/H2O mixtures, while for 100% H_2O it was increased to 110 °C. The results demonstrated that ASE significantly enhanced extraction yield, which ranged from 15.4 to 41.6 g/100 g dry weight. Extracts obtained under different conditions exhibited variable total phenolic content (25–43 mg GAE/g extract) and in vitro antioxidant capacity (199.4–302.4 mg TE/g extract), as well as notable UV-protective potential (SPF > 8 at 0.1 mg/mL). These findings highlight ASE as an efficient approach for producing high-value extracts from E. sphaerocephalus with potential applications in the pharmaceutical and nutraceutical fields. Furthermore, the PLE–EtOH extract exhibited pronounced superoxide scavenging activity in the PCL assay (122.2 mg TE/g E), significant antiglycation activity (IC50 = 0.74 mg/mL), and inhibitory effects against α-amylase, α-glucosidase, and pancreatic lipase (IC50 = 1.64–15.14 mg/mL). These bioactivities suggest that E. sphaerocephalus extracts may help reduce inflammation and oxidative stress and modulate pathways associated with metabolic disorders.

Keywords: Echinops sphaerocephalus; accelerated solvent extraction;

THIN-FILM POLYMER SYSTEM FOR DRUG DELIVERY

Felix Lücke[1], Šarūnas Žukauskas[1,3], Arūnas Ramanavičius[1,2], Almira Ramanavičienė[2,3]

[1]Center for Physical Sciences and Technology (FTMC)
[2]Vilnius University
[3]State Research Institute Centre for Innovative Medicine
felix.luecke@ftmc.lt

Conventional drug administration routes, such as oral and intravenous delivery, can be affected by poor bioavailability, limited patient compliance, and inadequate targeting ability. Moreover, many drug classes, including peptides, genes, and small molecules, are hindered by poor solubility and lipophilicity, enzymatic degradation, insufficient absorption within the body, and premature activation [1,2]. These challenges can be addressed by drug delivery systems (DDS) through improvements in drug stability and targeting ability, which expand the range of viable therapeutic targets, enhance safety, and reduce side effects [3].

For the development of a polymer-based DDS, initial efforts were directed toward establishing a reliable method for producing and depositing the desired polymer. Subsequently, a protocol for drug incorporation was established, and preliminary drug release tests under different conditions were performed as a proof of concept for a topical DDS. A general depiction of a topical DDS is shown in Figure 1. The finished DDS is intended for topical use; therefore, polypyrrole (PPY) was selected as the polymer matrix due to its biocompatibility, electroactivity, and availability.

To ensure repeatable and uniform polymer deposition, an extensive electrode preparation and polymer deposition protocol was designed. This protocol was focused on maximizing the amount of deposited polymer while minimizing overoxidation. Ibuprofen (Ibu) was selected as the model drug to be delivered. Integration of Ibu into the polymer matrix was achieved by its presence in the reaction solution during electrochemical polymerization. Drug release was monitored and analyzed using UV–Vis spectroscopy.

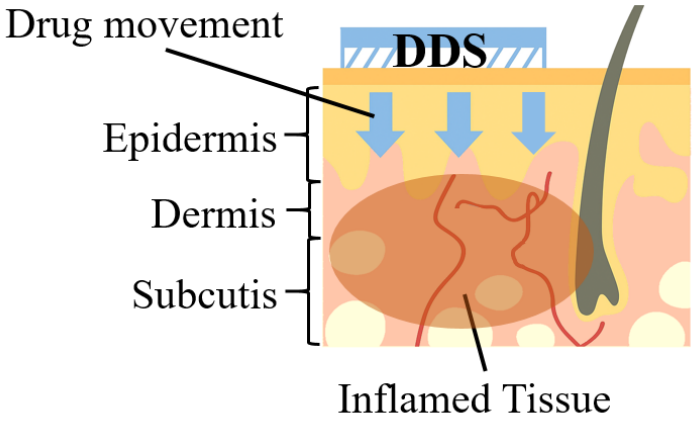


Fig. 1. Schematic of a topical Drug Delivery System and its stylized mechanism.

Acknowledgements
This project has received funding from the Research Council of Lithuania (LMTLT), project Nr. S-PD-24-121

[1] [1] C. A. Lipinski, “Drug-like properties and the causes of poor solubility and poor permeability,” Journal of Pharmacological and Toxicological Methods, vol. 44, no. 1, pp. 235–249, Jul. 2000, doi: https://doi.org/10.1016/s1056-8719(00)00107-6.
[2] [1] J. A. Barrett, W. Yang, S. M. Skolnik, L. M. Belliveau, and K. M. Patros, “Discovery solubility measurement and assessment of small molecules with drug development in mind,” Drug Discovery Today, Jan. 2022, doi: https://doi.org/10.1016/j.drudis.2022.01.017.
[3] [1] R. C. Maranhão, C. G. Vital, T. M. Tavoni, and S. R. Graziani, “Clinical experience with drug delivery systems as tools to decrease the toxicity of anticancer chemotherapeutic agents,” Expert Opinion on Drug Delivery, vol. 14, no. 10, pp. 1217–1226, Jan. 2017, doi: https://doi.org/10.1080/17425247.2017.1276560.

STIMULI-RESPONSIVE ALGINATE-BASED CONDUCTIVE HYDROGELSINCORPORATING PANI AND PEDOT FOR TUNABLE DRUG RELEASE

Shahbaz Khan[1,2], Šarūnas Žukauskas[1,3], Arūnas Ramanavičius[1,2], Felix Luecke[1]

[1]Center for physical sciences and Technology (FTMC)
[2]Vilnius University
[3]State Research Institute Centre for Innovative Medicine
shahbaz.khan@chgf.stud.vu.lt

Conductive and stimuli-responsive hydrogels offer promising opportunities for drug delivery systems by enabling both passive diffusion and stimulus-triggered release. In this study, alginate-based composite hydrogels incorporating polyaniline (PANI), poly(3,4-ethylenedioxythiophene) (PEDOT), and their combinations are being developed to investigate passive and active drug release mechanisms. Sodium alginate hydrogels are ionically crosslinked with calcium ions, and methylene blue is used as a model compound. The hydrogels are being characterized in terms of swelling behavior and electrical conductivity. Passive release studies under physiological conditions have demonstrated sustained, diffusion-controlled release behavior, while active release experiments are expected to evaluate the influence of electrical stimulation on release kinetics compared to passive diffusion. Hydrogels containing PEDOT and PANI-PEDOT are anticipated to exhibit enhanced conductivity and more pronounced electroresponsive release compared to PANI-only systems. Comparative analysis will be performed to elucidate the roles of polymer composition and stimulus type in governing release profiles.

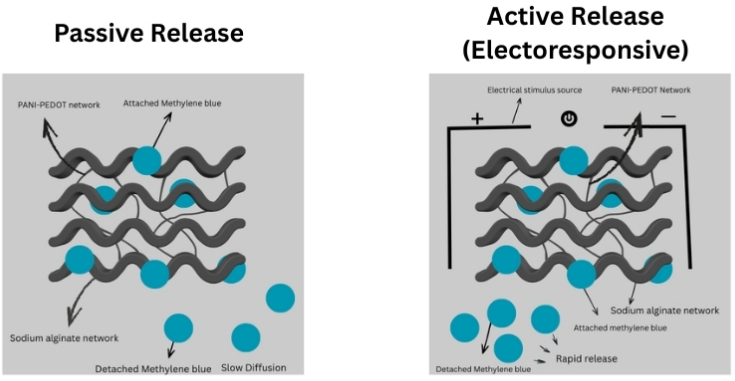


Fig. 1. Schematic Representation of Passive and active release

INVESTIGATION OF REAL-TIME INTERACTIONS BETWEEN DPP IV PROTEIN AND SPECIFIC ANTIBODIES

Justina Liesytė[1], Antanas Zinovičius[2], Ieva Plikusienė[1,2]

[1]Vilnius University, Faculty of Chemistry and Geosciences, Institute of Chemistry, NanoTechnas - Center of Nanotechnology and Materials Science, Naugarduko St. 24, LT-03225, Vilnius, Lithuania
[2]State Research Institute Centre for Physical Sciences and Technology, Department of Nanotechnology, Sauletekis Avenue 3, LT-10257, Vilnius, Lithuania
justina.liesyte@chgf.stud.vu.lt

Dipeptidyl peptidase-IV (DPP IV) is a protein encoded by the DPP4 gene in humans. It is a transmembrane glycoprotein which can also be found circulating in blood. DPP IV is important for T-cell stimulation and glucose metabolism. Renal, colon, prostate and thyroid human carcinoma tissues overexpress DPP IV and it can also be a diagnostic for lysosomal storage diseases [1]. Due to DPP IV being a biomarker for cancer and type 2 diabetes, the importance of developing a biosensor for its detection has been increasing.

This study aimed to use a combined method of spectroscopic ellipsometry (SE) and quartz crystal microbalance with dissipation (QCM-D) to investigate interactions between DPP IV and specific antibodies and to assess the thermodynamic properties of formed complex. Specific antibodies were immobilized through protein G for them to be well-oriented and able to freely interact with DPP IV protein. SE allowed to assess the thickness of protein monolayers and to calculate the surface mass density of proteins. The data obtained from QCM-D method allowed to assess the viscoelastic properties of antibody and DPP IV monolayers and to calculate the amount of PBS trapped in each monolayer. Moreover, the combined method of SE and QCM-D is non-destructive, label-free and allows to watch the interaction between specific antibodies and DPP IV in real time. The results present that interaction between specific antibodies and DPP IV was successful. The monolayer of specific antibodies was found to be rigid, while the monolayer of DPP IV protein formed during the interaction with antibodies presented viscoelastic properties.

[1] J. Valverde-Pozo et al., “Ratiometric Two-Photon Near-Infrared probe to detect DPP IV in human plasma, living cells, human tissues, and whole organisms using zebrafish,” ACS Sensors, vol. 8, no. 3, pp. 1064–1075, Feb. 2023, doi: 10.1021/acssensors.2c02025.

GOLD NANOPARTICLE-BASED STRATEGIES FOR IMPROVING SARS-COV-2 ANTI-RBD IMMUNOSENSOR SENSITIVITY

Agne Giniunaite[1], Asta Kausaite-Minkstimiene[1]

[1]Vilnius University, Faculty of Chemistry and Geosciences, Institute of Chemistry, NanoTechnas– Center of Nanotechnology and Materials Science, Naugarduko St. 24, LT-03225, Vilnius, Lithuania
agne.giniunaite@chgf.vu.lt

Although global management of COVID-19 has shifted into a post pandemic phase, the continued circulation of SARS-CoV-2 and the long-term consequences of infection highlight the need for ongoing monitoring of immune responses. Antibodies targeting the receptor-binding domain (RBD) of the SARS-CoV-2 spike protein remain key biomarkers for assessing immunity acquired through infection or vaccination. Accurate quantification of anti-RBD provides valuable insight into both naturally acquired and vaccine-induced immunity, enabling evaluation of an individual's immune status.

Surface plasmon resonance (SPR) immunosensors offer real-time, label-free detection of antigen–antibody interactions and show strong potential for sensitive serological analysis. However, further improvements in analytical performance are required to achieve lower detection limits in complex biological samples. Gold nanoparticles are widely recognized for their ability to enhance optical signals and amplify biosensor responses. Therefore, the aim of this work was to develop SPR-based immunosensors for quantitative anti-RBD detection by employing gold nanoparticles to strengthen the analytical signal and improve overall immunosensor sensitivity.

In this work, two SPR immunosensor variants based on an indirect sandwich-type detection format were developed. In the first design, commercially available streptavidin-modified gold nanoparticles were conjugated with biotinylated anti-IgG antibodies (anti-IgG$_{biot}$–SAv–AuNPs). In the second approach, gold nanoparticles synthesized via the Turkevich method were functionalized with a mixed self-assembled monolayer of 11-mercaptoundecanoic acid and 2-mercaptoethanol, activated using EDC/NHS chemistry, and subsequently modified with 3-aminoboronic acid (AuNPs-11-MUR/2-MEA-3-ABR). In both cases, the resulting nanoparticle conjugates were used to amplify the analytical signal during the second biorecognition step.

Both immunosensors enabled quantitative detection of anti-RBD antibodies over distinct concentration ranges and exhibited strong linear responses. The immunosensor employing anti-IgG$_{biot}$–SAv–AuNPs demonstrated sensitive detection within the picomolar to nanomolar range, while the immunosensor employing AuNPs-11-MUR/2-MEA-3-ABR achieved enhanced sensitivity in the low picomolar range. The latter approach provided a notably lower detection limit, highlighting the effectiveness of nanoparticle surface functionalization in improving analytical performance. Both immunosensors were successfully applied for anti-RBD antibody quantification in human serum samples, demonstrating high accuracy and excellent recovery values. These results confirm the suitability of the developed SPR immunosensors for sensitive and reliable estimation of SARS-CoV-2 anti-RBD antibody levels in biological samples.

ENVIRONMENTALLY RELEVANT EFFECTS OF PHOTOLUMINESCENT GOLD NANOCLUSTERS: LINKING NANOMATERIAL PROPERTIES TO AQUATIC BIORESPONSES

Agne Mikalauskaite[1], Živile Jurgelene[2], Danguole Montvydiene[3], Simonas Ramanavicius[4]

[1]State Research Institute Centre for Physical Sciences and Technology, Vilnius, Lithuania
[2]Nature Research Centre, Institute of Ecology, Vilnius, Lithuania
agne.sukoviene@ftmc.lt

Photoluminescent gold nanoclusters (Au NCs), composed of several to tens of gold atoms, represent a distinct class of quantum-sized nanomaterials exhibiting long-lived excited states, size-dependent electronic structure, and high colloidal stability. Their increasing use in biomedical and environmental applications highlights the need for integrated studies linking physicochemical characterization with biologically relevant effects under realistic exposure conditions. Strong red photoluminescence centered at 680–700 nm with an average lifetime of 1.4 μs was preserved for several weeks in aqueous and buffered media, indicating effective suppression of fluorescence quenching. Integration of Au NCs also enhanced saturation magnetization and increased the blocking temperature, demonstrating cooperative optical–magnetic behavior.

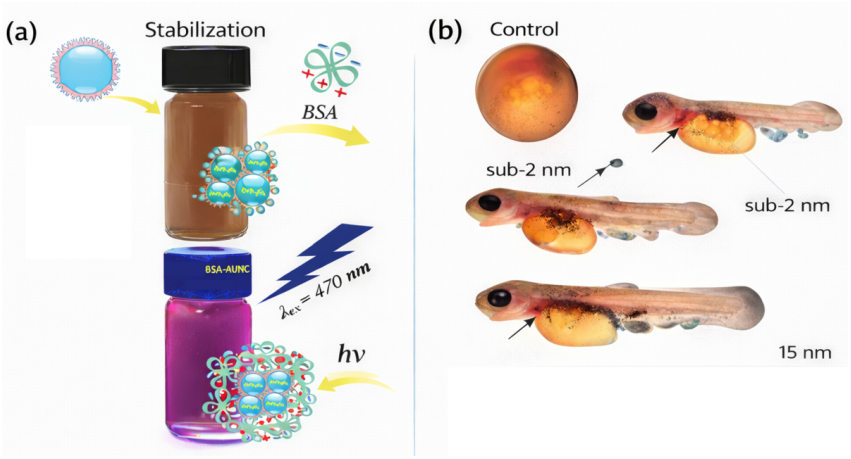


Fig. 1. Synthesis route, physicochemical properties, and biological interaction of hybrid gold nanocluster–based nanostructures.

To evaluate biological relevance, the effects of Au NCs were investigated using aquatic primary producers and consumers as model organisms. The freshwater green alga Desmodesmus communis and the cladoceran Daphnia magna were exposed to varying concentrations of Au NCs in standard laboratory media and in natural river water. In D. communis, Au NCs induced time- and concentration-dependent alterations in growth dynamics, colony structure, and photosynthetic pigment composition. After 96 h exposure, changes in chlorophyll a and carotenoid content accompanied by increased malondialdehyde levels indicated oxidative stress and membrane lipid peroxidation, with stronger effects observed in natural water matrices. In D. magna, Au NC exposure resulted in significant sub-lethal physiological and behavioral responses, including altered heart rate, swimming velocity, and total movement distance after 24–48 h. Behavioral endpoints proved more sensitive than acute toxicity, revealing early neurophysiological stress responses.

Overall, the combined physicochemical characterization and multi-species biological assessment demonstrate that the behavior and effects of Au NCs are governed by their quantum-scale structure, surface chemistry, and environmental context. These findings underscore the importance of integrating advanced nanomaterial characterization with environmentally relevant bioassays for realistic risk assessment and safe-by-design development of photoluminescent nanomaterials.

Keywords: Gold nanoclusters; Photoluminescence; Nanomaterial characterization; Aquatic toxicity; Algae; Daphnia

REDUCED GRAPHENE OXIDE AND CALCIUM-DEFICIENT HYDROXYAPATITE COMPOSITES: SYNTHESIS, STRUCTURAL AND ELECTROCHEMICAL ANALYSIS

Dovilė Burakovaitė[1], Greta Linkaitė[1], Inga Grigoravičiūtė[1], Justina Gaidukevič[1,2]

[1]Vilnius University, Faculty of Chemistry and Geosciences, Institute of Chemistry, Vilnius, Lithuania
[2]Center for Physical Sciences and Technology, Department of Nanoengineering, Vilnius, Lithuania
dovile.burakovaite@chgf.stud.vu.lt

Dopamine (DA) is one of the most important catecholamine neurotransmitters and deviations from its average dopamine concentration in blood are associated with Parkinson's and Alzheimer's diseases, depression, schizophrenia, hypertension, and heart failure [1]. Therefore, rapid and accurate determination of DA concentration is essential for the early diagnosis of these disorders. Electrochemical sensors are attracting increasing attention due to their high sensitivity, fast response, and relatively low cost, while their performance strongly depends on electrode surface properties [2]. Thus, electrode modification with graphene oxide (GO), combined with calcium-deficient hydroxyapatite (CDHA) due to its high ion adsorption capacity and biocompatibility, is expected to improve sensor stability, sensitivity, and selectivity [3].

The aim of this study was to synthesize GO/CDHA composites using wet and hydrothermal synthesis methods and to evaluate their structural and electrochemical properties for DA detection.

GO/CDHA composites were synthesized in two ways. By the wet synthesis method, a mixture of gypsum and GO (ratio 2:1) and disodium hydrogen phosphate was heated at 80 ℃ for 28 hours to obtain a CDHA rGO composite. By the hydrothermal synthesis method, a similar mixture of gypsum and GO (ratio 2:1) and disodium hydrogen phosphate was heated in a hydrothermal bomb at 180 ℃ for 12 hours to obtain a CDHA rGO hydr composite.

Structural and morphological characterization confirmed the successful synthesis of GO/CDHA composites. XRD analysis showed that the characteristic diffraction peaks of CDHA were preserved in the composite diffractograms. Raman spectroscopy revealed the presence of phosphate (PO_4^{3-}) bands of CDHA and the characteristic D and G bands of GO. Furthermore, XRD and Raman spectroscopy results indicated that samples synthesized by the wet synthesis method exhibited lower crystallinity and higher amorphousness compared to those synthesized under hydrothermal conditions. FTIR and XPS analyses confirmed the presence of functional groups and elements characteristic of both CDHA and GO in the composites.

Electrochemical studies were performed in a three-electrode cell using a phosphate buffer solution (pH 7.2). The GCE/CDHA rGO sensor demonstrated the highest sensitivity (11.11 μA $\mu M^{-1}\ cm^{-2}$) and the lowest limit of detection (LOD 100.35 nM) compared to the GCE/CDHA rGO hydr sensor. Also, this sensor showed good selectivity, as the DA current response changed slightly in the presence of other analytes, high stability – the current strength values almost did not change over 13 measurements and good repeatability – the relative standard deviation (RSD) was below 5 %. In the future, sensor performance could be further improved by expanding the linear range for analyte detection and reducing the LOD.

[1] M. Sajid, M. Baig, K. Alhooshani, "Chemically modified electrodes for electrochemical detection of dopamine: Challenges and opportunities," TrAC Trends in Analytical Chemistry, vol. 118, pp. 368-385, 2019.
[2] J. Jackowska, P. Krysinski, "New trends in the electrochemical sensing of dopamine," Anal Bioanal Chem, vol. 405, pp. 3753–3771, 2013.
[3] P. Šponer, M. Strnadová, K. Urban, "In vivo behaviour of low-temperature calcium-deficient hydroxyapatite: comparison with deproteinised bovine bone," Int Orthop, vol. 35, no. 10, pp. 1553-1560, 2011.

CHEMICALLY DRIVEN SURFACE MODIFICATION OF POROUS POLYCARBONATE MEMBRANES IN DUAL-CHANNEL MICROFLUIDIC SYSTEMS TO ENHANCE CELL ADHESION

Kamilė Kasperavičiūtė[1], Tadas Turonis[2], Wanessa Melo[1], Arūnas Stirkė[1]

[1]Center for Physical Sciences and Technology, Department of Functional Materials and Electronics, Vilnius, Lithuania
[2]Gediminas Technical University, Vilnius, Lithuania
kamile.kasperaviciute@ftmc.lt

Microfluidic and organ-on-chip technologies provide advanced platforms for in vitro modeling, however, insufficient cell adhesion on synthetic membranes remains a major technical challenge, particularly under dynamic flow conditions [1]. This study investigates multiple chemically driven surface modification strategies for porous synthetic polycarbonate (PC) membranes to enhance cell attachment, spreading uniformity, and long-term stability in dual-channel microfluidic systems [2]. PC membranes were functionalized using several chemical agents, including polyethyleneimine (PEI), dopamine hydrochloride, and other surface-active compounds, either alone or in combination with biological coatings such as collagen and fibronectin. Surface topography and physicochemical changes were characterized by atomic force microscopy (AFM) and Fourier-transform infrared spectroscopy (FTIR). Cell adhesion, morphology, and spatial distribution were evaluated using optical microscopy. Results demonstrate that chemically modified membranes exhibit significantly improved initial cell adhesion compared to untreated membranes, indicating the critical role of surface chemistry in regulating cell–material interactions. Different chemical functionalization strategies produced distinct adhesion profiles, reflected in variations in cell attachment efficiency, spreading behavior, and spatial distribution. Certain surface treatments promoted more homogeneous cell coverage and enhanced cellular spreading, suggesting improved surface compatibility. In several cases, combining chemical modification with additional surface coatings further increased attachment uniformity. Overall, this work highlights chemically driven surface functionalization as an effective strategy to overcome adhesion limitations of synthetic porous polycarbonate membranes, supporting the development of robust and reproducible dual-channel microfluidic and organ-on-chip platforms for long-term in vitro applications.

[1] S. Shrimali, D. Li, B. Knox, W. Tong, and B. Ning, “Microphysiological systems as an emerging in vitro approach for the evaluation of drug absorption, distribution, metabolism, and excretion and toxicity,” Drug Metabolism and Disposition, vol. 53, no. 12, p. 100187, Oct. 2025, doi: 10.1016/j.dmd.2025.100187.

[2] N. J. Douville, Y.-C. Tung, R. Li, J. D. Wang, M. E. H. El-Sayed, and S. Takayama, “Fabrication of Two-Layered Channel System with Embedded Electrodes to Measure Resistance Across Epithelial and Endothelial Barriers,” Analytical Chemistry, vol. 82, no. 6, pp. 2505–2511, Feb. 2010, doi: 10.1021/ac9029345.

ULTRA-TRACE DETERMINATION OF RHODIUM IN CAR EXHAUST SAMPLES USING UV PHOTOLYTIC DIGESTION AND DIFFERENTIAL PULSE VOLTAMMETRY

Islam Hassan[1,2,3], Rasa Pauliukaitė[2], Gerd-Uwe Flechsig[3]

[1]Vilnius University, Faculty of Chemistry and Geosciences, Institute of Chemistry, Vilnius, Lithuania.
[2]Centre for Physical Sciences and Technology (FTMC),Department of Nanoengineering, Vilnius, Lithuania.
[3]University of Coburg, Faculty of Applied Sciences and Health, Department of Analytical Chemistry, Coburg, Germany
Islam.hassan@chgf.stud.vu.lt

Rhodium released from automotive catalytic converters[1] has become an emerging environmental contaminant, particularly in urban particulate matter and road dust. Due to its ultra-trace concentrations and strong interactions with organic components in environmental matrices, the reliable determination of rhodium remains analytically challenging. Rhodium in environmental samples is often determined by advanced trace metal techniques, such as ICP-MS, which offer high sensitivity but rely on costly instrumentation and extensive sample preparation[2] In this study, an electrochemical approach based on adsorptive stripping voltammetry at a static mercury drop electrode (SMDE) was developed for the determination of rhodium. Particular emphasis was placed on sample pretreatment, as voltammetric measurements are strongly affected by organic interferences and limited electrochemical accessibility of metal species. To address this, ultraviolet photolytic digestion was used as a mild alternative to conventional chemical digestion, enabling effective oxidation of organic matter while minimizing contamination risk[3]. Key electrochemical parameters, including supporting electrolyte composition, solution pH, accumulation potential, and accumulation time, were evaluated. The proposed procedure provides a sensitive and cost-effective alternative electrochemical strategy for monitoring anthropogenic rhodium emissions, contributing to the environmental assessment of traffic-related pollution.

Keywords: Rhodium; Differential pulse voltammetry; Static mercury drop electrode; UV photolytic digestion; Car exhaust

[1] M. Niemelä, P. Perämäki, J. Piispanen, and J. Poikolainen, “Determination of platinum and rhodium in dust and plant samples using microwave-assisted sample digestion and ICP-MS,” Analytica Chimica Acta, vol. 521, no. 2, pp. 137–142, Jul. 2004, doi: 10.1016/j.aca.2004.05.075.

[2] K. Hašlová and S. Musil, “Sensitive and spectral Interference-Free determination of rhodium by photochemical vapor generation inductively coupled plasma mass spectrometry,” Analytical Chemistry, vol. 97, no. 6, pp. 3545–3553, Feb. 2025, doi: 10.1021/acs.analchem.4c05921.

[3] G. Woldemichael, T. Tulu, and G.-U. Flechsig, “Solar UV-treatment of water samples for stripping-voltammetric determination of trace heavy metals in Awash river, Ethiopia,” Heliyon, vol. 2, no. 3, p. e00091, Mar. 2016, doi: 10.1016/j.heliyon.2016.e00091.

COMPARATIVE STUDY OF TITANIA SUBSTRATE WETTABILITY TO PROMOTE MXENE ADHESION FOR WATER SPLITTING APPLICATION

M. Sajid[1], P. Gaigalas[1], O. Gogotsi[2], V. Klimas[1], S. Ramanavicius[1]

[1]State Research Institute Center for Physical Sciences and Technology, Department of Electrochemical Material Science, Sauletekio av. 3, LT-10257 Vilnius, Lithuania
[2]Materials Research Center, Krzhizhanovskogo street, 3, 03680, Kyiv, Ukraine
mohd.sajid@ftmc.lt

Renewable energy is widely recognized as the foundation of a sustainable and technologically advanced future. Among various clean energy modalities, hydrogen (H_2) is regarded as a promising next-generation fuel owing to its high energy density and the absence of carbon emissions upon utilization[1]. Given the abundance of water on Earth, it is considered an ideal large-scale hydrogen reservoir. Nevertheless, the realization of efficient and economically viable water splitting continues to constitute a central challenge in contemporary energy research[2], [3]. Although excellent performance in the hydrogen evolution and oxygen evolution reactions is exhibited by noble-metal-based electrocatalysts, practical implementation has been significantly constrained by their high cost. Consequently, emphasis has been placed on advanced materials and innovative engineering strategies to enable cost-effective and scalable hydrogen production. Two-dimensional (2D) materials have been identified as exceptional candidates for electrochemical water splitting, with MXenes recognized as among the most promising and rapidly expanding members of the 2D materials family[3], [4]. The development of hybrid electrodes that integrate conventional substrates with advanced nanomaterials is still regarded as challenging. The performance of electrochemical electrodes is governed by multiple interdependent factors, including structural integrity, long-term cycling stability, surface wettability to promote efficient water interaction, and robust adhesion between the catalytically active material and the underlying substrate[3], [4], [5], [6]. In this work, biocompatible and low-cost titania (TiO_2) was selected as the substrate, and a facile, solution-processed methodology was demonstrated to fabricate MXene-modified Ti electrodes with enhanced interfacial adhesion. To systematically improve the wettability and adhesion of MXene on titania, four distinct surface-modification strategies were implemented - anodization, plasma treatment, HF etching, and HF–HNO_3 surface activation, along with a multimodal surface-engineering approach. Through these treatments, the TiO_2 surface chemistry and morphology were optimized to strengthen MXene anchoring. Furthermore, the resulting Ti–MXene hybrid electrodes were comprehensively evaluated for applicability in electrochemical water splitting, and it was demonstrated that engineered interfacial properties contribute to enhanced electrode performance.

Keywords: Surface Functionalization, MXene, Adhesion, Water Splitting

[1] M. Sheng, X. Bin, Y. Yang, Z. Chen, and W. Que, 'A Green and Fluorine-Free Fabrication of 3D Self-Supporting MXene by Combining Anodic Electrochemical In Situ Etching with Cathodic Electrophoretic Deposition for Electrocatalytic Hydrogen Evolution', Adv. Mater. Technol., vol. 9, no. 3, Feb. 2024, doi: 10.1002/admt.202301694.

[2] M. Wang et al., 'A triple increase in global river basins with water scarcity due to future pollution', Nat. Commun., vol. 15, no. 1, p. 880, Feb. 2024, doi: 10.1038/s41467-024-44947-3.

[3] E. Y. Kim, J. H. Park, and G. Y. Han, 'Design of TiO2 nanotube array-based water-splitting reactor for hydrogen generation', J. Power Sources, vol. 184, no. 1, pp. 284–287, Sep. 2008, doi: 10.1016/j.jpowsour.2008.05.059.

[4] S. Ramanavicius and A. Jagminas, 'Synthesis, Characterisation, and Applications of TiO and Other Black Titania Nanostructures Species (Review)', Crystals (Basel)., vol. 14, no. 7, p. 647, Jul. 2024, doi: 10.3390/cryst14070647.

[5] R. V. Lakshmi, P. Bera, and C. Anandan, 'Surface treatment and its effect on the electrochemical behavior of Ti–15Mo–3Nb–3Al alloy', RSC Adv., vol. 6, no. 43, pp. 36345–36355, 2016, doi: 10.1039/C6RA00934D.

[6] T. Zhang et al., 'Activating Titanium Metal with H 2 Plasma for the Hydrogen Evolution Reaction', ACS Appl. Mater. Interfaces, vol. 13, no. 21, pp. 24682–24691, Jun. 2021, doi: 10.1021/acsami.1c02646.

ELECTROCHEMICAL INVESTIGATION OF POLYURETHANEBASED BINDERS FOR SODIUM ION BATTERIES

Paulina Nemaniutė-Daubarė[1], Nadežda Traškina[1], Jurgis Pilipavičius[1], Linas Vilčiauskas[1]

[1]Center for Physical Sciences and Technology, Department of Chemical Engineering and Technology, Lithuania
paulina.nemaniute@ftmc.lt

Sodium-ion batteries (SIBs) have emerged as a promising alternative to lithium-ion batteries due to the abundance and low cost of sodium precursors [1]. The development of optimal anode composition is crucial for enhancing the performance of SIBs, and polymer binders play a vital role in maintaining electrode integrity during cycling. Polyvinylidene fluoride (PVDF) is predominantly used as a binder due to its chemical stability, mechanical properties and ability to form a cohesive film [2]. Unfortunately, it is typically processed using toxic and volatile organic solvents, which raises environmental and health concerns [3]. Polyurethane (PUR) properties, such as strong adhesion, flexibility, and mechanical robustness [4], makes this polymer a promising alternative binder for sodium-ion batteries.

The aim of this work was to electrochemically investigate polyurethane in $NaTi_2(PO_4)_3$ (NTP) based electrodes in order to determine the viability as a binder for aqueous sodium ion batteries. As PUR polyol component polydiethylene glycoladipate (PDEA of 2700 g/mol) were diluted with polyethylene glycol (PEG of 200 g/mol), to decrease PDEA initial viscosity. Polyol was then reacted with a trifunctional adduct of hexamethylene -1.6- diisocyanate (HDI3) in 1.5 mol excess. Electrochemical properties of the prepared anode electrodes were evaluated by cyclic voltammetry and galvanostatic cycling.

Cyclic voltammetry measurements demonstrated that the prepared electrodes are electrochemically active, as evidence by the observed current response (Fig. 1). Galvanostatic charge/discharge cycling (GCD) was performed using beaker-type three electrode cell. The results showed quite high initial capacity.

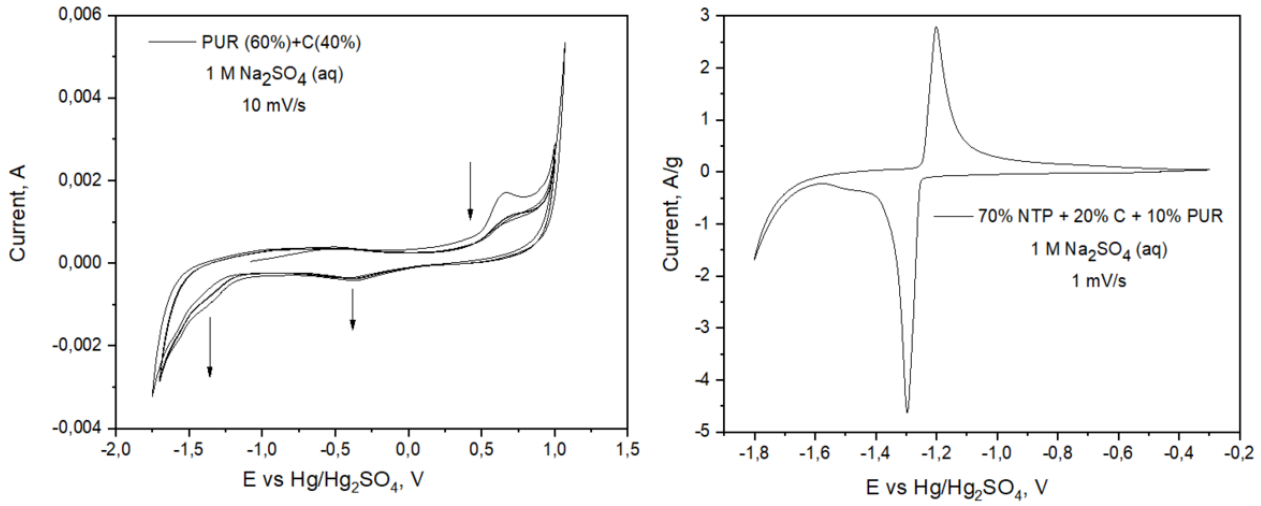


Fig. 1. Cyclic voltammograms of prepared electrodes without active material (left) and with active material (right)

[1] 1. P. Wang et al., “Suppressing the P2–O2 phase transition of NA0.67MN0.67NI0.33O2 by magnesium substitution for improved Sodium-Ion batteries,” Angewandte Chemie International Edition, vol. 55, no. 26, pp. 7445–7449, May 2016, doi: 10.1002/anie.201602202.

[2] S. Jiang, J. Zhou, H. Yang, S. Tan, Y. Wu, and C. Wang, “Ionic liquid fabricated PVDF binder for cathode toward stable and high-rate lithium-ion batteries,” Journal of Power Sources, vol. 633, p. 236439, Feb. 2025, doi: 10.1016/j.jpowsour.2025.236439.

[3] 3. S. Janakiraman, A. Surendran, S. Ghosh, S. Anandhan, and A. Venimadhav, “Electroactive poly(vinylidene fluoride) fluoride separator for sodium ion battery with high coulombic efficiency,” Solid State Ionics, vol. 292, pp. 130–135, Jun. 2016, doi: 10.1016/j.ssi.2016.05.020.

[4] F. Sun, S. Zhao, Y. Zhao, P. Zhou, and J. Zhou, “Optimizing carbonization temperature to achieve high-capacity and long-cycle hard carbon anodes from polyurethane precursors for sodium-ion batteries,” Journal of Energy Storage, vol. 132, p. 117722, Jul. 2025, doi: 10.1016/j.est.2025.117722.

POSTER SESSION 3

Laser Physics and Optical Technologies

Materials Science and Nanotechnology

Biology, Genetics and Biomedical Sciences

TIME-DEPENDENT PROPERTIES OF $ZnIn_2S_4$ THIN FILMS DEPOSITED FROM POWDER

Tautvilas Breive[1], Rokas Kondrotas[1], Arnas Naujokaitis[1], Vidas Pakstas[1], Asta Bronusiene[1]

[1]Center for Physical Sciences and Technology, Department of Characterization of Materials Structure, Lithuania
tautvilas.breive@ftmc.lt

Zinc indium sulfide (ZnIn2S4) is a promising ternary chalcogenide semiconductor for optoelectronic and energy applications due to its tunable bandgap and favorable charge carrier dynamics. Its performance in photocatalysis, photodetectors, and solar conversion is highly dependent on film stoichiometry, crystal structure, and surface morphology. This work investigates the influence of deposition duration and multi-stage temperature ramping on the quality of ZnIn2S4 thin films deposited via thermal evaporation from a powder source.

The films were deposited onto substrates using a precision-controlled temperature ramp to optimize nucleation and growth kinetics. To address initial elemental imbalances, as-deposited films underwent thermal annealing in a sulfur-rich atmosphere. This post-deposition treatment was critical for refining the grain structure and ensuring the structural integrity of the ternary phase.

Initial as-deposited films exhibited an amorphous structure and significant sulfur deficiency. While the thermal evaporation process yielded uniform, continuous films with complete coverage, post-deposition sulfurization was necessary to eliminate vacancies and achieve a near-ideal 1:2:4 stoichiometry. Experimental results indicate that increasing evaporation duration and employing a multi-step thermal profile positively correlate with stoichiometric ratio. Films deposited over extended durations reached a near-ideal ratio of 1:2:3.97. In contrast, rapid ”shock” deposition resulted in highly non-stoichiometric films (e.g., 1:1.49:3.15 and 1:2.16:4.2). This improvement is attributed to the exhaustive evaporation of the source material and the mitigation of thermal shock, ensuring a stable deposition pathway.

Structural analysis via X-ray diffraction (XRD) and Raman spectroscopy confirmed the formation of the crystalline ZnIn2S4 phase after annealing. Scanning Electron Microscopy (SEM) revealed well-defined growth patterns in the optimized films. Optical characterization demonstrated high transparency, with transmittance reaching 92% in the visible spectrum. These results showed that obtained ZnIn2S4 thin films are promising candidates for high-performance, transparent optoelectronic applications.

[1] J. Wang et al., “A review: Synthesis, modification and photocatalytic applications of ZnIn2S4,” Journal of Material Science and Technology, vol. 78, pp. 1–19, Nov. 2020, doi: 10.1016/j.jmst.2020.09.045.

[2] Z. Jing, Q. Wang, C.-M. Fan, X.-F. Yang, P.-Y. Tang, and B. Li, “ZnIn 2 S 4 -based heterostructure photocatalysts for solar energy conversion: a comprehensive review,” Journal of Materials Chemistry A, vol. 13, no. 24, pp. 18253–18282, Jan. 2025, doi: 10.1039/d5ta02501j.

[3] A. Khan, M. Danish, U. Alam, S. Zafar, and M. Muneer, “Facile Synthesis of a Z-Scheme ZnIn2S4/MoO3 Heterojunction with Enhanced Photocatalytic Activity under Visible Light Irradiation,” ACS Omega, vol. 5, no. 14, pp. 8188–8199, Apr. 2020, doi: 10.1021/acsomega.0c00446.

MODIFICATION OF MATERIAL PROPERTIES USING HIGH ENERGY ION BEAMS

Deividas Rūškys[1,2], Mindaugas Gaspariūnas[1], Vitalij Kovalevskij[1], Konstantinas Birzul[1]

[1]Center for Physical Sciences and Technology, Department of Nuclear Research, Savanorių av. 231, Vilnius, Lithuania
[2]Vilnius University, Faculty of Physics, Saulėtekio av. 9, Vilnius, Lithuania
deividas.ruskys@ftmc.lt

During the production of various semiconductor structures, it is sometimes necessary to change the properties of certain layers. This can be achieved by introducing additional defects, thereby changing the chemical or electrical properties of such structures. One of the effective methods for doping and modifying materials is ion implantation. This method of modifying semiconductor materials is one of the essential steps in the manufacturing process of integrated circuits, which form the basis of global communication and advanced computing capabilities [1]. Since the depth of the particles penetrated into the material depends on their energy, it is possible to selectively and locally modify the parameters of the structure only in a certain layer, therefore it is desirable to have the ability to implant various ions in a wide range of ion energies from few keV to several MeV. Therefore, it is essential to determine the elements and molecules sputtered from experimentally measured mass spectra of negative ion beams for different targets in low energy and acceleration branch chambers for further experiments.

In this work, a Tandetron 4100A (General Ionex Corporation, USA) tandem accelerator with a negative ion source Hiconex 834 was used. This technology is based on the use of atoms and molecules knocked out of surfaces, which, when focused into the beam, can be accelerated using high voltage. The particles are knocked out of a conical target of the desired material by a beam of positive cesium ions [2]. To determine the composition of the beam, an analyzing magnet is used, which, by changing the magnetic field strength, can deflect different ions or compounds along different trajectories. By scanning the ion beam at a selected interval, the deflected ions can be selected only by removing all unwanted ions [3]. At the same magnetic field strength, ions with a higher mass/charge ratio deflect less, and ions with a lower ratio deflect more, thus selecting the desired ions by choosing the appropriate magnetic field strength.

In mass spectrum (Fig. 1) the current value of the analyzing magnet can be used to determine which position the negative ion occupies. This value can be calculated using the formula $n\sqrt{mE}$, where n is the coefficient, m is the atomic mass (a.m.u.), and E - voltage sum of electronic focusing devices.

The measurements performed in this work can be used to implant negative ions into materials for modification and also to calibrate the parameters of the source equipment.

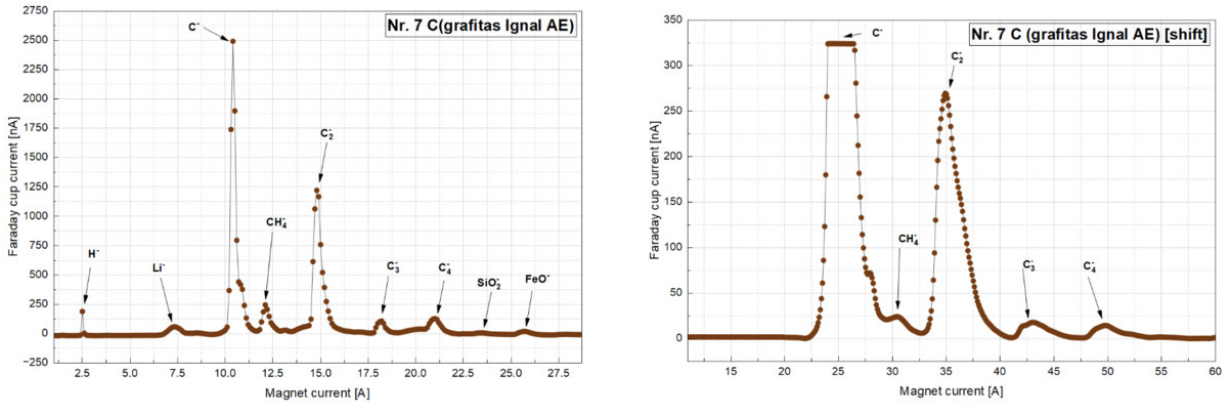


Fig. 1. Mass spectrum of a negative ion beam from a carbon target. (a) data obtained from the accelerator branch chamber, (b) - from the low energy chamber

[1] Y. Zhao et al., "Electrical spectroscopy of defect states and their hybridization in monolayer MoS2," Nature Communications, vol. 14, no. 1, p. 44, Jan. 2023, doi: 10.1038/s41467-022-35651-1.
[2] J. Ishikawa, "A heavy negative ion sputter source: Production mechanism of negative ions and their applications," Nuclear Instruments and Methods in Physics Research Section B Beam Interactions With Materials and Atoms, vol. 37–38, pp. 38–44, Feb. 1989, doi: 10.1016/0168-583x(89)90133-x.
[3] B. Schmidt and K. Wetzig, Ion beams in materials processing and analysis. 2012. doi: 10.1007/978-3-211-99356-9.

EXPERIMENTAL ESTIMATION OF HOT CARRIER TEMPERATURE IN P-N SOLAR CELLS

Jonas Petrokas[1], Jonas Gradauskas[1,2], Oleksandr Masalskyi[1,2,3], Ihor Zharchenko[1,3], Steponas Ašmontas[1], Algirdas Sužiedėlis[1], Aldis Šilėnas[1], Aurimas Čerškus[1]

[1]Center for Physical Sciences and Technology, Laboratory of Electronic Processes, Vilnius, Lithuania
[2]Vilnius Gediminas Technical University, Faculty of Fundamental Sciences, Vilnius, Lithuania
[3]Vilnius Gediminas Technical University, Faculty of Electronics, Vilnius, Lithuania
jonas.petrokas@ftmc.lt

Hot carriers (HC) are free carriers with excess energy higher than the crystal lattice temperature. In a semiconductor, light can heat the carriers in two cases. First, if the photon energy hv is lower than the bandgap E_g, the absorbed light contributes to heating through intraband transitions (Fig. 1, 1). Another possibility for creating HC is the interband absorption of photons with photon energy hv > E_g. The excess energy, hv – E_g, is used to heat the generated electron or hole (Fig. 1, 2).

The calculations of the efficiency of a single p-n junction solar cell (SC) absolutely ignore intraband absorption, which is treated as an intrinsic *"below E_g loss"* [1,2]. The indirect harmful impact of HC on the operation of a cell is considered only as a *"thermalisation loss"*; that is their excess energy is dissipated into the crystal lattice, thereby increasing lattice temperature and contributing to efficiency loss. On the other hand, despite their extremely short lifetime, HCs can provide benefits. An efficient hot carrier SC, a cell based entirely on the HC phenomenon, was proposed with efficiency reaching over 60% [3].

Thus, the role of hot carriers in photovoltaics remains ambiguous. Knowing the HC temperature is vital for modelling their influence and for guiding the design of next-generation photovoltaic devices. Various techniques were developed to determine the temperature of the hot carriers. The most of these techniques are technically demanding or strongly dependent on the material and sample structure.

This study presents an experimental method for determining the HC temperature by analyzing the hot carrier-induced photocurrent across a p-n junction [4]. The objects of investigation included industrial poly-Si solar cells manufactured by SoliTek, and GaAs p-n diodes grown by liquid-phase epitaxy. The samples were illuminated with pulsed laser radiation at wavelengths of 1.342 μm for Si and 1.064 μm for GaAs. I-V characteristics were measured at 300 K and 80 K temperatures. The temperature-induced shift of the I-V curves is quantified by the temperature coefficient. A model based on the temperature coefficient was developed providing a direct measure of hot carrier temperature [5,6]. The obtained HC temperature values are reasonable and consistent with results reported in other studies. These results advance the understanding of HC phenomena in photovoltaic devices.

Overall, the developed temperature-coefficient model offers an experimentally accessible route to determine hot carrier temperatures in solar cells. These findings enhance current insight into hot carrier generation and thermalisation, supporting future efforts to harness HC effects in advanced photovoltaic concepts.

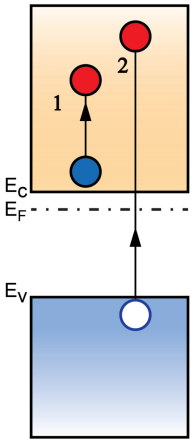


Fig. 1. Schematic illustration of hot carrier generation in a semiconductor by intraband (1) and interband (2) light absorption.

[1] W. Shockley and H. J. Queisser, "Detailed Balance Limit of Efficiency OFP-NJunction Solar cells," Journal of Applied Physics, vol. 32, no. 3, pp. 510–519, Mar. 1961, doi: 10.1063/1.1736034.
[2] L. C. Hirst and N. J. Ekins-Daukes, "Fundamental losses in solar cells," Progress in Photovoltaics Research and Applications, vol. 19, no. 3, pp. 286–293, Aug. 2010, doi: 10.1002/pip.1024.
[3] D. K. Ferry, V. R. Whiteside, and I. R. Sellers, "Pathways to hot carrier solar cells," Journal of Photonics for Energy, vol. 12, no. 02, Apr. 2022, doi: 10.1117/1.jpe.12.022204.
[4] F. Encinas-Sanz and J. M. Guerra, "Laser-induced hot carrier photovoltaic effects in semiconductor junctions," Progress in Quantum Electronics, vol. 27, no. 4, pp. 267–294, Jan. 2003, doi: 10.1016/s0079-6727(03)00002-8.
[5] I. Zharchenko, J. Gradauskas, O. Masalskyi, and A. Rodin, "Hot carrier photocurrent induced by 0.92 eV photon energy radiation in a Si solar cell," Opto-Electronics Review, p. 150181, Apr. 2024, doi: 10.24425/opelre.2024.150181.
[6] S. Ašmontas, O. Masalskyi, I. Zharchenko, A. Sužiedėlis, and J. Gradauskas, "Some Aspects of Hot Carrier Photocurrent across GaAs p-n Junction," Inorganics, vol. 12, no. 6, p. 174, Jun. 2024, doi: 10.3390/inorganics12060174.

INVESTIGATION OF HYDROGENATED GRAPHENE/Si JUNCTIONS USING LOW-FREQUENCY NOISE SPECTROSCOPY

Ingrida Pliaterytė[1], Justinas Glemža[1], Šarūnas Meškinis[2], Rimantas Gudaitis[2], Šarūnas Jankauskas[2], Asta Guobienė[2], Andrius Vasiliauskas[2], Sandra Pralgauskaitė[1], Jonas Matukas[1]

[1]Vilnius University, Institute of Applied Electrodynamics and Telecommunications, Vilnius, Lithuania
[2]Kaunas University of Technology, Institute of Materials Science, Kaunas, Lithuania
ingrida.pliateryte@ff.vu.lt

Graphene/Si junctions have attracted considerable interest for electronic and optoelectronic applications due to the combination of graphene's high carrier mobility and optical transparency with silicon's well-established fabrication technology. Direct and catalyst-free growth of both pristine and hydrogenated graphene is possible by plasma-enhanced chemical vapor deposition (PECVD). However, hydrogenated graphene can be deposited at significantly lower temperatures [1]. Moreover, hydrogenation partially opens a bandgap, enabling interface passivation and reducing dark current, making hydrogenated graphene/Si heterostructures promising for high-performance Schottky photodetectors and sensors [2]. Low-frequency noise measurements are a sensitive and non-destructive way to assess device quality and reliability, and to gain insight into underlying physical mechanisms. To date, no scientific reports have been found in the literature on the low-frequency noise characteristics of hydrogenated graphene or devices based on it. The aim of this work was to investigate the low-frequency noise characteristics of hydrogenated graphene/Si junctions and to evaluate the influence of different graphene synthesis conditions, used during the same low-temperature PECVD growth of graphene, on the observed noise behaviour.

Electrical noise measurements were performed in the 10 Hz – 60 kHz frequency range under forward and reverse bias in a wide temperature range. Depending on the different synthesis conditions used during graphene's growth, the junctions exhibited 1/f, Lorentzian (g-r), or both types of voltage noise spectra (Fig. 1). For samples that exhibited pronounced Lorentzian-type spectral components, temperature dependent noise spectroscopy was performed in order to find the charge carrier characteristic time and activation energy of the observed g-r processes, which was compared with the theoretically calculated value in [3]. Statistical analysis across multiple junctions of the same synthesis conditions samples revealed the highest noise intensity in samples where graphene was synthesized with the highest H_2/CH_4 flow ratio at the same low temperature.

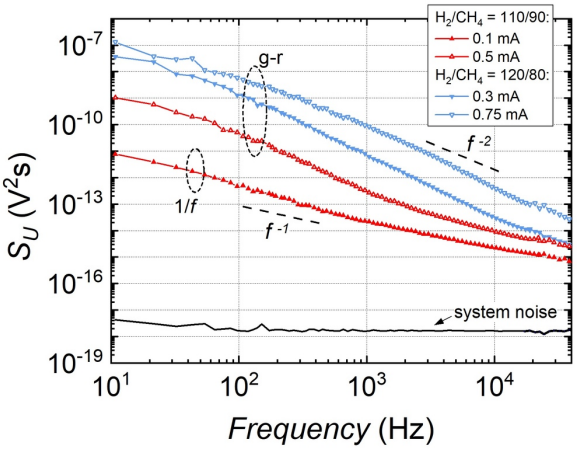


Fig. 1. Representative noise spectra at different forward currents for junctions with graphene, synthesized using different gas flow (sccm) ratios.

Keywords: fluctuations, graphene, low-frequency noise.

[1] Š. Meškinis, A. Lazauskas, Š. Jankauskas, A. Guobienė, and R. Gudaitis, "Advancing graphene synthesis: Low-Temperature growth and hydrogenation mechanisms using Plasma-Enhanced chemical vapor deposition," Molecules, vol. 30, no. 1, p. 33, 2024.
[2] J. Cong, A. Khan, P. Hang, L. Cheng, D. Yang, and X. Yu, "High detectivity graphene/si heterostructure photodetector with a single hydrogenated graphene atomic interlayer for passivation and carrier tunneling," Nanotechnology, vol. 33, no. 50, p. 505201, 2022.
[3] P. Wang et al., "Radiation-Induced Charge Trapping and Low-Frequency Noise of Graphene Transistors," IEEE Trans. Nucl. Sci., vol. 65, no. 1, pp. 156–163, 2018.

INVESTIGATION OF COPPER MICRO-PATH ELECTRODE DESIGN AND LINE SPACING ON ELECTROCHROMIC DEVICE FUNCTIONALITY

Dainius Balkauskas[1], Titas Tamošauskas[1], Modestas Sadauskas[1], Edita Voitechovič[1], Romualdas Trusovas[1], Karolis Ratautas[1], Alexandr Belosludtsev[1]

[1]Lithuania, Center for Physical Sciences and Technology, Department of Laser Technologies, Savanorių ave. 231, Vilnius 02300
dainius.balkauskas@ftmc.lt

Electrochromic devices (ECDs) are increasingly important for applications such as smart windows and adaptive optical systems, yet their performance and cost remain strongly dependent on the choice of transparent electrodes. This study addresses the challenge of replacing conventional indium-based conductors with low-cost copper while maintaining optical transparency, electrochemical stability, and device durability. The objective was to evaluate how copper line-pattern electrodes of varying geometries perform in ECDs employing PEDOT:PSS or WO_3 electrochromic layers and $LiClO_4$ or H_2SO_4 electrolytes. Transparent microscale copper electrodes were fabricated using the SSAIL technique, and devices were assembled and characterized through optical transmittance measurements, switching-speed analysis, and cycling stability tests. The results show that electrode geometry strongly influences optical modulation and switching kinetics, with narrower line spacing yielding higher transmittance but increased resistance. Electrolyte choice proved critical: PEDOT:PSS devices with $LiClO_4$ demonstrated stable operation with copper electrodes, while H_2SO_4 caused rapid copper degradation and loss of electrochromic functionality. These findings highlight the importance of electrode–electrolyte compatibility and provide practical guidelines for designing durable, cost-effective ECDs using copper-based transparent electrodes.

Keywords: Electrochromic device

ALCOHOLS OXIDATION OVER CoNb AND CoCe OXIDE-BASEDCATALYST SUPPORTS

Virginija Kepenienė[1], Raminta Stagniūnaitė[1], Jūratė Vaičiūnienė[1], Loreta Tamašauskaitė-Tamašiūnaitė[1]

[1]Center for Physical Sciences and Technology, Department of Catalysis, Vilnius, Lithuania
virginija.kepeniene@ftmc.lt

Growing environmental concerns, depletion of fossil fuels, and the demand for clean energy technologies have intensified interest in efficient and sustainable energy conversion systems. Alcohol fuel cells are considered promising alternatives due to their high energy density, low operating temperatures, ease of fuel storage, and near-zero harmful emissions [1-3]. The performance of alcohol fuel cells strongly depends on the activity, stability, and durability of the catalytic materials employed for alcohol oxidation reactions [1-3].

In this work, platinum-supported Co–Nb/C and Co-Ce/C catalysts were prepared by microwave irradiation heating to achieve uniform metal dispersion and enhanced metal–support interactions. Combintion Co–Nb and Co–Nb oxides as a supports contributed to improved catalytic performance and structural stability of prepared catalysts. The morphology and composition of the prepared catalysts have been investigated using X-ray diffraction (XRD), field-emission scanning electron microscopy (FE-SEM), and inductively coupled plasma optical emission spectroscopy (ICP-OES). Cyclic voltametry was used for investigation of PtCo–Nb/C and PtCo-Ce/C as electrocatalysts for ethanol, methanol and ethylene glycol oxidation.

The obtained results showed that the PtCo–Nb/C catalyst exhibits approximately twofold higher electrocatalytic activity toward alcohol oxidation reactions compared with the PtCo–Ce/C catalyst, highlighting the importance of catalyst design in developing efficient, low-emission energy technologies for future sustainable power generation.

[1] M. H. Nazir et al., “Liquid Metal Electrocatalyst with Ultralow Pt Loading for Ethanol Oxidation,” Small Science, vol. 5, no. 1, p. 2400370, Oct. 2024, doi: 10.1002/smsc.202400370.

[2] D. K. Madheswaran, M. Thangamuthu, S. Gnanasekaran, S. Gopi, T. Ayyasamy, and S. S. Pardeshi, “Powering the Future: Progress and Hurdles in developing proton Exchange membrane fuel cell components to Achieve Department of Energy Goals—A Systematic Review,” Sustainability, vol. 15, no. 22, p. 15923, Nov. 2023, doi: 10.3390/su152215923.

[3] M. Hren, M. Božič, D. Fakin, K. S. Kleinschek, and S. Gorgieva, “Alkaline membrane fuel cells: anion exchange membranes and fuels,” Sustainable Energy & Fuels, vol. 5, no. 3, pp. 604–637, Nov. 2020, doi: 10.1039/d0se01373k

COMPARATIVE ANALYSIS OF SAMARIUM AND GADOLINIUM DOPED CERIUM OXIDE SYNTHESIZED BY COMBUSTION AND CO-PRECIPITATION CHEMICAL METHODS FOR SOFC APPLICATION

Augustinas Zinkus[1], Mantas Sriubas[1], Tomas Šalkus[2], Brigita Abakevičienė[1]

[1]Lithuania, Kaunas, Kaunas University of Technology, Department of Physics, Institute of Materials Science
[2]Lithuania, Vilnius, Vilnius University, Faculty of Physics, Institute of Applied Electrodynamics and Telecommunications
augustinas.zinkus@ktu.lt

Hydrogen fuel cells are attracting considerable attention due to their ability to convert the chemical energy stored in hydrogen molecules into electrical energy without releasing harmful by-products into the environment. During electrochemical reactions, hydrogen is reduced to protons and oxygen is oxidized into ions, which generates an electric current and produces only heat and water [1]. This method of electricity generation helps to combat climate change because the energy produced is green. Solid oxide fuel cells (SOFCs) are highly efficient compared to other fuel cells, but their wide application is limited by their high operating temperature [2]. Reducing the operating temperature while maintaining high efficiency is a clear objective for materials scientists [3]. In this work, the electrolyte, which is responsible for ion conductivity in the cell, nanopowders are synthesized using two different chemical routes and the properties are compared respectively.

The electrolyte material is prepared by chemically synthesizing samarium and gadolinium oxide impurities into cerium oxide, obtaining nanopowders with stoichiometric formula of $Ce_{0.825}Sm_{0.0875}Gd_{0.0875}O_{2-\delta}$ (SGDC). Two different synthesis methods are used: glycine-nitrate precursor combustion and oxalate precursor co-precipitation. The produced nanopowders are examined using an X-ray diffractometer (XRD), a scanning electron microscope (SEM) and combined thermogravimetric and differential thermal analysis (TG/DTA). It has been determined that the synthesized powder must be calcinated to at least 700 °C for the crystal lattice to fully form and for the chemical residues from the synthesis to disappear (Fig. 1). It was found that nanomaterials obtained by co-precipitation reaction are more homogeneous and have a smaller average grain size than those obtained by combustion reaction. The results show that the choice of synthesis route influences the properties of the synthesized powders and must be taken into account when planning fuel cell production.

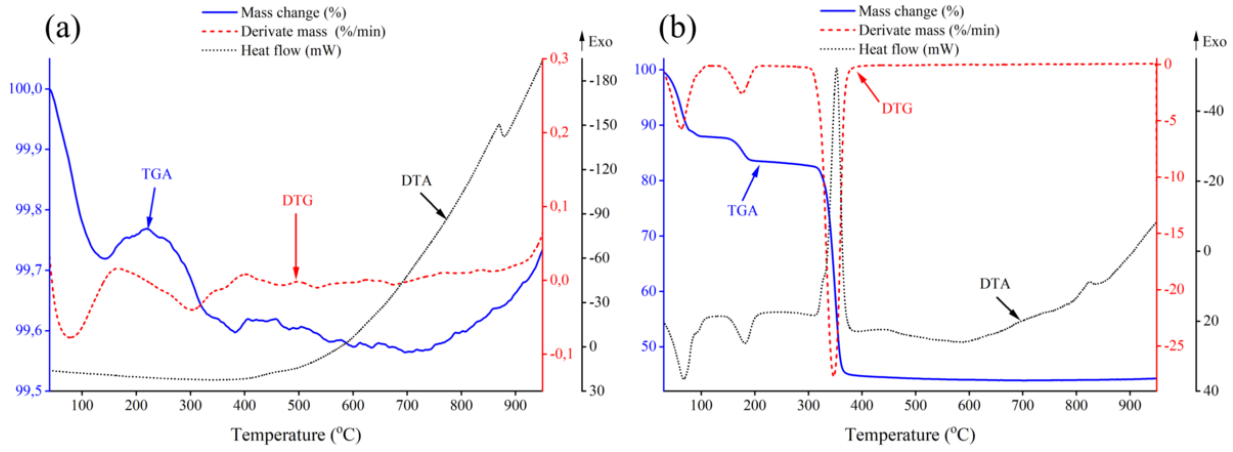


Fig. 1. Combined thermal analysis curves of SGDC nanopowders synthesised by (a) combustion and (b) co-precipitation methods

Acknowledgements

The research was funded by project No. S-MIP-24-8/2025 of the funding programme by the Research Council of Lithuania (LMT).

[1] S. Singhal, "Advances in solid oxide fuel cell technology," Solid State Ionics, vol. 135, no. 1–4, pp. 305–313, Nov. 2000, doi: 10.1016/s0167-2738(00)00452-5.
[2] A. Choudhury, H. Chandra, and A. Arora, "Application of solid oxide fuel cell technology for power generation—A review," Renewable and Sustainable Energy Reviews, vol. 20, pp. 430–442, Jan. 2013, doi: 10.1016/j.rser.2012.11.031.
[3] J. A. Kilner and M. Burriel, "Materials for Intermediate-Temperature Solid-Oxide fuel cells," Annual Review of Materials Research, vol. 44, no. 1, pp. 365–393, Apr. 2014, doi: 10.1146/annurev-matsci-070813-113426.

MANGANESE/COBALT-BASED CATALYSTS FOR METAL-AIRBATTERIES: SYNTHESIS, CHARACTERIZATION AND PROPERTIES

Kirill Grib[1], Loreta Tamašauskaitė-Tamašiūnaitė[2]

[1] Lithuania, Kaunas, Kaunas University of Technology (KTU), Faculty of Chemical Technology
[2]Lithuania, Vilnius, Center for Physical Sciences and Technology (FTMC)
kirill.grib@ktu.edu

In recent years, metal–air batteries have attracted considerable attention due to their outstanding energy storage potential, causing extensive efforts in their research and development. The oxygen reduction (ORR) and oxygen evolution (OER) reactions are key catalytic processes for sustainable energy technologies, such as water electrolysis, fuel cells or metal-air batteries. Researchers have focused on exploring various catalysts because their composition and structure strongly influence the electrochemical performance and overall efficiency of these systems. In this study, the synthesis of manganese and manganese-cobalt supported graphene composites was successfully accomplished through the utilization of microwave synthesis. The prepared samples were characterized using scanning electron microscopy, X-ray diffraction, and inductively coupled plasma optical emission spectroscopy. The composites were then used for ORR in a 0.1 M KOH solution and for OER in a 1 M KOH solution via linear sweep voltammetry (LSV). The findings indicate that the manganese-cobalt/graphene catalyst exhibits reduced overpotential and superior OER properties compared to the pure manganese/graphene catalyst. In contrast, the pure manganese/graphene catalyst exhibited a higher and more effective electrocatalytic activity toward ORR, with onset and half-wave potentials of approximately 0.86 V and 0.70 V, respectively, compared to manganese-cobalt/graphene (0.7 V and 0.6 V, respectively). These results suggest the presence of a four-electron electron transport pathway in an alkaline 0.1 M KOH solution. In contrast, a two-electron electron transport pathway was identified on the manganese-cobalt/graphene catalyst, indicating heightened hydrogen peroxide production activity.

Acknowledgements
This research was funded by a grant (No. P-SV3-25-1466) from the Research Council of Lithuania.

APPLICATION OF SPRAY DRYING FOR THE STABILIZATION OF NATURAL COLORANTS

Gabija Siaurusaitytė[1], Indrė Bernatavičiūtė[1], Rūta Gruškienė[1]

[1]Vilnius Gediminas Technical University, Faculty of Fundamental Sciences, Department of Chemistry and Bioengineering, Vilnius, Lithuania
gabija.siaurusaityte@stud.vilniustech.lt

Bio-colorants are natural pigments and dyes derived from renewable biological sources, such as plants, microorganisms and insects. They offer a sustainable, eco-friendly alternative to synthetic, petroleum-based colourants. Pigments such as chlorophylls, carotenoids and anthocyanins are used increasingly in the food, pharmaceutical and cosmetic industries [1]. Recently, vegetable residual materials have gained significant attention as a promising source of bio-colorants. Beetroot (Beta vulgaris L.) is a highly important source of natural red and purple colourants. Its characteristic colour is attributed to a group of water-soluble pigments known as betalains, which are considered to be safe, biodegradable and non-toxic alternatives to synthetic dyes. However, betalains are chemically unstable and sensitive to environmental factors such as light, oxygen, heat, pH and moisture [2]. These limitations reduce their shelf life and restrict their industrial application. One way to overcome these challenges is to encapsulate natural photochromic dyes to enhance pigment stability and protect them from degradation. Spray drying is the most commonly used encapsulation technique. It produces a stable powdered product and is already widely used in the food and pharmaceutical industries. Spray drying is considered an appropriate technique for thermosensitive compounds due to its short processing time and relatively mild thermal exposure [3]. The aim of this work was to obtain more stable betalain systems using κ-carrageenan as an encapsulating matrix and applying the spray drying method. To achieve this goal, more favorable spraying conditions were sought, such as sample composition, feed concentration and feed flow rate, inlet temperature, and spray gas flow. The most suitable spray drying conditions were selected based on the stability, antioxidant capacity and colour properties of the encapsulated dyes produced. A more detailed discussion of the results will take place during the poster session.

[1] A. Negi, “Natural Dyes and Pigments: sustainable applications and future scope,” Sustainable Chemistry, vol. 6, no. 3, p. 23, Aug. 2025, doi: 10.3390/suschem6030023.
[2] R. M. Martinez et al., “Betalains: A narrative review on pharmacological mechanisms supporting the nutraceutical potential towards health benefits,” Foods, vol. 13, no. 23, p. 3909, Dec. 2024, doi: 10.3390/foods13233909.
[3] N. F. N. N. A. Rahman, S. I. Zubairi, H. Hashim, and H. Yaakob, “Revolutionizing Spray Drying: An In-Depth analysis of surface stickiness trends and the role of physicochemical innovations in boosting productivity,” Journal of Food Quality, vol. 2024, no. 1, Jan. 2024, doi: 10.1155/2024/8929464.

DIELECTRIC SPECTROSCOPY OF PHOSPHATE-BONDED $BaTiO_3$ -$CoFe_2O_4$ MAGNETOELECTRIC CERAMICS.

Žygimantas Logminas[1], Artyom Plyushch[1], Jūras Banys[1]

[1]Vilnius university, Faculty of Physics, Institute of Applied Electrodynamics and Telecomunications, Vilnius, Lithuania
zygimantas.logminas@ff.vu.lt

In the era of artificial intelligence and machine learning, the growing need for compact, energy-efficient devices in consumer electronics and data storage has driven the search for innovative multifunctional materials that could replace conventional semiconductor technologies. Among the most promising candidates, multiferroic materials have attracted considerable attention over the past 15 years due to their exceptional physical properties and potential technological applications.

Multiferroics are materials that simultaneously exhibit two or more ferroic orders—namely ferroelectricity, ferromagnetism, and ferroelasticity. Their most important property is the magnetoelectric coupling effect, which enables magnetization to be controlled by an electric field and polarization to be influenced by a magnetic field. This coupling allows direct electrical control of magnetic properties and vice versa, paving the way for low-power devices such as magnetoelectric sensors, memory elements, spintronic components, microwave devices, and four-state logic systems, where magnetic storage bits (±M) are manipulated using electric fields (±E), thereby enhancing computing performance.

For the material to have appropriate multiferroic properties, both phases need to have a low tendency to react with each other. However, during sintering of such ceramics, they are subject to high temperatures upwards of 1000 °C. As a result unexpected and new phases may form due to interphasial diffusion and chemical reactions. Additionally, they have to retain their respective properties in the same temperature window. Such requirements reduce the possible combinations down to very few, like $BaTiO_3$ and $CoFe_2O_4$ or $NiFe_2O_4$. But even working with these materials researchers meet difficulties.

As a solution to these problems, an attempt was made to forgo the sintering step of production altogether by binding the ceramics with $AlPO_4$ – based glue. The samples were produced by dissolving $AlPO_4$ in water, which was then added to a mixture of $BaTiO_3$ and $CoFe_2O_4$ and homogenized in an agate mortar. The ceramics were formed by pressing the mixture uniaxially and then were left to cure. To speed up the curing process, samples were heated to a temperature of 300 °C for 1 hour, which is a way lower temperature than what is used during classic sintering process. In this work, dielectric properties of samples with differing grain sizes of $BaTiO_3$ and $CoFe_2O_4$ are investigated.

Keywords: Phosphate-bonded, ceramics, magnetoelectrics, non-sintered

PROCESSING AND PROPERTIES OF STARCH ESTER-BASED THERMOPLASTIC COMPOSITIONS

Klaudija Cerkaite[1], Ayodeji Amobonye[1], Joana Bendoraitiene[1], Dovile Liudvinaviciute[1], Muhammad Nasif[1], Laura Peciulyte[1], Deimante Rosliuk[1], Remo Merijs Meri[2], Shu-Kai Yeh[3]

[1]Kaunas University of Technology, Department of Polymer Chemistry and Technology, Lithuania
[2]Riga Technical University, Institute of Chemistry and Chemical Technology, Latvia
[3]National Taiwan University of Science and Technology, Department of Materials Science and Engineering, Taiwan
klaudija.cerkaite@ktu.edu

As worldwide demand for energy and consumer products continues to rise, the need for renewable resources to meet these requirements becomes increasingly urgent. For this reason, researchers are focusing on abundant, sustainable materials and exploring how they can be modified to replace products currently derived from non renewable sources. Among these materials, starch stands out as a major area of interest because it is plentiful, renewable, inexpensive, and easy to chemically and physically alter. However, the potential of natural starch to replace conventional plastics is limited because of being too hydrophilic, having poor mechanical properties and dimensional stability. By replacing the hydroxyl groups of starch with ester groups the hydrophobicity of molecules can be increased and number of hydrogen bondings reduced, thus increasing the molecular mobility and decreasing glass transition temperature of the polymer. Moreover, by incorporating plasticizers, this polymer can withstand extrusion process and can be shaped into various products.

In this study, thermoplastic starch esters were synthesized, mixed with plasticizer (polyethylene glycol or triacetin) and processed using twin-screw extrusion. The influence of the plasticizer and extrusion parameters on the properties of extrudates were evaluated.

Acknowledgements

This work was supported by the Project of Scientific Cooperation Program between Latvia, Lithuania, and Taiwan and received funding from the Research Council of Lithuania (LMTLT), agreement No S-LLT-25-4.

EFFECT OF ALKALINE TREATMENT ON STUCTURE OF HEMP SEED HULLS AND THE BIODEGRADABILITY OF THERMOPLASTIC BIOCOMPOSITES

Paulius Barvainis[1], Joana Bendoraitiene[1], Giedruna Pavuolyte[1], Laura Peciulytė[1], Dovile Liudvinaviciute[1], Ramune Rutkaite[1]

[1]Lithuania, Kaunas University of Technology, Department of Polymer Chemistry and Technology
barvainispaulius@gmail.com

Most conventional plastics originate from fossil resources and, if inadequately managed at the end of their life cycle, accumulate in the environment, contributing to greenhouse gas emissions and pollution [1,2]. Incorporating cellulose-based components, including modified cellulose and agricultural by-products such as hemp seed hulls, into biocomposite formulations not only reduces dependence on petroleum-based polymers but also supports circular-economy principles through the valorization of biomass residues.

The aim of this work is to evaluate the effect of alkaline treatment on the structure and biodegradability of biocomposites containing hemp seed hulls.

Biocomposites were obtained using hemp seed hulls (HH) as a filler in a cellulose diacetate matrix. The formation of biocomposites was carried out using a twin-screw extruder at a temperature range of 130-190 °C. To enhance interfacial adhesion between the filler and the polymer, the hulls were treated with alkali solutions at concentrations ranging from 4% to 16%. Alkaline treatment resulted in the removal of lignin, proteins and lipids from HH, thereby increasing their relative cellulose content. Hemicellulose content decreased most significantly, followed by a moderate reduction in lignin. During alkaline hydrolysis up to 29% of hemicellulose and 9% of lignin was removed without cellulose loss in HH biomass, demonstrating strong affinity between NaOH and amorphous cell wall components. However, even at higher NaOH concentrations, no evidence of cellulose mercerization was detected. XRD analysis confirmed the absence of the characteristic structural transition from cellulose I to cellulose II, indicating that alkaline treatment did not induce crystalline rearrangement in the hemp seed hulls. Instead, SEM analysis revealed pronounced surface degradation and increased roughness of the alkali treated hulls. The biocomposites with alkalized hemp hulls exhibited measurable biodegradation during the initial days of testing. Meanwhile, after 70 days approximately 29% biodegradation was reached under the applied conditions.

Obtained results show that that hemp seed hulls are suitable for the production of thermoplastic biocomposites. Alkaline treatment increases the surface roughness of the hulls, enhancing interfacial adhesion between the filler and the cellulose diacetate matrix. Moreover, biocomposites containing alkalized hulls exhibit improved biodegradability compared with untreated materials.

[1] “Plastics,” Environment. https://environment.ec.europa.eu/topics/plastics/
[2] S. Nizamuddin and C. Chen, “Biobased, biodegradable and compostable plastics: chemical nature, biodegradation pathways and environmental strategy,” Environmental Science and Pollution Research, vol. 31, no. 6, pp. 8387–8399, Jan. 2024, doi: 10.1007/s11356-023-31689-w.

ELECTRICAL PROPERTIES OF LLTO CERAMICS

Indrė Petkevičiūtė[1], Edvardas Kazakevičius[1], Dovydas Karoblis[2], Ona Balachninaitė[3]

[1]Vilnius University, Faculty of Physics, Institute of Applied Electrodynamics and Telecommunications, Vilnius, Lithuania
[2]Vilnius University, Faculty of Chemistry, Vilnius, Lithuania
[3]Vilnius University, Faculty of Physics, Laser Research Center, Vilnius, Lithuania
indre.petkeviciute@ff.stud.vu.lt

The subject of this research is lithium lanthanum titanate (LLTO). LLTO ceramics are known for their chemical stability as well as high ionic conductivity. These properties could allow for improvement of lithium-ion batteries by replacing the organic electrolyte with a solid one.

Current lithium-ion batteries have some drawbacks such as capacity loss during charge-discharge cycles causing degradation over time, as well as safety concerns. Liquid-free batteries could offer better thermal stability, absence of leakage, and a potentially longer lifespan, leading to less waste and pollution.

To learn of the physical properties of LLTO ceramics, both X-ray Diffraction (XRD) and Scanning Electron Microscopy (SEM) were used, while the electrical properties were investigated using Impedance Spectroscopy. Using these methods to investigate LLTO ceramics, a high grain boundary resistance was observed. That is not ideal and ways to lower it should be explored.

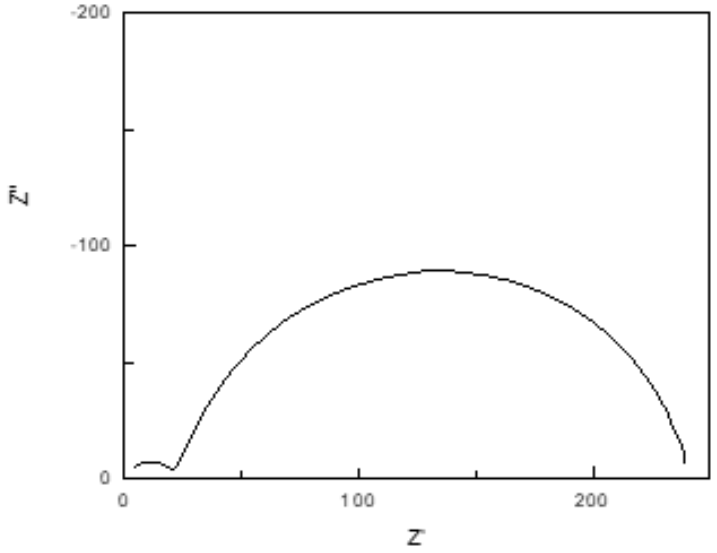


Fig. 1. Nyquist plot of LLTO ceramics at 300 K. The smaller semicircle indicates grains, while the bigger shows grain boundaries.

IMPACT OF HIGH PRESSURE ON THE STRUCTURE AND ELECTRICAL PROPERTIES OF LITHIUM VANADATE PHOSPHATE GLASS AND GLASS-CERAMICS

Łukasz Przeszłowski[1], Krzysztof Gadomski[1], Tomasz Pietrzak[1]

[1]Warsaw University of Technology, Faculty of Physics, Solid State Ionics Division, Warsaw, Poland
lukasz.przeszlowski.stud@pw.edu.pl

$LiVOPO_4$ is a promising material for battery cathodes because it can store a relatively large amount of electric charge. However, it conducts electricity poorly, which limits its practical use.

In this work, we investigate the electrical properties of $LiVOPO_4$ in glassy and glass-ceramic forms obtained by controlled thermal nanocrystallization. This synthesis approach has been systematically developed and optimized in our group over several years.

Phase formation in the synthesized materials was verified by X-ray diffraction (XRD). Thermal behavior, including glass transition and crystallization processes, was analyzed using differential thermal analysis (DTA) up to 700 °C.

To further modify the structure and enhance electrical conductivity, the samples were subjected to ultrahigh pressure and high temperature treatment (HPHT). The results reveal how extreme thermodynamic conditions influence the structure and electrical transport properties of $LiVOPO_4$-based materials.

OPTIMALIZATION OF ELECTRICAL PARAMETERS OF Bi_2O_3-Al_2O_3-SiO_2

Norbert Gąsior[1], Marcin Małys[1], Marek Wasiucionek[1], Tomasz K. Pietrzak[1], Maciej Nowagiel[1]

[1]Warsaw University of Technology, Faculty of Physics, Department of Solid State Ionics, Warsaw, Poland
01187721@pw.edu.pl

The δ phase of bismuth oxide (Bi_2O_3) is widely recognized as one of the most efficient oxide ion conductors, yet its stability is typically restricted to high temperatures above 730°C. Recent research has demonstrated that this fluorite-type phase can be effectively stabilized down to room temperature through the confinement of nanograins within an amorphous matrix [1]-[3]. The studies focused mainly on glass-ceramic composites of the ternary Bi_2O_3–Al_2O_3–SiO_2 system.

While preliminary investigations into these composites have shown promising oxygen ion transport numbers (0.89–0.94) and grain conductivities reaching 1 mS/cm at 507°C, the total conductivity remains more than an order of magnitude lower.

In this work, we aimed at bridging this gap by modifying the material's morphology through controlled thermal nanocrystallization of the glass.

A combination of in situ impedance spectroscopy, X-ray diffraction, and thermal analysis techniques allowed us to understand the processes responsible for changes in electrical parameters as a function of temperature.

Our study is the next step to enhance properties of Bi_2O_3 -based glass-ceramics, furthering their potential application as electrolytes in intermediate-temperature fuel cells.

[1] T. K. Pietrzak, J. E. Garbarczyk, and M. Wasiucionek, "Stabilization of the δ-Bi2O3-like structure down to room temperature by thermal nanocrystallization of bismuth oxide-based glasses," Solid State Ionics, vol. 323, pp. 78–84, May 2018, doi: 10.1016/j.ssi.2018.05.021.

[2] V. Vlasenko, M. Nowagiel, M. Wasiucionek, and T. K. Pietrzak, "Stabilization of δ-like Bi2O3 Phase at Room Temperature in Binary and Ternary Bismuthate Glass Systems with Al2O3, SiO2, GeO2, and B2O3," Materials, vol. 17, no. 16, p. 4023, Aug. 2024, doi: 10.3390/ma17164023.

[3] M. Nowagiel et al., "Towards a deeper insight into the stabilisation mechanism of δ-Bi2O3-like phase to low temperature by confinement of nanograins in glassy matrix," Ceramics International, Jan. 2026, doi: 10.1016/j.ceramint.2026.01.182.

SYNTHESIS OF $YFeO_3$ THROUGH OXIDE INTERMEDIATES

Evaldas Lugauskas[1], Dovydas Karoblis[1], Aivaras Kareiva[1]

[1]Vilnius University, Faculty of Chemistry and Geosciences, Institute of Chemistry, Naugarduko g. 24, LT-03225, Vilnius, Lithuania
evaldas.lugauskas@chgf.vu.lt

Yttrium ferrite ($YFeO_3$) is a material which is attributed to the perovskite structure and exhibits unique magnetic and photocatalytic properties, which are dependent on the obtained crystal structure (orthorhombic or hexagonal). Due to the stability of orthorhombic $YFeO_3$, the material has been widely studied and can be easily synthesized via various methods. In comparison, hexagonal $YFeO_3$ exhibits more intriguing properties (i.e. ferroelectric and ferromagnetic coupling [1]), but it is metastable at room temperature. To overcome this, more complicated synthesis methods need to be used.

There are two main ways to counteract the metastability of the desired material, either through utilizing fast synthesis methods to obtain the kinetic product (ultra-fast high-temperature sintering) or via thermodynamically stable byproduct formation (cometathesis). The first option has become quite popular over the last few decades, although it is difficult to control and to get reproducible results due to high temperature fluctuations [2]. On the other hand, cometathesis reactions have to be tailored for easy removal of said byproducts from the final mixture. In this work, the obtained byproducts are water-soluble calcium and magnesium salts, which can be easily washed out. Depending on the Ca and Mg precursor ratios, the synthesis temperature can be manipulated quite effectively, regarding the desired results [3].

The main goal of this research - to synthesize the hexagonal $YFeO_3$ phase, using various oxide precursors ($MgFe_2O_4$, $CaFe_2O_4$ and YOCl) in different ratios and to elucidate the dependence of the obtained product phase purity and physical properties on the synthesis conditions.

This research encompasses the synthesis and characterization of the precursor materials, their use for the synthesis of $YFeO_3$ and analysis of the obtained product.

[1] R.-L. Zhang, C.-L. Chen, Y.-J. Zhang, H. Xing, X.-L. Dong, and K.-X. Jin, “Ferroelectricity in hexagonal YFeO 3 film at room temperature,” Chinese Physics B, vol. 24, no. 1, p. 017701, Jan. 2015, doi: 10.1088/1674-1056/24/1/017701.

[2] G. C. Aragonez, M. F. Da Silva Soares, D. D. De Lima, L. F. Valandro, M. P. Rippe, and N. De Freitas Daudt, “Ultrafast high-temperature sintering of dental grade 4YSZ ceramics: Effects on microstructure and flexural strength,” International Journal of Applied Ceramic Technology, vol. 23, no. 1, Sep. 2025, doi: 10.1111/ijac.70070.

[3] A. Wustrow et al., “Lowering ternary oxide synthesis temperatures by Solid-State cometathesis reactions,” Chemistry of Materials, vol. 33, no. 10, pp. 3692–3701, May 2021, doi: 10.1021/acs.chemmater.1c00700.

PROCESS DESIGN OF MIGRATION-ENHANCED MOCVD GROWTH OF AlN AND AlGaN

Karolina German[1], Tadas Malinauskas[1], Arūnas Kadys[1]

[1]Vilnius University, Faculty of Physics, Institute of Photonics and Nanotechnology, Lithuania
karolina.german@ff.stud.vu.lt

III-nitride semiconductor membranes are promising for flexible and hybrid electronic and optoelectronic systems, enabling lightweight, transferable GaN-based devices. Graphene and van der Waals interfaces offer a route to detachable nitride layers. However, fundamental limitations restrict their practical implementation. In particular, pure remote epitaxy of GaN through graphene cannot be realized under conventional MOCVD due to graphene degradation in ammonia- and hydrogen-rich environments. GaN nucleation on graphene is difficult, leading to a low density of islands and necessitating thick overgrowth for coalescence, which is incompatible with thin membrane concepts. Low-temperature AlN provides an alternative nucleation layer with improved coverage on graphene, but shifts the growth toward a van der Waals–dominated regime limited by gas-phase parasitic reactions and reduced adatom mobility. This motivates the development of migration-enhanced MOCVD (ME-MOCVD).

This work aims to design and optimize ME-MOCVD growth of AlN and AlGaN layers for thin membrane applications. The process relies on temporal separation of metal-organic (MO) precursors (TMA, TMG) and ammonia (NH_3) exposure, combined with intermediate purge steps to suppress parasitic gas-phase reactions. Nitridation pulses of 10 s were used, while TMA and TMG were supplied either simultaneously or separately in 2 s pulses, followed by a 2 s purge after each MO and NH_3 exposure. This process design temporally separates precursor supply from surface reactions, thereby enhancing adatom mobility.

AlN and AlGaN layers were grown at 750 $^{\circ}\mathrm{C}$ and 100 mbar, with growth rates of $\sim$ 1.1 $\mathrm{\AA/s}$ for AlN and 1–1.4 $\mathrm{\AA/s}$ for AlGaN. For AlN growth, TMA flows of 35 and 17 $\mu\mathrm{mol/min}$ were used. The AlGaN composition was controlled by varying TMG flow from 8.4 to 38 $\mu\mathrm{mol/min}$ and TMA flow from 17 to 3.9 $\mu\mathrm{mol/min}$. The resulting AlN thickness was $\sim$ 105 nm, while AlGaN layers reached $\sim$ 250–340 nm. With a 16 s growth cycle, the growth per cycle corresponds to $\sim$ 6 AlGaN monolayers, exceeding typical optimal values and indicating the need for growth-rate reduction.

Finally, X-ray diffraction confirms crystalline, single-phase, c-axis-oriented AlN and compositionally tunable AlGaN layers. This study demonstrates that ME-MOCVD provides a viable and scalable pathway toward III-nitride membrane technology within conventional MOCVD, supporting flexible and hybrid electronic and optoelectronic systems.

Acknowledgements

This research was founded by the Research Council of Lithuania, project No. P-MIP-24-264, ”Development of free-standing, thin, and flexible III-nitride LED structures grown by remote epitaxy”.

Keywords: ME-MOCVD, graphene, AlN nucleation layer, heteroepitaxy.

EXCITATION-DEPENDENT PHOTOLUMINESCENCE IN GaN EPILAYERS WITH DIFFERENT DOPING CONCENTRATIONS

Aurėja Ertmanaitė[1], Jūras Mickevičius[1]

[1]Vilnius University, Faculty of Physics, Institute of Photonics and Nanotechnology, Lithuania
aureja.ertmanaite@ff.stud.vu.lt

Efficiency of light emission in GaN-based photonic devices is governed by the competition between radiative and nonradiative recombination. Both processes are strongly dependent on carrier density, including contributions from photoexcited carriers and background doping. Although GaN technology is well-established, unintentional doping remains present in GaN epilayers [1,2], complicating the interpretation of recombination dynamics. In this work, we investigate how variations in doping concentration affect the excitation-dependent photoluminescence (PL) behavior of GaN epilayers.

Twelve GaN epilayers with doping concentrations ranging from 2×10^{15} cm^{-3} to 6×10^{19} cm^{-3} were studied using PL spectroscopy. PL spectra were recorded at room temperature under excitation by a nanosecond laser (emission wavelength 266 nm) over a wide excitation power density range from 0.35 kW/cm^2 to 25 MW/cm^2. The emitted luminescence was detected using an ICCD camera, and the main emission band and its evolution was analyzed.

The PL measurements revealed clear excitation-dependent behavior, characterized by the spectral broadening, the redshift of the emission peak, and the decreasing spectral slope with increasing excitation. At the highest excitations, a narrow-stimulated emission band emerged. To quantify the overall emission response and to reveal doping-related differences, the PL spectra were integrated over the entire spectral range. As shown in Fig. 1 the integrated PL intensity exhibits a strong dependence on doping concentration, with lightly doped GaN layers displaying a steeper increase in emission intensity compared to heavily doped layers.

These results demonstrate that excitation-dependent PL behavior in GaN epilayers is strongly influenced by the background doping, especially at low excitations. Consequently, modeling of PL intensity or efficiency dependences has to explicitly account for the background carriers.

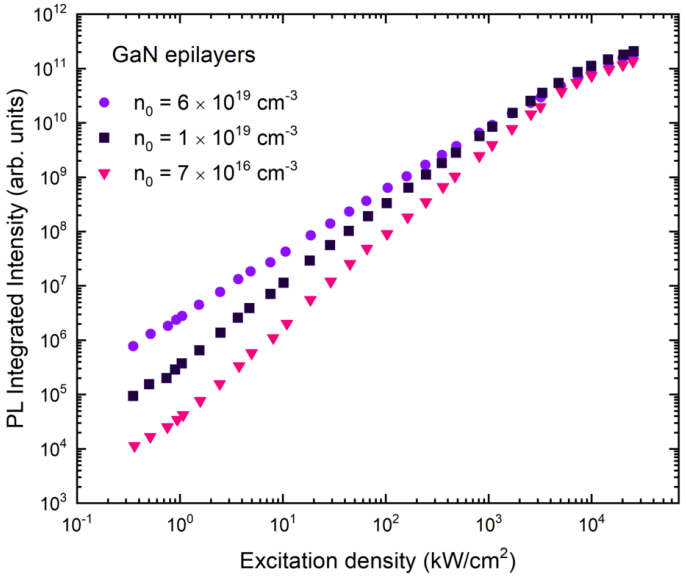


Fig. 1. Excitation dependence of integrated PL intensity for several GaN epilayers with different doping concentrations (indicated).

[1] P. Pampili and P. J. Parbrook, "Doping of III-nitride materials," Materials Science in Semiconductor Processing, vol. 62, pp. 180–191, Dec. 2016, doi: 10.1016/j.mssp.2016.11.006.
[2] T. Zhu and R. A. Oliver, "Unintentional doping in GaN," Physical Chemistry Chemical Physics, vol. 14, no. 27, p. 9558, Jan. 2012, doi: 10.1039/c2cp40998d.

STUDY OF SbSeI THIN FILM CRYSTALLIZATION

Deividas Vainauskas[1], Vidas Pakštas[1], Rokas Kondrotas[1]

[1]State research institute Center for Physical Sciences and Technology, Department of Characterisation of Materials Structure, Lithuania
deividas.vainauskas@ftmc.lt

Recently, antimony selenoiodide (SbSeI), one of the chalcohalide semiconductors that belongs to V-VI-VII class materials has been the subject of growing interest for applications, such as, solar cells, X-ray and γ-ray detection, photocatalysis, and in other optoelectronic devices. SbSeI enjoys additional benefits compared to other PV thin film systems, including the earth abundant and low toxicity chemical composition, high thermodynamic stability and large absorption coefficient (up to 10^5 cm^{-1}). Although SbSeI has very promising properties, there are few studies where this material has been used as an absorber layer in solar cells, and reported power conversion efficiency was low - 4,1 % [1]. One of the key challenges in synthesizing SbSeI thin film absorbers for PV application, is its tendency to form porous needle-like structure [2]. Because of quasi-1-dimensional crystalline structure of SbSeI, it has a preferred growth direction along [001] axis resulting in rod-shaped grain growth. The goal of this study is to find optimal annealing conditions to obtain continuous, uniform and compact morphology SbSeI thin films.

In this study we used a two-stage synthesis route where first precursor layers were deposited followed by annealing step. SbSeI precursors films were deposited under vacuum by thermal evaporation method to achieve amorphous, compact SbSeI thin film with Sb:Se:I molar ratio near 1:1:1. For crystallization stage, annealing under air atmosphere was performed with temperatures ranging from 140 ^{o}C to 190 ^{o}C with a graphite cover to prevent SbI_3 vaporisation. Properties of SbSeI thin films were characterised by XRD (θ-θ, Bragg-Brentano geometry), SEM, EDX and photoluminescence spectroscopy.

In situ XRD results showed that crystallisation onset of SbSeI begins at 100 ^{o}C , at the same time crystallinity of SbI_3 phase increases. The turning point was found about 140-150 ^{o}C, where steep drop in SbI_3 and increase of SbSeI phases was observed. SEM images of top and cross-section showed that best compact morphology was achieved at lower in 160-165 ^{o}C range. Photoluminescence studies revealed that PL signal was observed in samples annealed at temperature above 160 ^{o}C and intensity increased with increasing annealing temperature.

[1] R. Nie, M. Hu, A. M. Risqi, Z. Li, and S. I. Seok, “Efficient and Stable Antimony Selenoiodide Solar Cells.,” Advanced Science, vol. 8, no. 8, p. 2003172, Feb. 2021, doi: 10.1002/advs.202003172.

[2] I. Caño et al., “SbSeI and SbSeBr micro-columnar solar cells by a novel high pressure-based synthesis process.,” Journal of Materials Chemistry A, vol. 11, no. 33, pp. 17616–17627, Jan. 2023, doi: 10.1039/d3ta03179a.

DOPING CONTROL OF Si- AND Mg-DOPED GaN EPITAXIAL LAYERS FOR PIN DETECTOR APPLICATIONS

Gustė Jovaišaitė[1], Arūnas Kadys[1], Tadas Malinauskas[1], Dominykas Augulis[1]

[1]Vilnius University, Faculty of physics, Institute of Photonics and Nanotechnology, Vilnius, Lithuania
guste.jovaisaite@ff.stud.vu.lt

Gallium nitride (GaN) is a wide-bandgap semiconductor studied for radiation detection, optoelectronic, and high-power electronic applications due to its high radiation hardness, thermal stability, and favorable carrier transport properties [1]. In GaN PIN detector structures, precise control of dopant incorporation and free carrier concentration in epitaxial layers is essential for achieving stable and reproducible electrical performance, yet remains technologically challenging, particularly for p-type doping.

In this work, Si-doped n-GaN and Mg-doped p-GaN epitaxial layers were grown by metal–organic chemical vapor deposition (MOCVD) under varied growth temperature, pressure, and dopant precursor flow conditions. Dopant and background impurity concentration profiles were determined by secondary ion mass spectrometry (SIMS), while Hall effect measurements were employed to evaluate free carrier concentration and electron mobility in n-GaN layers. Comparison of n-GaN SIMS and Hall data reveals the influence of background donor impurities and parallel conduction paths, particularly at low intentional doping levels.

The results demonstrate that Si-doped n-GaN exhibits controllable dopant incorporation over a wide concentration range of approximately 10^{17} – 10^{19} cm^{-3}, with electron mobility values reaching up to 300 $cm^2/V{\cdot}s$ under optimized conditions. While optimized growth conditions provide the highest electron mobility, growth at elevated temperature and reduced pressure produces more uniform electrical properties across the sample surface (Fig. 1.).

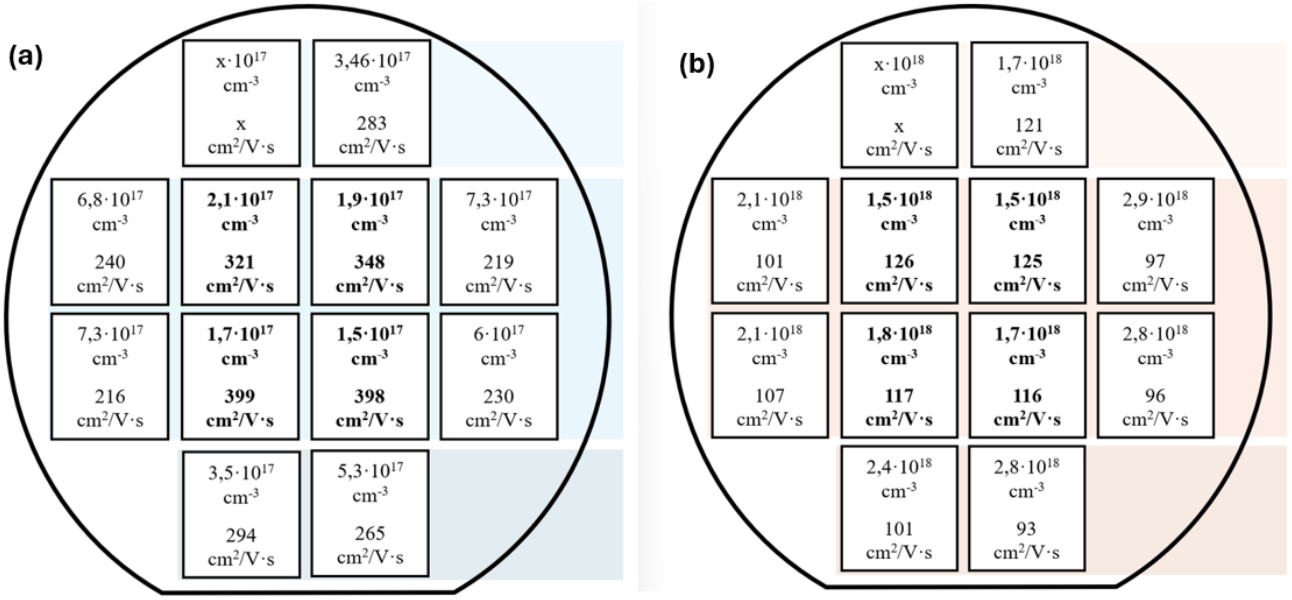


Fig. 1. Hall maps of n-GaN samples grown under the lowest SiH_4 flow rate (theoretical e^- concentration: $n=5{\cdot}10^{16}$ cm^{-3}). Electron concentration (cm^{-3}) and mobility ($cm^2/V{\cdot}s$) across the sample surface is displayed. Sample (a) was grown under 1050 °C and 800 mbar conditions, while sample (b) was grown under 1090 °C and 150 mbar conditions.

Additionally, Mg-doped p-GaN layers exhibit Mg concentrations sufficiently high for p-type operation (up to 10^{20} cm^{-3}). Nevertheless, p-type doping remains challenging due to pronounced Mg memory effects, resulting in significant Mg incorporation even in nominally undoped layers.

[1] F. Roccaforte and M. Leszczynski, Nitride Semiconductor Technology: Power Electronics and Optoelectronic Devices, p. 1-39, 2020

NARROW CAVITY CVD FOR MoS_2 FILM FORMATION FROM MoO_x PERCURSOR FILMS

Amelija Saulė Rupkutė[1], Mindaugas Kamarauskas[1], Tomas Daugalas[1], Vytautas Jakštas[1], Algimantas Lukša[1], Saulius Balakauskas[1], Ilja Ignatjev[2], Marius Treideris[1]

[1]Center for Physical Sciences and Technology, Department of Physical Technologies, Vilnius, Lithuania
[2]Center for Physical Sciences and Technology, Department of Organic Chemistry, Vilnius, Lithuania
amelija.rupkute@ftmc.lt

The future of integrated measuring systems for daily use and industry highly depends on silicon-photonics-based integrated sensors, consisting of a light source, photonic circuits and photodetectors. Typically, current systems operate in the near-infrared range. The extension of the working range into the mid-infrared range is still challenged by issues such as the low efficiency of current methods; however, such expansion would greatly improve the sensitivity of the systems and would create new possibilities for applications in various fields. From the perspective of photodetectors, on-chip 3–5 μm photodetectors and imagers with application-specific sensitivities are projected to be available by 2030 [1].

However, photodetectors functioning in the 3–5 μm range at room temperature with the possibility of integration into the silicon photonic integrated circuits (PIC) remain scarce - further research is required to find suitable materials and a design of the device's structure. In particular, Transition Metal Dichalcogenides (TMDs) are promising candidates as a material base for the infrared photodetectors. This is possible due to properties such as a high absorption coefficient and layer-dependent band gaps. Furthermore, van der Waals heterostructures allow stacking of different materials owing to weak interlayer interactions and the absence of epitaxial constraints, such as lattice constant matching [2].

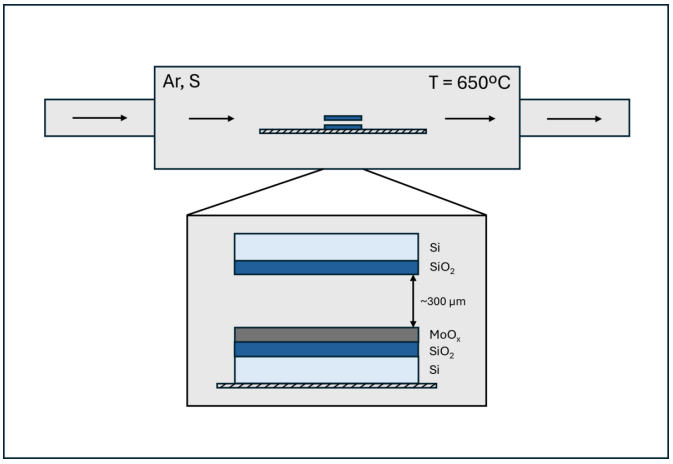


Fig. 1. Schematics of the narrow cavity CVD setup.

In this work, we present a novel narrow-cavity Chemical vapor deposition (CVD) method for the formation of MoS_2 films on SiO_2 dielectric and layer thickness control via a deposited MoO_x precursor layer. The idea is based on the sulfurization of relatively thick (5–50 nm) MoO_x films by formation of a narrow 300 μm cavity with the addition of another substrate (Fig.1).

CVD-grown MoS_2 layers were characterized by Raman scattering measurements. The resulting spectra showed typical MoS_2 layer peaks. Peak analysis showed that by controlling MoO_x precursor thickness, the resulting MoS_2 films can be obtained with a thickness ranging from 2-3 monolayers to more than 8 monolayers, with the film's crystallinity enhanced in comparison to standardized CVD sulfurization process with a single substrate setup.

[1] R. Chandrasekar, Z. J. Lapin, A. S. Nichols, R. M. Braun, and A. W. Fountain, "Photonic integrated circuits for Department of Defense-relevant chemical and biological sensing applications: state-of-the-art and future outlooks," Optical Engineering, vol. 58, no. 02, p. 1, Feb. 2019, doi: 10.1117/1.oe.58.2.020901.

[2] V. Selamneni and P. Sahatiya, "Mixed dimensional Transition Metal Dichalcogenides (TMDs) vdW Heterostructure based Photodetectors: A review," Microelectronic Engineering, vol. 269, p. 111926, Dec. 2022, doi: 10.1016/j.mee.2022.111926.

LOW MELTING TEMPERATURE LANTHANUM-LEAD-BISMUTH ALLOYS

Abdul Mannan Majeed[1], Sandra Stanionytė[2], Gediminas Kreiza[3], Šarūnas Vaitekonis[4], Vidmantas Kalendra[5], Patrik Ščajev[6], Algirdas Mekys[7]

[1]Vilnius University, Faculty of Physics, Institute of Photonics and Nanotechnology, Lithuania
[2]Center for Physical Science and Technology, Lithuania
[3]Vilnius University, Institute of applied electrodynamics and telecommunications, Lithuania,
mannan.majeed@ff.vu.lt

As a chemical element, La appears in many electronic applications, including superconductors, most notably LaH_{10}, which holds the record for a superconducting transition temperature of 230 K [1]. The fabrication of surface-engineered devices containing La sometimes requires handling the element in a solid form protected from atmospheric exposure. Elemental La is highly chemically reactive; however, when dissolved in alloys, it becomes protected against oxidation. In this work, La was incorporated into a so-called metal-flux alloy of Pb–Bi (45:55) at a much lower temperature (<300 °C) than the melting temperature of pure La (>900 °C). The resulting metal mixture demonstrates chemical stability against oxidation. Structural analysis using SEM, EDX, and XRD revealed non-equilibrium behavior of the melted alloys (in the temperature range of 180–420 °C), accompanied by elemental reorganization into more stable phases, namely Bi_2La (melting temperature 932 °C) and $Pb_{70}Bi_{30}$, as shown in Fig. 1. The newly developed soft La–Pb–Bi alloy enables safe handling and machining of La-rich materials at room temperature and opens new kinetic pathways for La–Bi phase formation, diffusion bonding, cold alloying, and liquid-metal-based delivery of La to substrates.

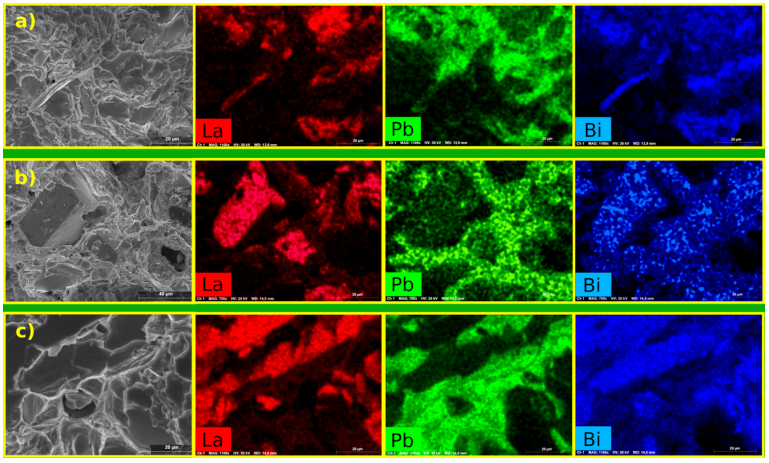


Fig. 1. Fig. 1. Visualization of chemical element distributions by SEM–EDX for three different alloys with La contents of 10 wt% (a), 20 wt% (b), and 22 wt% (c). Darker regions correspond to lower concentrations of the given element.

Acknowledgements
This research was funded by the Research Council of Lithuania, project No S-MIP-24-81.

Keywords: Superconductors, Alloys

[1] A. P. Drozdov et al., “Superconductivity at 250 K in lanthanum hydride under high pressures,” Nature, vol. 569, no. 7757, pp. 528–531, May 2019, doi: 10.1038/s41586-019-1201-8.

YAG-BASED HIGH-ENTROPY GARNETS: SYNTHESIS AND CHARACTERIZATION

Diana Vištorskaja[1], Artūras Katelnikovas[1], Aivaras Kareiva[1]

[1]Vilnius University, Faculty of Chemistry and Geosciences, Institute of Chemistry, Vilnius, Lithuania
diana.vistorskaja@chgf.vu.lt

The continuous engineering of advanced materials with tailorable properties remains a key scientific challenge, driven by the rapidly growing demands of modern industry and technology [1]. Since 2004, when a new alloy design strategy combining multiple elements in equimolar ratios was introduced, the term ”high entropy” has become widely used. This concept led to the development of high-entropy oxides (HEOs) – single-phase solid solution with five or more elements randomly distributed on equivalent lattice sites, in which the configurational entropy by mixing works as a driving force for stabilization [1, 2]. Multicomponent HEOs combine exceptional structural stability with a wide spectrum of functional properties, making them suitable for applications in energy storage, catalysis, optics, photothermal, and ferroelectric devices [1, 3].

Yttrium aluminium garnet (YAG) is a well-established optical host material, exhibiting broad optical transparency from the ultraviolet to the infrared region, high thermal and chemical stability [4]. The garnet structure, with general formula $A_3B_2C_3O_{12}$ and cubic space group, offers exceptional compositional flexibility through three distinct cation sublattices, enabling substitution of A-site yttrium(III) ions with various rare-earth elements and B/C-site aluminium(III) ions with transition or post-transition metals. This structural adaptability allows high lanthanide doping levels without concentration quenching, making YAG a key material for multicolour phosphors, solid-state lasers, and scintillators [5].

Recently, high-entropy strategies have emerged as a promising approach to tune the structural and optical properties of garnet-based materials. However, research on high-entropy rare-earth aluminium garnets remains at an early stage. In this work, high-entropy rare-earth aluminium garnets with novel chemical compositions were synthesized by the sol-gel method at 1000 degrees C. The sol-gel synthesis method was selected due to its ability to produce multicomponent systems with a high level of phase purity and homogeneity at relatively low temperatures. Furthermore, this approach has not previously been applied to the synthesis of YAG-based high-entropy oxides, thereby offering new insight and strong motivation for the present study. The structural properties of the obtained samples were characterized using XRD and FTIR techniques, while their morphology was evaluated by SEM analysis. Elemental composition was determined by SEM-EDX and ICP-OES methods. In addition, the optical properties of the synthesized materials were investigated by recording their emission and excitation spectra.

[1] J. Li, M. Fiato, and Y. Wu, “Transparent high entropy garnet ceramics by SPS,” Journal of the European Ceramic Society, vol. 44, no. 13, pp. 7846–7854, May 2024, doi: 10.1016/j.jeurceramsoc.2024.05.063.
[2] B. L. Musicó et al., “The emergent field of high entropy oxides: Design, prospects, challenges, and opportunities for tailoring material properties,” APL Materials, vol. 8, no. 4, Apr. 2020, doi: 10.1063/5.0003149.
[3] X. Gu, X.-B. Guo, W.-H. Li, Y.-P. Jiang, Q.-X. Liu, and X.-G. Tang, “High-Entropy materials for application: electricity, magnetism, and optics,” ACS Applied Materials & Interfaces, vol. 16, no. 40, pp. 53372–53392, Sep. 2024, doi: 10.1021/acsami.4c11898.
[4] B. Bettes and Y. Xie, “Synthesis and processing of transparent polycrystalline doped yttrium aluminum garnet: a review,” Materials Research Letters, vol. 11, no. 1, pp. 1–20, Sep. 2022, doi: 10.1080/21663831.2022.2109441.
[5] W. Cao et al., “Highly Nonstoichiometric YAG Ceramics with Modified Luminescence Properties,” Advanced Functional Materials, vol. 33, no. 14, Jan. 2023, doi: 10.1002/adfm.202213418.

VACUUM BASED SYNTHESIS OF $AgBiS_2$ THIN FILMS BY MAGNETRON SPUTTERING AND SULFURIZATION

J. Dubikaltis[2], R. Giraitis[1], M. Frankevičius[1], A. Sekskienė[1], V. Pakštas[1]

[1]Center for Physical Sciences and Technology (FTMC), Vilnius, Lithuania
[2]Vilnius University, Faculty of Physics, Vilnius, Lithuania
dubikaltis.juozas@gmail.com

Silver bismuth sulfide ($AgBiS_2$) is a promising lead-free ternary chalcogenide semiconductor for optoelectronic and photovoltaic applications due to its suitable bandgap (1.0–1.1 eV), strong optical absorption, and environmentally benign composition. In this work, $AgBiS_2$ thin films were synthesized on fluorine-doped tin oxide (FTO)–coated glass substrates using a vacuum-based approach combining magnetron sputtering and post-deposition sulfurization. Metallic precursor layers were sequentially deposited by magnetron sputtering using two different stacking orders: Ag (40 nm) / Bi (80 nm) and Bi (80 nm) / Ag (40 nm), followed by sulfurization in sulfur vapor at temperatures of 250, 350, and 450 °C for approximately 30 min. The structural properties and phase composition of the films were investigated by X-ray diffraction (XRD), while the surface and cross-sectional morphologies were examined using scanning electron microscopy (SEM). The results show that both sulfurization temperature and metal stacking order strongly influence $AgBiS_2$ formation and film quality. Films prepared using the Ag/Bi configuration exhibit more efficient sulfur incorporation, improved Ag–Bi interdiffusion, and a significantly more compact and uniform morphology compared to the inverse Bi/Ag configuration. Increasing the sulfurization temperature promotes the transformation of intermediate binary sulfides into the ternary $AgBiS_2$ phase, with optimal film quality obtained at intermediate sulfurization temperatures. The demonstrated synthesis route provides good control over film structure and highlights the importance of precursor design for scalable vacuum-based fabrication of $AgBiS_2$ thin films for sustainable optoelectronic and photovoltaic applications.

Acknowledgements
This research was supported by the Research Council of Lithuania (LMTLT) through Grant No. S-MIP-25-76.

Keywords: Green optoelectronic materials, Thin films, Magnetron sputtering

[1] C. Gao, S. Sun, J. Liu, T. Shen, and Y. Zhu, “Synthesis of magnetron sputtered AgBiS2 thin films,” Functional Materials Letters, vol. 14, no. 04, p. 2150017, Apr. 2021, doi: 10.1142/s179360472150017x.

OPTICAL DLTS STUDY OF RADIATION-INDUCED DEFECTS IN BORON-DOPED LGAD DETECTORS

Joris Plaščinskas[1], Tomas Čeponis[1], Jevgenij Pavlov[1]

[1]Vilnius University, Faculty of Physics, Institute of Photonics and Nanotechnology (IPN), Lithuania, Vilnius
joris.plascinskas@ff.stud.vu.lt

Boron-doped p-type LGAD detectors are expected to play an important role in future CERN experiments owing to their excellent timing performance [1]. However, these detectors remain sensitive to radiation damage, in particular to the so-called acceptor removal effect, in which irradiation leads to an apparent deactivation of dopant atoms [2]. The optical deep-level transient spectroscopy (O-DLTS) technique enables the investigation of irradiated LGAD sensors in cases where conventional DLTS methods are not applicable. Such sensors are promising for applications in high-energy physics experiments, advanced medical diagnostic technologies, and space applications [3]. DLTS measurements of irradiated LGAD structures are usually performed on PiN diodes designed to replicate the electrical properties of the LGAD multiplication layer. In this work, an alternative approach is proposed to obtain information on radiation-induced defects directly from LGAD detectors. The main challenge is the drastic decrease in capacitance observed in irradiated LGADs; however, background illumination can partially restore the capacitance and enable DLTS measurements.

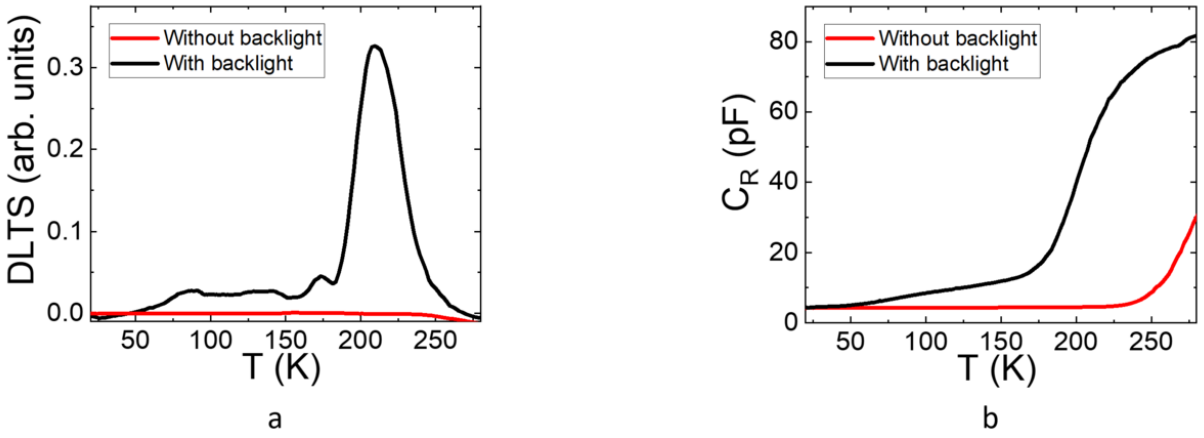


Fig. 1. a - DLTS spectra of proton-irradiated (Φ=1×1013cm-2) LGAD with and without backlight. b - The temperature dependence of the barrier capacitance (UR=25V) with and without backlight.

The measurements show (fig.1) that backlight illumination can help to take information from irradiated LGAD. The measurements demonstrate that background illumination provides an effective method for obtaining defect-related information directly from irradiated LGAD diodes. These results offer new insight into defect characterization in radiation-damaged semiconductor materials and will be presented and discussed at the conference.

Keywords: DLTS, LGAD, defects, semiconductor, Si.

[1] E. Curras, M. Fernandez, and M. Moll, “Gain suppression mechanism observed in low-gain avalanche detectors,” Nucl. Instrum. Methods Phys. Res. A, vol. 1031, p. 166530, 2022.
[2] M. Moll, “Acceptor removal—Displacement damage effects involving the shallow acceptor doping of p-type silicon devices,” Proc. Sci., Vertex2019, p. 27, 2020.
[3] W. Kruger, T. Bergauer, T. Galatyuk et al., “LGAD technology for HADES, accelerator and medical applications,” Nucl. Instrum. Methods Phys. Res. A, vol. 1039, p. 167046, 2022.

GERMANIUM(II) SULFIDE THIN FILMS FOR VISIBLE-LIGHT PHOTODETECTORS

Andrej Vedernikov[1,2], Audrius Drabavičius[1]

[1]Department of Characterization of Materials Structure, State research institute Center for Physical Sciences and Technology, Sauletekio av. 3, Vilnius, Lithuania
[2]Vilnius University, Department of Inorganic Chemistry, Naugarduko g. 24, Vilnius, Lithuania
andrej.vedernikov@ftmc.lt

The growing demand for ultra-low-light, high-gain, and energy-efficient visible-light photodetectors in imaging, sensing, and optoelectronic systems exposes fundamental limitations of conventional silicon-based CMOS technologies, particularly in the red and low-photon-flux regimes, where limited absorption depth and carrier collection efficiency restrict responsivity. Achieving high photoconductive gain at low operating voltages remains a key challenge, motivating the exploration of alternative semiconducting materials and device architectures. In this context, layered and quasi-two-dimensional materials offer enhanced light–matter interaction and tunable carrier transport, although scalable fabrication and defect control remain major obstacles. [1,2]

Polycrystalline germanium(II) sulfide (GeS) emerges as a promising low-toxicity, air-stable p-type semiconductor with a suitable bandgap (1.6 eV) for visible-light detection, enabling efficient photon absorption in the visible spectrum. In this work, GeS thin films are synthesized by rapid thermal evaporation (RTE), a simple and scalable deposition technique compatible with large-area device fabrication. [3] Thin films are deposited on quartz and interdigitated electrode substrates, followed by controlled post-deposition annealing to induce crystallization, grain growth, and defect redistribution. Furthermore, intentional doping is employed to modulate carrier concentration, trap density, and Fermi-level position, directly impacting photocarrier lifetime and transport.

Structural and morphological characterization using X-ray diffraction and scanning electron microscopy confirms the formation of homogeneous and reproducible polycrystalline GeS films after annealing. The optoelectronic performance of GeS-based photodetectors is evaluated through current–voltage measurements under visible-light illumination. Enhanced responsivity and specific detectivity are achieved through the combined effects of doping and thermal post-treatment, attributed to improved carrier mobility, reduced recombination, and increased photoconductive gain arising from trap-assisted charge transport.

These results demonstrate that rapid thermal evaporation, combined with post-deposition electronic structure engineering, provides a viable pathway toward low-power, high-gain visible-light photodetectors based on scalable polycrystalline GeS thin-film technology.

[1] Audrius Drabavičius et al., “High-Performance GeS Thin Film Photodetectors Obtained via Sulfurization and Boron Doping,” ACS Applied Optical Materials, vol. 3, no. 9, pp. 2232–2240, Sep. 2025, doi: https://doi.org/10.1021/acsaom.5c00312.
[2] E. Sutter, B. Zhang, M. Sun, and P. Sutter, “Few-Layer to Multilayer Germanium(II) Sulfide: Synthesis, Structure, Stability, and Optoelectronics,” ACS Nano, vol. 13, no. 8, pp. 9352–9362, Jul. 2019, doi: https://doi.org/10.1021/acsnano.9b03986.
[3] H. Song et al., “Rapid thermal evaporation of Bi2S3 layer for thin film photovoltaics,” Solar Energy Materials and Solar Cells, vol. 146, no. 0927–0248, pp. 1–7, Nov. 2015, doi: https://doi.org/10.1016/j.solmat.2015.11.019.

SURFACE ENGINEERING BY LASER BEAM IN PRISTINE AND PROTON IRRADIAED GaN

Mykolas Strigūnas[1], Jevgenij Pavlov[1], Tomas Čeponis[1]

[1]Vilnius University, Faculty of Physics, Institute of Photonics and Nanotechnology, Lithuania
mykolas.strigunas@ff.stud.vu.lt

Gallium nitride (GaN) is widely employed in optoelectronic and high-power electronic applications due to its wide bandgap, high breakdown field, and robustness in harsh environments [1]. Nevertheless, both native and radiation-induced defects are known to strongly influence its optical and electrical performance. In particular, proton irradiation is known to introduce vacancy-related and deep-level defects, which significantly alter carrier lifetime, recombination dynamics, and conductivity, posing critical challenges for GaN-based devices operating in radiation-rich environments. Previous studies have shown that thermal annealing can partially modify or anneal irradiation-induced defects in GaN; however, such processes lack spatial selectivity and require high global temperatures. In contrast, laser beam processing is considered a localized and contact-free approach to surface engineering, enabling precise energy delivery and potentially distinct defect-modification mechanisms compared to conventional thermal treatments [2].

In this work, a systematic study of laser-induced surface modification in both pristine and proton-irradiated GaN layers is proposed. The effects of laser–matter interaction on defect-related optical and electronic properties are intended to be investigated. By comparing laser-processed and unprocessed regions, the feasibility of laser irradiation as a controllable tool for defect engineering or partial damage mitigation in irradiated GaN is to be explored. Optical characterization techniques, including microwave photoconductivity and time-integrated photoluminescence, are planned to be employed to probe changes in carrier dynamics and defect activity. This study is intended to contribute to the understanding of laser-based surface engineering of GaN and its potential role in tailoring material properties for radiation-tolerant devices. The results will be presented at the conference.

[1] T. Ceponis et al., “Combined techniques for recovery of radiation damaged detectors,” Materials Science in Semiconductor Processing, vol. 168, p. 107863, Sep. 2023, doi: 10.1016/j.mssp.2023.107863.

[2] Y. Jiang, H. Tan, and Y. Zhao, “Improving Optical and Electrical Properties of GaN Epitaxial Wafers and Enhancing Luminescent Properties of GaN-Based Light-Emitting-Diode with Excimer Laser Irradiation,” Symmetry, vol. 13, no. 10, p. 1935, Oct. 2021, doi: 10.3390/sym13101935.

CHARACTERIZATION OF INITIAL DEFECT LANDSCAPES AND METHODOLOGY DEVELOPMENT FOR LGAD-RELATED P-TYPE SILICON APPLICATIONS

Faustina Kiaušaitė[1], Tomas Čeponis[1], Jevgenij Pavlov[1]

[1]Vilnius University, Faculty of Physics, Institute of Photonics and Nanotechnology, Vilnius, Lithuania
faustina.kiausaite@ff.stud.vu.lt

Low-Gain Avalanche Detectors (LGADs) represent a promising technology for high-energy physics, particularly for the ATLAS and CMS experiments at CERN, due to their high-precision timing performance. However, the radiation-induced deactivation of dopants - known as the Acceptor Removal Effect [1] - remains a critical challenge for the boron-doped gain layer.

This study was carried out within the CERN DRD3 WP3 (WG3) project [2], “Defect engineering in PAD diodes mimicking the gain layer in LGADs.” The project investigates the acceptor removal process (ARP) in irradiated LGAD gain layers to understand and parameterize its behavior as a function of boron, carbon, oxygen concentrations and irradiation fluence. The objective is to identify defect-engineering strategies that enhance radiation hardness.

Thermally Stimulated Current (TSC) spectroscopy was performed on non-irradiated and neutron irradiated p-type silicon PIN diodes to imitate the LGAD gain layer [3]. The sample set includes Diffusion Oxygenated Float Zone (DOFZ) and phosphorus-doped (P-plateau) substrates, with carbon co-implanted at fluences from 5×10^{12} to 5×10^{14} cm^{-2}. TSC was selected to bypass capacitance-related distortions in highly-doped structures, ensuring more accurate defect characterization compared to other transient methods [4].

A significant focus was placed on developing and optimizing the experimental setup for high-sensitivity TSC measurements. The setup used a Keithley 6430 electrometer and Lake Shore 336 controller, automated via custom LabVIEW. Samples were cooled under reverse bias, followed by trap filling through forward bias injection (60–360 s). During heating at a constant rate β, the resulting current I_{TSC} was recorded against temperature to characterize structural defects from spectral peaks [1].

Defect parameters, including activation energy (E_a) and capture cross-section (σ), are extracted from I_{TSC} signals using Arrhenius plots of $\ln(T_m^4/\beta)$ versus $1/T$. Trap concentration (N_t) is determined by integrating TSC peaks after background subtraction [4]. This initial characterization provides the baseline for investigating radiation-induced changes, with higher trap densities expected at the maximum carbon fluence of 5×10^{14} cm^{-2}.

Overall, carbon co-implantation combined with DOFZ substrates is expected to be the most effective strategy to withstand the acceptor removal effect and enhance radiation tolerance. These findings will be presented and discussed at the conference.

[1] A. Himmerlich et al., ”Defect characterization studies on irradiated boron-doped silicon pad diodes and Low Gain Avalanche Detectors,” Nucl. Instrum. Methods Phys. Res. A, vol. 1048, p. 167977, 2023.
[2] https://drd3.web.cern.ch/wg3
[3] G. Pellegrini et al., ”Technology developments and first measurements of Low Gain Avalanche Detectors (LGAD) for high energy physics applications,” Nucl. Instrum. Methods Phys. Res. A, vol. 765, pp. 12–16, 2014.
[4] P. Blood and J. W. Orton, The Electrical Characterization of Semiconductors: Majority Carriers and Electron States. San Diego, CA, USA: Academic Press, 1992

DIRECT CURRENT INJECTION EFFECTS ON RADIATION-INDUCED DEFECT DYNAMICS IN SILICON AND SILICON GERMANIUM SENSORS

Adelija Garšvaitė[1], Tomas Čeponis[1], Jevgenij Pavlov[1]

[1]Vilnius University, Faculty of Physics, Institute of Photonics and Nanotechnology, Vilnius, Lithuania
adelija.garsvaite@ff.stud.vu.lt

Silicon–germanium (SiGe) alloys exhibit strong potential for the fabrication of radiation-tolerant detectors intended for high-energy physics experiments, advanced medical diagnostics, and space applications. Despite their importance, the formation of radiation defects in p-type SiGe structures have not been fully explored, thus, analyzing how these defects can be manipulated or removed using methods such as current injection, annealing, etc. is remarkable for enhancing the durability of next-generation detectors [1].

This work investigates the effects of direct current injection on radiation-induced defects in p-type silicon (Si) and silicon–germanium (SiGe) diodes. The aim of the study is to determine changes in metastable and bistable defects induced by direct current injection in irradiated detectors using deep-level transient spectroscopy (DLTS). Si diodes grown by the Czochralski and epitaxial methods, as well as SiGe diodes containing 1% and 5% Ge, were irradiated with electrons and alpha particles.

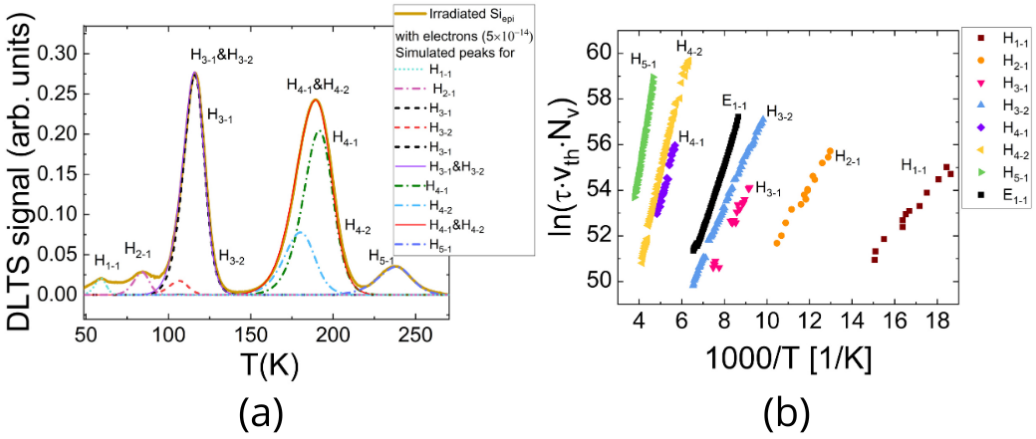


Fig. 1. a - DLT spectra of majority-carrier traps in the electron-irradiated epitaxial Si sample. b - Corresponding Arrhenius plots.

The experimental results demonstrate that direct current injection promotes the transformation of divacancy (V_2) defects into trivacancy (V_3) defects [2] and leads to an approximately twofold increase in the concentration of complexes involving two interstitial atoms and oxygen (I_2O). These findings provide insights into defect transformations induced by current in irradiated semiconductor materials and will be presented at the conference.

Keywords: Si, SiGe, radiation defects, DLTS, defect transformation, annealing.

[1] L. F. Makarenko et al., “Formation of a bistable interstitial complex in irradiated P-Type silicon,” Physica Status Solidi (A), vol. 216, no. 17, Jun. 2019.
[2] J. Coutinho et al., “Electronic and dynamical properties of the silicon trivacancy,” Physical Review B, vol. 86, no. 17, Nov. 2012.

SYNTHESIS AND CHARACTERIZATION OF NICKEL TUNGSTEN CATALYST

Lukas Šimkus[1], Gitana Valeckytė[1], Zita Sukackienė[1], Jūratė Vaičiūnienė[1], Loreta Tamašauskaitė-Tamašiūnaitė[1], Eugenijus Norkus[1]

[1]Center for Physical Sciences and Technology (FTMC), Department of Catalysis, Vilnius, Lithuania
lukassimkus99@gmail.com

Hydrogen is widely recognized as a key energy carrier for the transition toward a sustainable energy system [1,2]. However, the majority of hydrogen production currently relies on non-renewable fossil resources, resulting in significant carbon emissions [3]. While carbon capture technologies enable the transition from gray to blue hydrogen, truly sustainable green hydrogen production remains commercially limited [4]. As a result, alternative hydrogen generation routes that avoid direct CO_2 emissions are of considerable interest. One promising approach is the hydrolysis of borohydrides, which enables efficient hydrogen release without carbon byproducts [5]. The effectiveness of this process strongly depends on the availability of cost-efficient and active catalysts, particularly those based on non-noble metals. In this context, electrolessly deposited nickel–tungsten catalysts supported on copper substrates represent a viable and scalable solution for borohydride-based hydrogen generation.

In the present study, the synthesis of $Ni_{93}W_7$/Cu, $Ni_{91}W_9$/Cu, $Ni_{89}W_{11}$/Cu, $Ni_{87}W_{13}$/Cu, and $Ni_{85}W_{15}$/Cu catalysts was accomplished through the chemical method of metal deposition. The surface morphology, internal structure and chemical composition of the obtained catalysts were analyzed using field emission scanning electron microscopy, X-ray photoelectron spectroscopy and inductively coupled plasma optical emission spectroscopy. It was determined that the prepared coating particles consist of oval-shaped agglomerates. The composition of the catalysts was analysed, showing Ni loading ranging from 252.0 to 603.5 μg/cm^2 and W ranging from 43.0 to 64.9 μg/cm^2.

Table 1. The element al composition and metal loading of the prepared NiW/Cu coatings analyzed via ICP–OES.

Catalyst	Element, wt.%		Element Loadings, μg cm^{-2}		
	Ni	W	Ni	W	Ni + W
$Ni_{93}W_7$/Cu	92.94	7.09	603.5	46.0	649.5
$Ni_{91}W_9$/Cu	91.13	8.87	483.7	47.1	530.8
$Ni_{89}W_{11}$/Cu	89.04	10.96	527.0	64.9	591.9
$Ni_{87}W_{13}$/Cu	86.88	13.12	373.9	56.5	430.4
$Ni_{85}W_{15}$/Cu	85.40	14.60	252.0	43.0	295.0

[1] P.-A. Le, V. D. Trung, P. L. Nguyen, T. V. B. Phung, J. Natsuki, and T. Natsuki, “The current status of hydrogen energy: an overview,” RSC Advances, vol. 13, no. 40, pp. 28262–28287, Jan. 2023, doi: 10.1039/d3ra05158g.

[2] D. Guan et al., “Hydrogen society: from present to future,” Energy & Environmental Science, vol. 16, no. 11, pp. 4926–4943, Jan. 2023, doi: 10.1039/d3ee02695g.

[3] M. Hermesmann and T. E. Müller, “Green, Turquoise, Blue, or Grey? Environmentally friendly Hydrogen Production in Transforming Energy Systems,” Progress in Energy and Combustion Science, vol. 90, p. 100996, Feb. 2022, doi: 10.1016/j.pecs.2022.100996.

[4] V. A. Panchenko, Yu. V. Daus, A. A. Kovalev, I. V. Yudaev, and Yu. V. Litti, “Prospects for the production of green hydrogen: Review of countries with high potential,” International Journal of Hydrogen Energy, vol. 48, no. 12, pp. 4551–4571, Oct. 2022, doi: 10.1016/j.ijhydene.2022.10.084.

[5] N. Ruslan et al., “Review on Magnesium hydride and sodium borohydride hydrolysis for hydrogen production,” Crystals, vol. 12, no. 10, p. 1376, Sep. 2022, doi: 10.3390/cryst12101376.

ELECTROCHEMICAL SENSOR BASED ON MOLECULARLY IMPRINTED POLYMERS FOR PROTEIN DETECTION

Gintarė Ruginytė[1,2], Ernestas Brazys[1,3], Vilma Ratautaitė[1], Arūnas Ramanavičius[1,3]

[1]Lithuania, State Research Institute Center for Physical Sciences and Technology (FTMC), Department of Nanotechnology
[2]Lithuania, Vilnius University (VU), Life Sciences Center
[3]Lithuania, Vilnius University (VU), Faculty of Chemistry and Geosciences, Institute of Chemistry, Department of Physical Chemistry
gintare.ruginyte@gmc.stud.vu.lt

Proteins perform many important functions in living organisms. The selective detection of proteins is essential in clinical diagnostics, biomedicine, proteomics, etc. Conventional analytical methods, including enzyme-linked immunosorbent assay (ELISA), high-performance liquid chromatography–mass spectrometry (HPLC–MS), and fluorescence-based assays, offer high sensitivity but rely on costly instrumentation and complex sample preparation. These limitations have led to the development of biosensors, particularly electrochemical sensors, which offer rapid response and low cost [1]. Electrochemical sensors incorporating molecularly imprinted polymers (MIPs) have demonstrated potential for detecting a wide variety of analytes [2]. MIPs function as artificial receptors that mimic the molecular recognition behaviour of natural antibodies [3]. In this work, we report the development of an electrochemical sensor based on MIPs for selective protein recognition.

Molecularly imprinted polymers were electrochemically synthesised directly on the surface of screen-printed carbon electrodes (SPCE). Polymerisation of pyrrole was performed in the presence of bovine serum albumin (BSA), which was used as a model protein for system optimisation. During polymer formation, a conducting polymer, polypyrrole, was formed, and protein molecules were incorporated into its matrix. Following the removal of the template, complementary binding cavities were created within the polymer matrix. A non-imprinted polymer (NIP) was used as a control layer. The selective rebinding of BSA was assessed by monitoring the response using electrochemical impedance spectroscopy (EIS).

The MIP-modified electrochemical sensor showed a more pronounced impedance response to BSA than the non-imprinted polymer. The obtained results show the potential of MIP-based electrochemical sensors for the selective detection of proteins.

Acknowledgements

This project has received funding from the Research Council of Lithuania (LMTLT), agreement No. S-MIP-24-11.

[1] Z. Mazouz et al., “Computational approach and electrochemical measurements for protein detection with MIP-based sensor,” Biosensors and Bioelectronics, vol. 151, p. 111978, Dec. 2019, doi: 10.1016/j.bios.2019.111978.
[2] L. Wang, M. Pagett, and W. Zhang, “Molecularly imprinted polymer (MIP) based electrochemical sensors and their recent advances in health applications,” Sensors and Actuators Reports, vol. 5, p. 100153, Apr. 2023, doi: 10.1016/j.snr.2023.100153.
[3] B. Ö. Acet, T. İnanan, K. Salieva, B. Borkoev, M. Odabaşı, and Ö. Acet, “Molecular imprinted polymers: important advances in biochemistry, biomedical and biotechnology,” Polymer Bulletin, vol. 81, no. 12, pp. 10439–10459, Mar. 2024, doi: 10.1007/s00289-024-05238-5.

MOLECULAR IMPRINTED POLYDOPAMINE-BASED SENSOR FOR TETRACYCLINE DETECTION

Danish Khalid[1], Arūnas Ramanavičius[1,2], Ernestas Brazys[1,2], Vilma Ratautaitė[2]

[1]Vilnius University (VU), Faculty of Chemistry and Geosciences, Department of Physical Chemistry, Naugarduko str. 24, Vilnius LT-03225, Lithuania
[2]State Research Institute Center for Physical Sciences and Technology (FTMC), Department of Nanotechnology, Sauletekio Ave. 3, Vilnius LT-10257, Lithuania
danish.khalid@chgf.stud.vu.lt

Tetracycline (TC) is a broad-spectrum antibiotic produced by Streptomyces and is widely used in livestock because of its effectiveness, low cost, and ease of administration [1]. However, residual TC in animal-derived foods can enter the human body through the food chain, posing significant health risks [2]. Accurate detection of TC and other antibiotic residues is therefore essential for pharmaceutical quality control, food safety, and environmental monitoring. Although conventional detection methods offer high sensitivity, they require costly instrumentation and complex procedures, highlighting the need for simple, cost-effective sensing platforms [1]. Molecularly imprinted polymer (MIP)-based sensors are synthetic recognition systems that mimic biological “lock-and-key” interactions, enabling selective detection of target molecules used as templates during imprinting [3].

In the present study, a MIP-based sensor was developed for the selective determination of tetracycline, using dopamine hydrochloride as the functional monomer and tetracycline as the template, thereby generating recognition sites complementary to the target’s molecular structure. MIP fabrication was performed via drop-casting of polydopamine nanoparticles synthesized via auto-oxidation of dopamine hydrochloride in Tris buffer (pH 8.5) and electrochemical polymerization via cyclic voltammetry in phosphate-buffered saline (PBS, pH 7.4), with TC. Non-imprinted polymers (NIPs) were prepared using the same procedure but without a template and served as controls. Template removal was performed by solvent washing with an ethanol-acetic acid mixture (9:1, v/v). Rebinding studies using electrochemical techniques, including cyclic voltammetry and electrochemical impedance spectroscopy, confirmed that MIPs exhibited enhanced sensitivity and selectivity for tetracycline compared with NIPs, demonstrating the system’s potential for tetracycline detection.

Acknowledgements
This project has received funding from the Research Council of Lithuania (LMTLT), agreement No. S-LL-25-3.

Keywords: Molecular imprinted polymer, polydopamine, tetracycline, non-imprinted polymer

[1] Wang, J. Zhang, L. Chen, H. Liu, X. Yang, and Y. Li, “Novel fluorescence sensor for the selective recognition of tetracycline based on molecularly imprinted polymer-capped N-doped carbon dots,” RSC Advances, vol. 12, no. 38, pp. 24778–24785, 2022.
[2] W. Gao, P. Li, S. Qin, Z. Huang, Y. Cao, and X. Liu, “A highly sensitive tetracycline sensor based on a combination of magnetic molecularly imprinted polymer nanoparticles and surface plasmon resonance detection,” Microchimica Acta, vol. 186, no. 9, pp. 637–645, 2019.
[3] S. Akgönüllü, S. Kılıç, C. Esen, and A. Denizli, “Molecularly imprinted polymer-based sensors for protein detection,” Polymers, vol. 15, no. 3, pp. 629–645, 2023.

GREEN SYNTHESIS OF SILVER NANOPARTICLES USING LIPOPHILICITY-MODIFIED LINDEN EXTRACTS

Urtė Raubytė[1], Aistė Balčiūnaitienė[1], Jonas Viškelis[1]

[1]Lithuanian Research Centre For Agriculture and Forestry, Institute of Horticulture, Laboratory of Biochemistry and Technology
urte.raubyte@lammc.lt

Green synthesis of silver nanoparticles has emerged as a sustainable alternative to conventional chemical methods, particularly for antimicrobial and biomedical applications, yet achieving controlled stability and surface functionality using plant extracts remains challenging. This study aimed to evaluate whether modification of the lipophilic properties of Tilia cordata (linden) flower and leaf extracts can improve the reduction, stabilization, and surface energy control of silver nanoparticles synthesized via a green approach. Crude linden extract, Medusomyces gisevii–fermented extract, and enzymatically modified extract were employed as reducing and stabilizing agents, and the resulting nanoparticles were characterized using UV–Vis spectroscopy, SEM, TEM, SAED, XRD, FTIR, and colorimetric analysis. Antimicrobial activity was assessed against Gram-positive and Gram-negative bacteria and Candida albicans, while antioxidant capacity was evaluated using CUPRAC, ABTS, and DPPH assays; in addition, in vitro antifungal activity was tested on post-harvest table grapes. All extract variants successfully produced stable, predominantly spherical silver nanoparticles with nanometer-scale dimensions and defined crystallinity, while extract modification influenced particle size, aggregation behavior, and surface chemistry. Silver nanoparticle formulations exhibited markedly enhanced antimicrobial activity compared to crude extracts, with enzymatically modified nanoparticles showing the strongest broad-spectrum effects, whereas antioxidant activity displayed matrix-dependent changes following nanoparticle formation. Overall, the results demonstrate that tuning the lipophilicity of linden extracts is an effective strategy for controlling the physicochemical and biological properties of green-synthesized silver nanoparticles, highlighting their potential for sustainable antimicrobial and antioxidant applications.

Acknowledgements

The authors gratefully acknowledge the Research Council of Lithuania (LMTLT), agreement No. S-MIP-24-56, for the financial support provided for this research.

FUNCTIONALIZATION OF CoP AND CoFeP WITH GOLD NANOPARTICLES VIA GALVANIC DISPLACEMENT FOR ALKALINE WATER SPLITTING

Dmytro Shyshkin[1,2], Huma Amber[2], Loreta Tamašauskaitė-Tamašiūnaitė[2], Eugenijus Norkus[2]

[1]Vilnius University, Faculty of Chemistry and Geosciences, Naugarduko str. 24, LT-03225 Vilnius, Lithuania
[2]Center for Physical Sciences and Technology (FTMC), Department of Catalysis, Saulėtekio ave. 3, LT-10257 Vilnius, Lithuania
dmytro.shyshkin@ftmc.lt

Hydrogen is a clean and sustainable energy carrier with immense potential to replave fossil fuels. Overall water splitting (OWS), which involves both the hydrogen evolution reaction (HER) and the oxygen evolution reaction (OER), is an efficient method of producing hydrogen. Designing and developing innovative bifunctional electrocatalysts that exhibit both high catalytic activity and enhanced stability for both the HER and the OER is highly desirable and yet challenging. Transition metal phosphides (TMPs) are recognized as highly effective electrocatalysts due to their abundance of active surface sites, excellent electrical conductivity, and strong chemical stability. These characteristics are derived from the intrinsic high electrocatalytic activity of the metal (M) centers and phosphorus (P) sites. In this study, cobalt phosphide (CoP) and cobalt-iron phosphide (CoFeP) were directly deposited on copper (Cu) substrates via electroless deposition. The P source and reducing agent used in this process was sodium hypophosphite (NaH2PO2). Gold (Au) nanoparticles were subsequently anchored to the phosphides through a galvanic displacement strategy, thereby creating a composite material with enhanced properties. A comprehensive investigation was conducted to elucidate the morphology, composition, and crystal structure of the catalysts. This investigation utilized a range of analytical techniques, including scanning electron microscopy (SEM), energy-dispersive X-ray spectroscopy (EDS), X-ray diffraction (XRD), and X-ray photoelectron spectroscopy (XPS). The electrocatalytic bifunctionality of the materials for overall water splitting (OWS) was evaluated in a two-electrode setup using a 1 M KOH electrolyte.

The Au-CoFeP catalyst exhibited significant bifunctional activity, achieving a low cell voltage of 1.68 V at 10 mA cm-2. This performance was superior to that of the Au-CoP catalyst, due to the synergistic interaction among the Co, Fe, and Au elements. The combination of Au modification and bimetallic CoFeP composition led to lower overpotentials and enhanced stability, underscoring a practical and effective strategy for designing gold-modified transition metal phosphides as durable, efficient candidates for application in the field of electrocatalysis.

Acknowledgements
This research was funded by a grant (No. P-SV3-25-715) from the Research Council of Lithuania.

Keywords: gold nanoparticles; cobalt phosphide; cobalt-iron phosphide; electroless deposition; galvanic bifunctional electrocatalyst; alkaline electrolysis

GREEN SYNTHESIS OF SILVERNANOPARTICLES USING PROCESSED TILIA CORDATA EXTRACTS AND THEIR ENHANCEDANTIOXIDANT AND ANTIMICROBIAL ACTIVITIES

Syeda Hijab Zehra[1], Jonas Viskelis[1], Aiste Balciunaitiene[1]

[1]Lithuanian Research Centre for Agriculture and Forestry, Institute of Horticulture
hijab.zehra@lammc.lt

This work presents the green synthesis of silver nanoparticles using crude, fermented, and enzymatically modified linden Tiliacordata flower and leaf extracts, and thoroughly evaluates their functional properties. Experimental procedures included UV-Vis spectroscopy for nanoparticle confirmation, colorimetric analysis, SEM, TEM, XRD, and FTIR for morphological and chemical characterization, and assessment of total phenolic content. Antibacterial activity was tested against a panel of Gram-positive, Gram-negative bacteria and fungal strains using the agar diffusion method, demonstrating significant enhancement of antimicrobial properties in all AgNPs preparations versus unmodified extracts. Antioxidant capacity for all variants was quantified by CUPRAC, ABTS, and DPPH assays, revealing matrix-dependent changes after processing and nanoparticle formation. The data of this work suggest promising applications of this nanoparticle conjugated extracts in biomedical and therapeutic contexts due to their superior antioxidant potential compared to crude extracts alone. Further research could explore the mechanisms underlying these effects and there in vivo efficacy.

Acknowledgements

The authors would like to thank the Research Council of Lithuania, (LMTLT) agreement No. S-MIP-24-56, for the financial support given to achieve this work.

Keywords: Tilia cordata, silver nanoparticles, antimicrobial activity, Medusomyces Gisevii fungus, antioxidant activity

FABRICATION OF GRAPHENE FIELD EFFECT TRANSISTOR ARRAY FOR BIOSENSING

Ujjawal Malani[1], Aleksandra Širvinsytė[1], Vilius Vertelis[1], Skirmatas Keršulis[1], Nerija Žurauskienė[1]

[1]Center for Physical Science and Technology, Department of Functional Materials and Electronics, Vilnius, Lithuania
ujjawal.malani@ftmc.lt

Rapid, sensitive, and cost-effective biosensing technologies are essential for applications in medical diagnostics, environmental monitoring, and point-of-care testing. However, many existing biosensing platforms remain limited by high cost, complex instrumentation, and slow response times, restricting their widespread deployment. Current solutions include surface plasmon resonance (SPR) [1], quartz crystal microbalance (QCM) [2], microcantilever sensors [3], and giant magnetoresistance (GMR) devices [4].

Graphene field effect transistors (FET) or G-FET is type of FET which is formed using channels made from graphene layer. Graphene is a 2-D material composed of carbon atoms in HCP lattice. G-FET in the context of biosensing offers high surface sensing, fast, label free electrical sensing and readout, it is biologically inert, has CMOS integration possibilities, and a broad range of detection [5]. However, production of graphene-based FETs currently faces several challenges due to extremely delicate and sensitive graphene it requires complex functionalization, meticulous care and expensive equipment. Throughout this study a GFET device was fabricated by depositing and patterning metal electrodes on glass substrates using photolithography, followed by the transfer of graphene onto the metal contacts. This study focuses on developing an efficient and cost-effective technological production route to produce sub millimeter functionalized G-FET biosensors arrays.

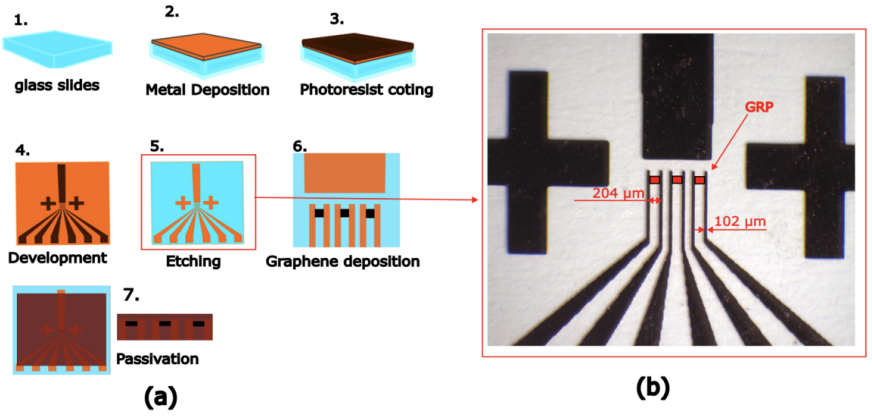


Fig. 1. (a) Technical route for the production of the sensor. (b) Micrograph of the base layer, where red marks labeled ”GRP” indicate the locations at which the graphene will be placed.

[1] T. Špringer, M. Bocková, J. Slabý, F. Sohrabi, M. Čapková, and J. Homola, “Surface plasmon resonance biosensors and their medical applications,” Biosensors and Bioelectronics, vol. 278, p. 117308, Feb. 2025, doi: 10.1016/j.bios.2025.117308.
[2] H. J. Lim, T. Saha, B. T. Tey, W. S. Tan, and C. W. Ooi, “Quartz crystal microbalance-based biosensors as rapid diagnostic devices for infectious diseases,” Biosensors and Bioelectronics, vol. 168, p. 112513, Aug. 2020, doi: 10.1016/j.bios.2020.112513.
[3] J. Wang, B. Xu, Y. Zhu, and J. Zhao, “Microcantilever sensors for biochemical detection,” Journal of Semiconductors, vol. 44, no. 2, p. 023105, Feb. 2023, doi: 10.1088/1674-4926/44/2/023105.
[4] K. Wu, D. Tonini, S. Liang, R. Saha, V. K. Chugh, and J.-P. Wang, “Giant magnetoresistance biosensors in biomedical applications,” ACS Applied Materials & Interfaces, vol. 14, no. 8, pp. 9945–9969, Feb. 2022, doi: 10.1021/acsami.1c20141.
[5] K. Aran, B. Goldsmith, and M. Moarefian, “Applications of graphene field effect biosensors for biological sensing,” Advances in Biochemical Engineering, Biotechnology, vol. 187, pp. 37–70, Jan. 2024, doi: 10.1007/10_2024_252.

MICROFLUIDIC SYNTHESIS OF CHITOSAN-TPP NANOPARTICLES FOR DRUG DELIVERY IN ANTIBIOFILM APPLICATIONS

Samanta Gelumbickytė[1], Adei Abouhagger[1], Arūnas Stirkė[1]

[1]Center for Physical Sciences and Technology, Department of Functional Materials and Electronics, Vilnius, Lithuania
samanta.gelumbickyte@ftmc.lt

Biofilms consist of dense bacterial communities embedded in an extracellular polymeric matrix that significantly restricts antibiotic penetration and reduce treatment efficacy [1]. Conventional antibiotic delivery strategies often fail to achieve sufficiently high local drug concentrations, while rapid drug clearance from tissues further limits therapeutic effectiveness [2]. These challenges highlight the need for novel approaches that can improve drug distribution and stability at the site of infection.

This study investigates microfluidic synthesis of chitosan-based nanoparticles, which enables precise control of diffusion and mixing within micrometer-scale channels, allowing more accurate and reproducible nanoparticle formation compared with traditional batch methods.

Tetracycline was incorporated into chitosan–TPP nanoparticles synthesized via ionic gelation, yielding uniform, positively charged particles suitable for interaction with biofilms. The antibiofilm activity of the nanoparticles was evaluated against *Staphylococcus aureus* and *Escherichia coli* biofilms. Encapsulated tetracycline exhibited concentration-dependent inhibition, with stronger suppression of *S. aureus* biofilm metabolic activity compared to the free drug, while *E. coli* biofilms showed higher tolerance. These findings demonstrate the potential of chitosan nanoparticles to modulate antibiotic–biofilm interactions and support their application in antibiofilm drug delivery systems.

[1] H. Y. Liu, E. L. Prentice, and M. A. Webber, “Mechanisms of antimicrobial resistance in biofilms,” Npj Antimicrobials and Resistance, vol. 2, no. 1, p. 27, Oct. 2024, doi: 10.1038/s44259-024-00046-3.

[2] K. E. Grooters et al., “Strategies for combating antibiotic resistance in bacterial biofilms,” Frontiers in Cellular and Infection Microbiology, vol. 14, p. 1352273, Jan. 2024, doi: 10.3389/fcimb.2024.1352273.

[3] A. Abouhagger, S. Gelumbickytė, M. Kirsnytė, T. Kavleiskaja, A. Stirkė, and W. C. M. A. Melo, “Microfluidic synthesis of tetracycline-loaded chitosan nanoparticles for antibiofilm applications,” Materials Research Express, vol. 12, no. 11, p. 115006, Nov. 2025, doi: 10.1088/2053-1591/ae1d40.

SURFACE PLASMON POLARITON APPLICATION FOR FLUORESCENT DYE LABELLED BOVINE SERUM ALBUMIN DETECTION

Ūla Elena Sauliūtė[1], Ernesta Bužavaitė-Vertelienė[1]

[1]Center For Physical Sciences and Technology, Department of Laser Technologies, Plasmonics and Nanophotonics Laboratory, Lithuania
elena.sauliute@ff.stud.vu.lt

Fluorescence-based biosensors have become an essential tool in biomedical applications and the life sciences, primarily due to their multiplexing capabilities and high sensitivity [1]. However, despite these advantages, fluorescence-based biosensing often encounters diminished optical output at low analyte concentrations where fluorescence signal is weak, which typically necessitates the use of expensive and bulky instrumentation to achieve functional dynamic range [1]. To overcome these limitations, surface plasmon polaritons (SPPs), which are electromagnetic waves propagating along the boundary between a metal and a dielectric, are utilized [2, 3]. By generating intense localized field enhancement, SPP allows detection of minuscule changes in refractive index at the metal-dielectric surface [3]. This interaction results in metal enhanced fluorescence significantly improving the quantum yield, excitation rate, radiation pattern and photostability of nearby fluorophores [1].

The excitation of SPP requires specific momentum-matching conditions to be satisfied. This is typically achieved through various coupling schemes such as prism coupling, grating diffraction and waveguide coupling. Nevertheless, SPPs possess certain qualities that impose technical constraints, most notably the dissipation of energy as heat in the metal and finite propagation length caused by attenuation [2]. Additionally, the efficiency of SPP enhancement is strictly distance-dependent: to prevent non-radiative quenching fluorophores must be placed at an optimal range from the surface which is typically between 10 and 50 nm [1]. By utilizing these plasmonic interactions and overcoming signal limitations, researchers are moving toward developing ultra-sensitive, portable point-of-care testing devices with low-cost detectors for early disease diagnosis [1].

In this work fluorescence microscopy and total internal reflection ellipsometry (TIRE) are used to evaluate properties of bovine serum albumin (BSA) conjugated with fluorescent CF680 molecules. The optical response of a structure consisting of a thin microscopic slide covered with 45 nm Au was measured using TIRE. Real-time measurements of bovine serum albumin labelled with CF680 dye adsorption to Au surface were performed. Formed BSA-CF680 layer emission pattern was measured with fluorescence microscopy setup. A new approach in labelled biomolecule detection is demonstrated through reduced losses of the SPP excitation when a layer of labelled BSA is covalently immobilized on sensing surface.

Keywords: biosensing, surface plasmon polaritons, fluorescence microscopy, total internal reflection ellipsometry

[1] D. Semeniak, D. F. Cruz, A. Chilkoti, and M. H. Mikkelsen, “Plasmonic fluorescence enhancement in diagnostics for clinical tests at Point-of-Care: A review of Recent technologies,” Advanced Materials, vol. 35, no. 34, p. e2107986, Mar. 2022, doi: 10.1002/adma.202107986.

[2] W. L. Barnes, “Surface plasmon–polariton length scales: a route to sub-wavelength optics,” Journal of Optics a Pure and Applied Optics, vol. 8, no. 4, pp. S87–S93, Mar. 2006, doi: 10.1088/1464-4258/8/4/s06.

[3] J. Homola, “Present and future of surface plasmon resonance biosensors,” Analytical and Bioanalytical Chemistry, vol. 377, no. 3, pp. 528–539, Oct. 2003, doi: 10.1007/s00216-003-2101-0.

ELECTROCHEMICAL IMMUNOSENSING OF DIPEPTIDYL PEPTIDASE IV:TOWARD SENSITIVE AND ACCESSIBLE CANCER-RELATED BIOMARKER DETECTION

Vejas Strelciunas[1], Antanas Zinovicius[2]

[1]National Center for Physical Sciences and Technology, Nanotechnology department, Vilnius, Lithuania
[2]Vilnius Gediminas Technical University, Faculty of Fundamental sciences, Department of Chemistry and Bioengineering, Vilnius, Lithuania
vejas.strelciunas@stud.vilniustech.lt

Dipeptidyl peptidase IV (DPP-IV, also known as CD26) is a multifunctional serine protease involved in immune regulation, metabolic homeostasis, and cancer-related signaling pathways. Altered levels of soluble DPP-IV have been reported in blood and other biological fluids in various oncological and metabolic disorders, suggesting its potential value as a clinically relevant biomarker [1] [2]. Despite this, the diagnostic utility of DPP-IV remains insufficiently explored, largely due to limitations of existing analytical approaches. Conventional detection methods, including chromatographic and optical techniques, often require complex instrumentation, labeled reagents, and extensive sample preparation, limiting their applicability for rapid, cost-effective, and decentralized diagnostics [3].

The objective of this study is to explore the potential of electrochemical immunosensing as an alternative approach for DPP-IV detection, addressing current methodological limitations and contributing to the development of sensitive and accessible biomarker detection platforms for early DPP-IV related disease diagnostics.

An electrochemical immunosensing platform based on screen-printed electrodes modified with gold nanostructures is proposed. The surface modification with gold nanostructures is intended to enhance electron transfer kinetics and improve antibody immobilization efficiency. The study focuses on the systematic evaluation of electrode surface modification strategies and their influence on immunosensor performance.

The study is expected to provide insight into how gold nanostructure-based surface modification influences the electrochemical response of immunosensing platforms toward DPP-IV recognition. Particular attention is given to evaluating trends in signal enhancement, surface-related stability, and reproducibility, which are critical parameters for reliable immunosensor performance. The anticipated findings will help identify key factors governing efficient electron transfer and biomolecular interactions at the electrode interface, thereby guiding the rational design of optimized electrochemical immunosensors.

This research aims to provide fundamental insights into electrochemical immunosensing strategies for DPP-IV detection and to support the development of portable and efficient biosensing tools. The proposed approach has the potential to contribute to future advances in early cancer diagnostics and biomarker-based electrochemical sensing technologies.

Keywords: DPP-IV, Electrochemical immunosensor, biosensor, biomarker, cancer

[1] P. Busek, J. S. Duke-Cohan, and A. Sedo, “Does DPP-IV inhibition offer new avenues for therapeutic intervention in malignant disease?,” Cancers, vol. 14, no. 9, p. 2072, Apr. 2022, doi: 10.3390/cancers14092072.
[2] X. Guo, H. Feng, L. Cai, J. Zheng, and Y. Li, “DPP-IV as a potential candidate in anti-obesity and obesity-related diseases treatment,” Biomedicine & Pharmacotherapy, vol. 180, p. 117464, Sep. 2024, doi: 10.1016/j.biopha.2024.117464.
[3] W. Li et al., “Dual-Probe Strategy-Enabled multiplex photoelectrochemical sensor for highly sensitive screening of diabetes and related complications,” Analytical Chemistry, vol. 97, no. 36, pp. 19949–19956, Sep. 2025, doi: 10.1021/acs.analchem.5c04320.

3D-PRINTED DIFFRACTIVE OPTICAL ELEMENTS USING GRAYSCALE MULTIPHOTON PRINTING

Paulius Semenauskas[1], Mangirdas Malinauskas[1], Maria Farsari[2], Gordon Zyla[1]

[1]Vilnius University, Physics Faculty, Laser Research Center, Lithuania
[2]Foundation for Research and Technology-Hellas, Institute of Electronic Structure and Laser, Greece
gordon.zyla@ff.vu.lt

Multiphoton printing (MPP) is a maskless, high-resolution 3D printing technique that exploits nonlinear light–matter interactions to induce localized polymerization in photosensitive materials, resulting in an ellipsoidal volume pixel known as a voxel [1]. Owing to its nonlinear nature, MPP allows dynamic modulation of the printing intensity, an approach commonly referred to as grayscale MPP, enabling precise control over voxel dimensions and fabricated geometry and particularly relevant for optical applications that require high structural fidelity [2].

Here, grayscale MPP was used to fabricate multilevel pixelated diffractive optical elements (DOEs) that manipulate the phase of transmitted light. The DOEs were designed from digital grayscale phase masks generated using computer-generated holography methods [3] to produce target far-field intensity distributions. During fabrication, each grayscale pixel was translated into a discrete height level by adjusting the local laser exposure dose, resulting in quasi-2.5D surface relief profiles. The fabricated structures achieved a minimum lateral pixel size of 2 x 2 μm^2 and comprised eight discrete height levels with a step height of approximately 80 nm. Surface topography and fabrication quality were characterized using optical profilometry and scanning electron microscopy, respectively (see Fig. 1, top). Optical characterization confirmed that the printed DOEs generate the intended far-field intensity distributions (see Fig. 1, bottom).

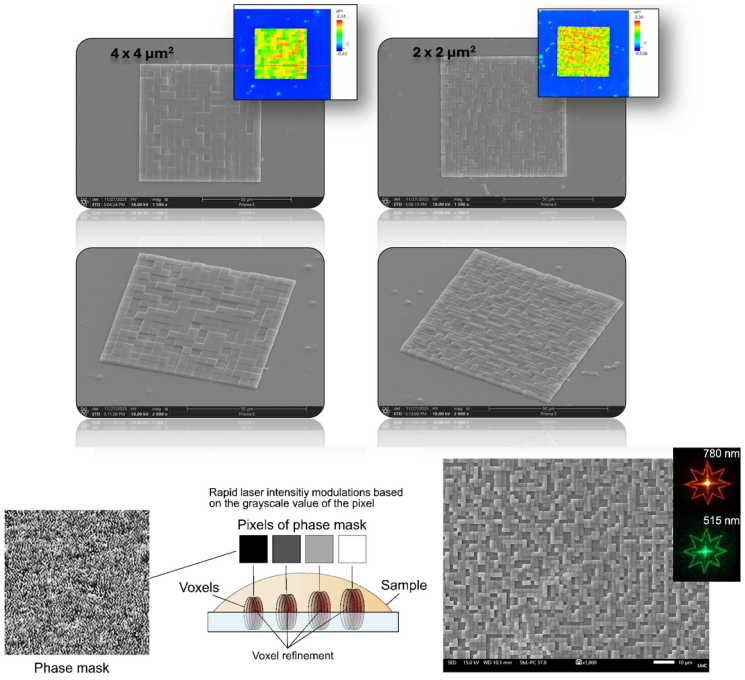


Fig. 1. Examples of multilevel pixelated structures and DOE printed by grayscale MPP

These results demonstrate that maskless grayscale MPP provides a flexible and cost-effective alternative to conventional lithographic techniques for the rapid fabrication of custom-designed DOEs, with potential applications in optical microscopy, laser beam shaping, and integrated optical systems [4].

[1] G. Zyla and M. Farsari, “Frontiers of Laser-Based 3D Printing: A perspective on Multi-Photon Lithography,” Laser & Photonics Review, vol. 18, no. 7, Mar. 2024, doi: 10.1002/lpor.202301312.
[2] G. Zyla et al., “3D micro-devices for enhancing the lateral resolution in optical microscopy,” Light Advanced Manufacturing, vol. 5, no. 2, p. 1, Jan. 2024, doi: 10.37188/lam.2024.019.
[3] Gerchberg, R. W. & Saxton, W. O., ”A practical algorithm for the determination of phase from image and diffraction plane pictures,” Optik 35, 237-246, 1972.
[4] S. N. Khonina, N. L. Kazanskiy, and M. A. Butt, “Exploring Diffractive Optical Elements and Their Potential in Free Space Optics and imaging- A Comprehensive Review,” Laser & Photonics Review, vol. 18, no. 12, May 2024, doi: 10.1002/lpor.202400377.

REAL-TIME DATA HANDLING FOR FAST LIDAR

Vaidas Šutas[1], Jonas Jurkevičius[1]

[1]Vilnius University, Faculty of Physics, Institute of Photonics and Nanotechnology, Vilnius, Lithuania
vaidas.sutas@ff.stud.vu.lt

Light Detection and Ranging (LiDAR) is a cornerstone technology for autonomous navigation and 3D environment mapping. Most beam-scanning LiDAR systems rely on moving mirrors and thus are limited by mechanical inertia.

An attractive alternative is employing akinetic scanning, where MHz line scans become possible without using moving parts. One candidate for such approach to LIDAR is spectro-temporal scanning [1], where a wavelength-swept laser source, such as an FDML laser [2] is used with a diffractive element to achieve a fast, akinetic line scan (see Fig. 1).

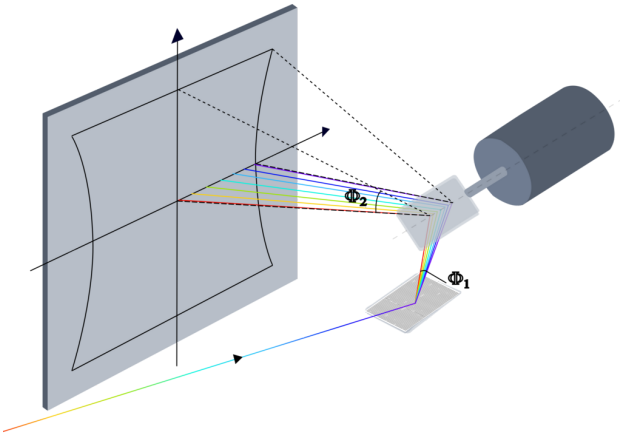


Fig. 1. A schematic of combined spectro-temporal and mechanical scanning. A wavelength-swept laser is directed towards a diffractive grating, producing an akinetic scan along the fast axis. A galvanometric mirror is used to scan along the slow axis.

While spectro-temporal scanning allows high framerate scanning, acquisition still relies on digitization of the signal of a fast photodetector. Thus, to enable 3D information recording by such akinetic LiDAR system from dynamic scenes or fast-moving objects, 3D data must be accurately and rapidly reconstructed from the 1D data stream.

In order to develop and validate high-throughput 3D data processing, we employed an approach based on photodetector signal emulation. An experimental setup was constructed using an arbitrary waveform generator that simulates detector signal waveform, corresponding to 3D data from a beam-scanned scene. The study utilized a high-performance C++ software framework to enable low-latency data transfer and real-time processing.

The custom algorithm was used for real-time image reconstruction, incorporating phase-shift synchronization and interpolation to map time-domain signals to spatial coordinates. The system achieved a data processing throughput of over 200 MS/s, exceeding the hardware limit of the digitizer (180 MS/s). The reconstruction accuracy was quantified using a root-mean-square error (RMSE) metric, confirming high signal fidelity (<2%).

This work demonstrates a software-hardware interface capable of handling the data rates required for future low-latency LiDAR applications.

[1] Y. Jiang, S. Karpf, and B. Jalali, “Time-stretch LiDAR as a spectrally scanned time-of-flight ranging camera,” Nature Photonics, vol. 14, no. 1, pp. 14–18, Dec. 2019

[2] R. Huber, M. Wojtkowski, and J. G. Fujimoto, “Fourier Domain Mode Locking (FDML): A new laser operating regime and applications for optical coherence tomography,” Optics Express, vol. 14, no. 8, p. 3225, Apr. 2006

TERAHERTZ METAMATERIAL ABSORBER BASED ON GRAPHENE PLASMONS

Mohammad Esmaeil Daraei[1], Mehdi Abedi-Varaki[2], Ignas Nevinskas[1]

[1]Center for Physical Sciences and Technology, Department of Optoelectronics, Vilnius, Lithuania
[2]Center for Physical Sciences and Technology, Department of Laser Technologies, Vilnius, Lithuania
esmaeil.daraei@ftmc.lt

Electromagnetic wave-matter interactions are considered fundamental to a wide range of modern photonic and electronic technologies, with particular significance attributed to the terahertz (THz) frequency regime [1] for applications including sensing, imaging, and wireless communication [2]. Within this spectral region, graphene [3] has been identified as a promising plasmonic platform due to its two-dimensional (2D) structure, electrically tunable carrier concentration, and capability to support surface plasmon polaritons (SPPs) exhibiting extreme subwavelength confinement and relatively low damping. A graphene metamaterial absorber (MMA) exhibiting near-unity, electrostatically tunable THz absorption was designed through finite element method (FEM) simulation. Graphene was represented using a surface conductivity formulation derived from the Kubo formalism. For highly doped graphene at THz frequencies, the conductivity is approximated by a Drude-like expression [4]:

$$\sigma_g = \frac{e^2 E_F}{\pi\hbar^2}\frac{i}{\omega + i/\tau} \tag{1}$$

where, ω, τ, $\hbar$, and E_F are defined as the angular frequency of the incident radiation, carrier relaxation time, reduced Planck constant, and Fermi energy, respectively.

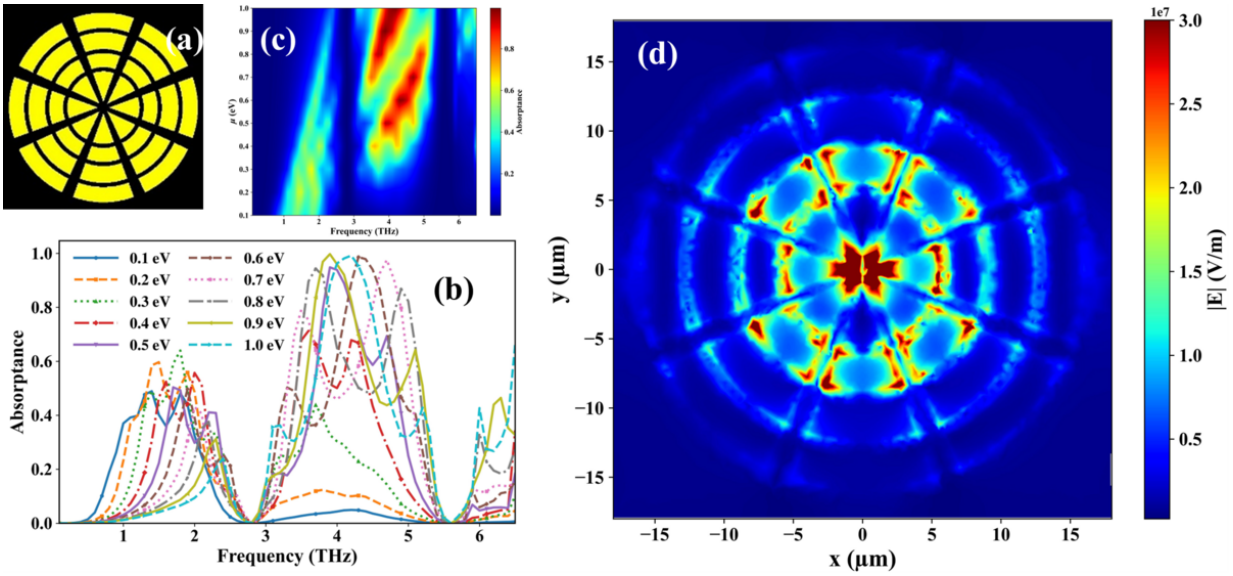


Fig. 1. Graphene-based metamaterial absorber: (a) 2D schematic of the structure; (b) chemical potential dependent absorption spectra; (c) absorption heatmap; and (d) electric field distribution at the resonance frequency (3.9 THz) for $\mu = 0.9\,\mathrm{eV}$.

The absorption response of the graphene-based MMA was evaluated for chemical potentials $\mu = 0.1\text{–}1.0\,\mathrm{eV}$. As illuatrated in Fig. 1(b), a pronounced blue shift of the dominant absorption resonance is induced with increasing μ, accompanied by a substantial enhancement of absorption, by which efficient electrostatic tunability is demonstrated.

The μ–frequency absorption heatmap presented in Fig. 1(c) provides a global representation of this behavior, wherein dispersive absorption bands are observed to shift monotonically toward higher frequencies as μ increases. The electric field distribution at resonance (Fig. 1(d)) is characterized by strong confinement within the graphene pattern, through which efficient plasmonic absorption is verified. Collectively, robust electrically tunable near-perfect absorption is demonstrated, and the suitability of the proposed structure for actively reconfigurable THz absorbers is established.

[1] I. Nevinskas et al., "Terahertz pulse emission from photoexcited bulk crystals of transition metal dichalcogenides," Journal of Physics D Applied Physics, vol. 54, no. 11, p. 115105, Nov. 2020, doi: 10.1088/1361-6463/abcc26.
[2] Y. Huang, Y. Shen, and J. Wang, "From Terahertz imaging to Terahertz wireless communications," Engineering, vol. 22, pp. 106–124, Sep. 2022, doi: 10.1016/j.eng.2022.06.023.
[3] C. T. Ellis et al., "Magneto-optical fingerprints of distinct graphene multilayers using the giant infrared Kerr effect," Scientific Reports, vol. 3, no. 1, p. 3143, Nov. 2013, doi: 10.1038/srep03143.
[4] S. Xiao, T. Wang, T. Liu, X. Yan, Z. Li, and C. Xu, "Active modulation of electromagnetically induced transparency analogue in terahertz hybrid metal-graphene metamaterials," Carbon, vol. 126, pp. 271–278, Oct. 2017, doi: 10.1016/j.carbon.2017.10.035.

A PM-PCF SAGNAC CONFIGURATION FOR HYBRID-WAVELENGTH PHOTON PAIR GENERATION

Gustas Liaugminas[1], Alexandr Belosludtsev[1], Julijanas Želudevičius[1], Kęstutis Regelskis[1]

[1]Center for Physical Sciences and Technology
gustas.liaugminas@ftmc.lt

Polarization-entangled photon sources are a key enabling technology for future quantum cryptography and secure communication based on Quantum Key Distribution (QKD) protocols [1]. Traditionally, entangled photon pairs are produced via spontaneous parametric down-conversion (SPDC) in periodically poled nonlinear crystals using free-space optical setups [2]. While such sources can exhibit high performance, fiber-based implementations are generally more robust and offer improved compatibility with existing optical fiber infrastructure, motivating the investigation of all-fiber alternatives. In this work, we present a fiber-based source for polarization-entangled photon pair generation based on spontaneous four-wave mixing (SFWM) in polarization-maintaining photonic crystal fiber (PM-PCF) in a Sagnac loop configuration. The Sagnac loop is pumped using 200 ps pulses at 1038 nm, generating nondegenerate photon pairs with signal and idler wavelengths at 831 nm and 1381 nm, respectively. This wavelength combination is particularly attractive for hybrid quantum networks, as it combines low-loss transmission in standard telecom fiber with compatibility with high-efficiency silicon single-photon detectors and quantum memory platforms operating in the near-infrared [3]. Polarization entanglement is produced by coherently superposing photon-pair generation processes from counter-propagating, orthogonally polarized pump pulses in the Sagnac interferometer. The experimental setup employs a fiber-based pump laser, pulse picking and amplification stages, and mutually twisted PM-PCF arms to ensure stable polarization control and phase matching. Signal and idler photons are separated using spectral filtering and detected with avalanche photodiodes, with polarization analysis performed using waveplates and polarizing beam splitters. The demonstrated source provides a compact, stable, and network-compatible platform for polarization-entangled photon generation, potentially suited for future hybrid quantum networking applications.

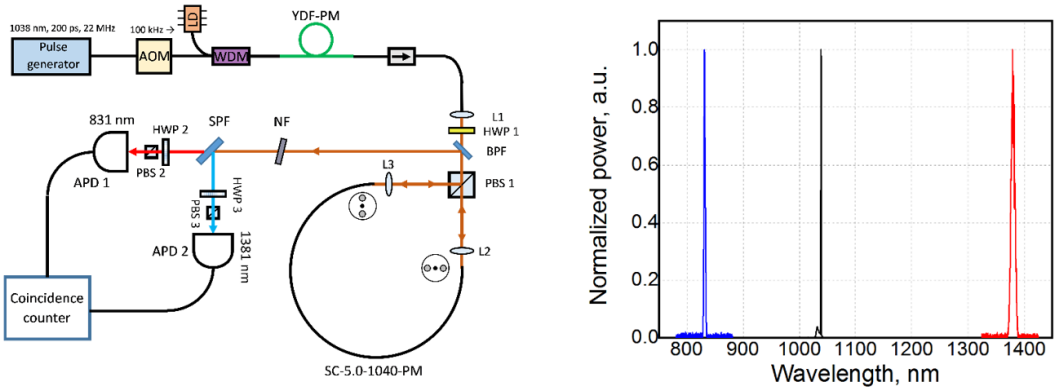


Fig. 1. Polarization-entangled photon pair generation setup (left). Spectra of pump, signal and idler waves generated in the PM-PCF (right).

Acknowledgements

This project has received funding from the Research Council of Lithuania (LMTLT), agreement No. [P-MIP-24-668]

[1] F. Xu, X. Ma, Q. Zhang, H.-K. Lo, and J.-W. Pan, "Secure quantum key distribution with realistic devices," Reviews of Modern Physics, vol. 92, no. 2, May 2020, doi: 10.1103/revmodphys.92.025002.
[2] P. G. Kwiat, K. Mattle, H. Weinfurter, A. Zeilinger, A. V. Sergienko, and Y. Shih, "New High-Intensity Source of Polarization-Entangled photon pairs," Physical Review Letters, vol. 75, no. 24, pp. 4337–4341, Dec. 1995, doi: 10.1103/physrevlett.75.4337.
[3] H. J. Kimble, "The quantum internet," Nature, vol. 453, no. 7198, pp. 1023–1030, Jun. 2008, doi: 10.1038/nature07127.

RAPID DEOXYGENATION OF TTA-UC SOLUTIONS USING BMTS SCAVENGER

Dominykas Likas[1], Steponas Raišys[1], Manvydas Dapkevičius[1]

[1]Vilnius University, Faculty of Physics, Institute of Photonics and Nanotechnology
dominykas.likas@ff.vu.lt

Triplet-triplet annihilation upconversion (TTA-UC) converts two low-energy photons into a single higher-energy photon in a paired sensitizer-annihilator system. After absorbing low-energy excitation light, the sensitizer generates a triplet exciton via intersystem crossing and transfers this energy to the annihilator through triplet-energy transfer. When two triplet-excited annihilators interact, one returns to the ground state while the other can form an excited singlet state. The emission from this state results in a photon of higher energy than that of excitation. [1]

Efficient TTA-UC depends on the long lifetime of triplet excitons. However, dissolved molecular oxygen under ambient conditions strongly quenches these triplet states, reducing upconversion emission and complicating the assessment of intrinsic photophysical parameters. [2] Traditional deoxygenation methods, such as inert-gas bubbling, freeze-pump-thaw cycles, or sample preparation in an oxygen-free environment (e.g., glovebox), are effective but time-consuming and require specialized equipment.

Chemical oxygen scavengers offer an alternative approach by irreversibly removing molecular oxygen through chemical reactions. After quenching the triplet state, molecular oxygen forms reactive singlet oxygen, which, in the presence of scavengers, reacts efficiently to produce stable oxidized products, thus lowering dissolved oxygen concentration.

In this work, various sulfur-based oxygen scavengers were investigated by measuring the emission onset of upconverting solutions under UV and 532 nm excitation. The compound containing three sulfur atoms (bis(methylthiomethyl) sulfide, BMTS) exhibited almost instant upconversion with an onset time of <1 s and a strong emission intensity.

The work examines the influence of the BMTS scavenger on UC quantum yields and lifetimes and determines the optimal scavenger concentration in the prepared TTA-UC solutions. The results of short- and long-term stability studies are also presented, which are essential for the practical application of this scavenger.

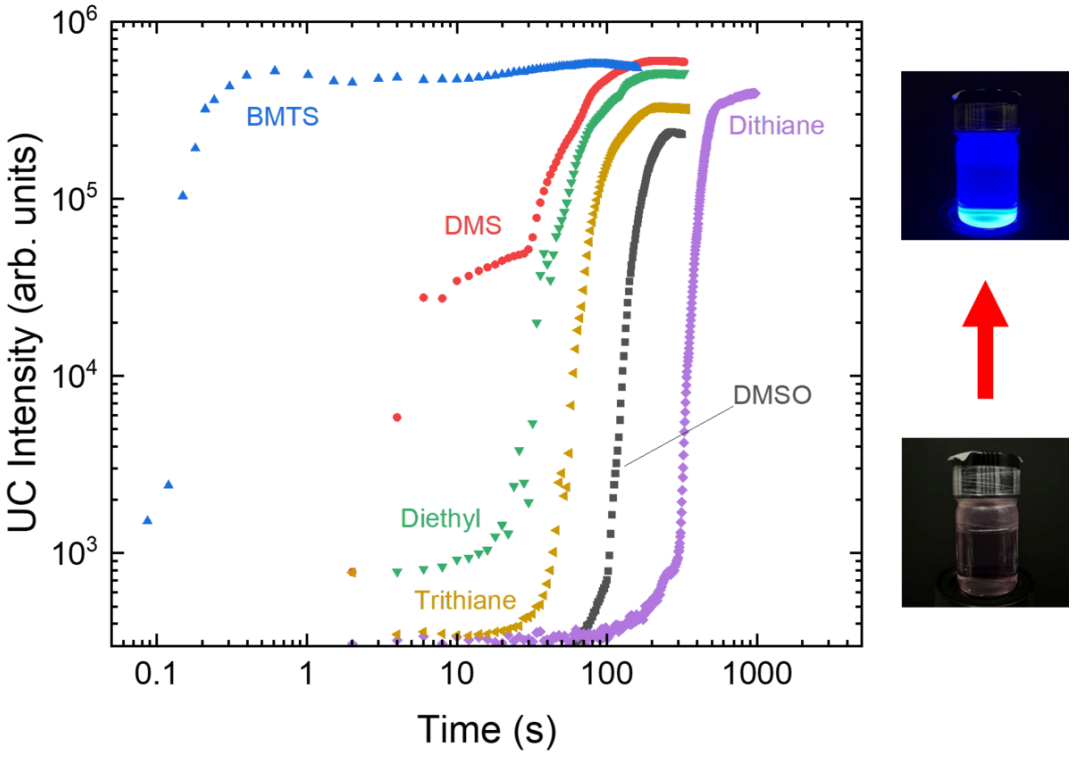


Fig. 1. UC intensity vs irradiation time of PtOEP-DPA in THF under ambient conditions with different oxygen scavengers.

[1] S. E. Seo, H.-S. Choe, H. Cho, H. Kim, J.-H. Kim, and O. S. Kwon, "Recent advances in materials for and applications of triplet–triplet annihilation-based upconversion," J. Mater. Chem. C, vol. 10, no. 12, pp. 4483–4496, 2022, doi: 10.1039/D1TC03551G.

[2] D. Dzebo, K. Moth-Poulsen, and B. Albinsson, "Robust triplet–triplet annihilation photon upconversion by efficient oxygen scavenging," Photochem. Photobiol. Sci., vol. 16, no. 8, pp. 1327–1334, Aug. 2017, doi: 10.1039/c7pp00201g.

MOLECULARLY IMPRINTED CONDUCTING POLYMER HYDROGEL COMPOSITES FOR TETRACYCLINE LOADING AND ELECTRICALLY RESPONSIVE DRUG DELIVERY

Samuel A. Kosoko[1,2], Ernestas Brazys[1,2], Vilma Ratautaite[1], Arūnas Ramanavičius[1,2]

[1]Lithuania, Centre for Physical Sciences and Technology (FTMC)
[2]Lithuania, Department of Physical Chemistry Vilnius University
samuel.kosoko@chgf.stud.vu.lt

Precise, on-demand drug delivery remains a critical challenge in modern therapeutics, particularly for localized treatments requiring high loading efficiency and spatiotemporal control. Electronic drug delivery systems (EDDS) based on electroactive materials offer programmable release profiles; however, their practical application is often limited by insufficient drug loading capacity and poor mechanical compliance. In this work, we report the development of a molecularly imprinted conducting polymer–hydrogel composite designed to address these limitations and enable electrically tunable drug delivery. The polypyrrole (PPy)–tetracycline complex was synthesized via chemical polymerization of pyrrole initiated by ammonium persulfate (APS). Polymerization was carried out for 24 h in an ice bath at approximately 0 °C. The template was subsequently removed using isopropanol and deionized water to obtain molecularly imprinted polypyrrole (MIP-PPy) powder. MIP-Ppy was incorporated at varying concentrations (0–2%) into a hydrogel matrix to enhance selective tetracycline recognition. Drug loading was quantified using UV–Vis spectroscopy at 360 nm, while swelling behaviour was evaluated to elucidate structure–property relationships. The composites exhibited reproducible tetracycline adsorption, with loading strongly dependent on PPy content. A low PPy concentration (0.2%) produced the highest adsorption capacity (≈381 μg g^{-1}). We attribute this to enhanced π–π and electrostatic interactions between tetracycline and the conducting polymer. In contrast, higher PPy contents (≥0.4%) led to reduced drug loading, which correlated with lower swelling ratios and greater network rigidity. Swelling systematically decreased from 84.1% for the PPy-free hydrogel to 71.3% at 2% PPy, highlighting the trade-off between binding selectivity and hydrogel permeability. These results demonstrate that careful optimization of conducting polymer content is essential to maximize drug loading while maintaining favourable hydrogel swelling properties. The presented molecularly imprinted PPy–hydrogel platform shows strong potential for integration into electroceutical systems, enabling high drug loading combined with electrically controlled, on-demand release.

Acknowledgements
This project has received funding from the Research Council of Lithuania (LMTLT), agreement No. S-LL-25-3.

Keywords: Molecularly imprinted polymers, conducting polymers, polypyrrole, hydrogels, tetracycline, electronic drug delivery.

[1] 1. Pérez-Nava, J. B. González-Campos, and B. A. Frontana-Uribe, “Conducting polymers for in situ drug release triggered via electrical stimulus,” ACS Applied Polymer Materials, vol. 6, no. 16, pp. 9375–9395, Aug. 2024, doi: 10.1021/acsapm.4c01013.
[2] 2. R. Liu and A. Poma, “Advances in molecularly imprinted polymers as drug delivery systems,” Molecules, vol. 26, no. 12, p. 3589, Jun. 2021, doi: 10.3390/molecules26123589.

DURABILITY AND SUSTAINED ANTIMICROBIAL ACTIVITY OF NANOCOMPOSITE COATINGS

Mindaugas Ilickas[1], Wanessa De Cassia Martins Antunes De Melo[2], Karolis Gedvilas[3], Asta Guobienė[1], Mantvydas Merkis[4], Simas Račkauskas[1], Arūnas Stirkė[2], Brigita Abakevičienė[1,5]

[1]Lithuania, Kaunas, Kaunas University of Technology, Institute of Materials Science
[2]Lithuania, Vilnius, State Research Institute Center for Physical Sciences and Technology, Department of Functional Materials and Electroni
[3]Lithuania, Kaunas district (Akademija), Vytautas Magnus University, Faculty of Natural Sciences
[4]Lithuania, Kaunas, Hospital of Lithuanian University of Health Sciences Kauno klinikos, Department of Radiology
[5]Lithuania, Kaunas, Kaunas University of Technology, Department of Physics
mindaugas.ilickas@ktu.lt

Durable antimicrobial coatings are critical for preventing pathogen transmission on frequently touched surfaces in healthcare and industrial environments. With antimicrobial resistance (AMR) posing a growing global threat – projected to cause up to ten million deaths and US$1 trillion in additional healthcare costs by 2050 [1] – developing long-lasting antimicrobial materials is urgent. Polyvinyl butyral (PVB)-based nanocomposites incorporating active agents such as silver nanoparticles (AgNPs), zinc oxide tetrapods (ZnO-Ts), and biocides (ampicillin, benzalkonium chloride, sodium pyrithione, triclosan) are promising candidates. This work reviews the durability and sustained antimicrobial performance of these coatings during aging.

AgNP-PVB coatings, produced via UV-mediated photochemical synthesis [2], generated AgNPs with average sizes of 15-118 nm depending on irradiation time. UV-Vis-NIR measurements after two years showed no significant shift in absorption bands, and water contact angles (WCAs) remained within ±5° of initial values. Antiviral assays against SARS-CoV-2 RNA confirmed sustained viral inactivation.

PVB-sodium pyrithione (NaPT) coatings demonstrated a unique “self-renewing” property: mechanical abrasion removed superficial polymer layers, exposing fresh biocide and increasing antibacterial efficacy against *E. coli* three-fold compared to unabraded surfaces. PVB-triclosan and PVB-NaPT coatings retained strong antiviral activity, achieving complete bacteriophage *φ6* inactivation and significant SARS-CoV-2 RNA degradation [3].

Synergistic PVB/ZnO-T/NaPT nanocomposites enhance durability and antimicrobial performance. The 3D tetrapod morphology [4] reinforces the PVB matrix mechanically, while ZnO-T and NaPT provide dual antimicrobial action via reactive oxygen species generation, Zn^{2+} ion release, and membrane depolarization. Smaller ZnO-T dimensions and higher NaPT concentrations lowered WCAs and increased efficacy, achieving $\log_{10}$ reductions up to 5.91 against *S. aureus*, *P. aeruginosa*, and *C. albicans*, and biofilm reductions of 87.7%. Surface free energy increased over four months (38.96 to 52.27 mN/m), reflecting aging-related polarity changes. Optimal tetrapod leg diameters approximately double the Debye length improved coating stability.

Overall, PVB-based nanocomposite coatings maintain structural integrity and high antimicrobial activity over time, offering a promising strategy for long-term protection of frequently touched surfaces.

Acknowledgements

This research has received funding from the Research Council of Lithuania (LMTLT), agreement no. S-A-UEI-23-1

[1] World Health Organization: WHO, “Antimicrobial resistance,” Nov. 21, 2023. https://www.who.int/news-room/fact-sheets/detail/antimicrobial-resistance
[2] M. Ilickas, A. Guobienė, K. Gedvilas, M. Merkis, and B. Abakevičienė, “UV-mediated photochemical synthesis and investigation of the antiviral properties of Silver nanoparticle-polyvinyl butyral nanocomposite coatings as a novel antiviral material with high stability and activity,” Applied Materials Today, vol. 38, p. 102203, Apr. 2024, doi: 10.1016/j.apmt.2024.102203.
[3] M. Ilickas, A. Guobienė, A. Stirkė, and B. Abakevičienė, “Development and characterisation of polyvinyl butyral-biocide nanocomposite coatings for antimicrobial applications,” Applied Materials Today, vol. 44, p. 102720, Apr. 2025, doi: 10.1016/j.apmt.2025.102720.
[4] M. Ilickas et al., “ZnO tetrapod morphology influence on UV sensing properties,” Nanotechnology, vol. 35, no. 1, p. 015502, Sep. 2023, doi: 10.1088/1361-6528/acfcbf.

OPTIMIZATION OF ANTIMONY SELENIDE DEPOSITION ON ZINC OXIDE BY VAPOR TRANSPORT DEPOSITION METHOD

Gerarda Jocytė[1], Rokas Kondrotas[1], Gintautas Jonkus[1], Vidas Pakštas[1]

[1]Lithuania, Center for Physical Sciences and Technology, Department of Characterisation of Materials Structure
gerarda.jocyte@ftmc.lt

Antimony selenide (Sb_2Se_3) is a one-dimensional crystalline material comprised of non-toxic and earth abundant elements. The band gap of this semiconductor is approximately 1.2 eV, the electron mobility in single crystals is between 10 and 40 $cm^2V^{-1}s^{-1}$, and absorption coefficient exceeds 10^4 cm^{-1} above the band gap. Due to these properties, Sb2Se3 has attracted considerable scientific interest for use in photovoltaic technologies, including thin-film solar cells, photodetectors, and photoelectrochemical systems. [1, 2]

A suitable electron transport layer material for fabricating Sb_2Se_3 solar cells is zinc oxide (ZnO) due to its tunability via magnesium doping, which allows control of optoelectronic parameters, such as the band gap, conduction band offset, carrier concentration and optical transmittance [3]. However, Sb_2Se_3 is rarely synthesized on ZnO layers, particularly using vapor deposition techniques. Despite the suitable properties of ZnO, the detailed physical and interfacial properties of this heterojunction remain underexplored.

In this work, the Sb_2Se_3 absorber was deposited by vapor transport deposition (VTD) in a three-zone tube furnace onto spin-coated ZnO substrates. The growth conditions were systematically varied, including the substrate temperature (400–520 °C), distance of the substrate from the heating zone (–4 to 0 cm), deposition duration, arrangement of evaporation source. The deposited samples were characterized using standard structural characterization techniques, including scanning electron microscopy (SEM), X-ray diffraction (XRD), and complementary optical and electrical measurement methods.

SEM analysis shows distinct variations in the morphology of the Sb_2Se_3 films between samples grown under varying conditions. When the source powder was placed in the middle zone of the furnace, decreasing the temperature from 440 °C to 420 °C resulted in an increase in whisker formation on the Sb_2Se_3 layer. In contrast, when the source powder and the substrate were positioned within the same furnace zone, the lower temperatures produced lower density of whiskers and higher open circuit voltage than samples grown in higher temperatures. Samples grown at 400 °C for 15 minutes exhibited poorer electrical performance compared to those grown for 30 minutes, indicating that the optimal growth conditions are at low temperature with a longer deposition process.

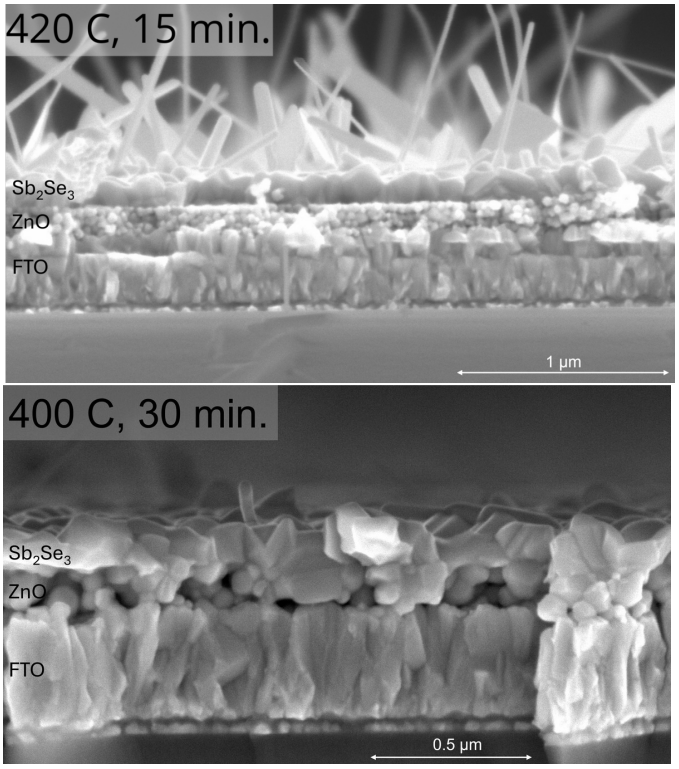


Fig. 1. SEM images of samples deposited under different conditions

[1] Wang, Liang, et al. "Stable 6%-efficient Sb2Se3 solar cells with a ZnO buffer layer." Nature Energy 2.4 (2017): 1-9.
[2] Mavlonov, Abdurashid, et al. "A review of Sb2Se3 photovoltaic absorber materials and thin-film solar cells." Solar Energy 201 (2020): 227-246.
[3] Rouchdi, Mustapha, et al. "Synthesis and characteristics of Mg doped ZnO thin films: Experimental and ab-initio study." Results in physics 7 (2017): 620-627.

INVESTIGATION OF ION-BEAM IRRADIATION EFFECTS ON THE ELECTRICAL PROPERTIES OF NOVEL N-TYPE LOW GAIN AVALANCHE DETECTORS

Margarita Biveinytė[1], Tomas Čeponis[1], Laimonas Deveikis[1], Miloš Manojlović[2], Vytautas Rumbauskas[1], Kęstutis Žilinskas[1]

[1]Vilnius University, Institute of Photonics and Nanotechnology, Lithuania
[2]Centro Nacional de Microelectrónica, IMB-CNM-CSIC, Cerdanyola del Vallès, Spain
margarita.biveinyte@ff.stud.vu.lt

Low Gain Avalanche Detectors (LGADs) are silicon sensors featuring internal signal amplification and are widely used in High-Energy Physics (HEP) experiments, particularly for precise timing measurements in environments with high particle fluences, such as those at Large Hadron Collider (LHC) at CERN. Conventional *p*-type LGADs have been optimized for the detection of highly penetrating particles but exhibit reduced gain performance for low penetrating radiation [1]. To address this limitation, *n*-type Low Gain Avalanche Detectors (nLGADs) have been developed to enhance sensitivity to low penetrating particles in silicon, such as soft X-rays, ultraviolet and visible photons, and low-energy charged particles [2]. Due to electron-initiated avalanche multiplication, nLGADs exhibit enhanced gain for surface-near energy deposition, making them particularly attractive for applications in medical physics, including ion beam cancer therapy, where accurate detection of low-energy charged particles is required [3]. However, the performance of nLGADs can be significantly affected by ionizing radiation through mechanisms such as donor removal, gain suppression, and modifications of the internal electric field [4].

In this work, we present an ongoing investigation of the effects of ion-beam irradiation on the electrical properties of novel *n*-type LGAD devices fabricated at the *Instituto de Microelectrónica de Barcelona* (IMB-CNM). A systematic irradiation campaign is combined with pre- and post-irradiation electrical characterization, including current–voltage (I–V) and capacitance–voltage (C–V) measurements, to study changes in leakage current, depletion region behavior, and gain-related parameters. The Transient Current Technique (TCT) is used to further investigate irradiation-induced modifications in charge collection efficiency and gain degradation.

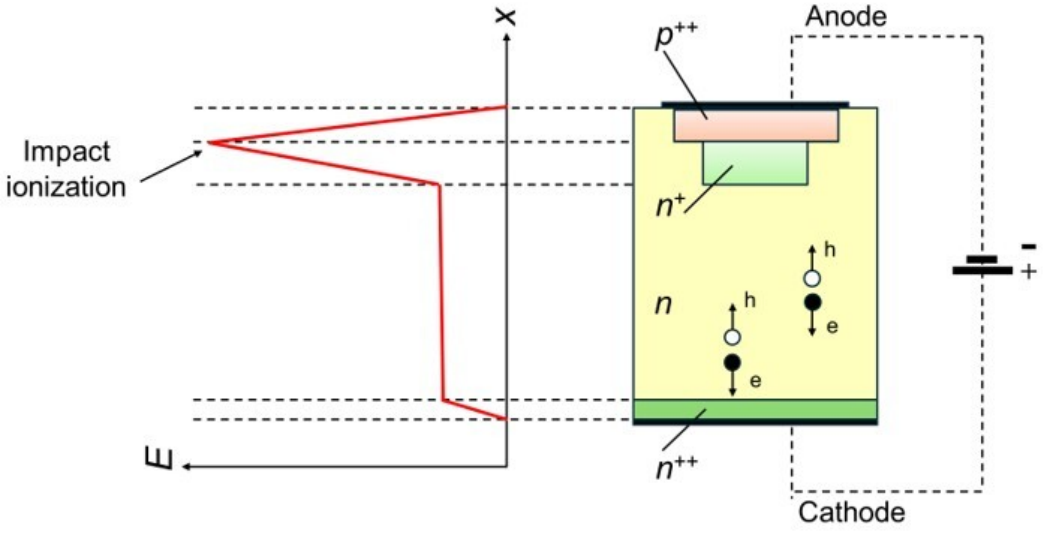


Fig. 1. A schematic representation of the nLGAD structure, implemented as $p^{++}n^{+}n$. A heavily doped gain layer generates a strong electric field (red solid line), enabling internal signal amplification for the detection of low-penetrating particles.

[1] V. Kraus, M. F. Garcia, S. Hidalgo, M. Moll, and J. Villegas, "Studies on the effect of low-fluence proton and neutron irradiation on n-type LGADs," Nucl. Instrum. Methods Phys. Res., Sect. A, vol. 1083, Art. no. 171138, Nov. 2025
[2] J. Villegas, N. Moffat, D. Maneuski, O. Ferrer, G. Pellegrini, and S. Hidalgo, "Gain measurements on NLGAD detectors," Nucl. Instrum. Methods Phys. Res., Sect. A, vol. 1055, Art. no. 168377, Jun. 2023
[3] M. Manojlović et al., "Gain response and ion beam-induced donor removal in NLGAD detector: Global gain quenching," IEEE Sensors J., vol. 25, no. 24, pp. 43985–43996, Oct. 2025
[4] V. Kraus, M. Biveinyte et al., "Investigating irradiation effects and space charge sign inversion in n-type low gain avalanche detectors," Nucl. Instrum. Methods Phys. Res., Sect. A, vol. 1080, Art. no. 170763, Jun. 2025

MODIFICATION OF GaN THIN LAYERS WITH HYDROGEN IMPLANTATION

Margarita Biveinytė[1], Šarūnas Vaitekonis[2], Vitalij Kovalevskij[2], Arūnas Kadys[1], Algirdas Mekys[1]

[1]Vilnius University, Institute of Photonics and Nanotechnology, Lithuania
[2]Center for Physical Science and Technology, Lithuania
margarita.biveinyte@ff.stud.vu.lt

Nowadays, the semiconductor material GaN is widely used in many electronic applications, including high-energy irradiation detectors [1]. However, its functionality is limited by material degradation during operation. To extend the applicability limits of such detectors, further research is required to improve the understanding of material interactions with high-energy particles that create structural damage.

Among various types of high-energy particles, hydrogen atoms (protons) are one of the most commonly used, and in this work the ion implantation technique was employed to generate defects in GaN using hydrogen. In addition to their availability, hydrogen atoms in the GaN crystal do not act as electrically active impurities and therefore do not introduce intentional doping; instead, they create defects by displacing host lattice atoms.

One of the most common methods for investigating irradiation-induced damage is electrical characterization of the material. Irradiation-induced defects modify the free carrier concentration and their drift mobility. The latter can be evaluated using the Hall effect method. However, the application of this method is not always straightforward and may lead to unusual results. In this study, the Hall mobility increases with irradiation dose, as shown in Fig. 1a, even though an increased defect density is generally expected to degrade carrier mobility.

The model explaining this behavior assumes that the defect generation probability depends on the pre-existing damage, leading to a non-uniform spatial distribution of defects, as illustrated in Fig. 1b. The resulting redistribution of the electric potential is responsible for the increased Hall voltage, as discussed previously [2].

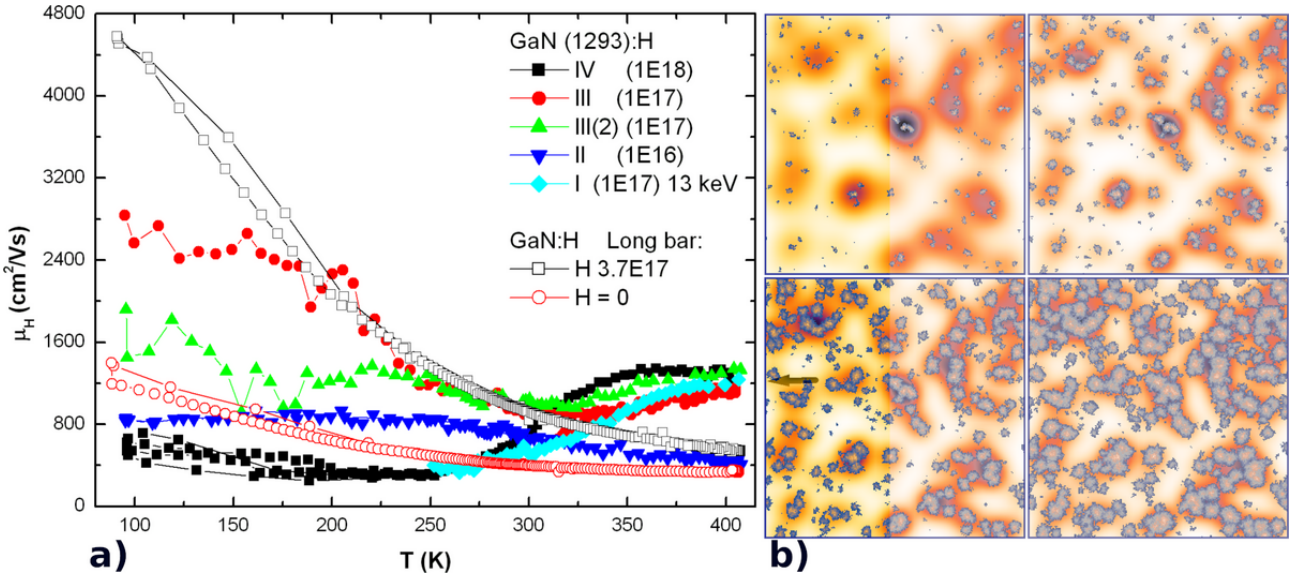


Fig. 1. (a) Temperature dependence of the Hall mobility for various implantation doses (cm^{-2}); (b) four modeled defect-generation time frames with increasing irradiation dose from left to right and from top to bottom.

Acknowledgements
This research was funded by the Research Council of Lithuania, project No S-MIP-24-81.

[1] J. Wang, P. Mulligan, L. Brillson, and L. R. Cao, "Review of using gallium nitride for ionizing radiation detection," Appl. Phys. Rev., vol. 2, no. 3, Art. no. 031102, Sep. 2015
[2] R. H. Bube, "Interpretation of Hall and photo-Hall effects in inhomogeneous materials," Appl. Phys. Lett., vol. 13, no. 4, pp. 136–139, Aug. 1968

BILAYER POLYSACCHARIDE FILMS CONTAINING FERMENTED AND NON-FERMENTED ARTHROSPIRA PLATENSIS EXTRACTS

Deimante Rosliuk[1], Dovile Liudvinaviciute[1], Ramune Rutkaite[1], Shahana Aboobacker[2], Vaida Kitryte-Syrpa[2], Michail Syrpas[2]

[1]Kaunas University of Technology, Faculty of Chemical Technology, Department of Polymer Chemistry and Technology, Kaunas, Lithuania,
[2]Kaunas University of Technology, Faculty of Chemical Technology, Department of Food Science and Technology, Kaunas, Lithuania,
deimante.rosliuk@ktu.lt

Orally disintegrating films (ODFs) are thin, flexible drug delivery systems that dissolve in the oral cavity to release active compounds locally [1]. Due to their rapid disintegration and ease of administration, ODFs are promising carriers for the local oral delivery of natural antioxidants in the treatment of oral cavity diseases such as periodontitis and gingivitis [2]. Arthrospira platensis extract is rich in proteins, phycocyanins, and phenolic compounds, and has been widely investigated as a source of antioxidant and anti-inflammatory agents [3]. These properties make it a promising bioactive material for incorporation into ODFs.

Main goal of this research work was the development of novel orally disintegrating bilayer films composed of polysaccharides and non fermented or lactic fermented Arthrospira platensis extracts and investigation of their properties. Bilayer films composed of a methyl cellulose and chitosan/hydroxyethyl cellulose layers, with glycerol and citric acid used as the plasticizer and crosslinker, respectively, were prepared using the solvent casting method. Non-fermented and lactic-fermented Arthrospira platensis extracts were immobilized in either layer. The main characteristics of the bilayer films including wetting, mechanical properties, bioactives release in a simulated salivary medium and antioxidant activities were evaluated.

Acknowledgements
This project has received funding from the Research Council of Lithuania (LMTLT), agreement No S-MIP-23-78.

[1] S. Mazumder, et al. “Quality by Design approach for studying the impact of formulation and process variables on product quality of oral disintegrating films,” International Journal of Pharmaceutics, vol. 527, pp. 151-160, 2017.
[2] S. Jacob, et al. “Orodispersible Films: Current Innovations and Emerging Trends,” Pharmaceutics, vol. 15, pp. 2753, 2023.
[3] N.K.Z. AlFadhly, et al. “Trends and Technological Advancements in the Possible Food Applications of Spirulina and Their Health Benefits: A Review,” Molecules, vol. 27, pp. 5584, 2022.

FABRICATION AND DYNAMIC MECHANICAL CHARACTERIZATION OF FLAX FIBER-REINFORCED HYBRID COMPOSITES

Robertas Gilys[1], Justas Ciganas[1], Urte Cigane[1]

[1]Siauliai State Higher Education Institution, Lithuania
robertas.gilys@stud.svako.lt

In recent years, increasing attention has been paid to the development of sustainable and environmentally friendly materials to reduce the environmental impact of synthetic composites [1]. This study investigated the fabrication of hybrid composites using natural flax fiber and bio-based epoxy resin. Dynamic mechanical analysis (DMA) was performed to evaluate the mechanical properties of the composite. The experimental study was performed according to the ISO 6721 standard [2]. The composites were manufactured using an open-molding technique, ensuring uniform fiber distribution within the matrix and good interfacial adhesion between the composite components. For comparison purposes, a UV-curable resin was also used as a reference material and was tested under the same conditions.

DMA tests were performed to evaluate the response of a material to cyclic mechanical load, since most materials today are subject to cyclic loading [3]. During the analysis, the storage modulus and loss modulus were determined, which allowed evaluation of the stiffness, elastic response, and internal energy dissipation of the composite. The results obtained showed that flax fiber reinforced composites exhibit different mechanical properties depending on the type of resin used. The highest stiffness, mechanical strength, and loss modulus values were determined for a hybrid composite consisting of flax fiber, bio-based epoxy resin, and UV-curable resin.

Although this hybrid composite exhibited good mechanical properties, at an excitation frequency of 40 Hz, the storage modulus decreased and the loss modulus increased. Considering the small dimensions of the tested specimens, changes in the storage and loss moduli were observed, which were not related to wave resonance phenomena but to internal relaxation processes and enhanced by interfacial interactions in the composite structure.

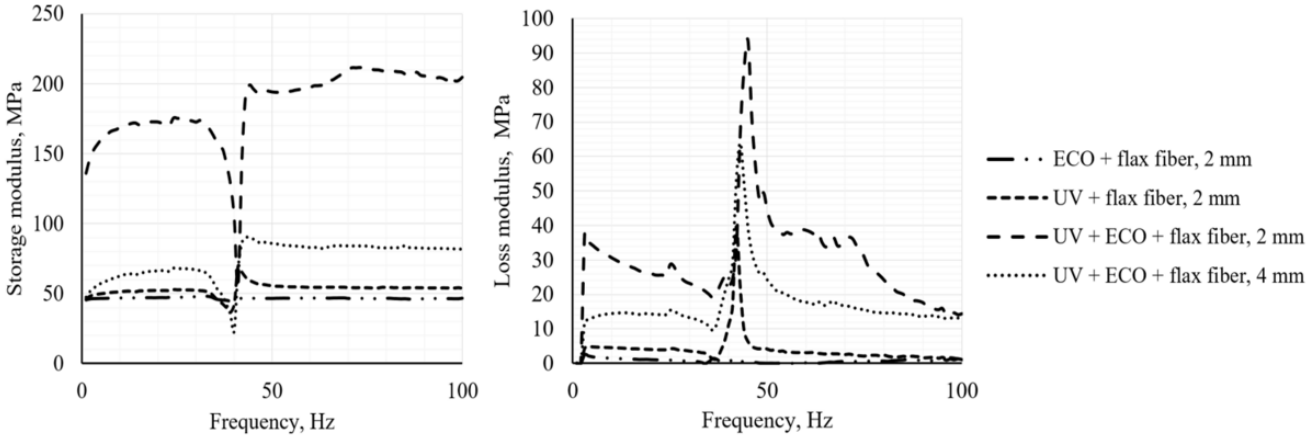


Fig. 1. Results of the storage and loss modulus

In summary, the results showed that single two-component epoxy resins do not exhibit sufficient dynamic mechanical properties. The development of a combined hybrid composite resulted in improved mechanical properties compared to composites prepared using individual resins. Therefore, bio-derived epoxy resins can be effectively used as modifiers in hybrid composite systems and are a promising alternative to conventional synthetic composites.

[1] C. Popescu, H. Dissanayake, E. Mansi, and A. Stancu, "Eco Breakthroughs: Sustainable materials transforming the future of our planet," Sustainability, vol. 16, no. 23, p. 10790, Dec. 2024, doi: 10.3390/su162310790.
[2] "ISO 6721-11:2019," ISO. https://www.iso.org/standard/74988.html
[3] S. P. Phansalkar, R. Mittakolu, B. Han, and T. Kim, "Enhanced DMA test procedure to measure viscoelastic properties of Epoxy-Based molding compound: multiple oscillatory strain amplitudes and monotonic loading," Micromachines, vol. 16, no. 4, p. 384, Mar. 2025, doi: 10.3390/mi16040384.

METAL HIGH-REFLECTIVE MIRRORS FOR SPACE APPLICATIONS

Alexandr Belosludtsev[1], Ignas Bitinaitis[1], Vitalij Kovalevskij[1], Karolis Stravinskas[1], Anna Sytchkova[2]

[1]Center for Physical Sciences and Technology, Vilnius, Lithuania
[2]ENEA Casaccia, Rome, Italy
Alexandr.Belosludtsev@ftmc.lt

The volume of information necessary to transmit on Earth, in space, and between satellites and ground stations is increasing. Satellites are planned to be connected to the global secured quantum network on low-Earth orbits, to be used for quantum communication at higher distances from our planet. Such applications require optical components like metallic mirrors for signal preparation and transfer. In recent study [1], we report a systematic investigation on the silver-aluminium (Ag-Al) mixed mirrors designed for space missions. We show the Ag-Al mixed coatings preparation process and investigate their properties for various Al concentrations up to 15%. It was found that optimize Al admixing leads to the formation of smooth mirrors with high reflectance (measured >90% vis-IR range). Mirrors were tested by low-energy proton irradiation at doses typical for interplanetary missions. Furthermore, we have coated an additive manufactured complex shaped mirror [2]. The performance under high-power laser irradiation was numerically studied.

Acknowledgements

This project has received funding from the Research Council of Lithuania (LMTLT), agreement No [P-MIP-24-15]. This work was carried out within the Space It Up! project funded by the Italian Space Agency (ASI) and the Italian Ministry of University and Research (MUR) under contract No. 2024-5-E.0, CUP No. I53D24000060005.

Keywords: Metal mirrors; Thin films; Radiation tests; Space Optics; Photonics; Quantum communication.

[1] A. Belosludtsev, et. al., Adv. Space Res. submitted (2026),
[2] I. Bitinaitis, et. al. Opt, Mater., 169, 117570 (2026).

SYNTHESIS AND CHARACTERIZATION OF ZINC SULFIDE FILMS ON FTO GLASS

Dominyka Zubrickaitė[1], Ingrida Ancutienė[1], Asta Bronušienė[1]

[1]Kaunas University of Technology, Department of Physical and Inorganic Chemistry
zubrickaite.dominyka@gmail.com

Zinc sulfide (ZnS) is a non-toxic, abundant semiconductor characterized by a wide direct band gap (3.65 eV) and excellent chemical stability against oxidation and hydrolysis [1]. Due to its unique optoelectronic properties, ZnS is widely utilized in solar cells, sensors, and light-emitting devices, while also serving as an efficient photocatalyst for the degradation of organic water contaminants [2]. Structurally, ZnS exists in two primary phases: the low-temperature stable zinc blende and the high-temperature wurtzite [3]. The aim of this work was to synthesize ZnS films on FTO glass using the Successive Ionic Layer Adsorption and Reaction (SILAR) method and to characterize them via X-ray diffraction (XRD), Grazing Incidence XRD (GIXRD), SEM, and EDX analysis. The deposition involved immersing a cleaned FTO substrate in a cationic precursor (0.1 M ZnCl2) for 30 s, followed by an anionic precursor (0.1 M Na2S) for 30 s, with intermediate rinsing in distilled water for 20 s. The process was performed in steps of 10 cycles up to a total of 40 cycles, with intermediate annealing after every 10-cycle increment to enhance film stability. XRD analysis identified a cubic ZnS phase (PDF No. 80-20) alongside SnO2 (PDF No. 46-1088) from the substrate surface, with ZnS peaks observed at 2θ= 28.28°, 48.23°, and 56.57°. As the number of deposition cycles increased, the intensity of the ZnS peaks also increased. Parallel analysis using GIXRD confirmed consistent ZnS peaks; however, the SnO2 substrate peaks were not detected in several diffractograms when using the grazing incidence method. In the 40-cycle sample, the SnO2 phase was entirely absent, indicating that the film thickness was sufficient to fully mask the surface of FTO substrate. SEM imaging revealed a clear evolution of the surface morphology as a function of the cycle count and thermal treatment. At 10 SILAR cycles, the unheated film exhibited a highly porous and fragmented structure consisting of loose aggregates with significant voids. Thermal treatment initiated the densification process, where particles began to rearrange into larger clusters. As the deposition progressed to 20 and 30 SILAR cycles, a distinct granular morphology emerged, characterized by more uniform and well-defined grains. By 40 SILAR cycles, the film reached its peak density and surface homogeneity, forming a continuous layer where individual grains merged to minimize porosity. These findings were further supported by EDX analysis, which showed the Sn signal from the FTO glass dropping to just 0.88 % at 40 SILAR cycles, while Zn and S concentrations reached 29.75 % and 19.22 %, respectively, confirming the formation of a dense, chemically mature, and uniform ZnS thin film.

[1] S. A. Saah, P. O. Sakyi, N. O. Boadi, F. A. Tieku, and A. K. Boampong, “Solventless Synthesis of Zinc Sulphide Nanoparticles from Zinc Bis(diethyldithiocarbamate) as a Single Source Precursor,” ChemistryOpen, vol. 13, no. 6, p. e202400050, May 2024, doi: 10.1002/open.202400050.

[2] N. Kaur et al., “A review on Zinc sulphide nanoparticles: from synthesis, properties to applications,” Journal of Bioelectronics and Nanotechnology, vol. 1, no. 1, Jan. 2016, doi: 10.13188/2475-224x.1000006.

[3] A. Chakrabarti and E. Alessandri, “Syntheses, properties, and applications of ZNS-Based Nanomaterials,” Applied Nano, vol. 5, no. 3, pp. 116–142, Aug. 2024, doi: 10.3390/applnano5030010.

MXENE BASED SCHOTTKY-JUNCTIONS FOR UNASSISTED PHOTOELECTROCHEMICAL WATER SPLITTING

Syeda Ammara Shabbir[1,8], Muhammad Haris[2,3], Sohaib Khalid[1], Carlos Ponce de Leon[8], Klaudijus Midverisa[2,3], Muhammad Younas[4], Hamid Latif[1], Imed Boukhris[5], M S alburiahi[6], Norah Salem Alsaiari[7], Tomas Tamulevičius[2,3], Sigitas Tamulevičius[2,3]

[1]Department of Physics, Forman Christian College (A Chartered University), Lahore, Pakistan
[2]Institute of Materials Science Kaunas, University of Technology, K. Baršausko g. 59, LT51423, Kaunas, Lithuania.
[3]Department of Physics, Kaunas University of Technology, Lithuania Studentų St. 50, LT, 51368, Kaunas, Lithuania
[4]Core Research Facilities, King Fahd University of Petroleum and Minerals, 3126, Dhahran, Saudi Arabia
[5]Department of Physics, Faculty of Science, King Khalid University, P.O. Box 9004, Abha, Saudi Arabia
[6]Department of Physics, Sakarya University, Sakarya, Turkey
[7]Department of Chemistry, College of Science, Princess Nourah bint Abdulrahman University, P.O. Box 84428, Riyadh 11671, Saudi Arabia
[8]Energy Technology Research Group, Faculty of Engineering and Physical Sciences, University of Southampton, Highfield Campus, Southampton, SO17 1BJ, UK
ammaraanwar@fccollege.edu.pk

The development of high performance self-powered photoelectrochemical (PEC) water splitting is greatly impacted by the screening of photoelectrodes with appropriate Fermi level difference. This work involved the merging of the Ti3C2/BiVO4 and Ti3C2/g-C3N4 based photoanodes and Ti3C2/MoS2 and Ti3C2/BiOI based photocathodes to create a dual-photoelectrode unassisted system for PEC water splitting. X-ray diffraction (XRD) and Scanning electron microscopic (SEM) analysis confirmed the structural and morphological analysis of fabricated photoanodes and photocathodes. MXene (Ti3C2) nanosheets produced distinctive Schottky junctions when combined with semiconductors (BiVO4, g-C3N4, BiOI and MoS2). These junctions modified Fermi energy levels, assisted in the separation of electron-hole pairs and increased light absorption and resulted in efficient conversion of water into hydrogen (H2) and oxygen (O2), analyzed through linear sweep voltammetry (LSV). The fabricated Ti3C2 MXene based Schottky junctions offered a base for the innovative building of dual-photoelectrode internal driven, independent of power, PEC water splitting platform with excellent performance.

Acknowledgements
This project has received funding from the Research Council of Lithuania (LMTLT), agreement no S-MIP-23-93.

CYANOPYRIDINE-BASED TADF EMITTERS FOR OLEDS AND OPTICAL SENSING

Akaki Kalatozishvili[1], Oleksandr Bezvikonnyi[1,2], Jurate Simokaitiene[1], Dmytro Volyniuk[1], Dalius Gudeika[1], Hlafira Krasnozhon[1,3], Juozas V. Grazulevicius[1]

[1]Kaunas University of Technology, Department of Polymer Chemistry and Technology, K. Baršausko st. 59, LT-51423 Kaunas, Lithuania
[2]University of Latvia, Institute of Solid State Physics, kengaraga iela 8, Latgales priekšpilsēta, LV-1063, Riga, Latvia
[3]Ivan Franko National University of Lviv, Faculty of Chemistry, Department of Organic Chemistry, Kyryla i Mefodiya st. 6, 79005, Lviv, Ukraine
akaki.kalatozishvili@ktu.lt

The technology of organic light emitting diodes (OLEDs) is rapidly growing. The main option to increase the efficiency of the devices is to effectively utilize triplet excitons in electroluminescence. Conventional phosphorescent OLEDs require the use of earth-rare metal complexes such as those of Ir, Pt, Au, etc. incorporated in the organic matrixes (hosts) [1]. Emitters exhibiting thermally activated delayed fluorescence (TADF) emerged as a cost-effective alternative to phosphorescent emitters [2]. TADF is a long-lived fluorescence based on upconversion of triplet excitons into singlet ones. Here, we report on the series of cyanopyridine derivatives as TADF emitters. The ionization energies estimated from the photoelectron emission spectra are in the range of 5.37-5.86 eV. Drift mobility of the charge carriers of the compounds measured by the techniques of time-of-flight and charge extraction by linear increase of voltage were evaluated to be up to 1×10^{-3} $cm^2/V{\cdot}s$ at an electric field of approximately 2.5×10^5 V/cm. TADF was detected for the toluene solutions of the compounds. Picric acid was added to the deoxygenated toluene solution of one of the compounds to test the sensitivity of its emission to the nitroaromatic explosive compound. The Stern-Volmer plot showed a linear correlation with the photoluminescence lifetime of the sample. The increase of the picric acid concentration to 20% resulted in the 5.8-fold decrease of the TADF lifetime of the solution. The emission peaks shifted from blue to green/yellow spectral regions for most of the compounds when they were molecularly dispersed in host 1,3-bis(N-carbazolyl)benzene. The photoluminescence and electroluminescence lifetimes of up to 0.5 ms were recorded. The thermal activation of TADF was confirmed from the analysis of photoluminescence decay curves recorded at the different temperatures. The fabricated OLEDs showed the external quantum efficiency of up to 30.6%.

Acknowledgements
This project has received funding from the Research Council of Lithuania (LMTLT), agreement No S-LU-24-6.

[1] Y. Patil, C. Demangeat, and L. Favereau, “Recent advances in room temperature phosphorescence of chiral organic materials,” Chirality, vol. 35, no. 7, pp. 390–410, 2023.
[2] E. Tankelevičiūtė, I. D. W. Samuel, and E. Zysman-Colman, “The blue problem: OLED stability and degradation mechanisms,” J. Phys. Chem. Lett., vol. 15, pp. 1034–1047, 2024.

SYNTHESIS AND PROPERTIES OF PHENANTHROIMIDAZOLE-BASED COMPOUNDS AS PROMISING EMITTERS FOR OLEDS

Svetlana Sargsyan[1], Viktorija Andruleviciene[1], Matas Guzauskas[1], Dmytro Volyniuk[1], Juozas Vidas Grazulevicius[1]

[1]Kaunas University of Technology, Faculty of Chemical Technology, Department of Polymer Chemistry and Technology, K. Baršausko st. 59, LT-51423, Kaunas, Lithuania.
svetlana.sargsyan@ktu.edu

In recent decades, organic light-emitting diodes (OLEDs) have attracted significant attention for their application in solid-state lighting and flat-panel display technologies, owing to their flexibility, cost-effectiveness, and high efficiency. The development of new organic emitters has therefore become essential to meet the increasing demand for high performance OLEDs in next-generation lighting and display applications[1]. Phenanthroimidazole-based fluorophores represent one of the most attractive families of compounds for organic electronic applications, owing to their tunable structures at the N1 and C2 positions. Furthermore, these compounds have rigid molecular skeletons, exhibit high charge-carrier mobilities, excellent thermal stability, and good film-forming properties. They are promising candidates for blue, green, and yellow emitters in high performance OLEDs [2]. Herein, we present the design and synthesis for four new phenanthroimidazole-derivatives prepared through a four-step procedure with high yields. The thermal and photophysical properties of the synthesized compounds are also reported. These compounds exhibit high glass-transition temperatures exceeding 150 °C. Photophysical properties of the solutions and of the solid films of the synthesized compounds were studied. The compounds demonstrated short fluorescence lifetimes, locally excited emission, and ionization potentials of ca.5.65 eV. Overall, the combination of favourable thermal stability, suitable ionization potential, and efficient short-lived emission makes these phenanthroimidazole derivatives promising materials for “fast” OLEDs.

[1] X. Tang, H. Liu, L. Xu, X. Xu, X. He, F. Liu, J. Chen, Q. Peng, Achieving High Efficiency at High Luminance in Fluorescent Organic Light-Emitting Diodes through Triplet–Triplet Fusion Based on Phenanthroimidazole-Benzothiadiazole Derivatives, Chemistry - A European Journal 27 (2021) 13828–13839. https://doi.org/10.1002/chem.202102136.

[2] H. Zhang, J. Zeng, W. Luo, H. Wu, C. Zeng, K. Zhang, W. Feng, Z. Wang, Z. Zhao, B.Z. Tang, Synergistic tuning of the optical and electrical performance of AIEgens with a hybridized local and charge-transfer excited state, J Mater Chem C Mater 7 (2019) 6359–6368. https://doi.org/10.1039/c9tc01453e.

MOLECULAR ENGINEERING OF ETHYLCARBAZOLE DERIVATIVES FOR HIGHLY EFFICIENT OLED HOST MATERIALS

Dovydas Blazevicius[1], Raminta Beresneviciute[1], Ernestas Kasparavicius[1], Julius Petrulevicius[1], Gintare Krucaite[1], Saulius Grigalevicius[1], Chih-Hung Ko[2], Cai-Fan Lo[2], Chih-Hao Chang[2]

[1]Lithuania, Kaunas University of Technology, Faculty of Chemical Technology, Department of Polymer Chemistry and Technology
[2]Taiwan, Yuan Ze University, Department of Electrical Engineering
dovydas.blazevicius@ktu.lt

Organic light-emitting diodes (OLEDs) have garnered significant scientific and industrial attention due to advantages ranging from innovative product design possibilities to highly efficient and sustainable light sources, creating amdemand for new high-performance materials. Although state-of-the-art OLEDs now exceed 30% EQE, challenges such as amorphous layer instability, exciton quenching, and efficiency roll-off persist, making device performance and operational stability strongly dependent on the molecular design of the organic layers. Among these, the host material in the emissive layer plays a particularly critical role, especially in phosphorescent and TADF OLEDs, where efficient management of both singlet and triplet excitons is required [1, 2].

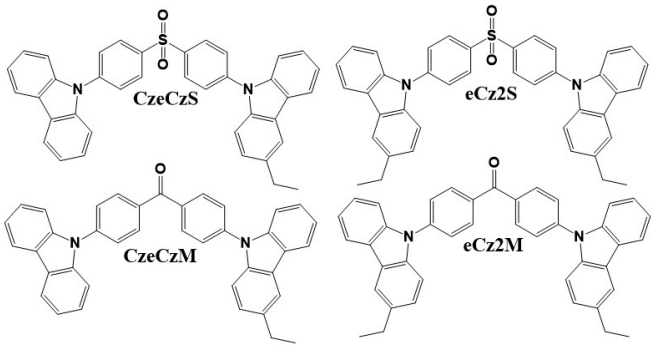


Fig. 1. Structures of newly synthesized ethylcarbazole derivatives

Addressing this need, new ethylcarbazole-based D-A-D host materials were synthesized using one- or two-step nucleophilic aromatic substitution routes and evaluated for their suitability in OLEDs. Materials had one (CzeCzS, CzeCzM) or two (eCz2S, eCz2M) ethylcarbazole units paired with either sulfonyl (CzeCzS, eCz2S) or methanone (CzeCzM, eCz2M) electron acceptors. Thermal and morphological analyses showed that all materials are highly resistant to degradation, with decomposition temperatures ranging from 393 to 436 °C, and they form stable amorphous films with high Tg values (89–112 °C). Photophysical measurements revealed high triplet state energies (2.71 – 2.90 eV), indicating that these compounds can serve as hosts for both green phosphorescent and yellow TADF emitters. Device studies highlighted that methanone-bridged hosts outperformed phenylsulfonyl analogues due to more balanced charge transport and improved exciton confinement. When applied as host materials to green phosphorescent emitter, maximum EQE of 16.5% was achieved. Incorporating these hosts into blended co-host architectures led to notable efficiency enhancements with external quantum efficiency values surpassing 20%. The best-performing device, based on the eCz2M:B3PyMPM co-host system, achieved an EQE of 20.3%, a luminance efficiency of 72.7 cd/A, and a power efficiency of 95.1 lm/W. Also, for yellow emitting TADF OLED prototype our co-host systems enabled to achieve an EQE of 10.3%. This work demonstrates that methanone-ethylcarbazole D-A-D structures are strong candidates for next generation efficient OLED host materials. This work provides fundamental knowledge for developing advanced host materials for both TADF and phosphorescent OLED technologies.

Acknowledgements

We acknowledge support from the Research Council of Lithuania (grant No. S-MIP-25-23) and for support from the Faculty of Chemistry and Chemical Technology of Kaunas University of Technology

Keywords: OLED; Organic Semiconductor; Host Materials.

[1] C. Van Hoesel, R. Coehoorn, and P. A. Bobbert, “Theoretical study of host-guest exciton-polaron quenching rates in phosphorescent OLED emission layers,” SPIE, p. 9, Jan. 2023, doi: 10.1117/12.2645104.

[2] G. Kreiza et al., “Suppression of benzophenone-induced triplet quenching for enhanced TADF performance,” Journal of Materials Chemistry C, vol. 7, no. 37, pp. 11522–11531, Jan. 2019, doi: 10.1039/c9tc02408e.

LINK BETWEEN SYNTHESIS PARAMETERS AND STRUCTURAL PROPERTIES OF ZINC OXIDE

Gintautas Jonkus[1], Vidas Pakštas[1], Rokas Kondrotas[1]

[1]State research institute Center for Physical Sciences and Technology, Department of Characterization of Materials Structure, Sauletekio av. 3, Vilnius, Lithuania
gintautas.jonkus@ftmc.lt

Zinc oxide is widely used in the field of optoelectronics as an electron transport layer in solar cells and light emitting diodes, as transparent conductive oxide, as an active material in photoconductor-type UV photodetectors etc.[1] Its intrinsic properties such as high band gap of 3,37 eV, high optical transparency in visible region and exciton energy of 60 meV are the qualities that make this material highly applicable in optoelectronic devices. ZnO thin films, depending on the application and required quality, can be synthesized by a wide range of methods - starting from a solution-based hydrothermal method to various physical vapour deposition approaches . [2] One of the highly perspective, low-cost solution-based deposition approach for ZnO thin films is the sol-gel method. In this method, the selection of solvents, ligands, precursors and their concentrations, and crystallization temperatures play a very important role in defining structural properties of ZnO thin films. In this study, we aim to establish the correlation between synthesis parameters and ZnO structural properties and its effect on the solar cell device characteristics.

This study investigates the effects of precursor concentration (spanning from 0.3 to 0.75M) and annealing temperatures (ranging from 400 to 525°C) on the preferential crystallographic orientation and morphological changes of ZnO nanostructures. Scanning electron microscopy (SEM) has been used in determining morphology and thickness of synthesised thin films. To determine the structural phases of the zinc oxide layers, X-ray diffraction measurements were conducted employing Bragg-Brentano θ-2θ geometry.

The results indicate a clear correlation between intensity of dominant (002) plane and the annealing temperature, increasing the temperature leads to the increase of (002) XRD peak intensity. We also observed that increasing the concentration of precursor can lead to larger nanostructures but does not have an impact on uniformity of the film. Synthesised thin films were employed in fabricating FTO/ZnO/Sb_2Se_3/Spiro-OMeTAD/Au solar cells which demonstrated 2.7% power conversion efficiency. Further work is planned to fine-tune ZnO properties by alloying it with Mg and thus to improve heterojunction quality.

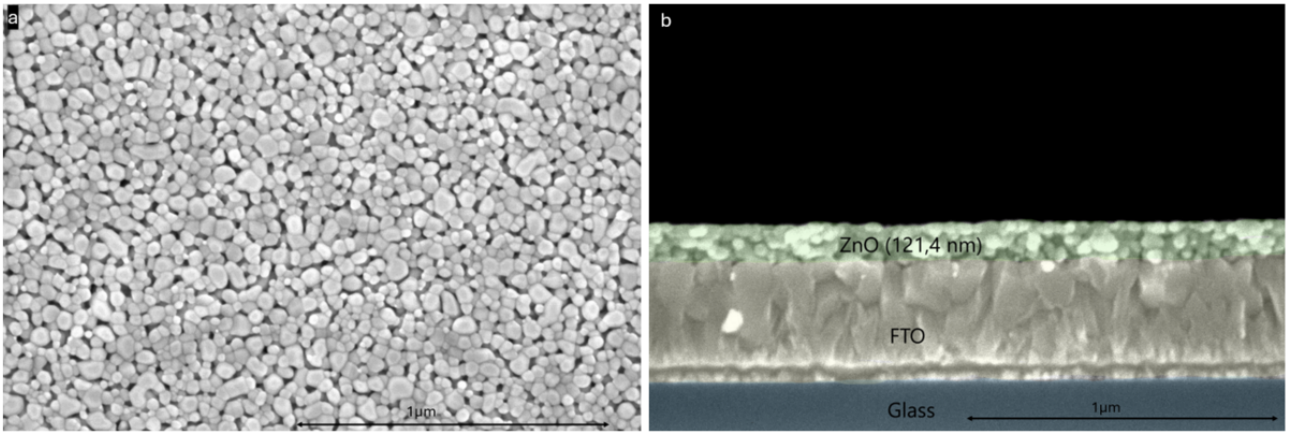


Fig. 1. SEM images of the synthesized ZnO thin films: (a) surface morphology and (b) cross-section.

[1] D. Buckley, A. Lonergan, and C. O'Dwyer, 'Review—ZnO-based Thin Film Metal Oxide Semiconductors and Structures: Transistors, Optoelectronic Devices and Future Sustainable Electronics', ECS J. Solid State Sci. Technol., vol. 14, no. 1, p. 015001, Jan. 2025, doi: 10.1149/2162-8777/ada3a2.

[2] F. T. Z. Toma, M. S. Rahman, and K. H. Maria, 'A review of recent advances in ZnO nanostructured thin films by various deposition techniques', Discov. Mater., vol. 5, no. 1, p. 60, Mar. 2025, doi: 10.1007/s43939-025-00201-1.

SELENIZATION OF THIN ANTIMONY FILMS FOR Sb_2Se_3 SOLAR CELLS

Linas Majauskas[1], Audrius Drabavičius[2], Vidas Pakštas[2], Rokas Kondrotas[2]

[1]Lithuania, Kaunas University of Technology, Faculty of Chemical Technology
[2]Lithuania, Center for Physical Sciences and Technology
linas.majauskas@ktu.edu

Given that today's dominant solar cells are mostly made from crystalline silicon, the limitations of this technology are becoming increasingly apparent. Also the rigid structure of silicon-based solar cells limits their applications where flexibility or integration into lightweight structures is required. One of the compounds that has received increasing attention in recent years is antimony selenide (Sb_2Se_3). This compound has a suitable energy bandgap (1.1–1.2 eV), a high light absorption coefficient, and good electron transport properties. In addition, the composition of Sb_2Se_3 is based on earth-abundant and less toxic elements. However, like many quasi-1D materials, Sb_2Se_3 is an anisotropic compound. To achieve efficient charge transport between the electrodes of a solar cell, it is necessary to form Sb_2Se_3 layers with a predominantly hkl (l≠0) crystallographic orientation. The aim of this work was to control the crystallographic orientation of Sb_2Se_3 thin films to expand the application possibilities of this material in solar cells.

This was achieved by two step synthesis: in the first stage antimony films were deposited using thermal evaporation method, systematically changing process parameters (current, evaporation time and the distance between substrate) to assess their influence on the quality of the layer. The coatings formed on SLG/FTO/TiO_2 substrates were characterized by X-ray diffraction (XRD). In the second stage, the deposited layers were selenized in a rapid thermal treatment (RTA) furnace, and the obtained samples were examined by XRD and scanning electron microscopy (SEM). The analysis allowed us to determine the dependence of the crystal quality, dominant orientation and surface morphology on technological parameters (temperature, time, pressure).

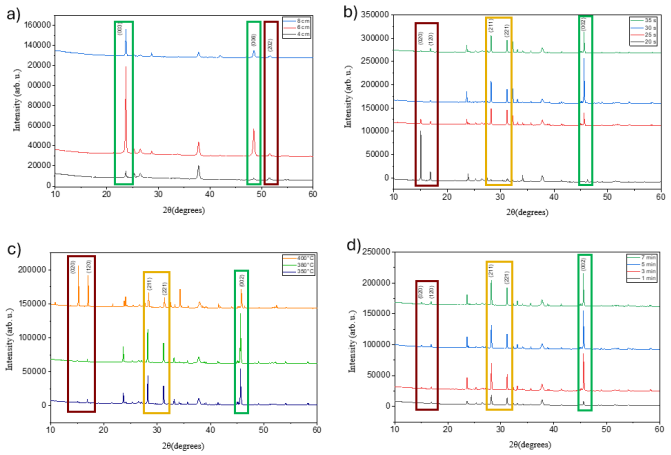


Fig. 1. a) X-ray diffraction pattern of Sb layers by varying the distance between the substrate and the Sb powder source; b)X-ray diffraction pattern of Sb_2Se_3 layers by varying the time of Sb deposition; c) X-ray diffraction pattern of Sb_2Se_3 layers by varying the temperature of selenization; d) X-ray diffraction pattern of Sb_2Se_3 layers by varying the time of selenization process

To conclude the experiments, we can highlight the key points:

1) The crystallinity of Sb layers directly depends on the distance between the substrate and the precursor material during thermal evaporation.

2) The predominant crystallographic orientation in the Sb_2Se_3 layers directly depends on the crystallinity of the Sb precursor layer.

3) It was not possible to completely avoid hkl (l = 0) oriented Sb_2Se_3 crystal planes, but after conducting a systematic study, we found that samples formed at a distance of 6 cm between the substrate and the precursor material and selenized at 380 ^{0}C for 3 minutes are characterized by an extremely low amount of them in the layer.

NANOCRYSTALLISATION OF AMORPHOUS ANALOGUES OF BSCCO SUPERCONDUCTORS

Maria Kacprzak[1], Tomasz K. Pietrzak[1]

[1]Warsaw Univeristy of Technology, Faculty of Physics, Poland
maria.kacprzak2.stud@pw.edu.pl

Superconductors are materials whose electrical resistivity becomes zero and which expel a magnetic field below a characteristic critical temperature (T_C). They can be divided into two main types. The first type is characterised by low-T_C (below 10 K) and the presence of the critical magnetic field above which superconductivity is destroyed. The second type includes materials in which, above a certain magnetic field B_1, the magnetic field penetrates the superconductor, leading to the formation of a mixed state. Above the critical field B_2, the superconducting state is destroyed. In addition, they often present high-T_C (above 100 K). It is worth noting that the type-I superconductors are mainly metals, whereas type-II superconductors are typically metal compounds and ceramics. Probably, the YBCO superconductor is known as the most popular type-II superconductor.

However, in the present study, attention is focused on the BSCCO superconductor. BSCCO is a family of high-temperature superconductors with a chemical formula $Bi_2Sr_2Ca_{n-1}Cu_nO_{2n+4+x}$. These compounds are well known for their high critical temperatures. There are three main types of BSCCO: 2201 (*n=1*) with T_C of approximately 10 K (very-low T_C phase), 2212 (*n=2*) with T_C≈85 K (low T_C phase) and 2223 (n=3) with T_C≈105 K (high-T_C phase). There is also a less common 4334 (n=4) phase, which exhibits even higher T_C values, though it has not been extensively studied yet.

Previous studies conducted by our research group have provided experience in developing highly conductive cathode materials for Li/Na-ion batteries via thermal nanocrystallisation of their amorphous analogues [1]. The intriguing properties of these nanomaterials originated from their microstructure, namely the presence of nanoscopic crystallites embedded in a residual glassy matrix.

In this research, the same approach was applied in order to obtain a nanocomposite with grains of the superconducting phase. Firstly, a glassy analogue of BSCCO 4334 was synthesised [2] using a standard melt-quenching approach. Then, the sample was examined using DTA (Differential Thermal Analysis) — to determine the glass transition and crystallisation temperature and XRD (X-Ray Diffractometry) — to verify amorphousness. Secondly, the samples were heated to induce thermal nanocrystallisation of superconducting phases. Eventually, the electrical conductivity will be examined, searching for the transition between the normal and superconducting state.

[1] T. K. Pietrzak, M. Wasiucionek, and J. E. Garbarczyk, “Towards higher electric conductivity and wider phase stability range via nanostructured glass-ceramics processing,” Nanomaterials, vol. 11, no. 5, p. 1321, May 2021, doi: 10.3390/nano11051321.

[2] M. Gazda, B. Kusz, L. Murawski, S. Stizza, and R. Natali, “(Bi,Pb)-Sr-Ca-Cu-O glass-ceramics – superconductor and granular metal,” Optica Applicata, vol. 38, no. 1, pp. 153–161, Jan. 2008.

STUDY OF RECOMBINATION CHARACTERISTICS OVER A WIDE FLUENCE RANGE IN REACTOR NEUTRON IRRADIATED Si

Justė Martinavičiūtė[1], Laimonas Deveikis[1], Tomas Čeponis[1]

[1]Vilnius University, Faculty of Physics, Institute of Photonics and Nanotechnology, Lithuania
juste.martinaviciute@ff.stud.vu.lt

Si is one of the most essential materials in high-tech applications, particularly in the fabrication of radiation-tolerant particle detectors and sensors used in high-energy physics and radiation monitoring. In these fields, the lifetime of non-equilibrium charge carriers is a critical parameter, as it serves as a sensitive indicator of material quality and lattice degradation [1]. Characterizing these recombination kinetics is essential for predicting the operational reliability and functional limits of semiconductor devices operating in harsh radiation environments.

In this work, Si samples were irradiated in the TRIGA Mark II reactor to induce displacement damage through the creation of primary Frenkel pairs and stable defect complexes, such as vacancies and related compounds [2]. These radiation-induced defects introduce deep energy levels into the bandgap that act as efficient recombination centers, directly dictating the speed of free charge carrier decay. To resolve these characteristics across a wide fluence range $(10^{12} - 10^{17}\,\mathrm{n/cm^2})$, two techniques were used. The microwave-probed photoconductivity (MW-PC) method was utilized for lower fluences to monitor nanosecond-range decay. However, at higher fluences, the increased density of recombination centers makes the kinetics ultrafast, exceeding the RC circuit constraints of the MW-PC system. Consequently, a femtosecond laser-based pump-probe (PP) method was required to resolve the picosecond-range kinetics in the most heavily irradiated samples. A comparative analysis of lower and higher irradiated Si was performed:

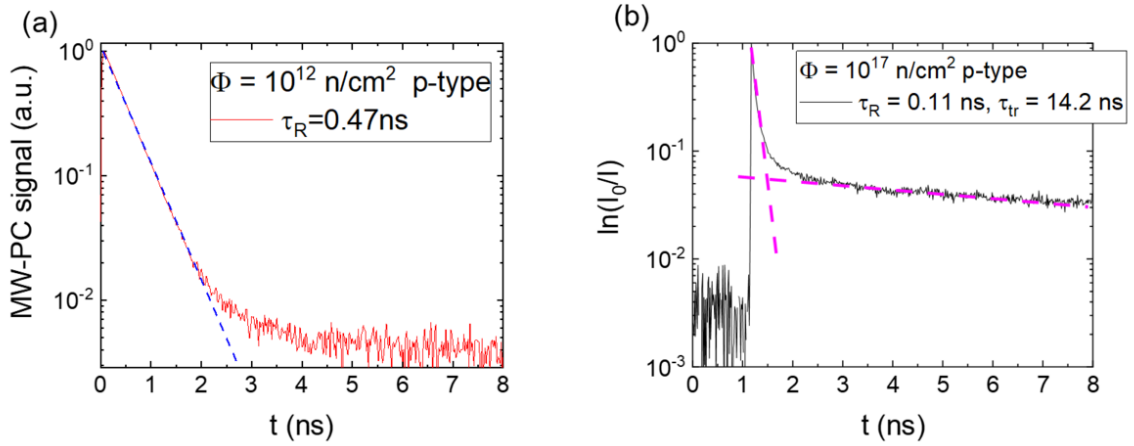


Fig. 1. (a) – MW-PC recombination kinetics at low fluence ($\varphi = 10^{12}\,\mathrm{n/cm^2}$). (b) – PP recombination kinetics at high fluence ($\varphi = 10^{17}\,\mathrm{n/cm^2}$).

Analysis of MW-PC and PP methods allowed us to determine the carrier lifetime in Si impacted by neutron irradiation. We found that the analysis of the recombination kinetics reveals a significant drop in carrier lifetime as the neutron fluence increases, from $0.47\,\mathrm{ns}$ at $10^{12}\,\mathrm{n/cm^2}$ to $0.11\,\mathrm{ns}$ at $10^{17}\,\mathrm{n/cm^2}$ fluence. A comparative analysis of these recombination characteristics and the methodology used to measure kinetics across a wide fluence range and various irradiation environments will be presented.

[1] E. Gaubas, E. Simoen, and J. Vanhellemont, "Review—Carrier Lifetime spectroscopy for defect characterization in semiconductor materials and devices," ECS Journal of Solid State Science and Technology, vol. 5, no. 4, pp. P3108–P3137, Jan. 2016, doi: 10.1149/2.0201604jss.

[2] A. P. Dolgolenko, P. G. Litovchenko, M. D. Varentsov, G. P. Gaidar, and A. P. Litovchenko, "Particularities of the formation of radiation defects in silicon with low and high concentrations of oxygen," Physica Status Solidi (B), vol. 243, no. 8, pp. 1842–1852, May 2006, doi: 10.1002/pssb.200541074.

OPTIMIZING QUALITY OF La:SrSnO3 FILMS VIA OXYGEN CONCENTRATION AND STOICHIOMETRIC CONTROL

Mindaugas Voznikas[1,2], Milita Vagner[1], Tomas Murauskas[2], Virgaudas Kubilius[2], Valentina Plaušinaitienė[2]

[1]Center for Physical Sciences and Technology, Department of Functional Materials and Electronics, Vilnius, Lithuania
[2]Vilnius University, Faculty of Chemistry and Geosciences, Institute of Chemistry, Vilnius, Lithuania
mindaugas.voznikas@chgf.stud.vu.lt

Lanthanum-doped strontium stannate (LSSO) is a promising material for transparent electronics due to its high electron mobility and thermal stability. Consequently, LSSO films are highly relevant in the development of high-performance power semiconductors and optoelectronic devices. A fundamental challenge in investigating lanthanum-doped SrSnO3 is the complex relationship between the doping level and intrinsic structural defects. Even minor deviations in oxygen stoichiometry or crystal lattice dislocations become dominant carrier scattering centers, hindering the achievement of high electron mobility. In this work, the influence of cation stoichiometry and oxygen partial pressure on the properties of LSSO films, grown via Metal-Organic Chemical Vapor Deposition, is investigated.

To evaluate the microstructure, morphology, and electron mobility of the films, scanning electron microscopy, X-ray diffraction, atomic force microscopy, and Hall effect measurement methods were employed. The study analyzes how varying precursor stoichiometric ratios and oxygen partial pressure affect surface roughness, structure, and carrier mobility. The results obtained allow for the determination of optimal values for cation stoichiometry and reactor oxygen partial pressure, providing new insights into how these parameters govern the final quality and electronic characteristics of LSSO films.

INVESTIGATION OF ENERGY CONVERSION IN FREQUENCY CONVERTERS FOR DIFFERENT PUMP SPATIAL PROFILE

Gabrielius Rusonis[1], Arūnas Varanavičius[1]

[1]Lithuania, Vilnius University, Physics Faculty, Laser Research Center
gabrielius.rusonis@ff.vu.lt

Efficient frequency conversion in nonlinear optics is essential for high-intensity laser systems, particularly in second harmonic generation (SHG) and optical parametric amplification (OPA). While Gaussian beams are commonly used due to their natural formation in laser resonators, flat-top (super-Gaussian) beams provide more uniform nonlinear interaction and improved energy conversion [1],[2]. This study aims to investigate how the spatial profile of the pump beam influences energy conversion efficiency in SHG and OPA processes.

Numerical simulations of three-wave nonlinear interactions using the CHI2D split-step propagation code were performed, coupled by custom Python code for pulse energy evaluation. SHG and degenerate OPA processes in beta-barium borate (BBO) crystals were modeled under varying pump intensities for Gaussian and 10th-order flat-top beams. Experimentally, a femtosecond Yb:KGW laser system (1030 nm, 300 fs) was used. Flat-top beams of 6th, 8th, and 10th super-Gaussian order were generated using a spatially varied wave plate (SVWP) with polarization control. Conversion efficiencies were measured for SHG and compared across beam profiles.

Simulations showed that flat-top beams significantly increased conversion efficiency compared to Gaussian beams. In SHG, the maximum simulated efficiency reached 86.18% for flat-top beams versus 58.96% for Gaussian beams, representing a 27.22% improvement. In OPA, flat-top pumping yielded a maximum efficiency of 41.89%, compared to 27.50% for Gaussian beams, corresponding to a 14.39% increase. Experimentally, SHG measurements demonstrated a 13.49–14.38% higher conversion efficiency for flat-top beams relative to Gaussian beams, with similar conversion achieved at substantially lower peak intensities. Although absolute efficiencies were lower than simulated values due to practical limitations such as phase mismatch and self-action effects, the observed trends were consistent with numerical predictions.

Flat-top pump beams enhance nonlinear conversion efficiency in both SHG and OPA compared to Gaussian beams, particularly by achieving higher efficiency at lower peak intensities.

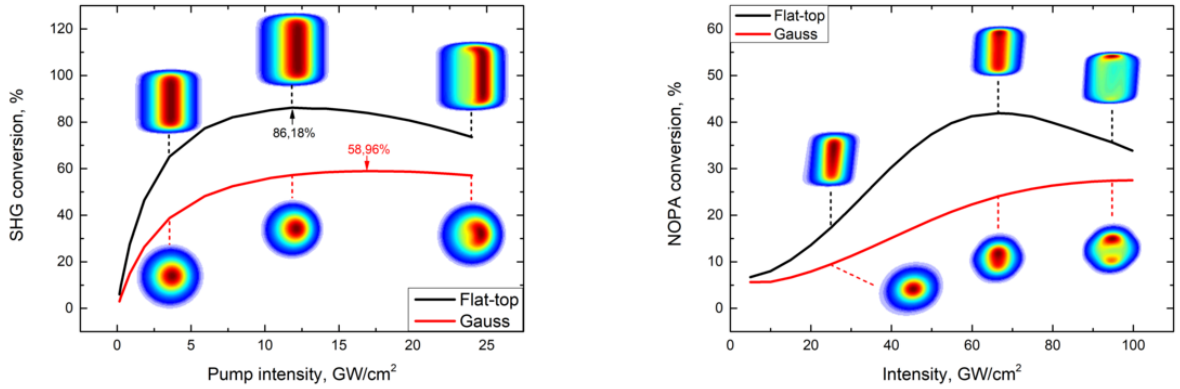


Fig. 1. SHG simulation results are presented in graph on the left, OPA simulation results are presented in graph on the right

[1] L. Wang and J. Xue, “Efficiency comparison analysis of second harmonic generation on flattened gaussian and gaussian beams through a crystal CSLIB6O10,” Japanese Journal of Applied Physics, vol. 41, no. Part 1, No. 12, pp. 7373–7376, Dec. 2002, doi: 10.1143/jjap.41.7373.

[2] S. Toth et al., “SYLOS lasers – the frontier of few-cycle, multi-TW, kHz lasers for ultrafast applications at extreme light infrastructure attosecond light pulse source,” Journal of Physics Photonics, vol. 2, no. 4, p. 045003, Jul. 2020, doi: 10.1088/2515-7647/ab9fe1.

OPTIMIZATION OF LASER CUTTING PARAMETERS FOR INCREASED CUTTING SPEED IN STAINLESS STEEL

Lukas Brundza[1], Mindaugas Gedvilas[1]

[1]Department of Laser Technologies (LTS), Center for Physical Sciences and Technology (FTMC), Savanorių Ave. 231, 02300 Vilnius, Lithuania
lukas.brundza@ftmc.lt

Laser cutting of thin stainless-steel sheets is widely employed in industry due to its precision and versatility. A key factor in process efficiency is the achievable cutting speed. Recently, a theoretical model was proposed to predict the maximum scanning speed for through-cutting thin materials, providing an explicit relationship between cutting speed, material properties, and laser parameters. While substantial progress has been made in optimizing ablation efficiency [1-8], achieving high cutting speeds in thin metal sheets remains challenging despite recent theoretical advances [9]. In this work, we refine the model by introducing adjustments to the critical speed equations that account for specific laser and material parameters, thereby extending its predictive capability. Building on this framework, we experimentally validate the model for stainless-steel sheets and identify the optimal cutting speed under practical conditions. Furthermore, we compare nanosecond and picosecond laser sources, analyzing their respective advantages and limitations for stainless-steel cutting. The results demonstrate the practical applicability of the improved theoretical model while also revealing distinct performance trade-offs between different pulse duration regimes.

Laser irradiation with a central wavelength of 1064 nm, controllable pulse durations of 4.5 ns or 13 ps, and a repetition rate of 400 kHz was used in the experiments. We determined that the maximum cutting speeds were 31 mm/s for nanosecond pulses at an average laser power of 38 W and 14 mm/s for picosecond pulses at an average laser power of 44 W for stainless steel sheets with a thickness of 0.3 mm at certain optimal fluence values using a slightly defocused Gaussian beam. The beam size optimization theoretical approach was adopted from [9] to explain the experimental data. These results will be valuable for industries requiring high-precision microfabrication, such as electronics, automotive, and medical device manufacturing, where speed and accuracy are most critical.

[1] G. Raciukaitis, “Use of high repetition rate and high power lasers in microfabrication: how to keep the efficiency high?,” Journal of Laser Micro/Nanoengineering, vol. 4, no. 3, pp. 186–191, Dec. 2009, doi: 10.2961/jlmn.2009.03.0008.
[2] A. Žemaitis, M. Gaidys, M. Brikas, P. Gečys, G. Račiukaitis, and M. Gedvilas, “Advanced laser scanning for highly-efficient ablation and ultrafast surface structuring: experiment and model,” Scientific Reports, vol. 8, no. 1, p. 17376, Nov. 2018, doi: 10.1038/s41598-018-35604-z.
[3] A. Žemaitis, M. Gaidys, P. Gečys, G. Račiukaitis, and M. Gedvilas, “Rapid high-quality 3D micro-machining by optimised efficient ultrashort laser ablation,” Optics and Lasers in Engineering, vol. 114, pp. 83–89, Nov. 2018, doi: 10.1016/j.optlaseng.2018.11.001.
[4] A. Žemaitis, P. Gečys, M. Barkauskas, G. Račiukaitis, and M. Gedvilas, “Highly-efficient laser ablation of copper by bursts of ultrashort tuneable (fs-ps) pulses,” Scientific Reports, vol. 9, no. 1, p. 12280, Aug. 2019, doi: 10.1038/s41598-019-48779-w.
[5] M. Gaidys, A. Žemaitis, P. Gečys, and M. Gedvilas, “Efficient picosecond laser ablation of copper cylinders,” Applied Surface Science, vol. 483, pp. 962–966, Apr. 2019, doi: 10.1016/j.apsusc.2019.04.002.
[6] A. Žemaitis, M. Gaidys, P. Gečys, M. Barkauskas, and M. Gedvilas, “Femtosecond laser ablation by bibursts in the MHz and GHz pulse repetition rates,” Optics Express, vol. 29, no. 5, p. 7641, Feb. 2021, doi: 10.1364/oe.417883.
[7] A. Žemaitis, M. Gaidys, P. Gečys, and M. Gedvilas, “Bi-stability in femtosecond laser ablation by MHz bursts,” Scientific Reports, vol. 14, no. 1, p. 5614, Mar. 2024, doi: 10.1038/s41598-024-54928-7.
[8] A. Žemaitis, U. Gudauskytė, S. Steponavičiūtė, P. Gečys, and M. Gedvilas, “The ultrafast burst laser ablation of metals: Speed and quality come together,” Optics & Laser Technology, vol. 180, p. 111458, Jul. 2024, doi: 10.1016/j.optlastec.2024.111458.
[9] X. Du and X. Yu, “Maximizing scanning speed in the ultrafast laser cutting of thin materials,” Optics Express, vol. 31, no. 6, p. 9750, Feb. 2023, doi: 10.1364/oe.478214.

AEROSOL CHARACTERIZATION DURING LASER ABLATION OF STRUCTURAL STEEL FOR NUCLEAR DECOMMISSIONING APPLICATIONS

Emilis Sadrejevas[1,2], dr. Artūras Plukis[2], dr. Rita Plukienė[2], Vilius Žalėnas[2], dr. Anton Koroliov[2], Jon Jeffrey Haist[2,3]

[1]VILNIUS TECH, Faculty of Mechanics, Department of Mechatronics, Robotics and Digital Manufacturing, Vilnius, Lithuania
[2]State Research Institute Center for Physical Sciences and Technology, Department of Nuclear Research, Vilnius, Lithuania
[3]Vilnius University, Faculty of Physics, Vilnius, Lithuania
emilis.sadrejevas@stud.vilniustech.lt

The nuclear industry faces a significant decommissioning challenge. It is estimated that by 2050, approximately 400 nuclear reactors will be closed and over 5 million tons of metallic scrap will be created [1]. For this reason laser ablation has been identified as a highly effective decontamination method due to its non-contact application and the reduction of secondary waste [2, 3]. However, the large-scale implementation of this technology depends on the successful mitigation of radioactive aerosol dispersion and this requires a closer look at exactly how these particles are generated [4].

In this study, aerosol size distribution and mass concentrations were characterized during the ablation of stainless and carbon steel surfaces. A nanosecond pulsed fiber laser, mounted on a linear motor stage, was used to perform controlled removal of material. Measurements obtained using a cascade impactor indicate that the resulting debris is concentrated primarily in the sub-micron range. Specifically, 80–90% of the total mass consists of ultrafine particles that are 1µm or smaller.

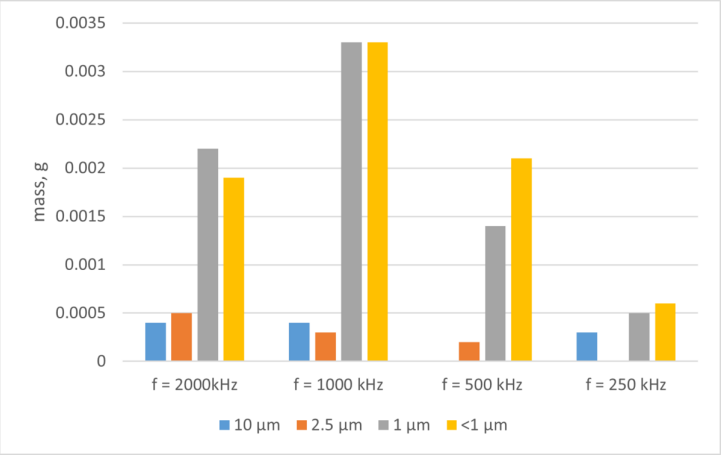


Fig. 1. Mass distribution vs. laser pulse frequency

Comparative analysis reveals that surface conditions significantly influence emission volumes. The ablation of painted layers was found to generate higher aerosol concentrations than unpainted substrates, which is caused by the increase of optical absorption [2]. Furthermore, filtration tests revealed that standard vacuum filters were insufficient to contain this debris, as nanometric particles were observed passing straight through. This failure highlights the necessity of specialized high-efficiency (HEPA) filtration, which is known to effectively capture such ultrafine aerosols by leveraging their ionization-induced electrostatic charge to ensure operational safety [3, 5].

Keywords: Laser decontamination, Nuclear decommissioning, Laser ablation, Aerosol characterization, Particle size distribution

[1] L. Zhong, J. Lei, J. Deng, Z. Lei, L. Lei, and X. Xu, “Existing and potential decontamination methods for radioactively contaminated metals-A Review,” Progress in Nuclear Energy, vol. 139, p. 103854, Sep. 2021, doi: 10.1016/j.pnucene.2021.103854.
[2] G. Greifzu, T. Kahl, M. Herrmann, W. Lippmann, and A. Hurtado, “Laser-based decontamination of metal surfaces,” Opt Laser Technol, vol. 117, 2019, doi: 10.1016/j.optlastec.2019.04.037.
[3] C. H. Jung, H. S. Park, H. J. Won, J. K. Moon, B. S. Choi, and W. K. Choi, “Size distribution and filtration property of particles generated from laser ablation decontamination process,” Environ Prog Sustain Energy, vol. 32, no. 3, 2013, doi: 10.1002/ep.11679.
[4] Q. Wang et al., “Laser decontamination for radioactive contaminated metal surface: A review,” 2023. doi: 10.1016/j.net.2022.09.020.
[5] X. Zhou et al., “Basic study on laser ablation surface cleaning of nuclear facility,” Surface Engineering, vol. 17, no. 5, 2001, doi: 10.1179/026708401101518051.

MICROFABRICATION OF TRANSPARENT POLYMER FOR INTRAOCULAR LENS BY FEMTOSECOND PULSES

Dainius Ratkus[1], Andrius Žemaitis[1], Arnas Vyšniauskas[1], Paulius Gečys[1]

[1]Department of Laser Technologies (LTS), Center for Physical Sciences and Technology (FTMC), Savanorių Ave. 231, 02300 Vilnius, Lithuania
dainius.ratkus@ftmc.lt

Polymer based Intraocular Lenses (IOL) are optical components applied for cataract treatment because the transmittance of differing wavelengths coincides with the lens of the human eye. The fabrication of such optics is carried out by using lathe cutting and tumble polishing. These methods are fast and can be applied for mass production. Nevertheless, the production of personalized lens by conventional methods are challenging due to diamond-based unyielding machinery. In addition, thermal disposition of the machinery can damage the materials transparent qualities, deeming the final product improper for use.

An alternative microfabrication of lenses can be realized by femtosecond pulses. Femtosecond laser (Ekspla, Femtolux 30) was utilized for ablation and polishing of polymer. This microfabrication technique, based on the cold-ablation approach, mitigates the thermal effect on the polymer and ensures transmittance of visible light to be adequate for the human eye. Moreover, femtosecond laser systems are non-contact and offer wide customization and sustainable micromachining [1, 2].

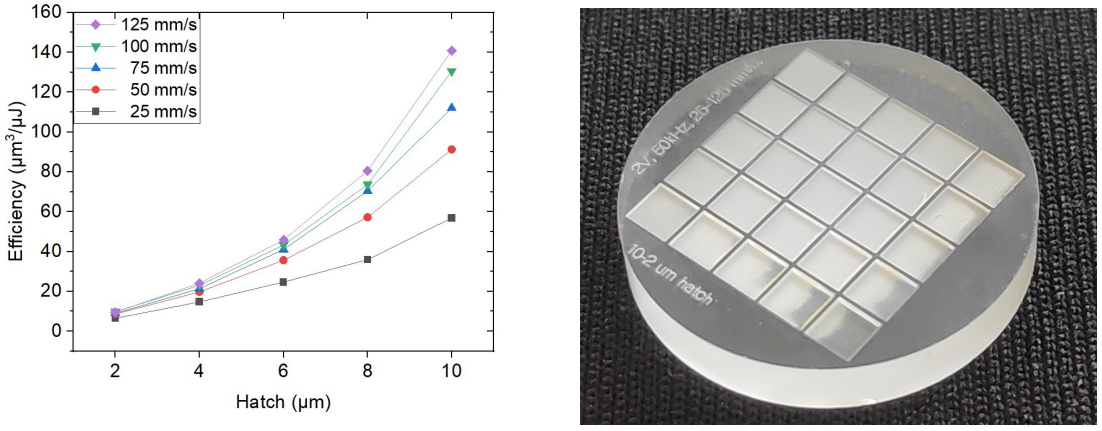


Fig. 1. Ablation efficiency of polymeric material versus hatch distance for various beam scanning speeds (left). Cavities ablated on the sample surface, laser fluence of 0.37 J/cm2, 50 kHz repetition rate (right).

[1] [1] Kerse, C., Kalaycıoğlu, H., Elahi, P. et al. Ablation-cooled material removal with ultrafast bursts of pulses. Nature 537, 84–88 (2016). doi: https://doi.org/10.1038/nature18619

[2] [2] Yu, Nan & Fang, Fengzhou & Wu, Bing & Zeng, Lan & Cheng, Ying. (2018). State of the art of intraocular lens manufacturing. The International Journal of Advanced Manufacturing Technology. 98. 1-28. doi: https://doi.org/10.1007/s00170-018-2274-5

LASER INDUCED DAMAGE THRESHOLD CHANGE IN TIME IN NANOSTRUCTURED GLAD ALL-SILICA HIGHLY REFLECTIVE OPTICAL MIRRORS

Adomas Strazdas[1], Lukas Ramalis[2]

[1]Center for Physical Sciences and Technology (FTMC), Department of Laser Technologies, Lithuania
adomas.strazdas@ftmc.com

Optical components are critical elements in laser systems, where they control and direct laser radiation. As the demand for high-power laser systems grows so does the need for highly resistive and durable optical mirrors. Nanostructured thin film mirrors deposited using the GLancing Angle Deposition (GLAD) technique [1] have emerged as a promising alternative to conventional mirrors, offering higher potential Laser Induced Damage Threshold (LIDT). Although GLAD coatings have issues, that may be solved only with more research and development.

The aim of this study is to investigate the change of LIDT in time of all-silica nanostructured high-reflectivity (HR) mirrors fabricated using the GLAD method. By applying GLAD method at 70°, self-shadowing effect is induced to form nanostructured layers which have lower effective refractive index. Combining porous layers with dense layers formed at 0° allows us to make Bragg mirrors from only SiO_2[1]. Conventional mirrors have a dielectric of a lower bandgap, which has a higher refractive index, thus limiting the maximum potential LIDT. In this case all-silica mirrors have an advantage. Although GLAD mirrors exhibit high potential, they are known to absorb water or other harmful particles from environment and reduce resistance to repeated laser exposure. This can be avoided with optimizations of manufacturing and storage processes.

In this work, six HR mirrors designed for operation at a wavelength of 355 nm (reflectance >95%) were investigated. The all-silica mirrors were fabricated using the GLAD technique. After deposition, all samples were stored in argon-filled PET-G boxes and sealed with Kapton tape, to suppress degradation [2]. LIDT 1-on-1 measurements were performed monthly by sequentially unsealing selected samples, allowing the degradation rate to be evaluated as a function of storage time, and to see if unsealing the mirror accelerates degradation. Another factor that will be experimented on, is whether the LIDT of conditioned [2] all-silica mirror will change over time.

The results show great LIDT (at 355nm laser wavelength) 1-on-1 results, the mirror survived 163.57 J/cm^2 laser shots, but damage occurred from 67 J/cm^2. After a month these values didn't change much, the maximum energy survived – 162.1 J/cm^2, and first damage – 56 J/cm^2. When compared to other 355nm wavelength mirrors, this degradation is quite slow, and unlike other mirrors, all-silica mirrors can be rejuvenated with laser conditioning [2].

Further investigation is required for solutions and insights into the nanoscale physical mechanisms responsible for coating degradation under sealed storage conditions and to optimize GLAD mirror designs and production sequences for long-term use in high-power and ultrafast laser systems.

[1] Tolenis T. et al., Scientific Reports, 7:10898 (2017)
[2] Ramalis L. et al., Science Direct, Optics 14 100616 (2024)

REAL-TIME FULL-FIELD VIBROMETRY USING A SMART-PIXEL LOCK-IN CAMERA

Florian Dötzer[1], Fridtjof Seufert[1], Stefan Sinzinger[1]

[1]TU Ilmenau, Department of Mechanical Engineering, Optical Engineering Group, Germany
florian.doetzer@tu-ilmenau.de

Full-field vibrometry techniques such as frequency shifted or phase modulated interferometry already offer considerably short acquisition times compared to scanning methods such as Laser-Doppler-Vibrometry when high spatial resolution is required. However, when measurements with picometer-sensitivity are to be performed, this can only be achieved by recording a large number of frames with a subsequent narrowband (lock-in) filtering during digital postprocessing. Due to the limited frame rate of regular CMOS camera sensors, the acquisition time then can be several seconds to minutes and the computationally intensive evaluation of the large image stack further adds to the measurement time.

Both problems are addressed by the use of a smart-pixel camera that implements an electric lock-in circuit in every pixel before AD-conversion [1]. It supports the demodulation of frequencies even beyond 100 kHz which means that the same number of oscillation periods can be acquired significantly faster compared to a regular camera. As illustrated in figure 1, the filtering is applied in the analogue domain and only a single frame is produced in the end, which can be instantly further processed compared to a whole stack of images that must first be processed and filtered digitally. This should enable such interferometric setups to perform even highly sensitive measurements in real-time (i.e. several measurements per second).

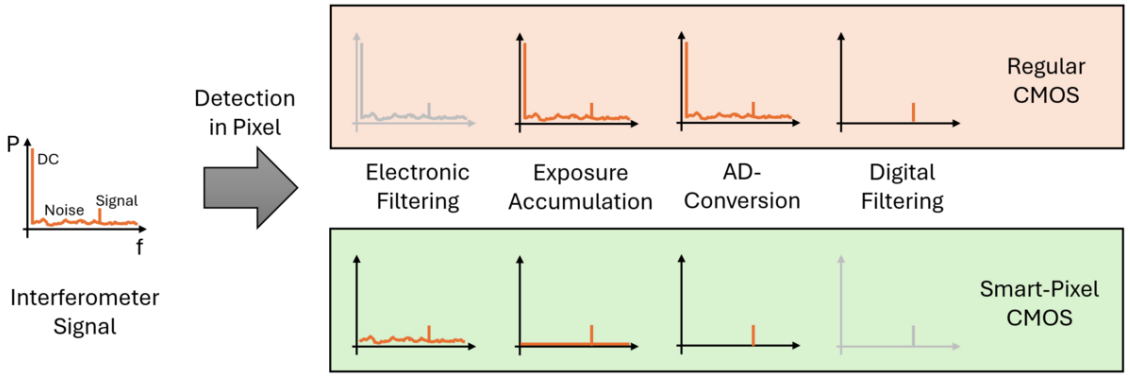


Fig. 1. Simplified signal filtering pipeline for lock-in detection with a smart-pixel camera compared to a regular one.

Additionally, there is also a second possible advantage regarding measurement noise. As the typical signal to be measured in such an interferometer is an extremely weak modulation in front of a much stronger DC background, the measurement can be assumed to be shot noise limited. In this case only a larger number of accumulated photons, i.e. a larger full well capacity (FWC) can increase the signal to noise ratio (SNR) for a conventional detector. The smart-pixel detector however filters out the DC component such that only the modulated part is accumulated in the potential well. Hence, the entire FWC and AD-converter bit depth is available for the modulated part only. This promises to provide a performance similar to a conventional detector with excessively large FWC and bit depth which should provide measurement results with superior SNR.

In this submission, we will present first measurements using the smart-pixel camera inside an established interferometric full-field vibrometry setup. We compare the results to the ones obtained with a conventional camera detector and discuss advantages and limitations.

[1] Heliotis AG, “C4 – Heliotis AG,” Heliotis AG. https://www.heliotis.com/c4/

LASER TREATMENT OF HYBRID TI-AU-AG THIN FILMS AND INVESTIGATION OF THEIR OPTICAL PROPERTIES

Kasparas Okleiteris[1], Evaldas Stankevičius[1]

[1]Center for Physical Sciences and Technology (FTMC), Department of Laser Technologies, Plasmonics and nanophotonics laboratory, Lithuania
kasparas.okleiteris@ftmc.lt

Plasmonic nanostructures are important for sensing and optical spectroscopy because localized surface plasmon resonance (LSPR) strongly controls light absorption and visible color. In this study, plasmon excitation and resonance in a hybrid Ti–Au–Ag thin-film system on soda-lime glass were investigated, focusing on how nanosecond laser processing modifies the optical response. A Ti/Au/Ag trilayer (10 nm per layer) was deposited by magnetron sputtering and subsequently patterned by laser irradiation, following established approaches for laser-induced plasmonic nanoparticle formation. [1] The average laser power (0.1–0.8 W) and lens–substrate distance (12.3–16.92 cm) were varied to generate colored nanoparticle regions. Six squares (K1–K6) showing the largest color differences were selected and analyzed using UV–Vis reflectance and transmittance spectroscopy, and extinction spectra were derived. All laser-processed regions exhibit a single dominant extinction band in the visible range, with peak positions spanning approximately 480–490 nm to 608 nm, consistent with the observed structural colors. Strongly red-shifted and broadened resonances indicate increased coupling and/or larger effective features, while shorter-wavelength peaks suggest a more Ag-like response. Overall, the results demonstrate that laser processing enables effective tuning of LSPR and color in Ti–Au–Ag layers, where both Au/Ag contribution and the titanium (or TiOx) environment influence the resonance position and bandwidth.

[1] V. Petrikaitė, I. Ignatjev, A. Selskis, G. Niaura, and E. Stankevičius, “Hybrid gold-silver nanoparticles synthesis on a glass substrate using a nanosecond laser-induced dewetting of thin bimetallic films and their application in SERS,” Opt. Laser Technol., vol. 168, Art. no. 109956, Jan. 2024, doi: 10.1016/j.optlastec.2023.109956.

FORMATION OF MICROSTRUCTURES IN GLASS USING LASER INTERFERENCE ABLATION AND CHEMICAL ETCHING

Daumantas Sriubas[1], Simonas Indrišiūnas[2]

[1]Vilnius University, Faculty of Physics, Center for Physical Sciences and Technology, Department of Laser research, Vilnius, Lithuania
daumantas.sriubas@ftmc.lt

Glass micropatterning is important in many novel technologies, such as microfluidics or fabrication of metasurfaces [1, 2]. This work investigated the possibility of fabricating microstructures in glass using direct laser interference ablation and wet chemical etching through a thin chromium mask. The fabrication process consists of three steps: selective removal of chromium film, using laser, etching through glass surface, removal of chromium film (Figure 1a). Using laser, holes were ablated in thin chromium film. Then the samples were etched in KOH solution for different time intervals. Lastly, chromium layer was dissolved in chromium etchant. After the experiment, the samples were investigated using Sensofar optical profiler, where the channel depth and its entrance width data were obtained. Dependence of dimple depth on number of pulses per spot (Figure 1b) and irradiation fluence was found.

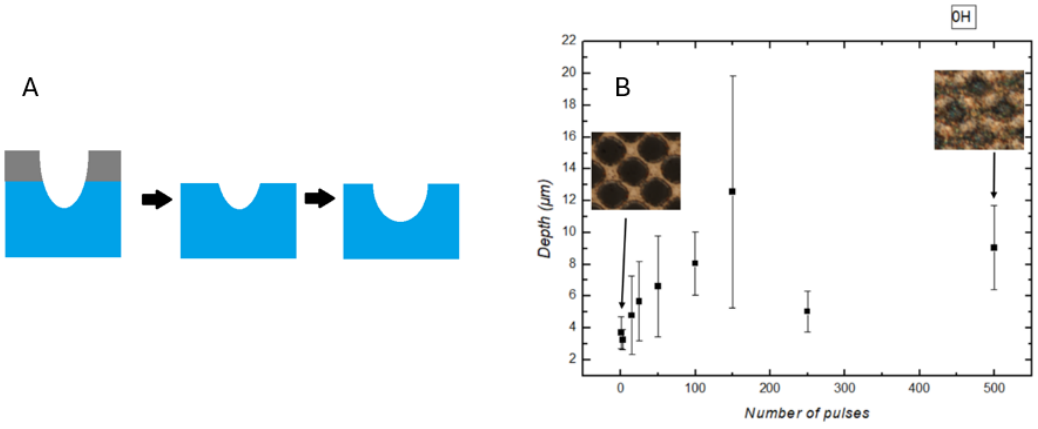


Fig. 1. a – fabrication of microstructures in glass using direct laser interference ablation and wet chemical etching after removing a thin chromium mask; b – dependence of microstructures depth on number of laser pulses per spot.

[1] 1. Patrice Genevet, Federico Capasso, Francesco Aieta, Mohammadreza Khorasaninejad, and Robert Devlin Recent advances in planar optics: from plasmonic to dielectric metasurfaces, Optica, 4(1), pp. 139-152 (2017).
[2] 2. Felix Sima and Koji Sugioka. ”Ultrafast laser manufacturing of nanofluidic systems” Nanophotonics, (9), pp. 2389-2406, (2021).

X-RAY EMISSION FROM A CU TARGET DRIVEN BY 2 µm FEMTOSECOND LASER PULSES

Miroslav Saniuk[1], Anton Koroliov[1], Artūras Plukis[1]

[1]Center for Physical Sciences and Technology (FTMC), Department of Nuclear Research, Vilnius, Lithuania
miroslav.saniuk@ftmc.lt

X-ray radiation is widely used in modern medicine, industry, and science. With the rising demand for sub-picosecond pulses, laser–plasma interaction has emerged as a compact alternative to large-scale accelerator facilities. In this process, a femtosecond laser pulse ionizes the target, creating plasma in which electrons are accelerated by the electromagnetic field. These electrons subsequently re-enter the target, producing bremsstrahlung and characteristic X-ray radiation.

In this study, X-ray generation from a copper target using 1 µm and 2 µm femtosecond laser systems was investigated. A femtosecond laser system “Pharos PH1-SP-1.5mJ” with center wavelength λ = 1028 nm and pulse duration τ = 158 fs, as well as an optical parametric amplifier (OPA) ORPHEUS MIR (“Light Conversion”) with a tunable wavelength range from 1300 nm to 11000 nm, were employed. The OPA was operated at a center wavelength of λ = 2000 nm with a pulse duration of τ = 36 fs. In both cases, the pulse energy was E_p = 0.135 mJ and the repetition rate was f = 4 kHz, resulting in an average laser power of P = 540 mW. X-ray emission was detected using a thermoelectrically cooled Si-PIN spectrometer Amptek X-123. Measurements were performed in reflection geometry, with the detector placed 150 mm from the target at angles ranging from 30° to 90° relative to the incident laser beam.

According to the literature, longer-wavelength laser radiation can enable more efficient X-ray generation due to the scaling law $I\lambda^2$[1]. Fig. 1 shows the copper X-ray spectra obtained using described laser systems. The characteristic Kα (8.04 keV) and Kβ (8.96 keV) emission lines, bremsstrahlung background, and pile-up effects are clearly observed. Contrary to expectations, the experimental results demonstrate a several-fold higher X-ray photon yield for the 1 µm laser. These findings are inconsistent with previously reported data [2]. For longer wavelengths, electrons interact with the plasma over a longer time, penetrate deeper into the target, and may be partially screened, resulting in reduced X-ray generation efficiency. Compensation for this effect requires higher laser pulse energies.

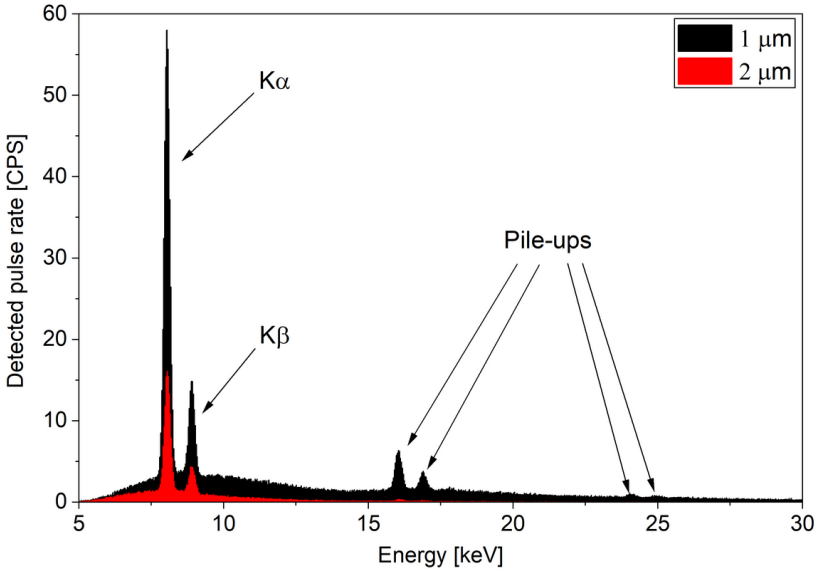


Fig. 1. X-ray spectra obtained using 1 µm and 2 µm laser systems. The detector was positioned 150 mm from the target at an angle of 45°. The detector active area is 25 mm^2.

[1] J. Weisshaupt, V. Juvé, M. Holtz, M. Woerner, and T. Elsaesser, “Theoretical analysis of hard x-ray generation by nonperturbative interaction of ultrashort light pulses with a metal,” Structural Dynamics, vol. 2, no. 2, p. 024102, Mar. 2015, doi: 10.1063/1.4915485.

[2] A. Koç et al., “Compact high-flux hard X-ray source driven by femtosecond mid-infrared pulses at a 1 kHz repetition rate,” Optics Letters, vol. 46, no. 2, p. 210, Nov. 2020, doi: 10.1364/ol.409522.

PARAMETRIC ANALYSIS OF FILAMENT ASSISTED X-RAY GENERATION

Šarūnas Logminas[1], Balys Momgaudis[1]

[1]Vilnius University, Faculty of Physics, Laser Research Center, Vilnius, Lithuania
sarunas.logminas@ff.stud.vu.lt

Laser-induced X-rays are of particular interest due to their potential as unique X-ray sources for time-resolved applications due to inherited ultrashort pulse duration. The generation of X-rays starts with laser light ionizing the metal atoms by the electromagnetic field. The produced free electrons are then further accelerated in the electric field to energies comparable to X-rays, which is then generated through characteristic radiation or bremsstrahlung (braking radiation).

In this work a new generation arrangement is investigated. A rotating steel target was irradiated with a loosely (f=∼2m) Ti:sapphire laser over a course of 5-15 minute intervals, during which X-ray photon count was measured every 10 s. The profile of the sample was measured at different points in time. The X-ray measurements were carried out with different parameters varied: pulse duration, sample position and pulse power. The measurements showed a rise in X-ray generation that coincides with the appearance of self-forming microstructures on the surface of the sample indicated by an increasing surface roughness (Fig 1). These structures are believed to act as local field enhancers and were found to amplify the X-ray radiance by up to ∼1000 times. After a certain point generation drops and surface roughness ceases to increase, believed to be related to surface oxidation. Pulse duration measurements revealed that longer pulses yield better efficiency as higher intensity pulses get more attenuated by the plasma while the beam is propagating through air.

The obtained results suggest that laser induced X-ray sources can be further optimized to yield more efficient generation by introducing laser structured surfaces.

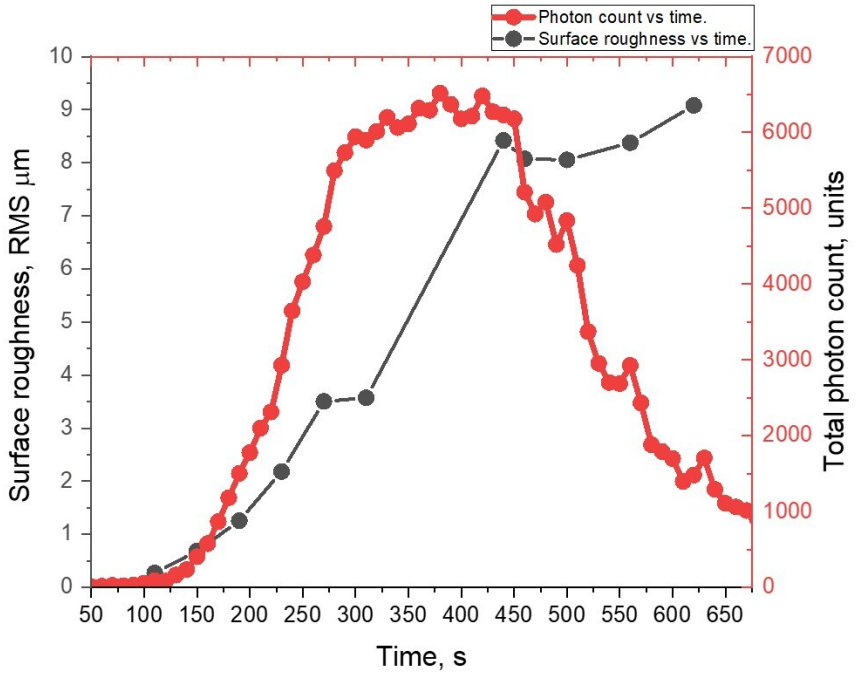


Fig. 1. X-ray generation and surface roughness over continuous laser-sample interaction.

IMPROVED SEAM STRENGTH IN ULTRASHORT PULSED LASER WELDING OF GLASSES VIA INTERFACE PRE-ROUGHENING

Neda Mažeikytė[1], Edgaras Markauskas[1], Paulius Gečys[1]

[1]Center for Physical Sciences and Technology, Department of Laser Technologies, Savanoriu Ave. 231, Vilnius, Lithuania
neda.mazeikyte@ftmc.lt

Laser-based glass welding is a joining technique that enables the formation of strong, hermetic joints by inducing highly localized melting in transparent materials through controlled laser-matter interactions, making it suitable for high-precision and long-term reliable applications [1]. The non-optical contact glass welding technique enables welding of glasses with interface gaps of up to several micrometres [2]. In addition, the use of relatively loose focusing can be employed, allowing the use of fast galvanometer scanners [2]. However, loose focusing shifts the welding process towards higher pulse energies and average power levels, often exceeding several watts [3]. These elevated power levels can lead to increased heat accumulation, resulting in higher residual stresses, more pronounced chipping and cracking, weakening the seam strength. Fortunately, glass surface pre-roughening has been shown to enhance laser absorption [4], potentially enabling lower welding power levels at non-optical contact welding conditions.

This study investigates non-optical-contact multi-scan welding of two 1 mm thick soda-lime glass plates using an ultrashort pulsed laser operating in burst mode at a wavelength of 1030 nm. Both the glass pre-roughening and welding processes were realized using the same laser source. Transition between the two regimes was achieved by adjusting the incident laser power and laser beam scanning strategies. After welding, longitudinal tensile tests were performed to determine the weld strength, while optical microscopy was used to evaluate the weld morphology.

The results (see Figure 1) demonstrate that glass interface pre-roughening improved weld strength compared to standard welding without the roughening step. Moreover, pre-roughening reduced the optimal laser power levels, increasing welding process efficiency.

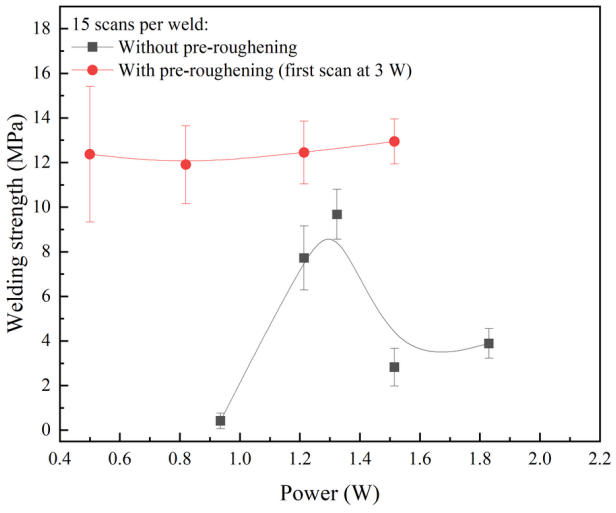


Fig. 1. *Welding strength dependence on incident laser power for samples processed with and without interface pre-roughening. Laser pulse duration 176 fs and 23 sub-pulses per burst. Dots are connected to guide the eye.*

[1] X. Jia et al., "Ultrafast laser welding of transparent materials: from principles to applications," International Journal of Extreme Manufacturing, vol. 7, no. 3, p. 032001, Jan. 2025, doi: 10.1088/2631-7990/ada7a7.
[2] Y. Huang et al., "Process study of picosecond laser welding of soda-lime glass," Optics & Laser Technology, vol. 182, p. 112095, Nov. 2024, doi: 10.1016/j.optlastec.2024.112095.
[3] X. Jia, K. Li, Z. Li, C. Wang, J. Chen, and S. Cui, "Multi-scan picosecond laser welding of non-optical contact soda lime glass," Optics & Laser Technology, vol. 161, p. 109164, Jan. 2023, doi: 10.1016/j.optlastec.2023.109164.
[4] L. Zubauskas, E. Markauskas, A. Vyšniauskas, V. Stankevič, and P. Gečys, "Comparative analysis of microlens array formation in fused silica glass by laser: Femtosecond versus picosecond pulses," Journal of Science Advanced Materials and Devices, vol. 9, no. 4, p. 100804, Oct. 2024, doi: 10.1016/j.jsamd.2024.100804.

METASURFACE OPTICS FOR APPLICATIONS ACCROSS THE INFRARED

Erika Jonaitytė[1], Klaudijus Midveris[1], Mindaugas Juodėnas[1]

[1]Kaunas University of Technology, Institute of Materials Science, Kaunas, Lithuania
erika.jonaityte@ktu.lt

Electromagnetic wave manipulation has long been dominated by the use of refractive optics. These solutions, however, face significant challenges in the mid-infrared (MIR) spectral region. Materials, such as germanium or chalcogenide glasses, used in MIR applications, are toxic, expensive and difficult to integrate into smaller systems. These challenges, coupled with the increasing need for more compact and lightweight optical systems, have created a demand for a novel solution – metasurfaces. They are ultrathin arrays of subwavelength nanostructures capable of shifting the phase, amplitude, and polarization of incident light. Metasurfaces offer remarkable capabilities that are unattainable by bulk optics, including monochromatic aberration correction and encoding multiple optical functions into a single element.

Despite the rapid advancements being made in the meta-optics for visible and near-infrared light regimes, MIR spectrum remains largely unexplored. This spectral range is critical for applications such as free-space communication, sensing technologies and molecular fingerprinting. Here, we explore the design, fabrication, and characterization of all-silicon meta-optical devices optimized for MIR operation. Our approach makes use of high refractive index silicon nanopillars that act as waveguides and shape light properties only through their geometric parameters.

To demonstrate the versatility of metaoptics, we fabricate a variety of optical components, ranging from fundamental elements to complex wavefront modulators. They include beam deflectors for beam steering, quarter-wave plates for the manipulation of the polarization state of light, axicons for Bessel beam generation, among others. Additionally, we developed holographic elements to demonstrate wavefront shaping capabilities.

Fabrication methodology is one of the critical points of this work. Nanostructures were designed using Rigorous Wave Coupled Analysis (RCWA) to optimize their transmittance and phase delay and were patterned using Electron Beam Lithography (EBL), ensuring precise dimensions and placement of the sub-micrometer features. The pattern was then transferred to the silicon wafer by Cryogenic Reactive Ion Etching (Cryo-RIE). Unlike the Bosch process, which produces scalloped walls that degrade the optical performance of the fabricated element, Cryo-RIE produces high-aspect ratio structures with smooth, vertical sidewalls. This sidewall profile is critical for minimizing losses.

The geometry of the fabricated metaatoms was analyzed using Scanning Electron Microscopy (SEM). The inspection revealed an excellent match to the designed dimensions, confirming the suitability of the fabrication protocol. The fabricated devices exhibit the structural integrity required for high-efficiency operation. We anticipate such silicon optical elements to overcome the limitations of bulk refractive optics and pave the way for a new generation of miniaturized optical systems.

Acknowledgements
This research has received funding from the Research Council of Lithuania (LMTLT), agreement No S-MIP-24-4.

LIFETIME MEASUREMENTS OF PLASMON-EXCITON POLIARITONIC EMISSION USING SUPERCRITICAL ANGLE FLUORESCENCE MICROSCOPY

Evita Spalinskaitė[1], Justina Anulytė[1], Vytautas Žičkus[1,2], Zigmas Balevičius[1]

[1]Center for Physical Sciences and Technology, Department of Laser Technologies, Plasmonics and Nanophotonics Lab., Saulėtekio av. 3, LT-10257 Vilnius, Lithuania
[2]University of Glasgow, School of Physics and Astronomy, Glasgow G12 8QQ, United Kingdom
evita.spalinskaite@ftmc.lt

Surface plasmon polaritons (SPPs) are electromagnetic waves that propagate along a metal-dielectric interface. Their excitation relies on the coupling between coherent oscillations of free electrons and photons, which can be drastically enhanced with the grating coupler approach [1]. Scattered light in the periodic arrays of metallic nanosotructures interfere constructively with damping of localized plasmon resonance (LPR) of individual structures, resulting in ultra-narrow plasmonic resonance known as a surface lattice resonance (SLR) [2]. SLR has a wide range of applications in sensing [3], but can also be used to enhance the spontaneous emission rates of organic fluorescent molecules deposited on top of structured metallic surface. In this work we present various energy exchange dynamics, differing in decay rates, by implementing a near-field collection via supercritical angle fluorescence (SAF) microscopy.

We investigate a metallic structure of gold bumps (period around 500 nm) on 50 nm thick gold, with drop-caster and evaporated fluorescent dye of rhodamine R6G, dissolved in water on top of the structure. The fluorescence was excited with a 515 nm femtosecond laser through oil immersion objective, collected in an epi-configuration and filtered at 600 nm. Additionally, a 4F optical system with an adjustable aperture was used for spatial filtering of the back focal plane (BFP) to select particular fluorescence signals (Fig. 1). Near-field and far-field emissions were examined and attributed to SAF and undercritical angle fluorescence (UAF) respectively. UAF mostly contains the uncoupled dye molecules in the bulk dye, thus exhibiting a longer fluorescence lifetime. On the contrary, the SAF decay is fastest and limited by the instrumental response function (IRF) of the detector. This is due to the combination of radiative energy enhancement and non-radiative fluorescence quenching in our sample [2]. The latter effect occurs when an excited-state fluorophore is in close proximity to a metal surface and an instant energy transfer to surface electrons is induced. As radiative and non-radiative decay rates increase, the total lifetime of SAF decreases. In addition, the first-order diffraction rings, formed from multidirectional leakage radiation by SLR, were also observed and had a mix of lifetimes due to UAF influence and filtering limitations.

The lifetime decay measurements were consistent with theoretical predictions, despite being IRF limited. Research on SLR-enhanced coherent emission can lead to development and improvement of quantum nanophotonic devices as well as advanced microscopy and optical biosensing [4].

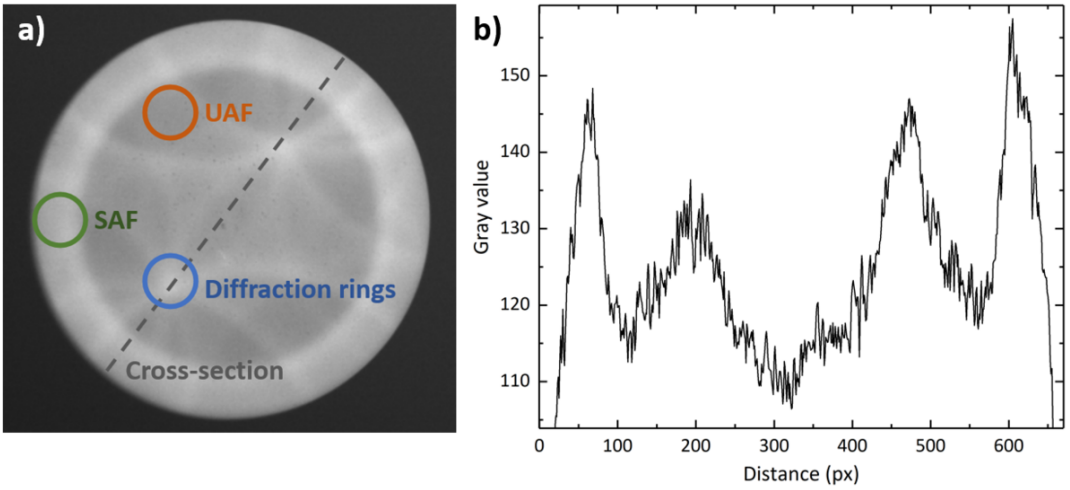


Fig. 1. a) BFP with standard filtering of examined sample, b) Corresponding cross-section taken from a).

[1] E. Stankevičius, K. Vilkevičius, M. Gedvilas et al., "Direct laser writing for the formation of Large-Scale gold microbumps arrays generating hybrid lattice plasmon polaritons in VIS–NIR range," Advanced Optical Materials, vol. 9, no. 12, Apr. 2021, doi: 10.1002/adom.202100027.
[2] P. Jurkšaitis, J. Anulytė, E. Spalinskaitė et al., "Plasmon–exciton polaritonic emission lifetime dynamics under strong coupling," Nanophotonics, vol. 14, no. 14, pp. 2485–2493, Jun. 2025, doi: 10.1515/nanoph-2025-0129
[3] U. F. S. Roggero, C. J. Rojas-Bejarano, C. A. Herreño-Fierro et al., "Surface lattice resonances for high-performance sensing: a study on gold nanoparticle arrays," Optics Express, vol. 33, no. 14, p. 30328, Jun. 2025, doi: 10.1364/oe.564444
[4] W. Deng and E. M. Goldys, "Plasmonic approach to enhanced fluorescence for applications in biotechnology and the life sciences," Langmuir, vol. 28, no. 27, pp. 10152–10163, May 2012, doi: 10.1021/la300332x

SUB-THZ BEAM FORMING FOR NEXT-GENERATION HIGH-FREQUENCY COMMUNICATION SYSTEMS USING DIFFRACTIVE OPTICAL ELEMENTS

Kotryna Nacienė[1], Kasparas Stanaitis[1], Ernestas Nacius[1], Linas Minkevičius[1]

[1]Department of Optoelectronics, Center for Physical Sciences and Technology, Vilnius, Lithuania
kotryna.naciene@ftmc.lt

The sub-terahertz (sub-THz) frequency band (below 300 GHz) has attracted great interest for applications in next-generation wireless communications, offering ultra-broadband channels far beyond today's microwave and millimeter-wave systems [1]. A major challenge, however, is the high free-space path loss at THz frequencies, which limits transmission distance and reliability. One way to overcome this is by using high gain focusing elements to direct and enhance THz signals. Conventional beam shaping approaches - like refractive lenses or parabolic mirrors - tend to be large, heavy and expensive, which limits their suitability for compact optical setups. In contrast, diffractive optical elements (DOEs) provide a compelling option, as they manipulate the wavefront through phase modulation to achieve highly efficient focusing in a thin, lightweight form factor.

In this work, we explore the use of 3D printable DOEs made of high impact polystyrene (HIPS) suitable for 93 GHz beam focusing. We designed a range of flat Fresnel lens type DOEs with various focal lengths (5-15 cm), apertures (5-15 cm diameters) and phase quantization levels (step-like profiles of 2, 4, 8, 16, 32 steps) and evaluated their ability to improve the signal directivity of a THz communication system. The key metrics of interest were the peak focal intensity and the focal beam width. For communications, a narrower, high-intensity beam is desirable to extend range and reduce interference. Such lenses could serve as compact antenna gain modules: for example, placed in front of a THz transmitter or receiver to significantly boost effective radiated power or receiver sensitivity.

Additionally, the antireflective (AR) structures can enhance transmission signal gain of such beam altering elements [2]. THz transmitters often have limited output power, so preserving as much of that power as possible is important. Using finite-difference time-domain (FDTD) electromagnetic simulations, DOEs combined with AR structures could be analyzed as it is important to find best matching case designed for 93 GHz signal enhancement. This could be used in the future for developing sub-THz antenna boosters, tailored to specific frequencies or beam requirements, at a low manufacturing cost. Therefore, it would find applications in indoor THz networks or fixed point-to-point links, where inexpensive plastic lenses could replace much heavier and costlier parabolic antennas.

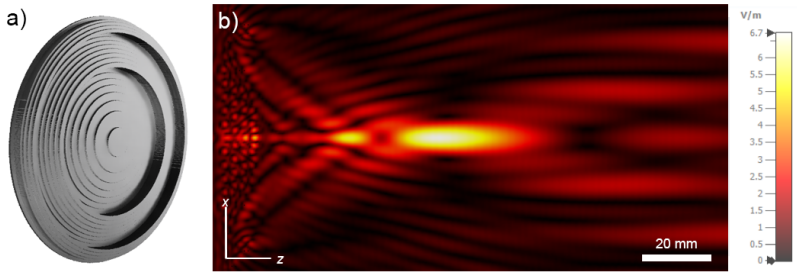


Fig. 1. a) Example of diffractive optical element model made of high impact polystyrene, having focal length of 100 mm and diameter of 100 mm, phase is quatized to 8 step-like profile. b) Simulated electric field distribution after the DOE when illuminated with a plane wave of 93 GHz.

[1] I. F. Akyildiz, J. M. Jornet, and C. Han, "Terahertz band: Next frontier for wireless communications," Phys. Commun., vol. 12, pp. 16–32, 2014.

[2] M. Tamošiūnaitė et al., "Focusing of terahertz radiation with laser-ablated antireflective structures," IEEE Trans. Terahertz Sci. Technol., vol. 9, no. 6, pp. 537–545, 2019.

FLUORESCENCE CONCENTRATION QUENCHING IN CHLOROPHYLL MOLECULE AGGREGATES

Liudas Ablačinskas[1]

[1]Lithuania, Vilnius University, Faculty of Physics, Institute of Chemical Physics
liudas.ablacinskas@ff.stud.vu.lt

Under laboratory conditions, fluorescence quenching is observed with increasing chlorophyll concentration. While this phenomenon is well known, its mechanism remains unclear. A full understanding of fluorescence behavior in laboratory systems is helpful for accurate interpretation of fluorescence in nature, where even in high concentrations, quenching is not observed.

In this work, continuing previous research [1], Monte Carlo simulations were used to model chlorophyll fluorescence decay kinetics. A three-dimensional model with randomly distributed chlorophyll molecules was employed, in which half of the molecules were randomly assigned as excitation traps. Fluorescence decay kinetics were obtained from 10000 simulations performed at concentrations of 0.02 mM, 5 mM and 30 mM.

The simulated decay kinetics were compared with experimental data obtained at the Physical Sciences and Technology Center, Department of Molecular Compound Physics. The results show that the random trap model reproduces experimental fluorescence decay at low chlorophyll concentrations. However, at higher concentrations, decay kinetics became more dispersed, and the simulations no longer matched the experimental data.

These findings indicate that while the random trap model is suitable at low concentrations, its parameters require adjustments at higher concentrations. An alternative, statistical pair model, may provide better results at higher concentrations.

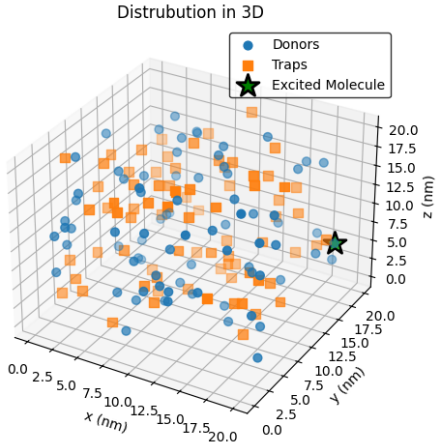


Fig. 1. 3D distribution of molecules

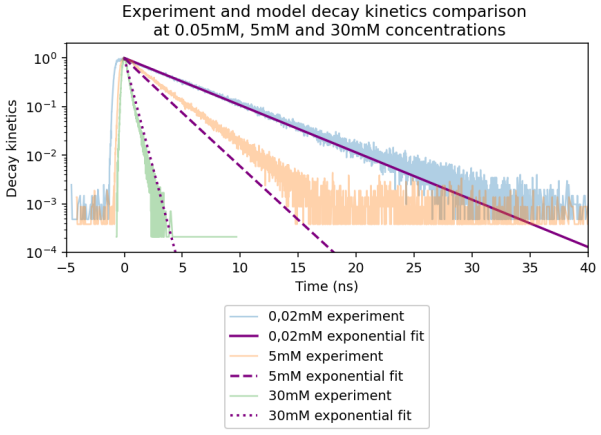


Fig. 2. Experiment and model decay kinetics comparison

Keywords: Fluorescence, Concentration quenching, Chlorophyll

[1] S. Barysaitė, J. Chmeliov, L. Valkunas, and A. Gelzinis, "Concentration quenching of fluorescence decay kinetics of molecular systems," The Journal of Physical Chemistry B, vol. 128, no. 20, pp. 4887–4897, May 2024, doi: 10.1021/acs.jpcb.3c08254.

MULTIFUNCTIONAL CARBON-BASED QUANTUM DOTS FOR ENVIRONMENTAL AND MEDICAL APPLICATION

Martynas Zalieckas[1], Hanna Maltanava[2], Nikita Belko[2], Polina Kuzhir[2], Renata Karpicz[1]

[1]Department of Molecular Compound physics, Center for Physical Sciences and Technology, Saulėtekio Ave. 3, LT-10257 Vilnius, Lithuania
[2]Department of Physics and Mathematics, University of Eastern Finland, FI-80100 Joensuu, Finland.
martynas.zalieckas@ftmc.lt

Modern environmental monitoring and medical diagnostics increasingly require functional materials that combine optical sensitivity, chemical stability, and compatibility with complex systems. Conventional fluorescent materials often suffer from limited stability, toxicity concerns or restricted tunability. Carbon-based quantum dots have emerged as promising candidates due to their low toxicity, chemical robustness, and strong photoluminescence [1]. Among them, carbon nitride quantum dots (CNQDs) are particularly attractive because of their unique electronic structure and surface chemistry, which can be exploited for interaction with chemical and biological environments relevant to sensing and imaging applications [2, 3].

In this study, we focus on investigating the stability and optical properties of CNQDs prepared from bulk graphitic carbon nitride (G-C3N4) using LiOH-assisted ultrasonic exfoliation followed by mild thermal treatment. The resulting dispersions were purified by dialysis and characterised using UV-Vis absorption spectroscopy, steady-state photoluminescence spectroscopy, fluorescence lifetime measurements and Fourier transform infrared (FT-IR) spectroscopy.

To assess the imaging compatibility, CNQD fluorescence was also examined under live-cell fluorescence microscopy conditions using HeLa cells, demonstrating detectable optical signals under standard imaging parameters without additional labelling.

By addressing fundamental optical response and imaging visibility at an early stage of material development, this study highlights the relevance of CNQDs as versatile building blocks for future multifunctional platforms.

Acknowledgements

This work was supported by the Horizon Europe FLORIN project (No. 101086142) and the Research Council of Lithuania (Grant No. S-MIP-23-70).

[1] B. Sen and H. Sarma, “Carbon quantum dots as multifunctional nanomaterials for sustainable optoelectronic biosensing and green photonics,” pp. 1–14, 2026, https://doi.org/10.1038/s43246-025-01056-y

[2] J. Dong et al., “Fabrication of Graphitic Carbon Nitride Quantum Dots and Their Application for Simultaneous Fluorescence Imaging and pH-Responsive Drug Release,” ChemistrySelect, vol. 3, no. 44, pp. 12696–12703, 2018, doi: 10.1002/slct.201802492.

[3] N. Azam, M. Najabat Ali, and T. Javaid Khan, “Carbon Quantum Dots for Biomedical Applications: Review and Analysis,” Front. Mater., vol. 8, no. August, pp. 1–21, 2021, doi: 10.3389/fmats.2021.700403.

DESIGN AND FABRICATION OF MINIATURIZED OPTICAL SYSTEMS VIA MULTI-PHOTON LITHOGRAPHY

Austėja Kvedaraitė[1], Dimitra Ladika[1], Mangirdas Malinauskas[1], Gordon Zyla[1]

[1]Vilnius University, Faculty of Physics, Laser Research Center, Lithuania
gordon.zyla@ff.vu.lt

Over recent years, the field of modern optics exploiting free-form optics and flat optics such as metasurfaces at the microscale has attracted increasing research interest. This grow is driven by the aim to miniaturize optical elements and enhance overall compactness of optical systems while maintaining effective control of light through integrated designs. [1] Within this context, one of the key technologies enabling fabrication of miniaturized optics is multi-photon lithography (MPL) - a maskless 3D lithography technique which, in combination with highly transparent photoresist, allows the realization of free-form micro-optical elements. [2]

At present, the practical extent to which micro-optical systems can be scaled down while still satisfying the assumptions of geometrical optics and the constraints imposed by MPL remains an open question. For instance, existing integrated optics designs report system lengths of several hundred micrometers to achieve sufficient beam diameter for effective light modulation. [3, 4] To explore the feasibility of further reducing the size of micro-optical system designs, this work investigates MPL fabricated micro beam expanders realized using an organic-inorganic hybrid photoresist - SZ2080^{TM}, which enables the fabrication of accurate three-dimensional structures with high fidelity.

Initial designs of classical type Galilean beam expanders enable approximately threefold reduction in length compared to existing light structuring approaches. In addition, multi-lens beam expander configuration also mitigates vignetting effect caused by rapid beam expansion over short propagation distances. The results indicate that translating conventional optics concepts to micro-scale via MPL offers a promising approach toward compact micro-optical systems, enabling efficient light structuring within confined system geometries. The optical designs were developed using Zemax software, while the quality of the fabricated structures was assessed by optical profilometry and scanning electron microscopy. Beam expansion performance was evaluated using a home-built setup.

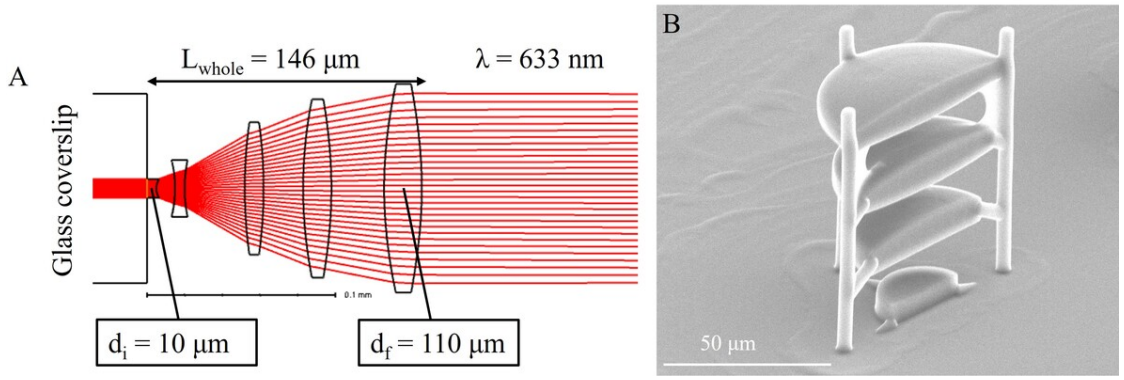


Fig. 1. A – Ray tracing of multi-lens beam expander with M = 10 expansion ratio using Zemax software. L_{whole} – overall structure length from substrate, d_i, d_f – diameter of first lens and last lens respectively. B – scanning electron microscopy image of multi-lens beam expander (M = 10).

[1] D. Gonzalez-Hernandez, S. Varapnickas, A. Bertoncini, C. Liberale, and M. Malinauskas, "Micro-Optics 3D Printed via Multi-Photon Laser Lithography," Advanced Optical Materials, vol. 11, no. 1, p. 2201701, 2023, doi: 10.1002/adom.202201701.
[2] G. Zyla and M. Farsari, "Frontiers of Laser-Based 3D Printing: A Perspective on Multi-Photon Lithography," Laser & Photonics Reviews, vol. 18, no. 7, p. 2301312, 2024, doi: 10.1002/lpor.202301312.
[3] H. Ren et al., "An achromatic metafiber for focusing and imaging across the entire telecommunication range," Nat Commun, vol. 13, no. 1, p. 4183, Jul. 2022, doi: 10.1038/s41467-022-31902-3.
[4] C. Li et al., "Metafiber transforming arbitrarily structured light," Nat Commun, vol. 14, no. 1, p. 7222, Nov. 2023, doi: 10.1038/s41467-023-43068-7.

LASER-INDUCED GRAPHENE FOR RADAR ABSORBING MATERIALS APPLICATIONS

Rokas Klimas[1], Augustas Koklevičius[2], Paulius Ragulis[3], Romualdas Trusovas[4]

[1]Vilnius University, Faculty of Physics, Institute of Photonics and Nanotechnology, Lithuania
rokas.klimas@stud.ff.vu.lt

Laser-Induced Graphene (LIG) has been widely studied in recent years. It is a porous nanomaterial produced by laser irradiation of polymer or organic materials. When appropriate irradiation parameters are applied, this method enables the formation of conductive structures in insulating substrates. LIG formation is a widely scalable technique, as laser irradiation can form conductive microstructures and process larger areas.

One possible application of LIG structures is in meta-surfaces as part of Radar-Absorbing Materials (RAM). In this work, LIG formation in Polyetherimide (PEI) material was investigated using 532 nm irradiation of nanosecond (Baltic HP, Ekspla) and femtosecond (FemtoLux, Ekspla) lasers. Laser microprocessing parameters, including irradiation power, scanning speed, and defocusing, were varied during the experiments. The sheet resistance of laser-processed samples was measured using the four-probe method. Meanwhile, the proposed meta-surface structure was modelled using CST Studio.

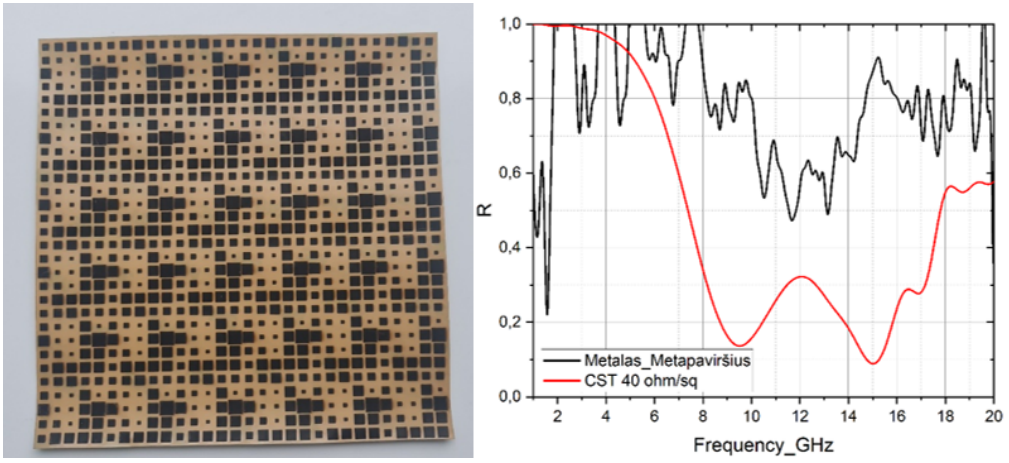


Fig. 1. LIG Meta-surface on PEI - left; Reflectance dependence on frequency – measurement(black), modelling (red) - right.

Finally, the LIG metasurface structure was fabricated and characterised in an anechoic chamber (Fig. 1). The most pronounced reduction in reflection is experimentally observed in the 8–15 GHz frequency range, which aligns well with theoretical calculations. The experimentally measured minimum reflectance reaches approximately R≈0.6, corresponding to a reflection reduction of about 3 dB (nearly twofold). The obtained results demonstrate that such graphene metasurfaces hold great promise for the development of ultrathin radar-absorbing materials (RAM) in the microwave frequency range.

DIRECT LASER WRITING OF PLASMONIC NANOSTRUCTURES ON AG-AU ALLOY FILMS

Marijus Mozdeikis[1], Evaldas Stankevičius[2]

[1]Center for Physical Sciences and Technology, Department of Laser Technologies, Plasmonics and Nanophotonics Laboratory, Vilnius, Lithuania
[2]Center for Physical Sciences and Technology, Department of Laser Technologies, Plasmonics and Nanophotonics Laboratory, Vilnius, Lithuania
marijus.mozdeikis@ftmc.lt

Plasmonic gratings and arrays composed of noble metals are actively studied due to their ability to support strong light–matter interactions and surface plasmon excitation. Such properties enable applications ranging from spectroscopy and sensing to photovoltaics and functional surface design [1]. These effects originate from plasmonic resonance, which occurs when incident light excites collective oscillations of free electrons at the metal surface. Since the momentum of incident photons is insufficient to directly couple to surface plasmons, additional momentum matching is required. This can be achieved by structuring the metal surface with wavelength-comparable features that act as a diffraction grating [2], enabling efficient light–plasmon coupling and the excitation of localized surface plasmon resonances (LSPR).

In this study, plasmonic nanostructures are formed using direct laser writing on glass substrates coated with silver–gold alloy films. Alloy compositions with silver-to-gold ratios of 50/50 and 80/20 and a coating thickness of 100 nm are investigated. The laser-induced surface patterning enables the formation of periodic structures with dimensions comparable to the excitation wavelength, which induces LSPR excitation. The plasmonic properties of the fabricated structures are analyzed using reflectance spectra measured under different polarization conditions in the visible to near-infrared spectral range. This work demonstrates that silver–gold alloy thin films can be effectively structured to support plasmonic resonances, highlighting their potential for tunable plasmonic devices and practical applications.

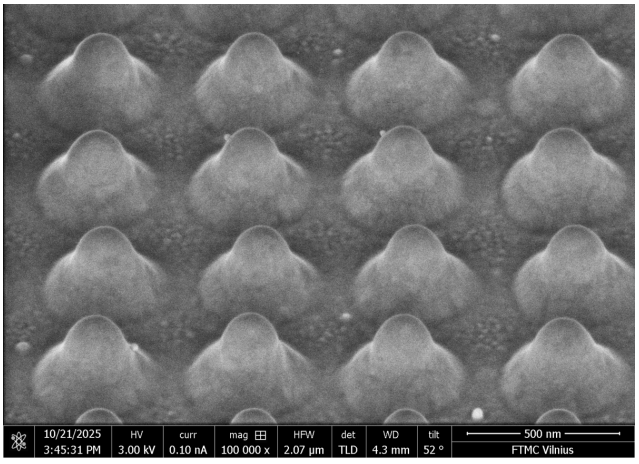


Fig. 1. Array of plasmonic nanostructures fabricated on a 100 nm thick Ag–Au (50:50) alloy film using a single-pulse energy of 0.7 nJ and a period of 0.5 µm

[1] R. Liudvinavičius, K. Vilkevičius, and E. Stankevičius, “High-quality grating-coupled surface plasmon resonances in silver and gold bumps arrays fabricated in thin metallic films using the third harmonic of femtosecond laser,” Applied Surface Science, vol. 711, p. 164127, Jul. 2025, doi: 10.1016/j.apsusc.2025.164127.

[2] K. Vilkevičius, A. Selskis, and E. Stankevičius, “Femtosecond laser Wavelength-Dependent formation of plasmonic gold nanostructures,” Applied Surface Science, vol. 617, p. 156629, Feb. 2023, doi: 10.1016/j.apsusc.2023.156629.

MULTI-PHOTON LITHOGRAPHY FOR PHOTONIC APPLICATIONS

Kristina Budiak[1], Gordon Zyla[1], Mangirdas Malinauskas[1], Dimitra Ladika[1]

[1]Laser Research Center, Physics Faculty, Vilnius University, Vilnius, LT-10223 Lithuania
dimitra.ladika@ff.vu.lt

Multi-Photon Lithography (MPL) is an advanced fabrication technique that allows direct, maskless writing of true 3D micro- and nanostructures using computer-aided design (CAD) models.[1] The process is based on multi-photon absorption in a photosensitive material, which occurs only upon tight focus of a femtosecond laser beam (Fig. 1A). After this absorption, free radicals are generated in the photoresist, which initiate polymerisation by bonding with monomers and eventually forming a solid polymer network. Therefore, stable 3D structures can be produced inside the bulk of the resist rather than being restricted to its surface (Fig. 1B). [2]

MPL photoresists are typically negative-tone materials, most commonly based on acrylate or epoxy polymers. In addition, hybrid organic–inorganic materials have gained increasing attention because they exhibit reduced polymerisation shrinkage and improved mechanical stability.[2] In this work, the hybrid organic–inorganic photoresist SZ2080 was used. It contains a zirconium-based inorganic component and Michler's ketone as a photoinitiator.

Due to its ability to fabricate complex free-form 3D geometries with high spatial resolution (down to hundreds of nanometres), MPL has been widely applied in fields such as micro-optics, photonics, mechanical metamaterials, and biomedical engineering. It is particularly promising for producing 3D photonic crystals with engineered band gaps, as well as micro- and nanostructures controlling the phase, amplitude, and polarisation state of light.[2] In this work, we aim to propose and demonstrate 3D printed nanostructures potentially capable of such light manipulation (Fig. 1C). Additionally, 3D photonic crystals, widely used in nanophotonic applications, are presented to demonstrate the capabilities of MPL in this context.

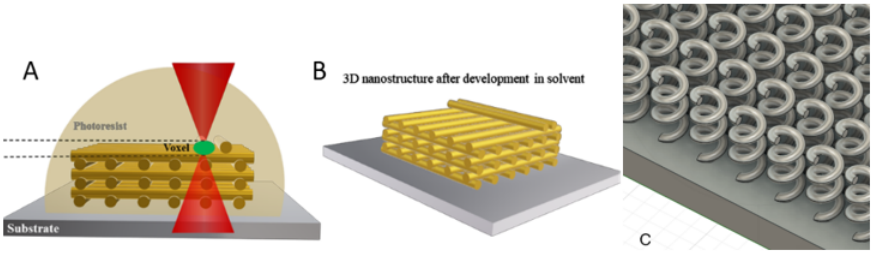


Fig. 1. *Schematic illustration of the MPL process: (A) representation of the tight focusing of the laser beam into the material. By moving the laser beam and translation stages along the x, y, and z axes, three-dimensional printing of the structures is performed. (B) Revelation of the printed structure after development in a solvent. (C) An STL image of the fabricated 3D spiral array structures.*

[1] G. Zyla and M. Farsari, "Frontiers of laser-based 3D printing: A perspective on multi-photon lithography," Laser & Photonics Reviews, vol. 18, no. 7, p. 2301312, 2024.

[2] H. Wang, W. Zhang, D. Ladika, H. Yu, D. Gailevičius, H. Wang, F. Pan, P. N. Suseela Nair, Y. Ke, T. Mori, J. Y. En Chan, Q. Ruan, M. Farsari, M. Malinauskas, S. Juodkazis, M. Gu, and J. K. W. Yang, "Two-photon polymerisation lithography for optics and photonics: Fundamentals, materials, technologies, and applications," Advanced Functional Materials, vol. 33, no. 39, p. 2214211, 2023.

DESIGN AND FABRICATION OF METASURFACES VIA MULTI-PHOTON LITHOGRAPHY

Jonas Vytautas Sviklis[1], Dimitra Ladika[1], Mangirdas Malinauskas[1], Gordon Zyla[1]

[1]Vilnius University, Faculty of Physics, Laser Research Center, Vilnius, LT-10223 Lithuania.
gordon.zyla@ff.vu.lt

Multi photon polymerization (MPL) features a maskless 3D printing method, that enables complex 3D design fabrication with feature sizes below 1 µm using femtosecond laser radiation [1]. As a manufacturing tool, MPL offers unmatched versatility and great adaptability for realizing advanced optical components on surfaces that are hard to access, such as optical fibers. This capability presents significant opportunities for developing optical applications in integrated optical scenarios [2].

Within the field of advances of optical components, metasurfaces – comprising individual nanostructures arranged in carefully designed patterns – have attracted considerable interest. These planar elements are often regarded as flat analogues of conventional optical components and enable precise tailoring of electromagnetic waves, fostering compact devices for precise light manipulation [3].

This work demonstrates the fabrication of metasurfaces operating at telecommunication wavelengths, with a specific focus on metalenses composed of isotropic unit cells formed by cylindrical nanorods, fabricated using MPL and organic-inorganic photoresists. Alongside the metalens design, its optical properties were simulated by finite-difference time-domain (FDTD) methods. For the fabrication of MPL, the metalens design was sliced into individual layers and hatched with defined spacing to generate the exposure paths for the laser radiation. The fabricated metalens exhibited high structural fidelity, with nanorod diameters of 0.6 µm (see Fig. 1). Structural characterization was performed using scanning electron microscopy. These results highlight the strong potential of MPL as a maskless fabrication approach for further exploring multi-layer metasurfaces with more complex unit cell geometry.

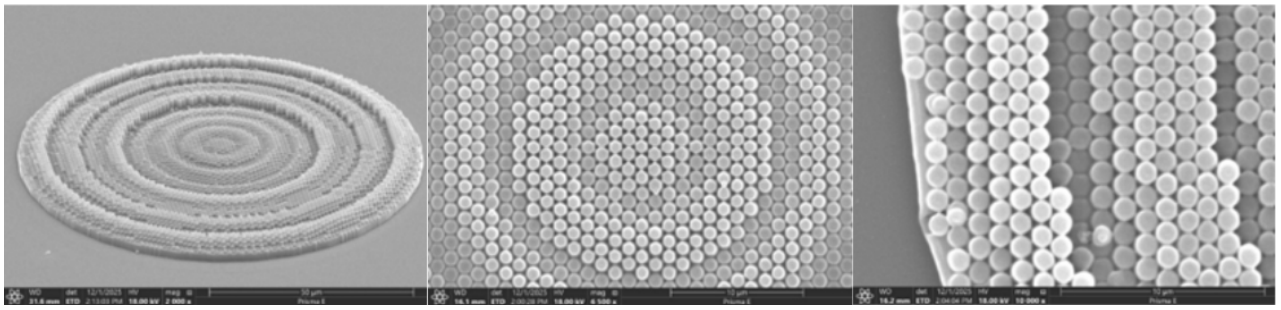


Fig. 1. Isotropic metalens, consisting out of a base and cylindrical nanorods of different heights, fabricated using laser output power of 1.4 mW, SEM pictures from different angles and magnification.

[1] A. H. Dorrah, “Compound meta-optics: there is plenty of room at the top,” Nanophotonics, vol. 14, no. 23, pp. 3835–3849, Apr. 2025, doi: 10.1515/nanoph-2024-0772.

[2] G. Zyla and M. Farsari, “Frontiers of Laser-Based 3D Printing: A perspective on Multi-Photon Lithography,” Laser & Photonics Review, vol. 18, no. 7, Mar. 2024, doi: 10.1002/lpor.202301312.

[3] H. Wang et al., “Two-Photon Polymerization Lithography for optics and Photonics: Fundamentals, materials, technologies, and applications,” Advanced Functional Materials, vol. 33, no. 39, Mar. 2023, doi: 10.1002/adfm.202214211.

[4] D. Gonzalez-Hernandez, S. Varapnickas, A. Bertoncini, C. Liberale, and M. Malinauskas, “Micro-Optics 3D printed via Multi-Photon Laser lithography,” Advanced Optical Materials, vol. 11, no. 1, Nov. 2022, doi: 10.1002/adom.202201701.

LASER-INDUCEDGRAPHENE FORMATION IN KEVLAR

David Bolanos[1], Romualdas Trusovas[1]

[1]Center for Physical Sciences and Technology, Department of Laser Technologies, Vilnius, Lithuania
david.bolanos@ftmc.lt

Wearable systems that integrate sensing, communication, and protective functions require materials that are lightweight, flexible, electrically conductive, and mechanically robust. Laser-induced graphene (LIG) has emerged as a promising platform for wearable electronics due to its scalable, mask-free fabrication and excellent electrical and electrochemical properties [1]. Recent studies have demonstrated direct laser writing of graphene on high-performance polymer fabrics such as Kevlar, enabling multifunctional textile electronics that combine structural durability with active device capabilities [2]. In particular, the transformation of Kevlar fibers into conductive LIG via photothermal laser processing has enabled flexible sensors, energy storage elements, and integrated protective garments capable of physiological monitoring and environmental sensing [3]. By leveraging the intrinsic mechanical strength and thermal stability of Kevlar alongside the functional conductivity of LIG, such fiber-based architectures offer a compelling route toward next-generation wearable electronics and personal protective systems [4]. In this work, we explore the direct formation of LIG on Kevlar fibers, combining the intrinsic mechanical strength, thermal stability, and impact resistance of aramid textiles with the functional conductivity of graphene.

Janus laser-induced graphene (LIG) was fabricated on two yellow Kevlar substrates using two distinct nanosecond laser regimes (wavelength 532 nm and 1064 nm) to investigate their effects on composite formation for wearable electronics and protective applications. Different scanning speeds were explored at different laser powers. Laser processing enabled simultaneous LIG formation on both surfaces of the Kevlar fibers, preserving the substrate's inherent mechanical strength and thermal stability while imparting enhanced electrical conductivity and flexibility. Sheet resistance measurements were carried out by the 4-probe method.

LIG-Kevlar composite was successfully fabricated in a range of 4,25-5,5 W and low scanning speed in a range of 10-50 mm/s. Laser regimes at 532 nm and higher scanning speeds didn't display positive results for janus composite, while positive data was obtained at 1064 nm wavelength, 13 ns pulse duration and 100 kHz repetition rate. The squared composite is more mechanically stable than the rectangled composite, due to fiber design and its thickness 0.5 mm and 0.3 mm, respectively. Reported sheet resistance values of 4.74-69.64 Ohms/Sq at 4.25-5.5 W for the LIG-Squared Kevlar and 0-14 mm defocusing; and 6.86-64.48 Ohms/Sq at 5-6.75 W for the LIG-rectangled Kevlar and 0-4 mm defocusing.

Further experimental characterization will reveal differences in LIG morphology, electrical performance, and mechanical integrity. corresponding to each laser regimes

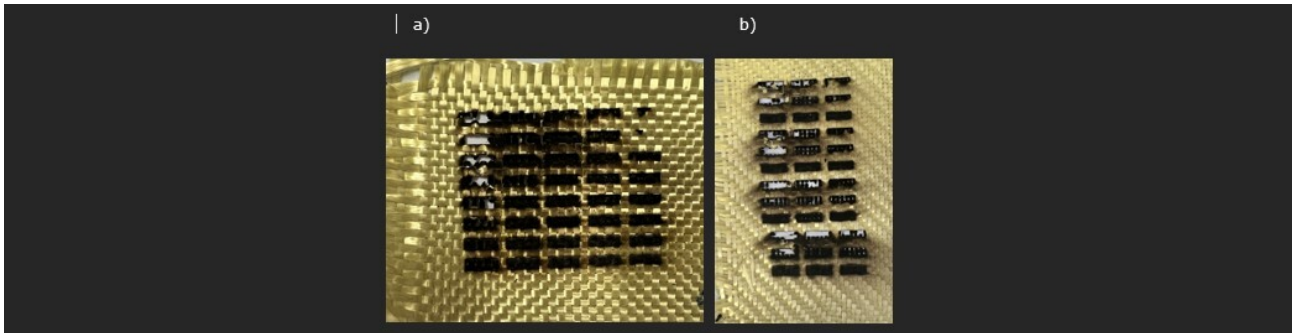


Fig.1 Formation of graphene on a Kevlar textile induced by laser writing. a) LIG-square Kevlar at 5.25 W, 100KHz, 10-50 mm/s, 0 – 14 mm defocusing. b) LIG-rectangle Kevlar at 30-50 mm/s scanning speed, 5-5.75 W power, 100KHz, 0 – 4 mm defocusing

Keywords: Laser-induced graphene, kevlar, janus composite

[1]] Y. Zou, Y. Wang, Y. Cao, Y. Li, and Z. Wang, "Flexible wearable strain sensors based on laser-induced graphene for monitoring human physiological signals," Polymers, vol. 15, no. 17, Art. no. 3566, Aug. 2023, doi: 10.3390/polym15173566.

[2]] H. Wang, Y. Wang, Y. Zhang, Y. Li, Z. Wu, and Z. Hu, "Laser writing of Janus graphene/Kevlar textile for intelligent protective clothing," ACS Nano, vol. 14, no. 3, pp. 3219–3226, Mar. 2020, doi: 10.1021/acsnano.9b08638.

[3] H. Wang et al., "Laser writing of Janus graphene/Kevlar textile for intelligent protective clothing," ACS Nano, vol. 14, no. 3, pp. 3219–3226, Mar. 2020, doi: 10.1021/acsnano.9b08638.

[4]] Y. Rao, X. Huang, J. Zhang, Y. Li, and Z. Wang, "Laser-scribed phosphorus-doped graphene derived from Kevlar textile for enhanced wearable micro-supercapacitors," J. Colloid Interface Sci., vol. 628, pp. 818–826, Jan. 2023, doi: 10.1016/j.jcis.2022.10.012.

STRUCTURAL AND OPTICAL PROPERTIES OF Eu^{3+} /Tb^{3+} CO-DOPED $GdPO_4$ NANOPARTICLES

Mirza Abdul Qudoos Baig[1], Eglė Ežerskyte[1], Artūras Katelnikovas[1], Živilė Jurgelenė[2], Vaidas Klimkevičius[1]

[1]Vilnius University, Faculty of Chemistry and Geosciences, Institute of Chemistry, Lithuania
[2]State Scientific Institute Nature Research Centre, Lithuania
qudoos.baig@chgf.stud.vu.lt

Lanthanide-doped gadolinium phosphate ($GdPO_4$) nanoparticles constitute a versatile class of inorganic nanophosphors whose functional properties are strongly governed by crystal structure, particle size, and morphology. Achieving precise control over these parameters remains challenging, particularly in multicomponent systems where dopant interactions can significantly influence crystal growth and structural order. In this study, Eu^{3+}/Tb^{3+} co-doped $GdPO_4$ nanoparticles were synthesized via a hydrothermal method to systematically investigate the effects of precursor stoichiometry and dopant concentration on their structural and morphological evolution. Four Ln^{3+}:PO_4^{3+} molar ratios (1:25, 1:50, 1:100, and 1:200) were examined, while the Eu^{3+} content was varied from 0 to 5 mol% in $GdPO_4$:20 mol% Tb^{3+} samples. X-ray diffraction analysis revealed a progressive increase in crystallinity and crystallite size with increasing phosphate excess and decreasing Eu^{3+} concentration, with the highest degree of structural order observed at a Ln^{3+}:PO_4^{3-} ratio of 1:200. These findings demonstrate that both precursor stoichiometry and activator concentration play a critical role in crystal growth. Furthermore, photoluminescence measurements showed that varying the Eu^{3+} concentration in $GdPO_4$:20 mol% Tb^{3+} enables controlled tuning of the emission color from green to red. The established structure-composition-morphology correlations provide valuable insight into the rational design of $GdPO_4$-based nanophosphors with tailored optical and physical properties for advanced functional materials.

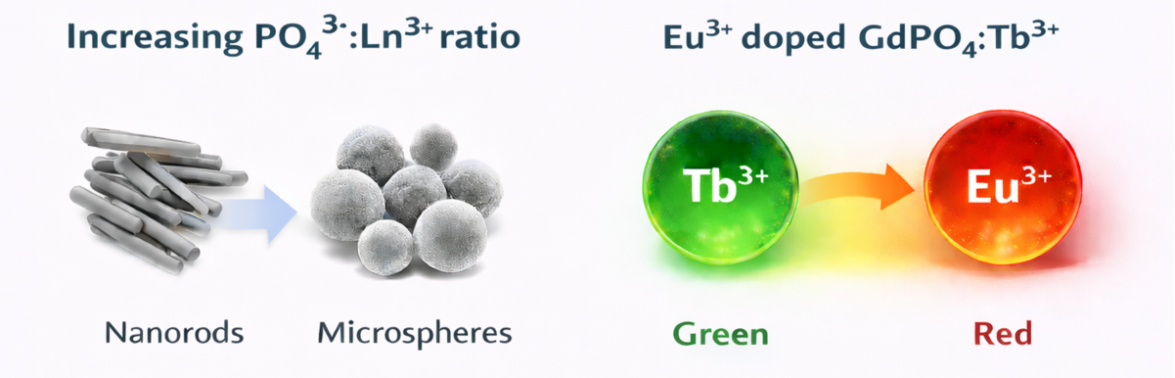


Fig. 1. Morphology evolution from nanorods to microspheres driven by Ln^{3+}:PO_4^{3+} ratio and gradual emission tuning from green to red via Eu^{3+} doping in $GdPO_4Tb^{3+}$ samples

Acknowledgements
This work was supported by the Research Council of Lithuania, agreement No. [S-MIP-24-92]

PROTOTYPE OF A WHITE LED WITH GLASSY NAF-AL_2 O_3-P_2O_5: EU PHOSPHOR

Mateusz Słotwiński[1], Agata Jarocka[1], Tomasz Pietrzak[1]

[1]Warsaw University of Technology, Faculty of Physics, Solid State Ionics Division, Warsaw, Poland
mateusz.slotwinski.stud@pw.edu.pl

One of the key research directions in modern optoelectronics and materials physics is the development of white LEDs with emission spectra closely resembling natural light, while maintaining low production costs. This work presents both the prototyping stage and the characterization of innovative luminescent materials based on a NaF-Al_2O_3-P_2O_5 glass matrix doped with europium.

The key element of the project is the utilization of the partial reduction of europium ions ($Eu^{3+} \rightarrow Eu^{2+}$) during synthesis via the melt-quenching method in a reducing atmosphere. Through precise control of temperature and melting time, it is possible to manage the concentration ratio of active centers, allowing for the seamless adjustment of the emission color—ranging from amaranth, through warm white, to cool white. In this system, the glass matrix plays a dual role: it serves as a stable substrate for the luminescent ions and acts as a durable mechanical shield.

As part of the research, a complete LED lamp prototype was designed and fabricated, consisting of:

- The glass phosphor,
- A steel housing and a dedicated stand with an adjustable beam angle,
- An aluminum reflector to optimize light extraction, utilizing a UV LED as the excitation source.

Furthermore, material characterization was conducted, including confirmation of the amorphous structure (XRD), determination of thermal parameters (DTA), and optical properties (absorption and photoluminescence spectroscopy).

The research results confirm that the use of europium-doped fluorophosphate glasses allows for a continuous and smooth emission spectrum, highly similar to sunlight.

Keywords: LED, optoelectronics, glass matrix, phosphor, photoluminescence, rare-earth metals, materials engineering, solid-state physics, materials physics, technical design

[1] A. Jarocka, B. Fetliński, P. Dębowski, T. K. Pietrzak, K. Jurak, and M. Wasiucionek, “Facile and cost-effective technique to control europium oxidation states in glassy fluorophosphate matrices with tunable photoluminescence,” Scientific Reports, vol. 12, no. 1, p. 18774, Nov. 2022, doi: 10.1038/s41598-022-21981-z.

[2] T. K. Pietrzak et al., “Photoluminescence of partially reduced Eu2+/Eu3+ active centers in a NaF–Al2O3–P2O5 glassy matrix with tunable smooth spectra,” Journal of Luminescence, vol. 208, pp. 322–326, Dec. 2018, doi: 10.1016/j.jlumin.2018.12.060.

EFFECT OF ORGANIC WASTE PARTICLE ADDITIVES ON THE PROPERTIES OF THERMOPLASTIC CELLULOSE ACETATE

Akvile Brazdauske[1], Laura Peciulyte[1], Ramune Rutkaite[1], Dovile Liudvinavičiūtė[1], Joana Bendoraitiene[1], Kastytis Pamakštys[2], Visvaldas Varzinskas[2]

[1]Kaunas University of Technology, Department of Polymer Chemistry and Technology, Kaunas, Lithuania
[2]Kaunas University of Technology, Research Center for Advanced Packaging Materials and Technologies, Kaunas, Lithuania
akvile.rekasiute@ktu.edu

With the continuous rise in synthetic polymer production, waste management is becoming an increasingly pressing global challenge. As a result, huge amounts of plastic end up in landfills and eventually migrate into natural ecosystems, where they disrupt the habitats of living organisms. Additionally, incinerating plastic waste contributes to higher greenhouse gas emissions. Biodegradable cellulose acetate (CA) offers a promising alternative to conventional synthetic plastics, as it can achieve comparable mechanical properties. However, a major limitation of CA is that its melting temperature is very close to its decomposition temperature, making melt processing difficult unless plasticizers are added. When appropriate plasticizers are incorporated, CA can be converted into thermally processable mixtures suitable for thermoplastic manufacturing. Additionally, agriculture and food production waste can be utilised as fillers to adjust product mechanical, thermal and/or hydrophobicity properties and reduce manufacturing cost.

In this study, compositions of thermoplastic cellulose acetate were obtained using ecofriendly plasticizer triacetin, and fruit waste particles. By varying the amounts of CA, plasticizer and filler particles, a set of thermoplastic mixtures was prepared and thermally processed using twin-screw extrusion, by estimation the extrusion parameters. By the means of injection molding and 3D printing the samples of novel bioplastics were obtained. The influence of the triacetin content on the mechanical properties of the extrudates is greater than that of the filler content. With an increase in the plasticizer content in the compositions, the tensile strength and elastic modulus values decrease both in the compositions with fruit waste filler and without filler, and the elongation, on the contrary, increases

Acknowledgements

Research was conducted as part of the execution of Project ”Mission-driven Implementation of Science and Innovation Programmes” (No. 02-002-P-0001), funded by the Economic Revitalization and Resilience Enhancement Plan ”New Generation Lithuania”.

PHOTOLUMINESCENCE STUDY OF InGaAs QUANTUM WELLS WITH LINEARLY AND PARABOLICALLY GRADED AlGaAs BARRIERS

Denis Goldobin[1], Aistė Štaupienė[1], Justas Žuvelis[1], Aivaras Špokas[1], Andrea Zelioli[1], Aurimas Čerškus[1], Evelina Dudutienė[1], Renata Butkutė[1]

[1]State research institute Center for Physical Sciences and Technology, Saulėtekio av. 3, Vilnius, Lithuania
denis.goldobin@ftmc.lt

InGaAs is a well-studied III–V ternary semiconductor with a tunable bandgap suitable for near-infrared (NIR) applications. Decades of progress in epitaxial growth have made it a reliable platform for systematic studies of barrier effects on optical properties of quantum wells (QW). In this work, we investigate the influence of graded AlGaAs barrier profiles on the emission of InGaAs QW structures, motivated by earlier reports of enhanced carrier capture and photoluminescence (PL) intensity in graded-index separate-confinement heterostructures [1,2].

The InGaAs QW samples were grown by molecular beam epitaxy on semi-insulating GaAs (100) substrates. Investigated structures include parabolically graded (PQW) and linearly graded (TrQW) AlGaAs barriers, with Al composition varying from 30% to 0%. Additional rectangular quantum well (RQW) samples with prolonged *in-situ* annealing were grown to separate effects of barrier design from high-temperature exposure. Optical properties were studied using temperature-dependent PL, supported by band-structure simulations performed with Nextnano. Room-temperature PL measurements reveal a clear enhancement of emission intensity in structures with graded AlGaAs barriers relative to conventional RQWs (see Fig. 1).

Temperature-dependent PL shows improved carrier confinement and suppressed thermal quenching in graded-barrier designs, with PQW structures exhibiting the highest PL intensity up to 300 K. Analysis of PL peak energies indicates moderate blueshifts associated with high-temperature exposure, attributed to In segregation, while simulations confirm higher In retention in the presence of Al-containing barriers. Arrhenius analysis of PL intensities identifies higher activation energies for nonradiative processes in graded-barrier structures, consistent with enhanced carrier trapping.

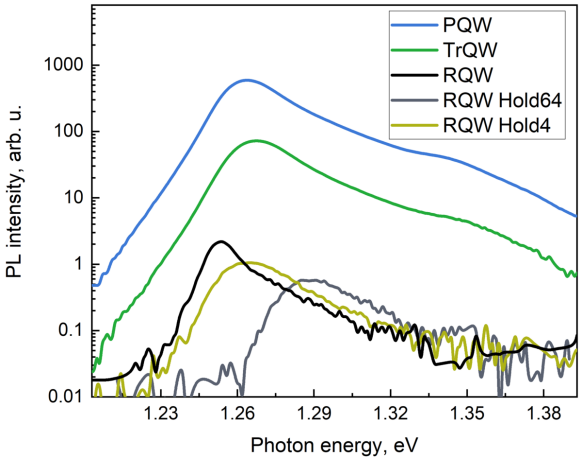


Fig. 1. Room-temperature PL spectra of all investigated InGaAs QW structures measured under the excitation of 5 kWcm^{-2}.

Keywords: InGaAs, quantum wells, photoluminescence, graded AlGaAs barriers, molecular beam epitaxy

[1] J. Feldmann et al., "Carrier trapping in single quantum wells with different confinement structures," Applied Physics Letters, vol. 51, no. 4, pp. 226–228, Jul. 1987, doi: 10.1063/1.98456.
[2] S. Pūkienė et al., "Enhancement of photoluminescence of GaAsBi quantum wells by parabolic design of AlGaAs barriers," Nanotechnology, vol. 30, no. 45, p. 455001, Jul. 2019, doi: 10.1088/1361-6528/ab36f3.

SPECTROSCOPIC INVESTIGATION OF GOLD NANOCLUSTERS UNDER DIFFERENT PH CONDITIONS

Jelizaveta Fedotova[1,2], Giedrė Grincienė[1], Renata Karpicz[1]

[1]Center for Physical Sciences and Technology, Department of Molecular Compound Physics, Lithuania
[2]Vilnius University, Faculty of Physics, Lithuania
jelizaveta.fedotova@ftmc.lt

Gold nanoclusters (AuNCs) have attracted significant interest due to their unique size-dependent optical properties, which make them promising materials for applications in sensing, bioimaging, and nanophotonics. The photophysical behavior and stability of AuNCs are known to be strongly influenced by their chemical environment, particularly by pH, which can affect surface chemistry, aggregation processes, and electronic structure. Understanding these effects is essential for the reliable use of gold nanoclusters in aqueous systems.

In this work, the influence of pH on the optical properties of AuNCs was investigated using spectroscopic methods. A series of solutions with pH values ranging from 1 to 13 was prepared, and AuNCs were introduced under identical conditions. Fluorescence and absorbance spectroscopy were employed to monitor the optical response of the nanoclusters immediately after mixing and as a function of time. The study aims to assess the pH-dependent stability and optical behavior of AuNCs and to identify conditions suitable for further spectroscopic and application-oriented studies.

Keywords: Fluorescence, Absorption, Gold nanoclusters, pH dependence.

INFLUENCE OF Co^{2+} IONS ON GYROLITE FORMATION UNDER HYDROTHERMAL CONDITIONS

Adrija Marija Paknytė[1], Tadas Dambrauskas[1]

[1]Kaunas University of Technology, Faculty of Chemical Technology, Department of Silicate Technology, Kaunas, Lithuania
adrija.paknyte@ktu.lt

As humanity faces various global challenges, such as climate change, biodiversity loss, and pollution, there is an increasing demand for new, environmentally friendly materials capable of reducing environmental harm, including greenhouse gas emissions and other pollutants [1, 2]. Such materials can be calcium silicate hydrates ($xCaO{\cdot}ySiO_2{\cdot}nH_2O$, where x, y, and n are molar coefficients). These materials are characterized by a high surface area and pore volume as well as thermal and chemical stability, making them suitable for use as thermal insulation materials, in the production of low-carbon cements, as adsorbents, and as catalysts supports [3, 4]. Compared to other calcium silicate hydrates, gyrolite [$Ca_8Si_{12}O_{30}(OH)_4{\cdot}7H_2O$] exhibits the largest distances between silicate layers 0.3 nm, i.e., sufficient to intercalate additional ions while maintaining charge neutrality. Thus, gyrolite is a promising material in advanced adsorption processes, for example, for the purification of wastewater from heavy metal ions, anions, and organic compounds; for the adsorption of carbon dioxide [5]. However, there are limited data on the synthesis and application of gyrolite with intercalated transition metal ions. Therefore, this study aimed to determine the effect of Co^{2+} ions on gyrolite formation during hydrothermal synthesis at 200 °C and on its main physical and chemical properties.

To synthesize gyrolite, calcium oxide and amorphous silicon dioxide were mixed to obtain a mixture with a molar ratio of CaO to SiO_2 equal to 0.66. This molar ratio corresponds to that of gyrolite. Then, 20 mL of distilled water or a cobalt nitrate solution (c_{Co}=10 g/L) was added to 2 g of the solid mixture to obtain suspensions (W/S = 10). The resulting suspensions were transferred into PTFE vessels for hydrothermal synthesis. The vessels were placed in a „Parr Instruments“ autoclave and treated at 200 °C, with the duration of isothermal treatment ranging from 0 h to 72 h. The obtained products were characterized by XRD, STA, FT-IR, AAS, and other methods.

It was found that Co^{2+} ions positively affected the formation of calcium silicate hydrates in $0.66CaO{-}SiO_2{-}H_2O$ mixture during hydrothermal synthesis. In the system without cobalt ions, pure gyrolite formed after 48 h and remained stable up to 72 h. Meanwhile, in the presence of Co^{2+} ions, the target product was the dominant phase after 16 h of synthesis and remained stable until 72 h. The analysis of the liquid medium showed that all Co^{2+} ions (100 mg of Co^{2+} per gram of initial mixture) were intercalated into the structure of gyrolite. Cobalt ions changed not only the formation sequence of calcium silicate hydrates but also the thermal stability of gyrolite.

[1] Guo, J., et. al. Chinese Chemical Letters, vol. 37, iss. 2, 2026
[2] Ameachi, C. V., et. al. Materials Today Sustainability, vol. 33, 2026
[3] Supriya, et. al. Journal of Cleaner Production, vol. 417, 2023
[4] Wu, Q., et. al. Desalination and Water Treatment, vol. 324, 2025
[5] Baltakys, K., et. al. Synthetic Gyrolite, Springer, 2024, p. 277

EVALUATION OF THE PHYSICO-CHEMICAL PROPERTIES OF HYDRAULIC CALCIUM SILICATE-BASED SEALER MODIFIED WITH CALCIUM HYDROXYAPATITE, FLUOROHYDROXYAPATITE, AND MAGNESIUM WHITLOCKITE

Paulina Mozūraitė[1], Goda Bilvinaitė[1,2], Saulius Drukteinis[1], Simas Šakirzanovas[2]

[1]Vilnius University, Faculty of Medicine, Institute of Dentistry, Lithuania
[2]Vilnius University, Faculty of Chemistry and Geosciences, Institute of Chemistry, Lithuania
paulina.mozuraite@mf.stud.vu.lt

Hydraulic calcium silicate–based sealers (HCSS) are widely used materials in modern endodontics due to their advantageous handling properties and clinical performance, mainly attributed to favorable biocompatibility and bioactivity. However, their relatively long setting time and insufficient chemical stability often lead to increased solubility and altered setting reactions, representing key limitations of HCSS. Further, the hydration products of HCSS differ from mineral phases naturally present in dental tissues, limiting their biomimetic properties. Although several attempts have been made to modify HCSS with conventional calcium hydroxyapatite (Ca-HAp, $Ca_{10}(PO_4)_6(OH)_2$), showing improved physico-chemical properties of HCSS, the influence of chemically distinct calcium phosphate phases – such as fluorohydroxyapatite (F-HAp, $Ca_{10}(PO_4)_6(OH)_{2-x}F_x$) and magnesium whitlockite (Mg-WH, $Ca_{18}Mg_2(HPO_4)_2(PO_4)_{12}$) – on HCSS modification remains unexplored. Nevertheless, both Mg-WH and F-HAp possess intrinsic physicochemical and biological properties that make them promising HCSS modifiers. Therefore, the present study systematically investigated and compared the physico-chemical properties of HCSS modified with Ca-HAp, F-HAp, and Mg-WH.

Ca-HAp, F-HAp, and Mg-WH were synthesized using chemical precipitation, chemical precipitation combined with pH cycling, and a low-temperature dissolution–precipitation method, respectively. Phase crystallinity and purity were analyzed by X-ray diffraction (XRD), while functional groups were identified using Fourier-transform infrared spectroscopy (FT-IR). Particle morphology was examined using scanning electron microscopy (SEM). The commercial and clinically used HCSS BioRoot RCS (Septodont, France) was then modified with Ca-HAp, F-HAp or Mg-WH. The chemical properties and ISO 6876:2012 standard parameters of unmodified and modified HCSS were evaluated. Setting time and flowability were determined following ISO 6876:2012 guidelines. Surface morphology and elemental composition were analyzed using scanning electron microscopy with energy-dispersive X-ray spectroscopy (SEM–EDX). Solubility was assessed by mass loss measurements, while ion release was quantified using inductively coupled plasma optical emission spectrometry (ICP-OES). Mechanical hardness was evaluated by compression testing, thermal stability by thermogravimetric analysis (TGA), and porosity by micro–computed tomography (micro-CT). Surface morphology, solubility, pH, ion release, thermal stability, and porosity were evaluated after 24 h and 7 d of incubation in Hank's balanced salt solution at 37 °C.

The applied experimental approach enabled a comprehensive evaluation of original and modified HCSS, allowing a comparative assessment of the effects of Ca-HAp, F-HAp, and Mg-WH on clinically relevant physico-chemical properties.

Acknowledgements

The study was supported by Angelė and Sigitas Kazlauskas Endowment Sub-fund managed by the Vilnius University Foundation.

CHEMICAL CHARACTERIZATION AND ANTIMICROBIAL ACTIVITY ASSESSMENT OF SPENT COFFEE GROUNDS USED IN BUILDING GYPSUM COMPOSITES

Neringa Matutytė[1], Rita Kazernavičiūtė[2], Aušra Šipailienė[2], Nora Kybartienė[1]

[1]Kaunas University of Technology, Faculty of Chemical Technology, Department of Silicate Technology, Kaunas, Lithuania
[2]Kaunas University of Technology, Faculty of Chemical Technology, Department of Food Science and Technology, Kaunas, Lithuania
neringa.matutyte@ktu.edu

The extensive global consumption of coffee results in significant quantities of spent coffee grounds (SCG) as a post-brewing residue. Such residue is usually disposed in landfills, raising environmental concerns and encouraging the need for sustainable reuse approaches [1]. The construction industry is a promising sector for the SCG valorisation, where they could be used as an additive in various building materials [2]. Although mechanical and physical properties of construction composites with organic additives are commonly evaluated, but information regarding antimicrobial behaviour of such additives, particularly for indoor construction applications, remains scarce. Additionally, treated SCG, despite containing potentially valuable bioactive compounds applied in other fields, remain mostly underutilised as well.

Therefore, this study aims to assess antimicrobial activity, bioactive compounds and mechanical properties of untreated and acetone or boiling water treated spent coffee grounds used as an additive in building gypsum composites.

The properties of two types of SCG were compared: collected from domestic manual brewing and from local coffee shop using machine brewing. The particle size used for further experiments of both types of SCG were lower than 0,5 mm. SCG treatment was performed with either 100 °C temperature boiling water, or with different concentrations of acetone solvent. Mechanical properties were determined by forming 2 × 2 × 2 cm specimens out of SCG and building gypsum, otherwise known as β-hemihydrate gypsum, and measuring their compressive strength. The chemical composition as well as antimicrobial activity of used organic additive was evaluated. Total phenolic content (TPC) of SCG, before and after treatment, was assessed using Folin-Ciocalteu assay, either directly from solid material by the QUENCHER method or from the methanolic SCG extracts.

[1] D. N. Dari, et al., “Spent coffee grounds: Insights and future prospects for bioenergy and circular economy applications“, Green Technologies and Sustainability, 3, 4, 100213, 2025.
[2] J. J. Yee, et al., “Spent coffee grounds enhanced compressive strength of cement mortar: an optimization study”, Discovered Applied Sciences, 6, 379, 2024.

DEVELOPMENT OF MOLECULARLY IMPRINTED POLYMER ON MAGNETIC PARTICLES

Gabrielė Slaboševičiūtė[1,2], Ernestas Brazys[1,3], Vilma Ratautaitė[1], Arūnas Ramanavičius[1,3]

[1]State Research Institute Center for Physical Sciences and Technology (FTMC), Department of Nanotechnology, Sauletekio Ave. 3, Vilnius LT-10257, Lithuania
[2]Vilnius Tech, Faculty of Fundamental Sciences, Department of Chemistry and Bioengineering, Sauletekio ave. 11, Vilnius LT-10223, Lithuania
[3]Vilnius University (VU), Faculty of Chemistry and Geosciences, Institute of Chemistry, Department of Physical Chemistry, Naugarduko str. 24, Vilnius LT-03225, Lithuania
gabriele.slaboseviciute@ftmc.lt

Molecularly imprinted polymers (MIPs) are synthetic receptors with highly specific recognition sites for target molecules. They have shown great potential as substitutes for biological receptors (e.g., antibodies and enzymes) in many areas, including molecular chemosensing, separation and purification, enzyme-like catalysis, drug development, and various biomedical applications. MIPs are stable, easy to make, and have high affinity and selectivity [1].

The typical molecular imprinting procedure consists of a few steps: 1) self-assembly of functional monomers, crosslinkers, and template molecules to create pre-polymerisation complexes; 2) chemical or electrochemical polymerisation; 3) removal of the template molecules from the obtained polymer, which generates the binding sites in the structure of the polymer, which are specific or complementary to the template molecules [2,3]. This characteristic is helpful for sensor development for specific detection. Traditionally, MIPs are prepared by bulk polymerisation as monoliths. However, this method has several drawbacks, such as a limited amount of binding sites near the surface, inaccessible recognition sites within the polymer bulk, or non-uniform morphology. In particular, imprinting of large, high-molecular-weight macromolecules, especially peptides and proteins, remains a significant challenge due to their large dimensions, complex structures, and limited solubility and stability in solution [1]. A solution to overcoming these disadvantages is the use of magnetic nanoparticles. This study presents some aspects of molecularly imprinted biosensor development, with polymerisation occurring on magnetic nanoparticles.

In this study, cobalt ferrite ($CoFe_2O_4$) magnetic nanoparticles (MNP) were employed as a platform to develop a MIP-based sensor. During chemical synthesis, MIP polymerisation was carried out directly on the surface of the magnetic nanostructures, followed by removal of the template molecules to generate specific recognition sites. The synthesised MIP-coated MNP were used for spectrophotometric and electrochemical measurements to determine the polymer-template interactions. The electrochemical measurements were carried out in a three-electrode electrochemical cell comprising magnetic glassy carbon working electrode (GCE), a platinum grid counter electrode, and an $Ag/AgCl_{3MKCl}$ reference electrode. The interactions of the MIP-coated MNP on GCE with the template molecule were investigated by cyclic voltammetry (CV), electrochemical impedance spectroscopy (EIS), and differential pulse voltammetry (DPV).

Acknowledgements

The authors are grateful to Aswathi Raveendran, Dr. Agnė Sukovienė, and Dr. Simonas Ramanavičius for the kind donation of the cobalt ferrite magnetic nanoparticles. This project has received funding from the Research Council of Lithuania (LMTLT), agreement No. S-LL-25-3.

[1] M. Dinc, C. Esen, and B. Mizaikoff, “Recent advances on core–shell magnetic molecularly imprinted polymers for biomacromolecules,” TrAC Trends in Analytical Chemistry, vol. 114, pp. 202–217, Mar. 2019, doi: 10.1016/j.trac.2019.03.008.
[2] E. Brazys, V. Ratautaite, E. Mohsenzadeh, R. Boguzaite, A. Ramanaviciute, and A. Ramanavicius, “Formation of molecularly imprinted polymers: Strategies applied for the removal of protein template (review),” Advances in Colloid and Interface Science, vol. 337, p. 103386, Dec. 2024, doi: 10.1016/j.cis.2024.103386.
[3] H. Zhang, “Molecularly imprinted nanoparticles for biomedical applications,” Advanced Materials, vol. 32, no. 3, p. e1806328, May 2019, doi: 10.1002/adma.201806328.

HIGH-ASPECT-RATIO c-Si METASURFACES FOR ULTRA-FAST PULSE LASERS

Klaudijus Midveris[1], Erika Jonaitytė[1], Gvidas Klyvis[1], Tomas Klinavičius[1], Andrius Žutautas[1], Mindaugas Juodėnas[1]

[1]Institute of Materials Science, Kaunas University of Technology, Lithuania
klaudijus.midveris@ktu.lt

Dielectric metasurfaces offer a transformative approach to wavefront engineering, yet their deployment in the ultrafast regime is frequently constrained by the complexities of managing group delay dispersion (GDD). While crystalline silicon (c-Si) is a premier platform due to its high refractive index and CMOS-compatible fabrication, its application with femtosecond pulses requires sophisticated strategies to balance phase accumulation against two-photon absorption (TPA) and nonlinear losses [1].

In this work, we demonstrate the fabrication and characterization of monolithic c-Si metasurfaces specifically engineered for low-power, ultrafast beam shaping. By utilizing monolithic integration, we realize exceptionally tall meta-atom geometries that significantly expand the parameter space for temporal and spatial optimization. To circumvent the limitations of aspect-ratio-dependent etching (ARDE), we employ a Pancharatnam–Berry (PB) phase design, ensuring a uniform local pattern density that is critical for high-fidelity fabrication [2].

Our fabrication process leverages deep reactive ion etching (DRIE) to achieve aspect ratios up to 15:1. This structural depth may enable substantial GDD tuning via propagation phase accumulation, a mechanism that operates independently of the geometric phase modulation provided by the PB orientation [3]. We experimentally validate our design by characterizing the transmitted pulse duration and evaluating the laser-induced damage threshold (LIDT). Our results demonstrate efficient spatial modulation with negligible temporal distortion, positioning high-aspect-ratio silicon metasurfaces as a robust, passive architecture for next-generation integrated ultrafast systems.

Acknowledgements
The work was supported by the Research Council of Lithuania (LMT) project No. S-MIP-24-4.

Keywords: Dielectric Metasurfaces, Monolithic Crystalline Silicon, Ultrafast optics, Pancharatnam–Berry, High-aspect-ratio

[1] M. Maiuri, A. Schirato, G. Cerullo, and G. Della Valle, “Ultrafast All-Optical Metasurfaces: Challenges and new frontiers,” ACS Photonics, vol. 11, no. 8, pp. 2888–2905, Aug. 2024, doi: 10.1021/acsphotonics.4c00776.
[2] B. Oliveira et al., “High-aspect-ratio, ultratall silica meta-optics for high-intensity structured light,” Optica, vol. 12, no. 5, p. 713, Apr. 2025, doi: 10.1364/optica.559278.
[3] Z. Yang et al., “Ultrafast Q-boosting in semiconductor metasurfaces,” Nanophotonics, vol. 13, no. 12, pp. 2173–2182, Feb. 2024, doi: 10.1515/nanoph-2023-0718.

PHOTOLUMINESCENCE STUDY OF n/InGaN/p SINGLE QUANTUM WELLS

Deimantė Jukneviičiūtė[1], Jūras Mickevičius[1]

[1]Vilnius University, Faculty of Physics, Institute of Photonics and Nanotechnology, Lithuania
deimante.jukneviciute@ff.stud.vu.lt

Optical properties of polar nitride quantum well (QW) structures are strongly influenced by the internal electric field arising from both spontaneous and piezoelectric polarizations [1]. In light-emitting diodes (LEDs), the active region QWs are sandwiched between p-type and n-type layers. The net electric field in the wells is therefore a superposition of the intrinsic polarization field and the junction field. This combined field distorts the QW potential, spatially separates electron and hole wavefunctions, and reduces the radiative recombination efficiency. One approach to mitigating these negative effects is the introduction of doped barriers [2,3], which can partially screen the polarization charges. The aim of this work is to investigate photoluminescence (PL) dynamics in InGaN/GaN QWs with varying structural parameters and junction configurations.

Eight InGaN/GaN QW structures grown by metal-organic chemical vapor deposition (MOCVD) on sapphire substrates were studied. The samples were divided into two groups, *p-n* and *n-n*, based on the barrier doping configuration. Each group contained four samples with QW widths ranging from 2.0 nm to 7.0 nm. The structures were characterized using PL spectroscopy with a 405 nm CW laser diode as the excitation source. Temperature-dependent PL measurements were performed under low excitation conditions in the range of 8-300 K, while excitation-dependent PL was measured at power densities from 32 mW/cm^2 to 20 W/cm^2.

The room-temperature PL spectra of the *p-n* InGaN/GaN QWs exhibit the redshift of the emission peak and spectral broadening as the QW width is increased (Fig. 1a). While PL intensities remain similar in narrow QWs, they decrease significantly in the wider structures. The characteristic S-shaped temperature dependence of the peak position shift (Fig. 1b) indicates strong carrier localization. Local minimums occur at different temperatures for different QW widths, and the magnitude of the redshift becomes more pronounced in the wider structures. For the widest QW, no local minimum is observed within the measured temperature range, suggesting a very broad distribution of localized states. A comparison of the two studied sample groups reveals similar trends for the *n-n* structures.

The obtained results indicate that, under low excitation conditions, the PL properties of the studied samples are governed primarily by the physical QW parameters rather than by the junction configuration.

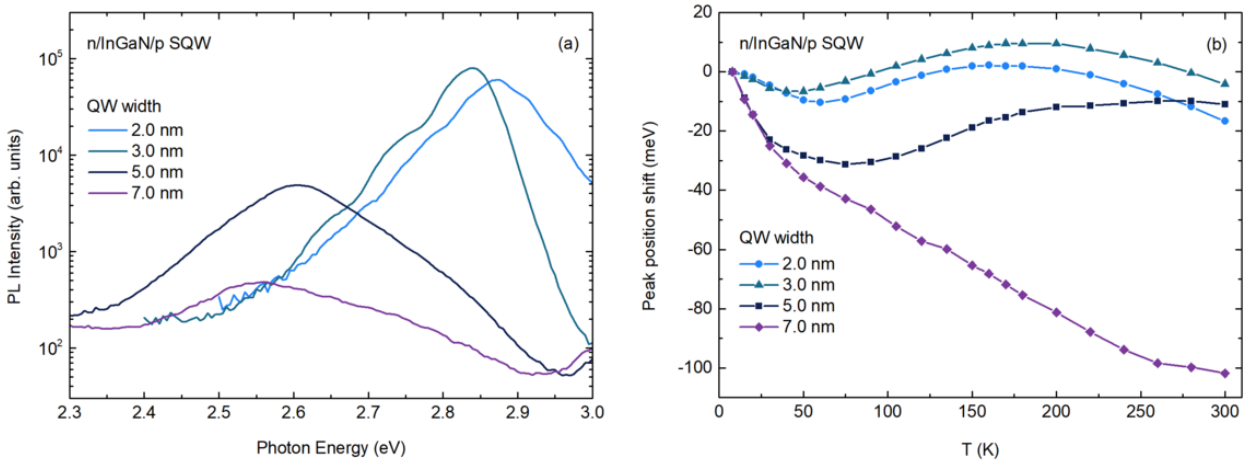


Fig. 1. (a) PL spectra of the studied *p-n* InGaN/GaN SQWs at 300 K. (b) Temperature dependence of the PL peak position shift for *p-n* InGaN/GaN SQWs.

[1] G. Muziol et al., "Beyond Quantum Efficiency Limitations Originating from the Piezoelectric Polarization in Light-Emitting Devices," ACS Photonics, vol. 6, no. 8, pp. 1963–1971, Jul. 2019, doi: 10.1021/acsphotonics.9b00327.
[2] Y. C. Chow et al., "Reduction of efficiency droop in c-plane InGaN/GaN light-emitting diodes using a thick single quantum well with doped barriers," Applied Physics Letters, vol. 119, no. 22, Nov. 2021, doi: 10.1063/5.0073741.
[3] Y. C. Chow, C. Lynsky, S. Nakamura, S. P. DenBaars, C. Weisbuch, and J. S. Speck, "Low-efficiency-droop c-plane InGaN/GaN light-emitting diodes through the use of thick single quantum wells and doped barriers," Journal of Applied Physics, vol. 133, no. 14, Apr. 2023, doi: 10.1063/5.0142035.

SULPHUR-ENHANCED REVERSE INTERSYSTEM CROSSING IN TADF AND MULTI-RESONANCE TADF BLUE EMITTERS

Mykolas Vaitilas[1], Goda Grybauskaitė[1], Giedrius Puidokas[1], Gediminas Kreiza[1], Domantas Berenis[1], Kenkera Rayappa Naveen[2], Karolis Kazlauskas[1]

[1]Vilnius University, Institute of Photonics and Nanotechnology, Vilnius University, Sauletekio av. 3 LT-10257, Vilnius, Lithuania
[2]Indian Institute of Technology, Roorkee, Roorkee - Haridwar High Hwy, Roorkee 247667, Uttarakhand, India
mykolas.vaitilas@ff.stud.vu.lt

Multi-resonance thermally activated delayed fluorescent (MR-TADF) emitters are leading candidates for BT. 2020-standard-compatible blue organic light-emitting diodes (OLEDs) because they combine intrinsically narrow emission spectra and high PL quantum yields [1]. Recent advances in boron–oxygen π-conjugated donor–acceptor architectures exhibiting multi-resonant characteristics have enabled PL quantum yields approaching unity while maintaining full widths at half maximum below 30 nm [2]. However, in TADF-sensitized fluorescence (TSF or hyperfluorescence) architectures, limited reverse intersystem crossing (RISC) in the terminal MR-TADF emitters can promote triplet accumulation, accelerating triplet–triplet and triplet–polaron annihilation and contributing to efficiency roll-off and reduced operational stability, particularly under high-brightness operation [2]. RISC is a thermally activated spin-flip process that enables the up-conversion of long-lived non-emissive triplet excitons into emissive singlet states when a sufficiently small singlet–triplet energy splitting is achieved. Because the RISC rate directly governs triplet depopulation, efficient RISC is essential not only for maximizing exciton harvesting efficiency but also for suppressing triplet–driven loss and other degradation pathways, thereby improving device stability.

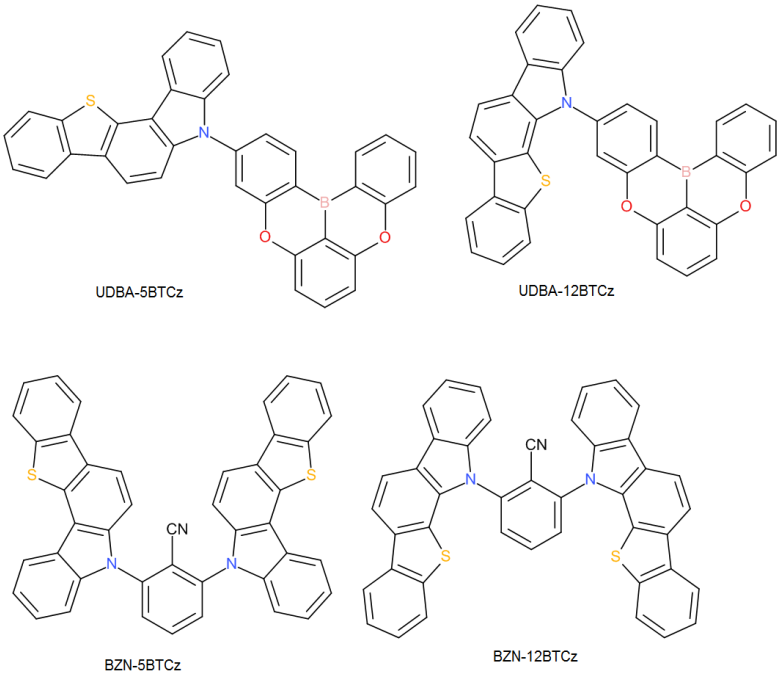


Fig. 1. Molecular structures of the studied materials.

In this work, a series of blue MR-TADF emitters (Fig. 1) was rationally designed to increase spin-orbit coupling via sulphur-containing structural motifs (internal heavy-atom/heteroatom effect) while preserving the rigid multi-resonant framework that underpins narrowband emission. To isolate the impact of this design element, these MR-TADF emitters were systematically compared with conventional TADF counterparts bearing the same sulphur functionality. Photophysical properties were comprehensively investigated in toluene solution and solid-state thin films using steady-state and time-resolved spectroscopic techniques. The newly developed emitters exhibit photophysical characteristics well-suited for application as terminal emitters in next-generation TSF devices.

[1] M. Liu, C. Li, L. Duan, and D. Zhang, “Recent advances in blue multiple-resonance thermally activated delayed fluorescence materials and their applications in organic light-emitting diodes,” Adv. Opt. Mater., vol. 14, no. 1, Art. no. e03140, 2026, doi: 10.1002/adom.202503140.
[2] D. Zhang, H. Dai, H. Zhang, and L. Duan, “Stable deep-blue organic light-emitting diodes based on sensitized fluorescence,” Nat. Photon., vol. 20, no. 2, pp. 136–150, 2026, doi: 10.1038/s41566-025-01810-1.

APPLICATION OF DIBENZOFURAN-BASED HOST MATERIALS FOR BLUE 3RD GENERATION THERMALLY ACTIVATED DELAYED FLUORESCENCE (TADF) ORGANIC LIGHT EMITTING DIODES

Goda Grybauskaitė[1], Kristupas Bagdonas[1], Domantas Berenis[1], Gediminas Kreiza[1], Edvinas Orentas[2], Eigirdas Skuodis[3], Karolis Kazlauskas[1], Dovydas Banevičius[1]

[1]Vilnius University, Faculty of Physics, Institute of Photonics and Nanotechnology, Vilnius, Lithuania
[2]Vilnius University, Faculty of Chemistry and Geosciences, Department of Organic Chemistry, Vilnius, Lithuania
[3]Kaunas University of Technology, Faculty of Chemical Technology, Department of Polymer Chemistry and Technology, Kaunas, Lithuania
goda.grybauskaite@ff.vu.lt

Over the past decade, intensive research has been carried out on organic light-emitting diodes (OLEDs) employing thermally activated delayed fluorescence (TADF) emitters, which enable achieving 100% internal quantum efficiency [1]. While green and red OLEDs used in industry exhibit excellent efficiency and operational stability, blue devices still suffer from unresolved stability issues [2]. One possible approach to improving the stability of blue emitters is the synthesis and incorporation of new host materials into the device structure. The emitter molecules are dispersed in a host matrix to suppress concentration quenching and enhance charge transport. Importantly, the triplet energy level of the host material must be higher than that of the emitter to prevent reverse energy transfer from the emitter back to the host [3–4].

The aim of this study was to evaluate the suitability of three newly synthesized dibenzofuran-based host materials—A0, A1, and A2—for the fabrication of efficient and stable blue TADF OLEDs. The triplet energy levels of the host materials were determined using absorption and photoluminescence measurements, while the optimal concentration of the emitter DMeCzIPN [5] was established based on photoluminescence quantum yield (PLQY) measurements. The OLED devices were fabricated by vacuum deposition and subsequently electrically and optically characterized.

It was found that the triplet energies of hosts A0 and A1 are similar to that of the emitter, while A2 possesses a higher triplet energy. The optimal emitter concentration in all hosts was 20%. The devices achieved a maximum EQE of 8.1% and an LT_{50} of 2.5h at ~1000 cd/m^2, likely limited by crystallization of the organic layers. At low voltages, a broad green emission was observed due to exciplex formation between DMeCzIPN and the adjacent Tris-PCz layer. Introducing a 10 nm mCBP interlayer suppressed exciplex formation, significantly improving efficiency to EQE = 27% and extending LT_{50} to 11h, while also reducing crystallization effects.

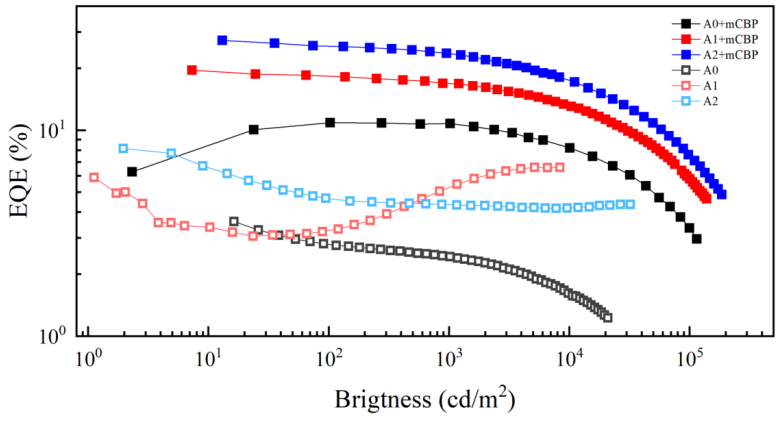


Fig. 1. External quantum efficiency curves as a function of brightness for OLEDs with A0, A1, and A2 host materials.

[1] H. Uoyama, K. Goushi, K. Shizu, H. Nomura, and C. Adachi, "Highly efficient organic light-emitting diodes from delayed fluorescence," Nature, vol. 492, no. 7428, pp. 234–238, Dec. 2012, doi: https://doi.org/10.1038/nature11687.
[2] D. Banevičius, G. Puidokas, G. Kreiza, S. Juršėnas, E. Orentas, and K. Kazlauskas, "Prolonging blue TADF-OLED lifetime through ytterbium doping of electron transport layer," Journal of Industrial and Engineering Chemistry, vol. 128, pp. 515–520, Aug. 2023, doi: https://doi.org/10.1016/j.jiec.2023.08.016.
[3] Eglė Tankelevičiūtė, Samuel, and E. Zysman-Colman, "The Blue Problem: OLED Stability and Degradation Mechanisms," The Journal of Physical Chemistry Letters, vol. 15, no. 4, pp. 1034–1047, Jan. 2024, doi: https://doi.org/10.1021/acs.jpclett.3c03317.
[4] M. Y. Wong and E. Zysman-Colman, "Purely Organic Thermally Activated Delayed Fluorescence Materials for Organic Light-Emitting Diodes," Advanced Materials, vol. 29, no. 22, p. 1605444, Mar. 2017, doi: https://doi.org/10.1002/adma.201605444.
[5] G. Kreiza et al., "High efficiency and extremely low roll-off solution- and vacuum-processed OLEDs based on isophthalonitrile blue TADF emitter," Chemical Engineering Journal, vol. 412, p. 128574, May 2021, doi: https://doi.org/10.1016/j.cej.2021.128574.

OPTIMIZATION OF MAGNETIC-FIELD QUANTUM SENSING WITH NV CENTERS

Vakaris Šilys[1], Julius Janušonis[1], Tadas Paulauskas[1]

[1]Center for Physical Sciences and Technology, Saulėtekio al. 3, 10257 Vilnius, Lithuania
vakaris.silys@ftmc.lt

Nitrogen-vacancy (NV) centers in diamond are a leading platform for room-temperature quantum sensing of magnetic fields, owing to their long spin coherence times and optical addressability [1,2]. In this work, we investigate how diamond crystal orientation and paramagnetic impurity concentration influence the coherence properties and magnetic sensing performance of NV centers. We present a comparative study of bulk diamond samples with different crystallographic orientations, specifically (111)- and (100)-oriented diamonds, as well as varying concentrations of substitutional nitrogen (P1 centers).

Using scanning confocal microscopy combined with optically detected magnetic resonance (ODMR) and pulsed microwave control, we characterize NV spin dynamics through Ramsey interferometry, Rabi oscillations, and longitudinal (T_1) and transverse (T_2) relaxation measurements. We analyse how crystal orientation affects NV axis alignment, ODMR contrast, and magnetic field sensitivity, while P1 center concentration is shown to play a critical role in spin decoherence and relaxation behaviour [2].

Our results demonstrate clear orientation- and impurity-dependent differences in coherence times and sensing performance, highlighting trade-offs between signal strength, spin bath interactions, and achievable sensitivity. These findings provide practical guidance for optimizing diamond material selection for DC and AC magnetic field sensing applications [1].

[1] C. L. Degen, F. Reinhard, and P. Cappellaro, “Quantum sensing,” Rev. Mod. Phys., vol. 89, art. no. 035002, Jul. 2017.
[2] M. W. Doherty et al., “The nitrogen-vacancy colour centre in diamond,” Phys. Rep., vol. 528, pp. 1–45, 2013.

DETERMINATION OF THE PROBABILITY OF SINGLET EXCITON FORMATION DURING TRIPLET-TRIPLET ANNIHILATION IN MODEL PHOTON UPCONVERSION COMPOUNDS

Manvydas Dapkevičius[1], Džiugas Krencius[1], Steponas Raišys[1], Justas Lekavičius[1], Karolis Kazlauskas[1]

[1]Lithuania, Vilnius University, Faculty of Physics, Institute of Photonics and Nanotechnology
manvydas.dapkevicius@ff.stud.vu.lt

Triplet-Triplet Annihilation (TTA) is a process where two low-energy triplet excitons combine to generate one high-energy singlet exciton. This mechanism holds significant potential for enhancing solar cell efficiency, deep-tissue phototherapy, 3D printing, and climate change mitigation [1-3]. An effective TTA system typically requires precise energy level alignment between two components: a long-wavelength absorbing sensitizer and a short wavelength emitter. Despite growing interest, existing literature frequently reports inconsistent photophysical parameters for identical TTA materials. These discrepancies come from varied measurement techniques and calculation methods, they hinder direct comparisons and experimental reproducibility. To address this, a systematic study of the most widely used TTA molecules was performed. By utilizing a single laboratory environment, uniform equipment, and standardized calculation protocols, a reliable and comparable dataset is provided.

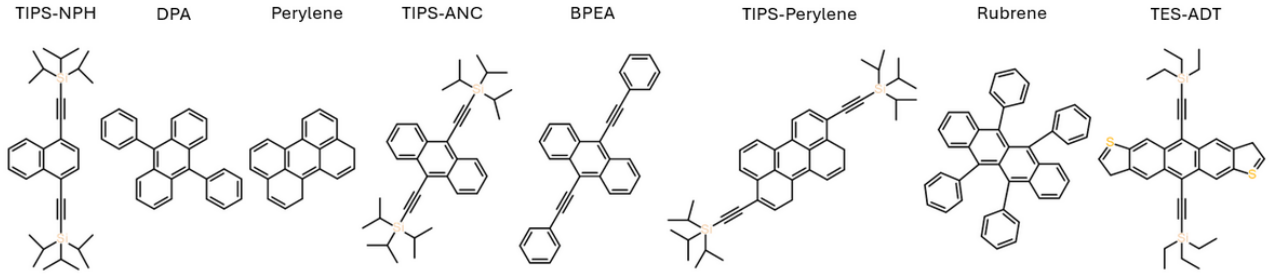


Fig. 1. Model triplet annihilators used in this work

The overall photon upconversion quantum yield, ϕ_{UC}, can be expressed as the product of several contributing processes:

$$\phi_{UC} = \frac{1}{2} f \phi_{ISC} \phi_{TET} \phi_{TTA} \phi_{FL} \tag{1}$$

In this expression, ϕ_{ISC} denotes the intersystem crossing efficiency of the sensitizer, ϕ_{TET} represents the efficiency of triplet energy transfer from the sensitizer to the emitter, ϕ_{TTA} is the efficiency of the triplet–triplet annihilation process, and ϕ_{FL} corresponds to the fluorescence quantum yield of the emitter. The factor f accounts for the spin statistical probability of singlet state formation. Deviations from literature values are primarily attributed to differences in the methodologies used to determine fluorescence and upconversion quantum yields, with relative actinometry generally being less reliable than absolute measurements performed using an integrating sphere.

[1] K. J. Ramírez-Escárcega, K. J. Amaya-Galván, J. C. García-Prieto, F. de J. Silerio-Vázquez, and J. B. Proal-Nájera, “Advancing photocatalytic strategies for microplastic degradation in aquatic systems: Insights into key challenges and future pathways,” Journal of Environmental Chemical Engineering, vol. 13, no. 2, p. 115594, Jan. 2025. Available: https://doi.org/10.1016/j.jece.2025.115594 . [Accessed February 2, 2026].

[2] S. N. Sanders et al., “Triplet fusion upconversion nanocapsules for volumetric 3D printing,” Nature, vol. 604, no. 7906, pp. 474–478, Apr. 2022. Available: https://doi.org/10.1038/s41586-022-04485-8 . [Accessed February 2, 2026].

[3] M. Klimezak et al., “Triplet-Triplet Annihilation Upconversion-Based Photolysis: Applications in Photopharmacology,” Advanced Healthcare Materials, vol. 13, no. 19, Apr. 2024. Available: https://doi.org/10.1002/adhm.202400354 . [Accessed February 2, 2026].

ENHANCING RISC IN NARROWBAND BLUE MR-TADF EMITTERS

Giedrius Puidokas[1], Lukas Deltuvytis[1], Gediminas Kreiza[1], Karolis Kazlauskas[1]

[1]Vilnius University, Faculty of Physics, Institute of Photonics and Nanotechnology, Lithuania
giedrius.puidokas@ff.vu.lt

OLEDs are widely used in displays due to their high contrast, wide viewing angles, and compatibility with flexible substrates. However, the development of efficient, long-lived blue OLEDs remains a critical bottleneck. Device degradation is closely linked to long-lived triplet excitons and their interactions (e.g., triplet–triplet and triplet–polaron annihilation), which can generate high energy excited states that may induce molecular decomposition [1].

This work examines structural modifications of two multi-resonant thermally activated delayed fluorescence (MR-TADF) emitters, DABNA [2] and v-DABNA [3] (Fig. 1). The derivatives are designed to balance high photoluminescence quantum yield (PLQY), efficient triplet harvesting via reverse intersystem crossing (RISC), and high color purity. Absorption and emission spectra, PLQY, and time-resolved photoluminescence are characterized in solution and thin films. Selected derivatives reach PLQY >80% and RISC rates up to 10^6 s^{-1} while maintaining narrowband emission (FWHM ≤20 nm).

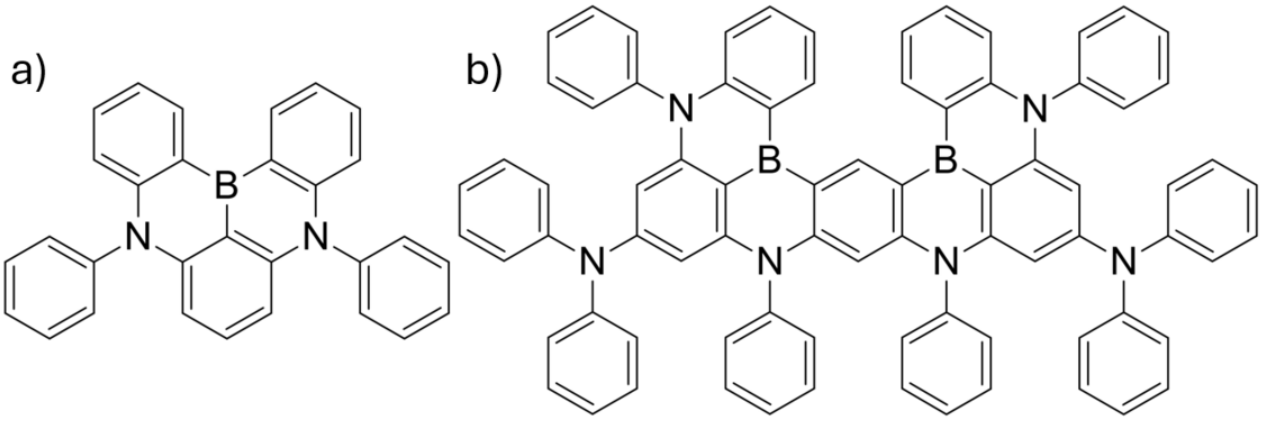


Fig. 1. (a) DABNA and (b) v-DABNA

Across the series, structural variations are assessed for their impact on emission spectrum, PLQY, and excited state dynamics, with π-extension, in particular, associated with narrower, red-shifted emission and enhanced RISC. At the same time, increased π-extension can exacerbate aggregation and concentration quenching in solid films, which are common challenges for MR-TADF emitters [1]. As a next step, selected derivatives could be used either as standalone emitters or as sensitizers in hyperfluorescent OLED architectures.

[1] X. Wu et al., "Comprehensive Review on the Structural Diversity and Versatility of Multi-Resonance Fluorescence Emitters: Advance, Challenges, and Prospects toward OLEDs," Chemical Reviews, vol. 125, no. 14, pp. 6685–6752, May 2025, doi: 10.1021/acs.chemrev.5c00021.
[2] T. Hatakeyama et al., "Ultrapure blue thermally activated delayed fluorescence molecules: efficient HOMO–LUMO separation by the multiple resonance effect," Advanced Materials, vol. 28, no. 14, pp. 2777–2781, Feb. 2016, doi: 10.1002/adma.201505491.
[3] Y. Kondo et al., "Narrowband deep-blue organic light-emitting diode featuring an organoboron-based emitter," Nature Photonics, vol. 13, no. 10, pp. 678–682, Jul. 2019, doi: 10.1038/s41566-019-0476-5.

INVESTIGATION OF THE DEPENDENCE OF PHOTOLUMINESCENCEPROPERTIES ON MAGNESIUM CONCENTRATION IN LuAG: CeSCINTILLATORS

Mikas Iršėnas[1], Augustas Vaitkevičius[1], Arnoldas Solovjovas[1], Saulius Nargelas[1]

[1]Vilnius University, Faculty of Physics, Institute of Photonics and Nanotechnology, Vilnius, Lithuania
mikas.irsenas@ff.stud.vu.lt

Cerium-doped aluminum garnet scintillators exhibit high light yield and strong resistance to ionizing radiation. They are used in high-energy particle physics experiments, medical diagnostics, and radiation safety applications [1]. However, these crystals are prone to the formation of antisite-type defects, which degrade the scintillation timing characteristics that are critical for their application in detector systems. One approach to addressing this issue is the growth of scintillating layer using the liquid-phase epitaxy (LPE) method, which, due to the lower processing temperatures, reduces the probability of defect formation [2]. Another approach is co-doping with Mg^{2+} ions, which introduce fast recombination pathways at the expense of reduced light yield [3].

The aim of this study is to measure and evaluate PLE grown LuAG: Ce photoluminescence parameters dependence on increasing magnesium concentration.

In this study, seven samples with magnesium concentrations ranging from 0 to 6000 ppm relative to lutetium were investigated. Spatial distributions of surface photoluminescence parameters were measured using a confocal scanning microscope, absorption spectra were recorded with a UV–VIS spectrophotometer, and the photoluminescence decay times of the Ce^{3+} $5d_1$ level were measured using a streak camera with femtosecond laser excitation.

The obtained results indicate that increasing magnesium concentration leads to enhanced absorption in the UV spectral region, reduction of Ce^{3+} $5d_1$ and $5d_2$ absorption peaks and a shortening of the photoluminescence decay time from 57 to 0.8 ns, when magnesium concentration increases from 0 to 6000 ppm. These effects are attributed to the stabilization of cerium ions in the tetravalent state due to the influence of Mg^{2+} on charge compensation within the crystal lattice. Ce^{4+} ions more effectively compete with electron trapping centers for conduction-band electrons, resulting in faster scintillation decay. However, this also introduces nonradiative recombination pathways that reduce the light yield [3]. In addition, a decrease in both the density and size of hexagonal and triangular surface defects in the epitaxial layer was observed with increasing magnesium concentration. Defect size decreased from 2338 μm^2 at 0 ppm magnesium to 314 μm^2 at 6000 ppm magnesium. This size reduction may be influenced by changes in ionic radii within the dodecahedral sublattice [4].

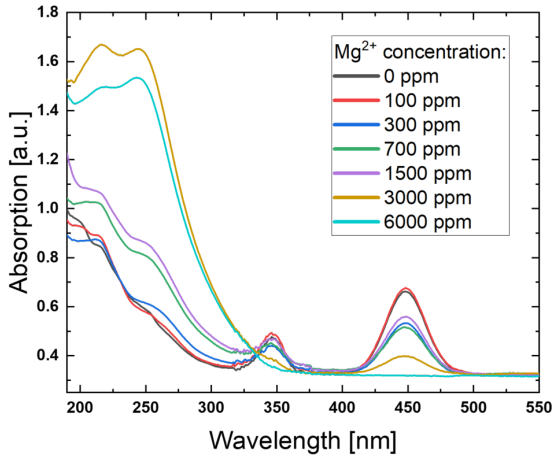


Fig. 1. LuAG: Ce, Mg absorption spectrum

[1] X. Chen, Z. Hu, M. Cao, et al., Influence of cerium doping concentration on the optical properties of Ce,Mg:LuAG scintillation ceramics, Journal of the European Ceramic Society, 2018, 38, 3246–3254
[2] E. Kuphal, Liquid phase epitaxy, Applied Physics A, 1991, 52, 380–409.
[3] M. Lucchini, O. Buganov, E. Auffray, et al., Measurement of non-equilibrium carriers dynamics in Ce-doped YAG, LuAG and GAGG crystals with and without Mg-codoping, Journal of Luminescence, 2018, 194, 1–7.
[4] D. Lu, Q. Jiang, X. Ma, Q. Zhang, X. Fu, and L. Fan, Defect-related etch pits on crystals and their utilization, Crystals, 2022, 12.

DESIGN OF NOVEL 3-(DIPHENYLAMINO)CARBAZOLE COMPOUNDS FOR MULTI-CHANNEL GREEN TADF OLEDs

Raminta Beresneviciute[1], Inesa Sasnauskaite[1], Zeyad Taher Abdou[1], Dovydas Blazevicius[1], Saulius Grigalevicius[1], Wanting Ju[2], Xiangqin Gan[2], Junqiao Ding[2], Kaspars Traskovskis[3]

[1]Kaunas University of Technology, Department of Polymer Chemistry and Technology, Kaunas, Lithuania
[2]Yuann University, School of Chemical Science and Technology, Kunming, P. R. China
[3]Riga Technical University, Faculty of Natural Sciences and Technology, Riga, Latvia
raminta.beresneviciute@ktu.lt

High-performance TADF emitters are currently in great demand for applications in full-color displays and solid-state lighting. These materials can reach up to 100% internal quantum efficiency without relying on noble metals. However, overall eficiency is still limited by slow and inefficient reverse intersystem crossing (RISC) processes [1]. Herein, we introduce a series of 3-(dephenylamino)carbazole-based compounds with a potential of multi-channel RISC. The structures of materials are shown in Fig. 1.

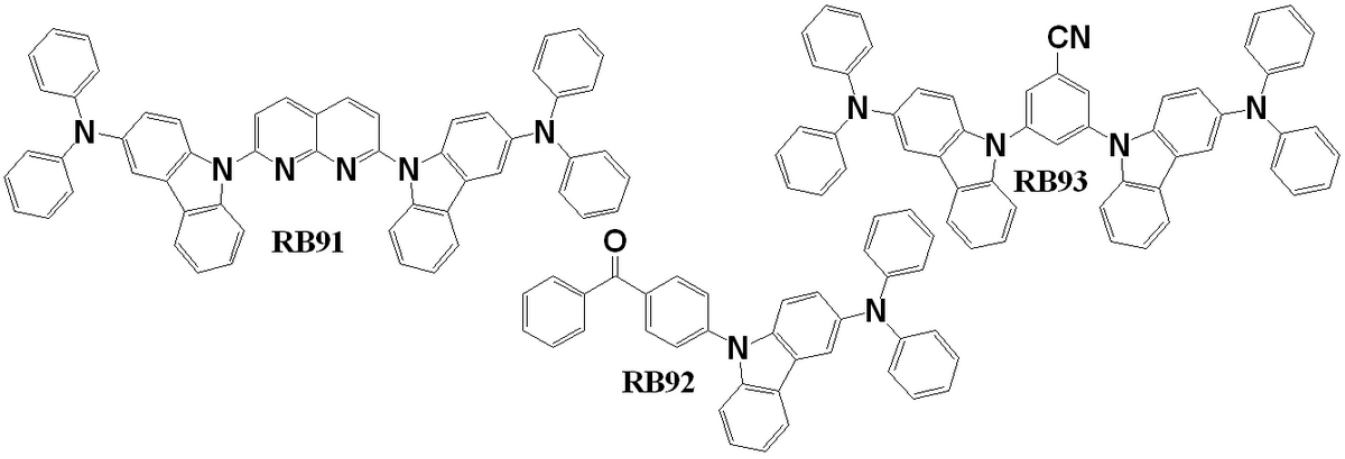


Fig. 1. Chemical structures of 3-(diphenylamino)carbazole-based derivatives

New compounds RB91, RB92, and RB93 were synthesized via Ullmann coupling and nucleophilic aromatic substitution. Their structures were confirmed by MS and NMR, and they showed excellent thermal stability (T_d > 350 °C) and good film-forming ability (T_g=90–145 °C). All compounds exhibited green photoluminescence (optical gaps: 2.66–3.10 eV) and TADF with microsecond-range delayed lifetimes. Theoretical studies supported the experimental findings. Twelve OLEDs were fabricated using these emitters. RB91 emerged as the top performer, achieving a peak EQE of 12.87%, and highest current/power efficiencies (37.24 cd/A, 41.34 lm/W). This performance stems from RB91's small ΔE_{ST} (0.14 eV) and optimized excited-state properties, enabling efficient RISC and low efficiency roll-off at high brightness.

Acknowledgements

We are obliged to the Research Council of Lithuania for the support (Grant. No. S-LLT-25-2). KT acknowledges the financial support of the Latvian Council of Science (project LV-LT-TW/2025/4).

[1] K. Kumar, "High-Efficiency Functional Materials: Challenges and developments in solution and dry processed green OLEDs," Reaction Chemistry & Engineering, vol. 9, no. 3, pp. 496–527, Jan. 2024, doi: 10.1039/d3re00410d.

STRUCTURE-PROPERTY RELATIONSHIPS IN ANTHRACENE ANNIHILATORS FOR TRIPLET-TRIPLET ANNIHILATION PHOTON UPCONVERSION

Džiugas Krencius[1], Justas Lekavičius[1], Manvydas Dapkevičius[1], Steponas Raišys[1], Edvinas Orentas[2], Karolis Kazlauskas[1]

[1]Vilnius University, Faculty of Physics, Institute of Photonics and Nanotechnology, Lithuania
[2]Vilnius University, Faculty of Chemistry and Geosciences, Institute of Chemistry, Lithuania
dziugas.krencius@vu.ff.lt

Triplet–triplet annihilation photon upconversion (TTA-UC) enables conversion of two low-energy photons into one higher-energy photon using a sensitizer/annihilator pair, offering routes to improved photocatalysis [1], bio-optical applications [2], and solar utilization [3].

Anthracene derivatives are among the most widely investigated TTA-UC annihilators, yet predictive design rules connecting substitution patterns to UC efficiency remain incomplete. This study aims to investigate how systematic structural modifications of anthracene annihilators (Fig. 1) affect the photophysical properties governing TTA-UC. A commonly used PtOEP was selected as the triplet sensitizer, with its relatively high triplet energy (1.94 eV), while explicitly accounting for sensitizer-related losses such as reabsorption/inner-filter effects. Steady-state spectroscopy and time-resolved upconversion/phosphorescence measurements reveal that increasing linker rigidity from a vinyl (C=C) to an ethynyl (C≡C) motif sharpens vibronic structure and narrows emission spectra, consistent with reduced conformational disorder. This substantially increases UC quantum yield from 3.9% for bTPhS(DB)-Anc to 15.6% for bTPhS(TB)-Anc. In general, symmetric 9,10-disubstituted anthracenes show higher fluorescence quantum yields and larger spin-statistical factors f (≥ 0.40), supporting reduced non-radiative losses and more productive triplet-pair pathways.

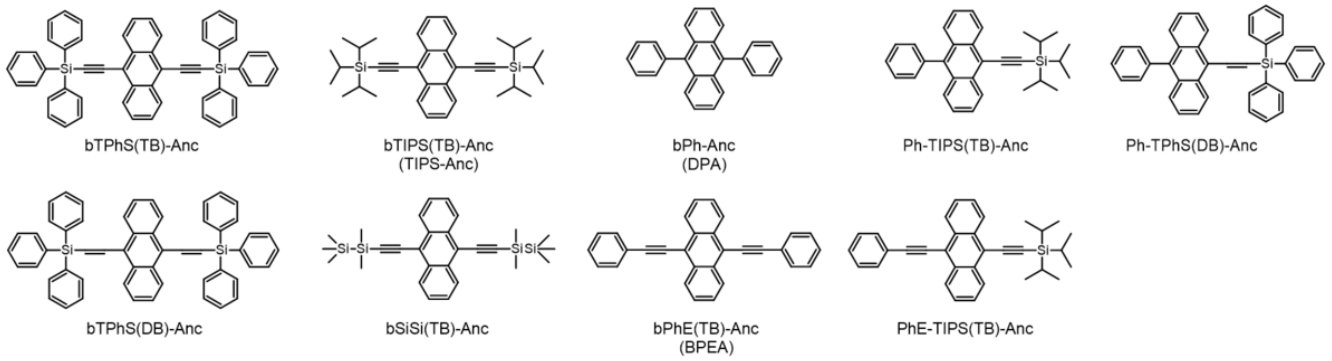


Fig. 1. Molecular structures of anthracene compounds.

These findings demonstrate that modest structural changes have a strong influence on TTA-UC performance, enabling rational design of annihilators beyond trial-and-error screening.

[1] S.-Y. Hwang, D. Song, E.-J. Seo, F. Hollmann, Y. You, and J.-B. Park, "Triplet–triplet annihilation-based photon-upconversion to broaden the wavelength spectrum for photobiocatalysis," Scientific Reports, vol. 12, no. 1, p. 9397, Jun. 2022, doi: 10.1038/s41598-022-13406-8.
[2] Y. Sasaki et al., "Near-Infrared Optogenetic Genome Engineering Based on Photon-Upconversion Hydrogels," Angewandte Chemie, vol. 131, no. 49, pp. 17991–17997, doi: 10.1002/ange.201911025.
[3] L. Naimovičius, P. Bharmoria, and K. Moth-Poulsen, "Triplet–triplet annihilation mediated photon upconversion solar energy systems," Materials Chemistry Frontiers, vol. 7, no. 12, pp. 2297–2315, Jan. 2023, doi: 10.1039/d3qm00069a.

PHOTOPHYSICAL STUDY OF POLYCYCLIC AROMATIC COMPOUNDS

Tautvydas Kairys[1], Kamilė Boguševičienė[1], Kasper Moth-Poulsen[2], Paulius Baronas[1], Saulius Juršėnas[1]

[1]Vilnius University, Faculty of Physics, Institute of Photonics and Nanotechnology, Lithuania
[2]Polytechnic University of Catalunya, Institute of Materials Science of Barcelona, Spain
tautvydas.kairys@ff.stud.vu.lt

Polycyclic aromatic compounds are widely studied for photonic and optoelectronic applications because their optical properties strongly depend on their environment. In particular, molecular photoswitches are of significant interest due to their ability to undergo reversible structural changes upon light irradiation. Light-induced isomerization can modify their electronic structure and, consequently, their optical and photophysical properties, enabling potential applications in smart materials and light-controlled devices. Understanding how solvent polarity and solid-state embedding affect such systems is therefore important for the design and usage of future functional materials [1].

The aim of this work was to investigate the photophysical properties of two compounds, NB18 and NB38, in toluene, acetonitrile and a PMMA matrix.

Absorption, fluorescence spectra, quantum yields (QY), fluorescence lifetimes, and femtosecond pump–probe measurements were performed. The main absorption maximum for both compounds was observed near 370 nm (Fig. 1). The results show a clear influence of solvent polarity on the optical properties of both compounds. Changing from polar acetonitrile to less polar toluene led to a significant increase in fluorescence efficiency and lifetime. For example, NB18 exhibited a quantum yield of only 0.13% in acetonitrile, which increased to 5.49% in toluene, while its lifetime increased from 59 ps to 283 ps. Similar trends were observed for NB38, where the compound exhibited moderate QY in both solutions (about 0.3%) and its lifetime increasing from 401 ps in acetonitrile to 591 ps in toluene. NB18 showed a moderate quantum yield in PMMA of (4.97%), while NB38 exhibited a significantly higher value in PMMA (40.67%). Such differences between the solvents and the polymer are drastically different because a more rigid environment does not allow them to rotate freely and thus restricts their motion. Fluorescence lifetimes were shortest in acetonitrile and increased in toluene and PMMA, reaching up to 1173 ps for NB38 in the polymer matrix. Pump–probe experiments showed weak transient signals, especially for NB38, while NB18 displayed clearer early-time dynamics indicating a signal for specific time-frames showing that it reaches an excited state.

These results demonstrate that solvent polarity and matrix immobilization strongly influence the optical efficiency and excited-state behavior of both materials.

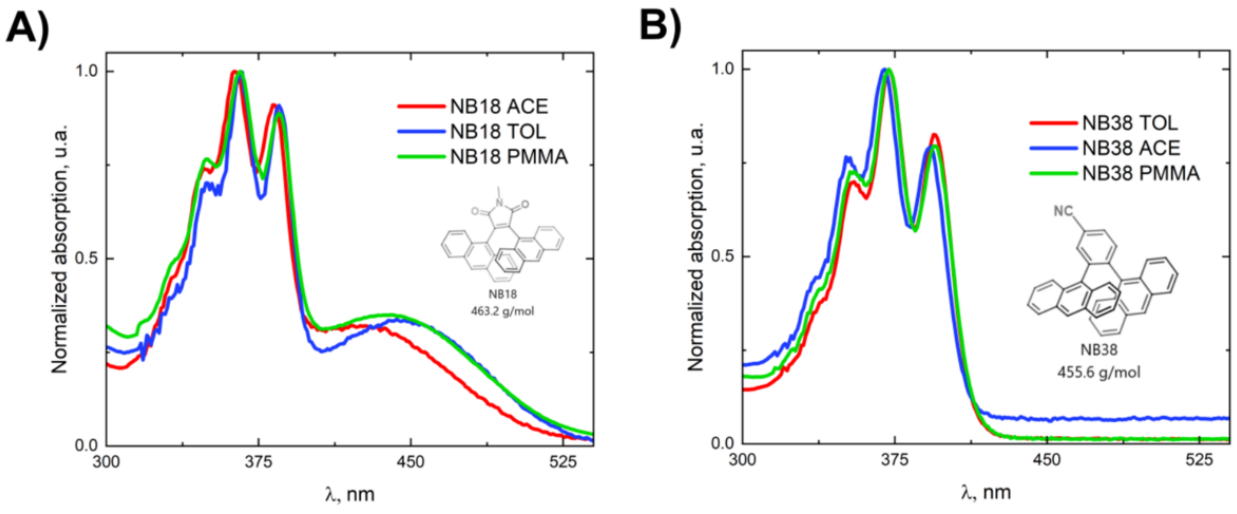


Fig. 1. A) Maximum absorption of the compound NB18, where the concentration is 10^{-5} mol L^{-1} in acetonitrile and toluene, and 10^{-2} mol L^{-1} in poly(methyl methacrylate), B) Maximum absorption of the compound NB38, whereas the concentrations are the same as for NB18.

[1] T. Nishiuchi, H. Sotome, K. Shimizu, H. Miyasaka and T. Kubo, "1,2,3-Tri(9-anthryl)benzene: Photophysical Properties and Solid-State Intermolecular Interactions of Radially Arranged, Congested Aromatic π-Planes," *Chemistry – A European Journal*, vol. 28, no. 5, p. e202104245, 2022, doi: 10.1002/chem.202104245.

CRYSTALLINE GETE THIN FILMS FOR INFRARED PHOTODETECTION

Pijus Kuliavas[1,2], Marius Franckevičius[1], Vidas Pakštas[1], Rokas Kondrotas[1], Audrius Drabavičius[1]

[1]Lithuania, Center for Physical Sciences and Technology, Saulėtekio av. 3, 10257 Vilnius.
[2]Lithuania, Vilnius University, Departament of Inorganic Chemistry, Naugarduko st. 24, 03225 Vilnius.
pijus.kuliavas@ftmc.lt

Rapid advances in optoelectronic technologies are driving the demand for infrared (IR) photodetectors capable of room-temperature operation while avoiding highly toxic materials and complex cooling requirements. State-of-the-art IR detector technologies based on HgCdTe and InSb remain limited by high cost, material toxicity, and the need for cryogenic operation [1], motivating the exploration of alternative semiconductor platforms. Germanium telluride (GeTe) is a promising candidate owing to its narrow bandgap (0.6 eV), high infrared absorption coefficient, and strong light–matter interaction, which are favorable for thin-film IR photodetection [2]. In addition to its well-known phase-change behavior, crystalline GeTe exhibits optical and electronic properties [3,4] that, combined with its chemical stability and compatibility with standard semiconductor processing, make it an attractive material for infrared optoelectronic applications.

In this work, the focus is placed on establishing and comparing fabrication strategies for crystalline GeTe thin films with controlled stoichiometry and structural quality, as a prerequisite for future device development. Two complementary deposition approaches are explored: rapid thermal evaporation from pre-synthesized GeTe sources and reactive diffusion based on vacuum-deposited Ge/Te multilayer stacks followed by thermal treatment. The resulting thin films are examined using X-ray diffraction, scanning electron microscopy, X-ray photoelectron spectroscopy, and Raman spectroscopy to assess phase formation, compositional uniformity, and microstructural evolution.

By systematically investigating the influence of deposition route and post-deposition processing on film structure and composition, this study aims to clarify process–structure relationships in crystalline GeTe thin films. The outcomes are expected to provide guidance for optimizing GeTe thin-film growth toward infrared optoelectronic applications and to support the longer-term development of room-temperature IR photodetectors based on non-toxic and scalable material systems.

[1] T. Luo et al., “Dual ligands-assisted oxidation strategy for suppressing dark current in PbS quantum dot infrared photodetectors,” Journal of Alloys and Compounds, vol. 1053, p. 186232, Feb. 2026, doi: https://doi.org/10.1016/j.jallcom.2026.186232. Available: Sciencedirect, https://www.sciencedirect.com/science/article/abs/pii/S0925838826003002 [Accessed: February 25, 2026]

[2] Y. Zhao et al., “Infrared photodetector based on GeTe nanofilms with high performance,” Optics Letters, vol. 45, no. 5, p. 1108, Feb. 2020, doi: https://doi.org/10.1364/ol.385280. Available: Optics letters, https://opg.optica.org/ol/viewmedia.cfm?uri=ol-45-5-1108&seq=0 [Accessed: February 25, 2026]

[3] G. Bruns et al., “Nanosecond switching in GeTe phase change memory cells,” Applied Physics Letters, vol. 95, no. 4, p. 043108, Jul. 2009, doi: https://doi.org/10.1063/1.3191670. Available: Applied Physics Letters, https://pubs.aip.org/aip/apl/article-abstract/95/4/043108/897618/Nanosecond-switching-in-GeTe-phase-change-memory?redirectedFrom=fulltext [Accessed: February 25, 2026]

[4] Nabil El-Hinnawy et al., “A Four-Terminal, Inline, Chalcogenide Phase-Change RF Switch Using an Independent Resistive Heater for Thermal Actuation,” IEEE Electron Device Letters, vol. 34, no. 10, pp. 1313–1315, Oct. 2013, doi: https://doi.org/10.1109/led.2013.2278816. Available: IEEE Electron Device Letters, https://ieeexplore.ieee.org/document/6587467 [Accessed: February 25, 2026]

SYNTHESIS AND INVESTIGATION OF PHENOTHIAZINE ORGANICSEMICONDUCTORS

Skirmantas Musteikis[1], Mantas Marčinskas[1], Tadas Malinauskas[1]

[1]Kaunas University of Technology, Faculty of Chemical Technology, Department of Organic Chemistry, Lithuania
skirmantas.musteikis@ktu.lt

As solar energy continues to receive increasing attention and investment, scientists are trying to develop better alternatives to the currently most widely used silicon solar cells. The production and energy costs of silicon solar cells are high, so there is a need for a new, more economical technology whose manufacturing would be cheaper, simpler, and more environmentally friendly. One of the most promising candidates is perovskite solar cells. They can be produced at lower cost using simpler fabrication methods, while the final product exhibits a similar power conversion efficiency (PCE).

For perovskite solar cells to operate efficiently, it is necessary to have layers that separate the positive and negative charge carriers generated in the perovskite light absorber. Materials that transport positive charges are called hole-transporting materials (HTMs), and they usually limit the efficiency of solar cells [1]. Currently, some of the most promising HTMs are those capable of forming a self-assembled monolayer (SAM). Solar cells employing SAM-based hole-transporting materials typically show high efficiency, low HTM consumption, and this architecture is suitable for the fabrication of tandem photovoltaic panels.

At present, lead-based perovskite technology is the most developed. This is because the use of lead results in the highest performance and stability. These solar cells are easy to fabricate and test, which is why this perovskite composition has received the most time and research attention. Although this technology is quite advanced, one major problem is immediately apparent – lead. Over time, during the use of these solar cells, a small amount of lead can leach into soil or drinking water, which would cause harm not only to the environment but also to humans.

In order to solve this problem, tin-based perovskite technology is being developed. Although this technology is relatively young and the solar cells currently achieve only about 16% PCE compared to 27% PCE for lead-based perovskites [2], the use of tin perovskites avoids lead entirely. To optimize tin-based solar cells, it is not sufficient to simply use existing hole-transporting materials, because their energy levels, geometry, and functional groups are tailored for lead-based perovskites.

Therefore, in order to enable broader and more efficient application of tin perovskites, it is important to synthesize new compounds that are compatible with the physical and chemical properties of this perovskite. In this project, a new phenothiazine compounds were synthesized, which not only could form SAM but also has additional functional groups for interaction with tin-based perovskite. With this technology, it can be expected to not only achieve higher efficiency, but also increased stability of said solar cells.

[1] [1] S. Liu, V. P. Biju, Y. Qi, W. Chen, and Z. Liu, “Recent progress in the development of high-efficiency inverted perovskite solar cells,” NPG Asia Materials, vol. 15, no. 1, May 2023, doi: 10.1038/s41427-023-00474-z.

[2] [2] Z. Xiong et al., “Homogenized chlorine distribution for >27% power conversion efficiency in perovskite solar cells,” Science, vol. 390, no. 6773, pp. 638–642, Nov. 2025, doi: 10.1126/science.adw8780.

TEMPERATURE-DRIVEN CROSSOVER OF CHARGE SEPARATION MECHANISMS IN NON-FULLERENE ORGANIC SOLAR CELL BLENDS

Rokas Jasiūnas[1], Nakul Jain[2], Titas Klepeckas[1], Andrius Gelžinis[1,3], Vidmantas Gulbinas[1]

[1]Center for Physical Sciences and Technology, Department of Molecular Compound Physics, Lithuania
[2]Linköping University, Department of Physics Chemistry and Biology (IFM), Sweden
[3]Vilnius University, Faculty of Physics, Institute of Chemical Physics, Lithuania
titas.klepeckas@ftmc.lt

Charge separation in non-fullerene organic solar cells (OSCs) is widely regarded as a central yet unresolved process, with ongoing debate over whether it is primaraly governed by thermally activated processes to overcome Coulombic binding or proceeds via a barrier-free, coherence-driven mechanisms. Resolving this question is essential for optimizing charge generation efficiency, suppressing recombination losses, and improving overall device performance. In this study, a temperature-dependent investigation of charge separation dynamics is presented for the three donor–acceptor blends exhibiting different highest occupied molecular orbital (HOMO) level offsets. Ultrafast transient absorption spectroscopy, combined with multivariate curve resolution analysis, was employed over a broad temperature range (50–350 K) to directly monitor the formation of charge-transfer and spatially separated charge states.

Accelerated charge separation was observed at lower temperatures for all investigated blends, contrary to expectations for thermally activated processes. At cryogenic temperatures, an ultrafast separation channel was found to dominate, whereas at elevated temperatures this this channel was progressively suppressed and replaced by slower, thermally activated charge separation, occurring on hundreds-of-picoseconds timescales. The enhanced low-temperature behavior in this work is attributed to reduced thermal disorder, by which electronic coherence and charge delocalization are preserved, enabling rapid escape from Coulombic attraction prior to charge localization.

These findings provide direct experimental evidence for non-relaxed, coherence-assisted charge separation in non-fullerene OSCs and reveal a temperature-driven crossover between coherent and thermally activated pathways. In doing so, previously conflicting models of charge separation are reconciled, offering new design principles for high-efficiency organic photovoltaic materials and devices.

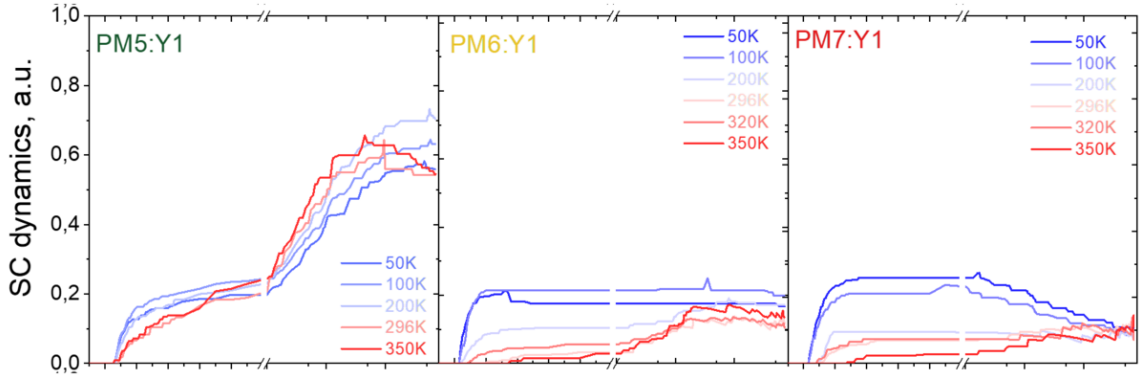


Fig. 1. Figure 1. Modeled temperature-dependent dynamics of separated charge (SC) state for PM5:Y1, PM6:Y1, and PM7:Y1 blends.

SUB-NANOSECOND PULSE PARAMETRIC AMPLIFICATION SYSTEM IN THE VISIBLE SPECTRUM RANGE

Ieva Baltrukonytė[1], Jonas Banys[1], Julius Vengelis[1]

[1]Vilnius University, Faculty of Physics, Laser Research Center, Lithuania
ieva.baltrukonyte@ff.vu.lt

Optical parametric systems pumped by Q-switched microlasers operating at kHz repetition rates enable the generation of μJ–mJ level pulses and are characterized by structural simplicity, low cost, high peak power, and stable performance [1]. In recent years, sub-nanosecond parametric systems based on periodically poled crystals with quasi-phase-matching (QPM) structures, such as multi-grating or fan-out geometries, have been demonstrated [2]. These systems are being actively developed due to their potential for applications requiring widely tunable sources in both the infrared and visible spectral regions.

However, the realization of parametric systems in the visible spectral range remains more challenging due to lower laser-induced damage thresholds, limited capabilities of QPM structures, and secondary effects in periodically poled crystals, such as linear and nonlinear absorption and noncollinear interactions [3]. Consequently, tunable OPA sub-nanosecond systems operating in the visible spectral range remain insufficiently studied.

In this work, we present, to the best of our knowledge, the first subnanosecond OPA system efficiently tunable in the visible spectrum range. An optical parametric generation (OPG) signal is first generated by pumping a periodically poled lithium niobate (PPLN) crystal with a second harmonic radiation. By combining crystal temperature tuning with multiple grating periods, continuous tunability of the OPG signal is achieved over the 670-2200 nm spectral range. Consequently, this OPG signal is later employed as a seed in OPA stage, based on lithium triborate (LBO) crystal pumped by third harmonic radiation. As a result, tunable μJ pulse energy output radiation in the visible spectral range from 420 to 710 nm was achieved, with a conversion efficiency ranging from 10% to 30%.

[1] J. J. Zayhowski, “Passively Q-switched Nd:YAG microchip lasers and applications,” Journal of Alloys and Compounds, vol. 303–304, pp. 393–400, May 2000, doi: 10.1016/s0925-8388(00)00647-2.

[2] J. Banys, S. Armalytė, J. Pimpė, O. Balachninaitė, V. Jarutis, and J. Vengelis, “Subnanosecond microlaser pumped fan-out grating design MgO:PPLN optical parametric generator continuously tunable from near- to mid-infrared,” Optics & Laser Technology, vol. 171, p. 110433, Dec. 2023, doi: 10.1016/j.optlastec.2023.110433.

[3] M. Simon, S. Wevering, K. Buse, and E. Krätzig, “The bulk photovoltaic effect of photorefractive $LiNbO_3$:Fe crystals at high light intensities,” Journal of Physics D: Applied Physics, vol. 30, no. 1, pp. 18–24, Jan. 1997, doi: 10.1088/0022-3727/30/1/004.

TOWARDS FDML-ENABLED FLOW-TROUGH QUANTITATIVE PHASE IMAGING

Laurynas Puškorius[1], Jonas Jurkevičius[2]

[1]Vilnius University, Faculty of Physics, Institute of Photonics and Nanotechnology, Lithuania
laurynas.puskorius@ff.stud.vu.lt

Recent advances in ultrafast two-photon imaging enable kHz-rate imaging of particles and cells in flow mode [1]. However, such high-throughput operation introduces a practical limitation: a large fraction of imaged objects may be irrelevant or unwanted, leading to inefficient use of imaging bandwidth and data processing resources. A lower-bandwidth imaging modality that would allow for label-free, phase-based discrimination of objects could provide an attractive solution for tandem operation, where only the objects meeting predefined selection criteria are directed to a high-speed two-photon imaging region and trigger data acquisition.

Multiplexed asymmetric-detection time-stretch optical microscopy (multi-ATOM) has been shown to provide such capability using a spectrally encoded line scan [2], a similarity shared with Spectrotemporal laser imaging by diffracted excitation (SLIDE) [3]. Instead of using time-stretch, we employ a Fourier-domain mode-locked (FDML) laser [4], as used in SLIDE, to realize spectro-temporal scanning. We report on an investigation into the applicability of FDML-laser-based spectro-temporal scanning for a multi-ATOM based flow-through quantitative phase imaging system.

[1] S. Karpf et al., “Harmonic imaging of stem cells in whole blood at GHz pixel rate,” Small, vol. 20, no. 40, p. e2401472, Jun. 2024, doi: 10.1002/smll.202401472.

[2] K. C. M. Lee et al., “Multi-ATOM: Ultrahigh-throughput single-cell quantitative phase imaging with subcellular resolution,” Journal of Biophotonics, vol. 12, no. 7, p. e201800479, Feb. 2019, doi: 10.1002/jbio.201800479.

[3] S. Karpf et al., “Spectro-temporal encoded multiphoton microscopy and fluorescence lifetime imaging at kilohertz frame-rates,” Nature Communications, vol. 11, no. 1, p. 2062, Apr. 2020, doi: 10.1038/s41467-020-15618-w.

[4] R. Huber, M. Wojtkowski, and J. G. Fujimoto, “Fourier Domain Mode Locking (FDML): A new laser operating regime and applications for optical coherence tomography,” Optics Express, vol. 14, no. 8, p. 3225, Apr. 2006, doi: 10.1364/oe.14.003225.

MODELING AND CHARACTERIZATION OF SPECTRAL PARAMETERS IN GLAD NANOSTRUCTURED THIN FILMS

Dovydas Šablinskas[1], Lukas Ramalis[1], Adomas Strazdas[1], Simas Melnikas[1]

[1]FTMC, Department of Laser Technologies, Optical Coatings Laboratory, Vilnius, Lithuania
dovydas.sablinskas@ftmc.lt

Low refractive index optical materials are essential for multilayer interference coatings, including antireflection coatings, high-reflectivity coatings, and structures designed to enhance total internal reflection [1]. Nanostructured low-refractive-index films fabricated by glancing angle deposition (GLAD) are of particular interest for high-power laser applications, as the technique allows wide-band-gap, low-absorption materials to be structured into coatings with an effective low refractive index [2]. However, accurate characterization of their optical response remains challenging.

Fundamental ambiguities arise when characterizing SiO_2 GLAD monolayers using thin-film optics based on Fresnel equations [3]. In such case GLAD layer effective refractive index value is limited between substrate and ambient medium refractive indices. Numerical modeling of light transmittance spectra reveals multiple refractive index solutions, as different refractive index values with the same optical thickness can produce nearly identical spectral responses (Fig. 1.). These non-unique solutions are most pronounced in the central region of the examined refractive index range, where alternative solutions cannot be reliably separated using transmittance data alone.

The results show that transmittance spectra by themselves cannot determine a unique refractive index solution in structured low refractive index films. Involving numerical modeling techniques enables to estimate the accuracy and limitations of such characterization for determination of optical constants.

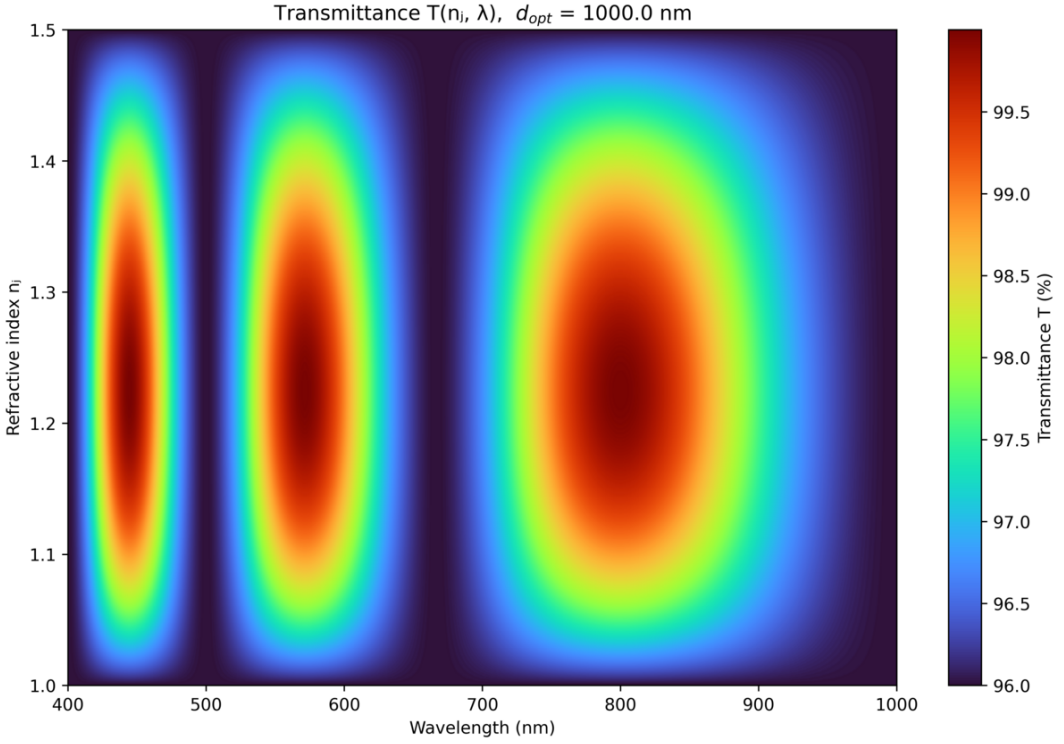


Fig. 1. Transmittance as a function of wavelength and intermediate refractive index for a single-layer thin film with air ($n = 1$) as the incident medium and a substrate refractive index of 1.5. The film has an optical thickness of 1000 nm.

Keywords: GLAD thin films, Nanostructured effective low refractive index films, Optical constants, High-power laser coatings, Fresnel thin-film optics

[1] Lukas Ramalis, Simas Melnikas, Deividas Buinovskis, Tomas Tolenis, Enhancement of total internal reflection in Nd:YAG crystals by multilayer nanostructured coatings, Optics & Laser Technology.

[2] Ramalis, Lukas & Norkute, Ugne & Grinevičiūtė, Lina & Buzelis, Rytis & Tolenis, Tomas. (2021). Sculptured thin film based all-silica mirrors for high power lasers. 43. 10.1117/12.2598667

[3] O. Stenzel, The Physics of Thin Film Optical Spectra: An Introduction, Springer Series in Surface Sciences, vol. 44, Springer-Verlag, Berlin–Heidelberg, 2005, pp. 81–95, Eq. (4.20).

POSTER SESSION 4

Ecology, Geology, and Environmental Sciences

Biology and Medicine

IMPACT OF BODY MASS INDEX ON ERYTHROCYTE MEMBRANE FATTY ACID COMPOSITION AND OXIDATIVE STRESS IN HEALTHY ADULTS

Inga Bikulčienė[1,2], Inga Fomčenko[3], Virginijus Šapoka[3], Arvydas Kaminskas[1], Dovilė Karčiauskaitė[1,2]

[1]Lithuania, Vilnius University, Faculty of Medicine, Institute of Biomedical Sciences
[2]Lithuania, Vilnius University, Faculty of Medicine, Translational Health Research Institute
[3]Lithuania, Vilnius University, Faculty of Medicine
inga.bikulciene@mf.vu.lt

The fatty acid (FA) composition of erythrocyte membranes reflects long-term dietary intake, metabolic status, and systemic inflammation, and may vary among individuals with different body mass indices (BMIs). This study aimed to investigate the relationships between BMI, erythrocyte membrane FA composition, and oxidative stress in healthy adults.

This cross-sectional study, conducted from May 2023 to June 2024, included 190 healthy men and women aged 29–43 years who attended the outpatient clinic at the National Centre of Osteoporosis in Vilnius, Lithuania. Based on BMI values, participants were categorised into one of four groups: underweight, normal weight, overweight, or obese. Blood samples were analysed for serum malondialdehyde (MDA) using high-performance liquid chromatography, and erythrocyte membrane FA composition was assessed using gas chromatography–mass spectrometry.

Across BMI groups, MDA levels were higher in the obese group than in the healthy weight group (107.8 ± 17.2 vs. 96.5 ± 16.6 ng/mL, $p = 0.007$). Underweight individuals had lower total SFA levels than those in the healthy weight group (60.9 (41.0, 62.5) vs. 81.2 (68.7, 88.6) %, $p < 0.001$), whereas healthy weight individuals had higher SFA levels than those in the obese group (81.2 (68.7, 88.6) vs. 47.4 (40.9, 65.0) %, $p < 0.001$). C16:0 was higher in the healthy weight group (52.5 (44.4, 58.6) %) compared with the overweight (36.4 (24.4, 39.0) %) and obese (28.6 (23.7, 40.8) %) groups ($p < 0.001$). Total MUFA levels were lowest in healthy weight individuals (14.0 (7.7, 16.6) %) and highest in the overweight (18.9 (13.5, 20.3) %) and obese (18.4 (15.8, 20.7) %) groups ($p < 0.001$), driven largely by increases in C18:1n-9. PUFAs were depleted in the healthy weight group (4.9 (4.1, 11.0) %) but elevated in the obese group (32.9 (17.4, 37.8) %, $p < 0.001$). Levels of n-3 PUFAs increased with BMI (5.7 (1.0–10.4) %), with the highest concentrations of C20:5n-3, C22:5n-3, and C22:6n-3 observed in the obese group. n-6 PUFA levels (mainly C18:2n-6) were lowest in the healthy weight group and highest in the obese group (3.8 (3.6, 25.8) % vs. 23.2 (12.6, 26.0) %, $p < 0.001$).

In conclusion, higher BMI was associated with increased oxidative stress. Alterations in erythrocyte membrane FA composition were observed, with obesity characterised by reduced SFA levels and elevated MUFA and PUFA levels. These findings suggest that excess adiposity is linked to membrane lipid remodelling in healthy adults.

EFFECTS OF MODULATING KDM5B EXPRESSION IN PROSTATE CANCER CELLS

Aukse Versekenaite[1], Ruta Maleckaite[1], Kristina Daniunaite[1]

[1]Vilnius University, Life Sciences Center, Institute of Biosciences, Vilnius, Lithuania
aukse.versekenaite@gmc.stud.vu.lt

Prostate cancer (PCa) remains one of the leading causes of death among men, with over 370,000 annual deaths worldwide [1]. It has become evident that epigenetics plays a significant role in the onset and progression of PCa, particularly histone methylation and its associated genes. One of these genes is *KDM5B*, a lysine-specific demethylase, which has been identified in recent years as an oncogene associated with many cancers [2]. In PCa, *KDM5B* is often overexpressed, which correlates with lower patient survival rates [3]. Therefore, lowering *KDM5B* expression in cancer cells could be a potential target for PCa treatment.

This study aimed to modulate *KDM5B* gene expression in PCa cells by transfection with small interfering RNA (siRNA) and to assess the induced potential changes in cell behavior. PC-3 and LNCaP cell lines were used for this study. The relative expression of *KDM5B* was measured using quantitative PCR, and commercial assays were used to assess cell viability, proliferation, invasiveness, and migration.

Our preliminary results demonstrated successful downregulation of *KDM5B* expression in both cell lines following siRNA transfection, with the statistically significant decrease observed in LNCaP cells ($P < 0.01$). Functional analyses revealed that *KDM5B* silencing reduced PC-3 cell viability and proliferation ($P = 0.0125$ and $P = 0.0190$, respectively), while no significant changes in apoptotic or necrotic cell populations were detected. Furthermore, decreased migratory capacity was observed in both PC-3 and LNCaP cells, suggesting a potential role of *KDM5B* in regulating prostate cancer cell motility.

In conclusion, our preliminary results indicate that siRNA-mediated downregulation of *KDM5B* expression in PCa cells reduces cell viability, proliferation, and migration, suggesting a potential role in PCa progression and its relevance for drug development.

[1] C. Boixareu, T. Taha, V. B. Venkadakrishnan, J. De Bono, and H. Beltran, “Targeting the tumour cell surface in advanced prostate cancer,” Nature Reviews Urology, vol. 22, no. 9, pp. 569–589, Apr. 2025, doi: 10.1038/s41585-025-01014-w.

[2] Y.-D. Fu et al., “Targeting histone demethylase KDM5B for cancer treatment,” European Journal of Medicinal Chemistry, vol. 208, p. 112760, Aug. 2020, doi: 10.1016/j.ejmech.2020.112760.

[3] B. Liu et al., “Evidence for context-dependent functions of KDM5B in prostate development and prostate cancer,” Oncotarget, vol. 11, no. 46, pp. 4243–4252, Nov. 2020, doi: 10.18632/oncotarget.27818.

EXPRESSION ANALYSIS OF THE COMPONENTS OF HIPPO SIGNALING PATHWAY IN OVARIAN CANCER

Kornelia Gurska[2], Rūta Čiurlienė[3], Rasa Sabaliauskaitė[1,2], Ieva Vaicekauskaitė[1,2]

[1]Lithuania, Vilnius, National Cancer Institute
[2]Lithuania, Vilnius, Life Science Center, Institute of Biosciences
[3]Lithuania, Vilnius University Hospital Santaros Clinics, National Cancer Center
kornelia.gurska@gmc.stud.vu.lt

Ovarian cancer is one of the most common women's reproductive system malignancies [1]. The most common subtype of ovarian cancer is high-grade serous ovarian carcinoma (HGSOC), which is characterized as an aggressively spreading malignancy. Furthermore, due to its non-specific symptoms, ovarian cancer is hard to diagnose in an early stage, which explains the high mortality rate of this disease.

Cancer development is often described by dysregulation of signaling pathways. Studies show that Hippo signaling pathway plays a crucial role in the ovary organ size control, development and regeneration [2]. Main components of this pathway are YAP, MST1/2, TAZ and LATS1/2 protein kinases, which control cell proliferation by regulating gene expression. Dysregulation of this pathway leads to uncontrolled cell proliferation and tumor progression.

This research aimed to analyze the expression of *YAP1*, *MST1*, *TAZ* and *LATS1* genes and identify their diagnostic potential. To achieve our aim, we performed a reverse transcriptase quantitative polymerase chain reaction (RT-qPCR) with 42 HGSOC, 14 other gynecological and 9 benign tumor tissue samples. The results were normalized to a reference gene *GAPDH*.

The ROC curve analysis when comparing HGSOC and benign cases showed an AUC of 0.94 for *TAZ*, 0.89 for *LATS1* and 0.87 for *YAP1* with a high sensitivity and specificity. Also, there was a high AUC, specificity and sensitivity rate when comparing HGSOC and other gynecological malignancies for *MST1* (AUC 0.74, specificity 0.79, sensitivity 0.71). Hippo pathway genes were downregulated in HGSOC and other tumor samples compared to benign cases ($p<0.05$).

Our research suggests that the components of Hippo signaling pathway could be considered as a potential biomarker for ovarian cancer diagnosis. Further research is needed to validate this suggestion.

[1] B. Smolarz et al., "Ovarian Cancer—Epidemiology, classification, pathogenesis, treatment, and estrogen receptors' molecular backgrounds," International Journal of Molecular Sciences, vol. 26, no. 10, p. 4611, May 2025, doi: 10.3390/ijms26104611.

[2] K. L. Clark et al., "Hippo signaling in the ovary: Emerging roles in development, fertility, and disease," Endocrine Reviews, vol. 43, no. 6, pp. 1074–1096, May 2022, doi: 10.1210/endrev/bnac013.

DNMT AND HDAC INHIBITION INDUCE DISTINCT TRANSCRIPTIONAL PROGRAMS AND ACTIVE CHROMATIN REMODELING IN CAR19-NK CELLS

Patricija Daugėlaitė[1], Veronika Viktorija Borutinskaitė[1]

[1]Vilnius University, Life Sciences Center, Institute of Biochemistry, Department of Molecular Cell Biology, Vilnius, Lithuania
patricija.daugelaite@chgf.stud.vu.lt

Chimeric Antigen Receptor Natural Killer (CAR-NK) cells are a novel and highly promising approach to cancer immunotherapy because of their strong cytotoxicity, favorable safety profile and reduced risk of graft-versus-host disease [1]. However, the clinical efficacy of this treatment is still constrained. Cellular exhaustion, insufficient antitumor activity and limited persistence necessitate further research [2]. Epigenetic regulation is a central determinant of immune cell identity and functional plasticity, yet its role in shaping transcriptional states of engineered CAR-NK cells remains incompletely understood, despite its potential to improve the therapeutic efficacy and persistence.

In this study, we examined how pharmacological inhibition of DNA methylation and histone deacetylation influences global gene expression patterns and active chromatin landscapes in CAR19-NK cells. CAR19-NK cells were treated with zebularine (a DNA methyltransferase inhibitor) or BML-210 (a histone deacetylase inhibitor), followed by transcriptome profiling using RNA sequencing. Comparative analysis revealed that the two epigenetic modulators induced partially overlapping but clearly distinct transcriptional programs. Zebularine predominantly affected genes associated with extracellular matrix interactions, focal adhesion, PI3K–Akt signaling, and immune-related pathways, suggesting transcriptional reprogramming linked to cellular interaction and environmental responsiveness. In contrast, BML-210 treatment resulted in broader transcriptional activation, with enrichment of pathways related to RNA processing, ribosome biogenesis, DNA replication, cell cycle progression, and chromatin remodeling, indicative of enhanced biosynthetic and proliferative capacity.

To mechanistically link these transcriptional changes with chromatin regulation, we performed chromatin immunoprecipitation followed by quantitative PCR (ChIP-qPCR) analysis of the active histone mark H3K4me3 at selected gene promoters. Epigenetic modulation led to differential enrichment of H3K4me3 at promoters of genes involved in immune regulation and differentiation (FOXO1, HOXA10, STAT5), as well as components of the Polycomb repressive complex 2 (EED, SUZ12, EZH2). Notably, pronounced H3K4me3 alterations at the HOXA10 and EZH2 promoters indicate remodeling of transcriptionally permissive chromatin states that may underlie the observed RNA-seq profiles.

Together, these data demonstrate that DNMT and HDAC inhibition drive distinct yet complementary transcriptional and chromatin-level responses in CAR19-NK cells. This integrated transcriptomic and epigenetic analysis provides mechanistic insight into how targeted epigenetic modulation can shape CAR-NK cell states, offering a rational framework for future optimization strategies in engineered NK-cell-based immunotherapies.

[1] M. B. Khawar and H. Sun, “CAR-NK Cells: From Natural Basis to Design for Kill,” Front. Immunol., vol. 12, p. 707542, 2021.
[2] Z. Pang et al., “Current Progress of CAR-NK Therapy in Cancer Treatment,” Cancers, vol. 14, no. 17, p. 4318, 2022.

CIRCULAR RNA QUANTIFICATION IN PROSTATE CANCER CELL LINES WITH MODIFIED EXPRESSION OF SELECTED MICRORNAS

Gerda Bertulyte[1], Ruta Maleckaite[1], Aukse Versekenaite[1], Arnas Stucinskas[1], Marta Tamosiunaite[1], Kristina Daniunaite[1]

[1]Vilnius University, Life Sciences Center, Institute of Biosciences, Vilnius, Lithuania
gerda.bertulyte@gmc.stud.vu.lt

Prostate cancer (PCa) remains a major global health burden, being the most frequently diagnosed malignancy among men in nearly two-thirds (118 of 185) of the countries worldwide [1]. Increasing attention has been directed toward noncoding circular RNAs (circRNAs), as their aberrant expression has been reported in various types of cancer and linked to tumor development or progression [2]. Some circRNAs can function as microRNA (miRNA) 'sponges' or interact with RNA-binding proteins, thereby influencing gene expression [3]. However, the regulatory interplay between various circRNAs and miRNAs in PCa cells remains poorly understood.

The aim of this study was to quantify selected circRNAs (circFOXO3, circFAT1, and others) in PCa cells with experimentally modified miR-155 and miR-137 expression. Firstly, a miRNA mimetic approach was used to induce the expression of selected miRNAs in PCa cells lacking endogenous expression. cDNA obtained from these cells was then analyzed using quantitative PCR (qPCR) to assess circRNA levels. Divergent primers were designed and applied to specifically amplify circular transcripts, allowing reliable discrimination between circular and linear RNA forms.

Our preliminary results confirm successful detection of circFOXO3, circFAT1 and circHIPK3 in both PC-3 and LNCaP cell samples. Differences in circRNA expression levels were observed between PCa cells transfected with miRNA mimetics and control cells lacking the selected miRNA expression. Notably, miRNA modulation appeared to be associated with circRNA-specific expression patterns, suggesting that individual circRNAs may respond differently to altered miRNA levels.

In conclusion, these preliminary findings indicate that experimental modulation of specific miRNA expression is associated with detectable changes in circRNA expression in PCa cell lines, indicating a potential regulatory interplay between circRNA and miRNAs that may be relevant to PCa biology.

[1] F. Bray et al., "Global cancer statistics 2022: GLOBOCAN estimates of incidence and mortality worldwide for 36 cancers in 185 countries," CA a Cancer Journal for Clinicians, vol. 74, no. 3, pp. 229–263, Apr. 2024, doi: 10.3322/caac.21834.

[2] S. Qu et al., "The emerging functions and roles of circular RNAs in cancer," Cancer Letters, vol. 414, pp. 301–309, Nov. 2017, doi: 10.1016/j.canlet.2017.11.022.

[3] A. Malviya and R. Bhuyan, "Circular RNAs in cancer: roles, mechanisms, and therapeutic potential across colorectal, gastric, liver, and lung carcinomas," Discover Oncology, vol. 16, no. 1, p. 5, Jan. 2025, doi: 10.1007/s12672-025-01743-9.

IN VITRO GENOTOXICITY ASSESSMENT OF POLYSTYRENE MICRO- AND NANOPARTICLES IN HUMAN ALVEOLAR EPITHELIAL CELLS (A549)

Vaiva Horbačauskaitė[1], Emilija Striogaitė[1], Juozas Rimantas Lazutka[1]

[1]Vilnius University, Department of Botany and Genetics, Institute of Biosciences, Vilnius, Lithuania
vaiva.horbacauskaite@gmc.stud.vu.lt

Polystyrene micro- and nanoparticles (PS-MNPs) are plastic particles widely distributed in the environment. Many studies with various test subjects have shown that polystyrene nanoparticles can enter living organisms, including humans, via multiple routes. This raises concerns about their potential adverse effects. In this work, the cytotoxicity and genotoxicity of 70 nm polystyrene nanoparticles and 1 μm polystyrene microparticles were investigated in the human alveolar adenocarcinoma cell line A549 in vitro. An oxidant-sensitive, fluorescent dye, 2,7-dichlorodihydrofluorescein diacetate (H2DCFDA), was used to evaluate cellular uptake and reactive oxygen species levels generated by PS-NMPs. A mixture of acridine orange and ethidium bromide dyes was used to determine the cytotoxic effects of PS-MNPs. The alkaline comet assay was used to evaluate primary DNA damage induced by PS-MNPs, and the enzyme-modified (Fpg) comet assay was used to evaluate oxidative DNA damage. Flow cytometry results showed that both polystyrene micro- and nanoparticles were efficiently absorbed by A549 cells. An increase in PS-MNP concentrations did not increase reactive oxygen species levels. The viability analysis showed that none of the concentrations caused cytotoxic effects in A549 cells. The alkaline and enzyme-modified comet assay showed that none of the polystyrene micro- or nanoparticle concentrations caused statistically significant changes in DNA damage. The obtained results suggest that PS-MNPs do not cause statistically significant DNA damage in A549 cells. However, since PS-MNPs were absorbed effectively by A549 cells, further research is needed.

ACTIVITY OF DOXORUBICIN AND 5-FLUOROURACIL IN HUMAN MELANOMA A375 SPHEROIDS FORMED BY DIFFERENT METHODS

Akvilė Žilytė[1], Vilma Petrikaitė[1]

[1]Lithuanian University of Health Sciences, Institute of Cardiology, Laboratory of Drug Targets Histopathology, Lithuania
akvile.zilyte@stud.lsmu.lt

Melanoma is the third most common form of skin cancer and is associated with a high risk of metastasis. Incidence and mortality rates are increasing each year, and it is predicted that the number of melanoma cases will continue to rise rapidly in the coming decades [1]. For these reasons, further research is required to improve our understanding of melanoma biology and to identify new effective anticancer drugs that could improve patient survival [2].

In this study, we evaluated the impact of in vitro 3D culture modelling of the human melanoma A375 on the activity of doxorubicin (DOX) and 5-fluorouracil (5-FU). These drugs were selected based on their differences in mechanism of action. DOX is a cytotoxic drug that inhibits topoisomerase II, causing DNA damage and cell death [3]. In contrast, 5-FU is a cytostatic drug that inhibits DNA and RNA synthesis, thereby suppressing cell proliferation [4]. Two of the most commonly used 3D culture formation methods were selected: the hanging drop method and the non-adhesive surface formation method [5].

Spheroid growth dynamics were assessed by phase-contrast microscopy through analysis of changes in spheroid diameter. To compare the effects of anticancer drugs in spheroids of different sizes, spheroids were generated using two initial cell numbers (250 and 2000 cells per spheroid). Following treatment with DOX and 5-FU,spheroids were incubated for 8 days. Drug activity was evaluated based on changes in spheroid diameter and cell viability, measured using the MTT assay. DOX transport into spheroids was assessed by measuring DOX fluorescence intensity over the total spheroid area using fluorescence microscopy.

In general, A375 spheroids formed using the non-adhesive surface method were more sensitive to DOX than spheroids formed using the hanging drop method. In smaller spheroids, 10 µM 5-FU inhibited viability more efficiently when spheroids were formed using the hanging drop method. DOX transport into spheroids varied depending on the concentration of DOX used. When spheroids were incubated with 10 µM DOX, accumulation was higher compared to incubation with 2 µM DOX. No statistically significant differences in DOX transport were determined in spheroids formed by different methods, nor in spheroids of different diameters (200 µm and 400 µm).

In conclusion, A375 spheroids formed using the non-adhesive surface method are more sensitive to DOX, while the effect of 5-FU varies depending on its concentration and the size of the spheroids. DOX transport into A375 spheroids does not depend on the formation method but is dependent on the DOX concentration used.

[1] L. A. Nurla and A.-M. Forsea, 'Melanoma epidemiology in Europe: what is new?', Ital. J. Dermatol. Venereol., vol. 159, no. 2, Apr. 2024, doi: 10.23736/S2784-8671.24.07811-3.

[2] S. M. Ostrowski and D. E. Fisher, 'Biology of Melanoma', Hematol. Oncol. Clin. North Am., vol. 35, no. 1, pp. 29–56, Feb. 2021, doi: 10.1016/j.hoc.2020.08.010.

[3] D. Salvador, V. Bastos, and H. Oliveira, 'Hyperthermia Enhances Doxorubicin Therapeutic Efficacy against A375 and MNT-1 Melanoma Cells', Int. J. Mol. Sci., vol. 23, no. 1, p. 35, Dec. 2021, doi: 10.3390/ijms23010035.

[4] J. Tian et al., '5-Fluorouracil efficacy requires anti-tumor immunity triggered by cancer-cell-intrinsic STING', EMBO J., vol. 40, no. 7, p. e106065, Apr. 2021, doi: 10.15252/embj.2020106065.

[5] R. L. F. Amaral, M. Miranda, P. D. Marcato, and K. Swiech, 'Comparative Analysis of 3D Bladder Tumor Spheroids Obtained by Forced Floating and Hanging Drop Methods for Drug Screening', Front. Physiol., vol. 8, p. 605, Aug. 2017, doi: 10.3389/fphys.2017.00605.

IN VITRO GENOTOXICITY OF POLYETHYLENE MICROPARTICLES IN HUMAN HEPATOMA (HEPG2) AND ADENOCARCINOMA (A549) CELL LINES

Emilija Striogaitė[1], Juozas Rimantas Lazutka[1]

[1]Vilnius University, Life Sciences Center, Institute of Biosciences, Vilnius, Lithuania
emilija.striogaite@gmc.vu.lt

The extensive use of plastics has raised ecological concerns, as they can persist in the environment for many centuries. Plastics may degrade into microparticles, and among MPs found in the environment, one of the most common is polyethylene microparticles (PE-MPs) [1]. Therefore, the potential negative impact of PE-MPs on human health should be explored.

This study aimed to assess the cytotoxicity and genotoxicity of polyethylene microparticles (1 µm) in human hepatoma (HepG2) and alveolar adenocarcinoma (A549) cells *in vitro*. The cellular uptake and levels of reactive oxygen species generated by PS-NPs were evaluated using the fluorescent, oxidant-sensitive dye 2,7-dichlorodihydrofluorescein diacetate (H_2DCFDA). Cytotoxicity was assessed using a mixture of acridine orange and ethidium bromide, based on cell integrity. Potential primary DNA damage under PE-MP exposure was tested by the alkaline comet assay, and potential induced oxidative DNA damage was tested by an enzyme-modified comet assay.

Flow cytometry analysis of HepG2 and A549 cells exposed to PE-MPs showed efficient uptake of these microparticles. The tested PE-MP concentrations were not cytotoxic to either cell line, but they did induce both primary and oxidative DNA damage.

These findings indicate that polyethylene microparticles can be effectively absorbed and possess genotoxic potential, raising concerns about plastic safety.

[1] J. Martín, J. L. Santos, I. Aparicio, and E. Alonso, “Microplastics and associated emerging contaminants in the environment: Analysis, sorption mechanisms and effects of co-exposure,” Trends in Environmental Analytical Chemistry, vol. 35, p. e00170, Jun. 2022, doi: 10.1016/j.teac.2022.e00170.

TDP-43 LIQUID-LIQUID PHASE SEPARATION AND PHOSPHORYLATION STUDY

Saulė Rapalytė[1], Dominykas Veiveris[1], Darius Šulskis[1]

[1]Vilnius University, Life Sciences Centre, Institute of Biotechnology, Amyloid Research Sector, Lithuania
saule.rapalyte@gmc.vu.lt

TAR DNA-binding protein 43 (TDP-43) is a multifunctional protein primarily localizing in the cell nucleus, where it binds to RNA and DNA [1]. It consists of 414 amino acids and is composed of four domains: N-terminal domain, two RNA-binding domains (RRM1 and RRM2), and low-complexity prion-like C-terminal domain [2]. RRM domains are flanked by nuclear export and import sequences, thereby enabling protein shuttling between the nucleus and cytoplasm [3]. In both the nucleus and cytoplasm, TDP-43 can form condensates through liquid-liquid phase separation (LLPS) – a biophysical process involved in the formation of membraneless organelles [4]. Due to LLPS, protein cleavage, mutations, and posttranslational modifications, such as hyperphosphorylation, TDP-43 can aggregate and form insoluble neurotoxic species, as well as disrupting downstream cellular processes [5]. TDP-43 aggregates are the hallmarks of several neurodegenerative diseases: amyotrophic lateral sclerosis and frontotemporal lobar degeneration [2]. However, latest studies have shown that phosphorylation of TDP-43 can greatly suppress the protein's propensity to undergo LLPS and slow TDP-43 aggregation into amyloid fibrils [6]. Therefore, we aim to identify key kinases implicated in neurodegeneration that can phosphorylate TDP-43 and elucidate their impact on its LLPS and aggregation.

In this study, we initially optimized the purification of full-length TDP-43. This protein is prone to degradation and forms aggregates after cleavage of the purification tag, making it difficult to purify. For LLPS studies, TPD-43 with mCherry fluorescent protein tag was purified and later used for fluorescent microscopy imaging. The kinetics of LLPS were analyzed by measuring the sample's turbidity with or without molecular crowder polyethylene glycol (PEG). For the phosphorylation assay, four different kinases were used: CK1α, PKA, PKR, and GSK3β. The phosphorylation effect was evaluated with SDS-PAGE electrophoresis.

The results demonstrate that TDP-43 is more prone to form condensates in the presence of molecular crowder. Higher PEG concentration resulted in more aggregates. For phosphorylation studies, we suggest that CK1α and PKR kinases were the most effective. However, we observed aggregates in almost all kinase treated TDP-43 samples, with fewer aggregates found in sample treated with CK1α. To further investigate these processes, we will optimize LLPS conditions and perform a more comprehensive analysis of kinase efficiencies and aggregate species.

[1] J. Song, "Molecular Mechanisms of Phase Separation and Amyloidosis of ALS/FTD-linked FUS and TDP-43," Aging Dis., vol. 15, no. 5, pp. 2084–2112, Aug. 2024, doi: 10.14336/AD.2023.1118.

[2] S. T. Kumar et al., "Seeding the aggregation of TDP-43 requires post-fibrillization proteolytic cleavage," Nat. Neurosci., vol. 26, no. 6, pp. 983–996, Jun. 2023, doi: 10.1038/s41593-023-01341-4.

[3] G. S. A. Wright et al., "Purification and Structural Characterization of Aggregation-Prone Human TDP-43 Involved in Neurodegenerative Diseases," iScience, vol. 23, no. 6, p. 101159, Jun. 2020, doi: 10.1016/j.isci.2020.101159.

[4] H. B. Schmidt, A. Barreau, and R. Rohatgi, "Phase separation-deficient TDP43 remains functional in splicing," Nat. Commun., vol. 10, no. 1, p. 4890, Oct. 2019, doi: 10.1038/s41467-019-12740-2.

[5] E. Buratti and F. E. Baralle, "TDP-43: gumming up neurons through protein–protein and protein–RNA interactions," Trends Biochem. Sci., vol. 37, no. 6, pp. 237–247, Jun. 2012, doi: 10.1016/j.tibs.2012.03.003.

[6] R. Haider, S. Penumutchu, S. Boyko, and W. K. Surewicz, "Phosphomimetic substitutions in TDP-43's transiently α-helical region suppress phase separation," Biophys. J., vol. 123, no. 3, pp. 361–373, Feb. 2024, doi: 10.1016/j.bpj.2024.01.001.

EXPRESSION, PURIFICATION AND ACTIVITY ASSESMENT OF RECOMBINANT ESCHERICHIA COLI PURINE DEAMINASES

Ugnius Kamandulis[1], Jaunius Urbonavičius[1], Daiva Tauraitė[1]

[1]Vilnius Gediminas Technical University, Department of Chemistry and Bioengineering, Lithuania
ugnius.kamandulis@stud.vilniustech.lt

Deaminases are enzymes that catalyze deamination reactions in purine metabolism and help to maintain purine homeostasis in cells. Disturbances in these pathways can contribute to harmful accumulation of purine-related metabolites and lead to metabolic imbalance. Purines themselves are essential biomolecules across all living systems. They are building blocks of DNA and RNA, central to cellular energy metabolism (ATP), and participate in intracellular and extracellular signalling through cyclic nucleotides and purinergic signalling networks [1]. Because altered purine metabolism and purinergic signalling have been associated with diverse pathological conditions, systematic biochemical characterization of enzymes involved in purine conversion remains relevant for both basic research and potential application-oriented work [2].

The aim of this study is to establish recombinant production and purification of Add and AdeC proteins in *Escherichia coli* and to confirm their functional activity using the adenine/adenosine and their modified derivatives as substrates, including product-formation analysis by the chromatography methods. *E. coli* Rosetta strains were transformed with expression constructs encoding Add and AdeC. Recombinant protein expression was induced with IPTG, and His-tagged proteins were purified using Ni^{2+} affinity chromatography. Expression and purity of proteins were assessed by SDS-PAGE. Enzymatic activities were tested using adenine/adenosine and their methylated conterparts as substrates, and TLC and HPLC were used to monitor substrate conversion and quantification of reaction products. HPLC analysis demonstrated enzymatic conversion of adenine to xanthine in the presence of the recombinant AdeC enzyme, indicating that the purified protein retained catalytic function after purification. However, the enzymatic activity was not detected when methylated adenine was used. Further experiments are aimed at the testing of the enzymatic activity of Add using the adenosine and it‘s methylated counterparts to establish the enzymatic activity and specificity of corresponding purine deaminases.

Acknowledgements

This project has received funding from the Research Council of Lithuania (LMTLT), agreement No [S-MIP-25-95].

Keywords: Adenine deaminase, purine metabolism, recombinant protein, enzymatic conversion.

[1] D. Wu, S. Yang, C. Yuan, K. Zhang, J. Tan, K. Guan, H. Zeng, C. Huang, “Targeting purine metabolism-related enzymes for therapeutic intervention: A review from molecular mechanism to therapeutic breakthrough,” International Journal of Biological Macromolecules, vol. 282, no. 1, p. 136828, Dec. 2024.

[2] Z. Huang, N. Xie, P. Illes, F. Virgilio, H. Ulrich, A. Semyanov, A. Verkhratsky, B. Sperlagh, S. Yu, C. Huang, “From purines to purinergic signalling: molecular functions and human diseases,” Signal Transduction and Targeted Therapy, vol. 6, no. 162, Apr. 2021.

PTTG1 RS2910200 POLYMORPHISM AS A POTENTIAL MARKER OF LOCALLY ADVANCED LARYNGEAL SQUAMOUS CELL CARCINOMA

Augustė Simanonytė[1], Enrika Pileckaitė[1], Vykintas Liutkevičius[2], Rasa Liutkevičienė[3]

[1]Lithuania, Kaunas, Lithuanian University of Health Sciences, Medical Academy, Neuroscience Institute, Laboratory of Ophthalmology
[2]Lithuania, Kaunas, Lithuanian University of Health Sciences, Department of Otorhinolaryngology
[3]Lithuania, Kaunas, Lithuanian University of Health Sciences, Medical Academy, Department of Ophtalmology
auguste.simanonyte@lsmu.lt

Laryngeal squamous cell carcinoma (LSCC) is the most frequent malignant tumor of the larynx and represents an aggressive disease with increasing incidence worldwide [1]. LSCC development is multifactorial, with growing evidence indicating that genetic variability, particularly single nucleotide polymorphisms (SNPs), contributes to tumor progression and clinical outcomes [2, 3].

Tumor extent, as defined by the TNM classification system, reflects the size of the primary tumor and its invasion into surrounding tissues. Locally advanced primary tumors with extralaryngeal extension represent an aggressive disease phenotype associated with extensive local invasion and poor prognosis [4]. Invasion and metastasis are the main contributors to LSCC-related mortality. Therefore, improved understanding of the molecular mechanisms underlying advanced locally invasive LSCC is essential for improving risk assessment and treatment planning.

Pituitary tumor-transforming gene 1 (*PTTG1*) regulates cell proliferation, differentiation and apoptosis. *PTTG1* has been implicated in tumor growth and metastasis [5]. However, the role of *PTTG1* genetic variation in the development of locally advanced primary tumors with extralaryngeal extension in LSCC remains poorly understood. Clarifying this association may improve understanding of tumor aggressiveness and support the identification of potential molecular markers of advanced local disease.

The aim of this study was to investigate the association between the *PTTG1* rs2910200 genetic variation and the development of locally advanced primary tumors with extralaryngeal extension in LSCC patients.

The study involved 30 LSCC patients with locally advanced primary tumors with extralaryngeal extension and 200 healthy controls. DNA samples from peripheral blood leukocytes were purified by DNA salting-out method. *PTTG1* rs2910200 SNP analyses was determined using real-time polymerase chain reaction (RT-PCR). Statistical analysis ware conducted using ”IBM SPSS Statistics 31.0” program.

Binomial logistic regression analysis revealed a statistically significant association under the over-dominant genetic model. The CT genotype, compared to the combined TT and CC genotypes, was associated with 2.3-fold increased odds of presenting with locally advanced primary tumors with extralaryngeal extension (OR = 2.297 95% CI: 1.049–5.030, $p = 0.037$, AIC = 175.682). No statistically significant associations were observed under other genetic models, including codominant, dominant, recessive and additive models ($p > 0.05$).

Our results indicate that LSCC patients carrying the *PTTG1* rs2910200 CT genotype are more likely to develop locally advanced primary tumors with extralaryngeal extension. These findings suggest that *PTTG1* genetic variation may serve as a potential biomarker for tumor aggressiveness, providing valuable information for prognosis and guiding clinical management.

Keywords: PTTG1, RS2910200, laryngeal squamous cell carcinoma, oncology

[1] J. Wang et al., “Unveiling the role of PPIF and macrophage subtypes in LSCC progression via single-cell and exosome RNA sequencing,” Scientific Reports, vol. 15, no. 1, p. 10141, Mar. 2025, doi: 10.1038/s41598-025-93584-3.
[2] J. Huang et al., “Updated disease distributions, risk factors, and trends of laryngeal cancer: a global analysis of cancer registries,” International Journal of Surgery, vol. 110, no. 2, pp. 810–819, Nov. 2023, doi: 10.1097/js9.0000000000000902.
[3] B. Verro et al., “Biomarkers in laryngeal squamous cell carcinoma: The Literature Review,” Cancers, vol. 15, no. 20, p. 5096, Oct. 2023, doi: 10.3390/cancers15205096.
[4] R. D. Rosen and A. Sapra, “TNM Classification,” StatPearls - NCBI Bookshelf, Feb. 13, 2023. https://www.ncbi.nlm.nih.gov/books/NBK553187/
[5] H. Wei, Y. Ma, S. Chen, C. Zou, and L. Wang, “Multi-omics analysis identifies PTTG1 as a prognostic biomarker associated with immunotherapy and chemotherapy resistance,” BMC Cancer, vol. 24, no. 1, p. 1315, Oct. 2024, doi: 10.1186/s12885-024-13060-5.

EXPRESSION OF KINESIN SUPERFAMILY MEMBERS KIF2C, KIF14 AND KIF20 AS DIAGNOSTIC BIOMARKERS FOR OVARIAN CANCER

Areta Petrauskaitė[1], Ieva Vaicekauskaitė[1,2], Rūta Čiurlienė[3], Rasa Sabaliauskaitė[1,2]

[1]Lithuania, Vilnius, Vilnius University, Life Sciences Center
[2]Lithuania, Vilnius, National Cancer Institute
[3]Lithuania, Vilnius, National Cancer Center
areta.petrauskaite@gmc.stud.vu.lt

Ovarian cancer is one of the most common malignancies of the female reproductive system [1] and has the highest mortality rate, with an overall five-year survival below 50% [2]. This is primarily due to late diagnosis caused by non-specific symptoms and the lack of effective screening methods [3]. KIF2C, KIF14 and KIF20A are mitotic kinesins involved in the regulation of mitosis and cytokinesis [4]. Given their involvement in cell cycle progression and reported associations with tumor development, altered expression of these kinesin superfamily genes represents potential as diagnostic biomarkers for ovarian cancer. This pilot study aimed to evaluate the diagnostic potential of *KIF2C*, *KIF14* and *KIF20A* by analyzing their gene expression levels and association with clinical features of ovarian cancer patients.

Gene expression levels were analyzed in 65 ovarian cancer samples, classified into three groups according to tumor histological type, using reverse transcription quantitative PCR (RT-qPCR). Association between gene expression and clinicopathological parameters were assessed, and diagnostic performance was evaluated using receiver operating characteristics (ROC) curve analysis.

Analysis of selected gene expression revealed statistically significant differences between the study groups. *KIF2C*, *KIF14* and *KIF20A* showed significantly higher expression in high-grade serous ovarian carcinoma compared with benign gynecological tumors (*KIF2C*, $p = 0,03$; *KIF14*, $p = 0,001$; *KIF20A*, $p = 0,02$). ROC analysis demonstrated that the gene expression biomarkers effectively distinguished between these two groups, with areas under the curve of 0,77, 0,91, and 0,82, respectively. These findings suggest that these genes could be potentially useful as diagnostic biomarkers for ovarian cancer.

Overall, *KIF2C*, *KIF14* and *KIF20A* from the kinesin superfamily emerge as promising candidates for ovarian cancer diagnosis. Variations in their expression levels could be associated with tumor histological subtype, as ROC curves demonstrate the ability to distinguish malignant from benign samples. Nonetheless, confirmation of these results through expanded and independent studies is needed to clarify their potential clinical relevance.

Acknowledgements
This study was supported by National Cancer Institute.

[1] W. Tian et al., “Extracellular vesicles in ovarian cancer chemoresistance, metastasis, and immune evasion,” Cell Death and Disease, vol. 13, no. 1, p. 64, Jan. 2022, doi: 10.1038/s41419-022-04510-8.
[2] U. Testa, E. Petrucci, L. Pasquini, G. Castelli, and E. Pelosi, “Ovarian cancers: genetic abnormalities, tumor heterogeneity and progression, clonal evolution and cancer stem cells,” Medicines, vol. 5, no. 1, p. 16, Feb. 2018, doi: 10.3390/medicines5010016.
[3] P. DiSilvestro and A. A. Secord, “Maintenance treatment of recurrent ovarian cancer: Is it ready for prime time?,” Cancer Treatment Reviews, vol. 69, pp. 53–65, Jun. 2018, doi: 10.1016/j.ctrv.2018.06.001.
[4] S. Petry, “Mechanisms of mitotic spindle assembly,” Annual Review of Biochemistry, vol. 85, no. 1, pp. 659–683, May 2016, doi: 10.1146/annurev-biochem-060815-014528.

LIQUID-LIQUID PHASE SEPARATION OF S100A4 PROTEIN

Arijus Jaloveckas[1], Darius Šulskis[1]

[1]Vilnius University, Life Sciences Center, Institute of Biotechnology, Lithuania
arijus.jaloveckas@gmc.stud.vu.lt

The main indications of Alzheimer's disease are the accumulation of aggregates called amyloids in the brain, which cause inflammation and neuronal damage [1]. One example are calcium binding and neuroinflammation associated S100A proteins, whose aggregates are found in Corpora Amylacea, spherical bodies of unknown function and origin, that form during the ageing process and several neurodegenerative disorders [2]. One of the initial causes that accelerates amyloid fibril formation is the liquid-liquid phase separation (LLPS) process, where proteins form membraneless droplets based on their affinity for each other and a crowded environment [3]. Presently, the relationship between LLPS and amyloid aggregation of S100 protein is unknown, therefore, the goal of this study is to determine whether a specific S100A4 member undergoes LLPS in a crowded environment and if it causes protein aggregation.

A construct S100A4 fused with an N-terminal eEGP construct was formed using restriction-free cloning. After successfully selecting positive colonies, plasmids containing eGFP-S100A4 insert were purified and sequenced. For protein expression, BL21 Star™ (DE3) E. coli cells were transformed with the pET28b plasmid, containing eGFP-S100A4. Cells were grown until 0.6 optical density and protein production was induced with 0.1 mM IPTG. Harvested cells were lysed using sonication, and the soluble medium was separated via centrifugation. Then, the protein was applied to the Ni-NTA column, and the eluted fractions were concentrated. eGFP-S100A4 was further purified by size exclusion and ion exchange chromatography. Amyloid aggregation was monitored using amyloid-specific ThT dye. LLPS assay was conducted using different concentrations of eGFP-S100A4 and S100A4 mixture (1:99 ratio) and different polyethylene glycol (PEG) concentrations, which were used to imitate cellular environment. LLPS assay was observed using Olympus IX83 fluorescence microscope.

Initially, we observed that S100A4 does not aggregate in a non-crowded environment, except at low pH conditions. The addition of PEG induced the formation of S100A4 droplets at all 4 different protein concentrations (25, 50, 75, 100 μM), although the most prominent droplets were found in 10% and 20% PEG solutions. After successfully perceiving LLPS of S100A4, further research will include characterization of S100A4 state (aggregates, oligomers) in the droplets and their effect on the neuronal cells.

[1] D. J. Selkoe and J. Hardy, 'The amyloid hypothesis of Alzheimer's disease at 25 years', EMBO Mol. Med., vol. 8, no. 6, pp. 595–608, Jun. 2016, doi: 10.15252/emmm.201606210.

[2] E. Augé, I. Bechmann, N. Llor, J. Vilaplana, M. Krueger, and C. Pelegrí, 'Corpora amylacea in human hippocampal brain tissue are intracellular bodies that exhibit a homogeneous distribution of neo-epitopes', Sci. Rep., vol. 9, no. 1, p. 2063, Feb. 2019, doi: 10.1038/s41598-018-38010-7.

[3] S. Mukherjee, M. Poudyal, K. Dave, P. Kadu, and S. K. Maji, 'Protein misfolding and amyloid nucleation through liquid–liquid phase separation', Chem. Soc. Rev., vol. 53, no. 10, pp. 4976–5013, 2024, doi: 10.1039/D3CS01065A.

DIFFERENT PHARMACOLOGICAL MODULATION OF TRPM6 AND TRPM7 PROTEINS IN HUMAN CARDIOMYOCYTES

Inga Andriulė[1], Regina Mačianskienė[1]

[1]Lithuanian University of Health Sciences, Institute of Cardiology, Laboratory of Membrane Biophysics, Kaunas, Lithuania
inga.andriule@lsmu.lt

TRPM7 and its homologue TRPM6 are part of the melastatin subfamily of TRP channels and are crucial for the cellular uptake of divalent cations such as Ca^{2+} and Mg^{2+}. Recently, we have found that both proteins are also present in human cardiomyocytes [1].

The goal of this study was to investigate various extracellular factors, such as medium ionic composition, acidosis, and TRP channel inhibitors (2-APB and carvacrol), on the expression of TRPM6 and TRPM7 in native cardiomyocytes.

In this study, immunofluorescence was used to detect TRPM proteins. Immunofluorescence was stronger in media containing divalent cations than in those without, and expression increased after 12 hours of incubation. Inhibitors like 2-APB and carvacrol reduced TRPM7 but increased TRPM6 immunofluorescence. At acidic pH, both proteins' expression increased in divalent cation conditions, but in divalent cation-free conditions, TRPM7 was suppressed.

This study confirms the presence of TRPM6 and TRPM7 in human cardiomyocytes and demonstrates that extracellular factors modulate their expression. Crucially, the results show that TRPM6 and TRPM7 are not interrelated into their regulation. Their divergent responses to external stimuli suggest that in cardiomyocytes, these proteins function independently and compose distinct channels.

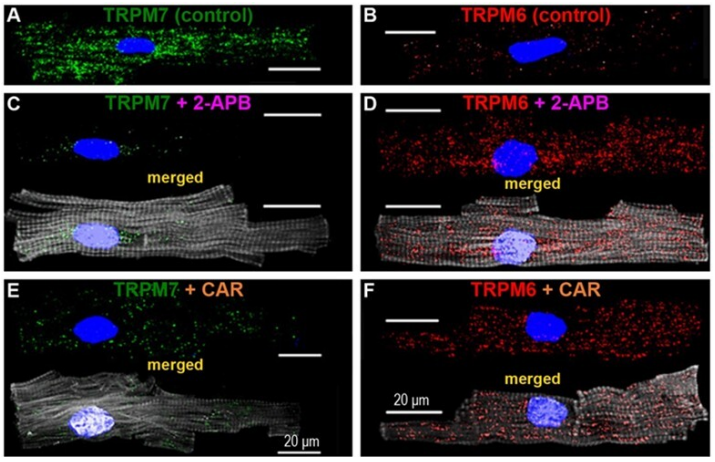


Fig. 1. Effect of 2-APB and carvacrol (CAR) on the immunofluorescence of TRPM6 and TRPM7 in human cardiomyocytes. Illustration of cardiomyocyte staining with anti-TRPM7 (A, C, E) or anti-TRPM6 (B, D, F) in the absence of drugs (A, B) and in the presence of either 2-APB (C, D) or CAR (E, F). Alexa Fluor 546 (*red*) – for TRPM6 protein; Alexa Fluor 488 (*green*) – for TRPM7 protein; Hoechst (*blue*) – for the nucleus; Alexa Fluor 405 (*surrogate grey*) – for F-actin cytoskeleton.

[1] I. Andriulė et al., „Evidence for the expression of TRPM6 and TRPM7 in cardiomyocytes from all four chamber walls of the human heart," Sci. Rep., vol. 11, no. 1, pp. 1–14, 2021.

MOONLIGHTING CHAPERONE ACTIVITY OF S100A12 WITHIN THE S100A FAMILY

Orestas Antipas Pelivanov[1,2], Darius Šulskis[1]

[1]Vilnius University, Life Sciences Center, Institute of Biotechnology, Lithuania
[2]Vilnius University, Faculty of Chemistry and Geosciences, Lithuania
orestas.pelivanov@chgf.stud.vu.lt

The S100A family consists of 24 calcium-binding proteins that participate in a wide range of cellular processes, including regulation of cell signaling, immune responses and other vital functions. Dysregulation of S100A proteins has been associated with inflammatory and neurodegenerative diseases [1], [2]. S100A8 and S100A9 are known to form amyloid-like oligomers, fibrils or amorphous aggregates [3], whereas the stability of S100A12 under physiological conditions is unknown, but has been proposed to exhibit moonlighting chaperone behavior as a secondary function [4]. Therefore, we investigated whether S100A12 can alter or inhibit the aggregation behavior of S100A8 and S100A9.

Protein aggregation was monitored in vitro using the amyloid-specific Thioflavin T (ThT) fluorescent probe in a microplate reader in the presence or absence of calcium ions. Protein thermal stability was determined by differential scanning fluorimetry (DSF) by monitoring the fluorescence of the 8-anilinonaphthalene-1-sulfonic acid (ANS) dye.

The results (Fig. 1) showed that in the absence of Ca^{2+}, S100A9 rapidly formed fibrils and S100A8 aggregated more slowly, matching previously reported data [3], whereas the S100A12 sample exhibited no increase in ThT fluorescence, indicating a lack of amyloid formation. On the other hand, co-incubation with S100A12 significantly reduced the aggregation of S100A9 in the presence of Ca^{2+}, while altering the aggregation of S100A8. Furthermore, the melting temperature of S100A12 was higher than that of S100A8 and S100A9, in agreement with the aggregation experiments. Overall, these results suggest that S100A12 can modulate the aggregation behavior of the S100A protein family and is a stable protein.

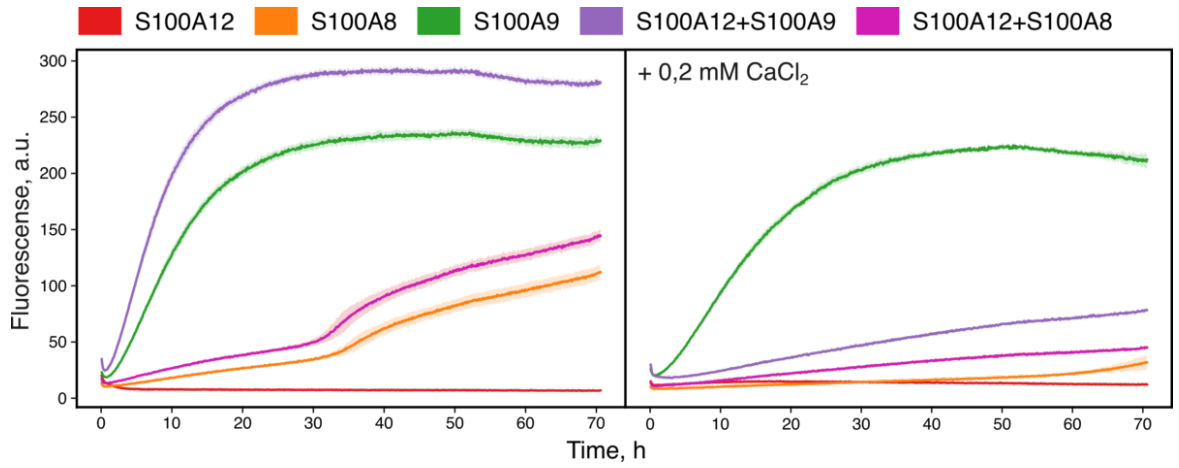


Fig. 1. ThT fluorescence kinetics of S100A8, S100A9 and S100A12 aggregation in the absence and presence of calcium ions

[1] J. S. Cristóvão and C. M. Gomes, "S100 Proteins in Alzheimer's Disease," Front. Neurosci., vol. 13, May 2019, doi: 10.3389/fnins.2019.00463.
[2] I. Marenholz, C. W. Heizmann, and G. Fritz, "S100 proteins in mouse and man: from evolution to function and pathology (including an update of the nomenclature)," Biochem. Biophys. Res. Commun., vol. 322, no. 4, pp. 1111–1122, Oct. 2004, doi: 10.1016/j.bbrc.2004.07.096.
[3] I. Baronaitė, D. Šulskis, A. Kopūstas, M. Tutkus, and V. Smirnovas, "Formation of Calprotectin Inhibits Amyloid Aggregation of S100A8 and S100A9 Proteins," ACS Chem. Neurosci., vol. 15, no. 9, pp. 1915–1925, May 2024, doi: 10.1021/acschemneuro.4c00093.
[4] T. Hatakeyama, M. Okada, S. Shimamoto, Y. Kubota, and R. Kobayashi, "Identification of intracellular target proteins of the calcium-signaling protein S100A12," Eur. J. Biochem., vol. 271, no. 18, pp. 3765–3775, 2004, doi: 10.1111/j.1432-1033.2004.04318.x.

REPROGRAMMING INHIBITOR-ENZYME RECOGNITION PROFILE VIA CHIMERIC CARBONIC ANHYDRASE I

Ignas Glušnys[1], Aurelija Mickevičiūtė[1], Daumantas Matulis[1], Joana Smirnovienė[1]

[1]Vilnius University, Life Sciences Center, Institute of Biotechnology, Department of Biothermodynamics and Drug Design, Vilnius, Lithuania
ignas.glusnys@gmc.stud.vu.lt

Achieving isoform selectivity in carbonic anhydrase (CA) inhibition is a persistent hurdle in pharmacology, primarily due to the high structural conservation among the twelve catalytically active human CA isoforms. Carbonic anhydrases catalyze the reversible hydration of carbon dioxide to bicarbonate and protons. Their isoforms play roles in numerous physiological and pathological processes by regulating the pH and bicarbonate balance [1]. While CA II serves as the prototypical drug target for conditions like glaucoma and epilepsy, the CA I isoform frequently acts as an unintended off-target, leading to undesirable systemic side effects. To isolate and validate the molecular drivers of this specific selectivity, a protein engineering strategy was employed to create chCA I, a chimera built upon the CA II scaffold but containing CA I-specific active site residues. The aim was to assess whether these mutations alone are sufficient to switch the inhibitor recognition profile from CA II to CA I and analyze structural differences between CA I and CA II.

The binding affinities of a focused set of sulfonamide-containing inhibitors were analyzed against human CA I, CA II, and the engineered chCA I. The binding constants (K_b) were determined using the fluorescent thermal shift assay (FTSA, also known as Thermofluor®). This method allows for the precise quantification of ligand-induced thermal stabilization, which correlates directly with binding affinity [2]. Data processing and parameter calculation were performed using the online Thermott software (Thermott.com, Figure 1) [3].

Analysis of the thermodynamic parameters revealed that the introduction of CA I-specific active site mutations in CA II caused the chimeric protein to recognize sulfonamide inhibitors with affinities closely mirroring those of native CA I. Compounds that exhibited high affinity for CA I but low affinity for CA II bound to chCA I with high affinity, effectively ”switching” the enzyme’s preference. The results demonstrate that a set of active site residues is sufficient to dictate the isoform-selective binding profile of CA I, since the chimeric CA I successfully mimics the ligand recognition properties of CA I. The characterized chCA I protein may therefore serve as a useful model for screening and designing highly CA I-selective inhibitors, potentially reducing off-target interactions in future therapeutic developments.

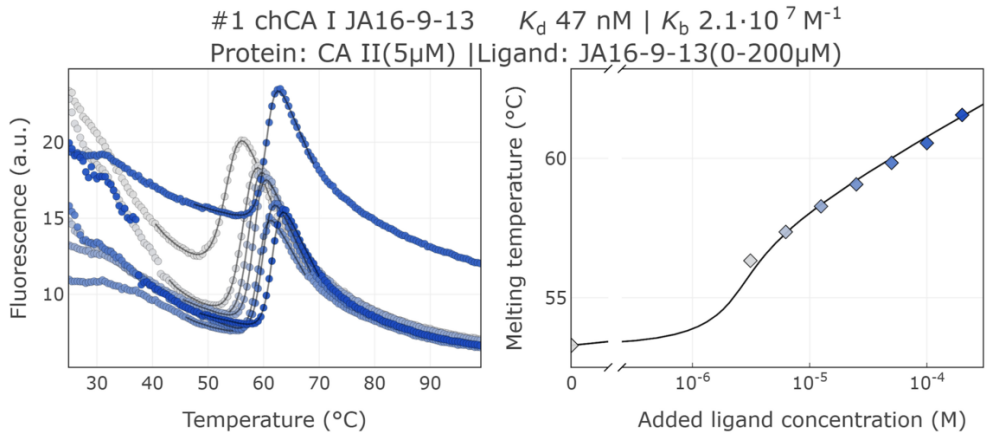


Fig. 1. Fluorescent thermal shift assay (FTSA) results of chimeric carbonic anhydrase I binding to compound JA16-9-13 – symbols correspond to experimental data, while the line shows fitting using the K_d determination model. Data fitted and figure prepared using Thermott [3].

[1] J. Smirnovienė et al., “Switching the Inhibitor-Enzyme recognition profile via chimeric carbonic anhydrase XII,” ChemistryOpen, vol. 10, no. 5, pp. 567–580, May 2021, doi: 10.1002/open.202100042.
[2] V. Petrauskas, E. Kazlauskas, M. Gedgaudas, L. Baranauskienė, A. Zubrienė, and D. Matulis, “Thermal shift assay for protein–ligand dissociation constant determination,” TrAC Trends in Analytical Chemistry, vol. 170, p. 117417, Nov. 2023, doi: 10.1016/j.trac.2023.117417.
[3] M. Gedgaudas, D. Baronas, E. Kazlauskas, V. Petrauskas, and D. Matulis, “Thermott: A comprehensive online tool for protein–ligand binding constant determination,” Drug Discovery Today, vol. 27, no. 8, pp. 2076–2079, May 2022, doi: 10.1016/j.drudis.2022.05.008.

FACTORS AFFECTING THE LONG-TERM COEVOLUTION OF STREPTOCOCCUS THERMOPHILUS AND ITS LYTIC PHAGE 2972

Yana Karnitskaya[1], Laurynas Vaitkus[1], Giancarlo Russo[1]

[1]Vilnuis University, Life Sciences Centre, VU-EMBL Partnership Institute for Genome Editing Technology, Vilnius, Lithuania
yana.karnitskaya@gmc.vu.lt

Clustered regularly interspaced short palindromic repeats (CRISPR) and CRISPR-associated protein (Cas) systems are widely recognized as advanced genome engineering tools. Their main function in nature is to provide adaptive immunity for bacteria and archaea. They achieve this by detecting and usually cutting specific DNA or RNA sequences that match unique spacers found between CRISPR [1]. While bacteria with CRISPR-Cas systems can coevolve with phages over time in nature, laboratory studies are constrained by limited model systems. Most bacteria do not develop CRISPR-based immunity against phages or plasmids in laboratory settings or do so at exceptionally low rates detectable only by deep sequencing. To date, only *Streptococcus thermophilus* and *Pseudomonas aeruginosa* reliably evolve CRISPR immunity under laboratory conditions [2].

This study aims to deepen our understanding of how *S. thermophilus* DGCC7710 and its lytic phage adapt to one another over time, thereby potentially forming innovative genome-editing strategies. To achieve this, long-term coevolution experiments have been conducted, along with the optimization of previously used methods for bacterial cell counting.

As a result, a new factor has been suggested as highly influential for the host-virus dynamics.

[1] J. Y. Wang, P. Pausch, and J. A. Doudna, “Structural biology of CRISPR–Cas immunity and genome editing enzymes,” Nat. Rev. Microbiol., vol. 20, no. 11, pp. 641–656, Nov. 2022, doi: 10.1038/s41579-022-00739-4.

[2] J. Common, D. Morley, E. R. Westra, and S. van Houte, “CRISPR-Cas immunity leads to a coevolutionary arms race between Streptococcus thermophilus and lytic phage,” Philosophical Transactions of the Royal Society B: Biological Sciences, vol. 374, no. 1772, p. 20180098, May 2019, doi: 10.1098/rstb.2018.0098.

BREWING DIVERSITY: PHENOTYPIC AND MOLECULAR CHARACTERIZATION OF YEAST FROM TRADITIONAL LITHUANIAN BEERS

Paulina Morkytė[1], Justina Stonytė[1], Rasa Pauliukaitė[1]

[1]Center for Physical Sciences and Technology (FTMC), Department of Nanoengineering, Lithuania
paulina.morkyte@ftmc.lt

Traditional farmhouse beers are products of spontaneous fermentation, which harbor diverse and local microbial communities [1]. In this study, yeast diversity was investigated in 19 unfiltered traditional Lithuanian home-brewed beer samples. Microorganisms were isolated and cultivated on Wallerstein Laboratory (WL) agar, where distinct colony morphologies were differentiated based on color, texture, and agar color reactions. In total, ten morphologically distinct yeast-like colony types were identified, indicating metabolic heterogeneity among isolates. Microscopic examination revealed predominantly oval to round yeast cells, with observable variation in cell size between different morphotypes. Molecular identification was performed by PCR amplification of the fungal internal transcribed spacer (ITS) region, confirming the presence of *Saccharomyces*-type yeasts as well as non-*Saccharomyces* representatives. The results demonstrate considerable diversity within traditional Lithuanian beer fermentations, highlighting microbial biodiversity preserved through traditional brewing practices.

[1] M. Iorizzo, F. Coppola, F. Letizia, B. Testa, and E. Sorrentino, “Role of Yeasts in the Brewing Process: Tradition and Innovation,” Processes 2021, Vol. 9, Page 839, vol. 9, no. 5, p. 839, May 2021, doi: 10.3390/PR9050839.

GENETIC STRUCTURE AND DIVERSITY OF RED DEER (CERVUS ELAPHUS) POPULATIONS IN LITHUANIA

Jokūbas Čypas[1], Evelina Genevičienė[1], Loreta Griciuvienė[1], Irma Ražanskė[1], Artūras Kibiša[1], Algimantas Paulauskas[1]

[1]Vytautas Magnus University, Lithuania
jokubas.cypas@stud.vdu.lt

The genetic structure of European red deer populations is influenced by both natural and anthropogenic factors, including historical and recent introductions. These processes may increase the risk of interspecific hybridization and contribute to uncertainty regarding the genetic status of local populations. Due to limited genetic monitoring, data on the genetic status and diversity of local red deer populations remain scarce in many regions. This study was aimed at assessing the genetic diversity of red deer (Cervus elaphus) in Lithuania using molecular genetic markers and identifying possible signs of heterogeneity in genetic origin.

In this study, molecular genetic markers were used, including an intron fragment of the Y-chromosome zfy gene and mitochondrial DNA sequences. Samples from red deer and individuals of unknown genetic origin were analyzed. The obtained sequences were compared with reference sequences available in the GenBank database, and phylogenetic analyses were performed using MEGA software.

The genetic data of Lithuanian red deer individuals showed close similarity to other European populations, including individuals from Scotland and Norway that have traditionally been classified as different subspecies (Cervus elaphus scoticus, C. e. atlanticus). Meanwhile, the genetic data of individuals of unknown origin exhibited higher genetic variability, possibly indicating a different genetic origin.

Overall, these preliminary results suggest that Lithuanian red deer are genetically similar to other European populations; however, more extensive sampling and additional genetic markers are required for a comprehensive assessment of population genetic structure and origin.

GENETIC DIVERSITY OF MICROORGANISM ASSOCIATED WITH MAKEUP FOUNDATIONS AND APPLICATION TOOLS

Ugnė Januškaitė[1], Saulė Norkutė[1], Asta Aleksandravičienė[1], Žaneta Maželienė[1], Giedrė Jarienė[1]

[1]Kauno Kolegija, Faculty of Medicine, Pramones pr. 20, LT-50468 Kaunas, Lithuania
ugne.jan529@go.kauko.lt

Decorative cosmetics, particularly makeup foundations and their application tools, are widely used in daily personal care routines and may serve as a source of microbial accumulation and transmission[1]. Microorganisms detected in these products may originate from the natural human skin microbiota as well as from environmental sources or improper usage practices, including potentially pathogenic species[2]. The genetic diversity of microorganisms in cosmetic products remains insufficiently explored, particularly in the context of long-term product use and repeated contact with the skin. Molecular analyses enabling the identification of bacterial genotypes are essential for understanding microbial diversity, tracking potential sources of contamination, and assessing possible health risks associated with cosmetic product use[3].

The aim of this study was to evaluate the genetic diversity of microorganisms found in makeup foundations and the application tools used with them.

Genomic DNA was extracted from bacterial isolates obtained from makeup foundation samples using the PureLink Genomic DNA Mini Kit according to the manufacturer's instructions. Bacterial identification was performed by PCR amplification of an approximately 1500 bp fragment of the 16S rRNA gene using universal primers 27F and 1541R, followed by agarose gel electrophoresis and visualization under UV light. Representative PCR products were purified, sequenced, and analyzed using MEGA X software, with sequence comparison performed against the GenBank database using NCBI BLAST.

A total of four microorganisms were identified in makeup foundations and their application tools, comprising two distinct fungal species and two bacterial species. The fungal species detected were Aspergillus oryzae and Penicillium hordei, while the bacterial species included Priestia aryabhattai and Achromobacter xylosoxidans. The presence of both fungal and bacterial taxa indicates mixed contamination patterns, likely influenced by repeated product use and environmental exposure.

The results of this study demonstrate the presence of both fungi and bacteria in makeup foundations and their application tools, which may contribute to the development of health-related issues, emphasizing the necessity for further research.

[1] M. Almukainzi, L. Alotaibi, A. Abdulwahab, N. Albukhary, and A. M. E. Mahdy, "Quality and safety investigation of commonly used topical cosmetic preparations," Scientific Reports, vol. 12, no. 1, p. 18299, Oct. 2022, doi: 10.1038/s41598-022-21771-7.

[2] I. K. Bedaida et al., "Makeup testers as reservoirs and transmission sources of antibiotic resistant bacteria," Infection Disease & Health, vol. 30, no. 3, pp. 211–216, Mar. 2025, doi: 10.1016/j.idh.2025.03.001.

[3] M. Ivashko, S. Burmei, L. Yusko, T. Chaikovska, and N. Boyko, "Microbiological diagnostics: From traditional to molecular genetic methods: A literature review," Bulletin of Medical and Biological Research, vol. 5, no. 4, pp. 34–41, Oct. 2023, doi: 10.61751/bmbr/4.2023.34.

PREVALENCE AND MOLECULAR CHARACTERIZATION OF ANAPLASMAPHAGOCYTOPHILUM IN TICKS FROM URBANIZED AND NATURAL HABITATS OF LITHUANIA

Queen Uyojo Omale[1], Justina Snegiriovaitė[1], Indrė Lipatova[1], Miglė Razgūnaitė[1], Algimantas Paulauskas[1], Jana Radzijevskaja[1]

[1]Vytautas Magnus University
queen.uyojo.omale@stud.vdu.lt

Anaplasma phagocytophilum is a tick-borne bacterium belonging to the family Anaplasmataceae, which causes human granulocytic anaplasmosis (HGA), tick-borne fever (TBF), and granulocytic infections in animals. While wild ruminants and small mammals play a central role in maintaining A. phagocytophilum in nature, a wide range of other animals (e.g., bears, foxes, wild boars, horses, and reptiles) may also act as occasional hosts or reservoirs. Across Europe, the pathogen shows broad geographic distribution and substantial genetic diversity with host and regional specificity. [1-2] However, data on the presence of A. phagocytophilum in ticks from urban environments remain limited, which is of particular concern given the pathogen's nonspecific clinical presentation and the potential risk it poses to human and companion animals health.

The aim of this study was to determine the prevalence and molecular characterization of A. phagocytophilum in ticks collected from urban and natural habitats in Lithuania. A total of 329 questing I. ricinus and D. reticulatus ticks were collected by flagging in two urban parks and one natural area (border of a wood) in Lithuania in 2023. The presence of A. phagocytophilum DNA in ticks was screened by real-time PCR for the msp2 gene. A. phagocytophilum strains were characterized based on the msp4 and groEL gene sequences.

The overall infection rate of A. phagocytophilum in ticks was 6.68% (22/329) and in different parks varied from 4.30% to 9.03%, while in the natural area, 4.94%. Anaplasma phagocytophilum was more frequent in I. ricinus (21/302) than in D. reticulatus (1/27). Two A. phagocytophilum ecotypes, ecotype I and ecotype II, were detected. Ecotype I has previously been detected in a wide range of hosts and is associated with HGA and TBF. In contrast, ecotype II has primarily been found in roe deer and moose and is currently considered non-zoonotic. [3]

Our findings confirm the presence of A. phagocytophilum in urbanized areas of Lithuania and the potential risk of anaplasmosis for city residents and their companion animals.

Acknowledgements
This study was supported by the Research Council of Lithuania (Grant No. S-MIP-23/19).

Keywords: Anaplasma phagocytophilum, ticks, urban parks, Lithuania

[1] S. Stuen, E. G. Granquist, and C. Silaghi, "Anaplasma phagocytophilum—a widespread multi-host pathogen with highly adaptive strategies," Frontiers in Cellular and Infection Microbiology, vol. 3, p. 31, Jan. 2013, doi: 10.3389/fcimb.2013.00031.

[2] S. Szekeres et al., "Candidatus Neoehrlichia mikurensis and Anaplasma phagocytophilum in natural rodent and tick communities in Southern Hungary," Ticks and Tick-borne Diseases, vol. 6, no. 2, pp. 111–116, Nov. 2014, doi: 10.1016/j.ttbdis.2014.10.004.

[3] J. Snegiriovaitė, I. Lipatova, M. Razgūnaitė, A. Paulauskas, and J. Radzijevskaja, "Molecular Surveillance of Neoehrlichia mikurensis and Anaplasma phagocytophilum in Ticks from Urbanized Areas of Lithuania," Pathogens, vol. 14, no. 7, p. 642, Jun. 2025, doi: 10.3390/pathogens14070642.

USE OF BACTERIAL OUTER MEMBRANE VESICLES IN COMBINED ANTIBIOTIC AND PHOTODYNAMIC THERAPY AGAINST ACINETOBACTER BAUMANNII

Ingrida Tarabildienė[1], Irina Buchovec[2], Jūratė Skerniškytė[1]

[1]Vilnius University, Life Sciences Center, Institute of Biosciences, Department of Biochemistry and Molecular Biology, Lithuania
[2]Vilnius University, Faculty of Physics, Institute of Photonics and Nanotechnology, Lithuania
ingrida.tarabildiene@gmc.stud.vu.lt

Acinetobacter baumannii is a Gram-negative opportunistic pathogen, which emerged as a prevalent cause of nosocomial infections. Due to the rise of multidrug-resistant strains and high morbidity and mortality, *A. baumannii* has been added to the World Health Organization priority list of drug-resistant bacteria [1].

Emerging strategies to address this challenge include advanced drug-delivery systems. Outer membrane vesicles (OMVs) naturally shed by Gram-negative bacteria could aid in the efficient transfer of antibiotics due to their structural similarity to bacterial membranes [2]. Another approach is antimicrobial photodynamic therapy (aPDT), in which a visible-light-activated photosensitizer generates reactive oxygen species (ROS) that cause lethal oxidative damage to microbial cells. Because ROS target multiple biomolecular structures in a non-specific manner, including membranes, proteins, and nucleic acids, classical antibiotic resistance mechanisms are effectively bypassed, minimizing the likelihood of developing further resistance [3].

In this study, we compared the susceptibility of two *A. baumannii* strains to aPDT and antibiotic therapy used in combination with OMVs. Gentamicin, a widely prescribed aminoglycoside, was used on both strains. The antibiotic was loaded into OMVs using sonication. Photosensitizers for aPDT were chosen to be water soluble and non-toxic: chlorophyllin – a semi-synthetic chlorophyll derivative, and riboflavin - also known as vitamin B2. Samples were irradiated using an LED light source (350 W/m^2), with activation wavelengths of 402 nm for chlorophyllin and 440 nm for riboflavin. Photosensitizer concentrations used for biofilms were tenfold higher than those applied to planktonic cells. The effects of aPDT and OMV-mediated delivery of antibiotics on bacterial viability were assessed by counting colony-forming units (CFUs).

The results demonstrate a 1.58 and 1.77 log_{10} CFU/mL decrease in planktonic cell viability after 4 h incubation with gentamicin encapsulated in OMVs compared to free gentamicin. The combination of aPDT and antibiotics reduced viability more (1.00–1.67 log_{10} CFU/mL) than either aPDT (0.02–0.87 log_{10} CFU/mL) or antibiotics alone (0.21–0.50 log_{10} CFU/mL). Gentamicin administration either before or after aPDT produced comparable effects. In contrast, no additional benefit of OMV-mediated antibiotic delivery was observed in biofilm-associated cells, which may be due to extracellular matrix interference with OMV penetration. These findings indicate that OMV-based antibiotic delivery is more effective against planktonic cells than biofilm-associated cells, whereas aPDT provides the most significant benefit in combined treatments targeting biofilms.

[1] C. A. Moubareck and D. H. Halat, “Insights into Acinetobacter baumannii: A Review of Microbiological, Virulence, and Resistance Traits in a Threatening Nosocomial Pathogen,” Antibiotics, vol. 9, no. 3, p. 119, Mar. 2020, doi: 10.3390/antibiotics9030119.
[2] S. M. Collins and A. C. Brown, “Bacterial outer membrane vesicles as antibiotic delivery vehicles,” Frontiers in Immunology, vol. 12, p. 733064, Sep. 2021, doi: 10.3389/fimmu.2021.733064.
[3] V. Bustamante and C. E. Palavecino, “Effect of photodynamic therapy on multidrug-resistant Acinetobacter baumannii: A scoping review,” Photodiagnosis and Photodynamic Therapy, vol. 43, p. 103709, Jul. 2023, doi: 10.1016/j.pdpdt.2023.103709.

A SECRET ALLIANCE BETWEEN SPLIT PROKARYOTIC ARGONAUTE PROTEINS AND TYPE I RESTRICTION - MODIFICATION SYSTEMS

Laura Juozepavičiūtė[1], Edvardas Golovinas[1], Mindaugas Zaremba[1]

[1]Vilnius University, Life Sciences Center, Institute of Biotechnology, Department of Protein-DNA Interactions
laura.juozepaviciute@gmc.vu.lt

The ability to discriminate host DNA from foreign genetic material at the molecular level is fundamental to bacterial survival and evolution. The bacterial defense forces against genetic elements of exogenous origin are frequently clustered within genomic regions known as defense islands. This pattern suggests that genes of unknown function, which are consistently found near established defense systems, likely serve protective roles or may work synergistically with adjacent systems [1], [2]. Three split prokaryotic Argonaute (pAgo) operons have been identified in the genomes of thermophilic bacteria. Unpublished bioinformatic analyses from our laboratory indicate that these split pAgos, together with associated HEPN domain-containing nucleases, are embedded within operons encoding type I restriction-modification (RM) systems (Fig.1). This genomic co-localization suggests potential cooperation between these defense pathways.

The objective of this study is to investigate whether split pAgos and their associated type I RM systems function cooperatively to enhance bacterial defense against exogenous genetic elements *in vivo*. To model this alliance, genetically modified *Escherichia coli* strains have been constructed using Argonaute-mediated homologous recombination to integrate relevant defense modules into the genome [3]. The further experimental workflow includes the assessment of cytotoxic effects of individual components and their combinations, followed by functional assays to evaluate protection against plasmid acquisition and bacteriophage infection.

Understanding such alliances may provide insight into how bacteria deploy layered immune strategies to limit the constant influx of invading genetic elements.

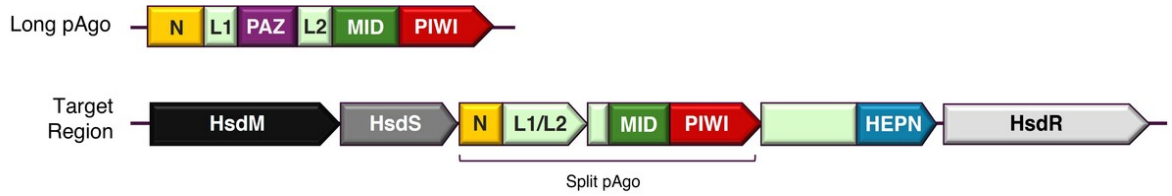


Fig. 1. Schematic representation of the genomic region encoding the target defense systems. For comparison, the domain architecture of a long pAgo is shown.

[1] S. Doron et al., "Systematic discovery of antiphage defense systems in the microbial pangenome," Science, vol. 359, no. 6379, Jan. 2018, doi: 10.1126/science.aar4120.

[2] K. S. Makarova, Y. I. Wolf, S. Snir, and E. V. Koonin, "Defense islands in bacterial and archaeal genomes and prediction of novel defense systems," Journal of Bacteriology, vol. 193, no. 21, pp. 6039–6056, Sep. 2011, doi: 10.1128/jb.05535-11.

[3] L. Fu et al., "The prokaryotic Argonaute proteins enhance homology sequence-directed recombination in bacteria," Nucleic Acids Research, vol. 47, no. 7, pp. 3568–3579, Jan. 2019, doi: 10.1093/nar/gkz040.

MOLECULAR DETECTION OF RICKETTSIA PATHOGENS IN ECTOPARASITES OF RED FOXES

Raminta Likšaitė[1], Ugnė Medikaitė[1], Indrė Lipatova[1], Justina Snegiriovaitė[1], Renata Špinkytė[1], Algimantas Paulauskas[1]

[1]Vytautas Magnus University, Kaunas, Lithuania
raminta.liksaite@stud.vdu.lt

The population of red foxes (Vulpes vulpes) has increased rapidly over recent decades, raising concerns about their role as reservoirs of parasites and pathogens of veterinary and medical importance [1,2]. Ectoparasites associated with foxes may contribute to the maintenance and transmission of zoonotic pathogens, including bacteria of the genus Rickettsia [3]. However, data on the occurrence of Rickettsia spp. in fox ectoparasites remain limited. The aim of this study was to evaluate the presence of Rickettsia spp. pathogens in ectoparasites collected from red foxes using molecular methods.

Ectoparasites were collected from nine red foxes and identified morphologically. DNA was extracted from individual ectoparasites, and Rickettsia spp. were detected using real-time PCR targeting the gltA gene. Positive samples were further analyzed by nested PCR amplifying a 381 bp fragment of the gltA gene, followed by sequencing for species identification.

A total of 109 ectoparasites were collected, including fleas (80.73%, n = 88) and ticks (19.27%, n = 21). Rickettsia DNA was detected in 9.52% of ticks (2/21) and 1.83% of fleas (2/88). Sequence analysis identified Rickettsia spp., Rickettsia helvetica,and Rickettsia conorii subsp. raoultii. These findings demonstrate the presence of several zoonotic Rickettsia species in fox-associated ectoparasites. The detection of pathogenic Rickettsia species in ectoparasites of red foxes highlights their potential role in the circulation of zoonotic pathogens. These results emphasize the importance of monitoring wildlife ectoparasites to better understand the epidemiology and public health risks associated with Rickettsia infections.

Acknowledgements

This research was partially supported by the Research Fund of Vytautas Magnus University (Kaunas, Lithuania) through project No. P-N-25-02.

Keywords: Rickettsia, Vulpes vulpes, ticks, fleas

[1] B. Goldyn, M. Hromada, A. Surmacki, and P. Tryjanowski, “Habitat use and diet of the red foxVulpes vulpes in an agricultural landscape in Poland,” European Journal of Wildlife Research, vol. 49, no. 3, pp. 191–200, Sep. 2003, doi: 10.1007/bf02189737.

[2] P. M. Lesiczka et al., “Red fox (Vulpes vulpes) play an important role in the propagation of tick-borne pathogens,” Ticks and Tick-borne Diseases, vol. 14, no. 1, p. 102076, Nov. 2022, doi: 10.1016/j.ttbdis.2022.102076.

[3] G. Liu et al., “Rickettsiae in red fox (Vulpes vulpes), marbled polecat (Vormela peregusna) and their ticks in northwestern China,” Parasites & Vectors, vol. 14, no. 1, p. 204, Apr. 2021, doi: 10.1186/s13071-021-04718-1.

REFINING PRECLINICAL SCREENING: 3D CELL CULTURE MODELS AS A TOOL FOR ASSESSING TARGETED THERAPIES IN ENDOMETRIAL CANCER

Laura Marija Račytė[1], Evelina Šidlovska[2], Margarita Montrimaitė[3], Gediminas Januška[3], Rūta Čiurlienė[3], Eglė Žalytė[1]

[1]Life Sciences Center, Institute of Biosciences, Department of Biochemistry and Molecular Biology, Vilnius, Lithuania
[2]National Center of Pathology, Vilnius, Lithuania
[3]National Cancer Center, Vilnius, Lithuania
laura.racyte@gf.stu.vu.lt

Endometrial cancer is one of the most common female cancers, with a high incidence in Europe, especially in Central and Eastern Europe [1]. The development of the disease is determined by a number of interrelated factors, including hormonal imbalances, metabolic disorders, genetic predisposition, higher body mass index and older age [2]. Despite the effectiveness of surgical treatment in the early stages of the disease, some patients require additional systemic treatment, the results of which are not always optimal.

Following surgical intervention, adjuvant chemotherapy or radiotherapy is administered to patients stratified with even a minimal risk of recurrence to improve oncological outcomes. Unfortunately, standard chemotherapy based on platinum compounds and taxanes often has limited selectivity and causes significant side effects. For these reasons, increasing attention is paid to targeted therapy strategies that affect specific molecular signaling pathways and provide the basis for more precise and personalized treatment [3]. The PI3K/AKT/mTOR pathway, receptor tyrosine kinases inhibitors, various cell cycle, proliferation and survival regulators, PARP polymerase and the nuclear transport system have been identified as potential targets for endometrial cancer therapy.

In order to evaluate the efficacy of such compounds, suitable preclinical models that can reflect the biological complexity of the tumor are necessary. For a long time, two-dimensional (2D) cell cultures have dominated cancer research, but they do not adequately reproduce the tumor microenvironment, cell-cell interactions, and spatial structure. In recent years, three-dimensional (3D) cell culture models, such as spheroids and aggregates, have become increasingly popular, which better mimic This *in vivo* conditions, including diffusion gradients, tumor heterogeneity, and extracellular matrix-dependent signaling pathways [4]. Due to these properties, 3D models are considered more suitable for studying drug response and tumor behavior.

In our previous studies the effects of targeted therapy compounds on 2D and 3D model systems of endometrial cancer cells were evaluated by analyzing the metabolic activity of the cells. In order to more fully characterize the biological effects of these compounds, this work was supplemented with fluorescence microscopy data, which allows us to distinguish between metabolic activity and cell death in 3D cultures. Additionally, quantitative PCR (qPCR) was employed to characterize 3D cultures by changes in the expression of endometrial cancer and stemness markers compared to 2D models. Such methodological expansion provides an opportunity for a more comprehensive assessment of the action of targeted therapies and a better understanding of the response of endometrial cancer cells to treatment.

Acknowledgements

This work was funded by Vilnius University Science Promotion Fund (project no. MSF-JM-17/2022), Future Biomedicine Fund (project no. (1.78) SU-442) and Research Council of Lithuania (project no. S-ST-24-101).

Keywords: endometrial cancer, spheroids, targeted therapy

[1] F. Bray et al., “Global cancer statistics 2022: GLOBOCAN estimates of incidence and mortality worldwide for 36 cancers in 185 countries,” CA a Cancer Journal for Clinicians, vol. 74, no. 3, pp. 229–263, Apr. 2024, doi: 10.3322/caac.21834.
[2] V. Makker et al., “Endometrial cancer,” Nature Reviews Disease Primers, vol. 7, no. 1, p. 88, Dec. 2021, doi: 10.1038/s41572-021-00324-8.
[3] M. Remmerie and V. Janssens, “Targeted therapies in Type II endometrial cancers: Too little, but not too late,” International Journal of Molecular Sciences, vol. 19, no. 8, p. 2380, Aug. 2018, doi: 10.3390/ijms19082380.
[4] Y. M. Salinas-Vera et al., “Three-Dimensional 3D culture models in gynecological and breast cancer research,” Frontiers in Oncology, vol. 12, p. 826113, May 2022, doi: 10.3389/fonc.2022.826113.

CRISPR-CAS SYSTEMS VALIDATION USING A FLUORESCENT REPORTER CELL LINE

Rugilė Tūskaitė[1,2], Neringa Daugelavičienė[1,2], Eimina Dirvelytė-Valauskė[1,2], Simonas Kutanovas[1,2], Urtė Neniškytė[1,2]

[1]Vilnius University, Life Sciences Center, VU LSC-EMBL Partnership for Genome Editing Technologies, Vilnius, Lithuania
[2]Vilnius University, Life Sciences Center, Institute of Bioscience, Vilnius, Lithuania
rugile.tuskaite@gmc.stud.vu.lt

CRISPR-Cas systems are molecular mechanisms in bacteria and archaea that are responsible for protecting these prokaryotes from mobile genetic elements. Owing to their programmable nuclease activity, these systems have become widely used tools for genome editing not only in prokaryotic cells, but also in mammalian cells. In bacteria, CRISPR-Cas systems are validated using plasmid interference, PAM depletion, and/or phage assays [1,3]. In mammalian cells, validation is performed by RT-qPCR, Western blot and sequencing [2,3]. These methods are time consuming and require specific equipment and skills, which is why a more straightforward way of validating new CRISPR-Cas systems is needed.

The aim of this study was to apply the mouse neuroblastoma Neuro-2a KI: EGFP-mRUBY2-PURO cell line, which was derived in our laboratory, for the validation of CRISPR-Cas systems. These cells stably express EGFP (green fluorescent protein) in their nuclei and mRuby2 (red fluorescent protein) in the membrane. To assess whether these cells can be used for screening new gene editing tools and evaluating their efficiency, Neuro-2a cells were transfected with a plasmid encoding SaCas9 and *EGFP*-targeting gRNA. *EGFP* knock-out efficiency was evaluated by fluorescence microscopy. EGFP fluorescence was analysed on days 3, 5, 7, and 10 after transfection to determine the optimal time point for *EGFP* knock-out analysis.

The results demonstrated that SaCas9 efficiently disrupted the *EGFP* gene at all analysed time points. On day 5 post-transfection, less than 10% of transfected cells remained EGFP-positive, compared to 91.78% in the control group. These findings indicate that fluorescent reporter cell lines may serve as a simple and effective platform for screening and validating novel CRISPR-Cas systems in mammalian cells.

[1] D. Burstein et al., “New CRISPR–Cas systems from uncultivated microbes,” Nature, vol. 542, no. 7640, pp. 237–241, Dec. 2016, doi: 10.1038/nature21059.
[2] J. Fueller et al., “CRISPR-Cas12a–assisted PCR tagging of mammalian genes,” The Journal of Cell Biology, vol. 219, no. 6, Mar. 2020, doi: 10.1083/jcb.201910210.
[3] Y. Wang et al., “Systematic evaluation of CRISPR-Cas systems reveals design principles for genome editing in human cells,” Genome Biology, vol. 19, no. 1, p. 62, May 2018, doi: 10.1186/s13059-018-1445-x.

AMNIOTIC FLUID STEM CELL-DERIVED EXTRACELULAR VESICLES MODULATE GENE EXPRESSION IN A miR-146a-5p-INHIBITED SH-SY5Y MODEL

Greta Bertašiūtė[1], Aistė Zentelytė[1], Rūta Navakauskienė[1], Giedrė Valiulienė[1]

[1]Vilnius University, Life Sciences Center, Institute of Biochemistry, Lithuania
greta.bertasiute@gmc.stud.vu.lt

Extracellular vesicles (EVs) contain biologically active molecules, such as microRNAs (miRNAs) and proteins, and have been emerging as a promising therapeutic strategy for neurodegenerative diseases [1]. One major advantage of EVs is their ability to cross the blood-brain barrier and efficiently deliver their cargo [2]. In this study, we investigated the molecular effects of EVs derived from human amniotic fluid stem/stromal cells (hAF-SCs) on SH-SY5Y neuronal cells that had reduced activity of the anti-neuroinflammatory microRNA miR146a-5p.

For this purpose, SH-SY5Y neuroblastoma cells were differentiated into a more mature neural phenotype using a specialized differentiation medium composed of BrainPhys™ neuronal medium supplemented with Penicillin/Streptomycin, serum- and antioxidant-free B-27™, 3.7 nM BDNF receptor agonist PG-003, and 10 µM retinoic acid. EVs were isolated from the hAF-SC conditioned media using size exclusion chromatography with qEVoriginal columns. The isolated EVs were characterized based on size using scanning electron microscopy (SEM) and nanoparticle tracking analysis (NTA) (Fig.1). Additionally, molecular markers were examined through western blotting (WB) and RT-qPCR. To inhibit the activity of miR146a-5p in the neuro-differentiated SH-SY5Y model, a mirVana inhibitor was utilized in combination with Lipofectamine RNAi/MAX transfection.

The results indicated that the most commonly detected particle size was 117.5 nm, and the EVs exhibited a round morphology. The extracted hAF-SC EVs were positive for typical EV markers, such as TSG101, CD63, and ALIX. Among the miRNAs tested, miR-16-5p, miR-146a-5p, and miR-210-3p showed the highest expression levels. Treatment of SH-SY5Y cells with 70,000 hAF-SC EVs per cell over 48 hours resulted in a significant increase in the expression of genes associated with neural processes, such as *NTN3, MAGEL2, GABRD, SLURP1, P2RY4,* and *SIX1* as revealed by mRNA sequencing analysis.

In conclusion, these findings support the potential of hAF-SC EVs as a cell-free strategy for targeting neuronal molecular pathways relevant to neurodegenerative and neuroinflammatory conditions.

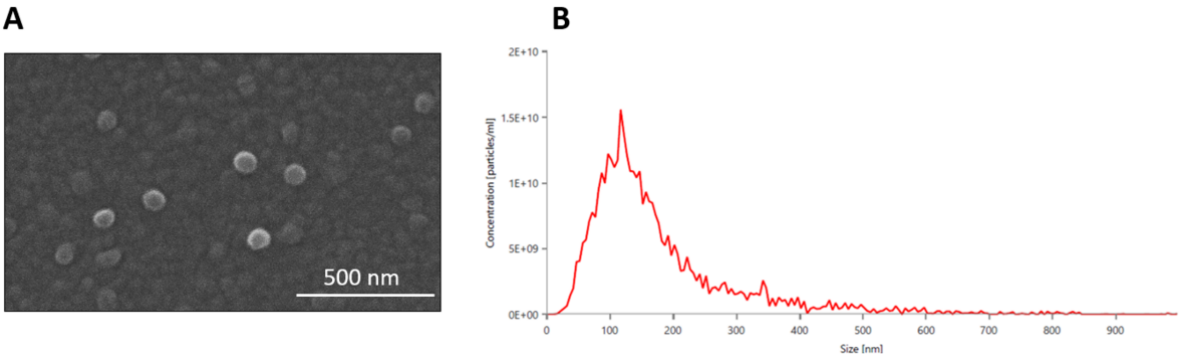


Fig. 1. Characterization of hAF-SC derived EVs. A. EV size and morphology by scanning electron microscopy (SEM); B. EV size distribution by nanoparticle tracking analysis (NTA).

[1] L. Wang, X. Zhang, Z. Yang, B. Wang, H. Gong, K. Zhang, Y. Lin, and M. Sun, "Extracellular vesicles: Biological mechanisms and emerging therapeutic opportunities in neurodegenerative diseases," Translational Neurodegeneration, vol. 13, no. 1, p. 60, 2024, doi: 10.1186/s40035-024-00453-6.

[2] X. Shi, W. He, A. Gupta, K. To, L. Clark, N. Mirle, T. Wynn, D. Wang, A. Ganesh, H. M. Zeng, and H. Wang, "Extracellular vesicles as drug and gene delivery vehicles in central nervous system diseases," Biomaterials Science, vol. 13, no. 5, pp. 1161–1178, 2025, doi: 10.1039/d4bm01394h.

ACTIVITY OF NOVEL HYDRAZONE DERIVATIVES IN 3D TUMOR SPHEROIDS AND SINGLE-CELL MIGRATION IN HUMAN BRAIN, TRIPLE-NEGATIVE BREAST, AND SKIN CANCER CELL LINES

Tomas Ragauskas[1], Juozas Kiltinavičius[2], Ingrida Tumosienė[2], Kristina Kantminienė[3], Vilma Petrikaitė[1]

[1]Lithuanian University of Health Sciences, Institute of Cardiology, Department of Drug Targets Histopathology, Lithuania
[2]Kaunas University of Technology, Department of Organic Chemistry, Lithuania
[3]Kaunas University of Technology, Department of Physical and Inorganic Chemistry, Lithuania
tomas.ragauskas@lsmu.lt

Triple-negative breast cancer accounts for less than 15% of all new cases of breast cancer, but due to its biologically aggressive and highly proliferative nature, it has a poor prognosis [1]. Melanoma is the most aggressive and severe form of skin cancer, which accounts for less than 2% of global cancer diagnoses and is the fifth most common cancer in the US [2]. The global incidence of glioblastoma is considered rare but one of the most aggressive and lethal brain tumors in adults and children, with a poor prognosis and a survival rate of 14-15 months [3]. Targeted drugs have led to major breakthroughs in cancer treatment. Therefore, hydrazone derivatives as potential kinase inhibitors are anticipated to contribute to cancer treatment. Our research aimed to evaluate the anticancer activity of hydrazone derivatives synthesized at Kaunas University of Technology (Lithuania) in human triple-negative breast, melanoma, and glioblastoma cell lines.

In our previous study, we investigated the activity of 22 hydrazone derivatives bearing substituted aromatic and different heterocyclic moieties on triple-negative breast cancer cell line MDA-MB-231, melanoma cell line IGR39, and glioblastoma cell line U87. Compounds IT199, IT207, and IT227 showed selectivity and a significant reduction of cell viability by MTT assay. In this study, we determined the compound effect on cell spheroid growth and viability at 5 μM concentration after 10 days of incubation, compared with anticancer drug dasatinib. We also investigated the impact on cell migration using a single-cell migration method in the presence of 5 μM of the tested compound during 8 hour period.

Compounds showed a lower viability-reducing effect on cancer cell 3D spheroids compared to their activity in a cell monolayer. Compound IT227 significantly reduced spheroid growth by up to 47% and viability by up to 86%, while another compound, IT207, inhibited only spheroid growth by up to 9%. IT199 reduced spheroid cell viability by up to 44% and showed little to no effect on spheroid growth. Dasatinib reduced MDA-MB-231 and U87 cell spheroid viability by approximately 49%, and IGR39 spheroid viability by less than 40%. Based on preliminary results from single-cell migration analysis, the average speed of cell migration was slightly reduced by compound IT227 on MDA-MB-231 cell line, while IT199 and IT207 had no significant effect on migration. A similar effect was observed with IGR39 and U87 cell lines.

In conclusion, compounds IT199, IT207, and IT227 showed generally weaker inhibition of spheroid formation compared to 2D monolayers. Among the tested compounds, IT227 exhibited the most pronounced anticancer activity, significantly reducing both spheroid growth and cell viability, as well as inhibiting cell migration in multiple cancer cell lines, thus indicating the compound as a promising candidate for further investigation.

Keywords: hydrazone; cell viability; tumor spheroids; cell migration

[1] A. M. Karim et al., „Triple-negative breast cancer: epidemiology, molecular mechanisms, and modern vaccine-based treatment strategies“, Biochemical Pharmacology, t. 212, p. 115545, Jun. 2023, doi: 10.1016/j.bcp.2023.115545.
[2] K. Saginala, A. Barsouk, J. S. Aluru, P. Rawla, and A. Barsouk, ‘Epidemiology of Melanoma’, Med Sci (Basel), vol. 9, no. 4, p. 63, Oct. 2021, doi: 10.3390/medsci9040063.
[3] F. Hanif, K. Muzaffar, K. Perveen, S. M. Malhi, and S. U. Simjee, ‘Glioblastoma Multiforme: A Review of its Epidemiology and Pathogenesis through Clinical Presentation and Treatment’, Asian Pac J Cancer Prev, vol. 18, no. 1, pp. 3–9, 2017, doi: 10.22034/APJCP.2017.18.1.3.

IN VITRO ANTICANCER ACTIVITY OF HYDRAZONE DERIVATIVES IN PANCREATIC CANCER CELLS UNDER NORMOXIA AND HYPOXIA

Digna Narkevičiūtė[1], Juozas Kiltinavičius[2], Ingrida Tumosienė[2], Kristina Kantminiene[3], Vilma Petrikaitė[1,4]

[1]Lithuania, Lithuanian University of Health Sciences, Department of Drug Targets Histopathology, Institute of Cardiology
[2]Lithuania, Kaunas University of Technology, Department of Organic Chemistry
[3]Lithuania, Kaunas University of Technology, Department of Physical and Inorganic Chemistry
[4]Lithuania, Vilnius University, Life Sciences Center, Institute of Biotechnology
digna.narkeviciute@stud.lsmu.lt

Pancreatic adenocarcinoma is one of the deadliest gastrointestinal cancers, accounting for over 90% of pancreatic malignancies and being frequently diagnosed at advanced stages due to late-onset symptoms and the lack of specific biomarkers [1,2]. Hypoxia within the tumor microenvironment plays a crucial role in pancreatic cancer progression by promoting aggressiveness and resistance to therapy [3].

This study aimed to evaluate the cytotoxic activity and selectivity of hydrazone derivatives synthesized at Kaunas University of Technology in human pancreatic cancer cells in vitro under normoxic and hypoxic conditions. The effects of 22 hydrazone derivatives were assessed in MIA PaCa-2 and PANC-1 cell lines using the MTT assay.

Several compounds significantly reduced cell viability, and IT199, IT206, IT207, and IT227 were selected for further analysis. Their EC_{50} values were determined in pancreatic cancer cells and human fibroblasts, with dasatinib used as a reference compound. Compared to dasatinib, the activity of the investigated hydrazone derivatives was 3–146-fold lower, depending on the cell line and oxygen conditions. Under normoxia, IT227 was the most active compound in MIA PaCa-2 (EC_{50}= 1.7 μM) and PANC-1 (EC_{50} = 4.3 μM) cells, whereas under hypoxia, IT207 (EC_{50}= 27.3 μM) and IT199 (EC_{50} = 21.7 μM) showed the highest activity. Under normoxic conditions, the compounds were largely non-selective toward cancer cells (SI ≤ 1), whereas under hypoxia, both potency and selectivity increased. Notably, IT227 demonstrated very high selectivity under hypoxia in both PANC-1 (SI = 15.9) and MIA PaCa-2 (SI = 30.3) cells, while IT207 (SI = 3.1) and IT199 (SI = 2.3) showed moderate hypoxia-associated selectivity.

In conclusion, the hydrazone derivatives exhibited differential cytotoxic effects against pancreatic cancer cell lines, with compounds containing a double hydrazone fragment showing higher activity. The most active compounds (IT199, IT206, IT207, and IT227) were 3–146-fold less potent than dasatinib. IT206, bearing a double hydrazone fragment with methyl and naphthalene substituents, demonstrated increased cytotoxic activity under hypoxic conditions but limited selectivity toward cancer cells (SI ≈ 1). Further studies are required to elucidate the mechanisms of action and therapeutic potential of the investigated compounds

Acknowledgements

I sincerely thank my supervisor for guidance and support, and Kaunas University of Technology for synthesizing the compounds used in this study.

[1] I. Skaraitė, E. Maccioni, and V. Petrikaitė, “Anticancer Activity of Sunitinib Analogues in Human Pancreatic Cancer Cell Cultures under Normoxia and Hypoxia,” International Journal of Molecular Sciences, vol. 24, no. 6, p. 5422, Jan. 2023, doi: https://doi.org/10.3390/ijms24065422.

[2] Raluca Roxana Grigorescu, Ioana Alexandra Husar-Sburlan, and C. Gheorghe, “Pancreatic Cancer: A Review of Risk Factors,” Life, vol. 14, no. 8, pp. 980–980, Aug. 2024, doi: https://doi.org/10.3390/life14080980.

[3] J. Tao et al., “Targeting hypoxic tumor microenvironment in pancreatic cancer,” Journal of Hematology & Oncology, vol. 14, no. 1, Jan. 2021, doi: https://doi.org/10.1186/s13045-020-01030-w.

SHORT-TERM PHARMACOLOGICAL MODULATION OFARTERIAL STIFFNESS IN PIGS IN VIVO

Ieva Lankutytė[1], Dominyka Adamonė[1], Vilma Zigmantaitė[1], Jonas Jurevičius[1], Regina Mačianskienė[1]

[1]Lithuanian University of Health Science, Institute of Cardiology, Laboratory of Membrane Biophysics, Sukilėlių pr. 15, Kaunas, Lithuania
ieva.lankutyte@lsmu.lt

Arterial stiffness, recognized as a marker of vascular aging, may also be influenced by various cardioactive drugs. However, the relationship between blood pressure and stiffness caused by different drugs has not yet been thoroughly characterized.

In anesthetized healthy pigs, the acute hemodynamic effects of nine vasoactive substances were systematically evaluated (Fig.1). A single intravenous bolus of each drug was administered via the ear vein, with measurements taken at peak, 5, and 30 minutes post-injection (n=3-5). Real-time measurements of systolic, diastolic, and mean arterial pressure (MAP), pulse pressure, heart rate, and carotid-femoral pulse wave velocity (PWV) were recorded and normalized to baseline. PWV was further normalized to MAP (PWV/MAP) to enable intergroup comparisons of the drug effects, revealing how the induced changes in blood pressure depend on vascular elasticity.

All compounds produced distinct, reproducible short-term hemodynamic profiles. α1 and β1 adrenergic stimulation increased PWV, whereas vasodilators and a β2-agonist decreased it. Regression modelling enabled us to evaluate the relationship between blood pressure and stiffness under different drug administrations. This study shows that arterial stiffness is dynamically regulated. We analysed how substances affecting hemodynamic properties can regulate blood pressure and vascular elasticity.

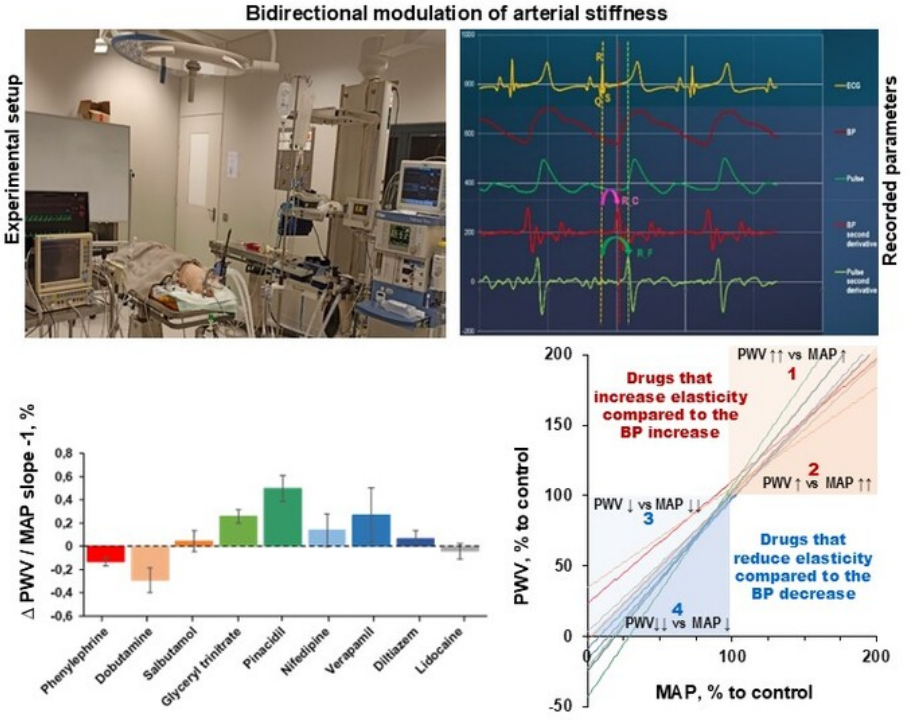


Fig. 1. Research on short-term hemodynamic modulation shows a relationship between arterial stiffness (PWV) and mean blood pressure (MAP), especially concerning substances that either increase or decrease blood pressure levels: (1) stiffness increased more than the increase in MAP, (2) stiffness increased, but less than the increase in MAP, (3) stiffness decreased, but less than the decrease in MAP, (4) and stiffness decreased more than the decrease in MAP.

RESISTANCE OF *ENTEROCOCCUS FAECIUM* BACTERIA TO COMMONLY USED DISINFECTANTS IN CLINICAL SETTING

Ernest Oleinik[1], Agnė Kirkliauskienė[2], Tatjana Kirtiklienė[1]

[1]Vilnius University, Life Science Center, Institute of Biosciences, Department of Microbiology and Biotechnology, Vilnius, Lithuania
[2]Vilnius University, Faculty of Medicine, Institute of Biomedical Science, Vilnius, Lithuania
ernest.oleinik@gmc.stud.vu.lt

Enterococcus faecium bacteria are facultative anaerobic gram-positive opportunistic pathogens responsible for healthcare-associated infections due to their exceptional ability to colonize abiotic surfaces and tolerate antimicrobial stress, promoted by commonly used disinfectants [2] [3]. Recent studies indicate that biofilm formation plays a critical role in the survival of pathogens under biocidal exposure and contributes to elevated resistance and environmental contamination [1] [4]. Hence, this study aimed to identify essential genes associated with resistance to biocidal agents and to assess the impact of disinfectants on biofilm formation.

In this study, 59 clinical *E. faecium* isolates were collected from two Lithuanian hospitals between January and November 2024. The multiplex PCR genetic characterization method was used to detect genes associated with tolerance mechanisms to disinfectants and antiseptics (*qacE*, *qacEΔ1*, *qacG*, *qacH*, *qacA*, *cepA*). Biofilm formation by enterococci was determined using the microtiter plate method. 42 biofilm-positive isolates were assessed after exposure to 50% ethanol, 50% isopropanol, and 5% sodium hypochlorite using the crystal violet microtiter plate assay. The effects of alcohol-based antiseptics and sodium hypochlorite on biofilms were evaluated after 5- and 10-min. exposure, and biofilm optical density (OD) was measured spectrophotometrically at 595 nm wavelength. Isolates were classified as non-biofilm-forming, weak, moderate and strong biofilm producers. Statistical analysis of disinfectant effect was performed using Fisher's and McNemar's Chi-squared tests.

Multiplex PCR assessment revealed 4 distinct biocidal resistance genes: *qacE*, *qacEΔ1*, *qacH*, *qacA*. Among these, the *qacH* gene was the most prevalent, identified in 19 isolates (67.8%). Exposure to an alcohol-based antiseptic resulted in a statistically significant reduction in biofilm producers after 5 min ($p < 0.001$), with a further reduction observed after prolonged exposure. In contrast, sodium hypochlorite resulted in less notable reduction of biofilm-forming isolates ($p < 0.001$). The detection of resistance genes suggests a potential contribution of genetic traits and tolerance to antiseptics. This research demonstrates the potential threat posed by *E. faecium* biofilms to tolerance of commonly used antiseptics in healthcare institutions and may be linked to underlying genetic determinants and healthcare-associated infections. These findings emphasize the need to design new and effective infection control strategies in clinical environments.

Keywords: gram-positive bacteria, disinfectants, resistance, tolerance, Multiplex PCR, biofilm formation, statistical analysis.

[1] B. Sadanandan and K. M. Yogendraiah, "Enterococcus faecalis Biofilm: A Clinical and Environmental Hazard," Medical Sciences Forum, p. 5, Aug. 2025, doi: 10.3390/msf2025035005.
[2] A. P. Pereira et al., "Unraveling Enterococcus susceptibility to quaternary ammonium compounds: genes, phenotypes, and the impact of environmental conditions," Microbiology Spectrum, vol. 11, no. 5, p. e0232423, Sep. 2023, doi: 10.1128/spectrum.02324-23.
[3] A. A. Alajlan et al., "Assessment of disinfectant efficacy in reducing microbial growth," PLoS ONE, vol. 17, no. 6, p. e0269850, Jun. 2022, doi: 10.1371/journal.pone.0269850.
[4] A. Oliveira et al., "Evaluation of antimicrobial activity against Enterococcus faecalis of activated chelating agents in different final rinse protocols: An ex vivo study," Journal of Clinical and Experimental Dentistry, vol. 14, no. 8, pp. e646–e651, Jan. 2022, doi: 10.4317/jced.59547.

THE EFFECT OF NOVEL SULFONAMIDE DERIVATIVES ON HUMAN PROSTATE AND TRIPLE-NEGATIVE BREAST CANCER CELL LINE VIABILITY UNDER NORMOXIA AND HYPOXIA

Kotryna Čiupkevičiūtė[1], Valdas Vainauskas[2], Birutė Grybaitė[2], Vytautas Mickevičius[2], Vilma Petrikaitė[1,3]

[1]Lithuanian University of Health Sciences, Institute of Cardiology, Department of Drug Targets Histopathology, Lithuania
[2]Kaunas University of Technology, Department of Organic Chemistry, Lithuania
[3]Vilnius University, Life Sciences Center, Institute of Biotechnology, Lithuania
kotryna.ciupkeviciute@gmail.com

Prostate cancer makes up 13,5% of diagnosed cancer wordwide, marking it as the fourth most widespread and the second most commonly diagnosed cancer in men [1]. Triple-negative breast cancer accounts for 10–15% of all new breast cancer cases, as it is an aggressive subtype with unfavorable prognosis [2]. Sulfonamide derivatives are potential anticancer agents with the ability to inhibit carbonic anhydrase IX, that are more expressed in cancer cells[3]. Research for new effective substances creates progress in the treatment of cancer. Our research aimed to evaluate the anticancer activity of sulfonamide derivatives synthesized at Kaunas University of Technology (Lithuania) on human prostate and triple-negative breast cancer cell line viability.

In our study, we investigated the activity of 23 sulfonamide derivatives bearing substituted aromatic and different heterocyclic moieties on prostate cancer cell line PC3 and triple-negative breast cancer cell line MDA-MB231. The effect on cell viability was determined by the MTT assay at 20 μM of compounds after 72 hours of incubation. The comparative compounds with significant cell viability-reducing capabilities were chosen for further studies, and the EC50 values were established.

Compounds 1, 4a, 4b, 4c, 7a, 7b and 12 reduced the viability of all cell lines by up to appr. 20-25%. These compounds were selected for the determination of EC50 values. The greatest difference in normoxia and hypoxia conditions were to MDA-MB231 cell line, as in hypoxia, viability was reduced by up to appr 70-90%. Compounds 1 and 4c are selective to the MDA-MB231 cell line, but compound 1 was more active under normoxia, while 4c was more active under hypoxia. Also, compounds 4b, 7a and 7b are only selective to MDA-MB231 cell line in hypoxia, although 7b had similar EC50 values in normoxia for both cell lines. Compounds 4a and 12 are more selective to the PC3 cell line in normoxia, but under hypoxia they become selective to the MDA-MB231 cell line.

In conclusion, compounds 1, 4a, 4b, 4c, 7a, 7b and 12 showed a significant reduction of cell viability by MTT assay. Compound 1, 7a and 7b are more effective in normoxia, while 4a, 4b, 4c and 12 reduce the viability higher in hypoxia. Especially effective in hypoxia are compounds 4a and 12 in the MDA-MB231 cell line.

[1] M. N. E. Almeeri, M. Awies, and C. Constantinou, “Prostate Cancer, Pathophysiology and Recent Developments in Management: A Narrative review,” Current Oncology Reports, vol. 26, no. 11, pp. 1511–1519, Oct. 2024, doi: 10.1007/s11912-024-01614-6.
[2] A. M. Karim et al., “Triple-negative breast cancer: epidemiology, molecular mechanisms, and modern vaccine-based treatment strategies,” Biochemical Pharmacology, vol. 212, p. 115545, Apr. 2023, doi: 10.1016/j.bcp.2023.115545.
[3] Y. Wan, G. Fang, H. Chen, X. Deng, and Z. Tang, “Sulfonamide derivatives as potential anti-cancer agents and their SARs elucidation,” European Journal of Medicinal Chemistry, vol. 226, p. 113837, Sep. 2021, doi: 10.1016/j.ejmech.2021.113837.

SUSTAINABLE MAGNETIC BUCKWHEAT HULL-Fe_3O_4 NANOCOMPOSITES FOR ENHANCED BIOSORPTION OF HEAVY METALS IN BINARY AND TERNARY CONTAMINANT MATRICES

Tayyab Tahir[1], Rūta Druteikienė[1], Zita Žukauskaitė[1], Rūta Barisevičiūtė[1], Jūratė Vaičiūnienė[2]

[1]Lithuania, Center for Physical Sciences and Technology, Department of Nuclear Research, Savanorių ave. 231, LT-02300 Vilnius
[2]Lithuania, Center for Physical Sciences and Technology, Department of Catalysis, Saulėtekio av. 3, LT-10257 Vilnius
tayyab.tahir@ftmc.lt

Water has always been essential for life on Earth. However, as a result of urbanization and industrialization, numerous contaminants, including mercury (Hg), lead (Pb), arsenic (As), cadmium (Cd), chromium (Cr), and nickel (Ni), have been introduced into aquatic systems. Due to their harmful effects on aquatic and marine ecosystems, these heavy metals have become a major environmental concern in both developed and developing countries [1]. Ion exchange, redox processes, electrochemical treatment, phytoremediation, and precipitation have been employed for the removal of toxic metals from water systems. However, these techniques have several limitations, including high cost, low efficiency, lack of selectivity, and labor-intensive operation. In contrast, adsorption is a cost-effective and environmentally friendly technique for the removal of heavy metals. It offers advantages such as high selectivity and the ability to remove metals even at low concentrations [2]. Bio adsorbents offer several advantages, including biocompatibility, affordability, biodegradability, and non-toxicity, making them among the most widely studied adsorbents in recent years. Due to their superparamagnetic and photocatalytic properties, and high specific surface area, and short diffusion distance which leads to fast kinetics, Fe_3O_4 nanoparticles have been extensively applied in water treatment. Magnetic adsorbents provide the additional advantage of facile separation from treated water through the application of an external magnetic field. Therefore, the development of magnetic adsorbents, such as those derived from buckwheat hulls, can enhance treatment efficiency by simplifying operational processes and improving overall productivity [3].

The objective of this research was to develop and assess a magnetic biosorbent derived from buckwheat hulls for the efficient elimination of multiple heavy metals from complex aqueous systems.

Buckwheat hull–Fe_3O_4 nanocomposites were synthesized and applied as a sustainable magnetic biosorbent for the efficient removal of heavy metals from binary and ternary aqueous systems. The characteristics of buckwheat hull–Fe_3O_4 before and after sorption were analyzed using SEM, EDX, FTIR, XRD, BET, and point of zero charge (pHpzc) techniques. The sorption performance toward Pb(II), Cd(II), and Cr(III) ions was investigated through batch experiments by varying operational parameters including contact time (30-1440 min), solution pH (2-9), biosorbent dosage (0.1 g-0.35 g), temperature (25–50 °C), initial each metal ion concentration (5-50 mg/L) and agitation speed 150 rpm. The biosorption behavior of Pb(II)/Cd(II) in binary systems and Pb(II)/Cd(II)/Cr(III) in ternary systems was further analyzed using kinetic, isotherm, and thermodynamic models.

The findings confirm that buckwheat hull–Fe_3O_4 nanocomposite exhibit strong potential for the efficient removal of metal ions from aqueous solution.

Keywords: Heavy metals biosorption, buckwheat hull–Fe_3O_4 nanocomposites, kinetics, equilibrium, thermodynamics

[1] H. Şensöz and R. Donat, “Biosorption study of Cd2+ ions onto activated carbon prepared from Posidonia oceanica Seagrass: Kinetics and thermodynamics studies,” Materials Science and Engineering B, vol. 314, p. 118067, Feb. 2025, doi: 10.1016/j.mseb.2025.118067.
[2] T. Tahir et al., “Biosorption of Lead (II) and cadmium (II) ions from aqueous solution by buckwheat (Fagopyrum Esculentum) hulls biosorbent: kinetic, equilibrium and thermodynamic studies,” Chemical Physics, vol. 602, p. 112997, Oct. 2025, doi: 10.1016/j.chemphys.2025.112997.
[3] S. S. Hosseini, A. Hamadi, R. Foroutan, S. J. Peighambardoust, and B. Ramavandi, “Decontamination of Cd2+ and Pb2+ from aqueous solution using a magnetic nanocomposite of eggshell/starch/Fe3O4,” Journal of Water Process Engineering, vol. 48, p. 102911, Jun. 2022, doi: 10.1016/j.jwpe.2022.102911.

ASSESSMENT OF METHANE EMISSIONS IN REWETTED SWAMPS USING STABLE CARBON ISOTOPE ANALYSIS

Laurynas Bučinskas[1], Ąžuolas Ivickas[1], Andrius Garbaras[1]

[1]Center for Physical Sciences and Technology, Department of Nuclear Research, Vilnius, Lithuania
laurynas.bucinskas@ftmc.lt

Rewetting of drained peatlands and swamps is increasingly promoted as a climate-mitigation strategy due to its potential to reduce carbon dioxide emissions and restore ecosystem functions [1]. However, rewetting may also enhance methane production, creating uncertainty about the overall greenhouse gas balance of restored wetlands [2]. Understanding the sources and formation pathways of methane in re-wetted systems is therefore essential for evaluating their climatic impact, yet field-based isotopic evidence from restored swamps remains limited. The objective of this preliminary study is to investigate changes of methane emissions following swamp rewetting using stable carbon isotope ratio ($\delta^{13}C$) measurements and to determine whether isotopic signatures can provide early indications of microbial methane generation in newly reestablished wet conditions.

In this study, methane samples were collected from a swamp site using and analyzed using a cavity ring-down spectroscopy (CRDS) analyzer (Picarro G1112-i). Preliminary $\delta^{13}C$ results indicated a greatly depleted isotopic signature typically associated with microbial methane production under anaerobic conditions. The observed isotopic composition provides initial evidence that suitable hydrological conditions promote microbial processes responsible for methane formation. The preliminary results also highlight the sensitivity of isotopic measurements for detecting early-stage changes in greenhouse gas dynamics of swamps.

[1] J. Leifeld and L. Menichetti, “The underappreciated potential of peatlands in global climate change mitigation strategies,” Nature Communications, vol. 9, no. 1, p. 1071, Mar. 2018, doi: 10.1038/s41467-018-03406-6.

[2] T. He et al., “Meta-analysis shows the impacts of ecological restoration on greenhouse gas emissions,” Nature Communications, vol. 15, no. 1, p. 2668, Mar. 2024, doi: 10.1038/s41467-024-46991-5.

SEASONAL VARIATION OF HYDROCARBON DEGRADATION GENES IN URBAN GREEN AREA SOILS OF VILNIUS

Aistė Pazikaitė[1], Nomeda Kuisienė[1]

[1]Lithuania, Vilnius, Vilnius University, Life Sciences Center, Institute of Biosciences, Department of Microbiology and Biotechnology
aiste.pazikaite@gmc.stud.vu.lt

Urban soils in green areas are frequently exposed to hydrocarbon pollution, particularly in environments influenced by road traffic, construction activities as well as other anthropogenic factors. Microorganisms play a crucial role in the natural degradation of these contaminants, and functional genes encoding degrading enzymes can serve as indicators of soil biodegradation potential. Despite their importance, the seasonal dynamics of these genes in urban environments remain poorly characterized. This study investigated the presence and seasonal variation of genes involved in hydrocarbon degradation in the urban green area soils of Vilnius. Soil samples were collected during autumn and spring seasons near four streets: Ševčenkos, Gerosios Vilties, Baltupių, and Antakalnio. Total DNA was extracted and PCR was used to screen for genes encoding enzymes involved in the degradation of aliphatic, aromatic, and polycyclic aromatic hydrocarbons. Quantitative real-time PCR (qPCR) was applied to assess seasonal changes in the relative abundance of the phenol hydroxylase gene (*phe*), and amplification specificity was confirmed by melting curve analysis. Results showed that the gene associated with aromatic hydrocarbon degradation (*phe*) was prevalent and detected in most samples, whereas genes for aliphatic and polycyclic aromatic degradation were not identified. Statistically significant seasonal differences in *phe* gene abundance were observed at the Baltupiai site, while no significant changes were detected at other locations. Sequencing analysis revealed that *phe* sequences were affiliated with bacterial genera such as *Pseudomonas*, *Rhodococcus*, and *Sphingomonas*, with a distinct dominance pattern observed in the Baltupiai spring sample. Overall, these results demonstrate that Vilnius urban soils harbor microorganisms with the genetic potential for aromatic hydrocarbon degradation and highlight the spatial and seasonal variability of this potential in urban green infrastructure.

IMPACT OF DIETARY MAGNETIC CHITOSAN AND PROBIOTICS ON OXIDATIVE STRESS BIOMARKERS IN COMMON CARP

Aida Bradauskaitė[1], Sergej Šemčuk[1,2], Renata Butrimienė[1], Danguolė Montvydienė[1], Natalia Matvienko[1], Vesta Skrodenytė-Arbačiauskienė[1], Živilė Jurgelėnė[1]

[1]State Scientific Research Institute Nature Research Centre, Vilnius, Lithuania
[2]Center for Physical Sciences and Technology, Department of Environmental Research, Vilnius, Lithuania
aida.bradauskaite@gamtc.lt

Magnetic chitosan nanocomposites (MCNs) possess a range of advantageous properties, including high surface area, magnetic responsiveness, and excellent sorption capacity, making them attractive candidates for various applications in industrial fields[1]. Due to their biocompatibility and ability to bind and deliver bioactive substances, MCNs have been proposed as carriers for functional feed additives, including probiotics. Their potential to enhance nutrient delivery, improve feed efficiency, and modulate the aquatic environment positions them as innovative tools in sustainable fish farming. Meanwhile, probiotics, live microorganisms that confer health benefits to the host, are increasingly used in aquaculture to improve gut health, immunity, and overall fish performance. However, despite their growing use, the effectiveness of probiotic supplementation, particularly in combination with nanocarriers such as MCNs, remains underexplored. A better understanding of how these agents interact within fish physiology is essential to assess their efficacy and ensure they do not induce unintended oxidative or physiological stress.

This study investigated the effects of dietary probiotics and MCNs on oxidative stress indicators in *Cyprinus carpio* L. over a 21-day feeding period. Fish were divided into four groups: control, probiotic-only, MCN-only, and a combination (MCN+P). Antioxidant enzyme activity and oxidative damage markers: superoxide dismutase (SOD), catalase (CAT), malondialdehyde (MDA), and hydrogen peroxide (H_2O_2) were measured in liver, gill, and muscle tissues.

The results indicated no significant increase in MDA levels across tissues, suggesting no enhancement in lipid peroxidation. H_2O_2 concentrations significantly decreased in gills in the MCN+P group, indicating reduced oxidative stress. SOD and CAT activities remained stable among groups, reinforcing the conclusion that neither probiotics nor MCNs induced oxidative stress under the tested conditions. These findings highlight the potential compatibility of probiotics and MCNs in aquaculture diets, offering a promising avenue for enhancing fish health without eliciting harmful oxidative responses.

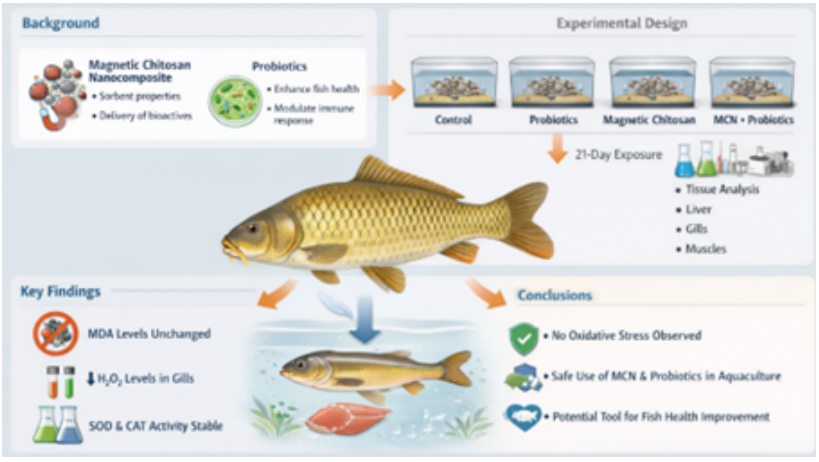


Fig. 1. Overview of the experimental design and key antioxidant enzyme responses in common carp (*Cyprinus carpio*) fed diets supplemented with MCNs and probiotics.

Acknowledgements
This work was supported by the Research Council of Lithuania, agreement No. S-PD-24-44.

[1] A. Benettayeb et al., "Chitosan nanoparticles as Potential Nano-Sorbent for Removal of toxic Environmental pollutants," Nanomaterials, vol. 13, no. 3, p. 447, Jan. 2023, doi: 10.3390/nano13030447.

THE EFFECT OF DIFFERENT RATES OF INDUSTRIAL WASTE (BIOFUEL ASH) ON CULTIVATED MAIZE IN ACIDIC SOIL

Gabija Žilytė[1], Kristina Bunevičienė[1], Urtė Čegytė[1,2]

[1]Lithuanian Research Centre for Agriculture and Forestry, Institute of Agriculture, Lithuania
[2]Vytautas Magnus University Agriculture Academy, Lithuania
gabija.zilyte@lammc.lt

In recent years, the rapid increase in fertilizer prices has raised growing concerns in the agricultural sector [1]. As economic pressure intensifies, it becomes essential to seek alternative, environmentally friendly, and sustainable solutions that can reduce the reliance on conventional fertilizers. One promising approach is the use of ash, as it contains a range of nutrients (Ca, K, P, S) required for plant growth [2]. Ash with low pollution levels should be used in agriculture and in the restoration of degraded land, rather than disposed of in landfills where its valuable properties would be lost [3].

The objective of this study was to evaluate the effect of different biofuel ash rates on the macroelement and microelement composition of soil and on the chemical and morphological properties of maize shoots and roots. The experiment was conducted in climate chambers. There were five variants: 0%, 1.25%, 2.5%, 5%, and 10% ash in the soil. All variants were fertilized with ammonium nitrate at a rate of 170 kg ha^{-1}. Samples were taken after 22 and 42 days. Root and shoot lengths were measured. During the experiment, physicochemical analyses were conducted on fertilization products, soil, and plants. Biofuel ash contains essential nutrients, notably high levels of Ca, K, P, and Mg. Increasing the application rate of biofuel ash significantly raises the levels of Ca, K, and P in both soil and plants, while changes in Mg and other elements remain minimal. Importantly, no heavy metals (such as As, Cd, Cr, Ni, and Pb) were detected in either the soil or the plants. The study determined optimal usage rates of 1.25% to 2.5%. Mentioned rates enhance nutrient availability and improve plant nutrition. However, applying biofuel ash at the highest rate of 10% is detrimental due to the excessively high pH.

Acknowledgements

This study was supported by the long-term research program „Productivity and sustainability agrogenic and forest soils", implemented by the LAMMC.

[1] C. Jian et al., "Effects of wood ash fertilizer on element dynamics in soil solution and crop uptake," Agronomy, vol. 15, no. 5, p. 1097, Apr. 2025, doi: 10.3390/agronomy15051097.

[2] G. Zając, J. Szyszlak-Bargłowicz, W. Gołębiowski, and M. Szczepanik, "Chemical characteristics of biomass ashes," Energies, vol. 11, no. 11, p. 2885, Oct. 2018, doi: 10.3390/en11112885.

[3] J. I. Odzijewicz, E. Wołejko, U. Wydro, M. Wasil, and A. Jabłońska-Trypuć, "Utilization of Ashes from Biomass Combustion," Energies, vol. 15, no. 24, p. 9653, Dec. 2022, doi: 10.3390/en15249653.

CHARACTERIZING ECOSYSTEM-SPECIFIC PATTERNS OF ANTIBIOTIC RESISTANCE IN ENVIRONMENTAL BACTERIA

Alper Melih Ucar[1,2], Juliana Lukša-Žebelovič[1,2], Elena Servienė[1,2]

[1]State Scientific Research Institute Nature Research Centre, Vilnius, Lithuania
[2]Vilnius Tech, Vilnius, Lithuania
a.ucar@stud.vilniustech.lt

Bacteria are a dominant component of environmental microbial communities and play an essential role in ecosystem functioning [1]. Antimicrobial resistance (AMR) is disseminated among diverse bacterial species, leading to the emergence of potential pathogenic antibiotic-resistant bacteria (ARB) that threaten both animal and human health [2]. Agricultural fields act as the hotspots for AMR, where resistance genes transfer across ARB in the interconnected environmental compartments including soil, water, and animal feed [3]. Understanding how ARB are distributed within farmland ecosystems is necessary to establish baseline resistance levels and to assess potential risks to animal and public health. This study examined the diversity, distribution, and antibiotic resistance profiles of environmental bacteria from ecological dairy farms in Lithuanian.

Bacteria strains resistant to at least one of the tested antibiotics (ampicillin, streptomycin, tetracycline, chloramphenicol) were isolated from soil, feed, and freshwater samples of three pastoral dairy farmlands. Isolates were identified by 16S rRNA gene sequencing and antibiotic resistance profiles were determined by quantitative minimum inhibitory concentration (MIC) assay. Associations between resistance patterns, bacterial genera, and habitat were evaluated using statistical analyses.

In total, 44 resistant isolates representing 14 bacterial genera were identified, with *Bacillus* and *Enterobacter* being the most prevalent. Antibiotic-resistant bacteria were most abundant in soil, followed by feed and freshwater. Resistance was highest to ampicillin (77.27%) and streptomycin (75%), moderate chloramphenicol (40.91%), and lowest to tetracycline (11.36%). More than 70% of isolates showed resistance to more than one antibiotic (Fig. 1). Resistance patterns differed among bacterial genera and were unevenly distributed across environmental compartments, indicating that habitat-specific factors influence both bacterial composition and resistance profiles.

The obtained results show that ecological farmland environments, particularly agricultural soils, support diverse bacterial populations with frequent multidrug resistance. Further work targeting a broader range of resistance genes would help clarify the mechanisms underlying the observed resistance patterns.

This project has received funding from the Research Council of Lithuania (LMTLT), agreement No S-MIP-23-7.

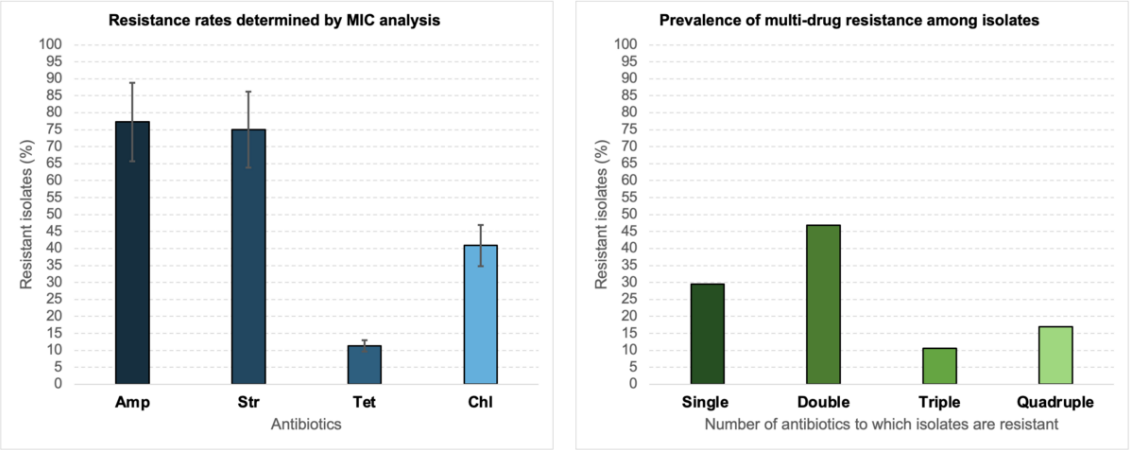


Fig. 1. Resistance behaviours of antibiotic-resistant bacterial isolates from farmland settings.

[1] L. Ma, C. Zhang, J. Feng, C. Yao, and X. Xu, "Distinct roles of plant and microbial communities in ecosystem multifunctionality during grassland degradation and restoration," Geoderma, vol. 459, p. 117381, Jul. 2025, doi: 10.1016/J.GEODERMA.2025.117381.
[2] S. Cleaveland, M. K. Laurenson, and L. H. Taylor, "Diseases of humans and their domestic mammals: pathogen characteristics, host range and the risk of emergence," Philos. Trans. R. Soc. Lond. B Biol. Sci., vol. 356, no. 1411, pp. 991–999, Jul. 2001, doi: 10.1098/RSTB.2001.0889.
[3] F. Wang et al., "Antibiotic resistance in the soil ecosystem: A One Health perspective," Curr. Opin. Environ. Sci. Health, vol. 20, p. 100230, Apr. 2021, doi: 10.1016/J.COESH.2021.100230.

HARNESSING THE POTENTIAL OF BACTERIA ISOLATED FROM CONSTRUCTION BY-PRODUCTS AS A SUSTAINABLE APPROACH TOWARDS ENVIRONMENTAL PROTECTION

Sabina Myrzakhmetova[1], Saloua Biyada[1]

[1]Vilnius Gediminas Technical University, Faculty of Fundamental Sciences, Department of Chemistry and Bioengineering, Lithuania
sabina.myrzakhmetova@stud.vilniustech.lt

With the rise of industrial progress, pollution has been and remains a major concern for the world. Scientific advances have contributed to the solutions of the given issue by suggesting various ways of encountering and reprocessing; the relatively operative methods include the employment of microorganisms. Bacteria exhibit great diversity in their forms, properties, and activities. For this reason, the current study encompasses the isolation of microorganisms from hostile environments with a greater adaptability, along with their application in solving major ecological issues. To this end, LB agar medium was used effectively in the isolation and purification of strains until pure colonies were obtained, the latter being subsequently molecularly identified.

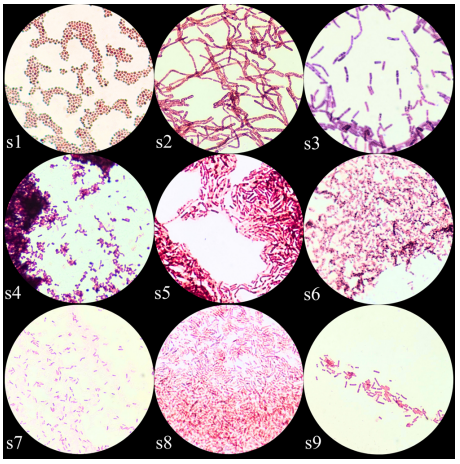


Fig. 1. Gram staining of isolated bacteria

In order to evaluate enzymatic activity, strains were screened and subsequently monitored for the predominant decomposition of substrates used. A total of 9 species were distinguished – 7 corresponding to lipase, 3 to gelatinase, 4 to pectinase, and 5 to cellulase activities – to represent the acquired bacteria. The promising outcomes were shown by strains “s3”, “s7”, and “s8”, sharing the results in almost every assessment, indicating their capability to metabolise a wide range of organic matter, speeding its degradation. Ultimately, given the nature of microorganisms, forward-looking considerations on the applications of bacteria active in the decomposition of oils, plastics, and industrial by-products have been specifically structured to address the problem of organic pollutants widespread.

Keywords: Construction by-product; Bacteria; Circular economy; Enzymatic activity.

OPTIMIZED BIOETHANOL PRODUCTION FROM SUNFLOWER (HELIANTHUS ANNUUS) HEAD WASTE USING SACCHAROMYCES CEREVISIAE

Sunil Kumar[1], Vilma Kaškonienė[1]

[1]Vytautas Magnus University, Instrumental Analysis Open Access Center, Lithuania
sunil.kumar@stud.vdu.lt

Agricultural waste pollutes the environment when dumped and is usually associated with health hazards. The agricultural waste contributes more than sixty percent of Lithuania's municipal solid waste, thus posing environmental concerns in both urban and rural areas. However, it is renewable and green source for bioethanol production because it contains generous amounts of reducing sugars, organic acids, and other essential nutrients. Therefore, this substrate can be considered as target for various valorisation techniques for proper management. In general, the usual management practices, such as landfilling, incineration, and open burning of agricultural waste, produce secondary waste. It therefore becomes necessary to control and recycle this waste for the sustainable production of useful products that reduce environmental pollution. Converting agricultural waste into bioethanol via fermentation provides an efficient and environmentally friendly method of eliminating this waste. The aim of the work was to analyze the ethanol content after pre-treating powdered sunflower heads (Helianthus annuus) with the commercial enzyme preparation Viscozyme under different substrate concentrations (10%, 15%, 20%, and 25% w/v). The Brix value was measured, and GC-FID analysis was employed to determine ethanol content. The results indicate that a 20% substrate loading ratio yields the maximum ethanol production (12.89±3.95%), with the Brix value decreasing from 8.6 after hydrolysis to 5.7 after five days of fermentation. This confirms that agricultural waste, particularly sunflower heads, can be a viable resource for bioethanol production, offering a sustainable waste-management solution that addresses both energy demands and environmental concerns.

The aim of the work was to analyze the ethanol content after pre-treating powdered sunflower heads (Helianthus annuus) with the commercial enzyme preparation Viscozyme under different substrate concentrations (10%, 15%, 20%, and 25% w/v). The Brix value was measured, and GC-FID analysis was employed to determine ethanol content. The heat treatment applied before enzymatic hydrolysis increased the Brix value from 2.5 to 6.73±0.97.The results indicate that a 20% substrate loading ratio yields the maximum ethanol production (12.89±3.95%), with the Brix value decreasing from 8.6 after hydrolysis to 5.7 after five days of fermentation. This confirms that agricultural waste, particularly sunflower heads, can be a viable resource for bioethanol production, offering a sustainable waste-management solution that addresses both energy demands and environmental concerns.

ADSORPTION OF POLYETHYLENE TEREPHTHALATE, POLYSTYRENE, AND POLYETHYLENE NANOPLASTICS FROM FRESHWATER SYSTEMS

Mahrosh Javed[1], Galina Lujanienė[1], Sergej Šemčuk[1], Vidas Pakštas[2], Martynas Talaikis[3], Aušra Selskienė[2]

[1]Center for Physical Sciences and Technology, Department of Environmental Research, Vilnius, Lithuania
[2]Center for Physical Sciences and Technology, Department of Characterization of Materials Structure, Vilnius, Lithuania
[3]Center for Physical Sciences and Technology, Department of Organic Chemistry, Vilnius, Lithuania
mahrosh.javed@ftmc.lt

Over 335 million tonnes of plastic have been produced worldwide. Plastic waste has been recognized as a global environmental problem, and improper handling of this waste has led to increasing amounts of plastic debris. Upon entering the aquatic environment, this debris undergoes chemical and physical processes caused due to aging by UV light and abrasion by waves, forming microplastics (>5 μm) and nanoplastics (>1 μm). Excessive release of these particles has polluted water systems. Ingestion of these plastic particles is reported to cause health risks to living cells. Therefore, removing nanoplastics from water systems is essential to ensure the safety of human health and aquatic [1]. Recent studies have employed various water treatment techniques to extract nanoplastics from water. Among these, adsorption offers several advantages, including the use of environmentally friendly materials, high efficiency, and simple operation. Various adsorbents, such as biochar, clay, silica, polysaccharides, zeolites, and graphene-based materials, have been used to remove nanoplastics. Graphene has also been reported to be a good adsorbent in the removal of pollutants with functional groups like carbonyl, hydroxyl, epoxy, and carboxyl. Nevertheless, graphene oxide (GO) has several layers, resulting in aggregation, thus complicating adsorption. In this regard, natural polymers like cellulose and chitosan (CS) can be functionalized to develop a composite with various functional groups and increased capacity of adsorption. Cellulose is an inexpensive and biodegradable substance that does not produce toxins, has a large adsorption capacity because of the presence of hydroxyl groups (-OH) in it, creating adsorption sites on its surface[1]. Because of a similar polysaccharide nature, chitosan also has these advantages and additional amino (-NH 2) groups obtained as a result of the chitin deacetylation process, and this further enhances its adsorption properties [2]. Microcrystalline cellulose (MCC) and chitosan (GO) composites were developed in this work to eliminate the nanoplastics, such as polyethylene terephthalate (PET), polystyrene (PS), and polyethylene (PE). GO was produced through a modified Hummer's method. MCC was first mercerised and then crosslinked with GO to create MCC-GO composites [3]. In the case of GO-CS, chitosan was dissolved in acetic acid and then crosslinked through glutaraldehyde [2]. SEM, XRD, and FT-IR were used to characterise the prepared composites. The nanoprecipitation method was used to produce nanoplastics, which were characterised by TEM and FT-IR. The surface charge of all the adsorbents prepared, as well as the nanoplastic,s was determined by calculating the point of zero charge (pHPZC). The synthesis of nanoplastics was confirmed by characterisation. The synthesised composites were used for nanoplasticadsorption. UV-VIS spectroscopy was used to monitor all the changes during the adsorption process.

Keywords: Nanoplastics, Adsorption, Water, Chitosan, Cellulose

[1] M. Javed and G. Lujanienė, "Nanoplastics in aquatic systems: challenges and advances in adsorptive removal technologies," Frontiers in Water, vol. 7, Jun. 2025, doi: 10.3389/frwa.2025.1611558.
[2] M. Sabzevari, D. E. Cree, and L. D. Wilson, "Graphene Oxide–Chitosan composite material for treatment of a model dye effluent," ACS Omega, vol. 3, no. 10, pp. 13045–13054, Oct. 2018, doi: 10.1021/acsomega.8b01871.
[3] A. Boudjellal, D. Trache, K. Khimeche, S. L. Hafsaoui, and M. S. Razali, "Preparation and characterization of graphene oxide-based natural hybrids containing alfa fibers or microcrystalline cellulose," Journal of Natural Fibers, vol. 19, no. 13, pp. 5321–5332, Feb. 2021, doi: 10.1080/15440478.2021.1875373.

EFFECT OF RAW MATERIAL COMPOSITION ON THE PHYSICALPROPERTIES OF SOLID ORGANIC FERTILIZERS

Gabija Aleksaitytė[1], Rasa Šlinkšienė[1]

[1]Lithuania, Kaunas University of Technology, Department of Physical and Inorganic Chemistry
gabija.aleksaityte@ktu.edu

Intensive agricultural practices have led to a gradual depletion of soil organic matter, highlighting the need to increase the input of organic materials to maintain soil health and productivity. At the same time, the accumulation of organic solid waste in landfills as a result of high consumption levels has become a serious environmental concern in many European Union countries, contributing to increased emissions of carbon dioxide and methane. In line with the objectives of the EU Green Deal, there is a growing emphasis on the development and implementation of technologies that promote nutrient recovery and material recycling from the food and agricultural sectors. In this context, organic fertilizers derived from secondary raw materials represent a promising solution, offering both environmental and agronomic benefits.

Organic waste, such as residues from buckwheat groats processing (buckwheat husks, their ash, and other biomass fractions), which are currently underutilized, can be used as raw materials for the production of organic fertilizers. When properly combined, these materials can be used to produce solid organic fertilizer formulations containing essential nutrients required for plant growth. However, the effectiveness and practical applicability of such fertilizers depend not only on their chemical composition but also on their physical properties, which are strongly influenced by the composition of the raw materials used.

The physical properties of solid organic fertilizers were studied using the following methods. Fractional composition, i.e., particle size distribution, was determined using woven sieves (RETSCH GmbH, Haan, Germany) in accordance with DIN ISO 3310-1, with mesh sizes of 0.2, 0.5, 1.0, 2.0, 3.15, 4.0, and 5.0 mm.

The static strength of granules was measured using an IPG-2 device (АО “УНИХИМ с ОЗ”, Yekaterinburg, Russia).

The hygroscopicity of granular organic fertilizers was evaluated using the gravimetric method by monitoring changes in mass over time under different conditions: at 98–99% relative humidity and 21.1–25.9 °C, and at 60–61% relative humidity and 20.6–25.0 °C.

The bulk density of loose granules was determined by the gravimetric method based on mass difference, according to CEN EN 1236:1995. The compacted bulk density was determined in accordance with DIN EN 1237.

Moisture content was determined using an electronic moisture analyzer (Kern MLS 50-3HA160N, Kern & Sohn GmbH, Balingen, Germany).

Fertilizer pH was measured using a pH meter (HANNA pH211, HANNA Instruments, Woonsocket, RI, USA).

ASSESSMENT OF WARM-SEASON SST TRENDS IN THE CURONIAN LAGOON USING REANALYSIS DATA

Gustė Gečaitė[1], Donatas Pupienis[1]

[1]Vilnius University, Faculty of Chemistry and Geosciences, Institute of Geosciences
guste.gecaite@chgf.stud.vu.lt

The increase in sea surface temperature (SST) is one of the most pronounced signals of climate change in oceans and seas. However, long-term SST trends in shallow Baltic Sea lagoons remain insufficiently studied [1-3]. Shallow lagoons are highly sensitive to changes in the heat balance, seawater exchange, river inflow, wind regime and other factors. As a result, climate change leads to pronounced seasonal and spatial heterogeneity in SST distribution within lagoon systems.

The aim of this study is to assess seasonal (May to September) changes and long-term trends in surface water temperature in the Curonian Lagoon using open-access reanalysis data from the Copernicus Earth Observation Programme for the period 1982 to 2024. The analysis is based on daily high-resolution (0.02°) Baltic Sea Sea Surface Temperature Reprocessed (L4) data provided by the Copernicus Marine Service [4]. Monthly trends in mean surface water temperature in the Curonian Lagoon were evaluated using the non-parametric Mann-Kendall test at a significance level of $p=0.05$.

The results show that surface water temperature in the Curonian Lagoon increased across the entire lagoon area at an average rate of 0.58 °C per year ($p>0.05$). The most pronounced SST increase was observed in June and July, reaching average rates of 0.82 and 0.77 °C per year, respectively ($p>0.05$). Spatial analysis revealed a non-uniform warming pattern within the lagoon. In June, the strongest warming was detected in the southwestern and northern, deepest parts of the lagoon. In contrast, during July the largest warming rates were identified in the shallower southeastern and eastern areas. In August, a statistically significant and spatially uniform warming of approximately 0.46 °C per year was observed throughout the lagoon, decreasing to an average of 0.37 °C per year in September.

These results highlight pronounced seasonal and spatial heterogeneity in SST warming within the Curonian Lagoon and emphasize the importance of long-term, high-resolution datasets for assessing the impacts of climate change in lagoon studies.

Keywords: Sea surface temperature, lagoon, reanalysis data

[1] I. Dailidienė, H. Baudler, B. Chubarenko, and S. Navrotskaya, “Long term water level and surface temperature changes in the lagoons of the southern and eastern Baltic,” Oceanologia, vol. 53, no. 1, pp. 293–308, 2011, doi: 10.5697/oc.53-1-ti.293.

[2] A. Galkus, “Vandens cirkuliacija ir erdvinė drumstumo dinamika vasarą Kuršių mariose ir Baltijos jūros Lietuvos akvatorijose,” Geografijos metraštis, vol. 36, no. 2, pp. 48–60, 2003.

[3] G. Umgiesser, P. Zemlys, A. Erturk, A. Razinkova-Baziukas, J. Mėžinė, and C. Ferrarin, “Seasonal renewal time variability in the Curonian Lagoon caused by atmospheric and hydrographical forcing,” Ocean Science, vol. 12, no. 2, pp. 391–402, Mar. 2016, doi: 10.5194/os-12-391-2016.

[4] E. U.-C. M. Service, “Baltic Sea- sea surface temperature reprocessed,” Mercator Ocean International. Jan. 01, 2015. doi: 10.48670/moi-00156.

ENVIRONMENTAL BEHAVIOR AND EFFECTS OF RARE-EARTH UPCONVERTING NANOPARTICLES TO FRESHWATER ALGAE

Taseer Mustafa[1], Živilė Jurgelenė[2], Danguolė Montvydienė[2], Vilius Poderys[3], Eglė Ežerskytė[1], Jūratė Karosienė[2], Artūras Katelnikovas[1], Augustas Morkvėnas[3], Lukrecija Miliūtė[2], Vitalijus Karabanovas[3], Vaidas Klimkevičius[1,3]

[1]Vilnius University, Faculty of Chemistry and Geosciences, Institute of Chemistry
[2]State Scientific Institute Nature Research Centre
[3]National Cancer Institute, Biomedical Physics Laboratory
taseer.mustafa@chgf.stud.vu.lt

Lanthanide-doped upconverting nanoparticles (UCNPs) are increasingly explored for biomedical and sensing applications, yet their behavior and biological effects in natural freshwater environments remain poorly understood. In this study, monodisperse $NaYF_4$:18%Yb^{3+}, 2%Er^{3+} UCNPs were synthesized via thermal co-precipitation and rendered hydrophilic through oleate removal. The stability and biological impact of the UCNPs were investigated using the freshwater green algae *Desmodesmus communis* in two exposure media: nutrient-rich MWC medium and natural river water from the Neris river. Optical characterization, including absorbance, fluorescence, and upconversion emission measurements, revealed progressive nanoparticle destabilization over a 0-96 hour exposure period in both media. Algal responses were more strongly influenced by the chemical composition of the exposure medium than by UCNP concentration. Pigment content showed limited sensitivity to nanoparticle exposure, whereas oxidative stress and antioxidant responses exhibited pronounced, medium-dependent variations. Confocal microscopy indicated that UCNPs predominantly associated with the algal cell surface, with only limited evidence of cellular internalization. Multivariate partial least squares discriminant analysis (PLS-DA) further distinguished response patterns, with oxidative and antioxidant variables dominating in artificial growth medium, while growth-related parameters were more influential in river water. These findings highlight the critical role of environmental chemistry in governing UCNP stability, aggregation, bioavailability, and biological effects, underscoring the importance of realistic exposure conditions in freshwater nanomaterial risk assessment.

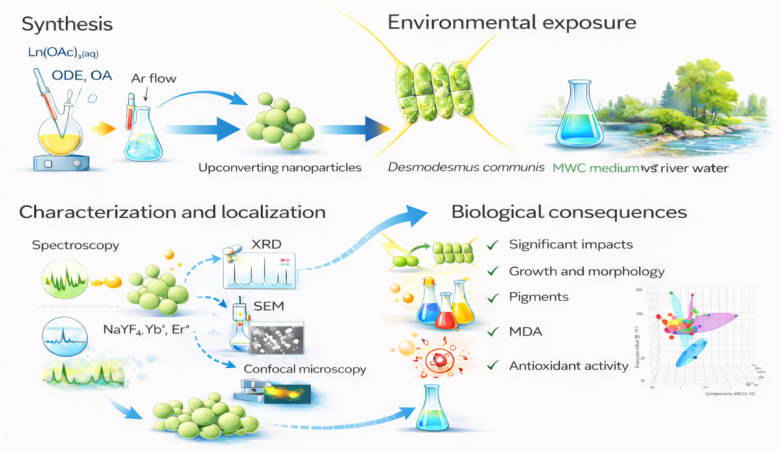


Fig. 1. Overview of nanoparticle synthesis, characterization methods, and with a focus on environmental exposure to Desmodesmus communis, and resulting biological effects

Acknowledgements
This work was supported by the Research Council of Lithuania, agreement No. [S-MIP-24-92].

INTEGRATING REMOTE SENSING AND MACHINE LEARNING TO RELATE GROUNDWATER LEVEL DYNAMICS WITH HYDROCHEMICAL VARIABILITY

Assemzhan Kunsakova[1], Vytautas Samalavičius[1]

[1]Lithuania, Vilnius University, Institute of Geosciences
assemzhan.kunsakova@chgf.stud.vu.lt

Sustainable groundwater management requires integrated evaluation of groundwater quantity and quality under changing climatic and anthropogenic pressures. This study combines satellite gravimetry, national monitoring data, and machine learning methods to investigate relationships between groundwater level (GWL) dynamics and hydrochemical variability across Lithuania. Groundwater level and hydrochemical data (2002 - 2024) were obtained from the Lithuanian Geological Survey and merged with terrestrial water storage anomalies derived from NASA's GRACE mission.

Machine learning models were applied to assess relationships between groundwater level fluctuations and key hydrochemical variables. The input chemical parameters used for modelling included chloride, calcium, and sulphate concentrations. The analysis aimed to identify three dominant chemical parameters showing the strongest correlation with groundwater level dynamics. Regularized linear models (LASSO and Ridge) were used to predict relative groundwater level variations at Well 283 (Fig 1). Both models show a moderate to strong positive correlation between observed and predicted levels ($r \approx 0.82$ - 0.83), with test performance of $R2 \approx 0.68$ - 0.69. While cross - validated R2 values were lower (≈ 0.33 - 0.35), indicating variability across samples, the results demonstrate that linear relationships explain a substantial fraction of short-term groundwater variability, with LASSO providing slightly improved generalization and model simplicity.

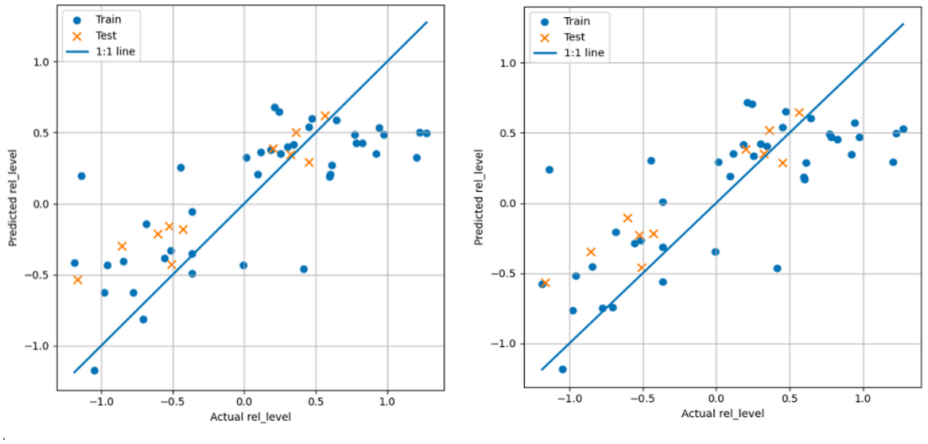


Fig. 1. Well 283 - RIDGE and LASSO results

The developed methodology supports improved groundwater resilience evaluation and contributes to the GRANDE-U project (Groundwater Resilience Assessment through Integrated Data Exploration for Ukraine), which promotes regional groundwater sustainability through advanced data integration. The GRANDE-U project unites researchers from six countries: the United States, Ukraine, Poland, Lithuania, Latvia, and Estonia. Vilnius University has received funding from the Research Council of Lithuania (LMTLT), agreement No. S-IMPRESSU-24-3.

Keywords: Machine Learning, GRACE, Ground Water Level (GWL).

INFLUENCE OF LANDFILL OPERATION AND TREATMENT PRACTICES ON LEACHATE TOXICITY TO DAPHNIA MAGNA

Tomas Makaras[1]

[1] State Scientific Research Institute Nature Research Centre, Lithuania
tomas.makaras@gamtc.lt

Landfill leachate toxicity is influenced by various physicochemical and landfill-related parameters, how these factors shape biological responses and how toxicity changes under different landfill operational conditions remain poorly understood [1,2]. In this study, a biological assessment was conducted using Daphnia magna exposed to leachates collected from non-hazardous and industrial landfills differing in operational status (active or inactive), precipitation exposure (protected or unprotected), and treatment stage (untreated, partially treated, or fully treated).

Acute effect concentrations (EC50) and low-effect equivalent concentrations (EC5 and its fractions: 1/4 and 1/16 EC5) were determined to enable comparisons among leachates and to link biological responses with physicochemical properties and landfill characteristics. This approach allowed the comparison of biologically equivalent exposure levels across sites and extended evaluation beyond standard endpoints by integrating biological responses.

Toxic effects were observed even at the lowest tested concentrations, including in treated leachates. Key physicochemical parameters driving leachate toxicity were identified, providing valuable insight for toxicity testing and environmental risk assessment. Based on toxicity unit (TU) values, the highest toxicity was observed in precipitation-protected leachate, followed by precipitation-unprotected leachates, leachate from non-operational landfills, and partially treated leachate after mechanical–biological treatment. No acute toxic effects were detected in fully treated leachate.

At the individual level, locomotor activity was assessed after 4 and 7 days using average velocity, angular velocity, and acceleration. Clear dose–response patterns were observed: exposure to some untreated leachates increased activity, whereas the most contaminated leachates caused pronounced hypoactivity. Significant effects occurred at 1/4 EC5 and EC5 concentrations. In contrast, acceleration remained unaffected, indicating that baseline locomotor activity was a more sensitive indicator of sublethal stress than phototactic or startle responses.

In raw leachates, elevated concentrations of of Cl^-, SO_4^{2-}, NH_4^+, K^+, total Cr, COD, BOD, TOC, and EC were closely associated with landfill operational status, site size, waste volume, and precipitation influence. Among these, K^+, TOC, COD, and EC showed the strongest associations with biological effects.

Overall, the results demonstrate that landfill age, waste composition, management practices, and treatment processes collectively determine leachate toxicity and associated biological responses. Further research is needed to elucidate contaminant interactions and assess the influence of landfill characteristics on long-term ecological risk.

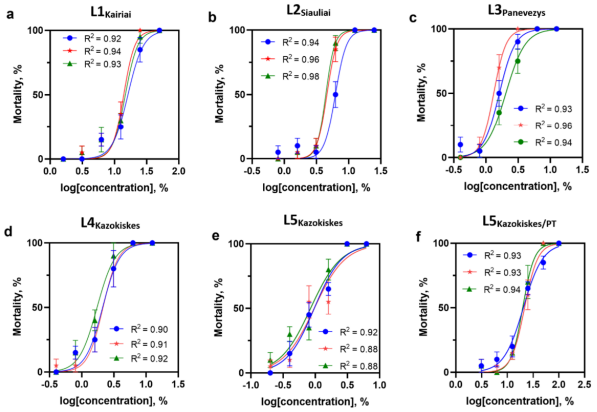


Fig. 1. Dose-response curves of D.magna exposed to different landfill leacahtes

[1] Kwarciak-Kozłowska, A. et al., J. Environ. Manag. 287, 112309 (2021).
[2] Rogers, E. R. et al., J. Environ. Manag. 284, 112031 (2021).

FIRST COMPREHENSIVE ASSESMENT OF MICROPLASTICS IN URBAN STREET DUST OF EASTERN SAUDI ARABIA: ABUNDANCE, TRAITS, AND HEALTH RISKS

Ali Ashry[1,2]

[1]Center for Physical Sciences and Technology (FTMC), Saulėtekio Ave. 3, LT-10257 Vilnius, Lithuania
[2]Sohag University, Faculty of Science, Department of Zoology, Sohag, Egypt, PO Box 82524
ali.ashry@ftmc.lt

Urban street dust has emerged as an important reservoir and secondary emission source of microplastics (MPs), yet evidence from arid regions remains scarce. This study provides a comprehensive assessment of MP contamination in street dust from two major cities in eastern Saudi Arabia, Alkhobar and Al-Dammam, integrating occurrence, physicochemical characteristics, and human health risk evaluation. Street dust samples were collected from 58 sites representing diverse land-use categories and analyzed using density separation, chemical digestion, stereomicroscopy, and ATR-FTIR spectroscopy. Microplastics were detected in all samples, with a mean abundance of 12.6 ± 13.8 items per 5 g of dust and pronounced spatial heterogeneity. Fragments were the dominant morphotype, followed by fibers and films, while medium-sized particles (300–999 µm) prevailed. Polymer analysis identified polyethylene (PE), polyethylene terephthalate (PET), and polypropylene (PP) as the most abundant polymers, alongside consistent contributions from high-toxicity polymers such as polyvinyl chloride (PVC) and polystyrene (PS). Diversity index (MDI) analysis revealed high heterogeneity in MP size and color across both cities. Human exposure assessment demonstrated that children experience substantially higher estimated daily and annual intake of MPs via both ingestion and inhalation compared with adults, particularly in residential and recreational areas. Polymer hazard index (H) classified several sites as high to very high risk, driven primarily by PVC and PS contributions. Overall, the findings identify urban street dust as a significant exposure pathway for hazardous microplastics in arid cities and provide critical baseline data for the Arabian Gulf region. These results highlight the need to integrate microplastic monitoring and polymer-specific risk control into urban dust management and public health frameworks in rapidly urbanizing arid environments.

Keywords: Microplastics (MPs) Street dust Human exposure risk Urban environment, Saudi Arabia

[1] H. A. Alharbi, A. Y. Bazeyad, Y. Al Naggar, B. K. Youssef, and A. Ashry, “First comprehensive assessment of microplastics in urban street dust of Eastern Saudi Arabia: abundance, traits, and health risks,” Journal of Hazardous Materials, 2026, Art. no. 141047.

RECYCLING INITIATIVES IN SUSTAINABLE POLYMER WASTE MANAGEMENT

Maksym Koliada[1], Viktoriia Plavan[2], Oleh Lozovyi[2,3]

[1]International Organization for Migration, Kyiv, Ukraine
[2]Kyiv National University of Technologies and Design, Faculty of Chemical and Biopharmaceutical Technologies, Department of Chemical Technologies and Resource Saving, Kyiv, Ukraine
[3]Polygreen plant, Biosphere Corporation, Fastiv Town, Kyiv Region, Ukraine
mkoliada@iom.int

The transition from landfilling and incineration to industrial recycling is a core priority of the European Union's circular economy policy and is particularly critical in humanitarian contexts, where emergency responses generate large volumes of plastic waste. Since 2022, humanitarian shelter operations in Ukraine have relied heavily on plastic tarpaulins for emergency roof repair and temporary shelter. While essential for protection, these materials create a significant secondary waste stream once damaged or no longer required.

This study explores the potential for transforming humanitarian shelter plastics into durable construction materials through organized recycling initiatives in Ukraine. According to EU Directive 2018/851 on waste, by 2035 the proportion of municipal waste sent to landfill should be reduced to 10%, while reuse and recycling rates should reach 65%. Achieving these targets requires a shift from disposal-based waste management toward industrial recycling systems.

In Ukraine, large-scale humanitarian assistance following Russia's full scale invasion in 2022 resulted in the distribution of millions of tarpaulins. These tarpaulins, typically composed of woven HDPE or polypropylene scrims coated with LDPE, are technically recyclable but logistically difficult to recover once dispersed across communities. This study applies qualitative and quantitative review methods to assess recycling feasibility, including analysis of estimated tarpaulin waste volumes generated between 2022 and 2025, and compatibility with conventional recycling technologies such as extrusion, compression moulding, and injection moulding.

An international comparative case is examined through a UNHCR pilot project in Lebanon that repurposed used plastic sheeting into shelter doors [1]. This case provides benchmarks for technical feasibility, cost efficiency, and product durability relevant to the Ukrainian context. The analysis indicates that Ukraine's humanitarian plastic waste stream is sufficiently large to support pilot and potentially industrial-scale recycling initiatives. Ukraine already possesses relevant industrial capacity. The Polygreen plant, the largest enterprise in Ukraine engaged in secondary processing of polyethylene film waste, demonstrates the feasibility of large-scale polyethylene recycling under domestic conditions. The material composition of tarpaulins distributed in Ukraine is compatible with existing recycling machinery, including equipment operated by Polygreen.

Beyond technical feasibility, institutional coordination is essential. Local authorities can support collection systems and integration into municipal waste services, while academic institutions while academic institutions can contribute to material testing and product design [2]. Recycling initiatives also create socio-economic benefits, including employment opportunities and community engagement in sustainability efforts [3].

Keywords: Humanitarian plastic waste; Polymer recycling; Circular economy; Ukraine

[1] D. Farres, "Repurposing plastic sheets into doors," in Proceedings of the Global Shelter Cluster Annual Meeting 2024, UNHCR, 2024. [Online]. Available: Google Slides: SESSION SUMMARIES.pptx. [Accessed: Nov. 30, 2025].

[2] United Nations, "They know what to do with your plastic," United Nations, 2025. [Online]. Available: https://ukraine.un.org/en/234857-they-know-what-do-your-plastic. [Accessed: Nov. 30, 2025].

[3] United Nations Development Programme, "Plastic waste management at the local level," 2021. [Online]. Available: https://www.undp.org/ukraine/projects/plastic-waste-management-local-level . [Accessed: Nov. 30, 2025].

UNRAVELING 4-HYDROXYPHENYLPYRUVATE METABOLISM IN CUPRIAVIDUS NECATOR H16

Monika Tamašauskaitė[1], Ingrida Sabaliauskė[1], Ernesta Augustinienė[1]

[1]Lithuania, Kaunas University of Technology, Bioprocess Research Center
monika.tamasauskaite@ktu.lt

Cupriavidus necator H16 is a metabolically versatile chemolithoautotroph capable of utilizing CO_2 and aromatic compounds [1]. The tyrosine-derived intermediate 4-hydroxyphenylpyruvate (4-HPPA) is a promising target for biosensor development and metabolic engineering. Here, we investigated the role of the *hppD* gene in 4-HPPA metabolism and its impact on inducible reporter activation.

A Δ*4hppD* mutant was generated via double homologous recombination using a suicide plasmid (pIK072). A red fluorescent protein (RFP) reporter plasmid (pPM014) was introduced into wild-type and mutant strains. Fluorescence responses to L-tyrosine, 4-HPPA, homogentisate, gentisic acid, and L-aspartic acid were quantified alongside growth monitoring.

Deletion of *hppD* did not affect bacterial growth (final OD_{600} 1.0 – 1.1) but markedly altered fluorescence induction. The Δ*4hppD* strain exhibited strong and sustained responses to L-tyrosine and 4-HPPA, with fluorescence intensities of 26.26 ± 4.36 and 30.90 ± 4.50 – fold, respectively (Fig. 1a). In contrast, the wild-type strain showed significantly weaker and transient responses (15.74 ± 1.92 and 16.35 ± 3.28 – fold) (Fig. 1b). Thus, fluorescence intensity in the wild type was approximately two times lower than in the Δ*4hppD* mutant. The prolonged induction in the deletion strain suggests intracellular accumulation of 4-HPPA due to disrupted conversion to homogentisate.

Our findings demonstrate that *hppD* is pivotal in controlling 4-HPPA metabolism in *C. necator* H16. The Δ*4hppD* strain represents an improved platform for 4-HPPA – responsive biosensing and metabolic engineering applications.

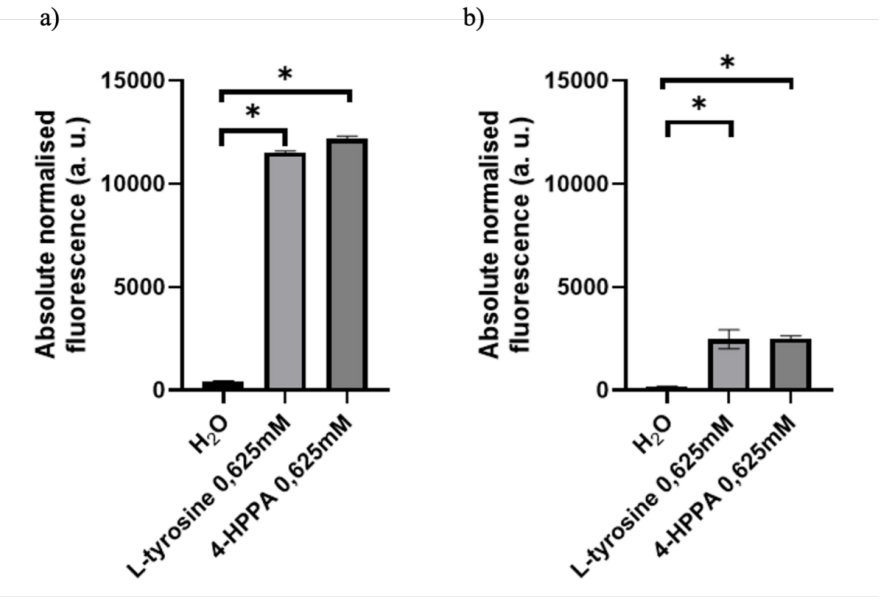


Fig. 1. Absolute normalised fluorescence of (a) *Cupriavidus necator* H16 Δ*4hppD* mutant and (b) wild-type strain, both carrying the pPM014 reporter plasmid. Data are presented as mean ± SD. Statistical significance was determined using an unpaired, two-tailed t-test (*p < 0.001).

[1] H. Pan, J. Wang, H. Wu, Z. Li, and J. Lian, "Synthetic biology toolkit for engineering Cupriviadus necator H16 as a platform for CO2 valorization," Biotechnology for Biofuels, vol. 14, no. 1, p. 212, Nov. 2021, doi: 10.1186/s13068-021-02063-0.

THE MECHANISMS OF TYPE I RESTRICTION-ENDONUCLEASES AT SINGLE-MOLECULE RESOLUTION USING MAGNETIC TWEEZERS

Farzaneh Alipoor Azizollahi[1], Paulius Toliušis[1], Mindaugas Zaremba[1], Algirdas Toleikis[1]

[1]Vilnius University, Life Sciences Center, institute of Biotechnology, Vilnius, Lithuania
farzaneh.alipoor@bti.stud.vu.lt

Restriction–endonuclease (RE) enzymes play a key role in the bacterial defense against foreign DNA invasion. NgoAVII is a type I RE enzyme composed of the restriction subunit with PLD nuclease and B3-like DNA-binding domains, and the helicase-like subunit, containing DEAD-box and Z1 domains.

Unlike traditional RE systems, it not only cuts the DNA but also translocates on the dsDNA using ATP. The translocation dynamics of NgoAVII is not fully understood, particularly how it is coordinated with DNA sequence recognition and cutting. To investigate the translocation, we use a custom-built magnetic tweezers microscope to study it at single-molecule level. We find that the translocation occurs via looping and unlooping events. We further investigate how translocation depends on force and the interaction between restriction and translocation subunits. We anticipate that the mechanical properties obtained in this study will provide valuable insight into the mechanisms of type I RE systems.

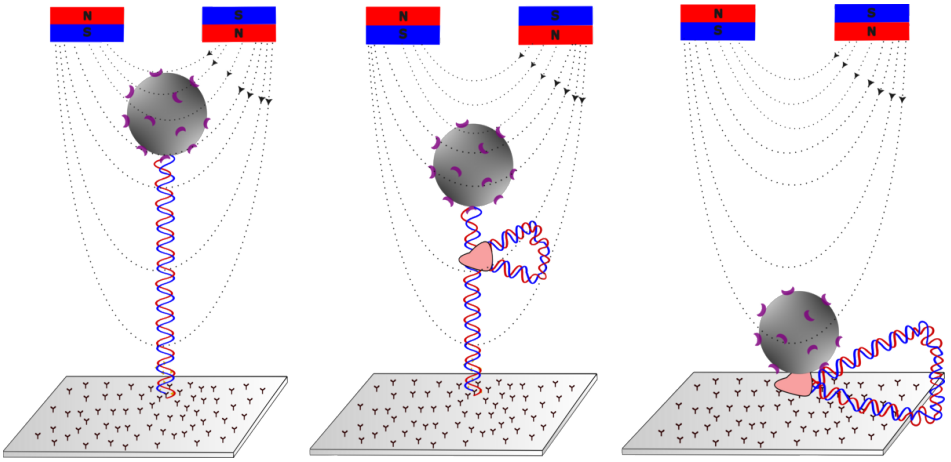


Fig. 1. A schematic of DNA and restriction-endonuclease enzyme in single-molecule resolution

APPLICATION OF MOLECULAR BIOLOGY METHODS FOR THE DETECTION OF BABESIA CANIS

Illia Hol[1], Miglė Razgūnaitė[1], Justina Snegiriovaitė[1], Indrė Lipatova[1], Karolina Jankauskaitė[2], Birutė Karvelienė[2], Algimantas Paulauskas[1], Jana Radzijevskaja[1]

[1]Vytautas Magnus University, Faculty of Natural Sciences, Donelaičio str. 52, LT-44243 Kaunas, Lithuania
[2]Lithuanian University of Health Sciences, Tilžės str. 18, LT-47181 Kaunas, Lithuania
migle.razgunaite@vdu.lt

Canine babesiosis is a widely distributed tick-borne infectious disease caused by the intraerythrocytic protozoan *Babesia canis*. During the past two decades, the number of cases of disease has increased across Europe, with a growing number also reported in Lithuania. Given the rapid spread of the disease, accurate diagnosis and effective treatment are becoming increasingly important. Conventional diagnostic approaches used in veterinary practice, including clinical examination and microscopic evaluation of blood smears, may lack sufficient sensitivity and often do not enable precise identification of the causative agent. This study aimed to assess the prevalence of *B. canis* isolated from shelter dogs in Lithuania through sequence analysis of the *B. canis Bc28.1* gene fragment. Blood samples were collected from 50 clinically symptomatic and asymptomatic shelter dogs between spring and autumn 2024. *B. canis* DNA was identified in 2 out of 50 samples (4%). Sequence analysis revealed identical *Bc28.1* gene fragments in both symptomatic and asymptomatic dogs. These findings highlight the value of molecular methods for detecting and characterizing *B. canis*, contributing to improved diagnostic accuracy and enhanced epidemiological surveillance of canine babesiosis.

Acknowledgements
This study was supported by the Research Council of Lithuania (Grant No. S-MIP-23/19).

Keywords: canine babesiosis, Babesia canis, shelter animals, Bc28.1 gene.

FUNCTIONAL CHARACTERISATION OF RECOMBINANT PSEUDOMONAS AERUGINOSA LIPOXYGENASE

Vytautė Blekaitytė[1], Dovilė Daunoraitė[1], Inga Matijošytė[1]

[1]Vilnius University, Life Sciences Center, Institute of Biotechnology, Sector of Applied Biocatalysis, Vilnius, Lithuania
vytaute.blekaityte@gmc.stud.vu.lt

In the industrial sector, there is an increasing reliance on biocatalysis, an approach that uses enzymes as catalysts, to enhance sustainability and process efficiency. Biocatalysis offers a greener alternative to traditional chemical methods by enabling highly selective reactions to be carried out under mild conditions, thereby reducing energy consumption and environmental impact. One particularly promising application of biocatalysis is the transformation of fatty acids into valuable compounds, including biofuels, polyols, and flavour compounds. In this context, lipoxygenases (LOX) have been identified as key enzymes in the peroxidation of polyunsaturated fatty acids. While most research has focused on human and plant LOX, the potential of bacterial LOX, which was only recently discovered, remains largely unexplored [1].

Among bacterial enzymes, *Pseudomonas aeruginosa* lipoxygenase (PaLOX) represents a promising candidate due to its reported stability and ability to oxidise a broad range of fatty acid substrates [2]. To better evaluate its suitability for biocatalytic applications, this study focused on the biochemical and functional characterisation of recombinant PaLOX. The *palox* gene was expressed in the yeast *Pichia pastoris*, enabling extracellular production of the recombinant enzyme. PaLOX was purified by immobilised-metal affinity chromatography. The effects of temperature, pH, and selected inhibitors on enzyme activity and stability were investigated. Enzymatic activity was measured using a spectrophotometric lipoxygenase activity assay. Further details of the study will be presented during the poster session.

[1] R. Chrisnasari, M. Hennebelle, J.-P. Vincken, W. J. H. Van Berkel, and T. A. Ewing, “Bacterial lipoxygenases: Biochemical characteristics, molecular structure and potential applications,” Biotechnology Advances, vol. 61, p. 108046, Oct. 2022, doi: 10.1016/j.biotechadv.2022.108046.

[2] C. Hashem, H. Stolterfoht, C. Rinnofner, S. Steinberger, M. Winkler, and H. Pichler, “Secretion of Pseudomonas aeruginosa Lipoxygenase by Pichia pastoris upon Glycerol Feed,” Biotechnology Journal, vol. 15, no. 11, p. e2000089, Aug. 2020, doi: 10.1002/biot.202000089.

EVALUATION OF THE ENZYMATIC ACTIVITY AND LYOPHILIZATION STABILITY OF SURFACE DISPLAYED ESTERASE FROM *GEOBACILLUS STEAROTHERMOPHILUS*

Viktorija Kurpickaja[1], Arūnė Verbickaitė[1], Antanas Padaiga[2], Vilius Malūnavičius[2], Renata Gudiukaitė[2], Rasa Petraitytė-Burneikienė[1]

[1]Vilnius University, Life Sciences Center, Institute of Biotechnology, Department of Eukaryote Gene Engineering, Vilnius, Lithuania
[2]Vilnius University, Life Sciences Center, Institute of Biosciences, Department of Microbiology and Biotechnology, Vilnius, Lithuania
viktorija.kurpickaja@gmc.stud.vu.lt

Yeast surface display is a powerful protein engineering technology which enables recombinant proteins to be immobilised on the surface of yeast cell. This offers significant advantages for biocatalysis and industrial applications. This strategy eliminates the need for enzyme purification, improves substrate accessibility and supports continuous enzymatic reactions while reducing the risk of contamination [1]. This study used the a-agglutinin based surface display system to express and display an extreme thermophilic esterase from This *Geobacillus stearothermophilus* [2] on the surface of This *Saccharomyces cerevisiae*. The target enzyme was fused to the Aga2 subunit, enabling stable immobilisation of the enzyme on the yeast cell wall via disulfide bonding with Aga1 [3].

Five different yeast expression vectors, each containing a different linker peptide between Aga2 and the esterase [4], were used to optimise the efficiency of enzyme display and the performance of the catalysis. Esterase activity was successfully detected and experimentally evaluated on the surface of yeast cells. Furthermore, yeast cells displaying the esterase were processed by lyophilisation. Notably, esterase activity was observed in the dried yeast cells, indicating that the immobilised enzyme retains its functionality after drying. This finding highlights the robustness of the system and its potential for long-term storage and practical industrial applications [5].

[1] Y. Li, X. Wang, N.-Y. Zhou, and J. Ding, “Yeast surface display technology: Mechanisms, applications, and perspectives,” Biotechnology Advances, vol. 76, p. 108422, Aug. 2024, doi: 10.1016/j.biotechadv.2024.108422
[2] R. Gudiukaite, M. Sadauskas, A. Gegeckas, V. Malunavicius, and D. Citavicius, “Construction of a novel lipolytic fusion biocatalyst GDEst-lip for industrial application,” Journal of Industrial Microbiology & Biotechnology, vol. 44, no. 6, pp. 799–815, Jan. 2017, doi: 10.1007/s10295-017-1905-4
[3] B. F. Mashangoane and E. N. Chirwa, “Cell surface display of palladium binding peptide on Saccharomyces cerevisiae EBY100 cells using the a-agglutinin anchor system developed for the biosorption of Pd (II),” Minerals Engineering, vol. 176, p. 107325, Dec. 2021, doi: 10.1016/j.mineng.2021.107325
[4] I. Šapronytė, „Acinetobacter baumannii Blp1 baltymo C-galinio fragmento eksponavimo mielių Saccharomyces cerevisiae ląstelių paviršiuje tyrimai“, Vilnius University, 2024
[5] E. Lee and J.-E. Lee, “Alterations in intracellular metabolites of Saccharomyces cerevisiae during freeze-drying and strategies for enhancing viability,” LWT, vol. 234, p. 118567, Sep. 2025, doi: 10.1016/j.lwt.2025.118567

CHARACTERIZATION OF A SYRINGIC AND VANILLIC ACID-INDUCIBLE GENE EXPRESSION SYSTEM IN SPHINGOBIUM SP. SYK-6

Miglė Loveikytė[1], Ernesta Augustiniene[1]

[1]Kaunas University of Technology, Faculty of Chemical Technology, Bioprocess Research Centre, Radvilėnų pl. 19, LT-50254 Kaunas, Lithuania
migle.loveikyte@ktu.edu

Phenolic acids such as syringic and vanillic acids are recognized as key intermediates in lignin depolymerization and are considered valuable bioactive compounds with applications in biotechnology, biorefinery processes, and synthetic biology. The aerobic alphaproteobacterium *SPHINGOBIUM* sp. SYK-6 is widely employed for the study of lignin-derived aromatic compound degradation because monoaryl and biaryl substrates can be utilized by this organism as sole carbon and energy sources. Despite the extensive characterization of lignin catabolic pathways in this bacterium, the transcriptional regulation of genes involved in syringic and vanillic acid metabolism has not been sufficiently understood [1,2]. In *SPHINGOBIUM* sp. SYK-6, syringic acid is converted to 3-methylgallic acid and is subsequently metabolized via the gallate cleavage pathway.

A powerful platform for the development of genetically encoded whole-cell biosensors is provided by transcription factor (TF)-based inducible gene expression systems, through which the detection and quantification of small molecules relevant to metabolic engineering and strain optimization can be achieved. Although biosensors responsive to several phenolic compounds have been reported, the development of a robust and specific syringic acid-inducible system has remained challenging [3].

In this study, a DesR-dependent inducible gene expression system from *SPHINGOBIUM* sp. SYK-6 that responds to syringic and vanillic acids was characterized. Genetic constructs containing desR and the promoter region upstream of desB were assembled and were evaluated in both native and heterologous bacterial hosts. New insights into the regulation of lignin-derived aromatic compound metabolism are provided by these results, and a foundation for the future design of syringic acid-responsive biosensors with potential applications in biotechnological and environmental monitoring platforms is established.

[1] T. Araki et al., “Regulation of vanillate and syringate catabolism by a MarR-type transcriptional regulator DesR in Sphingobium sp. SYK-6,” Scientific Reports, vol. 9, no. 1, p. 18036, Dec. 2019, doi: 10.1038/s41598-019-54490-7.

[2] Kamimura, N. et al., “Bacterial catabolism of lignin-derived aromatics: new findings in a recent decade,” Enviroinmental Biotechnology Reports, vol. 9, no. 6, pp. 679–705, Dec. 2017, doi: 10.1111/1758-2229.12597.

[3] E. Augustiniene, I. Kutraite, E. Valanciene, P. Matulis, I. Jonuskiene, and N. Malys, “Transcription factor-based biosensors for detection of naturally occurring phenolic acids,” New Biotechnology, vol. 78, pp. 1–12, Sep. 2023, doi: 10.1016/j.nbt.2023.09.004.

AUXOTROPH-BASED SCREENING STRATEGIES FOR MODIFIED HETEROCYCLIC BASE METABOLISM

Augustė Kavaliauskaitė[1], Ieva Petkevičiūtė[1], Daiva Tauraitė[1], Jaunius Urbonavičius[1]

[1]Vilnius Gediminas Technical University, Department of Chemistry and Bioengineering, Vilnius, Lithuania
auguste.kavaliauskaite@stud.vilniustech.lt

Purines and pyrimidines are fundamental heterocyclic molecules that emerged early in the evolution of life and therefore are concerved across all three Domains of Life. These compounds play essential role in nucleic acid structure, energy transfer and cofactor function, thereby regulating a wide range of cellular functions. In addition, heterocyclic base derivates are explored for their potential in pharmacological applications, as active ingredients in the theraphy for autoimmune diseases, cancer or viral infections [1]. Auxotrophic bacterial strains provide a powerful *in vivo* platform for metabolic studies, as their growth strictly depends on the restoration of specific biochemical functions. They help to determine the relationship between bacterial cell growth and protein synthesis, and the genes encoding corresponding metabolic functions [2]. During this study, different *Escherichia coli* auxotrophs were used to investigate the metabolism of modified heterocyclic bases using two complementary genetic strategies: metagenomic libraries and transposon mutagenesis.

Environmental genomic DNA isolated from soil samples was used to construct four independent metagenomic libraries in the pUC19 vector. These libraries were introduced into *E. coli ΔguaB::*Km and *E. coli ΔpurH::*Km auxotrophic strains, and growth complementation was assessed on minimal M9 medium supplemented with modified purine bases whose metabolic pathways remain poorly characterized in the literature. In parallel, specific growth phenotypes, including the ability of *E. coli ΔpyrF::*Km to utilize N^4-methylcytosine as uracil source [3] and *E. coli ΔguaB::*Km to grow in the presence of 2-amino-N^6-methylpurine, were investigated using transposon mutagenesis. Individual mutants were screened for loss of growth complementation, and selected candidates were subjected to genome sequencing for further analysis.

Overall, this study demonstrates the applicability of auxotroph-based systems for functional identification of enzymes involved in the metabolism of modified heterocyclic bases. Ongoing analyses aim to identify the genetic determinants underlying the observed growth complementation phenotypes.

Acknowledgements

This project has received funding from the Research Council of Lithuania (LMTLT), agreement No [S-MIP-25-95].

Keywords: Modified heterocyclic bases, auxotrophs, metagenomic libraries, transposon mutagenesis.

[1] M. G. Martina, L. Giannessi, and M. Radi, “Multicomponent Synthesis of Purines and Pyrimidines: From the Origin of Life to New Sustainable Approaches for Drug-Discovery Applications,” European Journal of Organic Chemistry, vol. 26, no. 2, Dec. 2022.

[2] J. Chen, Y. Wang, P. Zheng, and J. Sun, “Engineering synthetic auxotrophs for growth-coupled directed protein evolution,” Trends in Biotechnology, vol. 40, no. 7, pp. 773–776, Jul. 2022.

[3] J. Urbonavičius, A. Čekytė, and D. Tauraitė, “N4-Methylcytosine Supports the Growth of Escherichia coli Uracil Auxotrophs,” International Journal of Molecular Sciences, vol. 26, no. 5, p. 1812, Feb. 2025.

TNPB: A POTENTIAL TOOL FOR GENOME-EDITING IN E. COLI

Justė Dautaraitė[1], Gytis Druteika[1], Tautvydas Karvelis[1]

[1]Vilnius University, Life Sciences Center, Department of Protein-DNA Interactions, Lithuania
juste.dautaraite@chgf.stud.vu.lt

At present, bacterial genome editing frequently relies on CRISPR–Cas systems, which function as RNA-guided DNA endonucleases that introduce double-strand breaks in a PAM (Protospacer Adjacent Motif)-dependent manner. Despite their high efficiency, the application of these nucleases can be restricted under certain conditions due to cytotoxicity, potential off-target activity, and PAM sequence requirements [1]. Therefore, expanding the genome-editing toolkit in *E. coli* through the introduction of novel molecular tools that exhibit DNA cleavage activity as well as a wide range of target sequences may provide a foundation for advanced genetic manipulation and broader implementation in synthetic biology [2].

The aim of this study was to determine the DNA cleavage activity of selected TnpB proteins in *E. coli*. The analysis was conducted by performing a plasmid interference assay under IPTG-driven induction, in which nuclease activity led to the inhibition of cell growth, whereas inactive proteins did not cause any growth changes.

The results demonstrate that a set of tested TnpB nucleases with varying TAM sequences is capable of cleaving DNA in *E. coli*, leading to measurable growth inhibition. Growth reduction ranged approximately from one to three orders of magnitude compared to control reactions. These findings suggest that TnpB proteins, distinguished by their target sequence diversity, may represent valuable tools for advanced bacterial genome-editing together with the expansion of the target range.

[1] S. Cho, D. Choe, E. Lee, S. C. Kim, B. Palsson, and B.-K. Cho, “High-Level dCas9 Expression Induces Abnormal Cell Morphology in Escherichia coli,” ACS Synthetic Biology, vol. 7, no. 4, pp. 1085–1094, Mar. 2018, doi: 10.1021/acssynbio.7b00462.

[2] J. Luo et al., “STAGE: A compact and versatile TnpB-based genome editing toolkit for Streptomyces,” Proceedings of the National Academy of Sciences, vol. 122, no. 35, p. e2509146122, Aug. 2025, doi: 10.1073/pnas.2509146122.

AUXIN AND CYTOKININ PROFILES IN BARLEY TWEAKY SPIKE (tw) MUTANTS REVEAL AN AUXIN-SPECIFIC HORMONE DISTURBANCE

Dominykas Laibakojis[1], Tautvydas Žalnierius[1], Jurga Jankauskienė[1], Vėjūnė Pukenytė[2], Raimondas Šiukšta[2], Simonas Balčiūnas[3], Sigita Jurkonienė[1]

[1]State Scientific Research Institute Nature Research Centre, Laboratory of Plant Physiology, Lithuania
[2]Vilnius University, Institute of Biosciences, Lithuania
[3]Vilnius University, Department of Analytical and Environmental Chemistry, Lithuania
dominykas.laibakojis@gamtc.lt

Barley pleiotropic developmental tweaky spike (*tw*) mutants exhibit abnormal flower/inflorescence structure that has been associated with disturbances in auxin (Aux) physiology. Since spike development is regulated not by individual phytohormones but by their interactions in different spike segments, changes in Aux concentration may influence the distribution of other hormones along the spike axis and, conversely, Aux gradients may arise from imbalances in other phytohormone pathways. Barley inflorescence architecture is a key determinant of grain number and quality, and developmental mutants therefore provide an effective route to identify regulatory pathways controlling spike morphogenesis. The *tw* mutants comprise a recessive allelic series with pleiotropic spikes and floret defects, consistently associated with disrupted Aux regulation. In this study, we aimed to investigate the concentrations and distribution of phytohormones: indole-3-acetic acid (IAA) and cytokinins (CKs) among *tw* and wild-type backgrounds.

IAA and CKs concentrations were compared between *tw* mutants and their corresponding wild-type backgrounds in upper and lower spike segments. Across the *tw* alleles examined, mutants consistently had lower IAA levels than their corresponding wild types. In the 'Auksiniai 3' (A3) wild type, IAA was clearly higher in the upper spike segment than in the lower segment. In tw_9 and tw_{10} (A3 background), this gradient almost disappeared because the upper and lower segments contained very similar IAA levels. Therefore, the IAA distribution along the spike axis was much more even. In contrast, CKs profiles were largely stable at the segment level: cis-Zeatin was the main detectable CKs, while trans-Zeatin was inconsistent and isopentenyladenine/dihydrozeatin were mostly marginal, with no genotype-consistent directional change separating *tw* mutants from wild types.

Overall, the *tw* mutants show consistent Aux deficiency and disrupted IAA distribution, while CKs profiles remain broadly similar to wild types, indicating that the *tw* developmental syndrome is mainly associated with altered Aux homeostasis rather than major changes in CKs content.

Acknowledgements

This work was supported by a grant from the Lithuanian Research Council No. S-MIP-24-122 "Genetic mapping and characterization of barley developmental flower/inflorescence tweaky spike (tw) mutation".

ULTRASOUN-INDUCED CHANGES IN THE ABSORPTION SPECTRA OF MAGNESIUM AND COPPER CHLOROPHYLLINS

Dita Valiulytė[1], Irina Buchovec[1]

[1]Vilnius University, Faculty of Physics, Institute of Photonics and Nanotechnology, Lithuania
dita.valiulyte@ff.stud.vu.lt

Ultrasound is commonly used to influence the aggregation or self-assembly of molecules in solution, thereby directly affecting their nanostructure and optical properties.[1] However, there is limited data on how ultrasound exposure actually alters the absorption of metal-based chlorophyll derivatives such as chlorophyllins. The purpose of this study was to determine whether ultrasound treatment had any effect on the absorption spectra of magnesium (Mg-Chl) and copper (Cu-Chl) chlorophyllins. Furthermore, we wanted to test whether the central metal ion or solvent affected their stability and propensity for aggregation during sonication. Mg-Chl and Cu-Chl were selected as model metal-containing, photoactive chlorophyll derivatives to assess the influence of the central metal ion on spectral stability under ultrasonic conditions.

Absorption spectra were recorded using UV–Vis absorption spectroscopy in the wavelength range of 300–900 nm. The spectra were obtained before and after a defined ultrasound treatment of working solutions of Mg-Chl and Cu-Chl prepared in distilled water and in phosphate-buffered saline (PBS). Temperature of solutions was controlled during ultrasound treatment to reduce thermal artifacts. The influence of ultrasound treatment and solvent environment on spectral stability was evaluated by comparing pre- and post-exposure absorption profiles.

The results showed that the solvent environment had minimal impact on the spectral response of Cu-Chl to ultrasound. In both distilled water or PBS, the effect was nearly identical: a slight drop in Soret band intensity and a more noticeable decrease and broadening of the Q-bands. In contrast, Mg-Chl was much more sensitive to the choice of medium and was characterized by significantly greater reduction of the Soret band in PBS than in water. While Mg-Chl showed a larger overall drop in the Soret region compared to Cu-Chl, its Q-band maximum remained largely unchanged, which is quite different from what we observed with the copper derivative. These findings provide a basis for selecting the right chlorophyllin for ultrasound-assisted nanostructure formation, depending on whether distilled water or PBS is used as the solvent.

[1] J. H. Bang and K. S. Suslick, “ChemInForm Abstract: Applications of Ultrasound to the synthesis of nanostructured Materials,” ChemInform, vol. 41, no. 18, Apr. 2010, doi: 10.1002/chin.201018217.

CREATING INNOVATIVE ORGANIC BIODEGRADABLE SUBSTRATES FOR SEED GERMINATION

Eglė Didžiulytė[1], Rasa Šlinkšienė[1]

[1]Kaunas University of Technology, Faculty of Chemical Technology, Department of Physical and Inorganic Chemistry, Kaunas, Lithuania
egle.didziulyte@ktu.lt

In alternative farming, it is important to use only special pur-pose growing substrates, which used to consist largely of peat. The EU is working to reduce the use of peat, as peat-lands are essential for CO_2 capture and climate change miti-gation. 2020 European Green Deal aims promote a shift to-wards more sustainable alternative's biodegradable substrates and other sustainable products. As biogas production gener-ates large quantities of digestate (one biogas plant produces 10,000 m3/year of digestate, which has a chemical substrate that provides nutrients needed by plants), research has been carried out on how to use it in growing substrates instead of peat. Two digestates from Lithuanian companies (UAB "Tvari Energija" and UAB "Kurana"), also soil, peat, sapro-pel, and coffee grounds, were used to create the substrates with essential plant nutrients. Different ratios of raw materi-als were selected for the development of innovative sub-strates. These digestates contain not only primary and sec-ondary nutrients (N, P, K, Ca, Mg) also an organic carbon and organic matter. The germination of cucumber and tomato seeds improved in both speed and success when grown in a substrate containing UAB "Tvari Energija" digestate (40–60%), soil (20–30%), peat (10–20%), sapropel (5%), and coffee grounds (5%). The plants also exhibited greater growth over 30 days of cultivation compared to those grown with digestate substrates from UAB "Kurana". It is assumed that this digestate has a higher total nitrogen concentration, which burned the plants upon emergence. Consequently, a lower amount (20–30%) of UAB "Kurana" digestate was se-lected. This study confirms that digestate can be effectively used in seed germination substrates, thus recycling biogas production waste by reducing its disposal to landfills and conserving natural resources.

Keywords: Digestate, Substrates, Seed, Nutrients.

NOVEL POLYMER DOTS FOR FLUORESCENCE BIOIMAGING WITHIN THE SECOND NEAR-INFRARED WINDOW

Skaiste Talanovaite[1], Greta Tamoliunaite[1], Vilius Poderys[1], Simona Steponkiene[1], Yaw-Kuen Li[2,3], Tung-Kung Wu[2,4], Yang-Hsiang Chan[3], Vitalijus Karabanovas[1,5]

[1]National Cancer Institute, Biomedical Physics Laboratory, Vilnius, Lithuania
[2]National Yang Ming Chiao Tung University, Center for Emergent Functional Matter Science, Hsin-Chu, Taiwan
[3]National Yang Ming Chiao Tung University, Department of Applied Chemistry, Hsin-Chu, Taiwan
[4]National Yang Ming Chiao Tung University, Department of Biological Science and Technology, Hsin-Chu, Taiwan
[5]Vilnius Gediminas Technical University, Department of Chemistry and Bioengineering, Vilnius, Lithuania
skaiste.talanovaite@gmc.stud.vu.lt

The second near-infrared spectral window (NIR-II, 1000-1700 nm) offers significant advantages in deep-tissue penetration, reduces photon scattering and minimizes tissue autofluorescence. These advantages require development of emissive nanomaterials with broad absorption, efficient near-infrared emission and high photostability. Polymer dots (Pdots) represent a promising class of probes for NIR-II bioimaging due to their high brightness, strong resistance to photobleaching and low cytotoxicity [1]. In this study, we investigate the optical and physicochemical properties of novel polymer dots and to evaluate their suitability as NIR-II fluorescent probes for bioimaging applications.

Polymer dots composed of the semiconducting polymer DBT-4O-TTQ and surface-modified with DSPE-mPEG (40%) were characterized following dilution in aqueous media and measurements of absorption and fluorescence spectra, photobleaching, zeta potential and particle size distribution.

The Pdots exhibit broad absorption in the ultraviolet and visible regions, enabling efficient excitation at 808 nm. Under this excitation, a wide near-infrared emission band with a maximum at 930 nm was observed, extending toward longer wavelengths, relevant for NIR bioimaging (Fig. 1). Dynamic light scattering measurements reveal a hydrodynamic diameter of 85 nm with low polydispersity (PDI = 0.126), while zeta potential of -40 mV indicates good colloidal stability.

The acquired results indicate that Pdots combine broad spectral absorption, stable nanoscale morphology and near-infrared emission. The observed photophysical and optical properties highlights their potential as organic fluorescent probes for advanced bioimaging applications and motivates further NIR-II imaging studies in biological systems.

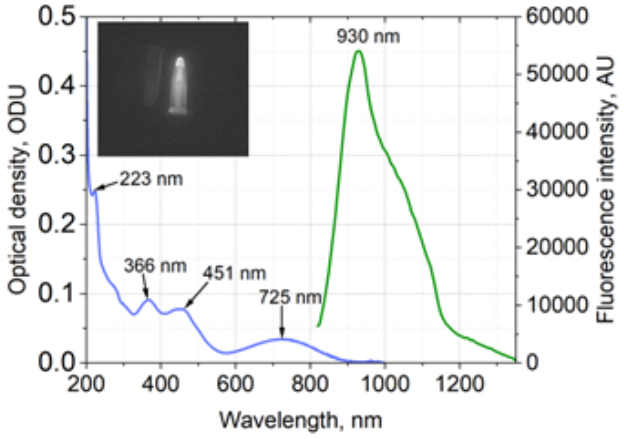


Fig. 1. Optical desnsity and fluorescence spectra (λ_{ex} = 808 nm laser, 95 mW) of Pdot

[1] R. Gupta et al., "Semiconducting Polymer Dots Directly Stabilized with Serum Albumin: Preparation, Characterization, and Cellular Immunolabeling," ACS Applied Materials & Interfaces, vol. 15, no. 48, pp. 55456–55465, Nov. 2023, doi: 10.1021/acsami.3c13430.

INVESTIGATION OF ENERGY TRANSFER AND SINGLET OXYGEN GENERATION IN BLOOD PLASMA PROTEIN GOLD NANOCLUSTERS-CE6-UCNP COMPLEXES

Greta Tamoliunaite[1], Skaiste Talanovaite[1], Vilius Poderys[1], Vaidas Klimkevicius[1,2], Vitalijus Karabanovas[1,3]

[1]Lithuania, Vilnius, National Cancer Institute, Biomedical Physics Laboratory
[2]Lithuania, Vilnius, Vilnius University, Institute of Chemistry
[3]Lithuania, Vilnius, Vilnius Gediminas Technical University, Department of Chemistry and Bioengineering
greta.tamoliunaite@gmc.stud.vu.lt

With photodynamic cancer therapy (PDT) being one of the clinically approved therapy strategies, its effectiveness greatly depends on the depth of the tumor and ability of light to reach photosensitizer that is accumulated in the tumor site. Near-infrared light (NIR) can penetrate deeper into tissues but lack energy to excite photosensitizers (PS). Upconverting nanoparticles (UCNPs) can offer a solution to this problem by converting NIR light in to higher energy VIS-UV photons, that are capable to excite PS molecules [1].

The goal of this study is to combine synthesized blood plasma protein gold nanoclusters (HSA-AuNC), PS Chlorin e6 (Ce6) and UCNPs to form complexes, that can be excited by NIR light, transfer energy to Ce6 and enable singlet oxygen generation. Gold nanoclusters were synthesized by reducing chloroauric acid in alkaline human blood serum environment [2]. The resulting HSA-AuNC were subsequently combined with Ce6 and UCNPs. The formation of the multicomponent complexes was confirmed using optical characterization techniques (Fig. 1). Energy transfer and singlet oxygen generation were investigated via photoluminescent decay, fluorescence anisotropy and singlet oxygen sensitive probes under VIS and NIR excitation conditions.

A red-shift of the Ce6 fluorescence emission and fluorescence anisotropy measurements confirms complex formation between Ce6 and HSA-AuNCs. Photoluminescence (PL) decay analysis reveals a pronounced shortening of the UCNP emission lifetimes in the UCNP–HSA-AuNC–Ce6 complex compared to free UCNPs, indicating efficient energy transfer from UCNPs acting as energy donors to Ce6 as the primary energy acceptor. Singlet oxygen generation, evaluated using fluorescence-based probe, under both VIS and NIR light demonstrates successful singlet oxygen generation.

Our investigations show promising potential for personalized therapeutic compounds, that can generate singlet oxygen, by being irradiated with deep-penetrating, low energy NIR light.

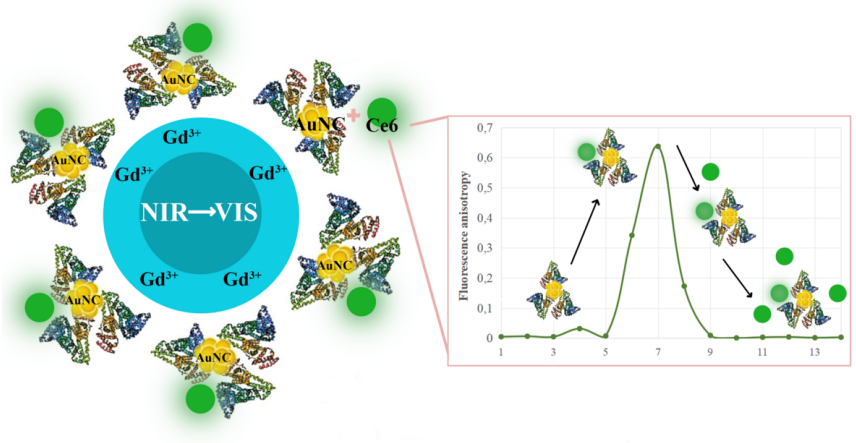


Fig. 1. Schematic depiction of HSA AuNC-Ce6-UCNP complex. FL anisotropy assessment of Ce6 adhesion to HSA-AuNC.

[1] H. Li, S. Song, W. Wang, and K. Chen, “In vitro photodynamic therapy based on magnetic-luminescent Gd2O3:Yb,Er nanoparticles with bright three-photon up-conversion fluorescence under near-infrared light,” Dalton Transactions, vol. 44, no. 36, pp. 16081–16090, Jan. 2015, doi: 10.1039/c5dt01015b.

[2] J. Xie, Y. Zheng, and J. Y. Ying, “Protein-Directed synthesis of highly fluorescent gold nanoclusters,” Journal of the American Chemical Society, vol. 131, no. 3, pp. 888–889, Jan. 2009, doi: 10.1021/ja806804u.

TIME-DEPENDENT STABILITY AND OPTICAL PROPERTIES OF RIBOFLAVIN AND MAGNESIUM CHLOROPHYLLIN MIXTURE IN SOLUTION

Urtė Mitrofanaitė[1], Irina Buchovec[2]

[1]Vilnius University, Life Sciences Center, Institute of Biosciences, Vilnius, Lithuania
[2]Vilnius University, Faculty of Physics, Institute of Photonics and Nanotechnology, Vilnius, Lithuania
urte.mitrofanaite@gmc.stud.vu.lt

The increasing prevalence of antibiotic-resistant foodborne pathogens highlights the urgent need for novel, non-toxic antimicrobial approaches. Antimicrobial photodynamic inactivation (API) is one such technology that is effective against a variety of pathogens that traditional disinfectants and preservatives have trouble with. API relies on three main components: a photosensitizer (PS), molecular oxygen, and light of an appropriate wavelength that corresponds with the absorption spectrum of the PS. Upon photoexcitation, the PS becomes photochemically active, generating reactive oxygen species (ROS) that cause lethal oxidative damage to microbial cellular components [1]. Since API performance hinges on PS physicochemical stability, shifts in absorption or aggregation behavior can directly compromise ROS generation, underscoring the importance of long-term stability. The present work aims to analyse how these conditions influence the spectral profiles of RF/Mg-Chl mixture, studying filtered and unfiltered aqueous systems and allowing the observation of aggregation effects as well as the influence of solution homogeneity on the recorded absorption spectra.

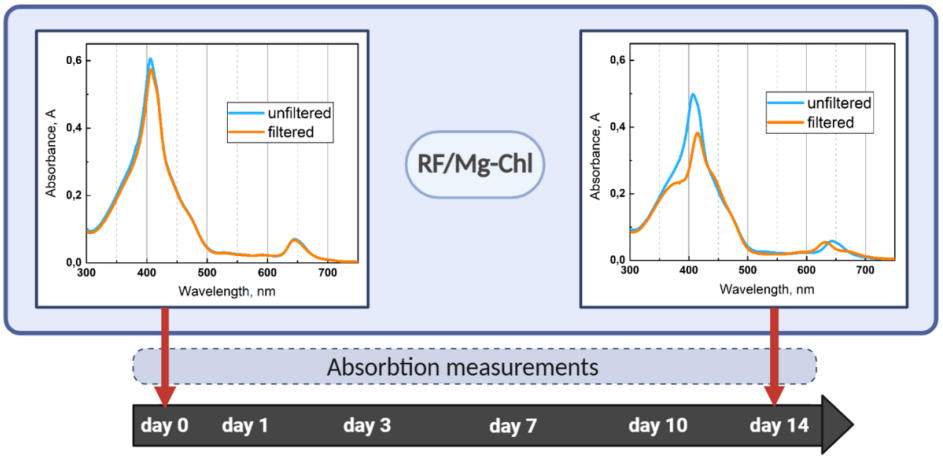


Fig. 1. Scheme of RF/Mg-Chl mixture absorption spectra monitoring in filtered and unfiltered systems over time.

To evaluate the stability of RF, Mg-Chl and their mixture, separate stock solutions of each PS were prepared in distilled water using compound-specific dissolution condition [1]. The stock solutions were used either after sterile filtration (0.22 µm) or without filtration. RF/Mg-Chl mixtures were then prepared from the corresponding filtered or non-filtered stocks and diluted to working concentration. Samples were stored under dark, low-temperature conditions and analysed over time. Spectrophotometric measurements were performed on days 0, 1, 3, 7, 10, and 14 to track the stability and changes in spectral peak positions, band shapes, and absorption spectra of RF/Mg-Chl mixture. On day 0, filtered RF/Mg-Chl solutions exhibited slightly reduced absorption compared to unfiltered samples, consistent with reduced scattering and partial removal of larger aggregates. After 14 days, absorbance decreases in both filtered and unfiltered solutions, indicating time-dependent aggregation processes. Filtered samples also showed small shifts in peak positions and modifications of the Soret band shape over time. These findings are essential for the design and standardization of preparation and handling protocols for PSs in future API studies.

Keywords: Photosensitizers, riboflavin, magnesium chlorophyllin, Antimicrobial Photodynamic Inactivation (API)

[1] I. Buchovec, E. Vyčaitė, K. Badokas, E. Sužiedelienė, and S. Bagdonas, “Application of Antimicrobial Photodynamic Therapy for Inactivation of Acinetobacter baumannii Biofilms,” International Journal of Molecular Sciences, vol. 24, no. 1, p. 722, Dec. 2022.

THE EFFECT OF DIETARY SUBSTRATES ON THE GROWTH OF THE YELLOW MEALWORM (TENEBRIO MOLITOR L.)

Felicija Kvedaraitė[1], Gabrielė Bumbulytė-Žukevičienė[2]

[1]State Scientific Research Institute Nature Research Centre, Laboratory of Chemical and Behavioural Ecology, Vilnius, Lithuania
felicija.kvedaraite@gmail.com

The escalating global human population demands strategies to reduce environmental pollution. Insects, valued in some Asian cultures as an alternative to conventional meat, offer rapid growth, low environmental impact, and high protein content, making them a promising protein source [1]. These advantages have fueled interest in large-scale insect farming, increasing the need for sustainable dietary substrates that reduce reliance on conventional feeds in mass rearing systems. The yellow mealworm *(Tenebrio molitor L.)* is a promising species for food and feed production; however, its growth performance is strongly influenced by diet composition. Therefore, identifying suitable food-derived waste substrates remains an important research objective.

This study evaluated the effects of different food-and-beverage-industry waste substrates on the growth of *T. molitor* larvae. The larvae were reared on diets composed of either 100% waste material or those containing 75% waste material supplemented with 25% wheat bran. Larvae were reared under controlled laboratory conditions, and their body weight was measured at regular intervals throughout development.

The results demonstrated that most food-and-beverage-industry waste substrates caused statistically significant differences in larval growth compared to the control. A more detailed overview of the substrate compositions and their effects on *Tenebrio molitor* larval growth will be presented during the conference.

[1] A. Orkusz, “Edible insects versus meat—Nutritional comparison: Knowledge of their composition is the key to good health,” Nutrients, vol. 13, no. 4, p. 1207, 2021.

INDIVIDUAL PHENOLIC COMPOUNDS COMPARISON OF BUCKWHEAT HONEY AND FLORAL SOURCE

Ernesta Zaksaitė[1], Mindaugas Liaudanskas[1,2], Vaidotas Žvikas[1,2], Sonata Trumbeckaitė[1]

[1]Lithuanian University of Health Science, Faculty of Pharmacy, Department of Pharmacognosy, Lithuania,
[2]Lithuanian University of Health Science, Faculty of Pharmacy, Institute of Pharmaceutical Technologies, Lithuania,
ernesta.zaksaite@stud.lsmu.lt

Honey's nutritional, physical, and bioactive characteristics are strongly shaped by the plant from which its nectar is collected. Variations in nectar sugars, phenolics, and volatiles substances – determine the honey's color, flavor, texture, and biological activity. Monofloral honeys reflect the properties of a single plant species, whereas polyfloral honeys show mixed profiles [1]. The aim of this study is to compare the phytochemical composition of buckwheat honey with that of its floral source.

Buckwheat honey samples were collected in 2023 from five apiaries, and buckwheat flowers were obtained from two Lithuanian fields. Extracts were prepared by extracting 1 g of each sample with 70% ethanol, sonicating for 20 minutes, filtering under vacuum into 10 mL flasks, and adjusting to volume with ethanol. Before UHPLC-MS/MS analysis, all solutions were filtered through 0.22 µm membranes. Statistical analysis was performed using MS Excel 2023, $P<0.05$ was taken as the level for significance.

Both samples: honey and buckwheat flowers contained quercetin, p-coumaric, ferulic, chlorogenic and protocatechuic acids. The amounts of quercetin, chlorogenic, and protocatechuic acids were markedly higher in flowers than in honey (36.33±3.17 vs. 2.43±2.85 µg/g; 330.07±25.35 vs. 0.74±1.02 µg/g; 22.11±1.75 vs. 0.64±0.58 µg/g, respectively). Quercetin was found mainly in the flowers (36.33±3.17 µg/g), while its concentration in honey was significantly lower (2.43±2.85 µg/g). In contrast, honey showed higher levels of p-coumaric and ferulic acids (6.82±1.98 and 2.34±3.04 µg/g) than flowers (0.12±0.15 and 0.93±0.16 µg/g). Isorhamnetin, acacetin, luteolin, kaempferol, and apigenin were detected only in honey (1.61±2.55, 0.90±0.23, 0.91±0.97, 0.64±0.42, 0.11±0.04 µg/g), likely reflecting pollen from other plant species. In addition to these compounds, several phenolics were detected exclusively in buckwheat flowers, including neochlorogenic acid, caffeic acid, vanillic acid, quercitrin, hyperoside, rutin, isoquercitrin, quercetin-3-O-arabinopiranoside, vitexin, isovitexin, kaempferol-3-O-rutinoside, kaempherol-3-O-glucoside, orientin, luteolin-7-O-rutinoside, luteolin-3,7-diglucoside, isorhamnetin-3-O-rutinoside, myricitrin, procyanidin B1, procyanidin B2, procyanidin C1, (+)-catechin, (−)-epicatechin, phloridzin.

In conclusion, buckwheat flowers demonstrated significantly higher concentrations of quercetin, chlorogenic and protocatechuic acids and a markedly broader spectrum of flavonoids and proanthocyanidins than honey, whereas the exclusive detection of specific flavonoids (acacetin, apigenin, isorhamnetin, luteolin, and kaempferol) in honey, together with elevated p-coumaric and ferulic acid levels, indicates contributions from other plant sources and underscores the complex botanical origin shaping its bioactive profile during nectar foraging.

Keywords: Biochemical properties, Buckwheat honey, Phenolic compounds, Buckwheat flowers, Biochemical profile

[1] Y. Cheung, M. Meenu, X. Yu, and B. Xu, "Phenolic acids and flavonoids profiles of commercial honey from different floral sources and geographic sources," International Journal of Food Properties, vol. 22, no. 1, pp. 290–308, Jan. 2019, doi: 10.1080/10942912.2019.1579835.

DETERMINATION OF BETULINIC ACID CONTENT AND IN VITRO ANTIRADICAL ACTIVITY IN JAPANESE QUINCE (CHAENOMELES JAPONICA (THUNB.) LINL. EX SPACH) FRUIT SAMPLES

Kornelija Kondrotaitė[1], Mindaugas Liaudanskas[1,2], Rima Šedbarė[1], Jonas Viškelis[3], Pranas Viškelis[3], Valdimaras Janulis[1]

[1]Lithuanian University of Health Sciences, Faculty of Pharmacy, Department of Pharmacognosy, Kaunas, Lithuania
[2]Lithuanian University of Health Sciences, Institute of Pharmaceutical Technologies, Kaunas, Lithuania
[3]Lithuanian Research Centre for Agriculture and Forestry, Institute of Horticulture, Babtai, Kaunas distr., Lithuania
kornelija.kondrotaite@stud.lsmu.lt

Japanese quince (*Chaenomeles japonica* (Thunb.) Lindl. ex Spach) belongs to the rose family (*Rosaceae* Juss.) and is rich in many active compounds, including triterpenic acids such as betulinic, corosolic, and ursolic acids. Betulinic acid is well known for its antiviral and anticancer activities [1]. The aim of this research was to determine the quantitative content of betulinic acid and the antiradical activity *in vitro* of Japanese quince fruit samples.

Japanese quince fruit samples were collected from 11 different regions of Lithuania. For extraction, 1 g of lyophilized fruit material was placed in dark glass bottles and extracted with 10 mL of acetone (100%, v/v). The samples were sonicated for 50 min in an ultrasonic bath (565 W, 80 kHz). The extracts were then vacuum-filtered and passed through 0.2 µm membrane filters prior to HPLC analysis. The quantitative composition of betulinic acid was determined using the HPLC method developed by Butkevičiūtė et al. [2]. Antiradical activity *in vitro* was assessed using the DPPH assay: 20 µL of ethanolic fruit extract was mixed with 3 mL of freshly prepared DPPH working solution and incubated in the dark for 30 min. Absorbance was measured at 517 nm using a UV–Vis spectrophotometer [3].

HPLC analysis showed that the betulinic acid content varied significantly among the Japanese quince samples from 310.98 to 1468.67 µmol TE/g. The highest amount (1468.67±88.35 µg/g, $p<0.05$) of betulinic acid was found in samples collected in the Vilkaviškis district and the lowest amount (310.98±20.98 µg/g) – in samples from the Šiauliai district. The betulinic acid amount in the analyzed Japanese quince fruit samples varied within a very wide range. The calculated coefficient of variation was 54.89%

The antiradical activity *in vitro* of the Japanese quince fruit extracts also varied across regions, ranging from 12.87 to 41.34 µmol TE/g. The weakest antiradical activity *in vitro* (12.87±0.01 µmol TE/g, $p<0.05$) was found in samples from the Biržai district, while the strongest antiradical activity was determined in samples from the Vilnius and Jonava districts (41.34±1.11 µmol TE/g and 38.84±1.13 µmol TE/g, respectively). The coefficient of variation, reflecting the relative variability of antiradical activity *in vitro*, across the investigated extracts, was 29.66%.

In conclusion, the highest betulinic acid amount was determined in Japanese quince fruits from the Vilkaviškis district, whereas the strongest antiradical activity *in vitro* was found in samples from the Vilnius and Jonava districts. The Japanese quince fruit samples collected in these districts may be valuable for further phytochemical and biological investigations.

[1] S. Lou, C. Dai, Y. Wu, L. Wang, Y. Jin, N. Shen, W. Lv, M. Wu, X. Xu, J. Han, and X. Fan, "Betulonic acid: A review on its sources, biological activities, and molecular mechanisms," European Journal of Pharmacology, vol. 998. 2025.

[2] Butkevičiūtė A, Liaudanskas M, Kviklys D, Zymonė K, Raudonis R, Viškelis J, Janulis V et al. Detection and analysis of triterpenic compounds in apple extracts. International Journal of Food Properties. 2018 Jan 1;21(1):1716–27.

[3] Raudonė L, Raudonis R, Liaudanskas M, Janulis V, Viškelis P. Phenolic antioxidant profiles in the whole fruit, flesh and peel of apple cultivars grown in Lithuania. Scientia Horticulturae, 2017;216:186–192.

CHANGES IN ANTIOXIDANT PROPERTIES OF BEE-COLLECTED POLLEN DURING STORAGE

Yelyzaveta Lopatina[1], Vilma Kaškonienė[1], Audrius S. Maruška[1], Neringa Sutkevičienė[2]

[1]Vytautas Magnus University, Instrumental Analysis Open Access Center, Akademija, Lithuania
[2]Lithuanian University of Health Sciences, Faculty of Veterinary Medicine, Animal Reproduction Laboratory, Kaunas, Lithuania
lizaa778899@gmail.com

Bee pollen is a natural product rich in carbohydrates, proteins, vitamins, fatty acids, and minerals, and is widely valued for its antioxidant and antimicrobial properties [1], [2]. These properties contribute to pollen quality and stability and may be influenced by processing and storage conditions. This study aimed to evaluate the stability of the antioxidant properties of bee pollen during four weeks of storage under various conditions, including differences in temperature, packaging material, pollen preparation (fresh or dried), and light exposure. Antioxidant activity was determined using spectrophotometric assays, including total phenolic content, flavonoid content, and free radical scavenging activity (DPPH) [3].

The effect of storage conditions on the antioxidant properties of fresh and dried bee pollen is shown in Figure 1. At the initial stage, dried pollen exhibited higher total phenolic and flavonoid contents as well as greater antiradical activity compared to fresh pollen, which can be attributed to concentration effects associated with moisture removal during drying.

After 4 weeks of storage, phenolics and flavonoid content remain stable in fresh pollen stored in the freezer, suggesting effective preservation of antioxidant properties under freezing conditions. While dried pollen samples showed slight variation depending on storage conditions, it is evident that storage had the highest impact on antiradical activity.

Further storage experiments are needed to clarify the long-term stability of these bioactive compounds under different environmental conditions. These results highlight the importance of optimized storage conditions to preserve the functional and sensory quality of bee-collected pollen.

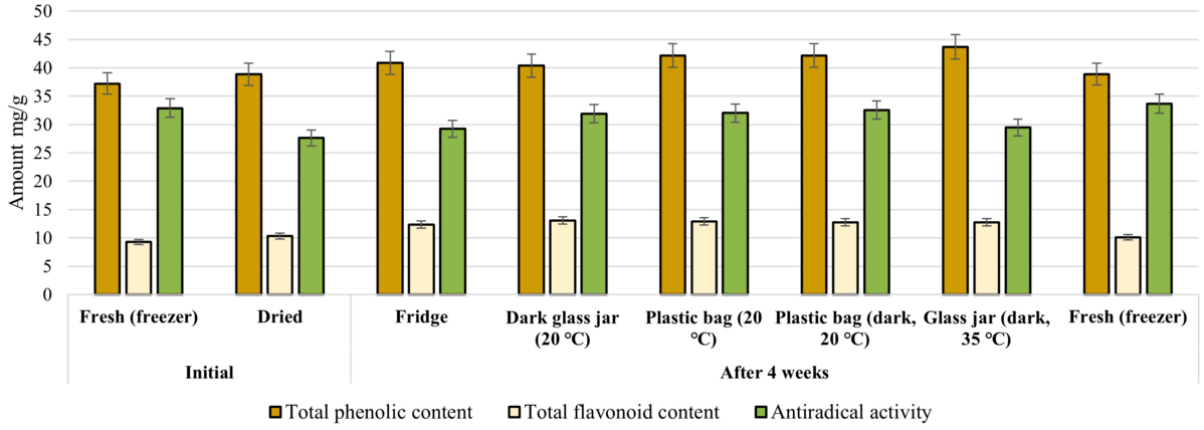


Fig. 1. Effect of storage conditions on the total phenolic content, total flavonoid content, and antiradical activity of fresh and dried bee pollen (results are expressed as mg of rutin equivalents per gram of fresh or dried bee pollen; n = 3, RSD ≤ 5.5%)

Acknowledgements
This work was funded by the Research Council of Lithuania (LMTLT), Grant No. S-ST-25-103.

Keywords: Bee pollen, antioxidant activity, storage conditions, total phenolic content, flavonoids, DPPH assay.

[1] S. A. M. Khalifa et al., "Bee Pollen: Current Status and Therapeutic Potential," Nutrients, vol. 13, no. 6, p. 1876, May 2021.
[2] M. Alcalá-Orozco, I. Lobo-Farfan, D. F. Tirado, and D. C. Mantilla-Escalante, "Enhancing the Nutritional and Bioactive Properties of Bee Pollen: A Comprehensive Review of Processing Techniques," Foods, vol. 13, no. 21, p. 3437, Oct. 2024.
[3] V. Kaškonienė, P. Kaškonas, and A. Maruška, "Volatile compounds composition and antioxidant activity of bee pollen collected in Lithuania," Chemical Papers, vol. 69, January, 2015.

EFFECTS OF CHRONIC PSYCHOLOGICAL STRESS ON FATTY ACID COMPOSITION IN RATS WITH TYPE 2 DIABETES MELLITUS

Justina Kežutytė[1], Justinas Baleišis[2], Romualdas Rudys[2], Inga Bikulčienė[2,3], Dovilė Karčiauskaitė[3]

[1]Lithuania, Vilnius University, Life Sciences Center
[2]Lithuania, Centre for Innovative Medicine, Department of Preclinical Research
[3]Lithuania, Vilnius University, Faculty of Medicine, Translational Health Research Institute
justina.kezutyte@mf.vu.lt

Chronic psychological stress is associated not only with psychiatric disorders but also with physical diseases. [1] Therefore, stress is increasingly recognised as a risk factor that may accelerate the development and progression of metabolic disorders, including type 2 diabetes mellitus (T2DM). [2] This chronic progression is closely related to lifestyle and environmental conditions. [3] However, limited data are available that directly link fatty acid (FA) composition to psychological stress in the context of T2DM. In this study, we investigated the effects of induced chronic psychological stress, using stroboscopic and water-avoidance stress models, on FA composition in a rat model of T2DM.

Levels of twenty-seven FAs were determined by gas chromatography–mass spectrometry. Fifteen of twenty-seven FAs were saturated fatty acids (SFA), six were monounsaturated fatty acids (MUFA), and six were polyunsaturated fatty acids (PUFA). Forty-eight adult male Wistar rats were used, and the study protocol was approved by the State Food and Veterinary Service (Approval No. B1-794). Rats were divided into five groups: control (n = 6), high-fat diet (HFD; n = 6), stress (n = 10), T2DM (n = 13), and T2DM + stress (n = 13).

Significant differences in FA composition between the T2DM and T2DM + stress groups were observed in PUFA, particularly in the ω-6 FA fraction (Fig. 1, A and B). Additionally, the percentage of C20:1 (ω-9) FA differed significantly between the T2DM and T2DM + stress groups and the remaining experimental groups (Fig. 1, C). There were also group-specific changes in selected MUFA and PUFA fractions when compared with control and non-stressed groups.

These results suggest that chronic psychological stress modulates FA composition in rats with T2DM, with the most pronounced alterations observed in MUFA and PUFA, especially ω-6 FAs. This stress-related shift in FA profile may contribute to metabolic dysregulation in T2DM.

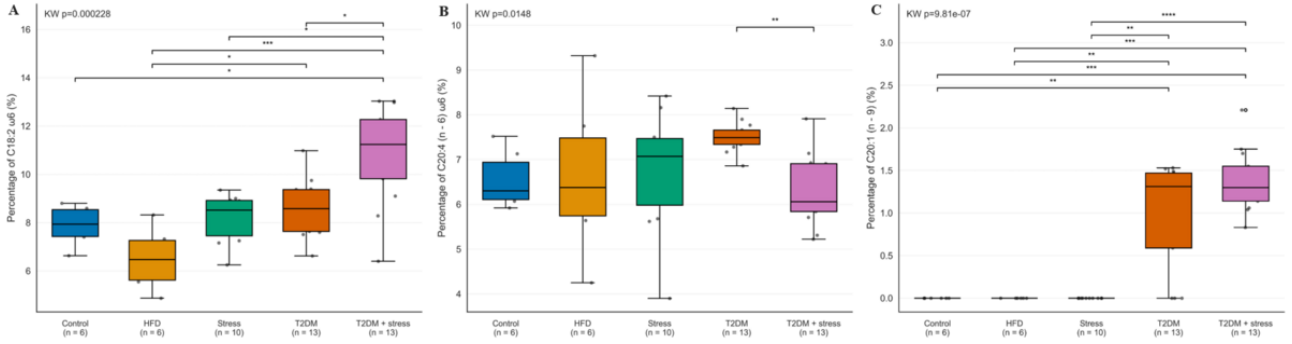


Fig. 1. Comparison of fatty acids between experimental groups. **A.** C18:2 (ω-6) *9,12-Octadecadienoic acid*, and **B.** C20:4 (ω-6) *5,8,11,14-Eicosatetraenoic acid* polyunsaturated fatty acids (PUFAs); **C.** C20:1 (ω-9) *13-Eicosenoic acid*, saturated fatty acid (MUFA).

[1] R. A. Hackett and A. Steptoe, "Type 2 diabetes mellitus and psychological stress - a modifiable risk factor," Nat. Rev. Endocrinol., vol. 13, no. 9, pp. 547–560, Sep. 2017, doi: 10.1038/nrendo.2017.64.
[2] "Diabetes." Accessed: May 30, 2025. [Online]. Available: https://www.who.int/news-room/fact-sheets/detail/diabetes
[3] H. Shiri et al., "Relationship between types and levels of free fatty acids, peripheral insulin resistance, and oxidative stress in T2DM: A case-control study," PLOS ONE, vol. 19, no. 8, p. e0306977, Aug. 2024, doi: 10.1371/journal.pone.0306977.

MATERNAL HIGH-FAT DIET EFFECT ON THE OFFSPRINGS VOLATILOME COMPOUNDS

Patricija Čepauskytė[1], Gintarė Urbonaitė[1], Mantas Norkus[4], Toma Petrulionienė[4], Urtė Neniškytė[1,3]

[1]Vilnius University, Life Sciences Center, Institute of Biosciences, Lithuania
[2]Vilnius University, Faculty of Medicine, Institute of Biomedical Sciences, Lithuania
[3]Vilnius University, Life Sciences Center, VU-EMBL Partnership Institute, Lithuania
[4]National Public Health Surveillance Laboratory, Chemistry Department, Instrumental Research Methods Unit, Lithuania
patricija.cepauskyte@gmc.vu.lt

One of the main global health concerns is the rising obesity rate. High-fat diet is known to induce physiological, metabolic, behavioral, and neurodevelopmental alterations [1]. During pregnancy and lactation, maternal diet-induced metabolic and inflammatory changes may be transmitted to offspring [2]. Previous animal studies have demonstrated that mothers fed a high-fat diet (HFD) exhibit impaired maternal care. As mice are highly olfactory animals, it is hypothesized that HFD disrupts the maternal olfactory system and may reduce the ability to recognize and distinguish their offspring. Altered olfactory cues may contribute to deficits in maternal behavior [3]. Offspring odor profiles are determined by metabolic activity and are reflected in the volatilome. Changes in the offspring volatilome may modify olfactory signals that are critical for maternal recognition and care [4]. However, the relationship between maternal diet, olfactory disruption, and offspring volatile profiles remains poorly understood. Investigating the offspring volatilome may provide novel insight into how maternal high-fat diet exposure influences maternal–offspring interactions and early-life programming of offspring metabolism and behavior.

Female C57BL/6J mice were fed either a control diet (CD, 10% fat) or a high-fat diet (HFD, 60% fat) from weaning through pairing, pregnancy, and lactation. Offspring were weaned onto a standard rodent diet. Postnatal day 6 (P6) pups were placed inside a glass container maintained on a temperature-controlled heating mat. Volatilome samples were collected using a sorbent tube and pump operating at a flow rate of 20 mL/min. Collected samples were analyzed at the National Public Health Surveillance Laboratory.

Volatilome samples from four litters of control diet (mCD) and high-fat diet (mHFD) offspring were analyzed. A total of 18 volatile compounds were identified and classified into eight functional groups. Some of these compounds, particularly nonanal, are inaturally occurring compounds commonly found on animal skin and in pheromone mixtures, where they play important roles in recognition, signaling, and communication between animals. Notably, offspring from mHFD did not emit specific compounds distinguished in mCD offspring. These findings suggest that maternal diet may alter offspring volatile profiles in ways that could affect olfactory-mediated maternal recognition and social interactions and require further investigation.

Keywords: Maternal obesity, high-fat diet, offspring, volatilome, neurodevelopment, olfaction, metabolic programming.

[1] Piché, M.-E., Tchernof, A., Després, J.-P., 2020. Obesity Phenotypes, Diabetes, and Cardiovascular Diseases. Circ. Res. 126, 1477–1500.
[2] Urbonaite, G., Knyzeliene, A., Bunn, F.S., Smalskys, A., Neniskyte, U., 2022. The impact of maternal high-fat diet on offspring neurodevelopment. Front. Neurosci. 16.
[3] Winther G, Elfving B, Müller HK, Lund S, Wegener G. Maternal High-fat Diet Programs Offspring Emotional Behavior in Adulthood. Neuroscience. 2018 Sep 15;388:87-101.
[4] Lacalle-Bergeron, L., Goterris-Cerisuelo, R., Portolés, T., Beltran, J., Sancho, J. V., Navarro-Moreno, C., & Martinez-Garcia, F. (2021). Novel sampling strategy for alive animal volatolome extraction combined with GC-MS based untargeted metabolomics: Identifying mouse pup pheromones. Talanta, 235, 122786.

EVALUATION OF ELECTROPORATION-INDUCED MYOCARDIAL LESION SIZE

Mantė Almanaitytė[1], Dominyka Adamonė[1], Ieva Lankutytė[1], Vilma Zigmantaitė[1], Jonas Jurevičius[1], Regina Mačianskienė[1]

[1]Lithuanian University of Health Sciences, Institute of Cardiology, Laboratory of Membrane Biophysics, Lithuania
Mante.Almanaityte@lsmu.lt

Electroporation (EP) is a promising technique for myocardial tissue modification, but its efficacy and safety depend on appropriate parameter selection, limited by the lack of practical methods for three-dimensional (3D) lesion assessment. This study aimed to establish a reliable framework for evaluating EP-induced myocardial lesions and identifying optimal EP parameters. Two complementary approaches were employed.

Microelectrode recordings at multiple sites within the EP-treated region determined transmural lesion depth by identifying where action potentials (AP) reappeared, and data from multiple experiments were integrated with AI-based analysis to reconstruct 3D lesion geometry. Lesion size was also assessed using optical mapping by analyzing optical action potential (OAP) amplitudes with depth-weighted exponential changes, and validated by ventricular wall sectioning and direct observation of AP propagation in the wedge.

Using near-infrared di-4-ANBDQBS fluorescent dyes (depth constant around 2.1 mm) enabled signal detection and 3D assessment of lesion zones. Both methods enabled precise characterization of lesion dimensions, and optical mapping amplitude analysis (Figure 1A) reliably delineated lesion boundaries and closely matched microelectrode-derived transmural profiles (Figure 1B), providing faster and more reproducible evaluation.

These findings demonstrate that OAP amplitude measurements can be routinely applied to assess EP-induced lesion 3D zones and guide the optimization of EP parameters for effective and reproducible myocardial EP.

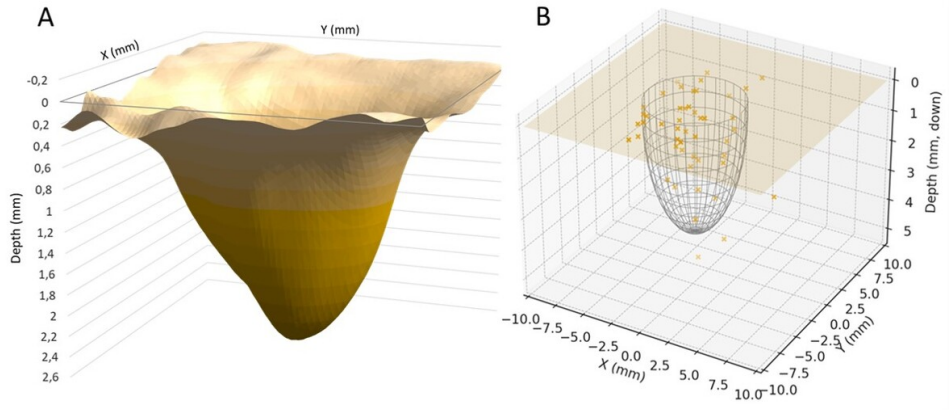


Fig. 1. Three-dimensional assessment of electroporation-induced myocardial lesions. (A) Optical mapping analysis showing lesion boundaries based on depth-weighted optical action potential (OAP) amplitudes, from a 10 × 10 mm area of the heart. (B) Reconstructed 3D lesion geometry from microelectrode recordings at multiple sites within the EP-treated region, from the same 10 × 10 mm heart area. Orange points indicate sites where action potentials reappeared, allowing determination of transmural lesion depth.

HS-SPME/GC-MS-BASED CHARACTERISATION OF VOLATILE COMPOUNDS IN AEGOPODIUM PODAGRARIA L. PARTS AND EVALUATION OF THEIR ANTIMICROBIAL PROPERTIES

Ugnė Gabrytė[1], Rūta Mickienė[1], Audrius Sigitas Maruška[1]

[1]Lithuania, Kaunas, Vytautas Magnus University, Faculty of Natural Sciences, Instrumental Analysis Open Access Centre
ugne.gabryte@vdu.lt

Aegopodium podagraria L. is a widespread member of the *Apiaceae* family, commonly found in forested areas throughout the country. This plant is invasive, spreads easily and outcompetes many plant species, which is why it is often considered disadvantageous [1]. Despite this, it has a long history of use in traditional medicine, with reported antioxidant, anti-inflammatory and even anticancer properties [2]. However, its pharmacological potential remains largely unexplored, even though it is abundant in the environment and easy to obtain. Only recently researchers have begun to recognize its potential, highlighting the need to further study the phytochemicals found in *A. podagraria* and their associated biological activity. To date, very little information is available on chemical composition of the plant, and it is not yet known which compounds contribute to its antimicrobial properties.

Thus, the aim of this study was to characterise volatile compounds present in leaves, stems, flowers and roots of *A. podagraria* using headspace solid phase microextraction (HS-SPME) coupled with gas chromatography-mass spectrometry (GC-MS) and to evaluate the antimicrobial activity of methanolic extracts of these plant parts against selected microorganism strains. The plant material used in the study was collected at 54.8208758 °N, 24.0492927 °E and air dried, extraction was performed by maceration method, and antimicrobial activity was assessed by well diffusion assay.

A total of 26 volatile compounds were identified across the parts of *A. podagraria*. Caryophyllene, α-pinene, β-pinene, cymene, and spathulenol were common to all plant parts, while β-farnesene and germacrene were major constituents in stems and flowers, with relative abundances of 8.84% and 45.01% for β-farnesene, and 28.00% and 14.97% for germacrene, respectively. β-bisabolene was predominant in roots. Stems exhibited the highest diversity of volatiles, whereas leaves showed the lowest. All extracts displayed antimicrobial activity against *E. coli* and *M. luteus*, with flower extracts being the most effective, correlating with higher concentrations of certain volatile compounds such as β-farnesene. Flower extract also demonstrated highest antimicrobial activity against *C. albicans*, with inhibition zone of 23.00 ± 2.00 mm.

The study highlights the composition and diversity of volatile compounds in *A. podagraria* and their contribution to antimicrobial activity. These findings support further exploration of the plant's bioactive potential and its application in research of antimicrobials.

[1] K. Jakubczyk, K. Janda, D. Styburski, and A. Łukomska, "Goutweed (Aegopodium podagraria L.) – botanical characteristics and prohealthy properties*," Postępy Higieny i Medycyny Doświadczalnej, vol. 74, pp. 28–35, Feb. 2020, doi: https://doi.org/10.5604/01.3001.0013.8551.

[2] S. Yılmaz Sarıaltın, D. Çiçek Polat, and C. Ö. Yalçın, "Cytotoxic and antioxidant activities and phytochemical analysis of Smilax excelsa L. and Aegopodium podagraria L.," Food Bioscience, vol. 52, p. 102359, Apr. 2023, doi: https://doi.org/10.1016/j.fbio.2023.102359.

INDUCTION OF APOPTOSIS AND PYROPTOSIS IN MACROPHAGES BY THE POLYSACCHARIDE CAPSULE OF ACINETOBACTER BAUMANNII

Joris Naujalis[1], Jūratė Skerniškytė[1]

[1]Vilnius University, Life Sciences Center, Department of Biochemistry and Molecular Biology, Lithuania
joris.naujalis@gmc.vu.lt

Acinetobacter baumannii is a Gram-negative opportunistic bacterium that causes difficult-to-treat nosocomial infections. Due to its multidrug resistance and persistence in clinical environments, *A. baumannii* is classified by the World Health Organization as a critical priority pathogen [1]. One of the key virulence factors of *A. baumannii* is the polysaccharide capsule, which enables evasion of host immune defences [2], [3].

Macrophages are among the first innate immune effectors and play an important role in controlling bacterial spread. These cells are involved in phagocytosis, antigen presentation, and regulation of inflammation [4]. During infection, macrophages can undergo different inflammatory and non-inflammatory forms of cell death. The balance between these pathways influences the outcome of the immune response [5]. This study aimed to investigate how the polysaccharide capsule of *A. baumannii* modulates apoptotic (non-inflammatory) and pyroptotic (inflammatory) cell death pathways in macrophages.

We used a capsulated clinical *A. baumannii* strain and its non-capsulated mutants. *In vitro* infections were performed using murine J774A.1 and human THP-1 macrophages. Viability of macrophages was assessed by fluorescence microscopy, while apoptosis and pyroptosis markers were analysed by Western blot. Apoptosis was evaluated by detecting activation of the effector caspase-3 (Casp-3), while pyroptosis was assessed by detecting formation of the N-terminal gasdermin D fragment (GSDMD-N) and secretion of the pro-inflammatory cytokine interleukin-1β (IL-1β).

The non-capsulated Δ*galU* mutant resulted in increased viability of J774A.1 and THP-1 macrophages and induced weaker activation of Casp-3 compared to the capsulated strain. To assess whether this effect is strain-dependent, Casp-3 activation was also analysed using another capsulated clinical isolate and its non-capsulated Δ*wza* mutant. The study revealed that the Δ*wza* non-capsulated mutant likewise induced significantly weaker Casp-3 activation. In contrast, loss of the polysaccharide capsule did not significantly affect GSDMD-N formation and IL-1β secretion in J774A.1 and THP-1 cells.

Our findings show that the loss of *A. baumannii* polysaccharide capsule significantly increased macrophage viability and reduced activation of the effector apoptotic caspase-3 in both cell lines. However, the loss of bacterial capsule did not affect pyroptotic responses. These results indicate that the polysaccharide capsule of *A. baumannii* induces apoptotic rather than pyroptotic signalling in J774A.1 and THP-1 macrophages during infection.

Acknowledgements

This project has received funding from the Research Council of Lithuania (LMTLT), agreement No S-MIP-23-109.

[1] S. Corcione et al., “Risk factors for mortality in Acinetobacter baumannii bloodstream infections and development of a predictive mortality model,” Journal of Global Antimicrobial Resistance, vol. 38, pp. 317–326, Jul. 2024, doi: 10.1016/j.jgar.2024.06.010.

[2] J. Skerniškytė, R. Krasauskas, C. Péchoux, S. Kulakauskas, J. Armalytė, and E. Sužiedėlienė, “Surface-Related Features and Virulence Among Acinetobacter baumannii Clinical Isolates Belonging to International Clones I and II,” Frontiers in Microbiology, vol. 9, p. 3116, Jan. 2019, doi: 10.3389/fmicb.2018.03116.

[3] R. Krasauskas, J. Skerniškytė, J. Martinkus, J. Armalytė, and E. Sužiedėlienė, “Capsule Protects Acinetobacter baumannii From Inter-Bacterial Competition Mediated by CdiA Toxin,” Frontiers in Microbiology, vol. 11, p. 1493, Jul. 2020, doi: 10.3389/fmicb.2020.01493.

[4] J. Brancewicz, N. Wójcik, Z. Sarnowska, J. Robak, and M. Król, “The multifaceted role of macrophages in biology and diseases,” International Journal of Molecular Sciences, vol. 26, no. 5, p. 2107, Feb. 2025, doi: 10.3390/ijms26052107.

[5] M. Kist and D. Vucic, “Cell death pathways: intricate connections and disease implications,” The EMBO Journal, vol. 40, no. 5, p. e106700, Jan. 2021, doi: 10.15252/embj.2020106700.

BIOCIDAL POTENTIAL OF YEASTS FROM PASTURE ENVIRONMENTS AGAINST OTHER YEASTS AND BACTERIA

Deividas Paliovkinas[1,2], Živilė Strazdaitė-Žielienė[1], Elena Servienė[1,2]

[1]State Scientific Research Institute Nature Research Centre, Vilnius, Lithuania
[2]Vilnius Tech, Faculty of Fundamental Sciences, Vilnius, Lithuania
deividaspaliovkinas@gmail.com

Microorganisms engage in intense competition within natural environments, leading many bacteria and yeasts to produce biocidal compounds that inhibit the growth of neighboring organisms. These naturally occurring antimicrobial agents are receiving increasing attention as potential alternatives to conventional antimicrobials, particularly in the context of rising resistance and the demand for environmentally sustainable biocontrol strategies. This study aimed to isolate microorganisms from environmental samples and evaluate their biocidal activity against selected microbial targets, followed by morphological and molecular identification of active strains. The study further sought to characterize the spectrum and potential genetic basis of the observed biocidal effects, with a particular focus on yeast-derived antimicrobial activity against both yeast and bacteria.

Water, feed, and soil samples were collected from pasture environments across Lithuania, and yeast isolates were obtained using standard cultivation techniques. Isolates were characterized morphologically and identified molecularly through PCR, RFLP, and PCR fragment sequencing. The biocidal activity of yeast strains was assessed on methylene blue agar at pH 4.0, 4.8, and 5.6 by embedding potentially sensitive yeasts from environmental samples or laboratory bacterial strains into the medium, followed by applying the putative biocidal yeast biomass onto the surface. Biocidal effects were evaluated based on the formation of growth inhibition zones. A total of 25 yeast strains were isolated, with the highest diversity observed in feed samples (16 isolates), followed by soil (6) and water (3). The predominant genera of isolated yeasts were *Wickerhamomyces* (36%) and *Debaryomyces* (20%). Twelve yeast strains exhibited biocidal activity, inhibiting the growth of 13 yeast strains and 3 laboratory bacterial strains. Biocidal yeast isolates belonged to the genera *Wickerhamomyces*, *Debaryomyces* and *Barnettozyma*. The strongest biocidal activity against yeasts was observed at pH 4.8, while activity against bacteria was highest at pH 5.6.

These findings indicate that pasture yeasts represent a promising source of pH-dependent biocidal activity against both yeasts and bacteria. Further characterization of the active compounds and their genetic determinants may facilitate the development of environmentally friendly antimicrobial or biocontrol applications.

HIDDEN DIVERSITY: SARCOCYSTIS PARASITES IN CATTLE (Bos taurus) RAISED IN LITHUANIA

Mingailė Stanionytė[1], Petras Prakas[2], Dalius Butkauskas[2], Donatas Šneideris[2], Naglis Gudiškis[2]

[1]Vilnius University, Life Sciences Center, Lithuania
[2]State Scientific Research Institute Nature Research Centre, Lithuania
mingaile.stanionyte@gmc.stud.vu.lt

Parasites of the genus *Sarcocystis* are widely distributed among domestic and wild animals, with cattle (*Bos taurus*) representing one of the most important intermediate hosts, making studies of these parasites highly relevant to both veterinary and public health [1]. In recent years, the increasing number of *Sarcocystis* species and their zoonotic potential have highlighted the need for more precise diagnostic methods, as morphological approaches are often insufficient for reliable identification of taxonomically closely related species [2]. In Lithuania, the prevalence and species diversity of *Sarcocystis* parasites in cattle are still insufficiently investigated using molecular methods, and infections often remain undetected due to the absence of clinical signs and the difficulty of detecting microscopic cysts [3].

The aim of this study was to evaluate the species diversity of *Sarcocystis* spp. parasites in cattle raised in Lithuania and to determine their genetic characteristics using microscopic and molecular methods. The analysis of stained and unstained muscle tissue samples was performed using the compression microscopy method to detect sarcocysts in tissues. Subsequently, genomic DNA was extracted from selected samples and used for molecular analysis. Parasite identification was carried out using nested polymerase chain reaction (PCR) targeting the cox1 gene as a genetic marker, the obtained PCR products were analyzed by electrophoresis.

A total of 28 bovine heart muscle samples were examined using the compression microscopy method. Sarcocysts were detected in 60.71% (17/28) of the samples. According to proposed classification by Bogush (1976) [4] and Malakauskas et al. (2001) [5], a low parasite burden was observed in most of positive the samples, while a moderate infection intensity was detected in only one sample (13 sarcocysts/g). The mean length of the detected sarcocysts was 650.93 µm (271,65–1052,90 ± 241,87, n = 28) and the mean width was 57.78 µm (29,49–85,02 ± 15,94, n = 28). Morphological characteristics were consistent with microscopic *Sarcocystis* species infecting cattle. Molecular analysis identified two species: *Sarcocystis cruzi* and *Sarcocystis bovifelis*, of which *S. cruzi* was dominant and detected in 75.0% (21/28) of the samples, whereas *S. bovifelis* was detected in 7.14% (2/28) of the samples.

The results further demonstrated a limited diversity of *Sarcocystis* species in Lithuanian cattle, highlighting the importance of molecular methods for accurate parasite identification and evaluation of zoonotic potential. In future studies, it is planned to expand the number of analyzed samples and to optimize molecular and viability assessment methods to more reliably evaluate the prevalence of these parasites in cattle and their significance for veterinary and public health.

[1] J. P. Dubey, E. Van Wilpe, R. Calero-Bernal, S. K. Verma, and R. Fayer, “Sarcocystis heydorni, n. sp. (Apicomplexa: Sarcocystidae) with cattle (Bos taurus) and human (Homo sapiens) cycle,” Parasitology Research, vol. 114, no. 11, pp. 4143–4147, Aug. 2015, doi: 10.1007/s00436-015-4645-2.

[2] J. J. Hu, S. Huang, T. Wen, G. W. Esch, Y. Liang, and H. L. Li, “Morphology, Molecular Characteristics, and Demonstration of a Definitive Host for Sarcocystis rommeli from Cattle (Bos taurus) in China,” Journal of Parasitology, vol. 103, no. 5, pp. 471–476, Jun. 2017, doi: 10.1645/16-187.

[3] P. Prakas et al., “Molecular identification of four Sarcocystis species in cattle from Lithuania, including S. hominis, and development of a rapid molecular detection method,” Parasites & Vectors, vol. 13, no. 1, p. 610, Dec. 2020, doi: 10.1186/s13071-020-04473-9.

[4] A. A. Bogush, Swine Muscle Parasitoses and Preventive Measures Against Them. Minsk, Belarus: Urodzhai, 1976.

[5] M. Malakauskas, J. Grikienienė, and G. Januškevičienė, “Mėsai medžiojamų žvėrių sarkocistozė,” Veterinarija ir Zootechnika, vol. 14, no. 36, pp. 36–43, 2001.

SPECIES DIVERSITY OF MESOSTIGMATID MITES FROM SMALL RODENTS IN SUBURBAN HABITATS

Violeta Šataitytė[1], Evelina Kaminskienė[1], Jana Radzijevskaja[1], Michal Stanko[2], Algimantas Paulauskas[1]

[1]Vytautas Magnus University, Department of Biology, Kaunas, Lithuania.
[2]Slovak Academy of Sciences, Institute of Parasitology and Institute of Zoology, Slovakia.
violeta.sataityte@vdu.lt

Small rodents are common hosts of ectoparasites and play an important role in the maintenance of parasite communities. Mites of the suborder Mesostigmata parasitizing small rodents represent a diverse group widely distributed across different environments. Rodent-associated mites are of ecological interest and may serve as potential vectors or reservoirs of microorganisms that cause disease in humans and animals. However, the species diversity of mesostigmatid mites parasitizing small rodents and their distribution in suburban habitats remains poorly documented. The aim of this study was to investigate infestation patterns of small rodent species with parasitic Laelapidae mites across suburban environments in Lithuania. A total of 290 Mesostigmata mites were collected from small rodents captured at ten suburban sites in Lithuania in 2020. Mites were recorded from *Apodemus flavicollis, Apodemus agrarius, Myodes glareolus, Microtus arvalis, Microtus oeconomus* and *Micromys minutus*. Based on morphological characteristics, seven Mesostigmata mite species and one genus-level taxon were identified: *Laelaps agilis, Laelaps jettmari, Laelaps hilaris, Haemogamasus microti, Haemogamasus nidi, Eulaelaps stabularis, Androlaelaps glasgowi*, and *Hirstionyssus* sp. Abundance and mean intensity of mite infestation varied among rodent species and study sites. Mites were detected on 20.1% of the examined rodents, with the highest number collected from *A. flavicollis*. The most abundant mite species was *L. agilis*, represented by 191 individuals, occurring predominantly on *A. flavicollis*. This study contributes to a better understanding of Mesostigmata mite diversity in suburban habitats, providing a foundation for future research on host–parasite interactions and pathogen-related processes.

BEHIND THE MUSCLES: SARCOCYSTIS PARASITES IN HORSES FROM LITHUANIA

Naglis Gudiškis[1], Mingailė Stanionytė[1,2], Petras Prakas[1], Eglė Rudaitytė-Lukošienė[1], Dalius Butkauskas[1], Donatas Šneideris[1]

[1]Vilnius University, State Scientific Research Institute Nature Research Centre, Laboratory of Molecular Ecology, Lithuania
[2]Vilnius University, Lithuania
naglis.gudiskis@gamtc.lt

Sarcocystis is a genus of cosmopolitan protozoa that parasitizes birds, reptiles, and mammals. Infected animal meat causes significant economic losses each year, due to unsuitability for human consumption or physiological changes in the animals themselves. In Lithuania, a moderate prevalence of sarcocystosis has been previously reported, but the species diversity of parasites has not been studied. To date, five *Sarcocystis* species have been described in equids: *S. asinus*, *S. bertrami*, *S. equicanis*, *S. fayeri*, and *S. neurona*. However, scientific debate continues regarding the classification of *S. bertrami* and *S. fayeri* as some researchers consider them a single species, while others argue they are distinct. Given these uncertainties, more detailed molecular studies on equids are essential to determine the true species diversity and distribution.

This study aimed to investigate the species diversity of *Sarcocystis* in the muscle tissues of domesticated horses (*Equus ferus caballus*) in Lithuania and to assess the intensity and prevalence of these parasites. Muscle tissue samples from 107 horses were examined using both methylene-blue-stained and unstained muscle squash microscopy, followed by isolation of individual sarcocysts, genomic DNA extraction, PCR amplification of multiple genetic markers, electrophoresis, and sequencing.

Microscopical analysis revealed that 23.4% of the investigated samples were *Sarcocystis* positive. The parasite load varied from one to 12 sarcocysts per gram of tissue ($\bar{x}$ = 3 sarcocysts/g; n = 25). Morphologically, sarcocysts observed in fresh squashed preparations were elongated and spindle-shaped, measuring 400–6000 × 30–225 µm (2036 ± 1374 × 108 ± 51 µm; n = 40) in size. The sarcocyst wall was thin with finger-like protrusions, measuring 1.0–1.9 µm (1.6 ± 0.9 µm; n = 40) in length. Cysts were septated, and their inner compartments were filled with elongated, banana-shaped bradyzoites measuring 10.0–16.0 × 2.0–4.0 µm (12.0 ± 1.2 × 2.6 ± 0.2 µm; n = 20) in size. Sequencing of the *cox1*, *18S* rRNA, and *28S* rRNA markers revealed the species present in Lithuanian horses as *S. bertrami*.

These findings confirm the presence of *S. bertrami* in horses in Lithuania and provide the first molecular characterization of this parasite in the country. However, the limited availability of comparative genetic data highlights the need for broader molecular investigations to resolve taxonomic uncertainties and better understand the diversity and distribution of Sarcocystis species in equids.

IMPROVING CELL INTACTNESS IN CRYOGENIC FLUORESCENCE SPECTROSCOPY MEASUREMENTS

Patricija Žemaitytė[1,2], Yaraslau Padrez[1,3], Claudia Büchel[4], Andrius Gelzinis[1,5], Lena Golubewa[1,5]

[1]State Research Institute Center for Physical Sciences and Technology, Department of Molecular Compound Physics, Vilnius, Lithuania
[2]Vilnius University, Life Sciences Center, Vilnius, Lithuania
[3]Jiaxing University, College of Medicine, Neuroscience Research Center, Jiaxing, China
[4]Goethe University Frankfurt, Department of Biosciences, Institute of Molecular Biosciences, Frankfurt, Germany
[5]Vilnius University, Faculty of Physics, Institute of Chemical Physics, Vilnius, Lithuania
patricija.zemaityte@ftmc.lt

Diatoms are unicellular algae with a distinctive photosynthetic apparatus that enables them to adapt to extreme changes in light intensity [1]. This allows the cells to efficiently utilize available light for photosynthesis and determines photoprotection mechanisms. *Cycclotella meneghiniana* is a convienient model for diatom analysis. Cryogenic fluorescence spectroscopy is a valuable tool for studying electronic excitation dynamics in photosynthetic apparatus on the whole-cell level. A mixture of glycerol and growth media is commonly used in cryogenic measurements to reduce ice crystal formation, which causes light scattering. However, evidence supporting the viability of cells in glycerol is limited, as most conclusions are based solely on fluorescence spectra shape [2]. The aim of this study is to assess the effects of glycerol on *C. meneghiniana* cell viability and reveal the differences in spectral features of cells in different functional states measured at cryogenic temperatures.

Cells were measured in either artificial seawater (ASP) or in medium for cryogenic measurements ASP:glycerol (2:3 ratio), and both steady-state fluorescence emission spectra and time-resolved fluorescence decays were measured at temperatures from 16K to room temperature (RT). Cell viability was assessed using propidium iodide, morphological changes in ASP and ASP:glycerol were assesed by fluorescence microscopy (Fig. 1a-b). Figure 1c-e contains representative data obtained at 77K. Diatoms exposed to ASP:glycerol exhibited rapid loss of viability, thylakoid membrane swelling (Fig. 1b), and longer fluorescence lifetimes, indicating disruption of the photosynthetic apparatus despite minimal changes in spectral shape. Medium exchange from ASP to ASP:glycerol led to significant changes in spectral features: the fluorescence spectrum peak position was red-shifted (Fig. 1c) and fluorescence lifetimes decreased, both for emission at 685 nm and 720 nm (Fig. 1d–e) in ASP:glycerol compared to ASP. In contrast, glycerol-free conditions preserved cellular integrity and produced a consistent, steadily changing fluorescence response from 16 K to 130 K (data not shown).

These results suggest that cryogenic studies using glycerol at the whole-cell level should be interpreted with caution, as cell viability needs to be confirmed.

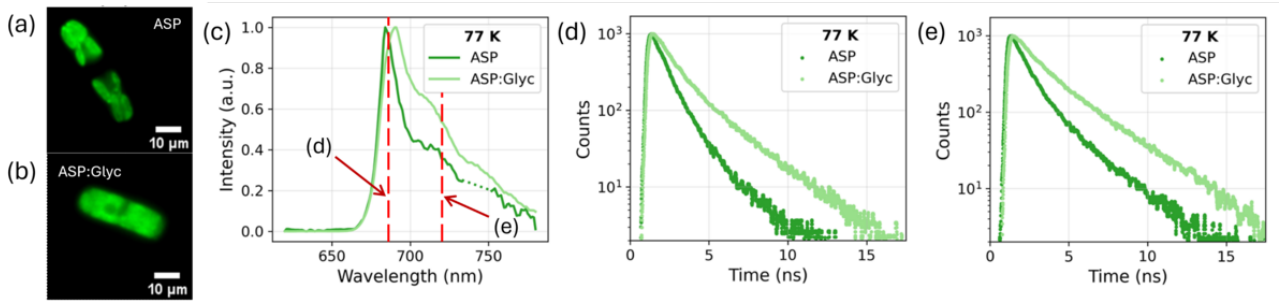


Fig. 1. Effects of glycerol on spectral features of diatoms: fluorescence microscopy images of cells in ASP (a) and ASP:glycerol (b) at RT; (c) fluorescence spectra of cells measured at 77 K; red dashed lines indicate the emission wavelengths used in (d) and (e); fluorescence decays of cells measured at 77 K, with excitation at 685 nm (d) and 720 nm (e). Fluorescence microscopy images were obtained with 405 nm excitation. Steady-state fluorescence spectra and fluorescence decays were measured with 375 nm excitation.

Keywords: Cryogenic fluorescence spectroscopy, Diatoms, Photosynthetic apparatus, Viability, Glycerol

[1] R. Goss, C. Wilhelm, and T. Jakob, “Photosynthesis in diatoms,” in Elsevier eBooks, 2020, pp. 217–229. doi: 10.1016/b978-0-12-818305-2.00013-9.
[2] M. Szabó, L. Premvardhan, B. Lepetit, R. Goss, C. Wilhelm, and G. Garab, “Functional heterogeneity of the fucoxanthins and fucoxanthin-chlorophyll proteins in diatom cells revealed by their electrochromic response and fluorescence and linear dichroism spectra,” Chemical Physics, vol. 373, no. 1–2, pp. 110–114, Mar. 2010, doi: 10.1016/j.chemphys.2010.03.001.

SELECTED TOOTH SAMPLE DEHYDRATION METHODOLOGY: LITERATURE REVIEW AND EXPERIMENTAL EXAMPLE

Robertas Virkėtis[1], Airida Elžbieta Žygytė[2], Artūr Harnik[3], Donatas Narbutis[4], Mangirdas Malinauskas[3], Irma Dumbrytė[2], Greta Merkininkaitė[1]

[1]Lithuania, Vilnius University, Faculty of Chemistry and Geosciences, Institute of Chemistry
[2]Lithuania, Vilnius University, Faculty of Medicine, Institute of Dentistry
[3]Lithuania, Vilnius University, Faculty of Physics, Laser Research Center
[4]Lithuania, Vilnius University, Faculty of Physics, Institute of Theoretical Physics and Astronomy
robertas.virketis@chgf.vu.lt

Enamel microcracks can contribute to tooth decay, reduced mechanical strength, and may act as precursors to larger structural fractures[1]. Accurate characterization of these microcracks using micro-computed tomography (μCT) and scanning electron microscopy (SEM) depends on careful sample preparation, including controlled dehydration. Improper dehydration can introduce artifacts such as contamination and dehydration-induced crack formation or enlargement, thereby compromising the reliability of microstructural analysis[2].

Although extracted teeth are widely used in μCT[1,2] and SEM studies[3,4], dehydration protocols are often insufficiently reported or systematically assessed. A systematic literature review identified 70 relevant articles published within the last decade; 31 studies passed initial screening, and only 4 met the final inclusion criteria, corresponding to ∼6% of the initially identified literature.

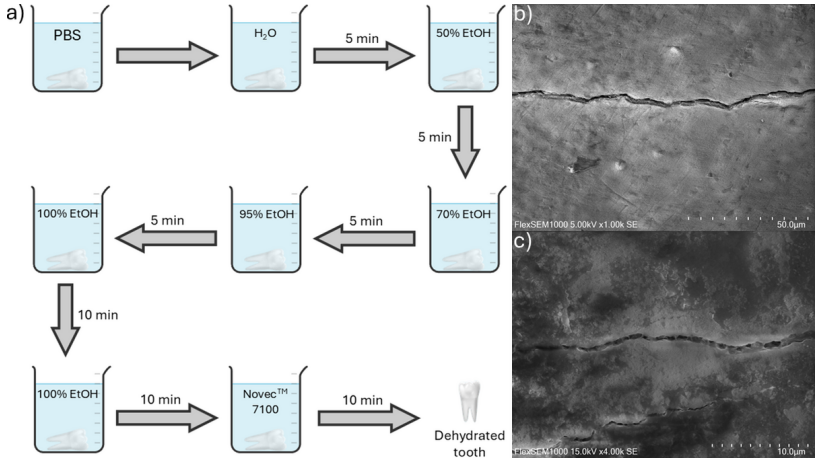


Fig. 1. a) Schematic illustration of the tooth dehydration process; SEM images of enamel microcracks after dehydration at b) ×1000 and c) ×4000 magnification.

Teeth are commonly stored in phosphate-buffered saline (PBS) to maintain chemical and physical stability prior to analysis. Water present within microscopic pores, interprismatic spaces, and microcracks can generate capillary stresses during rapid evaporation that may exceed the local mechanical strength of enamel, promoting crack propagation, particularly during vacuum-based analyses such as SEM. Based on these considerations, we present an experimental tooth dehydration protocol (Fig. 1 a) involving stepwise substitution of water with increasing ethanol concentrations, followed by immersion in a low–surface-tension liquid (Novec™ 7100) prior to air drying.

In conclusion, tooth storage and dehydration conditions are frequently underreported and insufficiently controlled in μCT and SEM studies, limiting data reliability and cross-study comparability. The proposed dehydration protocol provides a standardized and explicitly documented framework that minimizes dehydration-induced artifacts and supports preservation of native enamel microstructure for reliable microcrack analysis (Fig. 1 b, c).

[1] I. Dumbryte, A. Vailionis, E. Skliutas, S. Juodkazis, and M. Malinauskas, "Three-dimensional non-destructive visualization of teeth enamel microcracks using X-ray micro-computed tomography," Scientific Reports, vol. 11, no. 1, p. 14810, Jul. 2021, doi: 10.1038/s41598-021-94303-4.
[2] I. Dumbryte, D. Narbutis, M. Androulidaki, A. Vailionis, S. Juodkazis, and M. Malinauskas, "Teeth Microcracks Research: Towards Multi-Modal Imaging," Bioengineering, vol. 10, no. 12, p. 1354, Nov. 2023, doi: 10.3390/bioengineering10121354.
[3] I. Dumbryte, L. Linkeviciene, T. Linkevicius, and M. Malinauskas, "Enamel microcracks in terms of orthodontic treatment: A novel method for their detection and evaluation," Dental Materials Journal, vol. 36, no. 4, pp. 438–446, Jan. 2017, doi: 10.4012/dmj.2016-264.
[4] S. R. G. Swamy, "Ultrastructural analysis of incinerated teeth by scanning electron microscope – a short study," JOURNAL OF CLINICAL AND DIAGNOSTIC RESEARCH, vol. 10, no. 7, pp. ZC08-11, Jan. 2016, doi: 10.7860/jcdr/2016/18130.8101.

DETERMINANTS OF PHAGE SENSITIVITY TO THE OLOKUN ANTIPHAGE DEFENSE SYSTEM

Vincentas Raudys[1], Edvinas Jurgelaitis[1], Mindaugas Zaremba[1]

[1]Vilnius University, Life Sciences Center, Institute of Biotechnology, Department of Protein - DNA Interactions, Vilnius, Lithuania
vincentas.raudys@gmc.vu.lt

Bacterial and archaeal populations are constantly infected by bacteriophages, the most abundant biological entities on Earth [1]. Under this intense evolutionary pressure, prokaryotes have developed antiphage systems, while phages have developed countermeasures to overcome them. This coevolutionary “arms race” has led to a vast expansion in the diversity of antiphage systems, many of which possess unique and largely uncharacterised mechanisms of action. Several of these systems have been exploited for applications in science and medicine. For example, CRISPR-Cas systems have revolutionized genome editing, and restriction-modification systems have been used for DNA manipulation for more than half a century [2].

In this study, we lay the groundwork for elucidating a novel prokaryotic antiviral defence system – Olokun, discovered in the *E. coli* UMB0934 strain [3]. A phage-escaper workflow was applied to identify bacteriophage mutants capable of overcoming Olokun-mediated defence. Candidate mutant bacteriophages were isolated and validated. Following purification of phage genomic DNA, sequences were determined using next-generation sequencing. Raw sequencing reads were analyzed using bioinformatic approaches, leading to the identification of potential determinants of phage sensitivity to Olokun.

This work advances understanding of prokaryotic antiphage defence systems and their potential biotechnological applications.

[1] M. Zuppi, H. L. Hendrickson, J. M. O’Sullivan, and T. Vatanen, “Phages in the gut ecosystem,” Frontiers in Cellular and Infection Microbiology, vol. 11, p. 822562, Jan. 2022, doi: 10.3389/fcimb.2021.822562.

[2] H. Georjon and A. Bernheim, “The highly diverse antiphage defence systems of bacteria,” Nature Reviews Microbiology, vol. 21, no. 10, pp. 686–700, Jul. 2023, doi: 10.1038/s41579-023-00934-x.

[3] A. Millman et al., “An expanded arsenal of immune systems that protect bacteria from phages,” Cell Host & Microbe, vol. 30, no. 11, pp. 1556-1569.e5, Oct. 2022, doi: 10.1016/j.chom.2022.09.017.

INHIBITION OF THE CRISPR-CAS SYSTEM BY AN ANTI-CRISPRPROTEIN

Darija Andrušaitytė[1], Tomas Šinkūnas[1]

[1]Lithuania, Vilnius University, Life Sciences Center, Department of Protein-DNA Interactions
darija.andrusaityte@gmc.stud.vu.lt

The ongoing co-evolutionary arms race between bacteria and bacteriophages has led to the development of various defense and attack strategies. One of the bacterial defense systems against phages is CRISPR-Cas. This system detects and integrates invading DNA into the CRISPR array. The transcript of the CRISPR array is processed into small crRNA molecules, which together with Cas proteins form ribonucleoprotein effector complexes. Guided by crRNAs, these complexes recognize and cleave complementary phage DNA, thereby providing adaptive immunity [1]. To overcome CRISPR-Cas–mediated defense, bacteriophages have evolved anti-CRISPR (Acr) proteins that inhibit CRISPR-Cas activity, most commonly by preventing target DNA binding or nuclease function [2]. Beyond their biological relevance, Acr proteins have attracted considerable interest as regulators of CRISPR-Cas–based genome editing technologies [3,4]. Despite the rapid expansion in the number of identified Acr proteins, detailed molecular mechanisms of inhibition have been elucidated for only a small subset [4].

In this study, we analyse the inhibition mechanism of a previously uncharacterized AcrIF protein targeting the type I-F CRISPR-Cas system. *In vivo* activity assays demonstrate that this AcrIF protein inhibits the CRISPR ribonucleoprotein effector complex. The protein was purified using liquid chromatography, and its inhibitory activity was assessed through a series of biochemical assays. Our current data indicates a unique mode of action for this AcrIF protein, the molecular basis of which we aim to elucidate.

[1] G. Amitai and R. Sorek, “CRISPR–Cas adaptation: insights into the mechanism of action,” Nature Reviews Microbiology, vol. 14, no. 2, pp. 67–76, Jan. 2016, doi: 10.1038/nrmicro.2015.14.

[2] A. R. Davidson et al., “Anti-CRISPRs: protein inhibitors of CRISPR-CAS systems,” Annual Review of Biochemistry, vol. 89, no. 1, pp. 309–332, Mar. 2020, doi: 10.1146/annurev-biochem-011420-111224.

[3] G. Liu, Q. Lin, S. Jin, and C. Gao, “The CRISPR-Cas toolbox and gene editing technologies,” Molecular Cell, vol. 82, no. 2, pp. 333–347, Dec. 2021, doi: 10.1016/j.molcel.2021.12.002.

[4] N. Jia and D. J. Patel, “Structure-based functional mechanisms and biotechnology applications of anti-CRISPR proteins,” Nature Reviews Molecular Cell Biology, vol. 22, no. 8, pp. 563–579, Jun. 2021, doi: 10.1038/s41580-021-00371-9.

INVESTIGATION OF THE ACTIVATION MECHANISM OF SPLITPAGO PROTEINS AND ASSOCIATED HEPN EFFECTORS IN E. COLI

Rokas Bružaitis[1], Edvardas Golovinas[1], Mindaugas Zaremba[1]

[1]Vilnius University, Institute of Biotechnology, Department of Protein-DNA Interactions, Vilnius, Lithuania
rokas.bruzaitis@gmc.stud.vu.lt

As genome editing technologies progress, the scientific community is committed to enhancing the tools that facilitate this development. Presently, CRISPR-Cas systems lead the way in genome editing technologies, while limited research has been dedicated to their counterparts – pAgo systems. Nonetheless, recent discoveries regarding Argonaute protein research suggest that the HEPN domain is vital for the function of certain Argonaute systems [1], but their activation mechanisms are still unknown.

This research explores the potential interaction between prokaryotic Argonaute (pAgo) system and a plasmid with a CloDF13 origin of replication *(ori)* sequence. The pAgo system examined in this research includes a toxic effector protein, which contains a HEPN domain. This effector protein exhibits toxicity in the absence of its associated pAgo proteins. In some cases, pAgo systems can be activated by plasmids carrying a specific CloDF13 *ori* [2]. Through the investigation of an Argonaute–HEPN system with CloDF13 *ori* acting as a trigger, we aim to explore the activation mechanism of this system. This research not only lays the groundwork for future studies but also possesses significant potential for programmable DNA targeting in the field of biotechnology.

Investigating bacterial defense activation mechanisms provides critical insight of the intricate ways in which bacteria safeguard themselves against foreign DNA while also creating opportunities for advancements in biotechnology and genome editing tools.

[1] M. C. Pillon, K. H. Goslen, J. Gordon, M. L. Wells, J. G. Williams, and R. E. Stanley, “It takes two (Las1 HEPN endoribonuclease domains) to cut RNA correctly,” Journal of Biological Chemistry, vol. 295, no. 18, pp. 5857–5870, Mar. 2020, doi: 10.1074/jbc.ra119.011193.

[2] M. Zaremba et al., “Short prokaryotic Argonautes provide defence against incoming mobile genetic elements through NAD+ depletion,” Nature Microbiology, vol. 7, no. 11, pp. 1857–1869, Oct. 2022, doi: 10.1038/s41564-022-01239-0.

CHARACTERIZATION OF A NON-CANONICAL TYPE IV-A1 CRISPR-CAS SYSTEM

Gintarė Žvejytė[1], Rimvydė Čepaitė[1], Aistė Skorupskaitė[1], Patrick Pausch[1]

[1]Vilnius University, Life Sciences Centre, European Molecular Biology Laboratory (LSC-EMBL) Partnership Institute for Genome Editing Technologies, Vilnius, Lithuania
gintare.zvejyte@gmc.stud.vu.lt

CRISPR-Cas systems are used to provide adaptive immunity against mobile genetic elements in bacteria and archaea. Among these, type IV-A1 CRISPR-Cas systems are distinguished from other CRISPR types by the absence of canonical DNA or RNA nuclease activity. Instead, target DNA is unwound through the recruitment of a DinG helicase by these multisubunit complexes, resulting in transcriptional interference rather than cleavage and in this way preventing the infection [1][2].

Structural and biochemical studies have primarily been conducted on canonical type IV-A1 systems, in which a Cas8 homolog is employed in combination with Cas5 to mediate protospacer adjacent motif (PAM) recognition [3][4]. In contrast, a recently reclassified non-canonical type IV-A1 system – formerly designated type IV-A2 – has remained largely unexplored [1]. These systems were long thought to lack a Cas8 homolog, suggesting that an alternative mechanism of target recognition was used [5]. However, it has been shown that non-canonical type IV-A1 systems consistently co-occur with a small, conserved, *cas8-like* gene located adjacent to the *cas* operon and transcribed in the opposite orientation. Understanding of the function of the protein encoded by this gene may reveal a previously unrecognized component of type IV-A1 interference and expand current understanding of CRISPR-Cas systems diversity.

Here, initial insights into the structure and mechanism of a representative non-canonical type IV-A1 CRISPR-Cas system are presented.

[1] K. S. Makarova et al., “An updated evolutionary classification of CRISPR–Cas systems including rare variants,” Nature Microbiology, vol. 10, no. 12, pp. 3346–3361, Nov. 2025, doi: 10.1038/s41564-025-02180-8.
[2] V. M. Crowley et al., “A Type IV-A CRISPR-Cas System in Pseudomonas aeruginosa Mediates RNA-Guided Plasmid Interference In Vivo,” The CRISPR Journal, vol. 2, no. 6, pp. 434–440, Dec. 2019, doi: 10.1089/crispr.2019.0048.
[3] R. Čepaitė et al., “Structural variation of types IV-A1- and IV-A3-mediated CRISPR interference,” Nature Communications, vol. 15, no. 1, p. 9306, Oct. 2024, doi: 10.1038/s41467-024-53778-1.
[4] N. Cui et al., “Type IV-A CRISPR-Csf complex: Assembly, dsDNA targeting, and CasDinG recruitment,” Molecular Cell, vol. 83, no. 14, pp. 2493-2508.e5, Jun. 2023, doi: 10.1016/j.molcel.2023.05.036.
[5] R. Pinilla-Redondo et al., “Type IV CRISPR–Cas systems are highly diverse and involved in competition between plasmids,” Nucleic Acids Research, vol. 48, no. 4, pp. 2000–2012, Dec. 2019, doi: 10.1093/nar/gkz1197.

INFLUENCE OF BACTERIAL DEFENSE SYSTEM COMPONENTS ON CELL VIABILITY

Austėja Narkevičiūtė[1], Tomas Šinkūnas[1]

[1]Vilnius University, Life Sciences Center, Institute of Biotechnology, Vilnius, Lithuania
austeja.narkeviciute@gmc.stud.vu.lt

The ongoing arms race between bacteria and bacteriophages has led to the development of various defense strategies in bacteria. Prokaryotes have evolved mechanisms to terminate viral infection at multiple stages of the phage life cycle. Modification or masking of cell surface receptors prevents phage recognition, while superinfection exclusion systems (Sie) block the injection of bacteriophage nucleic acids if recognition occurs. Restriction-modification and the adaptive CRISPR-Cas systems target foreign nucleic acids that have entered the cell, and secondary metabolites can inhibit viral replication or transcription. Finally, abortive infection (Abi) systems halt bacteriophage propagation by inducing cell dormancy or programmed cell death [1].

It is now known that genes encoding these antiviral defense systems tend to cluster in regions called defense islands within the bacterial genome [2]. This observation has facilitated the discovery of previously unknown defense systems around already characterized defense genes. A four-gene operon, QatABCD, is one of the novel defense systems identified this way [3]. However, its precise mechanism of action remains unclear.

In this study, we investigate the effects of QatABCD components on *Escherichia coli* cell viability to determine a potential effector of the system. The growth of bacterial cells carrying plasmids with different deletion variants of the operon was monitored by measuring optical density in a plate reader under uninfected conditions. Additionally, phage infection dynamics were evaluated at varied multiplicities of infection (MOIs) using cells expressing the full QatABCD system. We find that specific QatABCD constructs differentially affect cell viability, pointing to candidate effector components of the system.

[1] A. B. Isaev, O. S. Musharova, and K. V. Severinov, “Microbial Arsenal of Antiviral Defenses – Part I,” Biochemistry (Moscow), vol. 86, no. 3, pp. 319–337, Mar. 2021, doi: 10.1134/s0006297921030081.

[2] K. S. Makarova, Y. I. Wolf, S. Snir, and E. V. Koonin, “Defense islands in bacterial and archaeal genomes and prediction of novel defense systems,” Journal of Bacteriology, vol. 193, no. 21, pp. 6039–6056, Sep. 2011, doi: 10.1128/jb.05535-11.

[3] L. Gao et al., “Diverse enzymatic activities mediate antiviral immunity in prokaryotes,” Science, vol. 369, no. 6507, pp. 1077–1084, Aug. 2020, doi: 10.1126/science.aba0372.

STUDY OF INTERACTIONS BETWEEN SHORT PROKARYOTIC ARGONAUTE AND HFQ PROTEIN

Jokūbas Šiaučiūnas[1], Edvinas Jurgelaitis[1], Evelina Zagorskaitė[1], Mindaugas Zaremba[1]

[1]Vilnius University, Life Sciences Center, Institute of Biotechnology, Vilnius, Lithuania
jokubas.siauciunas@gmc.stud.vu.lt

In recent years, bacterial antiviral defense systems have attracted significant global attention due to their role in uncovering prokaryotic biology and their potential applications in antibacterial therapies and genome editing. The diversity and complexity of these systems necessitate detailed investigation into their distinct mechanisms. Among them, some Argonaute proteins possibly exhibit interactive properties with a bacterial chaperone that modulates their activity.

This study aims to investigate the interaction between the widely conserved bacterial RNA chaperone Hfq and short prokaryotic Argonautes (pAgos). Hfq, an Sm-like RNA-binding protein, promotes base pairing between small RNAs (sRNAs) and their target mRNAs [1]. Because sRNAs are closely associated with stress response pathways, Hfq plays a critical role in bacterial adaptation to fluctuating environmental conditions. Although Hfq is primarily known for its role in translational regulation, evidence suggests functional interplay between Hfq and pAgo systems.

Short pAgos, together with toll/interleukin-1 receptor/resistance protein (TIR), form the heterodimeric abortive anti-infective defense system SPARTA. While the monomeric SPARTA complex detects phage infections through sensing foreign nucleic acid duplexes, the formation of an active tetrameric complex triggers nicotine adenine dinucleotide (NAD) depletion [2]. By analyzing interactions between Hfq and multiple SPARTA homologs, and assessing the influence of Hfq on SPARTA's NADase activity, this study seeks to clarify SPARTA's functional mechanisms and its dependence on auxiliary factors.

Investigating antiviral defense systems and their molecular interactions not only deepens our understanding of bacteria–phage dynamics but also opens new avenues for biotechnological applications and genetic engineering research.

[1] S. Park et al., "Dynamic interactions between the RNA chaperone Hfq, small regulatory RNAs, and mRNAs in live bacterial cells," eLife, vol. 10, Feb. 2021, doi: 10.7554/elife.64207.

[2] B. Koopal et al., "Short prokaryotic Argonaute systems trigger cell death upon detection of invading DNA," Cell, vol. 185, no. 9, pp. 1471-1486.e19, Apr. 2022, doi: 10.1016/j.cell.2022.03.012.

MONOCLONAL ANTIBODIES AGAINST STREPTOLYSIN O

Adrija Buturlakina[1], Indrė Kučinskaitė-Kodzė[1], Martynas Simanavičius[1]

[1]Vilnius University, Life Sciences Center, Institute of Biotechnology, Vilnius, Lithuania
adrija.buturlakina@gmc.stud.vu.lt

Streptolysin O (SLO) is a cholesterol-dependent cytolysin (CDC) produced by *Streptococcus pyogenes*. It is a main virulence factor of *S. pyogenes* that causes mild human infections such as pharyngitis, scarlet fever or severe infections such as necrotizing fasciitis and streptococcal toxic shock syndrome [1]. The pathogenic effect of SLO is based on its ability to form large pores approximately 30 nm in the cholesterol-containing cell membrane and induce host cell lysis [2]. Therefore, characterized SLO neutralising antibodies may provide valuable tools for reducing pathogenic effects.

In this study, a hybridoma collection (37 clones) producing monoclonal antibodies (MAbs) against SLO were characterized, evaluating their affinity, specifity, and potential applications in research. The MAbs were purified from a hybridoma growth medium using affinity chromatography. The purified MAbs were further characterized for specificity using enzyme-linked immunosorbent assay (ELISA), western blot (WB) and neutralizing activity determination methods. Among 37 MAbs, 16 were exclusively reactive with SLO, 21 MAbs were cross-reactive with perfringolysin O (PFO) and 22 MAbs were able to neutralize the cytolytic activity of SLO on a lung epithelial cell line. The overall results revealed four putative groups of the MAbs directed to different immunogenic regions of SLO. The selected MAbs from different groups will be further used for SLO epitope (recognizable sites) determination.

In conclusion, the characterized MAbs in this study may be useful for functional and structural studies of SLO and for the development of therapeutic or detection tools.

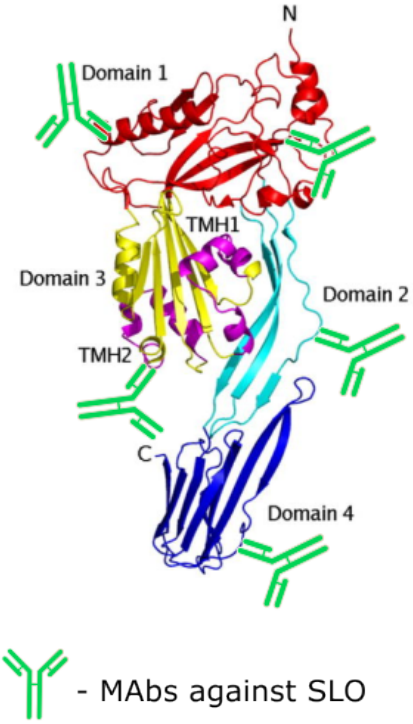


Fig. 1. SLO crystal structure [3]

[1] Walker, M. J., Barnett, T. C., McArthur, J. D., Cole, J. N., Gillen, C. M., Henningham, A., Sriprakash, K. S., Sanderson-Smith, M. L., & Nizet, V. (2014). Disease manifestations and pathogenic mechanisms of Group A Streptococcus. Clinical microbiology reviews, 27(2), 264–301. https://doi.org/10.1128/CMR.00101-13

[2] Stewart, S. E., D'Angelo, M. E., Paintavigna, S., Tabor, R. F., Martin, L. L., & Bird, P. I. (2015). Assembly of streptolysin O pores assessed by quartz crystal microbalance and atomic force microscopy provides evidence for the formation of anchored but incomplete oligomers. Biochimica et biophysica acta, 1848(1 Pt A), 115–126. https://doi.org/10.1016/j.bbamem.2014.10.012

[3] Feil, S. C., Ascher, D. B., Kuiper, M. J., Tweten, R. K., & Parker, M. W. (2014). Structural studies of Streptococcus pyogenes streptolysin O provide insights into the early steps of membrane penetration. Journal of molecular biology, 426(4), 785–792. https://doi.org/10.1016/j.jmb.2013.11.020

CHARACTERIZATION OF THE EC2APEA ANTIVIRAL PROTEIN THROUGH PHAGE INFECTIONS AND TOXICITY ASSAYS

Ema Ežerskytė[1], Jonas Juozapaitis[1], Giedrius Sasnauskas[1]

[1]Vilnius University, Life Sciences Center, Department of Protein-Nucleic acids Interactions, Vilnius, Lithuania
ema.ezerskyte@gmc.stud.vu.lt

The intense coevolutionary arms race between bacteria and phages has resulted in an unexpectedly wide and diverse array of antiphage defense systems [1]. While well-characterized antiviral systems such as CRISPR-Cas and restriction-modification directly target bacteriophage genetic material, abortive infection (Abi) systems function by activating toxic effectors upon infection, causing inhibition of metabolism or programmed death of the host cell to halt bacteriophage proliferation and protect the bacterial colony [2]. Many Abi systems rely on proteins containing HEPN (Higher Eukaryotes and Prokaryotes Nucleotide-binding) domain, which possesses endoribonuclease activity and is important in a variety of bacterial immune responses [3].

Our research focuses on one such Abi system ApeA which encodes a single protein ApeA with a HEPN domain variant as its key functional feature. While ApeA was previously shown to defend against a limited set of classic T phages [4], the molecular mechanisms were not yet clear. Our earlier work expanded the known antiphage spectrum of ApeA homologs and identified a highly active homolog Ec2ApeA. Structural analysis of Ec2ApeA revealed a loop, prominently changing its conformation during activation. The protein was also co-purified with a dinucleotide, suggesting a potential activation mechanism.

Here we aimed to explore the activation mechanism of Ec2ApeA further by assesing the functional importance of the structurally dynamic loop, as well as the potential dinucleotide signal in the cell. Targeted mutagenesis was used to evaluate the role of the conformationally dynamic loop and co-expression of a dinucleotide cleaving enzyme was employed to test the requirement of dinucleotides as signaling molecules in Ec2ApeA activation.

These experiments demonstrated that both the conformationally dynamic loop and the dinucleotide signal are critical for Ec2ApeA protein activation.

[1] H. Georjon and A. Bernheim, “The highly diverse antiphage defence systems of bacteria,” Nature Reviews Microbiology, vol. 21, no. 10, pp. 686–700, Jul. 2023, doi: 10.1038/s41579-023-00934-x.

[2] A. Lopatina, N. Tal, and R. Sorek, “Abortive Infection: Bacterial suicide as an antiviral immune strategy,” Annual Review of Virology, vol. 7, no. 1, pp. 371–384, Jun. 2020, doi: 10.1146/annurev-virology-011620-040628.

[3] V. Anantharaman, K. S. Makarova, A. M. Burroughs, E. V. Koonin, and L. Aravind, “Comprehensive analysis of the HEPN superfamily: identification of novel roles in intra-genomic conflicts, defense, pathogenesis and RNA processing,” Biology Direct, vol. 8, no. 1, p. 15, Jun. 2013, doi: 10.1186/1745-6150-8-15.

[4] L. Gao et al., “Diverse enzymatic activities mediate antiviral immunity in prokaryotes,” Science, vol. 369, no. 6507, pp. 1077–1084, Aug. 2020, doi: 10.1126/science.aba0372.

IN VITRO CHARACTERIZATION OF THE MOKOSH TYPE 1 ANTI-PHAGE DEFENSE SYSTEM

Matas Račickas[1], Edvinas Jurgelaitis[1], Arūnas Šilanskas[1], Mindaugas Zaremba[1]

[1]Vilnius University, Life Sciences Centre, Institute of Biotechnology, Department of Protein-DNA Interactions, VIlnius, Lithuania
matas.racickas@gmail.com

During the constant battle between bacteria and bacteriophages, bacteria have evolved a plethora of anti-phage defense systems. While restriction-modification, and CRISPR-Cas systems have been characterized to various extents, there remain completely uncharacterized and novel anti-phage defense systems. One of these systems, named after the Slavic goddess, protector of women's destiny, Mokosh, is a family of defense systems that is evolutionarily linked to eukaryotic immune system proteins, more specifically anti-transposon piwi-interacting RNA pathway proteins [1]. The Mokosh type I system is one of two in the Mokosh family and contains two proteins MkoA and MkoB, which contain four predicted domains (STK, RNA helicase, HTH, PLD, fig. 1) [2].

The primary aim of this study is to examine the specifics of each domain and its function. Here we present our findings on the Mokosh type I defense system, focusing mostly on *in vitro* experiments. Firstly, we optimized the expression of the proteins MkoA and MkoB in E. coli using different strains. Additionally, after successfully purifying both proteins together, two mutants were selected and purified as well. Subsequently, we tested different nucleic acid substrates using denaturing urea polyacrylamide gel electrophoresis, possible inhibitory mechanisms and nucleotide hydrolysis with microplate assays, as well as identifying possible oligomerization states using mass photometry and SEC-MALS.

This research unveils a new potential tool for biotechnology and could provide new insights into the evolution of eukaryotic immune system proteins. Our gathered data serves as a valuable first step in understanding the Mokosh type I anti-phage system and its mechanisms of action.

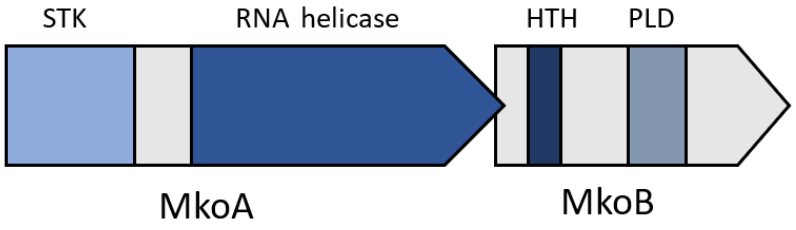


Fig. 1. Schematic representation of Mokosh type I predicted domain organization.

[1] Cury, Jean, et al. "Conservation of Antiviral Systems across Domains of Life Reveals Immune Genes in Humans." Cell Host & Microbe, vol. 32, no. 9, 28 Aug. 2024, pp. 1594-1607.e5, https://doi.org/10.1016/j.chom.2024.08.002

[2] Millman, Adi, et al. "An Expanded Arsenal of Immune Systems That Protect Bacteria from Phages." Cell, vol. 30, no. 11, 1 Nov. 2022, pp. 1556-1569.e5, https://doi.org/10.1016/j.chom.2022.09.017.

QCM-D/SE COMPARISON OF SB14 AND SB68 FC-FUSION NANOBODY IMMUNOCOMPLEX FORMATION WITH SARS-COV-2 VIRUS-LIKE PARTICLES

Mantvydas Usvaltas[1], Asta Lūčiunaitė[1,2], Vincentas Mačiulis[1], Ieva Plikusienė[1,3,4]

[1]State Research Institute Center for Physical and Technological Sciences, Sauletekio ave. 3 Vilnius, Lithuania.
[2]Vilnius University, Life Sciences Center, Institute of Biotechnology, Vilnius, Lithuania.
[3]Vilnius University, Faculty of Chemistry and Geosciences, NanoTechnas - Center of Nanotechnology and Materials Science, Naugarduko Str. 24, 03225 Vilnius, Lithuania.
[4]Vilnius University, Faculty of Medicine, Vilnius, Lithuania.
mantvydas.usvaltas@ftmc.lt

Macrophages may induce a strong inflammatory response when substantial amounts of inflammatory cytokines are secreted, which can lead to hyperinflammation and tissue damage [1]. This inflammatory response can be mediated by antibody-opsonized antigens called immunocomplexes (ICs). It has been experimentally confirmed that SARS-CoV-2 can activate this response, and antibody-opsonized SARS-CoV-2 particles can further enhance inflammation by promoting inflammasome activation [2]. The structural properties of immunocomplexes formed between an antibody and an antigen may affect IC interactions with FcR. Therefore, comparing how different antibodies form ICs with virus-like particles can help understand how IC structure may influence macrophage FcR engagement and support strategies to modulate macrophage responses in viral infections or antibody therapies, thereby avoiding adverse reactions.

In this work we compared how llama nanobodies fused with human IgG1 Fc - SB14 and SB68, form ICs with SARS-CoV-2 VLPs, which are assembled from the viral structural proteins and mimic the native virion. A self-assembled monolayer of 11-mercaptoundecanoic acid was used to covalently immobilize Protein G, enabling oriented capture of the Fc-fusion nanobodies and subsequent IC formation upon exposure to VLPs. By combining the quartz crystal microbalance with dissipation monitoring (QCM-D) and spectroscopic ellipsometry (SE) methods, we calculated the binding kinetics using a two-step interaction model, determined the wet and dry surface mass densities, and evaluated the viscoelastic properties of the formed VLP layers. A substantial difference was determined while comparing the viscoelastic properties of the formed layers: VLPs bound to SB68 produced a more viscoelastic layer, with an approximately two-fold larger frequency shift (ΔF) and higher dissipation (ΔD) than VLPs bound to SB14.

In this work, QCM-D and SE were used to compare SARS-CoV-2 VLP immunocomplex formation on SB14 and SB68 Fc-fusion nanobody layers. Surface mass density of the formed layers and binding affinity of the antigen-antibody interaction were evaluated which showed similar results for both nanobodies. ΔF and ΔD shifts revealed that the VLPs bound to SB68 formed a more viscoelastic layer than VLPs bound to SB14.

Acknowledgements

This work was supported by funded by Research Council of Lithuania, postdoctoral fellowship project No. [S-PD-24-156].

Keywords: antibody, viral antigen, QCM-D, SE

[1] D. Ragab, H. S. Eldin, M. Taeimah, R. Khattab, and R. Salem, “The COVID-19 cytokine Storm; What we know so far,” Frontiers in Immunology, vol. 11, p. 1446, Jun. 2020, doi: 10.3389/fimmu.2020.01446.

[2] C. Junqueira et al., “FcγR-mediated SARS-CoV-2 infection of monocytes activates inflammation,” Nature, vol. 606, no. 7914, pp. 576–584, Apr. 2022, doi: 10.1038/s41586-022-04702-4.

METABOLIC CHANGES IN VANDETANIB AND ROSMANTUZUMAB-TREATED HUMAN ENDOMETRIAL AND ENDOMETRIOTIC STROMAL CELLS

Žemyna Kazlauskytė[1], Rūta Navakauskienė[1], Aistė Zentelytė-Vilkė[1]

[1]Vilnius University, Life Sciences Center, Institute of Biochemistry, Department of Molecular Cell Biology, Lithuania
zemyna.kazlauskyte@gmc.stud.vu.lt

Endometriosis is a chronic inflammatory disease affecting about 1 in 10 women of reproductive age. Symptoms vary from pelvic pain and fatigue to nausea, depression, with severe cases causing infertility and organ adhesions. Currently, treatment for endometriosis is limited to hormonal therapy and surgical interventions. Hormonal therapy has side effects such as a reduction in bone density and is not suitable for every patient, while surgical methods are often invasive and not effective in preventing lesion regrowth [1].

New treatment strategies, including targeted pharmacological drugs, regenerative stem-cell therapy, immunotherapies, epigenetic and gene-based treatments, are being investigated [2]. To date, few studies have identified potential biomarkers and therapeutic targets for the disease. One recent analysis identified several potential markers and possible drug targets, including RSPO3 and EPHB4 proteins, which are important in lesion growth and angiogenesis, and it was proposed that the inhibition of these proteins could suppress lesion growth [3]. Rosmantuzumab and vandetanib are known inhibitors of RSPO3 and EPHB4, respectively, and the therapeutic potential of these drugs for endometriosis treatment remains unexplored.

Vandetanib modulates cellular metabolism through the inhibition of mTOR/HIF1α pathway. *In vitro* studies have shown that this inhibition leads to decreased GLUT1 and GLUT4 expression, resulting in reduced glucose uptake, thereby suppressing aerobic glycolysis [4]. Vandetanib has also been shown to reduce tumor glycolytic metabolism *in vivo*, as evidenced by decreased glucose uptake on 18F-FDG PET imaging [5]. RSPO3 enhances the Wnt/β-catenin pathway, which upregulates PDK1 and promotes glycolysis while suppressing oxidative phosphorylation [6]. Based on these mechanisms, we hypothesize that inhibiting EPHB4 with vandetanib and RSPO3 with rosmantuzumab will reduce glycolytic capacity and cell viability.

In this study, we aimed to determine the effects of rosmantuzumab and vandetanib treatments on cell viability (XTT assay), mitochondrial function, ATP production rate, glycolytic rate (Seahorse metabolic assays, Agilent), and gene expression (RT-qPCR) in both healthy endometrial and endometriotic stromal cells.

[1] L. García-Izquierdo et al., Int. J. Mol. Sci., 2024, 25(13), 7068.
[2] E. O. Tijani et al., Middle East Fertility Society Journal, 2025, vol. 30, no. 9.
[3] T. Tao et al., Front Endocrinol, 2024, 15:1416978.
[4] C. Sourbier, et al., Cancer Cell, 2014, 26(6):840–850.
[5] M. A. Walter, et al., J. Nucl. Med., 2011, 52(2):231–240.
[6] K. T. Pate, et al., EMBO J., 2014, 33(13):1454-73.

REAL-TIME INTERACTION STUDY OF COVALENTLY IMMOBILIZED SARS-COV-2 SPIKE PROTEIN AND SPECIFIC NANOBODIES

Smiltė Drobnytė[1], Mantvydas Usvaltas[2], Vincentas Maciulis[2], Asta Luciunaite[2], Ieva Plikusiene[2]

[1]Vilnius University, Faculty of Medicine, Pharmacy and Pharmacology Center, Vilnius, Lithuania
[2]State Research Institute Center for Physical and Technological Sciences, Sauletekio av. 3 Vilnius, Lithuania
Smilte.Drobnyte@gmail.com

The rapid evolution of SARS-CoV-2 and the emergence of variants with altered infectivity and immune escape properties continue to challenge existing therapeutic strategies. The viral spike (S) protein, which mediates host cell entry through interaction with the ACE2 receptor, remains a primary target for neutralizing monoclonal antibodies. Detailed characterization of spike–antibody interactions is therefore essential for the development and optimization of effective antibody-based therapies.

The aim of this study was to investigate and compare real time interactions between covalently immobilized SARS-CoV-2 spike protein with selected monoclonal antibodies and single-domain nanobodies. The SARS-CoV-2 spike protein was covalently immobilized on gold sensor surfaces using a self-assembled monolayer of 11-mercaptoundecanoic acid and EDC/NHS coupling surface chemistry. Real-time interaction analyses were performed using spectroscopic ellipsometry, quartz crystal microbalance with dissipation monitoring (QCM-D), and surface plasmon resonance. These complementary label-free techniques enabled monitoring of immobilization efficiency, antibody binding kinetics, and surface regeneration under controlled conditions.

During this study stable and reproducible conditions for immobilization of the spike protein were achieved. All investigated antibodies demonstrated specific binding to the immobilized antigen, with distinct interaction profiles. Quantitative analysis revealed differences in surface mass density and kinetic parameters among the antibodies, indicating variations in binding affinity and complex stability. Nanobody SB15 exhibited the strongest interaction with the spike protein, while CR3022 showed comparatively weaker binding .This study demonstrates the applicability of real-time, label-free biophysical methods for detailed evaluation of SARS-CoV-2 spike protein interactions with monoclonal antibodies. The obtained results provide valuable insight into antibody binding behavior and support the rational selection and design of antibody-based therapeutics against SARS-CoV-2 and its emerging variants.

PRODUCTION OF VB_ECOS_NBD2 BACTERIOPHAGE-ORIGINATED POLYTUBES USING DIFFERENT YEAST EXPRESSION HOSTS

Paulina Kočiūnaitė[1], Laima Čepulytė[1], Rasa Petraitytė-Burneikienė[1]

[1]Vilnius University, Life Sciences Center, Institute of Biotechnology, Department of Eukaryote Gene Engineering, Vilnius, Lithuania
paulina.kociunaite@gmc.stud.vu.lt

Virus-like particles (VLPs) are protein nanostructures that mimic viral morphology while lacking infectious genetic material. Their structural versatility and safety have positioned VLPs as promising platforms for biomedical applications, including vaccine development and immunotherapy [1]. Nonetheless, since no single structure is universally suitable for all applications, the identification of new VLPs remains essential. Among these, the nanostructures formed by the tail tube protein gp39 of bacteriophage vB_EcoS_NBD2 exhibit high potential due to their stability and immunogenicity [2].

Yeast-based recombinant systems represent an attractive approach, as they do not release endotoxins, allowing the production of recombinant proteins suitable for therapeutic use. Nevertheless, yeast strains differ in their characteristics, including glycosylation patterns, which can significantly influence downstream protein use [3]. The aim of this study was to analyse the suitability of different yeast species for producing recombinant bacteriophage tail tube protein gp39, as well as its purification and self-assembly into polytubes.

In this study, recombinant gp39 protein expression experiments were conducted using *Saccharomyces cerevisiae*, *Kluyveromyces lactis*, *Kluyveromyces marxianus*, and *Pichia pastoris* yeast. The sufficient expression was achieved only in the *K. lactis* and *S. cerevisiae* systems. Therefore, nanostructures were purified using sucrose density gradient centrifugation and analysed by electron transmission microscopy to assess VLP tube assembly. Furthermore, quantitative yield analysis demonstrated variations in gp39 production efficiency between yeast species.

The results show differences in bacteriophage gp39 expression and VLP assembly in yeast. *S. cerevisiae* was identified as the most effective platform for gp39-based VLP production, supporting their potential use in future experiments.

Acknowledgements
The research is funded by the Research Council of Lithuania (LMTLT), under agreement No. S-MIP-24-41.

[1] M. F. Bachmann, P. Van Damme, F. Lienert, and T. F. Schwarz, “Virus-like particles: a versatile and effective vaccine platform,” Expert Review of Vaccines, vol. 24, no. 1, pp. 444–456, May 2025, doi: 10.1080/14760584.2025.2508517.
[2] A. Avižinienė, “Bakteriofago vB_EcoS_NBD2 kilmės nanovamzdelių pritaikymas baltyminių fragmentų eksponavimui,” Ph.D. dissertation, Vilnius University, Vilnius, Lithuania, 2022.
[3] N. Kulagina, S. Besseau, C. Godon, G. H. Goldman, N. Papon, and V. Courdavault, “Yeasts as biopharmaceutical production platforms,” Frontiers in Fungal Biology, vol. 2, p. 733492, Sep. 2021, doi: 10.3389/ffunb.2021.733492.

PROTECTIVE PROPERTIES OF PLANT-DERIVED NANOVESICLES AGAINST VIRAL INFLAMMATION BY MODULATING MITOCHONDRIAL RESPIRATION

Vaiva Kurlytė[1], Emilija Mikalauskienė[1], Zbignev Balion[2], Aistė Jekabsone[1,2]

[1]Lithuania, Kaunas, Lithuanian University of Health Sciences, Faculty of Pharmacy, Institute of Pharmaceutical Technologies
[2]Lithuania, Kaunas, Lithuanian University of Health Sciences, Institute of Cardiology, Preclinical Research Laboratory for Medicinal Products
vaiva.kurlyte@stud.lsmu.lt

Based on data provided by the World Health Organisation, lower respiratory tract infections were the 5th most common cause of death in 2021 [1]. Research highlights the importance of mitochondrial respiration as a critical factor in the cellular immune response to viral inflammation [2]. Plant-derived nanovesicles (PDNV) have a unique structure – a double phospholipid layer - which protects bioactive substances inside the vesicle and improves their targeted delivery to affected cells [3].

This topic is relatively new, and therefore the aim of this study was to analyse the effect of PDNV on mitochondrial respiration during viral inflammation.

Methods: PDNV isolation by polymeric precipitation method; human bronchial epithelial cells (HBEC-3KT) cultivation; Seahorse XF Cell Mito Stress test; cell viability analysis with fluorescent microscopy using Hoechst 33342 dye and propidium iodide; Bradford method.

Cell viability analysis results revealed that none of the analysed Poly (I:C) concentrations (0.01, 0.025 ,0.05, 0.075, 0.1, 0.25, 0.5, 0.75 and 1 µg/ml) had a significant effect on cell viability. A concentration of 1 µg/ml Poly (I:C) was used for further experiments. It was determined that PNDV statistically significantly reduced the number of dead cells exposed to Poly (I:C) compared to a group affected by Poly (I:C) alone. A cellular mitochondrial respiration test showed that PNDV restored both maximum and baseline respiration in cells exposed to Poly (I:C) and PNDV, compared to a group exposed only to Poly (I:C)

Plant-derived nanovesicles have the potential to improve mitochondrial respiration during viral inflammation induced by Poly (I:C). These results indicate that PDNVs possess virus-fighting properties. Further research is needed to explore their potential applications in treating virus-induced lower respiratory infections.

[1] World Health Organization: WHO, “The top 10 causes of death,” Aug. 07, 2024. https://www.who.int/news-room/fact-sheets/detail/the-top-10-causes-of-death
[2] X. Li et al., “Viral infection modulates mitochondrial function,” International Journal of Molecular Sciences, vol. 22, no. 8, p. 4260, Apr. 2021, doi: 10.3390/ijms22084260.
[3] M. Chai et al., “Leveraging plant-derived nanovesicles for advanced nucleic acid-based gene therapy,” Theranostics, vol. 15, no. 1, pp. 324–339, Dec. 2024, doi: 10.7150/thno.104507.

CHARACTERIZATION OF A NOVEL BACTERIAL ANTI-PHAGE DEFENSE SYSTEM

Miglė Paulikaitė[1], Radvilas Bendorys[1], Patrick Pausch[1]

[1]Vilnius University, LSC-EMBL Institute for Genome Editing Technologies, Lithuania
migle.paulikaite@gmc.stud.vu.lt

Bacteriophages (phages) pose a constant threat to bacteria, driving the evolution of diverse anti-phage defense mechanisms. Among these strategies, recently identified anti-phage systems involve protein components related to eukaryotic ubiquitination pathways. Characterization of these proteins is essential for elucidating their roles in bacterial immunity and phage evasion.

In this study, we focus on the functional characterization of a bacterial anti-phage defense system using bacteriophage spot titer assays to evaluate protection against phage infection. By introducing and analyzing mutations in system proteins, we assess how specific protein components and their variants contribute to effective defense and directly link protein-level changes to antiviral function. Greater knowledge of this bacterial anti-phage system could help enable the use of its mechanisms as modulable tools in biotechnology.

EEG-BASED NEURAL VARIABILITY AND INHIBITORY CONTROL ACROSS THE MENSTRUAL CYCLE: A HORMONE-VALIDATED LONGITUDINAL STUDY

Gabrielė Kukytė[1], Monika Palaimaitė[1], Ingrida Zelionkaitė[1], Rimantė Gaižauskaitė[1], Lauryna Filatovaitė-Vyčienė[1], Ramunė Grikšienė[1]

[1]Vilnius University, Life Sciences Center, Institute of Biosciences, Vilnius, Lithuania
gabriele.kukyte@gmc.stud.vu.lt

Growing evidence in neuroimaging studies increasingly indicates that interactions between women's sex hormones and neural processes such as excitation–inhibition balance, emotional processing, and cognition vary across the menstrual cycle. One proposed mechanism involves allopregnanolone, a neuroactive metabolite of progesterone that acts as a potent modulator of the GABAergic system. Allopregnanolone enhances inhibitory neurotransmission and reduces neural excitability, potentially contributing to variability in cognitive control across the menstrual cycle. However, there is still a lack of densely sampled longitudinal data that would reveal the dynamics of electrophysiological parameters across the menstrual cycle, largely due to limited temporal sampling and insufficient hormonal confirmation.

This study implements a high-resolution longitudinal case design to examine phase-dependent variability in neural activity and inhibitory control across the menstrual cycle in a healthy woman. Data were collected at six time points: early and late follicular phases, ovulation and early, mid, and late luteal menstrual phases. Salivary samples were obtained at each session to quantify progesterone concentrations and enable more precise identification of luteal phase timing in the menstrual cycle.

Resting-state electroencephalogram (EEG) was recorded with eyes open and closed, to analyse alpha-band activity and the aperiodic slope as markers of global neural activity and excitation–inhibition balance. Inhibitory control and attentional processes were assessed using a Go/No-Go paradigm measuring response inhibition and reaction times (RT). Additionally, the Barratt Impulsiveness Scale (BIS-11) and the Well-Being Questionnaire (WBQ) were administered during the early follicular and late luteal phases. The late luteal phase is commonly associated with premenstrual symptoms and rapid progesterone changes, whereas the early follicular phase is typically linked to symptom attenuation and improved subjective well-being.

By combining dense temporal sampling with hormonal validation and multimodal neurobehavioral assessment, this study provides a fine-grained characterization of within-person variability across the menstrual cycle.

ANALYSIS OF IN VITRO GENOTOXICITY OF VARIOUS SIZE AND SHAPE GOLD NANOPARTICLES IN HUMAN HEPATOMA CELL LINE (HepG2)

Viltė Slančiauskaitė[1], Emilija Striogaitė[2], Juozas Rimantas Lazutka[3]

[1]Lithuania, Vilnius, Vilnius University, Institute of Biosciences, Department of Botany and Genetics
vilte.slanciauskaite@gmc.stud.vu.lt

Gold nanoparticles possess unique physical and chemical properties that can be modified for specific applications in various fields — from biotechnology to medicine [1]. They are especially promising in the development of therapeutic treatments and drug delivery systems [2].

However, as their use in medicine, science, and industry continues to grow, it becomes increasingly important to thoroughly assess the potential impact of nanoparticles on human health and the environment, with particular attention to their safety.

To determine the potential negative effects of gold nanoparticles in a human hepatoma cell line (HepG2), we assessed their cytotoxicity using a mixture of acridine orange and ethidium bromide. Genotoxicity was studied using alkaline and enzyme-modified comet assays. Gold nanospheres of 5 nm and 40 nm did not induce cytotoxic effects in HepG2 cells, indicating maintained cell viability. In contrast, exposure to 10 nm gold nanorods reduced cell viability by 76–98%, indicating cytotoxicity. Overall, treatment with 5 nm and 40 nm gold nanospheres did not significantly alter DNA damage levels in HepG2 cells, although a statistically significant reduction in DNA damage was observed at 2 µg/mL for 5 nm nanospheres and at 1.5–2 µg/mL for 40 nm nanospheres.

Overall, the results indicate that gold nanoparticle cytotoxicity depends on particle shape, with gold nanospheres demonstrating better biocompatibility than nanorods, making them promising for biomedical use and underscoring the need for further investigation of gold nanorod toxicity.

[1] M. A. Beach et al., “Polymeric nanoparticles for drug delivery,” Chemical Reviews, vol. 124, no. 9, pp. 5505–5616, Apr. 2024, doi: 10.1021/acs.chemrev.3c00705.

[2] D. Mundekkad and W. C. Cho, “Nanoparticles in clinical translation for cancer therapy,” International Journal of Molecular Sciences, vol. 23, no. 3, p. 1685, Feb. 2022, doi: 10.3390/ijms23031685.

MODULATION OF INTERCELLULAR COMMUNICATION THROUGH CARDIOVASCULAR CONNEXIN - 43 GAP JUNCTION CHANNELS BY ANESTHETIC PROPOFOL

Orestas Makniusevičius[1], Tadas Kraujalis[1,2], Mindaugas Šnipas[1,3], Lina Kraujalienė[1]

[1] Lithuania, Kaunas, Lithuanian University of Health Sciences, Medical Academy, Institute of Cardiology
[2]Lithuania, Kaunas, Kaunas University of Technology, Department of Applied Informatics
[3]Lithuania, Kaunas, Kaunas University of Technology, Department of Mathematical Modelling
orestas.makniusevicius@lsmu.lt

Propofol is a widely used intravenous general anesthetic characterized by rapid induction and recovery. One of its major side effects is a reduction in systemic vascular resistance, leading to hypotension, and in some cases inhibition of cardiac conduction, resulting in bradycardia. Although these effects have been recognized for decades, the underlying molecular mechanisms remain incompletely understood. Propofol has been shown to modulate muscarinic receptors, sinoatrial node activity, and cardiac conduction in a concentration-dependent manner, while also exerting protective effects against ventricular arrhythmias during myocardial ischemia.

Several studies suggest that propofol may modulate intercellular coupling via gap junction channels composed of connexin - 43 (Cx43), which play a critical role in vascular coordination and cardiac impulse propagation. The aim of this study was to investigate the effects of propofol on Cx43 gap junction channels. Gap junctional conductance was measured in HeLa cells expressing Cx43 using the dual whole-cell patch-clamp technique.

Our results demonstrate that propofol significantly inhibits Cx43 gap junction channels, with complete inhibition observed at 45 µM. Previous studies have suggested that propofol modulates Cx43 gap junction channels via protein kinase C (PKC) activation, which phosphorylates Cx43 and reduces intercellular coupling. Consistent with these findings, we observed that a PKC-specific inhibitor significantly attenuated the inhibitory effect of propofol, confirming a PKC-dependent regulatory mechanism. To further investigate propofol's mechanism of action, we performed experiments using a truncated Cx43 construct lacking the C-terminal domain, which is a primary site of phosphorylation involved in the regulation of channel opening and closing. Interestingly, our initial data show that 45 µM propofol still induced a complete blockade of these truncated channels. These findings suggest that propofol inhibits Cx43 gap junction channels through both indirect and direct mechanisms.

Keywords: propofol, connexin, gap junction, action mechanism

EXPLORING SPATIAL VARIATION OF THE URBAN HEAT ISLAND IN RELATION TO URBAN STRUCTURE USING MACHINE LEARNING

Mehri Davtalab[1], Steigvilė Byčenkienė[1]

[1]Lithuania,Center for Physical Sciences and Technology (FTMC), Department of Environmental Research
mehri.davtalab@ftmc.lt

With the growth of urban populations and increasing heat emissions, the Urban Heat Island (UHI) effect has become an increasingly severe issue, contributing to higher energy consumption, more frequent extreme weather events, worsening air pollution, and public health risks [1, 2]. Understanding the factors influencing UHI is critical for improving the urban thermal environment. Previous studies have shown that the spatial pattern of artificial impervious surfaces plays a significant role; however, the effects of the morphological spatial patterns of impervious surfaces on UHI intensity remain underexplored. This study quantified four built-up landscape pattern metrics, including Edge Density (ED), Largest Patch Index (LPI), Percentage of Landscape (PLAND), and Mean Patch Area (MREA-MN), along with built-up volume, built-up surface area, and greenery, to investigate their effects on UHI intensity at scale 500 m in Vilnius, Lithuania. Using an explanatory machine learning approach, non-linear relationships between these factors and UHI intensity were identified. Spatial Random Forest model was applied to quantitatively assess their relationships with UHI. Results indicate that LPI is strongly associated with UHI intensity. Interactions among key variables show that high values of LPI or PLAND combined with high built-up volume are associated with elevated UHI levels.

Acknowledgements

This research was funded by the Lithuanian Research Council LMT and is implemented under the Postdoctoral Fellowship agreement Nr. S-PD-24-137

[1] A. Guo, J. Yang, X. Xiao, J. Xia, C. Jin, and X. Li, “Influences of urban spatial form on urban heat island effects at the community level in China,” Sustainable Cities and Society, vol. 53, p. 101972, Nov. 2019, doi: 10.1016/j.scs.2019.101972.

[2] B.-J. He, J. Wang, J. Zhu, and J. Qi, “Beating the urban heat: Situation, background, impacts and the way forward in China,” Renewable and Sustainable Energy Reviews, vol. 161, p. 112350, Mar. 2022, doi: 10.1016/j.rser.2022.112350.

FOOT STRUCTURE ASSESSMENT AND MANAGEMENT OF FLAT FEET IN CHILDREN

Dominykas Ševelis[1], Raimonda Bružienė[1], Gintarė Petrošienė[1], Birutė Sinkutė[1]

[1]St. Ignatius Loyola College, Department of Health Sciences and Technologies, Kaunas, Lithuania
dominykas.sevelis@stud.ilk.lt

Flat feet in children aged 7–10 represent a relevant health concern, as the foot arch is expected to be fully developed at this stage. According to World Health Organization data, flat feet affect approximately 16–22% of children in this age group and are more often associated with functional or structural foot alterations rather than a temporary developmental condition. If left unaddressed, flat feet may contribute to postural problems, musculoskeletal discomfort, reduced physical activity, and long-term orthopedic complications. This study aimed to explore innovative approaches for the detection and management of flat feet in children. The research was conducted in a primary school in Kaunas and involved twenty-four 7-year-old pupils. Foot structure was assessed using an “Elinvision” foot scanner, and selected cases of children with flat feet were analysed in greater detail. In addition, information provided by parents was used to evaluate current management practices and intervention strategies. The findings revealed common patterns in foot structure alterations and highlighted gaps in early detection and management. The results underline the importance of timely screening and targeted preventive measures in primary school-aged children, suggesting that early identification combined with appropriate intervention may help reduce the risk of persistent foot deformities and associated complications later in life.

Keywords: flat feet, symptoms, scanner, innovations

INNOVATIVE APPROACHES TO THE DEVELOPMENT OF NEXT-GENERATION ORTHOPEDIC DEVICES

Minvydas Gražulevičius[1], Zigmas Bolzanas[1], Vaida Keršienė[1], Birutė Sinkutė[1]

[1]St. Ignatius Loyola College, Department of Health Sciences and Technologies, Lithuania
minvydas.grazulevicius@stud.ilk.lt

Orthopedic braces are commonly used orthopedic technical devices intended to support joint stabilization, alleviate pain, and assist rehabilitation following injuries, surgical interventions, or chronic conditions. The demand for these devices is steadily increasing as a result of the rising prevalence of musculoskeletal disorders, population aging, sports-related injuries, and the growing emphasis on preventive healthcare. Driven by the demand for non-invasive treatment solutions, the European orthopedic braces market is expanding at an estimated annual rate of 5–7%. Individuals over the age of 65 are particularly affected by conditions such as osteoarthritis, osteoporosis, and spinal disorders, which contributes to an increased need for braces designed for the back, foot, knee, and hip. At the same time, the growing popularity of recreational sports activities, including running and football, has led to a higher incidence of ligament injuries and post-surgical rehabilitation cases, further increasing the use of orthopedic braces and splints. Advancements in technology create new possibilities for the development of lightweight and "smart" braces incorporating sensor-based systems and manufactured using 3D printing technologies. In addition, the expansion of e-commerce and over-the-counter availability has improved the accessibility of orthopedic braces. Overall, the demand for these devices remains stable and continues to grow, particularly for preventive and rehabilitative applications. The aim of this study was to perform patient testing using next-generation equipment and to implement advanced manufacturing approaches for orthopedic braces. Biomechanical movement analysis was carried out using portable Digitsole Pro equipment. The biomechanical data obtained were subsequently applied in a targeted manner to the design and production of lower-limb orthopedic technical devices. Furthermore, the study highlights the potential and future prospects of 3D printing technologies in the manufacturing of orthopedic technical solutions.

EFFECTIVENESS OF ORTHOPEDIC TEXTILE COMPRESSION BRACES IN SCAR TREATMENT

Birutė Sinkutė[1], Vykinta Vaitiekūnaitė[1], Danutė Maurušaitienė[2]

[1]St. Ignatius Loyola College, Department of Health Sciences and Technologies, Lithuania
[2]UAB "Orthopaedic Clinic", Lithuania
birute.sinkute@ilk.lt

The treatment of keloid and hypertrophic scars is a topical issue that receives constant attention in medical practice. During surgery for diseases of the forearm and wrist, even minor injuries to the hand can result in large keloid and hypertrophic scars forming as the wounds heal, which can impair the function of the structures in the hand. To date, no single treatment method or set of rules and standards has been found that would completely cure keloid and hypertrophic scars. Furthermore, existing treatment methods, such as laser scar removal, have a temporary effect, as irritating the skin causes the body to promote keloid regrowth (Era Esthetic, 2020). The aim of the study is to produce and analyze the effectiveness of orthopedic textile compression braces with a silicone component for the treatment of surgical scars after planned operations for diseases of the forearm and wrist. The braces with silicone components are manufactured according to the parameters of the scar (size, volume, color, location). The structure of the compression fabric and the composition of the threads are tailored to the location and parameters of the scar. The braces are designed for long-term use, resistant to fluids secreted by the human body, characterized by hydrophilic and hydrophobic properties, elastic and providing a medically proven pressure therapy effect without restricting body segments, joint mobility, closely following the anatomical contours of the body. The splints are slightly elastic, i.e., up to 10% in the longitudinal direction in one direction of weaving and very elastic up to 200% in the perpendicular/transverse direction of weaving. The study involved 80 patients who underwent elective surgery in the forearm-wrist-hand area, with primary healing of the surgical wound. Two to three weeks had passed between the surgery and inclusion in the study. The patients' surgical wounds were up to 10 centimeters long. The patients were aged between 18 and 70 years. All patients were randomly divided into control and treatment groups. The control (comparison) group received a placebo—an orthopedic textile non-compression braces without an integrated silicone component, while the treatment group received textile compression braces with silicone components according to the size and location of the scar. All study participants were required to attend scar assessments after 1 week, 3 weeks, 3 months, and 6 months. The Vancouver Scar Rating Scale used in the study showed that orthopedic textile compression braces with silicone components are an effective and efficient treatment method for surgical scars after planned surgery for forearm and wrist disorders. The use of orthopedic textile compression braces with silicone components had a significant effect on the scars of the subjects in the treatment group. After 6 months, 100% of the subjects experienced a change in pigmentation, 83% in scar height, 42% in color, and as much as 90% in scar flexibility

IN SILICO PREDICTION AND VALIDATION OF TnpB AND Cas12a OFF-TARGETS IN THE HUMAN GENOME

Lukrecija Petrikaitė[1], Marius Baltramonaitis[1], Tautvydas Karvelis[1]

[1]Vilnius University, Life Sciences Center, Institute of Biotechnology, Vilnius, Lithuania
lukrecija.petrikaite@chgf.stud.vu.lt

The ability to modify a living organism's genome in a targeted way allows precise changes in phenotype, revolutionizing life science research and providing treatments for genetic diseases that act on the problem at its core [1]. CRISPR-Cas nucleases are the most widely used genome editing tools to date, known for their high efficiency and easy programming. These nucleases use RNA as a guide, recognizing the target via Watson-Crick base pairing and creating double-stranded breaks in DNA, which are then sealed by the cell's intrinsic repair mechanisms, resulting in random insertions or deletions that can inactivate the gene, or precise alterations if a repair template is provided [2]. However, their large size is incompatible with adeno-associated virus vectors widely used in gene therapy for *in vivo* delivery of functional genes into target cells [3]. In 2021, transposon-encoded TnpB proteins were identified as compact RNA-guided nucleases, about 3 times smaller than Cas9 or Cas12a, making it an appealing candidate for use in genome editing [4].

Being guided by RNA makes TnpB and Cas nucleases versatile, but it also means that DNA sequences similar to the target site might also be edited because of partial RNA-DNA complementarity. Off-target editing can be detrimental, especially if coding or regulatory sequences are modified, making deliberate RNA design and nuclease choice crucial. There are certain tendencies of RNA-DNA mismatch toleration for each nuclease that allow the prediction of potential off-target sites based on sequence similarity. Although bioinformatic tools for specificity analysis are powerful, the identified sites won't necessarily be modified inside a living cell, largely depending on chromatin accessibility. Because of this, further experimental validation is needed [5].

This study investigates the potential for off-target activity of TnpB and Cas12a nucleases in human cells. Multiple target sequences were examined, including one shared between both nucleases, revealing evidence of unintended editing. These findings offer preliminary insights into the specificity of selected nucleases, highlighting the importance of target site selection to minimize unintended off-target cleavage.

[1] M. P. Hirakawa, R. Krishnakumar, J. A. Timlin, J. P. Carney, and K. S. Butler, "Gene editing and CRISPR in the clinic: current and future perspectives," Bioscience Reports, vol. 40, no. 4, Mar. 2020, doi: 10.1042/bsr20200127.

[2] M. Pacesa, O. Pelea, and M. Jinek, "Past, present, and future of CRISPR genome editing technologies," Cell, vol. 187, no. 5, pp. 1076–1100, Feb. 2024, doi: 10.1016/j.cell.2024.01.042.

[3] D. Liu et al., "Adeno-associated virus therapies: Pioneering solutions for human genetic diseases," Cytokine & Growth Factor Reviews, vol. 80, pp. 109–120, Sep. 2024, doi: 10.1016/j.cytogfr.2024.09.003.

[4] T. Karvelis et al., "Transposon-associated TnpB is a programmable RNA-guided DNA endonuclease," Nature, vol. 599, no. 7886, pp. 692–696, Oct. 2021, doi: 10.1038/s41586-021-04058-1.

[5] X.-H. Zhang, L. Y. Tee, X.-G. Wang, Q.-S. Huang, and S.-H. Yang, "Off-target effects in CRISPR/Cas9-mediated genome engineering," Molecular Therapy — Nucleic Acids, vol. 4, p. e264, Jan. 2015, doi: 10.1038/mtna.2015.37.

PARAGEOBACILLUS THERMOGLUCOSIDASIUS AS A RECOMBINANT HOST: OPTIMIZATION STRATEGIES

Elina Guogytė[1], Rūta Kananavičiūtė[1]

[1]Vilnius University, Life Sciences Center, Institute of Biosciences, Lithuania
elina.guogyte@gmc.stud.vu.lt

Parageobacillus thermoglucosidasius, also known as emerging thermophilic cell factories, is receiving a lot of attention in the field of biotechnology. It is known that *P. thermoglucosidasius* can be an excellent producer of recombinant proteins. The proteins of thermophilic microorganisms are highly valued due to their greater thermostability, structural stability and solubility compared to mesophilic proteins. However, there are still problems with the use of these bacteria in industrial processes. There is a lack of suitable genetic tools, such as stable and high copy number vectors, and the low transformation efficiency of these bacteria [1]. For this reason, in this study, we present strategies that will facilitate the utilization of these bacteria. The main goal of the study is to increase the efficiency of the transformation of *P. thermoglucosidasius* and to expand the set of vectors for the manipulation of these bacteria.

The first strategy was to increase the transformation efficiency of *P. thermoglucosidasius* using differentially methylated plasmid DNA. We used the pG2K shuttle plasmid isolated from 3 *E. coli* strains characterized by different DNA methylation patterns (DH5α (*dam+, dcm+*), RR1 (*dam-, dcm+*) and GM2163 (*dam-, dcm-*) and from the *P. thermoglucosidasius* DSM 2542^T. A "lab-made" electroporator generating square wave pulses was used to transfer the pG2K plasmid into bacteria [2]. The obtained study data show that the *E. coli* RR1 (*dam-, dcm+*) strain and *P. thermoglucosidasius* DSM 2542^T cells are the most suitable for plasmid amplification before transferring them to *P. thermoglucosidasius*.

The second strategy was to expand the selection of plasmid vectors for *P. thermoglucosidasius*. For this, a vector with the minimal pGTG5 plasmid *rep5* replicon [3], isolated from bacteria of the genus *Parageobacillus*, was constructed. The target *rep5* replicon sequence was amplified and used to replace the *repBST1* replicon of the pG1AK-pRpls-GFP vector using restriction and ligation reactions. The resulting pG5AK-GFP construct is expected to be a 3.8 kb shuttle vector containing *CoIE1* (origin of replication for *E. coli*), *rep5* (replication initiation protein), *kanR* (kanamycin resistance gene) and MCS (multiple cloning site). Due to its relatively small size, the pG5AK-GFP vector is predicted to exhibit higher bacterial transformation efficiency, consistent with theoretical knowledge that smaller plasmids transform more efficiently.

These strategies may help to adapt *P. thermoglucosidasius* as a recombinant host and expand the spectrum of recombinant proteins already synthesized in these bacteria. Such proteins could be particularly valuable in industrial, medical, and environmental protection field.

[1] M. Paredes-Barrada, P. Kopsiaftis, N. J. Claassens, and R. Van Kranenburg, "Parageobacillus thermoglucosidasius as an emerging thermophilic cell factory," Metabolic Engineering, vol. 83, pp. 39–51, Mar. 2024, doi: 10.1016/j.ymben.2024.03.001.

[2] V. Novickij et al., "High-frequency submicrosecond electroporator," Biotechnology & Biotechnological Equipment, vol. 30, no. 3, pp. 607–613, Feb. 2016, doi: 10.1080/13102818.2016.1150792.

[3] R. Kananavičiūtė, E. Butaitė, and D. Čitavičius, "Characterization of two novel plasmids from Geobacillus sp. 610 and 1121 strains," Plasmid, vol. 71, pp. 23–31, Oct. 2013, doi: 10.1016/j.plasmid.2013.10.002.

EFFECTS OF GRNA STRUCTURE ON ASCAS12A ACTIVITY IN E. COLI

Gabija Magelinskaite[1], Jonas Kubilius[1], John P. Cooper[1], Stephen K. Jones Jr.[1]

[1]Vilnius University, Life Sciences Center, EMBL Partnership Institute, Vilnius, Lithuania
gabija.magelinskaite@gmc.stud.vu.lt

CRISPR–Cas-based genome editing is characterized by substantial variability in editing efficiency across different genomic targets. It is hypothesized that more predictable and stable editing outcomes can be achieved by tailoring the entire guide RNA (gRNA) sequence to each specific target. To test this hypothesis, the construction of large and diverse gRNA plasmid libraries is required, together with functional assays capable of reporting gRNA-dependent cleavage efficiency at scale. In this study, gRNA activity was investigated using an Escherichia coli cleavage assay. An original gRNA plasmid library was compared with libraries subjected to Cas-mediated cleavage under induced and non-induced conditions. Cas expression was controlled by IPTG induction during bacterial growth, allowing direct comparison of cleavage-dependent library depletion. Following library propagation, plasmid populations were analyzed by high-throughput sequencing, and changes in gRNA representation were quantified. Overall, a scalable workflow was established for linking gRNA sequence variation to cleavage outcomes, thereby supporting the development of more predictable CRISPR guide design rules.

DEVELOPMENT OF CELL-BASED SCREENING SYSTEM FOR TnpB GENOME EDITING TOOLS

Bartė Žiliukaitė[1], Marius Baltramonaitis[1], Tautvydas Karvelis[1]

[1]Department of Protein-DNA Interactions, Life Sciences Center, Vilnius University, Lithuania
barte.ziliukaite@gmc.vu.lt

The discovery of CRISPR-Cas systems revolutionized genome editing, making the development of treatments for genetic diseases more achievable than ever. Currently, Cas9 and Cas12a are the most widely applied nucleases due to their high efficiency in double-strand DNA break induction and specificity in target sequence recognition. However, the large size of these nucleases is incompatible with the limited packaging capacity of adeno-associated viruses that are commonly used in *in vivo* therapy, creating a demand for smaller nucleases.

Recent studies have shown that Cas12 nucleases are derived from TnpB proteins encoded in the bacterial IS200/IS605 family insertion sequences [1]. TnpB also exhibit RNA-guided nuclease activity and are smaller (∼400 amino acids) than Cas12 family nucleases (500–1500 amino acids), and therefore are attractive candidates to be used for genome editing. The widely studied TnpB from *Deinococcus radiodurans* (ISDra2) can cleave genomic DNA in eukaryotic cells, but demonstrates lower activity compared to modern genome-editing tools [2]. Therefore, TnpB protein engineering is an appealing strategy to increase its activity, which in turn demands an effective screening system.

In this study, we aimed to develop a cell-based system to identify the active TnpB variants. We demonstrate the feasibility of detecting TnpB nuclease activity in a cellular context and outline the principles of a cell-based platform for screening TnpB variants.

In the future, such cell-based screening could be applied to large-scale studies of protein evolution and to the development of other nuclease properties, such as target specificity or recognition of TAM sequences.

[1] G. Sasnauskas et al., “TnpB structure reveals minimal functional core of Cas12 nuclease family,” Nature, vol. 616, no. 7956, Art. no. 7956, Apr. 2023, doi: 10.1038/s41586-023-05826-x

[2] T. Karvelis et al., “Transposon-associated TnpB is a programmable RNA-guided DNA endonuclease,” Nature, vol. 599, no. 7886, pp. 692–696, Nov. 2021, doi: 10.1038/s41586-021-04058-1

PSILOCYBIN INDUCES SYNAPTIC REMODELING BY MODULATING MICROGLIA

Milda Markutė[1], Ieva Šiugždaitė[1], Louise Ellen Schuberth[2], Maxime Veleanu[2], Stefan Vestring[2], Urtė Neniškytė[1]

[1]Vilnius University, Life Sciences Centre, Vilnius, Lithuania
[2]University Medical Center Freiburg, Dept. of Psychiatry and Psychotherapy, Germany
milda.markute@gmc.stud.vu.lt

According to the World Health Organization, Major Depressive Disorder (MDD) affects 5.7% of adults, of which 30% have treatment-resistant depression; therefore psychedelics are being investigated as a potential new therapy. MDD presents itself with a decrease in brain structure volume and plasticity, especially prefrontal cortex, hippocampus and amygdala [1]. Microglial cells are brain immune cells, that also prune inactive synapses. It is also known that in MDD, microglial phagocytosis of synapses increases, which leads to reduced synaptic plasticity. Psilocybin is now being researched as a possible treatment for MDD since it increases neuroplasticity and alleviates depression symptoms [2]; however, the mechanism is still not known. It is known that psilocybin lowers microglial phagocytic activity and production of ROS and NO [2], [3]. We hypothesize that psilocybin induces the number of synapses by modulating microglial activity (Fig. 1). This study aims to compare the number of synapses in stressed and psilocybin-treated animals and to identify microglial involvement in this process.

Experiment included six mice groups: control, 1 mg/kg psilocybin, 2 mg/kg psilocybin, held while others experienced CDM and saline, stressed and saline, stressed and 1mg/kg psilocybin. The brains were cryosectioned and stained using immunofluorescence. To identify synapses, we used presynapse (anti-VGAT) and postsynapse (anti-GEPHYRIN) antibodies and microglial (anti-IBA1) in the dorsal hippocampus. Brains were imaged using the SP8 confocal microscope. The differences in synaptic density between groups are presented in 3D reconstruction images obtained using IMARIS software.

Understanding the mechanism of psilocybin-induced neuroplasticity could help understand microglia cell physiology and extend MDD treatment options.

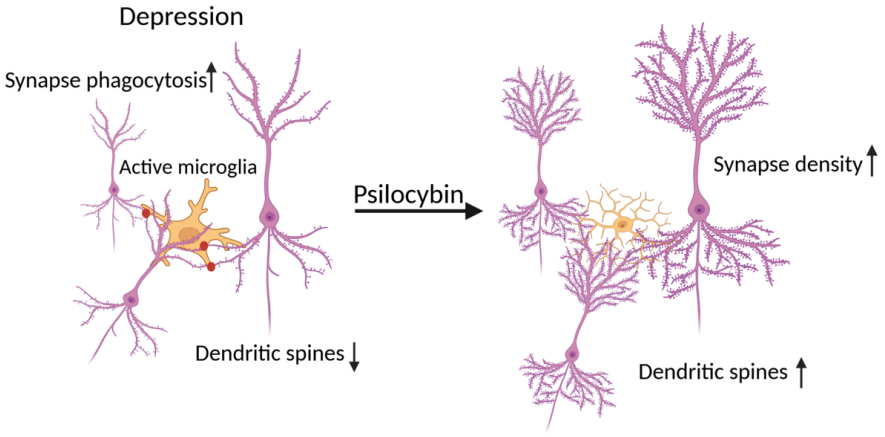


Fig. 1. In depression, the number of synapses decreases, which could be caused by their increased phagocytosis by microglia cells. We hypothesize that psilocybin increases the number of synapses by modulating microglial phagocytic activity. Created by BioRender.

Keywords: Microglia, depression, psilocybin, neuroplasticity

[1] V. M. Brown, S. Gujral, Y.-W. Chang, H. Galfalvy, K. Szanto, and A. Y. Dombrovski, "Brain volume reductions and relationship with depression and cognitive functioning in suicide in older adults: A cross-sectional and longitudinal study using Bayesian multilevel modeling," Biological Psychiatry Global Open Science, p. 100552, Jun. 2025, doi: https://doi.org/10.1016/j.bpsgos.2025.100552.

[2] B. Bassett et al., "Minocycline alleviates depression-like symptoms by rescuing decrease in neurogenesis in dorsal hippocampus via blocking microglia activation/phagocytosis," Brain, Behavior, and Immunity, vol. 91, pp. 519–530, Jan. 2021, doi: https://doi.org/10.1016/j.bbi.2020.11.009.

[3] K. R. Wiens, Noah, Ishvin Riar, B. K. Greuel, I. A. Lindhout, and Andis Klegeris, "Psilocin, the Psychoactive Metabolite of Psilocybin, Modulates Select Neuroimmune Functions of Microglial Cells in a 5-HT2 Receptor-Dependent Manner," Molecules, vol. 29, no. 21, pp. 5084–5084, Oct. 2024, doi: https://doi.org/10.3390/molecules29215084.

IN VIVO STUDY OF A NOVEL THOERIS EFFECTOR

Ignė Jačunskytė[1], Deividas Vilutis[1], Arūnas Šilanskas[1], Giedrė Tamulaitienė[1]

[1]Vilnius University, Life Sciences Center, Institute of Biotechnology, Department of Protein-Nucleic Acid Interactions, Vilnius, Lithuania
igne.jacunskyte@chgf.stud.vu.lt

Bacteria are constantly exposed to viral (bacteriophage) infections and have therefore evolved a diverse repertoire of innate immune defense systems [1]. Among these, the Thoeris antiviral defense system relies on Toll/interleukin-1 receptor (TIR) domain-mediated immune signaling [2]. Thoeris systems consist of two components: a TIR-domain-containing protein that senses phage invasion and generates a specific ADP-ribose-based immune signaling molecule, and an associated effector protein activated by this signal to induce cellular growth arrest or cell death, thereby aborting phage replication. Although several Thoeris system types have been characterized, large-scale genomic analyses have uncovered numerous Thoeris loci encoding previously uncharacterized effectorViln proteins with diverse domain architectures [3]. The frequent genomic association of TIR domains with genes encoding proteins of unknown function suggests that many Thoeris effectors act through yet undescribed molecular mechanisms.

In this study, we investigated the in vivo function of a previously uncharacterized Thoeris effector protein to define its role in TIR-mediated antiviral immunity. For functional analysis, the effector gene was cloned into E. coli expression vectors and introduced either alone or together with a TIR-domain–encoding gene via dual-plasmid electroporation, thereby establishing single-expression and co-expression conditions. Bacteriophage plaque assays demonstrated that expression of the effector alone did not confer antiviral protection, whereas co-expression with the TIR-domain protein resulted in phage resistance. These results indicate that the effector functions as a TIR-activated antiviral protein. Next, the effector protein was heterologously expressed in several E. coli strains, and expression was systematically evaluated across a range of induction conditions and growth temperatures to determine optimal protein production. Following optimization, the protein was purified by affinity chromatography.

These findings establish a functional framework for this previously uncharacterized Thoeris effector and lay the groundwork for future in vitro studies aimed at determining its molecular mechanism of action. Defining the function of this effector will expand our understanding of the mechanistic diversity of Thoeris defense systems and provide broader insight into conserved principles of TIR-mediated immune signaling across diverse biological domains.

[1] F. Tesson et al., “Exploring the diversity of anti-defense systems across prokaryotes, phages and mobile genetic elements,” Nucleic Acids Research, vol. 53, no. 1, Dec. 2024, doi: 10.1093/nar/gkae1171.

[2] S. Doron et al., “Systematic discovery of antiphage defense systems in the microbial pangenome,” Science, vol. 359, no. 6379, Jan. 2018, doi: 10.1126/science.aar4120.

[3] E. Yirmiya et al., “Systematic discovery of TIR-based immune signaling systems in bacteria,” bioRxiv, Dec. 2025, doi: 10.64898/2025.12.03.692087.

DESIGN AND CHARACTERIZATION OF A SYRINGE PUMP FOR MICROFLUIDICS

Mykolas Peleckis[1]

[1]Vilnius University, Faculty of Physics, Institute of Photonics and Nanotechnology
mykolas.peleckis@gmail.com

Microfluidic experiments require stable and accurate dosing of small volumes of fluid, which is why practical, easily modifiable, and inexpensive syringe pumps are an important part of laboratory equipment.

This work addresses the task of creating a prototype syringe pump for microfluidics, capable of repeatedly dispensing volumes of 0.1 – 10 ml and automatically converting the user-specified volume into stepper motor control steps.

The proposed solution is a self-designed mechanical structure manufactured using fused deposition modeling (FDM) 3D printing, using polylactic acid (PLA) plastic, acrylonitrile butadiene styrene copolymer (ABS) for the load-bearing joint, integrated with a NEMA17 stepper motor, a 0.56 mm step screw mechanism, Raspberry Pi 5 control (Python, GPIO), and an L298N driver. A 10 ml glass syringe filled with water was used for testing.

Experimental calibration showed that the optimal setting for a nominal 1 mL volume is 2370 steps/mL, and that dosing accuracy is primarily limited by mechanical backlash during direction reversal: 81.9 ± 2.6 steps, corresponding to a volume error of 0.034 ± 0.002 mL. It was found that, after calibration, changing the step delay (0.002 – 0.01) had no significant effect on volume accuracy, while adding tubing increased measurement variability and reduced accuracy.

The results confirm that the developed syringe pump is functional and suitable for laboratory microfluidic testing, providing repeatable dosing after calibration. Accuracy is mainly limited by backlash during direction changes, and added tubing increases variability; therefore, reducing mechanical play and increasing stiffness are key. Future work will optimize the drive and coupling, use lower-backlash components, and validate performance with different syringe sizes and real microfluidic channels.

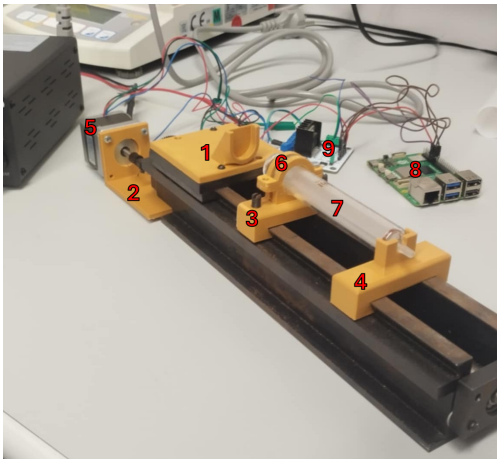


Fig. 1. Fully assembled syring prototype. 1 – syringe rear holder, 2 – motor mount to the system, 3 – syringe middle holder, 4 –syringe front holder, 5 – Nema 17 stepper motor, 6 – middle holder fastening, 7 – 10 ml glass syringe SIGMA–ALDRICH Z31458–1EA, 8 –Raspberry Pi 5, 9 – L298N driver.

MICROFLUIDIC FABRICATION OF ALGINATE MICRODROPLETS FOR PHOTODYNAMIC ANTIMICROBIAL THERAPY

Laura Milaknytė[1,2], Adei Abouhagger[1], Dr. Wanessa De Cassia Martins Antunes De Melo[1]

[1]Center for Physical Sciences and Technology, Department of Functional Materials and Electronics, Bioelectrics Laboratory, Lithuania
[2]Vilnius University, Life Sciences Center, Lithuania
laura.milaknyte@gmc.stud.vu.lt

Antimicrobial resistance has become a critical global health issue in 21st century, as bacterial tolerance to all currently used antibiotics has been detected and only a few novel medications are being developed [1]. In these circumstances antimicrobial photodynamic therapy (aPDT) has emerged as a promising alternative for the treatment of chronic wound infections. This method uses light-activated photosensitizers to generate reactive oxygen species (ROS) that kill pathogens without causing resistance. Methylene blue (MB) stands out among photoactive molecules because of its established clinical use, broad antimicrobial efficacy, and efficient absorption of red light (660–670 nm), which allows deeper tissue penetration [2].

To localize methylene blue exposure and support wound healing, the photosensitizer is commonly immobilized within alginate-based hydrogel systems. Alginate provides a biocompatible and optically transparent matrix that helps confine photodynamic activity and reduce off-target effects. However, most existing approaches rely on bulk hydrogels or polydisperse beads produced by batch emulsification, which result in broad size distributions and poorly controlled methylene blue loading. Therefore, photodynamic dosing remains undefined and difficult to reproduce. Moreover, despite the central role of ROS in aPDT, few researchers have quantified its output on a per-bead basis or evaluated how ROS generation evolves over repeated light activation cycles. These limitations restrict the predictability, optimization, and long-term applicability of alginate-based aPDT systems.

To address these challenges, a water-in-oil droplet microfluidic approach was developed for the fabrication of alginate microbeads. Highly monodisperse droplets were generated using a polydimethylsiloxane (PDMS) on glass microfluidic chip featuring a cross-junction geometry. Droplet formation and gelation were optimized by tuning aqueous and oil phase flow rates, alginate concentration, Tween 80 surfactant content in mineral oil, and calcium chloride crosslinking conditions. The resulting microbeads were characterized by optical microscopy to assess size, uniformity, and structural stability. Following methylene blue loading, reactive oxygen species generation was quantified on a per bead basis under controlled light activation, enabling direct evaluation of photodynamic behavior across microbead populations.

In summary, this work establishes a quantitative and reproducible framework for controlled antimicrobial photodynamic therapy dosing, enabling association between microbead design parameters and photodynamic output. Such an approach may facilitate the development of localized, reusable antimicrobial platforms, including wound dressings, catheter or implant coatings, and flow-based disinfection systems requiring precise photodynamic control.

Keywords: Microfluidics, Photodynamic Antimicrobial Therapy, Antimicrobial Resistance

[1] E. M. Darby et al., “Molecular mechanisms of antibiotic resistance revisited,” Nat. Rev. Microbiol., vol. 21, no. 5, pp. 280–295, May 2023, doi: 10.1038/s41579-022-00820-y.
[2] A. Solovieva et al., “Methylene Blue Solid Alginate Gels for Photodynamic Therapy: The Peculiarities of Production and Controlled Release of the Dye,” Polymers, vol. 16, no. 19, p. 2819, Jan. 2024, doi: 10.3390/polym16192819.

EVALUATION OF MICROBIAL CONTAMINATION IN USED MAKEUP FOUNDATION PRODUCTS AND ASSOCIATED APPLICATORS

Saulė Norkutė[1], Ugnė Januškaitė[1], Žaneta Maželienė[1], Asta Aleksandravičienė[1], Giedrė Jarienė[1]

[1]Kauno kolegija Higher Education Institution Pramones pr. 20, LT-50468 Kaunas, Lithuania
saule.nor302@go.kauko.lt

Nowadays, cosmetic products such as liquid and compact powder foundations play an important role in appearance and confidence improvement. Applicators maintaining direct contact with both the skin and the foundation products can transfer microorganisms, leading to bacterial colonization and cross-contamination [1]. In addition, the components contained in cosmetic products create favorable conditions for the growth and reproduction of bacteria and fungi [2]. Microbial contamination can lead to adverse skin reactions, particularly due to the presence of pathogenic bacteria, causing detrimental health effects in consumers [3]. According to previous investigations, Pseudomonas aeruginosa, Staphylococcus aureus, Escherichia coli, and different strains of Bacillus are the most common contaminants of makeup foundation products [4].

The aim of this study was to evaluate microbial contamination in used liquid and compact powder foundations, including their applicators. A total of 30 cosmetic samples were collected for analysis, equally divided into three categories: 10 compact powders, 10 liquid foundations and 10 makeup applicators. Inclusion criteria required all formulations to be within the manufacturer-specified expiration period (12–24 months). Furthermore, applicators were analyzed without prior cleaning following their most recent use. Collected samples were enriched in Eugon broth and inoculated onto selective nutrient media.

In 10 samples of compact powders, Bacillus spp. were identified in 100% of samples, S. aureus was identified in 10%, followed by coagulase-negative Staphylococcus spp. in 80% of samples. In 10 liquid foundations, Bacillus spp. were detected in 70%, while coagulase-negative Staphylococcus spp. were identified in 60% of samples. Lastly, in 10 samples of makeup applicators, Bacillus spp. were found in 100%, S. aureus in 10%, and coagulase-negative Staphylococcus spp. 90% of samples.

Results demonstrate that the bacteria species found in cosmetic products are Bacillus spp. and Staphylococcus spp. (including S. aureus) which may pose potential health risks to users. It is essential for manufacturers to strictly follow Good Manufacturing Practice (GMP) guidelines. Consumers should consider proper storage conditions of cosmetic products, avoid sharing them with others and observe the manufacturer's stated expiration dates in order to reduce microbial contamination.

[1] R. M. S. Attar and M. A. Imam, "Assessing the levels and types of bacterial contamination in cosmetic brushes: Implications for beauty and hygiene in Jeddah City," International Journal of Microbiology, vol. 2025, no. 1, p. 2128581, Jan. 2025, doi: 10.1155/ijm/2128581.

[2] J. D. Da Silva, F. a. M. Silva, and C. F. Rodrigues, "Microbial contamination in cosmetic products," Cosmetics, vol. 12, no. 5, p. 198, Sep. 2025, doi: 10.3390/cosmetics12050198.

[3] S. Akhand, A. Yadav, and D. K. Jain, "Potential contamination in cosmetics: a review.," EBSCOhost, Sep. 2023, doi: 10.31858/0975-8453.14.10.641-649.

[4] M. Ghias and L. Fozouni, "Assessment of microbial contamination and metabolite expo-sure in cosmetic products used in women's beauty salons," Iranian Journal of Public Health, vol. 53, no. 5, pp. 1175–1183, Jun. 2024, doi: 10.18502/ijph.v53i5.15599.

THE ABATEMENT OF MICROBIAL AIR POLLUTION USING IONIZATION TECHNOLOGIES

Patricija Kirvelaitytė[1], Justinas Masionis[1], Martynas Tichonovas[1], Dainius Martuzevičius[1]

[1]Lithuania, Kaunas, Kaunas University of Technology, Department of Environmental Technology
patricija.kirvelaityte@ktu.lt

Airborne viral and bacterial diseases represent a significant risk to public health, as demonstrated by global pandemics over the past century, including the ongoing COVID-19 pandemic and recurring seasonal influenza outbreaks. These events emphasize the importance of effective technologies for improving indoor air quality and reducing microbiological air pollution, particularly in healthcare environments such as hospitals and clinics, where airborne microorganism concentrations may be elevated [1].Common mitigation strategies include ultraviolet irradiation, chemical surface disinfection, and air filtration systems. However, their effectiveness varies, and additional technologies are required to ensure reliable air decontamination. Our main aim is to develop a technology that can ensure high efficiency in reducing microbiological air pollution. Ionization devices, such as unipolar and bipolar ionizers and their various types (needle ionizers, etc.) and plasma discharge devices, can improve air quality by up to 99% [2].

In this study, the efficiency of negative air ionization in reducing airborne bacterial contamination was investigated. A unipolar ionizer operating at a negative polarity voltage of 6 kV was used. A suspension of *Lactobacillus casei* containing 10^9 CFU mL^{-1} was aerosolized into a test chamber. Air samples were collected using an impinger after 5, 20, and 40 minutes with the ionizer switched ON and OFF. Collected samples were cultured on Petri dishes, incubated, and colony-forming units (CFU) were enumerated. Results are presented as mean values with standard deviation from three replicate measurements in Fig. 1.

The results demonstrate faster reduction of airborne CFU concentrations when ionization was applied compared to natural decay observed under control conditions. Fig. 1 shows the decrease in CFU over time when the ionizer is turned ON and OFF. After 40 minutes of ionizer operation, the reduction efficiency reached 95.06%. A gradual decrease in CFU was also observed when the ionizer was OFF, which can be attributed to natural sedimentation, gravitational settling, and desiccation of airborne bacteria. Ionization technology enhances this process by promoting the attachment of charged ions to bacterial cells, inducing oxidative stress and accelerating their removal from the air.

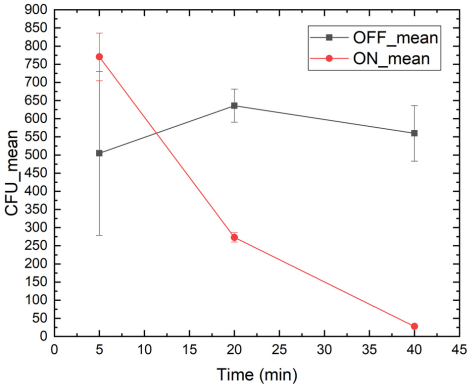


Fig. 1. Time-dependent variation of CFU with the ionizer ON and OFF.

The findings indicate that negative air ionization is an effective method for reducing microbiological air pollution and has strong potential for improving indoor air quality in enclosed environments, particularly in healthcare settings.

[1] L. Song et al., "Airborne pathogenic microorganisms and air cleaning technology development: A review," J. Hazard. Mater., vol. 424, Feb. 2022, Art. no. 127429, doi: 10.1016/j.jhazmat.2021.127429.

[2] R. Jangra, K. Ahlawat, A. Dixit, and R. Prakash, "Efficient deactivation of aerosolized pathogens using a dielectric barrier discharge based cold-plasma detergent in environment device for good indoor air quality," Sci. Rep., vol. 13, no. 1, Art. no. 37014, Dec. 2023, doi: 10.1038/s41598-023-37014-2.

ADVANCES IN ENGINEERING OF CHEMOLITHOAUTOTROPHIC BACTERIA FOR CARBON DIOXIDE FIXATION

Tasawar Abbas[1,2,3], Naglis Malys[1,2,3]

[1]Kaunas University of Technology, Faculty of Chemical Technology, Bioprocess Research Centre, Radvilėnų street 19, Kaunas, LT-50254, Lithuania
[2]Kaunas University of Technology, Faculty of Chemical Technology, Department of Organic Chemistry, Radvilėnų street 19, Kaunas, LT-50254, Lithuania
[3]Kaunas University of Technology, Faculty of Chemical Technology, Synthetic Biology and Biotechnology Research Group, Radvilėnų street 19, Kaunas, LT-50254, Lithuania
tasawar.abbas@ktu.edu

Chemolithoautotrophic bacteria utilize a hydrogen and other reduced compounds as electron donors for carbon dioxide (CO2) fixation offering an attractive alternative to light dependent photosynthetic systems. Seven natural metabolic pathways of CO2 fixation have been reported in chemolithoautotrophic bacteria including reductive pentose phosphate or Calvin-Benson-Bassham (CBB) pathway, reductive tricarboxylic acid (rTCA) or Arnon-Buchanan pathway, reductive acetyl Co-A or Wood-Ljungdahl (WL) pathway, 3-hydroxypropionate (3HP) bicycle or Fuchs-Holo pathway, 3-hydroxypropionate/4-hydroxybutyrate (3HP/4HB) pathway, dicarboxylate/4-hydroxybutyrate (DC/4HB) pathway and reductive glycine (rGly) pathway. Metabolic diversity in CO2 fixation by chemolithoautotrophic bacteria indicates their inherent potential for mitigation of climate change. Present work has investigated available literature on developments in detailed mapping and engineering of CO2 fixation metabolic pathways of chemolithoautotrophic bacteria through advanced strategies of metabolic engineering, systems biology, synthetic biology, genome sequencing and comparative genomics. Improvements in catalytic efficiencies of involved enzymes, energy supplies, redox cofactors, metabolic flux, heterologous expression of pathway genes, and systems level optimization of pathways are reviewed here. Special attention is dedicated to several synthetic pathways for CO2 fixation developed recently. Challenges of engineering the CO2-fixing organisms to reduce product toxicity, inhibition of competing pathways, and genetic stability are highlighted. Our findings highlight potential of chemolithoautotrophic bacteria for utilization in the sustainable carbon capture and circular bioeconomy.

Keywords: Chemolithoautotrophic bacteria, CO2 fixation, Metabolic engineering, Metabolic pathways, Biosynthesis, Synthetic Biology

NOTES

NOTES

NOTES

NOTES

NOTES

NOTES

NOTES

NOTES

ORGANIZERS

Faculty of Physics

CENTER FOR PHYSICAL SCIENCES AND TECHNOLOGY

OPTICA Advancing Optics and Photonics Worldwide | STUDENT CHAPTER VILNIUS UNIVERSITY

SPIE. STUDENT CHAPTER VILNIUS UNIVERSITY

EPS Young Minds

SPONSORS

LIGHT CONVERSION

THORLABS

EKSPLA

astrolight

OPTOMAN

Standa

Eksma Optics

LIDARIS LIDT Service

BARNAS MASS SPECTROMETRY

finance united
we count what really counts

BIOTECHA

Altechna

DMC Direct Machining Control

MONO SPEKTRA

senso life
Co-created in Lithuania

BOLDCUP